U.S. DEPARTMENT OF THE INTERIOR
U.S. GEOLOGICAL SURVEY

NATIONAL EARTHQUAKE HAZARDS REDUCTION PROGRAM, SUMMARIES OF TECHNICAL REPORTS VOLUME XXXIV

Prepared by Participants in

NATIONAL EARTHQUAKE HAZARDS REDUCTION PROGRAM

Compiled by

Muriel L. Jacobson

The research results described in the following summaries were submitted by the investigators in September 1991 and cover the period from April 1991 through October 1, 1991. These reports include both work performed under contracts administered by the Geological Survey and work by members of the Geological Survey. The report summaries are grouped into the four major goals of the National Earthquake Hazards Reduction Program.

Open File Report No. 93-195

The data and interpretations in these progress reports may be reevaluated by the investigators upon completion of the research. Readers who wish to cite findings described herein should confirm their accuracy with the author.

EARTHQUAKE HAZARDS REDUCTION PROGRAM

CONTENTS - VOLUME I

Goal I - Understanding what happens at the earthquake source

Why and how does a segment of a geologic fault suddenly slip and produce an earthquake? What physical conditions within the Earth control where and when an earthquake occurs?

Goal II - Evaluating the potential of future earthquakes

Where are future earthquakes likely? How large will they be? How often will they occur? When will they occur? Where are future earthquakes unlikely?

EARTHQUAKE HAZARDS REDUCTION PROGRAM

CONTENTS - VOLUME II

Goal II - Evaluating the potential of future earthquakes

Where are future earthquakes likely? How large will they be? How often will they occur? When will the occur? Where are future earthquakes unlikely?

Goal III - Predicting the effects of earthquakes

During an earthquake of a certain magnitude, how severely and for how long will the ground shake? Where will hillsides slide, and flatlands fissure and crack? On what types of ground will earthquake damage be concentrated? Which faults will offset the Earth's surface? By how much? Which coastlines will be elevated or submerged? Where will destructive sea waves be generated? What losses to structures are expected?

Goal IV - Using research results

What new hazard reduction strategies become possible as understanding of earthquake phenomena advances? What scientific information is needed and can be furnished to practitioners in the engineering, land-use planning and emergency managements communities? How can such information be most effectively communicated to these practitioners?

Regional Seismic Monitoring Along The Wasatch Front Urban Corridor And Adjacent Intermountain Seismic Belt

1434-92-A-0966

W. J. Arabasz, R. B. Smith, J. C. Pechmann, and S. J. Nava
Department of Geology and Geophysics
University of Utah
Salt Lake City, Utah 84112
(801) 581-6274

Investigations

This cooperative agreement supports "network operations" associated with the University of Utah's 81-station regional seismic telemetry network. USGS support focuses on the seismically hazardous Wasatch Front urban corridor of north-central Utah, but also encompasses neighboring areas of the Intermountain Seismic Belt. Primary products for this USGS support are quarterly bulletins and biennial earthquake catalogs.

Results (October 1, 1991 - September 30, 1992)

General accomplishments. During the report period, significant efforts related to: (1) implementation of a distributed computer system (4 SUN Sparc 2 workstations with associated peripherals) for processing and analysis of network data and data from portable seismographs; (2) implementation of a Concurrent 7200 computer for online data acquisition (our prior data acquisition computer, a PDP 11/34, was phased out in September 1992); (3) experimental use of 5 REF TEK digital recorders for supplementing regional-network data collection; (4) continued upgrading of site hardware and electronics at field stations that have been operating since the mid-1970s; and (5) installation and operation of five temporary telemetered stations and one REF TEK digital recorder in and around the source area of an M_L 5.8 earthquake in southwestern Utah.

Network Seismicity. Figure 1 shows the epicenters of 1241 earthquakes ($M_L \leq 5.8$) located in part of the University of Utah study area designated the "Utah region" (lat. 36.75°-42.5°N, long. 108.75°-114.25°W) during the period October 1, 1991 to September 30, 1992. The seismicity sample includes 31 shocks of magnitude 3.0 or greater (earthquakes of M_L 4.0 and greater are labeled in Fig. 1) and 19 felt earthquakes.

The largest earthquake during the report period was a shock of M_L 5.8 on September 2, 1992 (10:26 UTC), located 8 km ESE of St. George, in southwestern Utah. This earthquake caused structural damage in at least three localities within about 50 km of the epicenter, produced liquefaction along the nearby Virgin River, and triggered a massive, destructive landslide 45 km to the ENE in the town of Springdale. No surface faulting was observed. This earthquake was followed by remarkably few aftershocks. Other notable earthquakes that occurred during the report period included: (1) an M_L 4.2 shock on March 16, 1992 (14:42 UTC), located under the western Traverse Mts., the southern boundary of the Salt Lake Valley; and (2) a swarm of 34 locatable earthquakes, occurring on June 28-29, 1992, 11 km NW of Cedar City ($0.5 \leq M \leq 4.1$). Approximately 25% of the seismicity detected during the report period was associated with an area of ongoing coal-mining related seismicity, located within a 60 km radius of Price in east-central Utah (311 shocks, $1.2 \leq M \leq 3.7$). For more details about some of the larger earthquakes, see our companion research summary in this volume (R.B. Smith and others).

Reports and Publications

Nava, S.J. (1991). Earthquake Activity in the Utah Region, January 1 - March 31, 1991, *Wasatch Front Forum (Utah Geological and Mineral Survey) 7*, no. 3, 2.

Nava, S.J. (1991). Earthquake Activity in the Utah Region, April 1 - June 30, 1991, *Survey Notes (Utah Geological and Mineral Survey) 25*, no. 1, 7; also published in *Wasatch Front Forum (Utah Geological and Mineral Survey) 7*, no. 4, 2.

Nava, S.J. (1992). Earthquake Activity in the Utah Region, July 1 - September 30, 1991, *Wasatch Front Forum (Utah Geological and Mineral Survey) 8*, no. 1, 2; also published in *Survey Notes (Utah Geological and Mineral Survey) 25*, no. 2, 11.

Nava, S.J. (1992). Earthquake Activity in the Utah Region, October 1 - December 31, 1991, *Wasatch Front Forum (Utah Geological and Mineral Survey) 8*, no. 2, 2.

Christenson, G.E. (Compiler) (1992). The March 16, 1992 M_L 4.2 Western Traverse Mountains earthquake, Salt Lake County, Utah, *Utah Geological Survey Open-file Report 255*, 18 pp.

Arabasz, W.J., Nava, S.J., and Pechmann, J.C. (1992). Earthquakes near Cedar City, Utah, June 28-29, 1992, *University of Utah Seismograph Stations Preliminary Earthquake Report*, 5 pp; also published in *Wasatch Front Forum (Utah Geological and Mineral Survey) 8*, no. 2, 4-7.

Arabasz, W.J., Pechmann, J.C., and Nava, S.J. (1992). The St. George (Washington County), Utah, earthquake of September 2, 1992, *University of Utah Seismograph Stations Preliminary Earthquake Report*, 6 pp.

Arabasz, W.J., Pechmann, J.C., Nava, S.J., and Wallace, T.C. (1992). EERI Special Earthquake Report, St. George, Utah, September 2, 1992, *EERI Newsletter 26*, no. 10, 6-7.

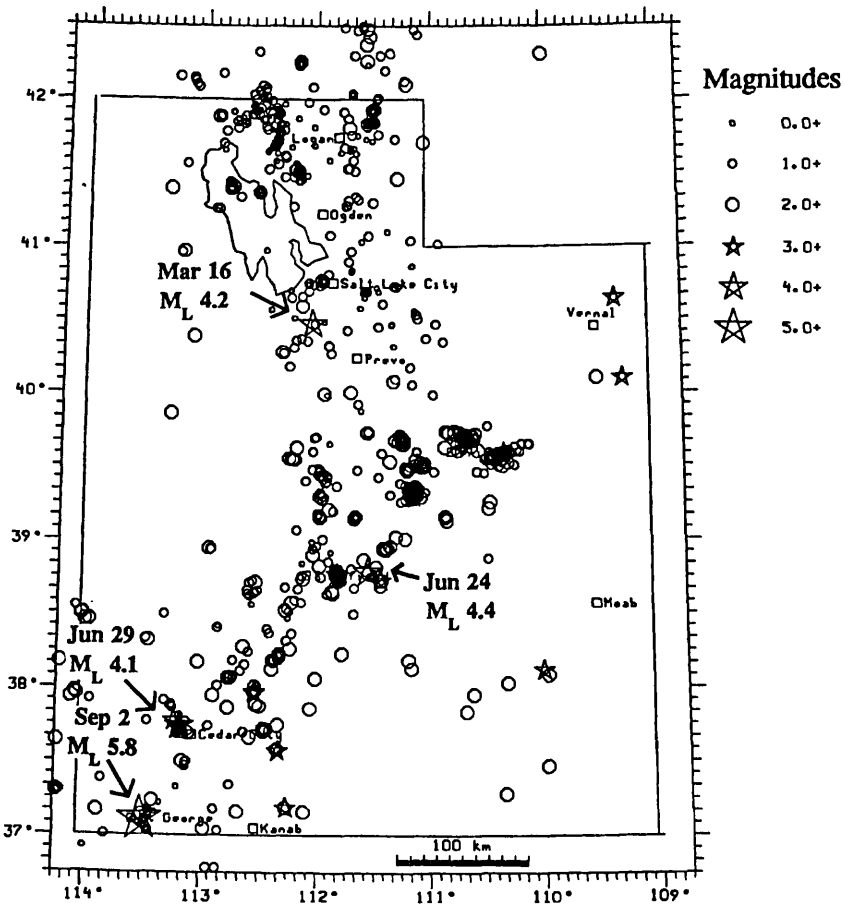

Figure 1. Earthquakes in the Utah region, October 1, 1991, through September 30, 1992. Shocks of magnitude 3.0 or greater are plotted as stars; those less than magnitude 3.0 as circles.

SPATIAL VARIATION OF STRESS DROPS OF LOMA PRIETA AFTERSHOCKS, DATED JANUARY 28, 1991

USGS 1434-92-G2204

Ralph J. Archuleta and Grant T. Lindley
Institute for Crustal Studies and Department of Geological Sciences
University of Calfiornia, Santa Barbara
Santa Barbara, CA 93106
(805) 893-4477 or x4893

Objective

The goal of this project is to measure source parameters of aftershocks of the October, 1989, Loma Prieta, California, earthquake and to study the variation of those source parameters with hypocentral location. In addition, the study has been broadened to examine the spatial variation of source parameters of aftershocks of the May, 1983, Coalinga, California, earthquake. The purpose is to study the spatial variation of source parameters of small earthquakes in order to better understand the nucleation and termination of large earthquakes. The ultimate goal is to be able to identify likely nucleation and termination zones of large earthquakes by analysis of small background earthquakes.

Results

Source parameters (stress drops and moments) have been determined for 392 aftershocks of the Loma Prieta earthquake and 108 aftershocks of the Coalinga earthquake. The data used in each case are digital recordings of aftershocks from portable instruments. The source parameters are determined from least-squares best fits to the Fourier amplitude spectrum of P- and S-waves. Parameters of the least-squares best fits to the Fourier spectra include the low-frequency spectral asymptote and the corner frequency. These parameters can be used to estimate the seismic moment and the stress drop of the aftershocks. Also included in the spectral fits is the parameter t* that determines the attenuation of the seismic waves. The parameter t* is the travel time divided by the quality factor of attenuation, Q. It is necessary to include attenuation in the spectral fits in order to accurately determine source parameters.

Cross sections showing stress drops of aftershocks of the Loma Prieta earthquake are shown in Figure 1. The darker areas show higher stress drop areas. A good correlation exists between the spatial variation of stress drop for P- and S-waves. The P- and S-wave spectral fits are independent of one another and the correspondence of the results is therefore important.

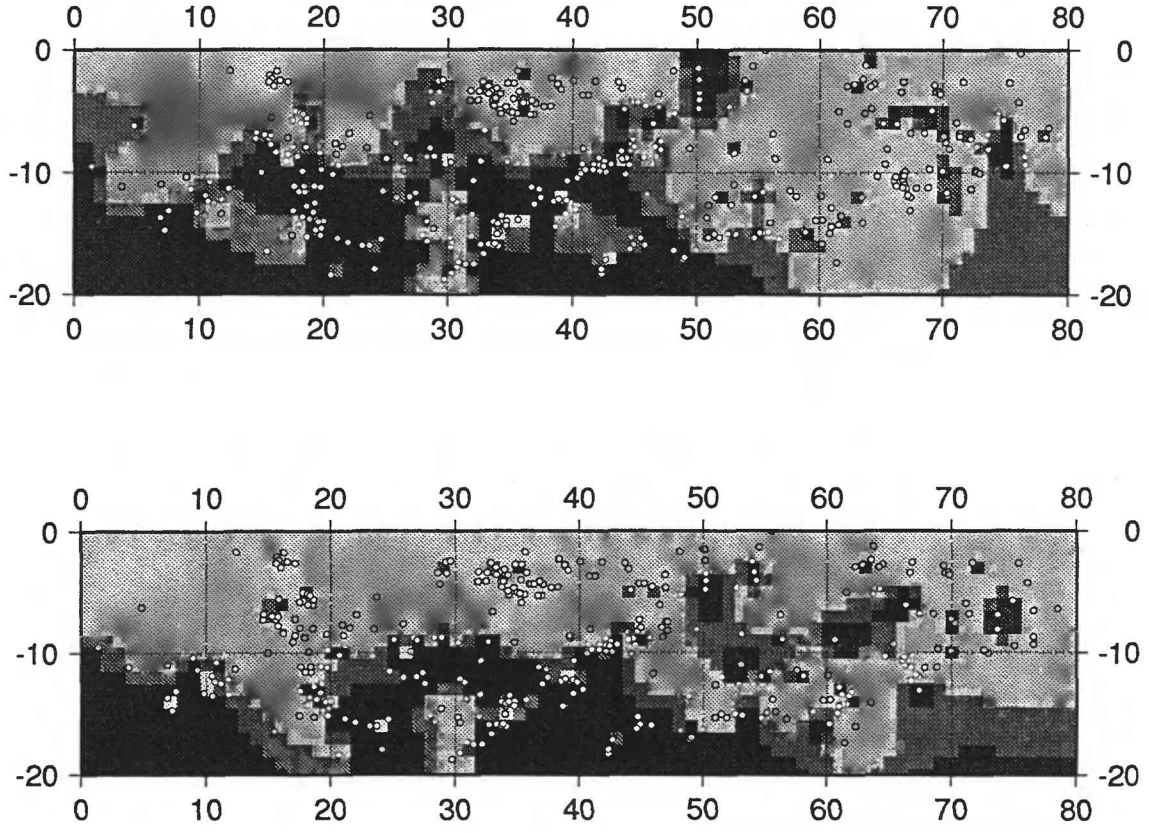

Figure 1. Cross sections along strike of the San Andreas Fault showing stress drops of Loma Prieta aftershocks: top) P-waves, bottom) S-waves. Higher stress drop areas are darker. Note the good correspondence of the P-wave and S-wave results.

Results at Coalinga indicate a high stress drop zone of aftershocks just above the main shock rupture zone (Figure 2). This high stress drop zone of aftershocks may indicate a high strength barrier that terminated the rupture of the main shock in the updip direction. The main shock hypocenter is located just below this zone of high stress drop aftershocks

and it is possible that the main shock nucleated at the edge of this high strength barrier. The cause for this high strength barrier is speculated to be the transition from a well-defined fault zone to intact rock. Also at Coalinga and Loma Prieta, there are several examples of high stress drop aftershocks that were followed by magnitude greater than five earthquakes located in nearly the same hypocentral locations. These results indicate that stress drops of small earthquakes may be useful in the identification of likely nucleation and termination zones of larger earthquakes.

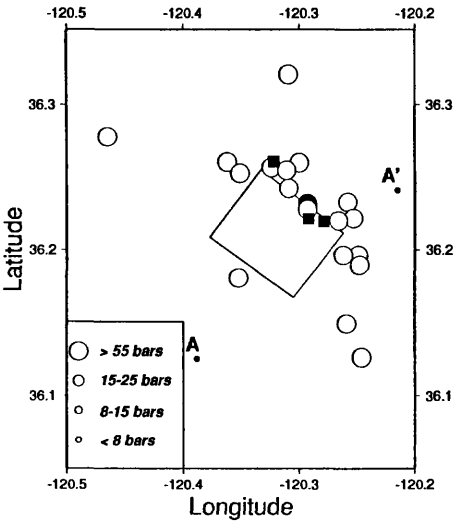

Figure 2. Map view shows twenty highest stress drop earthquakes. High stress drop earthquakes are concentrated to the north and east of the main shock rupture zone (rectangle) as identified by previous geodetic analysis. This zone is interpreted to be a high strength barrier that terminated the main shock rupture in the updip direction. Solid square shows the main shock hypocenter. Shaded circle and squares are magntiude >5 aftershocks.

Published Reports

Lindley, G. T. and R. J. Archuleta (1992). Earthquake source parameters and the frequency dependence of attenuation at Coalinga, Mammoth Lakes, and the Santa Cruz Mountains, California, *J. Geophys. Res.*, **97**, 14,137-14,154.

Lindley G. T. (1992). Spatial variation of aftershock source parameters and rupture process of the 1983, Coalinga, California, earthquake, submitted to *Bull. Seism. Soc. Am.*.

Lindley, G. T. and R. J. Archuleta (1991). Spectral analysis of Loma Prieta aftershocks to determine site and source effects (abstract), *Eos*, **72**, 338.

Seismic Source Analysis Using Empirical Green's Functions

9910-02676

John Boatwright and Leif Wennerberg
Branch of Engineering Seismology and Geology
U.S. Geological Survey, MS 977
Menlo Park, California 94025
(415) 329-5609, 329-5607

Investigations

(1) Seekins and Boatwright (1992) derived the relative site response as an function of frequency for a set of 11 accelerograph stations and 23 seismograph stations in the City of San Francisco. In general, the accelerographs recorded only the Loma Prieta main shock, while the seismographs recorded only aftershocks. The two data sets have been combined using recordings of aftershocks at four of the accelerograph sites. There is enough redundancy in the data set to make weak tests of the consistency of the strong and weak motion site response at these stations. We have grouped these 31 different sites according to the underlying rock-type: Franciscan sandstone, Franciscan serpentine, miscellaneous sand, and bay mud. Station MAS, sited in an ammunition bunker on Franciscan sandstone at Fort Mason, is used as the reference site. The relative site amplification for each rock-type appear to be remarkably consistent functions of frequency. The bay mud averages plotted in Figure 1 exhibit a peak at 1 Hz amplified by a factor of 5-6, a broad sidelobe at 2-3 Hz amplified by a factor of 3, and little relative amplification at 10 Hz. The sand averages have little relative amplification below 1 Hz, but are uniformly amplified by a factor of 2-3 at frequencies above 2 Hz. While these results are specific only to the limited range of rock-types and site conditions in San Francisco, this study is the first to demonstrate that site amplification can be regionally characterized using rock-specific functions of frequency.

(2) In FY91, Fletcher and Boatwright (1991) devised a spectral inversion technique to analyze the geometrical and anelastic attenuation using a line of stations sited along the axis of the San Francisco Pennisula from the Santa Cruz Mountains up to San Francisco. After fitting for source parameters and average attenuation parameters, the residuals are projected onto the set of stations and to a set of distances, resulting in a map of residual attenuation as a function of distance and frequency. These inversions are iterated until the misfit is minimized. This technique was applied to a set of vertical recordings of S-wave trains (that is, S, S_mS, S_n, and Lg) obtained from 1980 through 1990 on the Eastern Canadian Telemetered Network (ECTN). The 97 earthquakes analyzed range

in size from $3 < m_{bLg} < 6.5$; the epicentral distances range from 25 to 1000 km. The average S-wave attenuation for the data set is reasonably described by the function $R^{-\gamma}exp(\pi fT/Q)$ with $Q = 1997$ and $\gamma = 1$. The residual attenuation function is plotted in Figure 2. There is a single deep trough from 40 to 120 km which shallows with increasing frequency, then two ridges at 200 and 316 km which appear to represent energy that has been critically refracted from velocity discontinuities below the Moho. A broad region of relatively little variation extends from 200 to 800 km, indicating that recordings of the S-wave trains at this distance can be used to investigate source characteristics with minimal frequency-dependent effects.

Products

Boatwright, J., Regional propagation characteristics and source parameters of earthquakes in northeastern North America, submitted to *Bull. Seism. Soc. Am.*

Boatwright, J., L.C. Seekins, H-P. Liu, T.E. Fumal, and C.S. Mueller, Ground-Motion Amplification, in *The Loma Prieta, California, Earthquake of October 17, 1989 - Marina District, U.S. Geological Survey Professional Paper 1551-F*, Washington D.C., 1992.

Fletcher, J.B., and J. Boatwright, Source parameters of Loma Prieta aftershocks and wave propagation characteristics along the San Francisco peninsula from a joint inversion of digital seismograms, *Bull. Seism. Soc. Am.*, **81**, 1783-1812, 1991.

Seekins, L.C. and J. Boatwright, Ground-motion amplification, geology, and damage from the 1989 Loma Prieta earthquake in the City of San Francisco, submitted to *Bull. Seism. Soc. Am.*

Figure Captions

Figure 1. Average site amplifications for stations on bay mud (10 stations), sand (8), and Franciscan sandstone (8), plotted as a function of frequency. The shaded areas represent 68% confidence intervals. For reference, the range of fundamental frequencies for 2, 4, and 10-story buildings are shown at the bottom of the plot.

Figure 2. Residual attenuation of the S-wave trains, plotted as a function of hypocentral distance, as discerned from ECTN recorded at distances from 25 to 1000 km. The function is contoured in units of $\Delta \ln_e = 0.05$. The apparent high and low-frequency variations at the furthest distances are not statistically significant.

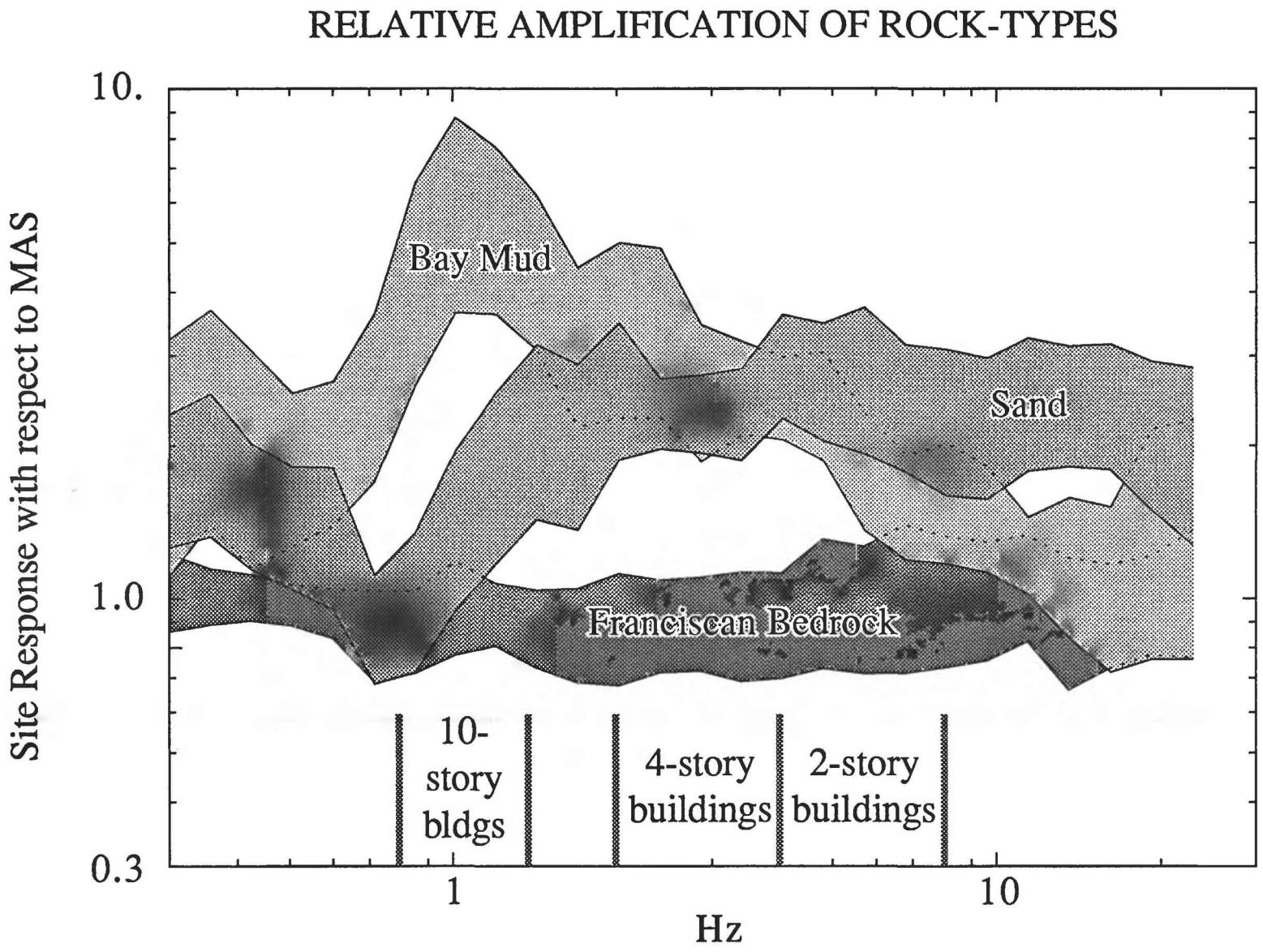
RELATIVE AMPLIFICATION OF ROCK-TYPES
Site Response with respect to MAS
10.
1.0
0.3
Bay Mud
Sand
Franciscan Bedrock
10-
story
bldgs
4-story
buildings
2-story
buildings
1
10
Hz

FIGURE 1

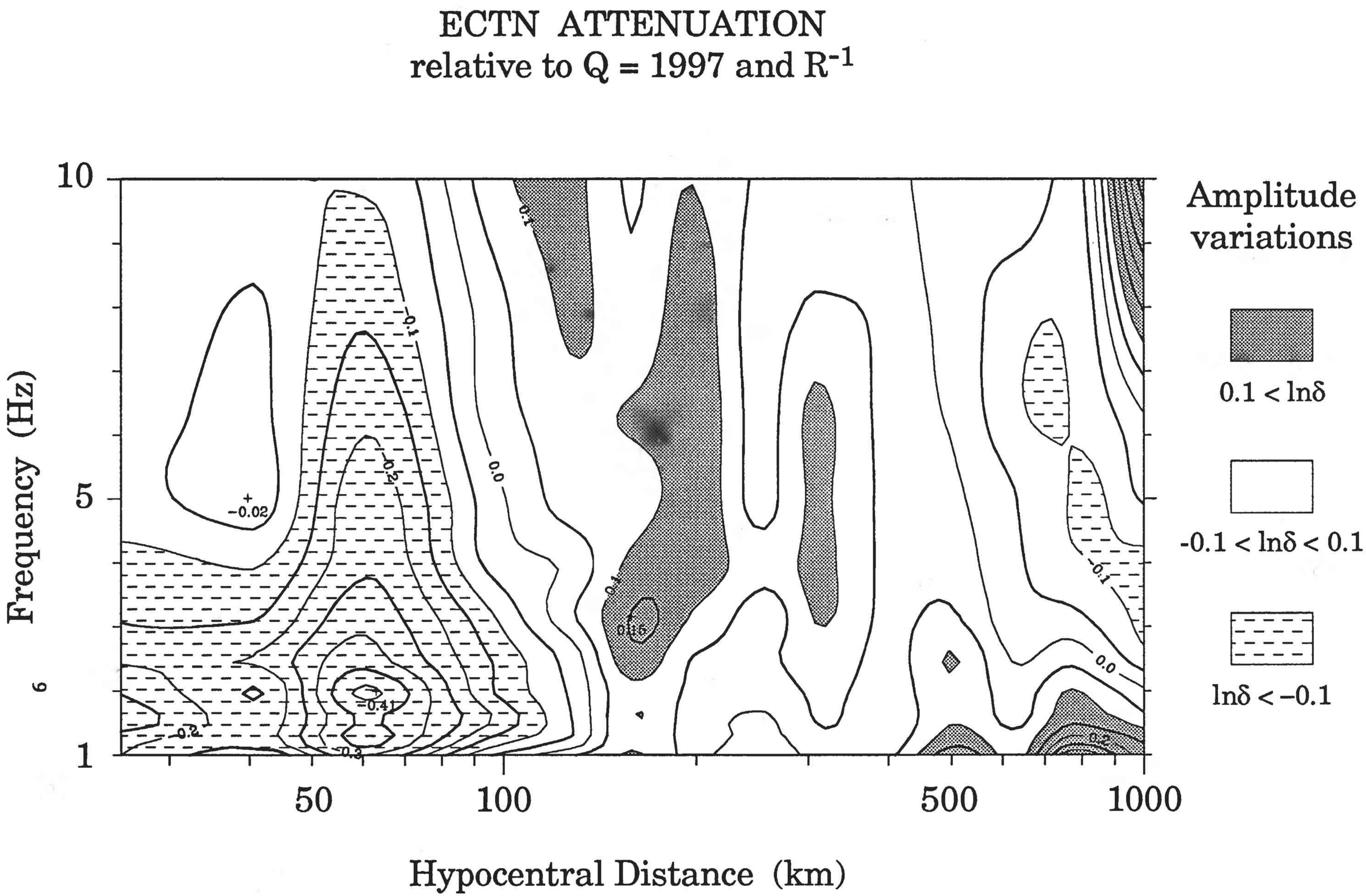

ECTN ATTENUATION
relative to Q = 1997 and R^{-1}
Frequency (Hz)
10
5
1
Hypocentral Distance (km)
50
100
500
1000
-0.02
-0.1
-0.2
-0.41
-0.3
-0.2
0.0
0.1
0.1
0.15
-0.1
0.0
0.2
Amplitude variations
0.1 < lnδ
-0.1 < lnδ < 0.1
lnδ < −0.1

FIGURE 2

9

I

SOUTHERN APPALACHIAN COOPERATIVE SEISMIC NETWORK

Award No. 1434-92-A-0971

G. A. Bollinger 703-231-9190
M. C. Chapman 703-231-5036
M. S. Sibol 703-231-4707
Seismological Observatory
Virginia Polytechnic Institute and State University
Blacksburg, Virginia 24061-0420

Objectives

This three-year cooperative project between Virginia Tech, Memphis State University, Tennessee Valley Authority and the University of North Carolina at Chapel Hill is designed to provide modern instrumental coverage of the Southern Appalachian Seismic Zone. The 32 stations of the Virginia Tech and Memphis State networks will be upgraded to three-component with high dynamic range by means of digital telemetry. Integration of the 19 station TVA network and the 5 station UNC network will result in the formation of a 56 station Southern Appalachian Cooperative Seismic Network (SACSN). There is to be common data formatting and access on computer networks to ensure near real-time waveform data sharing by the SACSN member institutions and accessibility to the general seismological community. This cooperative regional network is also scheduled to be fully integrated into the U.S. National Seismic Network.

Research objectives for the SACSN are focused on the Southern Appalachian Seismic Zone which is situated within a Paleozoic fold-and-thrust belt overlying a crystalline seismogenic basement weakened during Iapetan rifting. The research objectives include: earthquake detection and location and the study of seismogenic structures, earthquake source studies, wave propagation at local and regional distances, crustal velocity studies, temporal patterns of seismicity and seismic hazard assessment. Thus, the data and analyses from the SACSN are directed towards understanding the seismotectonics and assessing the seismic potential of the region.

The service objectives of the SACSN include the publication of an annual Seismicity Bulletin for the southeastern U.S. region, the development and maintenance of regional earthquake catalogs and general informational service to state/local governments and to the public.

Investigations

A high priority for this first year has been the development and implementation of a common data format and procedures for sharing seismic data in near real-time among the SACSN member institutions. Recognizing that there will never be total compatibility in acquisition packages due to differences in equipment, scale and logistics among the subnetworks, a more realistic goal is that member institutions have translation programs to convert from various data acquisition format(s) into a commonly agreed upon data format. Such "event" data, written in the agreed-upon format, is to be stored in accessible locations such as shared disk space or ftp-accessible partitions. Ideally, the data-exchange format will be the same as that used for analysis, and ultimately, we will want to ensure compatibility with other members of the USNSN.

As a first step, we have taken advantage of the fact that all of the SACSN member institutions have access to Sun Sparcstations with disk space which can be

dedicated to waveform data storage, and all have, or are in the process of installing, the LLNL Seismic Analysis Code (SAC) package. Accordingly, we have written translators for our two sources of digital data--a 32-channel short-period telemetered network and a three-component broadband GSE seismograph system at BLA--into both SAC data format and Center for Seismic Studies (CSS) data format. In addition, we have calibrated all channels and have the instrumental responses in both SAC-format pole-zero files and in frequency-amplitude-phase format. Data from recent events recorded with the Virginia Tech network have already been made available via our anonymous ftp directory on vtso.geol.vt.edu. For example, on August 21, a magnitude 4.1 shock occurred at 12:32 EDT northwest of Charleston, South Carolina. The NEIC released the location and size parameters for that event at 14:04 EDT. Our BLA broadband digital time series was available to SACSN in just over an hour after the USGS announcement and within three hours after the earthquake's origin-time.

Bulletin No. 26 of the *Seismicity of the Southeastern U.S.* for the calendar year 1991 was distributed this past June to over 230 institutions and individuals, including 40 foreign addresses. In addition to reporting the usual hypocentral parameters, magnitudes, etc. for the report period, the *Bulletin routinely presents a complete set of network catalog statistics for the 1977-1991 period* (see Tables 1 and 2 and Figures 1-5).

An investigation of the relationship between earthquake magnitude and the size of damage areas in the eastern and western United States has been concluded. To quantify damage area as a function of moment magnitude (**M**), 187 VI, VII, and VIII Modified Mercalli isoseismal areas for 112 earthquakes (76 in California and Nevada, 36 in the eastern United States and Canada) were measured. Regression of isoseismal areas versus **M** indicated that areas in the East were larger than in the West at all three intensity levels, by an average 4-5 times in the **M** 5 to 7 range. In terms of radii for circles of equivalent area, the results indicate that damaging ground motion from shocks of the same magnitude extend to twice the distance in the eastern United States compared to the West (see Figure 6).

To determine source and site parameters consistent with the above results, Response Spectral levels for eastern North America were stochastically simulated and compared to observed Response Spectral ordinates derived from recorded strong ground motion data in the western United States. Stress parameter values of 200 bars, combined with a surficial 2 km thick low velocity layer over rock basement, produced results that are compatible with the intensity observations, i.e., similar Response Spectral levels in the East at twice the western U.S. distance. These results suggest that ground motion modeling in eastern North America may need to incorporate source and site parameters different from those presently in general use. The results are also of importance to eastern U.S. hazard assessments as they require allowance for the larger damage areas in preparedness and mitigation programs. A paper presenting these results has been accepted by the **BSSA**, subject to revisions.

SEUSSN EARTHQUAKE CATALOG STATISTICS SECTION

TABLE 1

SEUSSN Report Period/Cumulative Earthquake Catalog Statistics

PERIOD: January through December 1991 (1 year)

	Tectonic	Reservoir
Number of Earthquakes with M ≥ 0.0	93	17
Number of Earthquakes with M ≥ 2.5	15	7
Number of Earthquakes with M ≥ 3.5	2	0
Number of Felt Earthquakes	11	10
Rate of Earthquakes with M ≥ 0.0 (per year)	93	17
Rate of Earthquakes with M ≥ 2.5 (per year)	15	7.0
Rate of Earthquakes with M ≥ 3.5 (per year)	2.0	0.0
Rate of Felt Earthquakes (per year)	11	10
Mean Earthquake Magnitude	1.8	2.2
Median Earthquake Magnitude	1.8	2.1
Number of Earthquakes with Known Dmin ≤ 5.0 km	7	12
Number of Earthquakes with Known Dmin ≤ 10.0 km	19	13
Number of Earthquakes with Known Dmin ≤ 25.0 km	51	13
Number of Earthquakes with Known ERH ≤ 5.0 km	81	14
Number of Earthquakes with Known ERZ ≤ 5.0 km	72	0
Number of Blasts or Questionable Events Reported	0	
Number of Events Outside the SEUSSN Area Reported	0	
Number of Seismograph Stations Operating	104	

Largest Earthquake: 15 March 1991; 06:54 - Sandy Hook, VA
mb(Lg)= 3.8, MDB= 3.3, MMI= V

PERIOD: July 1977 through December 1991 (14.5 years)

	Tectonic	Reservoir
Number of Earthquakes with M ≥ 0.0	1162	681
Number of Earthquakes with M ≥ 2.5	201	63
Number of Earthquakes with M ≥ 3.5	24	2
Number of Felt Earthquakes	136	20
Rate of Earthquakes with M ≥ 0.0 (per year)	80	47
Rate of Earthquakes with M ≥ 2.5 (per year)	14	4.3
Rate of Earthquakes with M ≥ 3.5 (per year)	1.7	0.1
Rate of Felt Earthquakes (per year)	9.4	1.4
Mean Earthquake Magnitude	1.6	1.4
Median Earthquake Magnitude	1.6	1.4
Number of Earthquakes with Known Dmin ≤ 5.0 km	85	75
Number of Earthquakes with Known Dmin ≤ 10.0 km	202	108
Number of Earthquakes with Known Dmin ≤ 25.0 km	628	140
Number of Earthquakes with Known ERH ≤ 5.0 km	1030	172
Number of Earthquakes with Known ERZ ≤ 5.0 km	861	116
Number of Blasts or Questionable Events Reported	182	
Number of Events Outside the SEUSSN Area Reported	12	

Largest Earthquake: 27 July 1980; 18:52 - Sharpsburg, KY
mb = 5.2, MMI = VII

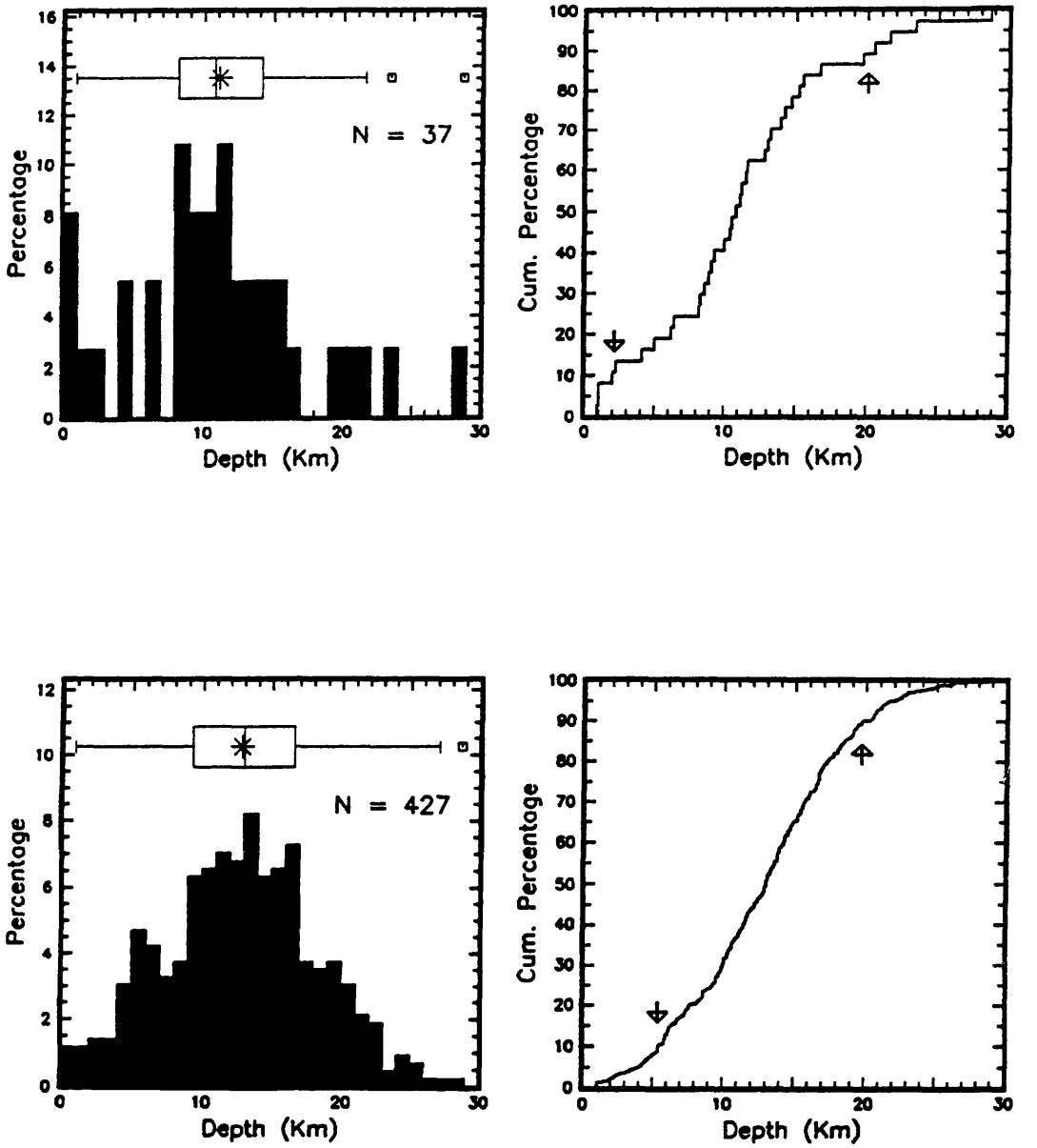

FIGURE 1. Focal Depth Distribution of Southeastern U.S. Earthquakes. The upper half of the figure shows the interval (left) and cumulative (right) depth distributions for the current report period while the lower half of the figure is a similar display for earthquakes reported during the period from July 1977 through this report period ($M \geq 0.0$, known ERZ ≤ 5.0 km, Dmin ≤ 20 km, and free depth determination). Displayed above both interval distributions is a box plot (Hoaglin and others, 1983, pp. 58-65). Indicated are the mean (star), the 25% and 75% quartile (box outline), the median (center bar), the upper and lower adjacent values (small vertical bars), and outliers (small squares). On the cumulative depth distributions arrows show the 10% and 90% depths.

COMPLETENESS ESTIMATES, MAGNITUDE DISTRIBUTIONS, AND RECURRENCE RELATIONS

TABLE 2

Completeness Estimates (Years) By Magnitude For The Southeastern U. S. And Subregions (Source: Bollinger and Others, 1989)

MAGNITUDE	2.25	2.75	3.25	3.75	4.25	4.75	5.25	5.75	6.25	6.75
Southeastern US	6	10	15	85	145	145	215	215	215	215
Valley & Ridge and Blue Ridge	9	10	20	75	110	215	215	215	215	215
Piedmont	10	10	115	215	215	215	215	215	215	215
Coastal Plain	10	10	60	145	145	215	215	215	215	215
Giles County, VA	10	15	15	30	30	215	215	215	215	215
Central Virginia	15	60	215	215	215	215	215	215	215	215
Eastern Tennessee	5	10	10	85	115	115	215	215	215	215
Charleston, SC	10	70	70	70	130	215	215	215	215	215

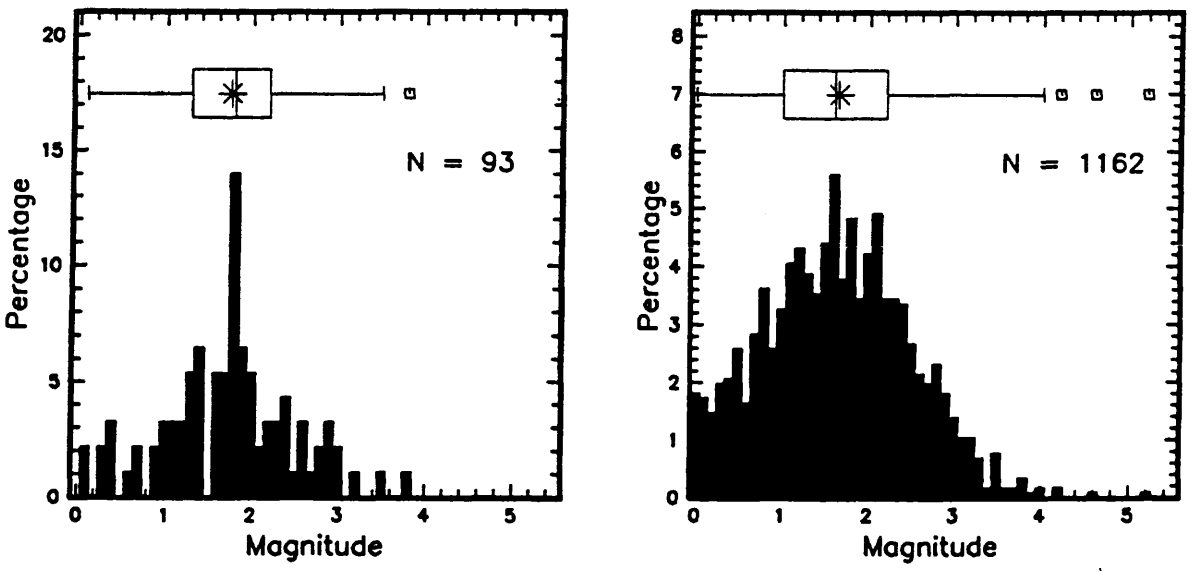

FIGURE 2. Magnitude Distributions of Southeastern U. S. Earthquakes. The left half of the figure shows the interval magnitude distribution for the report period while the right half of the figure shows a similar distribution for earthquakes from July 1977 through this report period. Displayed above both distributions is a box plot (Hoaglin and others, 1983, pp. 58-65). Indicated are the mean (star), the 25% and 75% quartile (box outline), the median (center bar), the upper and lower adjacent values (small vertical bars), and outliers (small squares).

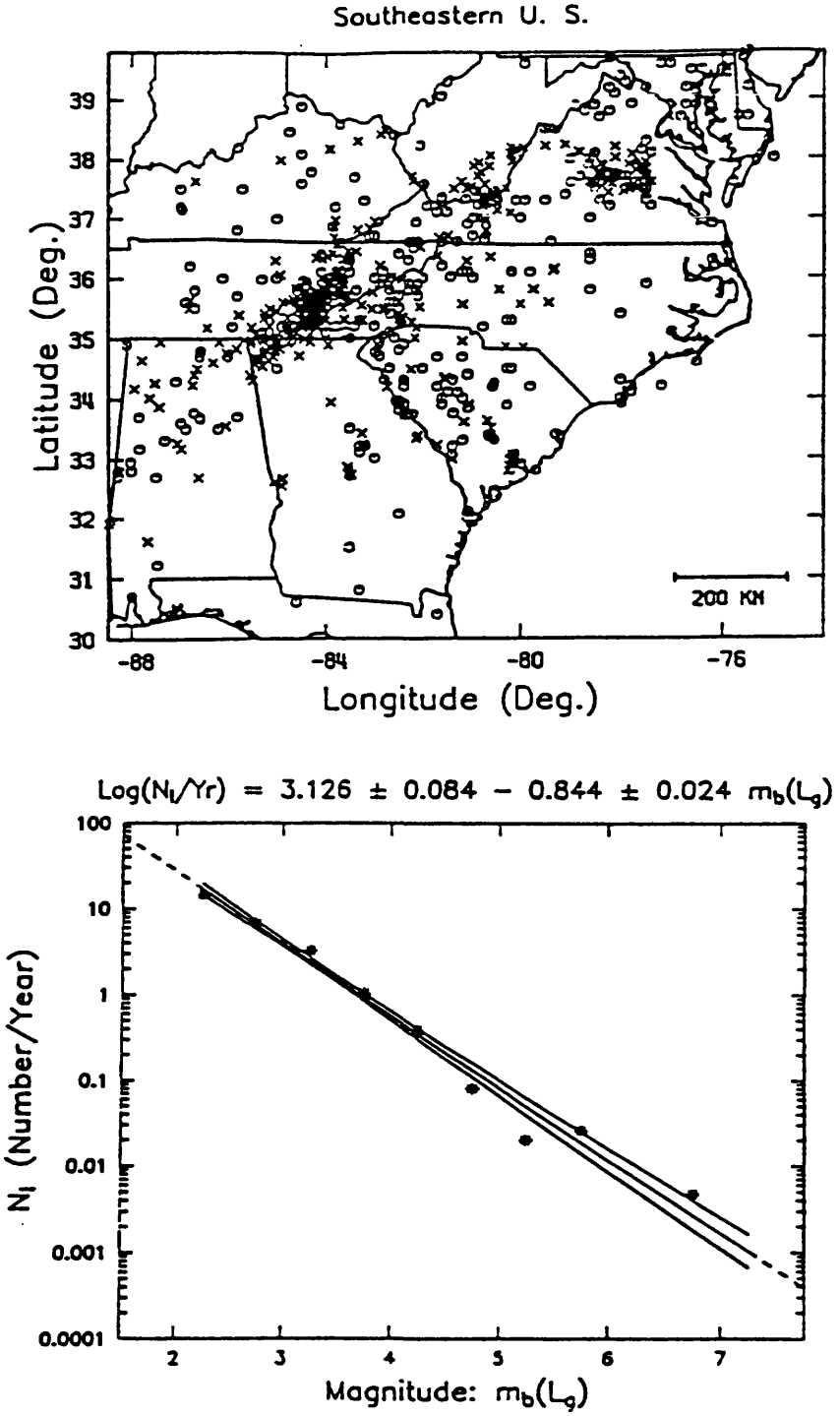

FIGURE 3. Magnitude Recurrence Relation For The Southeastern U. S. The upper half of the figure shows the seismicity map with historical (circles) and network (X's) epicenters for the time period 1772-1986. The lower half of the figure shows a plot of Log(NI) (interval number of earthquakes per year, m ± 0.25) versus mb(Lg) for the southeastern U.S. The maximum likelihood line includes 95% confidence intervals (Source: Bollinger and others, 1989).

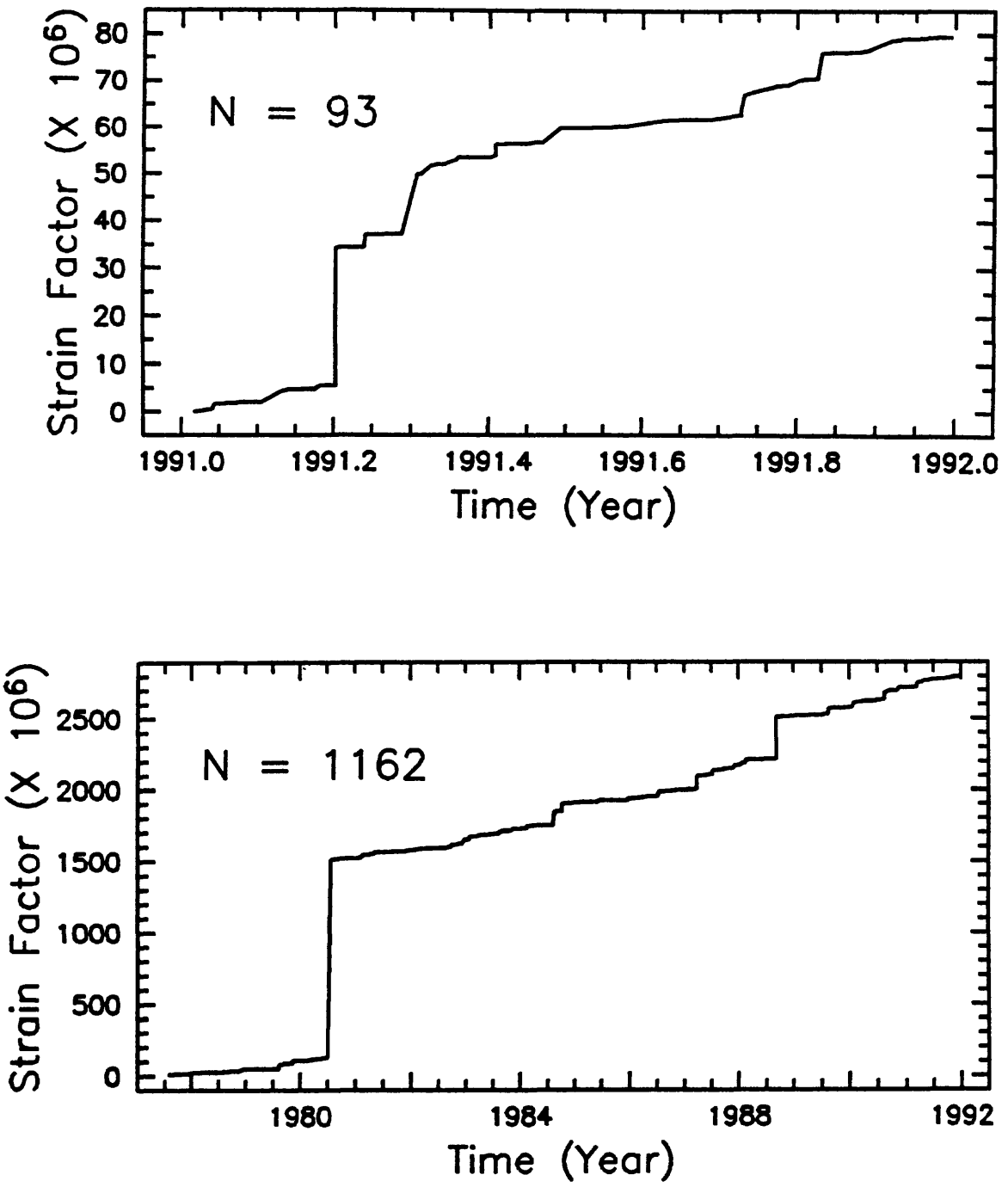

FIGURE 4. Cumulative Strain Factor History of Southeastern U.S. Earthquakes. The upper half of the figure shows the cumulative strain factor history for the report period, while the lower half of the figure shows a similar plot for earthquakes from July 1977 through this report period.

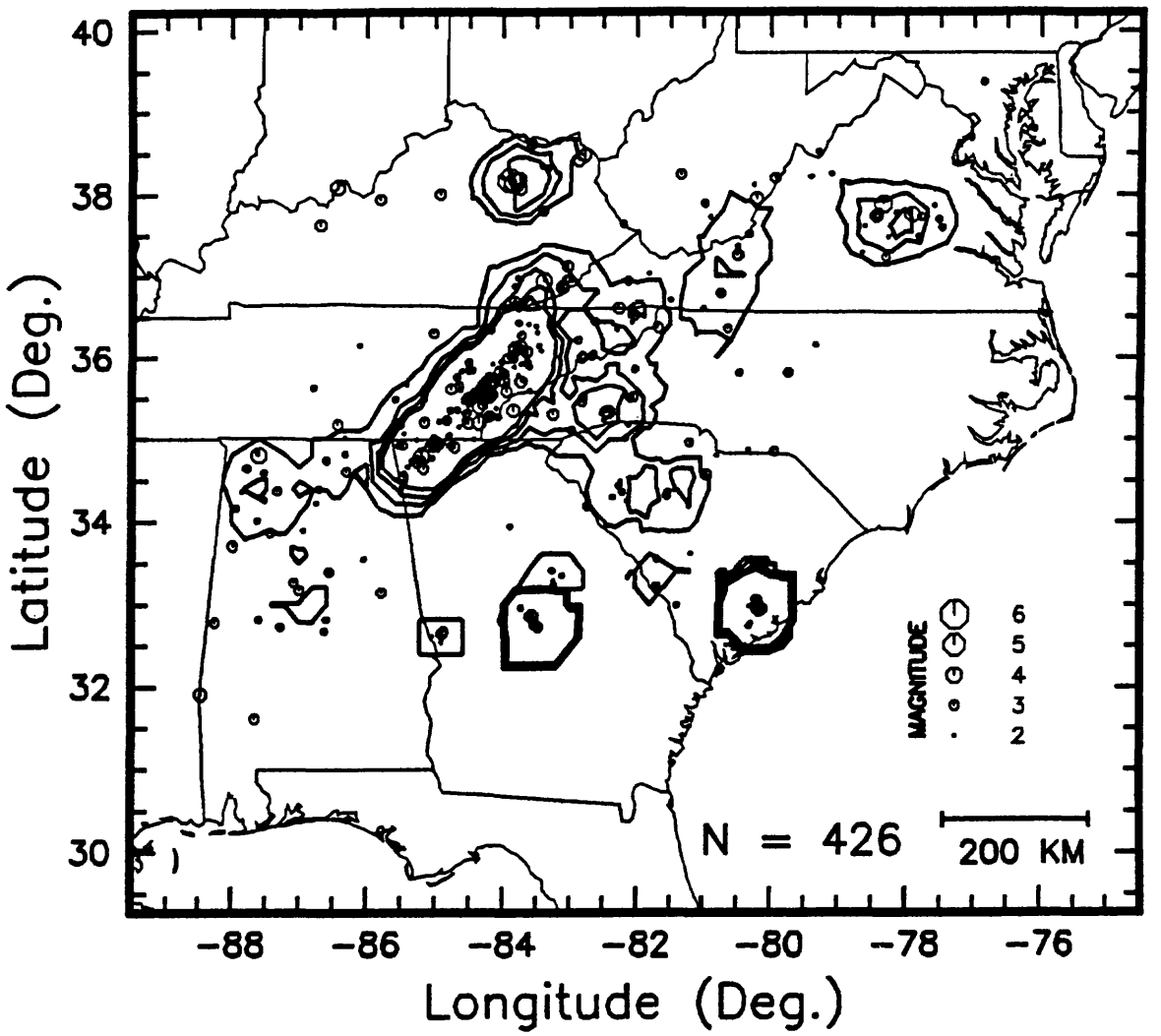

FIGURE 5. Epicenter Density Contour Map for Earthquakes (circles scaled to magnitude; M ≥ 2.0) in the Southeastern United States from July 1977 through this report period. Contours represent number of earthquakes within 50 km of a grid point scaled to number per 10,000 square km; grid spacing is 0.2 degrees. Lowest and highest contours are 5 and 20 events per 10,000 square km, respectively (contour interval is 5).

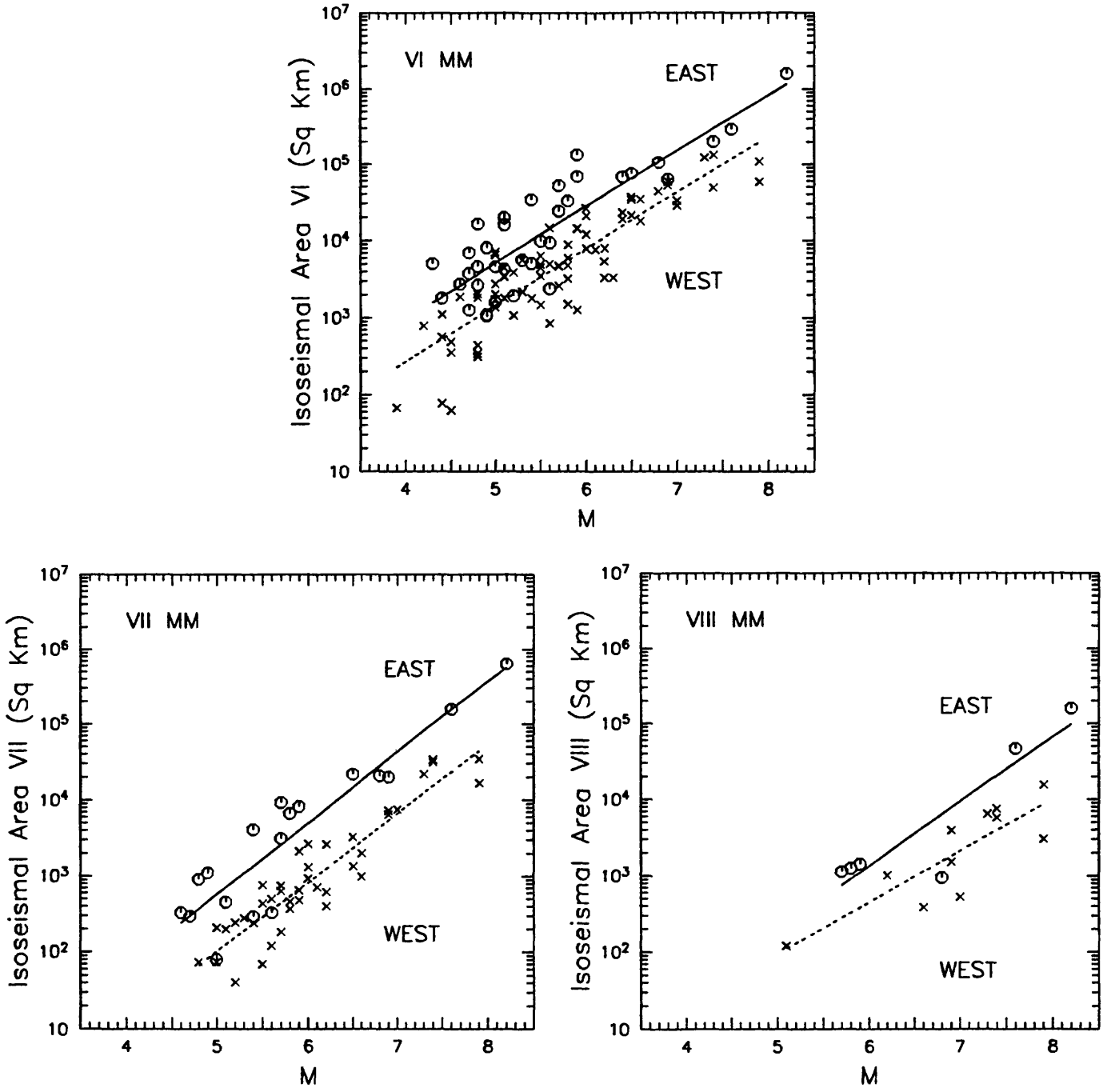

Figure 6. Isoseismal areas, at the MMI = VI, VII, VIII levels, versus moment magnitude for 112 VI areas, 58 VII areas and 17 VIII areas for 36 eastern North American earthquakes and 76 western U.S. earthquakes. ENA data = circles and WUS data = x's. The straight-line fits indicate that the ENA damage areas are about five times greater than those for the WUS.

Analysis of the 1957 Andreanof Islands Earthquake
14-08-0001-G1766

Thomas M. Boyd
Colorado School of Mines
Department of Geophysics
Golden, CO 80401
(303) 273-3522

Project Summary and Goals

Recent studies have indicated that the spatial distribution of moment release can be quite heterogeneous along any particular rupture zone. The most common explanation for this heterogeneity has been the rupture of strong patches, or asperities, along the fault plane [e.g., Ruff and Kanamori, 1983]. These strong patches could arise from spatial variations of the frictional characteristics along the fault or from geometrical barriers inherent to the fault's shape. Alternatively, the spatial distribution of moment release could have little to do with the physical characteristics of the fault's surface and may be related to the dynamics of slip and how regions of the fault interact with neighboring regions [e.g., Rundle and Kanamori, 1987; Horowitz and Ruina, 1989].

Distinctions between these two models can not be made from the analysis of single events [e.g., Thatcher, 1990]. Conclusive observations can only be drawn from a study of the moment-release distribution generated by several great earthquakes, all of which rupture the same fault segment. In this context, an excellent region of study is the central Aleutian Arc. In 1986, a magnitude 8.0 (M_W) earthquake occurred near the Andreanof Islands. Its slip distribution, aftershock, and preshock sequence have been described in detail in a number of recent studies. Prior to 1986, the central Aleutian Arc was ruptured by another great earthquake in 1957 ($M_W > 8.5$). The 1957 Andreanof Islands earthquake, however, remains poorly understood. Its seismic moment, slip distribution, and rupture area have not been well constrained.

The short time span between the 1957 and 1986 earthquakes provides us with a unique opportunity to study a complete seismic cycle bounded by two instrumentally recorded great earthquakes. In fact, it represents the only complete seismic cycle instrumentally observed along the Aleutian Arc. As briefly described in this summary, we are continuing our work on assembling and interpreting observations pertinent to the 1957 earthquake and the interseismic period between the 1957 and 1986 events. Progress can be summarized as;

1) We have constrained the rupture bounds of the 1957 earthquake using surface-wave directivity.

2) All seismicity occurring between 1957 and 1989 has been relocated.

3) A catalog of earthquake relocations is now available through anonymous FTP to the USGS in Golden or on the CD-ROM distributed as part of the Wadati Conference held in Fairbanks, Alaska in September, 1992.

Rupture Length Estimates

Accurate determinations of kinematic rupture parameters have been accomplished for some time using the so-called directivity function [e.g., Ben-Menahem, 1961; Ben-Menahem and Toksoz, 1962, 1963; Udias, 1971]. Unfortunately, because it is highly nonlinear, this function is difficult to invert. Using the simulated annealing method [Kirkpatrick et al., 1983], however, we have constructed an inversion process which is capable of extracting accurate estimates of kinematic rupture parameters and provides the probability distribution of their values.

A recent PhD. graduate who was supported by this project, David Lane, developed an ensemble approach in which several independent inversions are run simultaneously. The objective of each inversion is to maximize the joint probability distribution $P(\mathbf{M}=m|\mathbf{D}=d)$, where **M** represents the kinematic rupture parameters, and **D** represents the observed data. After several iterations the algorithm generates solutions distributed as $exp(-E/kT_j)$, where E represents the error between a possible solution and the observed data, and T_j is the control parameter of the *jth* inversion. We contend that the maximum likelihood estimate obtained during a single inversion is less important than the marginal distribution of rupture parameters. Since each of the inversions are independent we obtain the marginal distributions $P(M_i=n)$ by summing over the joint inversions. Figure 1 shows inversion results for the 1957 event using data recorded at Pietermaritzburg South Africa. As shown in Table 1., three solutions have been identified which match the observed directivity. These solutions rupture lengths of 874 km; 642 km to the east and 192 km to the west, 738 km; 550 km to the east and 188 km to the west; and 954 km, 601 km to the east and 354 km to the west. We are currently combining these results with those obtained by Satake under USGS grant 1434-92-G-2187 to obtain a final, consistent estimate of rupture length and moment-release distribution. Preliminary results from this portion of the project were presented at the 1990 Fall AGU meeting in San Francisco [Lane and Boyd, 1990] and recently at the 1992 Wadati Conference held in Fairbanks, Alaska [Boyd et al., 1992]. A paper by Lane in Boyd describing the results of this experiment is in preparation and will be submitted to BSSA within the next 3 months [Lane and Boyd, 1993].

Seismicity Relocations

We have relocated and cataloged seismicity recorded from 1957 through 1989 (March) with epicenters lying between 175°E and 160°W. Our relocations include epicenter-dependent, P-wave station corrections which account for near-source velocity structure. These corrections are calculated for 686 stations using a slab geometry detailed by a recent, teleseismic, travel-time study and the iasp91 travel-time model. Unless other information is available, source depths are constrained to 35 km. For events deeper than 50 km, station corrections are not applied and source depths are determined using both P and pP arrivals. Arrival times for earthquakes occurring between 1957 and 1963 are obtained by optically scanning of the ISS and BCIS bulletins. For this time period, magnitudes were available for only a small percentage of the relocated events. We calculated magnitudes for as many of these events as possible, using body- and surface-wave amplitudes recorded at Pasadena. For events recorded between 1964 and 1989,

arrival times and magnitudes are obtained from the ISC phase tapes.

The completed catalog consists of approximately 7300 earthquakes. Dividing the geographical distribution of observing stations into four azimuthal zones (Europe and the Arctic, North and South America, Asia, and the South Pacific), we classified earthquakes into one of four quality groups. Group A consists of events recorded by at least two stations in all four azimuthal zones. Group B consists of events recorded by at least two stations in three of the four azimuthal zones. Group C consists of events recorded by at least one station in three of the four azimuthal zones. Group D consists of all those events not meeting the requirements of groups A, B, or C. All events within groups A and B, 3200, have 90% error vectors of less than 25 km.

We determine the minimum magnitude of completeness for our catalog by plotting the number of events per magnitude increment. For this comparison, we have converted all of the observed magnitudes to Ms using a regression relationship derived from events for which both mb and Ms are available. Between 1964 and 1989, our catalog is complete above Ms=4.6. From 1957 through 1963, the minimum magnitude of completeness is 5.5. To uniformly sample the seismic record over the entire time period of our catalog, only events larger than or equal to 5.5 should be used. Also note that for each time period, earthquakes whose magnitudes are above the level of completeness are well located.

In Figure 2, we have plotted the epicenters of the shallow earthquakes listed in our catalog. Only events in groups A and B have been included. Notice that these events can be divided visually into two categories: 1) outer rise earthquakes (i.e., those events whose epicenters lie within or south of the trench), and 2) main thrust-zone earthquakes (i.e., those events whose epicenters lie between the trench and the arc massif). These two groups of earthquakes are separated by a clearly defined aseismic zone. The outer rise earthquakes are caused by deformation within the oceanic lithosphere whereas the main thrust-zone earthquakes are located at the coupled interface between the lithosphere and the overriding massif. Presumably, the aseismic region results from the presence of unconsolidated, overpressured sediments with strengths too low to support seismicity. Seismicity within the main thrust-zone, is bounded to the south and north by clearly defined seismic and aseismic fronts. In general, both the seismic and aseismic fronts are continuous, along-arc features. Five notable exceptions, however, can be observed. 1) The seismic front moves northward just south of Unalaska Island (166°W), and the level of activity within this region is lower than in surrounding regions. 2) Little seismicity has been detected over the past thirty years just east of the intersection point of the Amlia Fracture Zone with the trench at 173°W. We note, also, that the earthquakes within this region are large (Ms> 6.0), and occurred soon after the 1957 earthquake. 3) Near the Adak Canyon region (177°W), seismicity extends southward to the trench, while the aseismic front remains continuous. 4) Amchitka Pass (180°E) is aseismic. 5) The region near Murray Canyon (177°E) has generated very few earthquakes. Outer rise earthquakes occur along the entire arc, but cluster around a few specific regions: 178°E, 179°E, 177°W, 173°W, and 171°W. Most of the outer rise activity occurred soon after the large thrust faulting earthquakes of 1957 and 1965, with activity gradually decreasing from the time of the mainshock. Only one, well located, outer rise earthquake followed the 1986 event.

The space time distribution of main thrust-zone and outer rise earthquakes occurring within 30 days of the 1957 earthquake is shown in Figure 3. Except for the single event that occurred immediately after the mainshock near 165°W, earthquakes are initially

confined to a portion of the arc that lies between 167°W and 177°W. The initial aftershock area is consistent with the tsunami source area, and rupture length inferred from surface-wave directivity. Within a day after the mainshock, aftershock activity spread westward. Within three days, activity spread eastward. The final extent of the aftershock zone is some 1200 km. The larger events which extended the aftershock zone eastward all occurred within a small region east of Unalaska Island. Outer rise earthquakes are concentrated in three clusters; one each to the east and west of the intersection point of the Amlia Fracture Zone, and one south of Adak Canyon.

Figure 4 shows the epicentral locations of earthquakes occurring near Adak Island over three time periods; during the aftershock sequence of the 1957 earthquake, during the interseismic period between the 1957 and 1986 earthquakes, and during the aftershock sequence of the 1986 earthquake. Only shallow, well-located events larger than Ms=5.4 are included. The epicenters of the 1957 and and 1986 earthquakes are indicated by the largest filled circles in panels A and C.

The epicentral distribution of events is quite heterogeneous over time and space. During the aftershock sequence of the 1957 earthquake (Panel A, Figure 4), few events occurred along the main thrust-zone south of Amlia Island east of the epicenter of the mainshock. Many events occurred near Adak Canyon (177°W), southeast of Adak Island (176°W), and arcward of the intersection point of the Amlia Fracture Zone with the trench. Outer rise earthquakes cluster near the Amlia Fracture Zone and near the trenchward extension of Adak Canyon.

During the interseismic period (Panel B, Figure 4), many fewer outer rise events are detected, and those that did occur are clustered near the trenchward extension of Adak Canyon. As was observed for the 1957 aftershock sequence, few events are located along the main thrust-zone south of Amlia Island, while many events are observed arcward of the Amlia Fracture Zone, and southeast of Adak Island. Unlike the aftershock sequence, however, the region near Adak Canyon is seismically quiet during the interseismic period.

Aftershocks of the 1986 earthquake (Panel C, Figure 4) are concentrated near Adak Canyon, and south of Amlia Island. The section of the arc southeast of Adak Island that was seismically active during the 1957 sequence and during the interseismic period remains seismically inactive after the 1986 earthquake. Like the 1957 sequence, aftershocks of the 1986 event also cluster about the epicenter of the mainshock.

Studies of the moment distribution of the 1986 earthquake suggest that regions of high moment release generate few aftershocks. Seismic moment released during the 1986 event was concentrated in the regions just east of the mainshock's epicenter and along the western rupture extent, where few aftershocks occurred. Efforts are currently underway to constrain the seismic moment distribution of the 1957 earthquake independent of these speculations by modeling marigrams. Assuming an anti-correlation between aftershock locations and seismic moment release, we suggest that seismic moment was concentrated in an area bounded to the west by the mainshock's epicenter and to the east by the intersection with the Amlia Fracture Zone. Although a significant amount seismic moment may also have been released west of the mainshock to Adak Canyon, the concentration of the aftershocks southeast of Adak Island suggests this area did not generate significant slip during the 1957 earthquake.

Compared to the moment distribution of the 1986 earthquake, that which we have suggested for the 1957 earthquake different. If correct, regions of high seismic moment

release, asperities, may vary from earthquake to earthquake, suggesting that the moment distribution is not controlled by the strength distribution on the fault surface alone. Rather it is a consequence of the interaction of the fault's strength distribution with the dynamics by which rupture propagates.

Our relocation effort is complete, and a paper by Boyd, Engdahl, and Spence is in preparation. Preliminary results from this portion of the project were presented at the 1990 Fall AGU meeting [Boyd et al., 1990] and the 1992 Wadati Conference held in Fairbanks, Alaska [Boyd et al., 1992].

References

Ben-Menahem, A., and M. N. Toksoz, Source mechanism from spectra of long-period seismic surface waves, 1. The Mongolian earthquake of December 4, 1957. *J. Geophys. Res., 67,* 1943-1955, 1962.

Ben-Menahem, A., and M. N. Toksoz, Source mechanism form spectra of long-period surface waves, 2. The Kamchatka earthquake of November 4, 1952, *J. Geophys. Res., 68,* 5207-5222, 1963.

Boyd, T. M., E. R. Endgahl, and W. Spence, Aftershocks of the 1957 Aleutian Islands earthquake, *EOS, 71,* 1469, 1990.

Boyd, T. M., F. D. Lane, and E. R. Engdahl, Historical earthquakes: Rupture length estimates based on aftershock locations and surface wave observations, Abstract, *EOS, 72,* 189, 1991.

Boyd, T. M., E. R. Engdahl, and W. Spence, Analysis of seismicity associated with a complete seismic cycle along the Aleutian Arc: 1957 through 1989, Published in; Proceedings of the Wadati Conference on Great Subduction Earthquakes, University of Alaska, Fairbanks, AL, 43-51.

Boyd, T. M., E. R. Engdahl, and W. Spence, Analysis of seismicity associated with a complete seismic cycle along the Aleutian Arc: 1957 through 1989, to be submitted to, *J. Geophys. Res.*, 1993.

Dillinger, W. H., A. J. Pope, and S. T. Harding, The determination of focal mechanisms using *P-* and *S-wave* data, *NOAA Tech. Report NOS 44,* 56 pp., 1971.

Horowitz, F. G., and A Ruina, Slip patterns in a spatially homogeneous fault model, *J. Geophys. Res., 94,* 10,279-10,298, 1989.

Kirkpatrick, S., C. D. Gelatt, and M. P. Vecchi, Optimization by simulated annealing, *Science, 220,* 671-680, 1983.

Lane, F. D., and T. M. Boyd, A simulated annealing approach to the inversion of surface wave directivities: Application to the 1957 Aleutian Islands earthquake, *EOS, 71,* 1468, 1990.

Lane, F. D., and T. M. Boyd, Estimation of kinematic rupture parameters from historical seismograms, to be submitted to, *Bull. Seismol. Soc. Amer.*, 1993.

Ruff, L., and H. Kanamori, The rupture process and asperity distribution of three great earthquakes from long-period diffracted P-waves, *Phys. Earthq and Planet. Inter., 31,* 202-230, 1983.

Rundle, J. B., and H. Kanamori, Application of an inhomogeneous stress (patch) model to complex subduction zone earthquakes: A discrete interaction matrix approach, *J. Geophys. Res., 92,* 2606-2616, 1987.

Stauder, W., and A. Udias, S-wave studies of earthquake of the North Pacific, Part II: Aleutian Islands, *Bull. Seismol. Soc. Am., 53,* 59-77, 1963.

Thatcher, W., Order and diversity in the modes of Circum-Pacific earthquakerecurrence, *J. Geophys. Res., 95,* 2609-2624, 1990.

Udias, A., Source parameters of earthquakes from spectra of Rayleigh waves, *Geophys. J. R. Astr. Soc., 22,* 353-376, 1971.

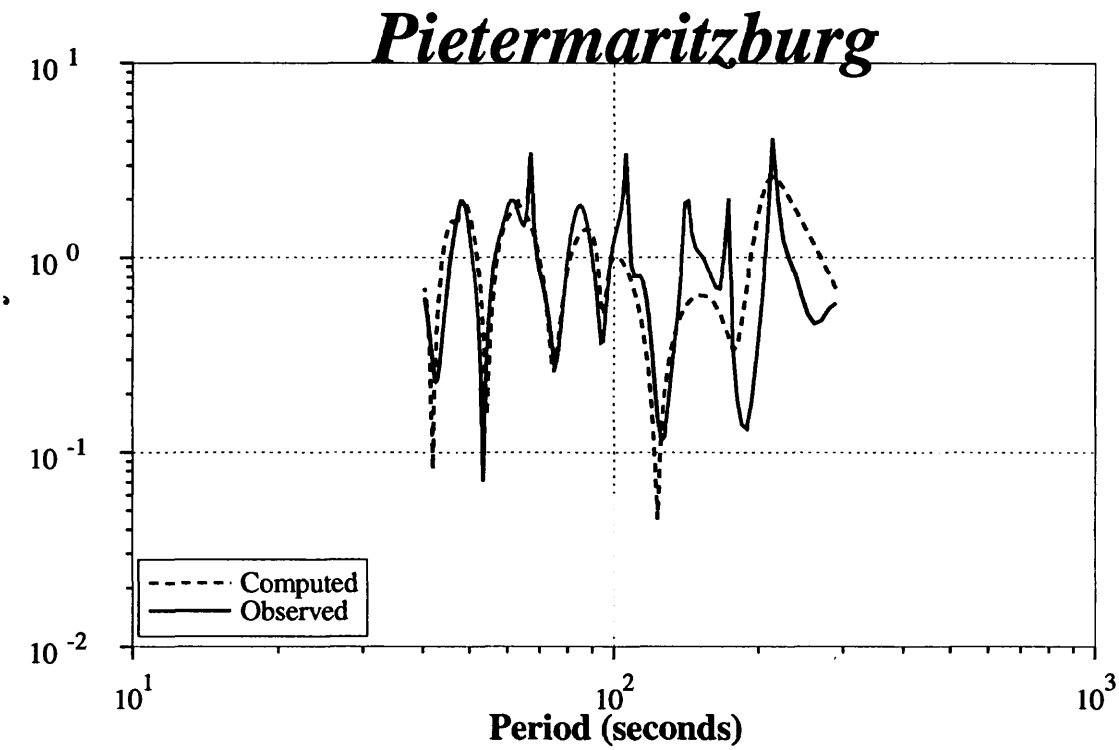

Figure 1: Computed, dashed line, and observed, solid line, directivity for the 1957 Andreanof Islands earthquake. Three different fault models were found that could produce the computed directivity shown above. The fault parameters for these three models are given in Table 1.

Table 1: Fault Parameter estimates

	Eastern Fault Length (km)	Western Fault Length (km)	Rupture Velocity (km/s)
Solution 1	682	192	2.2
Solution 2	550	188	1.9
Solution 3	601	354	2.1

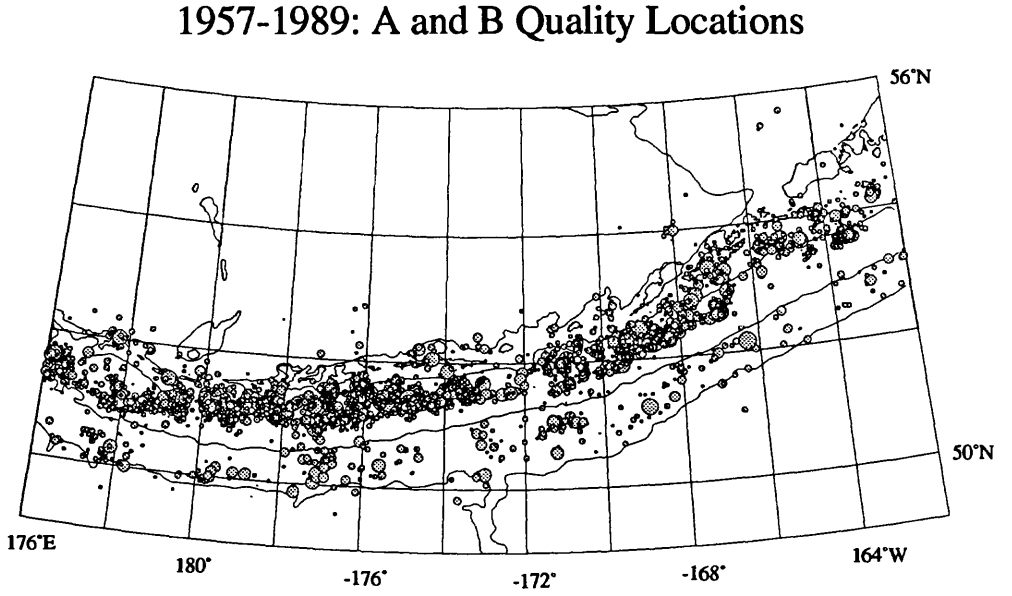

Figure 2: Epicentral locations of all earthquakes within groups *A* and *B* whose source depths are less than 50 km. Symbols are scaled by earthquake magnitude (M_S).

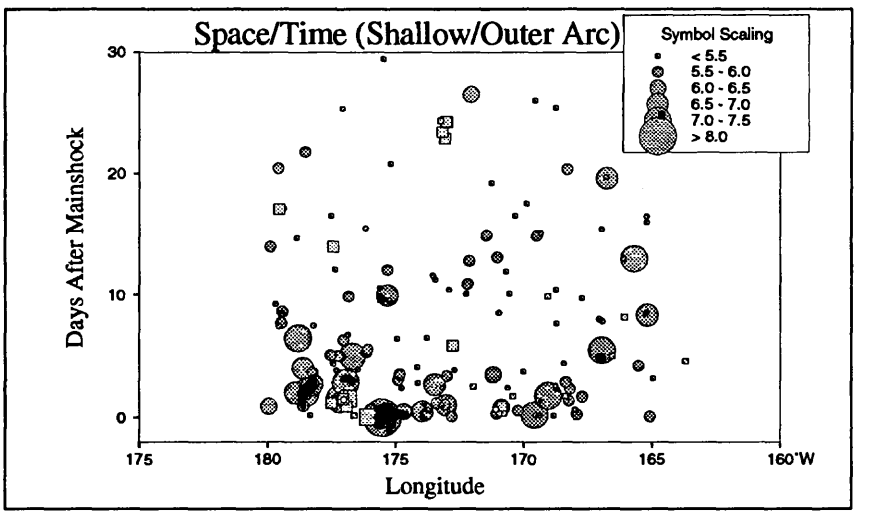

Figure 3: Space Time distribution of seismicity occurring within a month of the 1957 Aleutian Islands earthquake. Filled circles indicate earthquakes along the main thrust-zone, filled squares indicate outer rise earthquakes. The arrow indicates the rupture bounds of the 1957 event inferred from surface-wave directivity.

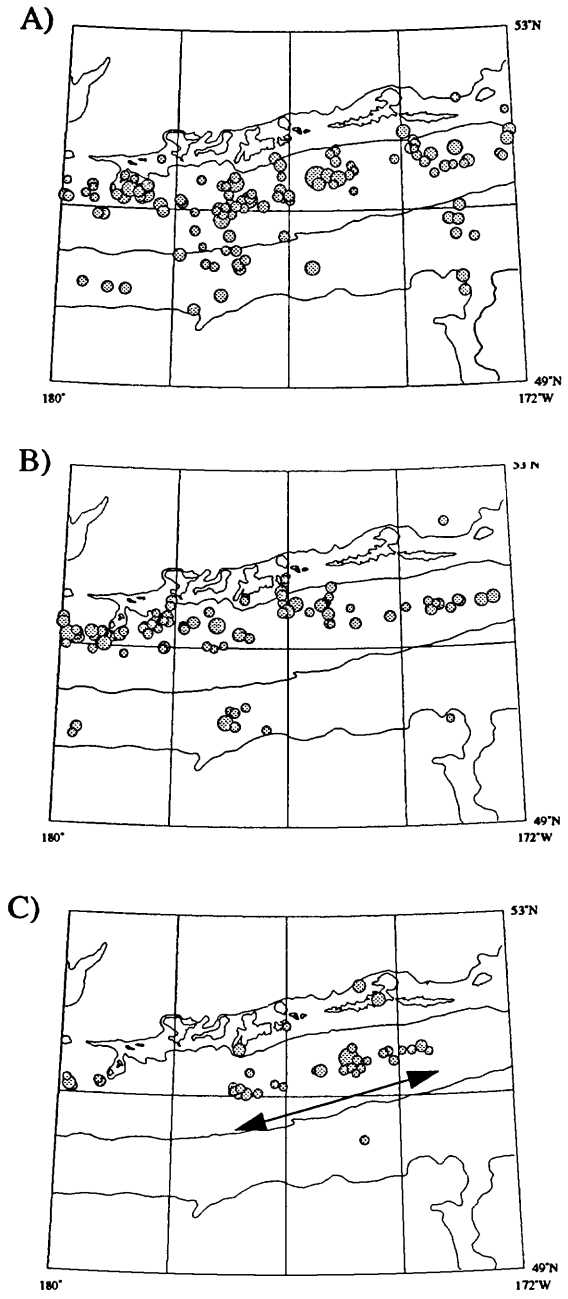

Figure 4: Well located earthquakes occurring around the rupture zone of the 1986 event with magnitudes above 5.4. Panel A shows events that occurred during the aftershock sequence of the 1957 earthquake (03/1957 - 05/1960). Panel B shows events occurring during the interseismic period (05/1960 - 05/1986). Panel C shows events occurring during the aftershocks sequence of the 1986 earthquake (05/1986 - 03/1989). Arrow indicates rupture bounds of the 1986 earthquake.

Characterization of Self-Similar Comminution and Slip Localization in Large-Displacement Faults for Application to Laboratory Fault Modelling

1434-92-G-2184

Frederick M. Chester

Department of Earth and Atmospheric Sciences, Saint Louis University
3507 Laclede Ave., St. Louis, MO 63103

James P. Evans

Department of Geology, Utah State University
Logan, UT 84322

Investigations

We are conducting a field geologic study of exhumed faults of the San Andreas system to infer the environmental conditions of faulting, the mechanisms of slip, and the physical and mechanical properties of fault zones at seismogenic depths. This type of research will help guide laboratory fault modelling efforts and ultimately will contribute to an understanding of the physics of the earthquake source. Up to this time we have focused our study to the North Branch San Gabriel fault because this fault segment is probably one of the most deeply exhumed and best exposed, large-displacement faults of the San Andreas system. To date we have conducted three related studies of the fault zone to characterize 1) mesoscopic scale subsidiary fault fabric, 2) mineralogic alteration and fluid/rock interaction, and 3) particle size distributions of the cataclastic fault rocks. The results of these studies have been integrated and used to develop a conceptual model for the internal structure and weakening mechanisms of the San Andreas fault and is presented by Chester et al. [1992]. The abstract of this paper is included below.

Our findings from the North Branch San Gabriel fault indicate localized but extensive evidence for fluid-rock interaction and mineralogic alteration contemporaneous with movement on the San Gabriel fault. This is in marked contrast with previous findings from petrologic study of several exposures of the San Gabriel fault west of our study localities [Anderson et al., *Tectonophysics*, *98*, 209-251, 1983]. Our most recent efforts have been directed toward trying to better characterize the differences in fault rock petrology along strike by expanding our study localities to include more western exposures of the San Gabriel fault in the Pacoima Canyon area. For several key localities of the San Gabriel fault we are investigating variations in bulk rock chemistry across and within the fault zone and surrounding host rock. Preliminary results indicate substantial mobility of some elements within the core of the faults and significant volume changes. We also have begun investigations of the San Andreas fault near Wrightwood so that we may better compare the characteristics of the San Andreas and San Gabriel faults.

Results

New observations of the internal structure of the San Gabriel fault (SGF) are combined with previous characterizations of the Punchbowl fault (PF) to evaluate possible explanations for the low frictional strength and seismic characteristics of the San Andreas fault (SAF). The SGF and PF are ancient, large-displacement faults of the SAF system exhumed to depths of 2 to 5 km. These fault zones are internally zoned; the majority of slip was confined to the cores of principal faults, which typically consist of a narrow layer (less than tens of centimeters) of ultracataclasite within a zone of foliated cataclasite several meters thick. Each fault core is bounded by a zone of damaged host rock of the order of 100 m thick. Orientations of subsidiary faults and other fabric elements imply that (1) the maximum principal stress was oriented at large angles to principal fault planes, (2) strain was partitioned between simple shear in the fault cores and nearly fault-normal contraction in the damaged zones and surrounding host rock, and (3) the principal faults were

weak. Microstructures and particle size distributions in the damaged zone of the SGF imply deformation was almost entirely cataclastic and can be modeled as constrained comminution. In contrast, cataclastic and fluid-assisted processes were significant in the cores of the faults as shown by pervasive syntectonic alteration of the host rock minerals to zeolites and clays and by folded, sheared, and attenuated cross-cutting veins of laumontite, albite, quartz, and calcite. Total volume of veins and neocrystallized material reaches 50% in the fault core, and vein structure implies episodic fracture and sealing with time-varying and anisotropic permeability in the fault zone. The structure of the ultracataclasite layer reflects extreme slip localization and probably repeated reworking by particulate flow at low effective stresses. The extreme slip localization reflects a mature internal fault structure resulting from a positive feedback between comminution and transformation weakening. The structural, mechanical, and hydrologic characteristics of the Punchbowl and San Gabriel faults support the model for a weak San Andreas based on inhomogeneous stress and elevated pore fluid pressures contained within the core of a seismogenic fault. Elevated fluid pressures could be repeatedly generated in the core of the fault by a combination of processes including coseismic dilatancy and creation of fracture permeability, fault-valve behavior to recharge the fault with fluid, post-seismic self-sealing of fracture networks to reduce permeability and trap fluids, and time-dependent compaction of the core to generate high pore pressure. The localized slip and fluid-saturated conditions are wholly compatible with additional dynamic weakening by thermal pressurization of fluids during large seismic slip events, which can help explain both the low average strength of the San Andreas and seismogenic characteristics such as large stress relief. In addition, such a dynamic weakening mechanism is expected only in mature fault zones and thus could help explain the apparent difference in strength of large-displacement faults from smaller-displacement, subsidiary seismogenic faults.

Reports

Chester, F.M., Subsidiary fault structure and paleostress of the San Gabriel fault zone, San Gabriel Mountains, California, Eos Trans. AGU, 72, 264, 1991.

Chester, F.M. , J.P. Evans, and R.L. Biegel, Internal structure and weakening mechanisms of large-displacement fault of the San Andreas system, Geol. Soc. Am. Abstr. w. Prog., 23, A103, 1991.

Evans, J.P., and F.M. Chester, Mechanisms of slip localization: No. Branch San Gabriel fault, CA, Eos Trans. AGU, 72, 435, 1991.

Chester, F.M., J.P. Evans, and R.L. Biegel, Internal Structure and Weakening Mechanisms of the San Andreas Fault, in press, J. Geophys. Res., 1992.

Friction Constitutive Behavior of Saturated Faults at Hypocentral Conditions

1434-92-G-2203

Frederick M. Chester

Department of Earth and Atmospheric Sciences, Saint Louis University
3507 Laclede Ave., St. Louis, MO 63103

Investigations

The goal of the project is to determine the friction constitutive behavior of water saturated faults at hypocentral conditions through laboratory experiments and constitutive modeling. I have focused my investigations on the temperature dependence of friction because this information is necessary to apply laboratory data to natural faulting and to identify the fundamental micromechanisms governing friction at hypocentral conditions. The results of this research should help to improve our understanding of earthquake faulting and provide the constitutive descriptions of fault zones that are necessary to formulate quantitative models of the earthquake source.

I completed the following tasks during the previous contract period: 1) formulation of a temperature-dependent constitutive relationship for friction in rock, 2) development of a multi-mechanism constitutive model that can describe frictional behavior at hydrothermal conditions, 3) experimentation with quartz gouge at hydrothermal conditions to determine constitutive behavior, and 4) experimentation with graphite to determine the rate- and temperature-depedent characteristics of the testing apparatus. The results of tasks (1) and (2) are reported by Chester and Higgs [1992]. Over the last year I have carried out a detailed analysis of the graphite experiments to quantify apparatus properties followed by an analysis of the quartz experiments to quantify constitutive behavior and to test the constitutive relationship that I formulated for temperature-dependent friction. Description of the experiments on quartz and graphite and the results of the analyses are summarized below and a manuscript is now in preparation [Chester, 1992].

Results

Thin layers of graphite powder and granular quartz were sheared in a gas confining medium, internally heated, triaxial apparatus using a standard triaxial shear configuration (Figure 1). The sample for both graphite and quartz experiments consisted of a cylinder of steel 32.8 mm in diameter cut in half along a plane inclined 35° from the cylinder axis. Either graphite or quartz was placed between the sample halves along the 35° inclined interface. The assemblies were sealed in metal sleeves and axially shortened at confining pressure. The metal sleeves consisted of copper foil (either 0.075 or 0.15 mm thick) centrally located within a lead foil totaling 2 mm thick. Confining pressure, pore fluid pressure, and axial shortening rate were servo-controlled during the experiments. Axial load was measured both inside and outside the pressure vessel. Axial shortening caused shear displacement of the sample halves and allowed measurement of the resistance of the graphite or quartz layers to shear.

Axial shortening of the assembly requires lateral motion of the sample halves. Lateral offset occurred along a single interface between steel spacers oriented perpendicular to the cylinder axis (Figure 1). In all experiments this spacer interface was ground smooth and separated by a layer of graphite approximately 0.2 mm thick. In addition to the lateral offset, shortening of the sample requires deformation of the metal sleeves used to seal the sample from the confining medium. Both the strength of the metal sleeves and the frictional resistance to slip along the spacer interface contribute to the total resistance to axial shortening of the sample. These two effects, though relatively small, were significant for the measurements of velocity and temperature dependencies of friction in the quartz layers. The metal sleeve, lateral slip surface, and the inclined interface are all coupled in the testing assembly and can not be isolated for characterization (Figure 1). However,

the behavior of each component can be determined by an appropriate parametric study because each has a different dependence on external parameters such as confining pressure, slip velocity, and temperature. The experiments on graphite were done primarily to characterize the two apparatus effects.

Axial displacement of the sample was measured with a displacement transducer located external to the pressure vessel. Displacement rate was specified with a 16 bit digital command signal generator and maintained by closed-loop servo control. The least significant bit of the command signal corresponded to 0.16 μm shear displacement, and I have verified through additional sensing transducers that the actuator achieved displacements at this level of precision. The displacement measurements over the course of an experiment were less accurate due to a number of factors including temperature-induced changes of the transducer outputs. Experiments were conducted by stepping shear velocity by a factor of ten between 4.0 and 0.04 μm s^{-1} in a standardized sequence. The step changes in velocity were essentially instantaneous.

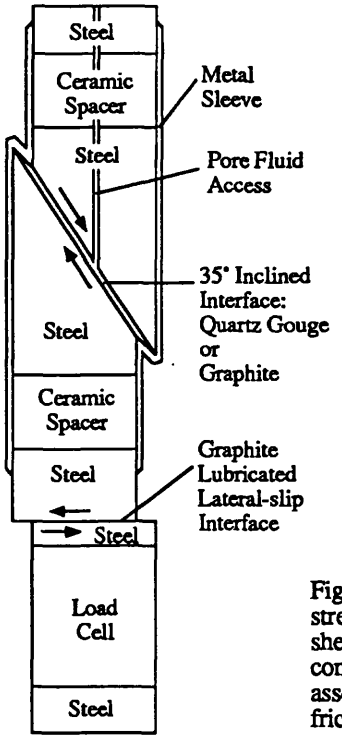

$$\mu_i = \frac{\tau_i}{\sigma_i} = \frac{\Delta\sigma_t(\cos\theta\sin\theta - \mu_{ls}\sin\theta) - \Delta\sigma_{ms}\cos\theta\sin\theta}{(P_c - P_p) + \Delta\sigma_t(\sin^2\theta + \mu_{ls}\cos\theta\sin\theta) - \Delta\sigma_{ms}\sin^2\theta}$$

μ_i = coefficient of friction of inclined interface

μ_{ls} = coefficient of friction of lateral-slip interface

$\Delta\sigma_t$ = total differential stress

$\Delta\sigma_{ms}$ = differential stress supported by metal sleeve

$(P_c - P_p)$ = effective confining pressure

$\theta = 35°$ = angle of inclined surface

Figure 1. Sample assembly for triaxial shear experiments. Shear strength of the inclined interface, strength of the metal sleeve, and shear strength of the graphite lubricated, lateral-slip spacer interface contribute to the total differential stress supported by the sample assembly and measured by the internal load cell. The coefficient of friction of the inclined interface is defined in terms of the other parameters by the equation above.

Elevated temperatures were achieved within the pressure vessel with a resistance furnace wrapped around the steel cylinder halves. The temperature of the furnace was controlled by a sensing thermocouple located at the furnace. The temperature of the specimen was monitored independently by a sensing thermocouple located at the gouge layer in the pore-fluid access hole. The temperature of the graphite lubricated, lateral slip surface also was monitored by a dedicated thermocouple. Temperatures in the center of the specimen were generally maintained to within 1°C. The cylinder halves were thermally insulated from the load column by Al_2O_3 ceramic spacers and from the confining medium and the pressure vessel walls by a ceramic fiber wrap. Insulation was not perfect, however, so other components of the load column such as the lateral-slip interface also experienced elevated temperatures. The furnace produced relatively small temperature gradients along the sliding surfaces and no restriction on the lateral motion of the sliding specimen halves. Temperature of the samples during tests were maintained constant at or stepped between room temperature (24° to 28°C), 57°C, and 82°C. By using steel cylinders with high thermal

conductivity and the proper sequence of variable power output by the furnace, an upward temperature step of 30°C to a new equilibrated temperature condition was achieved at the 35° inclined interface in approximately 100 s. Steps down in temperature from 82°C to 57°C took slightly longer, approximately 200 s. The lateral-slip interface took somewhat longer to reach equilibrium after temperature steps than the inclined interface. Temperature steps were conducted only during sliding at a constant velocity of 0.04 μm s^{-1}. Therefore, the shear displacement across the gouge layer during the temperature step was less than several μm. Based on the relatively rapid equilibration of pore fluid pressure in the samples, pore pressures were maintained constant during temperature steps.

Thermal expansion of the sample column during temperature changes was significant; expansion was approximately 1 μm axial lengthening per °C temperature change. The expansion was measured by the transducer used to generate the feedback signal for the displacement servo-control. Accordingly, the command signal was corrected to achieve a constant shear velocity of approximately 0.04 μm s^{-1} across the gouge layer during each temperature step. In practise, the average shear velocity during the temperature steps was maintained between 0.02 and 0.06 μm s^{-1}. Corrections to the command signal were based on separate calibrations conducted under load feedback that defined the thermal expansion of the sample column during temperature changes. To apply the proper correction to the command signal and achieve a constant shear velocity during the temperature steps, it was necessary to standardize the heating sequence during temperature steps. Due to slight variations in the furnace geometry between each sample assembly, it was necessary to calibrate the power requirements of the furnace and the heating sequence for each experiment. This calibration was done at confining and pore pressure and small differential load but prior to imposing shear displacement. The test assembly was permitted to equilibrate to the specified temperature of the experiment prior to initiating the shear displacement tests.

Analog and digital records of differential axial load, axial displacement, confining pressure, pore fluid pressure, pore volume changes, temperature along the 35° inclined interface, and temperature of the graphite lateral slip surface were collected for all experiments. Analog signals were digitized at 15 to 20 Hz with a 14 bit analog to digital converter. Digitized data was averaged and recorded by a computer every 3.0 μm of shear displacement during steady sliding and every 0.3 μm of shear displacement during friction transients associated with step changes in velocity, temperature, or pore-pressure. The least significant bit for digital records were 5.0 N axial load, 0.76 μm shear displacement, 10 kPa confining pressure, 0.24 kPa pore pressure, and 0.03 °C.

Graphite Experiments. In these tests the 35° inclined interface between sample halves and the thickness of the graphite along the interface was prepared the same as for the lateral-slip spacer interface. This simplifies the analysis of the experiments because the surfaces are described by the same constitutive relation. At the temperature and pressure conditions of the experiments, graphite lubricated interfaces are frictional in that they show a dependence of shear strength on pressure. In contrast, the strength of the metal sleeves is largely insensitive to pressure because they deform by intracrystalline plastic deformation mechanisms. Thus in these experiments the relative contributions of the graphite interfaces and the metal sleeves to the total strength of the sample assemblies varies with confining pressure. At high pressures the graphite surfaces support greater loads than the metal sleeves whereas at low pressures the opposite occurs. Accordingly, experiments were conducted at confining pressures ranging from 2 to 60 MPa. The dependence of the metal sleeve and of the graphite interfaces on temperature and velocity were defined by stepping velocity between 4, 0.4 and 0.04 μm/s and stepping temperature between 24 and 57 °C or 57 and 82 °C at a fixed confining pressure of 20 or 60 MPa. Samples with single- and double-thickness copper foil sleeves were used in both types of experiments.

By simultaneously modelling the results for all graphite experiments with single- and double-thickness metal sleeves at low and high confining pressure it is possible to define the relative contribution of the sleeves and the graphite to the temperature and velocity dependencies. I have found that the differential stress supported by the metal sleeves is insensitive to confining pressure and that the shear strength of the graphite lubricated interfaces is adequately described with a Coulomb relation ($\tau = C_0 + C_1\sigma$) over the range of normal stresses tested (Figure 2). Thus, the

coefficient of friction of graphite is a strong function of normal stress. Both graphite friction and metal sleeve strength are functions of displacement based on the results of fitting at three displacements. Steady-state graphite friction and metal sleeve strength increase with increased velocity (Figure 3) and decrease with increased temperature (Table 1). Although the dependence of

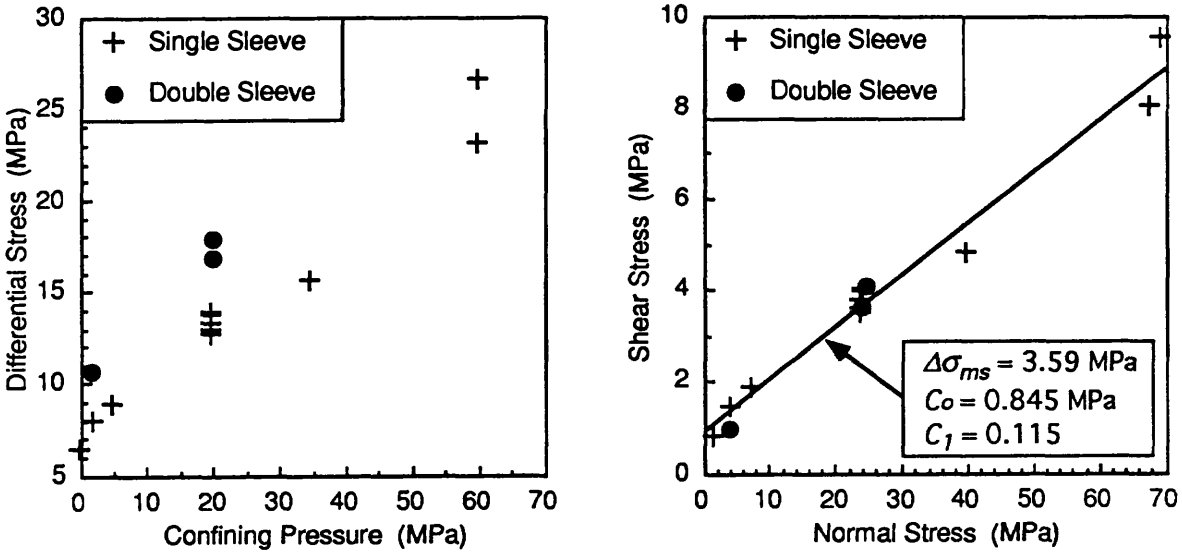

Figure 2. Results of graphite experiments conducted at slip velocity of 4 μm/s and room temperature. Plot on left shows total differential stress supported by the graphite assemblies at a shear displacement of 4.5 mm as a function of confining pressure and number of copper sleeves. Results clearly show that doubling the thickness of the sleeves increases assembly strength. Plot on right shows frictional strength of graphite on the inclined interface as a function of normal stress calculated from the same experimental data. Calculation of friction is based on equation shown in Figure 1 and assuming that the shear strength of graphite follows a Coulomb law and that the strength of the metal sleeve is a constant (see text). The best-fit values for sleeve strength and the Coulomb law are indicated.

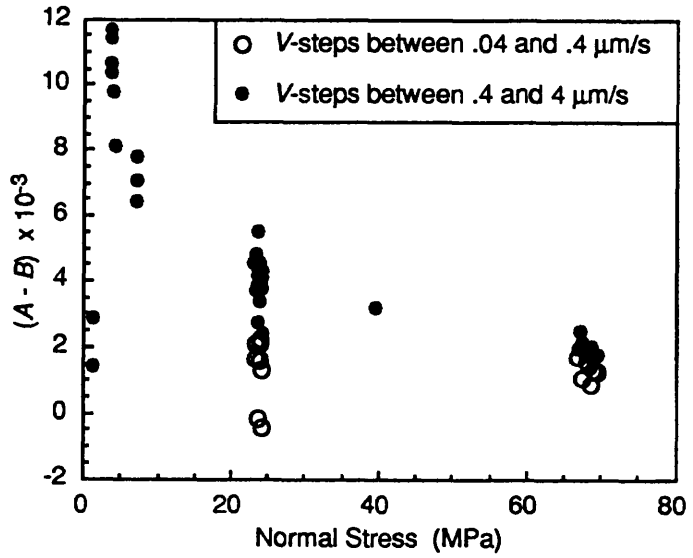

Figure 3. Steady-state velocity dependence of graphite friction at all temperatures and displacements as a function of normal stress. $(A - B)$ is equivalent to $d\mu^{ss}/d(\ln V)$. Although velocity dependence is a function of velocity, temperature and normal stress, it is fairly constant at normal stresses above 70 MPa. The normal stresses across the lateral-slip spacer interface in the quartz friction experiments is in the range of 80 to 100 MPa. Accordingly, steady-state velocity dependence of graphite friction can be assumed constant for purposes of calculating the coefficient of friction of quartz in the quartz gouge experiments (see text).

Table 1. Dependence of Graphite Friction on Temperature

Test #	P_c (MPa)	# Cu Sleeves	T-Step (°C)	Normal Stress (MPa)	$\frac{d\mu^{ss}}{d(1/T)}$
103	20	1	24 - 57	24	39.6
107	20	2	24 - 57	25	40.9
104	60	1	24 - 57	68	15.7
110	60	1	57 - 82 - 57	67	24.8

graphite friction on velocity changes with temperature and velocity at lower normal stresses, the velocity dependence is fairly constant at the high normal stresses appropriate for the apparatus corrections in the quartz experiments (Figure 3). The graphite experimental results indicate that the dependence of metal sleeve strength on velocity and temperature show little history effects, whereas the dependence of graphite friction on velocity and temperature shows significant history effects.

Quartz Experiments. For the quartz experiments, grooves with amplitude and periodicity of approximately 200 μm were ground into the 35° inclined interfaces. The grooves were oriented perpendicular to the cylinder axis and to the relative slip direction of the sample halves. These grooves caused the slip between sample halves to occur entirely within the 1.5 mm thick layers of fine-grained (< 100 μm diameter) granular quartz. For the tests without pore-water, the quartz was allowed to equilibrate at the laboratory conditions prior to testing. For the water-saturated tests, pore fluid access to the gouge layer was through a hole in the steel cylinder and pore pressure was maintained at a specified value by closed-loop servo-control. Pore pressure equilibration was sufficiently rapid within the gouge layers such that the pore pressure remained essentially constant over the range of velocity employed and during velocity and temperature steps. All quartz tests were conducted at an effective confining pressure of 20 MPa, and pore-fluid pressure was 5 MPa in the water-saturated tests. Each test involved a standardized sequence of velocity steps between 4, 0.4 and 0.04 μm/s and up to two temperature steps between 24 and 57 °C or 57 and 82 °C.

The coefficient of friction of quartz during each experiment was calculated from the differential stress versus displacement records using the formula shown in Figure 1. The calculations used the results of the graphite experiments to define the frictional properties of the graphite lubricated, lateral-slip interface and the strength of the metal sleeve. For the metal sleeve, the strength was calculated as a function of the displacement, velocity and temperature assuming a direct dependence on each parameter, i.e., the sleeve was always at steady-state. Coefficient of friction of the graphite lubricated lateral slip interface was defined by the displacement and the normal stress across the interface, and then modified to include the transient dependence of graphite friction on velocity and temperature, i.e., direct and history dependencies. Figure 4 shows a plot of the differential stress supported by a quartz gouge sample assembly in a typical velocity and temperature stepping experiment and the coefficient of friction calculated from that experiment as a function of displacement. Comparison of the two curves illustrate that corrections for apparatus effects is necessary to accurately determine the transient and steady-state frictional response of the quartz gouge to step changes in velocity and temperature.

In general, the water saturated quartz exhibits slightly lower coefficients of friction relative to the dry quartz at all displacements. All quartz experiments show a gradual increase in coefficient of friction with displacement superposed with the transient changes in friction associated with step changes in temperature and velocity. For purposes of analyzing the transient effects associated with velocity and temperature steps, the gradual slip hardening was modelled with a polynomial function and subtracted from the records. The polynomial was determined using the slope of the

friction record prior to the fourth and the sixth velocity steps. The polynomial and resulting detrended friction record for a representative experiment is shown in Figure 4.

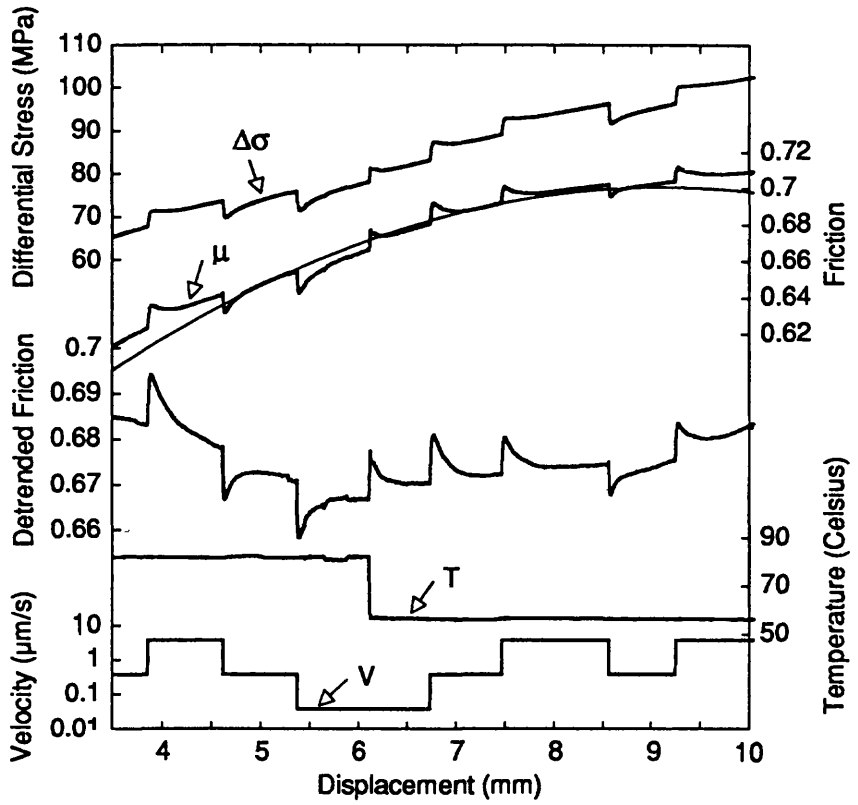

Figure 4. Representative results of an experiment on quartz gouge (hp106) at water saturated conditions. Velocity and temperature stepping sequence is shown. Total differential stress measured during the experiment and the coefficient of friction calculated are plotted as a function of shear displacement. The polynomial fit to the friction curve is shown by the thin line. The polynomial is used to remove the slip-hardening trend from the friction record to produce the detrended friction curve which is used for constitutive modelling.

Test of the Constitutive Model. I have proposed a temperature dependent friction constitutive relation based on the state variable friction constitutive relations developed by Dieterich [1979] and Ruina [1983]. Temperature dependence was added to the previous constitutive relations assuming velocity and temperature dependencies follow an Arrhenius relationship

$$\frac{d(\ln V)}{d(1/T)} = -\frac{Q}{R}$$

in which Q is the apparent activation energy for the rate limiting process [Chester, 1988, 1992; Chester and Higgs, 1992]. Following the notation of Dieterich and Linker [1992], the temperature and velocity dependent state variable friction relation is given by

$$\mu = \mu^* + A\left[\ln\left(\frac{V}{V^*}\right) + \frac{Q_a}{R}\left(\frac{1}{T} - \frac{1}{T^*}\right)\right] + B\Theta$$

$$\frac{d\Theta}{dt} = -\frac{V}{D_c}\left[\Theta + \ln\left(\frac{V}{V^*}\right) + \frac{Q_b}{R}\left(\frac{1}{T} - \frac{1}{T^*}\right)\right]$$

where $\Theta^{ss} = 0$ and $\mu^{ss} = \mu^*$ at $V = V^*$ and $T = T^*$. Previous versions of the temperature dependent friction relations presented by Chester [1988, 1992] and Chester and Higgs [1992] do not include the term with reference temperature T^*. All the relations are essentially the same except that $\Theta^{ss} = -Q_b/RT^*$ and $\mu^{ss} = \mu^* + (AQ_a - BQ_b)/RT^*$ at $V = V^*$ and $T = T^*$ in the previous versions. I prefer the version above because it adheres to original definitions of Θ^{ss} and μ^{ss} [e.g., Linker and Dieterich, 1992], and it is more consistent with the intent of the constitutive law to describe frictional behavior at or near steady-state conditions over a restricted range of velocity, temperature and normal stress conditions.

The proposed friction relation above predicts that 1) an abrupt increase in temperature induces a direct and transient change in friction similar to but in the opposite sense as that induced by a step increase in velocity, and 2) the characteristic distance for the transient response to evolve to a new steady-state coefficient of friction after step changes in temperature and velocity is the same. These two characteristics are evident from inspection of the friction versus displacement records of the quartz experiments (Figure 4).

I have modelled the frictional response of the quartz gouge experiments using the friction constitutive relations above in a simple spring slider system to quantify the friction parameters A, B, D_c, Q_a and Q_b. The modelling procedure is similar to that in previous studies [e.g., Marone et al., 1990; Chester and Higgs, 1992]. I compare forward models to the friction records during the velocity and temperature stepping sequence over the displacement range of 5 to 8 mm for each quartz experiment. The response to velocity steps was used to determine the parameters A and B, and the response to temperature steps to determine Q_a and Q_b. The response to all velocity and temperature steps was used to determine D_c. The results of the modelling are shown for two representative experiments (Figure 5).

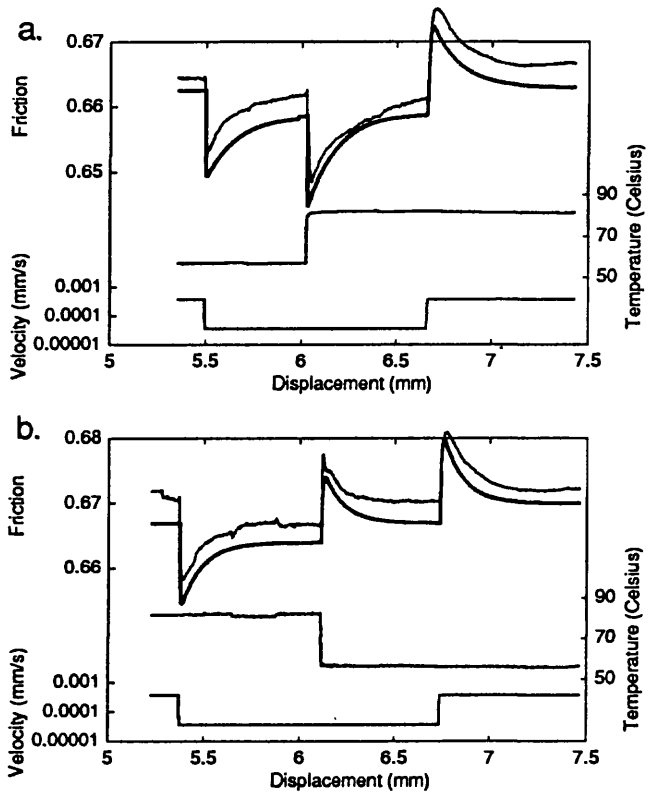

Figure 5. Example of model fits to friction data for velocity and temperature stepping experiments on water saturated quartz gouge. Velocity and temperature stepping sequence is shown. Thin lines at top of diagrams are the detrended friction records, and the thick lines are the model simulation. Model simulation is offset by .003 for ease of comparison. (a) experiment hp014. (b) experiment hp106.

Overall, the values of A, B and D_c are slightly larger and the values of Q_a and Q_b are slightly less for the water saturated tests relative to the dry tests as determined by modelling (Table 2). The variability in values for the apparent activation energies are sufficiently large that a difference in Q_a and Q_b can not be demonstrated. The magnitude of the average apparent activation energy in the water saturated tests (89 ± 23 kJ mol^{-1}) are similar to values determined for subcritical crack growth of quartz in hydrous environments [Atkinson, 1984] and for crack healing by diffusive mass transfer [Brantley et al., 1990]. The values are substantially larger than that determined by Chester and Higgs [1992] and Rutter and Mainprice [1978] for frictional slip at elevated temperatures and slow displacement rates where solution transfer processes are dominant. The activation energies in these experiments are significantly less than values typically determined for intracrystalline plasticity in quartz [e.g., Stesky, 1978]. Thus, the results of the quartz experiments are consistent with models of friction involving failure of contact junctions by sub-critical crack growth and time-dependent strengthening of contact junctions by either increasing the true area of contact through sub-critical cracking or by increasing the quality of contact junctions through healing.

Table 2. Model Parameters for Quartz Temperature and Velocity Stepping Experiments

Test #	T-Step (°C)	Q_a	Q_b	A	B	D_c (mm)
Dry						
hp011	24 - 57	87.1	139	.0035	.00246	.10
hp009	57 - 82	154	168	.0035	.00307	.11
hp105	82 - 57	60	43	.004	.00378	.10
Wet						
hp013	24 - 57	68.8	73.5	.0055	.00355	.13
hp014	57 - 82	101	143	.0062	.00446	.15
hp108u	57 - 82	89.2	113	.0062	.0042	.13
hp106	82 - 57	68.1	62.7	.006	.0047	.11
hp108d	82 - 57	85.7	82.2	.0062	.0042	.13

Average activation energies (Q_a and Q_b) for wet tests: 89 ±23 kJ mol^{-1}

Conclusions:

1. A sudden change in temperature results in both a sudden and transient change in the frictional resistance to sliding, similar to but in the opposite sense as the change in friction produced by a sudden change in slip velocity.
2. The dependence of friction on temperature can be described adequately with state-variable friction constitutive relations previously used to describe velocity dependence and modified to incorporate temperature dependence based on the assumption that slip velocity and temperature follow an Arrhenius relationship.
3. For experimental shear displacement of water-saturated, granular quartz at 50 MPa normal stress, 0.004 to 4 μm/s slip velocity, and between 24 and 82 °C, the apparent activation energy for the sudden and transient changes in friction following a change in temperature or slip-velocity is 89 ± 23 kJ/mol. These activation energies are similar to values previously determined for sub-critical crack growth in quartz by stress corrosion and for healing of microcracks in quartz by diffusive mass transfer. Thus, experimental results are consistent with models of friction involving failure of contact junctions by sub-critical crack growth and time-dependent strengthening of contact junctions by either increasing the true area of contact through sub-critical cracking or by increasing the quality of contact junctions through healing.

References

Atkinson, B.K., Subcritical crack growth in geologic materials, *J. Geophys. Res.*, *89*, 4077-4114, 1984.

Brantley, S.L., B. Evans, S.H. Hickman, and D.A. Crerar, Healing of microcracks in quartz: implications for fluid flow, *Geology*, *18*, 136-139, 1990.

Chester, F. M., Temperature and rate dependence of friction for faults, *Eos Trans. AGU*, *69*, 471, 1988.

Chester, F. M., Temperature-time relationships for frictional strength of quartz gouge, *Eos Trans. AGU*, *71*, 1579, 1990.

Chester, F. M., Temperature-, rate- and state-dependent friction constitutive behavior of quartz gouge, in press, *Eos Trans. AGU*, 1992.

Chester, F.M. and N.G. Higgs, Multimechanism friction constitutive model for ultrafine quartz gouge at hypocentral conditions, *J. Geophys. Res.*, *97*, 1859-1870, 1992.

Dieterich, J.H., Modeling of rock friction, 1, experimental results and constitutive equations, *J. Geophys. Res.*, *84*, 2161-2168, 1979.

Linker, M.F. and J.H. Dieterich, Effects of variable normal stress on rock friction: Observations and constitutive equations, *J. Geophys. Res.*, *97*, 4923-4940, 1992.

Marone, C., C.B. Raleigh, and C.H. Scholz, Frictional behavior and constitutive modeling of simulated fault gouge, *J. Geophys. Res.*, *95*, 7007-7025, 1990.

Ruina, A.L., Slip instability and state variable friction laws, *J. Geophys. Res.*, *88*, 10359-10370, 1983.

Rutter,, E.H., and D.H. Mainprice, The effect of water on the stress relaxation of faulted and unfaulted sandstone, *Pure Appl. Geophys.*, *116*, 634-654, 1978.

Stesky, R.M., Mechanisms of high temperature frictional sliding in Westerly granite, *Can. J. Earth Sci.*, *15*, 361-375, 1978.

SEISMIC PROPERTIES OF ROCK FORMATIONS IN THE PUGET SOUND, WILLIAMETTE LOWLAND REGION

Agreement No. 1434-92-G-2189

Nikolas I. Christensen
Purdue University
Dept. of Earth & Atmospheric Sciences
1397 Civil Engineering Bldg.
West Lafayette, IN 47907-1397

(317) 494-1643

Investigations Undertaken

This project is part of a cooperative study with USGS scientists to obtain high-resolution seismic refraction/wide-angle reflection profiles in western Washington and Oregon, concentrating on areas of high population in the Puget Sound Basin and the Williamette Lowland. The field study has been successfully deployed and preliminary crustal and upper mantle models have been obtained based on qualitative analyses of the data. At present, the data is being analyzed using forward modeling and inversion techniques. The models obtained by these studies will aid in the accurate evaluation of crustal earthquake mechanisms and substantially improve our ability to locate and evaluate earthquakes in the region.

Physical property measurements of rock formations along the seismic transect are currently being studied in the Purdue Rock Physics laboratory. Compressional and shear wave velocities, densities, Poisson's ratios and attenuation measurements are providing important constraints on the nature and distribution of structures and lithologies to the base of the crust and into the upper mantle. By providing information critical for the extension of surface geology to depth, the laboratory studies will facilitate the integration of geological and geophysical data of the region.

Results Obtained

Over 40 samples, representing a variety of lithologies along the transect, were collected this past summer for physical property measurements. Many of these samples have been prepared for velocity and density measurements. To investigate anisotropy, a minimum of three cores have been taken from each sample. Measurements of velocities to pressures of 1000 MPa (equivalent to 35 km depth) are currently underway. Cores of selected samples have provided attenuation measurements (Figure 1) at elevated pressures using a pulse echo technique.

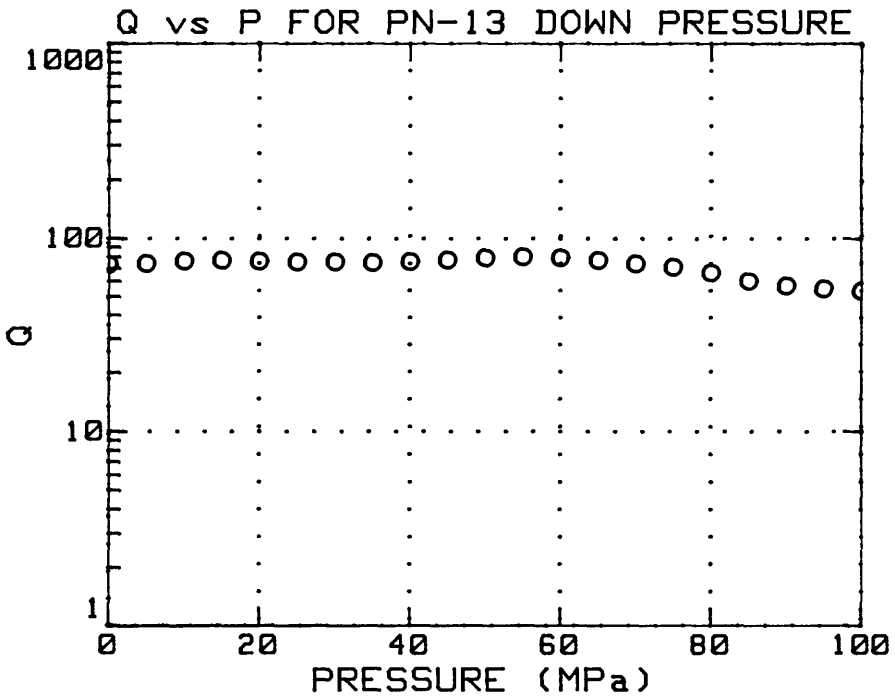

Figure 1. Q versus pressure for a western Washington basalt.

Publications

Luetgert, J., W.D. Mooney, E. Criley, A. Trehu, S.B. Smithson, C. Humphreys, N.I. Christensen, R. Clowes and I. Asudeh, Crustal velocity structure of the Pacific N.W.: The 1991 seismic refraction/wide-angle reflection experiment, Geol. Soc. Am., Cordilleran Section 1992 Abstracts with programs, 66, 1992.

Partial Support of Joint USGS-CALTECH Southern California Seismographic Network

#1434-92-A-0960

Robert W. Clayton
Egill Hauksson

Seismological Laboratory,
California Institute of Technology
Pasadena, CA 91125 (818-356-6954)

INVESTIGATIONS

This Cooperative Agreement provides partial support for the joint USGS-Caltech Southern California Seismographic Network. The purpose is to record and analyze data from more than 50,000 local earthquakes from October 1991 to September 1992 and generate a data base of phase data and digital seismograms. The primary product derived from the data base is a joint USGS-Caltech catalog of earthquakes in the southern California region. We also provide rapid response to media and public inquiries about earthquakes.

For more detailed information about data access, please contact:
Dr. Kate Hutton at (818)-356-6959;
or with E-mail: kate@bombay.gps.caltech.edu.

RESULTS

Network Operation

Southern California Seismographic Network. The SCSN has 230 remote sites (with 300 components) and gathers data from local, regional and teleseismic earthquakes. These data are used for earthquake hazards reduction as well as for basic scientific research. The earthquake hazards reduction effort has become more important as moderate-sized earthquakes continue to occur within densely populated areas in southern California. The largest damaging earthquake to occur was the (M_W=7.3) Landers earthquake of 28 June 1992, located in rural parts of San Bernardino County. It caused over $100 million in damage.

The average rate of 15 publications per year over the last 10 years using the network data illustrates the strength of the ongoing research activities that use the network data. Continued efforts to improve data quality and accessibility have created the arguably best regional earthquake data base in the world. The ongoing upgrading of the quality of the waveforms recorded by the short-period network and the addition of low-gain seismometers and accelerometers provide numerous new avenues of research. Most important of these is analysis of on-scale waveforms to determine source, path and site effects.

The USGS operates most of the remote stations in the SCSN. Caltech operates: 1) 24 short period telemetered stations; 2) 7 stations with local photographic recording of Wood-Anderson seismometers; and 3) 7 very broadband TERRAscope stations; in 1993 we plan to install 8 more TERRAscope stations. Caltech also maintains drum recorders and other equipment at the central site located in the Seismological Laboratory at Caltech.

The computer equipment at the central site has been upgraded and a switch-over to the new computers took place in January 1992. The SCSN data is recorded by two microVAX-III computers and the data processing is done on five VAX workstations using a VAX-4000 as a central server. The operation of this equipment is shared by Caltech and USGS personnel. To avoid duplication, software development is done in cooperation with the USGS in Menlo Park.

More than 50,000 earthquakes will be entered into the southern California earthquake catalog for this reporting period. Approximately 10.0-15.0 Mbytes of phase data and 100-150 Gbytes of seismograms will be archived. In addition to the data analysis we carry out software maintenance, hardware maintenance and other tasks necessary to complete the catalog. Caltech and USGS maintain a data base that includes: 1) earthquake catalog (1932-present); 2) phase data (1932-present); 3) photographic paper seismograms (1930-present); and 4) digital seismograms (1977-present). The earthquake catalog (1932-present) and phase data (1960-present) are available via dial-up and over INTERNET. Other data are available upon request. This data base is being made available to the DC/SCEC and will be the most voluminous part of the data stored in the DC/SCEC.

Near real-time reporting to USGS in Reston and the Governor's Office of Emergency Services and other response to any felt or damaging earthquake activity is provided by network personnel.

The Data Center of the Southern California Earthquake Center. This center has significantly increased the use of the data from SCSN for scientific research. The mass-store system, which became operational on 1 October 1991, provides on-line storage for more than 300 Gbytes of data. The availability of 60 years of catalog, 30 years of phase data, and 14 years of digital seismograms on both UNIX and VMS computers and on-line over INTERNET/NSFNET improves the access to the data.

Seismicity October 1991 - September 1992

The Southern California Seismographic Network (SCSN) recorded approximately 50,000 earthquakes during the 12 months from October 1990 through September 1991, an average of 4170 per month, making it the most active reporting period ever (Figure 1).

The (M_W6.2, 7.3, 6.3) 1992 Landers sequence that began on 23 April with the M_W6.2 1992 Joshua Tree preshock is the most substantial earthquake sequence to occur in the last 40 years in California. These earthquakes ruptured almost 100 km of both surficial and concealed faults and caused aftershocks over a 100 km wide and 180 km long area. The faulting was predominantly strike-slip and all three events had unilateral rupture to the north away from the San Andreas fault.

The M_W7.3 Landers mainshock occurred at 34°N13' and 116°W 26' at 11:58 GMT, June 28, 1992 with a seismic moment of $1x10^{27}$ dyne-cm (Figure 2). The distribution of more than 15,000 aftershocks, short period focal mechanisms, and onscale waveforms from TERRAscope illuminate a complex sequence of faulting (Hauksson et al., 1992). The aftershocks extend 65 km to the north of the mainshock epicenter along a system of at least five different surficial faults and 40 km to the south crossing the Pinto Mountain fault through the Joshua Tree aftershock zone, towards the San Andreas fault near Indio.

The aftershocks range in depth from near-surface down to 15-17 km depth. This is very different from the depth distribution observed in the 1979 Homestead Valley sequence indicating that the maximum depth of earthquake faulting is similar in this region as elsewhere in California.

A tight cluster of small foreshocks (M1.5-3.0) preceded the mainshock by 12 hours. The rupture initiated in the depth range of 5-10 km. The mainshock focal mechanism showed right-lateral strike-slip faulting with a strike of N8°W on an almost vertical fault. The rupture formed an arc-like zone defined by surficial faulting and aftershocks with more westerly faulting to the north. This change in strike is accomplished by jumping across dilational jogs connecting surficial faults with strikes rotated progressively to the west. The

most prominent off-fault aftershock cluster occurred 30 km to the west of the Landers mainshock.

The largest event within this cluster was the M_w6.3 Big Bear aftershock with a seismic moment of $3x10^{25}$ dyne-cm occurring at 34°N10' and 116°W49' at 15:05 GMT 28 June . It exhibited left-lateral strike slip faulting on a northeast striking and steeply dipping plane. The Big Bear aftershocks form a linear trend extending 20 km to the northeast with two lobes of aftershocks located within the dilational quadrants of the M_w6.3 rupture surface.

The faults that caused the Landers mainshock and the fault that caused the Big Bear aftershock are oriented 60° ap \rt, with the Camp Rock-Emerson fault at N10°W to N30°W and the fault for the Big Bear earthquake oriented at about N45°E. The Big Bear fault and the Camp Rock-Emerson fault form a conjugate set. The two faults form the legs of a triangle, the base of which is the Mission Creek strand of the San Andreas fault. The aftershock distributions of both faults touch the San Andreas at Yucaipa for the Big Bearfault and at Joshua Tree for the Landers fault. One earthquake, a M_L4.4 event on the first day, appears to have occurred on the San Andreas fault near Yucaipa with a N60°W fault orientation. The distance on the base of the triangle is approximately 70 km.

The M_w7.3 Landers mainshock occurred near the southernmost extent of the eastern Mojave shear zone, a 80 km wide and more than 400 km long zone of deformation. It extends into western Nevada and accommodates about 10-20% of the plate motion between the Pacific and North America Plates. The Joshua Tree preshock, its aftershocks, and Landers aftershocks form the previously missing link that connects the Mojave shear zone to the southern San Andreas fault.

PUBLICATIONS USING NETWORK DATA (ABSTRACTS EXCEPTED)

Biasi, G. P., and E. D. Humphreys, P-wave image of the upper mantle structure of central California and southern Nevada, *Geophys. Res. Lett., 19,* 1161-1164, 1992.

Hauksson, E., and L. M. Jones, The 1988 and 1990 Upland earthquakes: Left-lateral faulting adjacent to the Central Transverse Ranges, *J. Geophys. Res., 96,* 8143-8165, 1991.

Hull, A. G., and C. Nicholson, Seismotectonics of the northern Elsinore Fault zone, southern California, *Bull. Seismol. Soc. Amer., 82,* 800-818, 1992.

Magistrale, H., H. Kanamori, and C. Jones, Forward and inverse three-dimensional *P* wave velocity models of the southern California crust, *J. Geophys. Resl., 97,* 14,115-14,135, 1992.

Mori, J., Correlation of *P* wave amplitudes and travel time residuals for teleseisms recorded on the Southern California Seismic Network, *J. Geophys. Res., 97,* 6661-6674, 1992.

Nicholson, C., and J. M. Lees, Travel-time tomography in the northern Coachella Valley using aftershocks of the 1986 M_L 5.9 north Palm Springs earthquake, *Geophys. Res. Lett., 19,* 1-4, 1992.

Sung, L-Y., and Jackson, D. D., Crustal mantle structure under southern California, *Bull. Seismol. Soc. Amer., 82,* 934-961, 1992.

Vidal, A., and L. Munguia, Local magnitude and source parameters for earthquakes in the peninsular ranges of Baja California, Mexico, *Bull. Seismol. Soc. Amer., 81,* 2254-2267, 1991.

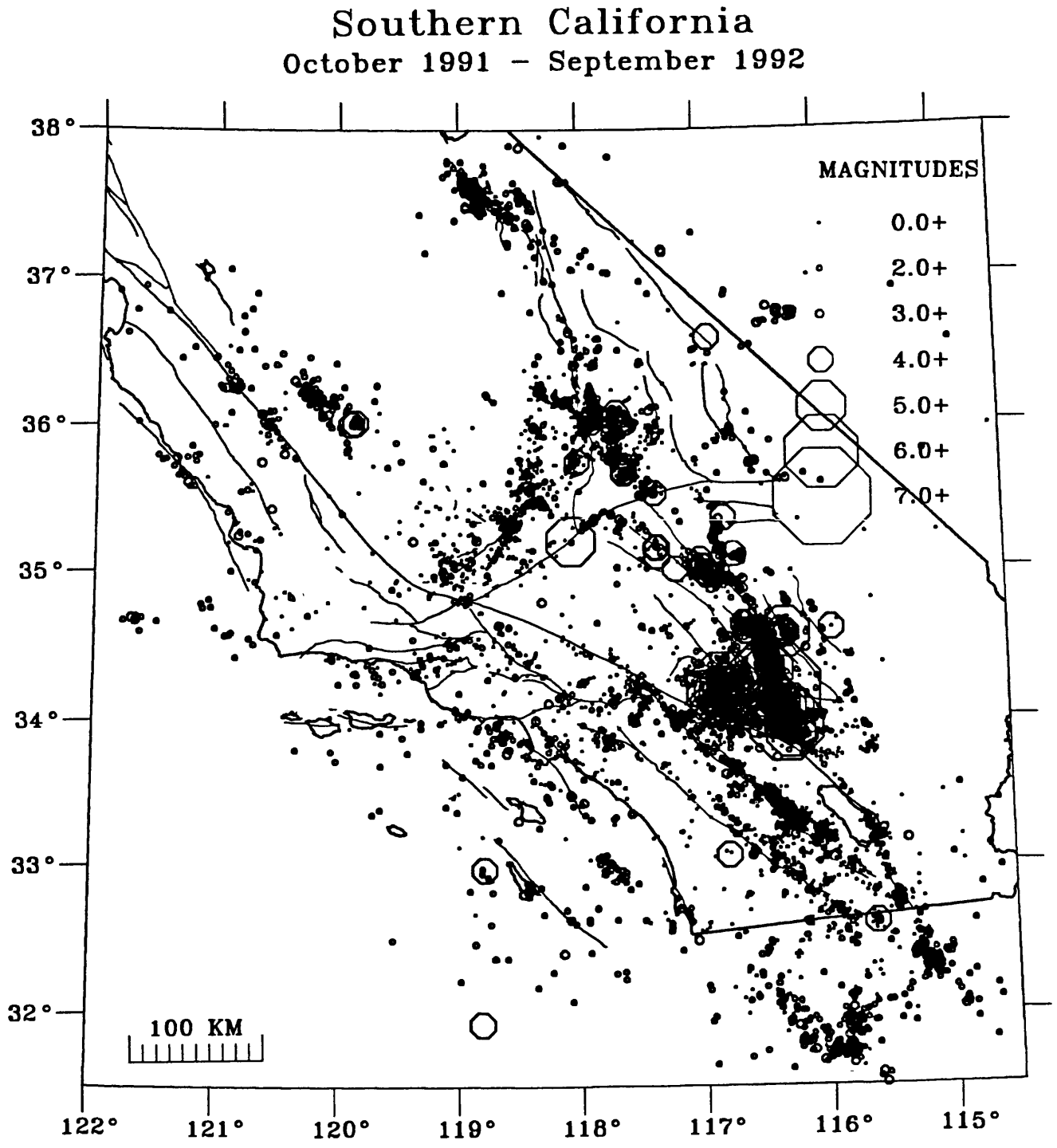

Figure 1. Map of epicenters of earthquakes in the southern California region, 1 October 1991 to 30 September 1992.

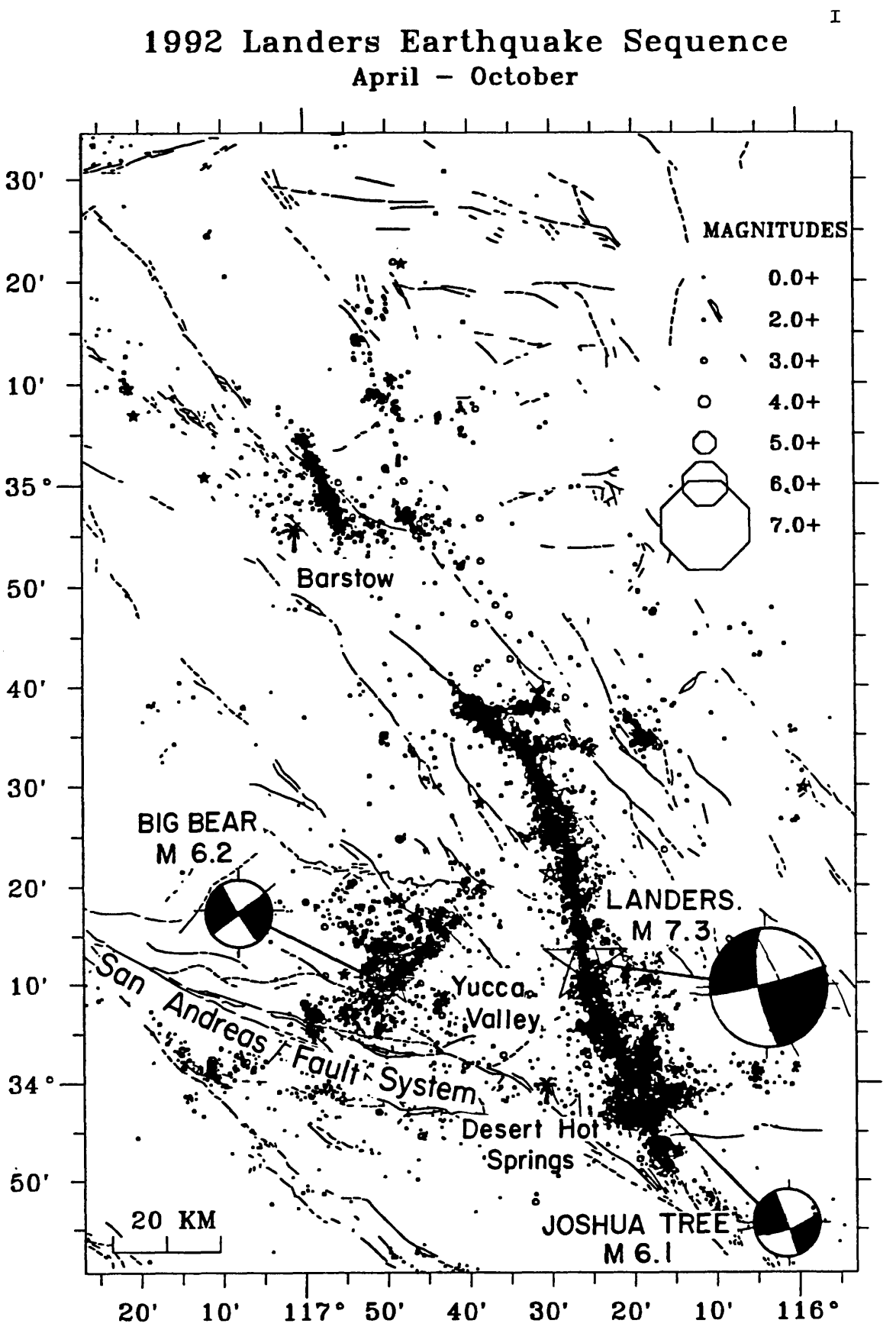

Figure 2. The 1992 Joshua Tree, Landers and Big Bear earthquakes and their aftershocks. The large spatial extent of this aftershock sequence is expected given the magnitude of the M_w7.3 mainshock. The strike-slip focal mechanisms of the M6.1 Joshua Tree, the M7.3 Landers mainshock and the M6.2 Big Bear aftershock are also included.

1. Regional Seismic Monitoring in Western Washington
1434-92-A-0964 R.S. Crosson, P.I.
and
2. Seismic Monitoring of Volcanic and Subduction Processes in Washington and Oregon
1434-92-A-0963 S.D. Malone and A.I. Qamar, P.I.s

R.S. Crosson, S.D. Malone, A.I. Qamar and R.S. Ludwin
Geophysics Program
University of Washington
Seattle, WA 98195
(206) 543-8020
Oct. 1, 1991 - Sept. 30, 1992

Investigations

Operation of the Washington Regional Seismograph Network (WRSN) and preliminary analysis of earthquakes in Washington and Northern Oregon continue under these contracts. Quarterly bulletins which provide operational details and descriptions of seismic activity in Washington and Northern Oregon are available from 1984 through the third quarter of 1991. Final published catalogs are available from 1970, when the network began operation, though 1986.

The University of Washington operates 81 stations west of 120°W under these agreements, 28 are supported under 1434-92-A-0964, 51 under 1434-92-A-0963, and 2 are operated jointly. This report includes a brief summary of significant seismic activity. Additional details are included in our Quarterly bulletins.

Network Operations and Outreach

Station WMO (Whale Mt.,OR) was replaced by BBO (Butler Butte, OR) and station APW (Alpha Peak, WA) was replaced by LCW (Lucas Creek, WA) during this contract period. We also installed a Guralp 3-component broad-band seismometer at Longmire, WA (funded under USGS contract #1434-92-G-2195) which is recorded on-site by a REFTEK digital data logger. Data of interest are retrieved from the data logger over telephone lines via modem.

Our processing scheme includes an automatic alarm for local events that initiates electronic mail or faxes to local emergency response agencies, operators of adjacent seismograph networks, and the National Earthquake Information Center in Colorado. When the event has been fully processed, the updated final information on it is also faxed or e-mailed. A taped message on our voice mail system (206) 543-7010 gives information on felt earthquakes in the last few days within our network, and a longer general message is available on earthquakes in the Pacific Northwest. In addition, locations of recent significant earthquakes can be obtained via modem by dialing (206)685-0889 and logging in as "quake" with password "quake", or via ethernet using the UNIX utility "finger quake@geophys.washington.edu".

We answer from 3-40 questions per day on Pacific Northwest seismicity and seismic hazards, and give about a half-dozen lab tours or presentations each month for a wide variety of age groups; students from elementary through post-graduate, retirees, science teachers, emergency educators, etc. Requests for information increased after the Landers and Big Bear earthquakes in southern California at the end of June.

Seismicity

The Washington Regional Seismograph Network processed 3,537 events between Oct. 1, 1991 and Sept. 30, 1992. Of these 2,613 were earthquakes or blasts within the network and the remaining events were either regional earthquakes (360) or teleseisms (564).

Figure 1 shows earthquakes (M_c ≥2.0) located in Washington and Oregon during this reporting period. Excluding blasts, probable blasts, and earthquakes outside the U. W. network, a total of 1,795 earthquakes west of 120.5°W were located between Oct. 1, 1991 and Sept 30, 1992. Of these, 631 were located near Mount St. Helens, which has not erupted since October of 1986. East of 120.5°W, 197 earthquakes were located.

During this reporting period there were 16 earthquakes reported as felt west of the Cascades, and 6 reported as felt to the east of the Cascades. No damage was reported. The largest earthquake within the area shown in Fig. 1 was a M_c 4.3 earthquake which occurred on November 28, 1991 at 01:08:59(UTC) at ~10 km depth. This earthquake was felt in the Walla-Walla, WA and Milton-Freewater, OR vicinity, and was followed by a few aftershocks. Other felt earthquakes in the same vicinity with similar mid-crustal depths also occurred on December 15, 1991 (M_c 3.3) and July 14 and Sept. 23, 1992 (M_c 4.1 and 2.8, respectively).

Reports and Articles

Benson, R., C.D. Lindholm, R.S. Ludwin, and A.I. Qamar, (in press), A Method for Identifying Explosions Contaminating Earthquake catalogs: Application to the Washington Regional Earthquake Catalog, Seis. Res. Lett.

Jonientz-Trisler, C. B. Myers, and J. Power, (in preparation), Seismic identification of gas-and-ash explosions at Mount St. Helens: capabilities, limitations, and regional application, in /flProceeding Volume, First International Symposium on Volcanic Ash and Aviation Safety,/fR USGS Bulletin 2047.

Ludwin, R.S., A.I. Qamar, S.D. Malone, C. Jonientz-Trisler, R.S. Crosson, R. Benson, and S. Moran (in preparation), Earthquake Hypocenters in Washington and Northern Oregon, 1987-1989, Washington State Dept. of Natural Resources.

Ludwin, R. S., S.D. Malone, R.S. Crosson, A.I. Qamar, (in press or submitted), Washington Earthquakes 1986, Washington Earthquakes 1987, Washington Earthquakes 1988, Washington Earthquakes 1989, in U.S. Earthquakes

Ludwin, R. S., C.S. Weaver, and R.S. Crosson, 1991, Seismicity of Washington and Oregon, Neotectonics of North America. Slemmons, D.B., E.R. Engdahl, D. Blackwell and D. Schwartz, editors; Decade of North American Geology Associated Volume CSMV-1;

Univ. of Wash. Geophysics Program, 1992, Quarterly Network Report 92-A on Seismicity of Washington and Northern Oregon

Univ. of Wash. Geophysics Program, 1992, Quarterly Network Report 92-B on Seismicity of Washington and Northern Oregon

Univ. of Wash. Geophysics Program, 1992, Quarterly Network Report 92-C on Seismicity of Washington and Northern Oregon

Abstracts

Qamar, A.I. and R.S. Ludwin, 1992, Stress directions in Washington and Northern Oregon inferred from earthquake focal mechanisms, Seis. Res. Lett., V. 63, No. 1, p. 28 (also in GSA 88th Annual Cordilleran Section, 1992 Abstracts with Programs, V. 24(5)).

Jonientz-Trisler, C. B. Myers, and J. Power, 1991, Seismic identification of gas-and-ash explosions at Mount St. Helens: capabilities, limitations, and regional application, in /fl First International Symposium on Volcanic Ash and Aviation Safety,/fR USGS Circular 1065, Program and Abstracts, Seattle WA, July 8 through 12, 1991.

Malone, S.D., (in press, Invited), Pacific Northwest earthquake hazards based on Historic seismicity, Report of the National Earthquake Prediction Evaluation Council, May 7-8, 1992.

Moran, S. C., S. D. Malone and S. E. Barker, 1991, Deep earthquakes at Mount St. Helens: evidence for a collapsing and dilating magma chamber (abstract), EOS, V. 72, p. 523.

Theses

Moran, S. C., 1992, Mount St. Helens, 1980-1992: The dynamics and evolution of an active magmatic system as inferred from earthquakes and focal mechanism, Master's thesis, Geophysics Program, Univ. of Wash., Seattle, WA.

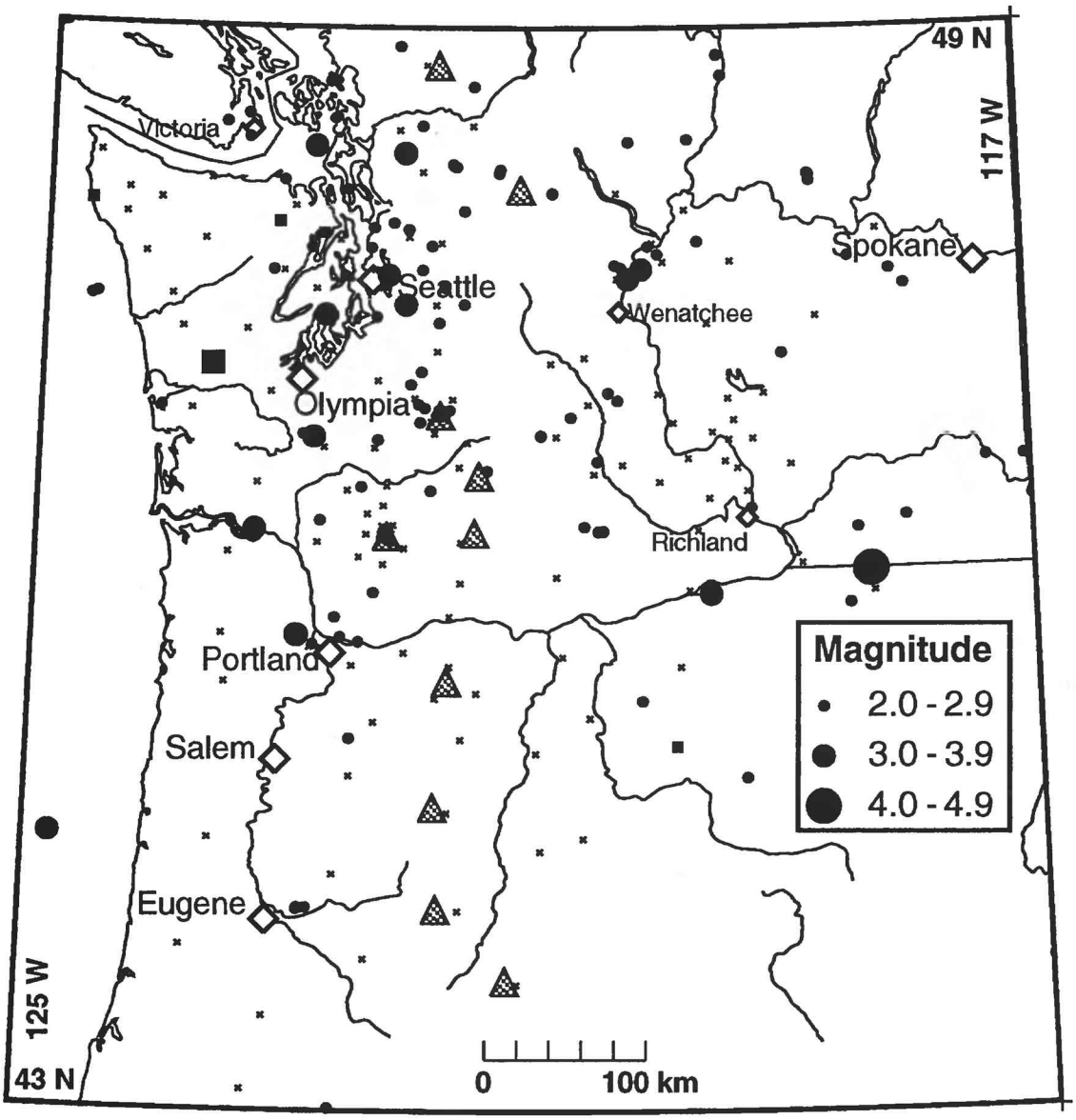

Figure 1. Earthquakes larger than magnitude 2.0 between October 1, 1991 and September 30, 1992. Locations of a few cities are shown as white-filled diamonds. Earthquakes are indicated by filled symbols, where the round symbols represent earthquakes at depths shallower than 30 km, and squares represent earthquakes at 30 km or deeper. Small "x" symbols indicate locations of seismometers operated by the WRSN at the end of September, 1992, and shaded triangles show the position of Cascade volcanos.

Stressing, Seismicity and Rupture of Slip-Deficient Fault Zones

14-08-0001-G1788

R. Dmowska and J. R. Rice (PI)
Division of Applied Sciences and Department of Earth and Planetary Sciences,
Harvard University, Cambridge, MA 02138
(617) 495-3452 and 3445

Investigations:

1.1 Stress transfers during the earthquake cycle in oblique subduction segments.

1.2 Modeling earthquake cycles in the Shumagins (Aleutians) subduction segment with seismic and geodetic constraints.

1.3 Physical modeling of earthquake cycles, asperity development, and characteristic earthquake response, considering lab-based friction, pore pressure and thermal structure.

1.4 Dynamics of rupture

Results:

2.1 Stress transfers during the earthquake cycle in oblique subduction segments have been studied. These transfers are between asperities along the interplate interface (zones of higher locking and high slip in large/great earthquakes) and outer-rise areas, adjacent to the rupture zones, as well as slab areas at intermediate depths, down-dip from the rupture zones. It has been shown previously in our work (Dmowska and Lovison, 1992) that locking of asperities during the cycle results in an uneven distribution of seismicity along strike, both in the outer-rise and at intermediate depth, with seismicity clustering next to asperities on the interplate interface. In subduction segments with direction of convergence approximately perpendicular to the trench (as, e. g., Alaska 1964, Valparaiso 1985) seismically active areas in the outer-rise and at intermediate depth are located next to asperities, along the direction of subduction. However, in study of oblique subduction segments in the western Aleutians (area of Rat Islands 1965 earthquake), we have found that the active areas of the outer-rise and of the slab at intermediate depth, associated with an asperity, locate next to asperities, but along directions somewhat between the convergence vector and the direction perpendicular to the trench. This is shown schematically in Figure 1, and is consistent with observations by Ekström and Engdahl (JGR,1989) that part of the trench-parallel component of subduction is accommodated in the thrust interface, and part in the strike-slip events in the back-arc region.

The position of the active areas seems to be independent of the time window during the cycle, even though the style of seismicity varies with time. E.g. the seismicity in the outer-rise would be tensional in the early part of the cycle and compressional (if at all present) in the later part; at intermediate depth, events after a great subduction earthquake could be compressional, but are tensional later in the cycle. We are planning 2D finite element modeling, somewhat analogous to that discussed next, to examine the magnitudes of cyclic stress transfers and to see what inferences about the stress state and failure process can be made from the seismicity locations.

The observations and computational results may provide better understanding of the mechanics of oblique subduction segments and outer-rise seismicity.

2.2 In continuation of recent work on assessing the seismic potential of the Shumagin Islands segment along the Aleutian subduction zone (Dmowska and Lovison-Golob, EOS, 72, 1991), we use a new 2D finite element model to analyze space- and time-dependent stress transfers in the area during the earthquake cycle. The model is a specific version of the one used by Rice and Stuart (EOS, 70, 1989), but tailored to the geometry of the Shumagins region as constrained by oceanic age and seismicity locations. It consists of an elastic oceanic plate dipping under an also elastic upper plate, into a viscoelastic mantle. The interplate interface undergoes periodically repeated slips and is otherwise locked. We are investigating different model possibilities, such as different geometries of the interplate interface as well as different locking depths (both, updip, between the trench and the upper part of the locked zone, and downdip), different viscosities of the mantle, thicknesses of oceanic and upper plates, etc.

We find that if approximately 15% of the convergence takes place seismically (consistent with $Mo = 1.7 \cdot 10^{20}$ Nm for the 1917 event, Estabrook and Boyd, 1992), if the thrust interface location is taken from seismicity data (Hauksson, BSSA, 1985) so as to dip at 30° beyond 30 km depth, after an initial approximately 10° dip, and is seismically coupled only between approximately 20 km and 50 km depth, but allowed to relax elsewhere (consistent with the finite-element mesh geometry of Figure 2), and if the mantle region relaxes on a time scale of order of 0.1 of the recurrence interval, then consistency with measured strain (Lisowski et al., JGR, 1988) and vertical displacement and tilt (Beavan, NEHRP Summary Reports, 1992) data is obtained, although the uplift and strain are slightly overpredicted. Figure 3 summarizes deformation predictions, with observational constraints shown as the short dashed-line segments. All deformation predictions are within observational ranges if, instead, just 10% of the convergence is assumed to take place seismically.

Our model simulations suggest that the Shumagins segment is capable of large earthquakes, and that the hypothesis of totally aseismic subduction is not consistent with current geodetic constraints.

2.3 A series of three-dimensional analyses have been completed (Rice, 1992a) of slip on a long vertical strike-slip fault between steadily driven elastic crustal blocks, based on depth-variable friction properties which are taken either as uniform along-strike at every depth or as perturbed modestly from uniformity . A rate- and state-dependent friction law governs motion on the fault; the law includes a characteristic slip distance L for evolution of surface state and slip-weakening. Because temperature and normal stress vary with depth, frictional constitutive properties (velocity weakening/ strengthening) do also, in a way constrained by data from Blanpied et al. (GRL, 1991) for granite under hydrothermal conditions. The governing equations of quasistatic elasticity and frictional slip are solved on a computational grid of cells as a discrete numerical system, and a viscous radiation damping term is included to approximately represent inertial control of slip rates during earthquake-like instabilities. The numerical results show richly complex slip, with a spectrum of event sizes, when solved for a grid with oversized cells, that is, with cell size h that is too large to validly represent the underlying continuous system of equations. However, in every case for which it has been feasible to do the computations (moderately large L only), that spatio-temporally complex slip disappears in favor of cycles of periodically repeated large earthquakes with reduction of cell size h. Further study will be necessary to determine whether a similar transition occurs when the elastodynamics of rupture propagation is treated more exactly. The transition from complex to ordered fault response occurs as h is reduced below a theoretically

derived nucleation size h* which scales with L but is $2 \cdot 10^4$ to 10^5 larger in cases considered. [It is given as $h^* = 2 L \mu / \pi (B - A)_m$, where μ = shear rigidity and $(B - A)_m$ is the maximum value on the fault of the velocity weakening parameter $- V d\tau_{ss}(V)/dV$.] Cells larger than h* can fail independently of one another whereas those much smaller than h* cannot slip unstably alone, and can do so only as part of a cooperating group of cells. The results contradict an emergent view that spatio-temporal complexity is a generic feature of mechanical fault models. Such generic complexity does apparently result from models which are inherently discrete in the sense of having no well-defined continuum limit as h diminishes. Those models form a different class of dynamical systems from models like the present one that do have a continuum limit. Strongly oversized cells cause the model developed here to mimic an inherently discrete system. It is suggested that oversized cells, capable of failing independently of one another, may crudely represent geometrically disordered fault zones, with quasi-independent fault segments that join one another at kinks or jogs. Such geometric disorder, at scales larger than h*, may force a system with a well defined continuum limit to mimic an inherently discrete system and show spatio-temporally complex slip at those larger scales.

In continuing study of this type, a fault zone with highly variable properties along strike is being modeled. This variation has been induced in different studies either by varying the degree of pore pressurization along strike, or by assigning an amplitude factor to multiply some particular depth-variation and letting the amplitude factor vary along strike (this might crudely represent lithological variation). In the case studied most extensively so far, the latter method was used to simulate Parkfield-like conditions, thus producing a creeping zone that is bordered by moderate earthquake zones (like Parkfield and San Juan Bautista) which are, in turn, bordered by zones of infrequent great earthquakes (1857 and 1906 rupture zones). To induce this type of behavior, with characteristic earthquake behavior of different segments, it was necessary to have very strong property variations. E.g., the amplitude factor varied by a factor of 10 between the creep zone and moderate earthquake zones, and by a further factor of 5 between the moderate and great earthquake zones, in the case studied. This may be stronger variation than necessary, although trial runs with weaker variation often show a tendency for phase locking between different zones, which thus lose their characteristic behavior. Presumably, strong geometric barriers at zone ends could induce characteristic-like behavior with weaker variation from zone to zone. The Parkfield-like events, in versions of the model studied thus far, are found to have highly variable moment release and recurrence intervals. One sequence of five such events, in the time span between adjacent great earthquakes, has a ratio of sample standard deviation to mean of the recurrence intervals of about 0.59, higher than 0.33 for the Bakun and McEvily (JGR, '84) Parkfield catalog.

2.4 Crack dynamics studies of a type reported previously (Rice, Ben-Zion and Kim, 1991), in which a scalar wave approximation to elastodynamics is used, are being continued to study crack advance along a plane on which there is variable resistance to cracking. In that work the resistance to cracking is given entirely by a spatially variable critical fracture toughness, and zero stress is assumed on the rupture surface. We have also begun studies of the dynamics of slipping faults which satisfy rate- and state-dependent friction on their surfaces. The work is being done for the 2D anti-plane strain case at present, and uses a numerical algorithm of Madariaga and Cochard (manuscript, 1992) which we have adapted to the rate- and state-dependent context. The aims here are to see what type of stress heterogeneity is left on a fault

surface after a rupture has propagated spontaneously and undergone a wave-mediated arrest of slip after encountering an unbreakable region, and also to see under what conditions the rupture propagation has the form suggested by Heaton (PEPI, 1990), with all slip taking place just near the advancing front of the rupture and relocking behind that.

Reports:

R. Dmowska, "Stress transfers during the earthquake cycle in oblique subduction segments" (abstract), EOS, Trans. Am. Geophys. Un., vol.73, N.43, supplement, p.361, 1992

R. Dmowska, L. C. Lovison-Golob and J. J. Durek, "Partial breaking of a mature seismic gap: The 1987 earthquakes in New Britain", *Pure and Applied Geophysics*, **136**, 459-477, 1991.

R. Dmowska and L. C. Lovison, "Influence of asperities along subduction interfaces on the stressing and seismicity of adjacent areas", *Tectonophysics* , **211**, 23-43, 1992.

Dmowska R., G. Zheng, J.R.Rice and L.C.Lovison-Golob, "Stress transfer, seismic phenomena and seismic potential in the Shumagin seismic gap, Alaska" (abstract), Wadati Conference on Great Subduction Earthquakes, abstract book, 150-152, Fairbanks, Alaska, Sept.16-19, 1992.

H. Gao, J. R. Rice and J. Lee, "Penetration of a quasistatically slipping crack into a seismogenic zone of heterogeneous fracture resistance", *Journal of Geophysical Research*, **96**, 21535-21548, 1991

H. Gao, J. R. Rice and J. Lee, "Configurational stability of the uniform upward growth of a shear crack along a strike-slip fault zone" (abstract), AGU 1991 Fall Meeting Program and Abstracts (supplement to 29 Oct. 1991 EOS), S31C-6, p. 325, 1991

M. F. Linker and J. H. Dieterich ,"Stability of fault slip under conditions of variable normal stress", (abstract), EOS, Trans. Am. Geophys. Un., vol.73, N.43, supplement, p. 511, 1992

M. F. Linker and J. R. Rice, "The effective viscosity of the San Andreas fault beneath the seismogenic zone: Constraints from the response to the 1989 Loma Prieta earthquake" (abstract), ibid, S21C-9, pp. 310-311, 1991

M. F. Linker and J. R. Rice, "Models of postseismic deformation and stress transfer associated with the 1989 Loma Prieta earthquake", manuscript intended for inclusion in USGS Professional Paper on the Loma Prieta Earthquake, 1992

J. R. Rice, "Spatio-temporal complexity of slip on a fault", *Journal of Geophysical Research,* in press, 1992

J. R. Rice, "Fault stress states, pore pressure distributions, and the weakness of the San Andreas fault" in *Fault Mechanics and Transport Properties of Rocks,* ed. B. Evans and T.-F. Wong, Academic Press, pp. 475-503, 1992

J. R. Rice, "Variable earthquake recurrence intervals at Parkfield" (abstract), EOS, Trans. Am. Geophys. Un., vol.73, N.43, supplement, p.407, 1992

J. R. Rice, Y. Ben-Zion and K.-S. Kim, "A first order perturbation solution for a dynamic planar crack with a non-uniformly moving front" (abstract), AGU 1991 Fall Meeting Program and Abstracts (supplement to 29 Oct. 1991 EOS), S31C-7, p. 325, 1991

G. Zheng, R. Dmowska and J. R. Rice, "Modeling earthquake cycles in the Shumagins (Aleutians) subduction segment with seismic and geodetic constraints" (abstract), EOS, Trans. Am. Geophys. Un., vol.73, N.43, supplement, p.367, 1992

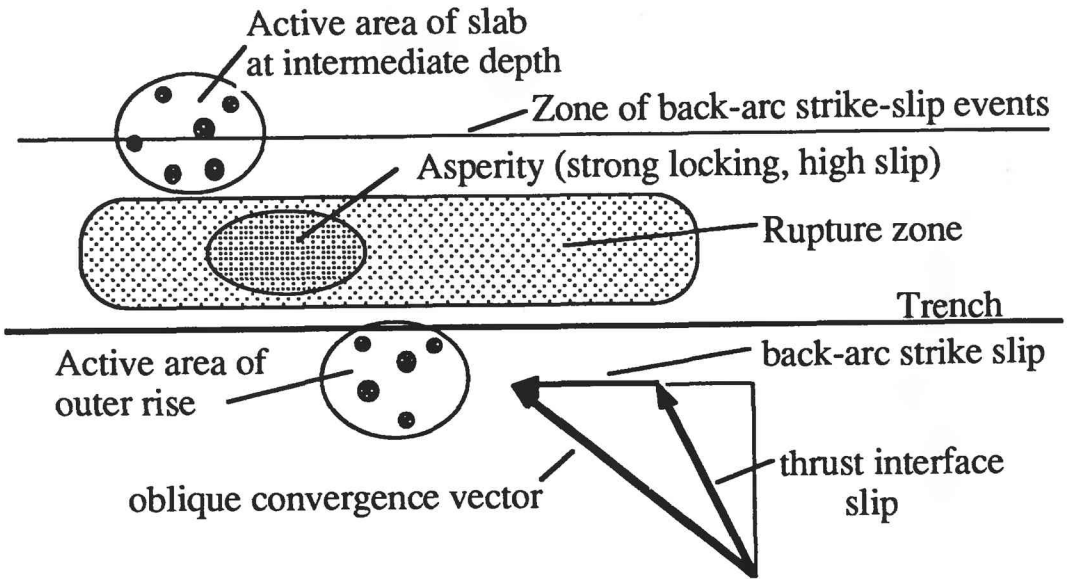

Figure 1: Oblique subduction and location of seismically active areas.

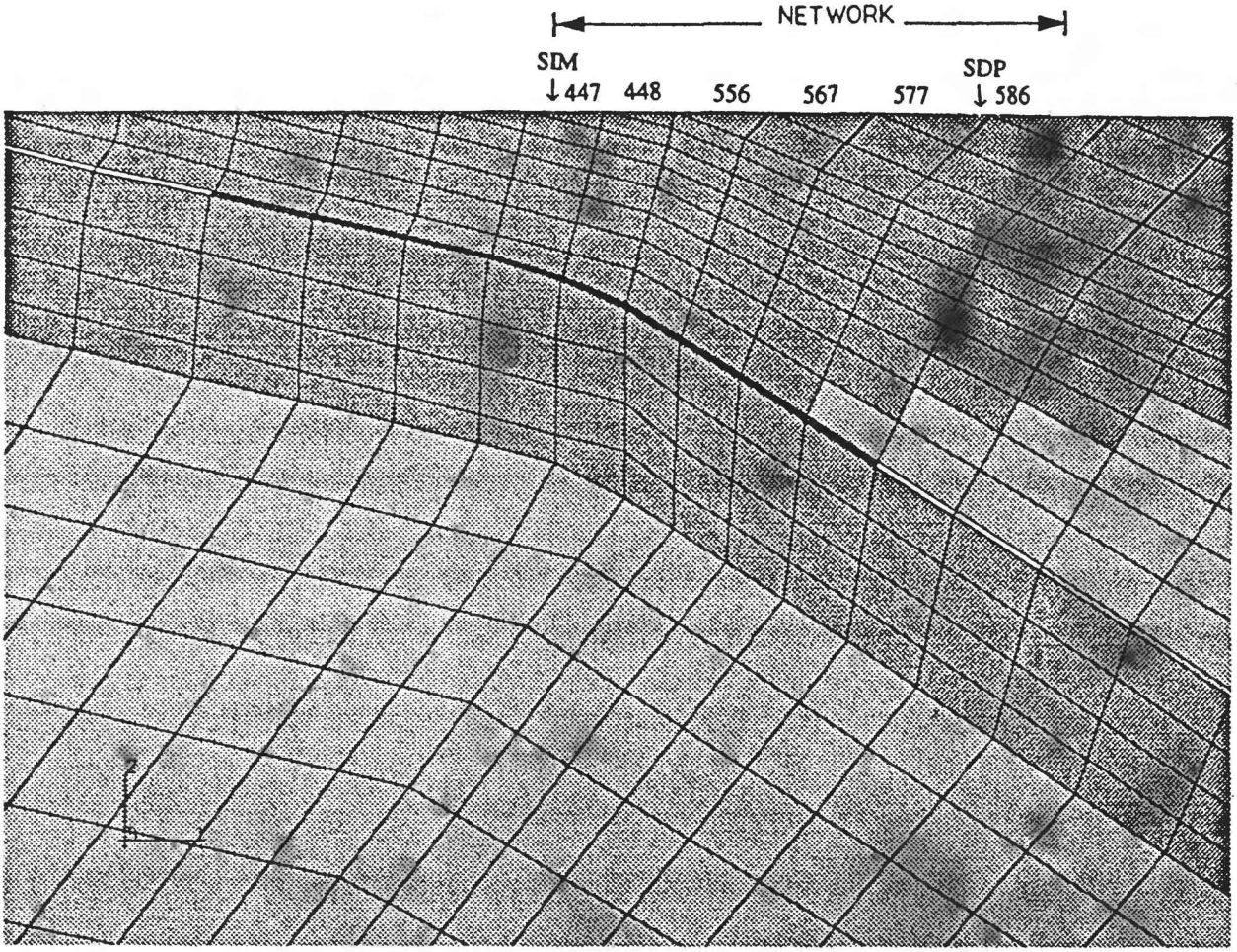

Figure 2: Finite-element mesh used for analysis of deformation at Shumagins subduction segment.

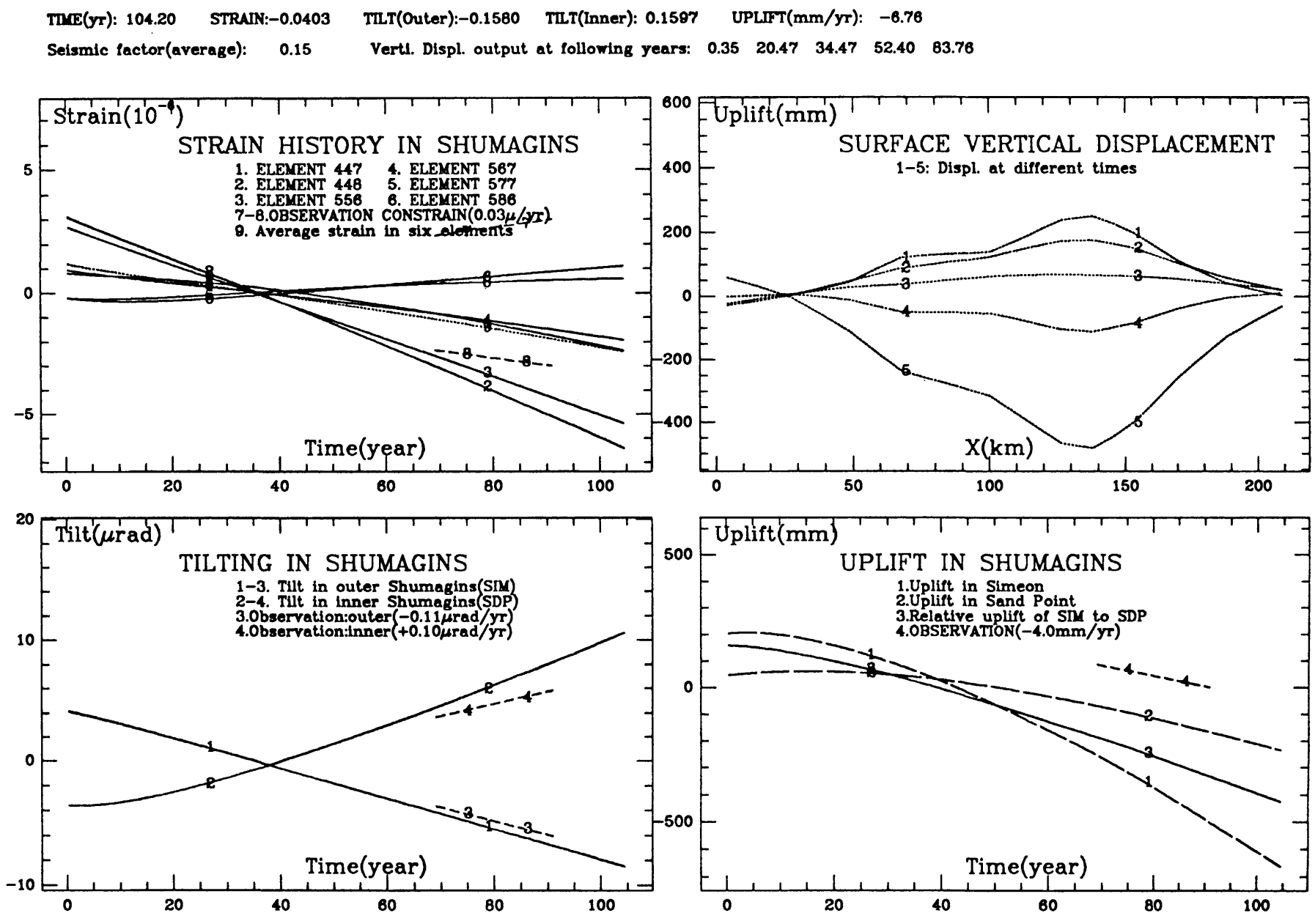

Figure 3: Deformation predictions in Shumagins area; preferred model with 15% seismic coupling.

The New England Seismic Network
Agreement No. 1434-92-A-0972

John E. Ebel
Weston Observatory
Department of Geology and Geophysics
Boston College
Weston, MA 02193
(617) 899-0950

Investigations

The operation of a regional seismic network to monitor earthquake activity in New England and vicinity is supported under this project. The purpose of this earthquake monitoring is to compile a complete database of earthquake activity in New England to as low a magnitude as possible in order to understand the causes of the earthquakes in the region, to assess the potential for future damaging earthquakes, and to better constrain the patterns of strong ground motions from earthquakes in the region. The New England Seismic Network (NESN) is cooperatively operated by Weston Observatory of Boston College and the Earth Resources Laboratory of the Massachusetts Institute of Technology (MIT).

Network Status

Weston Observatory presently has 30 seismic stations spread throughout New England, and in addition MIT is operating 9 seismic stations in New Hampshire and Massachusetts. At present, 26 of the Weston Observatory NESN remote seismic stations are single-component (vertical) stations (1 Hz velocity transducer geophones) linked via analog telephone telemetry to Weston Observatory where event triggering and recording is being done on a PC computer. The three other remote stations (at Moodus, CT, Gaza, NH and Milo, ME) are new PC-based stations, with digitizing and event triggering at the remote site and data telemetry via dial-up telephone connections. All three of these stations have three-component 1-Hz force-balanced sensors which are somewhat broader band than the standard velocity transducer. Weston Observatory and MIT are planning within the next year to install an additional 15 of these PC based stations throughout New England to replace the analog stations, all of which will lose their continuous telephone telemetry sometime during 1993.

Weston Observatory and MIT are presently archiving independently the waveform data for the seismic stations which they are presently operating. However, each institution now has the capability to convert these waveforms to SAC format for external distribution, and ftp accounts are being set up at each institution for easy external access to the waveforms as well as the event location data.

A satellite receiver to receive U.S. National Seismic Network (USNSN) waveforms has been installed atop Weston Observatory. Also, Weston Observatory is donating to the USGS a set of Streckheisen STS-1 seismometers for installation at its CBM site in northeastern Maine (at Caribou) as one of the new USNSN stations. When completely operational, there should be about 5 USNSN stations in New England in addition to the Weston Observatory/MIT regional network stations. Weston Observatory will act as a regional node with the capability of receiving and transmitting USNSN data.

Seismicity

Figure 1 shows the local and regional earthquakes recorded by Weston Observatory from October 1, 1991 to October 10, 1992. A total of 26 local earthquakes with magnitudes from 1.8 to 4.8 were detected and located by the network, five of which were felt. Also recorded on the new PC stations were several microearthquakes at Moodus, CT and at Milo, ME. Significant earthquakes during this time period included a $m_{Lg}(f)=3.4$ earthquake at Franklin, NH on October 6, 1992 which was felt throughout central New Hampshire. This was the latest and largest of several small shocks in that state during the past year. Also occurring was a $m_b=4.8$ earthquake centered on the continental slope south of Rhode Island and east of southern New Jersey. This earthquake was unusual in that it was very rich in low-frequency seismic energy and it was recorded teleseismically. Whether or not this earthquake represents a slump event on the continental slope, as has been proposed for the 1929 Grand Banks, Newfoundland earthquake, is being studied. Finally, a number of small earthquakes were recorded from central New Brunswick in the vicinity of the 1982 $m_b=5.7$ Miramichi aftershock zone. More than 10 years after the main shock, the seismic activity of this part of the northern Appalachians remains elevated above rates seen prior to 1982.

Publications

Doll, W.E., C.D. Rea, J.E. Ebel, S.J. Craven and J.J. Cipar, 1992. Analysis of shallow microearthquakes in the south Sebec seismic zone, Maine, 1989-1990, Seism. Res. Lett., 63, in press.

Zhu, H. and J.E. Ebel, 1992. Tomographic inversion for the seismic velocity structure beneath northern New England using seismic refraction data, submitted to J. Geophys. Res.

Abstracts

D'Annolfo, S.E. and A.L. Kafka, 1992. Lateral variation in the seismic velocity structure of the shallow crust beneath eastern Massachusetts and southern New Hampshire, Seism. Res. Lett., 63, in press.

Ebel, J.E., 1992. A revised Lg-wave magnitude scale for northeastern North America: Implications for seismic hazard assessment, Eos, Trans. Am. Geopyhys. U., 73, No. 14, 206.

Ebel, J.E., 1992. The $m_{Lg}(f)$ magnitude scale: A proposal for its use in northeastern North America, Seism. Res. Lett., 63, in press.

Jacobson-Carroll, M.R., and A.L. Kafka, 1992. Site effects on regional seismograms recorded in the vicintiy of Weston Observatory, Seism. Res. Lett., 63, in press.

Paulson, A.D. and J.E. Ebel, 1992. Analysis of the 1988 NYNEX seismic reflection/refraction data, Seism. Res. Lett., 63, in press.

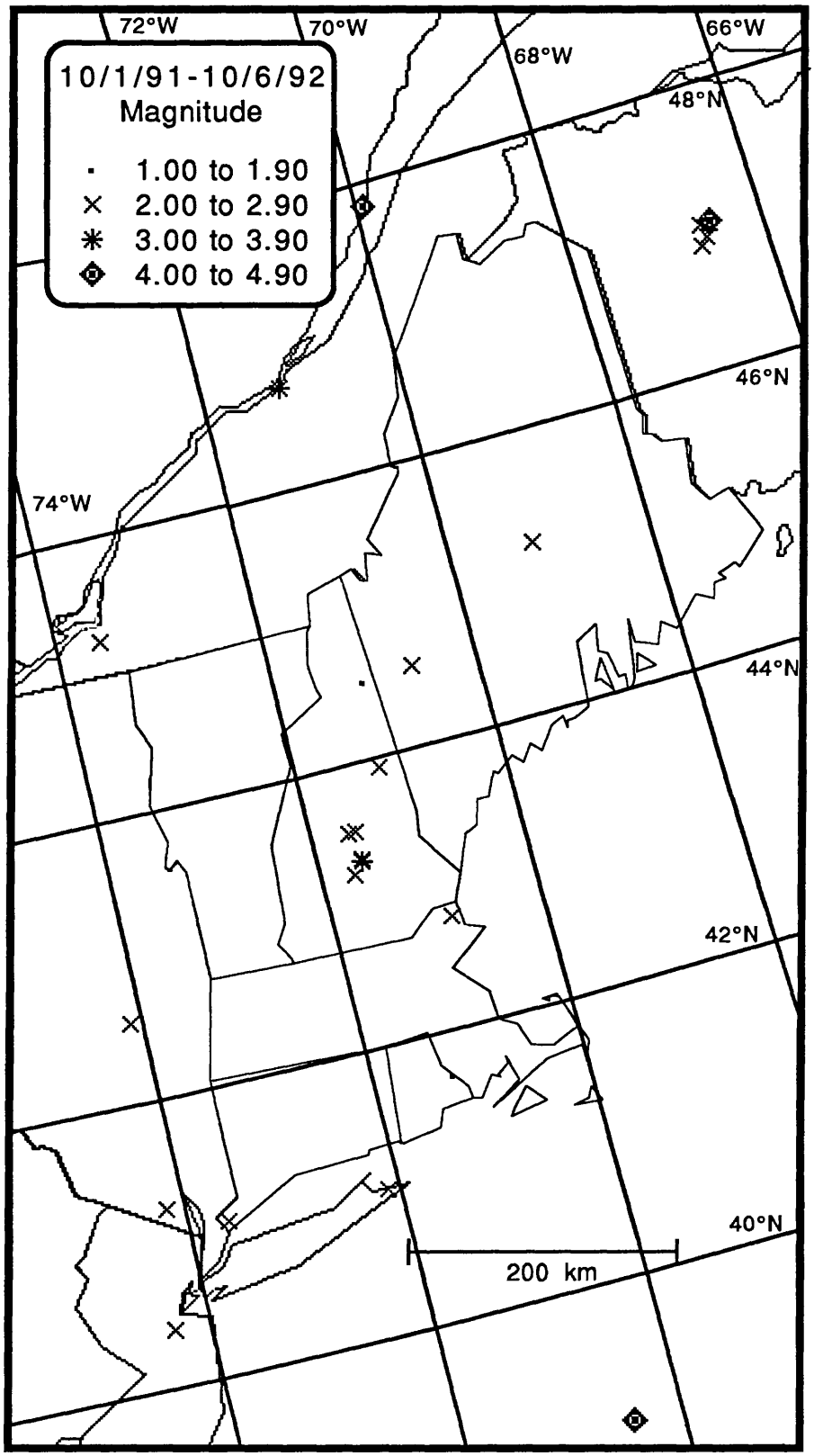

Figure 1. Seismicity recorded and located by the New England Seismic Network of Weston Observatory of Boston College from October 1, 1991 to October 10, 1992.

Central California Network Operations

9930-01891

Wes Hall
Branch of Seismology
U.S Geological Survey
275 Middlefield Road-Mail Stop 977
Menlo Park, California 94025
(415) 329-4730

Investigations

Maintenance and recording of 374 seismograph stations (474 components) located in Northern California, Central California and Oregon. Also recording 70 components from other agencies. The area covered is from the Oregon border south to Santa Maria.

Results

1. Site maintenance visits 550

2. Bench Maintenance Repair
   - A. seismic VCO units 310
   - B. summing amplifiers 38
   - C. seismic test units 13
   - D. VO2H/VO2L VCO units 63
   - E. dc-dc converters 30

3. Production/Fabrication
   - A. J512A VCO units 55
   - B. J512B VCO units 12
   - C. summing amplifier units 21
   - D. lithium battery packs 68
   - F. seismometer housing/cable 71

4. Rehabilitation:
   VCO enclosures 56

5. Computer site map plots
   - A. new 25
   - B. update 89

5. Discriminator repair and tuning (J120) 166

6. Revised and updated documentation on all wiring from telco input to disscriminator output. (cusp, RTP, Motorola, PC, helicorder, etc).

7. Ordered Parts for 175ea J512 VCO's and 100 ea J120 discriminators

8. Equipment Shipped:

   A. Cal Tech, Pasadena
      a. 60 ea. J601 DC-DC Convertors
      b. 1 J512B vco's
      c. 40 ea. J120 discriminators
      d. 1 ea. discriminator rack
      e. 6 ea. L4 seismometers
   B. University Washington

a. 15 ea. J512a vco's
b. 15 ea. J120 discriminators
c. 1 ea. discriminator rack

C. Hawaii Volcano Observatory
a. 20 ea. J512a vco's
b. 20 ea. J120 J120 discriminators
c. 1 ea. discriminator rack
f. 20 ea. summing amp PCB

D. University Utah
a. 25 ea. J120 discriminators

9. New installations

A.	CPI	(Pinole Ridge)
B.	JSB	(San Bruno Mountain)
C.	JCP	(Coyote Point)
D.	KSC	(Snow Mountain)
E.	KHB	Hayfork Bally)
F.	BPO	(Post Ranch Vertical)
	BPON	(Post Ranch North)
G.	OCR	(Cohasset Ridge)
H.	CGP	(Garin Park)
I.	CYB	(Yerba Buena Vertical)
	CYBN	(Yerba Buena North)
	CYBE	(Yerba Buena East)
	CYBZ	(yerba Buena Low Vertical)
J.	KTR	(Thompson Ridge)
K.	KCS	(Cold Spring)
L.	MBE	(Bear Mountain)
M.	MBU	(Bullion Mountain)

10. Stations discontinued.

A.	BPF	((Pfeiffer Point Vertial)
	BPFN	(Pfeiffer Point Horizontal)
B.	OCH	(Cohasset Ridge)
C.	CSC	(Silver Creek)
D.	HQR	(Quien Sabe)
E.	PRP	(Reason Peak)

THE USGS PARKFIELD DENSE SEISMOGRAPH ARRAY (UPSAR)

9910-03974

M. HELLWEG, L.M. BAKER, J.B. FLETCHER, P. SPUDICH, L.K. STECK
BRANCH OF ENGINEERING SEISMOLOGY AND GEOLOGY
345 MIDDLEFIELD ROAD, MS 977
MENLO PARK, CALIFORNIA 94025-3591
415/329-5654 FAX 415/329-5163

Investigations:

1. Temporal stability of coda Q at Parkfield, California.

2. Determination of transient dynamic stresses caused by the Landers, California, earthquake.

3. Investigations of scattering and multipathing of surface waves caused by large California earthquakes.

Results:

1. Since mid-1989, the USGS Parkfield Dense Seismograph Array, UPSAR, an array with 14 three-component seismographs located in a 1 km^2 area, has been recording seismicity in the Parkfield region. At present, it has recorded more than 600 local events. These earthquakes have occurred at all azimuths and at varying distances, and include spatial clusters as well as doublets. To test the temporal stability of the Qc measurement we used Haar's method (1989) to determine coda-Q of a cluster of 10 events that occurred between December 1989 and the present, all of which were located in a 1 km3 source volume. The use of events in a compact source volume minimized station-hypocenter variability in the coda-Q measurements. In the frequency bands 4-8 Hz and 8-16 Hz values of Qc did not vary from the mean values of 108 and 222, respectively by more than 10 per cent during this period. Qc differences between nearly simultaneous doublets was as large as the variation between temporally separate events. To improve the temporal coverage, we determined coda Q in the frequency bands, 2 4 Hz, 4-8 Hz, 8-16 Hz and 16-32 Hz, from a set of 68 events with epicentral distances of less than 60 km. Analysis of this set shows that there has been no significant variation in coda Q in the Parkfield region since December 1989.

2. The UPSAR accelerometers produced usable broadband records from many of the recent large California earthquakes, such as the Joshua Tree, Landers, Big Bear, Petrolia, and Ferndale events. In an attempt to understand the origins of the widespread earthquake triggering following the Landers earthquake, the UPSAR

acceleration records of the Landers event have been double-integrated to displacement and have been inverted to obtain the dynamic strains as a function of time produced at UPSAR (epicentral distance = 415 km) by this event. Preliminary inversion results yield peak shear strains of about 6 x 10^{-6}. Noise levels, inferred from displacement differences between the two closest stations of the array, are about 1 x 10^{-6}. The maximum strains occur during the surface wave train. To extrapolate surficial strains to seismogenic depths, we must account for the variation of the surface wave eigen functions with depth, which we are presently doing. A rough calculation shows that our observed strains correspond to transient dynamic stresses of about 1 bar at depth. This stress is about a factor of 50 larger than the stress changes induced by earth tides.

3. Records of the Landers event at UPSAR contain P_n, P_g, P_L, S_n, S_g, L_Q and L_R phases, as well as later-arriving scattered surface waves. On velocity seismograms, a number of distinct arrivals can be seen in both the P and S wave trains. Broad-Band Frequency-Wavenumber analysis shows that the first arriving P energy comes in at an azimuth of about 80 o s, whole the lower frequency S waves come in at 100 o s, closer to the expected value of 115 o 's. Fundamental mode Love and Rayleigh waves are observed to arrive from about 120 o 's. However, 200 s after the P-wave arrival, 10-20 s surface waves arrive from about 70 o 's azimuth. These waves are probably surface waves scattered from the Sierra Nevadas.

Reports:

Fletcher, J.B., Baker, L.M., Spudich, P., Goldstein, P., Sims, J.D., and Hellweg, M., 1992, The USGS Parkfield, California, dense seismograph array: UPSAR, Bull. Seismol. Soc. Am., v. 82, 1041-1070.

Hellweg, M. Fletcher, J.B., and Spudich, P., 1991, Coda coherence and Q from UPSAR, Parkfield, California, [abs.], EOS Trans. Am. Geophys. Un., v. 72, 483.

Hellweg, M. Spudich, P., and Fletcher, J.B., 1992, Coda Q in the region of Parkfield, California: a temporal and spatial investigation, [abs.], EOS Trans. Am. Geophys. Un., v. 73, 200.

Hellweg, M. Spudich, P., and Fletcher, J.B., 1992, Stability of Coda Q at Parkfield, California, [abs.], EOS Trans. Am. Geophys. Un., v. 73, 397.

Steck, L.K., Spudich, P., Hellweg, M., Baker, L., and Fletcher, J., 1992, Shear strain at Parkfield produced by the Landers earthquake, [abs]., EOS Trans. Am. Geophys. Un., v. 73, 374.

Source Characteristics of events along the Transverse Ranges

14-34-92-G2180

Donald V. Helmberger
Seismological Laboratory
California Institute of Technology
Pasadena, CA 91125

(818)356-6998

Investigations

A number of recent and historic earthquakes have occurred along the Transverse Ranges, causing significant damage to the greater Los Angeles region. Many of the historic events occurring in this region have been recorded (locally) by relatively low gain long period and short period torsion instruments operated by Caltech (1930 to 1960). Some of the larger events M>5 can be seen on the (Berkeley Galitzins) regionally while still larger events M>6 can be observed teleseismically, (De Bilt ,etc.).

To understand these seismograms or separate propagational distortions from source properties is relatively easy at teleseismic distances, but becomes more difficult at regional and local distances. Fortunately, the digital systems used in the TERRAscope array provides observations that greatly aid in establishing the nature of regional propagation. For example, the wide dynamic range allows motions from small events (aftershocks) to be compared with large events at the same site even though the motions can be different by several orders of magnitude. Signals at these distances have not suffered mantle attenuation and thus the broadband features of this system allow us to see obvious propagational effects (headwaves and critical reflections) and detailed source characteristics (near-field and source complexity).

Modeling attempts to date indicate that whole seismograms can be understood at ranges less than a few degrees with simple models. At larger ranges, the energy carried by direct S generally becomes scattered and difficult to model, presumably caused by shallow earth structure. Fortunately, at these larger ranges the mantle headwaves, Pn and Sn, become visible and we believe this beginning portion of records (excluding the surface waves) can be used in source estimation as demonstrated by our waveform inversion results.

Results

Several papers involving the Sierra Madre earthquake sequence have been published or "in press": (1) Source parameters of the Sierra Madre Earthquake from Regional and Local Bodywaves, Dreger and Helmberger (1991). (2) Strong motion and broadband Teleseismic Analysis of the 1991 Sierra Madre, California Earthquake, Wald (1992). (3) Impact of broadband seismology on Strong Motion Attenuation. Helmberger et al. (1992). (4) Broadband observations of rupture directivity for the 1991 Sierra Madre earthquake, Dreger and Helmberger (1992). In this summary we will emphasize the recent Landers earthquake and the complex faulting deduced from broadband modeling local, regional and teleseismic waveform observations, Wald et al. (1992).

We have determined a finite-fault source rupture model for the 1992 Landers earthquake consistent with both teleseismic and strong motion displacement data. The procedure followed is similar to previous efforts, see Wald et al. (1991). The fault model parameterization consists subfaults making up three separate fault planes, mimicking the mapped surface offset (Figures 1

and 2). Each subfault is 3 km across by 2.5 km down-dip, giving a total fault depth 15 km and a total of 186 subfaults. The hypocenter is assumed to be 9 km, as determined by the network location (star in Figure 2). The fault strikes of the Johnson Valley/Landers, Homestead Valley, and Emerson/Camprock Faults are 355°, 334° and 320°, respectively.

Currently our inversion employs a subset of 11 local strong motion records (including Amboy, Barstow, Big Bear, Lucerne Valley, Morongo Valley, and Joshua Tree) combined with near-regional TERRAscope data. We also use 11 teleseismic P waves and 10 SH waves. All data and synthetics were bandpassed between 20 seconds and 1.0 Hz. Shallow slip in our model is constrained to match that measured at the fault surface by assigning that slip value to the shallowest subfault elements. We have also performed a separated inversion of the teleseismic broadband data using the same fault parameterization.

Rupture models are consistent for both data sets: we found unilateral rupture with two main regions of slip, separated by about 35 km with a slip gap. This is in agreement with the measured surface offset. The effective rupture length is about 65 km and the seismic moment was computed to be about 0.8 - 0.85 x 10^{27} dyne-cm, with peak slips of nearly 7 meters. The seismic moments of slip for the three fault planes is about 0.20, 0.25 and 0.35 x 10^{27} dyne-cm. The rupture velocity is locally variable, but can be approximated with value of 2.5 km/sec, or about 75% of the local shear velocity.

We find the nucleation of the rupture to be a complex growth, perhaps stopping and restarting, as required by late teleseismic P wave arrivals as well as emergent local strong motion arrivals. This was accounted for in our modeling with the use of multiple time windows, i.e., allowing repeated rupture to occur on each subfault. The use of time windows also allows for the estimate of rupture duration. Local slip durations (rise time) are short, less than 2.0 sec on most of the fault, but may be up to 4.0 sec in region of maximum slip at depth.

References

Dreger, Douglas S. and D. V. Helmberger (1991). Source parameters of the Sierra Madre Earthquake from regional and local body waves, *Geophys. Res. Lett.*, **18**, 22015-2018.

Dreger, D. S. and D. V. Helmberger (1993). Broadband observations of rupture directivity for the 1991 Sierra Madre earthquake, *Bull. Seism. Soc. Am.* (in press).

Helmberger, D. V., D. Dreger, R. Stead, and H. Kanamori (1993). Impact of broadband seismology on strong motion attenuation, *Bull. Seism. Soc. Am.* (in press).

Wald, David J.(1991). Strong motion and broadband teleseismic analysis of the 1991 Sierra Madre, California, Earthquake, *Journal Geophys. Res.*, **97**, 11033-11,046.

Wald, D., D. Helmberger, and T. Heaton (1991). Rupture history of the 1989 Loma Prieta, California, earthquake, *Bull. Seism. Soc. Am.*, **81**, 1540-1572.

Wald, D. J. D. V. Helmberger and T. H. Heaton (1992). On developing a simgle rupture model for the 1992 Lander, California earthquake consistent with static, broadband teleseismic, regional and strong motions, *EOS*, American Geophysical Union (Fall Meeting).

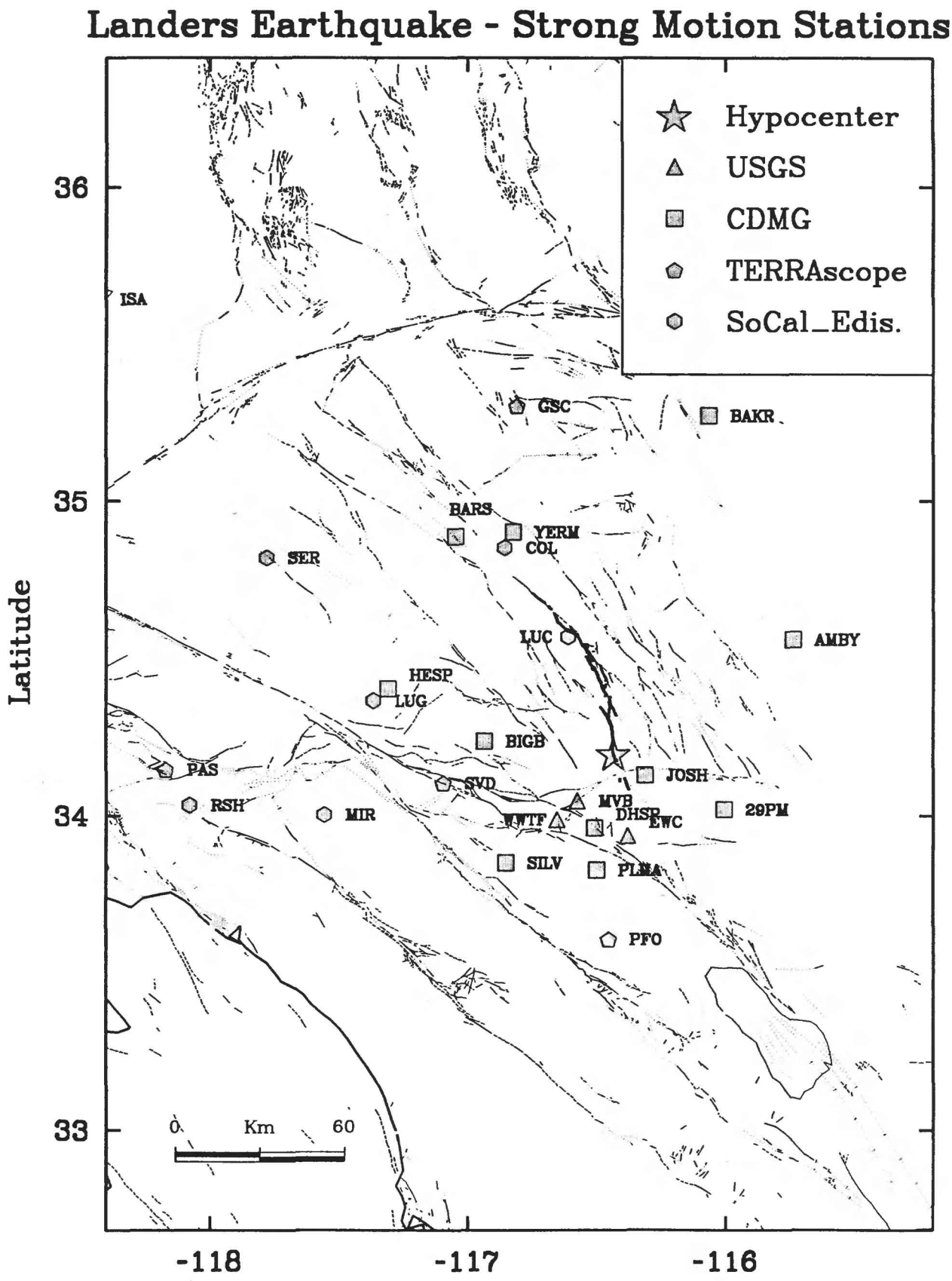

Fig. 1. Location map showing strong motion stations (solid symbols) for the Landers earthquake. Light lines are mapped faults and the thick line indicates surface offset from the Landers event (courtesy of K. Sieh, Caltech).

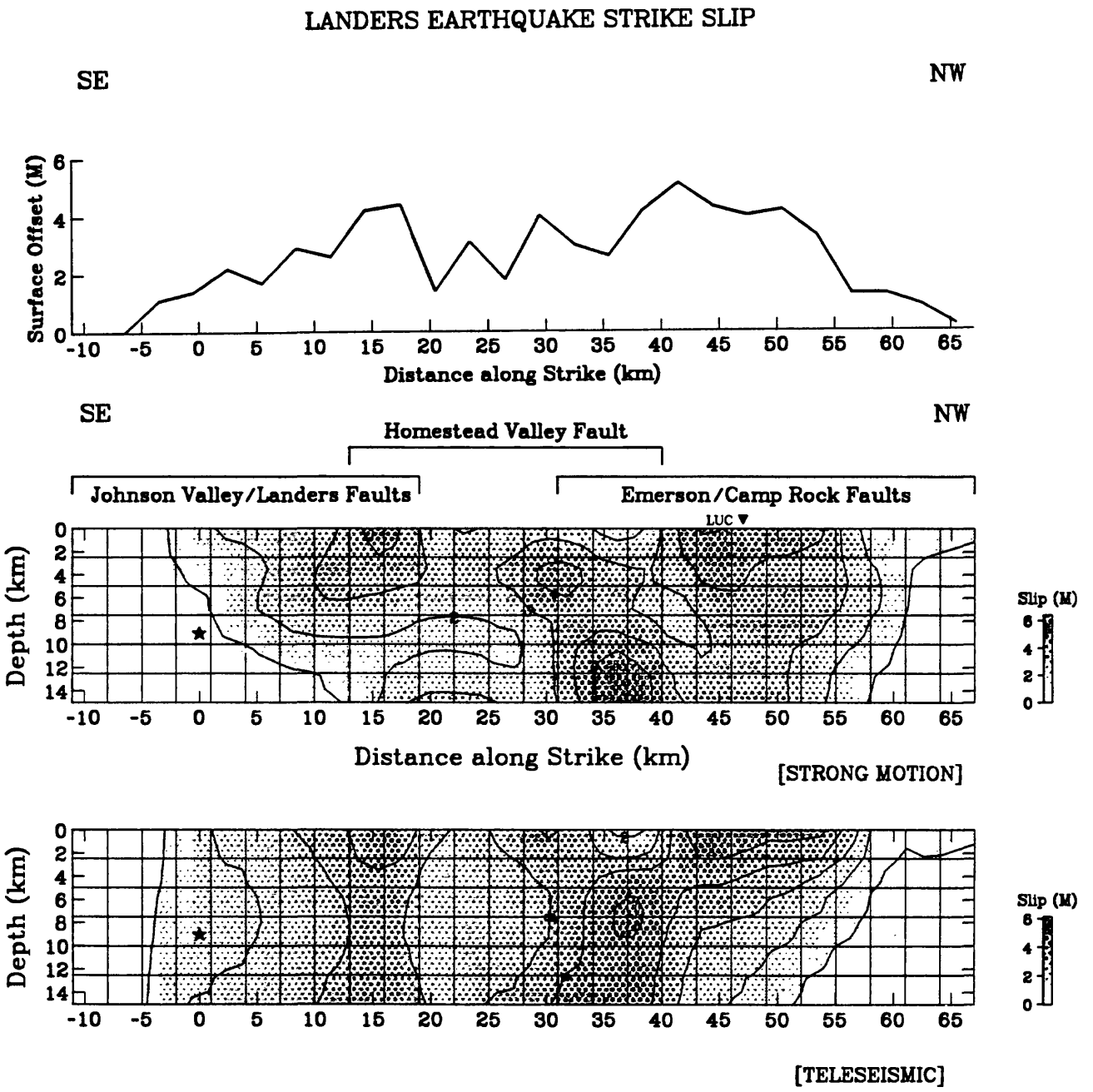

Fig. 2. Modeling results of the Landers earthquake showing strike-slip distribution. The three fault segments overlap as shown with braces and vertical dashed lines. Slip is given in meters with a contour interval of 1 meter. The observed surface slip, averaged over each 3 km horizontal subfault dimension is shown above (from K. Sieh).

Regional Microearthquake Network in the Central Mississippi Valley
14-08-0001-A0619

Cooperative New Madrid Seismic Network
14-34-92-A-0967

Robert B. Herrmann
Department of Earth and Atmospheric Sciences
Saint Louis University
3507 Laclede Ave.
St. Louis, MO 63103
314/658-3131, FAX 314/658-3117

Investigations

The purpose of the network is to monitor seismic activity in the Central Mississippi Valley Seismic zone, in which the large 1811-1812 New Madrid earthquakes occurred. The following section gives a summary of network observations during the last six months of 1991 and the first six months of 1992, as reported in Network Quarterly Bulletin Nos. 69 through 72.

Results

Event Location

From July 1, 1991 through June 30, 1992, 85 earthquakes, typically with magnitudes greater than 1.2, were located by the 40 station regional telemetered microearthquake network operated by Saint Louis University for the U.S. Geological Survey and the Nuclear Regulatory Commission. Figure 1 shows 77 earthquakes located within a 4° x 5° region centered on 36.5°N and 89.5°W. The magnitudes are indicated by the size of the open symbols. Figure 2 shows the locations and magnitudes of 68 earthquakes located within a 1.5° x 1.5° region centered at 36.25°N and 89.75°W.

During this time, 116 teleseisms were recorded by the PDP 11/34 microcomputer. Epicentral coordinates were determined by assuming a plane wave front propagating across the network and using travel-time curves to determine back azimuth and slowness, and by assuming a focal depth of 15 kilometers using spherical geometry. Arrival time information for teleseismic P and PKP phases has been published in the quarterly earthquake bulletin.

The significant earthquakes occurring from July 1, 1991 through June 30, 1992 include the following:

July 2, 1991 (0349 UTC). South-central Missouri. mbLg 3.3 <C.M.V.S.N.>.

July 7, 1991 (2124 UTC). Missouri-Arkansas Border Region. mbLg 4.0 (NEIS). 3.8 (TUL). Felt in Howell and Oregon Counties, Missouri. Also felt in northern Arkansas.

July 8, 1991 (2349 UTC). New Madrid, Missouri region. mbLg 2.9 <C.M.V.S.N.>.

October 3, 1991 (1146 UTC). New Madrid, Missouri region. mbLg 3.1 (GS). Felt (III) at Bladgett, Charleston and East Prairie. Felt (II) at New Madrid.

November 11, 1991 (0920 UTC). Southern Indiana. mbLg 3.8 (GS), 3.6 (TUL). Felt (III) at Bellmont, Birds, Claremont, Mt. Carmel, Newton, Noble, Parkersburg, Robinson, Sainte Marie, Sumner and West Liberty, Illinois. Also felt in the Lawrenceville, Illinois area.

November 13, 1991 (0943 UTC). Arkansas. <SLM-P>. MD 3.0 (SLM).

December 13, 1991 (1141 UTC). Arkansas. MD 2.8 (GS). Felt (IV) at Blytheville and (III) at Dell and Manila.

January 9, 1992 (0730 UTC). Felt in Tollesboro and Ribolt, Kentucky. MD 2.8 <K.D.S.N.>.

January 21, 1992 (1136 UTC). Central Missouri. Felt (IV) at Linn Creek. Felt (III) at Camdenton and Sunrise Beach. Also felt in the Osage Beach area. mbLg 3.2 <C.M.V.S.N.>.

March 3, 1992 (1230 UTC). New Madrid, Missouri region. Felt at Steele, Missouri. mbLg 2.6 <C.M.V.S.N.>.

March 27, 1992 (2157 UTC). Felt in Owingsville and Salt Lick, Kentucky. MD 2.4 <K.D.S.N.>.

April 3, 1992 (0306 UTC). Tennessee. <T.E.I.C.>. mbLg 3.5 (GS), 3.2 (TUL). Felt (IV) at Gates and Ripley. Felt (II) at Burlison. Felt in Dyer and Lauderdale Counties.

April 30, 1992 (0001 UTC). New Madrid, Missouri Region. mbLg 2.9 (TUL). Felt at Greenville, Piedmont, Poplar Bluff and Sikeston.

May 11, 1992 (0642 UTC). New Madrid, Missouri Region. mbLg 2.6. <C.M.V.S.N.>.

Data Acrhiving

As the seismic data acquisition has evolved from the PDP 11/34 to a PC based data acquisition and with the current upgrade to complete digital data acquisition, efforts have been made to ensure that all data digitally acquired since 1981 will be available for future reference and research.

This task involves many steps. First, all original time histories are reviewed, useless data are removed and all useful data are saved. The data are saved using the current formats, but a modern Center for Seismic Studies set of pointers into the binary data files is generated for the next generation of analysis software. The verified data set is then stored on optical disk with an exabyte backup. A master event list with pointers into the optical disk directories is also generated for rapid, automatic access of data.

During this report period, all teleseismic triggers have been stored on optical disk. This required reviewing about 1500 events and verifying their location parameters from the PDE. At the same time, system transfer functions have been documented to permit quantitative use of these data. This data set has already been used by a number of USGS investigators.

Future Plans

The archiving of digital recordings of all local and regional seismic events to optical disk will take place during the next year.

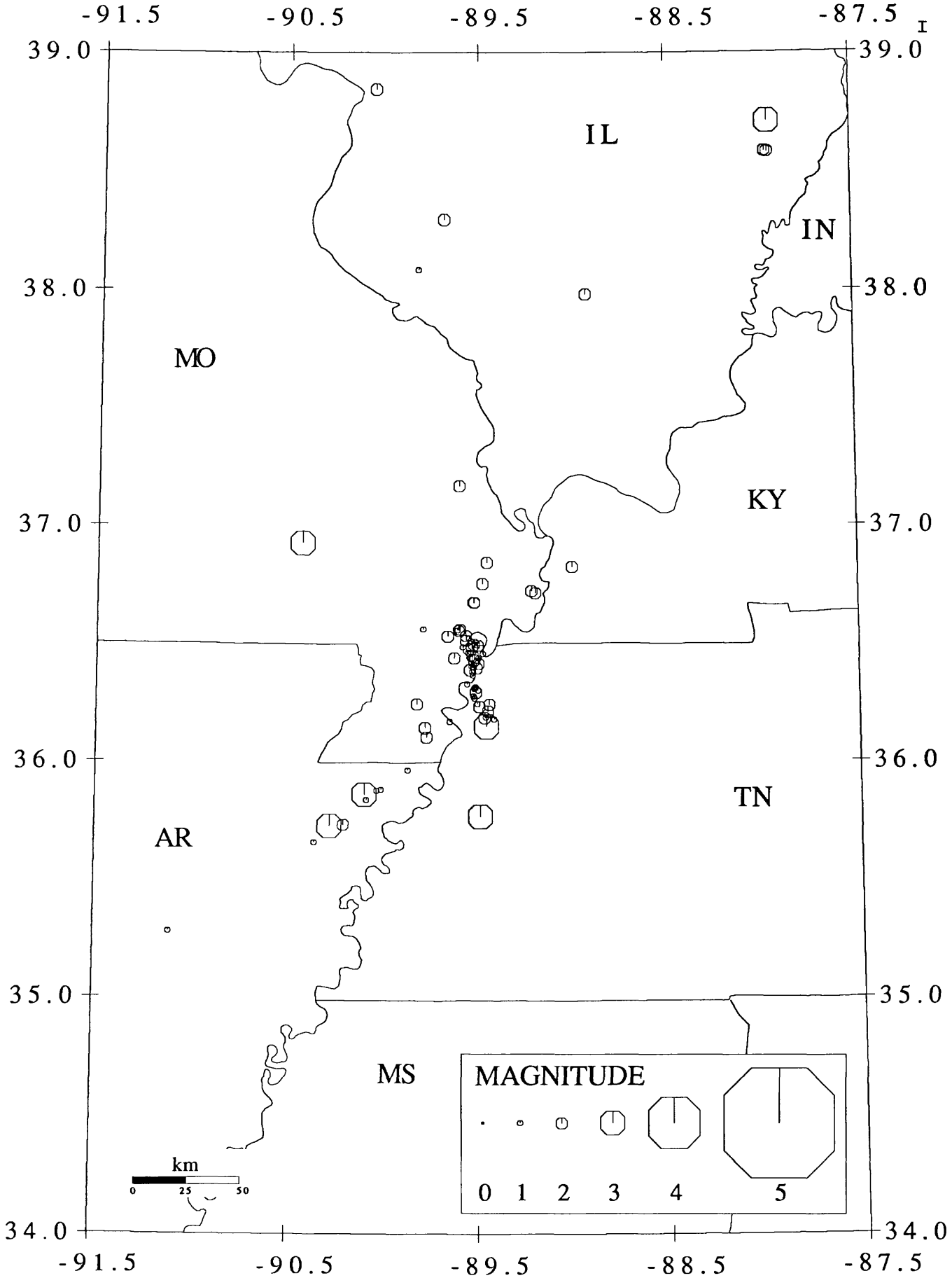

FIGURE 1

CUMULATIVE EVENTS 01 JUL 1991 TO 30 JUN 1992

LEGEND : △ STATION ⊙ EPICENTER

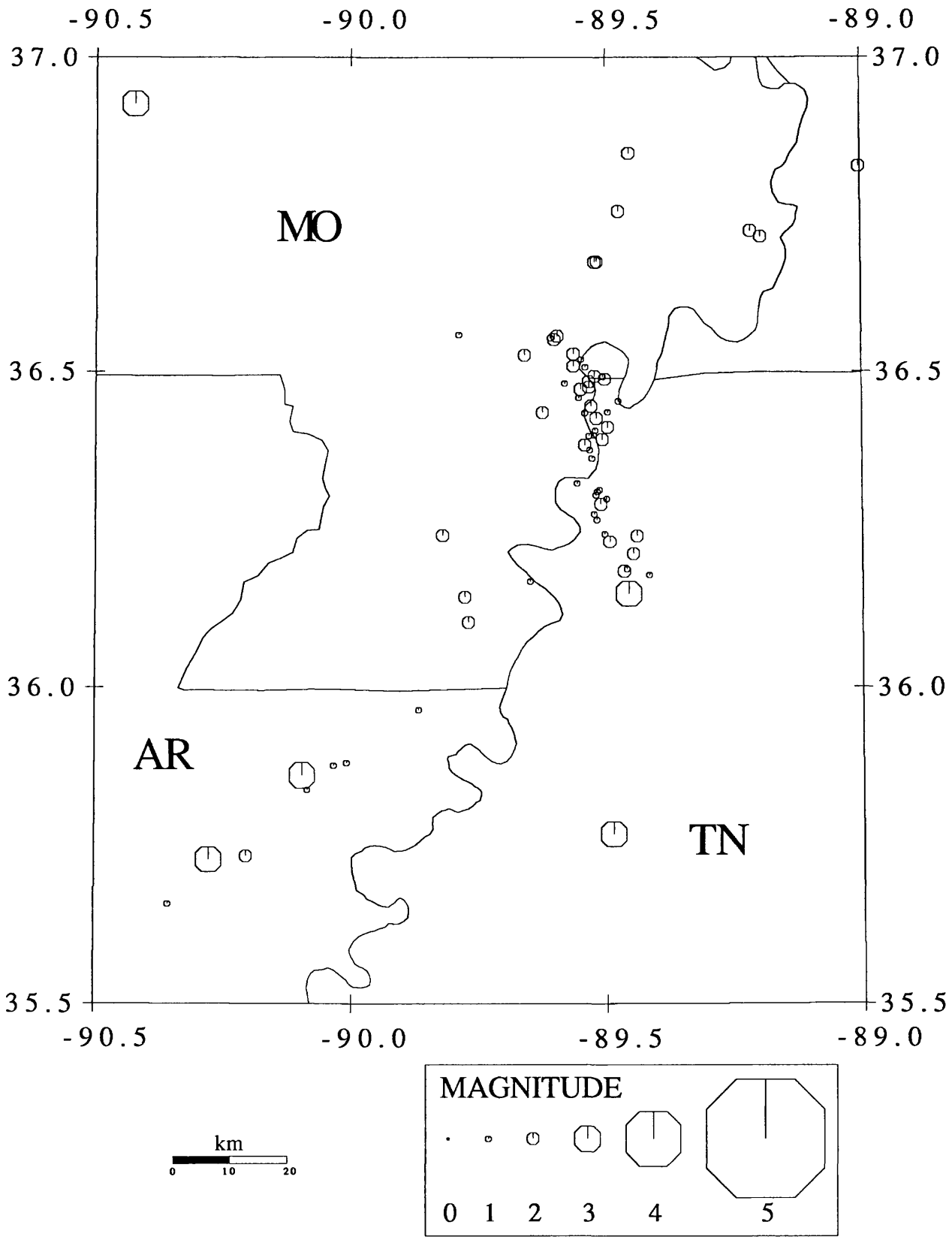

FIGURE 2

CUMULATIVE EVENTS 01 JUL 1991 TO 30 JUN 1992

LEGEND : △ STATION ⏲ EPICENTER

Cooperative New Madrid Seismic Network

14-08-0001-G1922
R. B. Herrmann
Department of Earth
and Atmospheric Sciences
Saint Louis University
3507 Laclede Avenue
St. Louis, MO 63103
(314) 658-3131

14-08-0001-G1923
A. C. Johnston, J. M. Chiu
Center for Earthquake
Research and Information
Memphis State University

Memphis, TN 38152
(901) 678-2007

Investigations

The object of this effort is to upgrade the regional seismic networks in the central Mississippi Valley to provide the data sets necessary for future research in the earthquake process and in earthquake generated ground motion.

In order to accomplish this, the satellite telemetry capability of the US National Seismic Network will be used to communicate between central data collection points at Memphis and St. Louis and the intelligent regional seismic network nodes to be placed at five sites in the region.

Major tasks involve the design and implementation of the data centers, the regional nodes at satellite uplink points, and the seismic sensors in the field. Data will be transmitted from the sensors to a node using all digital telemetry, 20 and 24 bit, to the extent possible with the present funding. The final network will consist of 5 nodes, each collecting data from a broadband sensor, an accelerometer and three-component seismometers.

Results

The previously reported PC based real time data acquisition for the current analog telemetry has proven very stable in over one year of service.

Current efforts are directed toward sending the seismic signals from a field unit using the USNSN packeting protocol.

Software development of the seismic data analysis system is underway. Given the expected data flow, data analysis will be performed without the use of a data base, using the computer file system as a simple flat file data base. All data acquired will be stored as created, and a Center for Seismic Studies "wfdisc" pointers into the data file will be used. The value of this is that data from a wide variety of sources can be analyzed by the same software, and also that all previously acquired network data can be so analyzed.

Discussions with local microwave networks and cable TV companies are underway for use of towers, network capacity, and grounds for satellite dishes.

Pressure Solution, Crack Healing and Crustal Stress

9960-04543

Stephen H. Hickman
U.S. Geological Survey
345 Middlefield Rd., MS 977
Menlo Park, CA 94025
(415) 329-4807

Investigations Undertaken

1. As part of a cooperative program between the USGS and the Russian deep scientific drilling organization, NEDRA, we are conducting an investigation of stress-induced borehole breakouts in a 4-km-deep well at Tyrnauz, Russia, in the Greater Caucasus Mountains. The Tyrnauz well is located within a granitic pluton in a region of active north-south crustal shortening associated with the collision of the Arabian and Eurasian plates. The goals of this study are to determine the nature of plate-interaction forces at a continent-continent collisional plate boundary and improve our understanding of the manner in which small- to intermediate-scale faults and topographic loads act to perturb the regional stress field. This work is being conducted in collaboration with Daniel Moos and Colleen Barton of Stanford University.

In a related investigation, we are collaborating with Carolyn Morrow and David Lockner of the USGS in Menlo Park in making measurements of permeability and resistivity on cores recovered from the 12-km-deep Kola well in Russia. Results from these measurements are discussed in the NEHRP Technical Summary by D. Lockner.

2. For many years, scientists affiliated with the USGS have performed a variety of experiments which involved making hydraulic fracturing stress measurements from drilling rigs deployed in tectonically active areas to constrain the mechanics of faulting and crustal deformation. To formulate a more viable and cost-effective in-situ stress program, beginning in Fiscal Year (FY) 1991 we have been building a wireline packer system that can be used without a drilling rig at depths of up to 1.5 km. The advantages of this wireline system over standard drill-pipe-deployed packer systems are threefold: (1) Because no drill rig is required during testing, the cost of making in-situ stress measurements is greatly reduced. (2) This wireline packer system is fully self-contained and therefore capable of making about twice as many measurements in a given amount of time as previously possible. (3) This wireline packer system measures both flow rate and fluid pressure downhole, improving the accuracy with which crucial test parameters such as shut-in and fracture-opening pressures (and, hence, in-situ stresses) can be determined.

3. We are conducting an experimental study of pressure solution and crack healing under load in simple quartz/water systems. These experiments employ single crystals in well-controlled model geometries inside a hydrothermal vessel equipped with an optical observation port. This port, in conjunction with a long-working distance microscope, allows the morphology and geometry of intergranular contacts and cracks to be continuously monitored. The goal of these experiments is to constrain the mechanisms and kinetics of solution-transport creep, asperity adhesion and crack healing and thereby provide fundamental constraints on processes controlling the spatial and temporal evolution of fault strength, permeability and other physical properties in the Earth.

Results Obtained

1. In the summer of 1991, we conducted a borehole televiewer log in the Tyrnauz well from a depth of 300 m to 3200 m. In FY 1992, we digitized this log to produce a continuous log of borehole radius and then analyzed this data to determine the orientations and widths of stress-induced borehole breakouts and natural fractures in this well.

Overall, the orientations of breakouts in the Tyrnauz well are extremely uniform, indicating that the direction of maximum horizontal compressive stress, S_{Hmax}, is N 13° E ± 10°, with an approximately 20° counterclockwise rotation in S_{Hmax} directions going down the well. This S_{Hmax} direction compares favorably with the NNW-NE range of P axis orientations determined from larger earthquakes in this region. Comparison to finite-element models of deformation in this region [*Oral et al.*, 1992] and relative plate motions [*Minster and Jordan*, 1978] shows that the orientation of S_{Hmax} at Tyrnauz is consistent with that expected if the source of the stress in the Greater Caucasus is the collisional force applied to the Eurasian plate by the northward-moving Arabian plate.

Applying the theory of *Moos and Zoback* [1990], in conjunction with laboratory measurements of uniaxial compressive strength on core obtained from this well, the observation that breakouts at Tyrnauz are nearly continuous below a depth of 400 m suggests that the horizontal stress magnitudes are very high and that the stress regime at this site is transitional from strike-slip to reverse faulting. This inference is in agreement with the occurrence of large- and intermediate-magnitude strike-slip and reverse-faulting earthquakes in the Greater Caucasus region.

At numerous depths in this well breakouts were observed to decrease in width or rotate near natural fractures or faults, suggesting localized perturbations to the regional stress field. In particular, theoretical modelling of a dramatic rotation in breakout azimuth observed above a fracture zone at about 3032 to 3045 m depth shows that this rotation can be accounted for by slip on faults observed to cut the well at this depth.

Most of the natural fractures observed in the televiewer log strike parallel to the S_{Hmax} direction at Tyrnauz and dip steeply (dips > 60°) to the west. These observations, together with the young age (2.5 Ma) of the granite in which this well is located, suggests that these fractures are tensile in origin and formed in response to the current tectonic stress field.

2. We completed construction of our wireline packer system in FY 92 and tested this system as part of two separate scientific studies: one in the Santa Cruz Mountains and the other in the Wawona area of Yosemite National Park.

Santa Cruz Mountains Experiment. Within minutes after the 1989 Loma Prieta earthquake, stream flows in the Santa Cruz Mountains immediately northwest of the epicenter began increasing by about a factor of 10 and ground-water levels in this area began to drop. One of the hypotheses advanced to explain these phenomena is that near-surface rocks in the Santa Cruz Mountains are under high ambient levels of deviatoric stress and that coseismic stress changes (dynamic and/or static) were sufficient to produce new fractures or reactivate pre-existing fractures, resulting in a dramatic increase in aquifer permeability (*Rojstaczer and Wolf*, 1992). In this experiment, which is conducted in collaboration with Stuart Rojstaczer of Duke University, we are using our wireline packer system and borehole televiewer to measure stress magnitudes and orientations, permeability and natural fracture orientations in shallow wells drilled in the Santa Cruz Mountains. We will then use these measurements, in conjunction with estimates of coseismic stress perturbations and simple rock failure criteria (both in shear and in tension), to test the Rojstaczer and Wolf (1992) model and determine the physical mechanisms responsible for these hydrologic changes. As part of this experiment, in July of 1992 we attempted to use our wireline packer system in two shallow wells located in highly fractured shales and sandstones near the top of the Santa Cruz Mountains, but problems with hole collapse and integrity of the surface casing in these wells prevented us from making any stress or permeability measurements. In February of 1993 we will attempt a similar suite of

experiments in shallow wells drilled in more competent and less fractured granitic rocks along the western flank of the Santa Cruz Mountains.

Wawona Experiment In this experiment we conducted hydraulic fracturing stress measurements and borehole televiewer logs in two shallow wells drilled by the National Park Service (NPS) in Yosemite National Park near the town of Wawona. This study, which is a multidisciplinary effort involving scientists from the USGS Water Resources and Geologic Divisions, private industry and the Lawrence Livermore and Los Alamos National Laboratories, is being conducted to ascertain if the ground water resources at Wawona are adequate to support relocation of NPS employees from the Yosemite Valley to the Wawona area. Our role in this study is to investigate the nature and origins of the shallow stress field and determine the extent to which these stresses control the orientations of permeable fractures and fault zones in the fractured granitic aquifer beneath Wawona.

Our field work at Wawona was quite successful and we obtained extremely high-quality hydraulic fracturing data from all 12 tests attempted. Although the field work was just completed in September of 1992, preliminary analysis of these data indicates that the shallow stresses at this site are transitional from a reverse faulting stress regime at depths of less than about 200 m to strike-slip faulting at depths of 200 to 300 m (the maximum depths of our tests). These data also indicate that the magnitudes of S_{Hmax} relative to the vertical stress at depths of 50 to 100 m are extremely high, being about twice as great as predicted using laboratory coefficients of friction and simple frictional faulting theory for reverse faulting. As Wawona is located in a topographically rugged area which has experienced rapid erosion, we attribute these high horizontal stresses to a combination of near-surface residual stresses and topographic effects. Based on borehole televiewer logs that we conducted in these wells, we hypothesize that high differential stresses can be maintained at Wawona because of the paucity of fractures in the shallow granite which are favorably oriented for reverse faulting. Our hydraulic fracturing tests indicate that the orientation of S_{Hmax} at Wawona is about N 55° W, an orientation that departs significantly from the roughly N-S to NNE regional trend and further suggests a local source for the stresses we measured in these wells.

Once in-situ permeability data collected at Wawona by scientists from the USGS Water Resources Division are analyzed, we will use these results to determine the relationship between permeability and the orientations and relative magnitudes of the in-situ stresses. In addition, our hydraulic fracturing tests were conducted while borehole seismometer and tiltmeter arrays were deployed in shallow boreholes at this site by scientists from the Los Alamos National Lab, the USGS and InfraSeismic Systems, Inc. The microseismic event locations and shallow tilts determined from these arrays will be used to delineate the geometry of some of our hydraulic fractures as they propagated away from the borehole, providing valuable constraints on the mechanics of hydraulic fracture propagation and an independent check on our determinations of stress orientations and relative magnitudes.

4. In FY 1992 we finished assembling and testing the pressure vessel, furnace and optical equipment to be used in the single-crystal pressure solution and crack-healing experiments. We are now adjusting the three-zone furnace while conducting temperature profiles of the pressure vessel at experimental conditions. Once this procedure is completed and the temperature gradients within the pressure vessel are minimized, we will begin conducting asperity adhesion and crack healing experiments in quartz.

References Cited

Minster, J. B., and T. H. Jordan, Present-day plate motions, *J. Geophys. Res., 83*, 5331-5354, 1978.

Moos, D., and M. Zoback, Utilization of observations of well bore failure to constrain the orientation and magnitude of crustal stresses: Application to continental, Deep Sea Drilling Project, and Ocean Drilling Program boreholes, *J. Geophys. Res., 95*, 9305-9325, 1990.

Oral, B. M., Reilinger, R. E., and Toksoz, M. N., Preliminary estimates of 1988 and 1990 GPS measurements in western Turkey and their tectonic implications, The Crustal Dynamics Project, Special Publications, AGU Monograph, 1992 (submitted).

Rojstaczer, S., and Wolf, S., Permeability changes associated with large earthquakes: An example from Loma Prieta, California, *Geology, 20*, 211-214, 1992.

Abstracts and Papers Published in FY 1992

Evans, B., and Hickman, S., Some experimental results on the effect of solution transfer processes on crack healing, cementation, and diagenesis, in *Proceedings 29th International Geol. Congress*, Kyoto, Japan, p. 456, 1992.

Hickman, S., and B. Evans, Growth of grain contacts in halite by solution transfer: Implications for diagenesis, lithification, and strength recovery, in *Fault Mechanics and Transport Properties of Rocks*, B. Evans and T.-F. Wong (eds.), Academic Press, pp. 253-280, 1991.

Hickman, S., D. Moos, C. Barton, and B. Khakaev, In-situ stress and borehole breakouts in the Tyrnauz Well, Caucasus Mountains, USSR, *EOS, American Geophysical Union Transactions, 72*, p. 511, 1991.

Hickman, S., D. Moos, C. Barton, G. Katz, G. Budkov, and E. Kim, 1992, Borehole breakouts and in-situ stress in the Tyrnauz well, Caucasus Mountains, Russia, *Proceedings Sixth International Symposium on Observation of the Continental Crust Through Drilling, BRGM, Paris*, p. 135, 1992.

Morrow, C., Hickman, S., Lockner, D., and Khakaev, B., Permeability of granodiorite cores from the Kola Superdeep Well, USSR, *EOS, American Geophysical Union Transactions, 72*, p. 475, 1991.

Morrow, C., Hickman, S., Lockner, D., and Khakhaev, B., Permeability of core samples from the Kola well, Russia, *Proceedings Sixth International Symposium on Observation of the Continental Crust Through Drilling*, BRGM, Paris, p. 189, 1992.

Zoback, M. D., and Hickman, S. H., Scientific rationale for drilling into the San Andreas fault zone, in *Proceedings 29th International Geol. Congress*, Kyoto, Japan, p. 31, 1992.

LATE QUATERNARY MOVEMENT ALONG THE HAT CREEK FAULT, NORTHEASTERN CALIFORNIA

9980-70338

Marie D. Jackson
Branch of Igneous and Geothermal Processes
U. S. Geological Survey
2255 North Gemini Drive
Flagstaff, Arizona, 86001
(602) 556-7186

Investigations

The Hat Creek fault, located about 30 km north of Lassen Peak, is composed of prominent NNW-trending escarpments that offset Quaternary and Pliocene volcanic rocks by more than 300 m. This fault, and the nearby McArthur, Pittville, and Mayfield faults (Wills, 1991) form an active system of normal faults, down-dropped to the west, that is the westernmost, and perhaps youngest, expression of Basin and Range normal faulting in northeastern California (Fig. 1). The Hat Creek escarpments, or rims, which are modified by erosion to a repose angle of about 35°, form the eastern side of an asymetric graben, along which the Hat Creek Basalt flowed during the Late Pleistocene or Early Holocene (Fig. 1) (Muffler *et al.*, submitted). The most recent slip along the fault forms a 20-km-long, left-stepping scarp as much as 30 m high cutting the Hat Creek Basalt (Fig. 2). Stream gravels, estimated to be no more than 15,000 years old (Muffler *et al.*, submitted), overlie the Hat Creek Basalt and were offset as much as 20 m by this youngest faulting. Monoclinal flexures with S-shaped axial planes link some of the left-stepping fault segments. The average Holocene vertical displacement along the fault has been about 2 mm per year, and the existence of this prominent young scarp in an area of low modern seismicity suggests that movement has been episodic with a periodicity of hundreds, or perhaps thousands of years (Muffler *et al.*, 1989).

This study uses field data and mechanical analysis to examine the structure of the Hat Creek fault and to evaluate its earthquake potential. In particular, this study investigates how a normal fault propagates and develops a surface rupture, and how its en echelon segments link to transfer predominantly dip-slip displacements. Field work undertaken includes 1:5000 mapping of the entire young Hat Creek scarp, detailed 1:1000 scale mapping of S-shaped monoclines at three large left-steps, and systematic measurement of structures resulting from fault-related flexure and fracture of the host basalt. Analytical work undertaken includes 1) mechanical analysis of the surface deformation over a growing normal fault and 2) analysis of interactions at left-steps using methods of fracture mechanics and plate bending theory.

Results

Geologic maps are the principal means of describing the structure of the young Hat Creek fault, and much progress has been made towards completion of these maps during the past year. Geologic field work is progressing well, following a productive three weeks of field work in May, 1992.

A preliminary map of the 20-km-long fault, compiled at 1:15,000 scale in winter and spring of FY'92 using a PG-2 stereoplotter, shows the overall structure of the young scarp. The young fault is composed of six left-

stepping segments (Fig. 2), 1.5- to 6.5-km-long, which offset the Hat Creek basalt. Some of these follow the older rim, and others extend past the older escarpments into the valley floor. Each of the long segments is composed of two or more 0.5- to 1-km-long, left-stepping segments which are, in turn, are made up of shorter, left-stepping segments, usually less than 100m in length. In this respect, the young scarp shows great similiarity to the recent Kaoiki earthquake ground ruptures on Mauna Loa Volcano in Hawaii (Jackson *et al.*, 1992).

S-shaped monoclines of warped and broken Hat Creek Basalt link all scales of the left-stepping segments. This year, the Flagstaff Photogrammetry group prepared detailed 1:1000 scale topographic maps of the three most prominent of these monoclines using an innovative method that does not require the use of surveyed control points. Geologic mapping of these monoclines in May 1992 shows that they are complex structures of flexed and faulted Hat Creek Basalt that have transferred both dip-slip and right-lateral displacements between adjacent left-stepping fault segments. The Photogrammetry Group has nearly completed a perspective digital image of one of the large monoclines, using digitized data from the topographic map and aerial photographs to show the three-dimensional structure of this area.

Along the fault segments, various left-stepping structures correlate with increased displacement. These include: 1) short, *en echelon* cracks that have small horizontal displacements, up to 0.5m, with components of both opening and right-lateral shear; 2) wider, longer, rubble-filled crack arrays with horizontal displacements of 0.5m to 2m; 3) low, 2- to 4-m-high scarps that are often expressed as gently faulted monoclines; 4) taller, scarp-parallel monoclines with steep limbs and larger wavelengths; and 5) high, long, near-vertical rubble-covered scarps.

Systematic measurements of the amplitude, wavelength and overall shape of the scarp-parallel monoclines, and detailed cross-sections across five of these, give important information about how these flexures developed and accomodated subsequent episodes of rupture. Large wavelength (>30m), high-amplitude (>10m) scarp-parallel monoclines may have formed during single large-magnitude seismic events. Subsequent faulting increased the vertical uplift of many monoclines. With continued seismic activity, however, some of the monoclines were strongly disrupted and collapsed into tall scarps covered with a rubble formed of broken columnar blocks of the host basalt.

To document the role of cracking and right-lateral shear in the propagation and transfer of slip along the ruptures, systematic field measurements of crack orientations, lengths and displacements were made in a manner similiar to that developed for the Kaoiki study (Jackson *et al.*, 1992). A 1:1000-scale map of a fascinating kilometer-long stretch of the Hat Creek fault gives a detailed picture of how the crack arrays coalesce to form short, left-stepping scarps and monoclines that are themselves linked by small S-shaped structures. These data form the basis of an interpretative map giving the lengths, vertical displacements and cross-cutting relationships of ruptures forming the young fault, and showing how motions along the scarp are related in time.

References cited

Jackson, M. D., E. T. Endo, P. T. Delaney, T. Arnadottir, and A. M. Rubin, 1992, Ground ruptures of the 1974 and 1983 Kaoiki earthquakes, Mauna Loa Volcano, Hawaii: Journal of Geophysical Research, v. 97, n. B6, p. 8775-8796.

Muffler, L. J. P., M. A. Clynne, and Holcomb, R. T., 1989, Late Quaternary faulting of the Hat Creek Basalt (Abs.): EOS (Transactions of the American Geophysical Union), v. 70, p. 1310.

Muffler, L. J. P., M. A. Clynne, and D. E. Champion, submitted, Late Quaternary faulting of the Hat Creek Basalt: Geol. Soc. Am. Bull..

Wills, C. J., 1991, Active faults north of Lassen Volcanic National Park, northern California: California Geology, p. 51-58.

Reports

Jackson, M. D., E. T. Endo, P. T. Delaney, T. Arnadottir, and A. M. Rubin, 1992, Ground ruptures of the 1974 and 1983 Kaoiki earthquakes, Mauna Loa Volcano, Hawaii: Journal of Geophysical Research, v. 97, n. B6, p. 8775-8796.

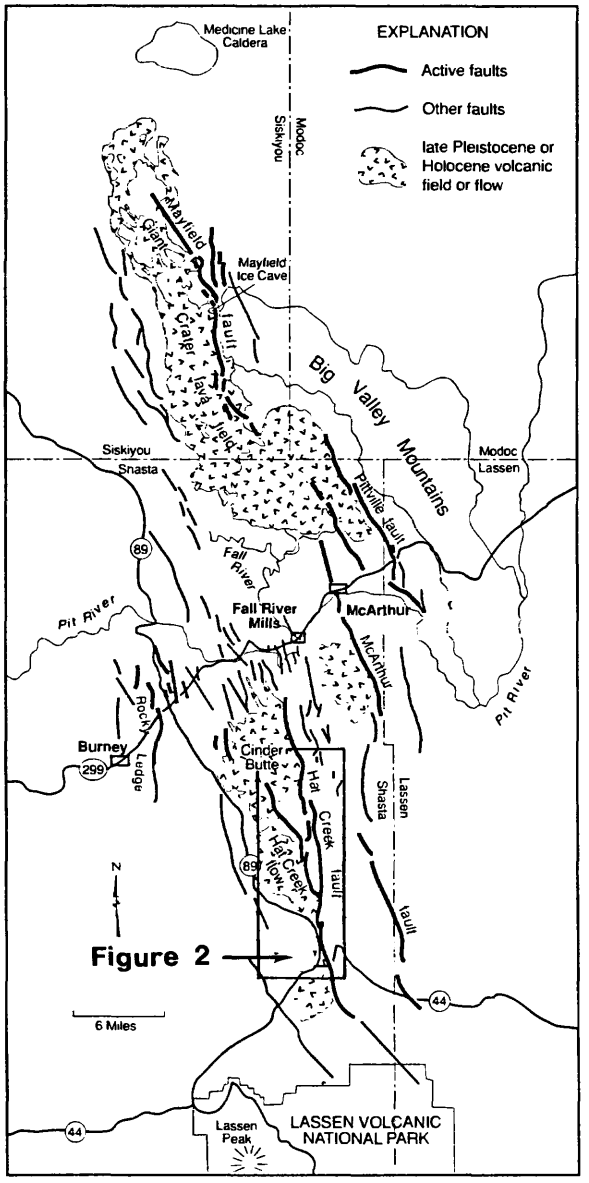

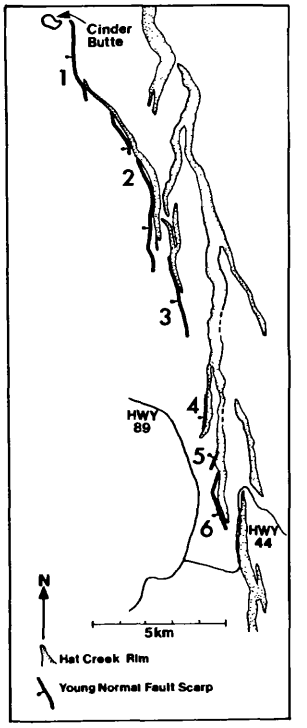

Figure 2. Sketch map of the Hat Creek Fault, showing the older escarpments and Late Quaternary ground rupture.

Figure 1. Simplified geologic map showing faults and young volcanic fields and flows between Lassen Peak and Medicine Lake volcano (after Wills, 1991).

State of Stress in the Rupture Zone of Large Earthquakes

Agreement No. 14-08-0001-G1773

Hiroo Kanamori
Seismological Laboratory
California Institute of Technology
Pasadena, California 91125

(818) 356-6914

Investigation

Investigation of the 1992 Landers, California, earthquake.

The 1992 Landers earthquake (M_S=7.5, M_W=7.3) was recorded at six TERRAscope stations in southern California. Peak accelerations ranged from 0.16 g at SVD (Δ=63 km) to 0.0092 g at ISA (245 km), decreasing with distance away from the fault zone. The peak velocity showed a different pattern reflecting the rupture directivity from south to north. The largest peak velocity, 19 cm/sec, was observed at GSC (Δ=125 km). Moment tensor inversion of long-period surface waves yielded a mechanism with M_0=1.1x10^{27} dyne-cm (M_W=7.3), dip=74°, rake=-176°, and strike=340°. Inversion of teleseismic *P* and *S* waves revealed two distinct sub-events of 6 and 8 sec duration and about 10 sec apart. The source parameters for the first and second events are: M_0=1.9x10^{26} dyne-cm, dip=83°, rake=179°, strike=359°; and M_0=6.1x10^{26} dyne-cm, dip=87°, rake=178°, strike=333°, respectively. The radiated wave energy, E_S, was estimated as 4.3x10^{23} ergs. The ratio E_S/M_0=3.9x10^{-4} corresponds to a stress drop of 280 bars, and suggests that the Landers earthquake belongs to the group of high stress drop earthquakes, and occurred on a fault with a long recurrence time. The rupture directivity can be seen clearly in the records from PFO (Δ=68 km) located to the south and GSC located to the north of the epicenter. The maximum displacement at PFO is only 13% of that at GSC despite the shorter epicentral distance to PFO than to GSC. The slip distribution determined with the empirical Green's function method indicates that the Landers earthquake consists of two distinct sub-events about 30 km apart, with the second sub-event to the north being about twice as large as the first one. This slip distribution is consistent with the teleseismic data and the surface offsets mapped in the field.

Publications

Hwang, L. J. and H. Kanamori, 1991, Rupture Processes of the 1987-88 Gulf of Alsaka Earthquake Sequence, J.G.R., in press.

Kanamori, H. and M. Kikuchi, The 1992 Nicaragua Earthquake -- Tsunami Earthquake?, Nature, submitted 1992.

Kanamori, H., Thio, H.-K., Dreger, D., Hauksson, E., Heaton, T., 1992, Initial Investigation of the Landers, California, Earthquake of 28 June 1992 Using TERRAscope, Geophys. Res. Lett., in press.

Kikuchi, M., H. Kanamori and K. Satake, Source complexity of the 1988 Armenian earthquake -- Evidence for a Slow After-Slip Event, Jour. Geophys. Res., submitted 1992.

Seismicity Patterns and the Stress State in Subduction-Type Seismogenic Zones

Grant Number 14-08-0001-G1810

Carl Kisslinger and Susanna Gross
Cooperative Institute for Research in Environmental Sciences
Campus Box 216, University of Colorado
Boulder, Colorado 80309-0216
(303) 492-6089

Research during the current grant year was directed to the following problems: (1) comparison of the seismicity rates and spatial patterns in the region monitored by the Central Aleutians Seismic Network (CASN) during 1988-1990 with those preceding the quiescence used a basis for the prediction of the May 7, 1986 great earthquake; (2) modeling the temporal behavior of aftershock sequences; (3) the effects of stress redistribution by moderate earthquakes on the spatial distribution of surrounding seismicity.

Comparison of Seismicity Rates in the Adak Region during 1988-1990 with those before and during the 1982-1986 Quiescence

A prediction of a major earthquake to occur near Adak Island, Alaska within six months of the end of October, 1985 was formulated and announced in 1985 (Kisslinger, et al. 1985, Kisslinger, 1986). The prediction was based on the observation, first noted in September, 1982, of strong and persistent quiescence in part of the seismic zone monitored by the CASN. On May 7, 1986, at the end of the time window specified in the prediction, a magnitude $M_S = 7.7, M_W = 8.0$ event did occur. Although the event that occurred differed in the details from the predicted parameters (magnitude was about 0.5 higher, rupture was in a section of the main thrust zone adjacent to that predicted), the preceding seismic quiescence observed with the local network was arguably related to this earthquake.

Questions have been raised about the validity of the prediction experiment, in particular whether the observed change in seismicity rate in parts of the seismic zone was natural or artificial. The principal concern has been that changes in instrumentation in mid-1982, designed to improve the detection capability of the network, may have inadvertently degraded the detection

threshold or introduced a shift in the magnitudes of events as determined in routine processing. The fact that the quiescence existed in all magnitude bands, the non-uniform distribution of the quiescence across the zone and the differences in the times of onset in different parts of the zone had been taken as evidence that the changes in rate were real. In an independent study, Wyss analyzed the reporting history of the CASN and concluded that the reported quiescence was most likely a natural phenomenon, but that this can not be proven beyond doubt.

It is impossible in principle to determine beyond doubt whether simultaneous changes occurred in both the real seismicity rate and in detection capability or analysis procedures, to produce an observed change in seismicity rate. However, under the hypothesis that a precursory quiescence ends with the occurrence of the strong earthquake. one test is a comparison of the seismicity rate several years after the mainshock with that prior to and during the interval of quiescence, with no changes in the instrumentation or data-processing procedures. The hypothesis is that a characteristic of the seismogenic cycle is that the seismicity rate should return to the pre-quiescence level after the aftershocks have ceased. It would be best to perform this test many years later, when there is confidence that the aftershocks have decayed to negligible numbers. However, the CASN has been terminated for financial reasons and the local data are available only through June, 1990. We, therefore, have compared the most recent documented seismicity with that prior to mid-1982, when the quiescence began, as well as during the interval of quiescence.

The data used cover the intervals 1977 through 1985 and September, 1988 through May, 1990. The year 1982 was eliminated because the strong quiescence began during that year at at time that is not easily fixed. The data were spatially grouped by the same geographic subregions used in the original analysis, Figure 1, and smoothed by counting events by quarters, from which mean monthly activity rates were calculated. Most of the work was done with a minimum duration magnitude of 2.3, the level determined earlier for catalog completeness. Tests were made in a number of magnitude bands, from 1.6 and above (known to yield an incomplete catalog) to 3.0 and above (complete catalog, but too few events for robust statistical confidence.)

The data since May 7, 1986 have been modeled to estimate the rate of aftershocks to be expected during the 1988-1990 interval. A newly developed program, in which the modified Omori relation is supplemented by adding

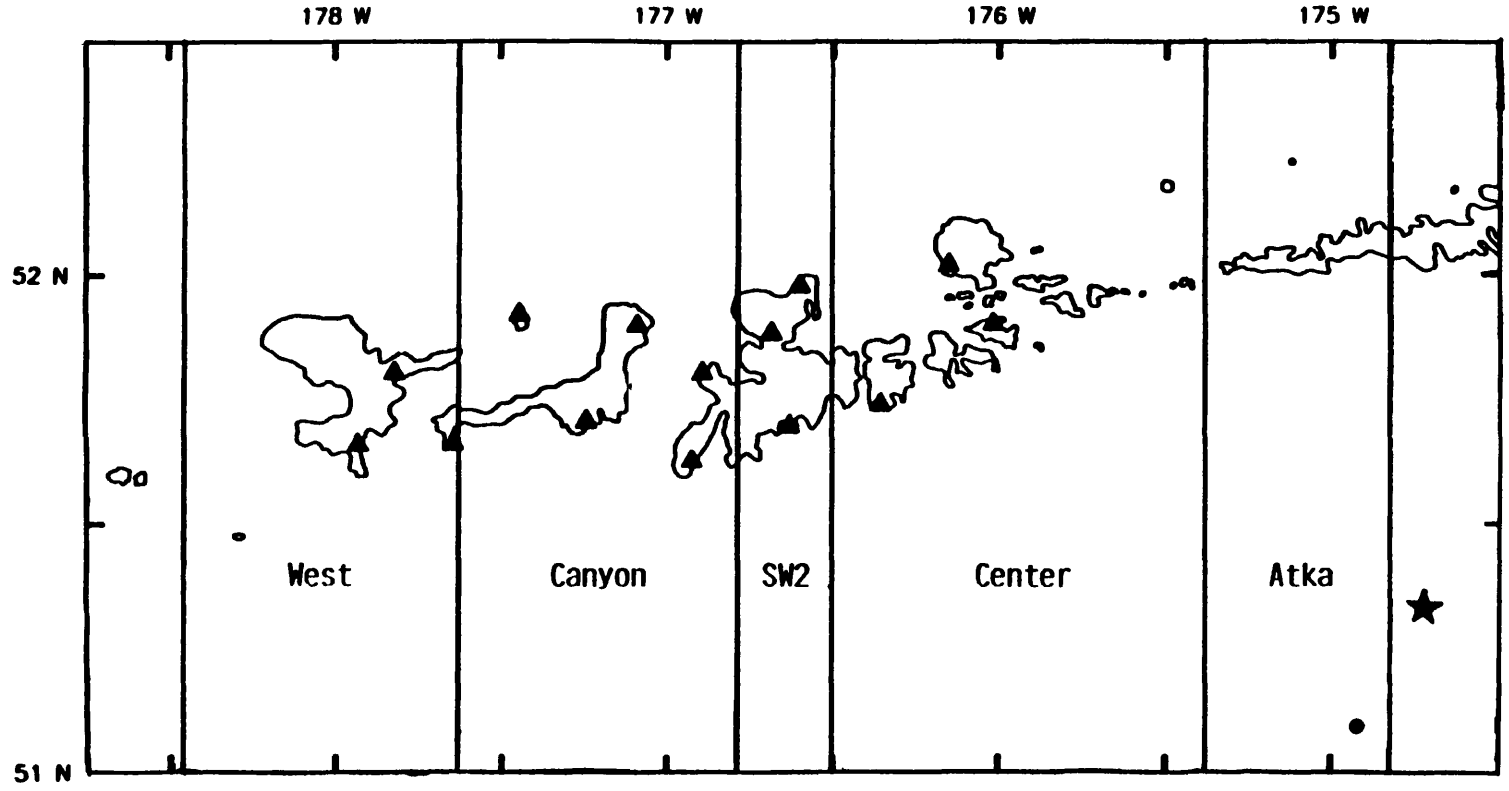

Figure 1. Map of the region monitored by the CASN. The network stations are marked by triangles. The star marks the epicenter of the May 7, 1986 $M_W = 8$ mainshock; the circle the epicenter of the March 12, 1990 $M_S = 6.2$ earthquake. The five subregions defined for the seismicity analysis are shown. The 1986 rupture terminated in SW2.

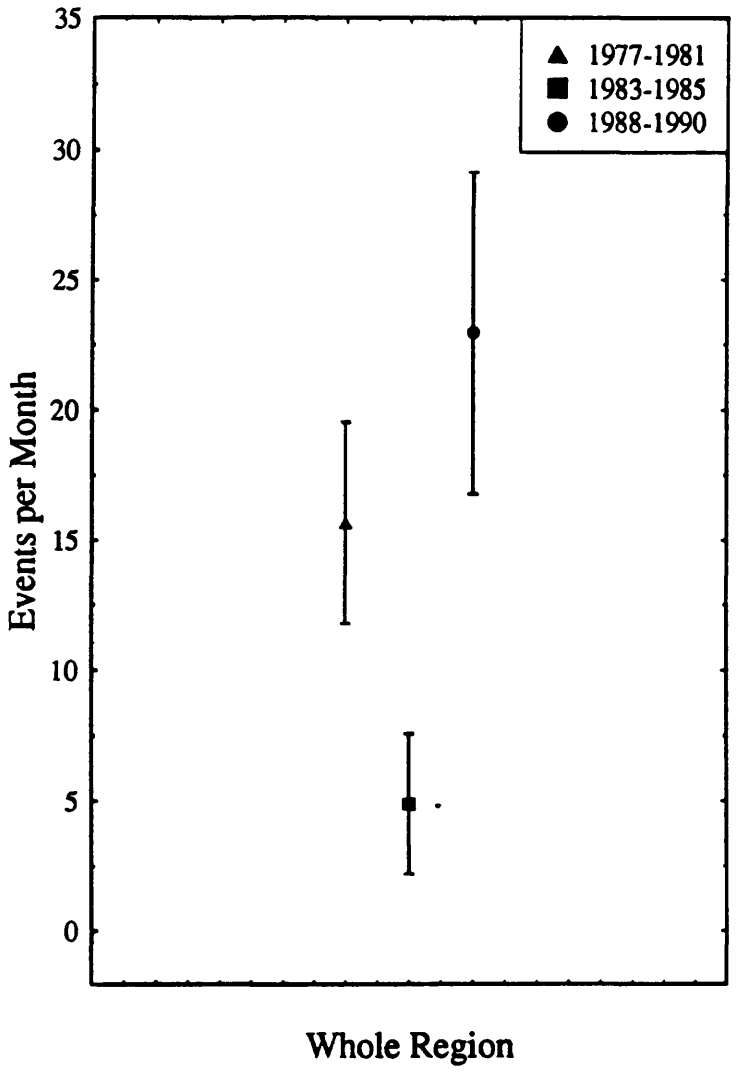

Figure 2: The mean monthly rates of activity for the entire region during the pre-quiescent interval, during the quiescence, and in the most recent interval for which CASN data are complete. The increased activity during 1988-90 (21 months) over 1977-81 agrees approximately with the rate of aftershocks of the May 7, 1986 event expected from a fit to the modified Omori relation.

a steady background rate of activity, was applied. We estimate that during the recent interval approximately 45aftershocks of 1986, superimposed on a steady rate close to that observed prior to 1982.

The principal result of this study is shown in Figure 2. Mean monthly rates for 1977-1981, 1983-1985, and September, 1988-May, 1990 for the whole Adak region are shown, with the standard deviation of the data. A more detailed breakdown will be given in the paper on this study now completed and to be submitted for publication. The pronounced quiescence on which the prediction was based is seen in the drop of mean rate from 15.65 per month to 4.89 per month. The recovery from the quiescence is shown by the recent rate of 22.24 events per month. The excess over the pre-quiescence interval, which is significant at the 98confidence level, is very close to the estimated fraction of aftershocks that were still in progress. The analysis also shows that the late aftershocks tend to be concentrated near the 1986 mainshock epicenter and near the western edge of the 1986 rupture zone.

The conclusion from this work is, if quiescence disappears after the mainshock and the previous rate is restored, the decrease in activity seen in 1982-1985 was a true quiescence and a precursor to the 1986 earthquake.

In an auxiliary study, two episodes of concentrated activity during 1989 and 1990 were examined. These occurred in the Atka subregion (Figure 1) and are interesting because the events filled a hole in the aftershocks of the 1986 earthquake, very near its hypocenter. The conclusion suggested by this observation is that the gap in aftershocks existed because the local strength was higher than the surrounding parts of the fault zone, so rupture was delayed.

Modeling Aftershock Sequences

The research on models of aftershock rate decay is completed. The work consisted of two parts: the investigation of the stretched exponential function as an alternative to the modified Omori relation, and the extension of both models to include a steady background rate of seismicity as an additional parameter in fitting the data. A paper on the first task is in press and scheduled for publication in the *Journal of Geophysical Research* in late 1992. A paper on the second task has been submitted to **JGR** and is in the review process. The results show that the widely-used modified Omori relation is a close approximation to the stretched exponential over the range of times usually used in aftershock studies. The stretched exponential is a general

relaxation law that has been found to describe relaxation processes in a variety of physical processes. The introduction of a steady background rate gives the best fit to the aftershock data in only some cases, principally those in regions of normally high seismicity. The techniques developed in this work are being applied to additional aftershock sequences and are applicable to foreshocks.

Influence of Earthquake-produced Stresses on Seismicity Distribution

This research involves models of stresses from a few dozen moderate magnitude (m_b about 4.7) earthquakes in the Central Aleutians and comparisons of the calculated stresses with the spatial distribution of seismicity observed by the Central Aleutians Seismic Network. The project represents both an attempt to find a deterministic element in the occurrence of earthquakes and an attempt to understand more about the physics of the earthquake process by selecting models with predictive power. The similarity between stresses and seismicity has been assessed through a quantitative measure of similarity based on a Student's t statistic.

The stress field has two elements, the background stress, and the stress due to the earthquake. The background stress is assumed to be homogeneous and appropriate for a dipping plate. The parameters defining it are the azimuth, plunge, and magnitude of the greatest principal stress.

$$\sigma_{\text{back}} = \begin{pmatrix} \sigma_1 & 0 & 0 \\ 0 & \frac{\sigma_1}{4} & 0 \\ 0 & 0 & 0 \end{pmatrix}$$

There are no free parameters in the earthquake stress, because the orientation of the double-couple which represents it is taken from the focal mechanism, and the magnitude provides an estimate of the moment.

$$\sigma_{xz} = \frac{\mu M_0}{4\pi\rho r^5}[(\frac{1}{\beta^2} - \frac{1}{\alpha^2})3(x^2 + z^2 - \frac{10x^2z^2}{r^2}) + \frac{1}{\alpha^2}(3y^2 - r^2)]$$

$$\sigma_{yz} = \frac{\mu M_0 3xy}{4\pi\rho r^5}[(\frac{1}{\beta^2} - \frac{1}{\alpha^2})(1 - \frac{10z^2}{r^2}) - \frac{1}{\alpha^2}]$$

$$\sigma_{zz} = \frac{\mu M_0 6xz}{4\pi\rho r^5}[(\frac{1}{\beta^2} - \frac{1}{\alpha^2})(2 - \frac{5z^2}{r^2}) - \frac{2}{\alpha^2}]$$

$$\sigma_{xx} = \frac{\mu M_0 6xz}{4\pi\rho r^5}[(\frac{1}{\beta^2} - \frac{1}{\alpha^2})(2 - \frac{5x^2}{r^2}) - \frac{2}{\alpha^2}]$$

$$\sigma_{xy} = -\frac{\mu M_0 3yz}{4\pi\rho r^5}[(\frac{1}{\beta^2} - \frac{1}{\alpha^2})\frac{10x^2}{r^2} + \frac{1}{\alpha^2}]$$

$$\sigma_{yy} = \frac{\mu M_0 6xz}{4\pi\rho r^5}[(\frac{1}{\beta^2} - \frac{1}{\alpha^2})(1 - \frac{5z^2}{r^2}) - \frac{1}{\alpha^2}]$$

The formula above applies to stresses induced by a double couple in an infinite elastic space. The coordinate system is centered on the double couple. The full model includes effects of the free surface by including an image source above the surface having opposite dip and rake. The model was checked by numerically computing the derivatives and computing the shear stress at the free surface. These two elements are rotated into geographic coordinates and added to give the total stress tensor.

In order to compare the resulting stress field with the seismicity, the tensor must be reduced to a scalar quantity which should influence the rate of occurrence of earthquakes. Physical models of fault geometry and properties provide many alternative approaches to how stresses could trigger earthquakes, and these fault and rupture models are the current focus of research in the project. Models explored so far include

- The magnitude of the greatest shear stress, independent of orientation, $\sigma_1 - \sigma_3$, which is thought to be appropriate for faults equally present in all orientations with substantial overburden pressure. This model has been quite successful.

- The magnitude of the shear stress on a particular weak plane. This model has the disadvantage of requiring two additional parameters to define the orientation of the plane. Its implications have just started to be explored.

- The magnitude of the pressure, or trace of the stress tensor $P = \sigma_{ii}/3$, which could act on faults through increases in the effective stress, $\sigma_{eff} - P$. This would be physically due to the contrast in bulk modulus between the rock and its pore fluids. The models incorporating this approach estimate the pore pressure field as a function of time by numerically convolving the Green's function for the diffusion equation (a gaussian) with the initial pressure field. These models show early

promise in predicting changes in the seismicity distribution. The fluid diffusivity enters as an extra parameter for these models.

- The rate of change of the pore pressure, dP/dt was postulated by Nur and Booker (1972) as a generator for aftershocks. In practical terms, this model is very close to those defined above, involving a different Green's function. The cases examined so far have not shown much resemblance to seismicity, but it merits more work.

It is postulated that the different fault and rupture models may be tested by comparing their ability to match the observed changes in spatial distribution of seismicity.

The actual comparison of stress models and seismicity is made using t-statistics. The quantities compared are changes in the triggering component of the stress evaluated at the hypocenters of surrounding earthquakes. The surrounding earthquakes are expected to occur more often in areas having high values of the triggering quantity and less often in areas with low values. The statistics are designed to compare sets of numbers and determine whether they are drawn from distributions having different means or not. The statistic used in this project does not assume that the standard deviations of the two sets, s_{before} and s_{after} are not equal:

$$t = \frac{\overline{\Delta\sigma_{\text{before}}} - \overline{\Delta\sigma_{\text{after}}}}{\sqrt{s^2_{\text{before}}/N_{\text{before}} + s^2_{\text{after}}/N_{\text{after}}}}$$

in which $\overline{\Delta\sigma}$ represents the average change in triggering component of stress at hypocenters of surrounding earthquakes. The statistics are calibrated by computing them for earthquakes that did not actually occur, so the clustering effects of real seismicity are included. Tests have shown that this approach is necessary, because clustering significantly changes the distribution of t-statistics.

The model also involves a temporal dimension which is just starting to be explored. The sets of surrounding earthquakes had formerly been defined in terms of numbers of events in the whole catalog. Typically the time window used for comparisons was 1000 events long, around 18 months. This definition has the advantage of reducing the effects of data gaps and magnitude shifts on the data, but the disadvantage of being unphysical. The model has been changed to allow temporal definitions of the before and after seismicity

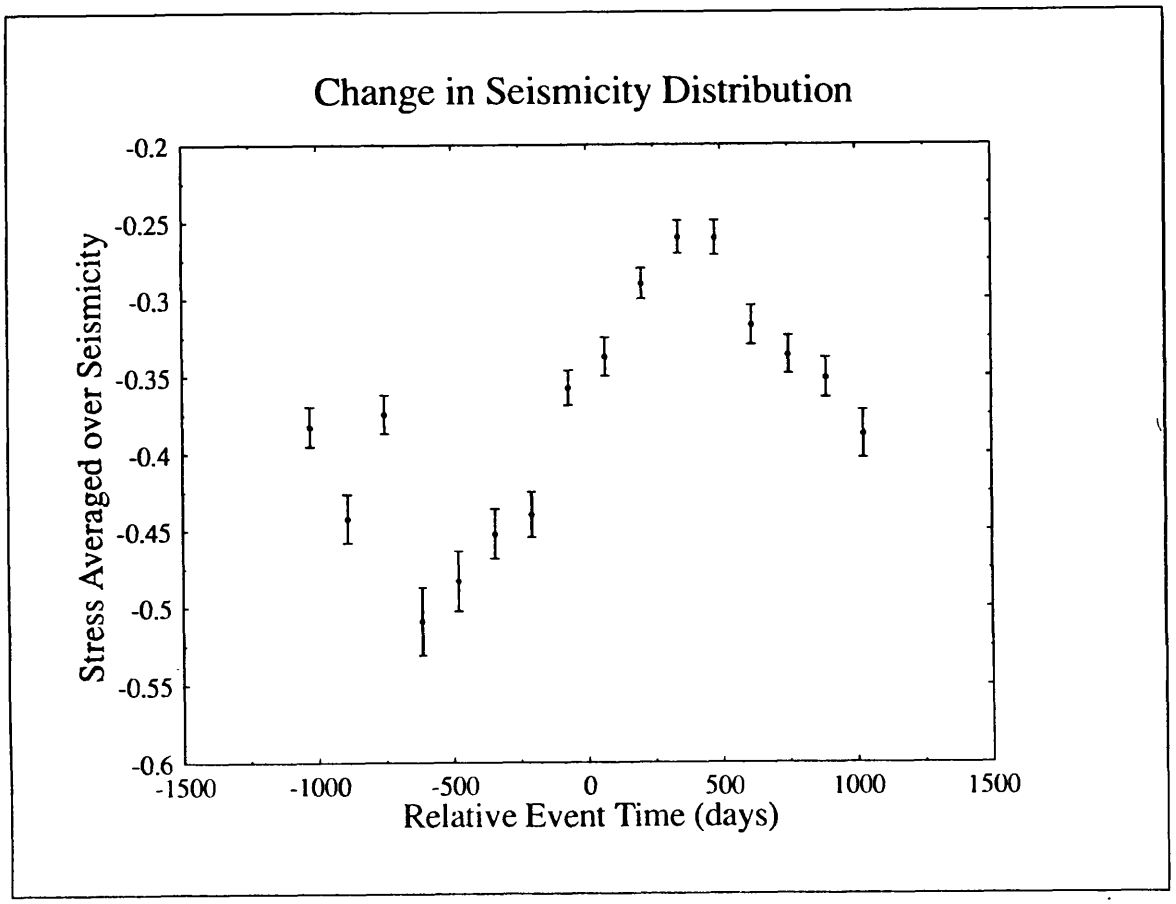

Figure 3: The average modeled change in shear stress at hypocenters of earthquakes surrounding 52 "target" events as a function of time relative to the target earthquake. The error bars apply to the standard deviation of the mean of the stress change, and may be slightly underestimated because the surrounding earthquakes are not independent of one another. The relatively lower values of stress before the earthquake imply that more of the seismicity is occurring in places which will experience larger decreases in maximum shear stress when the "target" earthquake occurs. After the target event, the seismicity moves to locations where the decrease in shear stress was less.

intervals. The most typical interval now used is 2 years. Longer intervals would probably be preferable, but limits in the catalog length would make statistics based on longer intervals harder to calibrate. The temporal signature of changes in the spatial distribution of seismicity which have been observed may be appreciated by examining Figure 3. This figure shows the average change in shear stress found at hypocenters of surrounding earthquakes as a function of time relative to the larger earthquake which caused the shear stress. All the data from the seismicity surrounding a set of 52 larger earthquakes has been combined on one plot. Changes in the average shear stress appear to be quite smooth, and vary most strongly around the time of the mainshock. The decrease in average shear stress before the event means that seismicity has become concentrated in those areas which will experience decreases in shear stress when the mainshock happens. The higher values afterwards mean that the seismicity has moved to occur in areas which have experienced shear stress increases.

Publications and Presentations based on the Research

Gross, S. and D. Schmerge, A Revised Duration Magnitude for the Central Aleutians Seismic Network (abs), *Seism. Res. Lett., 62*: 24, 1991.

Gross, S. J. and C. Kisslinger, A Subduction Stress Model Verified with Seismicity (abs), *Seism. Res. Lett., 63:* 66, 1992.

Gross, S. J., How Dependent are Earthquakes Upon One Another? Presented at the 1992 Seismological Society of America Eastern Section meeting.

Gross, S. J., A Test of the Fluid Diffusion Hypothesis of Aftershock Generation Using Changes in the Spatial Distribution of Seismicity (abs), *EOS, 73:* 389, 1992.

Gross, S. J. and C. Kisslinger, Tests of Models of Aftershock Rate Decay, *J. Geophys. Res.*, submitted, in review, 1993.

Huang, Z.X. and C. Kisslinger, Coda-Q before and after the 1986 Andreanof Islands Earthquake, *PAGEOPH, 138:* 1-16, 1992.

Kisslinger, C., The Stretched Exponential Function as an Alternative Model for Aftershock Decay Rate, *J. Geophys. Res., 97:* in press, 1992.

Kisslinger, C., Seismicity in Subduction Zones from Local and Regional Network Observations, *PAGEOPH,* accepted and in press, 1993.

Refinement of Pattern Recognition Procedures for Intermediate-Term Earthquake Prediction

1434-92-G-2214

L. Knopoff
Institute of Geophysics and Planetary Physics
University of California
Los Angeles, California 90024

(310)825-1885

Twenty-four of all of the 26 strong earthquakes in Southern and Central California and the Cape Mendocino area with magnitudes between 6 and 7.7 have been preceded by a significant increase in the rate of occurrence of intermediate magnitude earthquakes. The increased precursory activity takes place on an intermediate-term time scale that ranges from 2 to 10 years before the subsequent strong earthquake and scaled by the magnitude of the strong earthquake.

We began this study with an analysis of intermediate-magnitude earthquakes that precede strong earthquakes with $M_L \geq 6.4$, in Southern California, from the last half part of 1935 to the present. Seven out of 8 strong earthquakes in the magnitude range from 6.4 to 6.9 were preceded by a significant increase in the number of earthquakes with M_L in the range 4.8 to 6.3 in a window of 2 years duration; the peak persisted until 0 to 1 year before the strong earthquake (Fig. 1). We note particularly that the earthquakes that constitute the precursory spike are widespread over the entire extent of Southern California; in Fig. 2 we show the precursory seismicity of intermediate-magnitude events in the 10-year period before the Kern County earthquake. If the lower threshold for intermediate-sized earthquakes is lowered to 4.6 or raised to 5.0, the pattern persists. If we lower the threshold for definition of intermediate-magnitude earthquakes to 4.4, the correlation begins to vanish, and at a 4.0 threshold it has almost disappeared.

We hypothesize that an area of the seismogenic zone that is much larger than the dimensions of the future strong earthquake, has reached a critical threshold for fracture from 2 to 3 years before a strong earthquake, and hence that the precursory, intermediate-magnitude earthquakes are to be found over a broad region of elevated stress. We further hypothesize that the strong earthquake switches off the critical state over the larger region.

The correlation above failed to appear before the Landers earthquake at the threshold we had set for strong earthquakes in the M_L=6.3 to 6.9 range. We then made a hypothesis of self-similarity: the larger the future great earthquake, the larger all three parameters of the system would have to be, namely the size of the region in which precursory intermediate-sized shocks will occur, the time-window of anticipation, and the lower threshold for the definition of intermediate magnitude. With this redefinition, the Landers earthquake was also shown to be preceded by a spike in intermediate level seismicity.

However, the Landers earthquake was the only event of its size other than the Kern County earthquake (which was successfully fit by the original model), and to tailor a revision of the model to one event seemed unjustifiable. We therefore made the conjecture that the same change of scale in reverse, i.e., a reduced time window, a reduced area of interaction and a reduced magnitude

threshold for intermediate-magnitude events, would be appropriate for anticipation of strong earthquakes in the magnitude 6 to 6.3 range. In this application we were completely successful, except for one event with M_L=6.0 in 1940, that occurred within a few months of an earlier, stronger M_L=6.7 earthquake; in this case, the failure to fit the pattern was due to a feature of our model that resets the count of intermediate shocks to zero after a strong earthquake.

The model was then applied to earthquakes in the NEIS catalog (1965-1992) in Central California and the Pacific off Cape Mendocino, without change of parameters. NEIS magnitudes m_b were assigned equivalent M_L through a conversion derived from a comparison of (m_b, M_L) values for Southern California earthquakes. The Southern California pattern occurred in all cases in the other two regions without change of parameters; we summarize these results in Table 1. In the Table, we list the number of events in each region, followed by the number of times the anticipatory pattern described failed to appear.

Table 1

	Southern California	Central California	Mendocino
6.0 - 6.3	6/1*	2/0	1/0
6.4 - 6.9	8/1	1/0	3/0
7.0 - 7.3	0	1/0	2/0
7.4 - 8.0	2/0	0	0

* Failure to fit one event that was preceded by an earlier event within 7 months.

We comment on the case of the Loma Prieta earthquake. In this case there was sufficient precursory seismicity within 10 years and within 100 km of the epicenter of the strong shock that we would not have had to enlarge the space window as indicated; we could have continued to use the original Southern California space window without the modification to accommodate larger events.

The model has the following details: We remove aftershocks from the time series by the Gardner-Knopoff formula. (We have analyzed the complete catalogs, that is without removing aftershocks, and find that the model provides a fit that is almost as good as in the case in which aftershocks are removed.) For strong earthquakes in a range with M_o defined by its lower extreme (in Table 1 we have used M_o = 6.0, 6.4, 7.0, 7.4), we count the number of shocks in the relevant geographical area, with magnitudes between $(M_o - \mu, M_o - 0.1)$ in a τ year window sliding by 2 month increments. We construct a histogram of these values. We find that a spike threshold persists to less than 1 year before the strong event. A spike is considered to be a precursor if the count has a value greater than or equal to the nearest integer in the 10th to 25th percentile intervals of the histogram.

Details of the windows are given in Table 2. M_o is the lower cutoff magnitude for each strong magnitude band. The intermediate-magnitude earthquakes are defined in the interval from their lower bound listed in the second column to 0.1 magnitude units below M_o; the lower bounds for intermediate magnitudes can take on the broad range of values listed in column 2; our best fit is given in parentheses; μ is about 1.8. The widths of the sliding window are given in the third column. The range of distances in the fourth column is well-defined as the diameter of a circle in

the case of M_o=6.0; in the other cases, it is defined by the area covered by the catalog used. The number of strong shocks in each magnitude range in all three regions is given in the last column.

Table 2

M	$m \geq$	$\tau, years$	D,km	$Number$
6.0 - 6.3	4 - 4.4 (4.0)	2 - 5	200-300	9
6.4 - 6.9	4.6 - 5.0 (4.8)	2 - 5	500-600	12
7.0 - 7.3	5.0 - 5.4 (5.2)	5 -10	500-600+	3
7.4 - 8.0	5.4 - 5.8 (5.6)	5 -10	600-800	2

To summarize: The retrospective application of this model fit the occurrence of precursory seismicity before 14 out of 16 strong shocks (M=6.0) in Southern California between 1935-1992, and before all 10 such strong shocks in the Coast Range and Cape Mendocino areas between 1965-1992. The Landers, Loma Prieta and Kern County earthquakes are all successfully fit by the model. Of particular importance is our observation that the area of intensified activity in intermediate-magnitude events is much larger than the source dimensions of a subsequent strong earthquake and does not necessarily span it; this region is almost always distributed broadly in two-dimensions. If increased activity in the magnitude range (M_o - μ, M_o - 0.1) is spread out over even larger distances than D(M), it may be that the approach of an earthquake in a higher magnitude range is indicated.

The model is not a particularly strong prediction algorithm; the ratio of "alarm" times to total time is about 1:3 for earthquakes with magnitudes between 6.4 and 6.9. Measured in terms of the number of adjustable parameters, there are 5 degrees of freedom in this model; since this model is used to fit to 26 events, it is clear that we need additional data in the form of tests on additional seismically active regions of the world (in progress) or in the form of the future occurrence of clustering of seismic events in California, which is inevitable.

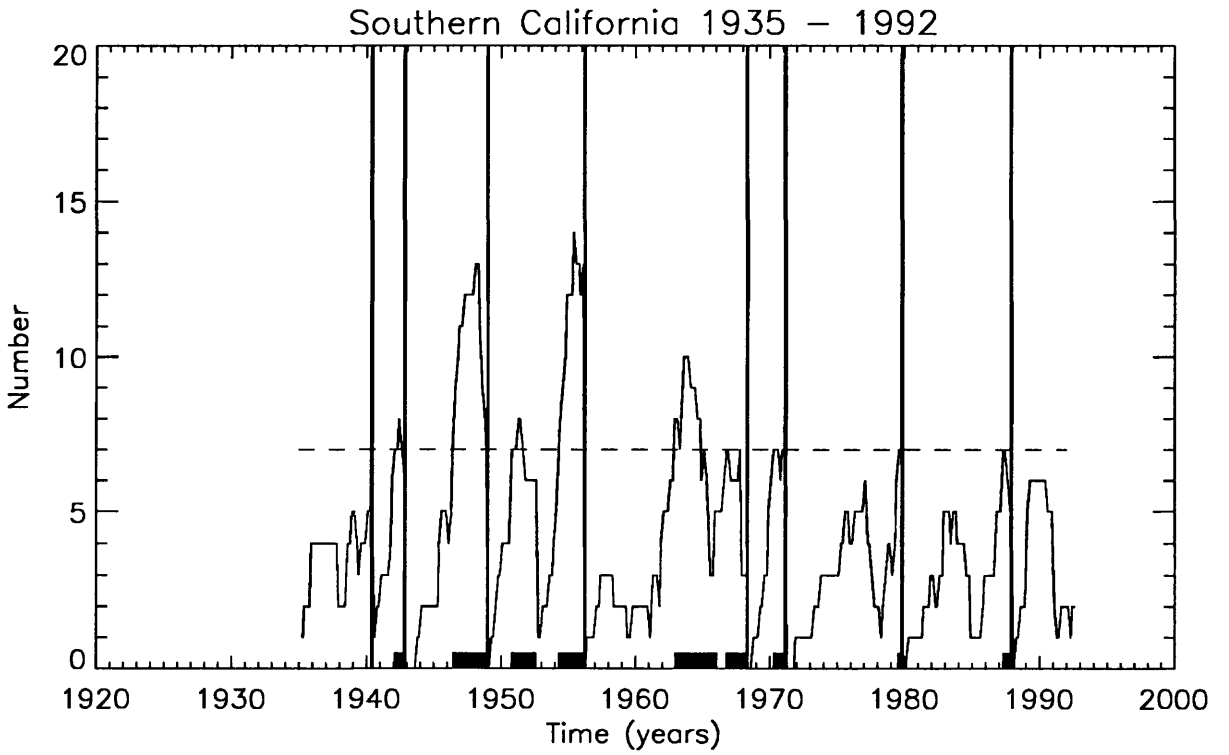

Number of intermediate magnitude events with $6.3 \geqq M_L \geqq 4.8$
in a 2 year sliding window. Dashed line is threshold.
Vertical lines are times of strong earthquakes with $6.4 \leqq M_L \leqq 6.9$.

Fig.1

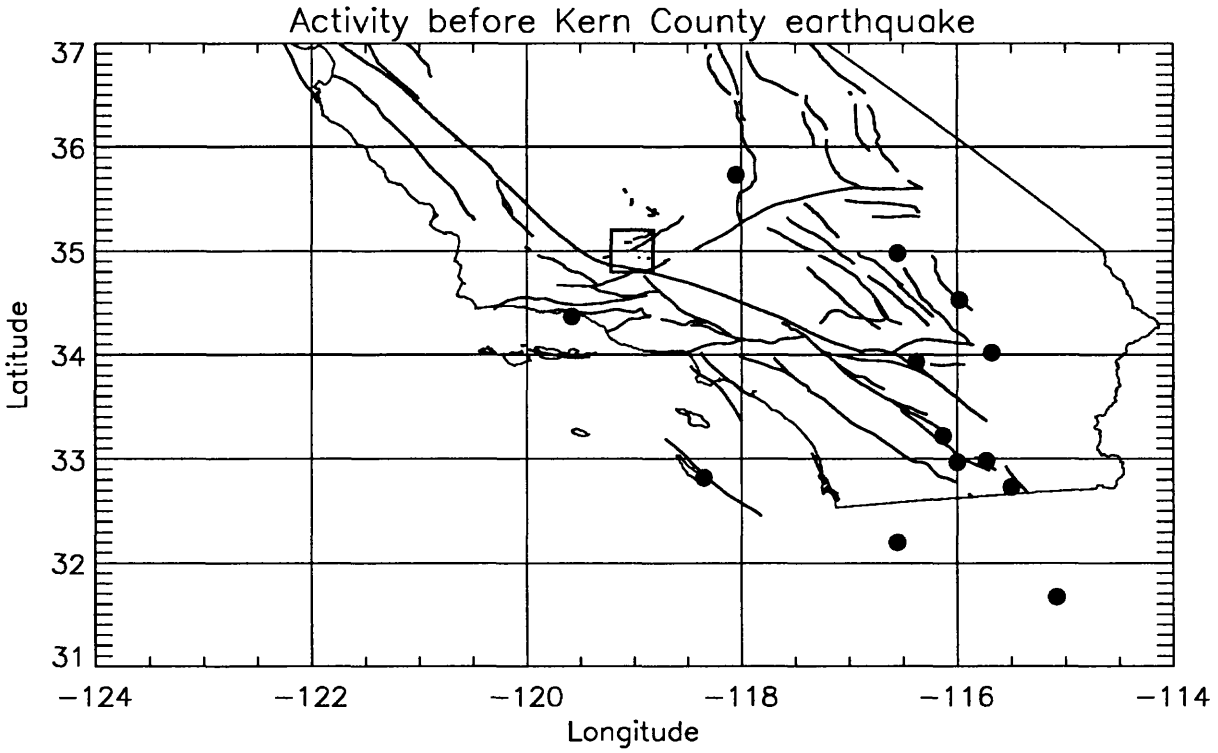

□ – Kern County earthquake (M =7.7);
• – intermediate magnitude events with magnitude M≧5.6 for ten years preceding August 21, 1952.

Fig.2

Stress and Anisotropy in Southern Hawaii

Contract No. 1434-92-G-2163

Clifford G. Munson and Clifford H. Thurber
Department of Geology and Geophysics
University of Wisconsin-Madison
Madison, WI 53706

608-262-6027

Investigations

From July to December 1990 four portable seismic arrays of 5-to-8 three-component PASSCAL instruments spaced approximately 1 to 2 km apart were deployed on the southeast flank of Mauna Loa (Figure 1). Seismic stations in the Bird Park array were located adjacent to the Mauna Loa Strip Road and Highway 11. The Ainapo seismic array was centered in the Keakapulu Flat area of the Kapapala Forest Reserve. The Waihaka and Punaluu Gulch arrays were located southeast of the Kau Forest Reserve in the Hilea region. Hundreds of microearthquakes were digitally recorded (100 sps and 60 s record) using 1 and 2 Hz seismometers. Two previous shear-wave anisotropy studies in southern Hawaii were done by Savage et al. [1989] (on Kilauea's south flank) and Booth et al. [1992] (in the Kaoiki area).

The Kaoiki seismic zone, situated between the volcanoes Kilauea and Mauna Loa, (Figure 1) has been subjected to frequent moderate to large earthquakes throughout this century. Crustal earthquakes in the Kaoiki seismic zone are a combination of shallow (< 9 km) strike-slip and deeper (9 to 12 km) low-angle seaward thrust events [Endo, 1985]. The neighboring Hilea seismic zone, to the southwest of Kaoiki along Mauna Loa's "exposed" southeast flank (Figure 1), is somewhat less active, but is thought to have been the locus of the great 1868 earthquake [Wood, 1914; Wyss, 1988]. The earthquakes in Hilea generally occur in the southern and eastern portion of the area between the southwest rift zones of Mauna Loa and Kilauea and are dip-slip events [Endo, 1985; Liang and Wyss, 1991]. The abundant seismicity indicates that significant levels of stress must be prevalent throughout the southeast flank of Mauna Loa.

Event locations provided by the Hawaiian Volcano Observatory (HVO) seismic network of the U.S. Geological Survey have allowed us to limit our analysis to arrivals from events within a 40° shear wave window (Figure 1). For obvious HVO network event mislocations, S - P times from our PASSCAL array data were used to relocate event hypocenters. The events analyzed ranged in depth from 1 to 14 km.

To estimate the shear wave polarization, we use a quantitative method based on a 3x3 particle motion covariance matrix decomposition [Jurkevics, 1988]. The polarization type and orientation of the particle motion is determined by computing a covariance matrix for the three components of motion in a selected time window. The orientation of the horizontal particle motion corresponds to the direction of the eigenvector for the largest eigenvalue of the covariance matrix projected onto the horizontal plane. Split shear wave arrivals are identified by their (1) rectilinear particle motion, (2) orthogonally polarized pulses, and (3) similar waveforms. Rectilinearity is measured by

$$1 - \frac{\lambda_2 + \lambda_3}{2\lambda_1}$$

where λ_1, λ_2, and λ_3 are the maximum, intermediate, and minimum eigenvalues [Jurkevics, 1988]. To estimate the time delay between the split shear wave arrivals (S_1 and S_2) we use the maximum value of the cross-correlation function derived from the two horizontal traces after rotation to the horizontal component of the S_1 polarization direction.

Results

Of the 381 arrivals that were examined, 311 had measurable leading shear wave polarization alignments and 106 showed clear evidence of shear wave splitting (i.e., a clear second shear wave arrival). Figure 2 shows the leading shear wave polarizations for each station among the four arrays. The measured S_1 polarizations for both of the arrays in the Kaoiki seismic zone show a high degree of alignment at each station as well as within the respective arrays (Bird Park N68°E ± 22° and Ainapo N99°E ± 11°). The measured S_1 polarizations for the Waihaka Gulch array are less aligned (N98°E ± 46°) both for the array as a whole and for individual stations. The number of observations at the Punaluu Gulch array is limited (24 arrivals), however the measured polarizations are strongly aligned (N172°E ± 20°). Table 1 shows the measured delay times for the four arrays. The delays vary from 100 msec to 270 ms, with a mean value of 187 ± 45 ms.

Focal mechanism studies in the Kaoiki and Hilea seismic zones [Wyss et al., 1992; Liang and Wyss, 1991] in addition to field measurement made in the vicinity of the 1974 and 1983 Kaoiki earthquakes [Jackson et al., 1992] lead us to conclude that the consistent leading shear wave polarizations for stations within the Bird Park, Ainapo, and Punaluu Gulch arrays are due to the presence of stress-aligned cracks. Wyss et. al [1992] determined the stress tensor orientation based on the inversion of 238 first motion fault plane solutions of earthquakes located in the 10-km radius Kaoiki crustal volume. The orientation of maximum principal stress, σ_1, for the southeast subarea of the Wyss et. al [1992] Kaoiki area is N83°E ± 7° and is near horizontal. This result agrees well with the leading shear wave polarizations for the Ainapo array (N99°E ± 11°) which was located in this subarea. Booth et al. [1992] also report a leading shear wave polarization of ENE-WSW for the three-component HVO station AIN which is near the Ainapo array. Field measurements of ground ruptures from the 1974 and 1983 Kaoiki earthquakes show that the mean strike of individual cracks is N91°E and N95°E respectively [Jackson et. al, 1992]. A focal mechanism study for the Bird Park array shows the orientation of σ_1 to be NE-SW and subhorizontal (P. Okubo, personal communication). The predominant S_1 polarization for events recorded by the Bird Park array is also NE-SW (N68°E ± 22°). Delaney et al. [1990] show that a reference baseline with a NW-SE orientation crossing the structural boundary between Mauna Loa and Kilauea (the Kaoiki fault zone) has been extending at a rate of 4.6 ± 0.5 cm per year since 1984, consistent with a NE-SW σ_1 orientation. Fault plane solutions for events near the Waihaka Gulch array (center subregion of Hilea) do not show a clear orientation for the maximum horizontal stress [Liang and Wyss, 1991]. Similarly, no predominant S_1 polarization is seen for events near the Waihaka Gulch array. For the center subregion of Hilea, Liang and Wyss (1991) report a maximum horizontal stress oriented approximately N144°E (with a dip angle of 7°) similar to the S_1 polarization for events near the Punaluu Gulch array (N172°E ± 20°).

For the 106 arrivals that show clear evidence of shear wave splitting, the average time between S_1 and S_2 is 187 ms with a standard deviation of 45 ms. For the 3-component HVO station AIN, Booth et al. [1992] were unable to measure a reliable delay between fast and slow shear wave arrivals due to interference by scattered or converted arrivals, although a few reliable arrivals indicate a time delay of approximately 190 ms. Savage et al. [1989] report delays ranging from 160 to 210 ms for the south flank of Kilauea. Thus our shear wave splitting observations are consistent with those of previous studies in southern Hawaii.

For the average event depth of 8 km, the time separation between split shear waves is 23 ms/km, the velocity anisotropy is about 7.5%, and the crack density is approximately 8% for the 8-km crustal section. However, a comparison of event depth vs. delay time shows that there is no increase in delay time with increasing event depth. This suggests that the observed delay times are caused by near-surface rather than pervasive anisotropy. Since shear wave splitting is observed for earthquakes as shallow as 3 to 4 km this indicates a transverse anisotropic velocity variation of about 14% and $e \approx 16\%$. For comparison, Leary et al. [1990] report a crack density range of 1 to 5% for most geolgical and tectonic regions and an extreme case of $e = 7\%$ for crystalline rock near an active normal fault in California. Thus our results indicate that the upper crust of the southeast flank of Mauna Loa is highly fractured.

TABLE 1. A Summary of Delay Times for the Four ALOHA Arrays

Array	Number	Delay Time (msec)
Bird Park	50	206 ± 37
Ainapo	36	166 ± 36
Waihaka Gulch	13	205 ± 47
Punaluu Gulch	7	123 ± 22

References

Booth, D. C., M. Wyss & D. Gillard, Shear-wave polarization alignments recorded above the Kaoiki fault zone, Hawaii, Geophys. Res Let. 19, 11, 1141-44, 1992.

Delaney, P.T., R. S. Fiske, A. Miklius, A. T. Okamura, & M. K. Sako, Deep magma body beneath the summit and rift zones of Kilauea volcano, Hawaii, Science 247, 1311-16, 1990.

Endo, E. T., Seismotectonic framework for the southeast flank of Mauna Loa, Hawaii, Ph. D. thesis, Univ. of Washington, Seattle, 349 pp., 1985.

Jackson, M. D., E. T. Endo, P. T. Delaney, T. Arnadottir, & A. M. Rubin, Ground ruptures of the 1974 and 1983 Kaoiki earthquakes, Mauna Loa volcano, Hawaii, J. Geophys. Res. 97, 8775-96, 1992.

Jurkevics, A., Polarization analysis of three-component array data, Bull. Seismol. Soc. Am. 78, 1725-43, 1988.

Leary, P. C., S. Crampin, & T. V. McEvilly, Seismic fracture anisotropy in the earth's crust: An Overview, J. Geophys. Res. 95, 11105-14, 1990.

Liang, B. and M. Wyss, Estimates of orientations of stress and strain tensors based on fault plane solutions in the epicentral area of the great Hawaiian earthquake of 1868, Bull. Seismol. Soc. Am. 81, 2320-34, 1991.

Savage, M. K., X. R. Shih, R. P. Meyer, & R. C. Aster, Shear-wave anisotropy of active tectonic regions via automated S-wave polarization analysis, Tectonophysics 165, 279-92, 1989.

Wood, H. O., On the earthquakes of 1868 in Hawaii, Bull. Seismol. Soc. Am. 4, 169-203, 1914.

Wyss, M., A proposed source model for the great Kau, Hawaii, Earthquake of 1868, Bull. Seismol. Soc. Am. 78, 1450-62, 1988.

Wyss, M., B. Liang, W. R. Tanigawa, & X. Wu, Comparison of orientations of stress and strain tensors based on fault plane solutions in Kaoiki, Hawaii, J. Geophys. Res. 97, 4769-90, 1992.

Contract Publications:

Munson, C. G., C. H. Thurber, & Y. Li, Seismic anisotropy in the Kaoiki and Hilea regions of southern Hawaii (abstract), Seismol. Res. Lett., 63, 59, 1992.

Munson, C. G., C. H. Thurber, and Y. Li, Observations of shear wave splitting on the southeast flank of Mauna Loa volcano, Hawaii, submitted to Geophys. Res. Lett., October 1992.

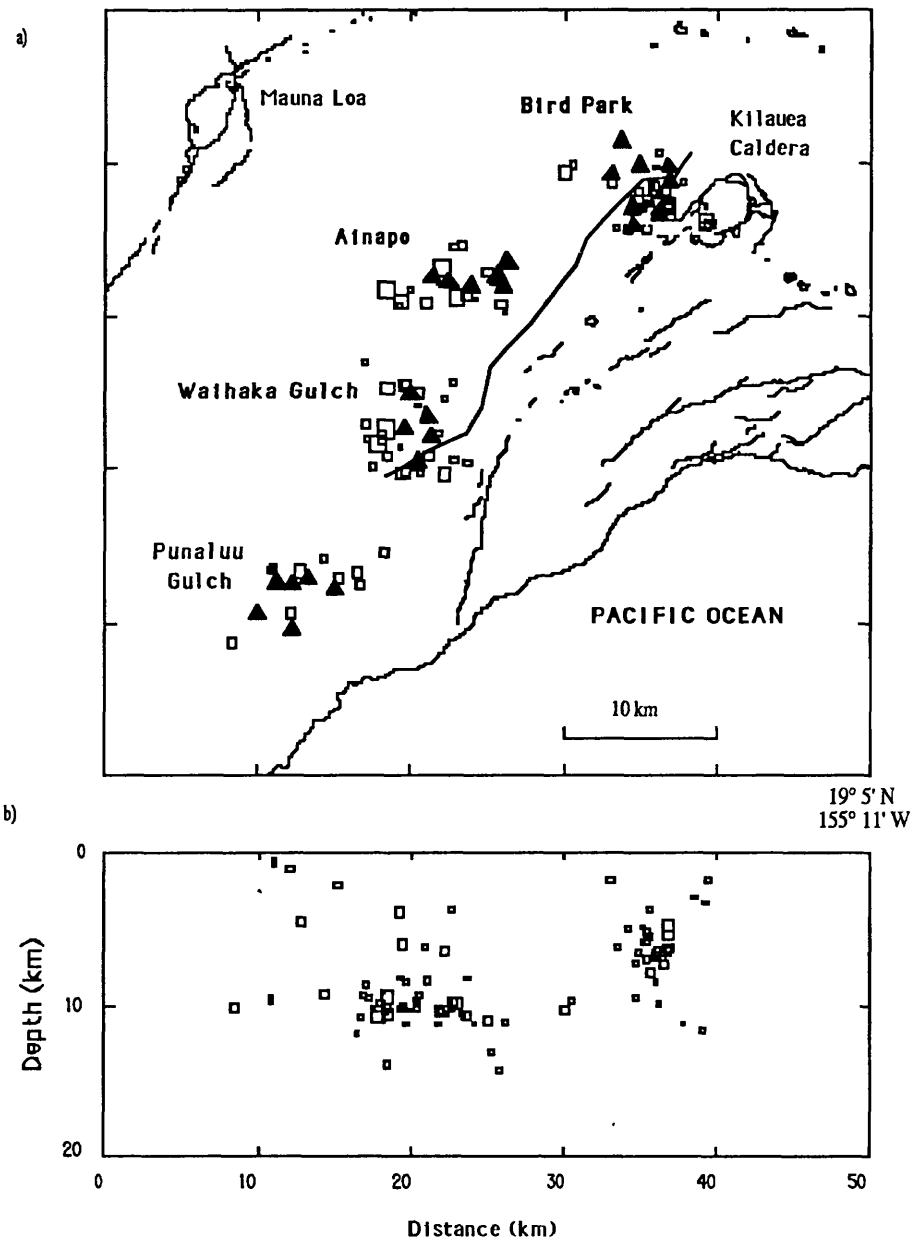

Figure 1. (a) A map of the Kaoiki and Hilea regions in Southern Hawaii, showing the locations of the PASSCAL stations (triangles) deployed from July to December 1990 and the events (boxes) that have been used in this study. The Bird Park and Ainapo arrays were located in the Kaoiki region and the Waihaka Gulch and Punaluu Gulch arrays were located in the Hilea region. The size of the boxes scale with magnitude; the smallest box represents a M = 0.5 earthquake, and the largest represents a M = 2.1 earthquake. (b) A cross section view of the 88 earthquakes showing the range of event depths.

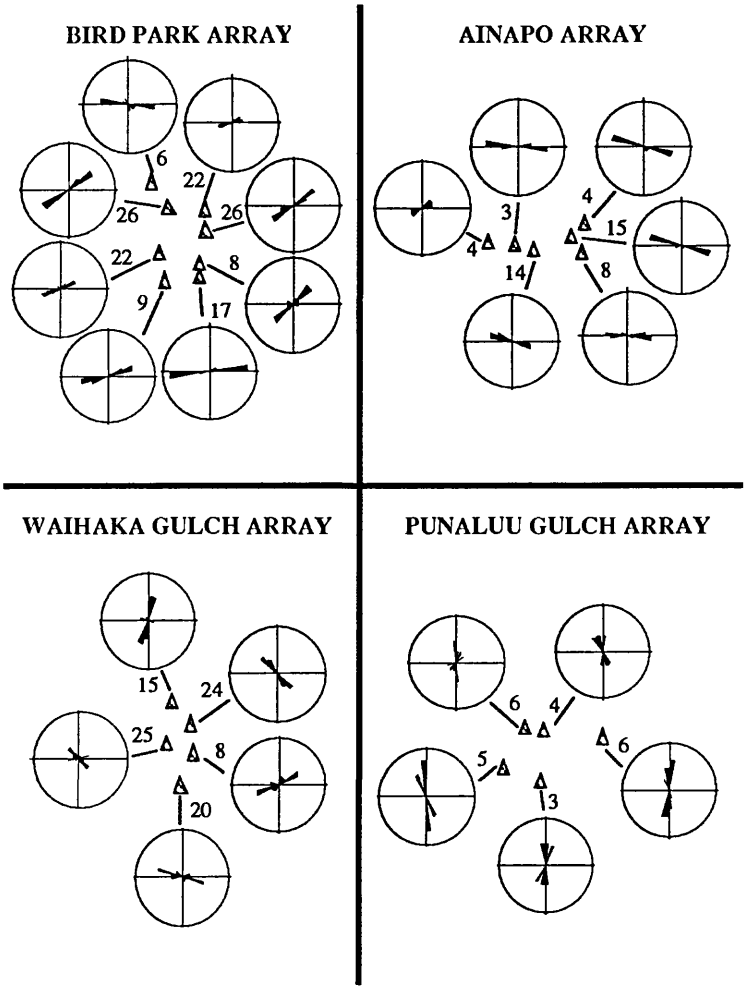

Figure 2. The measured polarization directions of the first-arriving shear wave from the four ALOHA arrays on Mauna Loa's southeast flank displayed as equal-area rose diagrams. The number of observations for each array ranges from 24 to 136.

Coupled Deformation-Diffusion Solutions for the Interpretation of Slip Induced Water Well Level Changes at Parkfield

Grant No. 1434-92-G-2164

J. W. Rudnicki
Department of Civil Engineering
Northwestern University
2145 Sheridan Road
Evanston, IL 60208-3109

(708)-491-3411

The purpose of this work is to develope more realistic coupled deformation-pore fluid diffusion solutions for fault slip and to use them to interpret observed water well level changes at Parkfield.

We have derived the coupled deformation diffusion solution for a plane strain slip that begins from rest, propagates a finite distance, and then stops. We intend to use this solution to explore the applicability of the previously used limiting cases of steady propagation [*Roeloffs and Rudnicki*, *PAGEOPH*, 1984/85] and simultaneous slip on a fault segment with a finite rise time [*Rudnicki and Hsu*, *JGR*, 1988]. The steady propagation solution idealizes cases in which the slip propagates primarily along strike. The simulataneous slip solution idealizes the case in which the slip propagates primarily from depth and reaches the surface essentially simultaneously at different positions along strike.

Earthquake Research in the Eastern Sierra Nevada Western Great Basin Region

Contract 14-08-0001-A0618

M. Savage, J. Anderson, J. Brune
Seismological Laboratory, MS 168
University of Nevada, Reno
Reno, NV 89557-0141
(702)784-4975

Investigations Undertaken

This contract supports continued research focussed on earthquakes in the eastern Sierra Nevada and western Great Basin region. We have investigated: 1) Quantitative determination of the probability that a moderate event will be a foreshock to a larger events; 2) Triggering of moderate earthquakes in Nevada following the M=7.5 June 28 1992 Landers, California earthquake; 3) The earthquake sequences of the M=5.6 June 29, 1992 Little Skull Mountain, Nevada, earthquake, and the M=5.0 October 24, 1990 Lee Vining, California, earthquake 4) The relation of precariously-balanced rocks in Nevada and California to past strong ground motion levels, with emphasis on using their presence to determine limits on past shaking 5) Microseismicity in the Mammoth Lakes, California and Yucca Mountain, Nevada region and the relation of microseismicity to the frequency of occurrence of larger events.

Results obtained

1) Foreshock Probabilities in the western Great-Basin eastern Sierra Nevada

We quantify foreshock occurrence probabilities in the eastern California/Western Nevada region by applying the empirical technique of Jones (1985) to the University of Nevada, Reno western Nevada-eastern California catalog from 1934 through 1991. We found it necessary to separate the Mammoth/Mono Lakes region from the rest of the catalog to determine the parameters that most effectively removed the aftershocks from the catalog. The probability that an $M \geq 3.0$ earthquake will be followed by an earthquake of larger magnitude within 5 days and 10 km is 10% in the Mammoth/Mono region and 6% in the Nevada region, and appears to be independent of the magnitude of the proposed foreshock. The probability that a mainshock at least one magnitude unit higher will occur decreases to about 2% in each region. These probabilities imply that the occurrence of an earthquake of $M \geq 4.0$ increases the possibility of a damaging earthquake of $M \geq 5.0$ by several orders of magnitude above the low background probability. Most mainshocks occur within a few hours after a possible foreshock, and the probability that a mainshock will still occur decreases logarithmically with time after the proposed foreshock. These properties are similar to those in southern California and in other parts of the world, with the exception that the Mammoth/Mono region, a volcanic area, exhibits more swarm-like behavior than does the southern California or Nevada region.

2) Earthquake Triggering from the Landers, California earthquake sequence

Within 24 hours after the Landers earthquake, there were 3 magnitude 3.4+ events in western Nevada and a general increase in the rate of small events. Based on the previous 25 year combined catalog for northern and southern Nevada, this level of widely scattered seismicity appeared quite unusual. Using a quantitative model that assumes statistical independence of these regions, the probability of this happening in a 24 hour period by random chance is less than once in 10^{10} years. Therefore, we conclude that there is a very high probability that these were triggered by the Landers event. The principal events that occurred were: Mina, 500 kilometers from Landers, M4.0, 36 minutes after Landers; Smith Valley, 590 kilometers from Landers, M3.4, 56 minutes after Landers; Little Skull Mountain, 280 kilometers from Landers, M5.6, 22.3 hours after Landers. These events are not associated with known volcanic activity or ongoing aftershock sequences. The evidence for triggering is particularly strong in the case of the Little Skull Mountain event, where an increased rate of microseismicity was evident as soon as small events could be identified in the coda of the Landers earthquake.

Earthquakes have been triggered in southern Nevada before, by nuclear testing and by filling of Lake Mead.

We speculate that these events are triggered by the dynamic low-frequency stress associated with surface waves propagating from the Landers earthquake. The distance dependence of static strain changes decrease as R^{-3} , which is much too rapid to cause a significant static strain change at the distances of the above events. Body wave amplitudes decrease more rapidly than surface waves with distance, so that the high-frequency strains associated with the body waves from the Landers earthquake would probably have been exceeded by other more local sources during the prior year. The above reasoning suggests that the cause of the distant triggering is the high amplitude, relatively longer period surface waves. Surface waves of a few seconds period have relatively high strains extending to a depth of more than 10 km. This mechanism for triggering satisfies the criterion of being a relatively rare phenomenon, since it is likely to occur only when a large surface wave is radiated into an area where strain has been building slowly toward the point where faults are unstable.

3a) The Little Skull Mountain, Nevada, earthquake sequence of June 29, 1992:

The Little Skull Mountain earthquake occurred about 20 km from the proposed high level nuclear repository at Yucca Mountain. The magnitude was 5.6, and the focal mechanism indicates normal faulting on a northeast trending structure. There is evidence that the earthquake was triggered by the magnitude 7.6 earthquake in Landers, California, which occurred less than 24 hours earlier. Preliminary locations of the hypocenter and several aftershocks define an "L" shaped pattern near the southern boundary of the Nevada Test Site. One arm trends to the northeast beneath Little Skull Mountain, and a shorter, more diffuse zone trends to the southeast. The aftershocks are mostly located at depths between 7 km and 11 km, and may suggest a southeast dipping plane. There is no clear correlation with previously mapped surface faulting. The strongest recorded acceleration is about 0.21 g at Lathrop Wells, Nevada, 15 km from the epicenter. An extensive network of aftershock recorders was installed by the Seismological Laboratory, University of Nevada, Reno, by the United States Geological Survey, Golden, Colorado, and by Lawrence Livermore Laboratory, Livermore, California. Aftershock experiments are ongoing as of November, 1992, and include experiments to improve location, depth, focal mechanism, and stress drop, study basin and ridge response near the epicenter and at Midway Valley, and study response of a tunnel at Little Skull Mountain. Analysis of this data, which includes thousands of aftershocks, has only begun.

3b) The October 24, 1990, Lee Vining, California Earthquake

On October 24, 1990, a magnitude 5.0 (Md) earthquake occurred near the town of Lee Vining, California. It was a strike-slip event with a hypocenter 5 km east and 11.5 km below the surface trace of the active (Holocene), vertically offset, Sierran frontal fault. A time domain deconvolution technique was used to obtain the source time function of this event using a small foreshock as an empirical Green's function. The resulting source time function indicates a simple rupture with a moderate stress drop of 31 bars. The distribution of aftershocks, duration of rupture, and lack of strong directivity observed in the first motion pulse widths, slightly favor bilateral rupture on a northwest striking vertical plane over unilateral rupture on a nearly vertical northeast striking plane. The Lee Vining main shock is the latest in a series of 27 magnitude 5.0 to 6.6 earthquakes to have occurred in the Walker Lane Belt since 1978. This is an area of diverse topography and numerous strike-slip faults which lies between the Sierra Nevada on the west and typical Basin and Range topography on the east. Between 86% and 91% of the cumulative moment released during these earthquakes was due to strike-slip motion (based on 20 available short-period focal mechanisms). Long-period mechanisms (centroid moment tensors) available for seven of the events also indicate a larger percentage of strike-slip than dip-slip motion. Slip ratios estimated for the two largest historic events in the Walker Lane Belt, the magnitude 7.7 Owens Valley earthquake and the magnitude 7.2 Cedar Mountains earthquake are consistent with these results. This indicates that the contemporary stress field has a significant component of horizontal shear.

4) Precarious Rocks

In several localized ares of California and Nevada there are large numbers of precariously balanced rocksrocks which could be knocked down by earthquake ground motion with peak accelerations of about 0.2g or less. In some cases geomorphic evidence indicates that these rocks have been in these precarious positions for thousands of years. In this study the locations of regions of precariously balanced rocks are compared with probability maps for strong ground motion, to help determine if the precarious rocks can be used as paleoindicators of peak acceleration. The following results are obtained:

1) No precarious rock zones are found within 15 km of known historic large earthquake rupture zones (e.g., Olinghouse, Fallon-Stillwater, Cedar Mountains, Nev.; Fort Tejon, Owens Valley, Borrego Mt., Tehachapi, Parkfield, Calif.)

2) Precarious rock zones have been found at the following sites: a) the region around Yucca Mountain, Nev., site of the proposed high level nuclear waste repository, b) the center of the Peninsular Ranges in southernmost Calif., c) 20 km north of San Gorgonio Pass, Calif., d) near Lida, Nev., 20 km southeast of the spectacular Holocene scarps in Fish Lake Valley, Calif., e) the West Walker River Canyon 15 km south of Walker, Calif., f) 25 km north of the ground rupture in the 1932 M=7.4 Cedar Mtn. earthquake.

3) In California these observations correlate well with published ground acceleration maps, but in Nevada there are significant discrepancies. The implications of these results for seismic hazard studies are discussed.

5) Microearthquakes

We set up four microearthquake stations near Mammoth Lakes, where we observed microearthquake rates of over 100 per day, most with S-P times of less than 3 sec. This confirms our previous expectations that in seismically active areas most events recorded on such instruments have S-P times of less than 3 sec. In a much less seismically active area, near Yucca Mountain, Nevada, there were many fewer events with short S-P times.

Publications

Refereed Journal Articles

Anderson, J. G., J. N. Brune, D. dePolo, J. Gomberg, S. C. Harmsen, M. K. Savage, A. F. Sheehan, K. D. Smith, Preliminary report: The Little Skull Mountain earthquake, June 29, 1992, *Proceedings of the ASCE Symposium on Dynamic Analysis and Design Considerations for High-Level Nuclear Waste Repositories, submitted.*

Brune, J.N., W. Nicks, and A. Aburto, Microearthquakes at Yucca Mountain, Nevada, *Bull. Seismol. Soc. Am.*, **82**, 164-174, 1992.

Horton, S., D. DePolo, and W. R. Walter, The October 24, 1990, Lee Vining, California earthquake and other recent moderate earthquakes in the western Basin and Range, *in revision, Bull. Seismol. Soc. Am.*, 1992.

Ozalaybey, S., and Savage, M.K. Inversion of double layers of anisotropy from waveforms of suites of seismograms, *to be submitted to Bull. Seismol. Soc. Am.*, 1992.

Savage, M.K. and P.G. Silver, Mantle deformation and tectonics: Constraints from seismic anisotropy in western United States, *Phys. Earth Planet. Int.*, in press, September 1992.

Savage, M.K., L. Li, J. Eaton, C. H. Jones, and J. N. Brune, Earthquake refraction profiles under the root of the Sierra Nevada, in preparation for submission to Geophysical Research Letters. (A draft is circulating among coworkers)

Savage, M.K., and D. DePolo, Foreshock probabilities in the eastern Sierra Nevada/Western Great Basin Region, *submitted to Bull. Seismol. Soc. Am.*, 1992.

Abstracts

Anderson, J., J. Louie, J. Brune, D. dePolo, M. Savage, and Y. Guang, Seismicity in Nevada apparently triggered by the Landers, California earthquake, June 28, 1992, *EOS, Trans. Am. Geophys. Union, 73,*, 393, 1992.

Brune, J.N. Distribution of precariously balanced rocks in Nevada and California: Correlation with probability maps for strong ground motion, *EOS, Trans. Am. Geophys. Union, 73,*, 351, 1992.

Brune, J. N. and J. W. Whitney, Precariously balanced rocks with rock varnish: Paleoindicators of maximum ground acceleration? *Seismol. Res. Lett., 63,*, 21

Horton, S.P., D. dePolo, and W. Walter, The October 24, 1990 Lee Vining, California earthquake and other recent moderate earthquakes in the western Basin and Range, *Seismol. Res. Lett., 63,*, 39

Li, L., M. K. Savage, J.N. Brune, J. Eaton, The Root of the Sierra Nevada: Evidence from Earthquake Refraction Profiles, *EOS, Trans. Am. Geophys. Union*73,, p. 369, 1992.

Ozalaybey, S. and M. Savage, Inversion of double layer anisotropy from SKS Phase, *EOS, Trans. Am. Geophys. Union, 73,*, 395, 1992.

Reasenberg, P.A., D. P. Hill, A. J. Michael, R. W. Simpson, W.L. Ellsworth, S. Walter, M. Johnston, R. Smith, S.J. Nava, W.J. Arabasz, J.C. Pechmann, J. Gomberg, J.N. Brune, D. DePolo, G. Beroza, S. D. Davis, J. Zollweg, Remote seismicity triggered by the M7.5 Landers, California earthquake of June 28, 1992, *EOS, Trans. Am. Geophys. Union, 73,*, 392, 1992.

Savage, M.K., and D. dePolo, Foreshock probabilities in the eastern Sierra Nevada/western Great Basin region, *Seismol. Res. Lett., 63,*, 21

Micromechanics of Rock Friction

Agreement No. USGS14-34-92 G2161

Christopher H. Scholz
Lamont-Doherty Geological Observatory
Columbia University
Palisades, New York 10964

(914) 359-2900

This is an experimental and theoretical study of rock friction in which the micromechanics of friction are studied by use of a model of the contact of random elastic surfaces.

In previous work the transition from partial to full sliding of the surfaces was studied. This takes place within the first 5-10 μm of sliding with the surfaces we study in the laboratory. Quantitative modeling show that this process can be well simulated with forward modeling based on measured topography of the experimental surfaces.

During the past year this has been extended through the stage of strong slip hardening until steady state friction is reached, in 0.1 to 1 mm of slip. To model this behavior we include the additional effects of oblique contacts (interlocking) and the evolution of surface topography during sliding (wear). This modeling successfully accounts for these later stages of friction and show that these processes account approximately equally to the additional friction that occurs after the onset of full sliding.

In order to facilitate the above study, an experimental study of the frictional wear of granite was also conducted. Modeling of the wear process allowed for the prediction of both transient and steady-state wear and the distinction to be made regarding the micromechanisms of 'riding up' and shearing through' to be distinguished for oblique contacts.

Work is continuing on scaling these processes to the geological scales, primarily through the scaling of the critical slip distance, D_c. Work is also continuing on the second order frictional effects, that of slip velocity and variable normal load.

Analysis of Seismic Anisotropy and Directional Site Resonance in the Loma Prieta Aftershock Zone

Agreement No. 14-08-0001 G2079

Susan Y. Schwartz
Institute of Tectonics, University of California, Santa Cruz, CA 95064
(408) 459-3133

Summary

The objectives of this research are twofold: to evaluate the existence, orientation and origin of crustal anisotropy in the aftershock zone of the 1989 Loma Prieta earthquake and to assess the influence of structural heterogeneities in the shallow crust on the seismic wavefield. To accomplish the first objective, we analyzed shear wave polarizations for evidence of seismic anisotropy using three-component digital recordings of Loma Prieta aftershocks recorded by PASSCAL instruments. Initial polarizations for over 60% of the records within the shear wave window (pre-critical arrivals) show clear evidence of shear wave splitting. Two fast directions of polarization parallel to the strike of the San Andreas Fault (290°-340°) and parallel to the direction of local maximum horizontal compressive stress (20°-45°) are observed. Stations located northeast of the San Andreas Fault predominantly show the fault parallel fast polarization direction which may result from mineral or fracture alignment caused by shearing along the plate boundary. Stations to the southwest of the San Andreas Fault show both fast directions of polarization. The direction perpendicular to the local axes of minimum horizontal compressive stress is consistent with the theory of extensive dilatancy.

Analysis of shear wave polarizations to investigate seismic anisotropy is often complicated by signal distortions produced by scattering and by the effects of shallow geology beneath the receiver. In order to understand these effects we investigate the site response and scattering properties of the shallow crust beneath one of our receivers. This investigation encompasses two experiments: the deployment of a 20-station small aperture array at station ZAYA to record five chemical explosions set off by the USGS in May of 1991, and a shallow refraction survey consisting of two orthogonal lines of geophones and both compressional and shear wave seismic sources. Analysis of three-component short-period recordings of the chemical explosions at our small array reveals: 1) smooth variations in shear wave polarization directions across the array, 2) a systematic bias of 30°-50° in the observed back azimuths of the P wave arrivals relative to known positions for the sources, and 3) a north-south preferred direction of arrival for P and S wave coda that is not consistent with the azimuth to the source. These results imply that the wavefield is strongly affected by regional velocity inhomogeneity beneath the receivers. To obtain more detailed information about the geology and seismic velocity layering beneath this array, we conducted a shallow refraction survey at ZAYA in August of 1992. This report describes the progress made in the first year of funding and the work we expect to accomplish during the second year.

Research Accomplished

1. Seismic Anisotropy in the Loma Prieta Rupture Zone

We have analyzed shear wave polarizations from three-component recordings of fifty-four aftershocks of the 1989 Loma Prieta earthquake for anisotropy induced shear wave splitting. Figure 1 shows the event-station geometry. Only events located at pre-critical distances from receivers (within the shear wave window) were analyzed to avoid distortions due to phase changes accompanying reflections and conversions from the free surface. We identify shear

wave splitting by: initial shear wave polarizations that abruptly change from linear to elliptical motion, consistent directions of initial linear polarization for many earthquakes with different focal mechanisms, and observations of the slow shear wave polarized in a direction orthogonal to the first arriving wave and delayed in time. To identify a transition from linear to elliptical particle motion at the onset of the shear wave, we plot the shear wave polarization vector as a function of time. Figures 2 shows horizontal component seismograms and polarization vectors plotted as a function of time, from two different earthquakes recorded at stations RADF and WVRD. Event 1 shows linear particle motion throughout the initial S arrival, as expected for propagation through isotropic material. S wave particle motion from event 2 is initially linear but abruptly changes to elliptical shortly after the S arrival. We interpret this behavior as evidence of anisotropy induced shear wave splitting, where arrival of the fast wave produces linear particle motion that changes to elliptical motion when the slow wave, polarized in the orthogonal direction, arrives.

For all events that show evidence of shear wave splitting, we determine the polarization direction of the fast wave directly from the polarization vector plot and compare it with directions determined by the aspect ratio (Shih *et al.*, 1989) and cross-correlation techniques. The aspect ratio method determines the initial polarization direction by searching through all azimuths for the maximum linear particle motion obtained from motions rotated onto a pair of orthogonal axes. The time separation between the fast and slow shear wave is estimated by advancing the slow wave by small time increments and searching for the time advance that yields the maximum linearity in particle motion. The direction indicated after this time shift represents the anisotropy corrected polarization direction, which we expect to be determined by the earthquake focal mechanism. The cross-correlation technique finds the azimuth and time delay that maximizes the waveform correlation between the fast and slow shear waves. For event 2 recorded at WVRD, the initial linear direction of polarization is 340° from the polarization vector plot (Figure 2), 330° from the aspect ratio technique (curve in Figure 3 marked with 0 delay time), and 335° from the cross-correlation method (Figure 4a). A delay time of 0.05 seconds between the fast and slow arriving waves results in the maximum aspect ratio (Figure 3) and a delay of 0.045 seconds produces the largest cross-correlation between the fast and slow waves. After correction for shear wave splitting of 0.05 seconds, the aspect ratio method indicates a direction of 285° (Figure 3). Before correction for shear wave splitting, linear particle motion persists for only .04 seconds from the onset of the shear wave (Figure 4b). After correcting for the .045 seconds indicated by the cross-correlation method, linear particle motion persist for over .2 seconds from the shear wave onset (Figure 4c). The direction after this correction is 290°. The shear wave polarization directions after correction for shear wave splitting indicated by cross-correlation and the aspect ratio technique are both consistent with the direction of 289° expected from the focal mechanism of this event.

For event 2, three methods of determing the initial polarization direction of the fast wave, and two methods to determine the time delay between the fast and slow wave are consistent providing confidence that the fast direction of polarization and the time delay until arrival of the slow wave are well determined. We are in the process of applying this methodology to 54 events recorded at 17 of the PASSCAL stations to look for evidence of anisotropy induced shear wave splitting and to evaluate the directions and time delays obtained. So far we have completed analysis at five stations which are indicated in Figure 1 using upward pointing triangles. Our results for four of the five stations are summarized in Figure 5 which shows the directions of initial polarization (solid lines) determined for many different earthquakes at each station. Polarization directions are plotted at the epicenter of the events for clarity. The range in delay time between the fast and slow shear waves observed at each station is indicated in milliseconds for each plot. At stations WVRD, WSWD and WAWA, all but one or two events show consistent directions of polarization that range between 140-160° at WVRD and WSWD and between 20-40° at WAWA. Results from station ZAYA are more mixed, with fast directions between 140-160° for only five of the nine events analyzed. Consistent directions of polarization at a particular station from events at different locations and with different focal mechanisms is diagnostic of anisotropy somewhere beneath the receiver. The observed directions of polarization are in most cases different from those originating at the source determined from P wave first

motion mechanisms of Oppenheimer (per. comm.). We are presently finishing our analysis on the remaining stations and looking for correlations between observed fast directions of polarization and known geologic information to isolate the origin of the seismic anisotropy. We are also correlating the delay times obtained with various parameters including focal depth, epicentral distance and azimuth. The different directions of fast polarization between stations WSWD and WAWA which are located very close to one another suggests that a component of the observed anisotropy occurs at very shallow depth. The mixed directions at ZAYA may result from strong velocity heterogeneity at shallow depth beneath this station that obscures any seismic anisotropy. The next sections of this report investigate the shallow velocity structure beneath the ZAYA station.

2. Dense Array Recording of Loma Prieta Rupture Zone Controlled Source Explosions

In an earlier study using data from the 6 element ZAYA sub-array of the 1989 Loma Prieta PASSCAL aftershock deployment (Figure 6), Bonamassa et al. (1991) found that in the frequency range between 1 and 20 Hz, different sites amplified ground motion in preferred directions that varied greatly between sub-array elements located only tens of meters apart. To further evaluate this phenomena, to investigate the relationship between the amplification and directionality of weak ground motions and microtremor at the same sites, and to study the scattering properties of the shallow crust, we deployed a dense array of 20 elements at the ZAYA site (Figure 6) and recorded five controlled source explosions located between 15 and 20 km from the array. Using several different array analysis techniques, we analyze the various signals from the explosions (including P wave arrivals and S wave coda) in the frequency band 2-26 Hz, to infer localized inhomogeneous velocity structure that may be associated with preferred polarization of ground motions.

Analysis of shear wave particle motions produced by the explosions showed that polarization directions changed smoothly across the 45 by 60 m array, and were more influenced by the site than by the location of the explosions. Lateral gradients in near-surface shear wave velocity are likely to cause these resonances. Changes in preferred polarization over short distances (<50 m) implies that the velocity heterogeneity responsible is located very near the receivers. Examination of explosion P wave arrivals also provide evidence of regional velocity inhomogeneity. We measured the arrival direction of the initial explosion P wave propagating across the array using three approaches: particle motion polarity, fitting a plane wavefront to relative arrival times, and frequency-wavenumber (f-k) analysis. Results of the three methods are consistent and reveal a systematic bias of 30-50° in the observed back azimuths of the P waves relative to known positions for the sources (Figure 7). It is unlikely that velocity structure far from the array is responsible for this strong deflection of the first arrival. Figure 8 shows a possible sub-array structure that may give rise to the observed bias. Quantitative modeling of potential structures is presently underway. We also analyzed the three-component signals throughout the P and S coda using f-k processing. We find a north-south preferred direction of coda arrival, which is not along the azimuth to the sources. We are using the three-component data to identify the polarization of these waves and to relate them to the preferred S wave polarizations.

3. Shallow Seismic Refraction Experiment

Our observations at ZAYA indicate that the seismic wavefield is strongly affected by local velocity inhomogeneity. In order to image the shallow velocity structure beneath ZAYA, we conducted a refraction experiment in August of 1992. Figure 6 shows the location of our two refraction lines relative to the dense array at ZAYA. The instrumentation consisted of a 64 channel, portable, PC-based recording system designed by W.H.K. Lee (Lee and Dodge, 1992), 23 Mark Products L-22, three-component geophones, an air-powered shear-wave generator designed by Liu et al. (1988) and a hammer P wave source. The source-receiver geometry is

shown in Figure 9 and consisted of two orthogonal rows of twelve sensors with 10 m spacings. Shear wave sources were detonated repeatedly at the ends of each line of geophones and at the center of the array (Figure 9). The sledge hammer source was used at each geophone location as well as at each of the shear wave source locations.

The air-powered, impulsive shear wave source and the hammer, produced clean, repeatable SH and P pulses. Multiple signals from each source location were stacked to improve the signal-to-noise ratio. Figure 10 shows profiles of stacked P and SH signals recorded on the north-south line with sources detonated at both the south end of the line (Figure 10a) and the north end of the line (Figure 10b). The reversed profiles reveal very different waveforms indicating a strongly varying velocity structure beneath the sensors. We will use this data to determine the shallow velocity structure beneath ZAYA and relate our results to the wavefield characteristics determined from the dense array.

References

Bonamassa, O., J.E. Vidale, H. Houston, and S.Y. Schwartz, 1991. Directional site resonances and the influence of near-surface geology on ground motion, *Geophys. Res. Lett, 18,* 901-904.

Lee, W.H.K., and D.A. Dodge, 1992. A course on: PC-based seismic Networks, U.S. Geol. Surv. Open-file Report 92-441, 535 pp.

Liu, H.P., R.E. Warrick, R.E., Westerlund, J.B.Fletcher, and G.L. Maxwell, 1988. An air-powered impulsive shear-wave source with repeatable signals, *Bull. Seismol. Soc. Am., 78,* 355-369.

Shih, X., R. Meyer, and J. Schneider, 1989. An automated, analytical method to determine shear-wave splitting, *Tectonophysics, 165,* 271-278.

Publications

Bonamassa, O., J.E. Vidale, W. Lee, and H. Liu, 1992. The Relation Between Ground Motions and Near-Surface Geology, Trans. Am. Geophys. Union, 73, 338.

Xu, Z., T. Lay, and S.Y. Schwartz, 1992. Seismic Wavefield Analysis Using a Very Small Dense Array, Trans. Am. Geophys. Union, 73, 367.

Zayante Seismic Experiment Team, 1992. Zayante Seismic Experiment: Data Report, U.S. Geological Survey Open-File Report, in press.

Zhang, Z. and S.Y. Schwartz, 1992. Seismic Anisotropy in the Crust of the Loma Prieta Rupure Zone, Trans. Am. Geophys. Union, 73, 402.

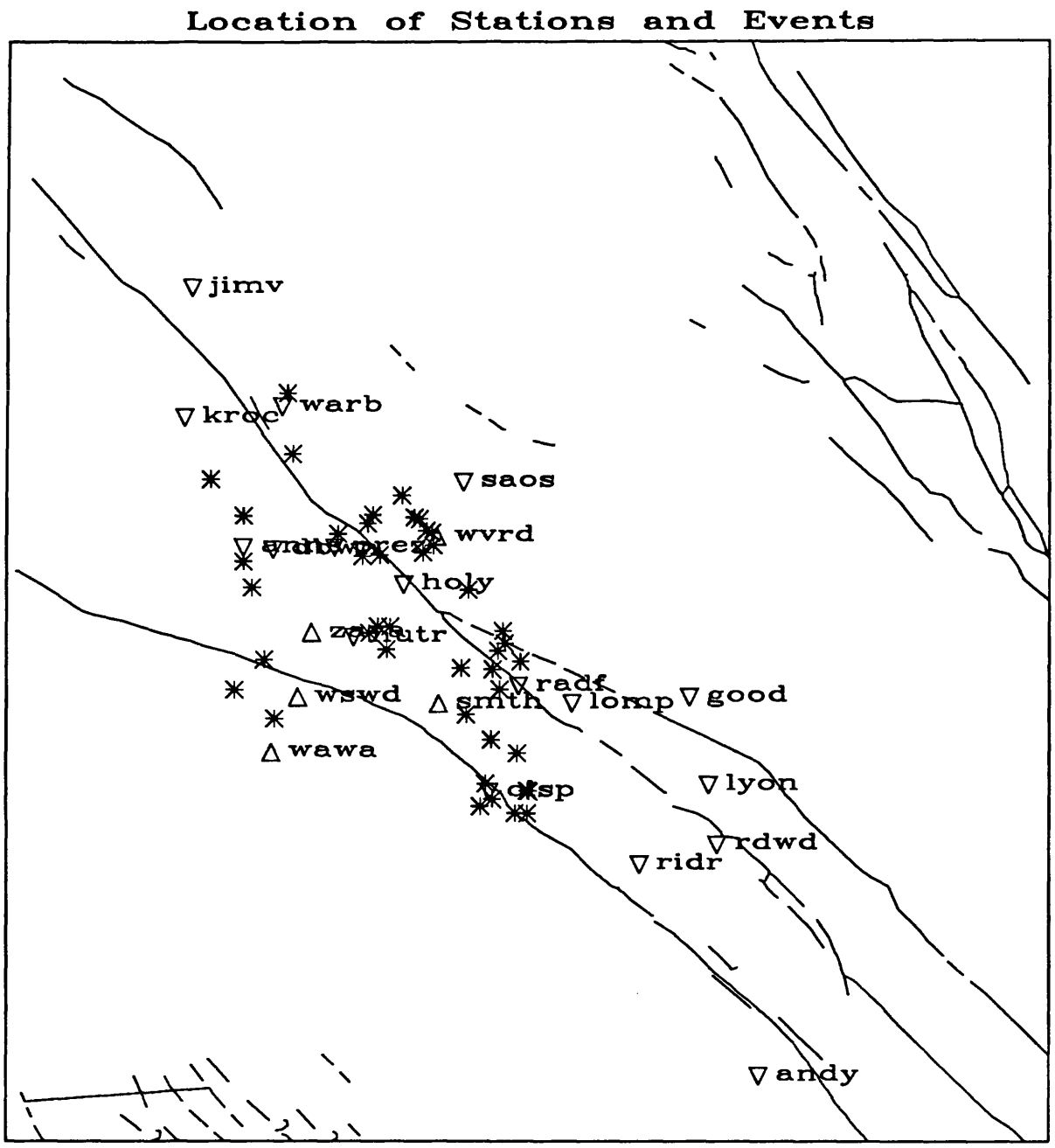

Fig. 1. Map showing location of Loma Prieta aftershocks (stars) and PASSCAL stations (triangles) used for the study of seismic anisotropy. Analysis on data from stations indicated with upward directed triangles has been completed and results are presented in this report.

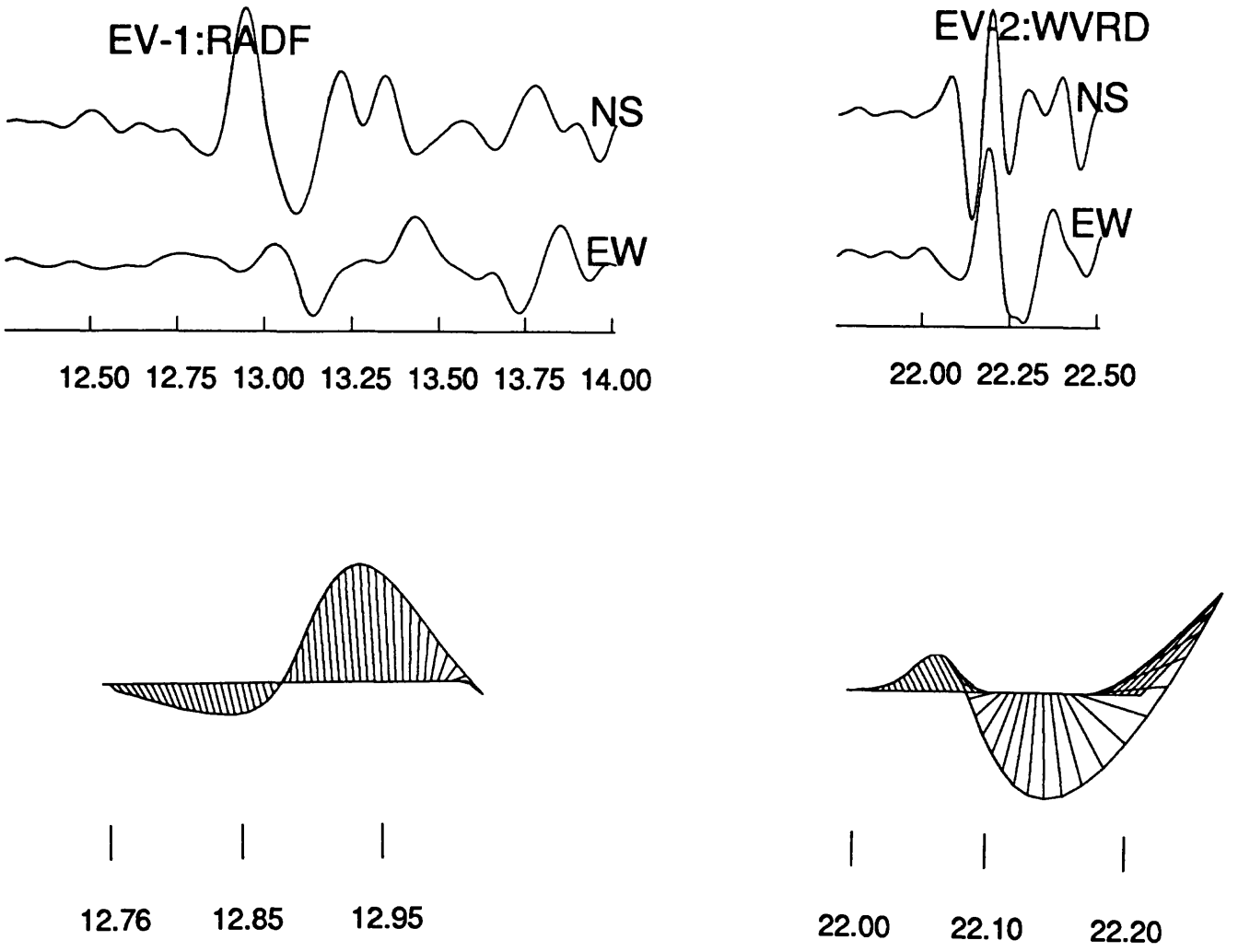

Fig. 2. Horizontal component S wave seismograms and polarization vector plots as a function of time for two earthquakes recorded at different stations. The polarization plot for event 1 indicates linear motion throughout the initial shear wave arrival. The polarization plot for event 2 indicates initial linear motion that abruptly changes to elliptical shortly after the onset of the shear wave. This behavior is suggestive of seismic anisotropy.

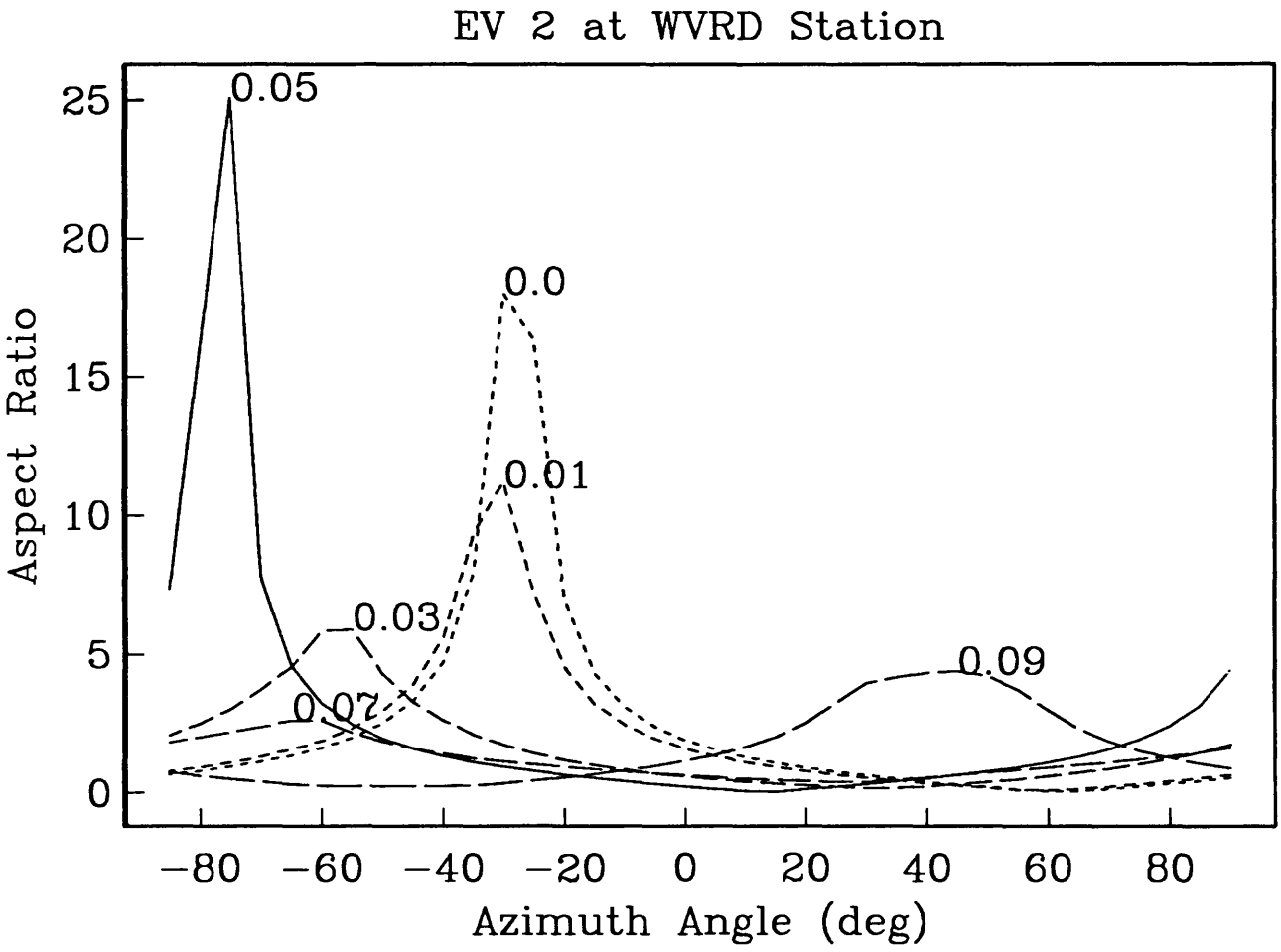

Fig. 3. Plot of aspect ratio versus polarization direction for initial shear wave as a function of different time delays of the fast wave. With no time delay, maximum linearity is obtained with a polarization direction of 330°. Maximum linearity is obtained when the fast wave is delayed by 0.05 s resulting in a polarization direction of 290°, consistent with the polarization at the source expected from the focal mechanism.

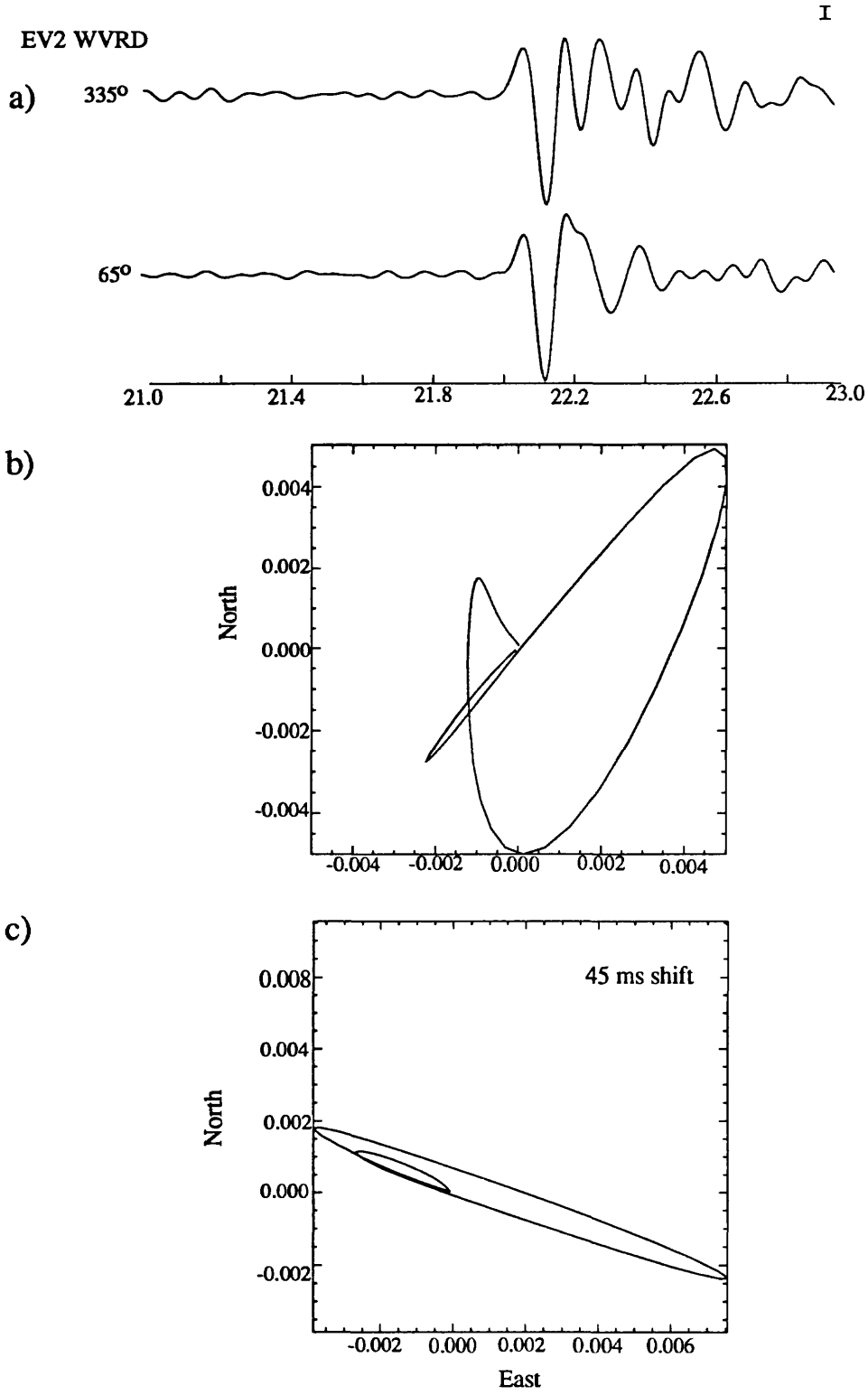

Fig. 4. a) A rotation of 335° and a delay time of 0.045 s yields the largest cross-correlation of horizontal component seismograms indicating this direction as the fast direction of polarization. b) Particle motion plot for the first 0.2 s of the shear wave before time shift shows an initial linear direction of 340°(first 0.04 s) that abruptly changes to elliptical motion after arrival of the slow wave. c) Particle motion for the same time window after delaying the fast wave by 0.045 s indicates linear motion with a direction of 290° as expected from the focal mechanism for this event.

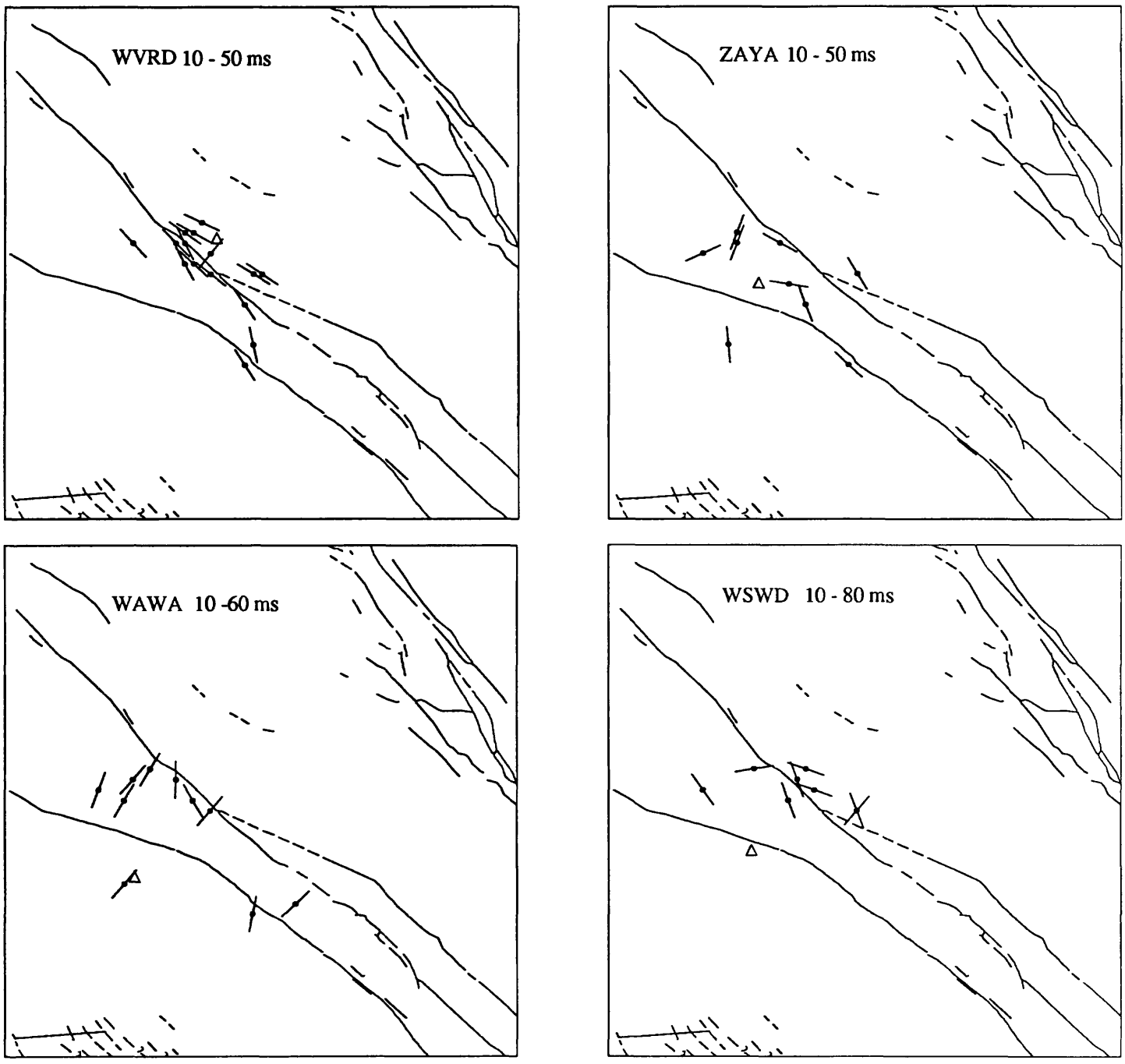

Fig. 5. Directions of initial polarization for many events determined at 4 stations. Polarization directions are plotted at the epicenter of each event for clarity. The range in delay time between the fast and slow wave at each station is indicated in milliseconds. Two dominant directions of polarization are observed, 140-160° and 20-40°.

Map of the 6-Station Array, Very Dense Array, and Shallow Refraction Seismology Lines in the Santa Cruz Mountains

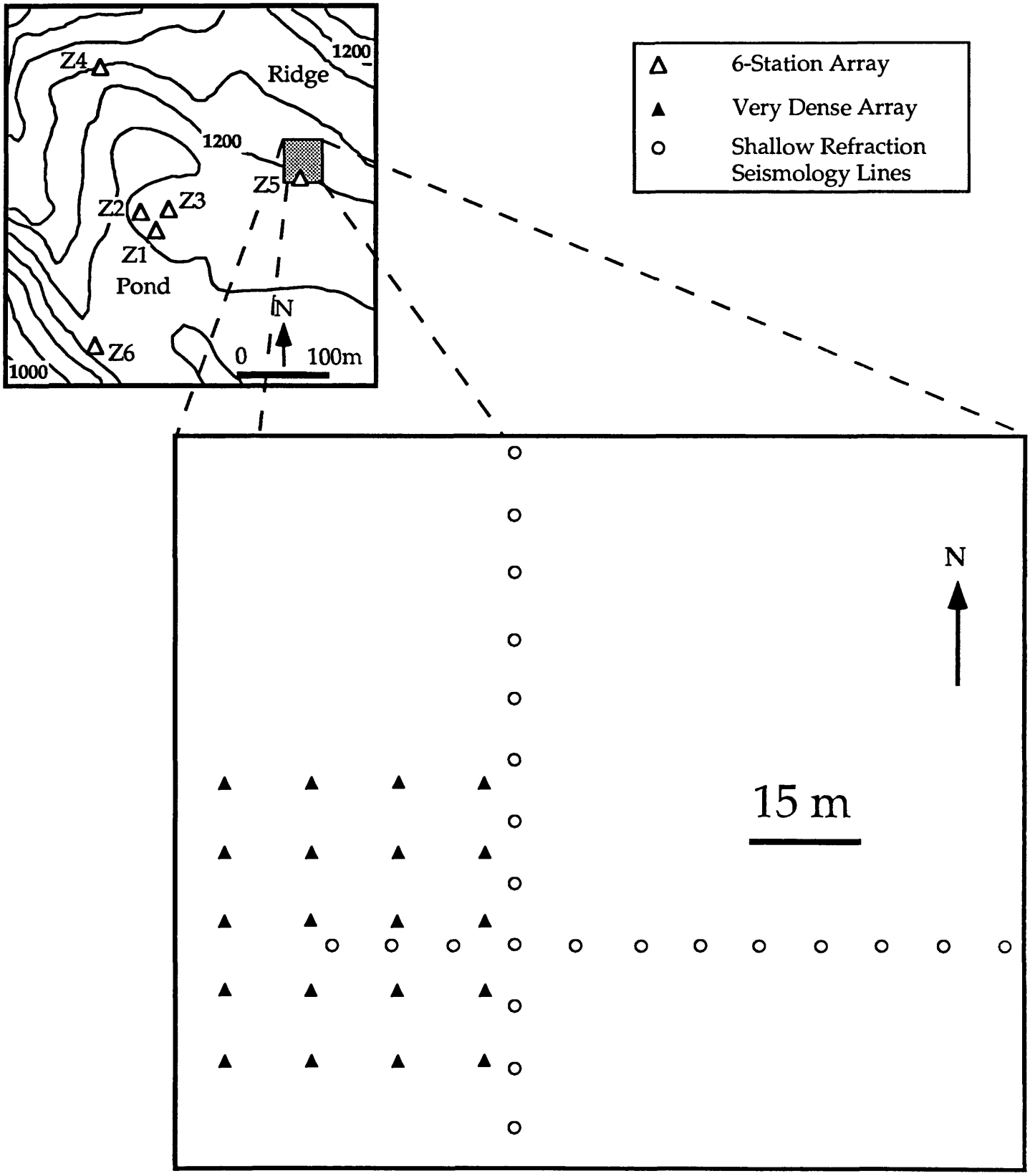

Fig.6 Map of the 6-station array, the very dense array, and the shallow refraction seismology lines deployed in the Santa Cruz Mountains.

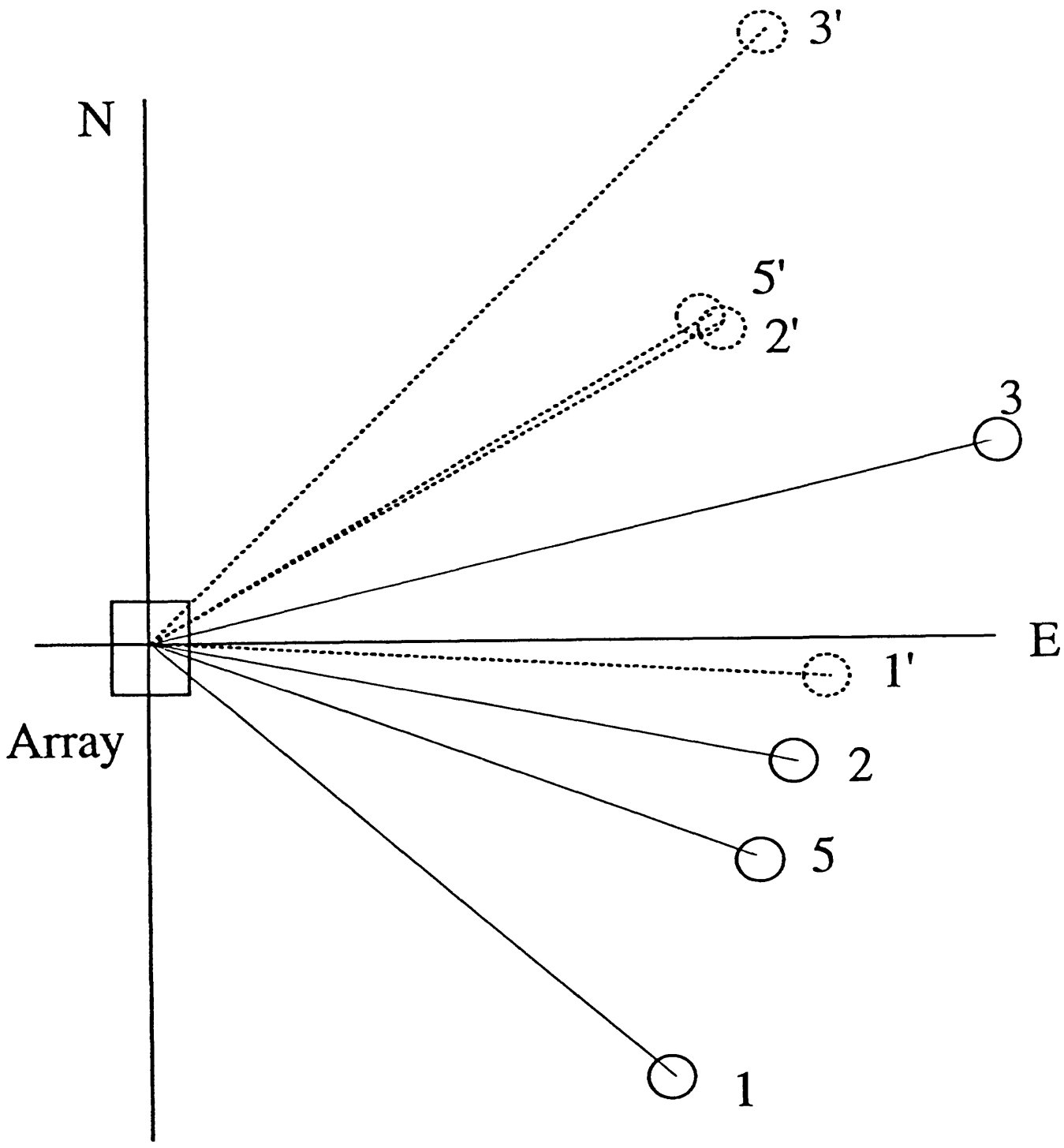

Fig. 7. Observed (dashed lines) and expected (solid lines) direction of back azimuth of the first P wave from 4 chemical explosions recorded at the dense ZAYA array. A systematic bias of 30-50° is observed for all 4 shots.

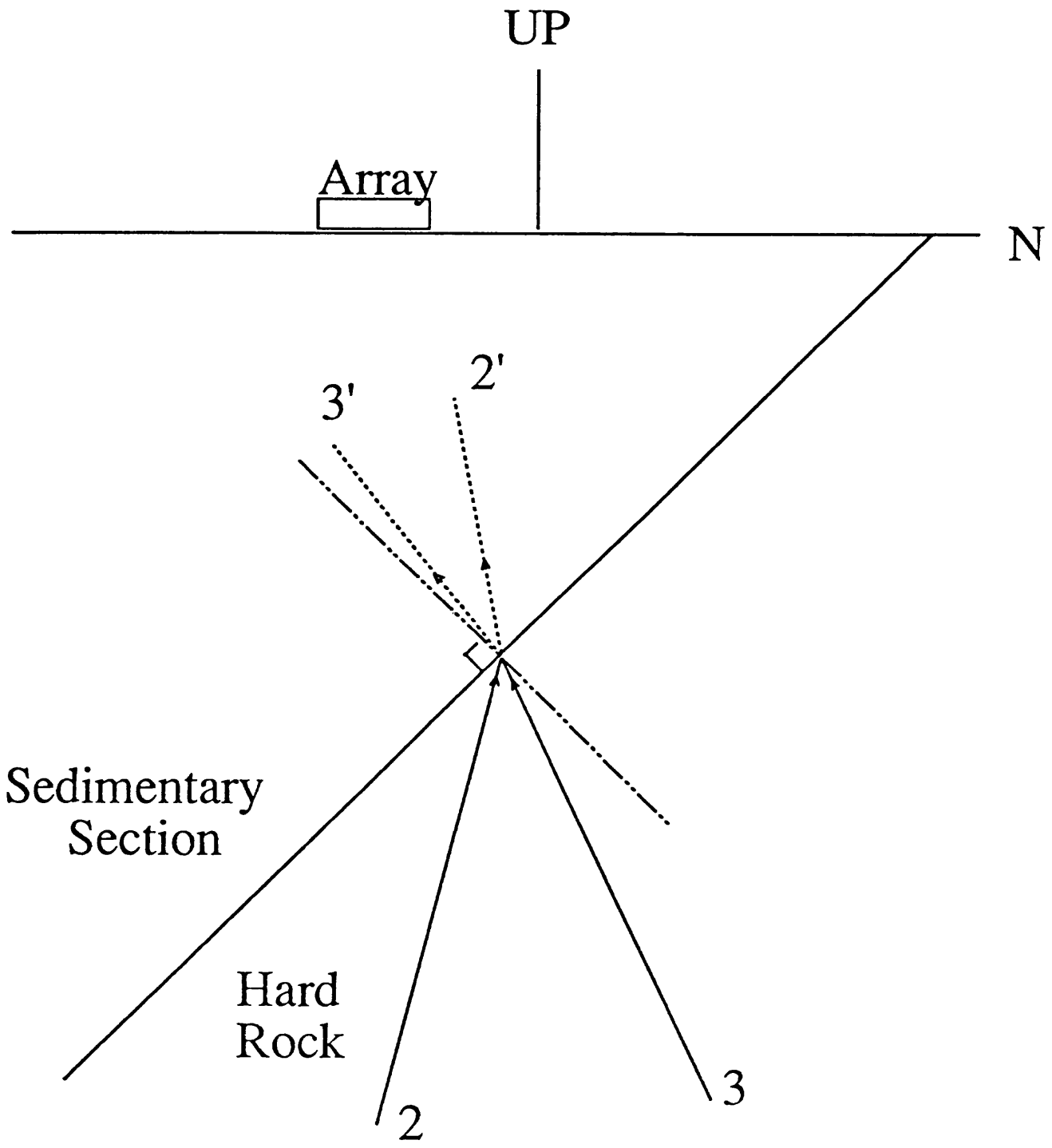

Fig. 8. Schematic cross-section of possible simple structure that may explain the systematic bias in back azimuth observations shown in Figure 7.

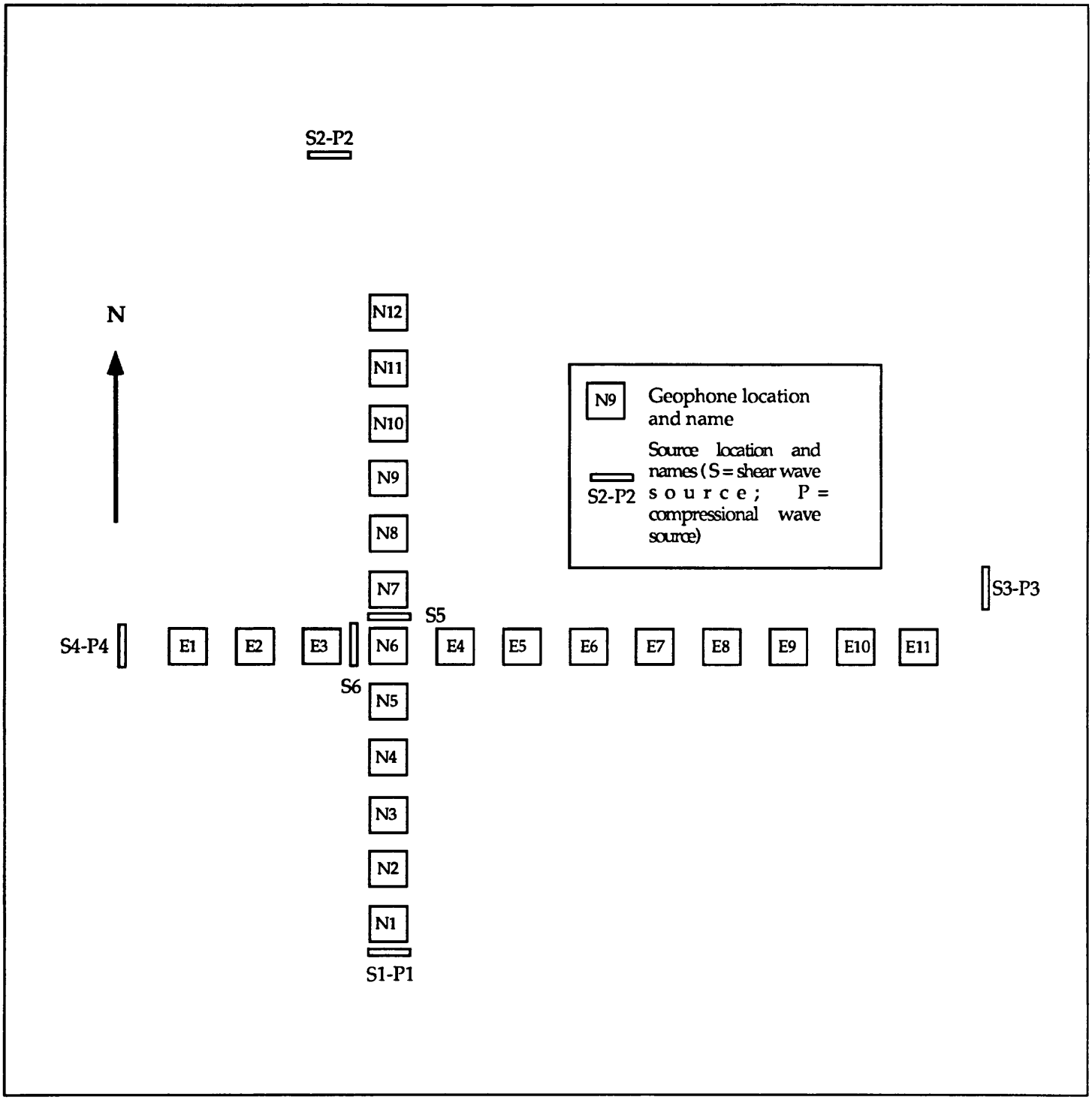

Fig. 9 Map of geophone and source geometries for refraction experiment. The map shows shear wave source locations and co-sited compressional wave sources. Compressional wave sources were also used at each geophone site (not shown).

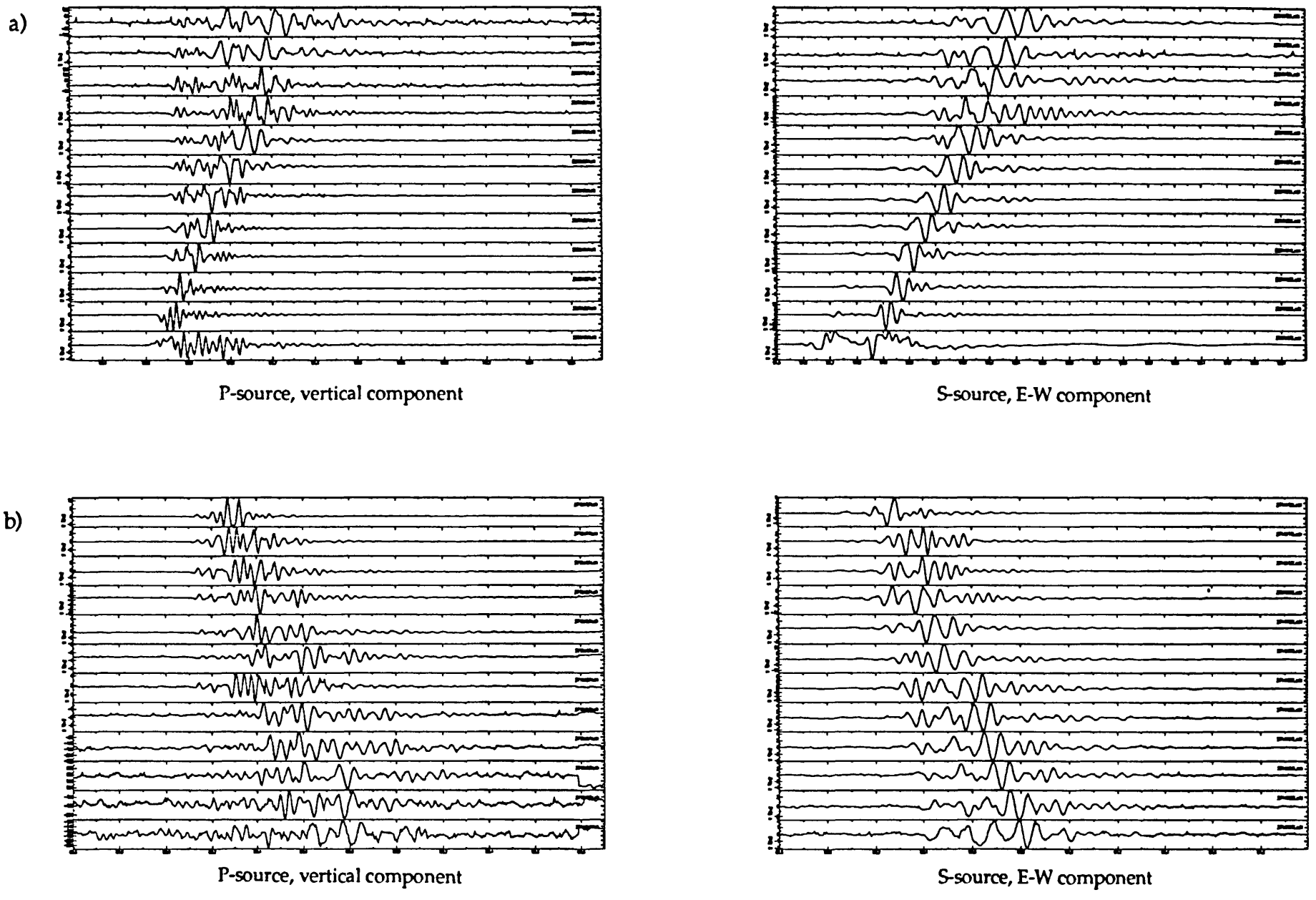

Fig. 10. Profile of normalized stacked signals recorded on the north-south line that lies along a topographic gradient. Sources are located at the south (a) and north (b) end of the line.

MECHANICS OF LITHOSPHERE PLATES

9960–03419

William D. Stuart and Ruth A. Harris
Branch of Tectonophysics
U. S. Geological Survey
Pasadena, California 91106
818 405-7816

Investigations

This project does theoretical analysis of earthquake faults. In FY92 we studied problems involving dynamic earthquake rupture across fault segments, static stress transfer to the San Andreas during the Landers earthquake sequence, interaction of large–scale tectonic plates, and precursory faulting at Parkfield.

2D and 3D Dynamic Rupture and Fault Segmentation

The magnitudes of most strike-slip earthquakes are controlled by their rupture lengths. Therefore if one could determine what controls the rupture length, one could determine the magnitude of a coming earthquake. The object of this study is to determine how fault geometry affects a propagating earthquake rupture. We specifically study 2D and 3D cases of parallel (non-collinear) strike-slip fault segments. The calculations simulate spontaneously propagating shear fractures. This work is with S. Day (SDSU).

Static Stress Changes from the June, 1992 Landers Earthquake Sequence

The goal of this study is to determine if coseismic slip of the Joshua Tree (M 6.1), Landers (M 7.5), and Big Bear (M 6.5) earthquakes loaded the nearby San Andreas fault closer to earthquake failure according to the Coulomb condition. The earth is represented by an elastic halfspace, and the appropriate stress components resolved on the San Andreas are calculated from static dislocation theory. This work is with R. Simpson.

Pacific-North America Plate Interaction

This work is an attempt to derive from mechanical principles the locations, slip rates, and lifetimes of major plate boundary faults in central and southern California since late Oligocene time. A special case is the present set of faults. The data most useful for testing the models for earlier times are measured offsets, rotations, and vertical motions of geologic units and crustal blocks. Results of this study may help explain average slip rates on modern seismically active faults, as well as apparent variations of brittle strength along strike.

Parkfield Precursors

A previously published model for earthquake instability at Parkfield has been modified to use the fault constitutive law developed by Dieterich, Kosloff, Liu, Ruina, Tse, and Rice. Instability models predict that precursory faulting occurs before the instability (mainshock). The anomalous fault slip causes ground deformation anomalies, which in some cases appear to be large enough to detect in field data before the mainshock. This work is with T. Tullis (Brown Univ.).

Results

2D and 3D Dynamic Rupture and Fault Segmentation

Two-dimensional finite-difference computer models were used to numerically simulate the interaction between an earthquake rupture and a geometrically segmented fault. Strike-slip earthquake ruptures are unlikely to jump across stepovers wider than 5 km. This conclusion assumes that the material in the stepover region is elastic, and that the faults do not merge at depth. When the effects of pore-pressure changes are included in the numerical simulations, changes in pore-pressure caused by a dynamically propagating earthquake rupture appear to inhibit an earthquake from jumping across dilational stepovers wider than 1 or 2 km. See Figure 1.

A 3D model for interaction between an earthquake rupture and a geometrically segmented fault was applied to the San Jacinto fault zone near Anza. Preliminary results for the Anza region suggest that if the dilational stepover at San Jacinto Valley is 4 km wide, and if the 1918 earthquake ruptured either the Claremont fault or the Casa Loma fault (both bound San Jacinto Valley), then the next Anza earthquake is unlikely to jump across San Jacinto Valley and rupture towards San Bernardino. The earthquake is unlikely to jump the step because the dynamic stress conditions will not be sufficient for failure.

Static Stress Changes from the June, 1992 Landers Earthquake Sequence

The Landers earthquake caused static normal stress changes of up to 10 bars on the San Bernardino segment of the San Andreas fault. These stress changes may have advanced the time of the next large earthquake on the San Bernardino segment of the San Andreas fault by 10–20 years. The location and mechanism of the Big Bear earthquake, which occurred 3 hours after Landers event, was consistent with loading by the coseismic Landers stress pulse.

Pacific-North America Plate Interaction

The plane–stress boundary value problem for several interacting plates has been posed and solved numerically. A plate may have any kind of boundary, i.e. transform, subduction, or ridge. Stresses are continuous across plate boundaries and satisfy a simple slip–rate dependent law. Displacement fields are continuous or discontinuous across plate boundaries, according to boundary type. Subducting plates have a fixed force representing slab pull. For the configuration of Pacific, North America, and Farallon plates in early to mid–Miocene time, and plausible assumptions of subduction pull, a southwest–northeast extensional stress field occurs in the part of the North America plate next to the Juan de

Fuca – Rivera transform boundary. This result could help explain the origin of eastern Mojave metamorphic core complexes.

A simplified version of the above model implies that the Garlock fault is caused, at least in part, by the stress concentration of the San Andreas bend near Gorman. Computed long term slip rate on the central Garlock is about 1/3 the San Andreas rate, in agreement with several reported field estimates.

Parkfield Precursors

Because the model simulates all stages of repeated earthquake cycles, one could in principle estimate values of model parameters (e.g. fault properties) using field data for a past stage and predict a future stage. At Parkfield we find that creep and trilateration data do not constrain model parameters well enough to predict the mainshock time with any useful precision. But if the next mainshock is assumed to have recurrence time and moment within the range of past values, predicted strain anomalies, as measured by extant borehole dilatometers and strainmeters, would be large enough to detect at least several weeks before the mainshock. Creep and trilateration precursors are too small to detect in this model, but were large enough to detect in a previous model based on a strain hardening and softening fault law. See Figure 2.

Reports

Banks, P. O., W. D. Stuart, and S. -W. Liu, Piezomagnetic fields of screw dislocation fault models, *Jour. Geophys. Res.*, *96*, 21,575–21,582, 1991.

Banks, P. O., W. D. Stuart, and Y. Sasai, Theoretical piezomagnetic field at Parkfield, (abstr.), *Eos Trans. AGU*, *73*, 397, 1992.

Eberhart–Philips, D., and W. D. Stuart, Material heterogeneity simplifies the picture: Loma Prieta, *Bull. Seismol. Soc. Am.*, *82*, 1964–1968, 1992.

Harris, R. A., Dynamic interaction of parallel strike-slip fault segment: some implications for the San Francisco Bay area, in Borchardt, G., et al., eds., *Proceedings of the Second East Bay Conference on Earthquake Hazards, CDMG Special Publication*, in press, 1992.

Harris, R. A., and S. M. Day, Dynamics of fault interaction: parallel strike–slip faults, *J. Geophys. Res.*, in press, 1992.

Harris, R. A., and R. W. Simpson, Static stress changes in southern California after the 1992 Landers earthquake (abstr.), *EOS Trans. AGU*, *73*, 373, 1992.

Harris, R. A., S. M. Day, and T. K. Rockwell, A 3-D dynamic rupture model of fault segmentation - with applications to the next Anza Gap earthquake (abstr.), *EOS Trans. AGU*, *73*, 389, 1992.

Harris, R. A., T. K. Rockwell, and S. M. Day, A 3-D dynamic rupture model for the next Anza Gap earthquake, (abstr.), *Seism. Res. Lett.*, *63*, 23, 1992.

Iyer, H. M., J. R. Evans, P. B. Dawson, and R. A. Harris, Seismic tomography of volcanic regions and individual volcanoes in western United States (abstr.), *Proceedings of the 29th International Geological Congress, Kyoto, Japan, 24 August - 3 September, 667*, 1992.

Roeloffs, E., and R. Harris, What will stop the next Parkfield earthquake? (abstr.), *EOS Trans. AGU*, *73*, 407, 1992.

Simpson, R. W., and R. A. Harris, Estimates of ongoing stress redistribution on southern California faults after the Landers earthquake (abstr.), *EOS Trans. AGU*, *73*, 373, 1992.

Stuart, W. D., Cause of the Garlock fault (abstr.), *GSA Abstracts with Programs*, *23(5)*, 198, 1991.

Stuart, W. D., Plate–induced Miocene extension in southern Calfornia (abstr.), *GSA Abstracts with Programs*, *24(7)*, 279, 1992.

Stuart, W. D., and T. E. Tullis, Instabilty model for repeated $M_W = 6$ earthquakes, (abstr.), *Eos Trans. AGU*, *73*, 406, 1992.

Tullis, T. E., and W. D. Stuart, Premonitory changes prior to a model Parkfield earthquake (abstr.), *Eos Trans. AGU*, *73*, 397, 1992.

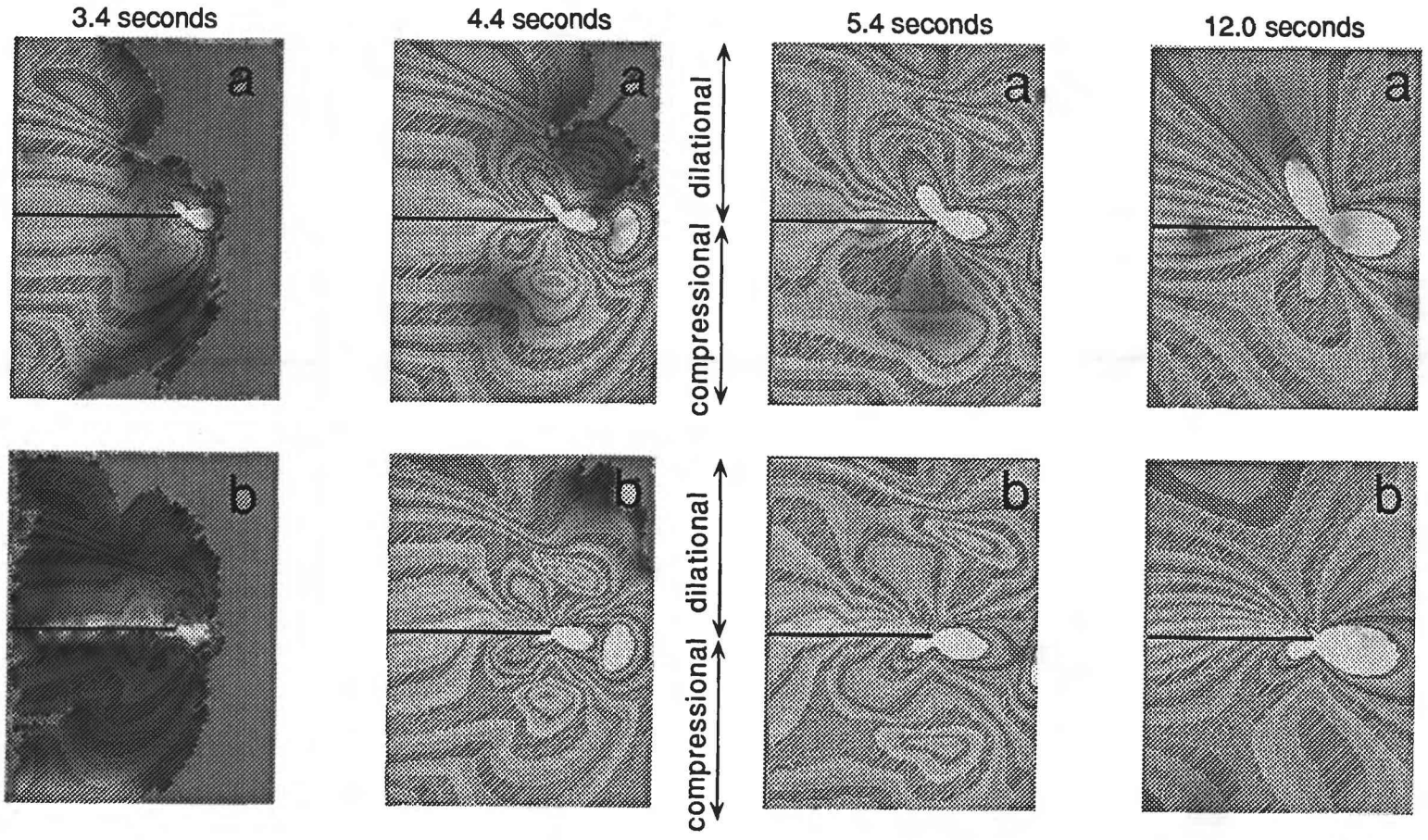

Figure 1. Two-dimensional failure stress for dynamically propagating ruptures [from *Harris and Day*, J. Geophys. Res., in press, 1992]. Case A assumes a 'dry' elastic medium and neglects the effects of changes in pore-fluid pressure, whereas case B includes the effects of pore fluid. For both cases, the dark line shows the location of the left-lateral strike-slip fault (shear crack), along which the rupture initially propagates. It takes the rupture 2.9 seconds to first reach the end of the fault. The light pattern shows where the rupture could jump to a second parallel fault segment, with regions above the dark line indicating locations of potential dilational stepovers, and regions below the dark line indicating locations of potential compressional stepovers. (a) This case assumes that the elastic medium between the two faults is 'dry', and ignores the effects of the dynamically propagating earthquake rupture on the pore fluids in the stepover region. The result is that wider dilational than compressional steps can be jumped, and that it takes longer to jump dilational steps than compressional steps (as can be observed by the time-dependent failure stress). (b) This case assumes that the elastic medium in the stepover region also contains 'undrained' pore fluids which are affected by the dynamically propagating rupture. The result is that the pore-pressure changes appear to inhibit jumps across dilational stepovers. The compressional stepovers appear to be relatively unaffected.

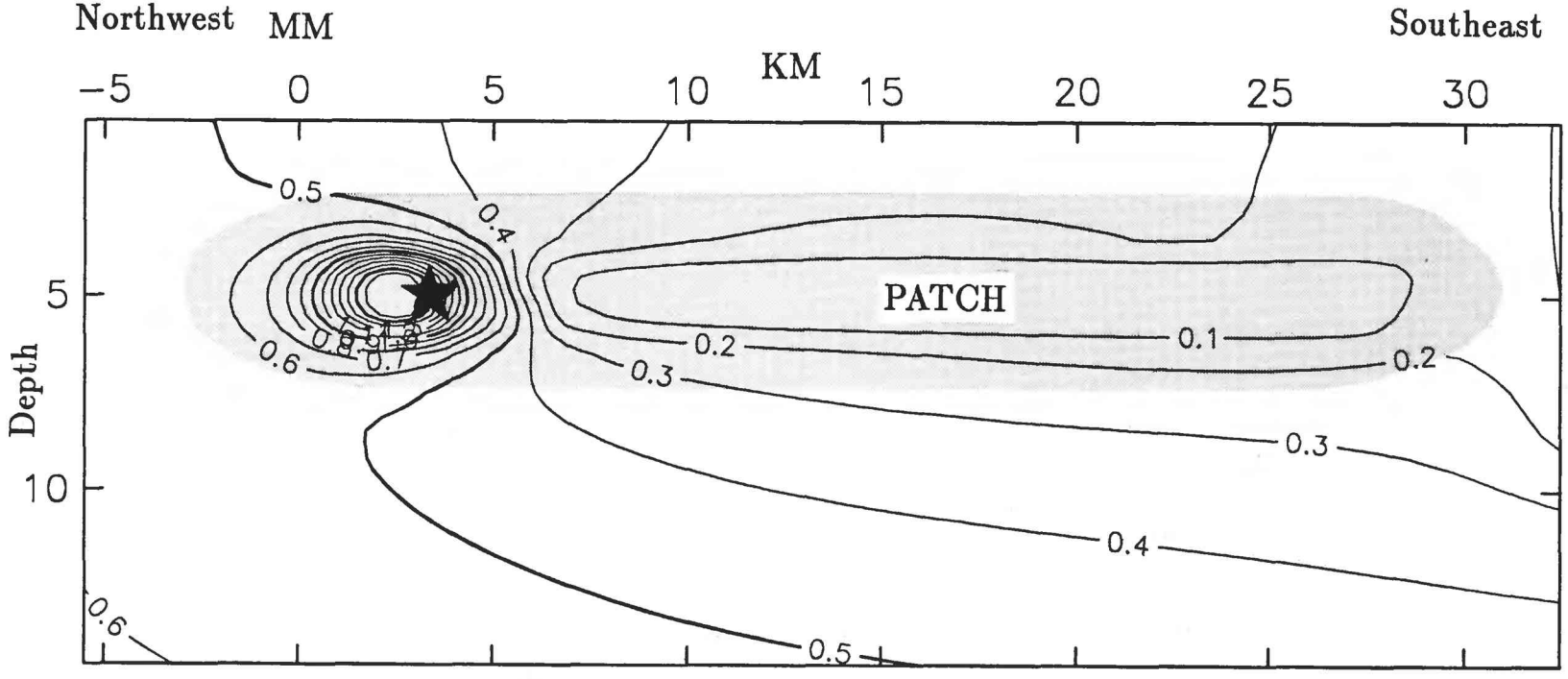

Figure 2. Accelerated preseismic slip on the San Andreas fault near Parkfield. Contours show fault slip velocity V scaled by plate slip rate $V_P = 35$ mm/yr at 0.1 yr before the model earthquake (instability). Anomalous slip rate $V/V_P > 0.5$ occurs near Middle Mt. (MM) and the theoretical focus (star). The anomalous slip rate increases with time and causes strain anomalies near the ground surface. The shaded area is a fault patch which fails before and during the mainshock.

INDUCED SEISMICITY AT BAD CREEK, SOUTH CAROLINA

1434-92-G-2199

Pradeep Talwani
Department of Geological Sciences
University of South Carolina
Columbia, South Carolina 29208
(803) 777-6449

INVESTIGATIONS:

(a) Field Studies: Monitoring of seismicity around Bad Creek Reservoir and Lakes Jocassee and Keowee was continued. Permanent stations were installed at JVW and CCK. Data from these and the Duke Power Company stations at BC, SMT, BG3 and MMC are collected at the Jocassee Dam (Fig. 1) and telemetered to USC, Columbia. These data are recorded digitally in an event triggered mode on a Puffin, and in an analog form on a tape recorder and on two Helicorders. The water levels at these lakes and Bad Creek Reservoir are monitored continuously as well as in the observation well OW3. OW3 is located about 1,000 feet (300m) from the reservoir and is open to a shear zone at a depth of 290 feet (88m) below the surface. The distance from the reservoir to the well along the shear zone is about 1,100 feet (335m).

(b) Modeling: (i) In view of the availability of detailed seismicity, groundwater, geological and in situ stress data at Monticello Reservoir, it was possible to study the role of elastic, undrained and drained responses in triggering earthquakes.

(ii) An analytical solution for the two-dimensional case of Biot's formulation for fluid infiltrated materials was developed. The model, similar to that of Roeloffs (1988) considers the changes produced in the environment of a reservoir due to a cyclic load. The mathematical solution was achieved by finding the eigenvalues and eigenvectors of the transformed system of equations expressed as function of stresses and pore pressure.

RESULTS:

The preliminary results of these investigations are summarized below.

(a) Groundwater Monitoring: Comparison of the water levels in OW3 and Bad Creek Reservoir (pool) following initial filling showed a systematic lag of about 80 hours. However, in 1992, there was a greater delay. Figure 2 shows a comparison of

pool and OW3 water levels for the period June 15 to August 29, 1992. The OW3 levels have been plotted on an enlarged scale to emphasize the similarity between the two curves. Cross correlation of the two time series showed that a lag of 98 hours fit the data well. In Figure 3 the pool levels have been shifted 98 hours. The two curves match rather well. These data imply a hydraulic diffusivity of about 3.2 x 10^3 cm^2/s. This value is towards the low end of diffusivity values found by Talwani and Acree (1984) for cases of reservoir induced seismicity.

The large fluctuations that were anticipated when the dam was built have not been realized so far. Compared to the largest drawdown possible (~100m) water level changes have not exceeded about 30m. The small change and the small volume of the reservoir are probable reasons why we have not observed an abrupt increase in seismicity.

(b) Seismicity Monitoring: Most of the events recorded near Bad Creek are small (magnitude <0.0). However, we are continuing to monitor both the lake levels and seismicity in anticipation of changed conditions.

(c) Modeling Studies: (i) The results of an analysis of seismicity that occurred following the impoundment of Monticello Reservoir were published recently (August, 1992 BSSA). They suggest that, during the filling period, the instability resulted from elastic, undrained, and possibly the onset of drained response. Subsequently, the seismicity showed a more consistent pattern associated with diffusion of pore pressure.

(ii) The 2D model was used to find the largest change in strength for different stress regimes. Variations in change in strength with different physical parameters (Skempton's constant, hydraulic diffusivity, Poisson's ratio and frequency of lake level change) affected not only the magnitude but also the spatial distribution of weakened regions. The largest changes were found to occur near the edge of the reservoir.

REPORTS PUBLISHED:

Kusala Rajendran and Pradeep Talwani, The role of elastic, undrained, and drained response in triggering earthquakes at Monticello Reservoir, South Carolina, Bull. Seis. Soc. Am., 82, 1867-1888, 1992.

Roberto G. Ruiz, Mathematical modeling and monitoring of pore pressure in fractured crystalline-rock following reservoir filling. Masters Thesis, Department of Civil Engineering, University of South Carolina, Columbia, 108 & vi pp, 1992.

Pradeep Talwani, Kusala Rajendran, Roberto Ruiz and John Dickerson, On the mechanism of reservoir induced seismicity, presented at Workshop on Induced Seismicity, 33rd US Symposium on Rock Mechanics, p 179, June 1992.

K. Rajendran, P. Talwani and E. Roeloffs, Do elastic models explain reservoir induced seismicity? (abstract), EOS Trans. AGU, 73(43), Fall Meeting Suppl., 405, 1992.

Pradeep Talwani, Roberto Ruiz, John Dickerson and K. Rajendran. Temporal pattern of reservoir induced seismicity. (abstract), EOS Trans. AGU, 73(43), Fall Meeting Suppl., 405, 1992.

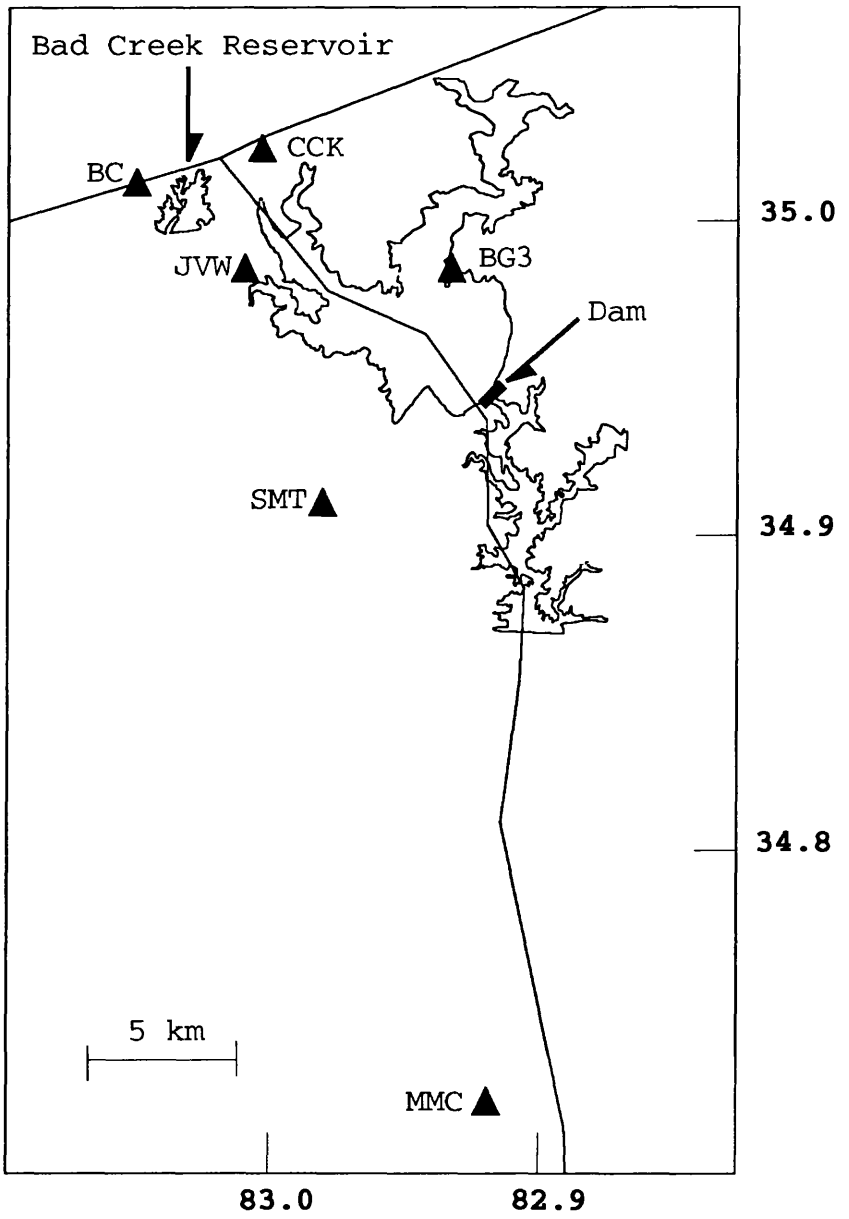

Fig.1 Locations of seismic stations near Bad Creek reservoir and Lake Jocassee. Data are collected at the Jocassee Hydro Dam and telemetered to USC.

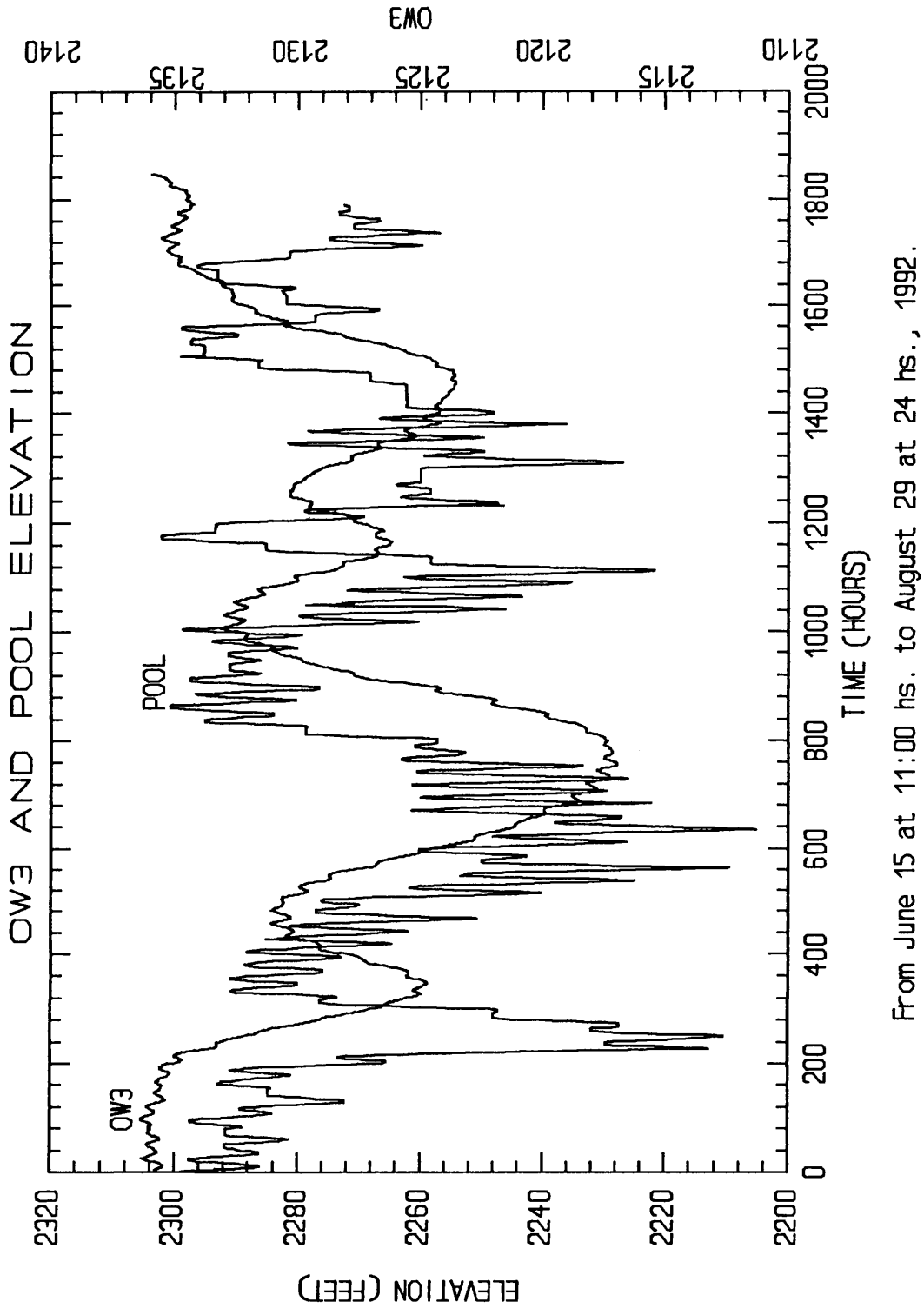

Figure 2. Water level in the pool and observation well OW3 for the period indicated. Note the difference in scale.

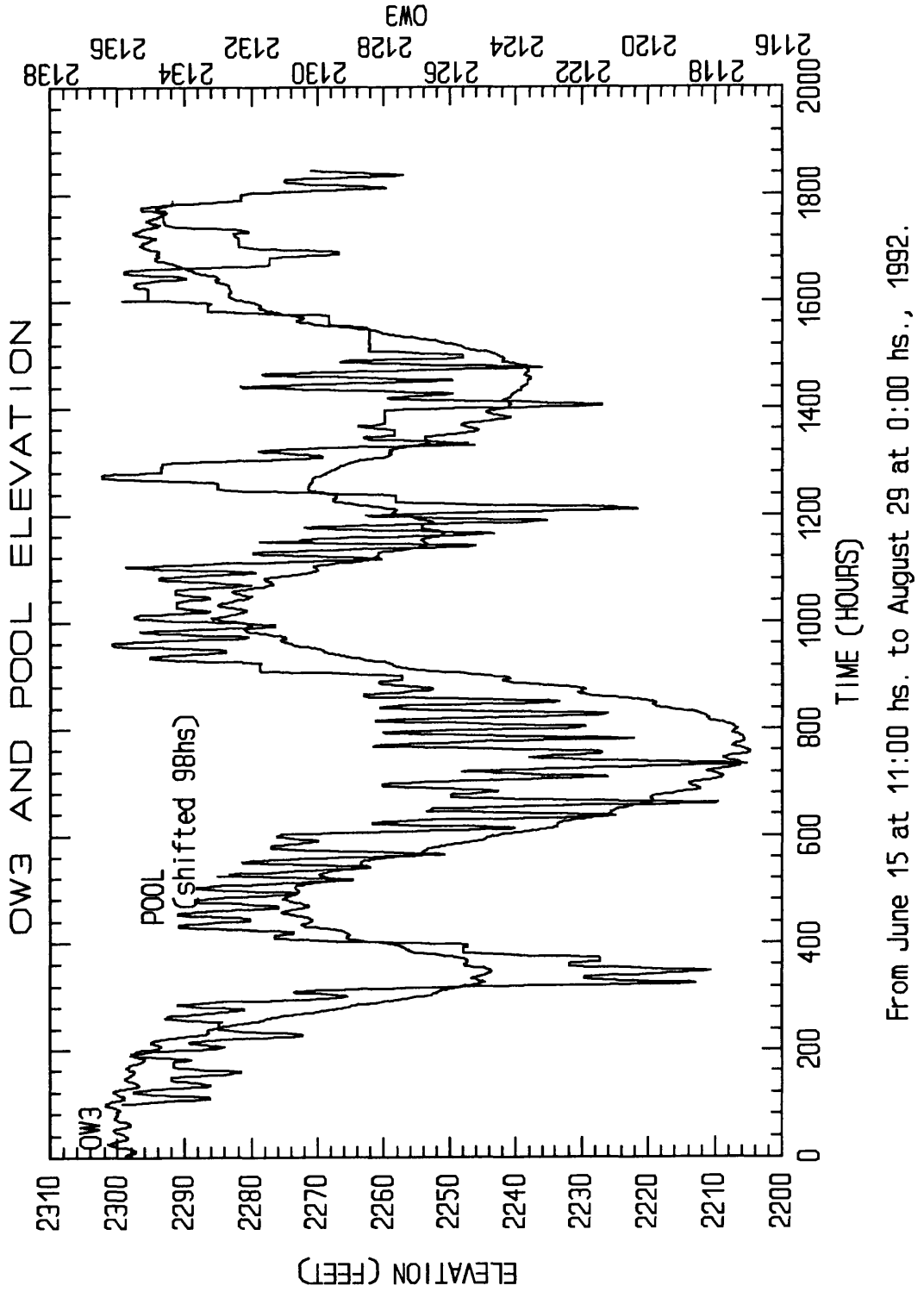

Figure 3. Same data as shown in Figure 2 with values for lake shifted 98 hours.

Earthquake Hazard Research in the Greater Los Angeles Basin and Its Offshore Area

Agreement # 14-08-0001-A0620

Ta-liang Teng and Thomas L. Henyey
Center of Earth Sciences
University of Southern California
Los Angeles, CA 90089-0740

BRIEF DESCRIPTION: This research is conducted in the Los Angeles metropolitan and offshore areas where urban centers of high population density coexists with high earthquake hazards. A special purpose seismic network has been established and has been in operation for the past 20 years. Against the noisy urban background, this network achieves its objective through deployment of both downhole and surface seismometers, through a diligent field instrument maintenance program, and through up-to-date data processing. Presently, the Los Angeles basin seismic network recording center at U.S.C. digitizes 70 channels of telemetered data from on land (surface and downhole) and offshore stations. This network is an important part of the research activity coordinated by the Southern California Earthquake Center (SCEC).

RESULTS OBTAINED: We have concentrated on advanced seismotectonic analysis based on data recorded by the network. This analysis goes beyond the conventional study of spatial and temporal distribution of seismic events. Shear-wave splitting and seismic waveform inversion are conducted using the network output for mapping of regional stress and source characteristics. A seismic database established for the Los Angeles basin is shown in Figure 1 (for the reporting year) and Figure 2 (for the period 1973 - 1992). Figure 3 shows the frequency of earthquake occurrence in the network coverage area. Clearly, 1991 is dominated by the occurrence of the mid-June M = 5.8 Sierra Madre earthquake and its aftershocks. Comprehensive studies have been continued on: S-wave splitting analysis; analysis of 3-D distribution of earthquakes along fault zones; seismotectonics of the Los Angeles basin; inversion analysis on the propagating fault rupture; site response and near-surface Q-values; and seismic response of a 2-D and 3-D sedimentary basin.

Recent improvements to the U.S.C. Los Angeles Basin Seismic Network (LABNET) consist of (1) operation of the PC-based backup recording system (16-bit 64-channel and expandable to 256 channels); (2) installation of the second generation of OTS (gain-ranging microprocessor-based telemetry) designed and constructed at USC to achieve an effective telemetry dynamic range of 120 dB; and (3) development and test the idea of neural network for intelligent event triggering in an urban environment and automation in seismic data processing.

Recent occurrences of the 1987 Whittier Narrows earthquake and the 1991 Sierra Madre earthquake present new views of the local seismotectonics. We have come to realize that:

1. Moderate-sized earthquakes do occur along faults previously deemed inactive, they do not necessarily occur along well-mapped universally recognized active fault strands.

2. These moderate-sized earthquakes have demonstrated that they are fully capable of producing higher than 0.5 g strong ground motion to the Los Angeles metropolitan area and can be very destructive.

3. These events are often located in the basement rocks beneath warps and uplifts in the overlying sedimentary section, which are common in the Los Angeles basin.

4. The Whittier Narrows earthquake occurred beneath a zone of uplifts stretching from Whittier, through downtown, to Malibu; these faults are collectively called the Elysian Park fault system. Other such zones may exist in the San Fernando Valley and South Bay area of Los Angeles

5. These kinds of earthquakes and their causal fault structures have not been adequately incorporated into earthquake hazards assessments for the Los Angeles area. For example, "design" earthquakes typically deal only with events on the San Andreas and the Newport-Inglewood faults.

RECENT RESESARCH FINDINGS:

Shear Wave Splitting and Stress Distribution in the Los Angeles Basin: On-scale short-period seismograms of numerous events of magnitudes between 2 - 4 from the portable RefTek recordings, from SCS array and from other field stations equipped with OTS telemetry are examined. Clear evidence of shear-wave splitting of 10-130 ms is found that implies a nearly NS regional compressional stress field. This finding is consistent with results from geological mapping and fault plane solutions. Furthermore, an inferred crack density of the crystalline basement is obtained. The quality of the on-scale seismic data from LABNET that makes this study possible(Figure 3).

Waveform Analysis: We are developing methodology that makes full use of waveform data from the LABNET with clear purpose of carrying out several significant scientific experiments. Short-period data is rich in information content and high in resolution when applied to the delineation of subsurface structures. However, the short-period waveforms can quickly lose their coherence in a complex medium where, beyond a certain frequency, a wavefield governed by a scattering process would then take over. The methodology we are working on spans a transition region between a deterministic approach where signals can be modeled as coherent propagating energy packets and a probabilistic approach where only the collective properties of the wavefield can be studied in a statistical sense.The frequency range of the transition region is probably covered by the band from 1 to 20 Hz -- a range that is mainly the operational band of current microearthquake networks. With large dynamic range and 3-component calibrated and matched seismic data provided by the OTS system, we plan to carry out a much more accurate study on coda waves. Moreover, we wish to explore the short-period limit on the applicability of waveform analysis and particle motion study that can only be performed over the coherent part of the signals. Available data from the LABNET are on-scale, matched 3-component, digital data from sources distributed throughout the Los Angeles basin and its offshore area. Different path combinations include paths through crystalline rocks, through basin sediments, and paths that traverse practically entirely inside a fault zone. The path differences are clearly manifested in the form of waveform differences.

REPORTS PUBLISHED

Li. Y.G., T.L. Teng, and T.L. Henyey, (1991) Shear-wave splitting observations and implications for the stress regime in the Los Angeles basin, Southern California, accepted with revision, Bull. Seism. Soc. Am.

Zeng, Y., K. Aki, and T.L. Teng, (1992) Mapping of high frequency source radiation for the Loma Prieta earthquake, California, Submitted to J. Geophys. Res.

Zeng, Y., K. Aki, and T.L. Teng, (1992) Source inversion of the 1989 Loma Prieta earthquake, California using isochron method, Submitted to Geophys. Res. Letters.

Zeng, Y., K. Aki, and T.L. Teng, (1992) Source inversion of the 1987 Whittier-Narrows earthquake, California using isochron method, Submitted to Bull. Seism. Soc. Am.

Chiu, H.C., Teng, T.L. , and Wong, H.L.(1991) Scattering effects on SH waves due to an irregular structure:A case at the SMART-1 Array site, Proceeding of the Geological Society of China, 34, 2, pp. 91-1110.

Su, F.,Aki, T., Teng, T.L., Zeng, Y., Koyonagi, S, and Mayeda, K. (1992) The Relation between site amplification factor and surficial geology in Central California, Bull. Seismol. Soc. Am., 82, No. 2, 580-602.

Wang, J. and T. L. Teng, (1992) Neural network-based detector for seismic triggering and P-picking, EOS, Trans. Am. Geophys. Union, 73

Teng, T.L., J. Qu, and J. Wang (1992) Propagation of surface waves in a 3-D basin, EOS, Trans. Am. Geophys. Union, 73

Qu, J. and T. L. Teng (1992) A constrained non-linear least squares method in the studies of seismic source, EOS, Trans. Am. Geophys. Union, 73

Li, Y.G. and T. L. Teng (1992) Seismic trapped waves along the San Jacinto fault at Anza, EOS, Trans. Am. Geophys. Union, 73

Li, Y.G., T.L. Teng and T.L. Henyey (1992) Shear-wave splitting in the Los Angeles basin, EOS, Trans. Am. Geophys. Union, 73

Henyey, T.L., Y.G. Li and T.L. Teng (1992) Observations of shear-wave splitting in source areas of 1992 Joshua Tree and Big Bear earthquakes, EOS, Trans. Am. Geophys. Union, 73

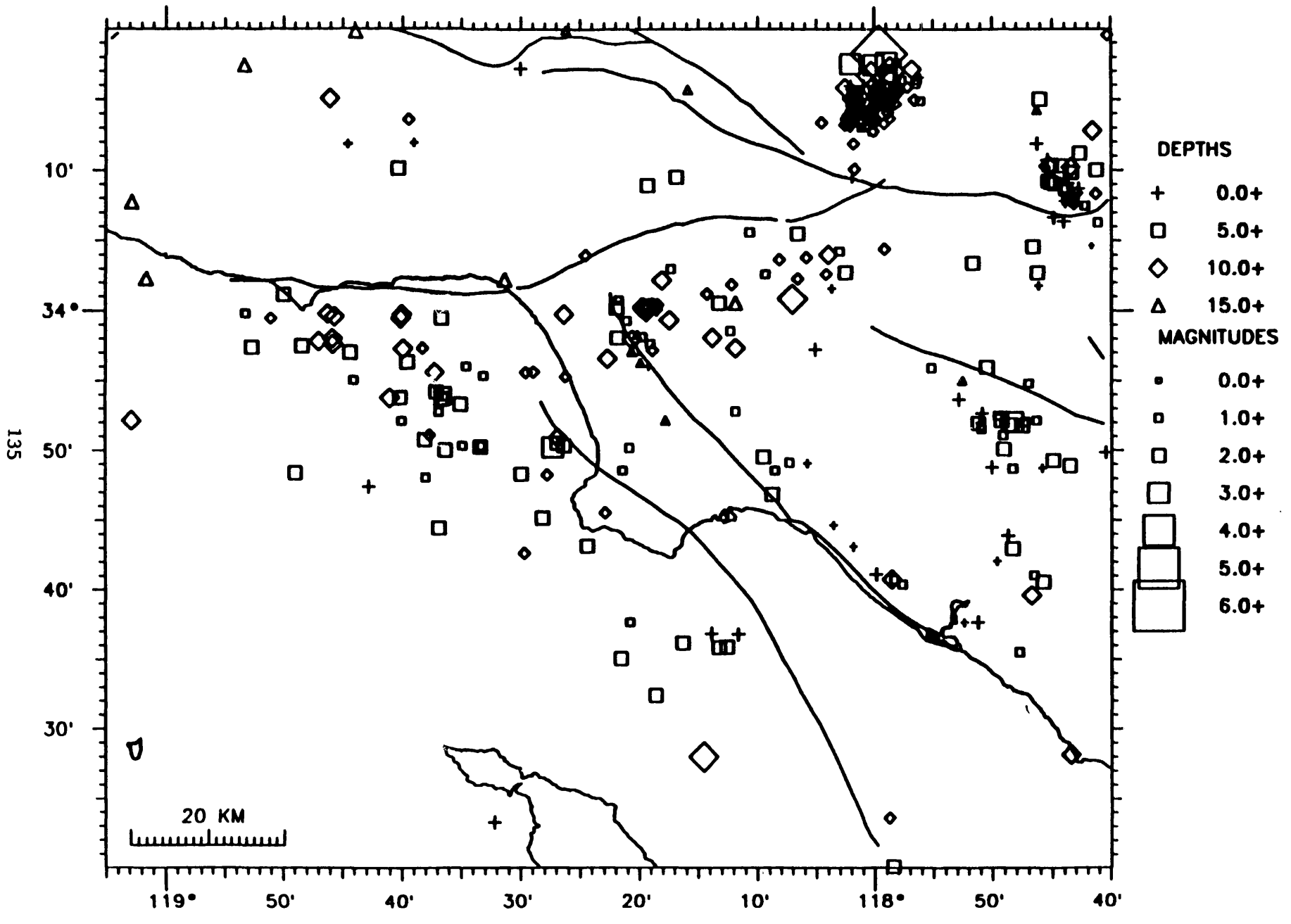
LOS ANGELES BASIN EARTHQUAKES
January - December 1991
DEPTHS
0.0+
5.0+
10.0+
15.0+
MAGNITUDES
0.0+
1.0+
2.0+
3.0+
4.0+
5.0+
6.0+
20 KM
10'
34°
50'
40'
30'
119°
50'
40'
30'
20'
10'
118°
50'
40'

Figure 1

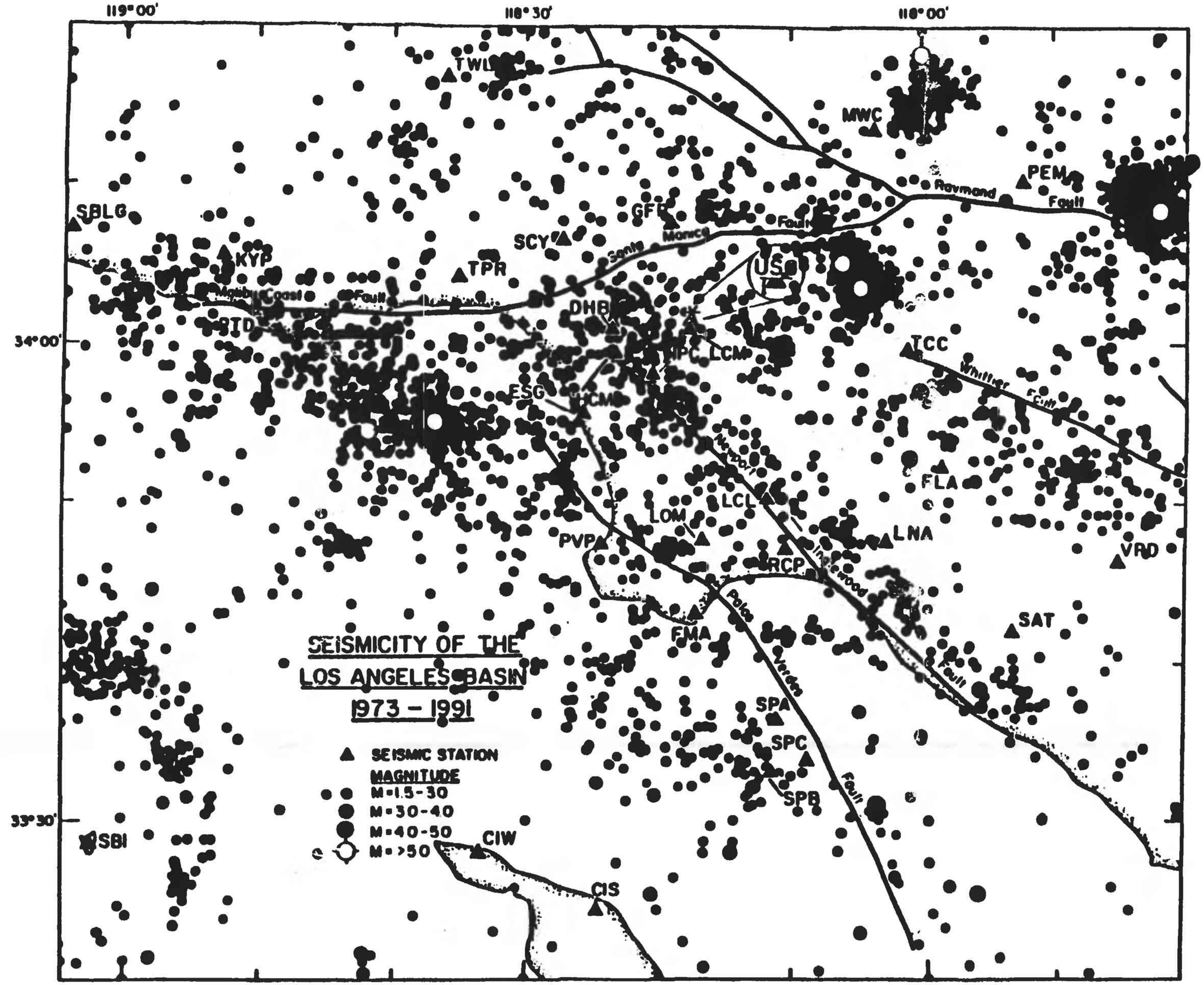
119°00'
118°30'
118°00'
34°00'
33°30'
SEISMICITY OF THE
LOS ANGELES BASIN
1973 - 1991
SEISMIC STATION
MAGNITUDE
M=1.5-30
M=30-40
M=40-50
M=>50
TWL
MWC
PEM
Raymond
Fault
SBLG
KYP
SCY
GFP
TPR
Santa Monica
Fault
USC
Malibu Coast
Fault
DHB
PTD
TCC
Whittier
Fault
LCM
ESG
FLA
LCL
LOM
PVP
LNA
VRD
RCP
Inglewood
Newport
Fault
Palos
Verdes
Fault
FMA
SAT
SPA
SPC
SPB
SBI
CIW
CIS

I

Figure 2

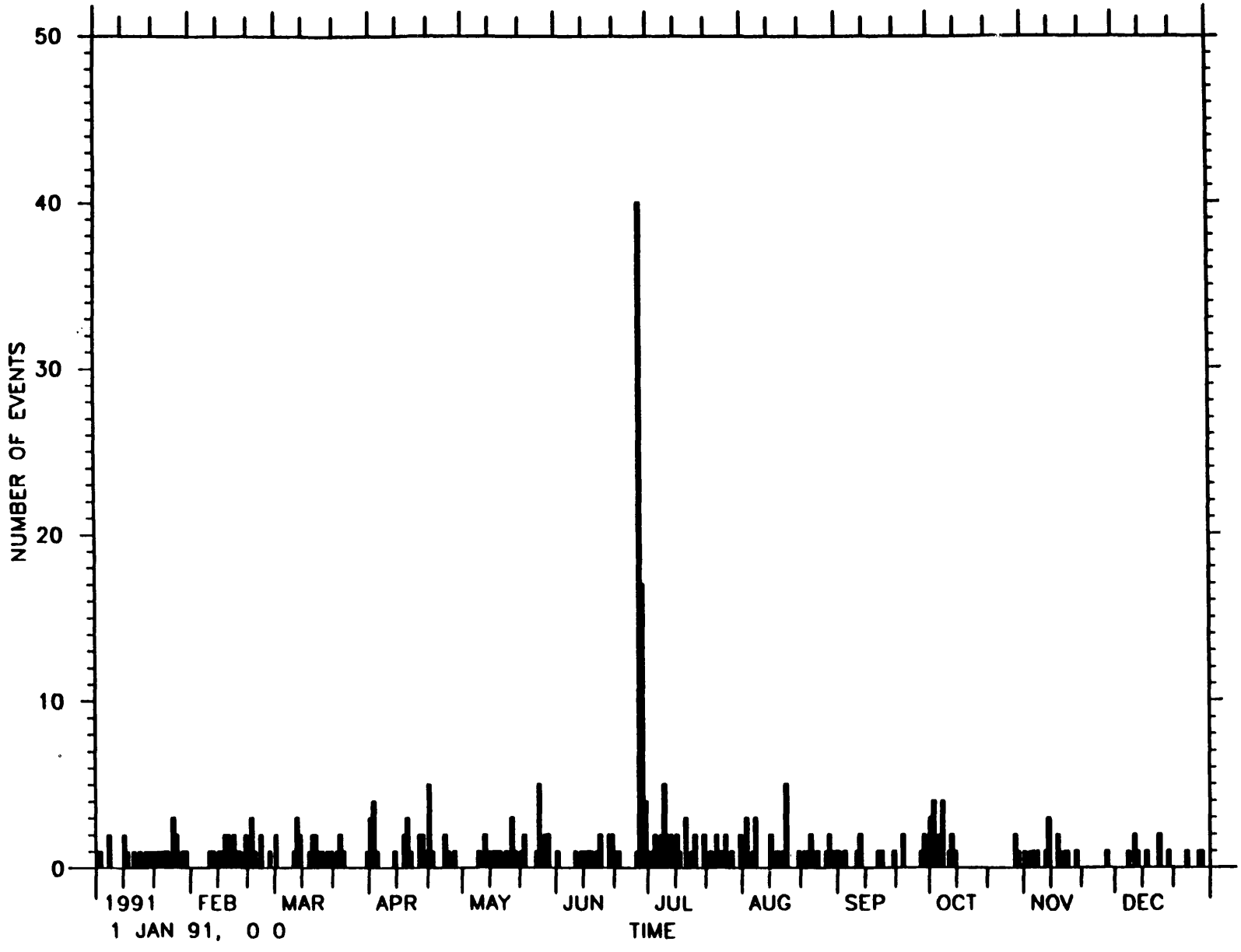
LOS ANGELES BASIN EARTHQUAKES
January – December 1991
NUMBER OF EVENTS
50
40
30
20
10
0
1991 FEB MAR APR MAY JUN JUL AUG SEP OCT NOV DEC
1 JAN 91, 0 0
TIME

Figure 3

The New England Seismic Network (Operated Collaboratively by M.I.T. and Boston College)

Contract no. 1434-92-A-0974

M. Nafi Toksöz
Massachusetts Institute of Technology
Earth Resources Laboratory
42 Carleton Street
Cambridge, Massachusetts 02142
(617)-253-7852

Investigations

The Earth Resources Lab at M.I.T. continues to maintain and operate the M.I.T. Seismic Network as part of the forty station New England Seismic Network under a collaborative arrangement with Weston Observatory of Boston College. The M.I.T. Seismic Network consists of nine digitally recorded short-period stations located in central and southern New Hampshire and eastern Massachusetts. Data from these stations are routinely analyzed to provide hypocentral, origin time and magnitude information for local earthquakes. Quarterly earthquake bulletins are published and available for the period October 1979 - March 1992. Figure 1 gives the station locations and seismicity for the reporting period January 1, 1992 - October 10, 1992. Two current research projects are focused on earthquake activity in central New Hampshire. One involves the relocation of earthquakes in that region, using a waveform correlation method, to search for significant changes in the spatial distribution of seismicity which might correlate with geologic structures. The second employs event pairs having similar hypocenters and focal mechanisms to estimate a source time function for the larger event. The source time function information can be used to study source parameters and the rupture process for the event.

Network Operations

The entire digital data archive (1980 to the present) is in the process of being converted to SAC binary format. The data will be archived on exabyte tape cartridges using the TAR tape facility to provide

convenient access for researchers at M.I.T. as well as other universities. In addition, an FTP anonymous account has been set up to provide on-line access to the most recent one year of digital waveforms and phase data files for local earthquakes. Details on accessing this account can be obtained by contacting Charles Doll at 617-253-7863 or doll@erl.mit.edu. The waveforms are in SAC binary format. These improvements will facilitate the transfer and analysis of seismic data between M.I.T. and Boston College using SAC, and will make the data available in a standard format used by many other institutions. To date, the procedure to download local earthquake data from our PC acquisition system to a Sun4 workstation and perform the basic analysis with SAC has been achieved, accelerating the process of locating earthquakes. Shortly, the same procedure will be implemented at Boston College, thus permitting new earthquake waveforms to be quickly exchanged between the two institutions and analyzed.

M.I.T. and Weston Observatory are conducting a joint project to upgrade and reconfigure the New England Seismic Network. Three-component wideband seismic systems will replace the present short-period, mostly vertical component only stations. On-site detection, digitization and recording will replace the present method of FM telemetry of analog signals and digitization at a central facility. Data transfer from the field unit to the central data collection node is accomplished through a modem-to-modem connection. These changes will improve the quality of data and greatly reduce the cost of data transmission. To date, three of these new units have been installed and are completely operational. With funds expected to be allocated by FEMA, M.I.T. and Boston College plan to begin deployment, during FY 1993, of an additional fifteen of these "new generation" seismic stations to replace the existing network.

Seismicity

Figure 1 shows the epicentral locations of local earthquakes within or adjacent to the M.I.T. Seismic Network for the period January 1 - October 10, 1992. Twelve earthquakes, with a magnitude range Mc 2.1 - 3.3, occurred during this period. No damage is known to have been caused by these events. Nine occurred in central New Hampshire, the area historically having the highest seismicity rate within the M.I.T. Seismic Network including two potentially damaging earthquakes in December 1940 (M_L=5.3 and 5.4; Ebel,

Somerville and McIver, 1986) and one in January 1982 (M=4.7) (Fig. 2). The recent nine and older events from this region (Fig. 2) suggest three linear trends of seismicity; A being ENE-WSW, B NNW-SSE, and C NE-SW. The purpose of relocating the seismicity is to test the validity of the proposed trends in Figure 2. Digitally recorded earthquakes along a trend are subdivided into clusters and relocated using a cross-correlation technique. This technique has been tested successfully with NORESS and New England explosion data. Figure 3 shows the raw data recorded at Station ONH for the three earthquakes making up the easternmost cluster of Trend A (Fig. 2). Figure 4 shows the correlation windows for P and S, the autocorrelation of these phases for event pair 1-1, and the cross-correlations of these phases for event pairs 1-2 and 1-3. Identical S-P times measured between the P and S peak correlation amplitudes for different event pairs indicates the same source to receiver distance for all three earthquakes. This procedure, repeated for different stations at nearly perpendicular axes, is used to constrain the event cluster to much closer relative locations. Preliminary results show closer clustering for some subgroups than previously determined by routine analysis using the Hypo inversion program. Further work is planned to relocate clusters for the other proposed trends, and then attempt to associate the spatial pattern of the relocated events with potential causative structures in that region. If these inferred linear trends of seismicity are related to faults, the comparable lengths of the trends imply the potential for future damaging earthquakes similar in size to the December 1940 or January 1982 events (Fig. 2). The M.I.T. Seismic Network detects more seismicity in central and southern New Hampshire than the Boston College network because of closer recording stations to the events.

Another technique employing event pairs relocated to similar hypocenters is being tested to estimate the source time function of the larger event of a pair. The smaller event (treated as an empirical Green's Function, EGF) is deconvolved from the larger one to obtain the estimate (e.g. Li and Thurber, 1988). On October 6, 1992, a magnitude 3.3 earthquake occurred and was followed by a magnitude 2.7 aftershock. The almost identical hypocenters and same first motion distributions for both events suggested a similar focal mechanism. This earthquake pair provided an excellent example where the source time function could be estimated quickly as part of the routine analysis. The result for this pair is shown in Figure 5. The source time function can be used to compute source

parameters and to study the rupture process. In the future, additional data for these events will be acquired for the Boston College stations to greatly expand the azimuthal coverage. The digital event locations in Figure 2 are divided into two periods corresponding to the approximate starting dates of digital recording at M.I.T. (1980) and Boston College (middle of 1985). Those events recorded beginning in 1986 will be used to expand the study discussed here. By computing estimates of the source time function using data recorded over a wide range of azimuths, we may be able to determine the rupture directivity for a given event. This information can help constrain which nodal plane of a fault plane solution is the probable fault, the result being correlated with the trends of mapped geologic faults in the source region, if present, or spatial patterns of the seismicity. The locations of the December 1940 and the January 1982 earthquakes along the trends proposed in Figure 2 illustrate the importance of collecting more data for these studies to thoroughly investigate the relationship between the spatial distribution and source parameters of the seismicity in central New Hampshire and potential causative structures. In the future, the EGF and relocation methods may be applied to other seismically active regions of New England, such as Moodus, Ct. and Milo, Me.

References

Ebel, J. E., P. G. Somerville, and J. D. McIver, 1986. A Study of the Source Parameters of Some Large Earthquakes of Northeastern North America. J. Geophys. Res. 91, 8231-8247.

Li, Yingping, and C. H. Thurber, 1988. Source Properties of Two Microearthquakes at Kilauea Volcano, Hawaii. Bull. Seis. Soc. Am. 78, 1123-1132.

M. I. T. Network Seismicity, January 1 — October 10, 1992

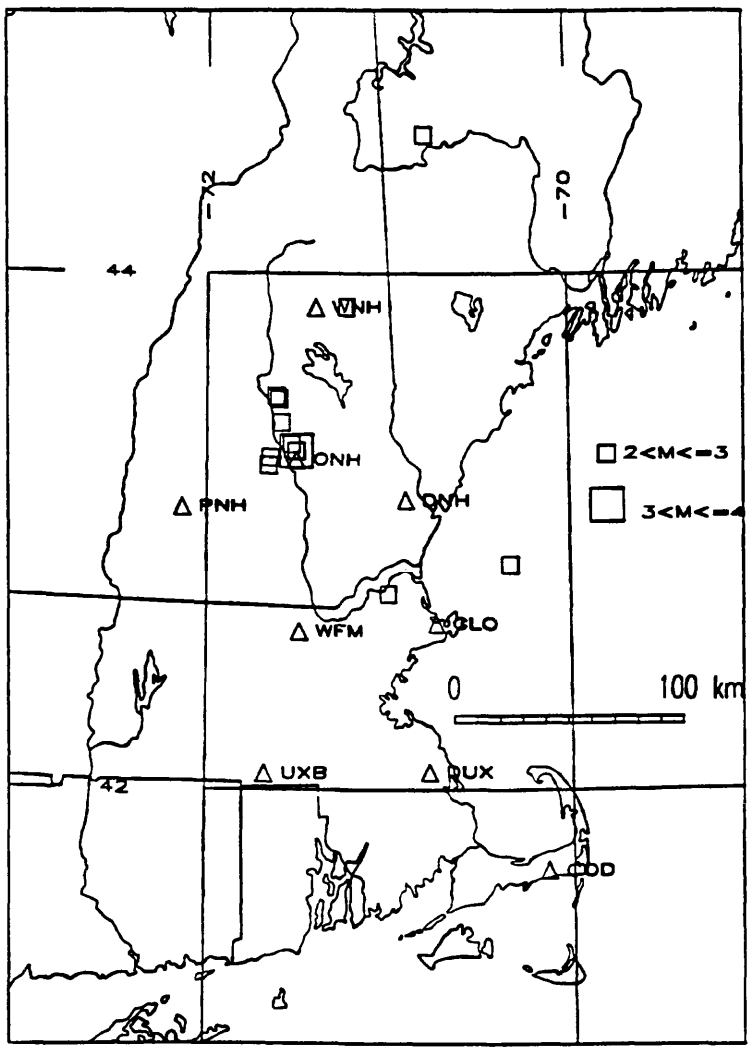

Fig. 1. Seismicity of New England recorded by the M.I.T. Seismic Network for the period January 1 - October 10, 1992. A majority of events is concentrated along a trend similar to that of the Merrimack River in central New Hampshire.

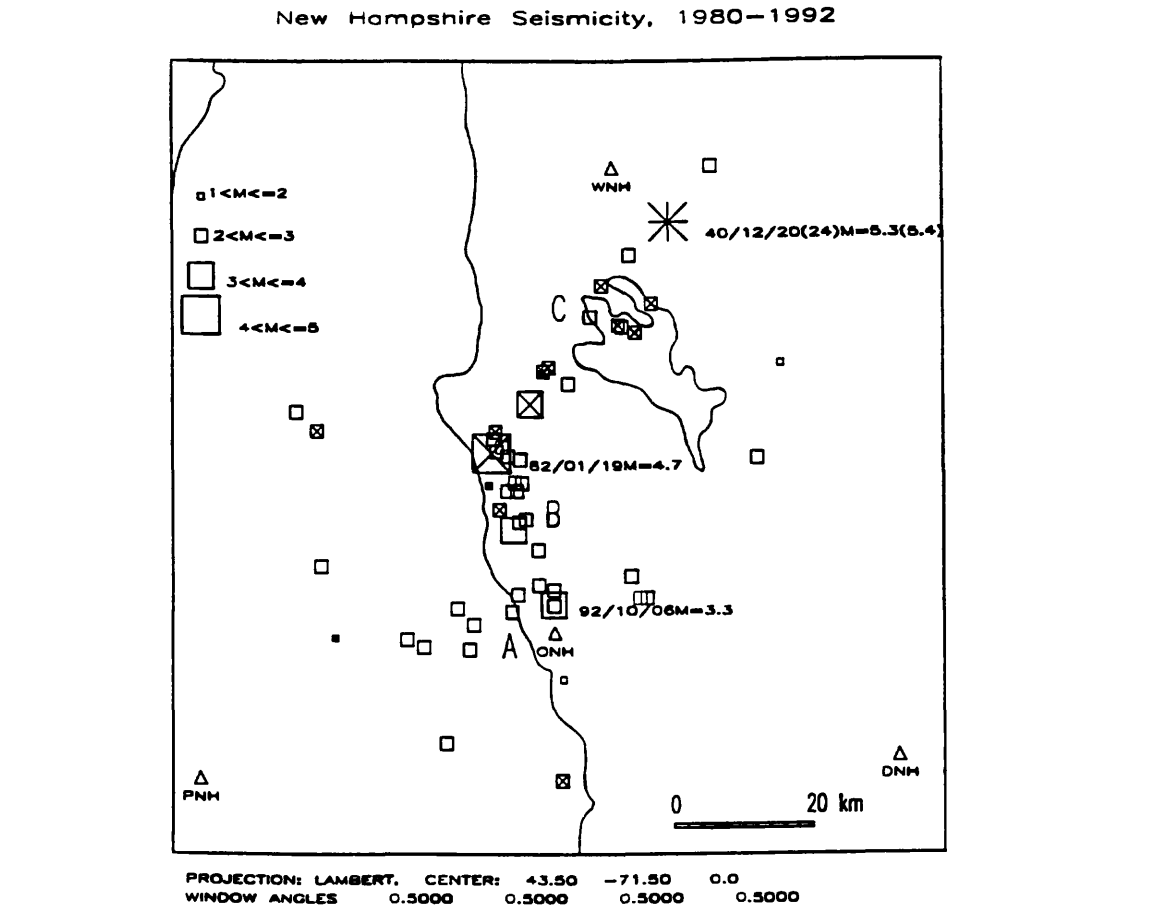

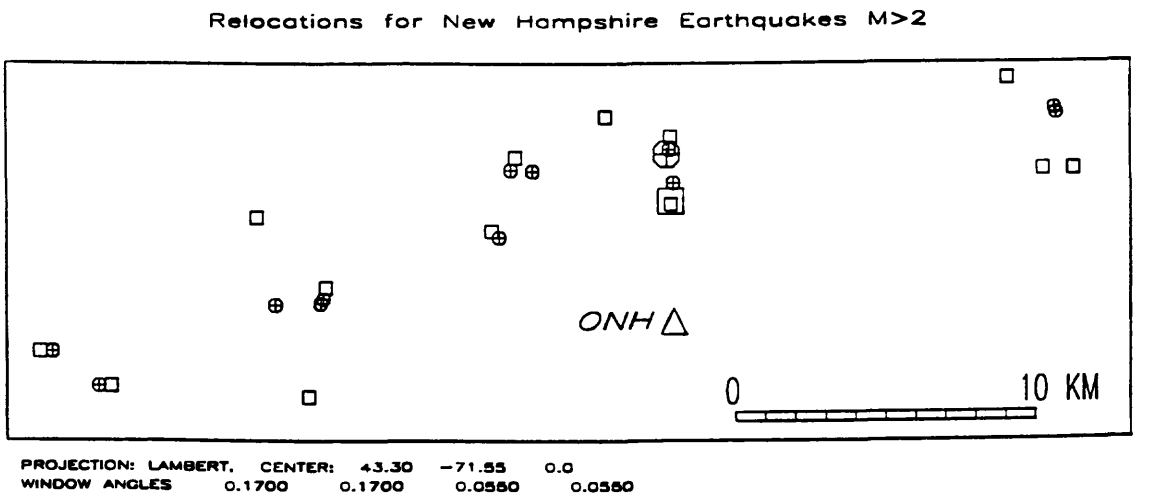

Fig. 2. Top figure is central New Hampshire seismicity recorded by the M.I.T. Seismic Network from 1980 - October 10, 1992. Three linear trends of seismicity are proposed. Trend A is ENE-WSW, B NNW-SSE, and C NE-SW. The boxes with an X and open boxes represent respectfully locations for digital events for 1980-1985 and 1986 to date. Bottom figure is original locations (boxes) and relative relocations (crosses) of clusters along trend A.

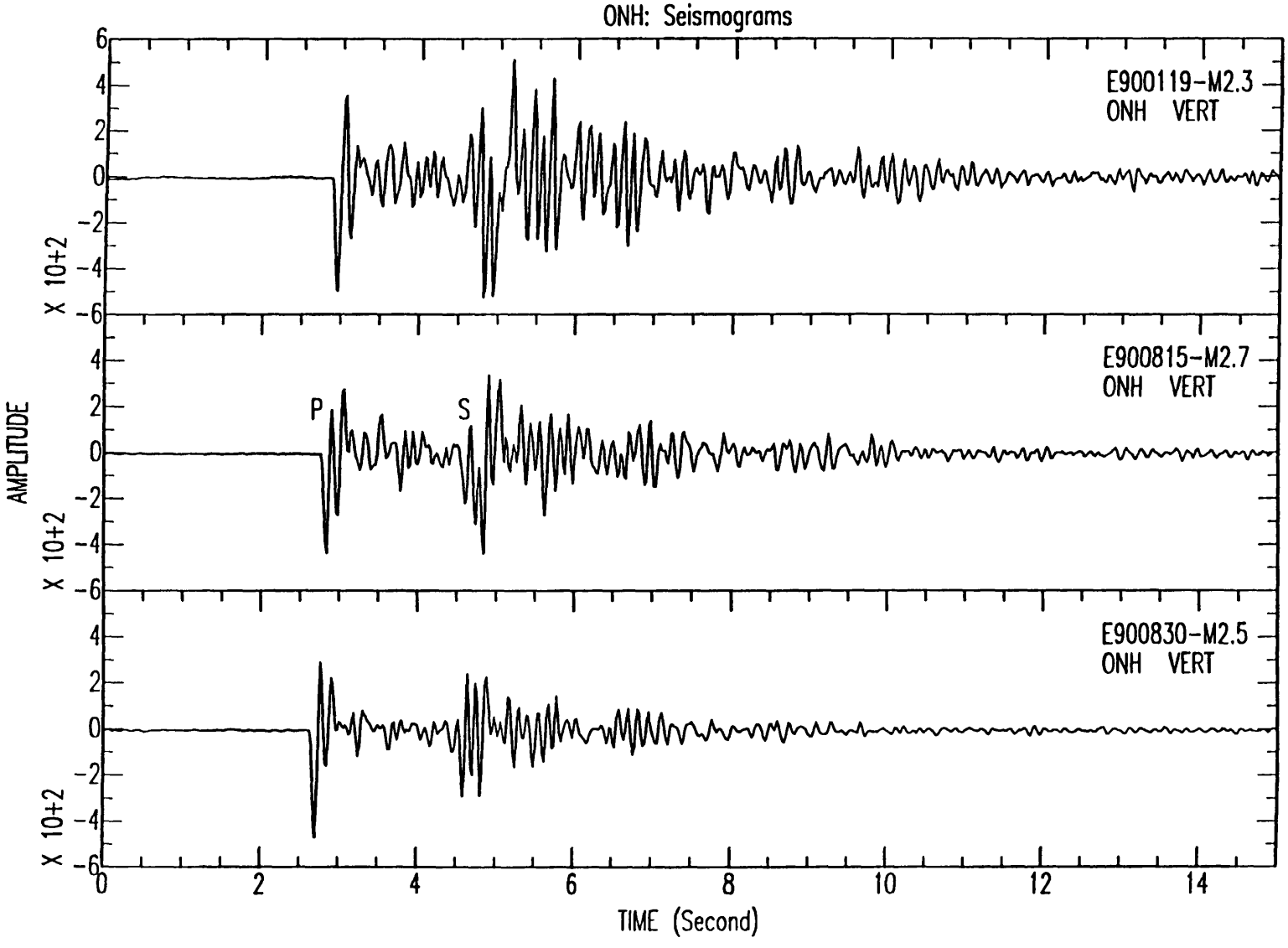

Fig. 3. Raw data recorded at station ONH for the easternmost cluster of three earthquakes of trend A in Fig. 2. The waveforms are similar.

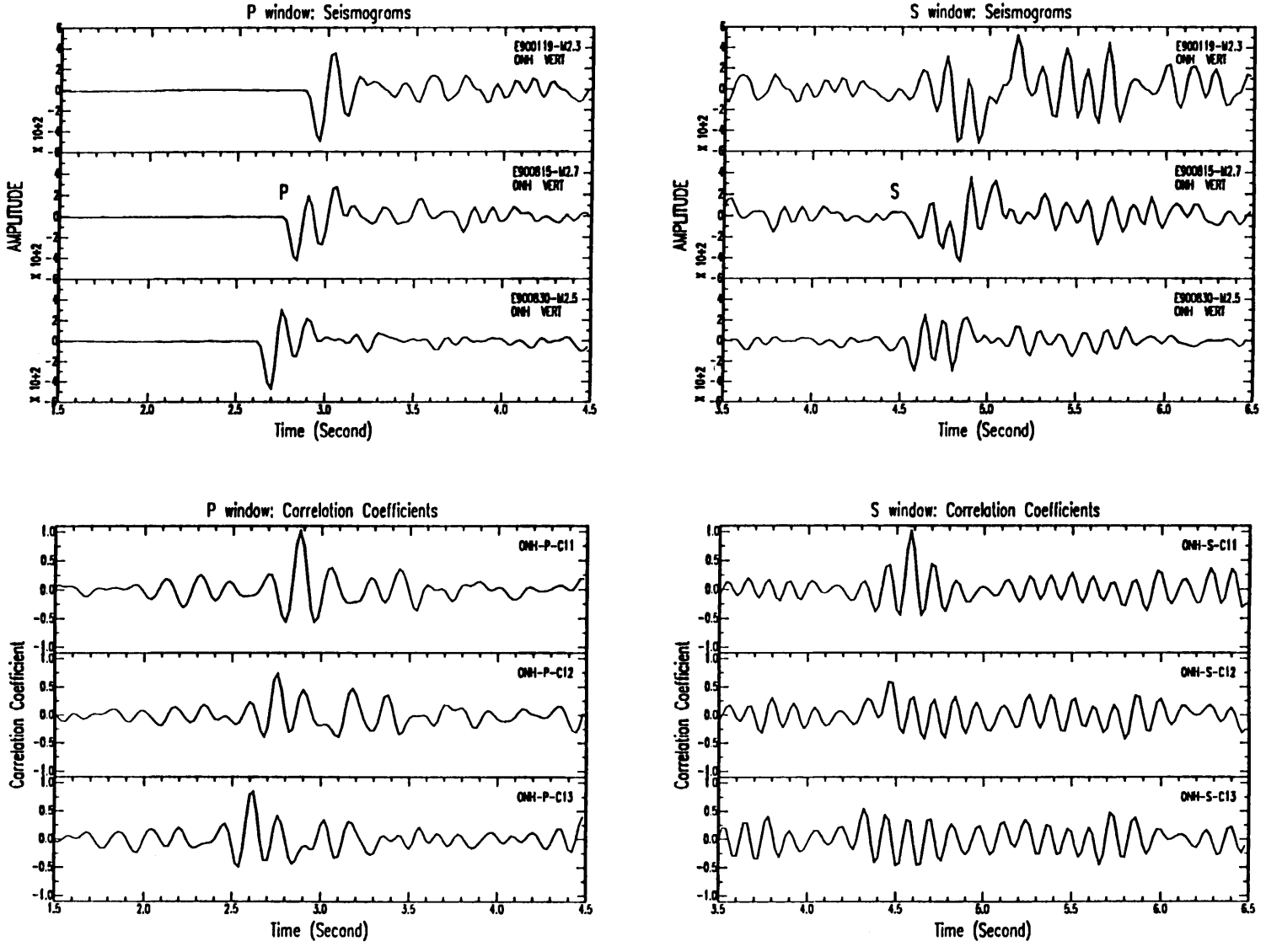

Fig. 4. Windowed P and S (top) and auto- and cross-correlations (bottom) of these phases for event correlation pairs C11, C12 and C13. Nearly identical time differences between S and P correlation peaks for these pairs suggest a similar location for the three events.

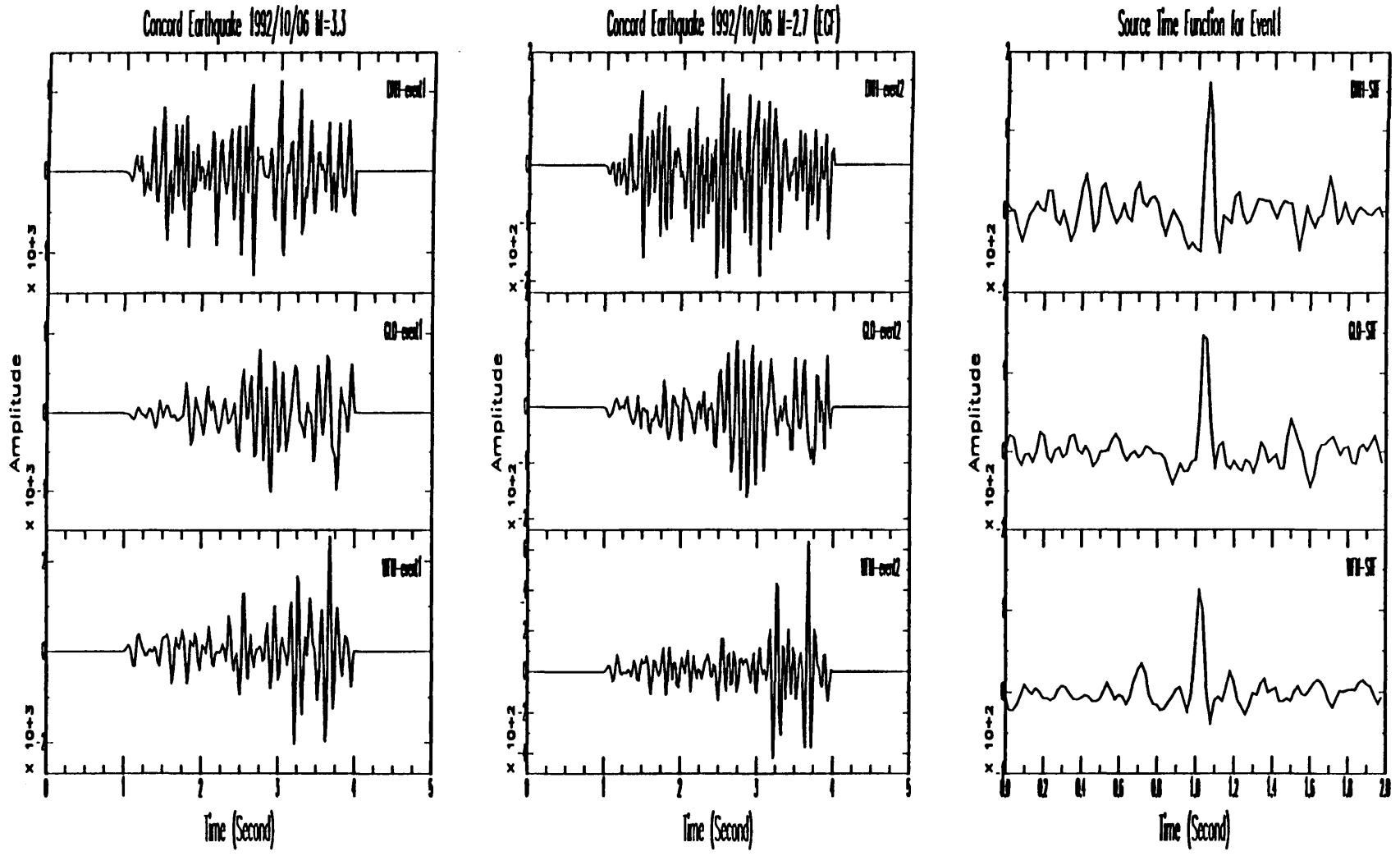

Fig. 5. Windowed P waves (for three stations) of a larger and a smaller event relocated to similar hypocenters. The smaller event (EGF = empirical Green's function) is deconvolved from the larger one to obtain the source time function estimate.

Earthquakes As Self-organized Critical Phenomena

Contract #1434-92-G-2165

Donald L. Turcotte
Department of Geological Sciences
Cornell University, Ithaca, New York 14853

(607) 255-7282

Investigations Undertaken

The objective of the research carried out is to understand whether earthquakes are an example of self-organized criticality. The approach is to develop analog models which are examples of self-organized criticality and which exhibit the important features of distributed seismicity. These models can then be examined for precursory behavior that can be predictive of major analog earthquakes. The results may provide the basis for new approaches to earthquake prediction.

The research is being undertaken in collaboration with Dr. Andrei Gabrielov who is on leave from the Institute for Theoretical Geophysics and Earthquake Prediction in Moscow and is spending the period of this grant at Cornell. Dr. Gabrielov was a leader in the development of the algorithems that successfully predicted the Armenian, Loma Prieta, and Landers earthquakes. One objective of our research is to test these algorithems on the analog SOC systems.

Results Obtained

It has been suggested that distributed seismicity is an example of self-organized criticality. If this is the case, the Earth's crust in an active tectonic zone is in a near-critical state and faults can interact over large distances. Observed seismicity and earthquake statistics are consequences of the dynamical interactions of seismic faulting over a wide range of scales. We address this problem by considering a two-dimensional array of slider blocks with static/dynamic friction. The two-dimensional system is treated as a cellular automaton such that only one slider block is allowed to slip at a given time and interacts only with its nearest neighbors through connecting springs. Because of this treatment, the amount of slip for each failed block can be obtained analytically, and the system is deterministic with no stochastic inputs or spatial heterogeneities. In many cases, the slip of one block induces the slip of adjacent blocks. The size of an event is specified by the number of blocks that participate in the event. The number of small events are close to a Poisson process, and gradually deviate towards periodicity for large events. The recurrence time statistics are generally insensitive to parameter variations. Large events may occur at stress levels considerably lower than the failure strength of an individual block, and the stress drops associated with large events are generally small. This may provide an explanation for observed low stress levels in tectonically active areas.

In the standard cellular-automata model for a fault an element of stress is randomly added to a grid of boxes until a box has four elements, these are then redistributed to the adjacent boxes on the grid. This redistribution may result in one or more of these boxes having four or more elements in which case further redistributions are required. On the average added elements are lost from the edges

of the grid. We have modified this model so that the boxes have a scale-invariant distribution of sizes. When a redistribution from a box occurs it is equivalent to a characteristic earthquake on the fault. A redistribution from a small (a foreshock) may trigger an instability in a large box (the main shock). A redistribution from a large box always triggers many instabilities in the smaller boxes (aftershocks). The frequency-size statistics for both main shocks and aftershocks satisfy the Gutenberg-Richter relation with $b = 0.835$ for main shocks and $b = 0.635$ for aftershocks. Model foreshocks occur 28% of the time.

Reports Published

1. B. Barriere and D.L. Turcotte, A scale-invariant cellular-automata model for distributed seismicity *Geophys. Res. Let.* **18**, 2011-2014 (1991)

2. G. Narkounskaia, J. Haung, and D.L. Turcotte, Chaotic and self-organized critical behavior of a generalized slider-block model *J. Stat. Phys.* **67**, 1151-1183 (1992)

3. G. Narkounskaia and D.L. Turcotte A cellular-automata, slider-block model for earthquakes. I. Demonstration of chaotic behavior for a low-order system, *Geophys. J. Int.*, in press (1992)

4. J. Huang, G. Narkounskaia, and D.L. Turcotte, A cellular-automata, slider-block model for earthquakes. 2. Demonstration of self-organized criticality for a two-dimensional system, *Geophys. J. Int.*, in press (1992)

QUATERNARY BLIND THRUSTING IN THE SOUTHWESTERN SACRAMENTO VALLEY, CALIFORNIA

Contract # 14-08-0001-G2059

Jeffrey R. Unruh (Lettis & Assoc., Oakland, CA; 510-832-3716)
Lewis P. Munk* (Dept. of Land, Air and Water Resources; 916-752-1406)
Bradley A. Loewen* (Dept. of Geology; 916-752-4950)
Eldridge M. Moores* (Dept. of Geology; 916-752-0352)
Randal J. Southard* (Dept. of Land, Air and Water Resources; 916-752-7041)

***all at*: University of California, Davis 95616**

OBJECTIVES

The goal of this investigation is to study Quaternary surface deformation related to movement on potentially seismogenic blind thrust faults in the Rumsey Hills/Dunnigan Hills region, southwestern Sacramento Valley, California. Our approach is to combine analysis of seismic reflection data with mapping of Quaternary tectonic-geomorphic features to infer the rate, timing and kinematics of late Cenozoic shortening. Additional studies have been undertaken to determine the origin of the blind thrust system beneath the southwestern Sacramento Valley, and to explore the relationship between anomalously high fluid pressures and active crustal shortening in western California.

INVESTIGATIONS UNDERTAKEN

Based on detailed surface mapping, analysis of seismic reflection profiles and drill hole data, we have developed a kinematically-restorable forward model for evolution of the blind thrust system in the Rumsey Hills/Dunnigan Hills region. The model is consistent with stratigraphic and structural relationships visible in deep seismic reflection profiles, and accounts for the development of angular unconformities in the section of Cretaceous-Tertiary forearc strata (Loewen and Unruh, 1992).

We conducted detailed field mapping and stratigraphic analysis of the late-Quaternary deposits and geomorphic surfaces in the Dunnigan Hills region to constrain the timing of the initiation of Quaternary deformation, and infer rates of tectonic uplift. Relative and absolute ages of the geomorphic surfaces and underlying sediments were determined via radiometric, (^{14}C, U/Th/Pa, K/Ar) magnetostratigraphic, geomorphic and tephrachronologic data. Soils underlying the geomorphic surfaces were described and sampled in 16 backhoe pits. Hundreds of additional obversations were made from natural exposures, auger holes and shallow pits. These data were used to develop soil morphological and chemical indices for the southwestern Sacramento Valley (Munk, 1992). Models for the development of the fluvial system of the Dunnigan and Rumsey Hills were developed based on field investigations and photo-interpretation.

We conducted field and aerial reconnaissance in order to map the locations of perennial saline springs emerging along thrust faults in the Rumsey Hills. The map data were combined with stable isotope analyses of the spring waters to relate spatial variations in fluid chemistry to distinct stratigraphic and structural horizons (Criss et al., 1992; Davisson et al., 1992).

RESULTS OBTAINED

Based on our structural studies, we conclude that the seismically-active blind thrust system beneath the southwestern Sacramento Valley initially evolved during progressive arcward-vergent contraction of the Mesozoic-Tertiary Great Valley forearc basin (Unruh et al., 1991). The youngest thrust fault in the study area is responsible for uplift and folding of the Rumsey Hills fault-propagation fold (Loewen, 1992). This young thrust roots in an older thrust fault, and folds

and deforms older structures. Displacement on this thrust has deformed the Plio-Pleistocene Tehama Formation (Loewen et al., 1992). Based on stratigraphic relationships in the Dunnigan Hills, we tentatively conclude that uplift, tilting and folding in this region began in middle Pleistocene and continued into the late Pleistocene (Munk, 1992).

Total late Quaternary displacement on the active thrust fault beneath the Rumsey Hills is estimated from the kinematic forward model and the structural relief on the deformed Tehama Formation. Based on a reasonable range of fault geometries and the age of the Tehama Formation, we calculate an average slip rate of 1-2 mm/yr. Using empirical relationships between fault area and earthquake magnitude, we estimate a maximum credible earthquake of Mw $6^1/_4$ for the blind thrust fault beneath the Rumsey Hills (Unruh and Loewen, 1992). Surface thrust or reverse faults in the Rumsey Hills that splay upward from the main thrust locally displace bedding contacts in the Tehama Formation approximately 0.5 m. These relationships yield a minimum estimate of cosesimic slip of 0.5 m. Assuming the slip rate calculated above, the recurrence interval for 0.5 m events is 250-500 yr. Paleoseismic investigations are neccessary to test these structurally-derived estimates.

Perennial saline springs emerge from thrust faults in the Rumsey Hills and are the surface expression of anomalously high fluid pressures generated by compressive forces and active shortening of Cretaceous marine sediments in the northern Coast Ranges (Unruh et al., 1992). The high fluid pressures may affect the mechanics of thrust displacement, and may also control the coseismic release of strain by blind thrusts (Ed Keller, personal communication, 1992). The perennial saline springs are aerially extensive and have been observed as far south as the northern Diablo Range (Criss et al., 1992). Discharge rates of individual saline springs in the Rumsey Hills are as high as 10 liters/minute and generally do not exhibit significant seasonal variations. Based on an estimated intergrated disharge rate throughout the Rumsey Hills, tectonic strain due to pore volume loss in this region may be locally as high as 10^{-7}/yr. The springs are rich in boron, and the high discharge rate suggests that the abnormally high boron concentrations in the potable groundwaters of the southwestern Sacramento Valley are probably due to contamination by fluids expelled from these saline springs.

REPORTS

Abstracts

Criss, R.E., Davisson, M.L., Loewen, B.A., Unruh, J.R., and Schaal, R.B., 1992, Occurrence of tectonically-driven, perennial saline springs in the eastern Coast Range, CA: Eos, Transactions, American Geophysical Union, Fall Meeting, V 73, #43.

Davisson, M.L., Presser, T.S., Criss, R.E., Unruh, J.R., and Loewen, B.A., 1992, Chemical and isotopic character of perennial saline springs in the eastern margin of the Coast Ranges thrust system, Rumsey Hills, California: Eos, Transactions, American Geophysical Union, Fall Meeting, V 73, #43.

Loewen, B.A., Unruh, J.R., Davisson, M.L., and Moores, E.M., 1992, Deformed Plio-Pleistocene fluvial deposits in the Rumsey Hills, California, and implications for late Cenozoic motion of an east-tapering underthrust wedge: Abstracts with programs, Cordilleran Section, Geological Society of America, p. 65.

Loewen, B.A., and Unruh, J.R., 1992, Kinematics and timing of progressive arcward-vergent contraction of the Mesozoic-Tertiary forearc basin, southwestern Sacramento Valley, California: Eos, Transactions, American Geophysical Union, Fall Meeting, V 73, #43.

Munk, L.P., and R.J. Southard. 1992. Soil stratigraphic relationships in a tectonically active landscape, Dunnigan HIlls, California. Abstracts. American Society of Agronomy, Annual Meetings, Minneapolis, MN, Nov. 1-6, 1992.

Unruh, J.R., Loewen, B.A., and Munk, L.P., 1992, Seismic hazard assessment of an active blind thrust fault beneath the Rumsey Hills, southwestern Sacramento Valley, California: Eos, Transactions, American Geophysical Union, Fall Meeting, V 73, #43.

Southard, R.J., and L.P. Munk. Quantitative clay mineralogy of a soil developmental sequence in a tectonic landscape.Abstracts. American Society of Agronomy, Annual Meetings, Minneapolis, MN, Nov. 1-6, 1992.

Theses and Dissertations

Loewen, B.A., 1992, Deformation of Lower Cretaceous through Tertiary strata in the Rumsey Hills-Capay Valley area: Implications for late Cenozoic motion of an east-tapering underthrust wedge: M.S. thesis, University of California, Davis, 84 p.

Munk, L.P., 1992, Stratigraphy, geomorphology, soils, and neotectonic interpretation of the Dunnigan Hills, California. Ph.D. dissertation, University of California, Davis.

Papers

Unruh, J.R., Ramirez, V.R., Phipps, S.P., and Moores, E.M., 1991, Tectonic wedging beneath forearc basins: ancient and modern examples from California and the Lesser Antilles: GSA Today, v. 1, p. 185-190.

Unruh, J.R., and Moores, E.M., 1992, Quaternary blind thrusting in the southwestern Sacramento Valley, California: Tectonics, v. 11, p. 192-203

Unruh, J.R., Davisson, M.L., Criss, R.E., and Moores, E.M., 1992, Implications of perennial saline springs for abnormally high fluid pressures and active thrusting in the southwestern Sacramento Valley, California: Geology, v. 20, p. 431-434.

Munk, L.P., and Southard, R.J., in press, Pedogenic and mineralogical implications of non-calcareous opaline pendants in some late-Pleistocene California Palexeralfs: SSSAJ, 57.

Unruh, J.R., Loewen, B.A., and Davis, D.L., in prep., Kinematics and timing of pregressive arcward-vergent contraction of the Mesozoic-Tertiary forearc basin, southwestern Sacramento Valley, California.

Unruh, J.R., Loewen, B.A., and Munk, L.P., in prep., Seismic hazard assessment of an active blind thrust fault beneath the Rumsey Hills, southwestern Sacramento Valley, California.

Phipps, S.P., and Unruh, J.R., in prep., Tectonic wedging beneath an imbricate roof thrust system, northern Coast Ranges, California.

Earthquake Prediction Experiments in the Anza-Coyote Canyon Seismic Gap

1434-92-A-0962

Frank Vernon
Institute of Geophysics and Planetary Physics
Scripps Institution of Oceanography
University of California, San Diego
La Jolla, California 92093
(619) 534-5537

Investigations: This report covers the progress of the research investigating the Anza-Coyote Canyon seismic slip gap for the period from January through November, 1992. The objectives of this research are: 1) To study the mechanisms and seismic characteristics of small and moderate earthquakes, and 2) To determine if there are premonitory changes in seismic observables preceding small and moderate earthquakes. This work is carried out in cooperation with Tom Hanks, Joe Fletcher and Larry Baker of the U. S. Geological Survey, Menlo Park.

Network status: During the period of this report, nine stations of the Anza Seismic Network were telemetering three component data. The network was set at a moderate gain so that a M=3.4 earthquake clipped the station directly over the hypocenter while the rest of the stations remained on scale. An STS-2 seismometer was installed at the PFO station to test the long term operational stability in preparation for the upgrade planned in 1993. The network has a front-end computer which allows the ANZA event data to be available over the INTERNET in near real time. No changes were made to the data logging software. Due to the abundance of aftershocks from the Joshua Tree -Landers - Big Bear earthquake sequence we now have a back log of P and S wave arrival picks and locations and focal mechanisms which need to be completed. The catalog is complete through April and we plan to be caught up by the end of December. The complete waveform data will also be loaded to the on-line optical disk storage system by the end of Decmeber.

Seismicity: Since the beginning of 1992, the ANZA network recorded 6270 events of which were large enough to locate and determine source parameters. This compares to 1437 from 1991. These events have magnitudes determined by of the Southern California Seismic Network from less than M=1.0 up to the Landers M=7.5 event. The seismicity pattern in the Anza region remained the same as in 1990. It is concentrated in two clusters located near the KNW and TRO stations respectively. These clusters have been active for the past 9 years while the ANZA network has been operational. The activity near TRO reached a maximum near the beginning of 1990 and is significantly higher than before 1989. The seismicity off the fault appears to be lower than the levels observed in the middle 1980s. It is also interesting that there is an apparent decrease in activity along the Anza segment of the San Jacinto fault after the Landers earthquake. We will investigate this further after completing our catalog for 1992.

A three-tiered investigation of seismicity and earthquake strains

Agreement No. 1434-92-6-2181

Steven N. Ward
Institute of Tectonics
University of California
Santa Cruz, CA 95064
404-459-2480

We have been attempting to revise the mean repeat time (T_{ave}) and coefficient of aperiodicity (ν) for segments of the San Andreas Fault by using models of synthetic seismicity. Primary inputs into the model are: 1) segment lengths and locations, 2) characteristic earthquake magnitudes, and 3) long-term slip rates. Of all the earthquake information available, these features are probably best constrained.

WGCEP (1990) has presented an eleven segment model for the San Andreas Fault. A slightly adjusted version containing 15 segments (Table 1) was employed to address the question: "Can the WGCEP segmentation reproduce observed SAF seismicity? If not, what needs to be done? If so, what can be said about T_{ave} and ν?" Figure 1 shows synthetic seismicity (*top*) and displacement (*bottom*) for a 1000 year piece of a 10,000 year run of the SAF model. Figure 2 (*stars*) overlays the synthetic seismicity with the observed annual rates (*boxes*) $N_{>}(M)$ and $N(M)$ of earthquakes within a 40 km wide band centered on the fault. The error bars show ±one standard deviation in the computed rates based upon 50, 200-year samples drawn from the 10,000 year history. We find that the synthetic seismicity model using the modified WGCEP segmentation is capable of generating the observed numbers of earthquakes over the magnitude range 4.5 to 8.0. Below we advance some recurrence statistics for the larger events.

Fault Averaged Results. Figure 3 plots cumulative probability of recurrence versus time for $M \geq M_o$ with M_o= 6.0 to 8.0. for the SAF model as a whole. Mean repeat time and spread parameter for a typical large event ($M \geq 7$) is 131 years and 1.1. It is important to recognize however, that both T_{ave} and ν are functions of magnitude; T_{ave} increases with M_o while ν decreases (bottom row, Table 2). Large earthquakes tend to be more periodic than small ones. Small ones tend to cluster early in the cycle. You can see this in the top panel of Figure 3, where the curves crowd to the left. The numerical value of ν bears directly on the concept of seismic gaps. If ν is less than 1.0, gaps behave normally in that the conditional probability of occurrence increases with gap time. If ν is greater than 1.0, the effect is reversed and conditional probability decreases as gap time increases. All of the models run so far show the same tendency; ν decreases from approximately 1.5 at M_o=6 to about 0.6 at M_o=7.75. The cross-over magnitude where gaps become a useful concept occurs around $M = 7$. Figure 4 visualizes this magnitude dependence of aperiodicity and clustering. In all instances the spread parameter that we find is much greater than the 0.21 value used by WGCEP.

Segment Specific Results. Earthquake aperiodicity, while on the average being a decreasing function of characteristic magnitude, is also dependent on the segment's relative location on the fault. Table 2 lists T_{ave} and ν for all of the SAF segments as a function of M_o. In scanning the columns, you can see that certain segments systematically behave more or less periodically than the fault as a whole. Generally, the more isolated a segment, the more periodic are its earthquakes. Note for instance, that the Parkfield segment tends to have a ν

less than the fault average. This segment borders the central creeping section to the north which provides a degree of isolation. Although very periodic failures of fault segments may exist, we find it difficult to make any segment conform to a spread value much less than 0.4. Given the information in Table 2 and the date of the last earthquake on a segment, the conditional probability of recurrence can be easily calculated. For the Parkfield segment [T_{ave}=27.6 and ν=1.12, 1966=previous quake], the conditional probability of recurrence of a $M \geq 6$ quake within the ten year Parkfield Prediction window beginning in 1983 is 29% (versus 95% estimated by Bakun and Lindh, 1985). Probability of recurrence in the 30 year WGCEP window starting in 1988 is 63% (versus > 90% estimated by WGCEP, 1988).

Verification. We have argued previously that unless the earthquake record contains at least ten recurrences, the estimated repeat time and aperiodicity coefficient will almost certainly be too low. Measured against this criteria, there are few data sets with which to compare (and correct) the model. Sieh (1989) reports nine recurrence intervals at Pallet Creek in the Mojave segment. Weibull function fits to these intervals give T_{ave} = 131.8 y and ν=0.84. Because it is not completely certain what magnitude earthquakes the paleoseismic data are detecting, we plot in Figure 5 (*dashed lines*) predictions for recurrence of M_o = 7, 7.25 and 7.5 quakes in the Mojave segment. The model reproduces both T_{ave} and ν quite well. Keep in mind that T_{ave} derives only from the segment length, characteristic magnitude, and slip rate. It is not an input parameter.

Weaknesses. Admittedly, products from synthetic seismicity models are easily attacked as nonunique or parameter dependent. We can't claim the contrary, but given the fact that there is almost a total lack of data on the recurrence statistics of SAF earthquakes, we believe that synthetic seismicity offers two unquestionable advantages over the real thing: 1) Synthetic seismicity can run as long as necessary to get a statistically significant sample. Individual products like "Segment X has a 50% chance of triggering Segment Y" may not agree with our limited historical sample, but at least there is a firm statistical basis for the statement. 2) Synthetic seismicity illuminates connections between physical parameters which otherwise would go unrecognized. Segment length, characteristic magnitude, mean repeat time and aperiodicity are linked; they can not be picked out of a hat. For instance, T_{ave} can not be arbitrarily decreased without cutting the characteristic magnitude or increasing slip rate. Likewise, the characteristic magnitude of a segment can not be reduced without (generally) increasing ν.

We believe that San Andreas earthquake recurrence statistics which derive from synthetic seismicity models such as these are as credible, if not more so, than any other method yet advanced.

Ward, S. N., 1992. An Application of Synthetic Seismicity in Earthquake Statistics: The Middle America Trench, *J. Geophys. Res.,97*, 6675-6682.

Segment	Length (km)	Characteristic Magnitude	Slip Rate (mm/y)
1. Medocino	100	7.0	15
2. North Coast	240	7.6	15
3. Mid Peninsula	41	7.0	18
4. N. Santa Cruz Mts.	20	6.5	15
5. S. Santa Cruz Mts.	39	6.9	15
6. Creeping Section	140	aseismic	30
7. Parkfield	30	6.3	36
8. Cholame	55	7.0	36
9. Carrizo	145	7.7	36
10. Mojave	100	7.4	30
11. San Bernardino	100	7.3	24
12. Coachella Valley	100	7.4	24
13. Brawley Seismic Zone	50	aseismic	30
14. N. Imperial Valley	30	6.5	30
15. S. Imperial Valley	30	6.6	30

Table 1. San Andreas Fault segmentation model. Slightly modified after WGCEP.

	$M \geq 6.0$		$M \geq 6.5$		$M \geq 7.0$		$M \geq 7.5$	
Segment	T_{ave} (y)	ν	T_{ave} (y)	ν	T_{ave} (y)	ν	T_{ave} (y)	ν
1. Medocino	86	1.4	90	1.4	122	1.1	278	0.5
2. North Coast	77	1.7	91	1.5	110	1.3	263	0.6
3. Mid Peninsula	74	1.4	78	1.4	137	1.0	476	0.4
4. N. Santa Cruz Mts.	43	1.4	60	1.2	117	1.0	530	0.5
5. S. Santa Crua Mts.	64	1.5	81	1.2	154	0.8	703	0.6
6. Creeping Section								
7. Parkfield	28	1.1	60	1.1	127	0.9	376	0.4
8. Cholame	52	1.4	63	1.2	124	1.0	362	0.4
9. Carrizo	158	1.5	175	1.3	188	1.2	326	0.5
10. Mojave	81	1.4	86	1.3	96	1.3	204	0.7
11. San Bernardino	60	1.5	69	1.3	86	1.1	203	0.7
12. Coachella Valley	91	1.5	107	1.3	134	1.0	273	0.4
13. Brawley Seismic Zone								
14. N. Imperial Valley	39	1.3	58	1.0	231	0.7		
15. S. Imperial Valley	44	1.2	55	1.0	231	0.7		
AVERAGE	57	1.5	75	1.3	131	1.1	315	0.6

Table 2. Predicted earthquake recurrence statistics for the San Andreas Fault segments for magnitudes greater than or equal to 6.0, 6.5, 7.0 and 7.5.

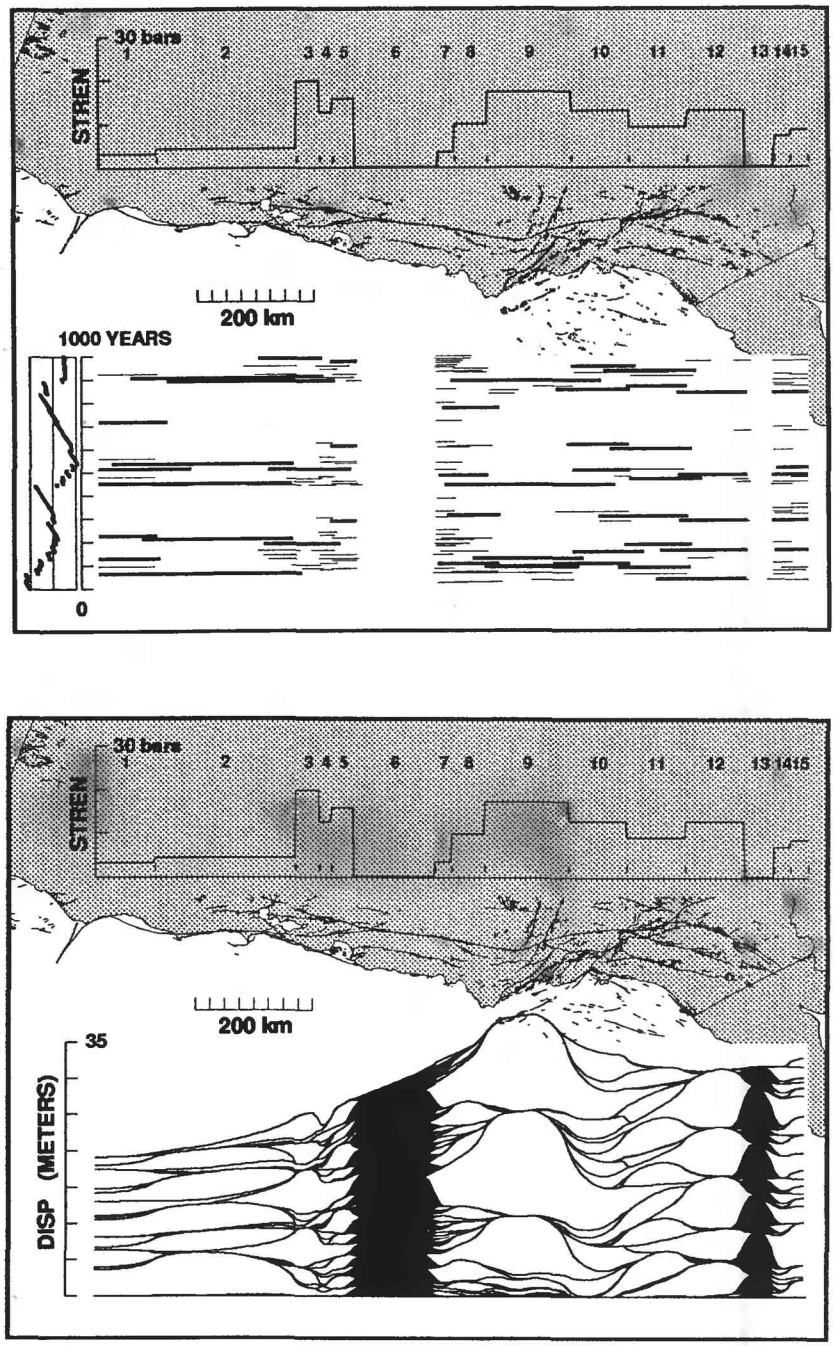

Figure 1. Synthetic seismicity (*top*) and displacement from the initial 1000 years of a 10,000 year run of a San Andreas Fault model based closely on the WGCEP segmentation. Length, position and strengths of the 15 segments are drawn along the top. Only events with $M \geq 6$ are shown. Bold line segments are $M \geq 7$ events. The blackened areas in the Central Creeping Section and Brawley Seismic Zone are aseismic slip. Note the mixture of characteristic and non-characteristic slip patterns in each segment.

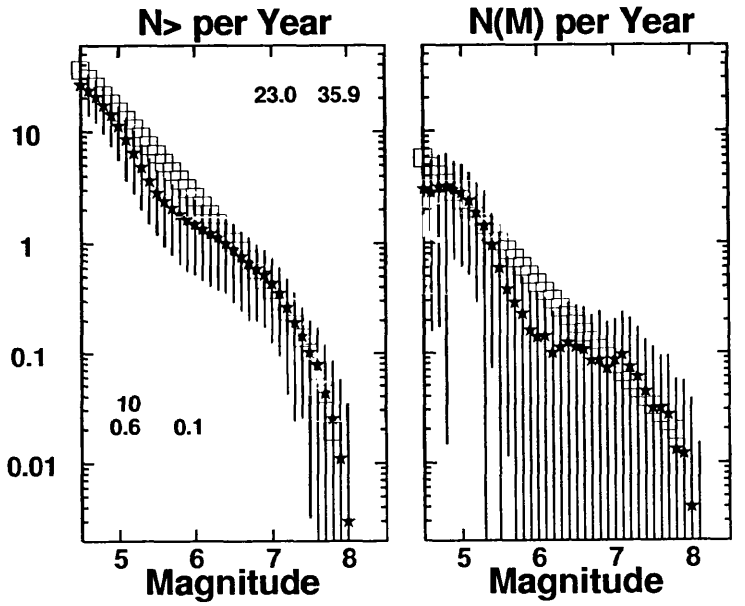

Figure 2. Observed seismicity (*boxes*) and synthetic seismicity (*stars*) from the model of Figure 1. The observed seismicity includes events within a 40 km wide band of the SAF. The modified WGCEP segmentation adequately represents observed seismicity.

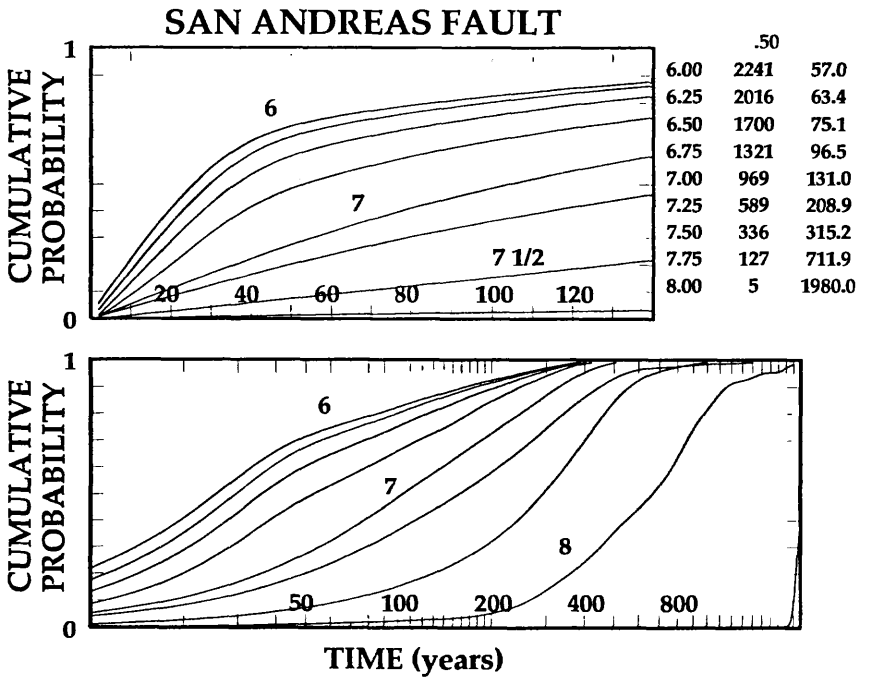

Figure 3. Cumulative probability for the recurrence of a $M \geq M_o$ earthquake within T years of a previous $M \geq M_o$ event. M_o covers the range M_o= 6.0 to 8.0 in 0.25 increments. Curves were tabulated from a 10,000 year run of synthetic seismicity for the SAF model. A segment is considered broken if more than 50% of its length slips during an earthquake. Numbers to the upper right give M_o, the number of segment recurrences, and the mean recurrence time. As can be seen in the steepening slopes of the curves, earthquakes tend to become more periodic with increasing magnitude. The concept of seismic gaps is useful for events of magnitude larger than about 7. For smaller quakes, increasing the gap time has little or diminishing effect on conditional probability of recurrence.

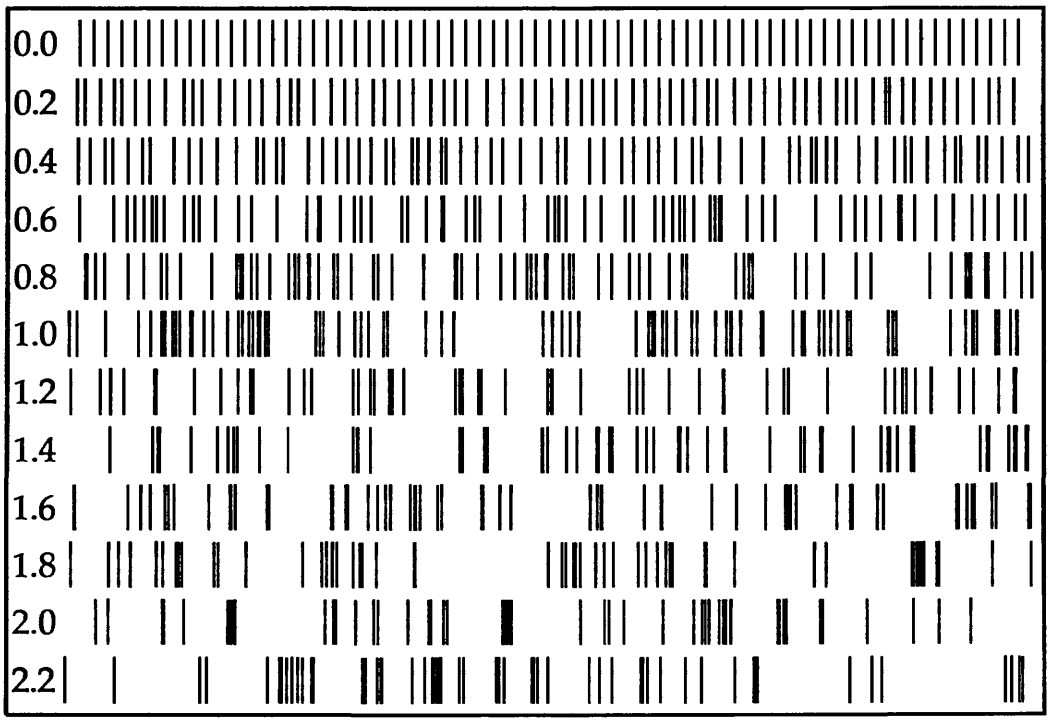

Figure 4. Visualization of the effect of the aperiodicity parameter ν on the recurrence of earthquakes. These 12 "bar code" lines show events drawn from a Weibull distribution of equal T_{ave} and ν increasing from 0.0 to 2.2. The trend toward temporal clustering of events as ν increases is obvious. Gap time is a useful concept only for time series with $\nu \leq 1$. We find: magnitude 6 events behave with $\nu \approx 1.5$; magnitude 6.5 events behave with $\nu \approx 1.3$; magnitude 7 events behave with $\nu \approx 1.1$; and magnitude 7.5 events behave with $\nu \approx 0.6$.

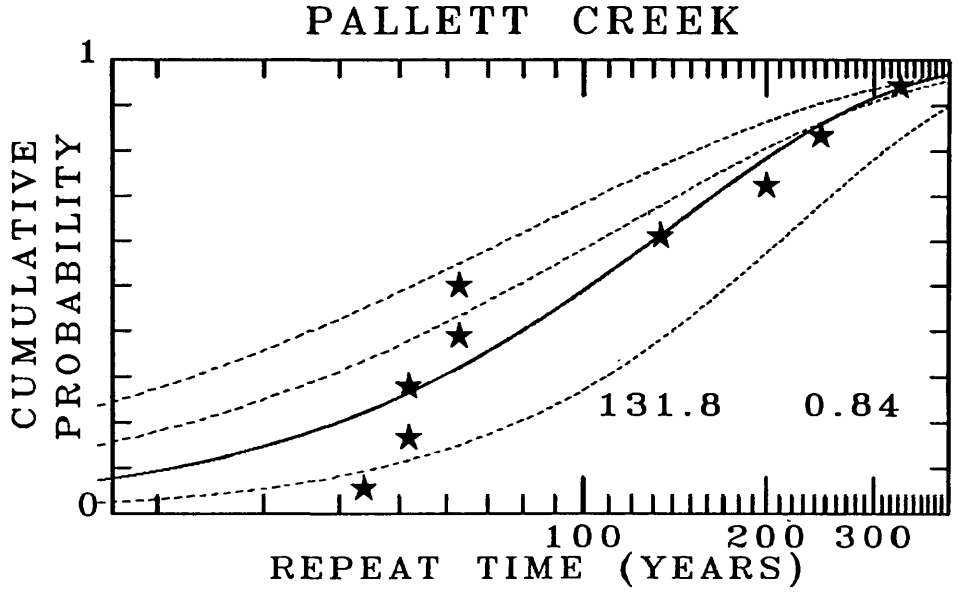

Figure 5. Cumulative probability Weibull fit (*solid line*) to the nine earthquake recurrence times given by Sieh (1989) for the Pallett Creek area of the Mojave segment. Left to right, the dashed lines are the predictions from the synthetic seismicity model for magnitudes greater than or equal to 7.0, 7.25 and 7.5. The predictions for events near 7.25 have no argument with the data.

Hayward Fault Recurrence Behavior: Trenching Studies, Fremont and Oakland California 14-08-0001-G2115

Patrick L. Williams and David L. Jones
Department of Geology and Geophysics
University of California
Berkeley, California 94720

Phone: (510) 486-7156
FAX: (510) 486-5686
e-mail: plw@geo.lbl.gov

Field work for the Tule Pond Paleosismic investigation is likely to finish in 1993. Substantial effort remains to establish age-control of offset strata. Our inventory of several hundred charcoal samples should allow us to accomplish this. Evidence remains good that at least seven paleoseismic events are recorded at Tule Pond.

FY1992 Accomplishments:

a) Logged two trenches at an additional paleoseismic site along the east flank of Tule Pond;
b) finished graphical representations of seven trenches;
c) collected and archived over 200 charcoal samples;
d) prepared over 40 charcoal samples for dating;
e) published Guidebook and Proceedings articles for the Second Conference on Earthquake Hazards in the Eastern San Francisco Bay Area;
f) presented case for dateable 1,100-foot offset of Strawberry Creek.

Recent Publications:

1991 Williams, P.L, Evidence of Late Holocene Ruptures, Southern Hayward Fault, California, *GSA Abstracts with Programs*, Spring 1991 SSA/GSA-Cordilleran meeting.

1992 Williams, P.L. and A.M. Hosokawa, Geomorphic features related to the Hayward fault at the University of California at Berkeley, in Taylor, C.L., Hall N.T. and Melody, M. eds., Field Trip Guidebook, Second Conference on Earthquake Hazards of the Eastern San Francisco Bay Area, 65-71.

1992 Williams, P.L., Earthquake recurrence studies at Tule Pond pull-apart, Fremont, California, in Taylor, C.L., Hall, N.T. and Melody, M. eds., Field Trip Guidebook, Second Conference on Earthquake Hazards of the Eastern San Francisco Bay Area, 179-189.

1992 Williams, P.L., Geological record of southern Hayward fault earthquakes, Proceedings, Second Conference on Earthquake Hazards of the Eastern San Francisco Bay Area, 1991-92, in press.

Acknowledgments

Preston Holland was co-leader of the 1992 investigations. Laurel Collins, Andrew Durham, Amy Hosokawa, and Laurie Schuur contributed to field and laboratory investigations.

CYCLIC STICK-SLIP INSTABILITY AS RELATED TO THE EARTHQUAKE CYCLE

USGS Grant #14-08-0001-G1807

Teng-fong Wong, Department of Earth and Space Sciences
State University of New York at Stony Brook
Stony Brook, NY 11794-2100
phone:(516) 632-8212; internet:tfwong@ccmail.sunysb.edu

Objectives

A physical understanding of the nonlinear dynamics of stick-slip instability as an analogue of earthquake rupture is of fundamental importance to earthquake mechanics. To this end, laboratory studies on rock friction can elucidate the friction constitutive relation, the micromechanics of frictional sliding and their relation to stick-slip instability behavior. In our previous study of cyclic stick-slip behavior of ultrafine quartz gouge [*Wong et al.*, 1992], we observed under high pressure a wide range of nonlinear oscillational and dynamic instability behavior which were in qualitative agreement with stability analyses and computer simulation of spring-slider system based on the Dieterich-Ruina type of friction law. The objective of the present study is to continue this line of research on simulated gouges of different mineralogy and particles size and to sliding surfaces of different roughness. Furthermore we proposed to pursue experiments in saturated samples under pore pressure, and to systematically investigate the deformation-induced microstructures.

Transition from stable sliding to cyclic stick-slip

The nonlinear dynamical behavior in the transition from stable sliding to cyclic stick-slip in two rock-gouge systems (sawcut Tennessee sandstone, and Tennessee sandstone with natural halite gouge) were investigated in a conventional triaxial configuration at confining pressures from 30 MPa to 110 MPa. The frictional sliding behavior was qualitatively similar to that of Westerly granite sandwiched with ultrafine quartz gouge. Induced by cumulative slip or load point velocity perturbation, the transition from stable sliding to cyclic stick-slip might involve several distinct sliding modes, including period doubling bifurcations and self-sustained periodic oscillations. The accumulation of slip may destabilize or stabilize the frictional sliding behavior, whereas an increase of load point velocity tends to stabilize the oscillational behavior. Apparently chaotic oscillations were also observed in the halite gouge. Details of the experimental observations were reported by *Gu and Wong* [1992a].

The experimental observations were interpreted using a spring-slider model with single degree of freedom. To reproduce the full range of sliding modes and their observed dependence on velocity perturbation, it was necessary to incorporate two state variables and high-speed cutoff of velocity dependence in the Dieterich-Ruina rate- and state-

dependent friction law. Analytic expression for the onset of Hopf bifurcation in such a system was derived. Stability boundaries dependent on stiffness, load point velocity, and friction constitutive parameters were established based on limit cycle oscillation modes observed in numerical simulations. Critical condition for the triggering of dynamic instability by sudden velocity perturbation was analyzed. The numerical simulation results were summarized by *Gu and Wong* [1993].

Development of Riedel shear localization in quartz gouge

Microstructures developed in ultrafine quartz gouge were compared with those in coarse quartz gouges. Several different country rocks (Westerly granite, Sioux quartzite, Frederick diabase and Blair dolomite) were considered. In the ultrafine quartz gouge, Riedel shear developed very early during frictional sliding, with density increasing with the cumulative slip and number of cyclic stick-slip events. In contrast, the Riedel shears were less developed in the coarser quartz gouge which underwent stable sliding, implying that comminution and compaction stablized the frictional sliding behavior. The detailed results will be presented by *Gu and Wong* [1992b].

Ongoing experimental studies

Ultrafine gouges of feldspar and crushed Westerly granite have been prepared. Frictional sliding experiments at confining pressures up to 400 MPa and at loading velocities between 0.1 to 10 μm/s are being conducted on sawcut Westerly granite samples sandwiched with the ultrafine gouges using our servo-controlled triaxial apparatus. Preliminary experiments have also been conducted on ultrafine quartz gouge under saturated conditions at pore pressures ranging up to 200 MPa. The drained and undrained behavior will be compared. In parallel, the permeability of the gouge will be determined as a function of normal stress and cumulative slip. The development of Riedel shear localization and comminution in the gouge layer will be characterized quantitatively.

References

Gu, J. and T.-f. Wong, The transition from stable sliding to cyclic stick-slip: effect of cumulative slip and load point velocity on the nonlinear dynamical behavior in three rock-gouge systems, in *Rock Mechanics Proceedings of the 33rd U. S. Symposium*, ed. J. R. Tillerson and W. R. Wawersik, A. A. Balkema, Rotterdam, 151-158, 1992a.

Gu, J. and T.-f. Wong, Development of shear localization in ultrafine and coarse grained quartz gouge, *EOS, Trans. Am. Geophys. Union*, **73**, No. 43 supplement, 516, 1992b.

Gu, J. and T.-f. Wong, Nonlinear dynamics of the transition from stable sliding to cyclic stick-slip in rock, submitted to "*Nonlinear Dynamics and Predictability of Critical Geophysical Phenomena*", ed. A. Gabrielov and W. Newman, Am. Geophys. Union Monograph, 1993.

Wong, T.-f., Y. Gu, T. Yanagidani and Y. Zhao, Stabilization of faulting by cumulative slip, in "*Fault Mechanics and Transport Properties of Rocks*", ed. B. Evans and T.-f. Wong, Academic Press, 119-143, 1992.

Collaborative Research (Tennessee Division of Geology and Vanderbilt University): Gravity Survey in the New Madrid Seismic Zone

USGS Grant Award No. 1434-92-G-2233

Ronald P. Zurawski
Tennessee Department of Environment and Conservation
Division of Geology
13th Floor, L & C Tower
401 Church Street
Nashville, TN 37243-0445
615-532-1504

Richard G. Stearns
Geology Department
Vanderbilt University
Box 1615, Station B
Nashville, TN 37235
615-322-2420

Investigations

We are performing a gravity survey of all of five and parts of three 7.5-minute quadrangles near the Mississippi river, north of Latitude 35.5 degrees and west of Longitude 88.5 degrees in Lauderdale and Tipton counties, Tennessee. We also propose to fill gaps in present coverage north of Latitude 35.75 degrees near the Mississippi River. Present coverage includes all of the area of the Mississippi Valley Graben (MVG) north of Latitude 35.75 degrees (over fifty 7.5- minute quadrangles); some of this work is published and some is in preparation.

This project will result in coverage of all of the area of the MVG in Tennessee. The 1.5 km station spacing will be about the same as the one mile spacing between flight lines in existing aeromagnetic maps. The eight quadrangle area of new coverage includes the edge of the MVG where it crosses the Mississippi River, the Chickasaw Bluffs lineament (a likely fault parallel to and close to the edge of the MVG) and other lineaments relating to that feature, and the magnetic high marking the Covington pluton, one of several plutons believed to be related to the edge of the MVG.

The gaps in present coverage are in areas that are difficult to approach, because they are in large farms, swampy areas, or isolated by such river-related features as sloughs or chutes. Reelfoot Lake (tectonically sunk during the 1811 earthquake) is mostly a large swamp accessible only by boat, and many of the areas near the Mississippi river can be best (or only) approached by boat. Gaps are important because they tend to be in areas of land subsidence (such as Reelfoot Lake) , or are near suspected faults (such as straight reaches of rivers).

The completed survey will consist of about 400 new stations, plus an estimated 100 reoccupations of old stations. There are already about 20 stations in each quadrangle (for which we have full original records). We also customarily reoccupy one or more old stations during each loop to check for bad loops. For fill-in surveys more reoccupations will be needed.

There are four base stations in or near the project survey areas. Gravity stations are occupied using loops and data will be reduced in the usual manner. Based on reoccupation statistics for surveys we have made so far, observed gravity will be better than 0.3 mgal standard deviation. Relatively low relief makes it likely that standard deviation of Bouguer anomaly will be near the same low value.

Results

Background

Gravity surveys have been made in the project area by Vanderbilt University since 1967 (Smith, 1967). This survey was incorporated into the regional survey of West Tennessee supported by USGS. Station spacing for this survey was about two miles (15-20 stations in each 7.5-minute quadrangle). Vanderbilt surveyed the area of West Tennessee west of 89 degrees Longitude and University of Kentucky (G. R. Keller, now at the University of Texas-El Paso) surveyed West Tennessee from 88-89 degrees Longitude. A regional map (Hildebrand and others, 1977) published by USGS and a map of West Tennessee (Stearns, Keller, and Templeton, 1980) published by the Tennessee Division of Geology resulted from this survey.

Soon after (1979-1982) more detailed surveys were made in the area working outward from the area of Reelfoot Lake in the northwest corner of Tennessee. A detailed gravity map was published by the Tennessee Division of Geology of the area close to Reelfoot Lake (Stearns, 1980). Surveys supported by the US Nuclear Regulatory Commission were published in NUREG documents (Keller, 1980; Stearns, 1986 and 1987).

These surveys used a variety of bases, and had sufficient data problems that Stearns judged that a thorough editing and possible recalculation was warranted. This task was carried on along with limited field work, including surveys of several quadrangles to square up the survey area. Once the editing job was completed, a project to make maps of the large area began with G. R. Keller at the University of Texas-El Paso, who had surveyed the area east of 89 degrees Longitude in 1978.

The entire area of the MVG now lacks only the data that will be acquired during this project.

Recent Work

During the first quarter of the project period we made 276 station occupations in eighteen 7.5-minute quadrangles. There were 34 loops; 4 to 15 stations in each loop. Every loop included at least one reoccupied old station (average of 2, range 1 to 10). There are 202 new stations and 74 reoccupations.

Stations were taken to fill gaps in earlier surveys, most in places hard to access because they are in the Mississippi River floodway, wetlands, or in large farms with few or no roads. Specific areas include:

Mississippi bank and floodway from Madrid Bend in Kentucky to the Cottonwood Point Quadrangle near 36 degrees Latitude.
Reelfoot Lake shore and wetland accessible by four-wheel drive vehicle.
Obion River bottoms upstream to the Rives and Rutherford quadrangles.
Part of the Forked Deer River bottom north of 36 degrees upstream to the Tatumville Quadrangle.

Future Work

Our plan is to continue the survey when weather and ground conditions improve. Our priorities are:

1- Survey of quadrangles south of 36 degrees in the bottoms, wetlands and floodway of the Mississippi and Hatchie rivers,
2- Finish some remaining gaps in the bottoms and wetlands of the Obion and forked Deer rivers, and
3- Reach some so-far inaccessible places by boat.

References Cited

Hildebrand, T. C., Stearns, R. G., and others, 1977, Bouguer gravity map of the Northern Mississippi Embayment, parts of Missouri, Arkansas, Tennessee, Kentucky and Illinois, U. S. Geological Survey Open File, Map No. 77-228.

Keller, G. R. and others, 1980, Bouguer gravity anomaly map of the east-central Midcontinent of the United States, U.S. Nuclear Regulatory Commission, NUREG/CR-1663, 12 p. with map, scale 1:1,000,000.

Smith, J. R., 1967, The Covington Pluton, unpublished Master's Thesis, Vanderbilt University, Nashville, Tennessee.

Stearns, R. G. and others, 1980, Gravity anomaly maps of Tennessee, West sheet, Tennessee Division of Geology, scale 1:250,000.

Stearns, R. G., 1980, Gravity anomaly map of the Reelfoot Lake Area, Tennessee (including a portion of southwest Missouri), Tennessee Division of Geology, scale 1:62,500.

Stearns, R. G., 1986, Post-Eocene fault near east edge of Reelfoot Rift in Lauderdale County, Tennessee, (with S. L. Wilson and S. J. Naval), U. S. Nuclear Regulatory Commission, NUREG/CR-4702, 36 p.

Stearns, R. G., 1986, One-dimensional gravity calculation and paleozoic structure and plutons at Reelfoot Scarp, (with S. L. Wilson), U. S. Nuclear Regulatory Commission, NUREG/CR-4703, 43 p.

Stearns, R. G., 1987, An integrated geological, geophysical and geochemical investigation of the major fractures on the east side of the New Madrid Earthquake Zone, (with A. L. Reesman), U. S. Nuclear Regulatory Commission, NUREG/CR-4936, 27 p., May.

Reports Published

None this reporting period.

Determination of earthquake source parameters from regional waveforms: Analysis of sparse network data in the Aleutians

1434-92-G-2200

Geoffrey Abers, Won-Young Kim
Lamont-Doherty Geological Observatory of Columbia University
Palisades, New York 10964
(914) 359-2900, 365-8828

Investigations Undertaken

We study wave propagation effects and develop appropriate procedures for calculating regional waveforms and determining source parameters in a subduction environment. We study amplitudes and phases observed in broadband and intermediate period seismograms recorded at stations in the east Aleutians, in particular the seismographic station at Sand Point, Alaska, for east Aleutian earthquakes. These waveforms and full waveform modeling methods are used to better understand propagation effects for these paths, and the sensitivity of these waveforms to earthquake source parameters. The goal of these studies is to characterize Aleutian propagation effects sufficiently to invert regional subduction zone seismograms for earthquake source parameters, and to develop appropriate inversions. In the future, such inversions may provide most of the information available for Aleutian earthquakes that are too small to study from teleseismic data, if monitoring in the Aleutians is based upon a sparse distribution of broadband stations.

Results Obtained

Work thus far has concentrated on assessing wave propagation properties to the station SAN in Sand Point, Alaska, where broad-band and intermediate-period digital waveforms have been recorded since 1982 (funding cuts forced the termination of digital data collection in the summer of 1992). The first part of this work has been to compile focal mechanisms from local network data, recently made possible by the determination of 3D velocity structure and accurate ray tracing through the model [Abers, 1992]. The most promising events are those that show interplate thrusting and events within the downgoing plate next to the interplate thrust events (Figure 1). The interplate thrust events are the most numerous and pose the most significant seismic hazard, so their evaluation is a high priority. The events below the thrust zone have different focal mechanisms and are 5-15 km deeper with similar epicenters; they are similar in depth and mechanism to events at the top of the downgoing plate in subduction zones where interplate thrust events are absent, such as Cascadia or the post-1964 Gulf of Alaska. Because paths are similar for these two sets of events but depths and mechanisms vary, they make a useful data set to test the ability of waveforms to recover source parameters.

Record sections have been constructed for interplate thrust events to station SAN, using broadband and intermediate period waveforms (Figure 2). These figures compare vertical and transverse seismograms, and show differences in arriving *P* and *SH* energy. These events are 25-40 km deep. Several types of complexity are apparent in these record sections:

- Waveforms make the transition at ~150 km range from impulsive seismograms, with most energy in the initial P/S cycle, to emergent records with energy dispersed over many cycles at longer ranges. The more distant class of seismograms will be much more difficult to model by direct waveform matching.
- Significant energy is observed on the transverse component soon after the initial *P* onset, in some cases (~90 km range) within a fraction of a second. Some of this energy has the form of discrete phases, and suggests specific scatterers. These arrivals will be impossible to model using a plane-layered propagation structure, and can be used to estimate the signal-generated noise level that will limit quality of seismogram fit.

• Distinct phases are seen to arrive on vertical component seismograms in the interval between *P* and *S*, the largest arriving 2-4 s before the transverse-component *S* arrival. These are probably *S*-to-*P* conversions, either at the free surface (e.g., Figure 3) or at other interfaces directly below the receiver (more likely for a phase 2-4 s before direct *S*). A successful Green's function must include the generation of these phases, because their amplitude is comparable to direct phases and ignoring them could lead to potentially large errors.

Several sensitivity tests have been conducted of seismogram matching. In one example, a complex plane-layered structure was used to generate seismograms at a series of depths (Figure 3). A prominent phase ~5 s after direct *P* is modeled as a *S*-to-*P* conversion at the free surface; timing of this phase is relatively independent of structure. Large amplitude variations are seen in synthetic seismograms in the first 5-10 s after direct S, due to crustal reverberation (labelled S1S). The amplitude variations of S1S can be equally well modelled by changes in depths to mid-crustal interfaces, comparable to direct *S* amplitudes, suggesting that the early S coda will hard to model without very good estimates of path structure. Another example demonstrates sensitivity to focal mechanism orientation, and shows that even a single seismogram may provide useful constraints on fault orientation (Figure 4).

Publications

Abers, G.A., and W.-Y. Kim, Potential of broad-band regional seismographs in the Aleutians, in Christensen et al., eds.,*Wadati Conference on Great Subduction Earthquakes*, U. Alaska Fairbanks, p. 154-155, 1992.

Abers, G.A., Plate configuration and seismogenic deformation of the Shumagin region, in Christensen et al., eds.,*Wadati Conference on Great Subduction Earthquakes*, U. Alaska Fairbanks, p. 147-149, 1992.

Abers, G.A., Relationship between shallow- and intermediate-depth seismicity in the eastern Aleutian subduction zone, *Geophys. Res. Lett.*, **19**, 2019-2022, 1992.

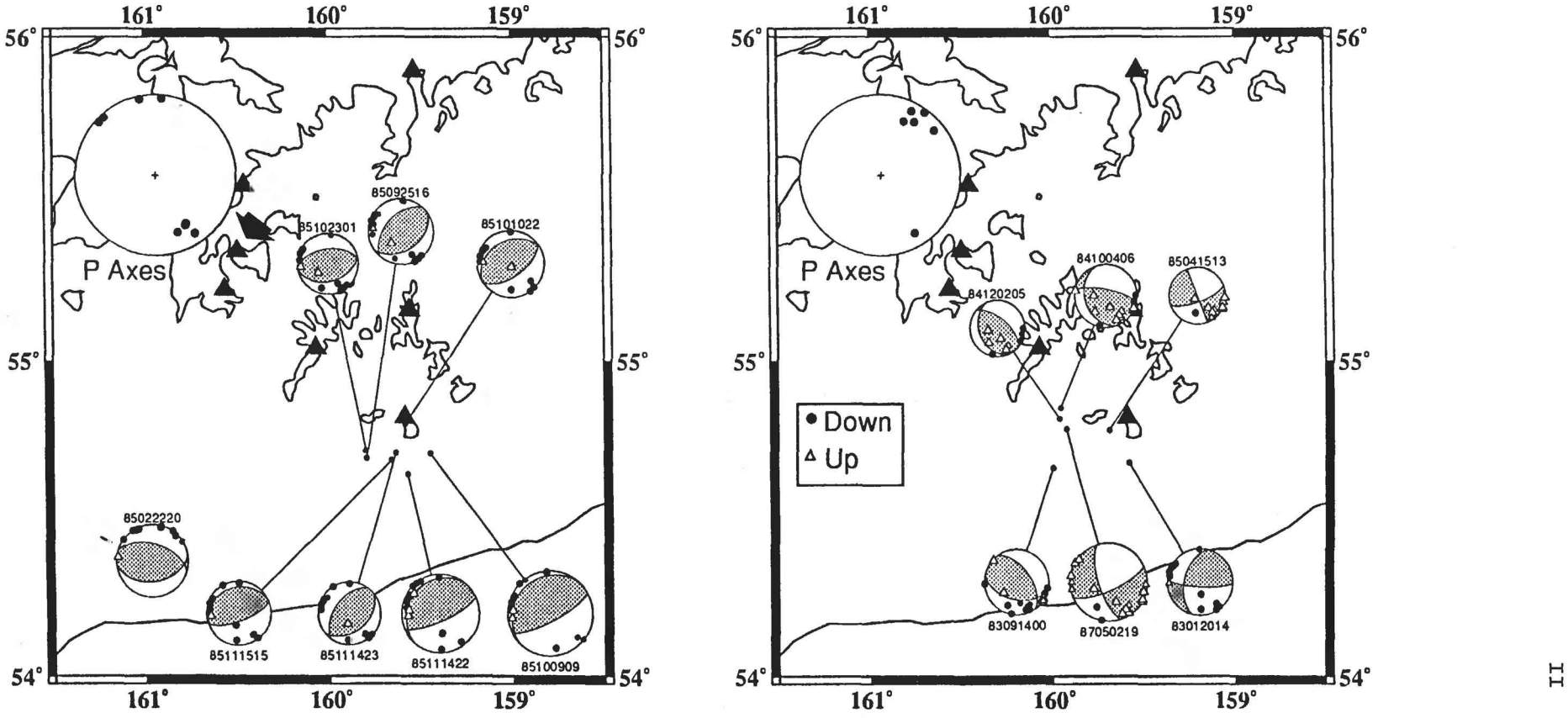

Fig. 1. First motion fault-plane solutions for events on and near the interplate thrust zone in the Shumagin Islands region. Open triangles are dilatations, circles are compressions. Events are relocated in 3D velocity model and rays are determined by exact ray tracing through the model. Events >5 km below main thrust zone show different mechanisms with rotated P axes. Solid triangles show network stations; SAN is indicated by large arrow. All results here are well-constrained by short-period arrival times and first motions; these events can be used to assess inversions of intermediate-period and broadband waveforms.

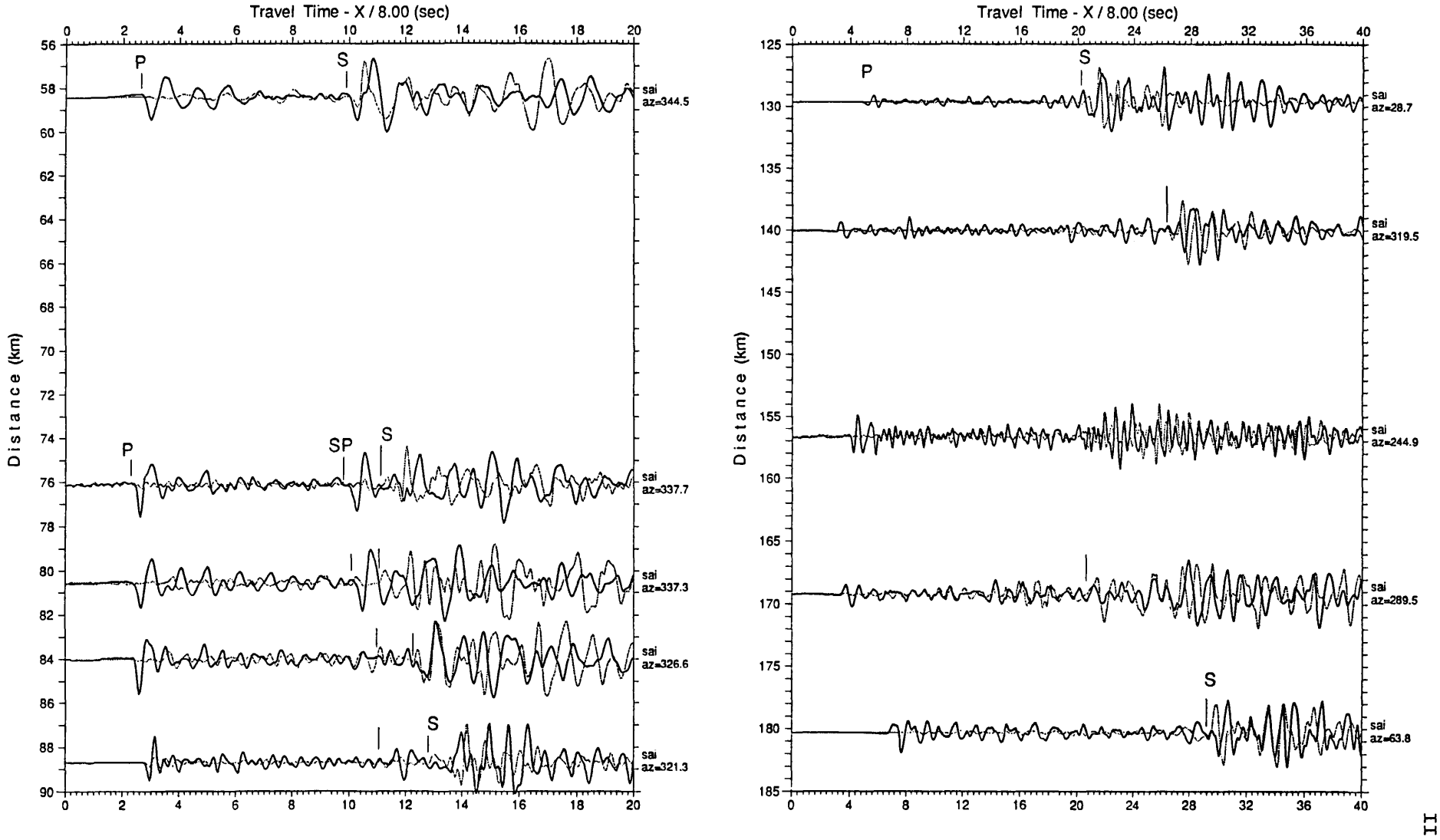

Figure 2. Record sections to station Sand Point (SAI) from interplate thrust zone earthquakes for distance range 56 to 90 km (**left panel**) and for distance range 125 to 185 km (**right panel**). For each event, vertical (*solid*) and transverse (*dotted*) components of intermediate-period records are plotted together for comparison. Records at 156.6 km are broadband. Major phases between P and S are probable converted phases and the most prominent phases (SP) arrive 1-2 sec before S with similar amplitude as S. Timing is modeled by S-P conversion ~10 km below station. Phase arrives too late for Sp free-surface critical refraction. These phases are large and are necessary to understand in modeling waveforms.

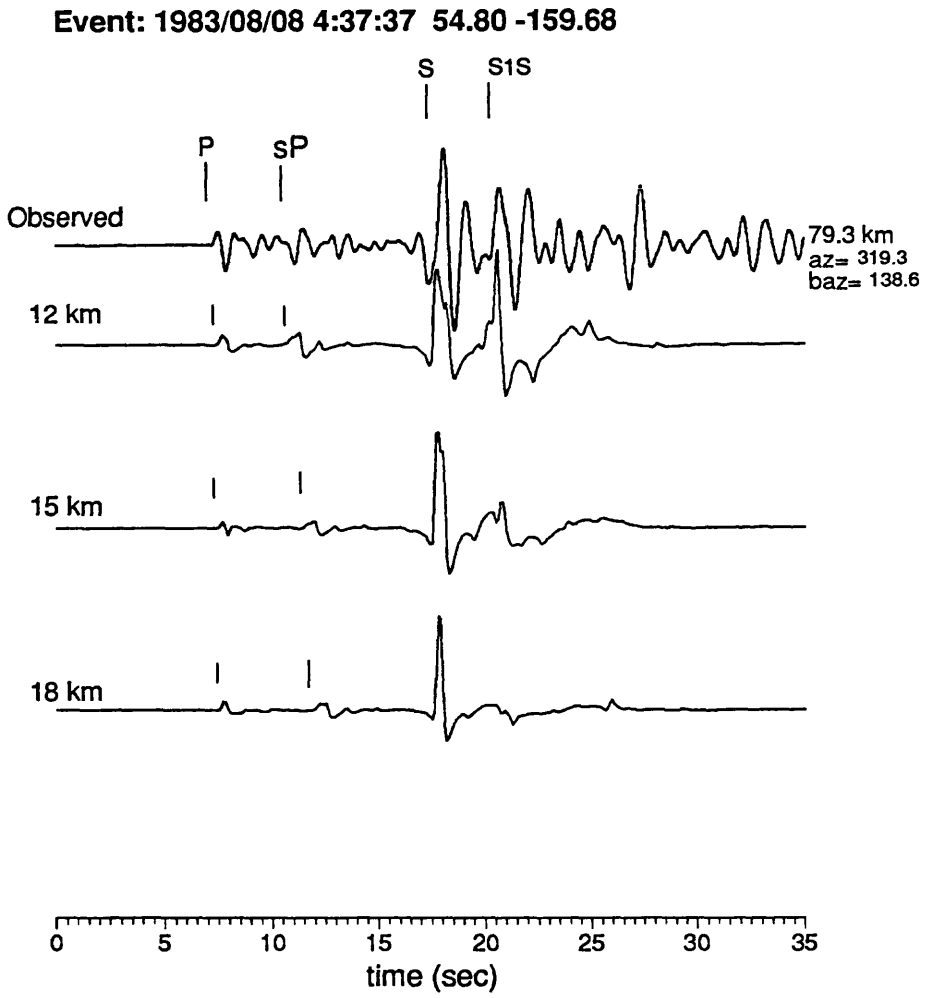

Figure 3. Observed and calculated vertical-component intermediate-period seismogram for event an upper-plate event 79 km from station at Sand Point, Alaska (event depth ~15 km from S-P times at station directly over event). Calculated seismograms are generated for mechanism consistent with first-motions, for depths of 12, 15, and 18 km. Calculation is a full-waveform seismogram using reflectivity and wavenumber integration, assuming a plane-layered structure similar to one determined from arrival-time inversion. The sP is the phase modelled as a S-to-P converted phase reflected off of the free-surface. Note relatively constant S-P times and 1 s change in sP-P times. Relative amplitudes of S to crustal reverberation S1S vary significantly with depth, because distance to nearest layer boundary changes (layer boundaries are at 10, 20, 30, 40, 75 km depth). Similar amplitude changes can be generated by moving interface with depth fixed, so if depth is known (from sP-P) then structure can be constrained.

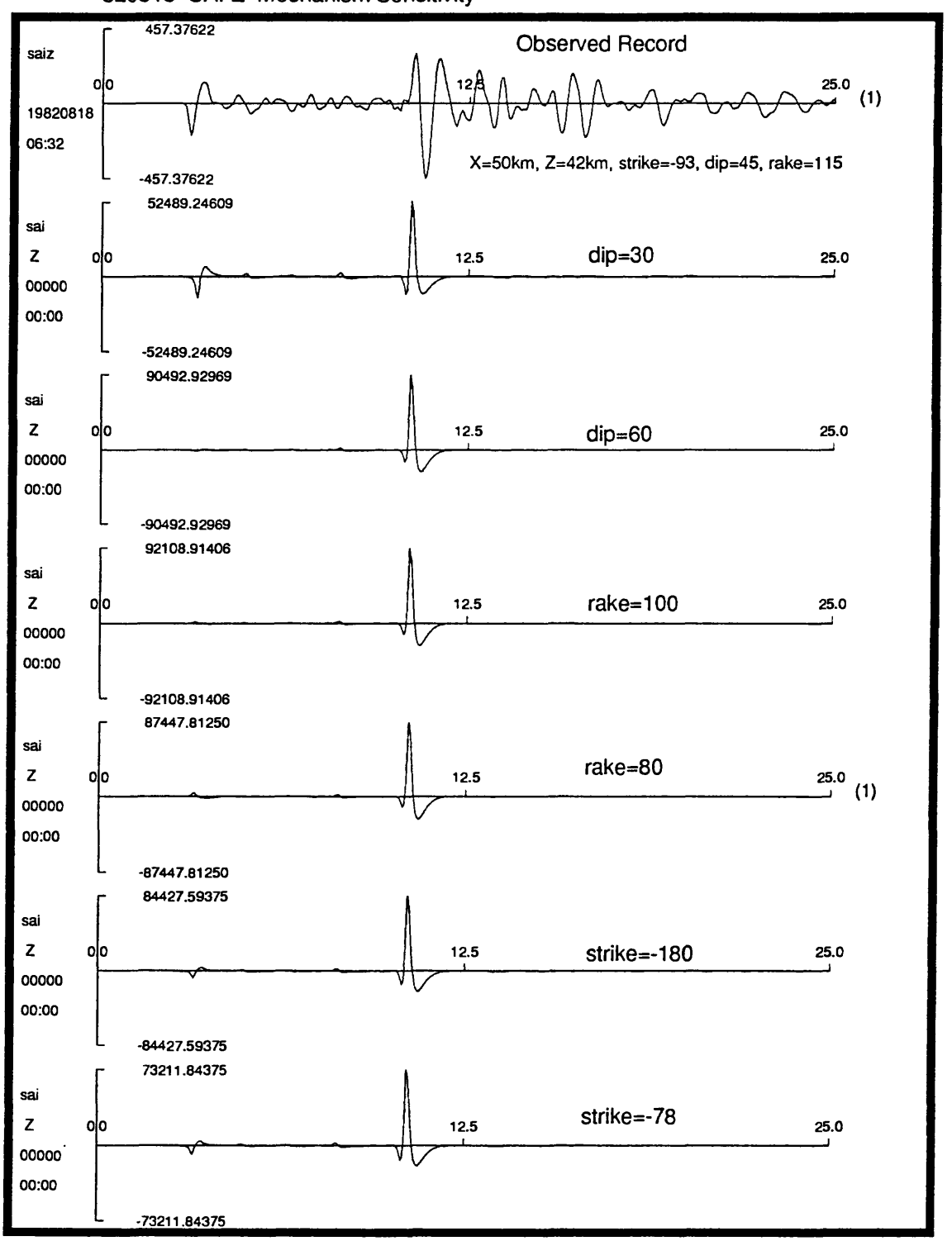

Figure 4. Vertical-component IP seismogram for event 820818 (42 km deep, 50 km distance) compared with seismograms calculated for varying mechanism. Mechanism determined from network first-motion polarities is oblique-reverse slip; parameters given at top. Observed seismogram is on top, followed by seismograms where each of strike, dip, slip is perturbed by 15 degrees. All seismograms are scaled by maximum amplitude. Velocity structure resembles that determined from inversion of arrival-times. Increase in rake or dip gives P arrivals that are too small.

Studies on Intrinsic Q^{-1} and Scattering Q^{-1} in Earthquake Source Regions

1434-92-G-2179
Keiiti Aki and Anshu Jin
Department of Geological Sciences, University of Southern California
Los Angeles, CA 90089-0740

INVESTIGATION

Introduction and objective

Attenuation of S-waves measured by Q^{-1} consists of contributions from scattering and absorption, namely, $Q^{-1} = Q_s^{-1} + Q_i^{-1}$, $Q_s^{-1}=k^{-1}\eta_s$ and $Q_i^{-1}=k^{-1}\eta_i$, where k is the wavenumber and η_s and η_i are the scattering and intrinsic attenuation coefficients, respectively. Hoshiba et al., (1991) have developed a method, called " multiple lapse time analysis", in which they consider energy for three consecutive time windows as a function of hypocentral distance to estimate the seismic albedo, $B_0=\eta_s/(\eta_s+\eta_i)$, and the total attenuation coefficient L_e^{-1}. Where $L_e=1/(\eta_s+\eta_i)$ is the extinction distance over which the primary S-wave energy is decreased by e^{-1}. Figure 1 shows how the energy determined for the three time windows varies as a function of source-receiver distance. They are calculated by Monte-Carlo simulations using homogeneously distributed scatterers in a full-space with uniform intrinsic attenuation under the assumption of isotropic multiple scattering for various B_0 and L_e (Hoshiba et al., 1991).

The objective of this study is to determine the intrinsic Q^{-1} and scattering Q^{-1} separately by applying the method of Hoshiba et al.(1991) to the broad-band high dynamic range seismograms of the TERRAscope network in southern California .

Data

Figure 2 shows the locations of the 6 TERRAscope seismic stations and the earthquakes used in this study. To obtain both the scattering and intrinsic Q^{-1} as a function of frequency, we selected earthquakes within 70 km for each station. Then we calculated, for each seismogram, the squared amplitude spectrum, $|F(\omega)|^2$ for the following three time windows: 0 to 15 seconds , 15 to 30 seconds, and 30 to 45 seconds measured from the onset of the S-wave arrival. We eliminated the effect of ambient noise by taking a noise sample of length 25 s prior to the P-wave arrival and subtracting the noise power spectra from the signal power spectra in each time window assuming that signal and noise are statistically independent. Data with signal power less than twice the noise was discarded. To normalize the observed energy for different magnitude earthquakes we chose a coda sample at a reference lapse time of 45 ± 2.5 seconds and calculated the squared amplitude spectrum, $|F^{ref}_{coda}(\omega)|^2$. The spectra for each lapse time window and the coda spectra at the reference lapse time (45 s) are averaged over three components and the normalized energy, $\frac{|F(\omega)|^2}{|F_{coda}(\omega)|^2}$, is calculated for each station - earthquake pair.

RESULTS

(1), No significant differences, neither in B_0 nor L_e^{-1}, have been found between the stations located on or near the San Andreas fault (such as station SVD, PFO, and PAS) and the stations far away from the fault (such as station ISA and GSC).

(2), Figure 3 shows the normalized energy, corrected for geometrical spreading by $4\pi r^2$ as a fuction of hypocentral distance for all stations at frequencies 0.75, 1.5, 3.0, and 6.0 Hz. The preliminary estimates of B_0 and L_e^{-1} for the whole of southern California, and corresponding scattering, intrinsic and total attenuation values, Q_s^{-1}, Q_i^{-1} and Q_t^{-1}, are listed in Table 1. Scattering dominates intrinsic absorption at low frequencies and vice versa at high frequencies. This is a universal observation for the frequency range 1 to 10 Hz.

Table 1

frequency (Hz)	Bo	δBo	L_e^{-1}	δL_e^{-1}	Q_s^{-1}	Q_i^{-1}	Q_t^{-1}
0.75	0.70	0.20	0.050	0.020	0.0223	0.0095	0.0318
1.5	0.50	0.12	0.075	0.025	0.0119	0.0119	0.0238
3.0	0.35	0.10	0.048	0.018	0.0027	0.0050	0.0077
6.0	0.30	0.07	0.048	0.018	0.0011	0.0027	0.0038

$B_0 = \eta_s L_e$, $L_e^{-1} = \eta_e = (\eta_i + \eta_s)$, where η_s, η_i, and η_e are the scattering, intrinsic and total attenuation coefficients, respectively. Attenuation was determined by: $Q_s^{-1} = \eta_s k^{-1}$, $Q_i^{-1} = \eta_i k^{-1}$, and $Q_t^{-1} = \eta_e k^{-1}$, where $k = 2\pi f/\beta$ and $\beta = 3.0$ km/s. δB_0 and δL_e^{-1} is the standard error of B_0 and L_e^{-1}, respectively.

Reference

Hoshiba, M, H. Sato, and M. Fehler, Numerical basis of the Separation of scattering and intrinsic absorption from full seismogram envelope, --a Monte-Carlo simulation of multiple isotropic scattering, Meteorology and Geophysics, 42, 65-91,1991.

Figure captions

Figure 1. Energy for the three time windows (0-15s, 15-30s,and 30-45s) plotted as a function of hypocentral distance r (km) for different pairs of L_e and B_0 predicted by Monte-Carlo simulations. Here the scatterers are statistically uniformly distributed in a full-space with uniform absorption coefficient. The scattering is assumed to be isotropic. (Following Hoshiba et al., 1991.)

Figure 2. Locations of the 6 TERRAscope seismic stations (the triangles) and the earthquakes used in theis study (the solid dots).

Figure 3. Plots of normalized energy corrected for geometrical spreading, $4\pi r^2$, as a function of hypocentral distance r (km), for frequencies 0.75, 1.5, 3.0, and 6.0 Hz (from the top to the bottom), measured at station SVD (right) which is located on the San Andreas fault, and ISA (left) which is located at a distance from the fault. E_1, E_2, and E_3 represent energy measurements for time windows of 0-15, 15-30, and 30-45 second, respectively.

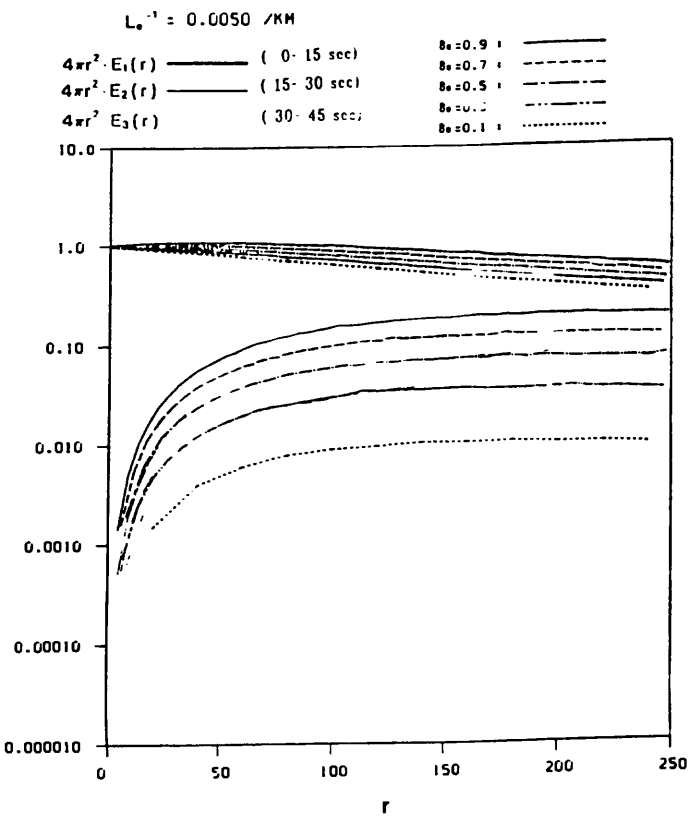
L_e^{-1} = 0.0050 /KM
$4\pi r^2 \cdot E_1(r)$ (0- 15 sec)
$4\pi r^2 \cdot E_2(r)$ (15- 30 sec)
$4\pi r^2 \cdot E_3(r)$ (30- 45 sec)
Be=0.9
Be=0.7
Be=0.5
Be=0.1
10.0
1.0
0.10
0.010
0.0010
0.00010
0.000010
0
50
100
150
200
250
r

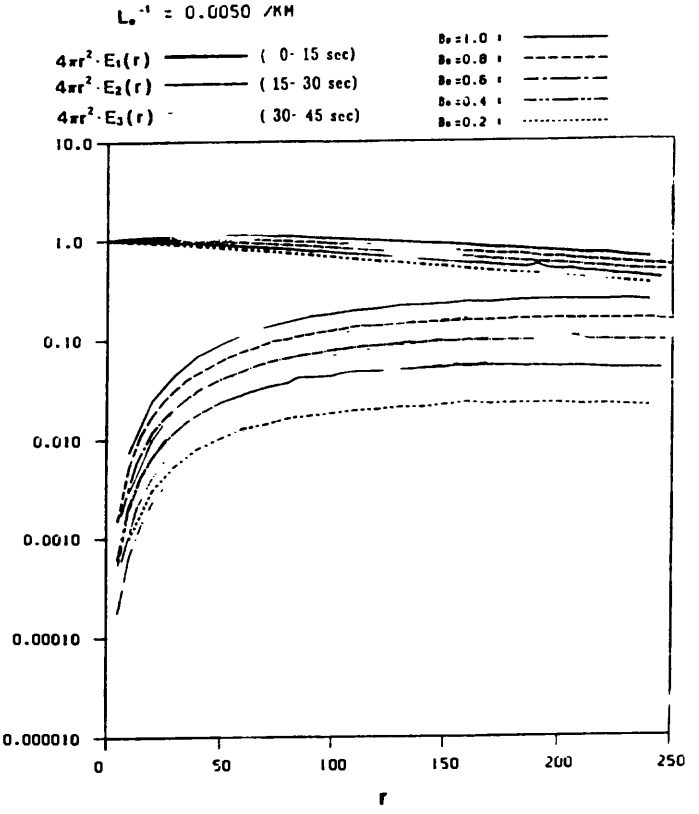
L_e^{-1} = 0.0050 /KM
$4\pi r^2 \cdot E_1(r)$ (0- 15 sec)
$4\pi r^2 \cdot E_2(r)$ (15- 30 sec)
$4\pi r^2 \cdot E_3(r)$ (30- 45 sec)
Be=1.0
Be=0.8
Be=0.6
Be=0.4
Be=0.2
10.0
1.0
0.10
0.010
0.0010
0.00010
0.000010
0
50
100
150
200
250
r

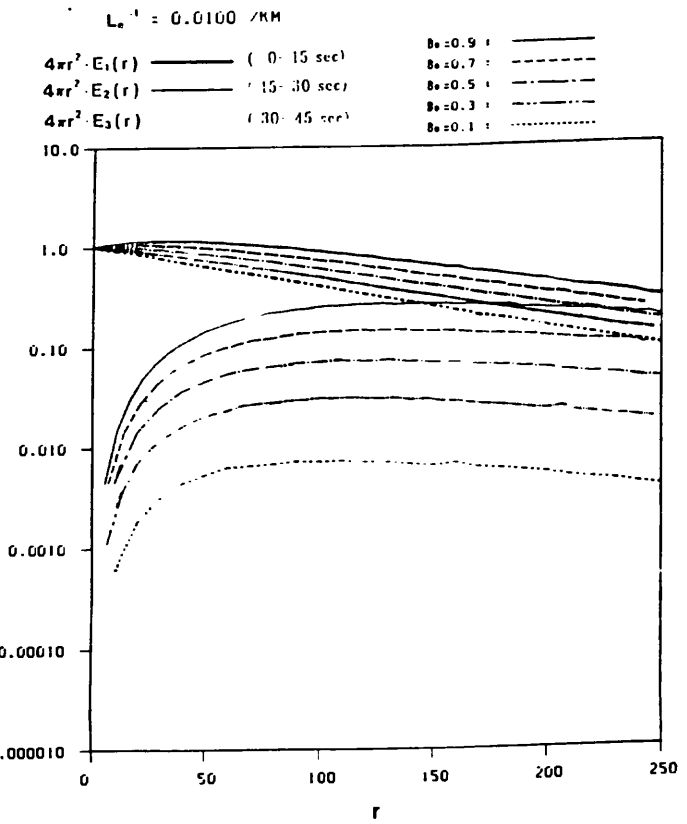
L_e^{-1} = 0.0100 /KM
$4\pi r^2 \cdot E_1(r)$ (0- 15 sec)
$4\pi r^2 \cdot E_2(r)$ (15- 30 sec)
$4\pi r^2 \cdot E_3(r)$ (30- 45 sec)
Be=0.9
Be=0.7
Be=0.5
Be=0.3
Be=0.1
10.0
1.0
0.10
0.010
0.0010
0.00010
0.000010
0
50
100
150
200
250
r

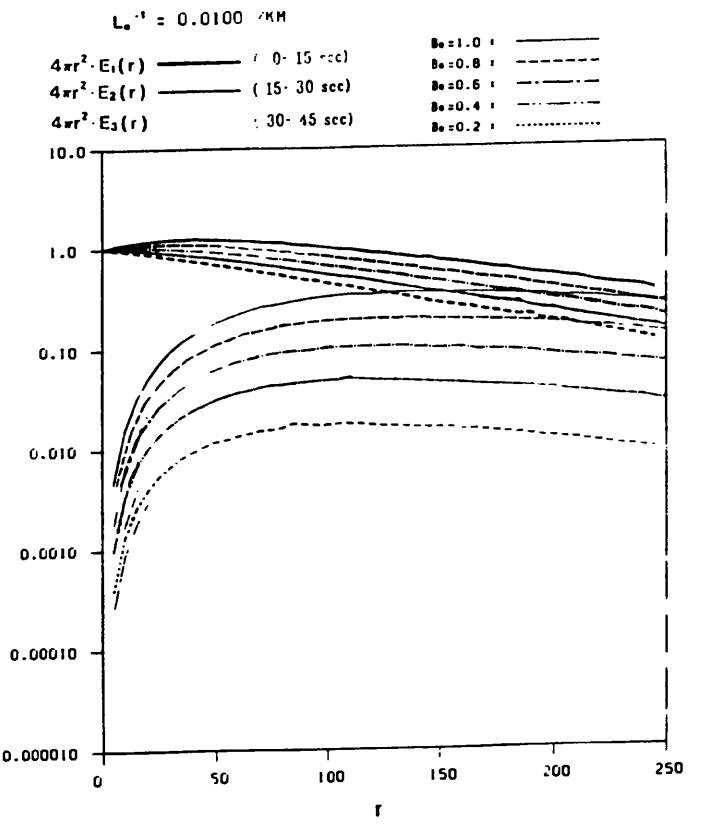
L_e^{-1} = 0.0100 /KM
$4\pi r^2 \cdot E_1(r)$ (0- 15 sec)
$4\pi r^2 \cdot E_2(r)$ (15- 30 sec)
$4\pi r^2 \cdot E_3(r)$ (30- 45 sec)
Be=1.0
Be=0.8
Be=0.6
Be=0.4
Be=0.2
10.0
1.0
0.10
0.010
0.0010
0.00010
0.000010
0
50
100
150
200
250
r

Figure 1

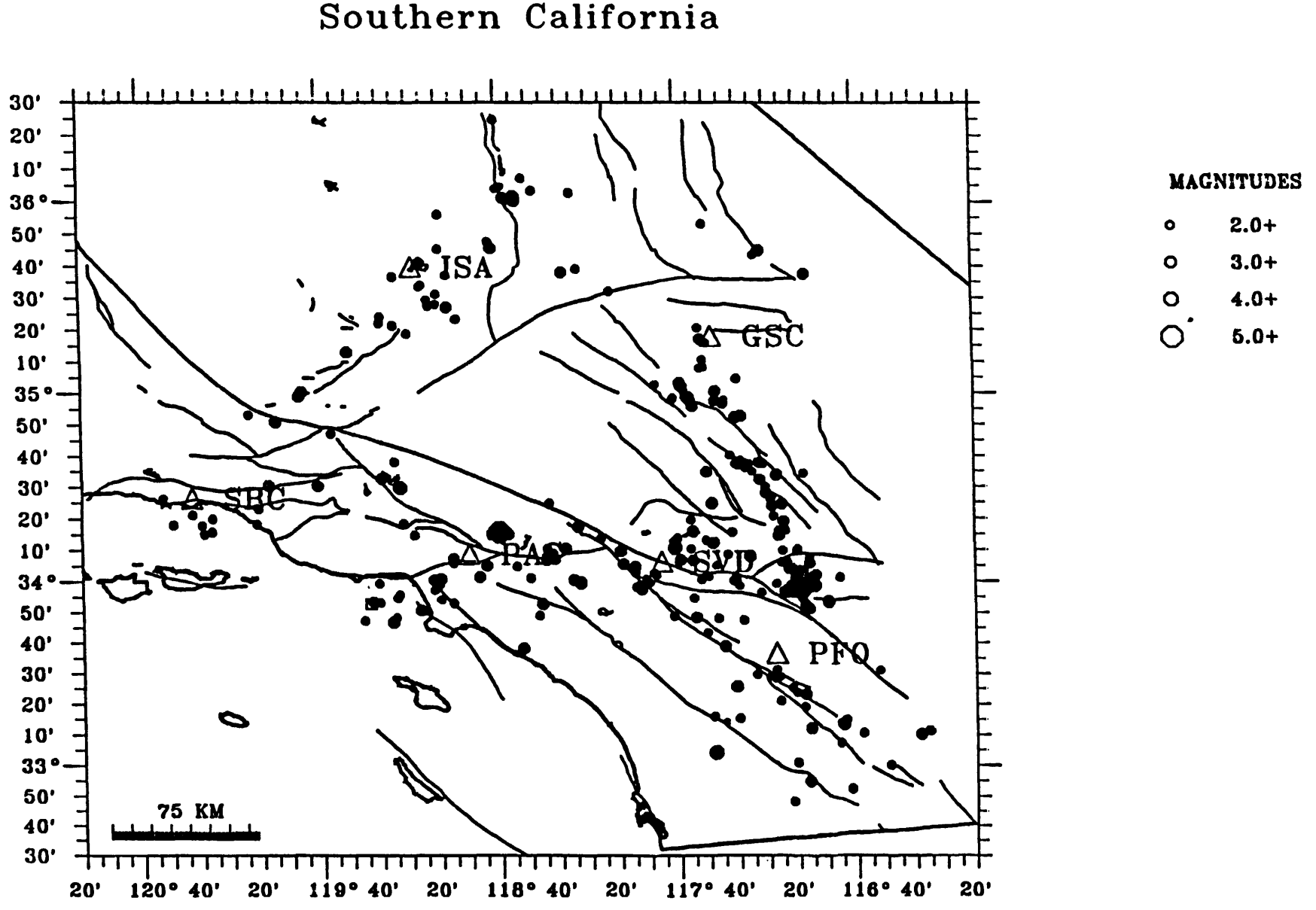
Southern California
MAGNITUDES
2.0+
3.0+
4.0+
5.0+
ISA
GSC
SBC
PAS
SVD
PFO
75 KM
30'
20'
10'
36°
50'
40'
30'
20'
10'
35°
50'
40'
30'
20'
10'
34°
50'
40'
30'
20'
10'
33°
50'
40'
30'
20'
120° 40'
20'
119° 40'
20'
118° 40'
20'
117° 40'
20'
116° 40'
20'

Figure 2

REGIONAL AND LOCAL HAZARDS MAPPING IN THE EASTERN GREAT BASIN

9950-01738

R. Ernest Anderson
Branch of Geologic Risk Assessment
U.S. Geological Survey
Box 20546, MS 966, Denver Federal Center
Denver, Colorado 80225
(303) 273-8578

INVESTIGATIONS

1. Studied the interrelations between Neogene strain and its bearing on horizontal extension and horizontal and vertical contraction at the eastern margin of the extensional orogen, Mormon Mountains area, Nevada and Utah.

2. Studied the interrelations between Neogene strain and its bearing on horizontal extension, and horizontal and vertical contraction at the transition zone of the Colorado Plateau and Basin and Range in the tricorner area of the Virgin River depression, Utah, Nevada, and Arizona.

RESULTS

1. Analysis of the distribution, geometry, and kinematics of structures of known or suspected Neogene age ranging in size from mountain blocks to outcrop scale between the southern Mormon Mountains and the Colorado Plateau shows that extensional deformation was accompanied by major vertical structural uplift and associated structural thinning (attenuation) and by extension-normal horizontal contraction. The vertical attenuation developed mainly by normal-sense displacements on steeply dipping to horizontal faults and appears to be most intense on the flanks of and above severely uplifted and tilted footwall blocks, several of which are major structural culminations that expose Precambrian crystalline basement rocks. Tilts of strata in these footwall culminations commonly exceed those in the hanging wall, suggesting convex-upward fault geometry. The faults either have curved traces concave upward toward the culmination or consist of two segments whose obtuse intersection angle faces the culmination. Stratigraphic throw either decreases abruptly away from the culmination axis or is fed abruptly into major transverse accommodation zones that possibly represent long-lived structural flaws. Typically, the culminations have strike lengths only two to three times their maximum throw, suggesting extreme lateral strain heterogeneity. Most are too small and have flanks that dip too steeply for isostatic uplift following tectonic denudation to be a cause of their formation. Also, in plan view, they tend to be arranged en echelon such that strain is not cumulative from one to the other along sections paralleling their kinematic axes. A major effect of hanging-wall structural attenuation adjacent to and above the culminations is to subdue the potential surface relief associated with uplift and tilting of the footwall.

2. The Virgin River depression and surrounding mountains in the Utah, Nevada, and Arizona tricorner area are Neogene features that are partly contiguous with the little-strained rocks of the structural transition to the Colorado Plateau province. This contiguity makes the area ideally suited for evaluating the sense, magnitude, and kinematics of Neogene deformation. Analysis along the strain boundary shows that, compared to the adjacent little-strained area, large-magnitude vertical deformation (both uplift and depression, locally exceeding 10 km) greatly exceeds extensional deformation and that there are tectonically significant amounts of lateral displacement approximately parallel tot he province

boundary. Extensional kinematics, the directions of lateral displacements, and the positioning and orientation of uplifts and one major depression are such that isostatic rebound following tectonic denudation is an unlikely direct cause of the strong vertical structural relief adjacent to the strain boundary. Instead, the observed structures are first-order features that define a three-dimensional strain field that formed in response to approximately east-west extension, vertical structural attenuation, and extension-normal shortening.

REPORTS

Anderson, R.E., and Barnhard, T.P., 1991, Relationship between Miocene plutonism, uplift, and extension Lake Mead area, northernmost Arizona and adjacent Nevada: Geological Society of America Abstracts with Programs, v. 23, p. A245.

____1992, Neotectonic framework of the central Sevier Valley area, Utah, and its relationship to seismicity: U.S. Geological Survey Professional Paper 1500-F, p. F1-F48.

____1992, Heterogeneous Neogene strain and its bearing on horizontal extension and horizontal and vertical contraction at the margin of the extensional orogen, Mormon Mountains area, Nevada and Utah: U.S. Geological Survey Bulletin B-2011, 113 p.

____(in press), Aspects of three-dimensional strain at the margin of the extensional orogen, Virgin Depression area, Nevada, Utah, and Arizona: Geological Society of America.

Anderson, R.E., and Hintze, L.F., 1991, Geologic map of the Dodge Spring quadrangle, Washington County Utah, and Lincoln County, Nevada: U.S. Geological Survey Open-File Report OF-360, scale 1:24,000

____1992, Geologic map of the Dodge Spring quadrangle, Washington County, Utah, and Lincoln County, Nevada: U.S. Geological Survey Quadrangle Map GQ-1721, scale 1:24,000.

Barnhard, T.P., and Anderson, R.E., 1991, Tectonic significance of dike orientations int he Lake Mead area of Nevada and Arizona: Geological Society of America Abstracts with Programs, v. 23, p. A233.

Analysis of Similar Earthquakes in Seismic Gaps

Award number 1434-92-G-2202

Richard C. Aster (P.I.)
Joseph A. Henton (Graduate Student)
Department of Geoscience/Geophysical Research Center
New Mexico Institute of Mining and Technology
Socorro, NM 87801
(505) 835-5924

Introduction

We utilize nearly identical microearthquake pairs recorded by the Anza, Parkfield, and Southern California seismic networks as quasi-repeating broadband sources at depth to probe seismic gaps in California for possible temporal variations in the seismic Green function. Significant progress has been made over the past year on the three principal goals of this project:
(1) Comprehensive identification of similar earthquake pairs and clusters in large microearthquake data sets.
(2) Development and evaluation of techniques for relative waveform analysis.
(3) Analysis of similar microearthquake seismograms to identify or establish limits on temporal variability in seismic Green's functions, specifically concentrating on seismic velocity, coda decay, and shear-wave anisotropy.

Progress

Comprehensive identification of similar earthquakes in large microearthquake data sets.

The first step in the project, now nearly completed, is to identify all earthquake pairs and clusters most suitable for similar earthquake analysis. One may, in principle, evaluate the complete upper-triangular matrix characterizing the waveform similarity of all of the earthquake pairs. For large data sets such as those considered here, however, this process may become prohibitively time consuming, as the amount of work required is proportional to $N(N-1)$. It is thus worthwhile to consider reasonable precomparison criteria which allow one to dismiss *a priori* those earthquake pairs which are highly unlikely to have similar seismograms.

Studies of waveform coherence from earthquake sources (e.g., Geller and Mueller, 1980; Thorbjarnardottir and Pechmann, 1987) suggest that a search for similar events would not need to consider earthquake pairs with interhypocenter separations of much more than a few times $\lambda_{max}/4$, where λ_{max} is the longest wavelength of interest. More recent work (Hutchings and Wu, 1990; Harris, 1991; Vernon, 1992; Scott, 1992) indicates that the $\lambda_{max}/4$ guideline is too restrictive in some cases, and that appreciable coherence can exist for interhypocenter separations of up to a few times λ. Thus, if one only examines seismograms from earthquake pairs with interhypocenter separations of $\Delta \leq \Delta_{max}$, where Δ_{max} is taken to be both several times the maximum dimension of a typical hypocenter error ellipse and several times λ_{max}, then essentially all highly similar earthquake pairs will be identified, despite a large reduction in computer time.

For the Anza network (Berger et al., 1984; Vernon, 1989) catalogue typical hypocenter errors are approximately 1 km (Scott, 1992; Scott et al., 1992), however, it is possible for an event to be mislocated by much more than this if one or more of the picks has an anomalously large picking error due to a phase misinterpretation. As a result of this problem, standard cluster studies based on nearly identical hypocenters may miss some nearly-identical pairs. Our algorithm can overcome this difficulty when a fairly generous value for Δ_{max} is chosen.

For the Anza data set, Δ_{max} was taken to be 10 km. To further reduce the work required to characterize waveform similarity, we eliminated from the analysis waveforms which were identified in the Anza data base as being unreadable. These precomparison criteria reduced the number of three-component seismogram pairs which needed to be cross-correlated by over an order of magnitude, from approximately 9×10^7 to approximately 5×10^6.

In general, any commutative measure may be chosen to quantify waveform similarity. For Anza network recordings which satisfied the above precomparison criteria, the three-component shear-wave seismogram cross-correlation peak between pairs of events (Aster et al., 1990) observed across the network was taken as the similarity measure. The median was chosen after trying several other operators. The minimum or mean cross-correlation was found to be unduly sensitive to low cross-correlation outliers which occasionally occurred when the S-wave arrival times used for the initial alignment of the two events exceeded the window length used in the cross-correlation at one or more stations. The maximum cross-correlation operator, on the other hand, tended to unduly emphasize the contribution of seismograms recorded at stations which were band-limited due to high near-surface attenuation (e.g., stations WMC and LVA; Hough and Anderson, 1988; Hough et al., 1988; Vernon, 1989).

The similarity measure for events j and k is thus $S_{jk} = \text{median}_i\{C_{ijk}\}$, where i is a station index and C_{ijk} is the three-component cross-correlation maximum. The time window used was 0.512 s ($M = 128$ samples) of the shear wave, beginning 0.128 s (32 samples) before the S arrival time pick. The S_{jk} were estimated for 1,121,332 earthquake pairs, requiring approximately 3 weeks of CPU time on a SUN sparc2 workstation. A plot of the S_{jk} versus estimated interhypocenter separation is shown in Figure 1.

The S_{jk} are quantitative measures of the degree of similarity between wavefield pairs, as spatially sampled by stations in the network. It is often the case that many mutually similar earthquakes will be generated in a small region, (e.g., Ishida and Kanamori, 1978; James and Savage, 1990). An equivalence class (EC) algorithm (e.g., Knuth, 1968; Press et al., 1986) was used to organize the pair similarity information into similar earthquake clusters. The EC procedure organizes the pair similarity catalogue into nonintersecting sets of events, the elements of which satisfy a commutative "sameness". In this application, the resulting event trees are open in that if earthquake pairs (A, B) and (B, C) both satisfy the sameness condition, then A, B, and C will be grouped into the same equivalence class, regardless of the similarity measure between A and C.

The sameness condition for the Anza network data was taken to be $S_{jk} \geq \beta$, where β is a value between 0 and 1. If β is close to 1, then the EC algorithm will identify a small number of tiny clusters consisting of earthquakes with extremely similar seismograms. As the β cutoff is reduced, new pairs become eligible for consideration, and are either incorporated into existing clusters or are assigned to new clusters. Additionally, two or more formerly separate clusters may coalesce into a single cluster. As β becomes close to the cross-correlation noise value, coalescence will eventually dominate, resulting in a small number of huge clusters containing almost all of the earthquakes. Because of the competing processes of new cluster formation and cluster coalescence, some value of β will produce a maximum number of clusters (there may be multiple maxima for some data sets).

To find a near-optimal β value for organizing events pairs into clusters, the number of event pairs, the number of equivalence classes, and the number of individual events were counted for $\beta = \{0.975, 0.950, 0.925, ..., 0.400\}$ (Figure 2). In the Anza data set, clustering was maximized ($N_{Equiv} = 290$) for $\beta \approx 0.725$ (1255 events; 1720 pairs). Figure 3 shows the locations of events in clusters with ten or more members, the largest of which occur along the Buck Ridge fault near Toro peak (number 276; 202 events) and in the Cahuilla Swarm zone, west of the seismic gap (number 212; 118 events). Both of these clusters have been sporadically active throughout the operational period of the Anza network (with pronounced peaks in activity during 1990 for the Buck Ridge cluster and during 1983 for the Cahuilla Swarm) and have produced similar earthquakes pairs with large temporal separations.

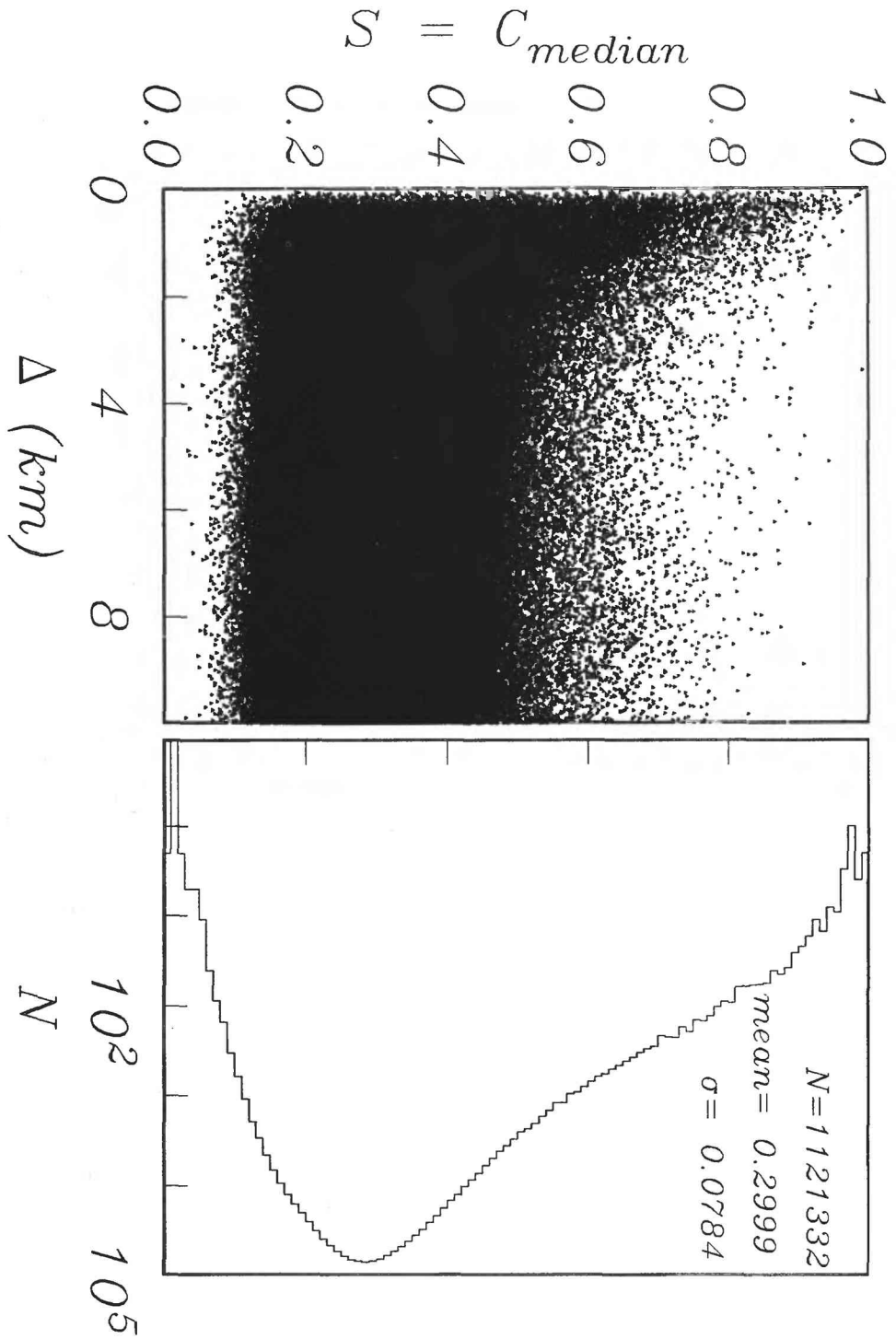

Figure 1. Median values of the shear-wave cross-correlation maximum, S, versus interhypocenter distance, $\Delta \leq 10$ km, for 1,121,332 Anza seismogram pairs satisfying the precomparison criteria (see text). The earthquakes were recorded between October, 1982 and April, 1992. A histogram of S values is shown at *right*. The wide range of S at small values of Δ indicates that small interhypocenter separations from network locations alone are insufficient to identify events with highly similar waveforms. The falloff of S values to background levels by about $\Delta = 3$ km indicates that $\Delta_{max} = 10$ km was sufficiently large for this data set to encompass almost all highly similar earthquake pairs.

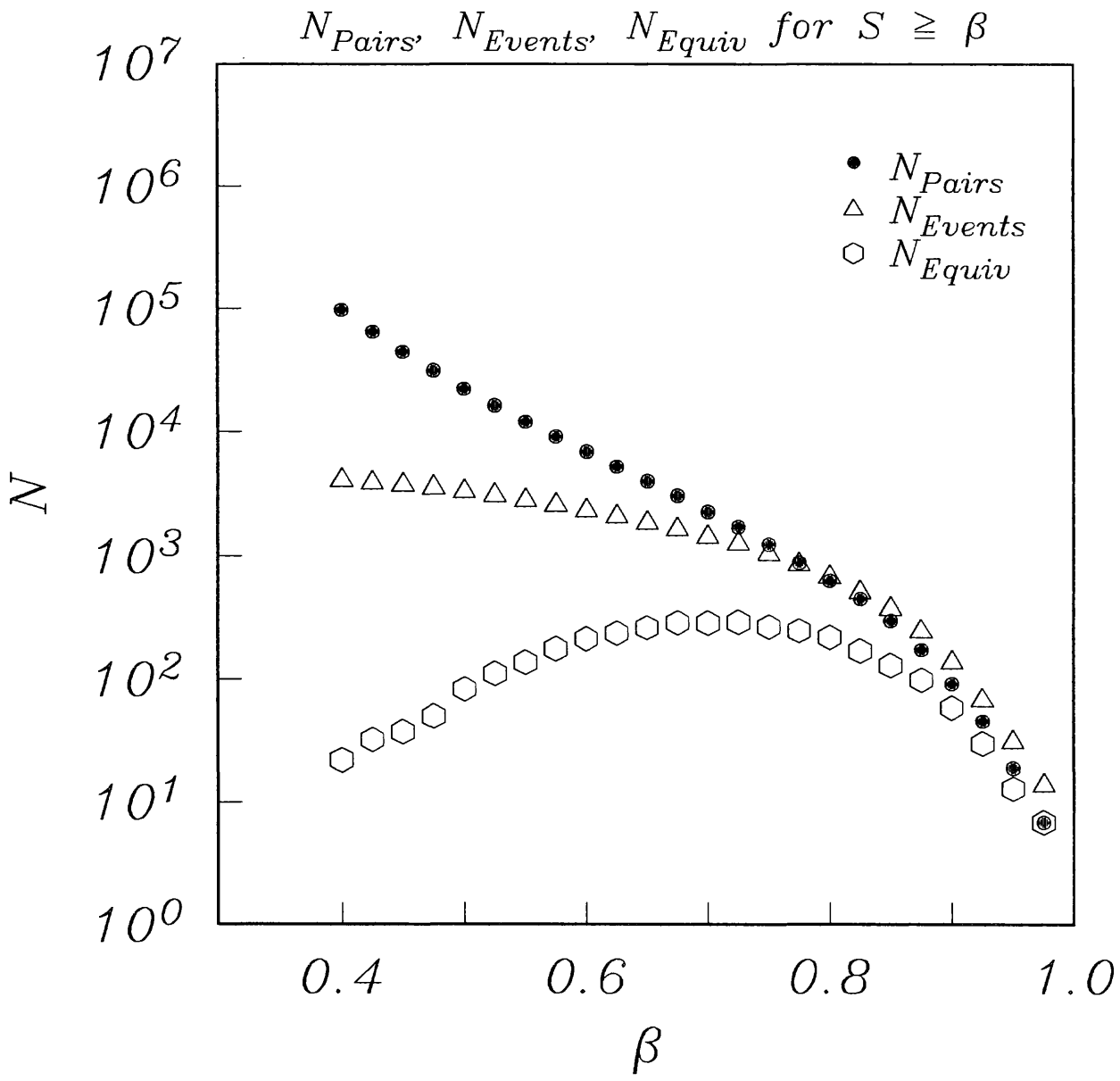

Figure 2. Number of earthquake pairs, events, and equivalence classes as a function of β, the minimum value of the median shear-wave crosscorrelation value (Figure 1). The number of clusters is maximized near β = 0.725).

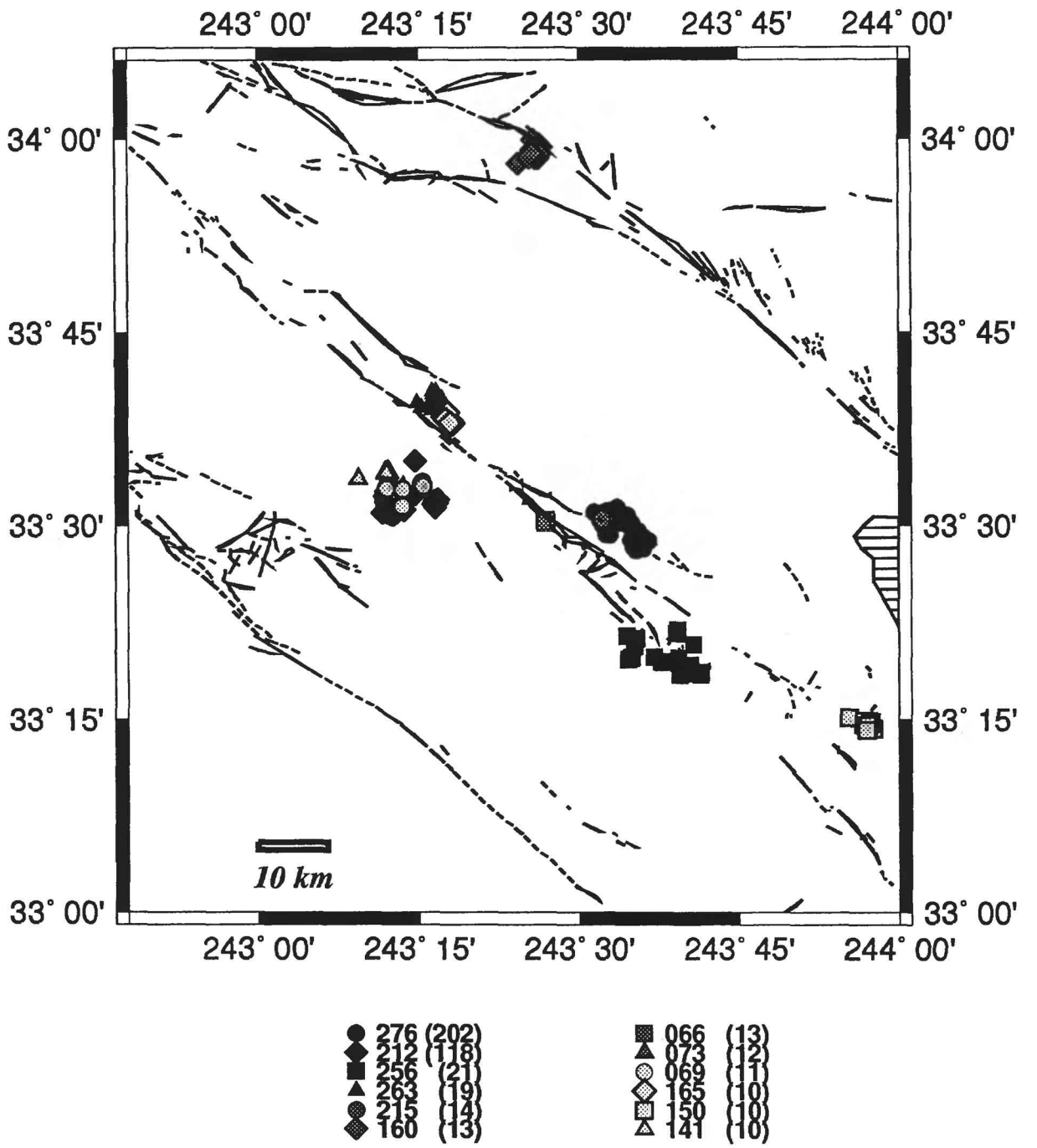

Figure 3. Network epicenters of the twelve largest ($N_{Equiv} \geq 10$) similar earthquake clusters identified at Anza for $\beta = 0.725$ (Figure 2). The legend denotes each cluster number and population.

This similar event identification algorithm is also currently being applied to obtain a comprehensive similar event catalog for Parkfield HRSN data by Bob Nadeau and Mike Antolik at U.C. Berkeley (Nadeau et al., 1991). This counterpart catalogue will ultimately enable direct comparisons between similar seismogram analyses at Anza and Parkfield.

Development and evaluation of techniques for relative waveform analysis.

The signal processing aspects of similar earthquake analysis generally involve two overlapping concerns. 1) Temporal alignment (or equivalently, lag estimation), either in moving windows or for entire seismograms. This type of measurement is especially appropriate for analyzing possible velocity variations in direct body phases and possibly for secondary phases buried in the coda (e.g., Verwoerd et al., 1992, Ellsworth et al., 1992). 2) Estimation of moving-window spectral ratios. This technique is most appropriate for coda or attenuation analysis, where one is testing for smooth variations in the Green function frequency response, such as might be induced by temporal variations in the degree of lithospheric microcracking.

When seeking to positively identify what may be very small variations in the response of the Earth to seismic waves, it may be essential to use the most robust and high-resolution techniques available on a large number of microearthquake pairs. We have progressed this year on developing the best possible techniques currently available for estimating relative lag times by testing both coherence-weighted phase slope methods (e.g., Poupinet et al., 1985) and Fourier interpolation methods (e.g., Aster and Shearer, 1992). We have also written and implemented multitaper spectral methods for estimating relative spectral amplitudes and coherence, as developed by Thomson (1982) and subsequently adapted for seismological applications by Park et al. (1987) and by Vernon (1989; 1992). Preliminary indications using a limited range of synthetic seismogram pairs suggest the the most robust estimates of relative times may be obtainable using Fourier interpolation and that the most robust spectral estimates are obtainable using multitaper Fourier analysis techniques.

Analysis of similar microearthquake seismograms to identify or establish limits on temporal variability in seismic Green's functions.

Our present emphases in relative seismogram analysis to assess any variability in seismic coda (Aster et al., 1992) and/or seismic velocities (Scott et al., 1992) using Anza network data from 1982 to present.

Temporal changes in seismic velocity. If temporal changes in seismic velocity exist due to stress-induced changes in or near the fault zone, they may be detectable in the variation of travel time residuals for rays which sample the same region at different times (Poupinet et al., 1984; 1985). Signals from nearly identical earthquakes in the Anza similar event catalogue are ideal for this type of analysis as differences due to path and source differences will be minimized. Scott et al. (1992) analyzed a highly similar pair of events with a 945 day time separation recorded at 8 stations. and found that relative travel-times of direct phases could be fit to less than 3 ms for P and less than 5 ms for S with an interhypocenter separation of 50 m. Preliminary indications are that temporal velocity changes for those ray paths sampled are less than about 0.1% for both P and S. Future work will also be extended to secondary phases in the coda

Temporal changes in seismic coda. Coda Q offers perhaps the brightest hope for finding definitively identifying temporal changes in Earth response. Besides having the advantage of sampling a large volume, coda analysis is especially intriguing because numerous reports (although none yet checked by using similar earthquakes) exist in the literature of reported temporal variations, some of which were precursory to large earthquakes (see Sato, 1988; Wyss et al., 1991). Regions with reported temporal changes include the Anza area; Haar (1989) analyzed 37 earthquakes recorded by the Anza network between June, 1984 and December, 1987 and reported an intriguing increase (at a confidence level of greater than 0.99) in the coda decay rate observed Anza network station KNW. This study noted an anomalously high attenuation, for earthquakes occurring in the 18 months before the North Palm Springs earthquake. A similar conclusion was reached by Su and Aki (1990) examining SCSN data. Our methodology for searching for temporal changes in seismic coda, assumes a single-scattering envelope decay function of the form (e.g., Aki and Chouet, 1975)

$$A(f,t) \propto S(f)\, t^{-m}\, e^{-\pi f t/Q} \tag{1}$$

where t is the time elapsed since the earthquake origin time and $S(f)$ is the source amplitude spectrum. A change in Q between two otherwise identical earthquake signals would thus appear as a change in time-varying exponential filtering. Specifically, an estimate of the change in Q^{-1} between similar earthquake seismograms observed at a given station can be obtained by aligning the two waveforms to sub-sample accuracy and examining moving-window estimates of the log of the spectral ratio as a function of time (e.g., Got et al., 1991; Got and Fréchet, 1992)

$$C(f,t) = \ln\left[\frac{A_1(f,t)}{A_2(f,t)}\right] = \pi\Delta Q^{-1} f t + \ln\left[\frac{S_1(f)}{S_2(f)}\right] = R(f,t) + W(f) \tag{2}$$

where $R(f,t)$ is an exclusively earth-dependent term and $W(f)$ is an exclusively source-dependent term.

We have recently implemented an algorithm which uses multiaper techniques to estimate $C(f,t)$, around N frequency points and M time points. Standard errors are obtained from bootstrap estimates (Efron and Tibshirani, 1986). Early indications are that the behavior of this estimate is remarkably similarly for different stations from the same event pair, which is suggestive of site-invariance, and is also similar across the three seismogram components, which suggests that the coda decay function is fairly independent of particle motion direction. An example of the output from the moving-window spectral ratio procedure is shown in Figure 4.

Differential measurements of changes in reciprocal Q and in the source spectral ratio term, $W(f)$, with error bars and significance levels can be estimated in the context of a discrete linear over-determined least-squares problem by fitting (2) to the estimated sonogram. The system to be solved is (unweighted for clarity):

$$\begin{bmatrix} C(f_1,t_1) \\ C(f_2,t_1) \\ \vdots \\ C(f_N,t_1) \\ C(f_1,t_2) \\ \vdots \\ C(f_N,t_M) \end{bmatrix} = \begin{bmatrix} \pi f_1 t_1 & 1 & 0 & 0 & \cdots & 0 \\ \pi f_2 t_1 & 0 & 1 & 0 & \cdots & 0 \\ & & & \vdots & & \\ \pi f_N t_1 & 0 & 0 & 0 & \cdots & 1 \\ \pi f_1 t_2 & 1 & 0 & 0 & \cdots & 0 \\ & & & \vdots & & \\ \pi f_N t_M & 0 & 0 & 0 & \cdots & 1 \end{bmatrix} \begin{bmatrix} \Delta Q^{-1} \\ W(f_1) \\ W(f_2) \\ \vdots \\ W(f_N) \end{bmatrix}. \tag{3}$$

For Anza data, signals from each of the component seismometers will be averaged by fitting the parameter vector to mean spectral ratio values from all three components.

Once relative estimates of ΔQ^{-1} are obtained for all pairs of events in a similar event cluster at a given station, a subsequent linear inverse problem can be cast to obtain the best set of absolute Q^{-1} values (with an arbitrary mean value), e.g. for a cluster of four earthquakes consistent with the available ΔQ^{-1} estimates from (3). For example, for a cluster consisting of four earthquakes the system to be solved is (again, unweighted for clarity):

$$\begin{bmatrix} \Delta Q_{21}^{-1} \\ \Delta Q_{31}^{-1} \\ \Delta Q_{41}^{-1} \\ \Delta Q_{32}^{-1} \\ \Delta Q_{42}^{-1} \\ \Delta Q_{43}^{-1} \end{bmatrix} = \begin{bmatrix} -1 & 1 & 0 & 0 \\ -1 & 0 & 1 & 0 \\ -1 & 0 & 0 & 1 \\ 0 & -1 & 1 & 0 \\ 0 & -1 & 0 & 1 \\ 0 & 0 & -1 & 1 \end{bmatrix} \begin{bmatrix} Q_1^{-1} \\ Q_2^{-1} \\ Q_3^{-1} \\ Q_4^{-1} \end{bmatrix} \tag{4}$$

A statistical test for detectable variability in Q^{-1} is thus whether or not a linear regression applied to the solution of (4) differs significantly from a zero-slope line.

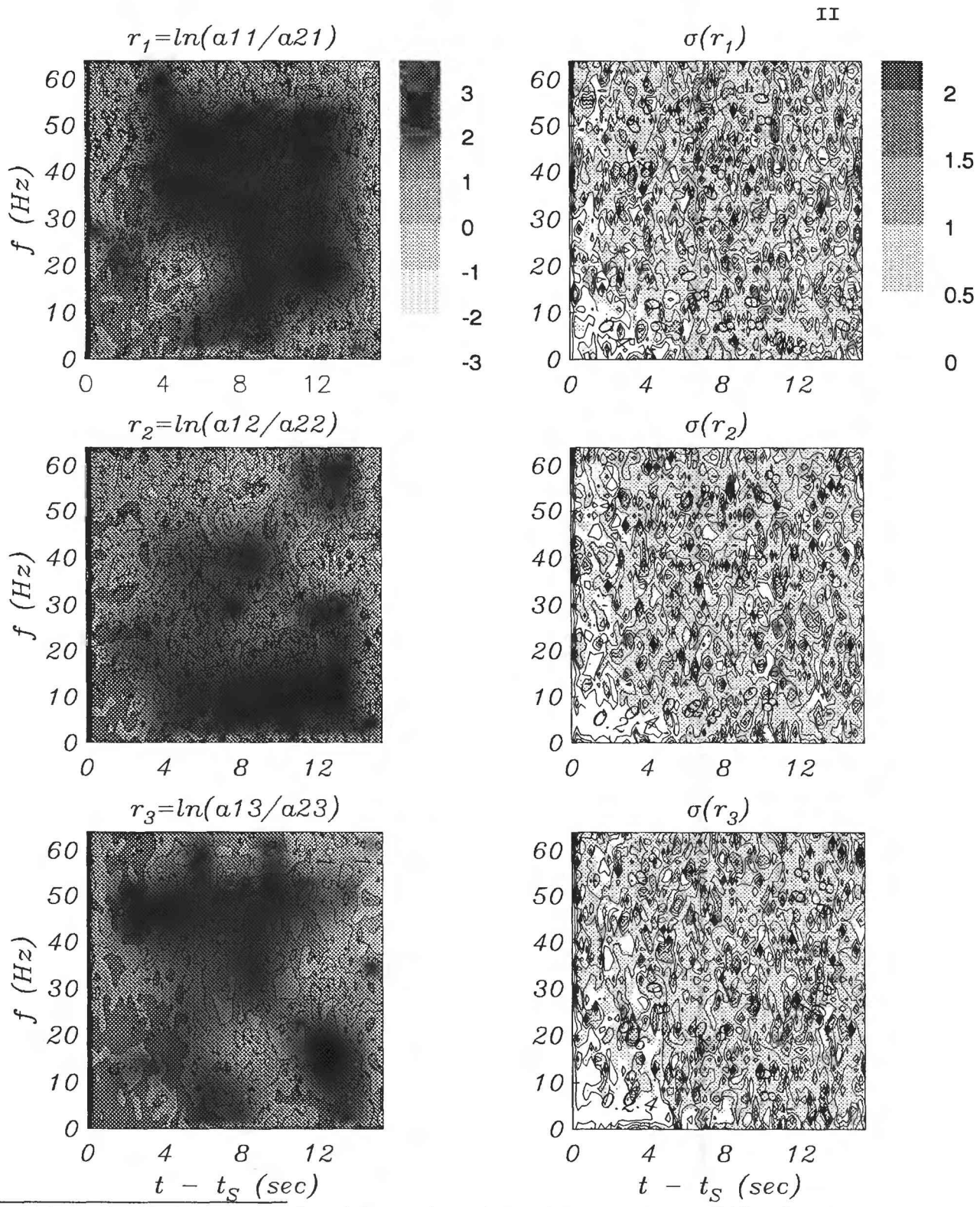

Figure 4. Shaded contour plot of the moving window log spectral ratio $C(f, t)$ and its standard deviation estimated for three components recorded at station WMC (vertical at top, NW-SE in the middle and NE-SW at bottom) for a similar earthquake pair from cluster 135 (5^{th} on the list shown in Table 1). Time is given relative to the S-wave arrival time. Multitaper spectral estimates using 8 prolate spheroidal taper functions were evaluated for 0.512 s 50% overlapping windows with a spectral averaging bandwidth of 8 Hz. Standard deviations were estimated using a statistical bootstrap with N=200 realizations.

Anza Similar Events ($\Delta t \geq 100$ days; $S \geq 0.86$; $N_{sta} \geq 3$)

Cluster	*event*$_1$	*event*$_2$	Δt *(days)*	Δh *(km)*	N_{sta}	S
276	aza001/82290101308	aza013/90057033115	2688.7	0.22	4	0.89
276	aza001/82290101308	aza013/90050151458	2682.2	0.53	5	0.90
174	aza002/84139101553	aza020/91094095001	2512.0	1.07	9	0.89
220	aza006/87307221107	aza024/91274052047	1427.3	0.54	5	0.89
135	aza005/86287100614	aza015/90105071049	1278.9	1.64	7	0.87
067	aza002/84175093325	aza006/87024033152	944.7	0.25	6	0.95
212	aza003/84306203243	aza005/86287175236	711.9	0.36	6	0.96
080	aza004/86182224033	aza008/88143113117	690.5	0.46	9	0.87
263	aza008/88292030028	aza018/90233080037	672.2	0.98	5	0.90
276	aza014/90095070015	aza025/91362100105	632.1	1.97	7	0.86
276	aza008/88206005916	aza013/90050055248	575.2	0.37	6	0.89
276	aza018/90239134028	aza025/91362100105	487.8	1.60	4	0.90
158	aza010/89307114605	aza018/90344061520	401.8	3.18	7	0.89
276	aza018/90334065756	aza025/91351083517	382.1	2.22	4	0.86
276	aza013/90052060711	aza019/91017103908	330.2	1.30	4	0.87
276	aza010/89279194452	aza018/90238224549	324.1	0.66	7	0.87
133	aza005/86240150620	aza006/87197222209	322.3	1.70	4	0.90
212	aza002/84191151716	aza003/85134220533	309.3	1.02	4	0.93
276	aza009/89108235416	aza013/90050105751	306.5	0.90	3	0.88
276	aza009/89108235416	aza013/90050055248	306.2	0.40	3	0.87
212	aza003/84207221148	aza003/85134220533	293.0	0.96	4	0.92
073	aza005/86200192301	aza006/87128153540	292.8	0.60	5	0.89
276	aza018/90334065756	aza023/91242203241	273.6	0.12	3	0.90
276	aza013/90050111412	aza018/90303163508	253.2	0.27	5	0.90
276	aza013/90050151458	aza018/90303042613	252.6	0.70	5	0.86
276	aza013/90050091713	aza018/90302141145	252.2	0.64	3	0.88
276	aza013/90050111412	aza018/90302141145	252.1	0.36	3	0.89
276	aza013/90051051508	aza018/90303042613	252.0	0.39	5	0.90
276	aza013/90051051508	aza018/90302141145	251.4	0.44	3	0.90
276	aza013/90052132750	aza018/90302141145	250.0	0.54	3	0.88
276	aza013/90057033115	aza018/90303163508	246.5	0.33	4	0.89
276	aza013/90057033115	aza018/90303042613	246.0	0.07	4	0.88
276	aza013/90057033115	aza018/90302141145	245.4	0.40	3	0.87
276	aza013/90059032744	aza018/90303042613	244.0	0.32	5	0.91
276	aza013/90059032744	aza018/90302141145	243.4	0.19	3	0.88
276	aza014/90092182003	aza018/90304031218	211.4	0.22	3	0.90
276	aza014/90092182003	aza018/90303042613	210.4	0.18	4	0.86
276	aza014/90095070015	aza018/90304031218	208.8	0.82	3	0.88
276	aza014/90095070015	aza018/90303042613	207.9	0.69	4	0.86
276	aza013/90050151458	aza018/90239134028	188.9	0.48	4	0.87
276	aza018/90304031218	aza021/91127062056	188.1	8.93	3	0.91
276	aza015/90115032939	aza018/90302141145	187.4	6.86	4	0.88
127	aza010/89230221814	aza013/90050234422	185.1	0.80	5	0.91
276	aza019/91062061528	aza022/91216110027	154.2	0.80	7	0.88
238	aza022/91212114921	aza025/91338212420	126.4	2.39	4	0.91
276	aza018/90239134028	aza018/90346211245	107.3	0.52	3	0.89
111	aza010/89260193523	aza011/89361113901	100.7	1.11	6	0.88

Table 1

Summary.

We have completed the compilation of a similar event catalogue for Anza network data from October 24, 1982 through April 15, 1992 and have programs in place for updating this catalogue as more recent seismograms and locations become available from UCSD (currently backlogged by the enormous number of events associated with the Landers/Big Bear earthquakes). We also have access to SCSN network seismograms through the Southern California Earthquake Center for these events which will be used to extend the geographic range of the study. A comparable organizational effort is also well underway at U.C. Berkeley for the Parkfield data set. A list of the "best" events from the Anza catalogue is shown in Table 1, where δh is the estimated hypocenter separation from network locations, N_{sta} is the number of Anza stations in common, and S is the median shear-wave crosscorrelation of 0.512 s of the aligned 3-component shear wave signal.

Work is presently proceeding on exploiting this catalogue to test waveform data for evidence of temporal variability in seismic velocities and seismic coda. An analysis of variation or stability in shear-wave splitting will also be performed using comparative techniques developed by Aster et al. (1990). Although the stable results of that study were negative with respect to one proposed precursor at a single station, the present state of data and programming organization now enables us to perform a far more comprehensive survey with relatively little additional effort.

We thus anticipate rapid progress during the next year on addressing the issue of Green function stability or variability at Anza and Parkfield. A future priority will be identifying and analyzing similar event pairs from the Anza and SCSN networks which sample the vicinity of the the Landers and Big Bear earthquakes of June 28, 1992.

Reports, Papers and Presentations Associated with this Project.

Aster, R., Scott, J., Comprehensive Identification of Similar Earthquakes in Microearthquake Data Sets, 1992. *Bull. Seism. Soc. Am.*, accepted for publication.

Aster, R., Scott, J., Shearer, P., Vernon, F.L., Analysis of near-repeating earthquake wavefields in the San Jacinto fault zone, southern California, 1991. *EOS trans. AGU*, **72**, no 44, p. 352.

Aster, R., Scott, J., Shearer, P., Vernon, F.L., Similar earthquakes in the Anza Seismic Gap, 1992. *Seism. Res. Lett.*, **63**, p. 63.

Aster, R., Henton, J., Scott, J., Shearer, P., Vernon, F.L., Comparative coda analysis of similar earthquakes with large temporal separations near the Anza seismic gap, southern California, 1992. *EOS trans. AGU*, **73**, no 43, p. 361.

Nadeau, R., Aster, R.C., McEvilly, T.V., Analysis of P and S wave polarizations at the Parkfield high-resolution seismic network (HRSN), 1991. *EOS trans. AGU*, **72**, no 44, p. 483.

Scott, J., Shearer, P., Aster, R., Constraints on temporal variations in velocity near Anza, California, from analysis of similar event pairs, 1992. *EOS trans. AGU*, **73**, no 43, p. 360.

Additional References

Aster, R., Shearer, P., and J. Berger (1990). Quantitative measurements of shear-wave polarizations at the Anza seismic network, southern California — implications for shear-wave splitting and earthquake prediction, *J. Geophys. Res.* **95**, 12,449-12,474.

Berger, J., L.N. Baker, J.N. Brune, J.B. Fletcher, T.C. Hanks, and F.L. Vernon (1984). The Anza array: a high-dynamic-range, broadband, digitally radiotelemetered seismic array, *Bull. Seism. Soc. Am.*, **74**, 1469-1481.

Efron, B., Tibshirani, R. (1986). Bootstrap methods for standard errors, confidence intervals, and other measures of statistical accuracy, *Statistical Science*, **1**, 54-77.

Ellsworth, W., Beroza, G., Verwoerd, M. (1992). Changes in crustal wave velocity associated with the 1989 Loma Prieta, California earthquake, *EOS trans. AGU*, **73**, no 43, p. 360.

Geller, R., and C. Mueller (1980). Four similar earthquakes in central California, *Geophys Res. Lett.*

7, 821-824.

Got, J.-L., Poupinet, G., and M.-J. Fréchet (1990). Changes in source and site effects compared to coda Q^{-1} temporal variations using microearthquake doublets in California, *PAGEOPH* **134**, 195-228.

Got, J.-L., Fréchet, J., 1992. Origins of amplitude variations in seismic doublets: Source or attenuation process?, *submitted for publication.*

Haar, R., 1989. *Spectra and Time Decay of Coda*, Ph.D. Thesis, Stanford University.

Harris, D. (1991). A waveform correlation method for identifying quarry explosions, *Bull. Seism. Soc. Am.* **81**, 2395-2418.

Hough, S., Anderson, J. (1988). High frequency spectra observed at Anza, California: Implications for *Q* structure, *Bull. Seism. Soc. Am.* **78**, 692-707.

Hough, S., J. Anderson, J. Brune, F. Vernon, J. Berger, J. Fletcher, L. Haar, T. Hanks, Baker, L. (1988). Attenuation at Anza, California, *Bull. Seism. Soc. Am.* **78**, 676-691.

Hutchings, L., and F. Wu (1990). Empirical Green's functions from small earthquakes: A waveform study of locally recorded aftershocks of the 1971 San Fernando earthquake, *J. Geophys. Res.* **95**, 1187-1214.

Ishida, M., and H. Kanamori (1978). The foreshock activity of the 1971 San Fernando earthquake, California, *Bull. Seism. Soc. Am.* **68**, 1265-1279.

James, D., and M. Savage (1990). A search for seismic reflections from the top of the oceanic crust beneath Hawaii, *Bull. Seism. Soc. Am.* **80**, 675-701.

Knuth, D. (1968). *Fundamental Algorithms, The Art of Computer Programming*, Addison-Wesley, Reading, Massachusetts.

Park, J., C. Lindberg, and F. Vernon (1987). Multiper spectral analysis of high-frequency seismograms. *J. Geophys. Res.* **92**, 12,675-12,684.

Poupinet, G., Ellsworth, W., and M.-J. Fréchet (1984). Monitoring velocity variations in the crust using earthquake doublets: An application to the Calaveras fault, California, *J. Geophys. Res.* **89**, 5719-5731.

Poupinet, G., Fréchet, M.-J., Ellsworth, W., Frémont, M.-J., and F. Glangeaud (1985). Doublet analysis: Improved accuracy for earthquake prediction studies, *Earthquake Predict. Res.* **3**, 147-159.

Press, W., Flannery, B., Teukolsky, S., and W. Vetterling (1986). *Numerical Recipes*, Cambridge University Press, Cambridge, U.K..

Scott, J. (1992). *Microearthquake studies in the Anza seismic gap*, Ph.D. thesis, Scripps Instit. Oceanogr., Univ. of Calif., La Jolla, California.

Scott, J., Masters, T.G., and Vernon, F. (1992). *Three-dimensional velocity structure of the San Jacinto fault zone near Anza, California, Part I: P waves submitted to Geoph. J. Int.*

Su, F., Aki, K. (1990). Spatial and temporal variation in coda Q^{-1} associated with the North Palm Springs earthquake of 1986, *Pure Appl. Geophys.*, **133**, 23-52.

Thorbjarnardottir, B., and J. Pechmann (1987). Constraints on relative earthquake locations from cross-correlation of waveforms, *Bull. Seism. Soc. Am.* **77**, 1626-1634.

Thomson, D., Spectrum estimation and harmonic analysis, *IEEE Proc.*, **70**, 1055-1096.

Vernon, F.L. (1989). *Analysis of Data Recorded on the Anza Seismic Network*, Ph.D. thesis, Scripps Instit. Oceanogr., Univ. of Calif., San Diego, La Jolla.

Vernon, F.L. (1992). Coherence vs. distance (abstract), *Seism. Res. Lett.*, **63**, 40.

Verwoerd, M., Ellsworth, W., Cole, A., Beroza, G. (1992). Changes in crustal wave propagation properties associated with the 1989 Loma Prieta, California earthquake: Implications for coda-Q as an earthquake precursor and for the mechanism of stress-induced velocity changes. (abstract), *Seism. Res. Lett.*, **63**, 71.

Holocene Paleoseismology in Western Washington

9540-10180
Brian F. Atwater
U.S. Geological Survey at University of Washington AJ-20
Seattle, Washington 98195
(206) 553-2927

Investigations:

My research in 1992 was focussed on four questions about great earthquakes that have been inferred for the Cascadia subduction zone:

1. **Did the ground really shake?** Great Cascadia earthquakes have been inferred primarily from coastal deposits that indicate abrupt subsidence, but evidence for shaking during this subsidence has proven elusive. In particular, few prehistoric liquefaction features of Holocene age have been found at the Cascadia subduction zone. In 1992, I looked for liquefaction features in a large excavation in Seattle, and I visited sites along the lower Columbia River at which Stephen Obermeier discovered liquefaction features of late Holocene age.

2. **What were the magnitudes?** (a) Work continued on maximizing the resolution of radiocarbon dating to test the coevality of subsidence along the Cascadia coast (B.F. Atwater, M. Stuiver, and D.K. Yamaguchi, *Nature*, v. 353, p. 156, 1991). The main goal in 1992 was a comparison of high precision radiocarbon ages on spruce stumps, southern Washington versus northern California (with Minze Stuiver, Gary Carver). (b) Work also continued on the death and survival of spruce trees near Portage, Alaska, that subsided into the intertidal zone during the 1964 Alaska earthquake (with David Yamaguchi, Eileen Hemphill-Haley). (c) Work began with the use of tree rings to put limiting minimum ages on the most recent great earthquake inferred for coastal Washington. This work consisted of coring live tidal-swamp spruce in parts of coastal Washington where spruce were killed by salt and (or) submergence from the most recent abrupt subsidence sometime between AD 1695 and 1710 (with Boyd Benson, David Yamaguchi).

3. **What were the recurrence intervals?** This also entails high-precision dating, for which sampling and dating continued in 1993 (with Minze Stuiver).

4. **What, if any, is their relationship to crustal earthquakes at Puget Sound?** This question has become important in light of recent findings, by Robert Bucknam and others, about prehistoric seismicity on structures in the North America plate near Seattle. I looked for tsunami deposits at Puget Sound to learn whether uplift near Seattle happened during an earthquake, as inferrred by Bucknam. I also sampled such deposits for plant fossils to obtain high-precision radiocarbon ages (with Minze Stuiver) and tree-ring correlations (with Gordon Jacoby).

Results:

1. **Shaking**--Atwater found gravel and sand intrusions less than 2000 years old in sewer excavation in Seattle (see 4, below). Independently, Obermeier found liquefaction features about 300 years old along the lower Columbia River.

2. **Magnitude**--(a) Stuiver supplied high-precision ages for spruce killed by the youngest abrupt subsidence event at Humboldt Bay, California. These ages are not statistically different from ages 600 km to the north, in southern Washington. The dating leaves intact the hypothesis of magnitude-9 earthquakes on the Cascadia subduction zone. The Washington ages were published in the *Nature* paper cited above; a manuscript on the California ages is in preparation. (b) Yamaguchi found that some of the spruce near Portage survived several months beyond the 1964 earthquake, as shown by partial 1964 growth rings. Implication for Cascadia: the season of tree death cannot be used with confidence to test coevality of subsidence. (c) At least a dozen Sitka spruce of modern tidal swamps in southern Washington contain more then 300 annual rings and thus should have survived any earthquake close to A.D. 1700. There is a chance that such trees would reveal the year and season of the most recent great earthquake in coastal southern Washington.

3. **Recurrence**--Samples for high-precision dating of earlier earthquakes were collected in July and August, 1992.

4. **Puget Sound seismicity**--A Puget Sound tsunami coincided, to the year, with abrupt tectonic subsidence in northern Seattle and with landslides into Lake Washington about 1000 years ago.

Reports

Atwater, B.F., 1992, A Seattle tsunami 1100 years ago [abstract]: *Geological Society of America Abstracts with Programs*, v. 24, no. 5, p. 4.

Atwater, B.F., 1992, Prehistoric earthquakes in western Washington [abstract]: *Geological Society of America Abstracts with Programs*, v. 24, no. 5, p. 4.

Atwater, B.F., and Moore, A.L., 1992, A tsunami 1000 years ago in Puget Sound, Washington: *Science* (in press).

Benson, B.E., Amidon, L., Yamaguchi, D.K., and Atwater, B.F., 1992, Limiting tree-ring ages for plate-boundary seismicity in southern coastal Washington [abstract]: Eos (in press).

Carver, G.A., Stuiver, M., and Atwater, B.F., 1992, Radiocarbon ages of earthquake-killed trees at Humboldt Bay, California [abstract]: Eos (in press).

SYNTHESIS OF DATA AND EXPLORATORY TRENCHING ALONG THE NORTHERN SIERRA NEVADA FAULT ZONE

1434-92-G-2217

John W. Bell, Alan R. Ramelli, Craig M. dePolo

Nevada Bureau of Mines and Geology
University of Nevada
Reno, Nevada 89557
(702) 784-6691

Objectives

1. Compile and synthesize existing data related to distribution and age of late Quaternary faulting along the northern Sierra Nevada fault zone (NSNFZ).

2. Conduct exploratory trenching of the southern portion of the NSNFZ (Genoa fault).

3. Estimate short- (Holocene) and long-term (late Quaternary) slip rates along the NSNFZ.

Results

Synthesis of fault data

Late Quaternary faulting within the Washoe City, Mt. Rose NE, Genoa, and Minden 7½-minute quadrangles was evaluated through analysis of aerial photography and existing geologic mapping. Definitive late Quaternary fault traces (primarily scarps) along the frontal fault zone in Washoe Valley to the northern edge of the Mt. Rose fan complex have been compiled and digitized using Generic CADD.

While the spatial distribution of active fault traces within the Washoe City and Mt. Rose NE quadrangles is fairly well represented on published maps, the age relations as shown are in some cases misleading or erroneous. For example, nearly continuous fault traces are assigned differing ages where they offset different-age deposits. Some scarps show greater offset of older surfaces suggesting recurrent faulting; however, displacement varies rapidly along strike of many traces, complicating such interpretations. Many of the scarps shown as "Donner Lake age" (~200 ka) on published maps in fact influence Holocene and active drainage patterns, indicating much more recent activity.

Late Quaternary faulting of the Mt. Rose outwash-fan complex forms a series of subparallel grabens traversing the outwash-fan, rather than being an antithetic (west-facing) system as described in previous work. These grabens generally trend north-south and are commonly sigmoidal-shaped. Northwest- to north-northwest-trending faults cutting the Mt. Rose outwash-fan commonly are linear and have a strong left-stepping en echelon pattern, suggesting right lateral movement. One northwest-trending fault cutting across the Mt. Rose fan appears to separate differentially deforming areas to the north and south. To the north, there are at least five subparallel grabens evenly spaced across the Mt. Rose fan, whereas to a south, faulting is mostly confined to the single complex graben lying between Steamboat Hills and Mt. Rose.

Exploratory Trenching

Three exploratory track-hoe trenches were excavated across portions of the Genoa fault in July, 1992 (Fig. 1), and the logging of the trenches has been completed by the Principal Investigators. The structural-stratigraphic relations exposed in all three trenches confirm that the Genoa fault is the most youthful segment of the NSNFZ and is currently believed to have the highest seismogenic potential of any fault in the Reno-Carson City urban corridor.

The most recent faulting event is displayed in the Jacks Valley and Sturgis trenches, respectively located near the northern and southern ends of the most recent surface rupture, where latest Holocene alluvial-fan deposits exhibit 4-4¼ m of total, single-event, stratigraphic throw. Topographic profiles across these respective fault scarps indicate that geomorphic surfaces also display about 4¼ m of vertical throw. Net dip-slip surface displacement is estimated to be about 5 m for this most recent event. Two events are exposed in the Walleys trench: the most recent event as well as an older event of comparable magnitude. A total of 7.6 m vertical throw of late Holocene deposits is recorded at the Walleys site, equivalent to about 9 m of dip-slip displacement.

Geomorphic and soils relations suggest that the faulted deposits at the three sites are late Holocene age. The complete lack of any significant soil horizonation in the most recently faulted deposits strongly suggests a numerical age for the youngest deposits of less than about 1,000 years. This is expected to be confirmed by radiocarbon dating of samples collected from all three trenches. The Jacks Valley and Sturgis trenches expose extensive sequences of faulted and unfaulted charcoal-rich horizons derived from repeated and alternating episodes of forest fires and debris- and flood-flow alluviation. A total of 49 charcoal samples has been collected from the Jacks Valley and Sturgis trenches, which will probably allow the precise bracketing of the age of the most recent 5 m displacement. A maximum age for the earlier event exposed in the Walleys trench will be estimated from dating two charcoal lenses preserved in the down-faulted block of alluvial-fan deposits. The presence of an incipient cambic (Bw) horizon in the faulted fan surface suggests that both events are less than a few thousand years in age.

Slip rates

Radiocarbon dating of samples (in progress) from the three trenches will allow estimation of mid- to late Holocene slip rates for the Genoa fault. Preliminary results based on ages inferred from soil and geomorphic evidence suggest that as much as 10 m of displacement associated with two major events has occurred during the mid- to late Holocene. This suggests that Holocene slip rates may be on the order of 1-2 mm yr^{-1}. Preliminary data also suggest that this rate may be greater than the longer-term (late Quaternary) average. At the Walleys trench site, alluvial-fan deposits estimated to be 100-200 ka on the basis of soil morphology are offset by a 20-m high scarp. Although this offset is a minimum value because of the likelihood of burial of the downthrown block, this offset suggests that the late Quaternary average slip rate for the Genoa fault is less than the Holocene rate, perhaps by as much as an order of magnitude.

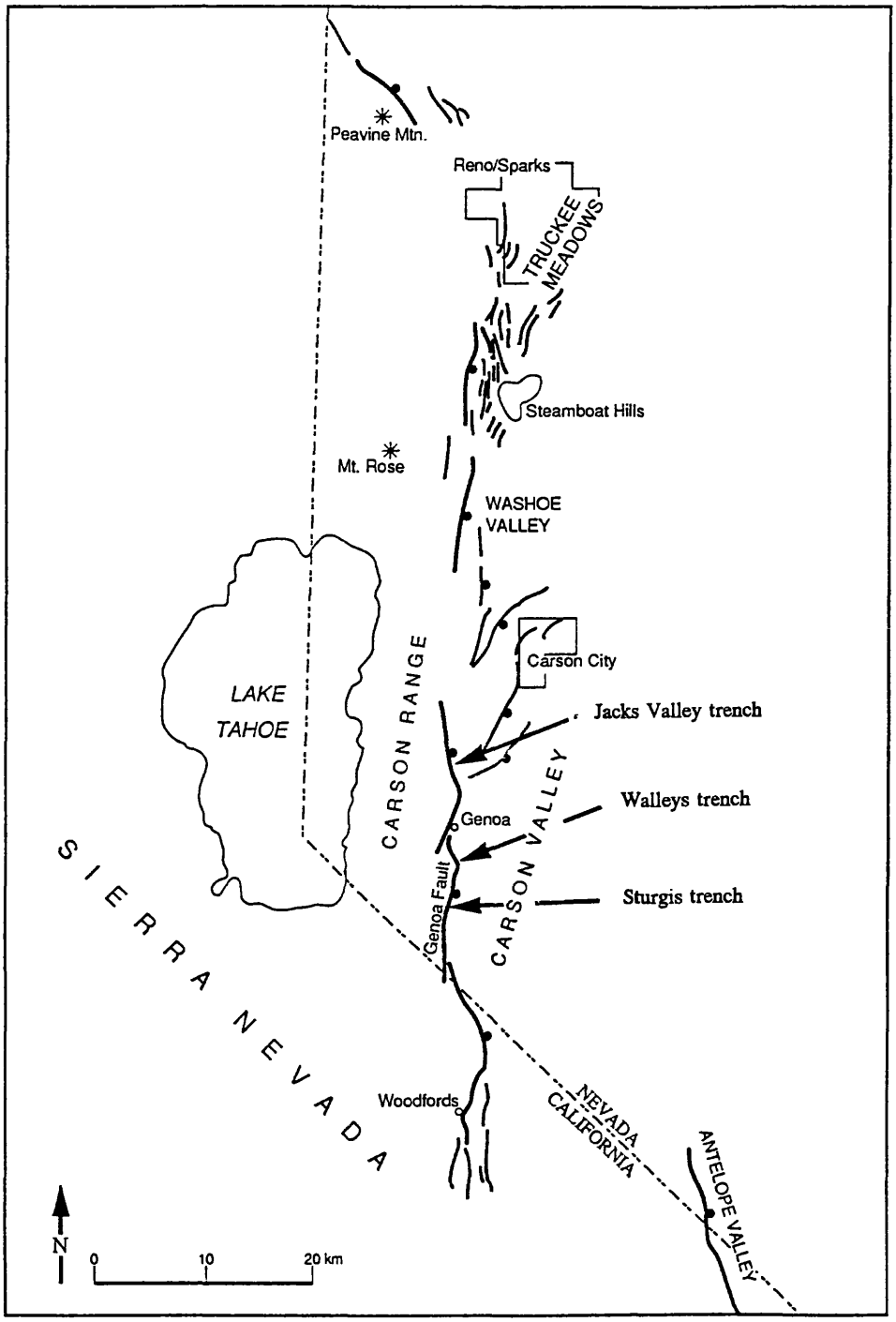

Figure 1. Generalized late Quaternary fault map of the northern Sierra Nevada fault zone showing the location of exploratory trenches across the Genoa fault. North-trending, east-facing faults form the main frontal fault zone of the Basin and Range-Sierra Nevada boundary at this latitude.

Detailed and Reconnaissance Finite Element Models of Four Fault Systems in the United States

Agreement No. 14-08-0001-G-1947

Peter Bird
Department of Earth and Space Sciences
University of California
Los Angeles, CA 90045

(310) 825-1126

Recent improvements in the technique of modeling fault networks with thin-plate finite elements yield fully-convergenced velocity/strain-rate/stress solutions, without any compromise in the representation of the frictional rheology of the upper crust or the transition to dislocation creep in the lower crust. Such models yield quantitative constraints on the rheologies of faults and crustal blocks, as well as specific predictions concerning long-term seismic risk.

Investigations Undertaken:

1. California: (The initial stages of this project were described in last year's report.) We applied these techniques to model the California region, incorporating all faults with estimated slip rate over 1 mm/yr, as well as variations in elevation, heat flow, and crustal thickness. Velocity boundary conditions on the model sides were based on the NUVEL-1 plate model and an approximation of deformation in the Great Basin. The frictional and dislocation-creep rheologic constants of the crust were calibrated to reproduce the observed variations in the maximum depth of seismicity, which occurs at model temperatures of 350-410 C. This left two free parameters: the coefficient of friction on faults, and the apparent activation energy for creep in the lower crust.
These parameters were systematically varied in three sets of 10, 81, and 64 experiments, respectively. The predictions of each model were tested against three published datasets: a set of 79 geologic limits on average slip-rate on faults, a set of 221 principal stress directions, and a set of 841 secular rates of geodetic baselines (both trilateration and VLBI).

2. New finite element code: The program referred to above, named FAULTS, includes only the crust in its model domain. This is appropriate where the crust is only weakly attached to the mantle lithosphere, as in California. However, it is not a good way to model regions of very thin crust (e.g., ocean basins) in which the crust is firmly bonded to the mantle lithosphere. Therefore, program FAULTS was modified to create the new program PLATES, in which the domain in the entire lithosphere. The approximations and assumptions are the same, except that the strength and density structure of the mantle lithosphere are included in all vertical integrals. This program was then used in the modeling of Alaska (below), where it was necessary to include the region of the Bering Sea.

3. Models of the Alaskan syntaxis: By modeling the region of the Alaskan syntaxis it may be possible to determine: (a) whether the extreme weakness of faults previously found in California is a general property of the Pacific margin; (b) how great is the seismic hazard to inland regions from faults within the North American plate; (c) whether terranes are continuing to flow around the syntaxis into the Aleutian forearc as they once did; and (d) what causes the observed radiation of principal stresses away from the syntaxis.

To reduce artificial edge effects, the models extend from Vancouver Island north to the Nansen Ridge, and west along the Aleutians to Kamchatka. The grid of 1500 nodes, 600 continuum elements, and 130 fault elements incorporates all mapped faults identified as active by Geist *et al.* (1988), Page *et al.* (1991), or Cooper *et al.* (1992). Topography is taken from the ETOPO5 digital dataset, and heat-flow from the GSA/DNAG map of Blackwell and Steele (1992). Crustal thickness is computed to achieve isostasy (outside the forearc), and mantle lithosphere thickness is derived from the heat-flow. Side boundary conditions are from NUVEL-1, and include an Okhotsk plate after Cook *et al.* (1986). The rheology is friction above the brittle ductile transition(s) (located separately in crust and mantle lithosphere) and dislocation creep below. The crustal creep parameters are taken from the study of California described above.

4. New Madrid seismic zone: In preparation for modeling the midcontinent (Mississippi Valley) seismic zone, references and maps have been collected from the literature.

Results Obtained:

1. California: The patterns of model scores indicate that the friction coefficient of major faults is only 0.17-0.25, or only 20-30% of the value (0.85) that is assumed for the friction in the intervening blocks. (The laser trilateration data taken alone would indicate a preference for a high-stress model, but this model is one with very little fault slip and seismicity, which can be rejected on other grounds.) In the final 3-parameter set of 64 models, we tested whether the anomalous weakness of faults is uniform or proportional to net slip. With slip-dependent weakening, there was a general reduction in prediction errors which supports the hypothesis. The geologic data and geodetic data agree in implying that fault weakness (e.g., friction of 0.17) is general, with an additional 30% slip-dependent weakening of the San Andreas (to friction of 0.12, or 14% of normal). However, the stress data is fit best if all weakness is slip-dependent (effectively, only the San Andreas is weak). Thus, the hypothesis that all weakening is slip-dependent should not be rejected.

The best models predict all available data with RMS mismatch of as little as 3 mm/yr (6% of the relative plate velocity), so their predictions may be useful for seismic hazard estimation, at least along faults where no data are available.

This study extends the finding of very low friction from subduction zones, where it was previously documented, to a dominantly strike-slip system in which underthrusting of wet sediment is not widespread. Return of previously subducted water from the mantle, and its chemical or physical binding in fine-grained gouge are possible explanations for the very low friction.

Results of these models may be useful for improving estimates of long-term seismic hazard, by contributing new limits on the long-term-average slip rate of each fault. Of course, it is necessary to give priority to actual geodetic and geologic data, and to only use computer models where data are absent or ambiguous. Also, it is necessary to consider the full range of rates displayed in a set of models (all those with reasonably good scores) in order to avoid giving a misleading impression of precision.

Following this philosophy, we have constructed Table 1, in which all available data are summarized and tentative conclusions offered. Space does not permit the listing of references in this table. Geologic slip rates are either from Bird and Rosenstock (1984) or manuscript #3 below. Where multiple studies gave overlapping rate windows, the common central segment is quoted. However, where multiple studies disagreed, the quoted range covers both opinions. Geodetic rates are all derived from laser geodimeter trilateration data of Lisowski et al. (1991) or Savage et al. (1990). (However, the assignments of equivalent slip rates to individual faults are our own subjective estimates.) The column "Good Models" gives the range of rates

found among the 30 models from group III which had global prediction errors of 4 mm/year or less. In combining the different kinds of limits, the highest weight is given to geodetic data, the geologic data are ranked second, and the models are considered the weakest.

Given these conservative rules, it is not surprising that these models add little to our knowledge of the intensively-studied San Andreas system. What we can add is some limits for minor branches: the Carneros fault of northern California probably does not exceed 6.6 mm/year, and the San Juan-Whiterock-Morales system of the southern Coast Ranges probably moves no more then 9 mm/year.

These models are most useful in suggesting estimates for offshore and coastal faults which are difficult to access, for thrust faults which typically 'bury their evidence', and for faults in less populous areas which have been given low priority in funding of studies. For example, these models address the controversy over the Hosgri fault, where Hamilton and Willingham (1977) inferred only 2-4 mm/year from geologic evidence, while Hall (1978) argued for 16-19. We never find rates over 3 mm/year on the San Gregorio-Carmel Canyon-Hosgri system in our models, so the lower rate is probably appropriate for seismic hazard evaluation (regardless of which is the correct mean rate for Pliocene-Quaternary time). In the southern California borderland, we confirm that the shoreline-cutting Newport-Inglewood-Rose Canyon-Vallecitos and Palos-Verdes-Coronado Bank systems are moving at no more than a few millimeters per year. One surprising result here is that we have good models in which the slip on the outer Santa Barbara Island-San Diego Trough-Agua Blanca system increases northwestward, from about 2 mm/year in Baja California to as much as 19 mm/year at the intersection with the Santa Barbara Channel structures. However, this result is not unique, as we have other good models where this system moves very slowly. Perhaps GPS observations at Santa Barbara and San Clemente islands can be used to resolve this.

It is important to estimate the slip rates of the thrust faults along the southern margin of the Transverse Ranges because of the high population densities there. Geodetic data are still inconclusive, and geologic rates must usually be treated as lower limits because of the tendency of thrusts to splay over a broad zone. Thus, it was ominous when Bird and Rosenstock (1984) used rigid-block kinematics to infer slip rates of 7-15 mm/year along this zone. Weldon and Humphreys (1986) showed an alternative kinematic model with slower thrusting, but did not resolve the new problems that this would create in the borderland. In this study, we find rates that are about half as great as Bird and Rosenstock's, but still indicative of real hazard. The Cucamonga fault slips at about 7 mm/year and the Sierra Madre fault rate is 3-6 mm/year. Along the southwest branch of this system (Santa Monica and Malibu Coast faults) the model rates are scattered, from under 1 to over 18 mm/year; however, since there is a geologic constraint showing slow motion (<1.1 mm/year) on the Santa Monica fault, this probably applies to the whole branch. On the northwest branch (Sierra Madre-San Fernando-Santa Susanna-San Cayetano-Red Mountain-Santa Barbara Channel faults) the models suggest an upper limit of 7 mm/year for the San Fernando fault and an upper limit of 3 mm/year for the Santa Barbara Channel fault. The fact that the fastest-slipping models just match the lower geologic rate limit (9 mm/year) on the central Red Mountain-San Cayetano fault segment suggests that these models may be the ones closest to reality.

All of these computations were completed before the two San Bernardino Mountains earthquakes of June 1992, so the new fault segments which they revealed are not included in our finite element grid. However, the grid does include the Pipes Canyon fault, which is parallel and close to the rupture of the larger event at Landers. Thus, the range of model slip rates that we found for the Pipes Canyon fault (0.2-2.1 mm/year) may be of interest to help place these events in context. Apparently, major events on these faults should have long recurrence times, and the fact that these

segments now appear to be more active than the adjacent San Andreas fault is only an artifact of the short instrumental record.

2. The new program PLATES passed all the validation tests previously applied to program FAULTS (which models the only the crust).

3. Models of the Alaskan syntaxis: In the first set of Alaskan experiments, the friction coefficient of faults was varied, while the friction within crustal blocks remained at 0.85. While the models have yet to be objectively scored against geologic, geodetic, and stress data, it is already apparent that:
A. The subduction traction on the base of the Aleutian forearc cannot exceed 10 MPa (or else the forearc bonds to the Pacific plate, and the effective plate boundary jumps to the volcanic arc).
B. Faults of the Alaskan interior (e.g., Denali, Tintina) would not be active at all if they did not have low friction.
If their friction coefficient is similar to that of strike-slip faults in California (0.17), then their time-averaged slip rates are approximately 5-10 mm/year. Thrusting at similar rates occurs on the Duke River fault, the Pamplona zone, and on the south branch of the Denali fault, beneath Mt. McKinley.
C. Trench-parallel compression develops in the forearc region of the syntaxis. This would tend to force crust westward along the forearc, but movement is blocked because the accomodating Castle Mt. and Bruin Bay faults are not mapped as continuous with arc-parallel faults further west.
D. All models confirm the rapid arc-parallel transport of the western Aleutian forearc that has been inferred from seismic slip vectors (Ekstrom and Engdahl, 1989).

4. New Madid seismic zone: We are prepared to create the finite elements grids for this region. Obviously, it is important to incorporate all major faults (or at least one fault from each family of subparallel strands) in order to give the model as many degrees of freedom as the real Earth. However, it remains unclear whether the Mississippi Valley fault system merely terminates in Illinois and Tennessee, or whether this cryptic sub-plate boundary continues in another direction. We currently plan to conduct two sets of model experiments. In the first, only mapped faults will be gridded, so that displacements will tend to go to zero at the northeastern end of the system. In the second grid, however, we will investigate the possibility that slip is transformed northwestward along a dextral strike-slip zone through central Missouri and into Kansas, to connect to the inactive(?) mid-continent rift marked by the well-known midcontinent gravity high.

Reports Published:

1. Bird, P., and X. Kong (1991) First accurate thin-plate models with faults (abstract), Eos (Trans. Am. Geophys. U.), 72, 121.
2. Bird, P. (1992) Computer simulations of neotectonics around the Alaskan syntaxis, Eos, 73, 504.
3. Bird, P., and X. Kong., Computer simulations of Calfornia tectonics confirm very low strength of major faults, submitted to Geol. Soc. Am. Bull., 8/92.

TABLE 1.

Final Slip-Rate Estimates for California Faults

(all figures in mm/year;
* marks conclusions which depend on computer models)

Fault	Geologic Rate	Geodetic Rate	Good Models	Best Model	Our Conclusion
Agua Blanca	2.4-5	---	0.2-1.3	0.7	~2.4
Anticline Ridge-Kettleman Hills	1.2-1.9	---	0.1-0.2	0.2	1.2-1.9
Avawatz Mountains	---	---	0-3.7	0.2	<3.7*
Banning	>1.7	---	0-0.3	0.2	~1.7
Black Mountain (Death Valley)	4.1-6.3	---	0.5-2.4	0.8	4.1-6.3
Brawley seismic zone	---	---	4.5-54	14.6	4.5*-54*
Calaveras (Gilroy)	---	12-22	0.1-26	18.0	12-22
Calaveras (Pleasanton)	~3	---	0-6.4	4.0	<6.4*
Carmel Canyon	---	---	0-2.7	0.6	<2.7*
Carneros	---	---	0.1-6.6	3.9	0.1*-6.6*
Cerro Prieta	---	---	22-42	31.9	22*-42*
Channel Islands (Santa Cruz I.)	>3	---	0.4-4.5	3.1	3-4.5*
Chino	0.1-0.4	---	0.4-5.3	1.5	~0.4
Cleghorn	0.9-2	---	0.1-3.1	2.9	0.9-2
Coronado Bank	---	---	0.1-1.9	1.1	0.1*-1.9*
Crystal Creek (N.San Bern.Mts.)	0.2-0.3	---	0.0-0.7	0.6	0.2-0.3
Cucamonga	>6.6	---	0.5-6.9	4.1	~6.6
Elk Hills	---	---	0-0.3	0.1	<0.3*
Elsinore	0.8-9	8-16	0.4-18	7.5	8-9
Furnace Creek	<0.7	---	0-1.1	0.2	<0.7
Garlock (Antelope Valley)	---	---	0.2-11	4.0	0.2*-11*
Garlock (Mojave)	---	---	0.3-9.9	2.8	0.3*-9.9*
Garlock (Searles Lake)	5.4-13	---	0.1-7.9	3.1	5.4-7.9*
Hayward	7-10	---	0.1-22	14.7	7-10
Hilton Creek	---	---	0.1-0.7	0.6	0.1*-0.7*
Honey Lake	---	---	0.1-10	2.2	0.1*-10*
Hosgri	2-19	---	0.2-3.1	2.1	0.2-3.1*
King City-Monterey Bay	---	---	0.1-1.7	1.4	0.1*-1.7*
Laguna Salada	---	0-4	0.5-21	10.4	0.5*-4
Lake Almanor-Mohawk Valley	---	---	0-0.1	0.0	<0.1*
Ludlow	---	---	0.6-2.8	1.9	0.6*-2.8*
Malibu Coast	---	---	0.7-8.6	6.1	0.7*-8.6*
central Mojave group (sum)	6-12	5.4-10	0.1-3.4	2.8	6-10
Montezuma-Birds Landing	---	---	0-0.1	0.0	<0.1*
Morales	---	---	0-9.0	5.3	<9*
Morongo Valley	---	---	0.1-6.2	3.5	0.1*-6.2*
Newport-Inglewood	0.4-0.8	---	0-0.2	0.0	~0.4
Ortigalita	---	---	0.1-0.9	0.8	0.1*-0.9*
Palos Verdes	0.7-1.4	---	0.3-2.4	1.9	0.7-1.4
Panamint Valley	1.6-6.1	---	0.3-2.5	1.5	1.6-2.5*
Pinto Mountain	>5.3	---	0.1-2.1	2.1	~5.3
Pipes Canyon	---	---	0.3-2.1	1.6	0.3*-2.1*
Pleito	---	---	2.4-17	16.1	2.4*-17*

Raymond	0.3-0.6	---	0.2-6.8	2.7	0.3-0.6
Red Mountain-San Cayetano	9.6-13.6	---	0.8-9.1	4.5	~9.6
Rinconada	3.5-12	---	0.1-10	8.6	3.5-10*
Rodgers Creek	>2.1	---	0-24	14.4	2.1-24*
Rose Canyon	1-2.2	---	0.1-1.2	0.6	1-1.2*
San Andreas (Mecca)	21-35	18-22	3.5-38	14.1	21-22
San Andreas (San Gorgonio)	13-28	12-20	0.4-36	4.4	13-20
San Andreas (San Bernardino)	<29	---	5.6-39	11.1	5.6*-29
San Andreas (Pearblossom)	35-60	18-30	16-33	22.0	18-30
San Andreas (Elkhorn Hills)	31-37	25-30	15-36	22.9	25-30
San Andreas (Parkfield)	32-59	16-40	24-38	29.2	32-38*
San Andreas (San Francisco)	10-38	16-24	8.3-46	18.1	16-24
San Andreas (Tomales Bay)	<25	---	5.2-38	15.1	5.2*-25
San Clemente Island	---	---	0.1-2.2	1.0	0.1*-2.2*
San Diego Trough	---	---	0.1-7.9	3.3	0.1*-7.9*
San Fernando	---	---	0.7-7.2	3.0	0.7*-7.2*
San Gregorio (sensu stricto)	---	---	0.1-3.5	2.1	0.1*-3.5*
San Jacinto	13.3-14	11-15	0.2-30	16.2	13.3-14
San Juan-Whiterock	---	---	0.1-5.3	3.5	0.1*-5.3*
San Pedro Martir	---	---	0.2-6.1	1.7	0.2*-6.1*
Santa Barbara Channel (N. side)	---	---	0.1-2.7	1.8	0.1*-2.7*
Santa Barbara Island	---	---	0.2-19	9.2	0.2*-19*
Santa Monica	0.8-1.1	---	0.3-18	10.8	0.8-1.1
Sierra Madre	2.8-7.1	---	0.1-5.7	1.6	2.8-5.7*
Sierra Nevada	0.3-1.5	---	0.1-6.9	0.9	0.3-1.5
Vallecitos	---	---	0.4-2.7	2.0	0.4*-2.7*
White Mountains	~0.9	---	0.6-9.1	3.1	~0.9
White Wolf	7.1-20	---	0.2-9.6	8.2	7.1-9.6*
Whittier	1-1.5	---	0.2-16	10.0	1-1.5

A Strategy for Obtaining High Temporal and Spatial Resolution of Crustal Deformation using GPS

USGS 1434-92-G2196

Yehuda Bock
Institute of Geophysics and Planetary Physics
Scripps Institution of Oceanography
La Jolla, CA 92093
(619) 534-5292
E-Mail: bock@bull.ucsd.edu

Objectives

GPS surveying has the potential to provide crustal deformation precursors for the prediction of large earthquakes and, in particular, to allow *frequent and dense* monitoring of coseismic and postseismic strain transients which would add to our fundamental understanding of the physics of the earthquake process. The goal of this research is to develop and evaluate the capability of surveying *spatially dense, local to regional scale, three-dimensional geodetic networks, in near real-time with several millimeter-level accuracy* using GPS in a continuously operating and kinematic-type modes.

Investigations Undertaken and Data Collected

Southern California Permanent GPS Geodetic Array

The Permanent GPS Geodetic Array (PGGA) has been operated in southern California since the spring of 1990 by SIO and JPL with assistance from Caltech, MIT and UCLA (Figure 1). Funding for the maintenance of the network is provided by NASA, NSF and USGS. The goals of the PGGA are to monitor crustal deformation related to the earthquake cycle in California, continuously, in near real-time and with millimeter accuracy, using a fully automated and economically viable system. The roles of the PGGA also include providing reference sites and precise GPS orbital and earth rotation information to support detailed GPS geophysical surveys in California. We have collected and analyzed an uninterrupted time series of data since 14 August, 1991. The Landers earthquake sequence generated the first real geophysical signals detected by PGGA. Data collected around the period of the Landers and Big Bear earthquakes have been studied extensively for coseismic and postseismic deformation. PGGA data has been a very important asset for our investigations of the spatial and temporal resolution of GPS under this award.

We have developed an automated system to collect, analyze and archive data from the PGGA sites at JPL, Piñon Flat Observatory (PFO), SIO, Goldstone and Vandenberg Air Force Base, and from a globally distributed set of about 30 GPS tracking stations (Figure 2). We monitor data at a 30 second sampling rate to all visible satellites, 24 hours a day, 7 days a week. All raw data in the SIO archive are translated into the Receiver Independent Exchange (RINEX) format for GPS data. These are archived on an optical storage device, the Epoch-1 Infinite Storage Server. All raw data collected to data are on-line and accessible via anonymous ftp.

Parkfield to Cholame Surveys

We have surveyed with GPS since 1990 several small networks along the San Andreas Fault between Parkfield and Cholame These surveys include measurements of (1) the

USGS GPS quadrilateral near Parkfield, (2) a 12-station fault crossing transsect through Parkfield, (3) the 10-station Kennedy Ranch Alinement Array [Genrich and Bock, 1992], and (4) a 12-station fault transsect along Highway 46 near Cholame. In October, 1992 we responded (at the request of USGS) to the level A alert at Parkfield by resurveying these four arrays [Genrich et al., 1992].

Japanese Permanent GPS Geodetic Array

We have analyzed 17 months of continuously monitored GPS observations collected at a ten station network in the Kanto-Tokai district in Japan by the National Research Center for Disaster Prevention. This is the first such network established in the world. Experience with these data have been invaluable in developing data analysis, handling and archiving algorithms for use in the California PGGA.

Results Obtained

Results from the Southern California Permanent GPS Geodetic Array

We have been estimating the position of the PGGA stations daily since August 1991. We perform, at twenty-four hour intervals, a simultaneous weighted least squares adjustment of the station positions and improved satellites ephemerides. During this period, we have also been generating precise satellite ephemerides and improved earth orientation parameters (polar motion) in support of GPS surveys in southern California. These products are available via anonymous ftp over Internet within 5-7 days of collection. We evaluate the precision of our satellite parameters based on overlapping orbital arcs and baseline repeatability. Our orbital ephemerides are sufficiently precise to support any crustal deformation GPS survey in California, thereby eliminating the time consuming and costly need for each investigator and/or analysis center to compute their own orbit improvements.

The time series of length determinations of the PGGA stations with respect to the DRAO site in Penticton, British Columbia more than 1700 km away is shown in Figure 3, indicating clearly interseismic deformation, and coseismic and postseismic signatures related to the Landers (M_S 7.5) and Big Bear (M_S 6.5) earthquakes on 28 June, 1992. The largest deformation was detected at PFO, which is situated about 80-90 km from the rupture zone, with respect to a reference frame defined by a globally distributed station of orbit tracking stations (Figure 4). We are able to detect significant "absolute" coseismic deformation of 1-5 cm with respect to the global frame (Figure 5), and postseismic deformation of nearly 1 mm/day at Goldstone for the two week period following the earthquakes (Figure 6). The details of our Landers analysis can be found in Bock et al. (1993).

As part of our PGGA efforts, we have made significant improvements to the GAMIT GPS software package in collaboration with investigators at MIT [King and Bock, 1992].

Results from the Japanese Permanent GPS Geodetic Array

Results from this extensive study are reported in Shimada and Bock [1992]. Although we obtained significant crustal deformation measurements in the region of central Japan, the primary thrust of our research related to this award was to demonstrate convincingly the power of regionally based, continuously monitoring GPS networks for obtaining temporally dense measurements of small horizontal and vertical crustal movements across plate boundary zones. This research has been invaluable for our work with the southern California PGGA.

Reports published (1992)

Journal articles

Genrich, J.F. and Y. Bock (1992), Rapid resolution of crustal motion with short-range GPS, *J. Geophys. Res.*,**97**, 3261-3269.

Shimada, S. and Y. Bock (1992), Crustal deformation measurements in central Japan determined by a GPS fixed-point network, *J. Geophys. Res.*, **97**, 12,437-12,455.

Bock, Y., D.C. Agnew, P. Feng, J.F. Genrich, B.H. Hager, T.A. Herring, K.W. Hudnut, R.W. King, S. Larsen, J.-B. Minster, K. Stark, S. Wdowinski and F.K. Wyatt (1993), Detection of crustal deformation from the Landers earthquake sequence using continuous geodetic measurements, *Nature*, in press.

Doctoral dissertations

Genrich, J.F., 1992: Geophysical applications of GPS kinematic techniques, Scripps Institution of Oceanography, Univ. of California San Diego.

Monographs and Conference Proceedings

Bock, Y., J. Zhang, P. Fang, J.F. Genrich, K. Stark and S. Wdowinski (1992), One year of daily satellite orbit and polar motion estimation for near real time crustal deformation monitoring, Proc. IAU Symposium No. 156, Developments in Astrometry and their Impacts on Astophysics and Geodynamics, Springer Verlag, in press.

King, R.W. and Y. Bock, 1992: "Documentation of the GAMIT GPS analysis software," Mass. Inst. of Technology and Scripps Inst. of Oceanography, September, 1992.

Abstracts

Bock, Y., J. Zhang, P. Fang, J. Genrich, J.B. Minster, K. Stark and S. Wdowinski (1992), Nine months of precise satellite ephemerides and high-frequency polar motion determined with an operational GPS global analysis system, *Eos, Trans. Amer. Geophys. Union, 73,* 85.

Genrich J., J.B. Minster, and Y. Bock (1992), Rigid body kinematics from multiple unit GPS pseudo range and phase measurements with applications to marine geophysical surveys, *Eos, Trans. Amer. Geophys. Union, 73,* 86.

Bock. Y. (1992), Towards a real-time crustal deformation monitoring system as a tool for earthquake hazards mitigation, *Eos, Trans. Amer. Geophys. Union, 73,* Vol. 43, 69.

Fang, P., Y. Bock, J.F. Genrich, V. Otero, K. Stark, S. Wdowinski, J. Zhang, T.A. Herring and R.W. King (1992), Determination of precise satellite ephemerides, high-frequency earth rotation, and crustal deformation before and during the IGS campaign, *Eos, Trans. Amer. Geophys. Union, 73,* Vol. 43, 134.

Hudnut, K.W., S. Larsen, M. Lisowski, K. Gross, J. Svarc, D. Jackson, Z. Shen, Y. Bock, and P. Fang (1992), Coseismic displacements in the Landers sequence: constraints from near-field geodetic data, *Eos, Trans. Amer. Geophys. Union, 73,* Vol. 43, 365.

Genrich, J.F., Y. Bock, S.S.O. Puntodewo, S. Wdowinski, and K. Hudnut (1992), GPS-determined slip rates across the San Andreas Fault near Parkfield, poster presented at AGU Fall Meeting, San Francisco.

Wdowinski, S., Y. Bock, P. Fang, J.F. Genrich, D.C. Agnew and F.K. Wyatt (1992), The 1992 Landers earthquake sequence: Detection of coseismic and postseismic surface displacement, *Eos, Trans. Amer. Geophys. Union, 73,* Vol. 43, 364.

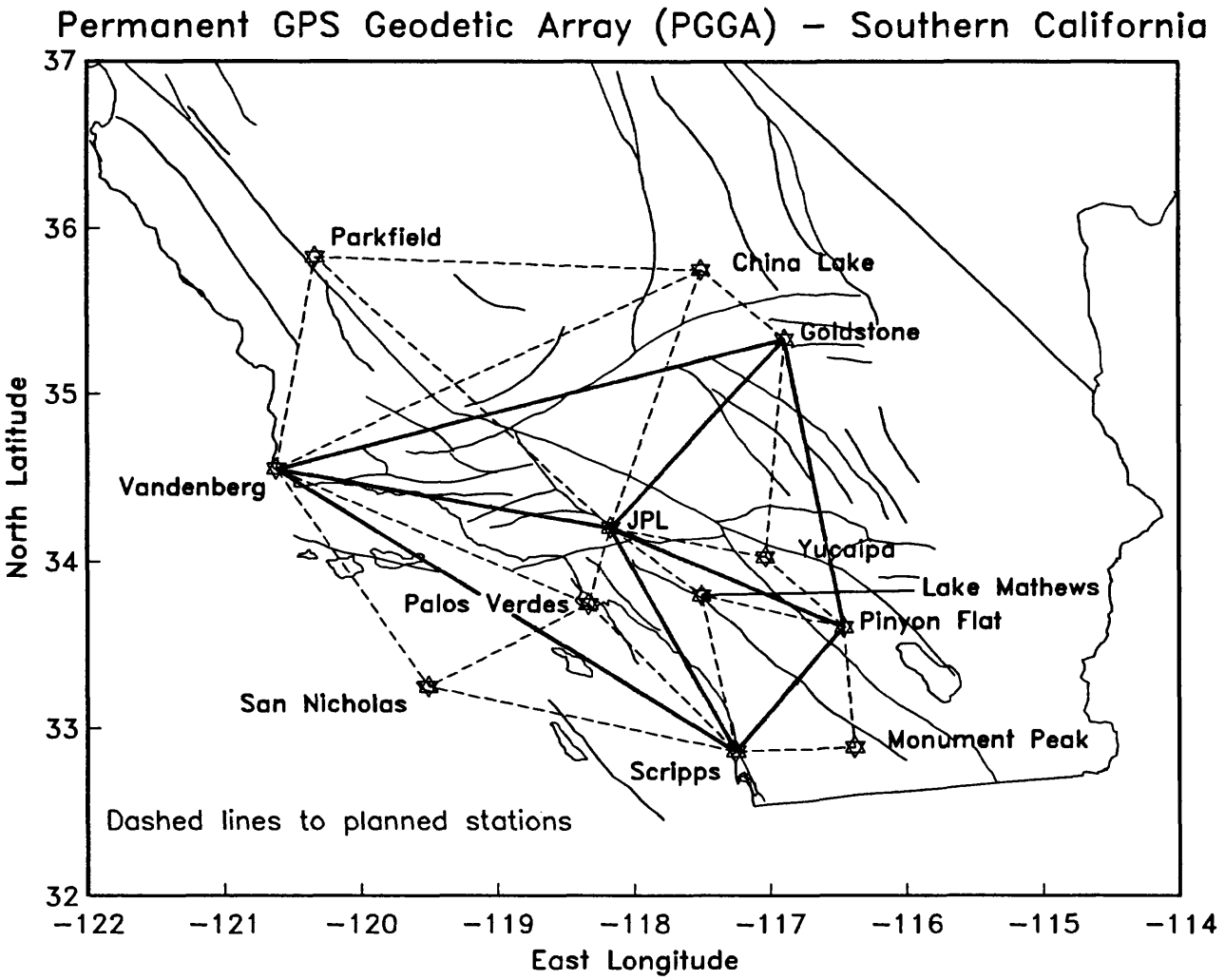

Figure 1: Operational and planned sites of the Southern California Permanent GPS Geodetic Array (PGGA) as of December 1992.

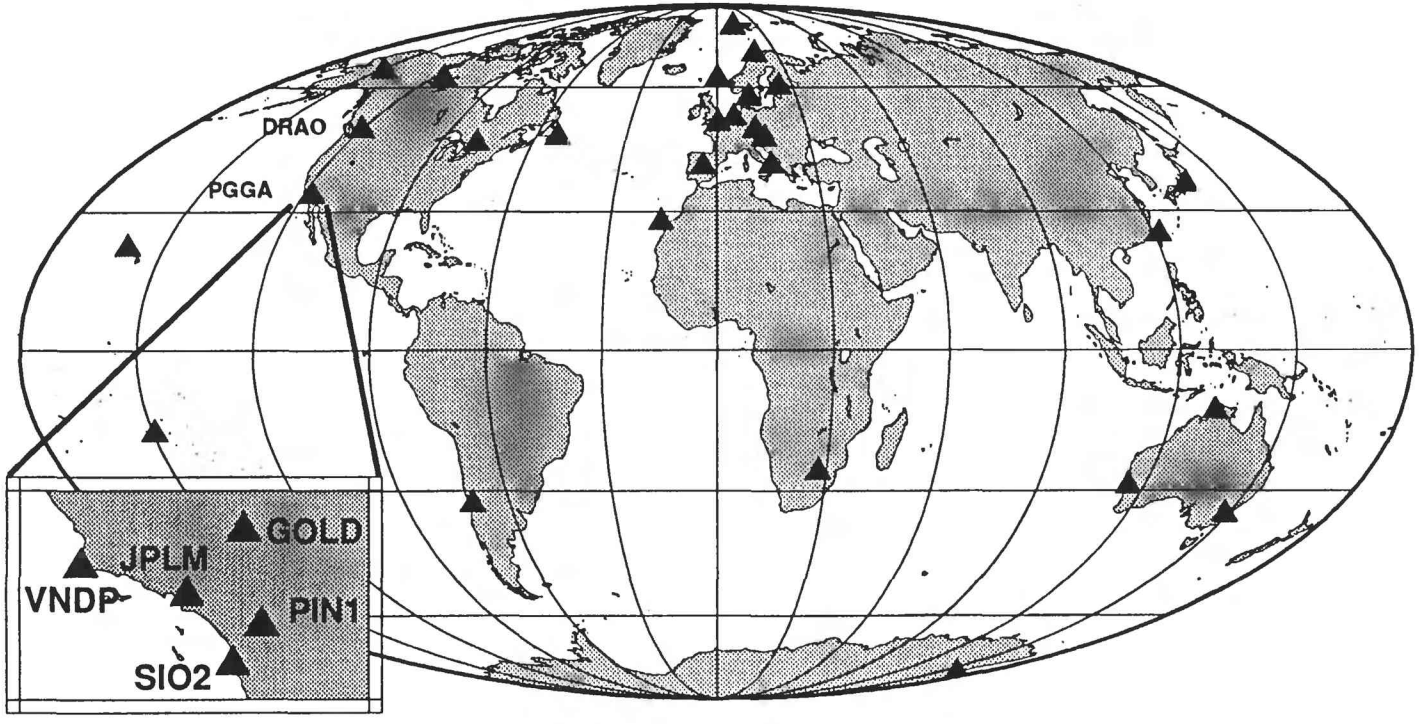

Figure 2: The current distribution of global GPS permanent tracking stations and the PGGA sites in southern California. The global tracking network is usually described by the acronyms CIGNET and FLINN for Cooperative International GPS Network and Fiducial Laboratories for an International Natural science Network, and more recently by the International GPS Service (IGS).

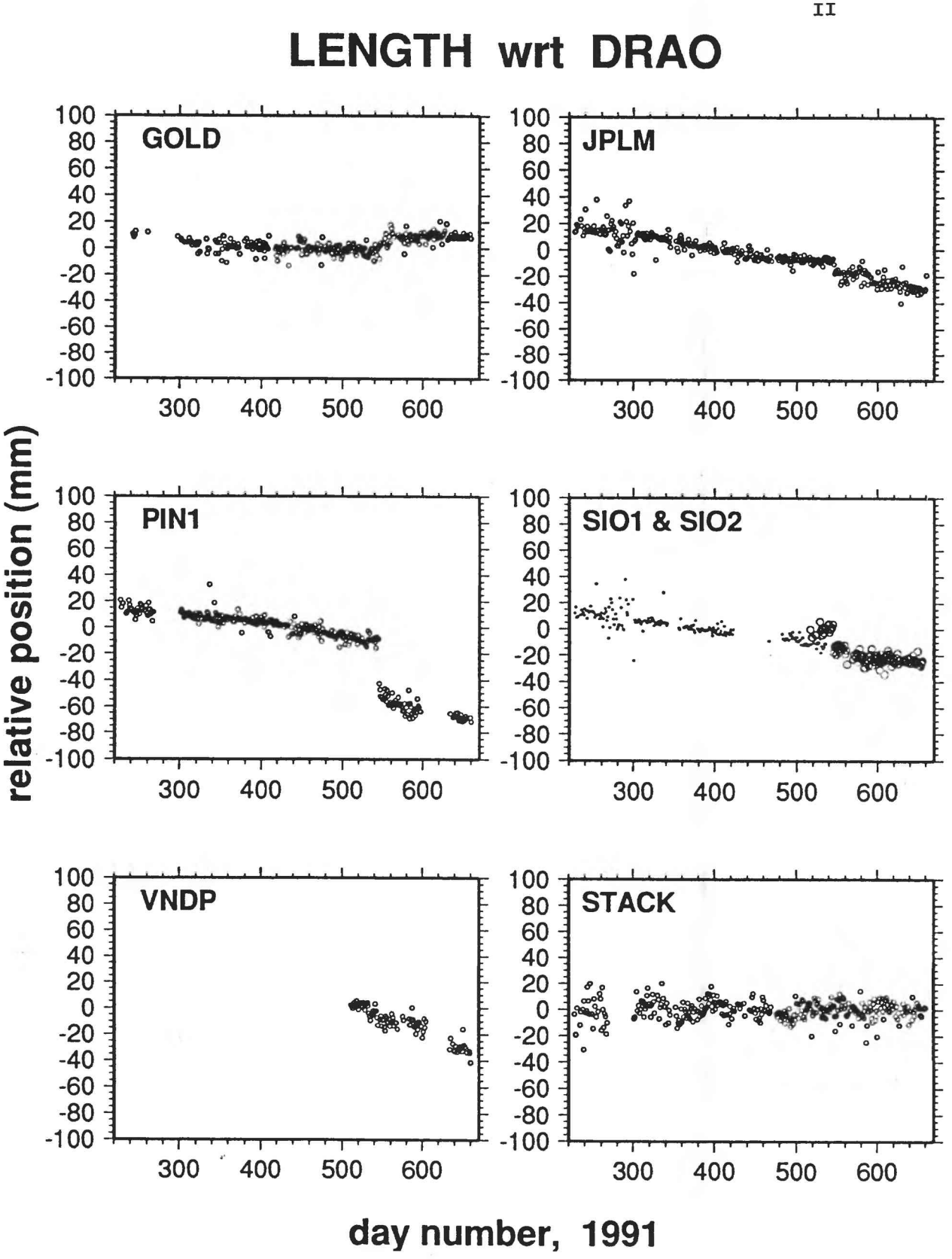

Figure 3: Time series of daily length determinations of the PGGA stations with respect to the DRAO site in Penticton, British Columbia from the time period August 1991 to October 1992. The baseline length is greater than 1700 km. From Wdowinski et al. [1992].

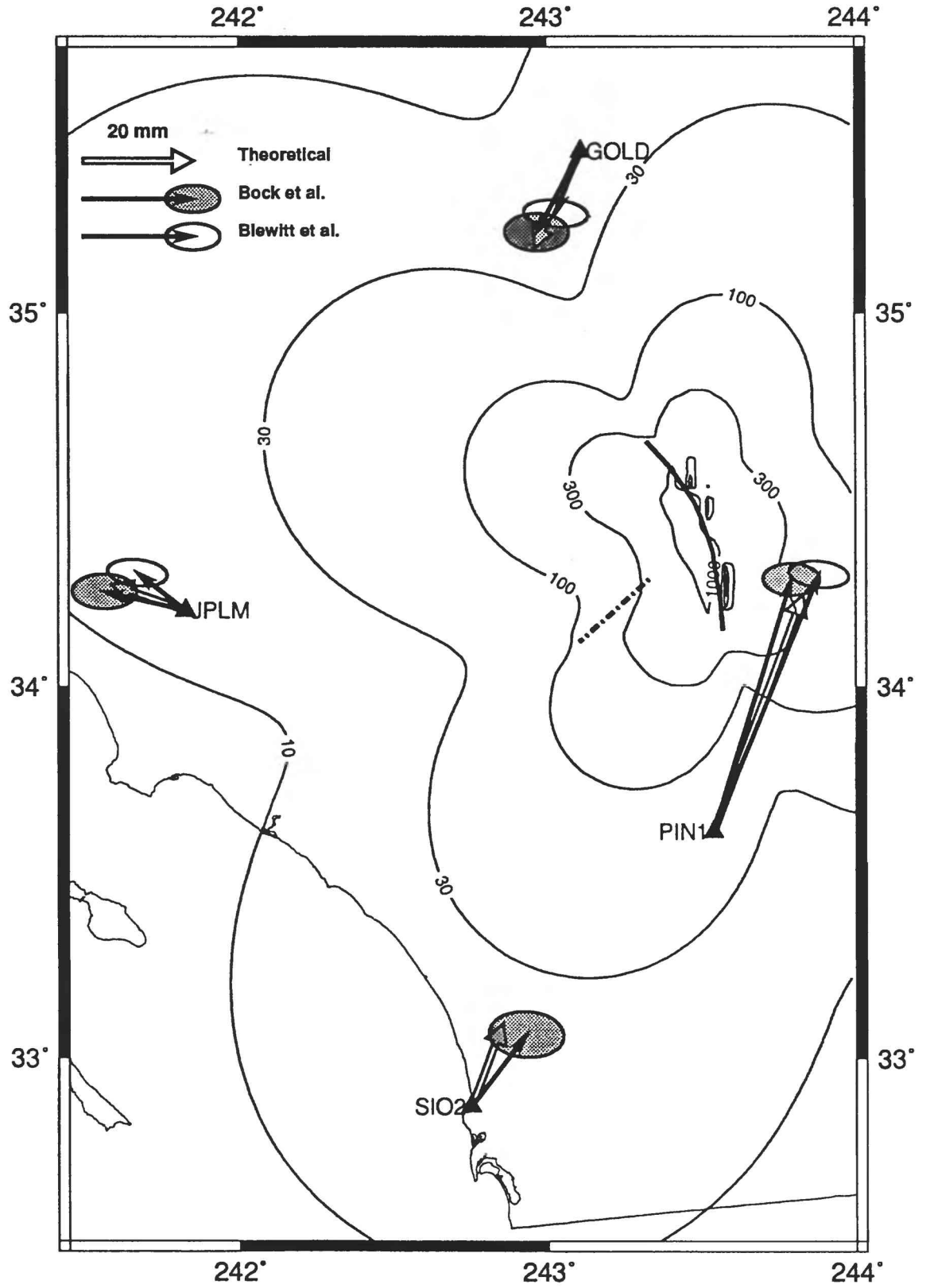

Figure 4: Plot showing the observed (solid arrows) and computed (open arrows) displacements at the PGGA stations, and a comparison of our results with Blewitt et al. at JPL. The contours (displacement magnitude), and the computed displacements are for an elastic halfspace (all units mm). The Landers earthquake break is indicated by a solid line and the Big Bear earthquake by a dotted line. Adapted from Bock et al. [1993].

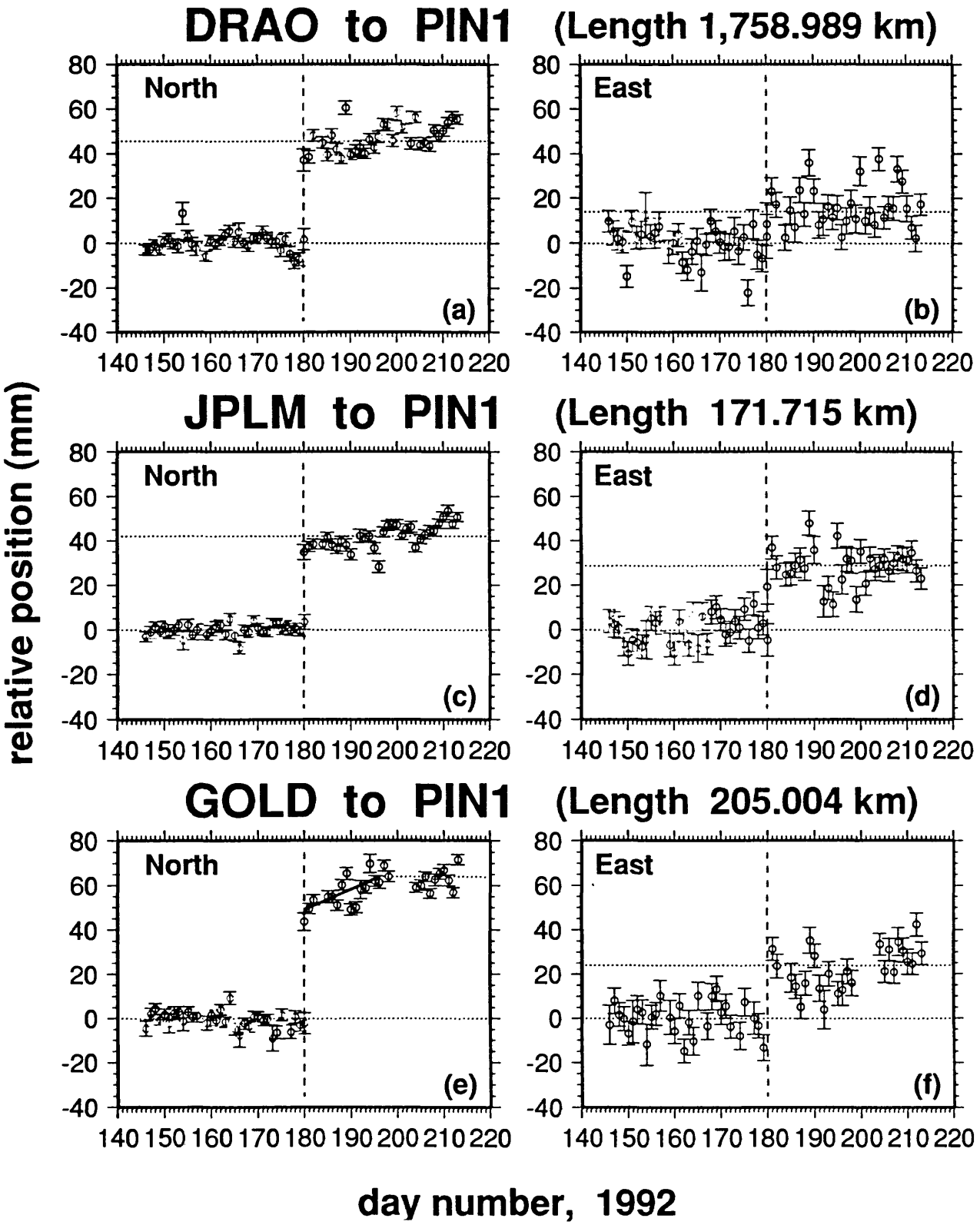

Figure 5: Time series of daily horizontal relative positions over a ten week period centered on the day of the earthquakes (day 180, 28 June 1992) for the DRAO to PIN1, JPLM to PIN1, and DRAO to GOLD baselines. The dotted horizontal lines are determined from the weighted means of the data points for the five week period before and after the earthquakes, and indicate the coseismic signature The error bars are one-sigma standard deviations. The apparent postseismic displacement between GOLD and PIN1 is fit by a solid line in the lower frame. Adapted from Bock et al. [1993].

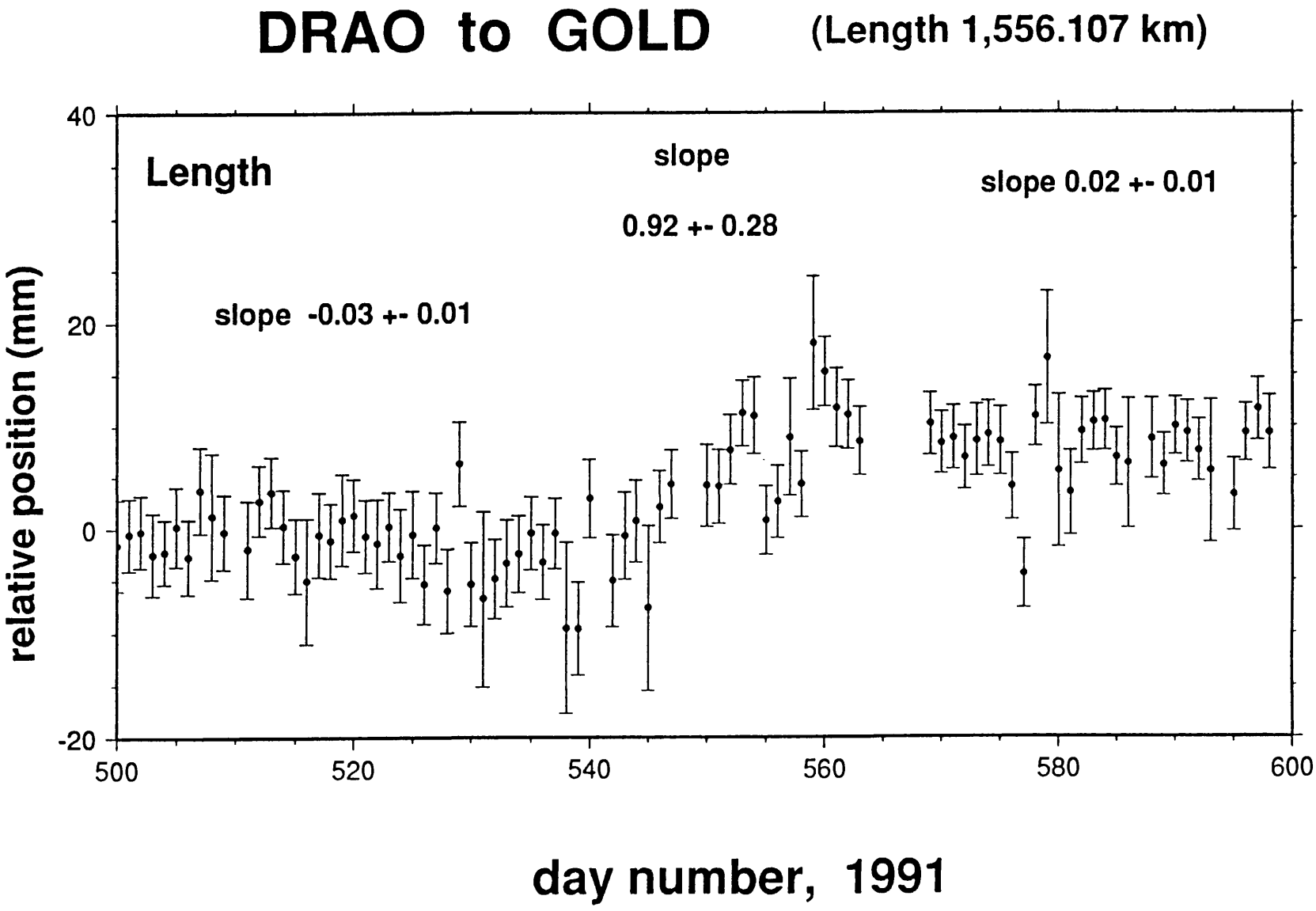

Figure 6: Apparent postseismic displacement at Goldstone with respect to DRAO for the two week period following the Landers earthquake [Wdowinski et al., 1992].

Surface Faulting Studies

9910-02677

M.G.Bonilla
Branch of Engineering Seismology and Geology
U.S. Geological Survey
345 Middlefield Road, MS 977
Menlo Park, CA 94025
(415) 329-5615

Investigations

Compilation and analysis of geologic information that can be used to evaluate and mitigate hazards from faulting and associated earthquakes on part of the San Andreas fault system. The focus is on the San Francisco South quadrangle, which contains the San Andreas and related faults, many landslides, and formations of widely different response to shaking, including Franciscan bedrock, Tertiary sediments, Bay mud, and artificial fills. A 1971 MF geologic map and a 1964 Open-File map showing contours on the bedrock surface are being revised. The revised maps are being compiled in GIS (ARC/ALACARTE) format and prepared for publication on a modern base. Emphasis is being placed on late Quaternary deformation, thickness and nature of unconsolidated deposits, and earthquake-related ground failure.

Results

Reviewed published and unpublished post-1971 reports and 1952-1964 field notes on geology of the quadrangle; searched for new artificial exposures of surficial materials and bedrock using 1989 aerial photos; made field reconnaissance of Serra thrust fault; selected site for augering to confirm probable Holocene displacement on Serra fault; looked for field evidence of possible Quaternary displacement on north part of the Hillside fault (none found to date); compiled information on and collected samples from a tunnel that is under construction near Lake Merced to use in interpreting late Quaternary geologic relations there; revised surficial/bedrock contact at northwest end of San Bruno Mountain; began compilation of new borings and geophysical data; began revision of map showing contours on the bedrock surface using GIS (ARC/ALACARTE) technology.

Revised paper on Marina District and technically reviewed several papers for the USGS Professional Paper on the Marina District.

Reports

Bonilla, M. G., 1992, Geologic and historical factors affecting earthquake damage, in O'Rourke, T.D., ed., The Loma Prieta, California, earthquake of October 17, 1989—Marina District: U.S. Geological Survey Professional Paper 1551-F, p. F7-F34.

11/92

Holocene Slip Rate of the Hayward Fault, Union City, California

Agreement No. 14-08-0001-G2078

Glenn Borchardt
Soil Tectonics
P.O. Box 5335
Berkeley, California 94705-0335

(510)654-1619

Objectives

This project was a cooperative effort with Jim Lienkaemper of the USGS to complete the Union City project. At Union City a stream cuts through the uplifted northeastern side of the fault near Masonic Home and debouches onto an alluvial fan on the southwest side of the fault. Excavations across the fan and parallel the fault uncovered an extremely complicated series of channel fills and interleaved soils. We had initially expected a simple record of successively older buried channel deposits laid down as the debouchment point moved to the northwest. Instead, the record shows a complex of buried alluvial fans having projected apexes of increasing age and offset. The relatively stable points of debouchment apparently were established in conjunction with several right-lateral offsets in the stream.

The preliminary slip rate for fan offset about 67 m was between 7 and 9 mm/yr for the last 8.3 ka. The preliminary slip rate for a fan offset about 43 m was between 6 and 10 mm/yr for the last 4.7 or 6.6 ka. To increase the precision and accuracy of these measurements, we needed to improve our knowledge of the sequence of events that would yield the precise time when each of the stream offsets was initiated.

Fortunately, the site had much datable charcoal and six major paleosols which will help in unraveling the depositional sequence. The paleosols formed on the stable portions of former fan surfaces at the same time as the channels were cutting still other portions of the same fans. Paleosols can be used as stratigraphic markers that constrain the ages of the channel fills that we use as piercing points. Many of these fills are by no means easy to recognize from trench-to-trench. When the size, morphology, and contents of a fill do not suffice, its relationship to the paleosol of the same age becomes the deciding factor in its identification.

Results

We obtained 115 soil samples and performed 55 particle size distribution analyses on 11 vertical sections taken in a 130-m trench. During the project period we completed the soil de-

scriptions and interpretations of the soil data in the context of the channel-fill sequence and 35 C-14 dates on disseminated charcoal (Fig. 1). The soil stratigraphic work supports the following conclusions:

1. The six major paleosols have the following pedochronology (Borchardt, 1992a):

	P1	P2	P3	P4	P5	P6
t_o, ka*	4.7	7.1	8.3	10.7	17.1	~23
t_b, ka	0.5	4.7	7.1	8.3	10.7	17.1
t_d, ky	4.2	2.4	0.8	2.4	6.4	~ 6

*t_o = age when soil formation or aggradation began, t_b = age when soil or strata was buried, and t_d = duration of soil development or aggradation.

2. The primary datum is the P3/P4 paleosol sequence formed during an extremely dry climatic period between 10 ka and 7 ka. These paleosols are easily distinguished by their unique Bk horizons, which contain nodular calcite.

3. Holocene soils at the site are gray brown and associated with varying fluvial conditions, while the Pleistocene soils are yellow brown and associated with relative landscape stability.

4. The youngest age in the G fan was 5.2 ka and the oldest age in the E fan was 5.1 ka. The E fan therefore was established at 5.15 ka. The 43-m offset yields a rate of 8.3 $\pm$1.0 mm/yr.

5. The youngest age in the I fan was 8.5 ka and the oldest age in the G fan was 8.3. The G fan therefore was established at 8.4 ka. The 67-m offset yields a rate of 8.0 $\pm$ 0.6 mm/yr.

6. The oldest age so far determined in fan I was 11 ky B.P. U/Th-corrected to 12.9 ka. The approximate 98-m offset yields a preliminary rate of 7.6 $\pm$ 0.4 mm/yr.

7. The average of the first two determinations yields a slip rate of 8.2 $\pm$0.8 mm/yr for the last 8 ka.

8. There has been no detectable change in the slip rate on the Hayward fault throughout the Holocene.

Reports Published in FY92

Borchardt, Glenn, 1992a, Pedochronology along the Hayward fault, in Galehouse, J.S., ed., Program and Abstracts: Second Conference on Earthquake Hazards in the Eastern San Francisco Bay Area, March 25-29, 1992, California State University, Hayward, p. 9.

Borchardt, Glenn, 1992b, Field trip contributions concerning the Hayward fault at Point Pinole Regional Park, Richmond, Contra Costa College and El Portal School, San Pablo, Hillside School and the University of California, Berkeley, Lake Temescal, Oakland, and Fremont Central Park, Fremont, in Taylor, C.L., Hall, N.T, and Melody, Moya, eds., Field Trip Guidebook, Second Conference, Earthquake Hazards in the Eastern San Francisco Bay Area, March 28-29, 1992: California State University, Hayward, California, p. 13-21, 23-24, 59, 61-63, 77-81, 191-197.

Borchardt, Glenn, Hirschfeld, S.E., Lienkaemper, J.J., McClellan, Patrick, Williams, P.L., and Wong, I.G., editors, 1992 (in press), Proceedings of the Second Conference on Earthquake Hazards in the Eastern San Francisco Bay Area: California Division of Mines and Geology Special Publication 113.

Borchardt, Glenn, and McClellan, Patrick, 1992, Highlights of the Second Conference on Earthquake Hazards in the Eastern San Francisco Bay Area: California Geology, v. 43, no. 4, p. 124.

Borchardt, Glenn, Lienkaemper, J.J., and Budding, K.E., 1992, Holocene slip rate of the Hayward fault at Fremont, in Galehouse, J.S., ed., Program and Abstracts: Second Conference on Earthquake Hazards in the Eastern San Francisco Bay Area, March 25-29, 1992, California State University, Hayward, p. 10.

Borchardt, Glenn, and Mace, Neal, 1992, Clastic dike as evidence for a major earthquake along the northern Hayward fault in Berkeley, in Galehouse, J.S., ed., Program and Abstracts: Second Conference on Earthquake Hazards in the Eastern San Francisco Bay Area, March 25-29, 1992, California State University, Hayward, p. 11.

Lienkaemper, J.J., and Borchardt, Glenn, 1992a, Hayward fault: Large earthquakes versus surface creep, in Galehouse, J.S., ed., Program and Abstracts: Second Conference on Earthquake Hazards in the Eastern San Francisco Bay Area, March 25-29, 1992, California State University, Hayward, p. 41.

Lienkaemper, J.J., and Borchardt, Glenn, 1992b, Holocene slip rate of the Hayward fault at Union City, California, in Galehouse, J.S., ed., Program and Abstracts: Second Conference on Earthquake Hazards in the Eastern San Francisco Bay Area, March 25-29, 1992, California State University, Hayward, p. 42.

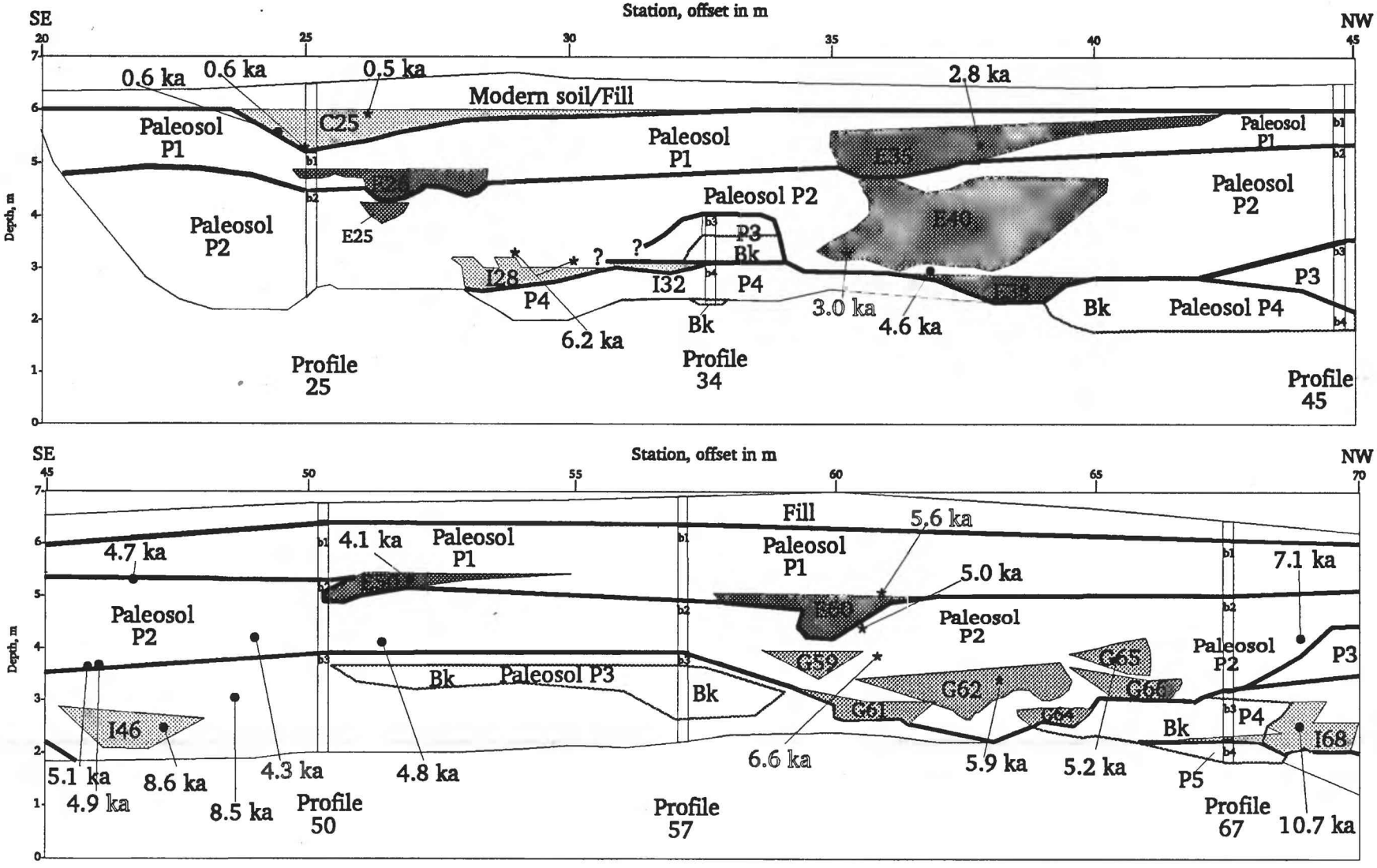

Figure 1. Simplified, reversed, and reduced-scale log of the soil and alluvial relationships parallel and southwest of the Hayward fault at Union City. 1989 trench used as the base. Only the most important channel fills and paleosols are shown. Abbreviations: G74 = channel fill from apex G at station 74; b1 = surface of buried soil; P3 = third youngest paleosol; ka = C-14 date corrected to thousands of calendar years; Bk = soil horizon containing calcite; * = charcoal from this exposure; o = charcoal from another exposure; open letters indicate discordant ages.

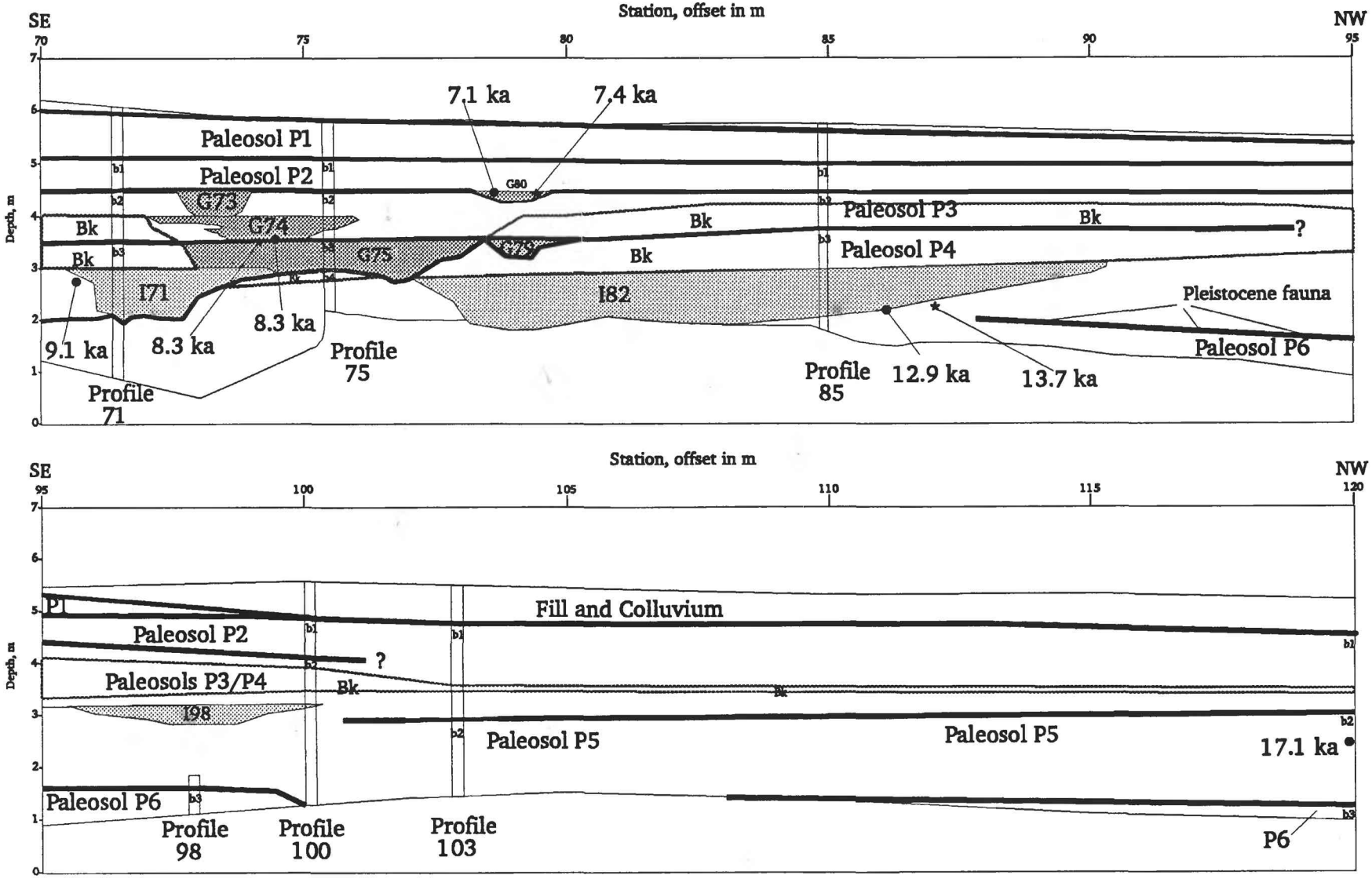

Figure 1. (continued)

ACCELERATION, VELOCITY, AND VOLUMETRIC STRAIN FROM PARKFIELD GEOS NETWORK

9910-02089

ROGER D. BORCHERDT, MALCOLM J. JOHNSTON,
C. DIETEL, G. GLASSMOYER, AND ALLAN LINDH
BRANCH OF ENGINEERING SEISMOLOGY AND GEOLOGY
U.S. GEOLOGICAL SURVEY
345 MIDDLEFIELD ROAD, MS 977
MENLO PARK, CALIFORNIA 94025
415/329-5619

Investigations

* Maintain GEOS array near Parkfield, CA, to serve as a strong-motion array to provide broad-band, high-resolution measurements of the mainshock as well as an array to provide measurements of pre-, co-, and post-seismic strain and displacement field perturbations for purposes of earthquake prediction.

* Maintain up-to-date archive of all events recorded in anticipated rupture zone.

* Develop theoretical basis and models to interpret collocated measurements of volumetric strain and seismic displacement fields.

Results

* An array of 13 stations is being maintained at 95% or greater reliability near Parkfield, CA. Array maintenance is being provided by C. Dietel. He is also maintaining an up-to-date digital data archive and providing summaries for monthly internal USGS reports. (See previous reports for detailed description of the array.) Events recorded along Parkfield segment of study zone during time interval indicated are summarized according to magnitude and depth (Table 1, Figure 1). Stations that triggered on the events are shown in Table 2.

* An example of magnitude 4.7 event recorded at all stations is shown in Figures 2, 3 4, and 5. Measurements of volumetric strain at the six dilatometer sites are arranged in record section format (Figure 2). Three-component measurements of ground acceleration velocity are shown in Figures 3, 4, and 5.

Reports

(see projects Borcherdt et al., [9910-02689 and 9901-03009] and Johnston for related reports.

TABLE 1

HYPO-71 LISTING: PARKFIELD EARTHQUAKES RECORDED ON ONE OR MORE GEOS STATIONS FROM OCTOBER 1, 1991 OCTOBER 20, 1992.

9110 3	547	10.42	35	55.70	120	28.46	4.78	0.83	11	147	3.1	0.03	0.4	0.7	
9110 9	1648	19.75	35	44.76	120	17.76	6.11	0.96	12	90	4.5	0.05	0.4	0.9	
911018	959	5.54	35	55.27	120	28.09	5.69	3.53	42	75	3.7	0.12	0.2	0.2	
911027	610	6.89	36	1.14	120	34.60	5.78	2.93	42	88	4.4	0.09	0.2	0.3	S
911029	628	34.05	35	59.12	120	33.77	9.73	0.94	11	116	3.5	0.11	0.6	0.7	S
911101	1909	36.48	36	1.08	120	34.56	5.63	3.0	28	131	4.	0.08	0.3	0.3	B
911102	0635	17.18	35	59.98	120	33.23	4.91	3.2	17	133	5.	0.04	0.3	0.5	B
911102	0652	16.33	35	59.75	120	33.82	5.56	2.3	21	94	4.	0.09	0.3	0.4	B
911108	0300	48.46	36	4.75	120	38.04	7.16	4.8	45	58	8.	0.12	0.2	0.4	B
911108	0301	25.16	36	4.77	120	37.93	7.46	3.3	20	133	9.	0.08	0.3	0.6	B
911116	1802	18.10	36	2.11	120	35.52	6.65	2.7	30	130	6.	0.08	0.2	0.4	B
911201	0012	30.35	35	57.88	120	30.62	7.40	1.4	15	161	1.	0.04	0.5	0.3	B
911201	0025	43.21	35	57.88	120	30.65	7.27	1.6	20	135	2.	0.05	0.3	0.3	B
911201	0140	12.99	35	57.98	120	30.46	7.40	1.9	24	137	1.	0.07	0.3	0.3	B
911217	0356	17.22	36	4.80	120	38.24	3.22	3.0	32	123	8.	0.08	0.2	0.8	B
911218	1442	19.58	35	57.90	120	31.08	11.57	3.0	37	132	2.	0.11	0.2	0.3	B
920104	1035	03.70	35	55.79	120	28.50	4.93	1.8	17	148	3.	0.04	0.4	0.4	B
920126	1712	51.31	35	59.47	120	33.89	4.92	1.8	24	91	3.	0.07	0.2	0.3	B
920206	0321	16.19	36	1.25	120	34.58	5.71	2.5	31	89	5.	0.07	0.2	0.3	A
920222	1410	50.12	35	48.17	120	21.35	9.04	2.2	27	72	5.	0.08	0.2	0.5	A
920224	1724	01.62	35	47.71	120	21.11	10.10	3.0	32	54	6.	0.12	0.3	0.7	A
920311	2051	35.70	35	52.95	120	25.67	5.95	2.0	26	128	2.	0.06	0.2	0.2	B
920317	1228	53.13	35	55.75	120	28.38	5.01	1.9	22	133	3.	0.05	0.3	0.3	B
920404	0311	16.64	35	58.47	120	31.13	7.55	1.5	20	137	3.	0.03	0.4	0.3	B
920404	0311	48.70	35	58.40	120	31.20	7.61	1.3	16	135	3.	0.02	0.5	0.4	B
920404	0830	17.74	35	55.73	120	28.42	5.02	1.0	17	148	3.	0.03	0.3	0.4	B
920408	1533	03.38	36	1.68	120	35.23	4.58	2.4	30	130	5.	0.11	0.3	0.5	B
920416	0633	54.03	35	58.87	120	31.73	8.03	3.1	14	175	4.	0.03	0.6	0.4	B
920529	1703	01.75	35	49.70	120	22.78	7.68	3.8	37	46	2.	0.13	0.2	0.3	A
920618	1154	35.04	36	3.40	120	36.19	5.54	2.1	29	130	8.	0.06	0.2	0.3	B
920618	1439	17.48	35	59.43	120	33.83	5.09	1.3	12	90	3.	0.07	0.3	0.7	A
920619	1118	55.03	35	47.63	120	20.86	9.15	1.5	21	65	7.	0.06	0.3	0.6	A
920703	0154	58.22	36	3.25	120	36.26	8.41	1.9	24	129	8.	0.07	0.3	0.4	B
920707	1335	53.71	36	1.75	120	35.70	8.25	2.6	31	150	5.	0.11	0.2	0.2	B
920711	0046	57.35	35	51.48	120	24.14	5.19	2.6	27	87	2.	0.07	0.1	0.2	A
920711	0158	15.39	35	51.47	120	24.07	5.25	2.7	29	89	2.	0.07	0.2	0.2	A
920724	1208	28.48	35	58.26	120	32.47	4.08	1.1	9	106	4.	0.09	0.4	1.6	B
920813	0757	08.20	36	.66	120	33.76	5.45	1.7	15	176	5.	0.05	0.4	0.3	B
920818	0703	53.10	35	48.53	120	21.39	5.06	2.1	26	77	5.	0.07	0.2	0.4	A
920819	2221	30.25	35	59.10	120	33.58	5.54	1.5	13	115	4.	0.07	0.3	0.6	B
920911	1351	41.64	36	2.77	120	36.51	10.46	2.8	33	91	7.	0.07	0.2	0.4	B
920914	1301	38.43	35	58.97	120	33.14	5.79	1.7	11	120	4.	0.08	0.4	0.5	B
920916	0525	13.52	35	52.91	120	25.62	5.94	3.4	37	133	5.	0.08	0.2	0.2	B
921001	0611	35.99	35	56.70	120	29.07	10.42	2.0	22	159	2.	0.07	0.3	0.4	B
921004	1816	57.32	35	55.65	120	28.18	9.79	4.0	39	76	3.	0.08	0.2	0.3	A
921005	0401	25.61	35	55.76	120	28.12	9.90	1.5	22	155	4.	0.05	0.4	0.3	B
921005	1859	32.18	35	55.73	120	28.22	9.76	3.3	35	82	3.	0.07	0.2	0.3	A
921007	1304	28.31	35	58.36	120	31.50	5.25	3.4	37	161	3.	0.09	0.3	0.2	B
921020	0528	08.91	35	55.69	120	28.26	9.91	4.7	46	70	3.	0.09	0.2	0.3	A
921020	0541	53.23	35	55.87	120	28.12	10.32	1.7	24	157	4.	0.06	0.3	0.3	B
921020	0548	04.11	35	55.67	120	28.36	9.99	2.7	27	146	3.	0.09	0.3	0.4	BC
921020	0555	54.39	35	55.75	120	28.07	10.21	1.9	26	156	4.	0.06	0.3	0.3	B
921020	0620	55.64	35	56.03	120	28.32	10.47	1.8	25	158	3.	0.06	0.3	0.3	B

TABLE 2

"WHERE" LIST OF TRIGGERED GEOS STATIONS FOR PARKFIELD EARTHQUAKES DURING THE TIME PERIOD OCTOBER 1, 1991 THROUGH OCTOBER 20, 1992.

	M	J	D	V	F	E	G	K	R	P	S	W	C	I
2760547	*													
2831648													*	
2910959	*	*	*	*	*	*	*	*		*		*		*
3000610	*		*		*	*								
3020628			*											
3051909	*		*		*	*		*		*				
3060635	*		*	*	*	*		*		*		*	*	
3060652	*		*							*				
3120300	*	*	*	*	*	*		*	*	*			*	
3120301					*									
3201802	*		*		*									
3350012			*		*									
3350025		*	*		*									
3350140		*	*		*									
3510356			*							*				
3521442		*	*	*	*	*		*		*			*	
0041035		*	*		*					*				
0261712			*											
0370321			*		*					*				
0531410		*			*	*		*					*	
0551724		*			*	*		*	*				*	
0712051		*			*	*		*						
0771228	*	*			*									
095031117	*		*		*									
095031148			*		*									
0950830	*	*	*											
0991533			*		*									
1070633			*		*									
1501702(3)	*		*	*	*	*	*	*		*			*	*
1701154											*			
1701439											*			
1711118								*						
1850154											*			
1891335	*	*	*		*					*	*			
1930046(7)		*	*		*	*	*	*		*				
1930158		*	*		*	*	*	*		*				
2061208											*			
2260757										*				
2310703							*	*						
2322221										*				
2551351			*		*					*	*			
2581301										*				
2600525	*	*	*	*	*	*	*	*		*				*
2750611		*	*		*									
2781816	*	*	*	*	*	*	*	*	*		*			*
2790401			*											
2791859	*	*	*	*	*	*		*			*			*
2811304	*	*	*	*	*	*		*			*			
2940528	*	*	*	*	*	*	*	*	*		*			*
2940541			*					*						
2940548	*	*	*	*	*	*	*	*			*			*
2940555			*		*			*			*			
2940620			*					*						
	M	J	D	V	F	E	G	K	R	P	S	W	C	I

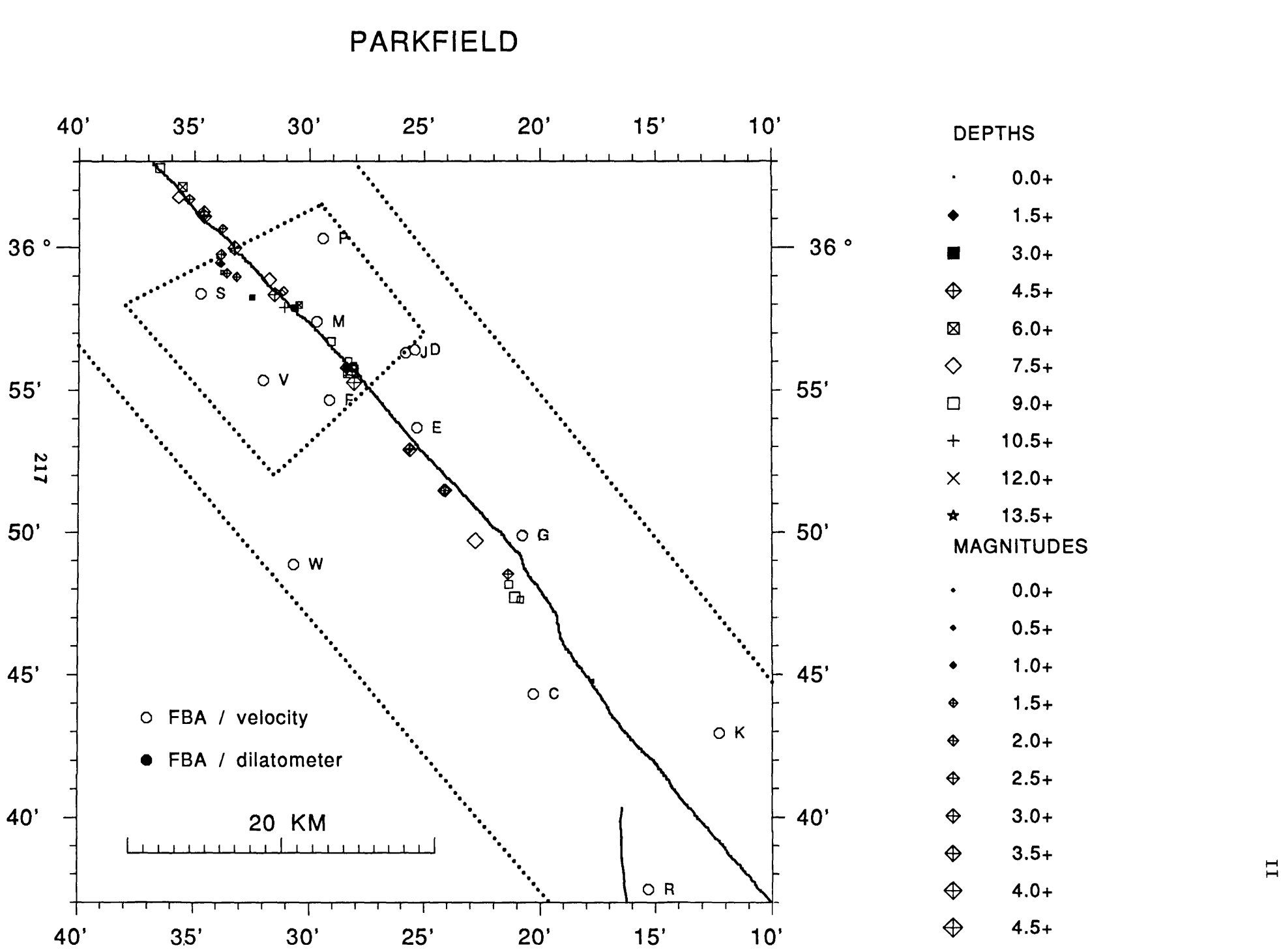
PARKFIELD
40'
35'
30'
25'
20'
15'
10'
36 °
55'
50'
45'
40'
P
S
M
JD
V
F
E
G
W
C
K
R
FBA / velocity
FBA / dilatometer
20 KM
DEPTHS
0.0+
1.5+
3.0+
4.5+
6.0+
7.5+
9.0+
10.5+
12.0+
13.5+
MAGNITUDES
0.0+
0.5+
1.0+
1.5+
2.0+
2.5+
3.0+
3.5+
4.0+
4.5+

217

Figure 1

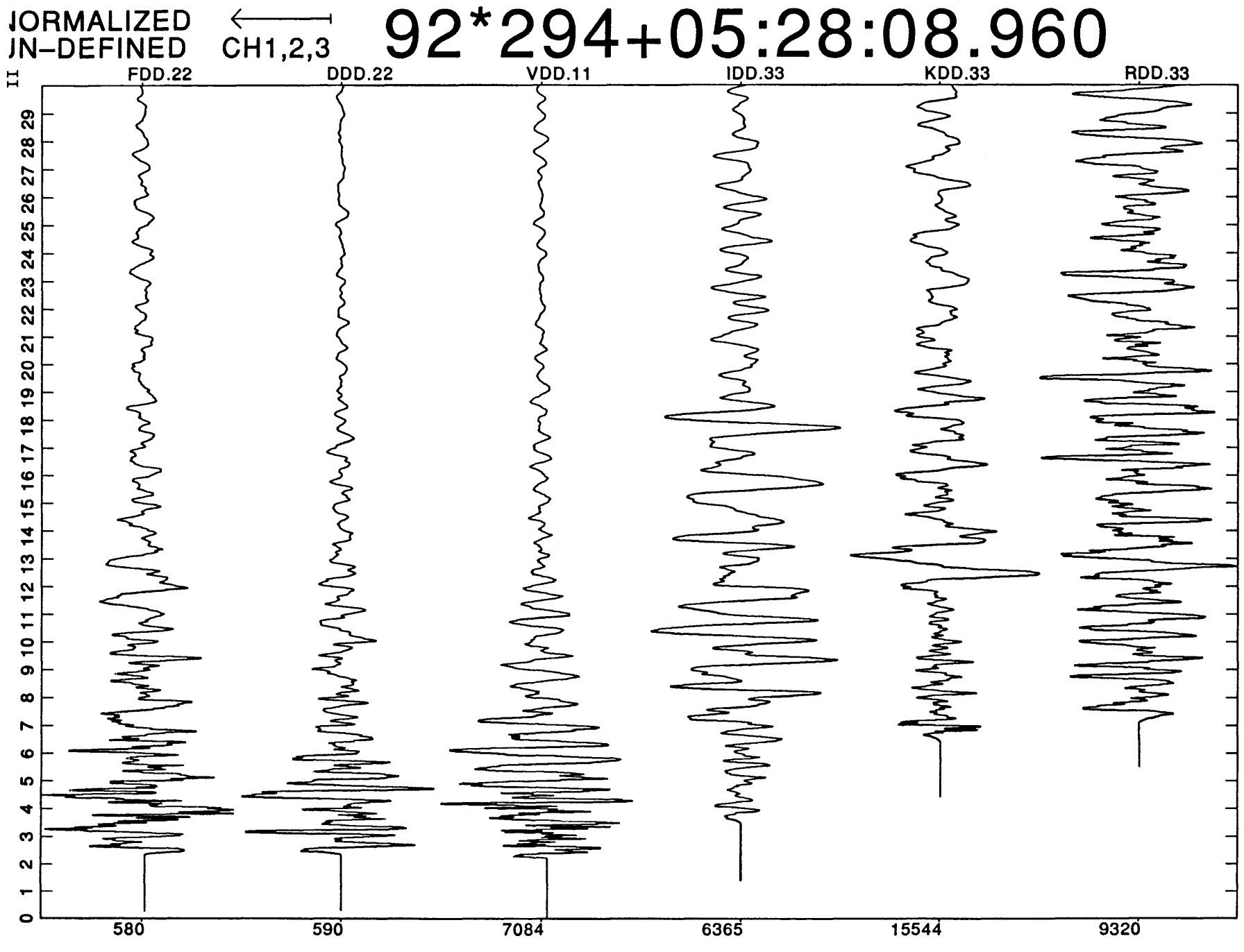
NORMALIZED
UN-DEFINED
CH1,2,3
92*294+05:28:08.960
FDD.22
DDD.22
VDD.11
IDD.33
KDD.33
RDD.33
0 1 2 3 4 5 6 7 8 9 10 11 12 13 14 15 16 17 18 19 20 21 22 23 24 25 26 27 28 29
580
590
7084
6365
15544
9320

Figure 2

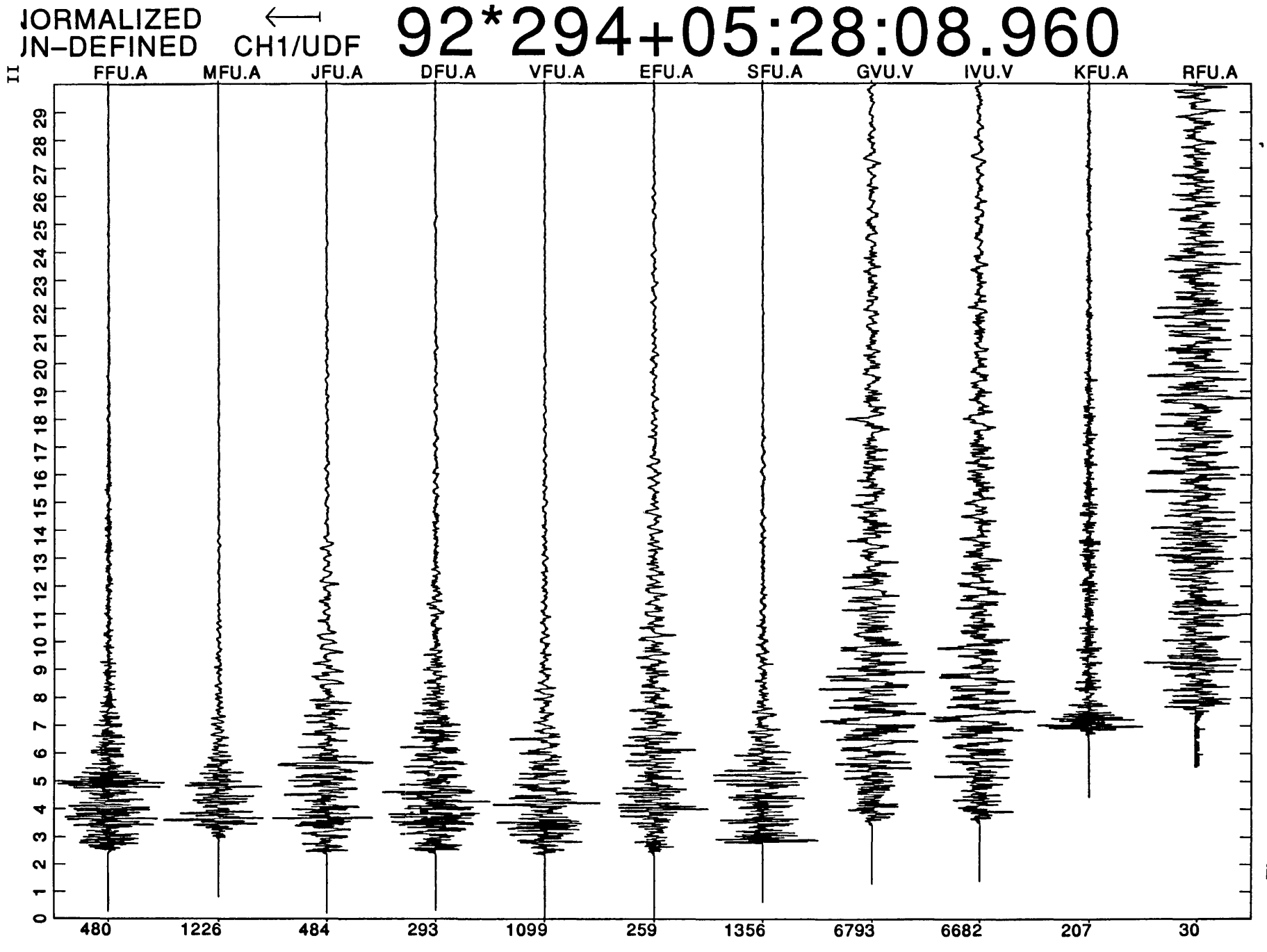
JORMALIZED
JN–DEFINED
CH1/UDF
92*294+05:28:08.960
FFU.A
MFU.A
JFU.A
DFU.A
VFU.A
EFU.A
SFU.A
GVU.V
IVU.V
KFU.A
RFU.A
0 1 2 3 4 5 6 7 8 9 10 11 12 13 14 15 16 17 18 19 20 21 22 23 24 25 26 27 28 29
480
1226
484
293
1099
259
1356
6793
6682
207
30

Figure 3

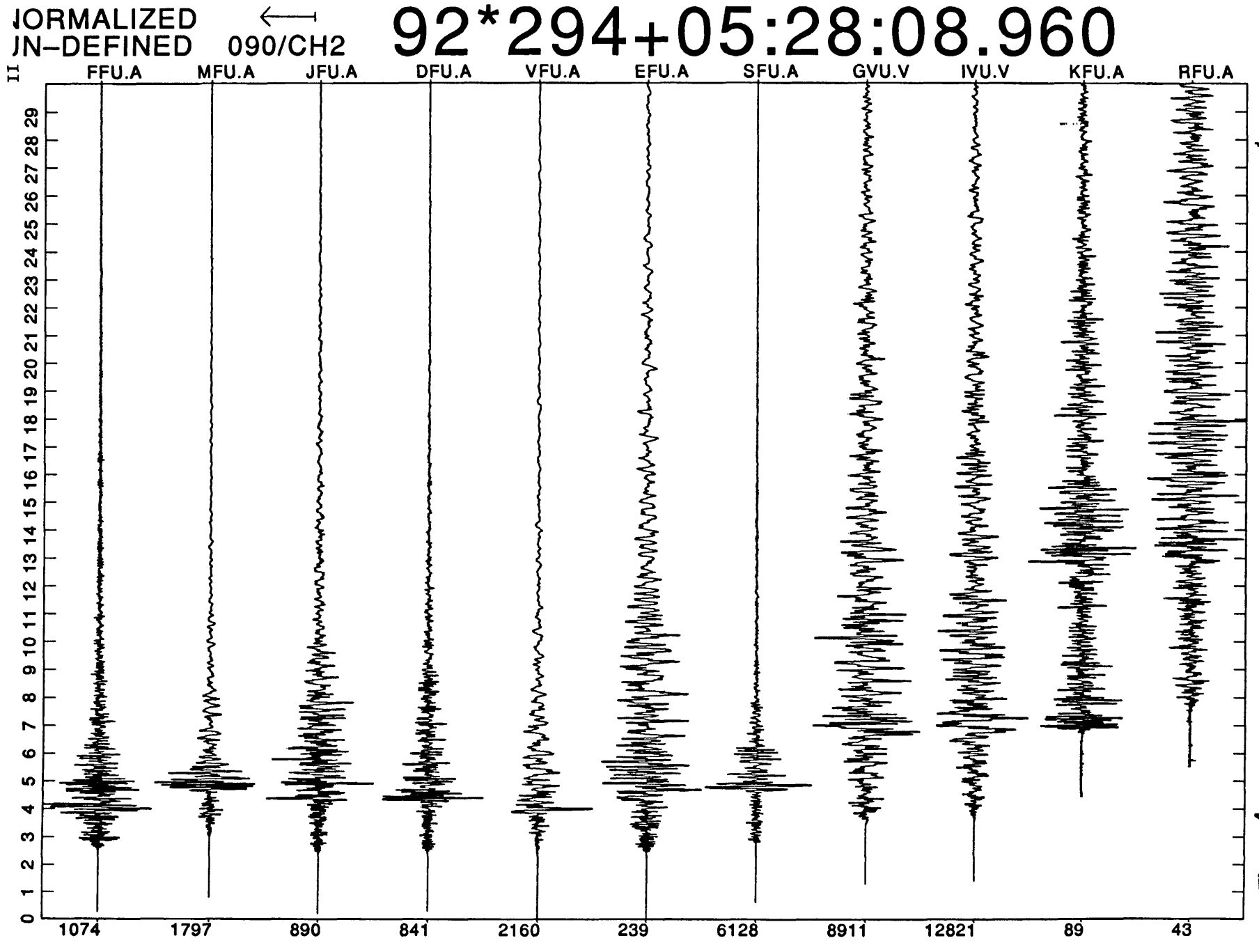
JORMALIZED
JN-DEFINED
090/CH2
92*294+05:28:08.960
II
FFU.A
MFU.A
JFU.A
DFU.A
VFU.A
EFU.A
SFU.A
GVU.V
IVU.V
KFU.A
RFU.A
0 1 2 3 4 5 6 7 8 9 10 11 12 13 14 15 16 17 18 19 20 21 22 23 24 25 26 27 28 29
1074
1797
890
841
2160
239
6128
8911
12821
89
43
220

Figure 4

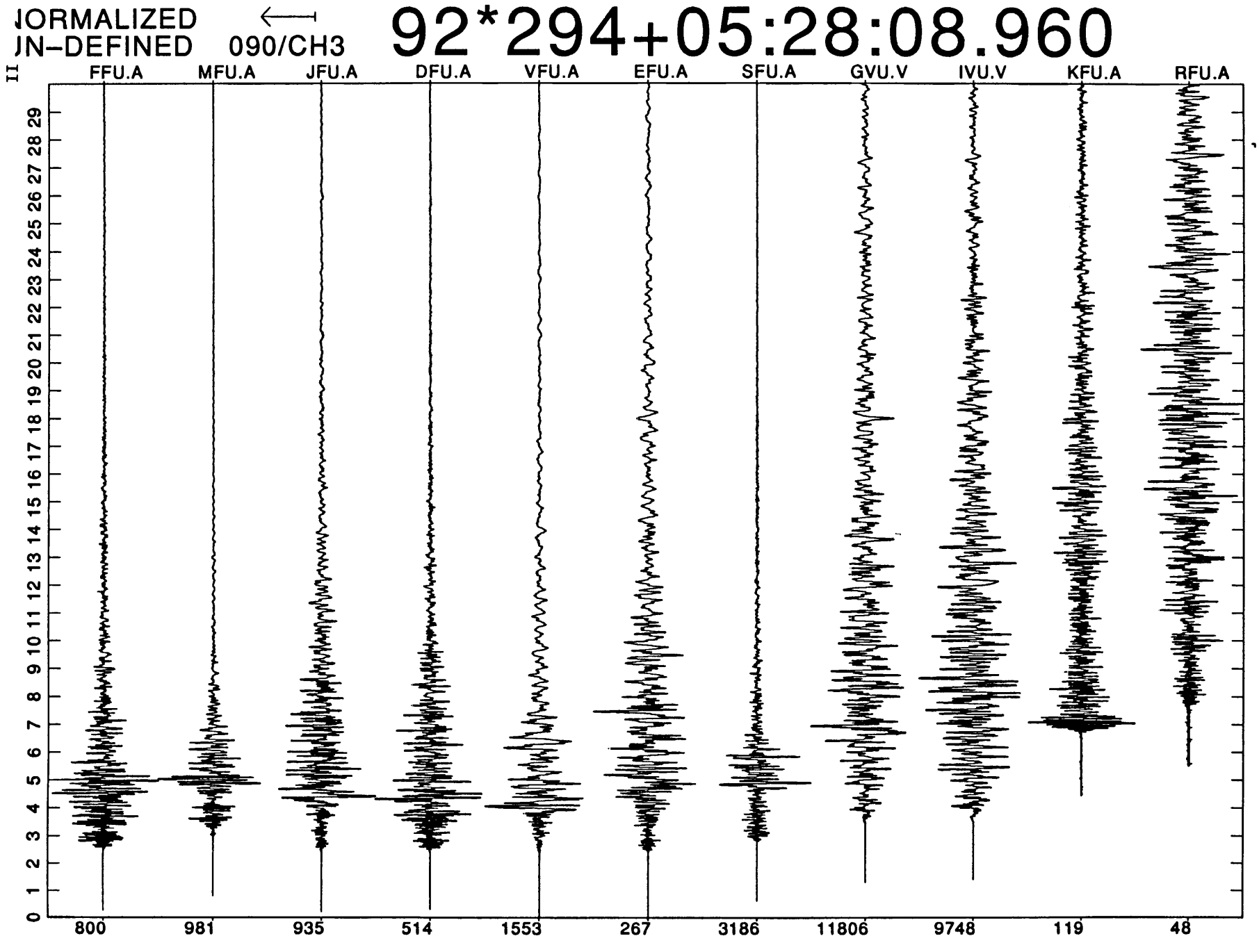
NORMALIZED
UN-DEFINED
090/CH3
92*294+05:28:08.960
FFU.A
MFU.A
JFU.A
DFU.A
VFU.A
EFU.A
SFU.A
GVU.V
IVU.V
KFU.A
RFU.A
0 1 2 3 4 5 6 7 8 9 10 11 12 13 14 15 16 17 18 19 20 21 22 23 24 25 26 27 28 29
800
981
935
514
1553
267
3186
11806
9748
119
48

Figure 5

ANALYSIS OF WIDE-ANGLE REFLECTION/REFRACTION RECORDINGS FROM THE BAY AREA SEISMIC IMAGING EXPERIMENT (BASIX[1])

Seismic Reflection Crustal Studies Project: Project No. 9930-70253 (formerly 04323)

T. Brocher
OEVE, Branch of Seismology
U. S. Geological Survey
345 Middlefield Road, MS/977
Menlo Park, California 94025
Telephone: (415) 329-4737
brocher@andreas.wr.usgs.gov

INVESTIGATIONS UNDERTAKEN

The primary goal of the Bay Area Seismic Imaging eXperiment (BASIX) was to image the subsurface geometry of the crust in the vicinity of the major earthquake producing faults in the San Francisco Bay Area. In September, 1991, BASIX obtained seismic reflection lines designed to provide a picture of the crust down to the base of the crust using a large airgun source and receivers moored to buoys in the water. At the same time, temporary seismic recorders were deployed throughout the Bay Area (see Figure 1) to record these airgun signals at large distances (wide-angles).

We have reduced and begun to analyze the high-quality wide-angle seismic data recorded using five-day recorders during the BASIX experiment. The analysis of these records has consisted of identifying and correlating arrivals recorded at each receiver, digitizing the travel times of these arrivals, and forward modeling and inversion of travel times. A primary goal of this research is to relate the velocity structure to seismic reflections observed in the BASIX multichannel seismic reflection profile. Copies of the five-day recorder data have been distributed to BASIX participants, including Kevin Furlong of Pennsylvania State University, Steve Holbrook of Woods Hole Oceanographic Institution, and Uri ten Brink of the USGS/Woods Hole.

Processing of the wide-angle data as near-vertical incidence reflection profiles represents a high priority for ongoing data processing and analysis. The 5 to 10 km spacing of 5-day and CALNET recorders along these lines, and the proximity of these recorders to the seismic lines, has permited us to generate a single fold seismic reflection line along these transects for comparison to the stacked marine multichannel reflection data acquired using the moored hydrophones. Plots of the wide-angle data as reflection gathers provide exciting images of the middle and lower crust in the Bay Area.

In addition, we have completed an similar wide-angle investigation conducted in the vicinity of Loma Prieta (Brocher et al., in review; Page and Brocher, in review).

---

[1]The BASIX Working Group includes: R. Anima, J. Childs, P. Hart, and M. Marlow of the Branch of Pacific Marine Geology; R. Clymer, D. Jones, E. Karageorgi, T. McEvilly, and P. Williams of UC Berkeley; T. Brocher, M. Moses and A. Michael of the Branch of Seismology; U. ten Brink of the Branch of Atlantic Marine Geology; S. Holbrook of Woods Hole Oceanographic Institution; S. Klemperer and G. Thompson of Stanford University; and K. Furlong of Pennsylvania State University.

RESULTS

Work to date has provided preliminary velocity and structural models for the Bay Area in the following areas: 1) the crustal block beneath SF Bay between the San Andreas and Hayward faults, 2) the crust beneath the East Bay faults between the San Andreas fault and the Great Valley, and 3) the San Andreas fault and continental shelf and slope offshore San Francisco. Similarly, velocity and structural models have been developed for the vicinity of the Loma Prieta earthquake.

San Francisco and San Pablo Bays

The block bounded by the San Andreas and Hayward faults is structurally high, having only a thin 100-200 m sediment cover, and has velocities less than 6 km/s to about 10 km, as one would expect for the Franciscan assemblage. The Hayward and Rodgers Creek faults bounded a 1.5 km deep basin filled with low velocity (2 km/s) sedimentary rocks. Franciscan rocks are thought to extend to a depth of about 16-18 km based on the analysis of the travel-time moveout of wide-angle reflections (Figure 2).

At a depth of about 16-18 km, San Pablo Bay and the northern end of San Francisco Bay are underlain by a prominent mid-crustal reflector (Figure 3), which in turn is thought to be underlain by a high-velocity (velocity about 7 km/s) mafic layer (Figure 2). This reflection can be identified on several recorders located in this portion of the Bay Area . The identity of the mafic layer is uncertain; it could represent a slab of subducted oceanic crust or a magmatically underplated unit.

The crustal thickness underneath this region is currently uncertain. Near-vertical reflections from both 9 and 11 s two-way travel time suggest that the crust may be either about 27 to 33 km thick. Additional wide-angle data acquired during BASIX must be analyzed to address this issue.

East Bay Faults and Crust

The Green Valley fault is also associated with a vertical offset of about 600 m, with the sense of motion being down to the east. From west to east between the Hayward to the Antioch faults, the top of the Franciscan plunges eastwards beneath younger sedimentary rocks to about 3 km depth (Figure 4). Velocities of the rocks to a depth of about 10 km are constrained by reversed Pg arrivals.

Unreversed Pn arrivals recorded by stations located in the Sierran foothills and eastern Great Valley suggest that the crust thins in the vicinity of the Antioch fault to about 24 km (Figure 4). Alternatively, these data, as well as compilations of previous refraction/reflection experiments by Fuis and Mooney (1990), suggest that the crust thickens towards the Coast Range and towards the Sierras. The crustal thinning occurs in the vicinity of deep seismicity near Antioch, and the depth to the base of seismicity can be traced to nearly the Moho near Antioch.

The San Andreas fault and Continental Shelf and Slope

Velocities in the shallow crust east of the San Andreas are lower than 6 km/s and are consistent with Franciscan rocks. The five-day data provide evidence for a low-velocity zone in the upper crust seaward of the San Andreas fault similar to that observed near Año Nuevo by

Brocher et al. (in review). The five-day recorder data obtained along Line OBS2 will be used by BASIX participants Holbrook and ten Brink to refine velocity models obtained from Ocean Bottom Seismometer recordings of this line.

Velocity Model near the Loma Prieta Epicenter

Wide-angle seismic reflection/refraction data obtained in the vicinity of the epicenter of the 1989 Loma Prieta earthquake provide evidence for a slab of oceanic crust extending from the deep sea floor to the San Andreas fault. During marine seismic reflection profiling of the north-central California margin in May 1990, two onshore recording arrays were deployed transverse to and straddling the San Andreas fault in the Santa Cruz Mountains and Diablo Range (Figure 5). Wide-angle reflections recorded by these arrays define the top and bottom of the oceanic crust as far east as the San Andreas fault. The wide-angle refraction data obtained by the arrays provide evidence that the oceanic crust, apparently connected to and inferred to represent Pacific plate, is overlain by a seaward tapering wedge of rocks having velocities between 6.0 and 6.6 $\pm$ 0.1 km/s (Figure 6). We interpret this wedge as being composed of slivers of San Simeon and Salinian (and perhaps other) rocks. The wide-angle data are consistent with a landward dip on the oceanic crust of between 8^{o} and 11^{o}. The velocity model inferred from these data suggests that the hypocenter of the magnitude 7.1 1989 Loma Prieta earthquake was located near the base of the interpreted wedge of Salinian rocks beneath the continental margin, but above the oceanic crust. On the basis of this geometry we infer that the top of the oceanic crust represents a detachment surface accommodating oceanward movement of North America. This oceanward movement mirrors the east-directed tectonic wedging observed beneath the Diablo Range and western Great Valley. An observed concave-upward geometry of the Moho in the vicinity of the San Andreas fault should strongly focus wide-angle reflections from the Moho which travel along the fault from earthquake sources on or near the fault.

Wide-angle seismic reflection and refraction data, mapped geologic structures, and marine magnetic anomalies provide evidence that oceanic crust underlies the coastal margin of California from Morro Bay northward beyond San Francisco. Page and Brocher (in review) interpret the presence of this oceanic slab to be the result of pseudo-subduction, i.e., underthrusting/ overthrusting of the Pacific and North America plates, during Pliocene-Quaternary time, well after the cessation of true subduction at this margin. Likely causes of this thrusting are the change in plate motions at about 3.5 Ma and extension in the Basin-and-Range Province.

Reports

Brocher, T.M., M. J. Moses, W.S. Holbrook, U.S. ten Brink, and S.L. Klemperer, Wide-angle seismic recordings of BASIX, EOS Trans. AGU, 73, 401, 1992.

Brocher, T. M., M. J. Moses, and S. D. Lewis, Wide-angle seismic recordings obtained during seismic reflection profiling by the S.P. Lee offshore the Loma Prieta epicenter, U. S. Geological Survey Open-file Report 92-245, 63 pp., 40 figs., 1992.

Brocher, T. M., M. J. Moses, and S. D. Lewis, Evidence for oceanic crust beneath the continental margin west of the San Andreas fault based on onshore-offshore wide-angle seismic recordings, U. S. Geological Survey Professional Paper on Loma Prieta, Vol. 1., in review.

Brocher, T.M., M. J. Moses, and J. McCarthy, Onshore-offshore wide-angle seismic recordings of BASIX, U. S. Geological Survey Open-file Report, in preparation.

Holbrook, W. Steven, U. S. ten Brink, and T. M. Brocher, Crustal structure beneath San Francisco Bay from BASIX wide-angle seismic data, EOS Trans. AGU, 73, 404, 1992.
Moses, M. J, and T.M. Brocher, Wide-angle seismic recordings of BASIX: Five-day recorder profiles, EOS Trans. AGU, 73, 404, 1992.
Page, B. M., and Brocher, T. M., Evidence for Pliocene-Quaternary pseudo-subduction, Coastal California, Geology, submitted to the journal for review.

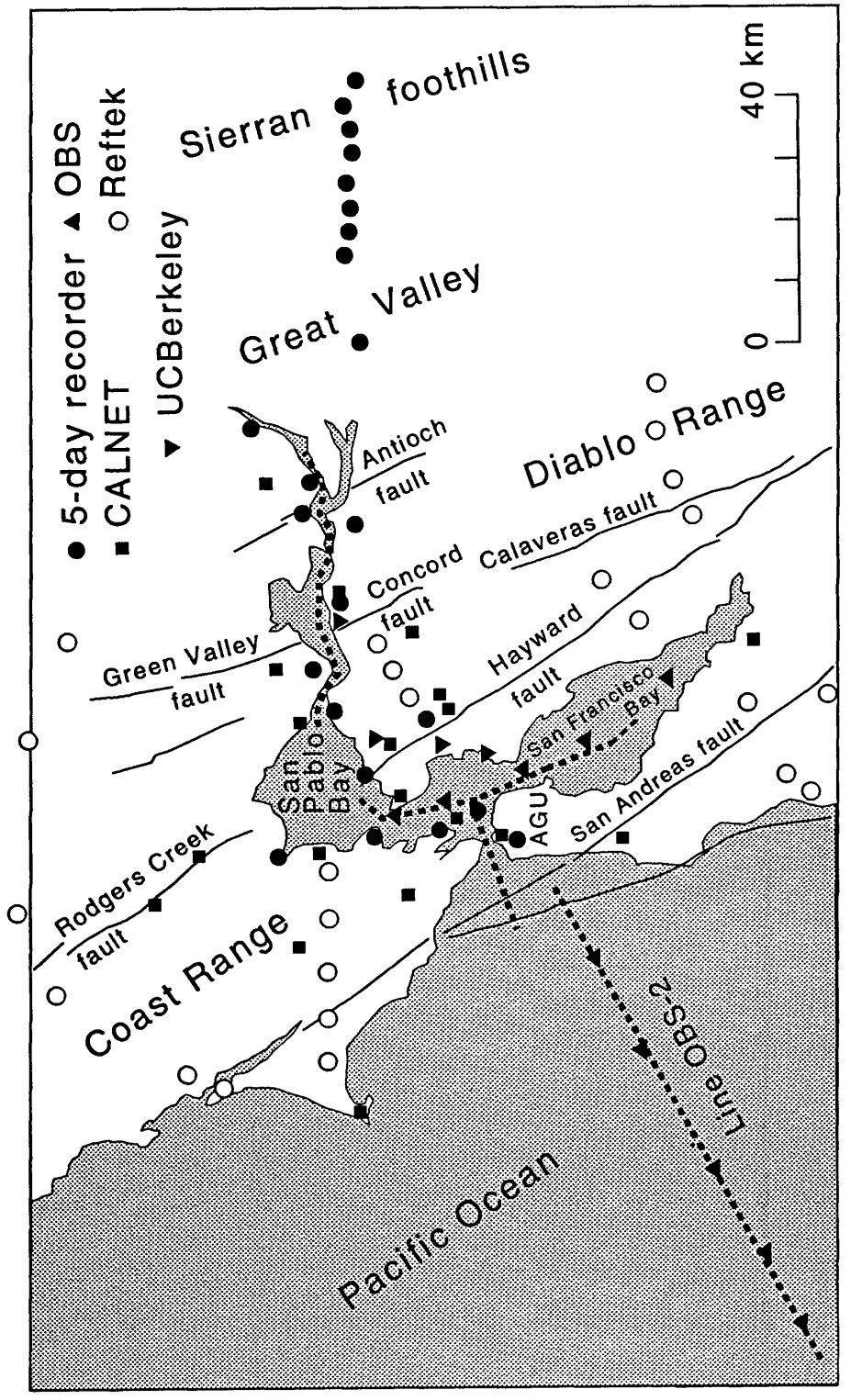

Figure 1. BASIX Seismic Reflection Lines and Wide-angle Recorders.

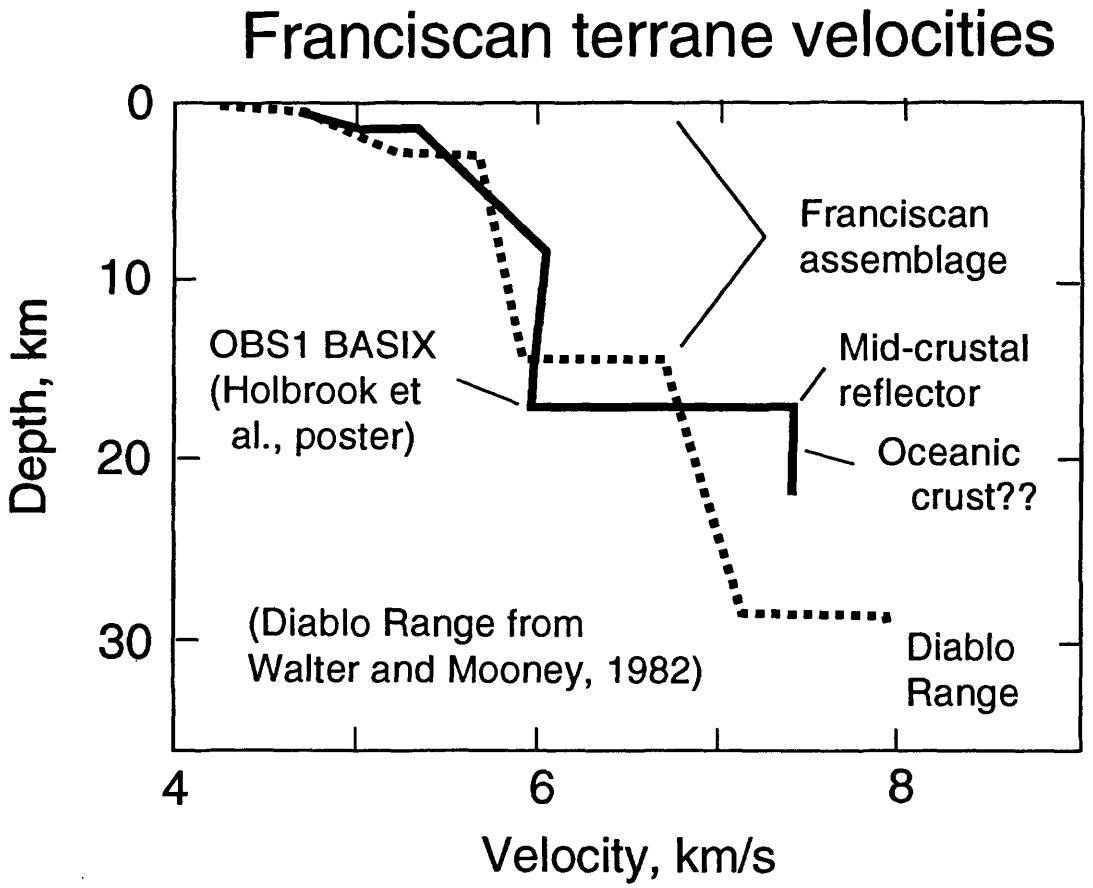

Figure 2. One-dimensional velocity model obtained for N-S line in San Francisco and San Pablo Bays compared to that from a previous strike-line in the Diablo Range (Walter and Mooney, 1982). Note the presence of a high velocity (7 km/s) layer beneath the prominent mid-crustal reflection at 6 s twtt (depth about 16-18 km).

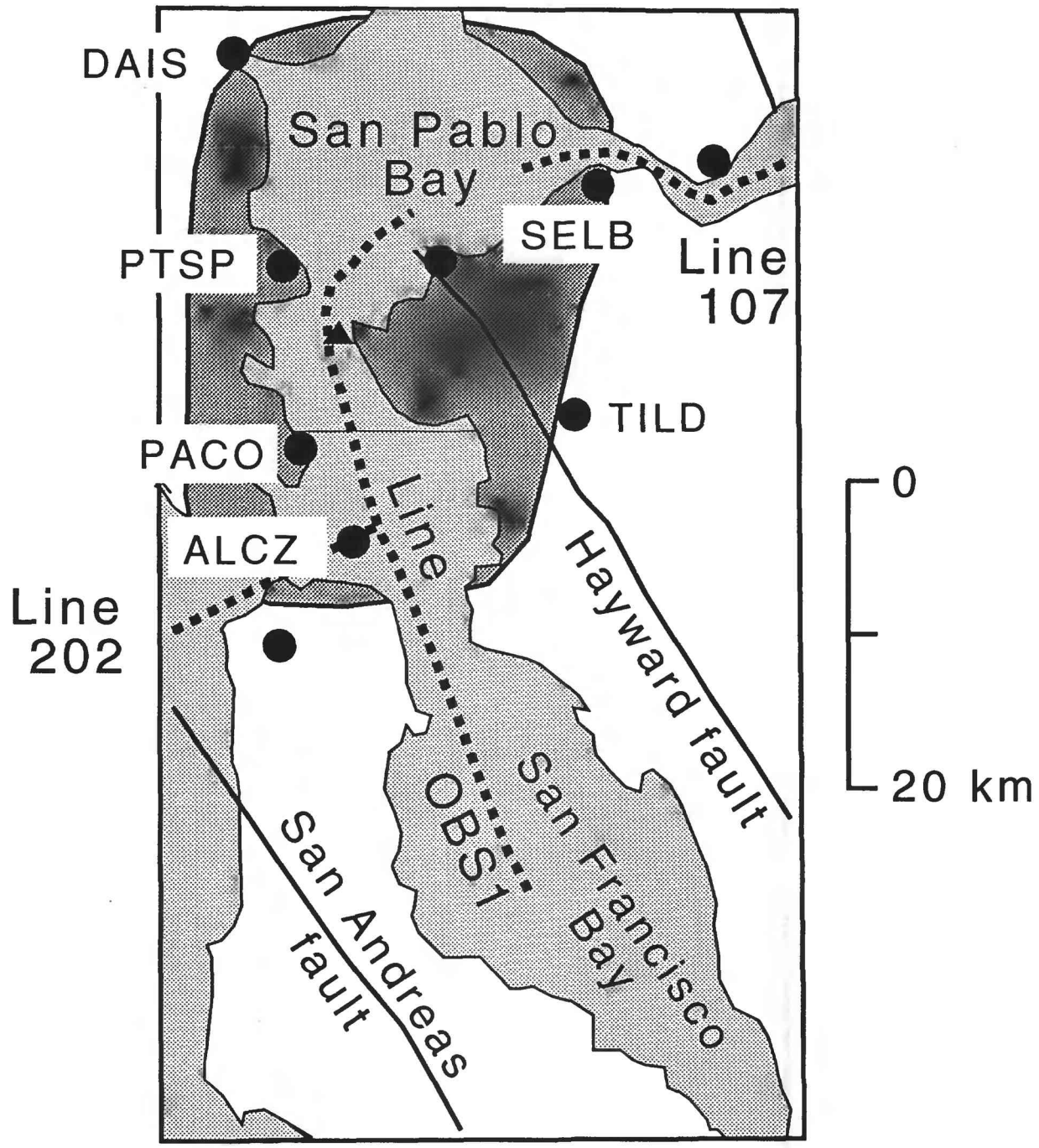

Figure 3. Extent of Mid-crustal Reflector.

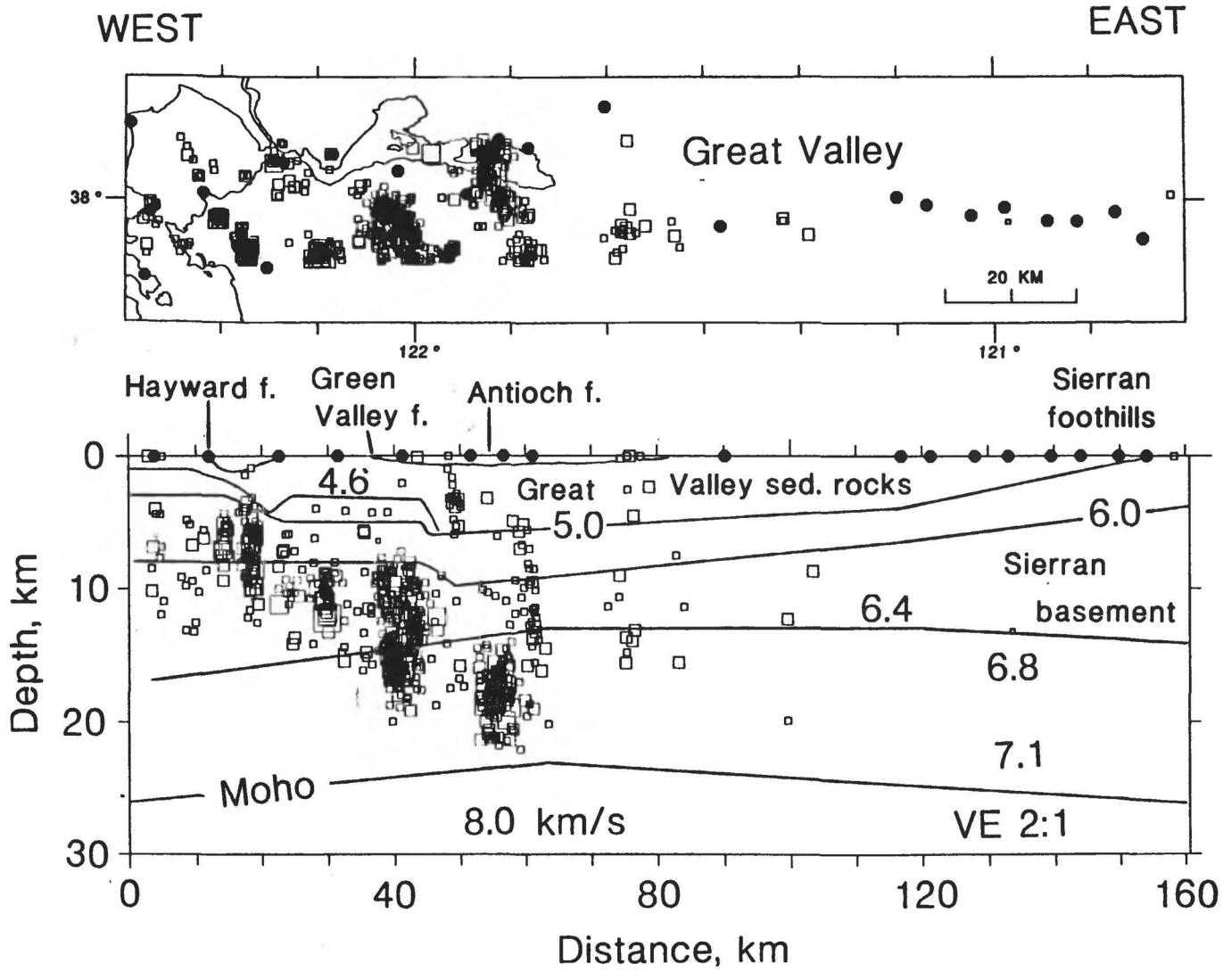
WEST
EAST
Great Valley
38°
20 KM
122°
121°
Hayward f.
Green Valley f.
Antioch f.
Sierran foothills
0
10
20
30
4.6
Great Valley sed. rocks
5.0
6.0
Sierran basement
6.4
6.8
7.1
Moho
8.0 km/s
VE 2:1
Depth, km
0
40
80
120
160
Distance, km

Figure 4.

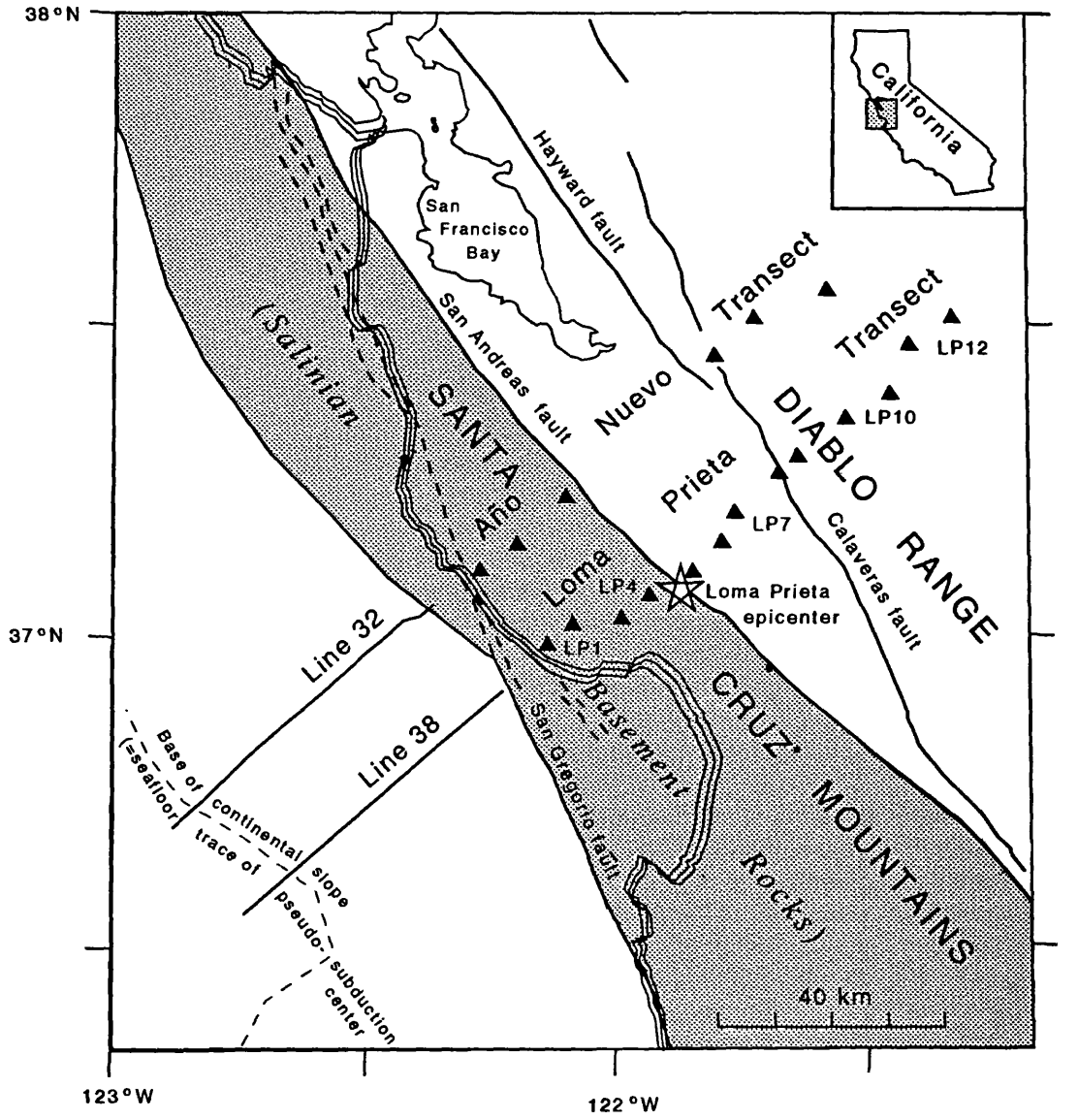

Figure 5. Location map showing seismic lines and recorder locations used for onshore-offshore wide-angle seismic experiment near the epicenter of the Loma Prieta earthquake.

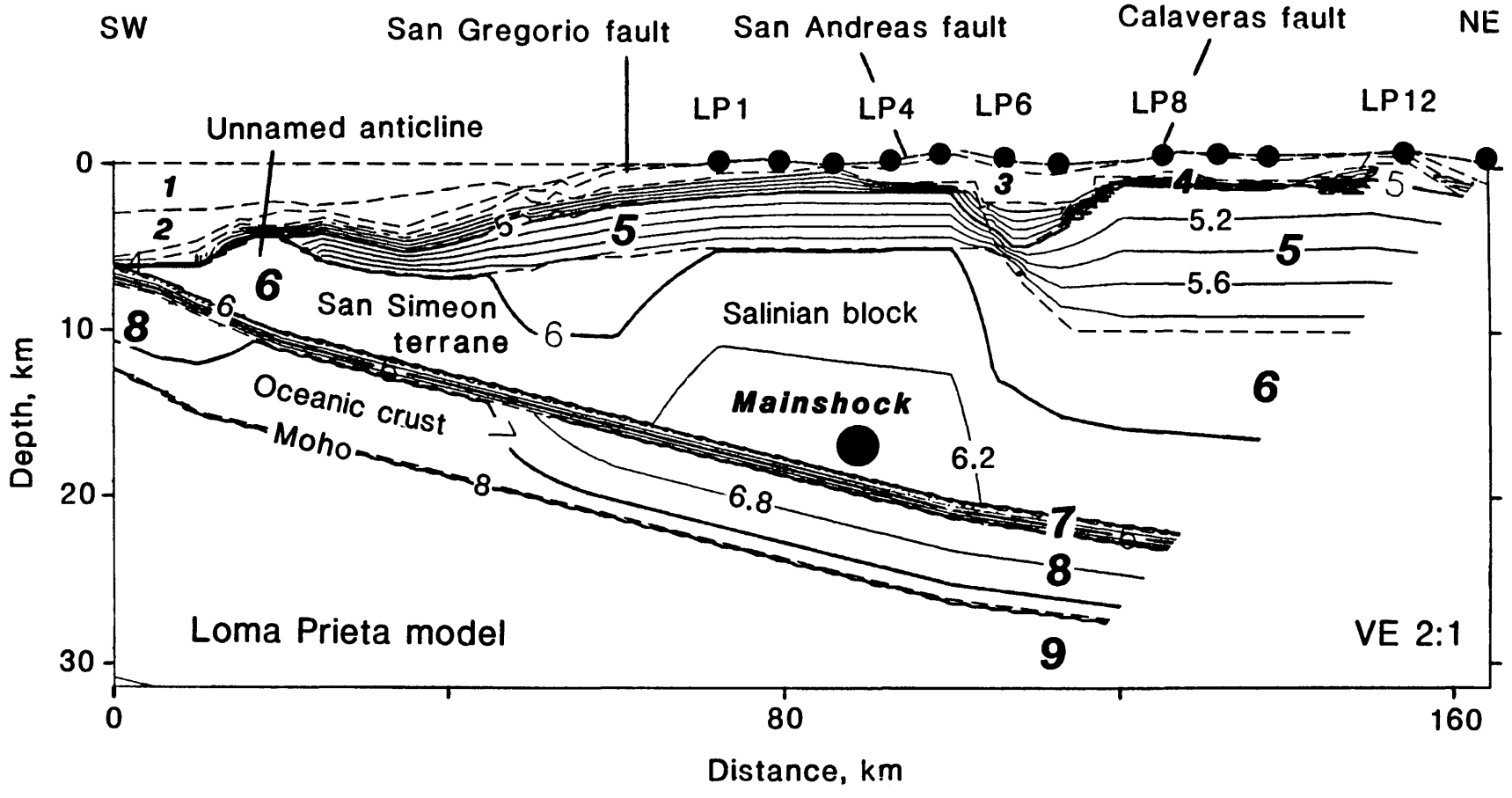
SW
San Gregorio fault
San Andreas fault
Calaveras fault
NE
LP1
LP4
LP6
LP8
LP12
Unnamed anticline
0
10
20
30
Depth, km
1
2
3
4
5
6
8
9
5.2
5.6
6.2
6.8
San Simeon terrane
Salinian block
Mainshock
Oceanic crust
Moho
Loma Prieta model
VE 2:1
0
80
160
Distance, km

Figure 6.

Northern San Andreas Fault System

9910-03831

Robert D. Brown
Branch of Engineering Seismology and Geology
U.S. Geological Survey
345 Middlefield Road, MS 977
Menlo Park, California 94025
(415) 329-5620

Investigations

1. Synthesis studies of the geology, seismology, and tectonics of the San Andreas fault system, especially in northern California.

2. Advisory activities for Bay Area Regional Earthquake Preparedness Project (BAREPP) and San Francisco Bay Conservation and Development Commission (BCDC), both of which are state agencies.

3. Research on applications of earth science-information, reviews of applications work by others, and interpretation of geologic and geophysical results for non-technical audiences.

Results

1. Revised paper, with D. Hill and R. Wallace, on the San Andreas fault system. Originally planned for book publication, the paper has been revised for publication in an issue of Annales Tectonicae that describes the geological character of active fault zones.

2. Late Holocene slope failures adjacent to the San Andreas fault in the Lakes district of Point Reyes National Seashore appear to document systematic tilting--up to the southeast--on a thrust fault that converges with the San Andreas fault north of Bolinas. Landslide blocks and other rocks above the fault plane exhibit structural complexities and compressed northwest-striking folds that contrast with relatively uniform, low, northwest dips beneath the fault. Relict ledges and patches of cemented iron-stained gravel that are attached to both bedrock and slide deposits at about 1 m above the present shoreline angle also suggest recent

uplift. G. K. Gilbert recorded evidence of vertical deformation near Bolinas and reactivation of some Lake district tension fractures immediately after the 1906 earthquake, but he observed no major reactivation of the landslides. The landforms and shoreline deposits predate the 1906 earthquake; one landslide is dated at about 3300 yr B. P. (Roger Byrne, personal communication, 4 March, 1992) and most of the other slides appear to be at least as recent. Evidence of coastal uplift along the San Andreas fault also occurs to the south along the San Francisco Peninsula and, of course, near the Loma Prieta earthquake of 1989. Thus, some earthquakes in this region may depart from the simple strike-slip model that is generally assumed. Any substantial component of vertical slip on this or other bay region faults introduces new and significant hazards during large earthquakes.

3. Continued to participate in activities of BAREPP and BCDC, but meetings of BCDC's Engineering Review Board were curtailed early in the year because of budgetary and staff shortages. Testified regarding USGS findings regarding Diablo Canyon Long Term Seismic Program at California State Senate hearings on nuclear power plants. Served as associate editor for Earthquakes and Volcanoes.

Reports

1. Brown, Robert D., 1991, Testimony *at* Hearing by California Senate Committee on Energy and Public Utilities regarding: California's Nuclear Power Plants: Their Safety, Environmental Impacts and Economic Costs, p. 75-81 and appendix.

11/92

PUGET SOUND PALEOSEISMICITY

9950-10175

Robert C. Bucknam
U.S. Geological Survey
M.S. 966, Box 25046
Denver, Colorado 80225
(303)273-8566

INVESTIGATIONS:

The primary objective of this project is to document and characterize Holocene deformation in the Puget Sound, Washington, region and develop an understanding of its structural and tectonic origins.

Work during the reporting period focused on an area of late Holocene uplift in central and southwest Puget Sound that has been inferred to have been the site of a large earthquake about 1000 years ago (Fig. 1). Paleontological analyses of diatoms from a core at Winslow collected in August 1991 were done by Eileen Hemphill-Haley, U.S. Geological Survey, Menlo Park, California. Analyses of plant macrofossils from the core were done by Estella Leopold and Daniel Ekblaw at the University of Washington. About 5 m of core was collected from another raised marsh at Restoration Point on Bainbridge Island, west of Seattle, in August 1992 for detailed paleoecological and radiocarbon age studies. Previous studies have shown that the section, which includes Mazama ash, was deposited during about the past 8,000 years. The long record offers an opportunity to study the history of relative sea level at the site and thus provides a means of determining if other large uplift events have occurred at the site in the past few thousand years.

Fieldwork at uplift sites in southwest Puget Sound in 1992 has provided additional constraints on the amount of uplift in that area.

RESULTS:

1. *Paleoecology of the Winslow marsh*

Two continuous 7.5 cm-diameter, 3-meter-long cores were collected in plastic pipe from a small coastal salt marsh near Winslow in August 1991. Previous work had shown that the marsh was present when about 7 meters of uplift occurred at Restoration Point, 5 km to the south, probably 1000 to 1100 years ago. Because of its proximity to the uplift area and to an inferred fault that crosses Puget Sound at Seattle, the site is a key to interpreting possible fault slip. Preliminary analysis of the core this year shows that organic mud at the Winslow marsh was deposited 1600 to 2100 years ago and contains diatoms characteristic of freshwater ponds. Gyttja overlying the mud was deposited 1400 to 1700 years ago and contains diatoms characteristic of fresh or slightly brackish water as well as seeds and fragments of freshwater plants. Several lenses of sand within the gyttja contain abundant foraminifera, including a high salt marsh species, suggesting that the site was at or near the level of high tide but probably isolated from Puget Sound by a storm bar. Peat deposited 700 to 900 years ago, after the uplift at Restoration Point, contains leaf bases and rhizomes of salt marsh plants showing that relative sea level rose at the Winslow marsh, probably as a result of subsidence during the time period of the nearby uplift at Restoration Point. The change from gyttja to overlying peat is marked by an abrupt contact. Additional detailed study of the section is underway to further characterize the timing and amount of possible subsidence at the Winslow marsh.

2. *Amount of uplift in southwest Puget Sound*

Relief on the surface of an uplifted tidal flat at Lynch Cove (Fig. 1) and the vertical range of shells that lived on the tidal flat shows that uplift there 1,000 to 1,500 years ago was greater than 2 m and less than 4 m. The former tidal flat surface slopes gently toward the central part of the cove. Plant fossils in freshwater peat that overlies the former tidal flat shows that before uplift, the highest point on the former tidal flat was below high tide, and after uplift the lowest point on that surface was above high tide. The relief between these two points, 2 m, is a minimum measure of the amount of uplift at the site. A shell-rich layer in the mud that underlies the former tidal flat contains abundant articulated remains of the Olympic oyster (Ostrea lurida). They commonly live between mean tide and low tide and are uncommon subtidally. The vertical range of their shells in the raised tidal flat mud at Lynch Cove limits the maximum amount of uplift to 4 m.

REPORTS PUBLISHED:

Bucknam, R.C., Hemphill-Haley, E., and Leopold, E.B., 1992, Abrupt uplift within the past 1700 years at southern Puget Sound, Washington: *Science*, in press.

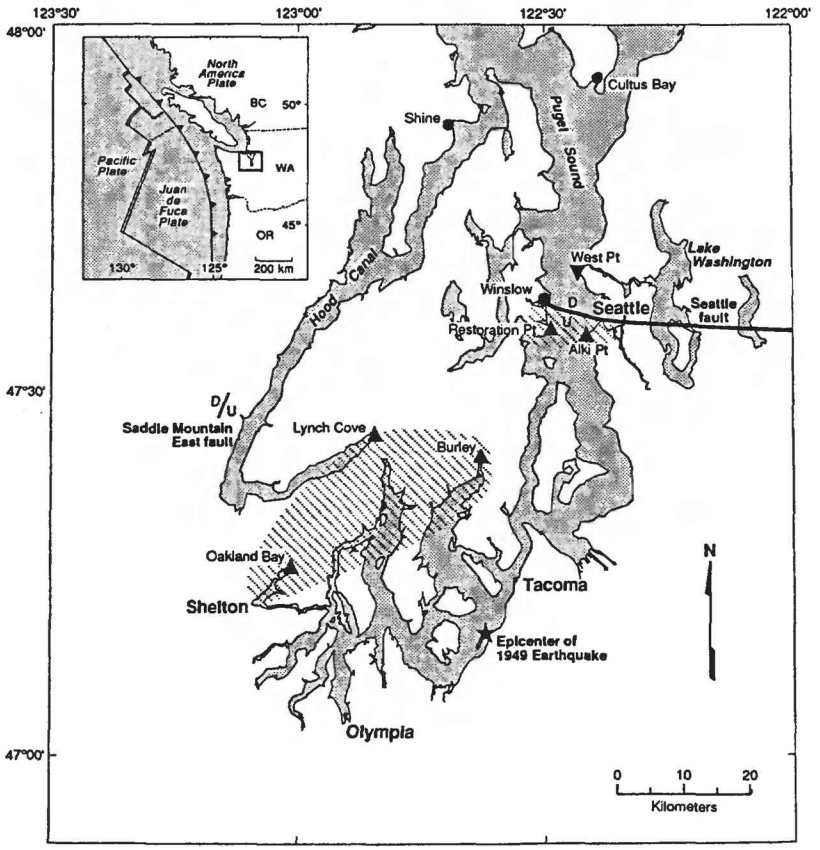

Figure 1. Diagonal ruling shows approximate minimum extent of late Holocene uplift in central and southwest Puget Sound. Sites with stratigraphic or geomorphic evidence of uplift shown by upward pointing triangles. Site with evidence of subsidence of 1 m or more shown by downward pointing triangle (After Atwater and Moore, *Science*, 1992). Stable sites (Cultus Bay; Atwater and Moore, Science, 1992; Shine; Eronen and others, Quaternary Research, v. 27) or sites with less than about 1 m subsidence shown by solid circles.

Global Seismograph Network

9920-10162

Howell M. Butler
Branch of Global Seismology and Geomagnetism
U.S. Geological Survey
Building 10002, Kirtland AFB-East
Albuquerque, New Mexico 87115-5000
(505) 846-5646

Investigations

The Global Seismograph Network (GSN) presently consists of the Global Digital Seismic Network (GDSN) 10 stations; the China Digital Seismic Network (CDSN) 10 stations; the Incorporated Research Institutions for Seismology Network (IRIS/GSN) 21 stations and the Worldwide Standardized Seismograph Network (WWSSN) 66 stations. Support is furnished at a level needed to keep the GSN at the highest percentage of operational time in order to provide the improved geographical coverage with analog and digital data from highly sensitive short-period and very broadband seismic sensor seismograph systems. This support includes provision of operational supplies, replacement parts, repair services, modifications, on-site system installation, maintenance, training and system calibration.

Results

The GSN continues with a combined total of 107 WWSSN/SRO/ASRO/DWWSSN/ CDSN/IRIS-1/IRIS-2 stations. Global seismic data coverage is provided to the National Earthquake Information Center (NEIC) and to other data centers and research organizations throughout the world.

IRIS-2 seismograph systems were installed at eight location: Narrogin, Australia (NWAO); South Pole, Antarctica (SPA); Rarotonga, Cook Islands (RAR); South Karori, New Zealand (SNZO); Yuzhno Sakhalinsk, Russia (YSS); Chiang Mai, Thailand (CHTO); Taipei, Taiwan (TATO); and Ankara, Turkey (ANTO).

On-site maintenance visits were required at the following locations: Albuquerque, New Mexico (ANMO); Guam, Mariana Islands (GUMO); College, Alaska (COL); Garni, Armenia (GNI); Toledo, Spain (TOL); and Grafenberg, Germany (GRFO).

Site surveys were performed at the following locations: Caico, Brazil (CAI); New Delhi, India (NDI); Kodaikonal, India (KOD); Magadan, Russia (MAG); Yakutsk, Russia (YAK); and Petropavlovsk, Komchalskiy (PET).

Aseismic Creep and Crustal Deformation of Large Normal Faults: Implications from the Teton Fault

USGS Grant #14-08-0001-G1970

John O.D. Byrd and
Robert B. Smith, Principal Investigator
Department of Geology and Geophysics
University of Utah
Salt Lake City, Utah 84112
gg-rbs@mines.utah.edu
(801) 581-7129

Investigations Undertaken: October 1, 1991-September 31, 1992

1. Analysis and boundary element modeling of 1st order leveling-line reobservations across the central portion of the Teton fault, collected in 1988, 1989, and 1991 (in a cooperative project with Dr. Arthur Sylvester of the University of California, Santa Barbara)

2. Reduction and two-dimensional modeling of detailed gravity profiles, in conjunction with construction and inversion of two-dimensional ray-tracing models of seismic refraction data across the hanging wall of the Teton fault to assess subsurface fault and hanging wall basin geometry.

Introduction

This study focuses on the mechanics of large normal faults and their seismogenic behavior as manifested by the Teton fault, Wyoming. The Teton fault is characterized by a generally continuous 55 km long series of Quaternary scarps, 3 m to 52 m in height, that offset post-glacial (~14,000 year) and younger deposits at base of the precipitous east side of the Teton Range (Figure 1). The Teton region is surrounded by zones of active seismicity including the historic scarp-forming 1959 M_S =7.5 Hebgen Lake, Montana, earthquake, and other zones of extensive Quaternary faulting. On the basis of fault segment lengths the Teton fault is considered a major seismogenic structure that has been assigned a maximum credible earthquake of M_S = 7.5. In addition, Quaternary deformation of the Teton fault

hanging-wall associated with prehistoric earthquakes on the fault appears to be expressed as asymmetric stratal tilt of the surface topography and Quaternary volcanic layers. We also note that the Teton fault coincides with one of the longest continuous zones of seismic quiescence within the Intermountain Seismic Belt. Information from our age-dating of the southern segment of the Teton fault suggests that it is overdue or "on schedule" for a major scarp-forming earthquake.

Results Obtained

Leveling Results:

The results of the three tectonic 1st-order surveys (Figure 1) in 1988, 1989, and 1991 have been discussed by Sylvester elsewhere in this volume and are only briefly summarized here. Arbitrarily fixing the west end, GT42, of the level line, the observed height changes (corrected for refraction errors by the National Geodetic Survey) between the 1988 and 1989 surveys indicate an anomalous 8 ± 0.7 mm of hanging wall uplift relative to the footwall block of the Teton normal fault (Sylvester and others, 1991). Comparison of the 1991 and 1988 surveys indicates this anomalous uplift persisted during the 1989-1991 two year interval, however, the maximum amplitude of the uplift decreased to 4 ± 0.7 mm (Figure 1a). The three surveys were conducted during a period of seismic quiesence at the M 3+ level, on the Teton fault, implying the observed deformation profiles are the result of aseismic or nontectonic mechanisms.

Comparison of the 1989 and 1991 survey results (Figure 1b) suggest subsidence of the hanging wall (the valley of Jackson Hole) was hinged at the Teton fault. The composite short wavelength-high amplitude, 5 km and 8 mm, component of the deformation signal centered around the Teton fault trace may be the result of near surface fault creep, or possibly differential subsidence of the hanging wall strata adjacent to the fault. However, the relatively long wavelength, 10 km, subsidence pattern of the hanging wall suggests large-scale aseismic creep may have occurred on the fault at depths up to 12 km.

Modeling Procedure:

In order to evaluate the nature of the observed 1989 to 1991 deformation profile, we have constructed a series of boundary element models followed the modeling procedure of King and others (1988) and King and Ellis (1991). The models invoke a stress-free elastic layer,

brittle layer, overrlying an inviscid fluid, plastic layer, where the elastic layer, region 1, is defined by two horizontal surfaces corresponding to a horizontal datum at the earth's surface, x_1=0 km, and a discrete lower boundary, x_1=12,15,18, or 20 km, representing the brittle-plastic transition. This elastic-layer is 'tethered' in the manner following King and Ellis (1991) where the horizontal displacement, u_3, and shear stress, σ_{13}, are set to zero along the vertical interface at x_3 = -60 km. Across the vertical boundary at x_3 = 48 km the shear and normal stresses, σ_{13} and σ_{33}, are set to zero. The block length is such that the boundary conditions at these boundaries do not affect the deformation imposed by faulting in the central portion of the block in the area of x_3 = 0 km.

A series of fault geometries, 30° to 75° E dips, and depths, 12 to 20 km, to the brittle-plastic transition were tested in the context of a simplified model of the footwall and hanging wall blocks determined from the ray-tracing and gravity modeling of the Teton fault and Jackson Hole. In each model run the fault -"ground surface" intersection, and hanging wall geometry were fixed. Variations in the fault dip and depth to the brittle-plastic transition resulted in changes in the vertical and horizontal stresses and displacement across the plane of the model. The variations in stress were discretized by dividing the hanging wall portion of the block model into a series of five vertical geometrically defined zones based on the hanging wall cut-off of the Tertiary strata at the fault, and the relationship of the deepest portion of the basin to the fault plane brittle-plastic transition intersection.

Modeling Results

The boundary element modeling results suggest the observed 1989 to 1991 height changes may be due to a combination of 3.5 cm and 5.0 cm of creep across a 60° E dipping planar normal fault zone at depths of 0.5 to 2 km, and 10 to 12 km, respectively (Figure 2a). The narrow wavelength and relatively large amplitude of the hanging wall subsidence adjacent to the fault restricts shallow slip to the upper 2 km. However, the average 4 mm subsidence of the hanging wall block at distances 10 km from the fault trace suggest this portion of the deformation signal is contributed by deep seated slip on the fault. Unfortunately, the short length of the level line relative to the wavelength of deformation associated with creep at depth on the fault it is very difficult to evaluate the possible contribution, or existence of this deeper seated signal.

Papers and Reports Published

Byrd, J.O.D. and R.B. Smith, 1991, Paleoseismicity, near-surface fault geometry, and segmentation of the Teton fault, Wyoming, (abs), Eos Trans. Amer. Geophys. Union, 72, 316.

Byrd, J. O. D., 1991, Paleoseismicity of the Southern Section of the Teton Fault, Wyoming, 1991 Abs. with Prog., 1991 Annual Meeting, Geol.Soc.Amer., 23, 5.

Meertens, C. M. and R. B. Smith, 1991, Crustal deformation of the Yellowstone caldera from first GPS measurements: 1987-1989, Geophys.. Res. Lett., 18, 1763-1766.

Sylvester, A.G., J.O.D. Byrd and R.B. Smith, 1991, Geodetic evidence for aseismic reverse creep across the Teton fault, Teton Range, Wyoming, Geop. Res.Lett, 18, 6, 1083-1086.

Smith, R. B. and W. J. Arabasz, 1991, Seismicity of the Intermountain Seismic Belt, in Seismicity of North America, editor E.R. Engdahl, Decade of North American Geology, Bull. Geol. Soc.Am. (in press).

Smith, R.B., J.O.D. Byrd, and D.D. Susong, 1993, Quaternary History, Neotectonics, and Earthquake Hazards of the Teton Fault, Wyoming, submitted to "The Geology of Wyoming", A. Snoke and J. Steidtmann *eds*, published by Wyoming Geological Association, in press.

Smith, R.B., K.L. Pierce, and R. J. Wold, 1993, Seismic Surveys and Quaternary History of Jackson Lake, Wyoming, submitted to "The Geology of Wyoming", A. Snoke and J. Steidtmann *eds*, published by Wyoming Geological Association, in press.

Figure 1A.

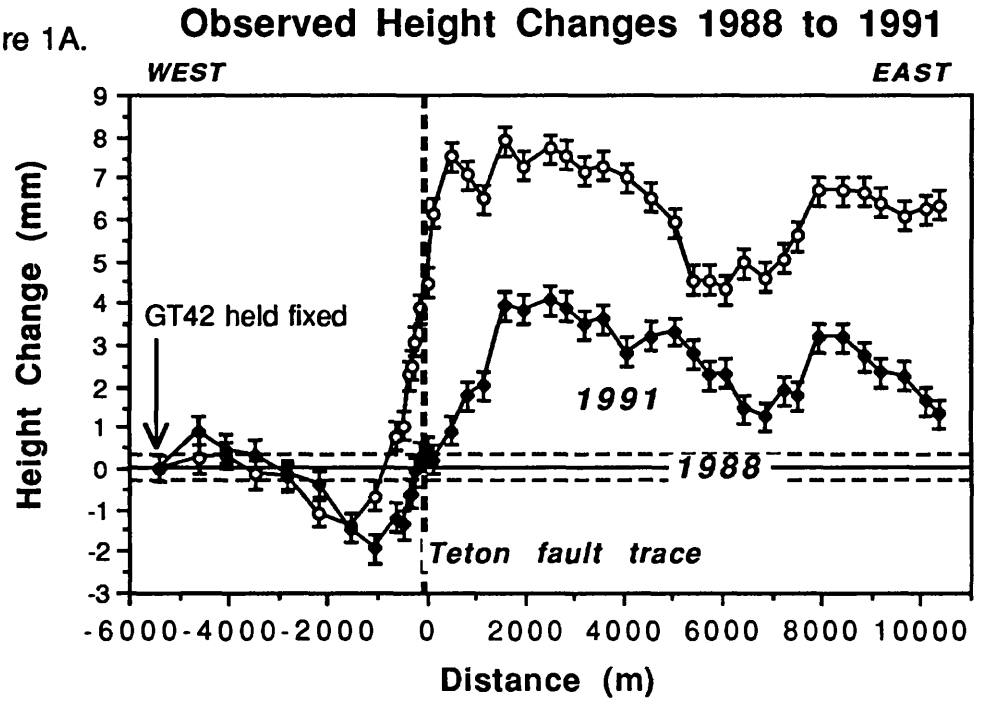

Figure 1B

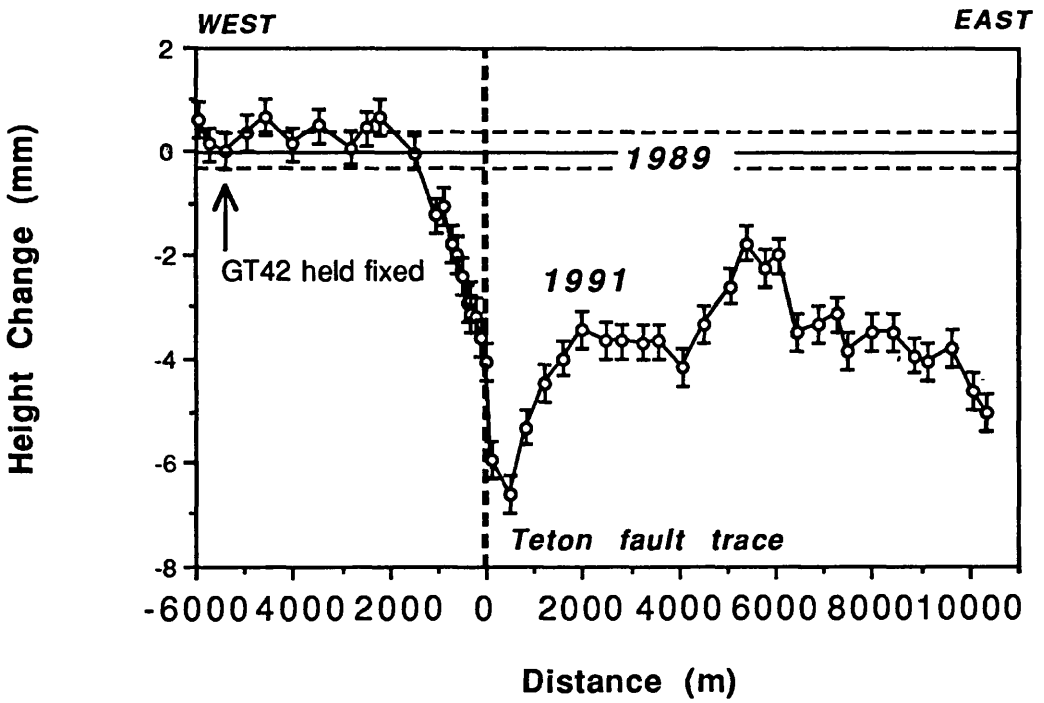

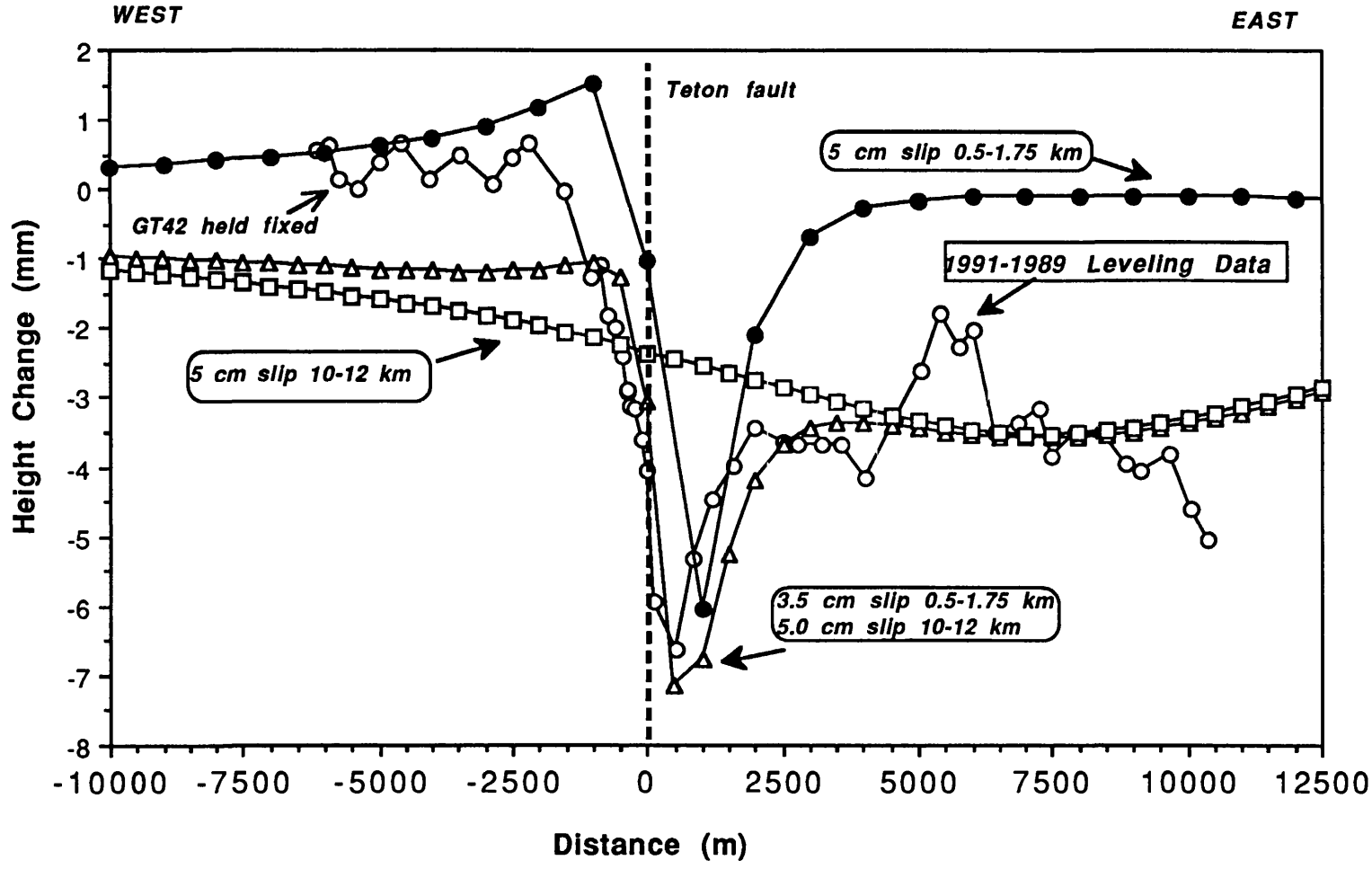
Surface Displacement 60° dip and 12 km bp
WEST
EAST
Teton fault
5 cm slip 0.5-1.75 km
GT42 held fixed
1991-1989 Leveling Data
5 cm slip 10-12 km
3.5 cm slip 0.5-1.75 km
5.0 cm slip 10-12 km
Height Change (mm)
Distance (m)
2
1
0
-1
-2
-3
-4
-5
-6
-7
-8
-10000
-7500
-5000
-2500
0
2500
5000
7500
10000
12500

Figure 2

SEISMIC REFRACTION/REFLECTION INVESTIGATIONS IN THE S. F. BAY AREA AND THE CENTRAL U. S.

Project Number: *1-9930-02102*
Investigator: *R. D. Catchings*
Institution: *U.S. Geological Survey, OEVE*
345 Middlefield Rd., MS 977
Menlo Park, CA 94025
FTS 459-4749; (415) 329-4749

Investigations Undertaken

In October and November of 1991, we acquired a 400-km-long seismic line between the cities of Memphis and St. Louis in order to look at long-range attenuation and strong ground motion in the Central U. S. These data are still being analyzed and are being compared with similar data from the Loma Prieta, CA area in order to estimate the effects of a M. 7.1 earthquake in the New Madrid region.

Investigations of strong ground motion and crustal structure of the San Francisco Bay area, as shown by active seismic experiments in May, 1991, continues . Specifically, we are examining the effect of crustal structure in influencing strong ground motion and attenuation during large earthquakes. In addition to the Loma Prieta earthquake, several other earthquakes are being examined, including the 1985 Mexico City earthquake.

Results Obtained

Data from the October/November 1991 Central U. S. experiment have been processed and plotted into seismic record sections. We have begun velocity analysis to determine the gross structure of the crust and the configuration of the Moho between Memphis and St. Louis. We have also calculated the ground motion from the shots to examine areas with unusually high amplitude variations. Those data have been directly compared with the type of data from the Loma Prieta area. We find that the ground motion resulting from a shot located near New Madrid, Missouri produces very strong amplitude seismic waves near the cities of Memphis and St. Louis. These amplitudes are significantly higher than those observed for shots in the Loma Prieta area. Thus, our data suggest that the cities of Memphis and St. Louis should should expect much more severe shaking from a M 7.1 New Madrid earthquake than San Francisco experienced during the 1989 Loma Prieta earthquake.

From the May 1991 San Francisco Bay area experiment, we have found very strong evidence that much of the damage from the 1989 Loma Prieta earthquake resulted from reflected energy from crustal interfaces and the Moho. The correlation between the geographical areas with high amplitudes from our seismic survey and those areas that experienced significant damage during the 1989 earthquake is striking. We have also correlated the wave propagation paths from the 1985 Mexico City earthquake and found strong evidence that reflected seismic energy was a major factor in the loss of 8000

lives and 4 billion dollars damage. A similar crustal configuration exists in the Pacific Northwest U. S., with implications for the safety of a large complex of Nuclear facilities.

Reports Published

(1) Catchings, R. D. and W. M. Kohler, (in press), Reflected Seismic Waves Damage Far from Earthquake Epicenters: An Example from the 1989 Loma Prieta Earthquake (in review, submitted to Science)

(2) W. M. Kohler, R. D. Catchings, and G. S. Fuis, (in press), Crustal Structure of the San Francisco Peninsula, (in review, submitted to*Bull. Seis. Soc. Am.*

(3) R. D. Catchings and W. D. Mooney, New Madrid and Central California Apparent Q from Seismic Refraction Data, *Seis. Res. Lett.*, **63**, 49 (1992)

(4) R. D. Catchings, W. M. Kohler, and G. S. Fuis, Influence of Crustal Structure on the 1989 Loma Prieta Earthquake and Associated Destruction, EOS Trans AGU, 1991

(5-7) Three abstracts in the 1992 AGU EOS. Several Abstracts to Eastern Meetings.

INSTRUMENTATION OF STRUCTURES

9910-04099

MEHMET ÇELEBI
BRANCH OF ENGINEERING SEISMOLOGY AND GEOLOGY
U.S. GEOLOGICAL SURVEY
345 MIDDLEFIELD ROAD, MS 977
MENLO PARK, CALIFORNIA 94025
415/329-5623

Investigations

1. The process of selection of structures to recommended for strong-motion instrumentation has continued in Hawaii, Puget Sound (Seattle), Reno (Nevada), and Puerto Rico.

2. The Veterans Hospital in Palo Alto, California, has been instrumented as a joint effort between VA and USGS.

3. Instrumentation at 575 Market Street, in San Francisco, California, has also been upgraded.

4. Agreements have been made with UCLA to convert the wind-monitoring system in the Theme Building in Los Angeles (previously financed by NSF) into a strong-motion monitoring system. Plans are being made to implement the conversion, whenever funds are available.

5. Studies of records obtained from instrumented structures are carried out. In particular, the records obtained during the October 21, 1987 Whittier Narrows earthquake from 1100 Wilshire Finance Building (Los Angeles), the Bechtel Building (Norwalk), and the Santa Ana River Bridge (base-isolated) are being investigated.

6. Studies of records obtained from instrumented structures during the October 17, 1989, Loma Prieta earthquake are carried out. In particular, Transamerica Building in San Francisco and Pacific Park Plaza in Emeryville have been investigated. Data from Embarcadero Building (San Francisco) has been studied. Papers are prepared.

7. Cooperative project with NIST on low-level amplitude tests of instrumented structures carried out and report and papers are prepared.

8. The instrumentation of building in Seattle completed.

9. Cooperative instrumentation of building in Olympia, Washington, in progress.

Results

1. The Hawaii Committee on strong-motion instrumentation of structures has completed its deliberations and a draft report is being prepared.

2. As final report of the Puget Sound (Seattle) advisory committee for strong-motion instrumentation has been completed.

3. Papers resulting from study of records obtained from structures are prepared.

4. Invited talks given at conferences and/or other gatherings.

Reports

Çelebi, M., and Şafak, E., 1991, Recorded seismic response of Pacific Park Plaza—Part I: Data and preliminary analysis: ASCE, July 1992.

Şafak, E., and Çelebi, M., 1991, Recorded seismic response of Pacific park Plaza—Part II: System identification: ASCE, June 1992.

Çelebi, M., Phan, L.T., and Marshall, R.D., 1992 Dynamic characteristics of five buildings determined from their response to the 10/17/1989 Loma Prieta (California) earthquake and low-level amplitude tests: in review, ASCE, 1992.

Çelebi, M., 1992, Coherency of free-field motions near a structure—a case study: (invited paper) ASCE Structures Congress, San Antonio, Texas, April, 1992.

Marshall, R.D., Phan, L.T., and Çelebi, M., 1990, Measurement of structural response characteristics of full-scale buildings: comparison of results from strong-motion and ambient vibration records: USGS Open-File Report 90-667 (also NISTIR 4884).

Çelebi, M., Lysmer, J., and Luco, E., 1992, Recommendations for a soil-structure interaction experiment: USGS Open-File Report 92-295, April 1992.

Çelebi, M., 1992, Earthquake response of an eccentrically braced tall building: Accepted by ASCE, Journal of Structural Division.

A Collaborative Research: Analysis of PANDA Data and Continuation of PANDA Experiment in the Central New Madrid Seismic Zone

#14-08-0001-G2143

Jer-Ming Chiu and Arch C. Johnston
Memphis State University
Center for Earthquake Research and Information
Memphis, TN 38152
901-678-2007

Robert B. Herrmann
Department of Earth and Atmospheric Sciences
Saint Louis University
3507 Laclede
St. Louis, MO 63103
314-658-3131

Investigations

Field work of the PANDA experiment in the central New Madrid seismic zone has been completed by the end of August 1992. More than 850 earthquakes with magnitude ranging from -2.0 to 4.6 were on-scale recorded by PANDA during the three years of field work. Prelminary analyses of portions of three-component high-resolution PANDA data have already produced significant new results that are impossible from any previous experiment in the region.

Results

Principal results obtained from preliminary analysis of PANDA data during field work period include:

(a) the identification of P to S and S to P converted waves from the bottom of the sedimentary basin from all three-component seismograms which enable a reliable imaging of 3-dimensional geometry of the sedimentary basin in the upper Mississippi basin.

(b) results of layered crustal structure inversion support a low velocity zone with Vp=4.83 km/sec at depth 2.5 to 5 km. Vp/Vs ratio inside this low velocity zone as determined from independent Vp and Vs inversion is 1.51 which may be due to the presence of fluid- or vapor-filled cracks and/or pores, probably under elevated pore fluid pressures. A large amplitude downward motion arrivals can be identified from the USGS explosions which provide a direct evidence of the existence of a low velocity zone at this depth.

(c) well-determined crustal velocity model for both P and S waves and unambiguous identifications of both P and S arrivals from all PANDA three-component seismograms allow reliable determination of earthquake hypocenters. The new data provides, for the first time, a clear 3-dimensional image of the active fault zones in the NMSZ (Figure 1). Our preliminary results corroborate the vertical (strike-slip) faulting of the southwest (axial), north-northeast, and western arms of the NMSZ and define two new dipping planes in the central NMSZ. The seismicity of the left-step zone between the NE-trending vertical segments is concentrated about a plane that dips at $\sim 31°$ SW; a separate zone to the SE of the axial zone defines a plane that dips at $\sim 48°$ SW. When these dipping planes are projected up dip, they intersect the surface along the eastern boundary of the Lake County Uplift (LCU) and the western portion of Reelfoot Lake. If these SW-dipping planes are thrust faults, then the LCU would be on the upthrown hanging wall and Reelfoot on the downthrown footwall.

(d) spectrum differences between the direct S and the converted P waves from the bottom of the sedimentary basin allow the determination of attenuation characteristics of seismic waves inside the sedimentary basin. These parameters (Vp, Vs, Qp, and Qs) will allow a reliable estimation of seismic response of the basin and what maximum

ground motion should be expected on the surface from active fault zones of known geometry beneath the sediments.

Papers Published and/or in Press

Imaging the active faults of the central New Madrid seismic zone using PANDA array data, in press (December 1992 issue), *Seismol. Res. Lett.*, J.M. Chiu, A.C. Johnston, and Y.T. Yang.

Papers in Review

Shear-wave splitting from microearthquakes in the New Madrid seismic zone, in press to be published in a special issue of Crustal Anisotropy, *Can. J. Expl. Geophys.*, H. Rowlands, D.C. Booth, and J.M. Chiu.

Crustal velocity structure studies in the New Madrid seismic zone from USGS explosion data recorded by the PANDA seismic array, submitted December 1992 to *Seismol. Res. Lett.*, Z.S. Liaw, J.M. Chiu, and A.C. Johnston.

Crustal velocity structures in the central New Madrid seismic zone using velocity inversion method and data collected by the PANDA array, submitted December 1992 to *Seismol. Res. Lett.*, Y.T. Yang, J.M. Chiu, and A.C. Johnston.

3-dimensional configuration of the sedimentary basin in the upper Mississippi embayment using S-to-P conversions, submitted December 1992 to *Bull. Seismol. Soc. AM.*, K.C. Chen, J.M. Chiu and A.C. Johnston.

$Q_p - Q_s$ relations in the sedimentary basin of the upper Mississippi embayment from the spectra ratio between the direct and the converted waves, submitted December 1992 to *Bull. Seismol. Soc. Am.*, K.C. Chen, J.M. Chiu, and A.C. Johnston.

3-dimensional color graphics presentation of the active fault zones in the New Madrid seismic zone, submitted December 1992 to *Nature*, J.M. Chiu, Y.T. Yang, and A.C. Johnston.

Abstracts

A high resolution PANDA experiment in the central New Madrid seismic zone, presented in the annual meeting of ESSA, Oct. 1990, J.M. Chiu, K.C. Chen, Y.T. Yang, S.C. Chiu, A.C. Johnston, and the PANDA Group.

The PANDA II - a PC-based seismic array, presented in the annual meeting of ESSA, Oct. 1990, J.M. Chiu, G.C. Steiner, R. Smalley, A.C. Johnston, and the PANDA Group.

The Cape Giradeau earthquake and its aftershock, presented in the annual meeting of ESSA, Oct. 1990, J.M. Chiu, A.C. Johnston, and the PANDA Group.

The CERI seismic networks in the New Madrid and the southern Appalachians, presented in the annual meeting of ESSA, Oct. 1990, A.C. Johnston, and J.M. Chiu.

A high resolution PANDA experiment in the central New Madrid seismic zone, presented in the annual meeting of GSA, Oct. 1990, J.M. Chiu, K.C. Chen, Y.T. Yang, S.C. Chiu, A.C. Johnston, and the PANDA Group.

A high resolution PANDA experiment in the central New Madrid seismic zone, *EOS*, Vol. 71, No. 43, 1435, presented in the Fall AGU, Dec. 1990, J.M. Chiu, K.C. Chen, Y.T. Yang, S.C. Chiu, A.C. Johnston, and the PANDA Group.

A gain-ranging and PC-based seismic array: PANDA II, presented in the annual SSA meeting, March 1991, *Seismol. Res. Let.*, 62(1), p. 22, J.M. Chiu, G.C. Steiner, R. Smalley, A.C. Johnston, and the PANDA Group.

The cooperative New Madrid seismic network - implementation of regional network nodes, presented in the annual SSA meeting, March 1991, *Seismol. Res. Let.*, 62(1), p. 33, E.J. Haug, R.B. Herrmann, and J.M. Chiu.

Fault zone geometry and crustal velocity structures in the central New Madrid seismic zone using the PANDA data, presented in the Spring AGU, May 1991, *EOS*, 72(17), p. 264, Y.T. Yang, J.M. Chiu, Z.S. Liaw, K.C. Chen, S.C. Chiu, A.C. Johnston, and the PANDA group.

Three-dimensional geometry of the sedimentary basin and its tectonic implications in the upper Mississippi embayment: results from the PANDA experiment, presented in the Spring AGU, May 1991, *EOS*, 72(17), p. 264, K.C. Chen, J.M. Chiu, Y.T. Yang, S.C. Chiu, A.C. Johnston, and the PANDA group.

3-dimensional fault zone geometry and sedimentary basin basin configuration in the central New Madrid seismic zone: determined from PANDA array data, presented in the annual ESSA meeting, Oct. 1991, J.M. Chiu, Y.T. Yang, K.C. Chen, Z.S. Liaw, S.C. Chiu, A.C. Johnston, and the PANDA group.

Determination of Q_p-Q_s relations in the sedimentary basin in the upper Mississippi embayment using converted phases, presented in the annual ESSA meeting, Oct. 1991, K.C. Chen, J.M. Chiu, Y.T. Yang, S.C. Chiu, A.C. Johnston, and the PANDA group.

Progress in implementing the cooperative New Madrid seismic network, presented in the annual ESSA meeting, Oct. 1991, R.B. Herrmann, E.J. Haug, A.C. Johnston, and J.M. Chiu.

The Risco, Missouri earthquake, May 4, 1991, presented in the annual ESSA meeting, Oct. 1991, S.C. Chiu, H. Hwang, J.M. Chiu, and A.C. Johnston.

3-Dimensional fault zone geometry and sedimentary basin configuration in the central New Madrid seismic zone determined from PANDA data, presented in the Fall AGU, Dec. 1991, *EOS*, 72(44), p. 429, J.M. Chiu, Y.T. Yang, K.C. Chen, Z.S. Liaw, S.C. Chiu, A.C. Johnston, and the PANDA group.

Seismological studies in the New Madrid seismic zone using the PANDA seismic array, presented in the Annual SSA meeting, April 1992, *Seismol. Res. Lett.*, 63(1), 49, J.M. Chiu, A.C. Johnston, Y.T. Yang, K.C. Chen, Z.S. Liaw, S.C. Chiu, J. Bollwerk, D. Reinbold, R.B. Herrmann, and the PANDA group.

3-D sedimentary basin configuration and seismic wave attenuation inside the sedimentary basin in the New Madrid seismic zone, presented in the Western Pacific Geophysical Meeting, August, 1992, *EOS*, 73(25), 50, K.C. Chen, J.M. Chiu, Y.T. Yang, S.C. Chiu, A.C. Johnston, and the PANDA group.

PANDA II and PANDA III seismic arrays and their applications in modern seismological observations, presented in the Western Pacific Geophysical Meeting, August, 1992, *EOS*, 73(25), 57, J.M. Chiu, G. Steiner, D. Xu, and D. Smith.

Imaging of fault zone geometry in the central New Madrid seismic zone using PANDA data, presented in the annual Eastern Seismological Society Meeting, Richmond, October, 1992, Y.T. Yang, J.M. Chiu, and A.C. Johnston

Crustal velocity studies in the New Madrid seismic zone from USGS explosions recorded by the PANDA seismic array, presented in the annual Eastern Seismological Society Meeting, Richmond, October, 1992, Z.S. Liaw, J.M. Chiu, and A.C. Johnston.

Three-dimensional color graphics presentation of the active fault zones in the New Madrid seismic zone, presented in the annual Eastern Seismological Society Meeting, Richmond, October, 1992, J.M. Chiu, A.C. Johnston, and Y.T. Yang.

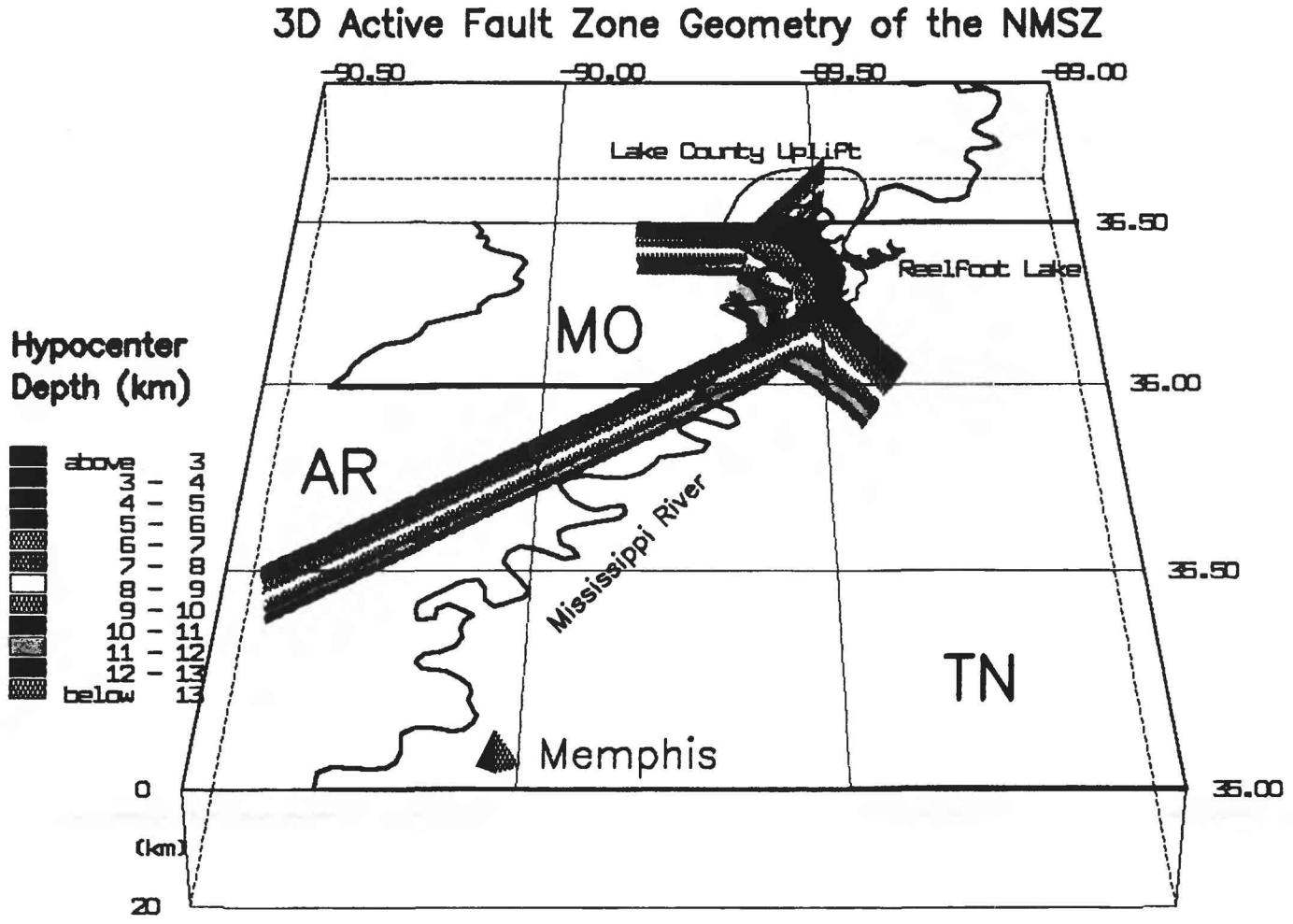

Figure 1. 3-dimensional configurations of the active fault zones in the New Madrid seismic zone showing the vertically dipping SW, NE, and NW segments and the gently southwest dipping central segment. Up-dip projection of the southwest dipping central segment will intersect with the surface between the Lake County Uplift and Reelfoot Lake. Relationships between these surface features and the underneath active zones are discussed in Chiu et al., (1992).

LATE QUATERNARY SLIP RATES ON ACTIVE FAULTS OF CALIFORNIA

9910-03554

MALCOLM M. CLARK
BRANCH OF ENGINEERING SEISMOLOGY AND GEOLOGY
345 MIDDLEFIELD ROAD, MS 977
MENLO PARK, CALIFORNIA 94025-3591
415/329-5624 FAX 415/329-5163

Investigations

1. Recently active traces of the Calaveras fault zone at Tres Pinos and San Felipe Creeks, California (K.J.Kendrick, J.W. Harden, M.M. Clark).

2. Recently active traces of Owens Valley fault zone, California (Sarah Beanland (NZGS), Clark).

3. Degradation of fluvial terrace risers along Lone Pine Creek, San Bernardino County (Kendrick, in conjunction with J.B.J. Harrison, L.D. McFadden (UNM), and R.J. Weldon (University of Oregon)).

4. Revision of slip-rate table and map of late Quaternary faults of California (Clark, Kendrick, J.J. Lienkaemper, K.R. Lajoie, C.S. Prentice, M.J. Rymer, D.P. Schwartz, R.V. Sharp, J.D. Sims, J.C. Tinsley, R.J. Weldon).

5. Late Quaternary evolution of the San Timoteo Badlands region, southern California (Kendrick, in conjunction with D.M. Morton and L.D. McFadden).

6. Post-earthquake investigations:
   a. Mono basin earthquake of 23 Oct 90 (Clark)
   b. Landers earthquake of 28 Jun 92 (Clark and Kendrick)

Results

2. Owens Valley fault zone. See v. 33, p. 202-3 of this publication for results summarized from our report, USGS Bulletin 1982, *in press,* listed below. This Bulletin features a 1 :24,000-scale strip map of the Owens Valley fault zone, a table of characteristics and measurements of active traces at 40 sites along the fault zone from Owens Lake to north of Big Pine, and text.

5. The degree of soil development associated with geomorphic surfaces in San Timoteo and Reche Canyons near the San Jacinto fault in the San Timoteo Badlands is comparable to that of nearby, dated soils and allows correlation of the surfaces. Twenty soil profiles have been described and sampled, including four surface soils and two buried soils associated with surfaces in San Timoteo Canyon (Q1-Q4), and

to surface soil associated with two surfaces in Reche Canyon (Q2, Q3). Soil development indices, based on field descriptions as well as laboratory analysis, provide a basis for comparison of these soils to each other and to dated soil chronosequences at Cajon Pass, Merced, and Anza.

The soils in the San Timoteo Badlands region record a complex tectonic and climatic history. Evidence includes buried soils, tilting and warping of both buried and surface soils, calcium carbonate coatings on manganese oxide and clay films, and the presence of silica cementation of soils in Reche Canyon, but not in the adjacent San Timoteo Canyon. The San Timoteo Badlands include preserved surfaces intermediate in soil development to those at Cajon Pass, and do not preserve a record of the major late Pleistocene to early Holocene aggradational event observed elsewhere in the region. In spite of the variability of the surfaces in this study area, soil development is similar to that of soils at other sites. With time the profiles develop progressively thicker argillic horizons, and increase in soil rubification, total mass of clay and crystalline iron oxides, and content and thicknesses of clay films.

The composition and content of iron species in soils of the San Timoteo study area is similar as in nearby sites, including the Cajon Pass chronosequence, Little Tujunga Canyon, Arroyo Seco Canyon, San Gabriel River, Day Canyon, Duncan Canyon, and the San Gorgonio Wash. With increasing soil age, there is an increase in the ratio of dithionite-extractable iron to total iron, a decrease in the ratio of ferrous to ferric iron, and a decrease in the ratio of oxalate- to dithionite-extractable iron, though all these trends are more subdued in the San Timoteo study area than elsewhere in the region. These patterns suggest that the slightly higher temperature and lower precipitation of the San Timoteo Badlands region may be responsible for both a slower rate of transformation of ferrihydrate to hematite and a shift in the maximum content of oxalate-extractable iron towards older soils.

Weighted means of soil development indices and rubification index values are used to compare the soils of this study to those at Cajon Pass, Merced, and Anza. Wide-range age estimates are determined using the maximum limits of these values, and result in 27.5-305 ka for Q1, 67-570 ka for Q2, and 305-700 ka for Q3 and Q4. Best estimates of age are determined by directly correlating soils with the same degree of soil development between this study and the closest chronosequence, Cajon Pass. This method constrains the time of formation of the Q1 surface to between 27.5-67 ka and the Q2 surface to 43-67 ka, and does not change the age estimates of the older surfaces.

Distinctive clast assemblages, identified by Morton and Matti (in press) are present along a limited section of the NE side of the San Jacinto fault, and are preserved on two surfaces within Reche Canyon, on the SW side of the fault. Subsequent displacement along the fault has resulted in offsets of approximately 1 and 4 km (Morton and Matti, in press). Age estimates based on comparisons of soil development allow us to better constrain these offsets, with resulting slip rates of 7-13 mm/yr since the formation of Q3, and 13-26 mm/yr since the formation of Q2.

6a. Mono Basin earthquake of 23 Oct 90. See K.R. Lajoie's results in v. 33, p. 381-2 of this publication.

6b. Landers earthquake of 28 Jun 92. We helped organize the post-earthquake geologic investigation and obtain existing and new aerial photos, and we contributed to the early mapping of surface ruptures.

Reports

Beanland, Sarah, and Clark, M.M., The Owens Valley fault zone, eastern California, and surface rupture associated with the 1872 earthquake: U.S. Geological Survey Bulletin 1982, *in press.*

Harrison, J.B.J., Kendrick, K.J., Weldon, R.J., and McFadden, L.D., 1992, Spatial and temporal variation in terrace scarp catinas in the Transverse Ranges, southern California: Catina, *in press.*

Kendrick, K.J., Harrison, J.B.J., McFadden, L.D., and Weldon, R.J., 1992, An evaluation of a non-linear diffusion equation as a model for determining the rate of scarp degradation in Cajon Pass, southern California (abs.); in Mörner, N.A., Owen, L.A., Stewart, I., and Vita-Finzi, C., eds., Neotectonics—recent advances: Abstracts vol., Quaternary Research Association, Cambridge.

Lajoie, K.R., Clark M.M., Hill, D.P., Lindh, A.G., Oppenheimer, D.H., and Yount, J.C., 1991, Mono Basin earthquake of October 23, 1990: U.S. Geological Survey administrative report.

Staff, USGS and CDMG, 1992, Pattern of surface ruptures associated with the June 28, 1992, Landers earthquake (abs.): EOS Trans. AGU, v. 73, no. 43, Fall Meeting Suppl., page 357-8.

INVESTIGATION OF PEAT STRATIGRAPHY IN ESTUARINE FLATS NEAR ANCHORAGE, ALASKA, AS A MEANS OF DETERMINING RECURRENCE INTERVALS OF MAJOR EARTHQUAKES

14-08-0001-G1949

Rodney A. Combellick and Richard D. Reger
Alaska Division of Geological & Geophysical Surveys
794 University Ave., Suite 200
Fairbanks, Alaska 99709
(907) 474-7147

Investigations

The goal of this project is to investigate the subsurface stratigraphy and sedimentology of estuarine deposits along the eastern shore of Cook Inlet (fig. 1) to obtain a record of subsidence events associated with major earthquakes. The results of this study, together with results of similar studies in the Prince William Sound, Copper River delta, and Middleton Island areas, are helping to develop estimates of the recurrence frequency of coseismic vertical tectonic displacements during the late Holocene.

Borehole drilling along Turnagain and Knik Arms in upper Cook Inlet during 1985-1989 revealed multiple submerged peat layers, possibly associated with six to eight coseismic subsidence events during the past 4,700 calendar years (Combellick, 1991b). In the current program, we have extended regional data coverage by drilling additional boreholes and examining tidal-channel exposures in estuaries of Fox River (Kachemak Bay), Kasilof River, Kenai River, and Chickaloon Bay. We also reexamined exposures at Girdwood and Goose Bay that have become more visible because of tidal erosion.

During 1991, we drilled nine hollow-stem boreholes and eight hand-auger holes at Fox River flats, four boreholes at Kenai River flats, and two boreholes at Kasilof River flats. Additionally, we examined extensive river-bank exposures at Kenai and Kasilof River Flats and tidal-bank exposures at Girdwood. We prepared and submitted 54 peat, wood, and organic silt samples for radiocarbon dating, and completed grain-size analyses of 83 samples to assist in interpreting depositional environment. During 1992, we examined tidal-channel exposures at Chickaloon Bay, Girdwood, and Goose Bay, and submitted an additional 17 organic samples for radiocarbon dating.

Results

A borehole at Portage, near the area of maximum 1964 subsidence, revealed the largest number of buried peat layers among all boreholes and exposures observed in this study. If all six peat layers at this site were buried as a result of pre-1964 coseismic subsidence, they imply an average recurrence interval of about 800 yr during the late Holocene. This value may underestimate the recurrence interval if some peats were

buried as a result of nonseismic processes and may overestimate the interval if some large subduction earthquakes did not result in peat burial at this site.

A buried peat layer indicating regional submergence between about 700 and 900 yr ago is present at Girdwood, Portage, Palmer Hay Flats, Goose Bay, and Chickaloon Bay. At Girdwood, this layer includes rooted stumps of trees that were probably killed by salt-water influx in the same manner as modern trees at Girdwood and Portage were killed as a result of the 1964 great earthquake. Evidence for coseismic uplift during the same period is present at Copper River Delta and at Cape Suckling. Although we cannot prove that submergence at all of these sites was coeval, the data strongly suggest that the most recent great earthquake prior to 1964 was about 700-900 yr ago.

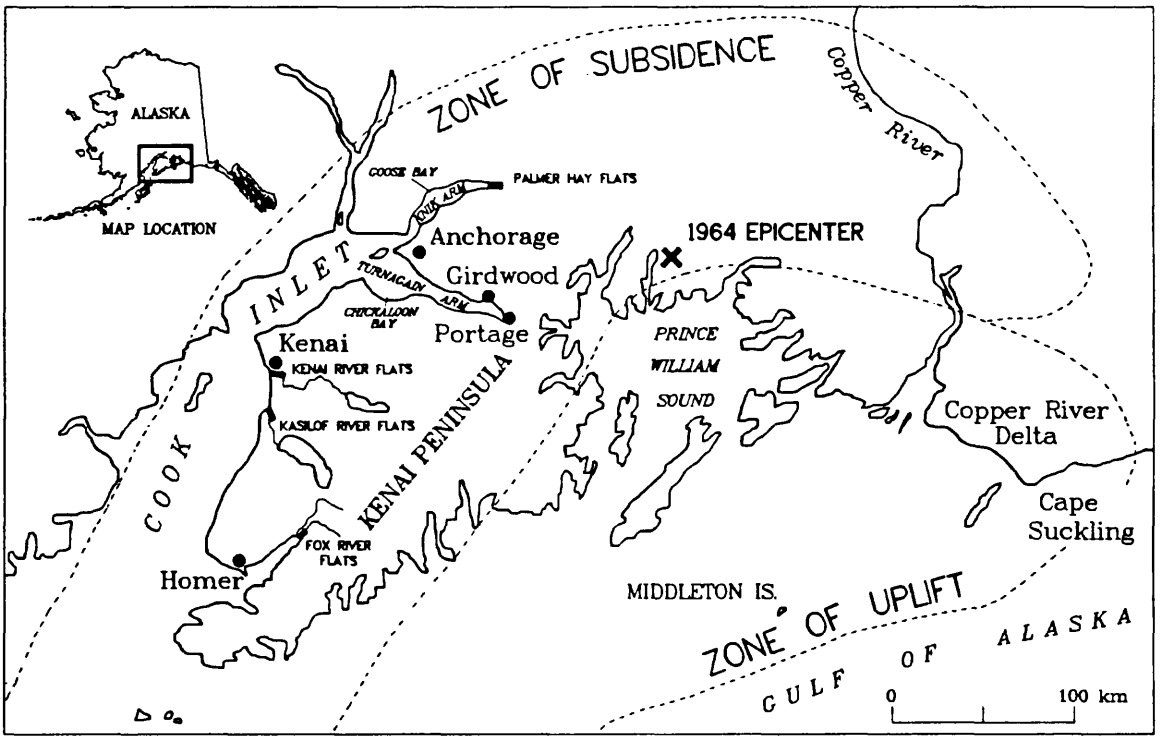

Figure 1. Study region in southcentral Alaska, showing zones of uplift and subsidence during the 1964 great earthquake.

Other than the postulated 700-900-yr event, the regional radiocarbon data set does not provide precise ages of all paleoseismic events. Uncertainty in age correlations among sites results from large standard deviations, some stratigraphic discordances and lateral inconsistencies, and the possibility that some ages may represent nonseismic events or local earthquakes (Combellick, 1991b; Bartsch-Winkler and Schmoll, 1992). However, if the data set is reduced to calibrated radiocarbon ages that appear coeval in two or more marshes, they cluster roughly into six to eight age groups during the past 5,000 yr, implying an average recurrence interval of about 600-800 yr (Combellick, 1992b).

A freshly eroded tidal-bank exposure near Girdwood corroborates previous radiocarbon data and reveals an extensive but formerly unrecognized peat layer with a radiocarbon age of 1,380±60 yr B.P. This layer may represent coseismic submergence that

is coeval with uplift dated at 1,350±200 yr B.P. at Middleton Island (Plafker and Rubin, 1967). Tidal-bank exposures at Goose Bay and Chickaloon Bay show as many as three submerged peat layers that pre-date the 1964 event, including the most recent regional event 700-900 yr ago. At Goose Bay and Palmer Hay Flats, there is evidence of a possible local event about 400-600 yr ago, perhaps an earthquake on the Castle Mountain fault, about 20 km north.

At Fox River flats, 17 boreholes and several shallow exposed sections failed to reveal any buried peat layers like those observed in upper Cook Inlet. The estuarine sediments are sandier, indicating that deposition may be dominated by the fluvial system of Fox River and Sheep Creek and that their deltas may be prograding over and reworking the tidal flat. The ages of some organic-rich horizons agree with ages of buried peats elsewhere, but we are reluctant to conclude that they are related to coseismic subsidence. Other ages are anomalously old (5-7 ka) for their shallow depth (less than 2 m) and we suspect that they may be contaminated by detrital coal, which is abundant in exposures of Tertiary rocks in the drainage basin.

At Kenai and Kasilof River flats, which are near the arcward limit of 1964 deformation, a thick (2 m), near-surface peat sequence spanning the late Holocene from about 1,000 to 7,000 yr B.P. is largely devoid of interseismic mud layers, indicating minimal coseismic subsidence in this area. Radiocarbon ages of several samples at the interface between the top of this thick peat and overlying intertidal mud indicate probable submergence about 1,300 yr B.P. (uncalibrated), which may correspond to similarly dated submergence at Girdwood and uplift at Middleton Island. The 700-900-yr-B.P. event is not represented by a buried peat layer in intertidal sections that we observed at Kenai or Kasilof. Vertical variations in vegetation type within the thick peat include alternations between forest and brackish marsh that may reflect responses to small coseismic vertical changes, but these cannot be accurately dated. The long-term relative stability of the Kenai-Kasilof area (near the zero isobase of 1964 subsidence) and repeated large subsidence at Portage (near the area of maximum 1964 subsidence) imply that coseismic deformation during late-Holocene events was generally similar to deformation during the 1964 earthquake (Combellick, 1992b).

Project Reports

Combellick, R.A., 1986, Chronology of late-Holocene earthquakes in southcentral Alaska: Evidence from buried organic soils in upper Turnagain Arm [abs.]: Geological Society of America Abstract with Programs, V. 18, no. 6, p. 569.

Combellick, R.A., 1990, Evidence for episodic late-holocene subsidence in estuarine deposits near Anchorage, Alaska: Basis for determining recurrence intervals of major earthquakes: Alaska Division of Geological & Geophysical Surveys Public-Data File 90-29, 67 p.

Combellick, R.A., 1991a, Paleoseismicity of the upper Cook Inlet region, Alaska, as recorded by peat stratigraphy in nine tidal-flat boreholes [abs.]: Geological Society of America Abstracts with Programs, v. 23, no. 2, p. 15.

Combellick, R.A., 1991b, Paleoseismicity of the upper Cook Inlet region, Alaska: Evidence from peat stratigraphy in Turnagain and Knik Arms: Alaska Division of Geological & Geophysical Surveys Professional Report 112, 52 p.

Combellick, R.A., in press, The penultimate great earthquake in southcentral Alaska: Evidence from a buried forest near Girdwood, *in* Solie, D.N., ed., Short Notes on Alaskan Geology, 1992: Alaska Division of Geological & Geophysical Surveys Professional Report.

Combellick, R.A., 1992a, Paleoseismicity of the upper Cook Inlet region, Alaska [abs.]: Geologic Reason--A Basis for Decisions Affecting Society, Symposium and Annual Meeting, Lake Tahoe, NV, Sept. 27-30, 1992, American Institute of Professional Geologists, p.18.

Combellick, R.A., 1992b, Coseismic and long-term tectonic subsidence in the Cook Inlet region, Alaska [abs.]: EOS, in press (abstracts of the December 1992 annual meeting).

Other Reference Cited

Bartsch-Winkler, Susan, and Schmoll, H.R., 1992, Utility of radiocarbon-dated stratigraphy in determining late Holocene earthquake recurrence intervals, upper Cook Inlet region, Alaska: Geological Society of America Bulletin, v. 104, no. 6, p. 684-694.

Plafker, George, and Rubin, Meyer, 1967, Vertical tectonic displacements in south-central Alaska during and prior to the great 1964 earthquake: Journal of Geosciences, Osaka City University, v. 10, no. 3, p. 53-66.

TECTONICS OF SEISMIC SOURCE ZONES, CENTRAL INTERIOR OF THE UNITED STATES

9950-04542

ANTHONY J. CRONE
Branch of Geologic Risk Assessment
U.S. Geological Survey
Box 25046, MS 966,
Denver, Colorado 80225
(303) 236-1595

PURPOSE OF PROJECT

This multidisciplinary project involves studies that provide basic geologic and geophysical information on the distribution, characteristics, and frequency of large earthquakes in the central interior of the United States and contribute to a better understanding of the structural features that might produce large, potentially damaging intraplate earthquakes. Individuals that contributed to this report include Donley S. Collins, Anthony J. Crone, Richard L. Dart, Sharon F. Diehl, William L. Ellis, Meridee Jones-Cecil, Donald T. Rodbell, and Henri S. Swolfs.

INVESTIGATIONS

Subsurface Stratigraphy and Structure—New Madrid Seismic Zone (NMSZ)

D.S. Collins completed an analysis of the insoluble residues from cuttings of the Strake Petroleum #1 Russell drill hole and the lithologies in the Killan #1 Pattinson drill hole, both in Pemiscot Co. Mo. These studies helps define the stratigraphy, depositional history, and tectonic framework of the Lower Paleozoic rocks in southeastern Missouri. This stratigraphic information combined with similar data from other deep drill holes in the New Madrid region aids in clarifying structural relations by improving correlations of Lower Paleozoic rocks in the Reelfoot rift. A report describing these relations is nearly complete.

A.J. Crone completed his initial analyses of about 135 km of industry Vibroseis seismic-reflection data across the Crittenden County fault zone in northeastern Arkansas and finalized a manuscript describing the results of this study for publication in *Seismological Research Letters*. (See also related investigations listed below.)

R.L. Dart has completed a series of subsurface structure-contour, isopach, and geologic subcrop maps and companion stratigraphic cross sections of the upper Mississippi embayment region. This work will be published as a Miscellaneous Field Studies Map. The process of updating the subsurface geologic database from which these maps and cross section were generated has been completed and a revised version of the drill-hole catalog has been prepared for publication as a USGS Open-File Report. The database has been converted to a GIS ARC/INFO data format, which provides the opportunity to merge and plot these data with other GIS databases.

Dart also made inquiries to the National Geodetic Survey (NGS) regarding the location and availability of recent geodetic data in the New Madrid region. He also requested information about the necessity and methods of applying various standard corrections to older leveling data.

S.F. Diehl continued her analyses of authigenic minerals and microstructural fabric of rocks in the Reelfoot rift and adjacent terrains. These studies revealed petrographic evidence of deformational and fluid-migration events in the rift that help characterize the rift's complex structural history. Specific investigations include petrographic studies of drill-hole samples from the USGS-New Madrid Test well in Pemiscot Co., Mo., and the Dow Chemical #1 Garrigan drill hole in Mississippi Co., Ark., and of lamprophyres from the Dow Chemical #1 Wilson drill hole in Mississippi Co., Ark.

In collaboration with C.K. Throckmorton, (Br. Central Regional Geology), and C.W. Clendenin (private consultant and former quarry employee), S.F. Diehl mapped the English Hill fault that is exposed in the Grays Point Quarry, near Scott City, southeastern Mo., and sampled the fractured Paleozoic rocks adjacent to the fault. The mapping determined the attitude of bedrock fractures and the relation of the fractures to the fault. These studies are part of an effort to clarify the relations between diagenetic events and periods of tectonic movement.

Diehl also completed revisions of two manuscripts. One report, which is coauthored with F.A. McKeown, discusses the spatial coincidence of high fluid pore pressure and contemporary seismicity in the New Madrid seismic zone. The second report, which is coauthored with M.B. Goldhaber (Br. of Geochemistry), documents the flow of acidic fluids out of the Reelfoot rift and into adjacent areas by mapping the regional extent of dissolved authigenic potassium feldspar.

H.S. Swolfs completed his analysis of structural features in the Dow Chemical #1 Garrigan drill hole to clarify the origin, evolution, and extent of deep-seated seismogenic structures that underlie and are perhaps associated with structurally high features in the Reelfoot rift. This drill hole is on the southeastern flank of the Blytheville arch, a major structural feature that coincides with the narrow, 120-km-long, southwest-trending zone of seismicity of between Caruthersville, Mo., and Marked Tree, Ark. The results of this study are being published in a special issue of the *Seismological Research Letters.*

Quaternary Deformation and Paleoseismicity—NMSZ

D.T. Rodbell completed two investigations: a) the distribution, age, and downvalley gradient of the alluvial terraces along the Obion River in northwestern Tennessee, and b) the distribution of probable 1811-12 liquefaction features that are present on these terraces and the number of seismic events recorded by these features. Reports describing these studies are in press.

Distribution of Stress—NMSZ

W.L. Ellis revised a manuscript titled "Summary and discussion of crustal stress data in the region of the New Madrid seismic zone," which will be submitted for publication as a chapter in the forthcoming USGS Professional Paper on current research in the New Madrid region.

Investigations of the Meers Fault, Southwestern Oklahoma

M. Jones-Cecil finalized her analysis of the magnetic field in the area of the Meers fault, southwestern Oklahoma, to examine subsurface structural relations and how they may affect the fault's seismic potential. Jones-Cecil finalized models of eight ground-magnetic profiles across the fault and three regional profiles across the entire Frontal Wichita fault system (FWFS) using aeromagnetic data. The FWFS separates the Anadarko basin to the northeast from the Wichita uplift to the southwest. The models incorporate *in situ* and laboratory magnetic susceptibility measurements, paleomagnetic data from drill core of holes adjacent to the Meers fault (on loan from Ken Luza of the Oklahoma Geological Survey), and petrologic information from the core (see below).

D.S. Collins examined the petrography of 28 thin sections and hand samples from the core of three aligned drill holes across the Meers fault. The petrographic data on the lithologies and mineral alterations of igneous rocks adjacent to the fault zone provide important constraints on the models of magnetic data near the fault. The net result is to refine the models and help clarify the structural relations of rocks across the fault zone.

Related Investigations

Although not directly funded by NEHRP, M. N. Machette (Br. Geologic Risk Assessment) and Crone, in conjunction with J.R. Bowman, completed two comprehensive USGS Bulletins that present their detailed field data and describe the results of their G.K. Gilbert Fellowship studies on the paleoseismicity of the 1986 Marryat Creek and 1988 Tennant Creek, Australia intraplate earthquakes. These Bulletins contain lithologic/structural maps of six trenches, detailed site maps,

scarp profiles, and the results of thermoluminescence and electron-spin resonance dating of Quaternary deposits in the two areas. The Bulletins document the long recurrence time between successive earthquakes on these faults and discuss the implications of these long recurrence times on seismic hazards in stable continental tectonic settings. Machette and Crone also presented the results of these studies at the 1991 Geological Society of America annual meeting (10/91) and at a workshop on "Cratonic Seismicity and Strain" sponsored by the USGS, the Nuclear Regulatory Commission, and the Electric Power Research Institute (7/92).

RESULTS

Subsurface Stratigraphy and Structure—NMSZ

(Collins) Analyses of the insoluble heavy minerals from the Strake Petroleum #1 Russell drill hole reveal that igneous rocks were exposed in the source area during deposition of Cambrian pre-Bonneterre rocks and the lower part of the Upper Cambrian Bonneterre Formation. In contrast, both igneous and high-grade, metamorphic rocks provided sediment during deposition of the upper part of the Bonneterre Formation and the overlying Lower Ordovician Eminence or Potosi Formations. The heavy minerals that indicate metamorphic rocks in the source area include kyanite, sillimanite, zoisite, and staurolite; the minerals that indicate an igneous source area include brookite, anatase, augite, ilmenite, magnetite, chromite, phlogopite/biotite, apatite, hornblende, wolframite, scheelite, garnet, zircon, and tourmaline. It is significant that the heavy mineral suites from neither the Dow Chemical Co. #1 Garrigan drill hole, which is about 90 km south of the Strake drill hole, nor the Killam #1 Pattinson drill hole, which is about 5 km southeast of the Strake drill hole contained evidence of metamorphic rocks in the sediment source areas. This suggests the presence of isolated depocenters that had different source terrains in the Reelfoot rift during the Early Paleozoic. The closest known major source of metamorphic rocks is the central Missouri high, which is about 240 km west of the Strake drill hole. The Precambrian igneous rocks that are exposed on the west side of the St. Francois Mountains may have been the main source of igneous detritus for Early Paleozoic rocks in the Strake, Killam, and Garrigan drill holes. These studies show that insoluble residues cannot be used to correlate the Early Paleozoic rocks on the carbonate platform along the northwestern flank of the Reelfoot rift with the dominantly siliciclastic rocks in the interior of the rift.

(Dart) R.L. Dart has completed revising his series of 14 subsurface maps and 11 stratigraphic cross sections that were derived from his database of subsurface information in the New Madrid region. These maps and cross sections will be published as a three-part series of USGS Miscellaneous Field Studies maps. Part 1 will contain three maps showing a variety of geologic and geophysical information about the subsurface geology of Paleozoic and Precambrian rocks. Part 2 will be a series of 10 structure contour, isopach, and subcrop maps of individual systems within the Paleozoic stratigraphic section. The third part will contain 11 northwest-southeast and northeast-southwest stratigraphic cross sections of the area.

Dart's inquiries to the NGS concerning new leveling data from the Mississippi embayment revealed that, in recent years, several new leveling lines have been completed along previously leveled routes. His inquiries concerning the need to apply corrections revealed that the necessary routine corrections have been applied to all data that is in the NGS vertical-control database. Upon request, the NGS can generate level profiles for any releveling route within the Mississippi embayment from their vertical-control computer database. Level profiles are fundamental tools for the recognition of recent vertical crustal deformation using geodetic data. The NGS's ability to produce level profiles and apply corrections to all old leveling data supersedes Dart's study of these data that was done in the early 1980's. However, Dart's earlier compilation and profiles of the leveling data from the Mississippi embayment can be used to make a preliminary identification of areas of possible crustal deformation.

(Dart & Swolfs) The principal objective of this research is to collectively interpret all of the available geological and geophysical subsurface data in the area of abundant seismicity to identify fault-related features and to evaluate the tectonic significance of these features. The comprehensive subsurface database and the resultant subsurface maps and cross sections permit preliminary structural interpretations that will lead to working hypotheses about the geological setting of seismically active fault zones. A three-dimensional image of the Precambrian bedrock surface shows previously unrecognized large-scale topography on the floor of the Reelfoot rift. The image shows a northwest-trending trough in northeastern Arkansas that is flanked on the northeast by a 2-km-high ridge. These major features are oriented normal to the northeast-trending rift axis and correlate well with similar structures expressed on a recently compiled depth-to-magnetic-basement map (Hildenbrand and Hendricks, USGS Professional Paper). The upward projection of the gently southwest-dipping boundary between the trough and ridge may be expressed in the subcrop maps of the Cambrian and Ordovician surfaces as mapped by Dart (in prep.) and Schwalb (1971), respectively. Along this boundary, key stratigraphic horizons are all displaced down to the southwest. The nature and tectonic significance of this boundary remains to be resolved, but in Precambrian basement rocks, it coincides with the southwestern terminus of the NMSZ and the end of the Blytheville arch near Marked Tree, Ark. During the past few decades, some of the largest earthquakes in the NMSZ have occurred in this area. This intra-rift basement structure may concentrate stress and/or act as a structural barrier that limits the seismicity at the southwestern end of the axial fault zone.

(Diehl) Paleozoic carbonate rocks from the USGS-New Madrid Test well, which is near the crest of the Pascola arch, are brecciated and enriched with sulfide and rare-earth minerals (Crone, 1981; Goldhaber and others, 1993). Petrographic analysis of samples from the drill hole shows that the sulfide mineralization is concentrated along intersecting fractures and stylolites. Scanning-electron-microscope mapping of the sulfides using the IPP program, which can selectively map as many as 8 different elements, shows an alignment of epigenetic minerals along fractures and demonstrates that fluid flow in the rock was controlled by internal structures.

The direct evidence of alkaline igneous activity in the Reelfoot rift has been limited to the presence of lamprophyric dikes and syenite penetrated in a few deep drill holes, but new petrographic studies of the sedimentary rocks in the region provide indirect evidence of alkaline magmatism and related metasomatism. These studies show that fluorite and elevated fluorine concentrations are present in several drill holes in the rift. Furthermore, the presence of fluorapatite, inclusion-rich potassium feldspar cement, monazite, and other rare-earth minerals suggests that metasomatism by alkaline magmatic fluids has occurred in these rocks.

Mapping along the segment of the English Hill fault that is exposed in the Grays Point quarry revealed evidence of fault movement during the Middle-Late Ordovician, which is earlier than the Devonian age of fault movements that is commonly interpreted throughout southeastern Missouri (Harrison and Schultz, 1992). In the quarry, the fault offsets the Ordovician Plattin, Decorah, and Kimmswick Formations, but the Ordovician Maquoketa Shale and undeformed Thebes Sandstone fill a synform along the fault. The fault is not mineralized by carbonate-rich fluids, but adjacent carbonate-filled fractures contain evidence of three periods of movement: (1) formation of fractures that were sealed by authigenic cement, (2) renewed deformation and partial recrystallization of subrounded breccia clasts, and (3) another episode of brecciation that produced angular clasts and allowed carbonate-rich fluids to precipitate minerals in fractures and vugs. Each successive fluid-flow event produced coarser authigenic mineral cement than the preceding event.

(Swolfs) The study of the cores from the Garrigan well was initiated to improve our understanding of the origin and extent of deep-seated seismogenic faults that underlie and are perhaps associated with the Blytheville arch in the Reelfoot rift (Swolfs, 1992). Two additional manuscripts are in various stages of preparation and contain, respectively, a detailed descriptive lithologic log of the oriented core (90% complete), and a summary of the methods used to obtain and record directional data in the oriented core (60% complete). A compendium of published and unpublished geologic information on the sub-Cretaceous rocks in the Reelfoot rift, obtained from studies of about twenty drill holes in this region, is ready for branch review. The subsurface data

compiled in this progress report includes information ranging from biostratigraphy to drill-stem test results, and its intended purpose is to complement the catalog of drill-hole data prepared by R.L. Dart (in prep.).

(Crone) The preliminary interpretation of recently purchased industry seismic-reflection data in the vicinity of the Crittenden County fault zone in northeastern Arkansas documented the structural relations that exist across the rift-bounding fault zones. Several profiles in this data set contain groups of prominent moderate to strong reflectors in the upper crust at depths that are below the top of crystalline basement. Many of the reflections are still visible at the base of the industry-processed record sections (5.0 sec two-way travel time), which corresponds to depths of approximately 15 km. These groups of strong reflectors, which are continuous for distances of several kilometers, typically have gentle dips. These data are being reprocessed (in collaboration with T. Pratt, Br. Geologic Risk Assessment) to yield 12-sec-long record sections; initial reprocessing shows that groups of strong reflectors are present in the crust to depths of about 20 km.

Quaternary Deformation and Paleoseismicity—NMSZ

(Rodbell) The terrace study, the results of which have been submitted for publication as a U.S. Geological Survey Bulletin, has led to the recognition of three terrace levels along the Obion River, thus corroborating the findings of Saucier (1987). In addition to elevation above the modern stream, these terraces can be differentiated by the number of loess units that mantle their surfaces and by how extensively they are dissected by tributary streams. These parameters permit correlation of the terraces and thus provide a method to test Saucier's (1987) two hypotheses concerning possible Quaternary deformation in the eastern uplands adjacent to the Mississippi River. Several cores, which were retrieved from these terraces using a hydraulically powered drill rig, contained radiocarbon datable materials from the base of the loess mantle. The youngest terrace is named the Finley terrace, and is mantled by Peoria loess. A radiocarbon date of 21.6 ka from the terrace alluvium beneath the loess indicates that the Finley terraces formed during the late Wisconsin rather than during the early Wisconsin as previously postulated (Saucier, 1987). The next older terrace is the Hatchie terrace, which is mantled by the Peoria and Roxana loesses. The presence of these two loesses indicates that these terraces are early Wisconsinan in age. The oldest terrace is the Humboldt terrace. A single core from this terrace near the edge of the bluffs penetrated more than 8 m of Peoria and Roxana loess and did not penetrate the underlying alluvium. Based on its extensive geomorphic modification, the Humboldt terrace believed to be pre-Wisconsinan in age.

Results of the liquefaction study are reported in a USGS Miscellaneous Field Studies Map (Rodbell and Bradley, in press) and in a note in the *Bulletin of the Seismological Society of America* (Rodbell and Schweig, in press). In this study, we excavated three trenches across sand blows that formed in sandy alluvial deposits underlying the Finley terrace in western Tennessee. The deposits are susceptible to liquefaction and have been in a geomorphic setting that is favorable for liquefaction for at least the past 21.6 ka. The lack of significant soil development on numerous sand-blow deposits exposed in three exploratory trenches indicates that the sand blows probably formed during the multiple episodes of strong ground shaking from the 1811-12 earthquakes. We found no convincing evidence of prehistoric liquefaction in our trenches. These results imply that shaking strong enough to cause liquefaction has not occurred at this site in at least the past 10,000 years. This result is consistent with the results of similar studies elsewhere in the NMSZ (Wesnousky and Leffler, 1992).

Investigations of the Meers Fault, Southwestern Oklahoma

(Jones-Cecil) The Meers fault is one of the few examples of an exposed, recently reactivated fault in the central and eastern U.S. Hence, understanding its structural role within the Frontal Wichita fault system (FWFS) and the Southern Oklahoma aulacogen, its orientation relative to the current regional stress field, and the degree of deformation and alteration within the fault zone may reveal reasons for the late Holocene reactivation of the fault. The possible causes of reactivation help to

characterize other potentially seismogenic faults in the vicinity of the Southern Oklahoma aulacogen, and, in turn, advances our understanding of intraplate seismicity.

The objective of the geophysical study of the fault was to examine its geometry and its relationship to other faults within the FWFS and to the present-day regional stress field. This study clearly demonstrates the importance of preexisting structures in controlling the location of the reactivated part of the fault. The last major episode of movement on the fault occurred in Late Paleozoic time. The northwestern limit of the Holocene rupture appears to have been controlled by splaying of the older Meers fault that occurred at a left step in the primary fault. At least two scarps of secondary reactivated faults coincide with minor faults that were modeled from the magnetic data. This result exemplifies of the extent to which preexisting structures apparently controlled the reactivation of even small-scale faults. The Meers fault's linear surface trace, trenching studies, and shallow seismic-reflection data all show that the fault has a near-vertical dip in the shallow subsurface. Models of the magnetic data also constrain the dip to be near-vertical to about 0.5 km depth. The up-to-the-north movement during Holocene faulting is qualitatively more compatible with a near-vertical dip at depth in the present-day regional stress field than with reactivation on a moderate southwest-dipping fault that was interpreted from COCORP reflection data (Brewer and others, 1983). If this qualitative assessment is true, then there are few faults with similar strikes and steep dips in the FWFS and within the area of the Southern Oklahoma aulacogen, and therefore few that are favorably oriented to be reactivated in the current regional stress field.

A dikelike body immediately south of the fault has been interpreted from magnetic data (Purucker, 1986) to extend along almost half the length of the Quaternary scarp. The Oklahoma Geological Survey (OGS) drill holes across the fault cored diorite/gabbro that has high magnetic susceptibility and is at the appropriate depth and location to be the probable source of the magnetic anomaly. Rock in the core is highly altered and sheared and has a high clay content. Preliminary detailed gravity profiles show a 1 mGal high associated with the dikelike body, implying that the alteration is limited to the near-surface. The presence of the dikelike body along the fault may localize stresses along the fault.

(Collins) Core samples from three OGS drill holes contain igneous rock of intermediate(?) composition probably from the Roosevelt Group, diorite and gabbro from the Roosevelt Group, and rhyolite from the Carlton Rhyolite Group. These rocks could not be correlated between the drill holes because of pervasive alteration and/or because each of the core holes penetrated different bodies of igneous rock. Differences in the amount of intragranular fracturing and degree of alteration between the drill holes suggest that the block of igneous rock sampled by the core holes is bounded on the north by the Meers fault and on the south by a subsurface fault that has no surface expression. Four types of fractures common in the core samples are from oldest to youngest: 1) breccia-filled fractures, 2) clay-filled fractures, 3) iron-oxide filled fractures, and 4) open (unfilled) fractures. Crosscutting relations of the fractures suggest that an early faulting event(s) was followed by at least three later extensional events.

Related Investigations

Results of Machette's and Crone's Gilbert Fellowship research on the Marryat Creek and Tennant Creek scarps in central Australia (Crone and others, 1992; Machette and others, in press) show that these historical earthquakes reactivated ancient faults and that the recurrence time of major earthquakes these faults is measured in time scales of many tens of thousands to hundreds of thousands of years, or possibly longer. Six trenches across the historical ruptures revealed no clear evidence of prehistoric scarp-derived colluvial deposits. Furthermore, we did not find compelling geomorphic evidence ancient scarps along the ruptures. These field studies and our brief examination of a trench across the 1968 Meckering (Western Australia) scarp suggest that surface ruptures on Australian intraplate faults have very long repeat times. If this is true for most faults in the stable interior of continents, then the concept of recurrence intervals may not be appropriate in characterizing the behavior of these faults. A more realistic model for earthquake-hazard assessment of continental interiors might be based on infrequent but moderate- to large-

magnitude earthquakes that can occur on any suitably oriented fault, rather than basing the assessments on only those faults that have Quaternary movement.

REFERENCES CITED

Brewer, J. A., Good, R., Oliver, J. E., Brown, L. D., and Kaufman, S., 1983, COCORP profiling across the southern Oklahoma aulacogen--Overthrusting of the Wichita Mountains and compression within the Anadarko basin: Geology, v. 11, p. 109-114.

Crone, A.J., 1981, Sample description and stratigraphic correlation of the New Madrid Test Well-1-X, New Madrid County, Missouri: U.S. Geological Survey Open-File Report 81-426, 26 p.

Harrison, R.W., and Schultz, A.P., 1992, Faulting at Thebes Gap, MO.-ILL.—Implications for New Madrid tectonism: Geological Society of America Abstracts with Program, v. 24, no. 7, p. A191.

Hildenbrand, T.G., and Hendricks, J.D., Geophysical setting of the Reelfoot rift and relations between rift structures and the New Madrid seismic zone: U.S. Geological Survey Professional Paper.

Purucker, Michael, 1986, Interpretation of an aeromagnetic survey along the Wichita Frontal fault zone *in* Gilbert, M.C., ed., Petrology of the Cambrian Wichita Mountains igneous suite: Oklahoma Geological Survey Guidebook 23, p. 129-136.

Saucier, R. T., 1987, Geomorphological interpretations of late Quaternary terraces in western Tennessee and their regional tectonic implications: U. S. Geological Survey Professional Paper 1336-A, 19 p.

Schwalb, Howard, 1971, The northern Mississippi embayment—A latent Paleozoic oil province, *in* Proceedings of symposium on future petroleum potential on NPC region 9 (Illinois basin, Cincinnati arch, and northern part of Mississippi embayment): Illinois State Geological Survey, Urbana, IL, Illinois Petroleum 95, p. 44-56.

Wesnousky, S.G., and Leffler, L.M., 1992, The repeat time of the 1811 and 1812 New Madrid earthquakes—A geological perspective: Bulletin of the Seismological Society of America, v. 82, p. 1756-1785.

REPORTS

Collins, D.S., 1992, A petrographic study of igneous rock from three drill holes near the Meers fault, Oklahoma: U.S. Geological Survey Open-File Report 92-411, 25 p.

Collins, D.S., Taylor, M.E., Repetski, J.E., and Palmer, A.R., 1992, New sedimentological data for the Dow Chemical #1 B.L. Garrigan drill hole, Mississippi County, Arkansas: U.S. Geological Survey Open-File Report 92-6, 38 p.

Crone, A.J., 1992, Structural relations and earthquake hazards of the Crittenden County fault zone, northeastern Arkansas: Seismological Research Letters, v. 63, no. 3, [in press].

Crone, A.J., Machette, M.N., and Bowman, J.R., 1992, Geologic investigations of the 1988 Tennant Creek, Australia, earthquakes--Implications for paleoseismicity in stable continental regions: U.S. Geological Survey Bulletin 2023-A, 52 p.

Dart, R.L., Drill-hole data catalog of Paleozoic subsurface geology in the upper Mississippi embayment - A revision of Open-File Report 90-260: U.S. Geological Survey Open-File Report, [in press].

Dart, R.L., Maps of the Paleozoic and Precambrian rocks of the Mississippi embayment from drill-hole and seismic reflection data: U.S. Geological Survey Miscellaneous Field Studies Map, [in press].

Diehl, S.F., Throckmorton, C.K., and Clendenin, C.W., 1993, Significance of recurrent fault movement at Grays Point, Missouri (abs): Geological Society of America Abstracts with Programs, North-Central Section, March 29-30, 1993, [submitted].

Diehl, S.F., and Goldhaber, M.B., Feldspar diagenesis in Cambrian clastic rocks of the southern Ozarks and Reelfoot rift, southeast Missouri and northeast Arkansas--Implications for Mississippi Valley-type ore genesis, *in* Day, Warren, and Lane, Diane, eds., Strategic and critical minerals of the midcontinent, U.S.A.: U.S. Geological Survey Bulletin 1989, [in press].

Goldhaber, M.B., Diehl, S.F., Flohr, Marta, and Sutley, S., 1993, Evidence for alkaline igneous activity and associated metasomatism in the Reelfoot rift: Geological Society of America Abstracts with Programs, North-Central Section, March 29-30, 1993, [submitted].

Jones-Cecil, Meridee, Total-field aeromagnetic and derivative maps of the Lawton area, southwestern Oklahoma: U.S. Geological Survey GP-998-A, 2 sheets, scale 1:100,000, [in press].

Jones-Cecil, Meridee, Donovan, R. N., and Bradley, L.-A., Structural framework of the Meers fault and Slick Hills area, southwestern Oklahoma, based on magnetic data, *in* Johnson, K.S, Structural styles of the southern mid-continent--a symposium: Oklahoma Geological Survey Circular, [Director's approval 7/92].

Jones-Cecil, Meridee, and Robbins, S.L., Bouguer and isostatic residual gravity anomaly and derivative maps of the Lawton area, southwestern Oklahoma: U.S. Geological Survey GP-998-B, 3 sheets, scale 1:100,000, [in press].

Machette, M.N., Crone, A.J., and Bowman, J.R., Geologic investigations of the 1986 Marryat Creek, Australia, earthquake--Implications for paleoseismicity in stable continental regions: U.S. Geological Survey Bulletin 2032-B, [in press].

Repetski, J.E., Taylor, M.E., Collins, D.S., Palmer, A.R., and Wood, G.E., 1992, Cambrian and Ordovician paleontological studies in the Reelfoot basin, southern Midcontinent, U.S.A. [abs.]: Fifth North American Paleontological Convention, Field Museum of Natural History, Chicago. (unpaginated).

Rodbell, D.T., and Bradley, L.A., Logs of exploratory trenches through liquefaction features on late Quaternary terraces in the Obion River Valley, northwestern Tennessee: U.S. Geological Survey Miscellaneous Field Studies Map, [in press].

Rodbell, D.T., and Schweig, E.S., III, The record of seismically-induced liquefaction on late Quaternary terraces in northwestern Tennessee: Bulletin of the Seismological Society of America, [in press].

Rodbell, D.T., Subdivision, subsurface stratigraphy, and estimated age of fluvial terraces in northwestern Tennessee: U.S. Geological Survey Bulletin, [submitted].

Swolfs, H.S., 1992, Structural features in the Dow Chemical B.L. Garrigan No. 1, Mississippi County, Arkansas, and their paleotectonic implications: Seismological Research Letters, v. 63, no. 3, [in press].

Earthquake Hazard Investigations in the Pacific Northwest and southern Alaska using network data

14-08-0001-G1803

R.S. Crosson and K.C. Creager
Geophysics Program
University of Washington
Seattle, WA 98195
(206) 543-8020

October 1, 1991 - September 30, 1992

Investigations

This research focuses on earthquake hazards in the Pacific Northwest, including large scale plate interactions, through the study of regional structure and tectonics. Current investigations by our research group include determining source scaling and moment estimation using coda amplitudes, completing work on subduction kinematics of the subducting plate, investigating P-wave multiplets arising from teleseismic arrivals reflected from the subducting plate, and refraction interpretation of earthquake travel times.

Source moment estimation and magnitude determination using S-coda amplitude:

We wish to provide accurate automated estimates of earthquake magnitude using regional or local (mainly vertical component) short-period data. The current technique for determining magnitudes from short-period data is to use S-wave coda duration. However machine algorithms to automatically assign coda durations are far from satisfactory due to variations in noise level and signal frequency.

We have developed a method to base magnitudes on coda amplitude rather than duration. Using standard coda amplitude models based on scattering theory (e.g. Aki and Chouet, 1975), we can relate the amplitudes back to the source spectrum and hence directly to moment. Magnitudes can then be derived directly from the moment estimates.

S-wave coda amplitudes from local earthquakes recorded by the regional network were used with the single-scattering coda model of Aki and Chouet (1975) to estimate source spectra in a narrow frequency band. We found an omega-square, constant stress drop scaling model provided the best fit to the source spectra estimate. Using an event with a known seismic moment, moment estimates for subsequent events can be determined.

We feel this method of moment estimation provides better source size estimates for locally recorded earthquakes than S-wave coda duration. The method is being prepared for routine testing on data from the WRSN (Washington Regional Seismograph Network).

Kinematic Modeling:

Several aspects of the surface geology of the Pacific Northwest, such as volcanism and crustal deformation, are related to mantle flow associated with subduction. Along-arc variations in the geology require a three- dimensional analysis of convection. In order to make a three-dimensional flow calculation both tractable and interpretable, we consider the limiting case that the subducting slab is very thin, and that its viscosity far exceeds that of the surrounding crust and mantle. With these assumptions, we have developed a non-linear finite-element optimization scheme to find the slab configuration with the least amount of membrane (in-plane) deformation rate while satisfying boundary conditions such as the known relative plate convergence rates, and partial geometric constraints obtained from Wadati-Benioff earthquake locations. Because of a concave-oceanward bend in the trench axis located seaward of the Olympic Mountains, the subducted Cascadia slab has a geometric space problem analogous to a table cloth hanging over the corner of a table. This induces along-arc compression within the slab surface which can be relieved by forming an arch or by an along-arc buckling structure. Our numerical experiments suggest that the arch-like structure, revealed from seismic observations, is a natural consequence of the subducted slab responding to the concave-

oceanward bending of the trench. The locus of points where both the observed and theoretical slab dips are less than 10° is offshore everywhere except along the arch, beneath the Olympic Mountains. According to the Critical Taper Theory, the height of an accretionary wedge will grow landward until the slab dip exceeds about 10°. This provides a plausible explanation for the origin and geographic location of the Olympic Mountains accretionary prism. The concentration of seismicity beneath the Puget Sound area appears to be the result of bending the already arched slab. The computed deformation is dominated by N-S compression in the Puget Sound area and the peak compressional strain-rate is around $2\times10^{-16}s^{-1}$ which is comparable to the value estimated from seismic moment release rates of the last century. A manuscript describing the results will be submitted to JGR.

Like Cascadia, the trench off Alaska has concave-oceanward curvature. Given this geometry and the assumption that the slab is continuous, our calculations (Creager and Chiao, 1992) predict that the slab under central Alaska should have a shallow dip relative to the dip under the Aleutian Islands to the west and under the Wrangell Mountains to the east. Our models also predict along-arc compressive strain rates under Alaska and along-arc extensional strain rates under the central Aleutians. The observed subduction geometry and the orientations of seismic moment tensors are in close agreement with our models.

Preliminary Investigation of P multiples from Teleseisms

We are using teleseismic P waves incident on the subducted Juan de Fuca slab to investigate local dipping structure through multiple P reflections. The potential advantage of using this method for regional networks is that:

a) A single component vertical short period station can be used;

b) Vertical structure information can be obtained for a large number of network stations, allowing lateral variations in structure to be mapped; and

c) Signal stacking and other array processing techniques can be applied to leverage the structure information using large numbers of stations.

We first investigated the expected amplitudes of multiple reflections using standard ray tracing techniques. These results indicated that amplitudes were sufficient that stacking techniques could be used to increase the signal-to-noise ratio. However, because earthquakes have individual source-time functions the source signals must be deconvolved prior to stacking.

We found that source signals could be approximately estimated using network averaging, and each source was deconvolved using its average signal. We immediately found strong signal coherence in the deconvolved signals for similar source distances and back azimuths. We are currently working on modeling some particularly strong coherent phases on selected stations using dipping interface models.

Work is continuing on improving our methods of source estimation and deconvolution in order to reduce the "noise" in the deconvolved signals and improve the stacking results. In addition, we are continuing work on modeling identified phases.

Refraction Interpretation of Earthquake Travel Times

In an attempt to gain a better understanding of the crust and upper mantle transition across the Cascade Range, we are using techniques of refraction interpretation with earthquakes as sources. We have constructed a profile from the central Puget Sound region southwest of Seattle to a point near Walla Walla in eastern Washington. There are a number of moderate sized earthquakes along the profile and near each of its ends, which can be well located with network stations. We are using these events as "sources" by assuming their locations are known, but allowing their origin times to float to minimize residuals. The advantage of earthquakes over man-made sources is that sources located at depth provide more information on velocities at depth. This advantage is at least partially offset by the uncertainties of the source locations and origin time.

Our analysis is being done using the forward and inverse modeling program developed by Colin Zelt. Both reflections and refractions can be utilized with this method. Preliminary results suggest that we will be able to produce an improved model of the Cascadia transition structure.

Articles

Chiao, L.-Y., and K. C. Creager (in preparation) Geometry and lateral membrane rate of the subducting Cascadia slab, to be submitted to JGR

Dewberry, S.R. and R.S. Crosson, (in preparation), Source scaling and moment estimation for the Washington Regional Seismograph Network using coda amplitudes, to be submitted to BSSA.

Lees, J.M. and R.S. Crosson, (1991), Bayesian ART versus conjugate gradient methods in tomographic seismic imaging: An application at Mount St. Helens, Washington, in *Spatial Statistics and Imaging*, A. Possolo, editor, Inst. of Math. Statistics, Hayward, CA, V. 20, p. 186-208.

Ma, L., R.S. Crosson, and R.S. Ludwin, 1991, Focal Mechanisms of western Washington earthquakes and their relationship to regional tectonic stress, USGS Open File OF-91-441-D, will also be published in a USGS Professional Paper.

Ma, L., R.S. Crosson, and R.S. Ludwin, (submitted), Focal Mechanisms of western Washington earthquakes and their relationship to regional tectonic stress, in: USGS Professional Paper "Assessing and Reducing Earthquake Hazards in the Pacific Northwest")

Mundal, I., M. Ukawa, and R.S. Crosson, (in press), Normal and anomalous P phases from local earthquakes, and slab structure of the Cascadia Subduction zone, BSSA

VanDecar, J.C., R.S. Crosson and K.C. Creager, (in preparation), Travel-time inversion for subduction zone structure: I. The effect of three-dimensional ray tracing on resolution analysis, to be submitted to JGR.

Abstracts

Carroll, D. C., and K. C. Creager, 1992. Mapping seismic discontinuities under central Alaska by stacking receiver functions, Seismol. Res. Lett.,V. 63, p. 36.

Creager, K. C. and L.-Y. Chiao, 1992, Membrane Deformation Rate and Geometry of Aleutian-Alaska Subduction, Wadati Conference on Great Subduction Earthquakes, Geophysical Institute, University of Alaska, Fairbanks, Alaska.

Creager, K.C. and Chaio, L.Y, 1992, Relationships among surface geology, seismicity, and three-dimensional models of Cascadia Slab Flow, GSA 88th Annual Cordilleran Section, 1992 Abstracts with Programs, V. 24(5), p. 17.

Crosson, R.S. and R.S. Ludwin, 1992 (Invited), Cascadia Subduction Zone: Constraints on slab structure from seismic observations, GSA 88th Annual Cordilleran Section, 1992 Abstracts with Programs, V. 24(5), p. 18.

Crosson, R.S., and J.C. VanDecar, 1992, Cascadia Subduction Zone: Large scale structure from receiver function analysis, seismicity, and teleseismic arrival time tomography, Wadati Conference on Great Subduction Earthquakes, Geophysical Institute, University of Alaska, Fairbanks, Alaska.

Dewberry, S.R. and R.S. Crosson, 1992, Source scaling and moments for the Washington Regional Seismic Network data using coda amplitudes, Seism. Res. Lett., V. 60, p. 71-72.

VanDecar, J.C., R.S. Crosson, and K.C. Creager, (in press), Teleseismic travel-time inversion for Cascadia subduction zone structure employing three-dimensional ray tracing (extended abstract), presented at the XXII General Assembly, European Seismological Commission, Barcelona, Spain, Fall, 1990.

Seismic Potential of Major Offshore Faults in the Santa Monica and San Pedro Basins

Agreement No. 1434-92-G-2167

James K. Crouch
J.K. Crouch & Associates, Inc.
3463 State St., Suite 282
Santa Barbara, CA 93105

(805) 967-2892

Introduction:

During the past 20 years, numerous small (M_L = 2.5-4.9) earthquakes and three moderate-sized (M_L = 5.0-5.9) earthquakes have occurred within or along the margins of the Santa Monica and San Pedro basin, offshore southern California (e.g., Hauksson and Saldivar, 1989; Hauksson, 1990). In addition, the epicenter of the 1930 Santa Monica (M_L = 5.2) earthquake has been relocated to a position along the shelf, several kilometers south of Malibu (Hauksson and Saldivar, 1986), and a 1912 M_L = 5.0 event is inferred to have occurred offshore, about 20 kilometers due west of Point Dume (Davis et al., 1989). The mainshock-aftershock sequences of the three more recent of these moderate-sized events (i.e., the 1973 Pt. Mugu and the 1979, 1989 Malibu earthquakes) are dominated by reverse focal mechanisms. These events, as well as the earlier 1912 and 1930 events, have all been associated with either the Anacapa-Dume or Santa Monica faults that extend offshore along the northern margin of the Santa Monica basin (Yerkes and Lee, 1979; Hauksson and Saldivar, 1986, 1989; Davis et al., 1989). These structures are known to be predominantly reverse faults that generally strike east-west and dip steeply to the north. The offshore location of these faults, however, is based upon a limited number of high-resolution, relatively shallow-penetration, single-channel seismic-reflection profiles (e.g., Junger and Wagner, 1977). Hence, along much of their length, the locations and down-dip directions of these, as well as other major faults within this offshore region are largely inferred and only in limited places, has their surface or near surface trace been imaged. Moreover, because the known mainshock hypocenters of the moderate-sized events occurred at depths of 12.1 to 13.8 km and the aftershocks occurred at depths that generally range from 9 to 16 km (Hauksson and Saldivar, 1989; Hauksson, 1990), significant extrapolation is required in order to correlate these events to offshore faults that have only been mapped at or near the sea-floor.

Investigations:

The primary focus of this investigation is to more precisely determine the location and character of major structures in the offshore Santa Monica and San Pedro basins by augmenting the existing U.S.G.S. high-resolution grid with an 860 km grid of more closely-spaced, deeper penetration (5.0 sec.), migrated, CDP seismic-reflection data shot by industry. This information is, in turn, being used to improve correlations between well-located offshore earthquakes and their causitive faults. Additional investigations include: 1) determinations of the tectonic framework and history of this offshore region, 2) estimates of the nature, timing, and

amount of offset on major faults along with the history of associated folds, and 3) estimates of the length and segmentation (if any) of major faults. The objective of this investigation is to improve our understanding of the seismic potential of major active faults in the offshore Santa Monica and San Pedro basins and thereby, improve estimates of the seismic risk that these structures pose to nearby coastal communities.

Results:

Within the offshore Santa Monica and San Pedro basins there are three mapped faults or fault zones that can be categorized as active, major, and a potential seismic risk to nearby coastal communities. These faults include: 1) the west-trending Dume fault (also referred to as the Anacapa-Dume fault), which chiefly follows the base of the slope along the northern margin of the Santa Monica basin, but crosses the Malibu-Santa Monica shelf where it appears to merge with (or connect to) the offshore extension of the Santa Monica fault zone, 2) the relatively straight, northwest-trending San Pedro basin fault, which bisects the long axis of the basin, and 3) the Palos Verdes fault, which crosses the Palos Verdes Hills onshore and extends offshore, both northwestward across the Santa Monica shelf and southeastward across the San Pedro shelf (e.g., Junger and Wagner, 1977). In addition to these well-kown major faults that extend to or near the sea-floor, more recent interpretations of the geometry and kinematics of the upper crust (0-20 km) using retrodefomable cross sections strongly suggest that a number of concealed (blind), seismogenic thrusts, thrust ramps, backthrusts, and a subhorizontal regional detachment probably exist at depth, beneath the central and marginal parts of the offshore Santa Monica and San Pedro basins (e.g., Davis et al., 1989; Namson and Davis, 1991).

Although the available CDP data in the offshore Santa Monica and San Pedro basins were collected and processed to 5.0 seconds, the relatively deep, low-angle thrust faults are not imaged and the planes of previously mapped major faults are generally only interpretable to depths of <3 km below the seafloor. Large anticlines or anticlinoria associated with (overlying) these faults, however, generally extend to or near the seafloor and these structures are well-imaged to subsea depths as great as 5 km. These are chiefly fault-bend and fault-propagation folds, and detailed mapping of their geometry, axes, and lengths is leading to improved constraints on both mapped reverse faults and concealed low-angle thrust faults. More importantly, this information is providing better control for the correlation of well-located earthquake hypocenters to causitive faults within the offshore Santa Monica and San Pedro basins.

Our work is also leading to proposed revisions in previously reported correlations between earthquakes located offshore and causitive faults, and to new estimates of the seismic activity and potential of specific faults in this offshore region. For example, the 1979 Malibu (M_L = 5.0) mainshock-aftershock sequence has previously been correlated to an inferred eastern extension of the north-dipping Anacapa-Dume fault (Hauksson and Saldivar, 1986), and more recently, to the north-dipping Elysian Park thrust (Davis et al., 1989; Hauksson and Saldivar, 1989). The Elysian Park thrust is interpreted to be responsible for the development and uplift of the Santa Monica Mountains anticlinorium, and it is also interpreted to be the source of the 1987 Whittier Narrows (M_L = 5.9) earthquake, as well as a number of other moderate-sized events that have occurred along the Santa Monica uplift zone (Davis et al., 1989). Detailed mapping of the offshore with CDP data, however, suggest that neither the Elysian Park thrust nor the Anacapa-Dume fault are the causitive source of the 1979 Malibu event. According to our study, the relocated epicenter of the 1979 Malibu mainshock and the tightly clustered

aftershocks epicenters (Hauksson and Saldivar, 1986) are respectively 5 km and 2-7 km south of the surface trace of the north-dipping Anacapa-Dume fault.

Because the 1979 Malibu mainshock occurred at a depth of 12.2 km and the mainshock-aftershock sequence define a west-northwest-trending hypocentral zone at depths ranging chiefly from 10-15 km (Hauksson and Saldivar, 1989), the Elysian Park thrust (Davis et al., 1989) would seem to be a more likey candidate for this event. However, the north-dipping nodal plane for the 1979 Malibu event, favored by Hauksson and Saldivar (1986,1989) and Hauksson (1990), dips 55 to 60 degrees to the north, whereas the geometric constraints of the Elysian Park thrust suggest that, along its entire length, this fault dips to the north at angles that are probably no greater than about 25 degrees (see Davis et al., 1989; Namson and Davis, 1991).

Structural mapping with CDP data in the offshore suggests that the 1979 Malibu earthquake most likely occurred on a blind, south-dipping, backthrust that underlies the northernmost end of the Palos Verdes anticlinorium (i.e., an extension of fault A interpreted and depicted in Davis et al., 1989 and Namson and Davis, 1991). Although the Palos Verdes anticlinorium is deeply incised by several cross cutting submarine canyons, and is mantled by numerous small amplitude and several large amplitude folds, the principal axial trend of this large northwest-trending structure can be tracked with a fair degree of confidence. It extends over a distance of about 80 km, from the southernmost end of the San Pedro shelf (near Lasuen Knoll) across the Palos Verdes Hills and Santa Monica shelf projection and into the Santa Monica Bay where it finally terminates. The epicentral locations of the 1979 Malibu earthquake sequence cluster around the northernmost axial trace of the Palos Verdes anticlinorium, where it plunges and appears to die out beneath the Santa Monica Bay. Moreover, the alternative nodal plane determined for the 1979 Malibu earthquake by Hauksson and Saldivar (1986), which dips between 30 to 38 degrees to the south and strikes between 100 and 120 degrees, corresponds reasonably well with the inferred dip of the backthrust (fault A) and the strike of the overlying Palos Verdes anticlinorium. The 1989 Malibu (M_L =5.0) earthquake, which occurred about 6.5 km to the southeast of the 1979 event and had very similar characteristics (Hauksson, 1990), most likely was a result of rupture on fault A as well. Finally several slightly smaller (M_L = 4.0-4.5) south-dipping thrust earthquakes that occurred in 1982, 1984, and 1988 (Hauksson, 1990) also appear to be associated with fault A. Two of these occurred at the southern terminus of the Palos Verdes anticlinorium and one occurred on the slope seaward of the San Pedro shelf; all occurred at depths that range from 9.3-11.7 km (Hauksson, 1990).

The 1979, 1989 Malibu events, together with these three events and numerous smaller thrust events (see Hauksson, 1990), strongly suggest that fault A may pose a much greater seismic risk than the mapped surficial faults along the northeast flank of the Santa Monica and San Pedro basins (e.g., the Palos Verdes fault). Assuming that fault A is 80 km long (the length of the overlying Palos Verdes anticlinorium) and, as interpreted by Davis et al. (1989), 11 km wide, this thrust ramp could potentially have a rupture area of 880 km^2 and could potentially generate a rather destructive event, on the order of M = 6.8.

References Cited:

Davis, T.L., Namson, J., and Yerkes, R.F., 1989, A cross section of the Los Angeles area: Seismically active fold and thrust belt, the 1987 Whittier Narrows earthquake, and earthquake hazard, J. Geophys. Res., vol.94, p.9644-9664.

Hauksson, E., 1990, Earthquakes, faulting, and stress in the Los Ageles basin. J. Geophys. Res., vol.95, p.15365-15394.

Hauksson, E., and Saldivar, G.V., 1986, The 1930 Santa Monica and 1979 Malibu, California, earthquakes, Bull. Seismol. Soc. Am., vol.76, p.1542-1559.

Hauksson, E., and Saldivar, G.V., 1989, Seismicity and active compressional tectonics in Santa Monica Bay, southern California, J. Geophys. Res. vol.94, p.9591-9606.

Junger, A., and Wagner, H.C., 1977, Geology of the Santa Monica and San Pedro basins, California Continental Borderland, scale 1:250,000, U.S. Geol. Surv. Misc. Field Stud. Map, MF-820, 5 sheets, 1 pamphlet.

Namson, J., and Davis, T.L., 1991, Late Cenozoic thrust ramps of California, Final Report to the Southern California Earthquake Center, 26p., 18 Figs.

Yerkes, R.F., and Lee, W.H.K., 1979, Maps showing faults and fault activity and epicenters, focal depths and focal mechanisms for 1970-1975 earthquakes, western Transverse Ranges, California, U.S. Geol. Surv. Misc. Field Studies Map, MF-1032.

Reports:

Crouch, J.K., and Suppe, J., in press, Neogene tectonic evolution of the Los Angeles basin and inner borderland: a model for core complex-like crustal extension, submitted to the Geol. Soc. Am Bull.

Using High-Accuracy VLBI to Improve Estimates of the Vertical from GPS

Agreement No. 1434-92-G-2170

James L. Davis
Harvard-Smithsonian Center for Astrophysics
60 Garden St., MS 42
Cambridge, Massachusetts 02138
617-496-7640

Arthur E. Niell
Haystack Observatory
Massachusetts Institute of Technology
Westford, Massachusetts 01886
508-692-4764

Investigations

(1) Improvements in the model for the atmospheric propagation delay in order to improve estimates of site position obtained from space geodetic data.
(2) Comparison of a series of estimates of site position obtained independently from Global Positioning System (GPS) data and from very long baseline interferometry (VLBI) data.

Results

We have investigated numerically the effects of stochastic atmospheric refractive index fluctuations on the estimates of gradient parameters obtained from GPS, VLBI, and WVR data. We have found that significant differences in estimated parameters can be obtained, even when no gradient is present, due to the different spatial and temporal sampling of each technique. Since the second investigation involves comparison of data and results from the two geodetic techniques, an algorithm for comparison of the estimated parameters needs to be developed.

We have analyzed GPS and VLBI data obtained at the times of the NASA VLBI "R & D" experiments. The GPS data were all obtained from Rogue receivers and processed at JPL using the GIPSY analysis software. The VLBI data were processed at the CfA using the SOLVK analysis software. As a preliminary step, we have compared all the length estimates from the common baselines for the experiments performed during January–August 1992. (Length estimates are insensitive to differences in the reference frames used by each analysis group.) For these experiments, there were three common baselines: Fairbanks–Kauai (4,728 km), Fairbanks-Wettzell (6,857 km), and Kauai–Wettzell (10,358 km). No effort was made to "tie" the GPS and VLBI reference

points together at each site. For each series of estimates for a given baseline, we formed residuals of the estimated lengths around a best-fit straight line constrained to change at a rate obtained from a VLBI "global solution." The fits were performed independently for the GPS estimates and for the VLBI estimates.

The results are given in Figure 1 for each of the three baselines. The plots are presented as residual length obtained from VLBI vs. residual length obtained from GPS. For each set of estimates, the value of the weighted correlation coefficient is given. The weighted correlation coefficients range (in absolute value) from 0.07 to 0.94. The high correlation was obtained on the Kauai-Wettzell baseline, and it indicates that over 90% of the scatter of the length vs. time results could be explained by scatter which is common to both the VLBI and GPS length estimates. If we use the residuals in the VLBI estimates to "correct" the GPS estimates, we obtain a reduced χ^2 of 0.1. The probability of this occurring due solely to random error is less than 2.5%. This result could indicate that both the VLBI and the GPS results are dominated by a common error, e.g., atmosphere. It will be interesting to see if this correlation continues to hold as more data are obtained. Our goal is to use such correlations to isolate and eliminate errors in both techniques.

Acknowledgements

The analysis of the VLBI data was performed in part by Pan Rongshi at the Harvard-Smithsonian Center for Astrophysics. The analysis of the GPS data was performed by M. Heflin and G. Blewitt at the Jet Propulsion Lab.

Publications and Reports

Davis, J.L., G. Elgered, A.E. Niell, and I.I. Shapiro, Horizontal gradients in the "wet" atmospheric propagation delay, to appear in Proceedings of the Symposium on the Refraction of Transatmospheric Signals in Geodesy, Netherlands Geodetic Commission, The Hague, May 19–22, 1992.

Davis, J.L., The effect of turbulence on atmospheric gradient parameters determined from ground-based radiometric and space geodetic measurements, *Geophys. Res. Lett.*, *19*, 2183–2186, 1992.

Ronghsi, P., J.L. Davis, A.E. Niell, M.B. Heflin, G. Blewitt, A comparison of VLBI and GPS estimates for long baselines, paper delivered at the 1992 Fall AGU Meeting, San Francisco, December 7–11, 1992.

Davis, J.L., G. Elgered, A.E. Niell, C.E. Kuehn, Ground-based measurements of gradients in the "wet" radio refractive index of air, submitted to *Radio Science*, 1992.

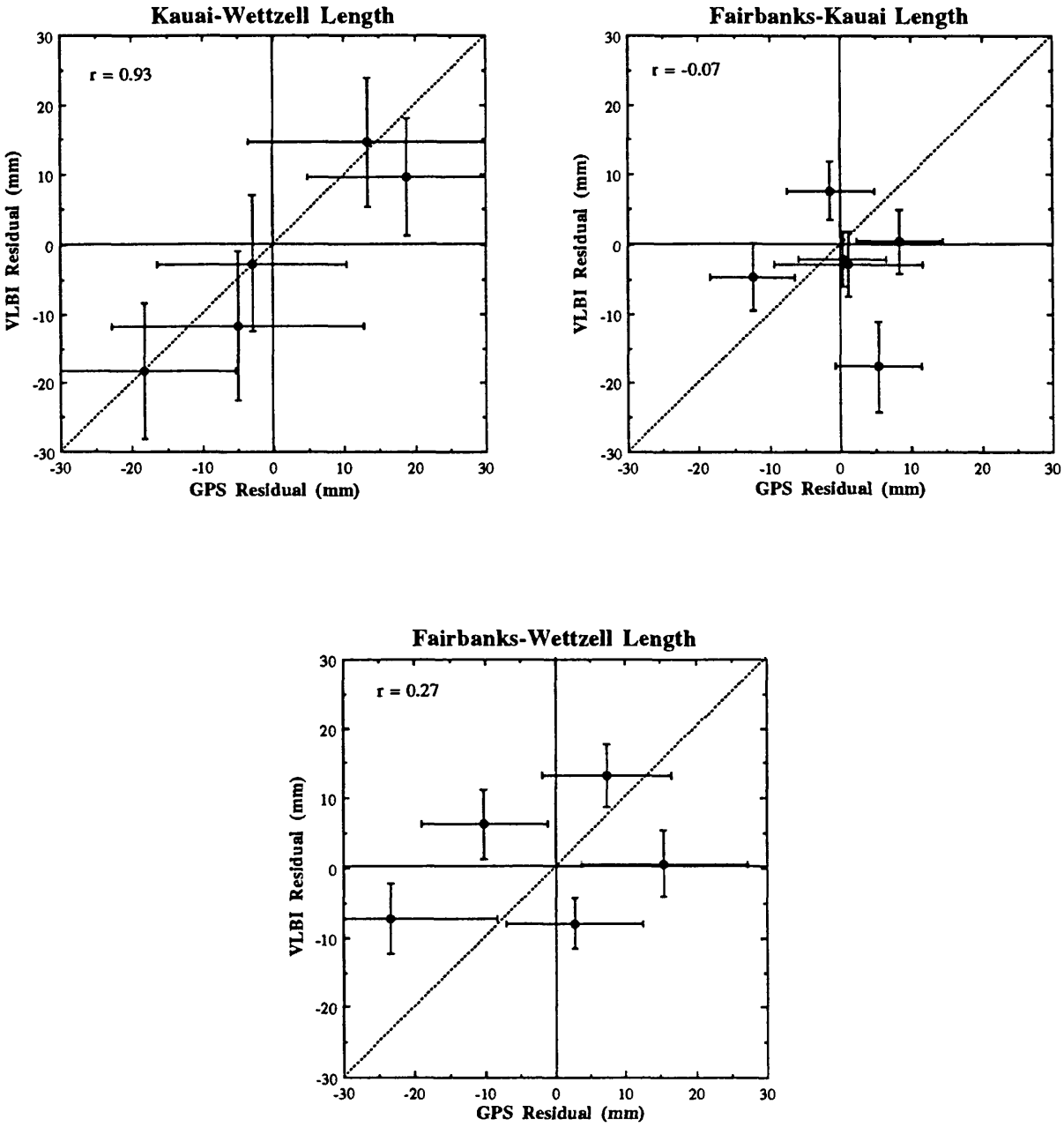

Figure 1. Plots of GPS vs. VLBI residual length (see text). Values of the weighted correlation coefficient are shown.

Reanalysis of Instrumentally Recorded United States Earthquakes

9920–10122

J. W. Dewey
and
William Spence
Branch of Global Seismology and Geomagnetism
U.S. Geological Survey
Denver Federal Center
Box 25046, Mail Stop 967
Denver, CO 80225
(303) 273–8419

Investigations

1. Describe the seismicity before and after the M_W 8.7, 1957 Aleutian arc earthquake to better understand the earthquake cycle in subduction zones. This major undertaking also will answer numerous questions concerning the size and probable rupture characteristics of this important earthquake (William Spence with extra-project colleagues T. Boyd and E. R. Engdahl).

2. Interpret the seismicity before and after the M_S 7.8, 1974 Peru earthquake to clarify the nature of subduction at this complex convergence zone (William Spence with extra-project colleague C. J. Langer).

3. Study the stress-loading process responsible for great thrust earthquakes (i.e., catastrophic slip between subducting and overriding plates at coupled subduction zones), with emphasis on understanding the relationship between seismicity patterns seaward of the trench and regional stress fields associated with the rupture of plate-coupling asperities (Steve Mueller and W. Spence with extra-project colleague G. Choy).

4. Quantify the compressional stress seaward of the asperity that controlled the M_S, 1985 Valparaiso, Chile, earthquake, and quantify the compressional stress seaward of the Shumagin seismic gap in the Aleutian arc (S. Mueller and W. Spence with extra-project colleague G. Choy).

5. Relocate epicenters, recompute magnitudes, and evaluate the tectonic implications of teleseismically recorded earthquakes from Yellowstone Park, Wyoming, and adjacent Montana and Idaho, including shocks associated with the Hebgen Lake earthquake (M_S 7.5) of August 1959 (J. W. Dewey).

Results

1. Magnitudes and relocations have been determined for nearly 7,000 earthquakes in the region of the great 1957 Aleutian arc earthquake for the period 1950–present. The catalog for the 1957 aftershocks is complete above magnitude 5.5.

2. The October 3, 1974, Peru earthquake filled a major seismic gap. Aftershocks were recorded by a temporary seismic network deployed within a week of the main shock. C. Langer and Spence have determined focal mechanisms for aftershock clusters and have relocated all aftershocks using the joint hypocenter determination (JHD) method. Focal mechanisms for aftershocks located at the shallow-dipping interface between the Nazca and overriding plates indicate continued underthrusting of the Nazca plate. Focal mechanisms for earthquakes downdip of the shallow-dipping interface indicate right-lateral, strike-slip motion on planes approximately parallel to the local plate convergence direction. This subsidiary deformation may be due to rebound of the overriding plate, as these earthquakes are associated with the location of greatest displacement during the main shock (as based on recent modeling by S. Hartzell and C. Langer).

3. It has been proposed that compressional seismicity within the outer rise complex indicates the presence of a substantial compressional stress field and, thus, and imminent great thrust earthquake near the trench axis. The modeling of Mueller, Spence, and Choy indicates that such a relationship cannot be universal. Compressional events within the subducting plate may occur in the complete absence of a compressional regional stress field, either during "unbending" of the inelastic lithosphere or the relaxation of a tensional stress field. Such a conclusion is supported by the fact that, worldwide, only 4 out of 30 hitherto identified compressional outer-rise events have actually been followed by great thrust earthquakes. Mueller et al. have developed a simple method that may allow innocuous (i.e., non-precursory) compressional outer-rise events to be distinguished from similar events that are potentially ominous.

4. Yield envelopes, which characterize lithospheric strength as a function of depth and loading history, have been used to infer the stress origin of the 20 km-deep M_S 7.2, 1981 reverse-fault earthquake that occurred at the Chilean outer trench wall. This earthquake is shown to result from stress concentration at the interplate asperity that ruptured in the M_S 7.5 Valparaiso underthrust earthquake, rather than being due to bending of the subducting Nazca plate.

5. J. Dewey completed reanalysis of 250 teleseismically recorded earthquakes that occurred in the Yellowstone/Hebgen Lake area in 1947–1989. The earthquakes were relocated with respect to calibration events recorded in the period 1973–1981 by a local network of stations run by A. M. Pitt (USGS, Menlo Park).

The relocated epicenter of the Hebgen Lake main shock of August 18, 1959 (M = 7.5 is at or near the east edge of the zone of surface faulting associated with the shock, at the margin of the zone of maximum subsidence and near the edge of the geodetically inferred fault plane. The location of the point of nucleation on the margins of, rather than within, the site of maximum moment release is consistent with observations that have recently been made on a number of large earthquakes for which accurate hypocenters and moment-release maps are available.

The zone of early aftershocks to the 1959 earthquake corresponds quite closely to the region of most intense activity in the decades following 1959. Early aftershocks occurred in a broad zone that trends west from the Norris Geyser Basin through the Hebgen Lake region to the southern Gravelly Range, Montana; most later activity has occurred in the same zone, though, with passing years, there has been a tendency for more activity to occur at greater distances outside of the 1959 aftershock zone. Dewey currently favors the hypothesis that the correspondence of later activity with the 1959 aftershock zone is due to the later activity having been part of the transient response of the Earth's crust to the 1959 earthquake.

Reports

Boyd, T.M., Engdahl, E.R., and Spence, W., 1992, Analysis of seismicity associated with a seismic cycle along the Aleutian arc—1957 through 1989 [abs.]: Wadati Conference on Great Subduction Earthquakes, Fairbanks, p. 43–50.

Dewey, J.W., and Suarez, G., 1991, Seismicity of Middle America, in Slemmons, D.B., Engdahl, E.R., Zoback, M.D., and Blackwell, D., eds., Neotectonics of North America: Boulder, Colorado, The Geological Society of America, DMV–1, p. 309–321.

Mueller, S., Choy, G.L., and Spence, W., 1992, Regional stress seaward of subduction zone asperities: Nature (submitted).

Spence, W., Herrmann, R.B., Johnston, A.C., and Reagor, G., 1992, Responses to Iben Browning's prediction of a 1990 New Madrid, Missouri, earthquake: U.S. Geological Survey Circular 1083, approximately 300 p. (in press).

Seismic Studies of Fault Mechanics

9930-02101

William L. Ellsworth
David A. Castillo, Alex Cole, and Lynn Dietz

Branch of Seismology
U.S. Geological Survey
345 Middlefield Road - MS 977
Menlo Park, California 94025
415-329-4784

Investigations

1. Analysis of preshocks, mainshock, and aftershocks of the 1989 Loma Prieta earthquake.
2. Temporal variations in wave propagation associated with the 1989 Loma Prieta earthquake.
3. Seismotectonics of the San Andreas fault system in northern California.
4. Earthquake monitoring along the Hayward fault.
5. Prototype rapid earthquake notification system for the San Francisco Bay Area.

Results

1. The standard approach to the imaging of the earthquake source solves an inverse problem in which far-field velocities (or displacements) are linearly related to the space-time distribution of slip acceleration (or velocity) on the fault through the de Hoop-Knopoff representation theorem. I am developing a complementary procedure for recovering some aspects of the rupture process that relies solely upon forward operations on the data. The basic idea is to stack the observed seismograms, with correction for the source radiation pattern, at each point of interest in the focal region to form a space/time image of the rupture. Stacking the data in this manner is equivalent to pre-multiplying the representation theorem convolution of the source time history and Green's functions with the transpose of the travel time delay operator. The stack adds coherently when the fault is radiating, as each unknown Green's function will be in phase. When no radiation is occurring at the image point, the stacked seismograms will tend to cancel due to incoherence between the Green's functions from station to station. Thus, the method works best at frequencies where the Green's functions may be considered a stochastic process. In this case, the stack will have a Gaussian distribution at times when no seismic radiation is taking place, and signal detection can be based upon their *a priori* probability of occurrence. The method is particularly well suited for use with clipped (sign bit) data. In this case, the phase but not absolute amplitude of slip acceleration (or velocity) can be determined. The computational efficency of the method make both detailed 2-D and 3-D sampling of the source volume practical.

   Application of the method to 256 heavily clipped short-period, vertical component Calnet seismograms ($1 \leq \Delta \leq 500$ km) of the 1989 Lake Elsman (M 5) and Loma Prieta (M 7) earthquakes yields detailed images of rupture nucleation and growth in the 1-10 Hz frequency band. The former is a simple rupture with a duration of about 0.8 s. In contrast,

the Loma Prieta earthquake begins with at least three acceleration pulses in the first 1.6 s ("the foreshock"), before the rupture begins to propagate away from the initial hypocentral region at a velocity of 3 km/s.

2. We use pairs of nearly identical earthquakes (doublets) to search for changes in high frequency wave propagation through the Earth's crust in the vicinity of the 1989 Loma Prieta, California earthquake, with a moving window cross-correlation technique capable of detecting traveltime changes of less than 2 msec. We analyze 36 events from 21 individual source zones, recorded during the interval 1979-1991. We find a strong change in traveltime for time windows containing the early shear wave coda for all doublets that span the Loma Prieta mainshock. The direct shear wave arrival time, however, is stable to within 1-2 msec. In each case, and for all stations that show an anomaly, traveltimes were greater after the Loma Prieta mainshock than they were before it. Time shifts exceed 35 ms at some stations, which amounts to a 0.3% path-averaged velocity change. The region of reduced velocity coincides with the aftershock zone of the earthquake, and has very sharp boundaries, particularly on its northeast side. Doublets occurring after the mainshock indicate that velocity has not recovered in the post-seismic period. Shear wave arrival times measured in the pre-seismic interval, from ten years to 4 days before the mainshock, varied by no more than 0.05%. Seismograms for pre-event doublets recorded at stations near the earthquake weakly display decreasing traveltimes in the coda, suggestive of an increasing shear wave velocity. It remains to be demonstrated, however, that this pre-seismic change has a precursory relationship to the Loma Prieta earthquake.

   We are also examining the hypothesis that temporal changes in shear wave attenuation are related to large earthquakes through the study of pairs of nearly identical earthquakes (doublets) located in the vicinity of the M_w 6.9 1989 Loma Prieta, California earthquake. The high coherency of waveforms for the doublets make them an ideal tool for searching for changes in seismic wave amplitude. By forming the spectral ratio of short windows of seismogram for each station observing the doublet, we can measure amplitudes with a precision of about 10% over a 1 Hz bandwidth from 1-15 Hz. Multiple samples of each pair of seismograms, obtained by moving the analysis window along the trace from the S-wave arrival into the coda, permit us to determine the change in coda Q (δQ_c) in multiple frequency bands and with a precision of about 5%. The measurement of δQ_c obtained in this way differs in some respects from Aki's method for determining Q_c, since our measurements utilize the near-shear wave coda waves out to about twice the shear wave traveltime, in contrast to beginning the measurement at twice the shear wave traveltime.

   Our Results indicate that Q_c is very stable over the time interval from 1978-1991. Doublets which span in time the occurence of the Loma Prieta earthquake display no evidence for systematic temporal or spatial variations in Q_c ($\pm$5%). These results are in sharp contrast to the large and systematic reduction in path-averaged shear wave velocity (0.3%) caused by the earthquake we have found using cross-spectral timing of the same doublet seismograms.

3. Focal mechanisms of earthquakes occuring along the northernmost and relatively youthful members of the San Andreas fault system between Point Arena and Cape Mendocino show that strike slip motion predominates both on and off of the major faults. by the San Andreas fault to the west and the Bartlett Springs fault to the east. The San Andreas fault north of Point Arena has been virtually aseismic in recent decades. In contrast, dense clusters of microearthquakes locate along . Seismicity at the northern ends of these faults zones terminates above the southern edge of the subducted Gorda Plate. Mechanisms from the Maacama and Bartlett Springs faults are dominated by right-lateral fault planes that dip 60°-80° to the northeast, rather than along vertical faults which is the norm along more mature faults within the San Andreas fault system. Although the San Andreas is virtually aseismic in this region, there are a few events located near enough to it to be on the fault, given location uncertainties, and these events have vertical nodal planes striking parallel to the fault. Focal mechanisms along and near the Maacama fault, and near the San Andreas were inverted separately to determine the orientation of the stress tensor. Both regions are in a strike slip regieme. The angle between the greates horizontal stress and the strike of the Maacama fault is 35°, suggesting a normal frictional strength for this fault. For the San Andreas fault, this angle is 60°, intermediate between high and low friction.

4. As part of the Bay Area Future Earthquakes Project, a new all-digital seismic network is being installed along the Hayward fault in the eastern San Francisco Bay region. This work is being done in cooperation with Malcolm Johnston and Paul Spudich (U.S.G.S.), and Tom McEvilly and Barbara Romanowicz (U.C. Berkeley). Downhole installation of sensors developed by Tom McEvilly at borehole strainmeter sites along the southern Hayward fault by Malcolm Johnston is now complete. Delivery of our digital field acquisition hardware and central site recording hardware has begun, and we anticipate conducting conducting acceptance tests of the hardware in early 1993.

5. A multi-year partnership has been formed between the U.S. Geological Survey and Pacific Gas and Electric Company for development and improvement of prototype rapid earthquake notification and response capabilities, initially focused on the greater San Francisco Bay region. Experience with recent California earthquakes illustrates the gap between earthquake occurrence and the delivery of accurate, appropriate seismological information to diverse private and public users. The goals of the partnership are to improve the seismological quantification of earthquakes, to speed the broadcast of this information, and to develop an increasing capability for recipients to wisely and rapidly use the notifications for knowledgeable and effective emergency response. The development strategy includes (1) maximizing the use of existing seismic resources (high-gain, short-period networks, real-time processors, broad-band and strong-motion stations); (2) integrating user requirements for information (location and severity) with scientific information (e.g., P-wave arrival times, spatial distribution of ground motion values); and (3) conducting an iterative development to assure balanced growth between user experience and acceptance, and increasingly rapid and sophisticated notification broadcasts.

Reports

Castillo, D.A., and Ellsworth, W.L., in press, Seismotectonics of the San Andreas fault system between Point Arena and Cape Mendocino in Northern California: implications for the development and evolution of a young transform: Journal of Geophysical Research, 45 p.

Ellsworth, W.L., and Heaton, T.H., 1992, Real-time analysis of earthquakes for early-warning and rapid post-event damage assessment: Proceedings Sensors Expo, Helmers Publishing, Inc. Peterborough, NH, p. 255-259.

Ellsworth, W.L., 1992, Imaging fault rupture without inversion (abs): Seismological Research Letters, v. 63, p. 73.

Verwoerd, M.C., Ellsworth, W.L., Cole, A.T., and Beroza, G.C., 1992, Changes in crustal wave propagation properties associated with the 1989 Loma Prieta, California earthquake: implications for coda-Q as and earthquake precursor and for the mechanism of stress-induced velocity changes (abs): Seismological Research Letters, v. 63, p. 71.

White, R.A., and Ellsworth, W.L., in press, Near-source short-to intermediate-period ground motions prior to the October 18, 1989 Loma Prieta M_S 7.1 earthquake: U.S. Geological Professional Paper on the Loma Prieta Earthquake, v. 1, 30 p.

Global Seismology

9920–70212

E. R. Engdahl
and
E. A. Bergman
Branch of Global Seismology and Geomagnetism
U.S. Geological Survey
Denver Federal Center
Box 25046, Mail Stop 967
Denver, CO 80225
(303) 273–8422

Investigations

1. **Travel-Time Tables.** Develop new standard global travel-time tables to locate earthquakes.

2. **Arrival-Time Data.** Coordinate planning for an International Seismological Observing Period (ISOP)—a time interval during which there would be enhanced reporting of arrival-time data.

3. **Earthquake Location in Island Arcs.** Develop practical methods to accurately locate earthquakes in island arcs.

4. **Subduction Zone Structure.** Develop techniques to invert seismic travel times simultaneously for earthquake locations and subduction zone structure.

Results

1. **Travel-Time Tables.** A major international effort within IASPEI over the last three years has led to the construction of two new global travel-time models for earthquake location and phase identification (iasp91, Kennett and Engdahl, 1991; and SP6, Morelli and Dziewonski, 1992). These radially stratified models have been constructed so that the travel times for the major seismic phases are consistent with the observations for events in the ISC Bulletin for 1964–1987. The baseline for the P-wave travel times in the iasp91 model has been adjusted to provide only a small bias in estimated origin time for independently constrained events at the main nuclear testing sites around the world. A set of algorithms has been developed (Buland and Chapman, 1983) that provides rapid calculations of the travel times of an arbitrary set of phases in these models for a specified source depth and epicentral distance.

Generally, differences in predicted travel times between the iasp91 and SP6 models are not significant—a few tenths of seconds. There are, however, certain classes of arrivals where the discrepancies are larger and the phase is important enough that the differences should be better understood. This presents a fundamental problem: exactly how lateral heterogeneity (and anisotropy) in the Earth's mantle and core contributes to the global variance in the teleseismic travel times of individual phases is not well understood. The differences between iasp91 and SP6 could therefore simply reflect the particular choices made in data selection and processing. It is quite possible that for many phases the global variance is large enough so that, for the current global data set, the two models are equally satisfactory.

To clarify these issues, a simple experiment is performed. First, a modified ISOP event-selection algorithm is applied to the ISC Catalog for 1964–1989. The selection algorithm has been designed so that selected earthquakes are not only rich in later phases, but also provide a relatively even global distribution of phase ray paths for the sampling of Earth structure. The selected events are then relocated in both models using P, pP and PKP arrivals to reduce errors in depth determination which are common for locations based solely on P-wave data. The relocation is performed for each model in an interactive manner and includes a re-identification of phases after each iteration. Since the upper and lower mantles in each model are virtually identical, the two models do not produce significantly different hypocentral parameters.

The emphasis in this work is to clarify the effects of lateral heterogeneity on the global travel times. Travel-time data for both P- and S-type phases are plotted globally over selected depth ranges to reveal effects produced by structure in different regions of the Earth. The plots clearly isolate systematics which are related to the lateral heterogeneity of the mantle. The data for direct P and S waves are surprisingly well correlated and illuminate features of the upper and lower mantle which are common to both data sets. Effects of lateral heterogeneity in the core are more problematic, as the travel times of core waves are seriously contaminated by lateral variations in the structure of the overlying mantle. Removal of these effects is a challenging problem that is now overcome only by using differential travel-time data for core phases.

2. **Arrival-Time Data.** Current seismological practice relies heavily on a complex, worldwide infrastructure, based on the efforts of thousands of people in over 100 countries, for the collection, processing, and dissemination of seismic data. Measurements reported by the existing global network of seismic observatories and compiled by agencies such as the National Earthquake Information Center (NEIC) and the International Seismological Center (ISC) have led to scientific discoveries of the first magnitude.

The accumulated observatory data continue to provide new information about earthquakes and Earth structure of fundamental importance to the Earth sciences. Yet progress toward the solution of a number of important problems in seismology is impeded largely by the lack of appropriate, globally distributed data sets. A set of important seismological problems are identified whose solutions require improvements of operational practice in the spirit of the ISOP. These problems include the detailed structure and lateral variations of major internal boundaries (e.g., the 400- and 650-km discontinuities and the core-mantle boundary), the need for improved resolution and wider sampling in tomographic studies of the Earth's three-dimensional structure, and the detection of small-scale structures deep in the Earth. Further progress on many of these problems will require the use of phases other than P. Such data are relatively scarce, not because they are weak phases, but because they are infrequently reported. The ISOP would be particularly effective in extending the sampling of later phases.

The current practice of most seismological agencies is to use the arrival times of short-period P waves to estimate earthquake origin times and hypocenters which are used in turn for such diverse purposes as analyzing seismic risk and studying Earth structure. Accurate locations are vital for many of these applications, yet it is well known that current procedures often lead to inaccurate and biased hypocenters especially in subduction zones. Additional problems may arise when inferences concerning source processes of larger earthquakes are made from the spatial and temporal offsets between the hypocentroid (point of initial rupture) and the source moment centroid, which is estimated independently from long-period waveform data. All of these problems suggest the use of phase information supplementary to P.

The enhanced reporting of times of first- and later-arriving, high-frequency seismic phases will be an important ISOP activity: first, because such data have a clear role to play in resolving important seismological issues, and, second, because the organizational structure planned for this purpose also supports a number of other ISOP initiatives which, in the long run, may have even greater significance to the Earth sciences.

Under the ISOP project, observatory personnel will receive training necessary to take advantage of the rapid spread of digital seismograph systems. The ISOP project can also serve as a stimulus for observatories to upgrade their instrumentation, communications links, and routine operations. The training and assistance which will be provided to participating seismologists and observatories represents a much-needed investment in the infrastructure of seismology, particularly in developing countries. The return on this investment will be counted in the form of a general enhancement of the quantity and quality of data available for global seismological studies of all types, in an increased capacity for seismologists in all countries to effectively monitor local seismic hazards, and in the cultivation of young seismologists of talent and energy.

3. **Earthquake Location in Island Arcs.** During the past 35 years, the central and eastern portions of the Aleutian Arc have been ruptured by two great earthquakes. The first, which occurred in March 1957 (M_W = 8.6), generated aftershocks along a 1200-km long segment of the arc, the largest length extent ever observed for an aftershock sequence. This event nucleated south of Amlia Island and ruptured bilaterally. The second occurred in May 1986. This smaller earthquake (M_W = 8.0) nucleated within a few tens of kilometers of the epicenter of the 1957 earthquake and re-ruptured a 250-km long portion of the arc. The short time span between the 1957 and 1986 earthquakes provides a unique opportunity to study a complete seismic cycle bounded by two instrumentally recorded, great earthquakes. In fact, it represents the only complete seismic cycle instrumentally observed along the Aleutian arc. Published and ongoing research activities have focused mainly on the final two thirds of this rupture cycle. To supplement our picture of the tectonic processes involved during the entire rupture cycle, to test recently proposed seismic hazard estimates, and to shed light on the connection between the seismic moment distributions observed for great earthquakes and the mechanical nature of the plate interface, a more fundamental understanding of the rupture characteristics of the 1957 earthquake and the nature of seismicity between the 1957 and 1986 earthquakes are needed.

   Seismicity recorded from 1957 through 1989 (March) with epicenters lying between 175° and 160° W have been relocated and cataloged. The relocations include epicenter-dependent, P-wave station corrections which account for near-source velocity structure. These corrections are calculated for 686 stations using a slab geometry detailed by a recent, teleseismic, travel-time study and the iasp91 travel-time model. Unless other information is available, source depths are constrained to 35 km. For events deeper than 50 km, stations corrections are not applied, and source depths are determined using both P and pP arrivals. Arrival times for earthquakes occurring between 1957 and 1963 are obtained by optically scanning of the ISS and BCIS bulletins. For this time period, magnitudes are available for only a small percentage of the relocated events. Magnitudes for as many of these events as possible are calculated using body- and surface-wave amplitudes recorded at Pasadena. For events recorded between 1964 and 1989, arrival times and magnitudes are obtained from the ISC phase tapes.

   The completed catalog consists of approximately 7,300 earthquakes. Dividing the geographical distribution of observing stations into four azimuthal zones (Europe and the Arctic, North and South America, Asia, and the South Pacific), the earthquakes are classified into one of four quality groups. Group A consists of events recorded by at least two stations in all four azimuthal zones. Group B consists of events recorded by at least two stations in three of the four azimuthal zones. Group C consists of events recorded by at least one station in three of the four azimuthal zones. Group D consists of all those events not meeting the requirements of groups A, B, or C. All events within groups A and B, 3,200, have 90 percent error vectors of less than 25 km. Catalog entries for earthquakes with groups A and B have been distributed on a CD–ROM.

The minimum magnitude of completeness for this catalog is determined by plotting the number of events per magnitude increment. For this comparison, all of the observed magnitudes are converted to M_S using a regression relationship derived from events for which both m_b and M_S are available. The log of the number of events per 0.2 M_S magnitude unit is plotted. The distribution of the events per incremental magnitude unit should be linear above the magnitude of completeness. Between 1964 and 1989, the catalog is complete above $M_S = 4.6$. From 1957 through 1963, the minimum magnitude of completeness is 5.5. To uniformly sample the seismic record over the entire time period of our catalog, only events larger than or equal to 5.5 can be used. Also, earthquakes whose magnitudes are above the level of completeness for each time period can be expected to be well located.

4. **Subduction Zone Structure.** Compressional body waves from earthquakes in the central part of the Tonga-Kermadec subduction zone arrive very early in New Zealand stations (Ansell and Gubbins, 1986), and the waveforms of these phases are often characterized by an emergent high-frequency precursor. Examples of these slab phases have been collected from short-period seismograms of SRO station SNZO in Wellington, and from Leeds' POMS array of nine 3-component broad-band seismometers in the Tararua Mountains, New Zealand.

   Gubbins and Snieder (1991) explained both the early arrivals and the body-wave dispersion by P-wave propagation through a high-velocity layer in the Tonga-Kermadec subduction zone. The absence, however, of detailed information about the morphology of the Tonga-Kermadec subduction zone prohibited the establishment of the relation between slab structure and observed waveforms.

   With the objective to further investigate the relation between the frequency characteristics of the digital seismograms and propagation through subducted slab, a tomographic study is performed to determine the morphology of the Tonga-Kermadec subduction zone. For the tomographic study, an approach similar to that described by Van der Hilst et al. (1991) is followed. The earthquakes are relocated in the iasp91 model for P- and S-wave velocities (Kennett and Engdahl, 1991) and computed travel-time residuals for P and pP phases relative to the iasp91 travel-time tables computed. In the linear inversion for aspherical Earth's structure, about 1,100,000 P and 35,000 pP data were used. By incorporating data of the pP phase, the sampling of shallow slab structure is improved, in particular below regions where only few seismological stations are located. New tomographic images depicting aspherical variations in P-wave velocity associated with the Tonga-Kermadec subduction zone are constructed.

Reports

Hwang, L.J., and Clayton, R.W., 1991, A station catalog of ISC arrivals—Seismic station histories and station residuals: U.S. Geological Survey Open-File Report 91–295, 3187 p.

Kennett, B.L.N., and Engdahl, E.R., 1991, Travel times for global earthquake location and phase identification: Geophysical Journal International, v. 105, p. 429–465.
Van der Hilst, R.D., and Engdahl, E.R., 1991, On the use of PP and pP data in delay time tomography: Geophysical Journal International, v. 106, p. 169–188.
Van der Hilst, R.D., Engdahl, E.R., Spakman, W., and Nolet, G., 1991, Tomographic imaging of subducted lithosphere below northwest Pacific island arcs: Nature, v. 353, p. 37-42.

Teleseismic Tomography of the Loma Prieta Region

Project 9930-01172

John R. Evans and H. M. Iyer
U.S. Geological Survey
Branch of Seismology
345 Middlefield Road, MS-977
Menlo Park, California 94025
415-329-4753

Investigations Undertaken

This Project is completing a teleseismic tomography study of the Loma Prieta region, using data we recorded late in 1990 in a large field experment. Data from this experiment also have been used by other Projects for local-earthquake tomography. This FY was consumed by extensive software development and the massive data-reduction process.

Early parts of FY 1992 also included an extended operational test of our PC-based trigger for teleseisms. Our aim was to ready the PC for assisting the capture of these events by CUSP. We successfully demonstrated the efficacy of this system for reliably capturing even very small teleseisms and for assisting with network maintenance and the capture of rare low-frequency local earthquakes known to occur beneath several parts of the network.

Results Obtained

Loma Prieta: Understanding the lower crust and upper mantle provides NEHRP with boundary conditions and structural information prerequisite to any master model of this transverse plate-boundary system. Understanding the detailed structure and state of the lower crust and upper mantle below the depths resolvable by local-earthquake tomography is necessary for understanding that fraction of the plate boundary that is responsible for earthquake hazards. Loma Prieta teleseismic tomography targets the source region of the 1989 earthquake to clarify the condition and location of the controlling plate boundary and to delineate the root structure of the imbricate thrust system bounding the Santa Clara Valley. This thrust system is now recognized as both a major, poorly understood structural feature and as a significant seismogenic zone in its own right.

We operated a 31-site portable seismograph network through December, 1990. This network augmented CalNet in the target region around Loma Prieta, forming nested oval shaped networks centered on the seismogenic zone. Three types of seismographs were used in this study, but most of the the data were recorded by the old "5-day" recorders. Digitizing and processing these data is very labor intensive and again consumed most of our efforts in FY92. At this writing, the data are 100% digitized and 50% analysed. Reaching this point has consumed about 2.5 person-years of effort. The USGS currently owns no other equipment suited to this type of work, and must rely on IRIS equipment for which NSF-funded projects take precedence. Three GEOS recorders tested at Loma Prieta recorded fewer than half the requisite events.

CUSP Teleseismic Triggering: In the first half of FY 1992 we performed an extended operational test of a PC-based trigger for teleseisms. CUSP routinely fails to capture most of these events; our aim was to use the PC as a specialized trigger to assist CUSP. We successfully demonstrated the efficacy of this system for reliably capturing even very small events while maintaining acceptable false-alarm rates. It is now clear that network telemetry glitches are a principal contributor of the false alarms that do occur. These glitches generally do not trigger CUSP, hence, the PC can assist technicians with identifying network trouble spots in addition to capturing teleseisms. Our PC teleseism effort was discontinued on Branch Chief orders, in lieu of planned changes directly to CUSP algorithms. No system is now in place for recording teleseisms reliably. Instead, we are investigating the efficacy of this system for capturing rare low-frequency events that occur in several parts of CalNet.

We have captured four of the five low-frequency events in the last six months at Mammoth Mountain, even recording a very small one missed in a scan by the best analyst the USGS has (Figure 1).

Reports Published

No reports were produced in FY92, excepting our contribution to W. H. K. Lee's Open-File Report of PC software. Most resources were applied to processing the largest teleseismic tomography data set yet collected by this Project, to software development, and to testing the PC teleseismic trigger system for CUSP. Data reduction was hampered seriously by Branch reassignment of a principal technician to other Projects.

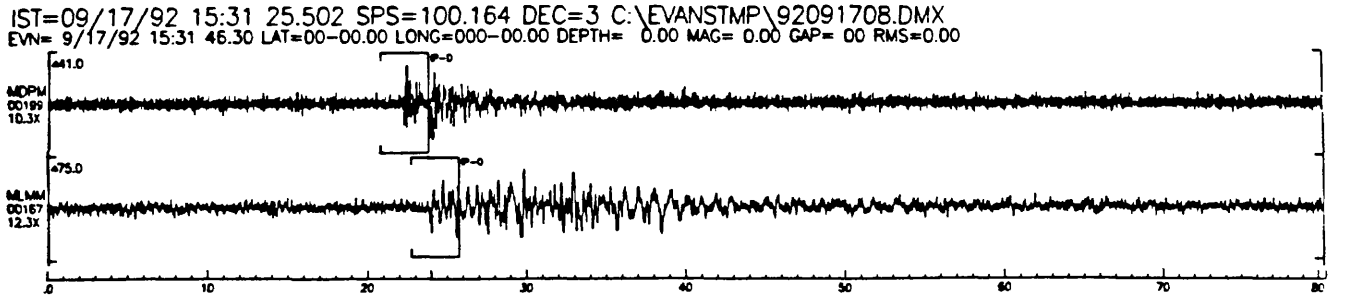

This low-frequency event occurred during a film change but triggered the PC successfully.

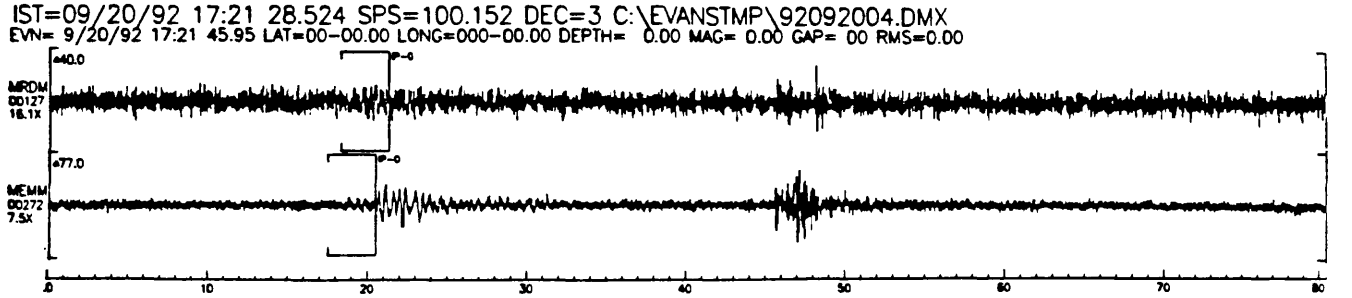

A very small low-frequency event missed by analyst.

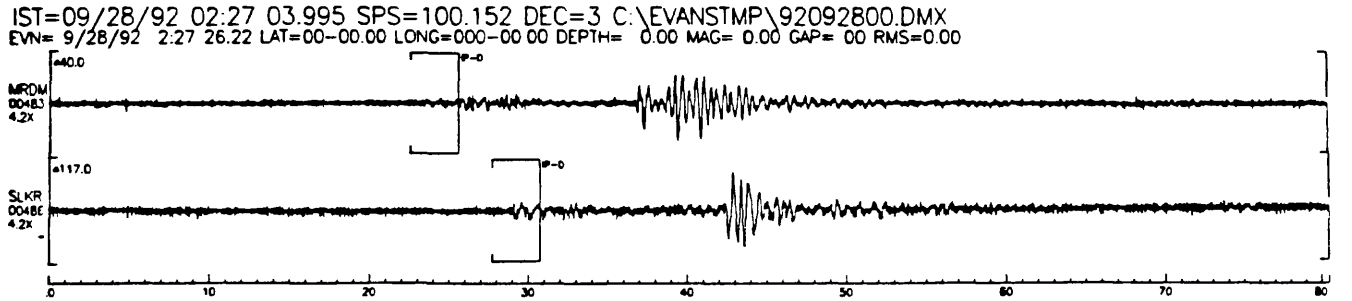

Both the analyst and the PC found this event pair.

PC missed a large low-frequency event at 09/28/92 03:12, probably disregarding it because of its modest high-frequency component. (The trigger attempts to discard high-frequency local earthquakes to avoid swamping the recording system.) The analyst found it easily; trigger parameters have been modified accordingly.

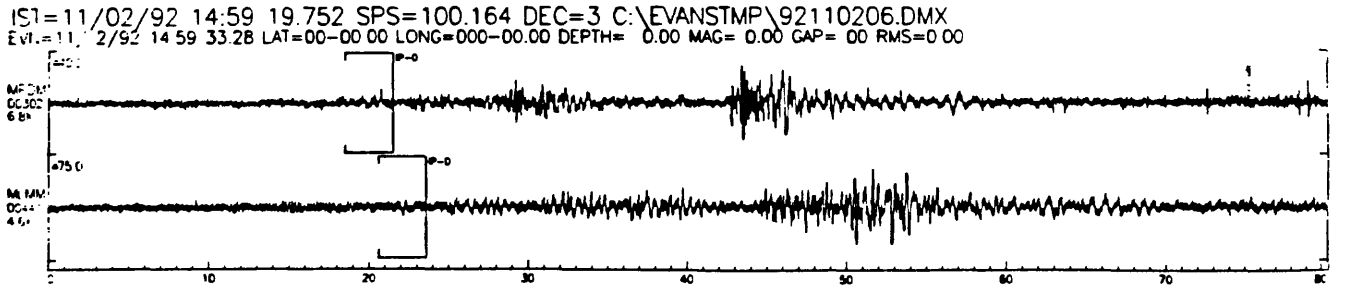

Both the analyst and the PC found this event.

Figure 1: Examples of the small low-frequency earthquakes occurring near Mammoth Mountain, east central California. These mid-crustal events are thought to be associated with the movement of magma.

THEODOLITE MEASUREMENTS OF CREEP RATES ON SAN FRANCISCO BAY REGION FAULTS

Grant Number 14 - 08 - 0001 - G1992

Jon S. Galehouse
Department of Geosciences
San Francisco State University
San Francisco, California 94132

(415) 338-1204

We began to measure creep (aseismic slip) rates on San Francisco Bay region active faults in September 1979. Over the past 13.2 years, we have made nearly 1300 creep measurements, with about 450 of these occurring in the three years following the Loma Prieta earthquake (LPEQ). Amount of slip is determined by noting changes in angles between sets of measurements taken across a fault at different times. This triangulation method uses a theodolite to measure the angle formed by three fixed points to the nearest tenth of a second of arc. Each day that a measurement set is done, the angle is measured 12 times and the average determined. The amount of slip between measurements can be calculated trigonometrically using the change in average angle. The precision of our measurement method is such that we can detect with confidence any movement more than 1-2 mm between successive measurement days.

We presently have measurement sites at 23 localities on active faults in the San Francisco Bay region (see Figure 1). We also have a measurement site on the San Andreas fault in the Point Arena area and one on the Maacama fault in Willits that do not appear on Figure 1. We remeasure most sites about once every two to three months. Most sites span a fault width of about 50-225 m, but a few must span a greater width because of site considerations. These distances are noted on Figures 2 through 5 as the IS (Instrument Station) to ES (End Station) distances. These figures also show the average rate of movement at each site as determined by the slope of the least-squares line which also appears on each of the graphs. The graphs also show the time of the 17 October 1989 LPEQ as a vertical line. The following is a brief fault-by-fault summary of our results through 30 November 1992.

SAN ANDREAS FAULT (see Figure 2) - We have been measuring horizontal slip on the San Andreas fault at Site 14 at the Point Reyes National Seashore Headquarters for 7.7 years and at Site 10 in South San Francisco for 12.7 years. Both sites have shown virtually no net slip and neither was affected by the LPEQ thus far.

In November 1989, we began measuring a USGS site (our Site 22) in Woodside that had not been remeasured for many years. Our results compared to unpublished USGS measurements in 1977 show that virtually no surface slip occurred between 16 February 1977 and 4 November 1989 and very little has occurred since. We also established in November 1989 Site 23 on the San Andreas fault near the

southeastern end of the LPEQ aftershock zone and northwest of San Juan Bautista. Very little slip has occurred at this site.

In July 1990, we established Site 25 on the San Andreas fault just southeast of San Juan Bautista and the aftershock zone. This site is on the central creeping portion of the fault and has been moving at a rate of 14.5 mm/yr for the past 2.2 years. This is considerably faster than the longer-term pre-LPEQ rate of about 7-8 mm/yr as determined by a USGS creepmeter at this site (Schulz, 1989).

Site 18 in the Point Arena area has averaged 1 mm/yr of right slip in the 11.1 years between 9 January 1981 and 31 January 1992.

In summary, the San Andreas fault at our measurement sites (18, 14, 10, 22, 23) along the previously locked portion of the fault both northwest and southeast of the LPEQ aftershock zone does not appear to have been affected by the LPEQ in the three years since October 1989. This portion of the San Andreas fault has remained virtually locked, with 1 mm/yr or less of creep occurring along it. In contrast, the post-LPEQ creep rate on the northern portion of the central creeping segment of the fault near San Juan Bautista is about twice the longer - term creepmeter average.

HAYWARD FAULT (see Figure 3) - We have been measuring horizontal slip at five sites along the Hayward fault for 12.2 to 13.2 years and have determined that the overall right-lateral creep rate is about 4.3 to 4.8 mm/yr. Although the creep characteristics (steady or episodic) differ from site to site, the overall rates are quite similar. A detailed discussion of the pre-LPEQ and post-LPEQ creep rates on the Hayward fault is in Galehouse (1993).

Since we began measuring Site 1 in Fremont in September 1979, the fault has moved rather episodically. Typical surface movement characteristics are relatively rapid right slip of about a cm over a few months time alternating with relatively slower slip over a period of two or more years. The fault at Site 1 was in one of the relatively slower phases of movement prior to the LPEQ and the slower phase has now persisted for about 4.5 years with virtually no net slip during this time. The creep rate before the LPEQ was 5.4 mm/yr but this present slow phase has brought the overall average down to 4.7 mm/yr for the past 13.2 years.

In February 1990 we established Site 24 on the Hayward fault on Camellia Drive in Fremont, about four km southeast of Site 1 (see Figure 1). Although relatively rapid creep had been reported for this site in recent years, we have measured virtually no creep at all. Perhaps the fault at this site moves episodically (similarly to nearby Site 1) and has been in a slower, dormant phase since we began measuring it 2.8 years ago.

Movement along the Hayward fault at Site 2 in Union City has been much more continuous and much less episodic than movement at Site 1. Site 2 has been moving at a fairly uniform rate of about 4.6 mm/yr for the 13.2 years since we began measurements in September 1979.

Extremely uniform movement characterizes Site 12 on D Street in Hayward. Two active traces of the Hayward fault occur here and their combined movement rate has been about 4.6 mm/yr for the 12.4 years since we began measurements in June 1980. Our nearby Site 13 on Rose Street in Hayward has a similar overall average rate of movement (4.8 mm/yr) since June 1980, but the movement is much more episodic than at Site 12.

In the 12.2 years since we began measurements in August 1980 in San Pablo (Site 17) near the northwesterly end of the Hayward fault, the overall average rate of

right slip (about 4.3 mm/yr) has been slightly slower, but similar to the overall rates at the other Hayward fault sites. However, superposed on the overall slip rate in San Pablo are changes between some measurement days of up to nearly a cm in either a right-lateral (more common) or left-lateral (less common) sense. This pattern was more pronounced between mid-1980 to mid-1986 and has been somewhat less pronounced since.

In summary, the creep rates on the Hayward fault from Union City to San Pablo are about the same as they were before the LPEQ. However, the southern portion of the fault in Fremont has shown virtually no post - LPEQ net slip.

CALAVERAS FAULT (see Figure 4) - We have been measuring horizontal slip at two sites on the Calaveras fault in the Hollister area for 13 years. Slip at both sites has been rather episodic with intervals of relatively rapid right slip typically lasting a couple months or less alternating with longer periods of time when little net slip occurs. The LPEQ occurred during an interval of slower movement that had persisted for about a year at Site 4. The earthquake apparently triggered up to 14 mm of right slip at Seventh Street (see Figure 4). Overall the rate of right slip is about 7.1 mm/yr for the past 13.1 years.

Slip at Site 6 along Wright Road just 2.3 km northwest of Site 4 is also episodic. The LPEQ occurred during an interval of slower movement that had persisted for about a year at Wright Road (similar to the situation at Seventh Street). The earthquake apparently triggered up to 12 mm of right slip. The overall rate of slip at Wright Road is about 11.0 mm/yr for the past 13.0 years. Except for our relatively new site (25) on the central creeping portion of the San Andreas fault, this rate is the fastest of any of our sites in the San Francisco Bay region. It is about 4 mm/yr faster than the rate at nearby Seventh Street. Either the creep rate decreases significantly from Wright Road southeast to Seventh Street or undetected surface movement is occurring outside our 89.7 m-long survey line at Seventh Street.

After the rapid slip triggered by the LPEQ, both sites in the Hollister area returned to a slower mode of movement which has now persisted for more than three years. At the present time, there appears to be a "slip deficit" of about 2 cm at Site 6. A more detailed discussion of the effect of the Loma Prieta earthquake on the Calaveras fault in the Hollister area was published in Geophysical Research Letters shortly after the quake (Galehouse ,1990). This paper also discusses the effect of the Morgan Hill earthquake in 1984. No immediate surface displacement had occurred at either of our Hollister area sites when they were measured the day after the Morgan Hill earthquake. However, within the following 2.5 months, both sites showed over a cm of right slip which was followed by a relatively long interval of slower slip (see Figure 4). A more detailed discussion of the longer-term effect of the LPEQ on the Calaveras fault is in Galehouse (1993).

In contrast to our sites in the Hollister area, Site 19 in San Ramon near the northwesterly terminus of the Calaveras fault was not affected by the LPEQ. It has remained virtually locked throughout our 12.0 years of measurements.

CONCORD - GREEN VALLEY FAULT (see Figure 5) - We began our measurements at Site 3 and Site 5 on the Concord fault in the City of Concord in September 1979. It appears that typical movement characteristics at both sites are intervals of relatively rapid right slip of about 7-10 mm over a period of a few months alternating with intervals of relatively slower right slip of about 1-2 mm/yr over a period

of several years. For the past 13 years, the overall average creep rate along the Concord fault in the City of Concord is about 3 mm/yr (3.4 at Site 3 and 2.6 at Site 5).

It appears that the LPEQ and the 1990 swarms of earthquakes near Alamo (between the southeastern end of the Concord fault and the northwestern end of the Calaveras fault) had little or no effect on the Concord fault at our measurement sites in the City of Concord.

We began measuring Site 20 on the Green Valley fault near Cordelia in June 1984. Large variations tend to occur at this site between measurement days, possibly because logistical considerations resulted in our survey line being particularly long (335.8 m). However, our results suggest that the Green Valley fault behaves similarly to the Concord fault i.e., relatively rapid right slip in a short period of time (months) alternating with relatively slower slip over a longer period of time (years). The Green Valley fault was in a period of relatively slower movement for the first 20 months of our measurements, averaging a few mm/yr of right slip. In early 1986, however, the fault slipped right-laterally more than a cm. This was followed by about three years in which the net slip was less than 1 mm/yr. Sometime after 6 August 1989, the Green Valley fault entered into another phase of relatively rapid right slip that totaled about 15 mm by 22 April 1990. For the past 2.5 years, there has been virtually no net slip on the Green Valley fault. The overall average rate of movement has been 5.3 mm/yr for the past 8.4 years.

Regarding the relationship between the Green Valley and Concord faults, the episodes of relatively rapid slip and relatively slower slip do occur at different times and the rate of slip is higher on the Green Valley fault. The episodic nature of the slip and the duration of the faster and slower intervals, however, are similar. Based on these similarities and the small step between their respective trends, we consider the Concord and Green Valley faults to be different names for the southeastern and northwestern segments of the same fault system.

RODGERS CREEK FAULT - We measured a site (16) on the Rodgers Creek fault in Santa Rosa from August 1980 until we had to abandon it for logistical reasons in January 1986. During these 5.4 years of measurements, no significant surface slip occurred and we concluded that the Rodgers Creek fault was not creeping at this site.

In September 1986, we established Site 21 on the Rodgers Creek fault near Penngrove (see Figure 1). The average at Site 21 is about 1-2 mm/yr for the past 6.1 years. Because variations of several mm tend to occur from one measurement day to another, it is difficult to know whether the Rodgers Creek fault is really creeping slowly or whether it is not moving much at all and our average rate at this point in time is due to the "noise" level at this particular measurement site. Perhaps the results will become less ambiguous as we continue our measurements over a longer period of time. The LPEQ does not appear to have had any effect on the Rodgers Creek fault at Site 21.

WEST NAPA FAULT - We began measurements at Site 15 in the City of Napa in July 1980. Similarly to the situation at Site 21 on the Rodgers Creek fault, there tends to be a lot of surface "noise" at this measurement site. However, the average rate of right slip on the West Napa fault over the past 12 years is only 0.4 mm/yr. In other words, the West Napa fault is virtually locked at the surface with no creep occurring. The LPEQ does not appear to have had any effect on our results for the West Napa fault.

SEAL COVE-SAN GREGORIO FAULT - We began measurements at Site 7 on the Seal Cove fault segment in Princeton in November 1979. The least-squares average indicates that virtually no creep has occurred at this site over the past 13 years. We began measuring Site 8 on the San Gregorio fault segment in May 1982. This site shows very large variations from one measurement day to another, probably due in part to the particularly long distance (452 m) between the IS and ES. The least-squares average shows no creep for the past 10.5 years. Therefore, the Seal Cove-San Gregorio fault is not presently creeping and the LPEQ does not appear to have had any noticeable effect on the rate of movement at either of our sites on this fault system.

ANTIOCH FAULT - We began measurements at Site 11 in the City of Antioch in May 1980. The average rate of movement has been virtually zero for the past 12.5 years. Site 9 just south of town showed 1.7 mm/yr for the 7.6 years from 21 November 1982 to 1 July 1990. New construction then destroyed our measurement array at this site. We have noted that much subsidence and mass movement creep occur both inside and outside the Antioch fault zone in the area of our two measurement sites and it is probable that these nontectonic movements are influencing our measurement results. If any tectonic creep is occurring along the Antioch fault, it is probably at a very low rate. The LPEQ does not appear to have had any noticeable effect at either of our sites on the Antioch fault.

MAACAMA FAULT - The Maacama fault extends from northern Sonoma County to north of Laytonville in Mendocino County and is the northwesterly continuation of the Hayward-Rodgers Creek fault trend. We began measurements at Site 26 in Willits in November 1991. Preliminary results over the past year indicate that the Maacama fault is creeping at about 5 mm/yr which is similar to the creep rate on the Hayward fault.

REFERENCES CITED

Galehouse, J.S., 1990, Effect of the Loma Prieta earthquake on surface slip along the Calaveras fault in the Hollister area: Geophysical Research Letters, v. 17, no. 8, p. 1219-1222.

Galehouse, J.S., 1993, Effect of the Loma Prieta earthquake on fault creep rates in the San Francisco Bay region: in U.S. Geological Survey Professional Paper (Postseismic Effects), in review.

Schulz, S.S., 1989, Catalog of creepmeter measurements in California from 1966 through 1988: U.S. Geological Survey Open-File Report 89-650, 193 p.

1992 PUBLICATIONS

Galehouse, J.S., 1992, Creep rates and creep characteristics on certain North and East Bay faults: 1979-1992: Program and Abstracts, Second Conference on Earthquake Hazards in the Eastern San Francisco Bay Area, p. 24.

Galehouse, J.S., 1992, Creep rates and creep characteristics of Eastern San Francisco Bay Area faults: 1979-1992: in Borchardt, G. and others, editors, Proceedings of the Second Conference on Earthquake Hazards in the Eastern San Francisco Bay Area, California Division of Mines and Geology Special Publication 113, in press.

Lienkaemper, J.J., Galehouse, J.S., and Simpson, R. W., 1992, Hayward fault, California: longterm creep rates versus slower creep since 1989 Loma Prieta earthquake: EOS, Transactions, American Geophysical Union, v. 73, no. 43, p. 119.

Galehouse, J.S., Sowma-Bawcom, J.A., and Prentice, C.S., 1992, The Maacama fault: preliminary creep and paleoseismic data, Mendocino County, California: EOS, Transactions, American Geophysical Union, v. 73, no. 43, p. 123.

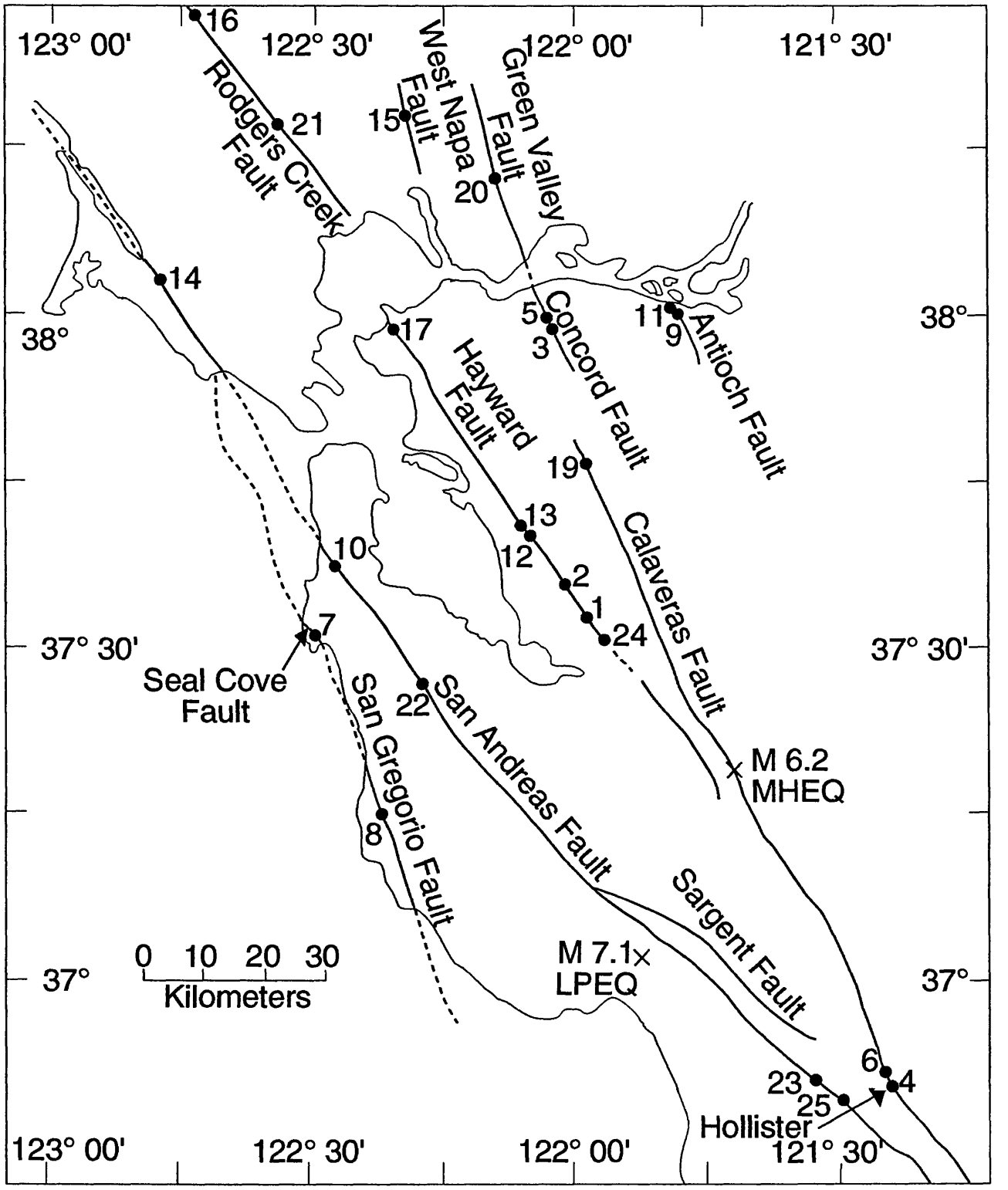

Figure 1. Numbered dots are San Francisco State University theodolite measurement sites.Epicenters and magnitudes are indicated for the 24 April 1984 Morgan Hill earthquake (MHEQ) and the 17 October 1989 Loma Prieta earthquake (LPEQ).

SAN ANDREAS FAULT

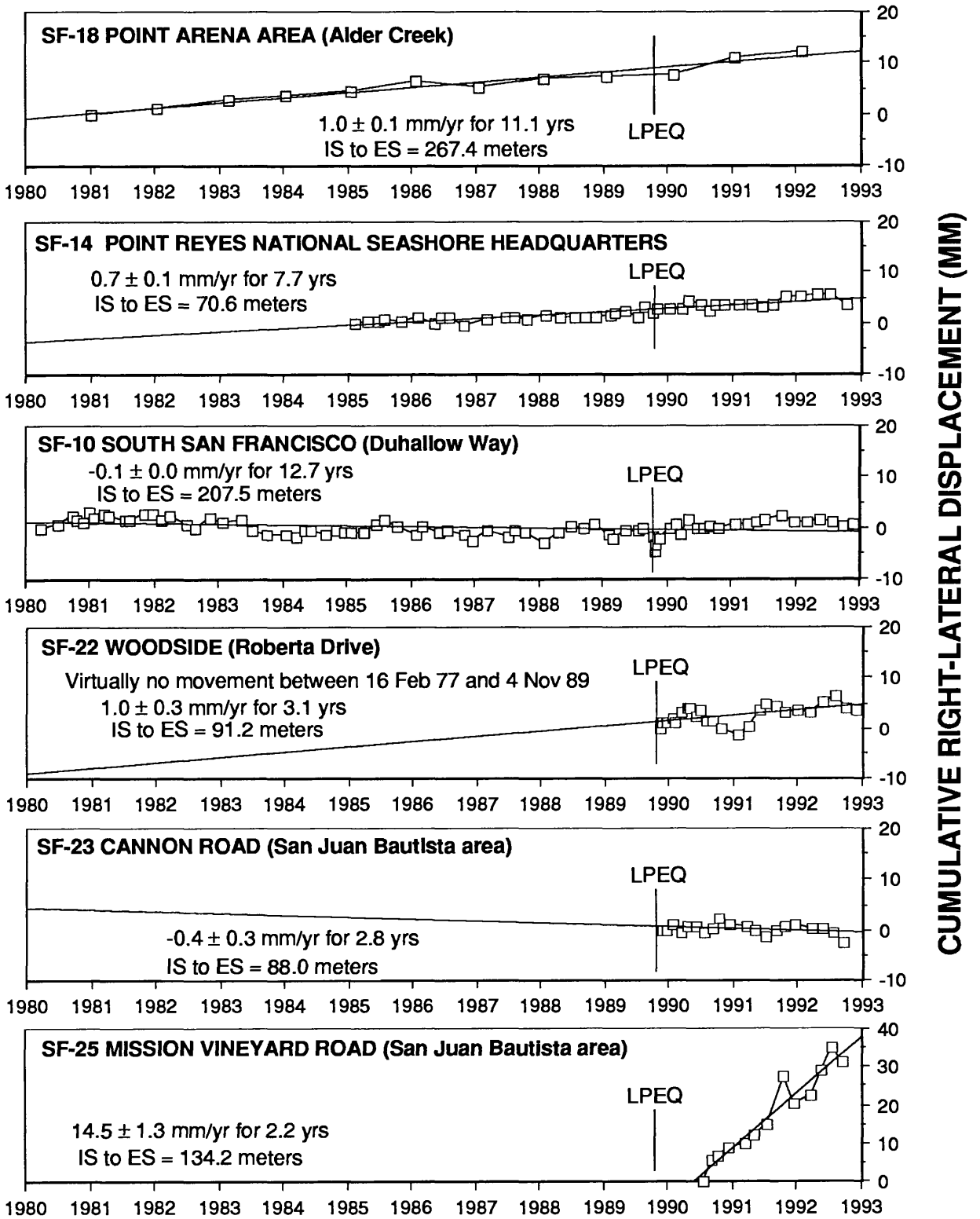

LPEQ = Loma Prieta Earthquake of 17 Oct 89

Figure 2. San Andreas Fault Displacement (1980 - 1992)

HAYWARD FAULT

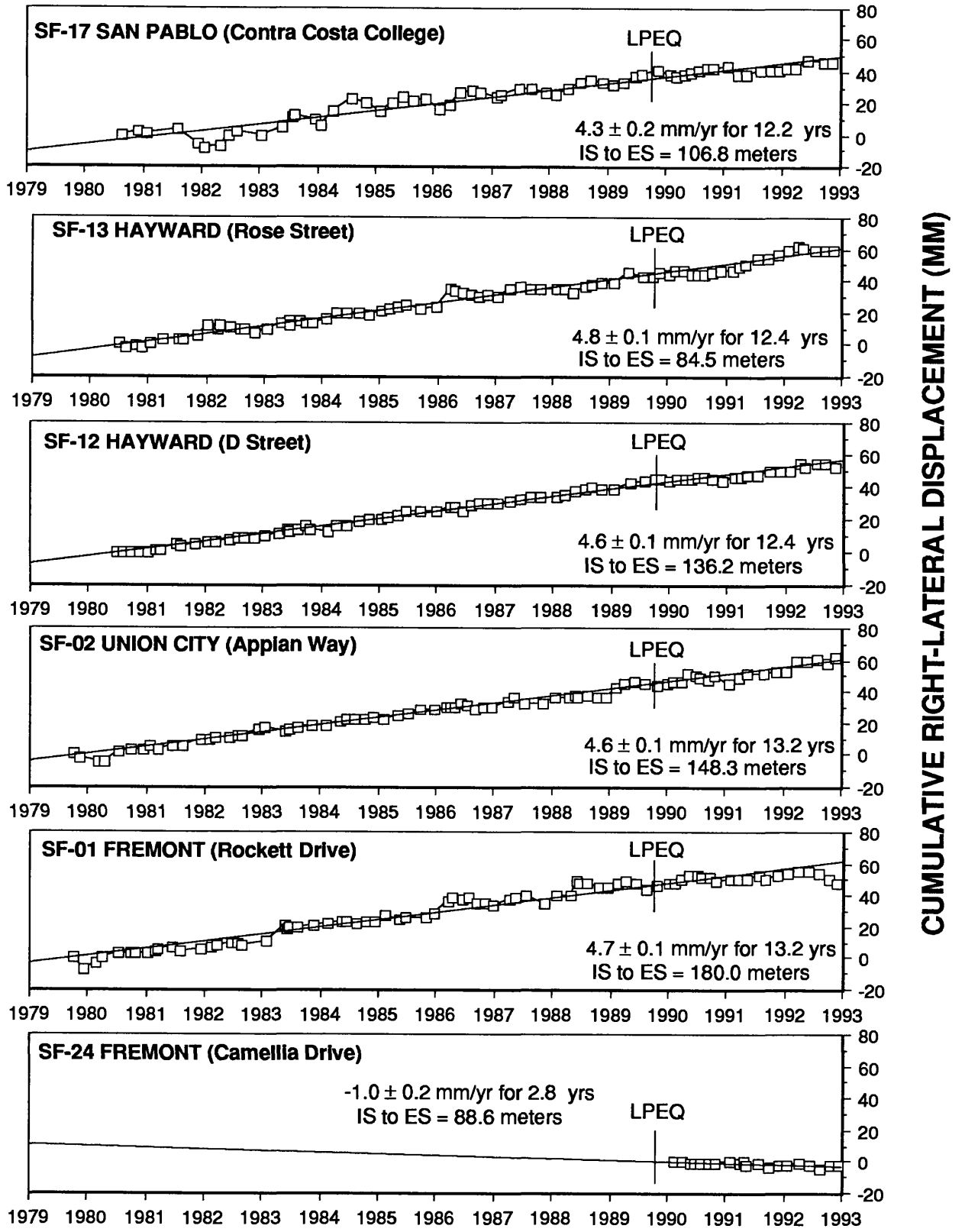

LPEQ = Loma Prieta Earthquake of 17 Oct 89

Figure 3. Hayward Fault Displacement (1979 - 1992)

CALAVERAS FAULT

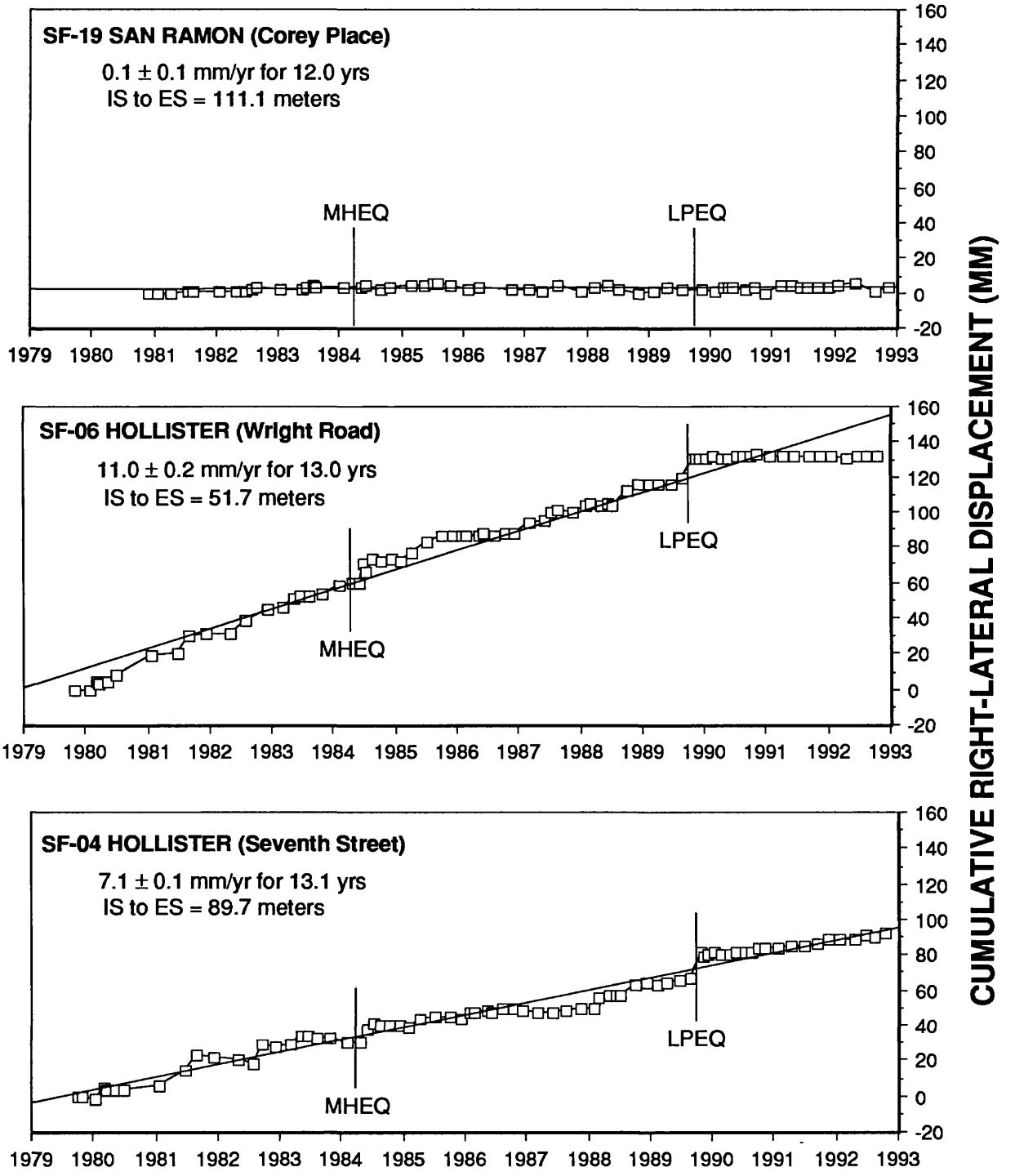

MHEQ = Morgan Hill Earthquake of 24 Apr 84
LPEQ = Loma Prieta Earthquake of 17 Oct 89

Figure 4. Calaveras Fault Displacement (1979 - 1992)

CONCORD - GREEN VALLEY FAULT

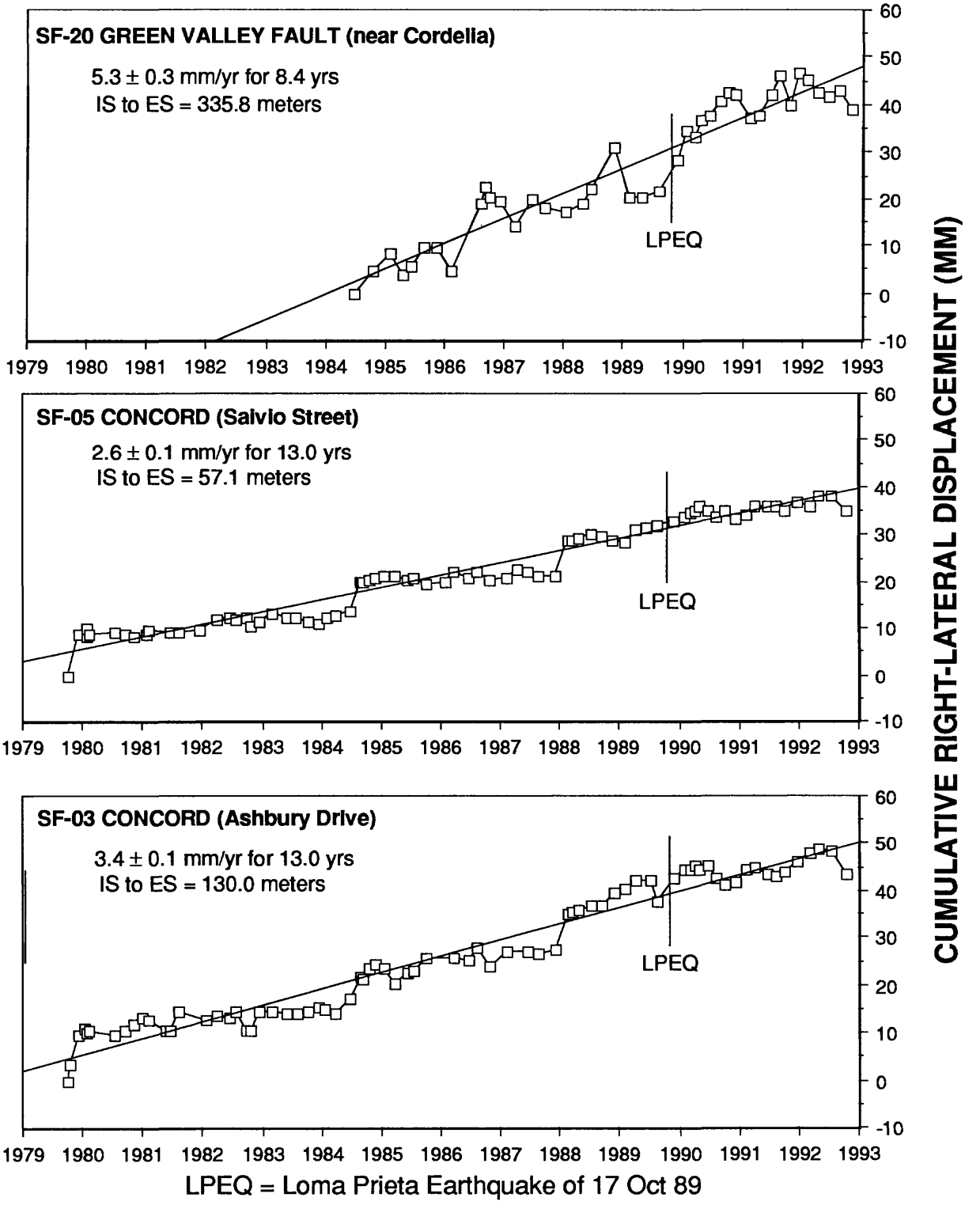

Figure 5. Concord - Green Valley Fault Displacement (1979 - 1992)

DEEP BOREHOLE PLANE STRAIN MONITORING
14-08-0001-G1812

Michael T Gladwin,

Department of Physics
University of Queensland
St.Lucia, 4067
AUSTRALIA.
ph. (+ 617) 3652473

ACTIVITIES

Two data processing procedures were refined further during 1992. Removal of dual exponentials (one of short time constant relating to grout cure effects and a long time constant exponential related to long term hole deformation processes) has been successfully implemented for data from the San Juan instrument. This procedure has been extended to the consideration of long term strain data from other U.S instruments, one at Pinon Flat (PFT) and three at Parkfield (EDT, FLT and DLT). Such a process is generally feasible, and yields residuals which give a much clearer picture of medium term strain anomalies present in the data. The tidal calibration procedure developed for analysis of the San Juan dataset has been extended to data from Parkfield (EDT and DLT), and will be used routinely in data reported from these sites. A paper detailing this calibration procedure is under preparation, in conjunction with D. Agnew and F. Wyatt from U.C.S.D., who are incorporating a comparison of tidal calibration of our Pinon Flat data with data from the laser strainmeter also located at that site.

The Pinon Flat instrument has registered strain steps associated with a number of earthquakes in that region during 1992. In particular strain steps coseismic with the Joshua Tree earthquake M_L 6.1 (April 23) and the Landers M_L 7.4 and Big Bear M_L 6.5 earthquakes (June 28) were inverted to determine most likely source dislocation parameters using seismically determined locations.

A detailed review of strain data from the three Parkfield instruments has been undertaken for inclusion in the special Parkfield review session of the Fall 1992 AGU. In particular coseismic steps associated with the M_L 4.7 Middle Mountain earthquake of 28 October, a series of strain steps correlated with nearby creepmeter events, a significant event common to both Eades and Donalee data during April 1989, and long term strain changes on all three instruments have all been investigated.

During November two further tensor strain instruments were installed as part of a borehole strain array situated in the vicinity of the Hayward fault east of San Francisco Bay. These instruments have been providing data (initially dominated by grout curing effects) since November 1, and data from these is now being processed as part of the routine processing of all U.S. instruments. Calibration of data from these two sites, one near Lake Chabot (CHT) and one in Garin State Park (GAT), will be conducted after some months of settling.

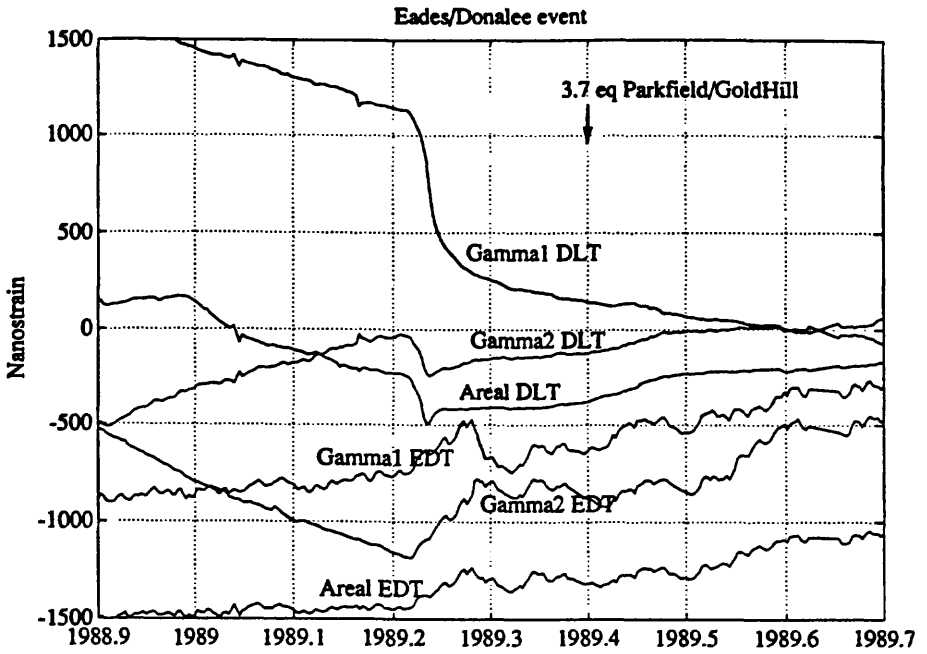

Figure 1. Detrended strain data from Eades and Donalee tensor strain instruments during 1989. The time of the M_L 3.7 earthquake is indicated.

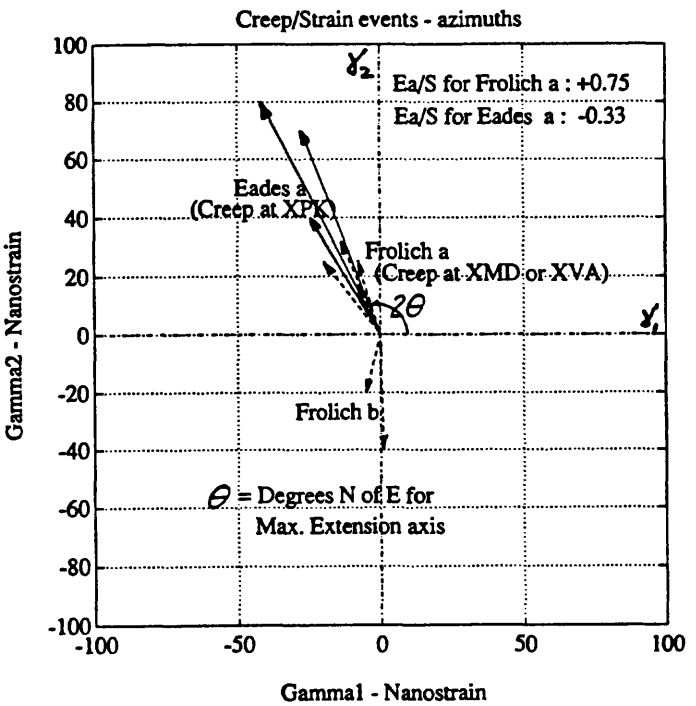

Figure 2. Plot of some representative strain steps during 1991-92 at Eades and Frolich. For each step, shear strain γ_1 is plotted against γ_2. The resulting vector has length corresponding to the size of the maximum shear strain, and orientation 2θ where θ = azimuth of the maximum extension axis north of east. Note the similarity of maximum shear and azimuth for the three groups Eades(a), Frolich(a) and Frolich(b).

RESULTS

Two papers were published during the year. In the first paper we analysed the continued shear strain anomaly in SJT data following the Loma Prieta earthquake, and proposed that the observed strain accumulation results from increased slip around a nearby locked section of the fault, this slip arising from loading by the failed Loma Prieta source region to the north. This model suggests an increased probability of a moderate earthquake near San Juan Bautista, and that interactions between fault regions are critical in earthquake processes. In the second paper, published jointly with A. Linde of D.T.M., Carnegie Inst. of Washington and M. Johnston of U.S.G.S., Menlo Park, we reported the absence of any changes in M_2 and O_1 tidal amplitudes precursory to the Loma Prieta earthquake, and estimated that any large scale changes in Young's modulus must have been less than about 2%. A further paper detailing investigation of episodic creep/strain events in the San Juan strain data over the period 1986-1992 has been completed in conjunction with K. Breckenridge of U.S.G.S, Menlo Park.

Strain steps observed in the Pinon Flat shear strain data were in broad agreement with those predicted from consideration of the seismically determined fault plane solution for the Joshua Tree Earthquake. Strain signals following the Landers earthquake in June indicated a large decay of order some hundreds of Nanostrain over a few days after the event, correlating with similar decays observed on co-located instruments such as the Pinon Flat laser strainmeter.

The anomaly present in the strain data from Eades and Donalee in April/May 1989 is shown in Figure 1. An anomaly in the same period was reported by S. Park (*J.G.R. 96(B9), pp14211-14237*) for resistivity measurements, and by E. Karageorgi (*B.S.S.A. 82(3), pp1388-1415*) in shear wave velocity. Preliminary investigation of a series of correlated creep/strain events during 1991-92 present mainly in the Eades and Frolich data indicates remarkably similar strain fields associated with the steps (see Figure 2), and suggests similar source regions.

Use of seismically determined source parameters for the M_L 4.7 earthquake near Middle Mountain on 28 October predicted strain steps in reasonable agreement with observed steps in all three tensor instruments, as shown below:

	Modelled *(Nanostrain)*			**Measured Dilatometer** *(Nanostrain)*	**Measured)) Tensor BCSM** *(Nanostrain)*		
Station	ε_a	γ_1	γ_2	ε_a	ε_a	γ_1	γ_2
DLT	+12	+15	-5	+9.5	+12 ±1	+12 ±1	-16 ±1
EDT	+10	+18	+2		+5 ±1	+20 ±1	+13 ±1
FLT	-5	+15	-1.5	-18.0	-10 ±5	+10 ±5	+1 ±5

Analysis of long-term data indicates no excursions in shear strain likely to be precursive to the expected M_L 6 earthquake, however the 5 year baseline of data will

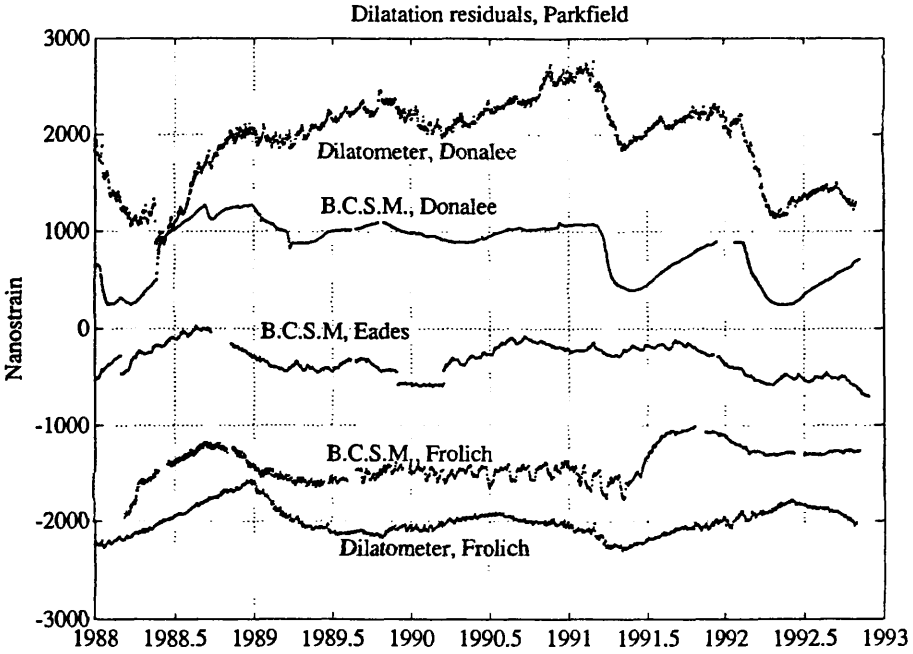

Figure 3. Long term dilatation at Frolich and Donalee and Eades as measured by tensor strain meters and by dilatometers (long term exponentials have removed from data).

provide a reliable determination of strain changes associated with an event of such magnitude. Comparison of long term dilation strains measured by the tensor instruments at Frolich and Donalee with dilatometer data from colocated instruments suggests an overall correspondence in the resulting data (see Figure 3) and provides strong evidence of consistency in the measurement of borehole strain by the two types of instrument.

RELEVANT PUBLICATIONS

Gladwin, M. T., High Precision multi component borehole deformation monitoring. *Rev.Sci.Instrum., 55*, 2011-2016, 1984.

Gladwin, M.T., Gwyther, R., Hart, R., Francis, M., and Johnston, M.J.S., Borehole Tensor Strain Measurements in California. *J. Geophys. Res. 92.* B8 pp7981-7988, 1987.

Gladwin, M. T. and Hart, R. Design Parameters for Borehole Strain Instrumentation. *Pageoph.,123,* 59-88, 1985.

Gladwin, M. T. and Wolfe, J. Linearity of Capacitance Displacement Transducers. *J.Sc.Instr. 46,* 1099-1100, 1975.

Johnston, M.J.S., Gladwin, M.T., and Linde, A.T. Preseismic Failure and Moderate Earthquakes. *I.A.S.P.E.I.* , Tokyo, August 19-30, S7-65, 35 , 1985.

Johnston, M. J. S., Linde, A.T., Gladwin, M.T., and Borcherdt, R.D. Fault Failure with Moderate Earthquakes. *Tectonophysics.* 144, 189-206, 1987.

Gladwin, M. T., Hart, R., and Gwyther, R. L. Continuous Deformation Measurements prior to the Loma Prieta Earthquake. *EOS, (Trans. Am. G. Un.) 71,* p 1461, 1990

Gwyther, R. L., Gladwin, M.T. and Hart, R.H.G., A Shear Strain Anomaly Following the Loma Prieta Earthquake. *Nature 356,* 142-144, 1992.

Linde, A.T., Gladwin, M.T. and Johnston, M.J.S. The loma Prieta Earthquake, 1989 and Earth Strain Tidal Amplitudes: An Unsuccessful search for Associated Changes. *Geo. Res. Lett., 19(3),* 317-320, 1992.

Gladwin, M.T., Gwyther, R.L., Higbie, J.W. and Hart, R.G., A Medium Term Precursor to the Loma Prieta Earthquake? *Geo. Res. Let. 18* #8 pp 1377-1380, 1991.

Gladwin, M. T., Breckenridge, K.S., Hart, R., and Gwyther, R. L. Recent Accelaration of Characteristic Creep-Strain Events at San Juan Bautista. *EOS, (Trans. Am. G. Un.) 72* p 484, 1991.

Gladwin, M.T., Borehole Strain Arrays: Insights from Parkfield, *EOS, (Trans. Am. G. Un.) 73* p 407, 1992.

Gwyther, R. L., Gladwin, M.T. and Hart, R., Interpretation of Continued Shear strain anomalies of the Loma Prieta Earthquake. *EOS, (Trans. Am. G. Un.) 72* p 310, 1991.

Seismicity and Crustal Structure in an Active Collisional Orogen, Central Asia

14-08-0001-G1802

Michael W. Hamburger, Gary L. Pavlis,
Haydar J. Al-Shukri, Emmanuel G. Ramos
Department of Geological Sciences, Indiana University
Bloomington, Indiana 47405
(812) 855-2934

Terry L. Pavlis
Department of Geology and Geophysics
University of New Orleans
New Orleans, Louisiana 70148
(504) 286-6797

Investigations

This program focuses on the highly active seismic zone between the Pamir and Tien Shan mountain belts in Soviet Central Asia. The Garm region is located directly atop the collisional boundary between the Indian and Eurasian plates, and is associated with a dense concentration of both shallow and intermediate-depth earthquakes. The fundamental aims of this collaborative research project with the Russian Academy of Sciences include: (1) elucidation of the structures and processes involved in active deformation of a complex collisional plate boundary, and (2) examination of the temporal variations in seismicity near Garm, in the form of changing spatial, depth, and stress distribution of microearthquakes that precede larger events. The seismological data base for this study includes the combined resources of the global, regional, and local seismic networks. Geological structures in the Garm region have been studied using compilation of published geological information, analysis of satellite imagery, and geological field work in the Peter the First, Gissar, and Darvaz mountain ranges near Garm.

Results

Geological Structure. The outbreak of a civil war in Tadjikistan during the late spring of 1992 led to cancellation of our plans for the 1992 field season. That work is now planned for 1993 if the political conflinct is resolved, but if hostilities continue we anticipate moving our field effort to the neighboring republic of Kyrgyzstan, where structures similar to the Garm region are exposed. In the absence of a field season in 1992 we concentrated our effort on the completion of a 1:100,000 scale geologic map and cross-sections for the Garm region. This effort and an accompanying manuscript are nearing completion and should be submitted for publication by early 1993. The map was produced by a combination of: 1) photo interpretation of two SPOT satellite images acquired in 1991, and 2) a compilation of our field observations together with those of Dr. V. Schevchenko who assisted us in the compilation during a visit to New Orleans in April 1992. Two major conclusions have arisen from this effort.

First, the present day structure of the Peter the First Range (Figure 1) is dominated by dextral transpression. This conclusion is indicated by both seismicity data [Ramos *et al.*, 1991; Ramos, 1992] and surface geology [Pavlis *et al.*, 1992]. The geological manifestations that support this conclusion include: 1) a system of south-vergent thrusts along the axis of the Peter the First Range that are both very young and form an *en echelon* array suggestive of dextral slip; 2) the general structure and topography of the Peter the First Range have all the characteristics of a classic "positive flower structure" with a prominent north and south-vergent thrust system forming an *en echelon* array centered on a topographic high.

Second, the present deformation front appears to be an erosionally controlled system, along which thrust systems are actively overriding a Quaternary surface generated by stream erosion. This conclusion is indicated primarily by the observation that throughout the Garm region, the present deformation front is marked by a major river valley (formed by the Surkhob River) with the Tien Shan Mountains forming a topographic barrier along its northern flank. The coincidence between the river and the deformation front suggests that the deformation front is dynamically maintained by stream erosion. That is, as thrust sheets advance toward the topographic wall of the Tien Shan Mountains, most of the mass delivered by the thrust systems is carried laterally by stream erosion.

The balance between thrust sheet advance and fluvial erosion has important implications for the interpretation of subsurface structure beneath the Peter the First Range, where most of the earthquake activity occurs in the Garm region. Our analysis of structures exposed at the deformation front suggests that the thrust systems have advanced faster than erosion could remove the material laterally. That is, projection of surface geology along the southern margin of the Tien Shan mountains southward (beneath the deformation front of the Peter the First Range) suggests that the complex geologic structure of the Tien Shan has been overridden by thrusts. This observation suggests that these structures were beveled by stream erosion and then overriden by the thrust sheets. One potential implication of this observation is that the dextral transpressional structures found along the axis of the Peter the First Range may represent the surface expression of a strike-slip fault system that originally developed along the southern edge of the Tien Shan mountains, but which has now been overriden by thrust sheets advancing from the south.

Seismicity and Focal Mechanism Studies. In order to study the style of active deformation in the Peter the First Range--the most seismically active portion of the Garm region--we examined the spatial patterns of high-quality hypocentral locations and the orientations of principal stresses determined from earthquake focal mechanisms in Garm. We first recalculated the hypocentral locations for about 60,000 earthquakes using the data collected by the Complex Seismological Expedition (CSE) network for the period 1969 to 1990 (Figure 2). A systematic method for evaluating relative quality of hypocentral locations, based on number and distribution of recording stations, standard error ellipsoid calculations, and RMS residuals was applied to the relocated earthquake catalog [Hamburger *et al.*, 1992*b*]. Earthquake focal mechanisms were determined for over 14,000 well recorded events in the Garm region [Ramos *et al.*, 1991; Ramos, 1992].

One salient feature of the earthquake mechanisms in the Garm region is that the diversity of focal mechanisms prevents the construction of reliable composite focal mechanism solutions, even along a single, well constrained seismogenic structure. This pattern mirrors that observed in the Transverse Ranges of California [Nicholson, 1986; Pechman, 1987; Real, 1987]. Our analysis also suggests that the compressional axes of focal mechanisms in Garm exhibit a more consistent orientation than the extensional axes, as observed in the Transverse Ranges [Pechman, 1987]. We have used this consistent orientation of the P-axes as an aid in delineating the seismically active structural features of the area. The well defined, sub-parallel orientation of the P-axes can be used as a guide in tracing the structures, particularly in areas where the dispersed distribution of the events masked the actual geometry of the faults (Figure 3). The resulting structural map was then correlated with the structures mapped on the surface and with other geological and geophysical observations in the region.

Among the most significant of our results is the delineation of a seismically active, vertical fault in the middle of the Peter the First Range. This structure, the Petrovsky Thrust (Figure 4) is presently the most active seismogenic feature in the Garm region. We have also identified other seismogenic structures in the region (Figure 5), including: a near-horizontal structure, the Nimich Fault, located at about 5 km depth near the boundary of the Peter the First Range and the Tien Shan; the intersecting Yasman and the Obi-Khabut faults near the 1949 Khait earthquake (M=7.4) epicenter; and segments of the Darvaz-Karakul Fault, which appear to be associated with more dispersed, but deeper, seismicity. The surface traces of most of the structures that we have

identified from the seismicity and P-axis distribution coincide with faults previously delineated based on geologic mapping and macroseismic effects of historical earthquakes. We have also used the orientation of the P-axes relative to the mapped structures in order to infer the dominant sense of slip along these faults. The inferred sense of motion along these faults (Figure 6) suggests that the ongoing deformation in Garm is dominated by westward oblique slip of crustal material along the mapped faults. This westward transport of materials appears to be a consequence of the north-south convergence of the Pamir and Tien Shan ranges, resolved along the oblique boundaries that define the margins of these two tectonic features.

Related Seismological Investigations. We are continuing are ongoing work on related studies of seismicity, crustal structure, and earthquake prediction investigations. These include: (1) regional velocity structure of the crust and upper mantle of the Pamir-Tien Shan region, based on teleseismic travel-time inversion [Mellors *et al.*, 1991; Hamburger *et al.*, 1992*c*]; (2) work on 1- and 3-dimensional velocity structure of the Garm region, using local earthquake travel-time inversion [Hamburger *et al.*, 1991; 1992*b,c*]; (3) study of the temporal distribution of earthquakes associated with moderate- and large mainshocks in the Garm region [Zheng *et al.*, 1991; Eneva *et al.*, 1992*a*; Zheng, 1992]; and (4) analysis of magnitude distribution and completeness of the Garm catalog [Eneva *et al*, 1990; 1992*b*].

References

Eneva, M., R. E. Habermann, M. W. Hamburger and G. A. Popandopulo, 1990, Man-made changes in the earthquake catalog of the Garm region, Soviet Central Asia [abs.], *EOS, Trans. Am. Geophys. Un., 71*, 1453.

Eneva, M., M. W. Hamburger and G. A. Popandopulo, 1992*a*, Spatial distribution of earthquakes in the Garm region, Soviet Central Asia, *Geophys. J. Intl., 109*, 38-53.

Eneva, M., R. E. Habermann, and M. W. Hamburger 1992, Man-made changes in the earthquake catalog of the Garm region, Soviet Central Asia, *Geophys. J. Int.*, in review.

Hamburger, M. W., H. J. Al-Shukri, G. L. Pavlis, and G. A. Popandopulo, 1991, P-wave velocity structure of the crust beneath the Garm region, Soviet Central Asia [abs.], *EOS, Trans. Am. Geophys. Un., 72*, 350.

Hamburger, M. W., D. E. Sarewitz, T. L. Pavlis and G. A. Popandopulo, 1992*a*, Structural and seismic evidence for intracontinental subduction in the Peter the First Range, Soviet Central Asia. *Geol. Soc. Amer. Bull., 104*, 397-408.

Hamburger, M. W., W.A. Swanson and G.A. Popandopulo, 1992*b*, Velocity structure and seismicity of the Garm region, Soviet Central Asia, *Geophys. J. Intl.*, in review.

Hamburger, M. W., H. J. Al-Shukri, R. J. Mellors, G. L. Pavlis. A. A. Lukk, and G. A. Popandopulo, 1992*c*, Crustal and upper mantle velocity structure in the Pamir-Tien Shan region, Central Asia [abs.], *Seismol. Res. Lett., 63*, 43.

Nicholson, C., L. Seeber, P. Williams and L. R. Sykes, 1986, Seismicity and fault kinematics through the eastern Transverse Ranges, California: Block rotation, strike-slip faulting, and low anlge thrusts, *J. Geophys. Res., 91*, 4891-4908.

Mellors, R.J., H.J. Al-Shukri, M.W. Hamburger, A.A. Lukk and G.A. Popandopulo, 1991, Velocity structure of the crust and upper mantle in the Pamir-Tien Shan region, Soviet Central Asia [abs.], *EOS, Trans. AGU, 72*, 203.

Pechman, J. C., 1987, Tectonic implications of small earthquakes in the central transverse ranges in recent reverse faulting in the transverse ranges, California, *U.S. Geol. Surv. Prof. Pap. 1339*, 97-112.

Ramos, E. G., 1992, Seismic expression of faults within the Peter the First Range, an active fold-thrust belt in Central Asia, *M.S. Thesis*, Indiana University, Bloomington.

Ramos, E. G., M. W. Hamburger, G. L. Pavlis, S. L. Yunga, and A. A. Lukk, 1992, Seismic expression of faults within the Peter the First Range, an active fold-thrust belt in Central Asia [abs.], *EOS, Trans. AGU, 73*, 213.

Pavlis, T.L., R.D. Myers, G.L. Pavlis, J.H. Holbrook, M.W. Hamburger, A.A. Lukk, and S.L. Yunga, Transpressional tectonics in the Peter the First Range, Soviet Tadjikistan [abstract], *EOS, Trans. Am. Geophys. Un., 72*, 514.

Real, C. R., 1987, Seismicity and tectonics of the Santa Monica-Hollywood-Raymond Hill fault zone and northern Los Angeles Basin in recent reverse faulting in the Transverse Ranges, California, *U.S. Geol. Surv. Prof. Pap. 1339*, 113-124.

Zheng, B., 1992, Temporal Variations in Seismic Activity in the Garm Region, USSR: Evidence for Quiescence Preceding a M = 6.3 Earthquake, *M.S. Thesis*, Indiana University, Bloomington.

Zheng, B., M.W. Hamburger, G.L. Pavlis, and G.A. Popandopulo, 1991, Temporal variations in seismic activity in the Garm region, USSR: Evidence for quiescence preceding a M=6.3 earthquake [abs.], *EOS, Trans. AGU, 72*, 322.

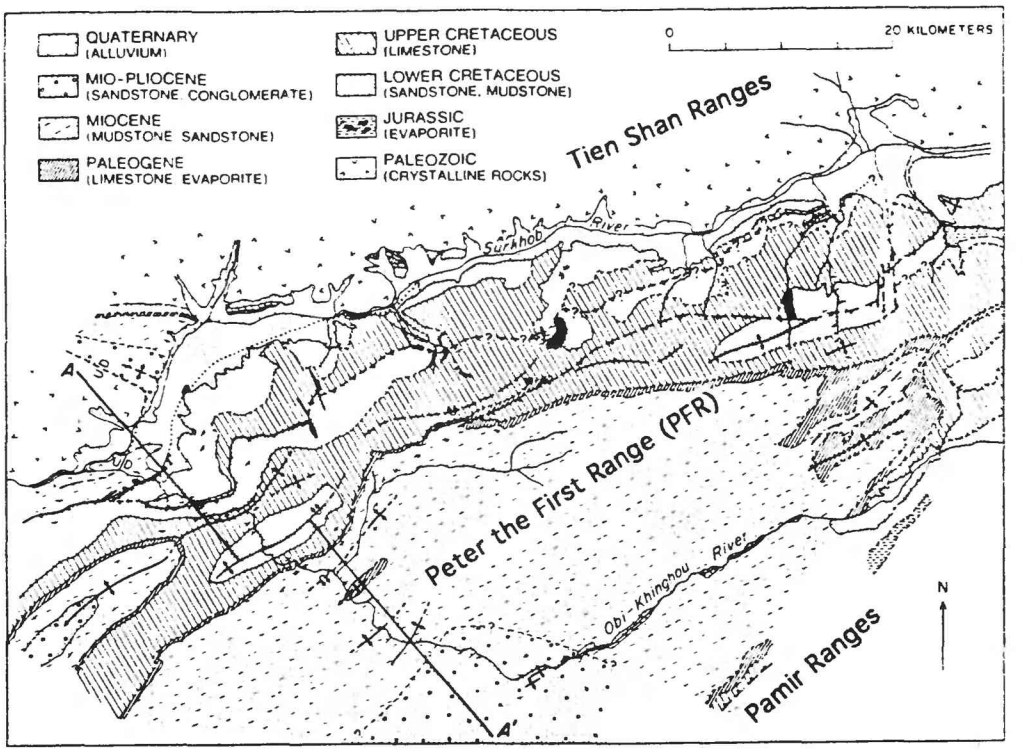

Figure 1. Reconnaissance geologic map of the Garm region based on field mapping, satellite imagery interpretation, and field data collected by V. I. Shevchenko. Contacts and structures are shown as solid where well constrained, dashed where approximate, queried where uncertain, and dotted where inferred. Drainage network is shown as dot-dash line (from Hamburger et al., 1992).

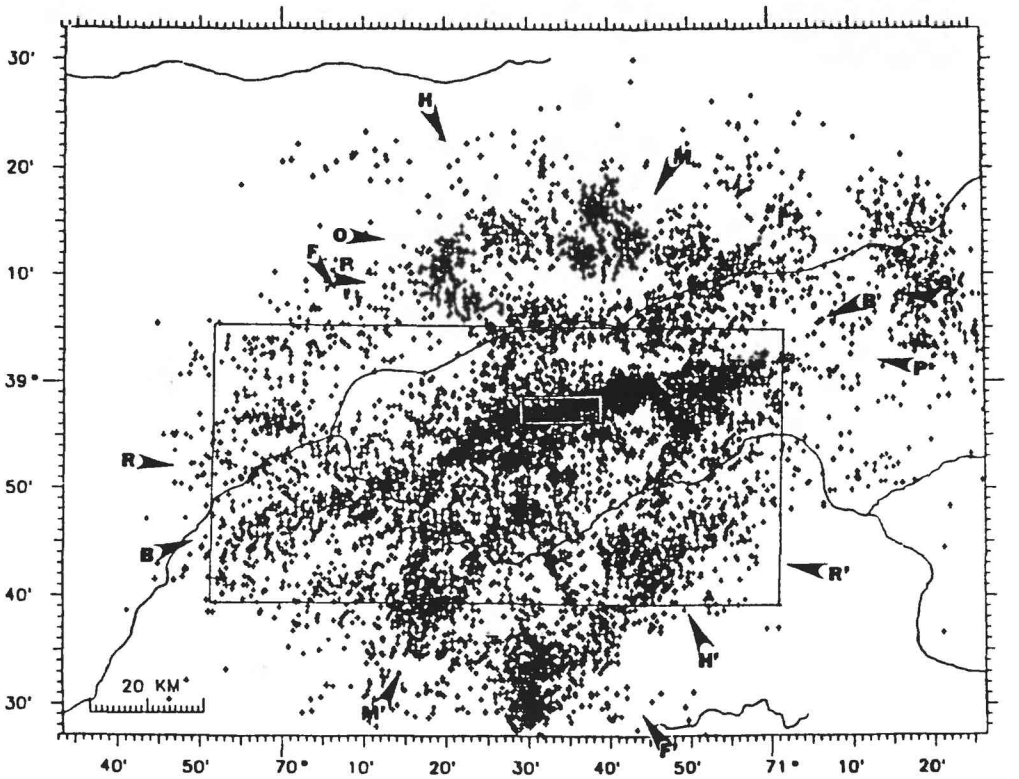

Figure 2. Plot of earthquakes located by the CSE network from 1969-1989, for which focal mechanism solutions have been determined. Note the dense concentration of events along the ridge of the Peter the First Range. Compare distribution of events with the structural map shown in Figure 5. Large rectangle shows area covered by Figure 3. Arrowheads labeled F and F' mark the cross-section line shown in Figure 4.

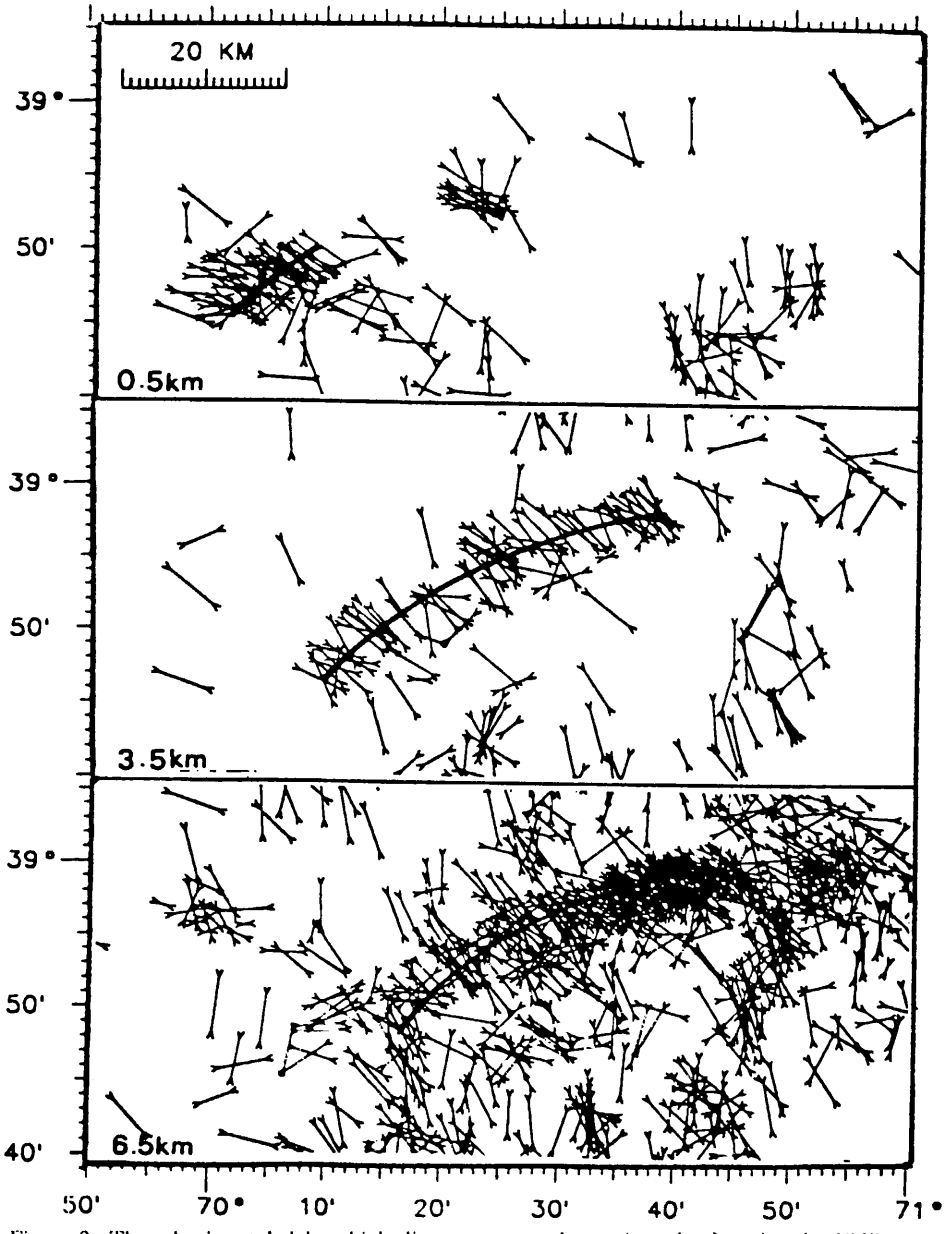

Figure 3. Three horizontal, 1-km thick slices constructed at various depths using the 1969-1989 focal mechanism catalog, showing the sub-parallel orientation of the P-axes under the PFR. The alignment of events with uniformly oriented P-axes is shown by a heavy line for each depth-slice. On the central part of the PFR, this alignment coincides at all depths indicating a vertical structure. In the west, this alignment shifts, indicating a southeast-dipping structure. The location of the slices is shown in Figure 2.

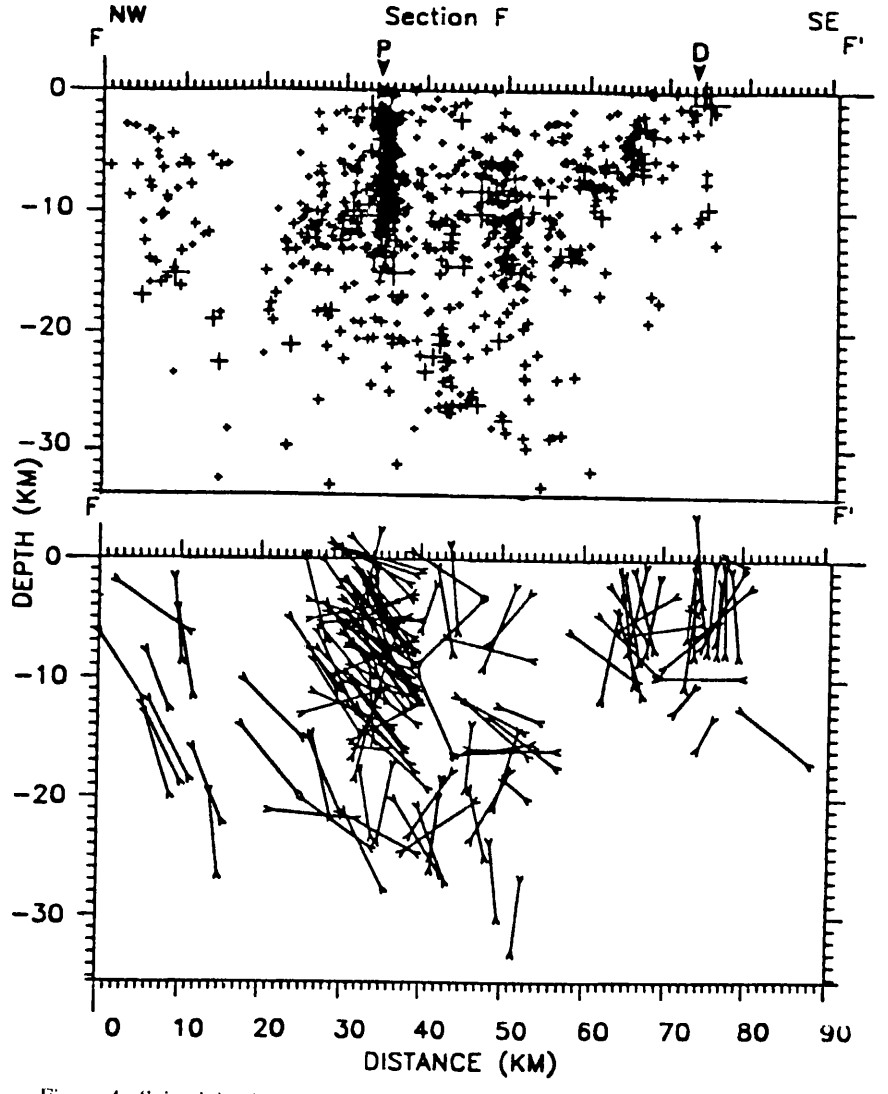

Figure 4. Seismicity (top) and P-axes (bottom) cross sections along line F-F' shown in Figure 2. Note the vertical cluster marking the Petrovsky Fault (marked P) and the dispersed seismicity near the Darvaz-Karakul Fault (D). The sections are 2 km thick. The orientation of the P-axes, here showing an apparent northerly upward thrust for the Petrovsky Fault cluster, was used to infer the relative motion of blocks along the faults.

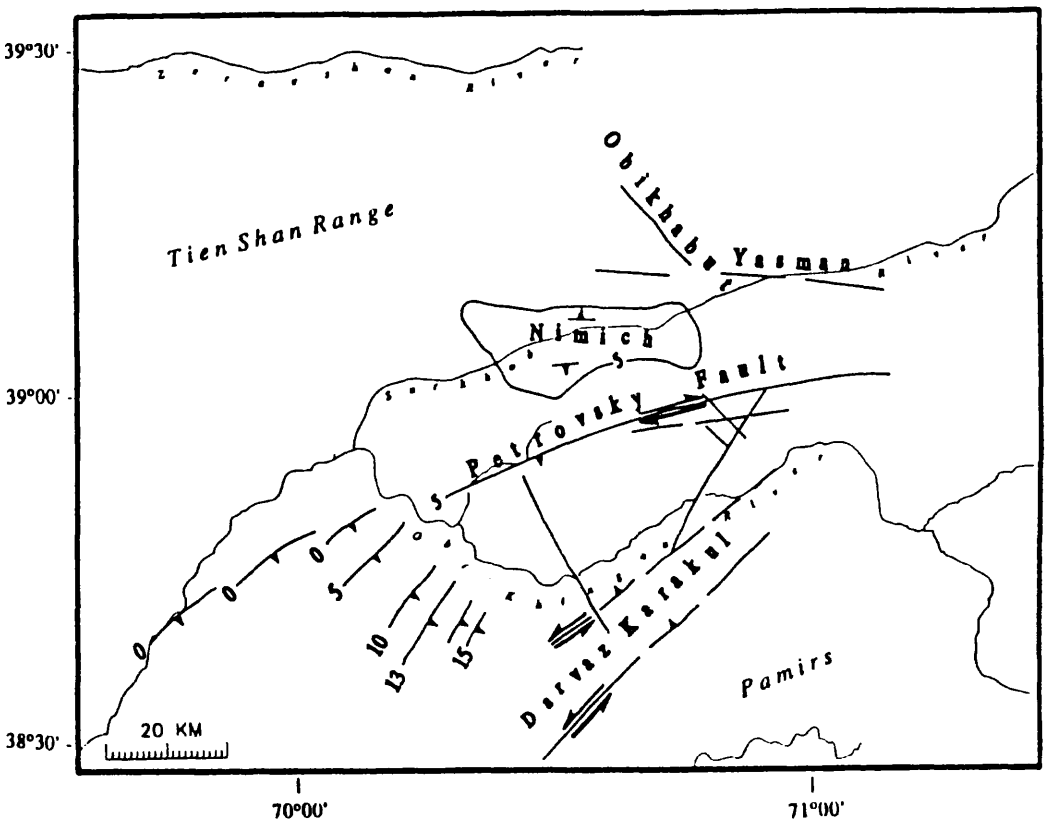

Figure 5. Structural interpretation of the P-axes and hypocenter distribution. The numbers near each structure indicate the depth of the respective segments of the faults. Note that the Petrovsky Fault along the axis of the PFR does not extend above ~5 km depth. The extent of the seismicity marking the horizontal Nimich Fault is shown as an outline at 5 km. The parallel lines along the Darvaz-Karakul Fault mark the outside boundaries of its seismogenic zone.

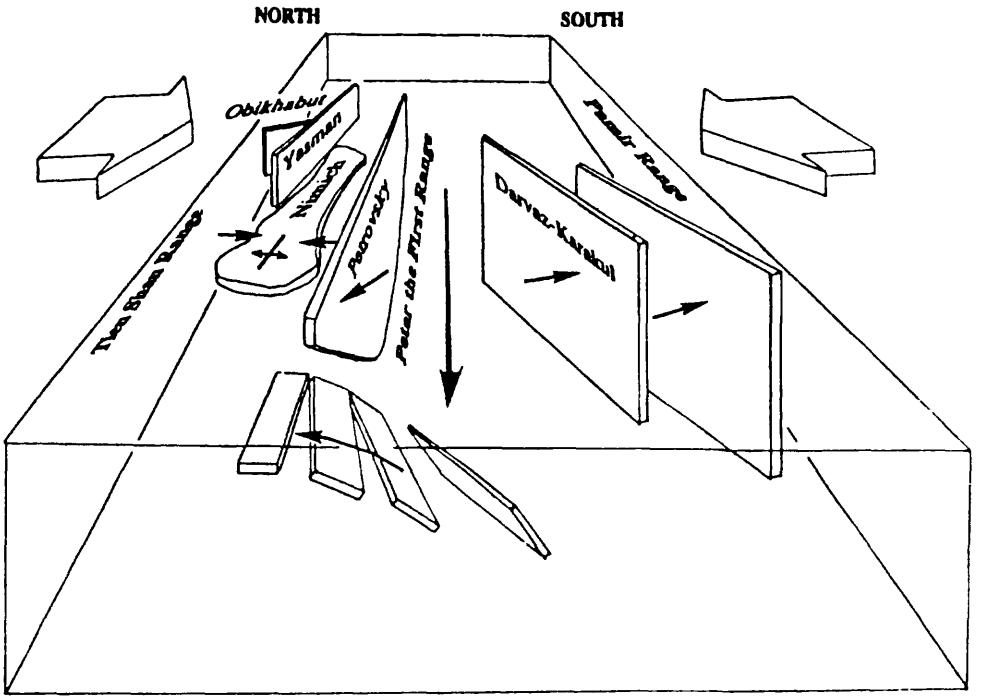

Figure 6. A perspective model of the active deformation in the Garm region. The large horizontal arrows show the north-south compression due to the collision of the Pamirs with the Tien Shan Range. The faults are shown as thin zones of weakness along which motion of crustal blocks (thin arrows) occur. The small discontinuous zones in the foreground are the imbricate, dipping thrusts of the Petrovsky Fault. A net westward motion of the southern PFR is suggested by the overall sense of transport along these faults (long horizontal arrow).

Analysis of Earthquake Data from the Greater Los Angeles Basin and Adjacent Offshore Area, Southern California

#14-08-0001-G1761

Egill Hauksson

Seismological Laboratory,
California Institute of Technology,
Pasadena, CA 91125
818-356 6954

INVESTIGATIONS

Seismotectonic analysis of earthquake data recorded by the CIT/USGS and USC networks during the last 16 years in the greater Los Angeles basin. Improve models of the velocity structure to obtain more accurate earthquake locations including depth and to determine focal mechanisms. Studies of the earthquake potential and the detailed patterns of faulting along major faults in the metropolitan area and adjacent regions.

A comprehensive study of the velocity structure of the Los Angeles basin is in progress. We have also analyzed aftershock data from the 1992 M6.1 Joshua Tree, M7.3 Landers, and M6.2 Big Bear earthquake sequence although it is located outside of the Los Angeles basin. Below we report some of the preliminary results.

RESULTS

Three-Dimensional Velocity Model of the Los Angeles Basin

Preliminary results of our work were presented at the 1992 SSA meeting (Hauksson, 1992). Arrival time data from 530 earthquakes and two blasts have been inverted for the P-wave velocity structure of the Los Angeles basin. An initial one-dimensional velocity model was specified at 648 nodes forming a sparse grid with 21 km horizontal spacing between grid points at depths of 1, 4, 8, 12, and 16 km. The velocity model from the sparse grid was interpolated and used as input for an inversion for a second set of 2048 grid nodes with 6 km horizontal spacing. Both grids are rectangular and centered on the basin proper. The velocities at most of the nodes of the dense grid are well resolved except to the northwest where the resolution is below average. .

Because the starting model is one-dimensional the final three-dimensional model can be correlated with the local geologic structures. Preliminary results of the inversion show high velocities in the crystalline rocks beneath the Santa Monica mountains and to the southeast. The flanks of the basin, where thrust faulting and folding is observed, can be recognized in the three-dimensional velocity structure and are characterized by intermediate velocities. The lowest velocities reflect the shape of the basin and form a gently dipping zone extending from Palos Verdes to the center of the basin. The more steeply dipping northeast flank of the basin can also be seen where the northeast trending velocity model cross section is compared to the north-northwest trending geologic cross section from Davis et al. [1989]. In the deepest part of the central basin low velocities extend down to 8-10 km depth. Some shallow basement velocity contrast exists across the Palos Verdes and the Newport-Inglewood faults. The most prominent low velocity zone associated with thrust faulting exists adjacent to the Sierra Madre fault zone.

Wright (1991) provided an excellent summary of the geology of the Los Angeles basin. Figure 1, from Wright (1991), is an index map that shows major structural features and the location of geologic cross section A through F. We have made similar cross sections through our preliminary three-dimensional model and made an overlay with the geologic cross sections from Wright (1991). Figure 2 is an overlay of our velocity model and geologic cross sections A, B, C, and D Wright (1991; Figure 8). These overlays show

remarkable agreement between the geology and the preliminary velocity model. The bottom of the basin is clearly reflected by velocities of 6 km/s or higher. The near-surface sediments correspond to low velocities of 3.0 km/s or less. The west flank of the basin is clearly defined by higher velocities at shallower depth than beneath the center of the basin. The east flank of the basin that consists of metamorphic rocks has lower velocities than the west flank and hence is not as well defined as the west flank.

The next step is to use the final three-dimensional model to improve hypocenters and focal mechanisms. Results from such inversions for the greater Los Angeles basin combined with results from our focal mechanisms studies, will provide a more comprehensive picture of the geological structure and seismotectonics of the Los Angeles basin than available before.

The M7.3 Landers Mainshock Rupture

The 1992 Mw7.3 Landers mainshock ruptured along separate segments of five major surficial faults. The rupture began at the epicenter, approximately 8 km south of the community of Landers (Figure 3). It proceeded along the Johnson Valley fault for a distance of 17 km. It used the newly named Landers fault to step the slip over to the Homestead Valley fault. The rupture continued for a distance of 25 km along the Homestead Valley fault and stepped over a broad shear zone to the Emerson fault. The final step over was from the Emerson fault to the Camp Rock fault.

The spatial distribution of aftershocks along the mainshock rupture is complex and appears to be 5-20 km wide in places. (Figure 3) The distribution is characterized by tight spatial clusters of aftershocks, wide diffuse distributions extending away from the rupture surface, and small areas where no aftershocks occur but where surface slip was reported. This complexity may in part be explained by: 1) the rupturing of subparallel and overlapping fault segments; 2) the large amount of slip causing an aura of large strains around the rupture; 3) the change in strike of the rupture, starting with northerly strike near the epicenter and gradually rotating to north-west; 4) roughness or small steps along individual fault segments; and 5) variations in slip along the mainshock rupture surface. None of these explanations are mutually exclusive and all may contribute simultaneously to the observed distribution of aftershocks.

Near the epicenter of the mainshock the aftershock distribution forms a simple north trending zone. A small cluster 8 km to the north of the mainshock epicenter is associated with a small right-step in the Johnson Valley fault. Some of the largest clusters of aftershocks occur between subparallel fault segments such as the Johnson Valley and Homestead Valley faults. This cluster also crosses the Homestead Valley fault where it coincides with a few kilometer wide slip gap identified independently from TERRAscope data by Kanamori et al., [1992]. A large aftershock cluster between the Emerson and Camp Rock faults may be associated with the change in strike to the north of the Emerson fault and transfer of slip to the Camp Rock fault.

The aftershock distribution extends from the surface to depths of 12-14 km. Four different depth cross sections along the mainshock rupture and five orthogonal cross sections are shown Figure 3. The large or M>4.0 aftershocks occur usually at the edges, bottom or top, of the mainshock rupture. The almost vertical dip and less than 2 km width of the aftershock zone where two strands do not overlap is illustrated in cross sections such as E-E'.

PUBLICATIONS and REPORTS

Hauksson, E. and L. M. Jones, The 1988 and 1990 Upland earthquakes: Left-lateral faulting adjacent to the central Transverse Ranges, *J. Geophys. Res.*, *96*, 8143-8165, 1991.

Hauksson, E., Seismotectonics, US National Report to International Union of Geodesy and Geophysics 1987-1990, *Reviews of Geophysics*, Supplement, 721-733, 1991.

Hutton, L. K., L. M. Jones, E. Hauksson, and D. D. Given, Seismotectonics of southern California, Slemmons, D. B., Engdahl, E. R., Zoback, M D., and Blackwell, D. D., eds., *Neotectonics of North America*, Boulder, Colorado, Geological Society of America, Decade Map Volume 1, 133-152, 1991.

Hauksson, E., K. Hutton, K. Douglass, and L. Jones, Earthquake atlas for southern California, 1978-1990, *Engineering Geology Practice in Southern California,* Belmont, California, Association of Engineering Geologists, B. Pipkin and R. J. Proctor, eds., 181-190, 1992.

Hauksson, E., Seismicity, faults, and earthquake potential in Los Angeles, southern California, *Engineering Geology Practice in Southern California*, Belmont, California, Association of Engineering Geologists, B. Pipkin and R. J. Proctor, eds., 167-179, 1992.

Hauksson, E., Hutton, K., and Jones, L. M., Preliminary Report on the 1992 Landers Earthquake Sequence in Southern California, *Landers Earthquake of June 28, 1992 San Bernardino County, California Field Trip Guidebook,* So. Calif. Section of the Association of Engineering Geologists, Ed. D. Ebersole, 23-32, 1992.

Hauksson, E., The 1991 Sierra Madre earthquake: Seismological and tectonic analysis, submitted to *J. Geophys. Res.*, 1992.

Landers Earthquake Response Team, (E. Hauksson, among 19 authors), Near-field investigations of the Landers earthquake sequence, April-July, 1992, submitted to *Science*, 1992.

Qian, H. X., E. Hauksson, and L. M. Jones, The Effect of the 1992 M7.5 Landers Earthquake on the Seismicity of the Southern San Andreas Fault, (Abstract), submitted to Fall AGU Meeting, 1992.

Hauksson, E., K. Hutton, H. Kanamori, S. Bryant, H. Qian and K. Douglass, L. M.Jones, D. Eberhart-Phillips, J. Mori and T. Heaton, Overview of the 1992 (M6.1,7.5,6.6) Landers Earthquake Sequence in San Bernardino County, California, (Abstract), submitted to Fall AGU Meeting, 1992.

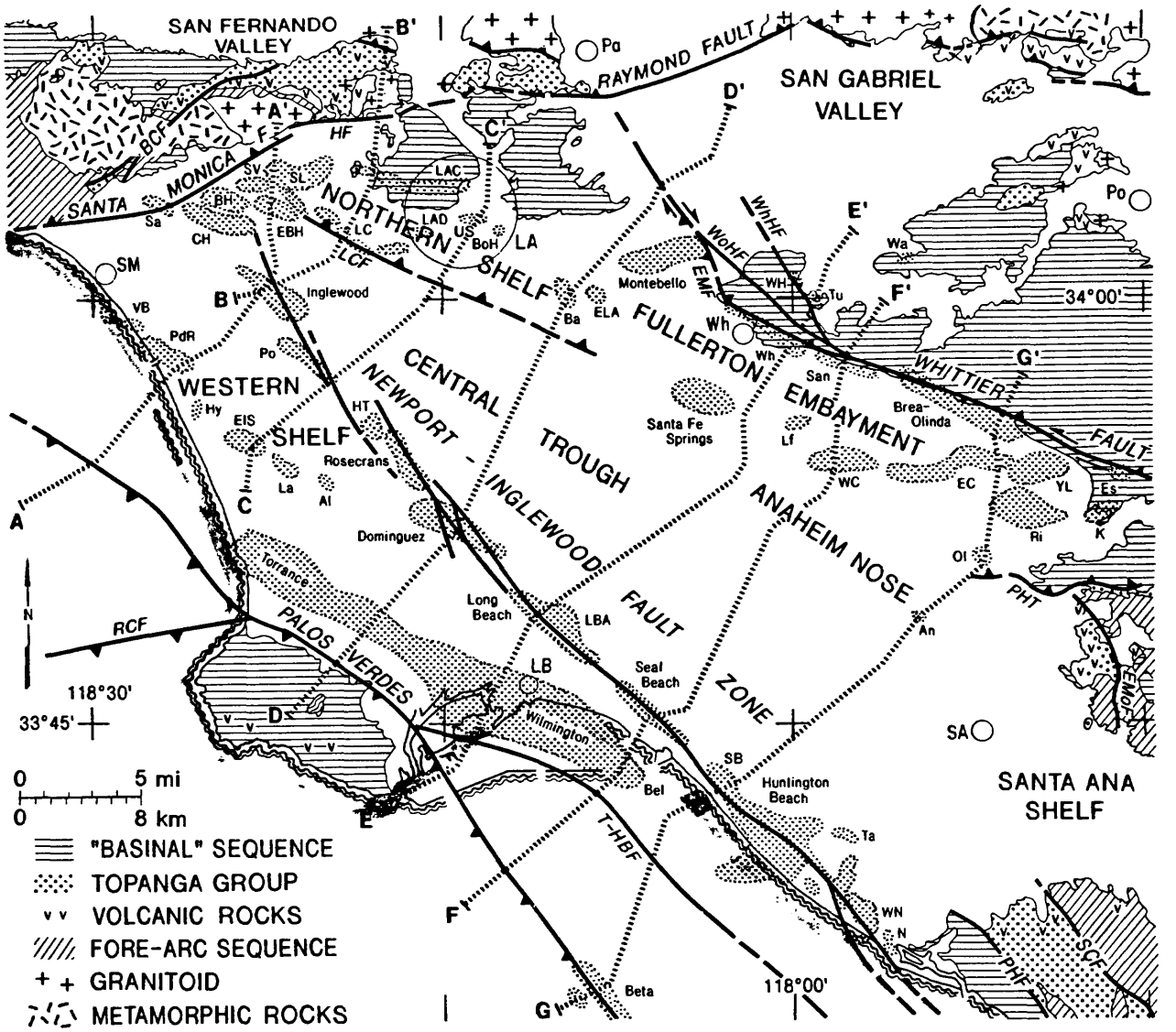

Figure 1. From Wright (1991). An index map that shows major structural features and the location of cross section A through F.

Wright, T. L., Structural geology and tectonic evolution of the Los Angeles basin, in *AAPG- Volume on Active-Margin Basins*, vol. 52, edited by K. T. Biddle, pp. 35-134, 1991.

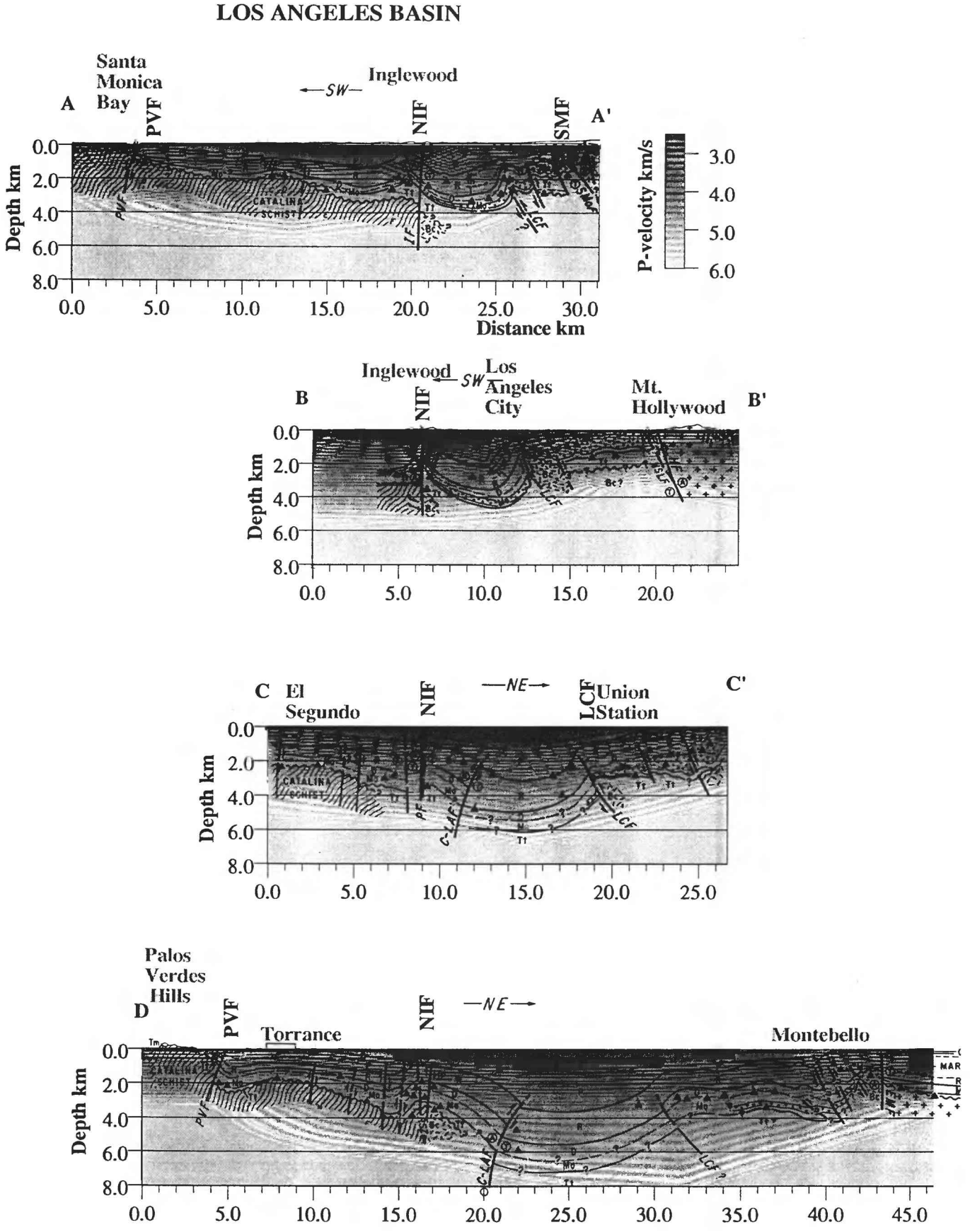

Figure 2. Overlay of our preliminary 3-D velocity model and geologic cross sections A, B, C, and D from Wright (1991; Figure 8).

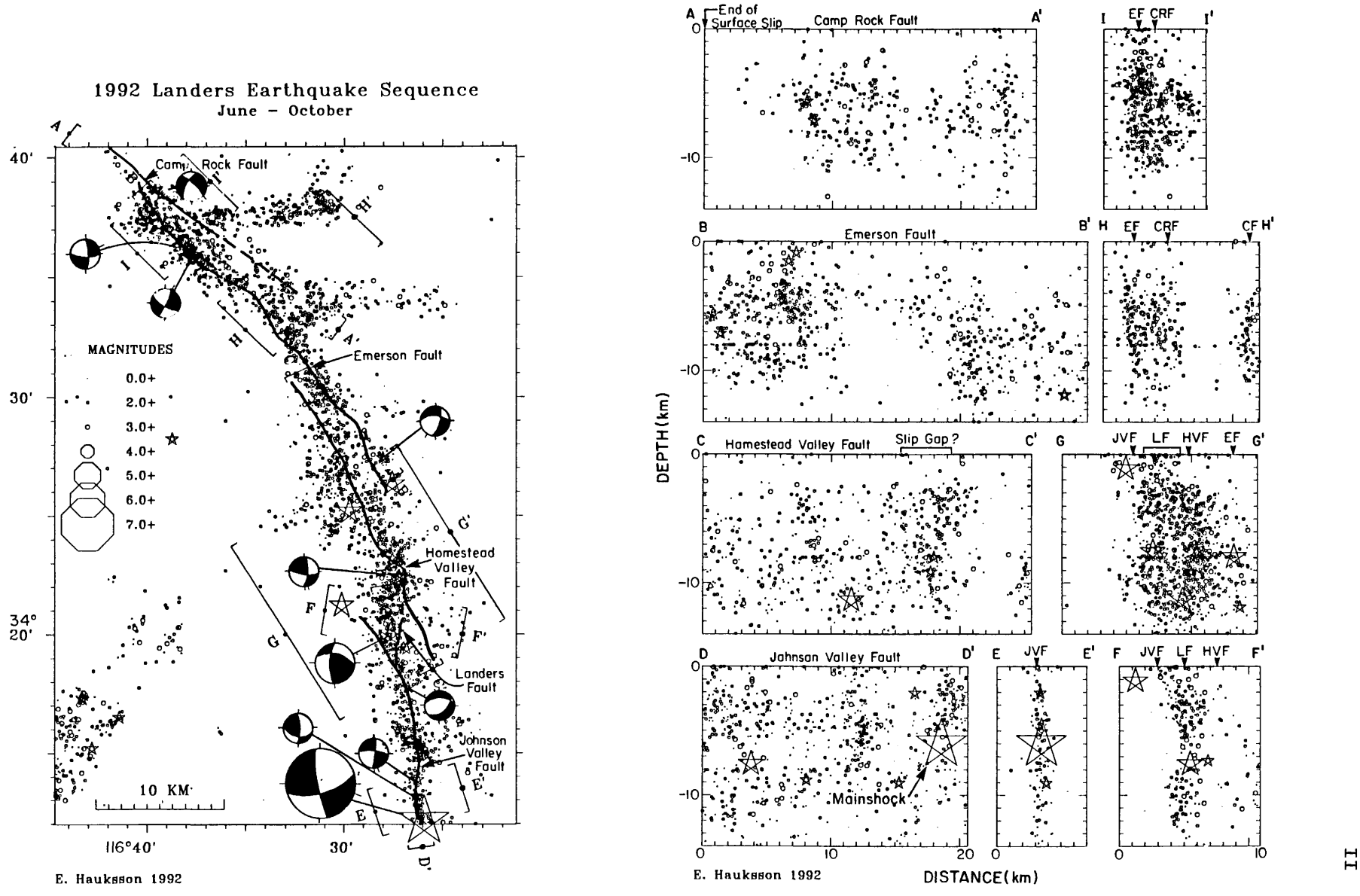

Figure 3. (Left) Map of 1992 M7.3 Landers mainshock and aftershocks and selected focal mechanisms. Surface rupture (provided by K. Sieh) is also shown. (Right) cross sections parallel to the fault strands (A-D) and across the fault strands (E-I). Note how the different fault strands overlap.

Assessment of Quaternary Deformation Between the Hayward and Calaveras Faults, San Francisco Bay Region, California

Award Number: 1434-92-G-2209

Mark A. Hemphill-Haley
Woodward-Clyde Consultants
500 12th Street, Suite 100
Oakland, CA 94607-4014
(510) 874-3269

Keith I. Kelson
William Lettis and Associates, Inc.
1000 Broadway, Suite 612
Oakland, CA 94607-4014
(510) 832-3716

Investigations

We are investigating the distribution and style of deformation within the complex intersection between the Hayward and Calaveras fault zones in the southern East Bay Hills of the San Francisco Bay region. The amount and mode of strain transfer from the central Calaveras fault zone onto the Hayward and northern Calaveras fault zones are poorly understood. The purpose of this investigation is to provide information about the mechanisms of slip transfer between these two major seismogenic faults, and thus to help define potential seismic hazards in the southern San Francisco Bay region.

Our research is designed to address: 1) the distribution and style of Quaternary deformation between the Calaveras fault in Sunol Valley and the Hayward fault in Fremont, where slip is transferred from the central Calaveras fault onto the southern Hayward fault, and 2) the nature and loci of Holocene deformation along a microseismically defined fault splay between the southern Hayward and Mission faults (Wong and Hemphill-Haley, 1992). We anticipate obtaining the following information from this investigation:

- Paleoseismologic data on the northwestern projection of the Mission fault in Fremont
- Structural relations of surficial lineaments along the mapped trace of the Mission fault, its northwestern extension, and a microseismically defined splay of the southern Hayward fault (Wong and Hemphill-Haley, 1992)
- Geologic and geomorphic assessments of the loci and nature of Quaternary deformation between the Calaveras fault in Sunol Valley and the Hayward fault in Fremont

Our data collection consists of two tasks: 1) interpretation of aerial photography, field reconnaissance, and paleoseismologic investigations of the Mission fault and the microseismically defined splay of the Hayward fault, and 2) quantitative geomorphic and geologic analyses of Quaternary deformation between the Hayward and Calaveras faults. These analyses include investigations of deformation of late Quaternary fluvial terraces flanking Niles Canyon and a possible late Tertiary to early Quaternary paleovalley (Mission Pass) through analysis of aerial

photography, field mapping, shallow drilling, and construction of envelope, subenvelope, and residual geomorphic maps.

Results

Paleoseismologic Investigations - Through our analysis of aerial photography and field reconnaissance, we identified a potential trace of the Mission fault along its northwestern projection in the Mission District of Fremont. We selected a trench site for paleoseismologic studies on an alluvial fan within an abandoned orchard on Ohlone College property, based on the presence of a strong tonal lineament, a subtle topographic swale, and a vegetation lineament possibly related to a fault-induced groundwater barrier. Based on our analysis of aerial photographs and field studies, this lineament is the most prominent feature possibly related to Holocene movement on the Mission fault on the alluvial fan complex in Fremont. In addition, the presence of the lineament across Holocene and late Pleistocene alluvial fan deposits suggested that a trench would expose datable surficial deposits. Our intent with the trench was to expose stratigraphic and structural relations associated with the swale and lineament, and determine if the lineament is related to late Quaternary movement on the Mission fault.

In April 1992, we excavated, logged, and backfilled a trench across the margin of the topographic swale that was approximately 18 m long, 1 m wide, and up to 3.5 m deep. Historic, Holocene, and late Pleistocene fluvial overbank and channel deposits were exposed in the trench, based on the presence of cultural remains (i.e., nails, bricks) and a probable late Pleistocene jaw bone of a horse. We observed no evidence of tectonic displacement of the fluvial deposits. The trench was reviewed informally by personnel with the U.S. Geological Survey (USGS) and Lawrence Berkeley Laboratory (LBL).

Based on analysis of aerial photography and field reconnaissance with personnel from the USGS, LBL, and the University of California at Berkeley, we identified another potential trench site in the southern East Bay Hills near Mission Peak. We are currently assessing the site to determine if investigation would be fruitful.

Quantitative Geomorphic Analyses - We have obtained 1:20,000-scale, black-and-white aerial photography taken in 1939 and 1940 of the southern East Bay Hills between the Calaveras fault in Sunol Valley and the Hayward fault in Fremont, and are currently interpreting the distribution of fluvial terrace surfaces flanking Niles Canyon on these photos. In addition, we are using these photographs to assess the presence of possible fluvial deposits or surfaces associated with the Livermore and Santa Clara/Irvington Gravels in the vicinity of Mission Pass. We are testing the hypothesis that the topographically low part of the southern East Bay Hills near Mission Pass is a paleovalley associated with these gravels. If so, this paleovalley may provide a long-term indicator of strain across the range, as may terraces along Niles Canyon.

As part of the quantitative analysis of the range, we have constructed an envelope map of the southern East Bay Hills at a scale of 1:62,500 (Lettis and Kelson, 1992), which is a generalized topographic contour map that ignores present-day valley incision. We are currently constructing a subenvelope map of the same area, which is a contour map drawn on the valley floors of second-order drainages. We anticipate that the quantitative difference between these two maps (a residual map) will yield information on the amount and distribution of erosion in the range, which in turn can be interpreted as a function of tectonic uplift. In addition, we are researching the feasibility of using digital elevation models (DEMs) and appropriate software to digitally construct these maps at a scale of 1:24,000.

Reports

Lettis, W.R., and Kelson, K.I., 1992, Distribution of geologic slip along faults in the San Francisco Bay and Santa Maria Basin Regions: Abstracts for American Geophysical Union Chapman Conference, Tectonics and Topography, Snowbird Utah, p. 37.

Wong, I.G., and Hemphill-Haley, M.A., 1992, Seismicity and faulting near the Hayward and Mission fault: *in* Galehouse, J.S. (ed.), Program and Abstracts, Second Conference on Earthquake Hazards in the Eastern San Francisco Bay Region, California State University, Hayward; also, in press, *in* Borchardt, G. (ed.), Proceedings, Second Conference on Earthquake Hazards in the Eastern San Francisco Bay Region, California Division of Mines and Geology Special Publication 113.

Collaborative Research: Analysis of PANDA data and continuation of PANDA experiment in the Central New Madrid Seismic Zone

14-08-0001-G2138

Robert B. Herrmann
Department of Earth and Atmospheric Sciences
Saint Louis University
3507 Laclede Avenue
St. Louis, MO 63103
(314) 658-3131

Investigations

The purpose of this segment of the collaborative effort is to learn as much as possible about the dynamics of the earthquake process in the New Madrid Seismic Zone by using data from the dense PANDA deployment of three component sensors on top of the seismicity in the central seismicity trend between New Madrid, Missouri, and Dyersburg, Tennessee.

Results

Since Booth *et al* (1991) reported on observable shear-wave splitting in the PANDA data set, and since this splitting could possibly affect the inference of focal mechanism parameters, a program for determining the Zoepritz coefficients for plane waves in a general anisotropic media was developed to determine how the peak amplitude of the shear wave from the source is affected by the anisotropy. This background work was essential prior to modeling the observed waveforms in terms of earth structure.

The other problem affecting analysis is the effect of the Q structure in the thick (600 m) sediments beneath the PANDA stations. Two different analysis techniques were applied. The first was that of Anderson and Hough (1984) whereby an attenuation operator was derived from the acceleration spectra. This was done for the P-wave on the vertical component and for the S-wave on the transverse component. The problem with technique is the effect of the unknown corner frequency upon the inference. The other technique follows Clouser and Langston (1991) to determine a differential attenuation between the P- and S-wave in the sediments. This is possible since an S-wave incident at the base of the sediments is converted into a P-wave which appears on the vertical component and into an SV-wave that appears on the radial component. Since the effect of source spectrum and crustal path drop out in the spectral ratio, the second technique yields stabler numbers than the second.

If the attenuation operator is given by $\exp(-\pi\kappa f)$, then we estimated $\kappa_S = 0.03 \pm 0.01$, $\kappa_P = 0.008 \pm 0.02$ by the Anderson and Hough technique , and $\Delta\kappa = 0.02 - 0.03$ by the Clouser and Langston technique. The individual station estimates showed an excellent correlation with sediment thickness,

this permitting another estimate by looking at the slope with respect to depth. Making reasonable estimates of the mean P- and S- wave velocities in the sediments permits and estimate that $Q_P = Q_S = 25 - 40$.

References

Booth, D. C., H. J. Rowlands, and J.-M. Chiu (1991). observation of shear-wave splitting in the New Madrid seismic zone, eastern USA (abs), *Seism. Res. Letters* **62,** 163.

Clouser, R. H., and C. A. Langston (1991) Q_P and Q_S relations in a sedimentary basin using converted phases, *Bull. Seism. Soc. Am.* **81,** 733-750.

Anderson, J. G, and S. E. Hough (1984). A model for the shape of the Fourier amplitude spectrum of acceleration at high frequencies, *Bull. Seism. Soc. Am.* **74,** 1969-1993.

Publications

Liu, Z., M. Wuenscher and R. B. Herrmann (1993). Attenuation of body waves in the New Madrid seismic zone, *Seism. Res. Letters.* **64,** (in review).

Ground Motion Estimation For The Central U. S.

14-08-0001-G2142

Robert B. Herrmann
Department of Earth and Atmospheric Sciences
Saint Louis University
3507 Laclede Avenue
St. Louis, MO 63103
(314) 658-3131

Investigations

The purpose of this effort is to improve strong ground motion prediction methodology for the central United States. Current techniques rely on early and dated work by Nuttli and Herrmann or random process theory techniques which do not take into account the effects of local structure, especially for sites in the Mississippi Embayment.

Results

Ou and Herrmann (1990a, 1990b) proposed extensions to random process theory to account for the effect of crustal structure on signal duration and level. Their technique included the direct and all supercritical S arrivals, but did not account for the reflection and transmission coefficients as the rays propagated through the crust. They calibrated their simple technique for the actual earth model by using wavenumber integration techniques.

Their work has been upgraded to use asymptotic ray theory for the estimation of individual ray amplitudes. This permits the following:

a) Estimates of peak motion for the vertical, radial, transverse, and vectorial horizontal time histories.

b) Use of a distance - focal mechanism dependent source excitation factor

c) Direct computation high frequency asymptotic seismograms that incorporate crustal complexity.

Other than generating peak motion estimates for realistic plane layered crustal models, the new technique permits sensitivity tests for changes in stress parameter, source depth, and source mechanism. Figure 1 presents the result of a set of simulations for a hard rock site for m_{Lg} = 5.0 and 7.5, for two mid-continent earth models, for four source depths, 5, 10, 15 and 20 km, for two stress parameter values, 100 and 200 bars, and for three mechanisms. One mechanism consisted of predominantly vertical strike slip source, another predominantly 45° dip slip sources, and the last all mechanisms having dip angles between 30° and 90° and which had either the P- or T-axis within 22.5° of the horizontal. The *mLg* values were determined by synthesizing vertical component WWSSN short period peak motions.

The peak motions presented in Figure 1 are peak transverse acceleration, velocity and PSRV at 1 and 10 Hz for 5% damped oscillators. Several features

are noted: first since all simulations had the same target *mLg* values, which is determined at distances greater than 100 km, there is very little dispersion in the estimates at large distances. The effects of different crustal structure are seen at 100 km distance where the first supercritical Moho reflection arrives. The major variation is at short distances, where the focal depth effect is profound.

Another interesting result is that, for fixed seismic moment and corner frequency, when compared to the other two focal mechanism simulations, the predominantly vertical strike slip source has an m_{Lg} 0.15 - 0.20 magnitude units smaller, while the peak transverse motion is about a factor of 1.3 - 1.4 times larger. Thus for a fixed m_{Lg}, the transverse motions of a vertical strike slip source will be about a factor of 2 times larger at large distances than the other mechanisms. At short distances, this difference is overwhelmed by the SH-wave excitation. This implies that specification of expected focal mechanism is important for hazard analysis. This may be difficult for older events where the magnitude is based on intensity, since the magnitude thus derived is probably related more to horizontal motions.

References

Ou, G.-B., and R. B. Herrmann (1990a). Estimation theory of peak ground motion, *Seism. Res. Letters* **61**, 99-107.

Ou, G.-B., and R. B. Herrmann (1990b). A statistical model for ground motion produced by earthquakes at local and regional distances, *Bull. Seism. Soc. Am.* **80**, 1397-1417.

Publications

Herrmann, R. B. and G.-B. Ou (1993). Random process theory and synthetic seismograms, *Bull. Seism. Soc. Am.* (in review).

Boore, D. M., K. W. Campbell, and R. B. Herrmann (1993). Characterization of strong ground shaking, in *Earthquake Hazard Assessment in the Central and Eastern US*, S. T. Algermissen and G. A. Bollinger, eds, EERI.

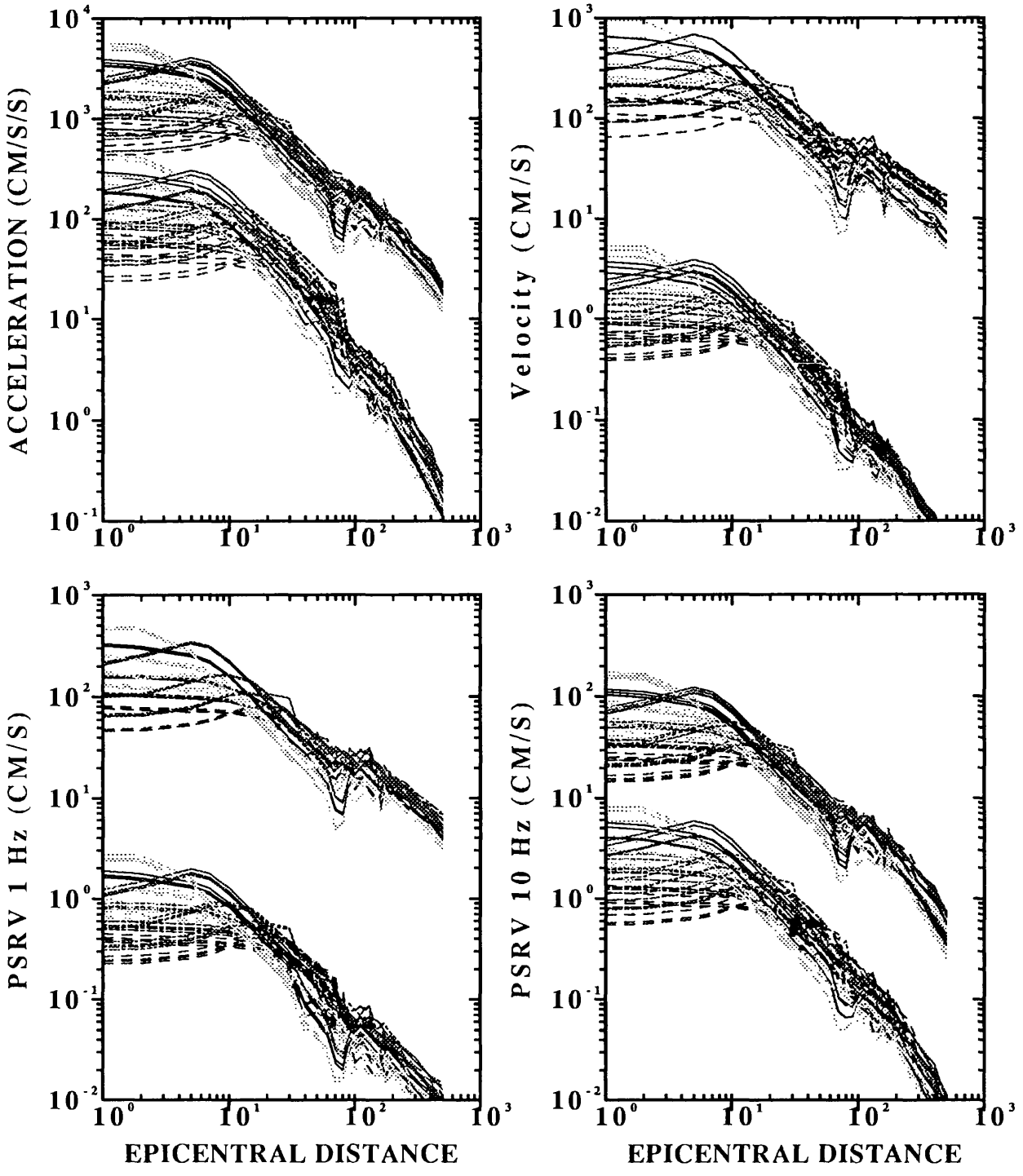

Figure 1. Sensitivity test to depth, model, stress drop and mechanism.

ACTIVE SEISMIC STUDIES OF VOLCANIC SYSTEMS

9930-01496

D.P. Hill, H.M. Benz, J.A. Olson, J.E. Vidale
Branch of Seismology
U.S. Geological Survey
345 Middlefield Road, MS 977
Menlo Park, California 94025
(415) 329-4795

Investigations

Over the last decade, this project has focussed on the activity in Long Valley caldera and coordination of associated monitoring research, and hazard reduction activities. Because project funding has come from the Volcano Hazards Program, the project has not been a regular contributor to the NEHERP semi-annual technical reports. For current reporting period, however, the following efforts funded under NEHERP have been administratively associated with this project in addition to the on-going coordination of Long Valley caldera monitoring and research:

1) Applications using the regional seismograph networks in the western United States for array studies of seismic scattering from upper mantle structures (J.E. Vidale and H.M. Benz).
2) Seismicity patterns associated with the Loma Prieta segment of the San Andreas fault (J. Olson and D.P. Hill).
3) Analysis of the geometry of seismogenic strike-slip and normal faults and its significance for fault strength and stress levels in the brittle crust (W. Thatcher and D.P. Hill).

Results

Long Valley Caldera (D.P. Hill)

Monitoring activities in Long Valley caldera through FY92 showed continued inflation of the resurgent dome at a strain rate of 2 to 3 microstrain per year and an uplift rate of 2 to 3 cm per year based on both two-color geodimeter measurements (see Langbein's report and Langbein et al., in press) and occupation of the leveling network within the caldera and along Highway 395 between Lee Vining and Tom's Place. Earthquake activity within the caldera persists at modest levels with occasional swarms of $M \leq 3$ events in the south moat and in the Sierra Nevada block south of the caldera. A most remarkable development in caldera seismicity occurred on June 28 when earthquake activity increased abruptly following the $M = 7.5$ earthquake at 4:58 AM (PDT) near Landers in southern California over 400 km to the south. This

dramatic increase in activity following the Landers event within the caldera and at multiple other sites in the western United States (as distant as Yellowstone National Park) is the first unambiguous example of a large earthquake triggering remote seismicity. In collaboration with a number of co-authors, Paul Reasenberg and I are preparing a manuscript describing the remote seismicity triggered by the Landers earthquake, which we intend to submit to Science for publication.

Figure 1 illustrates the abrupt increase in seismicity rate within the caldera at the time of the Landers earthquake. By applying a 5- to 30-Hz band-pass filter to the data from caldera seismic stations, Andy Michael was able to show that the onset of this triggered seismic activity began approximately 40 seconds after the S wave from the Landers mainshock passed through the area (or just over 2 minutes after the origin time of the Landers event). The first of the triggered events was located in the swarm area near the southwest margin of the resurgent dome. Seismicity spread to the other common centers of swarm activity in southern half of the caldera and parts of the Sierra Nevada block to the south over the next few hours. Notably, no activity was triggered beneath Mammoth Mountain, which had sustained a six-month-long swarm in 1989.

The triggered activity included over 300 earthquakes within the caldera before it gradually died out five to seven days after the Landers mainshock (Figure 1). Several $M \approx 3$, locally felt earthquakes occurred as part of the triggered activity, the largest of which was a $M = 3.7$ earthquake at 10:37 PM (PDT) on the 28th.

Loma Prieta seismicity patterns (J.A. Olson and D.P. Hill)

We examine the spatial distribution of the well-located earthquakes in the twenty years preceding the Loma Prieta earthquake, and their association with faults, along a 100-km-long extent of the southern Santa Cruz Mountains. Several faults in the area are clearly associated with background seismicity since 1969. Notably, however, the principal southwest-dipping portion of the Loma Prieta rupture below 10-km depth was virtually aseismic. Most of the seismicity in the area was associated with the creeping segment of the San Andreas fault south of Pajaro Gap and adjacent faults to the east. The area near the intersection of the San Andreas and Sargent fault traces, however, also produced persistent seismicity albeit at a much lower rate. This seismicity includes the 1988 (M5.3) and the 1989 (M5.4) Lake Elsman earthquakes, which have fault plane solutions consistent with oblique strike-slip and reverse-slip components on a plane that dips about 65^0 NE. These events stand out because they are a full magnitude unit larger than other events within a 15-km radius for at least 74 years, and because they occurred within 15 months and 2 1/2 months, respectively, of the Loma Prieta earthquake. Aside from these two Lake Elsman events, the seismicity patterns in the twenty years prior to the Loma Prieta earthquake were essentially stable showing no clear precursory changes. In the preceding twenty five years, however, two other $M \geq 5$ events occurred along the Loma Prieta rupture zone, near its southern end:

the 1964 (M5.0) and the 1967 (M5.3) Corralitos earthquakes.

Fault orientation and fault strength (D.P. Hill and W. Thatcher)

In a short note to the Bulletin of the Seismological Society of America (Hill, in press), I extended the definition of apparent friction used in Hill and Thatcher (1992, Bull. Seismol. Soc. Am., v. 82, pp. 883-897) to include ambient pore pressure, P_a, in the rock surrounding a fault zone with a fault-confined pore pressure, P_f. The modified definition is of the form

$$\mu^* = \mu(1 - \lambda'_n) = \mu\frac{(\sigma_n - P_f)}{\sigma_n - P_a)}$$

where

$$\lambda'_n = \frac{\Delta P}{\sigma'_n} = \frac{(P_f - P_a)}{\sigma_n - P_a)}$$

and σ_n is the normal stress across the fault plane. This form of the definition emphasizes that the upper bound on the apparent coefficient of friction, μ^*, for slip on a fault of arbitrary orientation, θ, in the presence of a second fault with the optimum, Coulomb orientation, θ_0 may be accommodated by variations in the intrinsic coefficient of friction, μ, and / or the pressure excess ΔP, of the fault-confined pressure over the ambient pore pressure.

Array Studies of Seismic Scattering (J.E. Vidale and H.M. Benz)

See separate summary by John E. Vidale and Harley M. Benz for project no. 9930-01496.

Publications

Hill, D.P., (in press), A note on ambient pore pressure, fault-confined pore pressure, and apparent friction: Bull. Seismol. Soc. Am.

Langbein, J.O., D.P. Hill, T.N. Parker, and S.K. Wilkinson, (in press), An episode of re-inflation of the Long Valley caldera, eastern California; 1989-1991; Jour. Geophys. Res.

Olson, J.A., and D.P. Hill, (in press), Seismicity in the southern Santa Cruz Mountains in the twenty years preceding the 1989 Loma Prieta, California, earthquake; in M.J.S. Johnston, ed., The Loma Prieta, California, Earthquake of October 17, 1989; Chapter C, Preseismic Observations, U.S. Geol. Survey Prof. Paper I - Earthquake Occurrence.

LONG VALLEY CALDERA — SEISMICITY
June 1 — July 2 1992

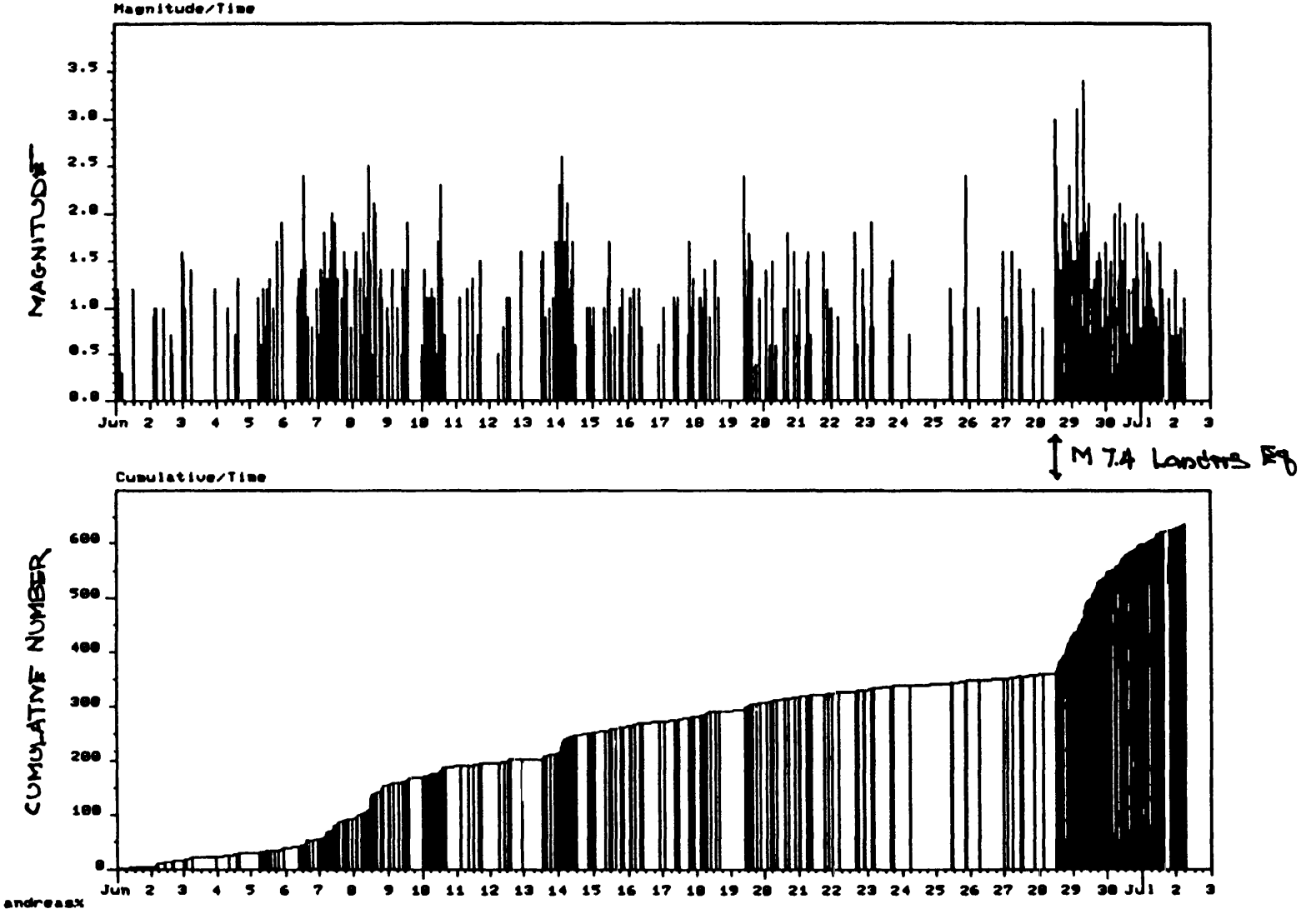

FIGURE 1

Computer Support Project

9920–10262

Roger N. Hunter
Branch of Global Seismology and Geomagnetism
U.S. Geological Survey
Denver Federal Center
Box 25046, Mail Stop 967
Denver, Colorado 80025
(303) 273–8472

Investigations

This project provides assistance to branch personnel in the area of IBM personal computers (hardware and software) and VAX programs. Primary focus has been on hardware procurement and graphics programs. The project also produces programs of its own as described below.

Results

Ethernet cards were procured for all branch PCs and are currently being installed. The net will link all PCs, Macintoshes, SUN workstations, and VAX computers using the TCP/IP network protocol.

The Interactive Mapping Program (IMP) is being sold to the public. IMP will plot the user's data on a Mercator map with a wide range of options. Two or three world outline sets are available (depending on the version). IMP was intended as an adjunct to the EPIC CD–ROM and reads those output files by default.

Two holograms were completed which use computer-generated images to display seismic information. They depict the seismicity in the San Francisco area. The first shows the Loma Prieta aftershock sequence and was featured on the cover of the special edition of the Bulletin of the Seismological Society of America (BSSA) distributed in October 1991. The second is a wider view of the San Francisco Bay area as seen from the northwest. These holograms are the second and third time that seismic information has been holographically displayed. (We also produced the first hologram representing seismic information.)

A PC-based Bulletin Board System (BBS) continues to serve as a focal point for seismic and geomagnetic information to the general public as well as participating scientists. It can be accessed by calling (303) 273–8508. We hope to add an 800 number in the future which will make the call less burdensome to the public. The BBS is used to permit the public to access the Quick Epicenter

Determination files and to leave messages to branch staff. Scientists can use it to leave seismic information or messages. The intent is to take some of the workload off of the VAX and to reduce the danger to the VAX from hackers. In order to promote amateur seismology, we have added an area for such purposes in the BBS and have allowed Mr. Robert Samuelson of New Hope, Minnesota, to post his programs and files there. Mr. Samuelson has built his own seismometer and is recording digital waveforms on his PC. He has also written a program to display the waveforms which can then be enlarged or shifted as needed. While this may have no immediate usefulness to the branch, we feel that amateur interest in seismology should be encouraged.

Global Seismograph Network Evaluation and Development

9920-68152

Charles R. Hutt
Branch of Global Seismology and Geomagnetism
U.S. Geological Survey
Albuquerque, New Mexico 87115-5000
(505) 846-5646

Investigations

Continued work in support of the US/USSR Joint Seismic Program.

Results

Equipment was ordered, assembled, and tested for a new Global Seismograph Network (GSN) station at Yuzhno-Sakhalinsk and two engineers from the station were trained over a two-week period at the Albuquerque Seismological Laboratory. The equipment and installation team were flown to Yuzhno-Sakhalinsk in May on a chartered Aeroflot plane and a successful installation was completed in June. Site visits were made to Petropavolvsk-Kamchatsky and Yakutsk to formulate agreements and to discuss actions needed to prepare these sites for installation of GSN systems in 1993. Both sites will require the construction of new vaults. A visit was also made to Magadan to meet with members of the seismological organization and inspect facilities to assess the feasibility of the future installation of a GSN station. Equipment has been ordered for the stations to be installed in 1993 and plans are being made for a training program.

Geophysical Framework
San Francisco Bay Earthquake Hazards

9380-03074

Robert C. Jachens and Andrew Griscom
U.S. Geological Survey MS 989
345 Middlefield Road
Menlo Park, CA 94025
(415) 329-5300

Investigations Undertaken

1) Gravity surveys were conducted in the Santa Cruz Mountains to fill in regional data gaps and to define the gravity anomalies along profiles critical to understanding the subsurface structure and lithology.

2) A new detailed aeromagnetic survey of northern San Jose and the east San Francisco Bay area was received from the contractor and merged with previous detailed surveys of San Jose, Menlo Park, and the San Francisco Peninsula.

3) A compilation of rock density and magnetic susceptibility was begun on samples from outcrops in the San Francisco Bay Area and surrounding mountains.

4) Most of our effort this past year was devoted to an interpretation of the structure of the upper crust surrounding the focus of the Loma Prieta earthquake. The main goals were to define the geophysical framework of this event and to examine the possible influence of crustal structure on fault movement and the distribution of aftershocks. This interpretation is based primarily on surface geology and modeling of gravity and magnetic anomalies constrained by information from seismic tomography and aftershock distributions. The interpretation is focused on the upper ten kilometers in the region bounded by the San Gregorio Fault to the west, the Gabilan Range to the south, the Calaveras and Silver Creek Faults to the east, and the latitude of the southern tip of San Francisco Bay to the north.

Results Obtained

1) The newly merged aeromagnetic map of the greater San Francisco Bay Area provides a detailed portrayal of the geomagnetic field in an area that extends from south of Santa Cruz to north of San Pablo Bay and from the west edge of the Great Valley nearly to the Pacific Coast. This map contains

detailed information on the subsurface distribution of plutonic rocks of the Salinian block southwest of the San Andreas Fault, mafic and ultramafic rocks of the Franciscan and younger terranes northeast of the San Andreas and Pilarcitos Faults, Cenozoic volcanic rocks throughout the region, and magnetic sedimentary strata mainly in the Diablo Range and the Santa Cruz Mountains. The new map displays prominant anomalies related to the Hayward Fault under San Pablo Bay and the northward continuation of the structures exposed at Mount Diable, anomalies which will provide additional insights into the crustal structure imaged by the BASIX experiment.

The new detailed aeromagnetic map has been merged with less detailed (1 km grid) aeromagnetic data to produce a statewide map of the geomagnetic field at an effective height of 300m above the earth's surface. This map provides a regional perspective for the highly detailed San Francisco Bay area survey and allows local structures to be interpreted within a regional context.

2) Combined interpretation of the geology, gravity, magnetic, and seismic data has resulted in substantial progress toward a model of the geology and structure of the upper 10 km of the crust of the Santa Cruz Mountains and adjacent Santa Clara Valley. The region southwest of the San Andreas Fault is made up of fault-bounded blocks floored by Mesozoic intrusive rocks. The La Honda Basin, wedged between the San Andreas and Zayante-Vergeles Faults, contains up to 6 km of Tertiary sedimentary rocks that overly a gabbroic basement probably related to ophiolitic rocks exposed at the southern end of the Sierra Nevada batholith. The Zayante-Vergeles Fault dips to the southwest, with Salinian block granitic rocks overriding the La Honda Basin block by as much as 10 km in places. In contrast the San Gregorio Fault farther southwest under Monterey Bay dips to the northeast.

Immediately northeast of the San Andreas Fault, the magnetic data have been critical in defining the upper crustal structure of the Franciscan and overlying terranes, and interpretations based on the gravity and magnetic anomalies indicate a tectonic history that includes obduction, uplift, tectonic wedging, dismemberment, and major lateral transport. One implication of this interpretation is that tectonic wedging has played a major role in the development of the Santa Cruz Mountains and that, unlike along the Great Valley-Coast Range boundary where the wedging is mostly confined to the subsurface and only revealed through geophysical and geologic inference, here the tectonic wedges have been tilted and eroded, providing exposed cross sections along which to study the phenomenon.

Still farther to the northeast but southwest of the Silver Creek Fault, the structural style within the Franciscan terranes is characterized by sedimentary blocks interleaved with flatlying sheets of serpentinite and mafic metavolcanic rocks. We infer that the Silver Creek Fault dips to the southwest.

3) A comparison of our crustal model with the distribution of aftershocks of the Loma Prieta earthquake leads us to the following observations and conclusions:

a) Many of the aftershocks that in plan view plot northeast of the San Andreas Fault trace, probably occurred on this fault. Although the distribution of aftershocks defines a major southwest-dipping zone of activity that most likely defines the San Andreas fault in the subsurface, the magnetic interpretation indicates that locally the San Andreas Fault must dip to the northeast in the top few km. The location of the inferred northeast dip coincides with a place where the aftershocks plot northeast of the fault trace.

b) Some isolated clusters of aftershocks southwest of the San Andreas Fault coincide with the inferred southwest subsurface projection of the Zayante-Vergeles Fault and probably reflect minor movement on this fault.

c) Many aftershocks appear to be associated with the Sargent Fault, which according to our crustal model cuts across the major structural boundaries in the Sierra Azule and underlying blocks. None of the inferred major structural boundaries are significantly offset by the Sargent Fault, suggesting that total offset on this fault is no more than a few kilometers

d) Some aftershocks near the northwest end of the aftershock zone probably occurred on a suite of southwest-dipping thrust faults in the vicinity of Cupertino.

e) The La Honda basin is floored by a coherent gabbroic block that is bounded on the northeast by the San Andreas Fault from just south of Logan quarry on the south to Lexington reservoir on the north. This reach coincides closely with the Loma Prieta "kink" in the San Andreas. The gabbroic block, as defined by the magnetic data, is remarkably free of aftershocks.

4) We now have a physical property data base with nearly 1300 elements, containing information on rock type, formation name, age, location, density, and magnetic susceptibility.

Reports Published

Jachens, R.C., and Griscom, Andrew, in press, Geologic and geophysical setting of the 1989 Loma Prieta earthquake, California, inferred from magnetic and gravity anomalies: U.S. Geological Survey Professional paper.

Jachens, Robert C., Griscom, Andrew, and McLaughlin, Robert J., 1992, Anatomy of the San Francisco Bay region: An evolving 3-D crustal model based on surface geology, and gravity and magnetic anomalies (abs.): EOS, Transactions, American Geophysical Union v. 73, p. 401.

Jachens, R.C., and Roberts, C.W., 1992, Aeromagnetic map of the San Francisco Bay area, California: U.S. Geological Survey Geophysical Investigations Map GP-1007, 1 sheet, scale approximately 1:286,500.

Roberts, C.W., and Jachens, R.C., 1992, Isostatic residual gravity map of the San Francisco Bay area, California: U.S. Geological Survey Geophysical Investigations map GP-1006, 1 sheet, scale approximately 1:286,500. (on satellite image, with interpretive text)

U.S. Geological Survey, 1992, Aeromagnetic map of Livermore and vicinity, California: U.S. Geological Survey Open File Report 92-531, 1 sheet, scale 1:250,000.

Wentworth, C.M., Jachens, R.C., Simpson, R.W., and Michael, A.J., 1992, Structure of the Parkfield region, CA, from geology and geophysics compiled in a geographic information system (GIS) (abs.): EOS, Transactions, American Geophysical Union v. 73, p. 396.

Instrument Development and Quality Control

9930-01726

E. Gray Jensen
Branch of Seismology
U.S. Geological Survey
345 Middlefield Road - Mail Stop 977
Menlo Park, California 94025
(415) 329-4729

Investigations

This project supports other projects in the Office of Earthquakes, Volcanoes and Engineering by designing and developing new instrumentation and by evaluating and improving existing equipment in order to maintain high quality in the data acquired by the Office. Tasks undertaken during this period include production of a 20 digital seismic telemetry field stations, support and maintenance of Seismic Group Recorders operations, development of a new Real Time Processor (RTP) for CALNET and supporting the establishment of an instrument center among other things.

Results

Twenty digital seismic telemetry (DST) field station a nearing completion. A prototype unit has been in field operation for some time monitoring a borehole seismic station. All printed circuit boards for the field station have been created. Final assembly and testing of the 20 production units is proceeding. In anticipation of deployment of these and other commercial digital stations, this project has been instrumenting and monitoring new borehole seismometers along the southern Hayward Fault. Use of portable recorders has proved the lower noise capability of the borehole sensors and revealed which sensors are not functioning in the preliminary test holes.

Development of an new RTP has shifted from Rex Allen's design based on transputers to a broader project based on multiple PCs or Suns connected by networks. In addition to picking and locating events on CalNet, we would like to integrate data from other sources such as new digital seismic stations. The goals for system output have been expanded to include rapid notification of event parameters to a variety of users.

The PASSCAL Instrument Center was established at this office late in 1991. The center now has over 100 3-channel, 195 megabyte seismic recorders for refraction and other experiments. This project has supported the establishment and operation of this IRIS center.

The Seismic Group Recorders have been busy during the last year. They were used in projects in the Pacific Northwest, southern California, Mexico, Canada, Montana, Nevada and the California north coast. This project supported most of these operations with instrument maintenance and some field support.

Piñon Flat Observatory: Comparative Studies and Geophysical Investigations

14-08-0001-G1763

Hadley O. Johnson, Frank K. Wyatt,
Duncan C. Agnew, James W. Happer
Institute of Geophysics and Planetary Physics
Scripps Institution of Oceanography
University of California, San Diego
La Jolla, CA 92093-0225
(619) 534-2411

This grant provides support for collaborative studies with several USGS-sponsored investigators conducting research at Piñon Flat Observatory (PFO). We briefly describe here a few of the projects we have been engaged in during the previous year. Each of these turns out to involve, in one way or another, GPS geodesy; while this has not been our primary focus in the past, we have found it very useful to examine this widely-used technique. Much of the work in this field has been, quite reasonably, on applying the technique to solving tectonic problems. Instead, our focus under this grant has been to try to fully understand the capabilities and error sources involved with this technique.

A particularly interesting study we have undertaken is a comparison between GPS and the two-color EDM data of Dr. John Langbein from his networks at Pinyon Flat and Anza—both near the San Jacinto Fault in southern California. Figure 1 shows the relative locations of the two-color and Geodolite (one-color EDM) networks to PFO. Over the span of these networks (1—10 km), the two-color system has been shown to have 1 mm or better precision, something we would like to be able to duplicate with GPS. But in order to understand how to process GPS data over these distances, we need a standard for comparison; the two-color data provide this.

The comparison is not straightforward, however, because of the nature of the 2-color Terrameter measurements.[1] This system does not in fact measure the absolute distance; unlike most EDM's it does not measure the phase of a signal modulated at different frequencies, but instead adjusts the modulation frequency until a null is found, meaning that there are an integer number of modulation wavelengths, N, in the optical path. This is done for two colors, red and blue, giving two frequencies f_i^r and f_i^b for the measurement over the i-th line. If f_i^r and f_i^b are separated by approximately 42 kHz (which is forced by the operator), N will be the same for both (because of the dispersive nature of the atmosphere). The relationship between the line distance d_i and the measurements is then

$$d_i = N_i \frac{c}{2}\left[\frac{1}{f_i^r} - A_i^r\left[\frac{1}{f_i^b} - \frac{1}{f_i^r}\right]\right] + C_\tau \equiv N_i \lambda_i + C_\tau$$

where c is the speed of light, A^r is related to the ratios of the index of refraction of red and

[1] We have received much help on this from Dr. Langbein, and have also found the thesis of Slater (1975) very useful.

blue light (and is found from end-point meteorological data), λ_i is the (defined) modulation wavelength, and C_τ is an instrument (and reflector) constant. If the instrument is used to find only changes in d_i, as it usually is, C_τ drops out and we need only a rough estimate of N, which is calculated using a measurement over a nearby parallel line with an HP3808 EDM. However, if we seek to compare absolute lengths, we need to know both N_i and C_τ—and neither of these is known *a priori*. (Note that for measurements on i lines there will always be $i + 1$ unknowns.)

Now suppose that we have measured GPS distances g_i over M lines; assuming that the 2-color measurement is error-free, we have $d_i = g_i + e_i$, e_i being the error in the GPS distance. Then N is given as a function of C_τ and e_i by

$$N = \frac{g_i + e_i - C_\tau}{\lambda_i}$$

For any value of C_τ we must select a set of e_i to make the N found by this formula an integer. This does not constrain C_τ at all, but we may do so by minimizing the variance of the GPS errors, that is by choosing C_τ to make $S(C_\tau) = \sum_{i=1}^{M} e_i^2$ a minimum. For each survey line, the curve of e_i as a function of C_τ will be periodic with period λ_i (see figure 2). Since for the actual measurements λ_i is always 5 cm to within a few parts per million, S will have this same periodicity. We can uniquely determine the minimum GPS error, and will then find C_τ to "modulo" 5 cm. Of course, our method chooses a distribution of e_i's centered on zero; any length-independent bias in the GPS results will bias our estimate of C_τ.

In April 1992 we conducted a GPS survey of most of the lines in the two-color network across Pinyon Flat, in two eight-hour sessions in the afternoon and evening of the same day. The data were processed using the GAMIT software and orbits provided by Dr. Yehuda Bock at UCSD from the PGGA network.[2] One line (Green to the fixed station PIN2) was common to both surveys. The ionosphere-free observable LC was used for final processing, even though the lines were all less than 5 kilometers long; this gave the most consistent results for the two surveys of this one repeated line. Data from two EDM surveys conducted in January and May 1992 were used for comparison. (The two EDM surveys used different two-color instruments which have different error characteristics and different instrument constants.) Figure 2 shows the process of comparing the GPS and EDM data sets. The left panels show the individual traces of e_i^2 as a function of C_τ for each line (each two-color line is actually shown twice, since the USGS crew routinely makes two measurements on successive nights during each survey, resulting in two independent estimates of the line length.) The right panels show $S^{1/2}$ as a function of C_τ ; the minima are well-defined and lead to estimates for the rms error of the GPS measurements of 1.2 mm and 1.5 mm—impressively small misfits. The best estimates for C_τ are 2.052 m and 2.061 m for the two EDM instruments used; these particular values were chosen over the other equally good ones based on Dr. Langbein's previous best estimates for the C_τ.

We have thus determined the precision of these GPS measurements over distances of a few kilometers, as well as the instrument constants of two of the Terrameter instruments. We

[2] The Permanent GPS Geodetic Array (PGGA) is a continuous GPS network covering the southern California region and operated as a joint project between a consortium of universities and the Jet Propulsion Laboratory.

have yet to fully reduce the data for the two-color networks near the town of Anza, but the field work has been completed, and the computer work is progressing nicely. We will examine these additional data to check their consistency with the results from the PFO net. Since some of the Anza lines are up to 12 kilometers long it will be interesting to see what GPS errors appear at these longer distances. In comparing these longer GPS results with the two-color data we can use the instrument constant derived from the shorter network around Piñon to see if any bias appears in the GPS results at longer distances; we can also see if the scatter goes up to the level that we expect from our repeat measurements over a 14-kilometer continuous line (briefly described below).

We are also in a position to help others use the two-color net at PFO for testing precise GPS techniques; in particular, the lack of obstructions at PFO means that a kinematic survey of the two-color marks could be done as easily as a more conventional one. Finally, the determination of C_τ means that the absolute line-lengths of other two-color measurements can be found to a few mm as long as they are known to within 5 cm: an easy task using conventional EDM or GPS. (With more data for our comparisons we should be able to reduce this few mm uncertainty to less than 1 mm.)

The favorable results from our comparison work with the two-color EDM system lead one to the issue of benchmark stability. With the level of precision that is possible with modern geodetic techniques, it is important to be sure that the data are not degraded because the ground mark moves in response to local soil instabilities. The construction of well-stabilized monuments is something that our long-term focus on strain and tilt measurements has caused us to be interested in, and we have tried to apply our knowledge to create several designs of highly-stable marks (Figure 3). These designs have as a basic principle the concept of bracing the mark using several inclined rods cemented into holes; this is an extension of the NGS "rod mark," which uses a single vertical rod. The angled rods form a space frame, making their intersection point very resistant to applied forces, including forces applied by the near-surface material especially as the monument is nearly free-standing over its upper 6 m. This gives deep-ground stability to a near-surface mark in both the horizontal and the vertical directions.

We have constructed three deeply-anchored monuments to be used by the two-color EDM at Pinyon Flat. One, at Green (Green c), is intended to replace the existing central monument; a second one (PF5c) is near PF5, and the third (PIN3c) is adjacent to the existing GPS marks at PFO, with which it can thus be compared. These new marks have already been surveyed twice by the USGS crew (both before and after the Landers earthquake of June 1992) and accurately tied to the previous measurements.

Finally, since May 1991 we have operated a continuously tracking "GPS strainmeter" between two receivers located near PFO as a joint project with Dr. Yehuda Bock and Dr. David Jackson at UCLA (see figure 1 for locations). The receivers are located on an almost directly east-west line of 14 km length—a length scale of particular interest for fault mechanics studies. During the last year this instrument has operated well and is providing an unparalleled understanding of the true spectrum of the errors associated with GPS measurements. From our work with this data, it appears that the day-to-day scatter of the GPS positioning estimates is approximately ±5 mm E-W, ±4 mm N-S, and ±12 mm U-D (over a 14 km line). These uncertainties are comparable to those attained by the USGS single-color Geodolite EDM program. As a comparison of the relative detection capabilities of the GPS strainmeter, figure 4 presents a series of East-West GPS distance estimates (converted to strain) and data from the three

long-baselength laser strainmeters we operate at PFO (the modulation seen on the laser strainmeter data are the earth tides). Clearly, and even with averaging, the strainmeters can detect much smaller signals, by a factor of 100 to 1,000, than the GPS data can over the relatively short time-span of this figure. Last year's report presents more details of this experiment.

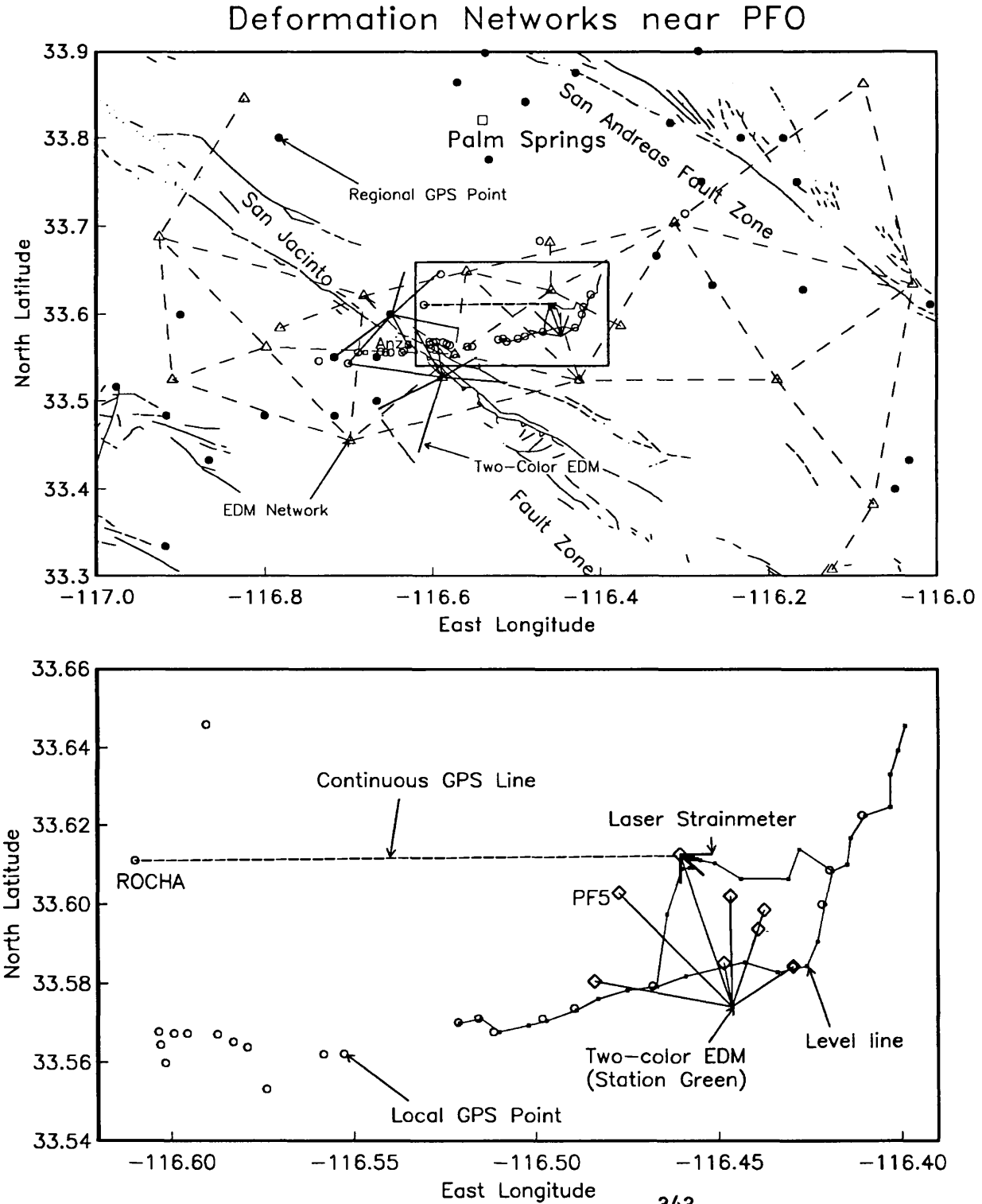

Figure 1.

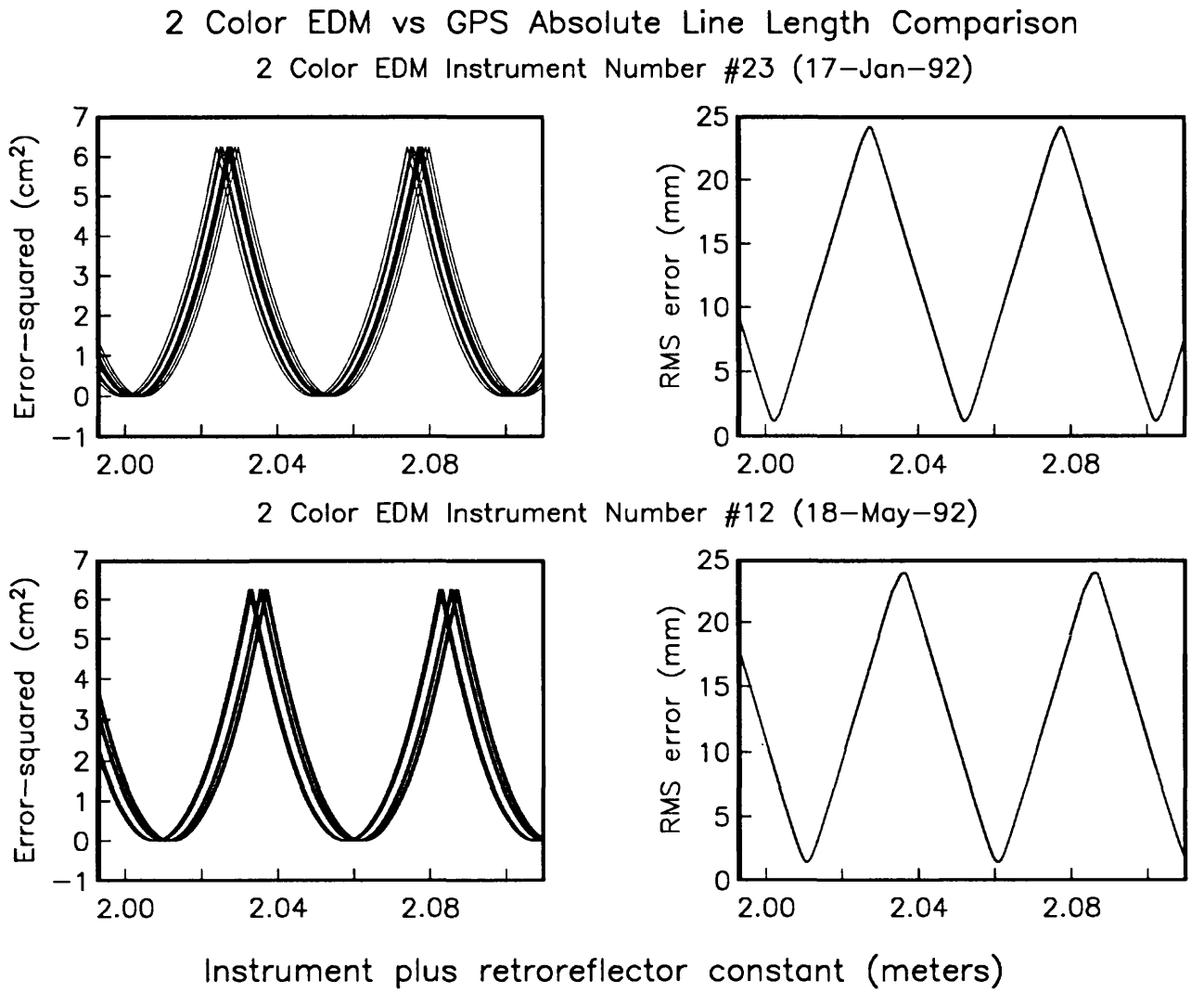
2 Color EDM vs GPS Absolute Line Length Comparison
2 Color EDM Instrument Number #23 (17-Jan-92)
Error-squared (cm²)
RMS error (mm)
2 Color EDM Instrument Number #12 (18-May-92)
Error-squared (cm²)
RMS error (mm)
Instrument plus retroreflector constant (meters)

Figure 2.

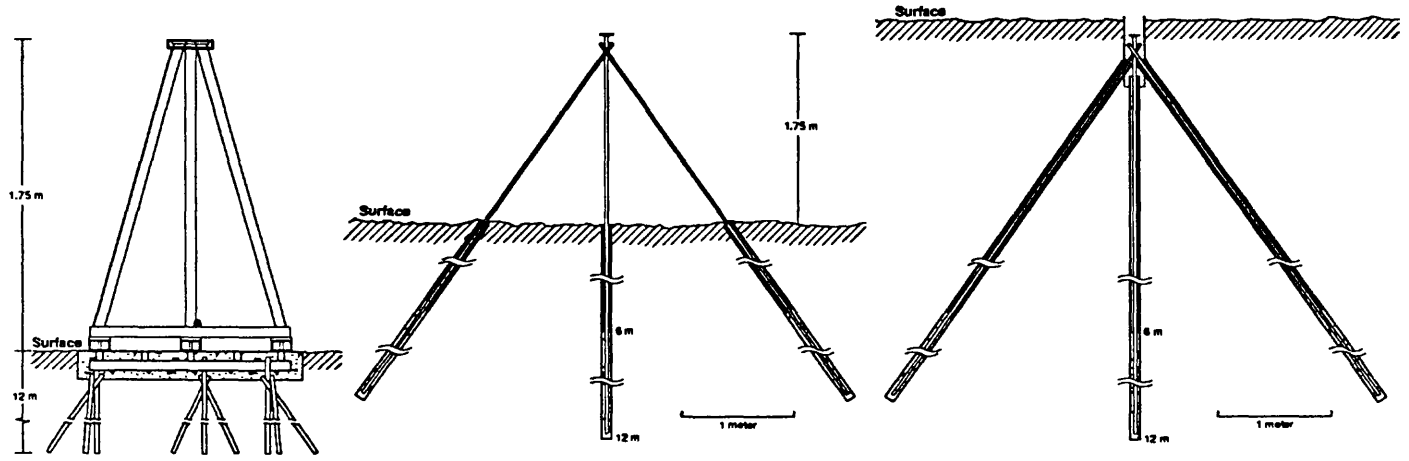

Figure 3.

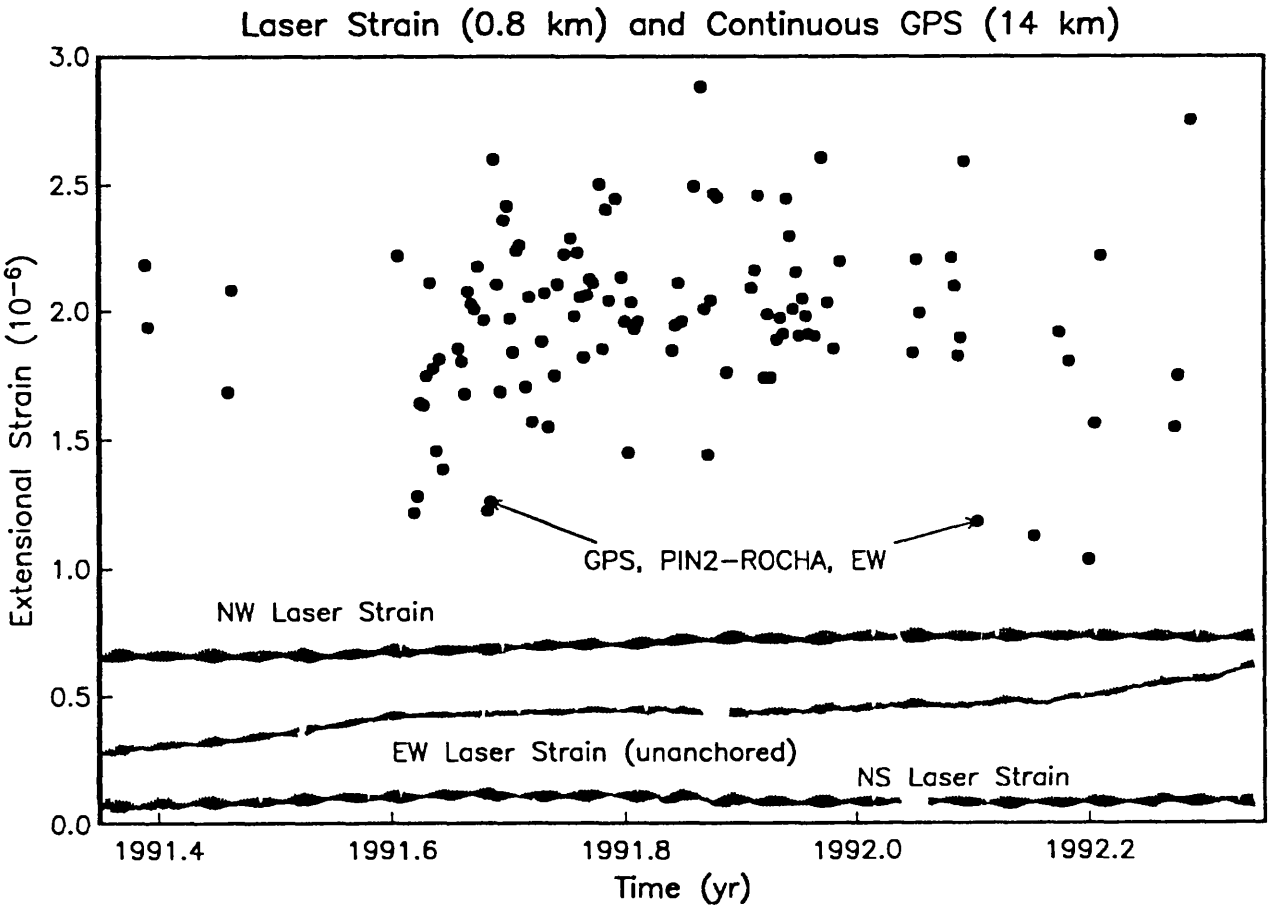

Figure 4.

Source Parameters of the 1957 Aleutian Earthquake from Tsunami Waveforms

Agreement No. 1434-92-G-2187

Jean M. Johnson and Kenji Satake
University of Michigan
1006 C.C. Little Building
Ann Arbor, MI 48109-1063
(313) 763-4069

I. Introduction

On 9 March 1957 a great earthquake (M_S=8.1) occurred in the central Aleutian Islands at 51.63°N, 175.41°W at 14:22 GMT. There are little seismic data available for this earthquake because it occurred before the introduction of the WWSSN stations. Due to this dearth of high quality data, this earthquake has been poorly understood. Elementary source parameters such as rupture area, seismic moment and slip distribution have not been well determined.

The source area of an earthquake is often identified as the region containing the aftershocks, which often delineate the fault rupture plane. The aftershock zone of the 1957 earthquake is the longest of any earthquake ever recorded. It stretches 1200km along the Aleutian Trench from approximately 164°W to 180°W (Figure 1). Both Sykes (1971) and Kanamori (1977) used the 1200km long aftershock zone of the 1957 earthquake in estimating the seismic moment. But these estimates are an order of magnitude different. Sykes' estimate of 30×10^{20}Nm is derived from the length of the aftershock zone and an average slip on the fault of 0.45m. Kanamori estimated the moment as 585×10^{20}Nm based on the relationship between source area and moment release, making the 1957 earthquake the third largest this century. However, House*et al.* (1981) argued that the easternmost area of the aftershock zone near Unalaska Island is anomalous and suggested that this area did not rupture in the 1957 main earthquake. In any case, the aftershock zone is an indirect means of deriving the moment.

The moment of the 1957 earthquake has also been estimated by more direct methods. Abe (1979) used the relationship between maximum tsunami height and earthquake moment to assign a tsunami magnitude of M_t=9.0 to the 1957 earthquake. The equivalent moment is 400×10^{20}Nm. Ruff *et al.* (1985) used the single

available surface wave record from the 1957 earthquake to estimate the slip distribution and determined a moment of 100×10^{20}Nm. However, the response of the instrument in Pietermaritzburg, South Africa where the surface wave was recorded, is poorly known, making results from this seismic data suspect. Lane and Boyd (1990) have studied the surface wave directivity of this surface wave record by a nonlinear inversion (simulated annealing), but they could only determine the rupture length of the earthquake.

From this brief review it is obvious that many questions about the basic source parameters of the 1957 Aleutian earthquake remain. Moment estimates range from $30\text{-}585 \times 10^{20}$Nm. Even the rupture area is not well established. Lack of seismic data has hampered past efforts to determine these parameters precisely. There is, however, a good quality data set available for this earthquake. The tsunami generated by the earthquake was recorded on tide gauges all around the Pacific Ocean. The tsunami waveforms can be used to determine the source parameters of the 1957 earthquake.

2. Computation of Tsunami Propagation

A tsunami which is generated by a large earthquake and propagates across the ocean can be treated as a linear long wave because the wavelength is much larger than the water depth. The wave equation for the small amplitude, linear long wave is

$$\nabla h^2 = \frac{1}{c^2}\frac{\partial^2 h}{\partial t^2}$$

where $c = \sqrt{gd}$, h is the height of water displaced from the equilibrium position, g is the acceleration of gravity, and d is water depth. Equivalently, the equation of motion and the equation of continuity are

$$\frac{\partial Q}{\partial t} = -gd\nabla h$$

$$\frac{\partial h}{\partial t} = -\nabla \cdot Q$$

where Q is the flow rate vector.

Given an initial condition, or water height, the equation of motion and equation of continuity can be solved by finite-difference calculations on a staggered grid system. Using highly accurate, digital bathymetry of the Pacific Ocean, the tsunami velocity and thus tsunami propagation can be calculated very accurately.

The initial condition is specified by the deformation of the ocean floor due to a buried fault as given by a program like Okada's (1985). This provides the initial condition in the source area. The tsunami propagation is calculated and a synthetic waveform is computed at the location of the tide gauges where the tsunami was actually observed.

Obviously, the tsunami velocity depends only on the water depth; therefore, the synthetic waveform is very sensitive to the bathymetry. The more accurate the bathymetry, the more accurate the computation. This suggests that a fine grid system be adopted in which to calculate the tsunami propagation. However, very fine grid-spacing on the entire northern Pacific Basin would be impractical due to the enormous computational effort. For the majority of the deep Pacific Ocean where the bathymetry changes slowly, the grid space need not be any finer than 5' (approximately 10 km). However, near coastal areas, the bathymetry changes much more rapidly. Also, islands and harbors where tide gauges are located cannot be adequately represented by 5' grid spacing. Therefore, in coastal areas, 1' (less than 2 km) grid spacing is used. Bathymetry of 1' accuracy is used for the west coast of North America, the Hawaiian Islands, and around the tide gauges in Alaska. Figure 2 shows the difference between 5' and 1' grid spacing around the island of Unalaska. With 5' bathymetry, Dutch Harbor, where the tide gauge is located, completely disappears.

3. Tsunami Source Area

As stated previously, the aftershock zone of the 1957 earthquake is the longest of any earthquake ever recorded. The eastern end of this aftershock zone has very few aftershocks, and it has been suggested that this area did not rupture in the 1957 main event. An alternative to equating the aftershock area and the source area is to determine the source area by tsunami data.

The tsunami source area can be located by a backward computation of the tsunami travel time from the source to the tide gauge. An initial condition is given at the tide gauge location. The tsunami propagates from the tide gauge for the duration of the observed tsunami travel time to that tide gauge. The location of the leading wavefront, or travel time arc, gives the origin point of the tsunami that reached that tide gauge. When many such travel time arcs from tide gauges distributed around the earthquake are combined, they bound a region that is the source area of the tsunami. Hatori (1981) used this method to determine the source area (Figure

3). Hatori's source area includes the eastern end of the aftershock area. However, this estimate may be unreliable. Few of the available observations were used. Also, the travel time arcs associated with both Unalaska Island and Sitka are questionable. The travel time used by Hatori for Sitka does not agree with any published travel time, nor does it agree with the apparent arrival time on the Sitka tide gauge record. Hatori's travel time arc for Unalaska is not compatible with a backward travel time of 83 minutes from Dutch Harbor where the tide gauge is located. Without these two travel time arcs, there is no constraint on the eastern end. But most significantly, Hatori drew the inverse refraction diagrams for all the travel times manually from large-scale bathymetric maps of the Pacific Ocean.

Our numerical calculation done on a fine grid of the actual Pacific Ocean bathymetry gives more reliable results. We computed travel time arcs from tide gauges in Alaska, N. America, and Hawaii. Figure 4 shows the travel time arcs and source area. Our source area is approximately 850km long, from 180°E to 168°W, and does not include the eastern end of the aftershock zone. Similar results were obtained by Lane and Boyd (1990) using surface wave directivity.

This supports the theory of House *et al.*(1981) that the 1957 earthquake ruptured a smaller section of the arc than can be assumed from the aftershock area.

We further performed forward modeling on two different fault models, with different lengths as shown in Figure 5. The longer fault is 1100km and covers the entire aftershock area, while the shorter is 600km and covers the western half of the aftershock area. The other parameters are the same for both (W=150km, δ=30°, and average slip S=1m). The results for one tide gauges is shown in Figure 6. The observed tsunami waveform from Dutch Harbor, Unalaska Is. is shown with synthetic waveforms from the short and long fault models. Clearly, the arrival time for the long fault model synthetic waveform is inconsistent with the observed tsunami arrival time. This again supports the hypothesis that the eastern end of the aftershock zone was not involved in the 1957 event.

5. Tsunami Waveform Inversion

Method

The best way to determine the source area and moment distribution of the 1957 earthquake is to directly invert the waveforms. We can obtain the slip distribution on the 1957 rupture zone, which will give an estimate of the moment and source area.

The method for inverting tsunami waveforms has been used previously by Satake (1989) for determining the slip distribution of the 1968 Tokachi-Oki and the 1983 Japan Sea earthquakes. Those studies used local and regional tsunami data, while this study is the first to determine slip distribution from far-field tsunami waveforms. However, the method is the same.

The fault area is divided up into subfaults. The latitude, longitude, strike, dip, depth, and area of each subfault is specified. The vertical deformation of the seafloor from unit displacement on each subfault is calculated. This bottom deformation is then used as the initial condition, and a waveform is calculated at each tide gauge from each subfault. This results in Green's functions for each tide gauge. The observed waveform is a linear superposition of the Green's functions, so the displacement on each subfault can be determined by solving the linear equation

$$A_{ij} \cdot x_j = b_i$$

where A_{ij} is the computed Green's function at tide gauge i for unit slip on subfault j, b_i is the observation at tide gauge i, and x_j is the unknown slip on subfault j. This equation can be solved by least-squares method by minimizing the misfit between the observed and synthetic waveforms.

Results

We divided the aftershock zone of the 1957 earthquake into eleven subfaults. The fault parameters were the same for each subfault. The parameters were L=100km, W=150km, δ=15°, and depth to the top of the subfault 1km. Figure 9 shows the location of the subfaults in relation to the Aleutian Arc. Each subfault has unit displacement in the direction of Pacific Plate motion relative to N. America. The displacement direction was determined for each subfault individually from the Euler pole at 48.7°N, -78.2°E with rotation rate of 0.78 deg-m.y.$^{-1}$ (DeMets *et al*, 1990). This means that the slip changes from pure dip-slip in the eastern end of the rupture zone to nearly equal components of dip-slip and strike-slip in the west. The tsunami waveform was then computed for each subfault. Figure 7 shows an example of the resulting Green's functions for the tide gauge at Massacre Bay, Attu Island.

Next we inverted the waveforms from 12 tide gauges from Alaska, the Aleutians, Hawaii, and N. America. These tide gauges are Attu, Unalaska, and Yakutat, AK; Neah Bay, WA; San Francisco, Alameda, San Pedro, Los Angeles Harbor, Newport Bay, and San Diego, CA; and Hilo, HI. The waveform data at each tide gauge station

consists of an average of 110 time points (dt=1 min) and the total number of data points is 1312. Figure 8 shows the observed and computed waveforms from some of these tide gauges. We performed both a free inversion (least-squares with no constraints on the solution), and an inversion with a positivity constraint. The slip distribution from the solution with a positivity constraint can be seen in Figure 9. It shows that the greatest slip occurred in the western half of the aftershock zone between 174°W and 180°E. The greatest slip occurred on subfault 4 (7m) and subfault 5 (5m) between 174° and 177°W. There is very little slip in the eastern half of the aftershock zone, with subfault eight having the only appreciable slip. There is no slip in the easternmost subfaults (aside from negligible slip on subfault 11) from 164° to 169°W, which corresponds to the results from determination of the tsunami source area. The results for both free and constrained solutions are compared in Table 1. The slip distributions in the western half of the rupture zone for both inversions are fairly compatible. In the eastern half the negative values in the free inversion are almost all zero under the positivity constraint. The RMS values for both inversions are almost the same. However, the synthetic and observed waveforms match more closely in the constrained solution, particularly for Dutch Harbor, as shown in Figure 10. The positivity constraint forces the slip in subfaults 10 and 11 to zero to match the Dutch Harbor waveform.

It is obvious from Figures 9 and 10 that the solutions from both the free and constrained inversion are unable to match the first positive pulse at Unalaska and San Francisco. A large displacement on subfault 8 can explain the pulse at Unalaska, and a large displacement on subfault 9 can explain the first pulse at San Francisco. However, large displacements in either of these subfaults is incompatible with the large amplitude wave at Hilo. We hypothesized from an examination of first arrival times at the three tide gauges in question that a large displacement on a subfault of smaller area and at the down-dip edge of subfault 8 or 9 might be compatible with all three waveforms. Accordingly, we divided subfaults 8 and 9 into smaller faults. Figure 11 shows the position of the additional subfaults 12 and 13. These subfaults have parameters L=50km, W=75km, δ=15°, and depth to the top of fault 20.4km. Green's functions were computed for these additional faults, and the inversion was performed again. The results are listed in Table 2. Figure 10 shows that a displacement of 3.3m on subfault 12 matches the first pulse on the Unalaska waveform and is still compatible with the Hilo waveform. However, the first pulse on the San Francisco waveform is still poorly matched. The solution for 13 subfaults is

compatible with our hypothesis of concentration of slip on a smaller subfault in the eastern half of the rupture zone. It is also compatible with the total average slip for the entire rupture zone, as the slip on subfault 12 is approximately four times the slip on subfault 8 from the solution for eleven subfaults.

Error Estimates

The formal statistical errors for a standard least-squares inversion are not considered a good estimate of the actual errors (Tichelaar and Ruff, 1989). Further no formal errors can be estimated for a non-negative least-squares inversion. Therefore, we applied a resampling technique to determine the errors. We reinverted the tsunami waveforms twelve times, each time dropping one waveform from each of the tide gauge stations from the data. This gives twelve estimates of the slip distribution, and a mean and standard deviation for the slip on each subfault can be determined. The results are listed in Tables 1 and 2 for each of the four inversions described in the previous section. The error estimates are almost all less than a meter. The errors show that the data is well-resolved, except for subfault 11. Therefore, the concentration of slip in the western half of the rupture zone and the small slip in the eastern half are real.

This technique for determining the errors is similar to the jackknifing technique described by Tichelaar and Ruff (1989). In jackknifing, a fixed number of random data points are deleted to produce a resample that is then inverted for the model parameters. Our technique is a pseudo-jackknife because we treat each waveform as a single data point. The resulting standard deviations of this pseudo-jackknifing technique are the same as the standard deviations derived above. If we treat each waveform as 110 data points out of a total of 1312 data points, then we must consider our resample as a delete-110 jackknife with corresponding errors. These errors are simply the standard errors derived above multiplied by a scale factor. In our case, that scale factor is approximately 3. This increases the errors we have determined enormously. However, since we delete an entire waveform at a time, rather than 110 random data points, the errors determined can be strongly influenced by the presence or absence of certain waveforms. Hence, we cannot compare directly the errors from the pseudo-jackknife to the true jackknife errors.

6. Discussion

As stated in the introduction, estimates of the seismic moment release in the 1957 earthquake vary by as much as an order of magnitude. With slip distribution as determined by tsunami waveforms, the seismic moment can now be accurately estimated. Table 1 summarizes the moment as determined by the four inversions. The highest of these estimates is 88×10^{20}Nm and the lowest is 67×10^{20}Nm. These estimates give a moment magnitude of M_W=8.5-8.6. This is much smaller than the estimate of Mw=9.1 originally assigned by Kanamori (1977). However, this estimate is in good agreement with the later estimate of 100×10^{20}Nm by Ruff *et al.* (1985), which was determined from the surface wave record. Although the magnification of the Pietermaritzburg instrument is only poorly known, the results from surface wave studies are more reliable than determining the moment purely from the aftershock area which has already been shown to be smaller than the actual rupture area. Ruff *et al.* also determined the moment distribution as shown in Figure 12. It shows that the greatest moment release occurred in the western half of the aftershock zone and that little moment was released in the eastern half. Again this is similar to results from the tsunami waveform inversion. Therefore, the estimates from the surface wave record and the tide gauge records confirm each other. It should be noted, however, that Boyd *et al* (1992) have speculated from the aftershock sequence that moment release was concentrated in the eastern section of the aftershock zone from 167° to 175°W rather than in the western section.

7. Conclusions

We studied the source parameters of the 1957 Aleutian earthquake using the tsunami waveform data recorded on tide gauges around the Pacific Ocean. Using a finite-difference computation, this tsunami can be numerically simulated. The tsunami source area was estimated by backward computation of the tsunami. The tsunami records were inverted for the slip distribution on the rupture area. Results show that slip was concentrated in the western half of the aftershock zone with a maximum displacement of 7m. The moment computed from the slip distribution is 88×10^{20}Nm, giving the 1957 earthquake a moment magnitude of M_W=8.6. Both the backward computation and the waveform inversion confirm that no slip occurred in the Unalaska Island area, making this area a possible

seismic gap with a potential to rupture in a great earthquake and generate a Pacific-wide tsunami.

8. References

Abe, K., Size of great earthquakes of 1873-1974 inferred from tsunami data , *J. Geophys. Res., 84*, 1561-1568, 1979.

Boyd, T.M., E.R. Engdahl, and W. Spence, Analysis of Seismicity Associated with a Complete Seismic Cycle Along the Aleutian Arc: 1957-1989, in Wadati Conference on Great Subduction Earthquakes, Sept. 16-19, University of Alaska (43-50 in extended abstracts).

DeMets, C., R.G. Gordon, D.F. Argus, and S. Stein, Current plate motions, *Geophys. J. Int., 101*, 425-478, 1990.

Hatori, T., Tsunami magnitude and source area of the Aleutian-Alaska tsunamis, *Bull. Earthq. Res. Inst., Univ. of Tokyo, 56*, 97-110, 1981.

House, L.S., L.R. Sykes, J.N. Davies, and K.H. Jacob, Identification of a possible seismic gap near Unalaska island, eastern Aleutians, Alaska, in *Earthquake Prediction - An International Review*, edited by D. W. Simpson and P. G. Richards, 81-92, American Geophysical Union, 1981.

Kanamori, H., The energy release in great earthquakes, *J. Geophys. Res., 82*, 2981-2987, 1977.

Lane, F.D., and T.M. Boyd, A simulated annealing approach to the inversion of surface wave directivities, *EOS, 71*, 1468, 1990.

Okada, Y., Surface deformation due to shear and tensile faults in a half-space, *Bull. Seism. Soc. Am., 75*, 1135-1154, 1985.

Ruff, L., H. Kanamori, and L.R. Sykes, The 1957 great Aleutian earthquake, *EOS, 66*, 298, 1985.

Satake, K., Inversion of tsunami waveforms for the estimation of heterogeneous fault motion of large submarine earthquakes: the 1968 Tokachi-oki and the 1983 Japan Sea earthquakes, *J. Geophys. Res., 94*, 5627-5636, 1989.

Sykes, L., Aftershock zones of great earthquakes, seismicity gaps, and earthquake predicion for Alaska and the Aleutians, *J. Geophys. Res., 76*, 8021-8041, 1971.

Tichelaar, B. W., and L. J. Ruff, How Good are Our Best Models? Jackknifing, Bootstrapping, and Earthquake Depth, *EOS, 70*, 593,605-606, 1989.

Table 1 Inversion results for 11 subfaults

	non-negative LS		standard LS	
subfault #	slip	error	slip	error
1	1.1	0.66	1.3	1.93
2	1.5	0.51	1.3	1.17
3	3.7	1.00	3.6	1.31
4	7.0	1.07	6.1	1.15
5	5.2	0.59	4.5	0.74
6	0.0	0.00	-1.4	0.37
7	0.0	0.16	-0.25	0.44
8	0.76	0.32	0.81	0.27
9	0.0	0.35	-0.45	0.47
10	0.0	0.00	-2.5	0.54
11	0.08	0.27	2.5	0.53

RMS error, cm	10.02	9.67
average slip, m	1.77	1.42
Mo, 10^{20} Nm	87.6	70.3

Table 2 Inversion results for 13 subfaults

	non-negative LS		standard LS	
subfault #	slip	error	slip	error
1	1.5	0.74	1.7	1.77
2	1.3	0.46	0.99	1.30
3	4.0	1.04	4.0	0.53
4	6.9	1.10	6.0	1.01
5	4.8	0.56	3.6	0.65
6	0.0	0.00	-1.4	0.43
7	0.0	0.01	-0.12	0.37
8	0.0	0.13	-0.30	0.75
9	0.0	0.32	-0.55	0.46
10	0.0	0.00	-2.8	1.76
11	0.32	0.27	3.0	1.67
12	3.3	0.26	5.1	0.64
13	0.0	0.03	-1.6	1.49

RMS error, cm	9.75	9.25
average slip, m	1.70	1.36
Mo, 10^{20} Nm	84.2	67.3

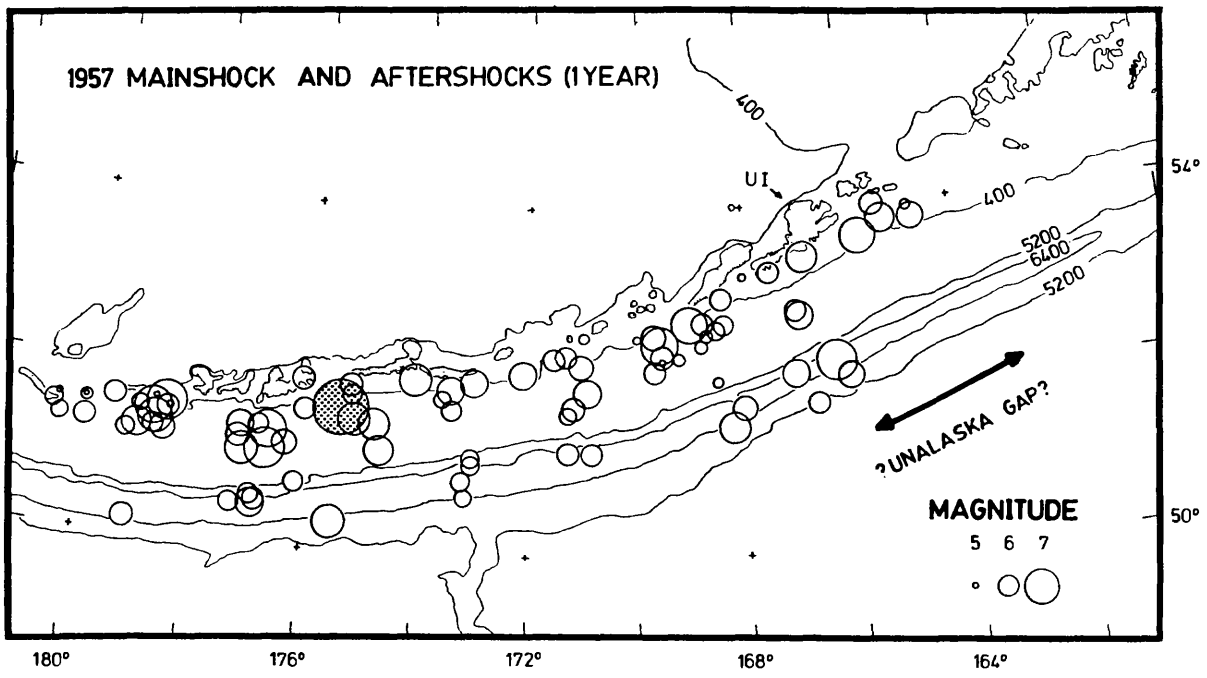

Figure 1: Detailed plot of the 1957 main shock and aftershocks over a period of 1 year. Aftershocks of March 1957 relocated by Sykes [1971] are supplemented by aftershocks located by the International Seismological Summary and the U.S. Coast and Geodetic Survey. Size of symbols is scaled to magnitude; only events assigned a magnitude of 5 or larger are plotted. The 1957 main shock is shaded and is plotted with a symbol appropriate for its surface wave magnitude (M_S) of 8.1 rather than its M_W of 9.1. UI indicates the location of Unalaska Island. Bathymetry is in meters. (from House *et al*, 1981)

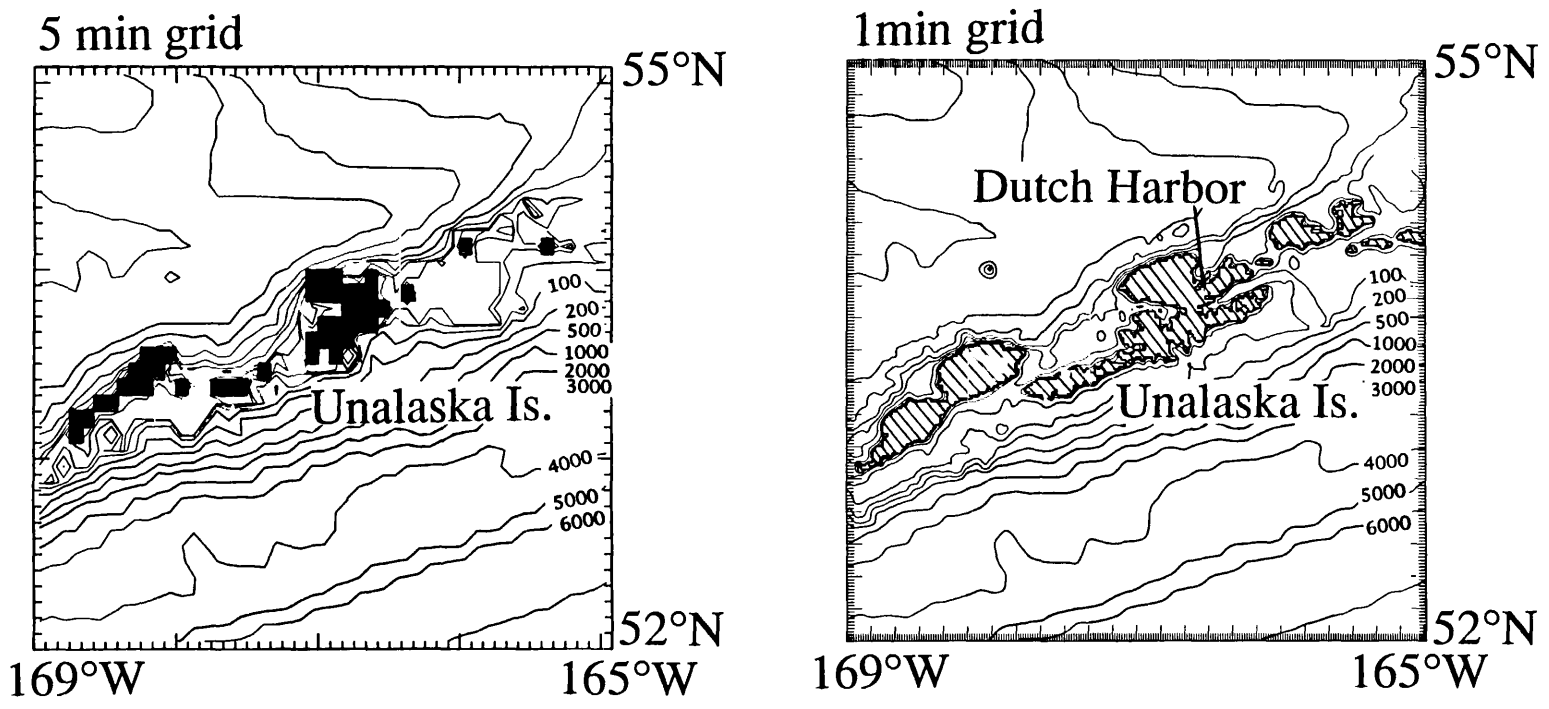

Figure 2: Comparison of detailed bathymetry near Unalaska Island using 5 minute grid size and 1 minute grid size. Bathymetry of the deep ocean is identical at 1 min or 5 min, but the islands cannot be well-represented at 5 min. The location of Dutch Harbor is indicated in the figure with 1 min grid size; at 5 min it disappears entirely. Bathymetry is in meters.

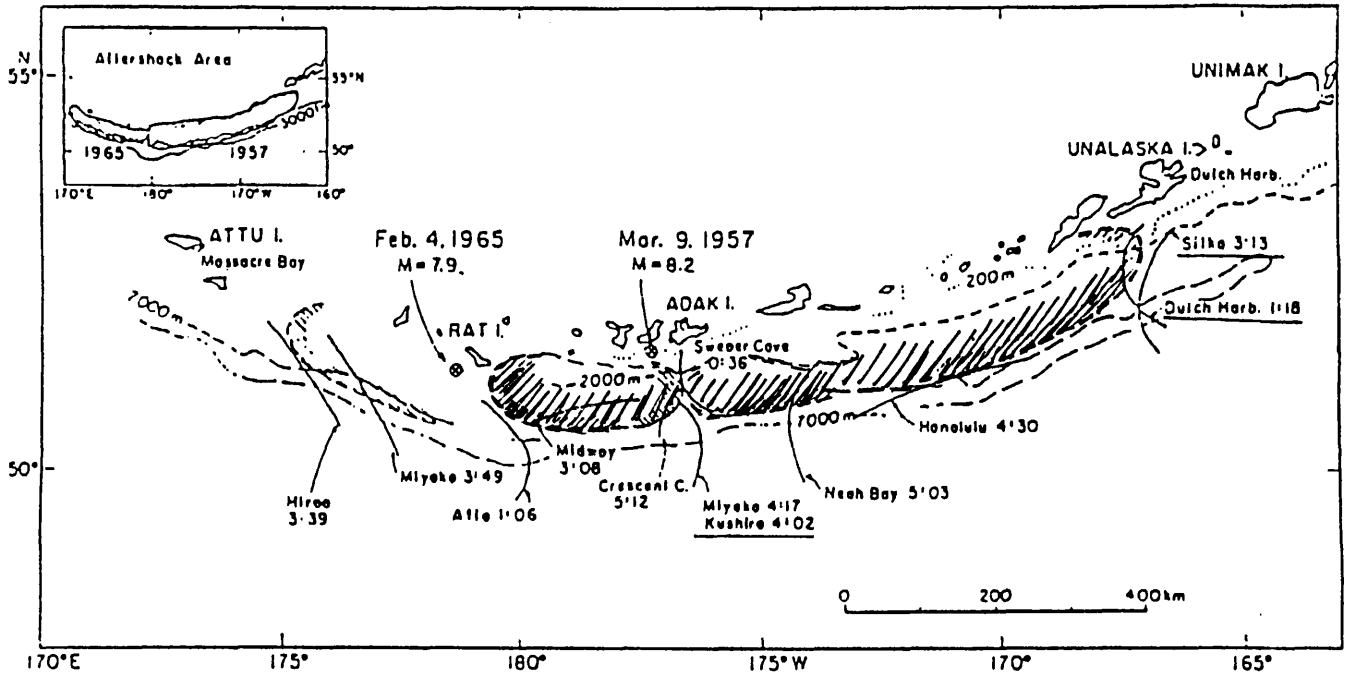

Figure 3: The tsunami source area of the 1957 and 1965 Aleutian earthquakes estimated by Hatori (1981).

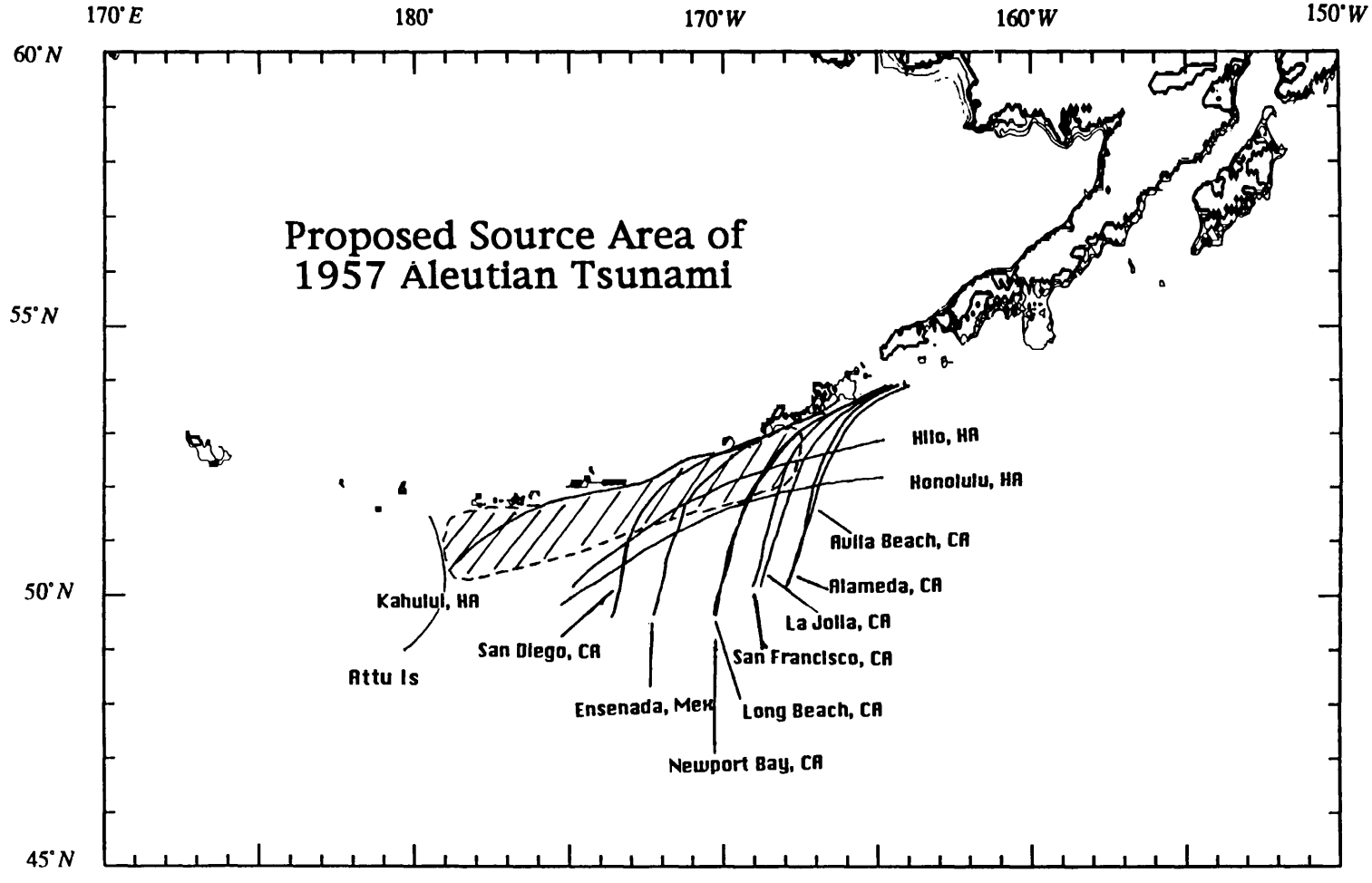

Figure 4: The source area of the 1957 Aleutian earthquake estimated by backward computation (finite-difference) of the tsunami.

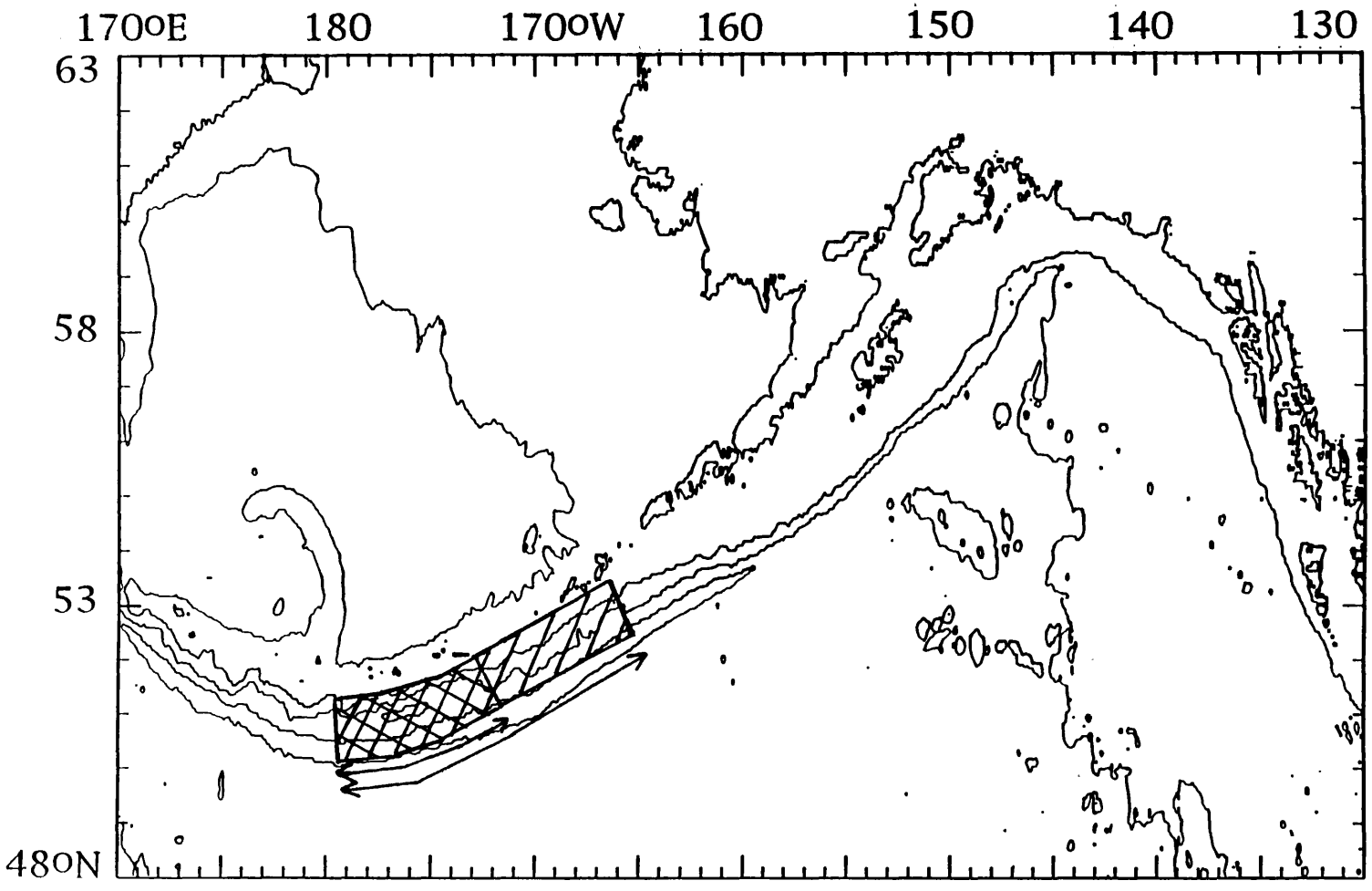

Figure 5: Long and short fault models for forward modeling of tsunami. The short fault is 600km long, the long fault is 1100km long. Both models have width 150km, and dip 30°.

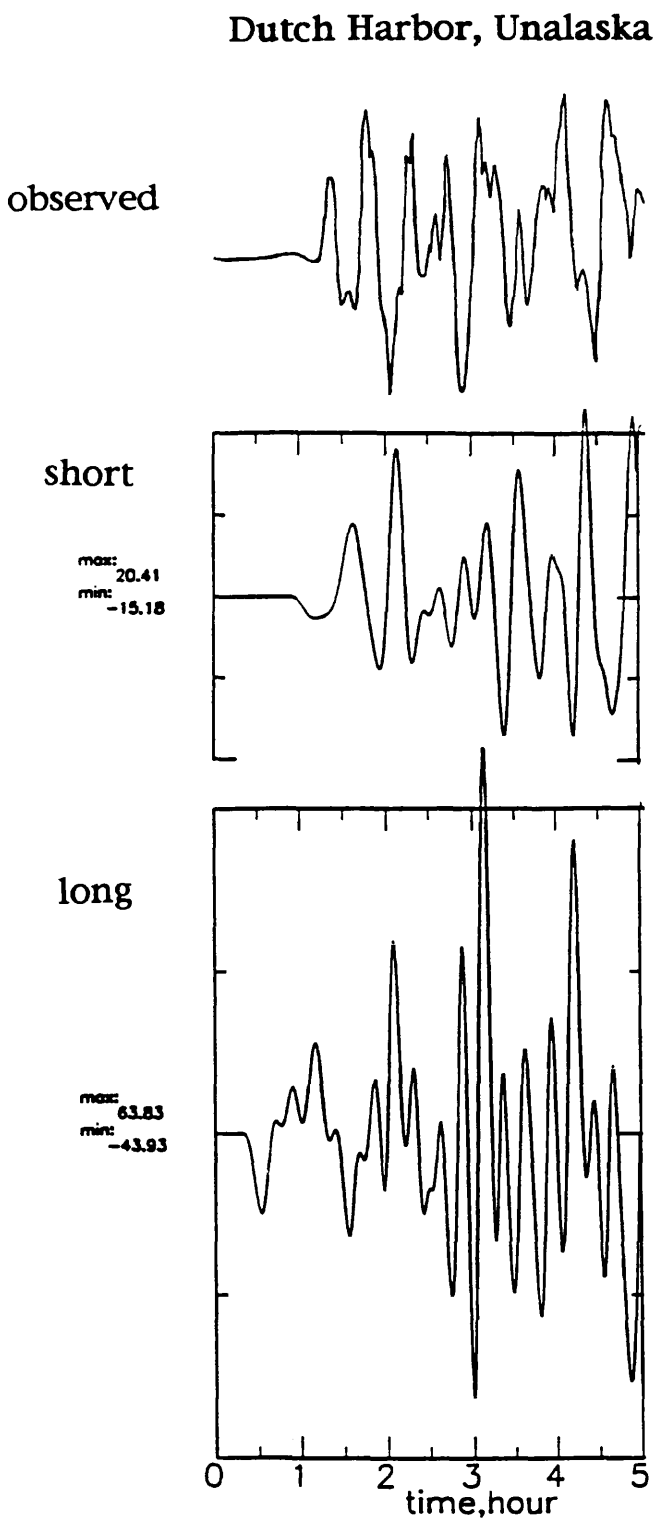

Figure 6: Results of forward modeling. The upper figure is the observed tsunami waveform recorded at Dutch Harbor, Unalaska. The middle figure is the synthetic waveform from the short fault model, the lower figure is the waveform from the long fault model. The amplitude is given in centimeters.

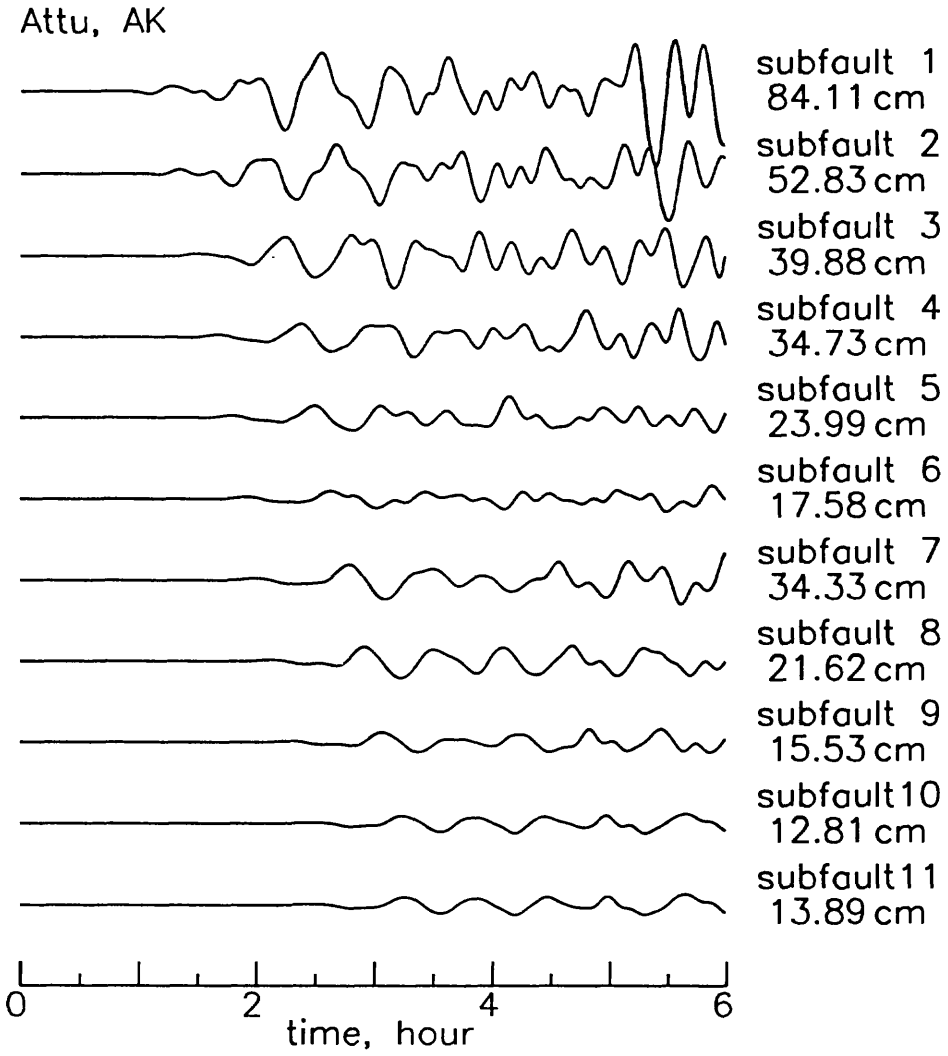

Figure 7: Computed waveforms from each subfault for Attu Island, AK. Amplitude is maximum peak-to-peak amplitude in centimeters.

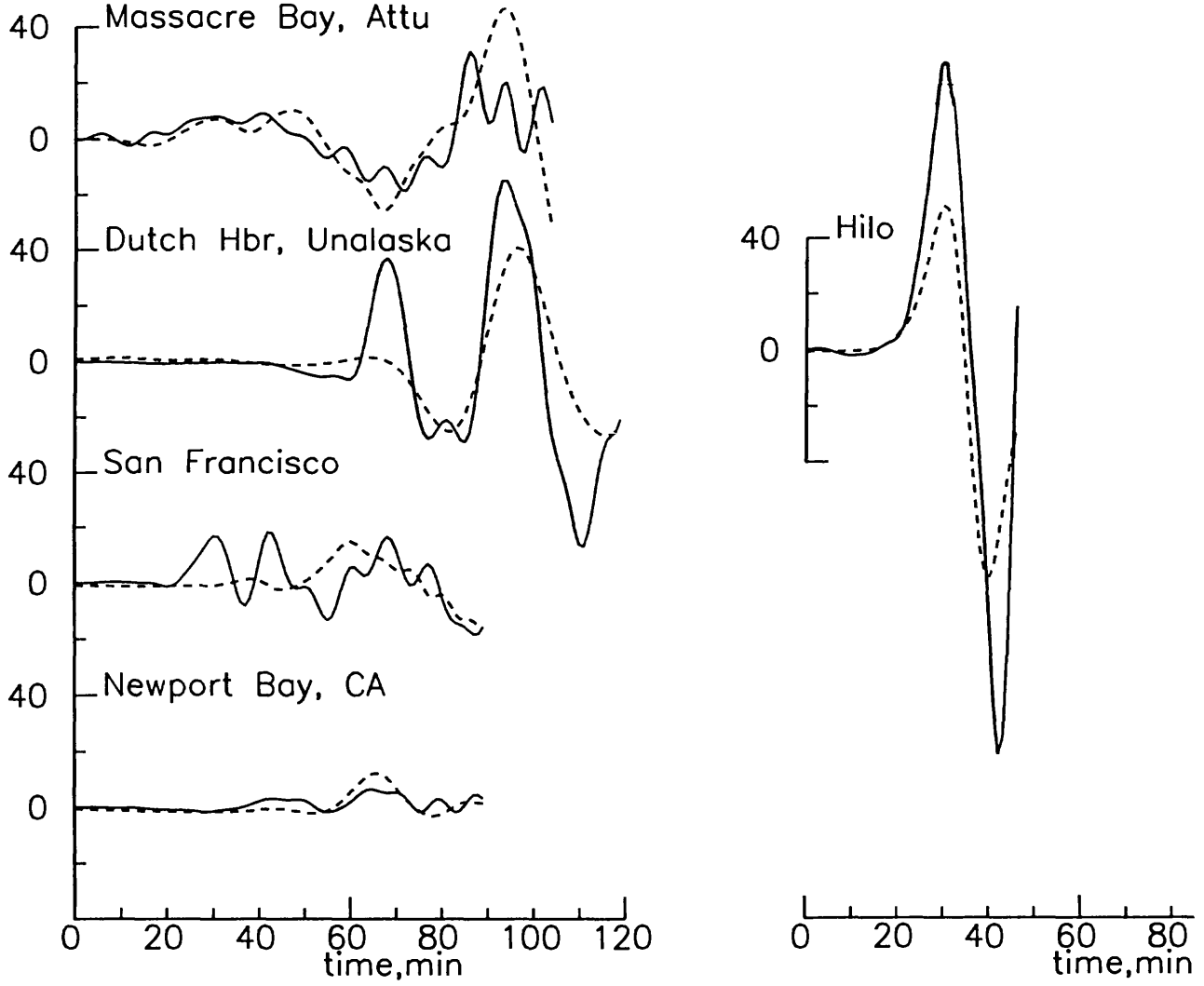

Figure 8: Observed and synthetic waveforms from non-negative least squares inversion for eleven subfaults. The solid line is observed and dashed is synthetic. Amplitude is in centimeters. Start time of each waveform is different.

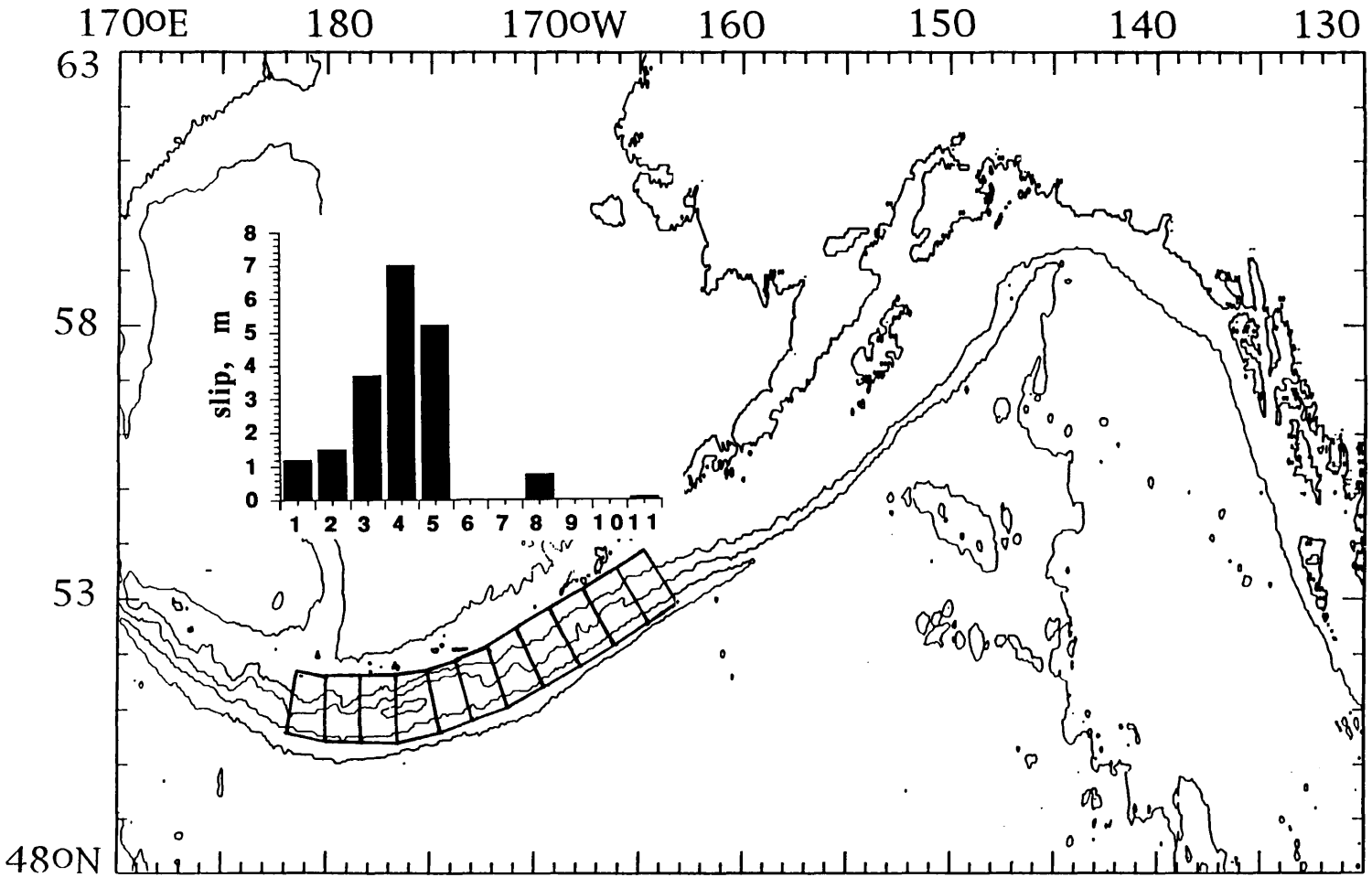

Figure 9: Slip distribution on rupture zone of 1957 earthquake from non-negative least-squares inversion on eleven subfaults. The numbered segments correspond to the subfault immediately below.

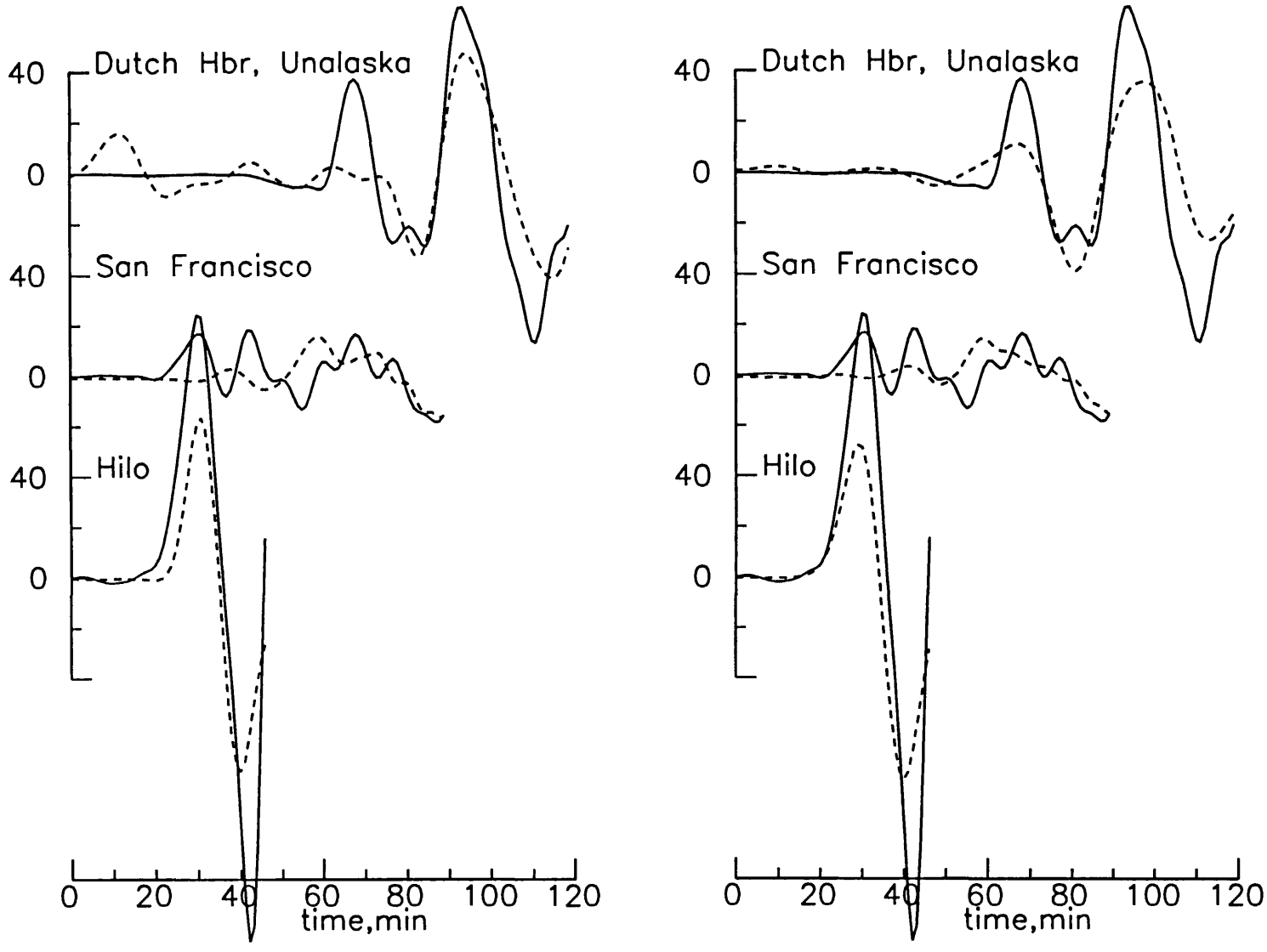

Figure 10. Observed and synthetic waveforms from (left) standard least squares inversion for eleven subfaults and (right) nonnegative least squares inversion for 13 subfaults. Solid line is observed and dashed is synthetic.

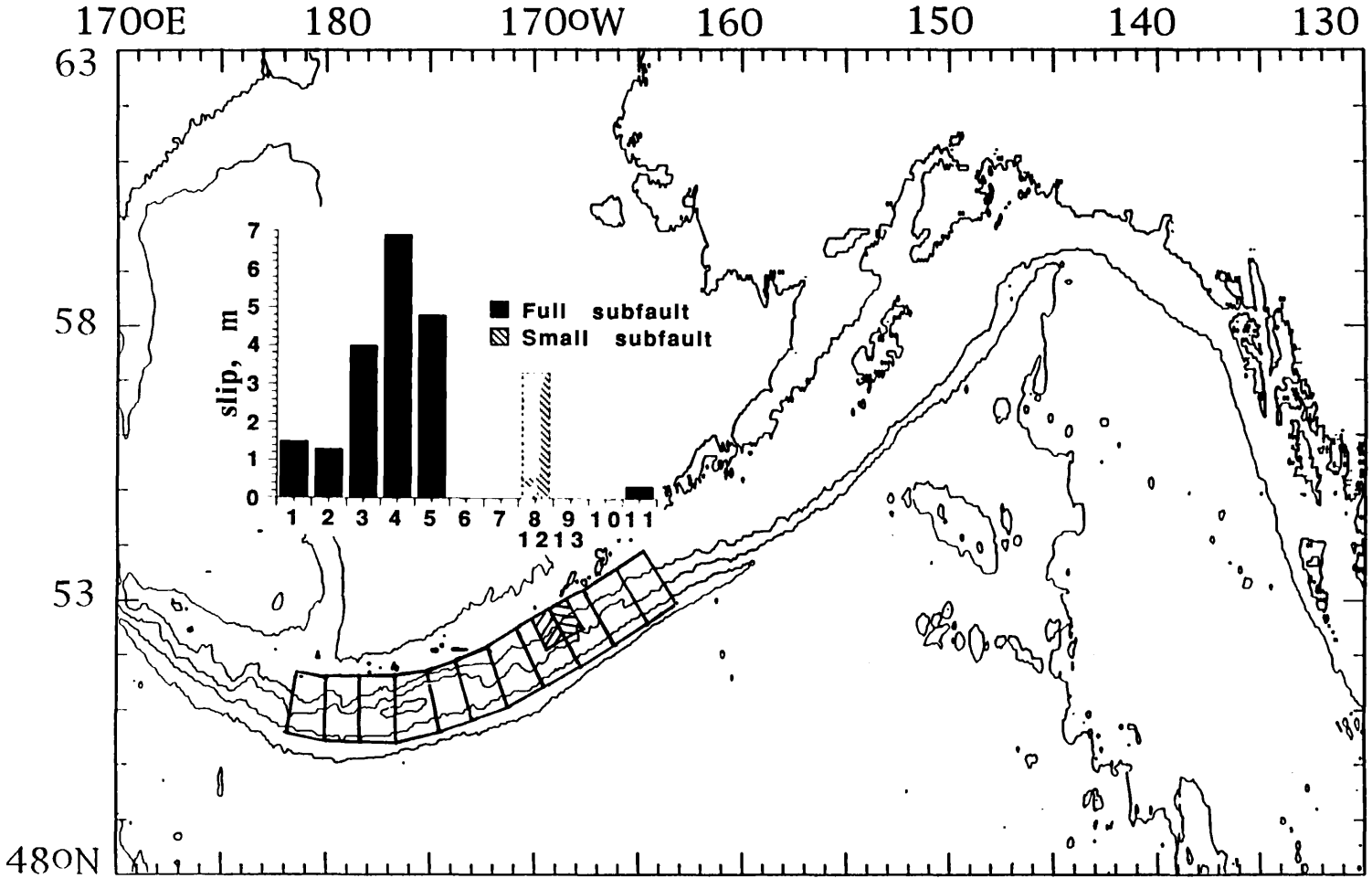

Figure 11: Slip distribution on rupture zone of 1957 earthquake. The numbered segments correspond to the subfault immediately below. The subfaults corresponding to 12 and 13 are shaded.

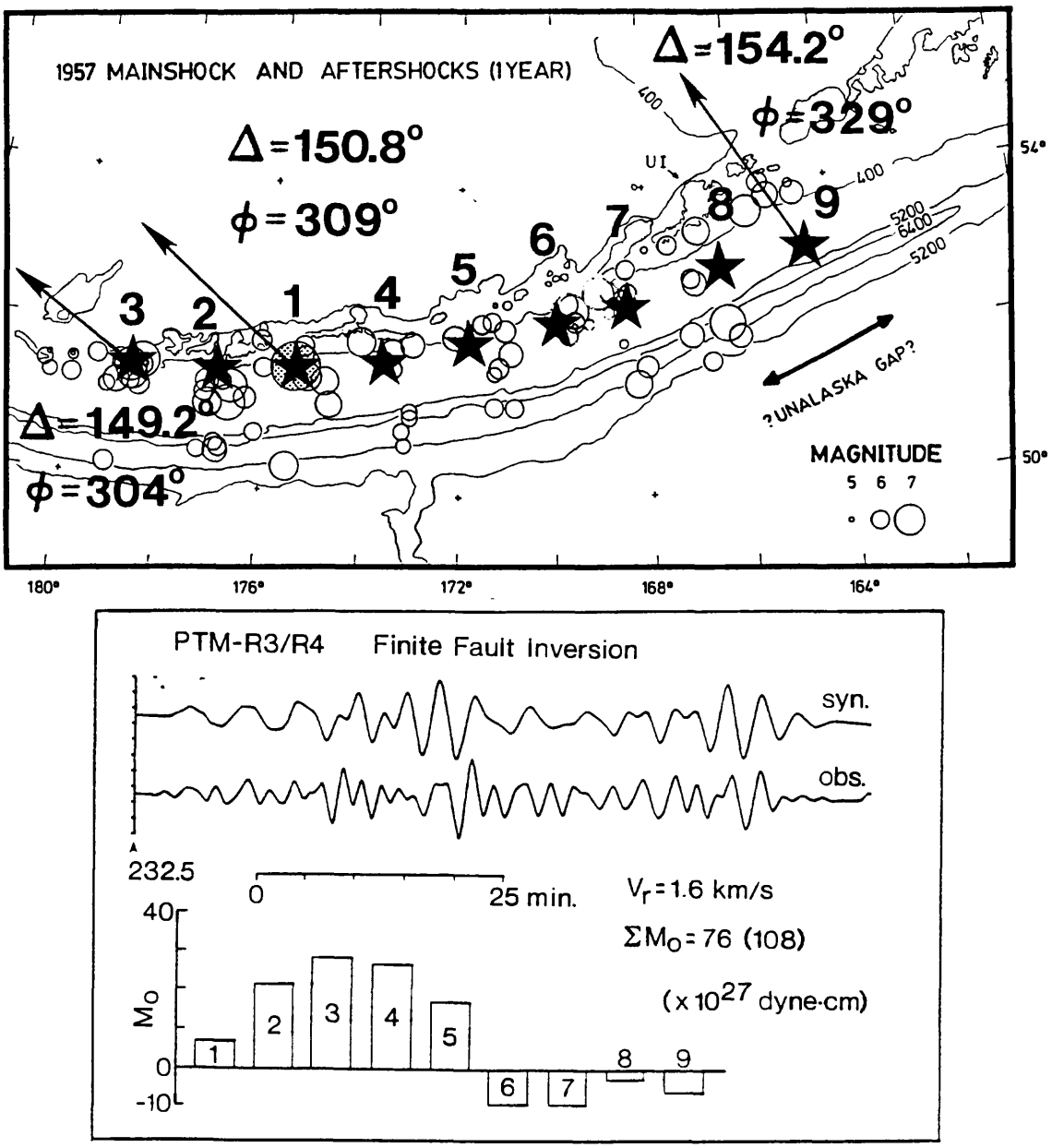

Figure 12: Slip distribution for the 1957 Aleutian earthquake by Ruff *et al.,* (1985) based on PTM record. The grid points in the lower figure corresponds to those in the upper map.

CENOZOIC TECTONIC AND PALEOGEOGRAPHIC EVOLUTION OF THE PUGET LOWLAND SEISMIC ZONE

9450-50551

Samuel Y. Johnson
Branch of Sedimentary Processes
U.S. Geological Survey
MS 939, Box 25046, DFC,
Denver, Colorado 80225
(303) 236-1545

Investigations

This research is designed to describe and interpret the stratigraphy, sedimentology, petrology, and age of Cenozoic units within and bounding the Puget Lowland seismic zone (fig. 1), with the goal of reconstructing the Cenozoic paleogeography of the region. Questions posed include the following: What sedimentary basins formed, what was their geometries, what were the tectonic controls on their origins, and at what rates did they subside? What is the petrology of Cenozoic sediments and in what environments were they deposited? How deeply were sediments buried as determined by thermal maturity and diagenetic studies? Where, when and how were Cenozoic strata deformed?

When these data are collected and analyzed, other important questions can be posed. Are there juxtaposed, mismatched, sedimentary facies, petrofacies, or burial-history trends across the Puget Lowland seismic zone that indicate significant lateral offset or horizontal shortening? If so, what units or features can be used as piercing points or markers in constraining amounts, rates, and timing of offset? Is there evidence for large throughgoing fault systems that have displaced units and(or) influenced depositional patterns? Are offsets distributed across wide zones? Do identified structures coincide with known zones of recent seismicity? If not, should identified structures be considered zones of potential seismicity?

Continuing project investigations in FY92 consisted of analyzing data collected in FY91, collecting additional field and borehole core data from Eocene sedimentary rocks, soliciting relevant seismic reflection data from industry, and studying/modeling Cenozoic subsidence in several areas within the Puget Lowland. These investigations are also sponsored by the USGS Evolution of Sedimentary Basins Program.

A significant amount of the field sedimentologic and stratigraphic data collected in FY91 has been plotted on vertical profiles; these data are being used to document and reconstruct depositional environments and systems. In FY92, additional detailed stratigraphic and sedimentologic studies were undertaken in the Morton anticline area, the Tiger Mountain area, the Black Diamond area, the northeastern Olympic Peninsula, and in the Centralia coal mine (fig. 1). Reconnaissance field studies were undertaken in the Vader-Ryderwood area. Five cores from the Jackson Prairie area in the Chehalis Basin were also described and cuttings were collected from the Mobil Kingston and So-Cal Whidbey wells (fig. 1). Cumulatively, stratigraphic sections totalling more than about 5,000 m were measured and sampled in FY92.

Petrologic data needed to provide constraints on paleogeography and sediment dispersal patterns were collected from thin sections of 63 samples collected in FY91, and 36 thin sections were point counted. Thin sections are now being made on an additional

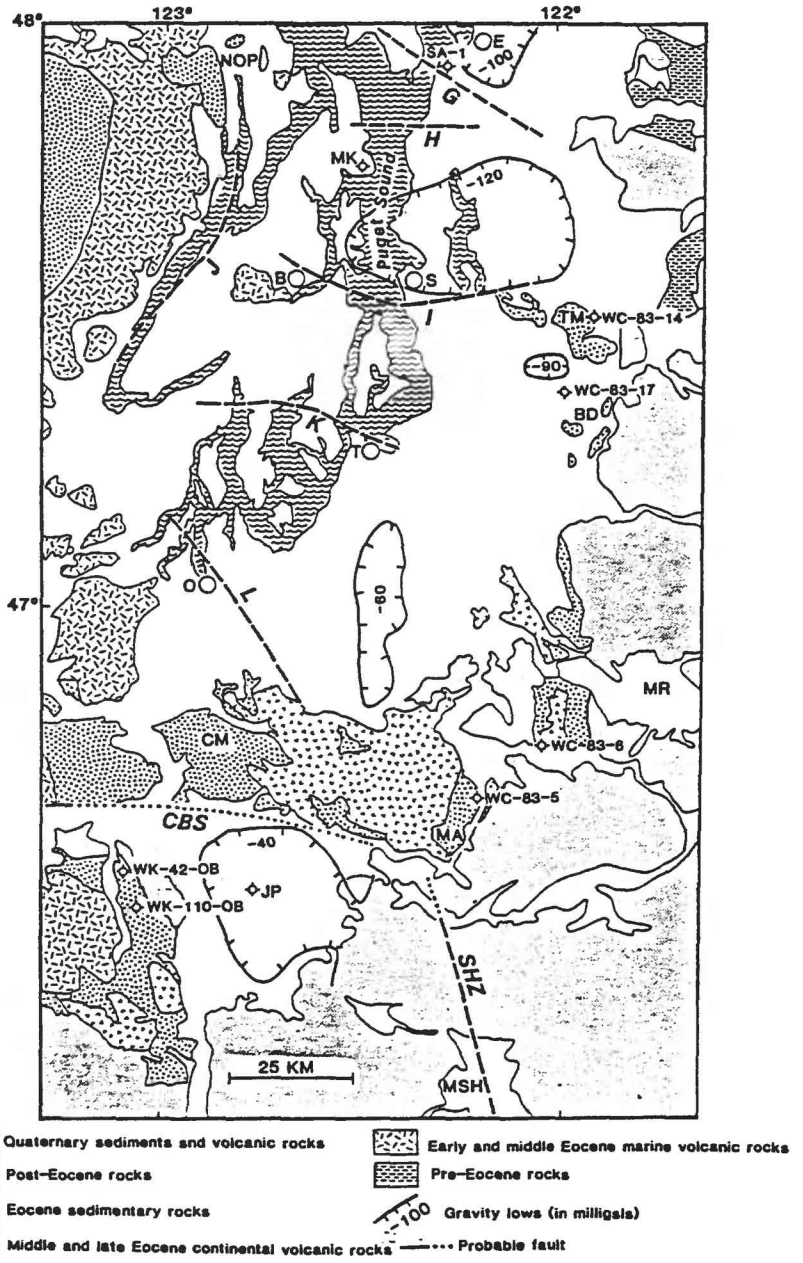

Figure 1. Schematic geologic map of the Puget Lowland seismic zone, showing locations of concentrated FY91 and FY92 field work (TM, MA, CM, BD, NOP) and borehole cores described and sampled (for example, WC-83-14). Probable faults include structures *G, H, I, J, K,* and *L* of Gower and Yount (1985), the Saint Helens seismic zone *(SHZ)* of Weaver and Smith (1983), and an inferred structure on the northern margin of the Chehalis sub-basin *(CBS)*. Other abbreviations as follows: B, Bremerton; BD, Black Diamond; CM, Centralia Mine; JP - Jackson Prairie; MA, Morton anticline area; MK - Mobil Kingston well; MR, Mount Rainier; MSH, Mount Saint Helens; NOP - northeastern Olympic Peninsula; O, Olympia; S, Seattle; T, Tacoma; TM, Tiger Mountain. Gravity data from Bonini and others (1974).

105 samples collected in FY 92. About 15 samples have been given to a colleague for analysis of heavy mineral content, which should further aid provenance and correlation studies. Geochronologic studies continue. Fifteen FY91 samples were submitted for mineral separation; five of these samples yielded sufficient zircons for dating and are in the hands of a colleague for fission-track dating. An additional six samples collected in FY92 have been submitted for mineral separation. Tephra correlation studies of Eocene strata also continue. Working with Paul Hammond of Portland State University, 141 samples have been submitted for XRF and INAA geochemical analyses; partial results have been obtained for 93 of these samples. Finally, the burial and thermal histories of these strata are being examined by vitrinite reflectance analysis (44 samples submitted, results back for twenty samples) and organic geochemical analysis (twelve samples submitted, results obtained for six samples).

In order to integrate and correlate the outcrop and well data and develop a coherent paleogeographic/paleotectonic model, a major effort was made to solicit regional seismic reflection data from industry. This effort has resulted in significant contributions (with some publication rights) from Mobil, Chevron, and L.B. Industries in late FY92. Chris Potter and I have also laid the groundwork for a multi-USGS Program (NEHRP, Evolution of Sedimentary Basins, and Deep Continental Studies) purchase of commercial seismic reflection data from the southern Puget Lowland in FY93.

Results

Published results of FY92 investigations are in Johnson (1992) and Johnson and Yount (1992). Johnson (1992) describes the stratigraphy and sedimentology of the lower? and middle Eocene Raging River Formation in the east-central Puget Lowland, and provides key information for understanding regional paleographic and tectonic evolution. The Raging River Formation is especially significant because (among other things) it provides the only surface analog for the conductive rocks (the SWCC) that underlie a large part of the southern Washington Cascade foothills and occur in other deep Eocene basins of the Puget Lowland area. Stanley and others (1987, 1991, 1992) have inferred the SWCC has significant control on regional seismicity and volcanism. Three informal stratigraphic units (designated 1 to 3 from base to top) are here recognized in the Raging River Formation based on distinctive sedimentary facies and lithologies. Unit 1, approximately 230 m thick, consists of interbedded sandstone, mudstone, and conglomerate of inferred nonmarine (lower part) and transgressive shallow-marine (upper part) origin. Unit 2, approximately 185 m thick, consists of interbedded conglomerate, sandstone, and mudstone, and is inferred to be of mainly alluvial origin. A significant transgression is recorded by Unit 3 (about 300 m thick), which consists of gray silty mudstone and lesser sandstone, and was deposited in a marine shelf (lower part) and bathyal slope (upper part) setting. This transgression reflects local tectonism and not fluctuating eustasy. The Raging River Formation is overlain by prodelta(?) marine shelf deposits in the lower part of the Tiger Mountain Formation. Three sandstone petrofacies were identified in the Raging River Formation and lower part of the Tiger Mountain Formation. These petrofacies reveal an upward evolution in sediment source from Mesozoic basement rocks of oceanic affinity (petrofacies 1), to lower Tertiary volcanic rocks (petrofacies 2), to a mixed provenance including Mesozoic oceanic rocks, lower Tertiary volcanic rocks, and more distal plutonic or crystalline rocks (petrofacies 3). This report will be formally published when colleagues provide additional heavy mineral analyses and isotopic dates.

Johnson and Yount (1992) discuss constraints on the Cenozoic paleogeography of the Puget Lowland based largely on new geologic data and subsidence models (fig. 2). Following up on Johnson (1984, 1985), they suggest the Puget Lowland was the site of Eocene dextral strike-slip faulting along the Puget fault zone, a structure inferred from

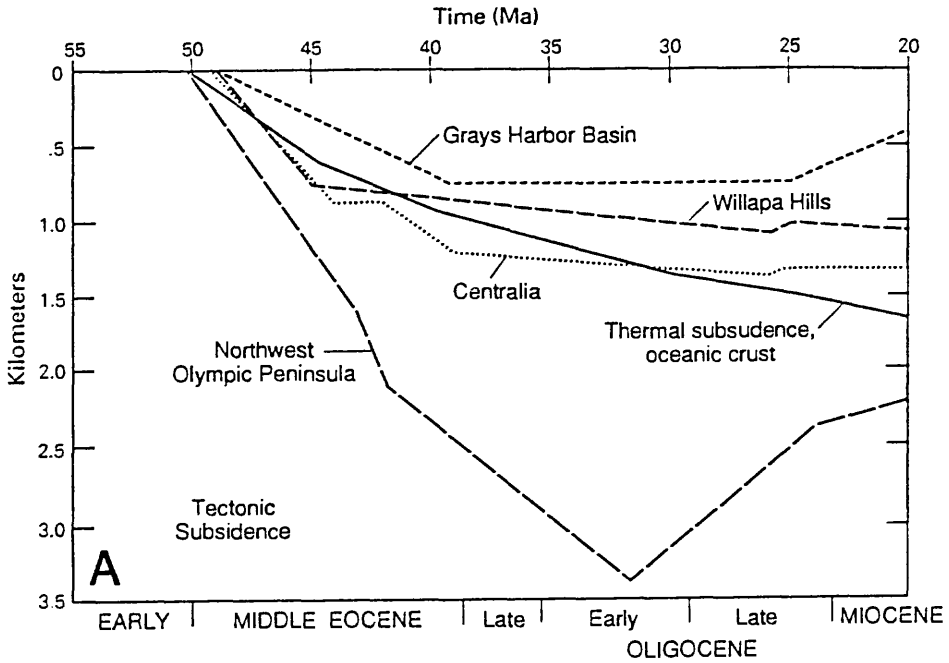

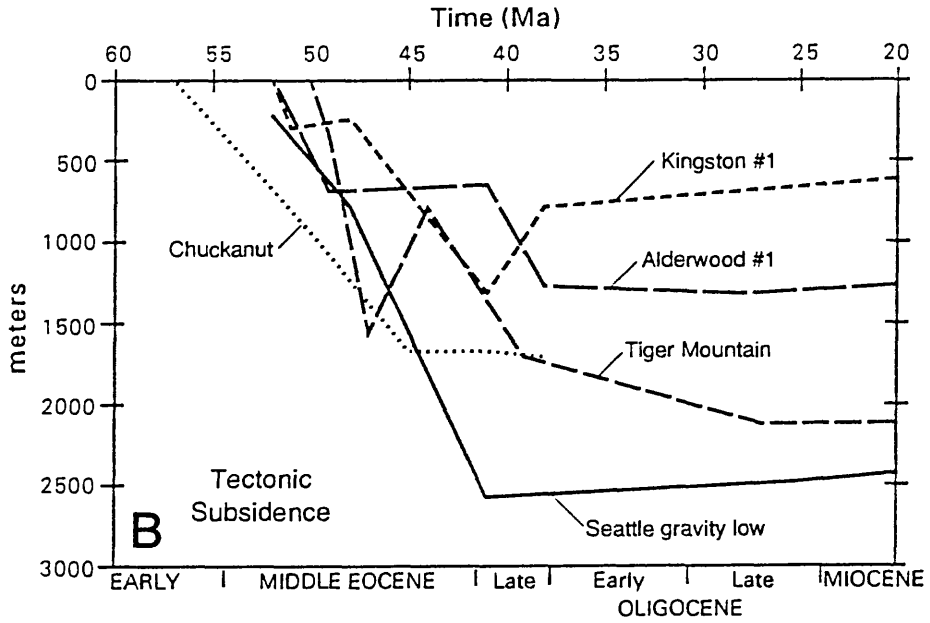

Figure 2. Diagrams showing subsidence histories of (A) three sites in the southwest Washington Coast Range, one site on the northern Olympic Peninsula, and the idealized thermal subsidence curve for oceanic crust; and (B) four sites in the central Puget Lowland and one site in the Bellingham area, northern Puget Lowland. Subsidence curves are corrected for the load induced by the weight of sediment and water through time. Paleobathymetry is approximate and based on foraminiferal data provided by Weldon Rau.

patterns and contrasts in basin evolution, and from facies and petrographic mismatches. This inferred fault zone forms the boundary between pre-Tertiary basement rock of the Cascades to the east and early and middle Eocene marine basaltic basement rock (Crescent Formation) of the Coast Range to the west. The inferred fault zone extends northward from Mt. St. Helens through the Puget Lowland and Puget Sound and bends northwestward into a zone of transpressive, south-directed thrust faults on southern Vancouver Island. The fault zone was initiated about 55 Ma when the Crescent Formation was erupted in a marginal rift basin (Wells and others, 1984; Snavely, 1987; Babcock and others, 1992). Northward movement of the Coast Range probably continued into the Neogene. Eocene-Oligocene subsidence of Crescent basement in southwest Washington is inferred to be mainly of thermal origin; much higher subsidence rates for Crescent basement on the northern Olympic Peninsula (fig. 2A) require an additional driving force, inferred to be loading from southern Vancouver Island thrust sheets. Some offset on the Puget fault zone was transferred eastward to the Straight Creek fault, leading to development of a broad, rapidly subsiding, pull-apart basin in the eastern Puget Lowland and Cascade foothills. Local sub-basins, such as the prominent gravity low near Seattle, formed within or adjacent to the Puget fault zone. Intrabasinal tectonics is reflected in local unconformities, abrupt facies change, and highly variable subsidence histories within limited geographic areas (fig. 2B). Much of the modern crustal seismicity in the Puget Lowland appears to be concentrated along the structural boundary described above between the Crescent Formation and pre-Tertiary basement. Documentation of the geometry and kinematics of this zone will enhance understanding of the modern seismic hazard.

Field studies conducted in FY92 have yielded several preliminary observations and interpretations relevant to understanding the regional geologic framework. Two problems addressed by these field studies are discussed below:

Morton anticline: FY91 studies indicate that Eocene sedimentary strata in the Morton anticline area consist of thick, alternating intervals of nonmarine and less common marine strata. FY92 studies provide further documentation of these facies and the presence of numerous tuffs that will be dated isotopically and correlated geochemically. Cross sections across the anticline indicate that far more section is present on the west flank than on the east flank, requiring the presence of an east-dipping normal fault or a west-dipping reverse fault in the anticline core. A steep east-dipping fault would project very close to the focus of the magnitude 5.5 (1987) earthquake below Storm King Mountain. Continuing analysis of field and seismic reflection data collected from the Morton anticline will provide documentation of its structure and stratigraphy and enhance understanding of the connection between surface faults and modern seismicity.

Comparison of Eocene stratigraphy in the Tiger Mountain--Black Diamond area (eastern Puget Lowland) and the Northeastern Olympic Peninsula: (western Puget Lowland) In FY92, I examined in detail the Eocene Puget Group in the Tiger Mountain-Black Diamond area and the correlative Lyre and Twin River Formations on the northeastern Olympic Peninsula. Puget Group strata consist of nonmarine to minor marginal marine sandstone, mudstone, and coal. Sandstone is mainly arkose and lithic arkose. In contrast, the Lyre and Twin River Formations consist of coarse-grained conglomerate, sandstone, and mudstone deposited in deep marine settings. Conglomerates contain abundant chert and basalt clasts and sandstones are rich in lithic detritus. These rocks are correlative with mainly nonmarine and marginal marine strata exposed in the Tiger Mountain-Green River Gorge area in the eastern Puget Lowland but have very different petrologies and represent very different sedimentary facies. The present geographic positions of these disparate correlative rocks and their variable subsidence histories (fig. 2B)suggests significant Eocene tectonism in the central Puget Lowland. Ongoing analysis of outcrops, wells, and seismic reflection data will lead to understanding Eocene structural features. These

prominent features have likely been reactivated repeatedly through time, and their documentation is essential to an understanding the modern structure and seismic hazard.

Publications

Johnson, S.Y., 1992, Stratigraphy and sedimentology of the Raging River Formation (Early? and Middle Eocene), King County, Washington: U.S. Geological Survey Open File Report 92-581, 38 p.

Johnson, S.Y., and Yount, J.C., 1992, Toward a better understanding of the Eocene paleogeography of the Puget Lowland, western Washington: Geological Society of America Abstracts with Programs, v. 24, p. 36.

References

Babcock, R.S., Burmester, R.F., Engebretson, D.C., and Warnock, A., 1992, A rifted margin origin for the Crescent basalts and related rocks in the northern Coast Range volcanic province, Washington and British Columbia: Journal of Geophysical Research, v. 97, p. 6799-6821.

Bonini, W.E., Hughes, D.W., and Danes, Z.F., 1974, Complete Bouguer gravity anomaly map of Washington: Washington Division of Geology and Earth Resources, Geologic Map GM-11.

Gower, H.D., and Yount, J.C., 1985, Seismotectonic map of the Puget Sound region, Washington: U.S. Geological Survey Map I-1613.

Johnson, S.Y., 1984, Evidence for a margin-truncating transcurrent fault (pre-late Eocene) in western Washington: Geology, v. 12, p. 538-541.

Johnson, S.Y., 1985, Eocene strike-slip faulting and basin formation in Washington, *in* Biddle, K.T., and Christie-Blick, N., Strike-slip deformation, basin formation, and sedimentation: Society of Economic Paleontologists and Mineralogists Special Publication 37, p.283-302.

Snavely, P.D., Jr., 1987, Tertiary geologic framework, neotectonics, and petroleum potential of the Oregon-Washington continental margin, *in* Scholl, E.W., Grantz, A., and Vedder, J.G., eds., Geology and resource potential of the continental margin of western North America and adjacent ocean basins, Beaufort Sea to Baja California: Circum-Pacific Council for Energy and Mineral Resources, Earth Science Series, v. 6, p. 305-335.

Stanley, W.D., Finn, C., and Plesha, J.L., 1987, Tectonics and conductivity structures in the southern Washington Cascades: Journal of Geophysical Research, v. 81, p. 810-820.

Stanley, W.D., Gwilliam, W.J., Latham, F., and Westhusing, K., 1992, The southern Washington Cascade conductor -- A previously unrecognized thick sedimentary sequence? American Association of Petroleum Geologists Bulletin, v. 76, p. 1569-1585.

Stanley, W.D., Finn, C.A., Williams, J.L., and Weaver, C.S., 1992, Tectonics and seismicity of the Mount Rainier region: EOS, Transactions, American Geophysical Union Fall Meeting, p. 526.

Weaver, C.S., and Smith, S.W., 1983, Regional tectonic and earthquake hazard implications of a crustal fault zone in southwestern Washington: Journal of Geophysical Research, v. 88, p. 10,371-10,383.

Wells, R.E., Engebretson, D.C., Snavely, P.D., and Coe, R.S., 1984, Cenozoic plate motions and the volcano-tectonic evolution of western Oregon and Washington: Tectonics, v. 3, p. 274-294.

TILT, STRAIN, AND MAGNETIC FIELD MEASUREMENTS

9960-70146
M. J. S. Johnston, R. J. Mueller, G. D. Myren
Branch of Tectonophysics
U. S. Geological Survey
Menlo Park, California 94025
415/329-4812

Investigations

[1] To investigate the mechanics of failure of crustal materials using data from both deep borehole tensor and dilational strainmeters and near surface strainmeters, tiltmeters, and arrays of absolute magnetometers.

[2] To develop physical models of incipient failure of the earth's crust by analysis of real-time records from these instruments and other available data.

Results

[1] A FOCUSED FAULT MONITORING EXPERIMENT ON THE HAYWARD FAULT

The identification of reliable short- and intermediate-term precursors to damaging earthquakes remains an critical challenge to the earthquake hazard reduction program. To this end, a focused fault monitoring experiment has been installed on the southern segment of the Hayward fault. Instruments used in this experiment include, dilational strainmeters, tensor strainmeters, water well monitors, creepmeters, continuous GPS displacement monitors, seismic velocity and acceleration transducers. The strainmeters and seismometers are installed in boreholes at about a 200 m depth. At this depth, measurement precision about 20 dB below that of surface instruments can be attained. Short-term strain changes less than one ppb can easily be identified. The borehole array of eight strainmeters has been installed along the segment of the Hayward fault between San Leandro and Milpitas with most sites at distances from 2 km to 7 km from the Hayward Fault. These sites are shown in Figure 1. Data are being transmitted using digital satellite and radio telemetry to Menlo Park, Ca. for analysis and display. Various other geophysical and geological data were also collected during the borehole drilling program. The overall array design was influenced by the form and amplitude of strain and displacement fields calculated from simple models of various possible damaging earthquakes that might occur on either the southern segment of the Hayward fault, or on the Calaveras fault.

[2] RECENT SEISMOMAGNETIC AND VOLCANOMAGNETIC EVENTS: IMPLICATIONS FOR PHYSICAL MECHANISMS

Recent seismic and volcanic events for which focussed magnetic and electromagnetic monitoring data have been obtained occurred on the Izu Peninsula in Japan, the Long Valley volcanic region in California, on the San Andreas fault, and on Mt. Unzen, in Japan. An example from Long Valley, California is shown in Figure 2.

For volcanic events (ie eruptions, intrusions, etc), contributions from different physical processes with different time durations can be identified. These processes include slow, near-surface thermal demagnetism effects, piezomagnetic effects, and effects from rotation/displacement of magnetized material. Second-order effects such as electrokinetic effects and changes in the telluric current system that result from

modification of the electrical conductivity structure, may also occur but critical parameters such as pore pressure gradients, zeta potentials, etc, are rarely measured and are poorly constrained. Well level measurements were obtained during the current deformational episode shown in Figure 1 but have remained essentially unchanged during this time. This suggests that the simplest expectation from electrokinetic processes are not a major contributor to the observed magnetic field changes for this event.

For seismic events, zero-frequency or coseismic contributions are instantaneous with no indication of short-term response effects with a decay time constant as expected for fluid driven electrokinetic processes. An example from the North Palm Springs earthquake is shown in Figure 2.

Simple piezomagnetic dislocation models using parameters determined geodetically or seismically generally match the observed zero-frequency signals in size and sign but other possibilities can not be completely discounted. Transient, higher frequency signals might be driven by localized dynamic changes in electrical conductivity, localized charge generation mechanisms, and electrokinetic effects. However, signals that appear to occur prior to a significant local earthquake but do not occur coincident in time with the earthquake, should generally be considered suspicious since many other data indicate that moment release prior to and earthquake is minor compared with that during the rupture. In other words, calibration with coseismic moment release is an important test of the reality of observed coseismic signals.

Unusual ULF signals were recorded predominately in the frequency band 1 Hz to 0.01 Hz at three different times during the month prior to the October 18, 1989, Loma Prieta M_s7.1 earthquake (Fraser-Smith et al., 1990). Three physical mechanisms are considered relevant if these signals are assumed to be generated in the hypocentral region. These are: 1) dynamic changes in electrical conductivity due to strain driven crack opening and closure, 2) dynamic charge generation due to strain, hydrodynamic, and gasdynamic processes, and 3) electrokinetic effects due to dynamic pore pressure variations.

Since the electrical conductivity varies between 1 S/m and 0.01 S/m and the seismic attenuation factor (1/Q) is about 0.03 in this region, dynamic magnetic, seismic and strain signals are attenuated comparably in the 1 Hz to 0.01 Hz frequency band. The absence of detectable seismic or strain signals on nearby seismometers and borehole strainmeters at the 10 micron/sec and 10^{-11}/sec level, respectively, strongly limits the size (i.e. the moment) of the source region driving the mechanisms above.

Models of these processes suggest dynamic stress gradients and pore pressure gradients exceeding 1 Kbar/km and 1 bar/km, are required to generate crack oscillation and electrokinetic effects, respectively, but associated strain oscillations from these gradients should be readily detectable unless the region effected is quite small. These problems, together with the inherent difficulty in maintaining charge separation continuously within this conducting region for long enough and over a large enough area, suggest that these ULF electromagnetic signals were generated relatively close to the receiver.

[3] MAGNETIC FIELD OBSERVATIONS IN THE NEAR-FIELD OF THE JUNE 28, 1992 M_L 7.5 LANDERS, CALIFORNIA, EARTHQUAKE.

Recent reports suggest that large magnetic field changes occur prior to, and during, large earthquakes. Two continuously operating proton magnetometers, LSBM and OCHM, at distances of 13.3 km and 21 km, respectively, from the epicenter of the June 28, 1992, M_L 7.5 Landers earthquake, recorded data through the earthquake and its aftershocks. These two stations are part of a differentially connected array of proton magnetometers that has been operated along the San Andreas fault since 1976. The instruments operate at a sensitivity of 0.25 nT of better and transmit data every 10 minutes through the GEOS satellite to the USGS headquaters in Menlo Park, CA.

Seismomagnetic offsets of -0.5 nT and -0.2 nT were observed at these sites. In contrast, offsets of 1.2 nT and 0.3 nT were observed during the July 8, 1986 M_L 5.9 North Palm Springs earthquake although this earthquake occurred right beneath the magnetometer sites.. The observations are generally consistent with a seismomagnetic model of the earthquake in which right-lateral rupture is assumed on four connected fault segments that roughly match the location of the surface rupture. The length of the segments from south to north are 15 km, 23 km, 22 km, and 23 km, the widths are 13 km, 17 km, 17 km, 17 km, and the assumed slip is 3 m, 4m, 4m, 5m, respectively. The average magnetization is assumed to be 1 A/m in general agreement with observations of surface magnetization at the two sites that range between 1.0 A/m and 0.1 A/m. An alternate explanation in terms of electokinetic effects seems unlikely since the changes are complete within a 10 minute period.

[4] ON THE DECTECTION OF SHORT-TERM STRAIN EVENTS - A COMPARISON OF THE SENSITIVITIES OF GPS AND BOREHOLE STRAIN MEASUREMENTS

For detection of short term deformation events which take place at or below seismogenic depths along the San Andreas Fault system we compare the capability of a network of GPS receivers with that of an array of Sacks-Evertson borehole strainmeters. We have compared the two techniques using different assumptions for the station distribution with respect to the location of the event, including cases where the sites have the most favorable geometry for detection. We also use the locations (now partially occupied) for the planned array of borehole sites along the Southern Hayward Fault. Since Earth strain noise level increases with period, we also allow the duration of the slip event to vary. We have concentrated on strike slip sources of deformation, but have also considered dip slip dislocations.

While many may be aware that for short duration signals (less than months) strain monitoring provides greater sensitivity than does GPS, the quantitative difference in threshold level is not widely perceived. For example consider how much right lateral slip, over a duration of 1 day, must occur on 1 km^2 of fault at a depth of 10 km for detection by an ideally located instrument array. The borehole strain array will provide a clear signal for a displacement of about 2 cm; the position monitoring will require about 10 m (assuming a detection threshold of a few mm) -- a ratio of 500. The strain threshold increases with period and the crossover period is about several months, depending on the characteristics of individual sites. At shorter periods the threshold ratio increases in favor of strain monitoring (5000 at 1 hour). This explains the apparent inability of the GPS net in southern California to detect the coseismic change due to the Sierra Madre (1991) earthquake (Hudnut *et al* & Zumberge *et al*, 1991 Fall AGU) which produced a very large offset on the nearest borehole instrument. Continuous strain monitoring should be an integral component of any program to detect possible short term earthquake precursors.

[5] BOREHOLE STRAIN ARRAY IN CALIFORNIA

A network of 15 borehole strainmeters along the San Andreas fault zone and in the Long Valley Caldera continues to be monitored and maintained. All instruments are installed at depths between 117-m and 324-m and all are between 1-km and 5-km from the the surface trace of the fault. High frequency dilatometer data in the frequency range 0.005 Hz to 100 Hz are recorded on 16-bit digital recorders with least count noise less than 10^{-11}. Low frequency data from zero frequency to 0.002 Hz are transmitted through the GOES satellite to Menlo Park, CA, using a 16-bit digital telemetry system. At the USGS in Menlo Park the data are displayed in "almost real time" and are continuously monitored with detection algorithms for unusual behavior. Least-count noise is about $5*10^{-12}$ for the on-site digital recordings, and about $2*20^{-11}$ for the satellite telemetry channels. Earth strain tides, strain transients related to fault creep and numerous strain

seismograms from local and teleseismic earthquakes with magnitudes between -1 and 6 have been recorded on these instruments. Static moments and total earthquake moments are determined from the co-seismic strains and total strain changes observed with the larger events.

[6] **REVIEW OF CONTINUOUS NEAR-FAULT AND NEAR-CONTINUOUS 2-COLOR DEFORMATION DATA AT PARKFIELD, CALIFORNIA: 1986-1992.**

Continuous strain along a 36-km segment of the San Andreas fault zone near Parkfield California is monitored with a network of 8 borehole dilatometers and 3 borehole tensor strainmeters (precision $<10^{-9}$). Near-continuous strain and fault displacement is also monitored with a 2-color laser geodimeter (precision $<10^{-7}$) using a 17-line array of 1-km to 9-km lines emanating from Carr Hill. The most remarkable features of these data during the last six years (1986-1992) are:

[1] The relative absence of short term strain transients greater than 10^{-7} that are coherent across the networks and can thus be clearly related to fault activity. Some coherent strain transients are observed on a limited scale, particularly on the more northern borehole instruments though these do not appear directly related to patterns of microseismicity during this time. The largest earthquake that occurred was a magnitude 4 just southeast of Parkfield on August 29, 1986. This generated coseismic strainsteps of a few nanostrain on the nearest instruments in agreement with expectations from dislocation theory.

[2] The smooth gradient in fault slip from about 20 mm/a in the north to 3 mm/a in the south and the overall linear nature of the slip time-history at each location.

[3] A broad scale geodetically determined strain rate of about 0.2 ppm/a that is significantly lower than the near-fault shear strain accumulation rate of about 1 ppm/a although the near-fault measurements may be contaminated by the effects of fault slip beneath Carr Hill..

[4] The relative absence of strain transients on the borehole strainmeters greater than 10–9, or on the 2-color lines greater than a millimeter or so, at the times of nearby creep events. Exceptions occur at two sites; one where a strainmeter is within 0.75 km of a creepmeter and the second where coupling appears to occur between a secondary fault near the strainmeter and the San Andreas fault.

The apparent invariance of the slip geometry and slip distribution during this time period is curious. Modeling of the expected nucleation region of the next Parkfield earthquake indicates that changes in fault slip of only a few millimeters over a square kilometer at depths of 5 km to 8 km would be readily detected by this array. The absence of short period transients (duration less than 1 day) on both geodetic and borehole strain at the times of surface creep observations indicates a complicated and spatially variable near-surface response to relatively uniform deep slip.

[7] **DIFFERENTIAL MAGNETOMETER ARRAY IN CALIFORNIA**

We continue investigations of local magnetic fields and relationships to crustal strain and seismicity in the Parkfield region and in southern California. The network consists of 9 stations which are all sampled synchronously every 10 minutes and transmitted with 16-bit digital telemetry to Menlo Park, CA through the GOES satellite. Data are monitored daily with particular attention to the seven stations operating in the Parkfield region of central California and the three stations operating in the Long Valley caldera. At these latter sites a magnetic field anomaly first became obvious in late 1989 and in continuing to the present in concert with anomalous 2-color geodetic strain measurements and spasmodic swarms of minor earthquakes.

Reports

Fenoglio, M. A., A. C. Fraser-Smith, G. Beroza, M. J. S. Johnston, 1992, Comparison of Ultra-Low Frequency Electromagnetic Signals with Aftershock Activity During the 1989 Loma Prieta Earthquake Sequence. Bull. Seis. Soc. Am. (in press)

Valdes-Gonzalez, C. M., B. Armstrong, J. D. Leaird, and M. J. S. Johnston, 1992, Low Strain Level Acoustic Emission Due to Seismic Waves and Tidal/Thermoelastic Strains Observed at the San Francisco Presidio, IBM PASC Report G320-3572, 28pp.

Johnston, M. J. S., R. J. Mueller, and J. O. Langbein, 1992, Ongoing Volcanomagnetic, Geodetic, and Seismicity Anomalies Observed from Mid-1989 in Long Valley Caldera, California, *Trans. Am. Geop. Un.*, **73**, 60.

Park, S. K., M. J. S. Johnston, T. R. Madden, F. D. Morgan, and H. F. Morrison, 1992, Electromagnetic Precursors to Earthquakes in the ULF Band: A Review of Observations and Mechanisms, Report to NSF, IGPP 92-15.

Johnston, M. J. S., G. D. Myren, R. J. Mueller, A. T. Linde, and M. T. Gladwin, 1992, A Focused Earthquake Prediction Experiment on the Southern Hayward Fault: Detection Array and Expected Strains and Displacements during Fault Rupture. . Proc. Second Conference, Earthquake Hazards in the Eastern San Francisco Bay Area, March 25-29, 1992, Cal. Div. Mines Geol. (in press).

Johnston, M. J. S., and A. T. Linde, 1992. Near-Field High Precision Strain Prior to the October 18, 1989 Loma Prieta M_L 7.1 Earthquake. USGS Prof. Paper on Loma Prieta Earthquake (in press).

Mueller, R. J. and M. J. S. Johnston, 1992. Seismomagnetic Effect generated by the October 18, M_L 7.1 Loma Prieta, California, Earthquake. USGS Prof. Paper on Loma Prieta Earthquake (in press).

Linde, A. T., M. T. Gladwin, and M. J. S. Johnston, 1992 Tidal Strain Response Before the 1989 Loma Prieta Earthquake: An Unsuccessful Search For Variations in Mechanical Properties. USGS Prof. Paper on Loma Prieta Earthquake (in press).

Mueller, R. J., M. J. S. Johnston, J. O. Langbein, and K. S. Breckenridge, 1992, Local Differential Magnetic Fields at Parkfield, California: July, 1985 to January, 1992, Proc. U.S.-China Conf. San Juan Bautista, (in Press).

Johnston, M. J. S., and J. Langbein, 1992, Review of Continuous Near-fault Strain and Near-Continuous 2-Color Deformation Data at Parkfield, California: 1986-1992, *Trans. Am. Geophys. Un.* (in press)

Johnston, M. J. S., R. J. Mueller and Y. Sasai, 1992, Magnetic Field Observations in the Near- Field of the June 28, 1992, M_L7.5 Landers, California, Earthquake, 1992, *Trans. Am. Geophys. Un.* (in press)

P. A. Reasenberg, D. P. Hill, A. J. Michael, W. L. Ellsworth, R. W. Simpson, S.

Walter, M. J. S. Johnston, R. Smith, S. J. Nava, W. J. Arabasz, J. C. Pechmann, J. Gomberg, J. N. Brune, D. DePolo, G. Beroza, S. D. Davis, and J. Zollweg, 1992, Remote Seismicity Triggered by the M7.5 Landers, California, Earthquake of June 28, 1992, *Trans. Am. Geophys. Un.* (in press)

Linde, A. T., I. S. Sacks, and M. J. S. Johnston, 1992, On the Detection of Short Term Strain Events - A Comparison of the Sensitivities of GPS and Borehole Strain Measurements, *Trans. Am. Geophys. Un.* (in press)

Park, S. K., M. J. S. Johnston, T. R. Madden, F. D. Morgan, and H. F. Morrison, 1992, Electromagnetic Precursors to Earthquakes in the ULF Band: A Review of Observations and Mechanisms, *Rev. Geophysics*, (submitted).

B. H. Armstrong, C. M. Valdes-Gonzalez, M. J. S. Johnston, and J. D. Leaird, 1992, Low Strain Level Acoustic Emission Due to Seismic Waves and Tidal/Thermoelastic Strains Observed at the San Francisco Presidio, Phys. Earth. Planet. Int. (Submitted).

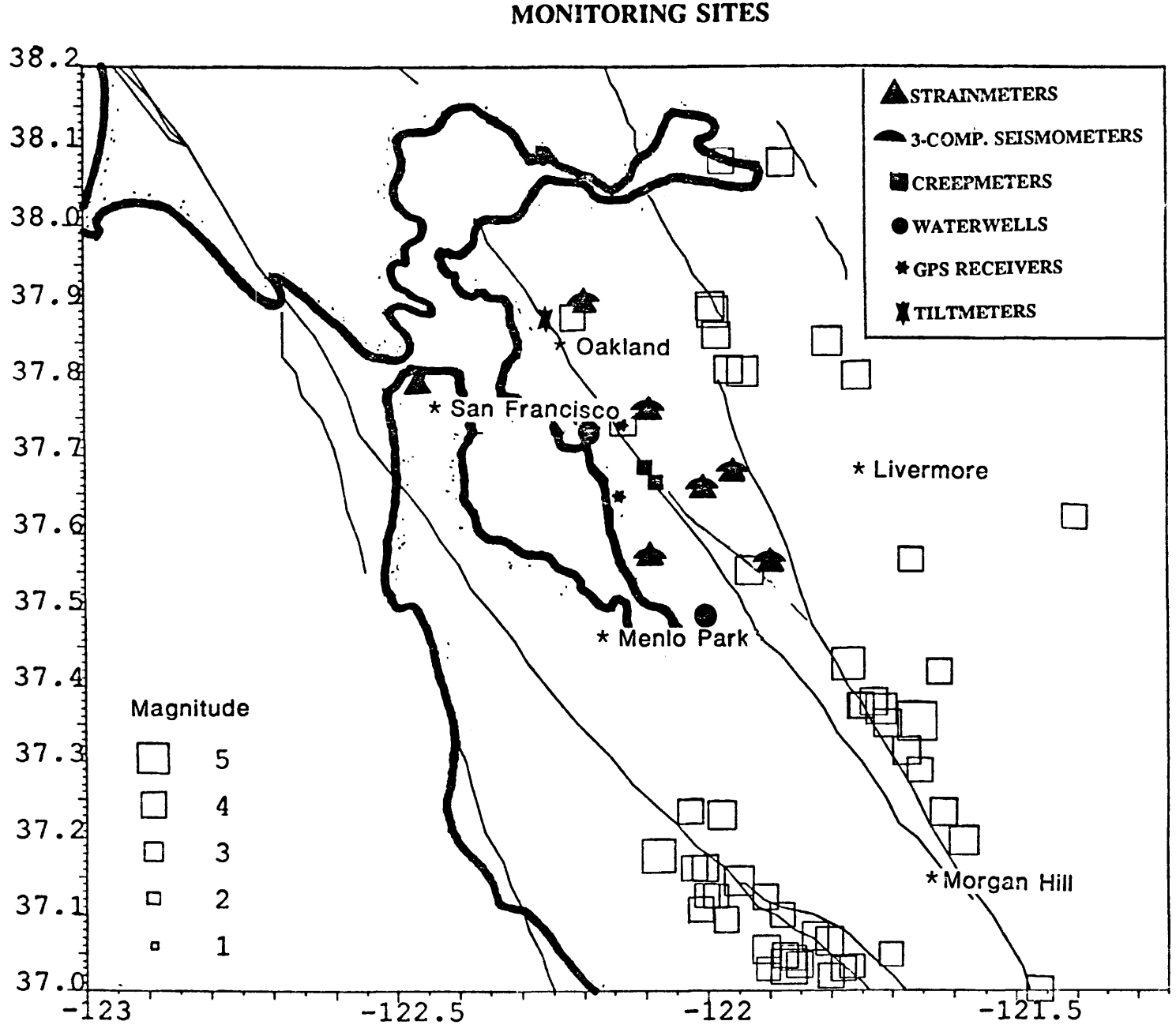

Figure 1. Monitoring instruments in the San Francisco Bay Area.

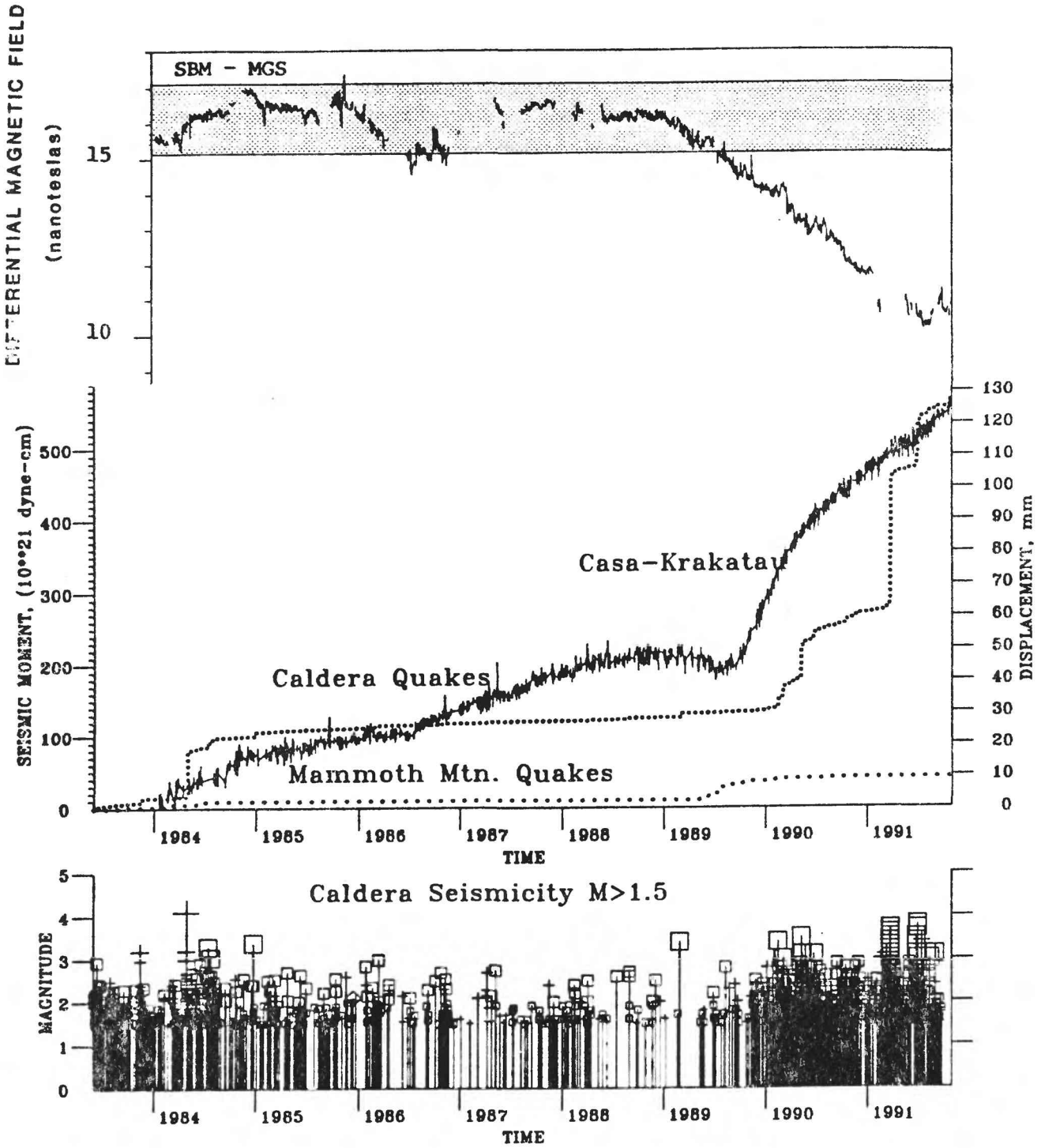

Figure 2. Magnetic, geodetic and seismic data from the Long Valley Caldera preceding and following. the start of volcanic activity in 1989.

Earthquake and Seismicity Research Using SCARLET and CEDAR

Agreement No. 14-08-0001-G1774

Hiroo Kanamori , Robert W. Clayton, and Leon T. Silver
California Institute of Technology
Pasadena, California

(818) 356-6914

Investigation

Determination of Earthquake Energy Release and M_L Using TERRAscope

We estimated the energy radiated by earthquakes in southern California using on-scale very broadband recordings from TERRAscope. The method we used involves time integration of the squared ground-motion velocity and empirical determination of the distance attenuation function and the station corrections. The time integral is typically taken over a duration of 2 min after the *P*-wave arrival. The attenuation curve for the energy integral we obtained is given by $q(r) = cr^{-n}\exp(-kr)$ $(r^2 = \Delta^2+h_{ref}^2)$ with c=0.49710, n=1.589, k=0.0089 km^{-1}, and h_{ref}=8 km, where Δ is the epicentral distance. A similar method was used to determine M_L using TERRAscope data. The station corrections for M_L are determined such that the M_L values determined from TERRAscope agree with those from the traditional optical Wood-Anderson seismographs. For $1.5<M_L<6.0$, a linear relationship $\log E_S = 1.96M_L+9.05$ (E_S in ergs.) was obtained. However, for events with M_L >6.5, M_L saturates. The ratio E_S/M_0 (M_0: seismic moment), a measure of the average stress drop, for six earthquakes, the 1989 Montebello earthquake (M_L=4.6), the 1989 Pasadena earthquake (M_L=4.9), the 1990 Upland earthquake (M_L=5.2), the 1991 Sierra Madre earthquake (M_L=5.8), the 1992 Joshua Tree earthquake (M_L=6.1) and the 1992 Landers earthquake (M_w=7.3) are about 10 times larger than those of the others that include the aftershocks of the 1987 Whittier Narrows, the Sierra Madre earthquake, and the Joshua Tree earthquake and the two earthquakes on the San Jacinto fault. The difference in the stress drop between the mainshock and their large aftershocks may be similar to that between earthquakes on a fault with long and short repeat times. The aftershocks, which occurred on the fault plane where the mainshock slippage occurred, had a very short time to heal, hence a low stress drop. The repeat time of the major earthquakes on the frontal fault systems in the Transverse Ranges in southern California is believed to be very long, a few thousand years. Hence, the events in the Transverse Ranges may have higher stress drops than those of the events occurring on faults with shorter repeat times, such as the San Andreas fault and the San Jacinto fault. The observation that very high stress-drop events occur in the Transverse Ranges and the Los Angeles Basin has important implications for the regional seismic potential. The occurrence of these high stress drop events near the bottom of the seismogenic zone strongly suggests that these fault systems are capable of supporting high stress that will eventually be released in major seismic events.

Characterization of earthquakes in terms of the E_S/M_0 ratio using broadband data will help delineate the spatial distribution of seismogenic stresses in the Los Angeles basin and the Transverse Ranges.

Publications

Kanamori, H., 1992, Locating Earthquakes with Amplitude--Application to Real-Time Seismology--, Bull. Seismol. Soc. Am., in press.

Kanamori, H., and E. Hauksson, 1992, A Slow Earthquake in the Santa Maria Basin, California, Bull. Seismol. Soc. Am., 82, 2087-2096.

Kanamori, H., E. Hauksson, T. H. Heaton, L. K. Hutton and L. M. Jones, 1992, Determination of Earthquake Energy Release and M_L Using TERRAscope, Bull. Seismol. Soc. Am., in press.

Jones, C., H. Kanamori and S. W. Roecker, Missing Roots and Mantle "Drips": Regional P_n and Teleseismic Arrival Times in the Southern Sierra Nevada and Vicinity, California, J.G.R., submitted 1991

Magistrale, H., Kanamori, H., Jones, C., Forward and inverse three-dimensional P-wave velocity models of the southern California crust, Geophys. Res. Lett., submitted August 1991.

Paleoseismicity in the Puget Sound Area as Recorded in Sediments from Lake Washington

Agreement No. 1434-92-G-2188

Robert Karlin
Mackay School of Mines/168
University of Nevada, Reno
Reno, NV 89557

(702) 784-1770

Brief Description of Project

This study was undertaken to evaluate the sediments of Lake Washington as a possible recorder of earthquake activity during the Holocene. Initial analyses show that a series of terrigenous silt layers have been episodically deposited throughout the lake. The objectives of this research have been to ascertain the timing, sources, and causes of the quasi-periodic disruptions in sedimentation. The work involves textural analysis, compositional characterization, and paleo/rock magnetism on gravity and piston cores. Radiocarbon dating supplemented by tephrachronology was used to establish an absolute time scale for several of the cores. If the layers are confirmed to be of seismogenic origin, the results from this study could provide an estimate of earthquake recurrence intervals for western Washington for the last 11,000 years.

Results

The first year's work concentrated on characterizing and dating eleven 3-m gravity cores which span the last 3,000 years. Magnetic susceptibility profiles, X-radiography, petrography, chemistry, and grain size analyses show that turbidites have been deposited episodically and can be readily correlated throughout the lake. These layers are characterized by highs in magnetic susceptibility, relatively coarse grain sizes, increases in aluminosilicate content and relative decreases in organic matter and biogenic silica. The sedimentary disturbances are most easily explained as the result of slumping of the steep-sided basin walls and increased detrital flux from landslides in the drainage basin as a result of large earthquakes. Because of the drainage configuration and analyses of modern major flood events, it is unlikely that these layers are caused by floods or other climatic phenomena.

One prominent turbidite layer was deposited in response to a major seismic event at about 1100-1200 yrs BP. Downcore patterns in susceptibility for this event can be readily correlated throughout the lake and suggest that near-simultaneous slumping occurred in at least three separate locations, two of which now contain submerged forests. The age of this event agrees with high

resolution radiocarbon dating and tree ring correlations of submerged trees (Jacoby et al., 1992). The event also coincides with >7 m of uplift at Alki and Restoration Points in south Seattle, submergence at Winslow Harbor and West Point (Bucknam et al., 1992), rock avalanches in the Olympic Mountains, (Schuster et al., 1992) and tsunami deposits at West Point and Whidbey Island (Atwater et al., 1992). All of these lines of evidence suggest a large magnitude 7 earthquake due to movement on the nearby Seattle Fault.

The susceptibility records from throughout the lake are suggestive of a correlation of Lake Washington disturbances with events observed elsewhere. In addition to the 1100 year event, sedimentary disturbances are found in the gravity cores 300 to 400, 1600 to 1700, 2200 to 2400, and 2800 to 3100 years ago. The latter three intervals correspond with periods of landsliding deduced from the dating of drowned trees in the lake (Jacoby et al., 1992). Major seismic events of the same age have also been reported from coastal marshes along the Washington coast (Atwater, 1987, 1992; Darienzo and Peterson, 1990). The event about 300 years ago is synchronous with probable coseismic submergence of marsh grass and trees along the Washington coast (Atwater, 1992; Atwater and Yamaguchi, 1991). Our results have been published in a report in *Science* (Karlin and Abella, 1992a) and were presented at the 1992 Fall meeting of the American Geophysical Union in San Francisco, California (Karlin and Abella, 1992b).

Piston cores provide a longer record of sedimentation extending to about 13.4 ka. Magnetic susceptibility profiles show remarkably consistent downcore patterns which can be readily correlated throughout the lake. A characteristic series of magnetic peaks is observed that correspond exactly with ash horizons and X-ray opaque intervals containing terrigenous layer which appear to be turbidites. From the size and lithologies of the turbidites and their areal distribution, these deposits are not due to flooding or local slides, but must represent basinwide disruptions such as associated with seismic activity. In 11 piston cores, more than fourteen sedimentary disturbances have occurred since deposition of the Mazama Ash at 6850 BP. If these events are all of seismic origin, the sediment record from Lake Washington suggests that large earthquakes occur on average about every 500 years in the Puget Sound region.

References

B. F. Atwater, *Science* **236**, 942 (1987).
B. F. Atwater and D. K. Yamaguchi, *Geology* **19**, 706-709 (1991).
B. F. Atwater, *J. Geophys. Res.* **97**, 1901 (1992a).
B.F. Atwater and A.L. Moore, *Science*, **258**, 5088, 1614 (1992).
R.C. Bucknam, E. Hemphill-Haley, E.B. Leopold, *Science*, **258**, 5088, 1621 (1992).
M. E. Darienzo and C. D. Peterson, *Tectonics* **9**, 1 (1990).
G. Jacoby, P. Williams, and B. M. Buckley, *Science*, **258**, 5088, 1621 (1992).
R.E. Karlin and S.E. Abella, *Science*, **258**, 5088, 1617 (1992).
R.E. Karlin and S.E. Abella, EOS **73**, 43, 527 (1992b)
R.L. Schuster, R. L. Logan, and P. Pringle, *Science*, **258**, 5088, 1620 (1992).

Proposal to Collaborate with the USGS Deep Continental Studies Group on the North Deployment of the Pacific Northwest Refraction Experiment

14-08-0001-G2073

G. R. Keller, K. C. Miller, J. M. Gridley
Department of Geological Sciences
University of Texas at El Paso
El Paso, Texas 79968
(915) 747-5501
e-mail address: keller@garrett.geo.ep.utexas.edu

Investigations

This research focuses on delineating the crustal structure of western Washington state and studying its implications for seismicity patterns in the Pacific Northwest. Key objectives addressed by this work are:

- Shallow crustal structure of the Pacific Northwest - What is the geometry of the sedimentary basins of the Puget Sound Basin? What is the nature and structure of terrane boundaries?

- Definition of the deep crustal structure - What is the along-strike geometry of the continental and oceanic Mohos? How is the crustal structure related to the subduction zone?

- Relationship of crustal structure to seismicity patterns - Are there north-south changes in crustal structure that correlate with seismicity patterns? Are there additional structural boundaries which have not yet been inferred from seismicity patterns?

Current investigations by our research group include determining seismic velocity structure by forward and inverse modeling of refraction/wide-angle reflection seismic data, constrained by analyses of gravity and magnetic data.

Seismic data were collected as part of the Pacific Northwest Seismic Experiment of 1991. The data set consists of two 300 km long

north-south deployments in the Willamette Lowlands of Oregon and the Puget Basin of Washington. Seismic data were acquired in collaboration with the U.S. Geological Survey Deep Continental Studies Group, Canadian Geological Survey, Oregon State University and several other academic contributors. This report addresses the north deployment in the Puget Basin of Washington (Figure 1). Approximately 485 instruments were deployed at intervals of 600 meters. Nine borehole shots were successfully detonated as the sources (~30 km intervals) over the length of this transect.

Results

The field program was successfully completed in September, 1991. In spite of some noisy recording conditions due to the high population density in the area, first arrival energy was seen to distances exceeding 280 km. In general, the data contain clearly identifiable first arrivals. Later phases such as PmP and Pn have less energy and are more difficult to identify.

To enhance arrivals, deconvolution, bandpass filtering, and three different gain corrections have been applied to the data, using a conventional reflection seismic data processing package. This processing effort has significantly enhanced PmP and Pn arrivals as well as some later phases. True amplitude records, records with automatic gain control applied, and trace normalized records, have been generated for each shot. Figures 2 to 4 show examples of this processing for the northernmost shot. Each type of record has been used in the phase identification process.

To date, preliminary crustal velocity models have been produced using first-arrival, PmP, and Pn picks. The velocity field has been interpreted using the seismic velocity inversion outlined by Zelt and Smith (1992). This analysis has resulted in a multilayered velocity model for the crust (Figure 5). The model shows upper crustal velocities to range from 2.50 km/s to 6.30 km/s and middle crustal velocities to range from 6.10 km/s to 6.80 km/s. Upper crustal velocities in the model are comparable to upper crustal velocities found by Taber et al. (1986) in an area southwest of this study area. Middle crustal velocities are within a +/- 0.2 km/s range of velocities found by Crosson (1976). The middle crust shows a significant lateral velocity gradient. Velocities from north to south increase from 6.20 km/s to 6.30 km/s at ~10 km depth and 6.50

km/s to 6.80 km/s at ~20 km/s. Lower crustal velocities range from 7.15 km/s to 7.40 km/s. Lower crustal velocities show a lateral velocity change from 7.40 km/s to 7.25 km/s north to south, respectively. Significant topography on the Moho has also been detected. Depth to Moho varies from ~36 km to ~48 km along the transect.

The inversion results have been used as a basis for forward modeling more subtle features in the data. The method of forward ray trace modeling is from Luetgert (1992). This model (Figures 6 & 7) uses the generalized seismic velocity structure from the inversion results and adds the constraints from known geology, gravity and magnetic data. Figures 6 & 7 show an example of the ray trace model from the northernmost shot. These results (Figures 6 & 7) better define the velocity structure of the surface structure and particularly the Puget Basin. Velocities in the Puget Basin range from 2.00 km/s to 5.50 km/s. Along this transect, the basin has a maximum depth of 8 km. Velocities used to define the basin range from 2.00 km/s to ~4.80 km/s. Velocities of the upper crust beneath the Cascades ranges are significantly faster at 4.50 km/s at the surface to 6.00 km/s at ~10 km depth. The mid-crustal lateral velocity gradient remains unchanged from the inversion model. Forward modeling of the Moho results in a more smoothly varying interface than that produced by the inversion model.

Study of true amplitude records (e.g. Figure 2) indicate significantly lower amplitudes in the southern part of the profile. This pattern of lower amplitudes to the south is seen on every shot in the experiment. Reflectivity analysis is being used to study the origin of these diminished amplitudes.

At present, phases later than PmP are being interpreted. This includes a wide-angle reflection that may represent the top the subducted Juan de Fuca plate. 2 1/2 - D gravity modeling is being done in concert with the seismic velocity modeling. Reflectivity analysis has also begun in an effort to resolve the origin of amplitude changes along the profile.

References

Crosson, R. S., 1976, Crustal modeling of earthquake data; 2, Velocity structure of the Puget Sound Region, Washington: Journal of Geophysical Research, v. 81, p. 3047-3054.

Luetgert, J. H., 1992, MacRay Interactive Two-Dimensional Seismic Ray Tracing for the Macintosh®, U. S. Geo. Survey Open-File Report 92-356, 43 p.

Taber, J. J., Jr., Lewis, B. T. R., 1986, Crustal structure of the Washington continental margin from refraction data: Bulletin of the Seismological Society of America, v. 76, p. 1011-1024.

Zelt, C. A., and Smith, R. B. 1992. Traveltime Inversion for 2-D Crustal Velocity Structure, Geophysical Journal International, vol. 108(1), p. 16-34.

Reports

Luetgert, J. H., Mooney, W.D., E. Criley, G. R. Keller, J. Gridley, K. Miller, A. Trehu, J. Nablek, S. B. Smithson, C. Humphreys, N. I. Christensen, R. Clowes, and I. Asudeh, 1991. Crustal Architecture of the Pacific NW: The 1991 Seismic Field Experiment, EOS, 72(44), p.323.

Mooney, W.D., Luetgert, J. H., E. Criley, G. R. Keller, J. Gridley, K. Miller, A. Trehu, J. Nablek, S. B. Smithson, C. Humphreys, N. I. Christensen, R. Clowes, and I. Asudeh, 1991. Crustal Architecture of the Pacific NW: The 1991 Seismic Field Experiment, EOS, 72(44), p.326.

Luetgert, J. H., Mooney, W.D., E. Criley, G. R. Keller, J. Gridley, K. Miller, A. Trehu, J. Nablek, S. B. Smithson, C. Humphreys, N. I. Christensen, R. Clowes, and I. Asudeh, 1992. Crustal Velocity Structure of the Pacific NW: The 1991 Seismic Refraction/Wide-Angle Reflection Experiment, 1992 Abstracts with Programs, Geological Society of America, Cordilleran Section, May 11-13, 1992, Eugene, Oregon, p.66.

Trehu, A. M., Nabelek, S., Azevedo, T. M., Brocher, J., Luetgert, J. H., Mooney, Asudeh, I., Clowes, R., Keller, G. R., Miller, K., Nakamura, Y., 1992, Crustal Structure of the Cascadia Subduction Zone Beneath Western Oregon, 1992 Abstracts with Programs, Geological Society of America, Cordilleran Section, May 11-13, 1992, Eugene, Oregon, p.87.

Gridley, J. M., Keller, G. R., and Miller, K. C., 1992, Crustal Structure of Western Washington State: Results of the Pacific Northwest Seismic Experiment 1991, (In Press), EOS, 1992 AGU Fall Meeting.

Miller, K. C., Roberts, D. G., Gridley, J. M., and Keller, G. R., 1992, Upper Crustal Structure of Northwestern Washington State: Integration of 3-Component Reflection Spread with Wide-angle Results, (In Press), EOS, 1992 Fall AGU Meeting.

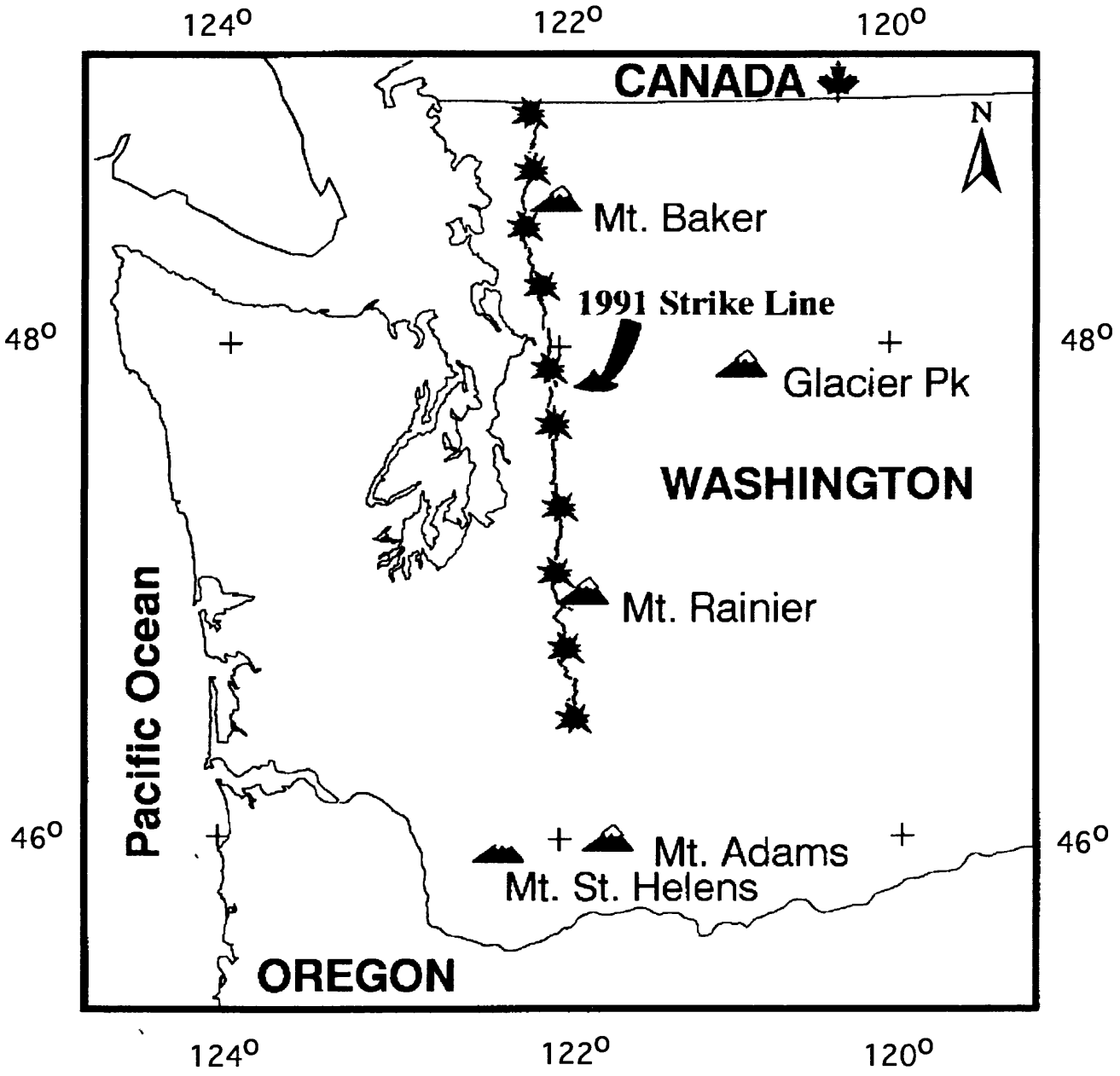

Figure 1. Location map of the profile recorded in 1991.

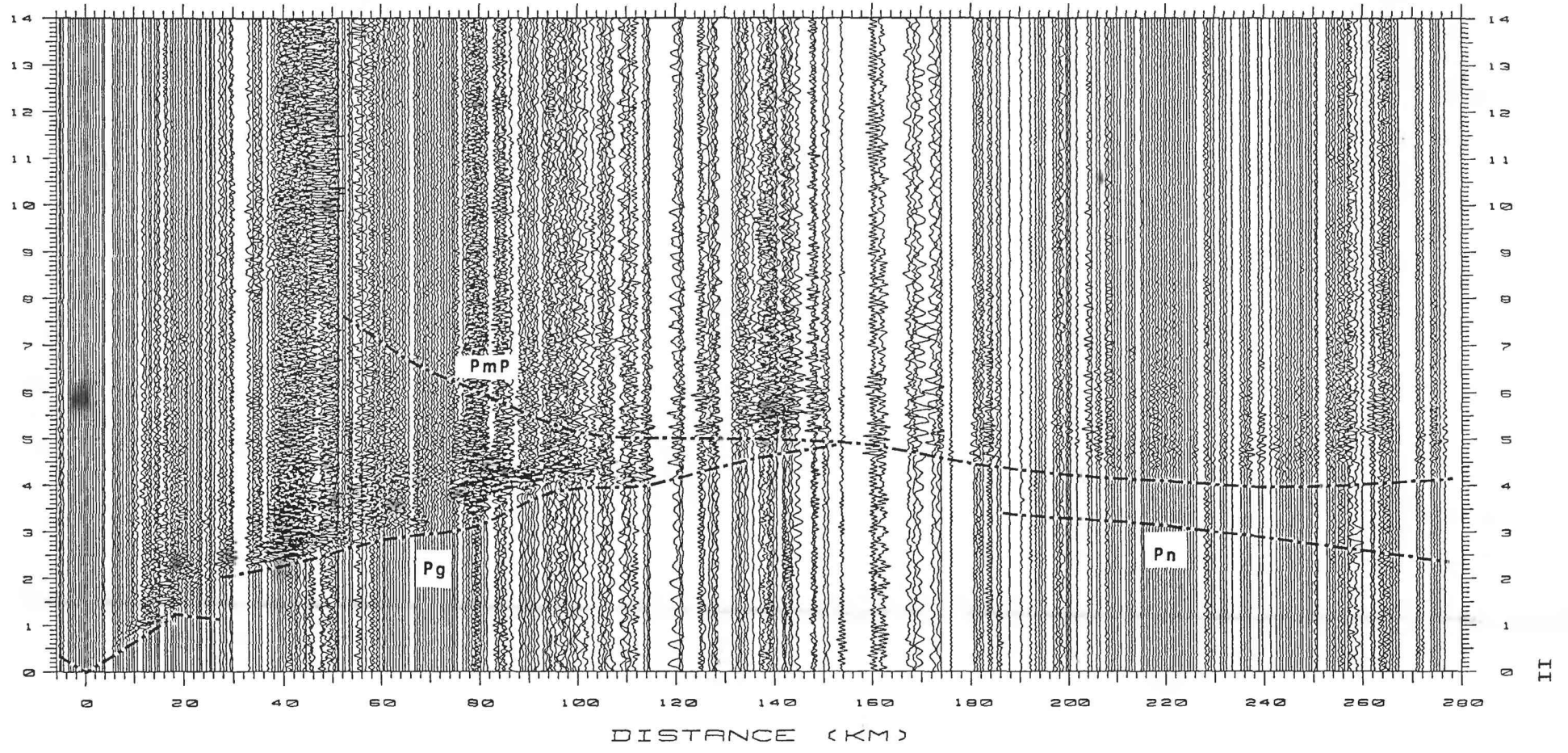

Figure 2. Seismic record of shot 1 with Pg, Pn and PmP arrivals denoted by the dashed line. This has been bandpass filtered, deconvolved and corrected for spherical spreading and plotted as true amplitude.

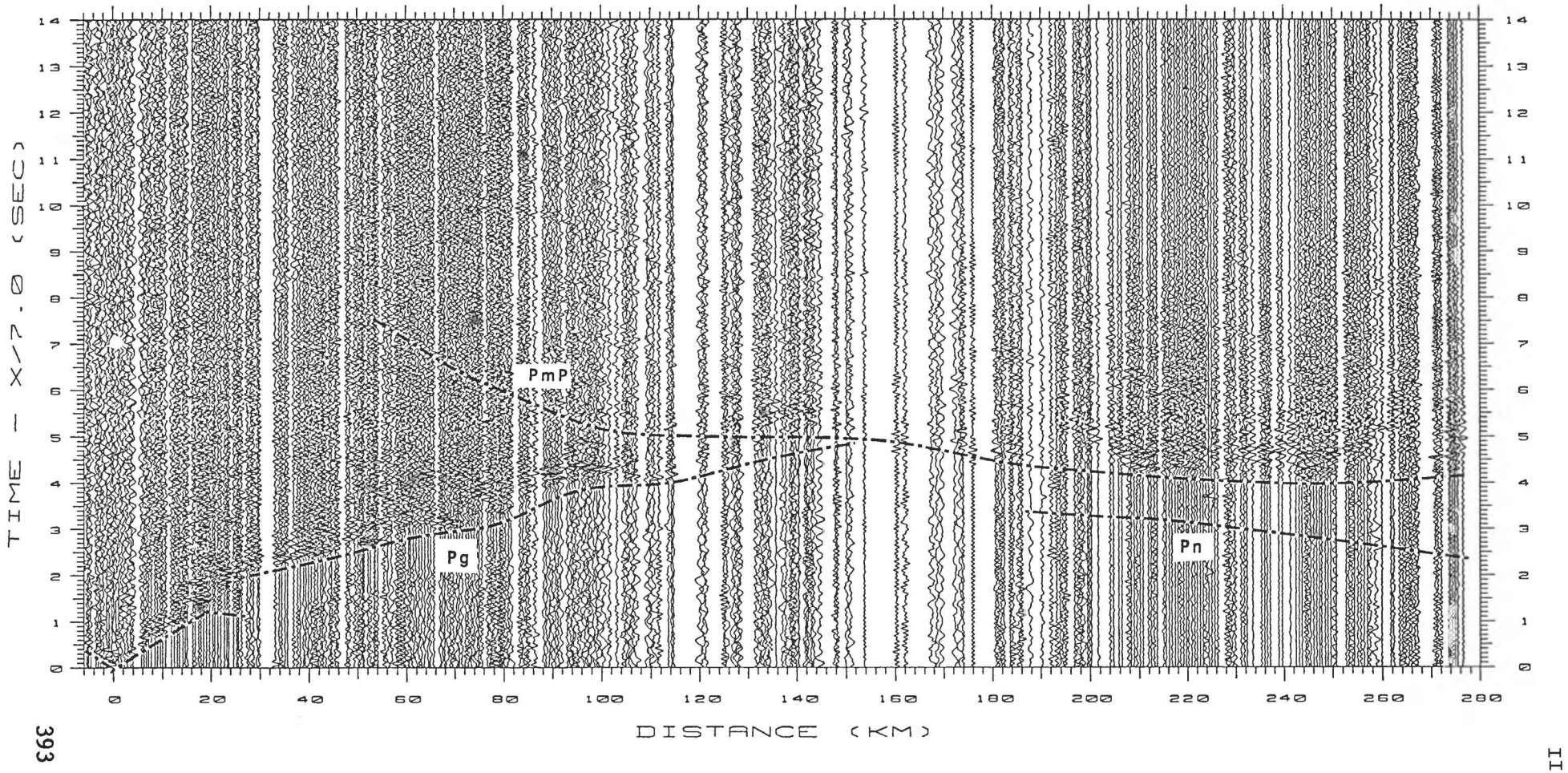

Figure 3. Seismic record of shot 1 with Pg, Pn and PmP arrivals denoted by the dashed line. This has been bandpass filtered, deconvolved and an automatic gain control has be applied.

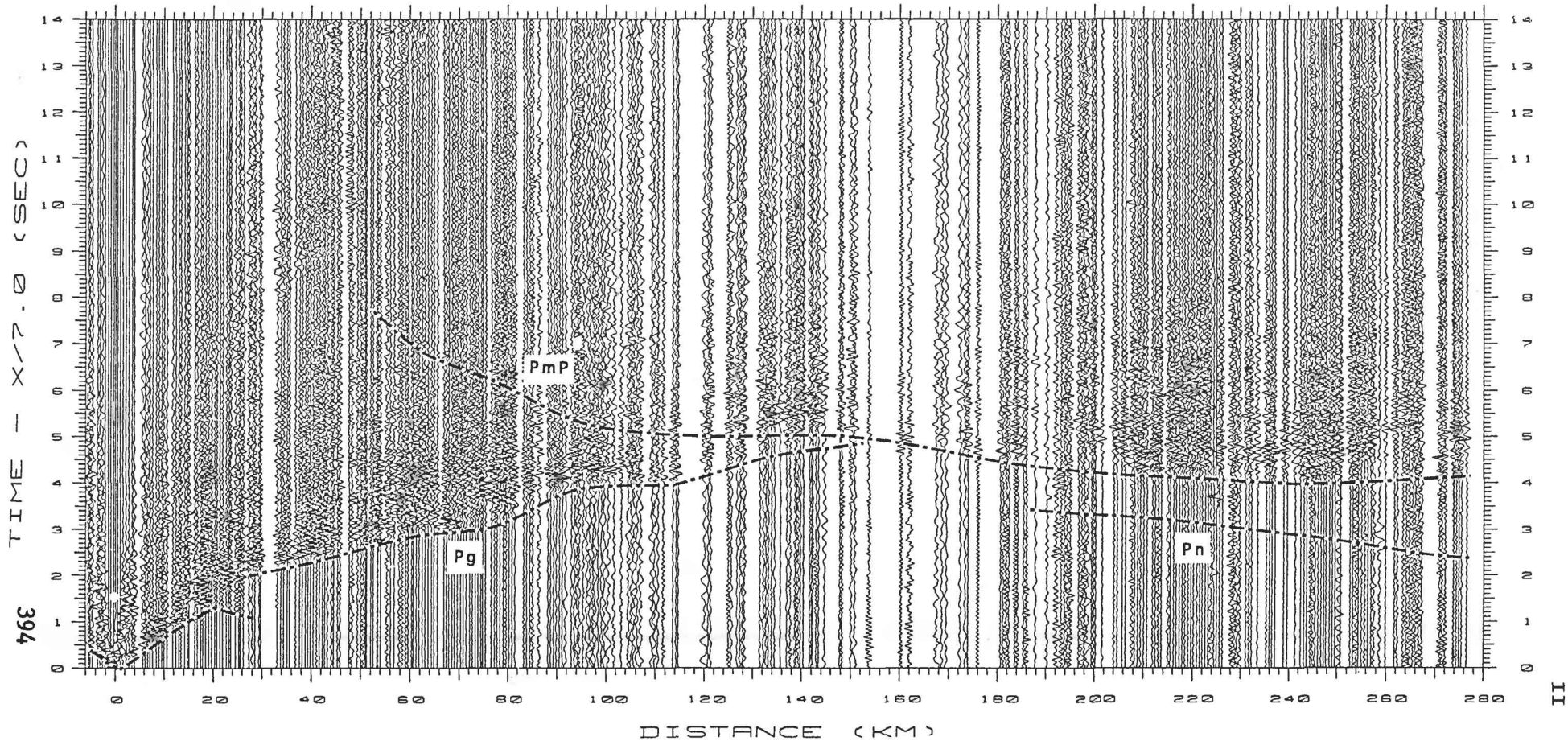

Figure 4. Seismic record of shot 1 with Pg, Pn and PmP arrivals denoted by the dashed line. This has been bandpass filtered, deconvolved and plotted with trace normallization.

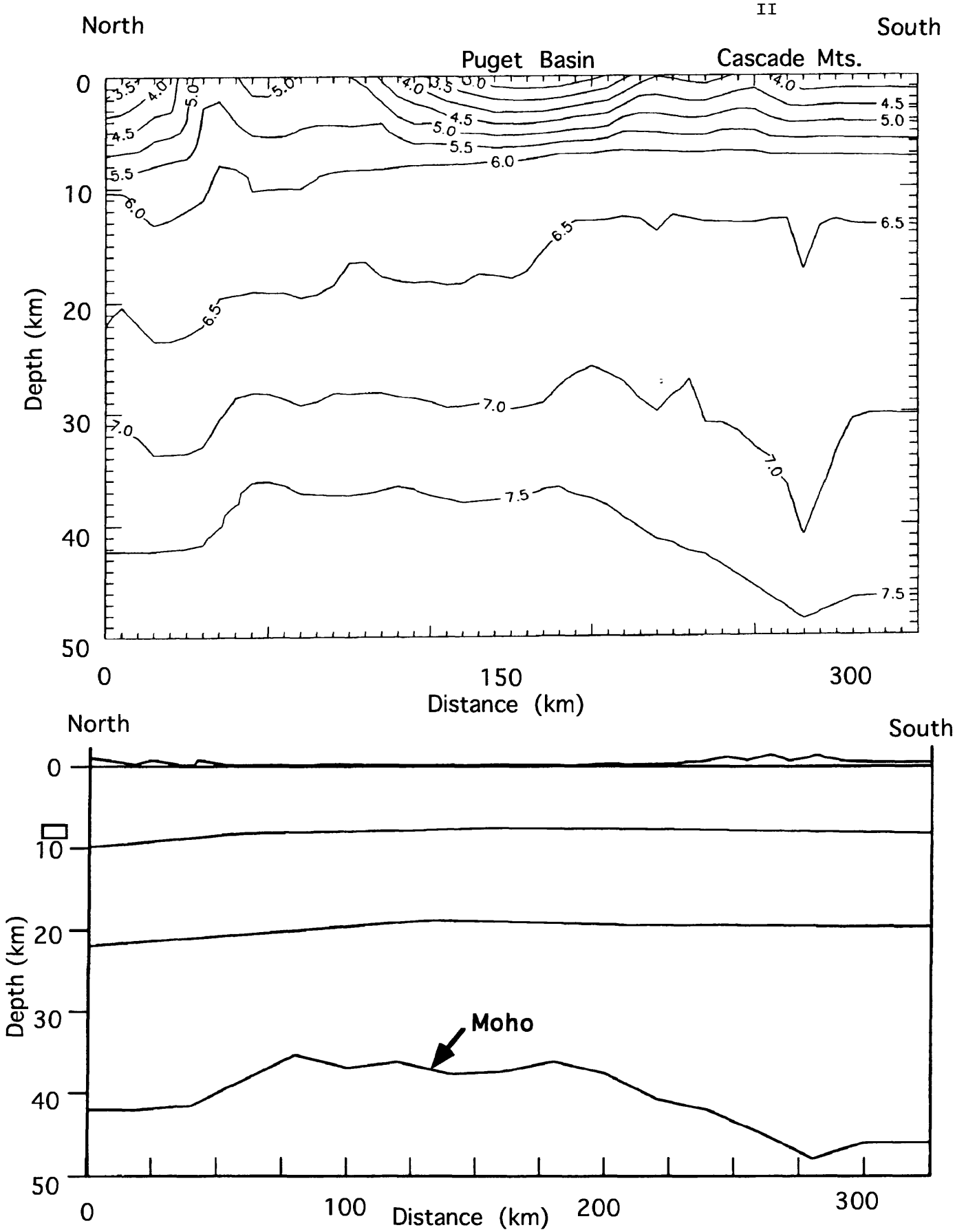

Figure 5. Seismic velocity model produced from inversion results of Pg, PmP and Pn arrivals. Upper figure shows the velocity field and the lower figure shows structure. Velocities are in km/s.

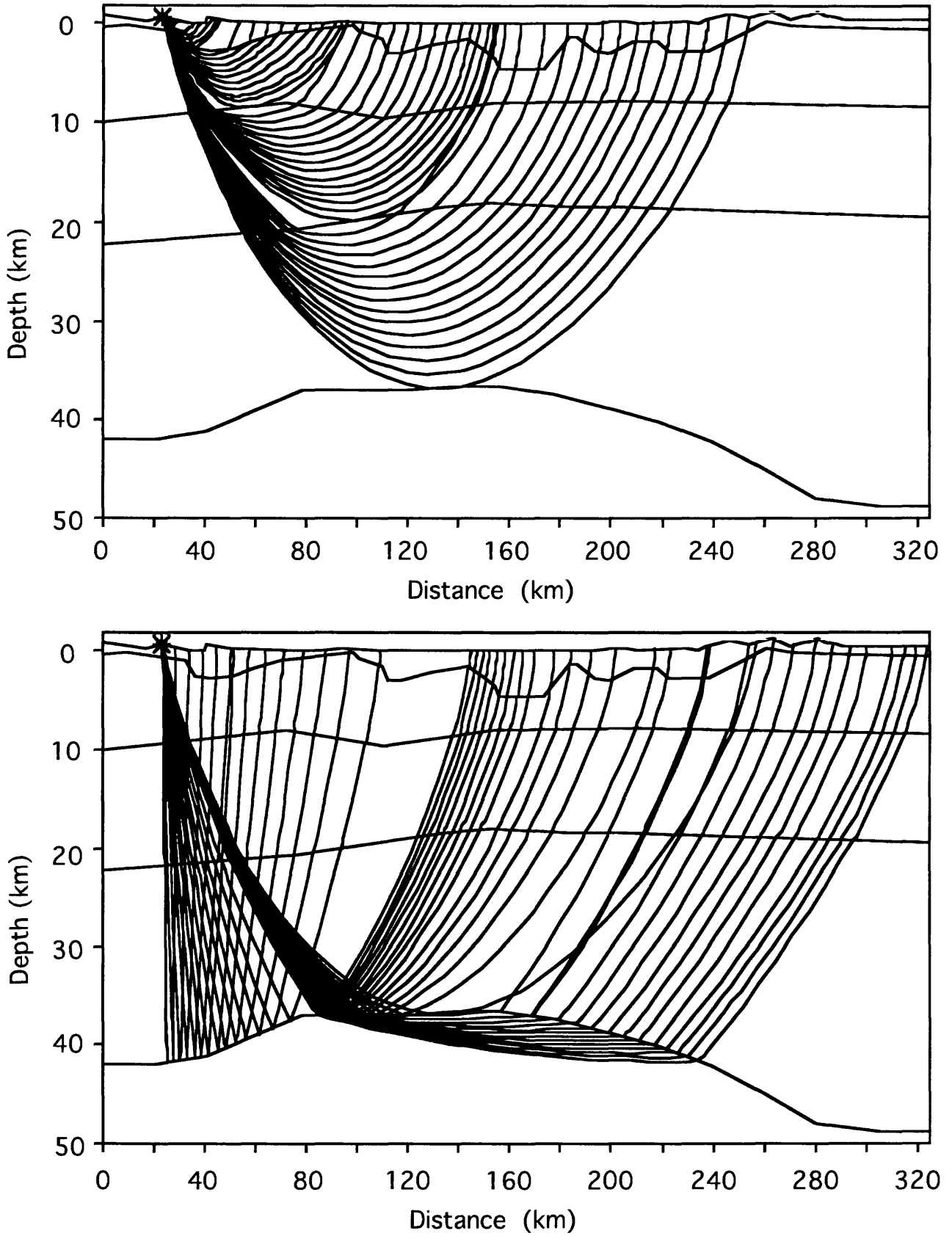

Figure 6. Forward ray trace model of the northern most shot. Upper figure is Pg arrivals and the lower figure is PmP and Pn arrivals.

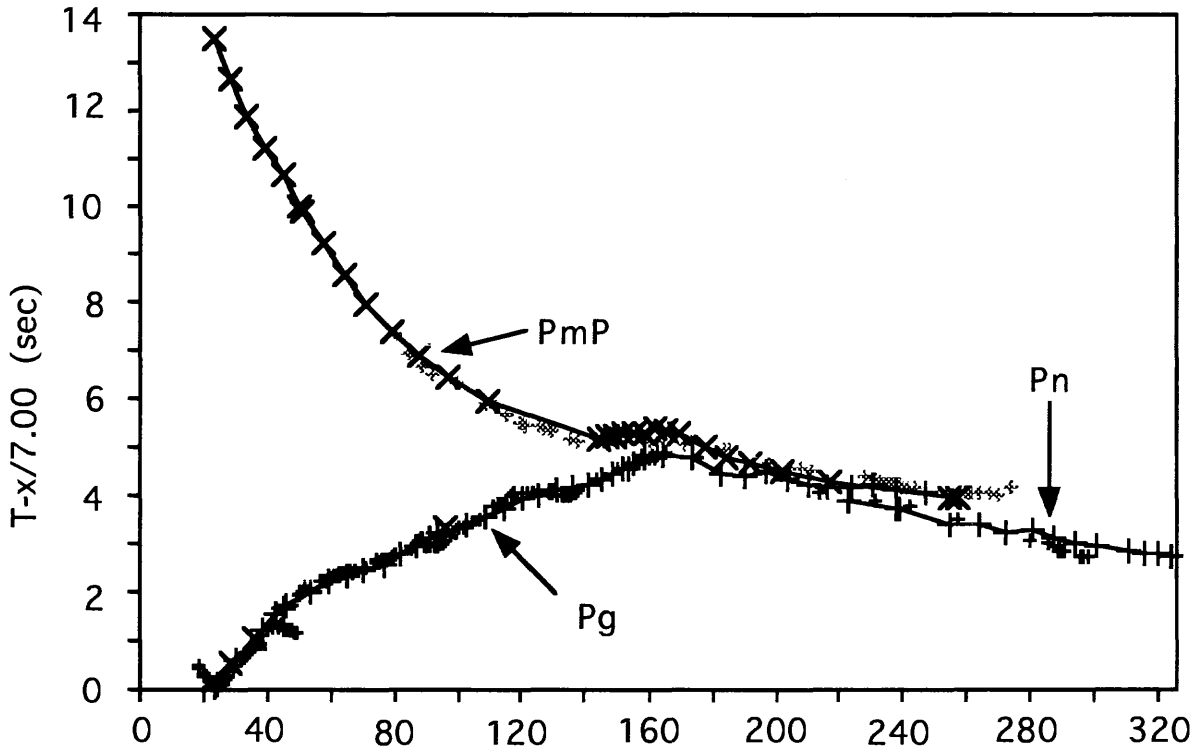

Figure 7. Forward ray trace model arrival fit for arrivals in Figure 6.

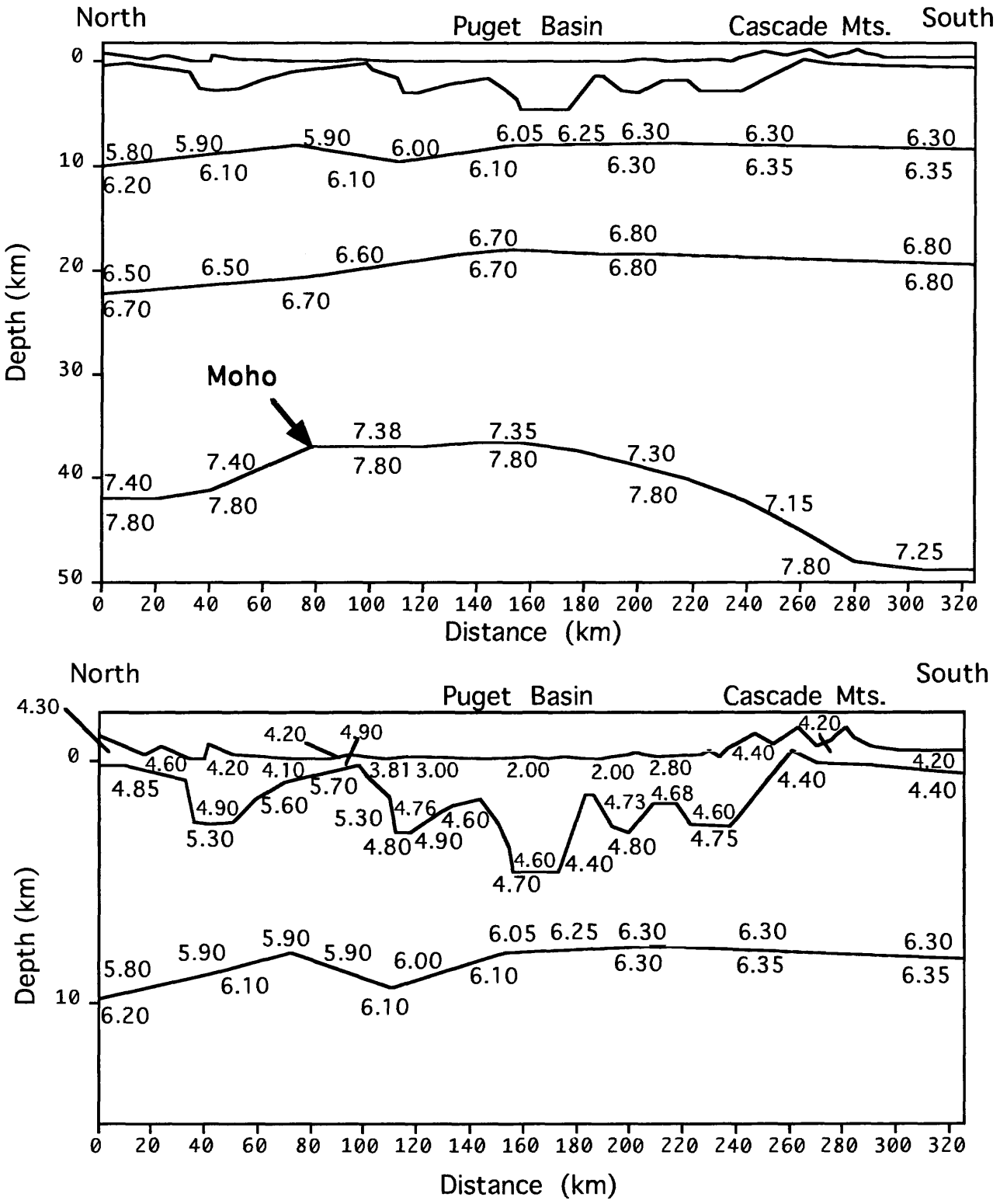

Figure 8. Top portion of the figure is the middle and lower crustal velocity structure from the forward ray trace model in Figures 6 & 7. Lower portion of the figure an is an elargement of the upper crustal velocity structure. Velocities are in km/s.

FAULT MECHANICS AND CHEMISTRY

9960-01485

C.-Y. KING
Branch of Tectonophysics
U.S. Geological Survey
345 Middlefield Road
Menlo Park, CA 94025
(415) 329-4838

Investigations

[1] Water temperature and radon content were continuously monitored at two water wells in Parkfield, California.

[2] Water level was continuously recorded at six other wells in central California.

[3] Water temperature and electrical conductivity were periodically measured, and water samples were taken from most of these wells and two springs in San Jose for Chemical analysis.

[4] Radon content of soil gas was surveyed across several faults.

Radon Surveys across Active Faults in California

Radon emanation is known to be anomalously high along active faults in many parts of the world. To check whether this is so for various faults in California, in late July and early August of 1992 we conducted soil-gas radon surveys with a portable radon meter (FD-3017, Shanghai Electronic Instruments, Inc.) across two creeping segments and one locked segment that was coseismically offset nearly three meters in the epicentral area of the magnitude 7.5 Landers earthquake on June 28, 1992.

Across the two creeping segments (Calaveras fault at Seventh Street in Hollister and San Andreas at Nyland Ranch in San Juan Bautista), the emanation was not anomalously high in the fault zones themselves, which are several meters wide, but was so on both sides of the fault. The survey lines were about 400 meters long and the maximum values, which are 5 to 8 times the background values, were measured at 10 to 55 meters from the center of the fault zones. This feature may indicate a relatively low permeability of the fault-gouge zone and high permeability of fractured rocks on both sides for terrestrial gases under pressure to escape into the atmosphere.

Along a 144-m survey line cross the currently locked segment of the San Andreas fault at the Earthquake Trail near Olema, the emanation was indeed anomalously high in the fault zone, by a factor of two above background values. However the maximum values (3 to 6 times background) were still recorded on the sides, about 10 meters away.

Alongside two roads (Encantado and Reche) that were offset by the Landers earthquake, the emanation at the two main breaks of the fault zone was an order of magnitude higher than background values measured over a distance of 300 and 420 meters, respectively.

Reports

King, C.-Y., (Group Chairman), 1991, Statements and recommendations (5 pages), in *Advisory Group Meeting Report on Isotopic and Geochemical Precursors of Earthquakes and Volcanic Eruptions,* reported by V. Dubinchuk, International Atomic Energy Agency, 1991.

King, C.-Y.,1991, Hydrological land geochemical approaches to earthquake prediction in *Proceedings of Symposium on Geology and Seismology of the Taiwan Strait and its Coasts,* China Ocean Press, 243-246.

King, C.-Y., Earthquake mechanism and predictability shown by a laboratory fault: *Journal of Geophysical Research,* (submitted), 40 Pages. (Branch Chief Approval, December 1991).

King, C.-Y., 1992, Earthquake-Prediction techniques: Encyclopedia of Earth system *Science, 2,* 111-118, *Academic Press Inc.*

King, C.-Y., 1992, Advances in Geophysical Research Vol. (Book review): Earthquake Spectra, v. 8, p. 637-639.

King, C.-Y., 1992, Earthquake-prediction techniques, *Proceedings of International School Symposium on Earthquake Prediction and Earthquake Engineering,* Plovdiv, Bulgaria, 16-23 April 1990.

King, C.-Y., 1992, Gas-geochemical approaches to earthquake prediction, *Proceedings of International School Symposium on Earthquake Prediction and Earthquake Engineering*, Plovdiv, Bulgaria 16-23 April 1990, p. 236-266.

King, C.-Y., Thermal stress in meteoroids by aerodynamic heating. *Journal of Geophysical Research,* (submitted), 23 pages. (Branch Chief approval, December 1991).

King, C.-Y.,Comment on "^{222}Rn premonitory signals for earthquakes" by R.L. Fleischer and A. Mogro-Campers: *Eos, American Geophysical Union Transactions,* (in press), 9 pages.

King, C.-Y., Basler, D., Minissale, A., Presser, T.s., Evans, W.C., and White, L.D., 1992, Hydrogeochemical measurements on Hayward fault (under review).

King, C.-Y., 1992, Thermal stress in meteoroids by aerodynamic heating, presented at *29th International Geological Congress*, Kyoto, Japan 24 August - 3 September, 1992, (abstract), v. 3, p. 641.

King, C.-Y., and Zhang W., 1992, Radon surveys across active faults in California, (abstract) *Supplement to Eos, American Geophysical Union Transactions,* 1992 Fall Meeting pl 362.

Minissale, A., and King, C.-Y., 1992, Seasonal variability of radon concentration in soil gas in central California (under review).

CASCADIA SUBDUCTION ZONE: NEOTECTONICS OF THE ACCRETIONARY WEDGE AND ADJACENT ABYSSAL PLAIN OFF OREGON AND WASHINGTON

CONTRACT 14-08-0001-G1800

Principal Investigator: LaVerne D. Kulm*
Co-Principal Investigator: Robert S. Yeats**
Graduate Research Assistant: Chris Goldfinger**

*College of Oceanography
**Department of Geosciences
Oregon State University
Corvallis, OR 97331
(503) 737-5211

Investigations

The overall objective of this project is to characterize and determine the timing of deformational events in the subducting Juan de Fuca plate (abyssal plain), deformation front (accretionary prism), and forearc basins (continental shelf) of the Cascadia convergence zone off Oregon and Washington. Field studies in 1992 were concentrated on potential active deformational zones identified in the recently completed neotectonic map of the Oregon margin. New sidescan sonar images and submersible dives discovered several active fault zones on the Oregon continental shelf and upper slope. We are continuing to identify and characterize discrete strike-slip fault and flexural-slip zones and relate them to potential fault and fold zones in the adjacent coastal region where co-seismic subsidence events in coastal bays are believed to be associated with large earthquakes in the Cascadia subduction zone. Alternatively, these co-seismic events may be related to local structures, rather than, or in addition to the unflexing of the plate margin.

Results

1. New Data Acquisition

Approximately 15,000 km of pre-existing oil industry multi-channel and single-channel seismic reflection records were acquired for the Oregon and Washington margins in 1992. In addition, biostratigraphic data were made available for surface outcrops cored on the shelf and slope. The Oregon records were used to construct the Oregon neotectonic map described below. We also obtained unprocessed BS^3 swath bathymetry from NOAA's National Ocean Service (NOS) for the submarine banks on the central and northern Oregon continental shelf and uppermost slope which allows the three-dimensional modeling of these features. SeaBeam swath bathymetry is now available in digital form for the Oregon continental slope and adjacent abyssal plain from NOAA/NOS.

In March 1992 we acquired a modest amount of funding from NOAA's National Undersea Research Program (NURP) to conduct a sidescan sonar and submersible dive project on the Oregon continental shelf and uppermost slope. Primary emphasis was placed on potential active fault zones. The NURP program provides funding chiefly for marine data acquisition, which was completed July 27 to August 4, 1992. The USGS's National Earthquake Reduction Program (NEHRP) provided the funding for data analyses and interpretation in this joint research program.

2. Neotectonic Map of Oregon Margin

We have completed the neotectonic map of the Oregon continental shelf, slope and adjacent abyssal plain that is the fundamental framework of our Oregon research program (Fig. 1, modified version of colored map; Goldfinger et al., 1992). The interpretation and correlation of the marine features on the map draws upon a combination of SeaBeam swath bathymetry, GLORIA long-range sidescan sonar, high-resolution SeaMARC-IA sidescan sonar, multi-channel and single-channel seismic reflection records, and DELTA and ALVIN submersible dives. This map will be published by the Oregon Department of Geology and Mineral Industries (DOGAMI) late in 1992. Several papers, which provided information to and utilized information from this map, were published during 1992 (Appelgate et al., 1992; Goldfinger et al., 1992a, 1992b; MacKay et al., 1992).

3. Active Faults of the Oregon Continental Shelf

In July-August 1992, we began a new and detailed study of selected active fault and fold structures of the Oregon continental shelf and upper slope which were previously identified in the Oregon neotectonic map (Goldfinger et al., in press). The objective of this program is to investigate active structures on the Oregon shelf and to determine their relationship to previously studied accretionary wedge active structures to the west and the active deformation of the Oregon coastal region to the east. The oil industry multi-channel seismic reflection profiles were combined with the field data from high-resolution 50 kHz Klein sidescan sonar surveys and DELTA submersible dives to locate, ground truth and map in detail the active structures. Three distinct styles of active deformation occur on the Oregon continental shelf: (1) active folding and associated flexural-slip faulting; (2) active strike-slip faulting; and (3) broad vertical deformation that may or may not be associated with individual faults. Each of these styles plays a role in the vertical and horizontal deformation of the Oregon shelf, and we infer, the adjacent coastal region. These structures also may be a seismic hazard to coastal communities in addition to or independent of the Cascadia plate interface.

Flexural-slip thrust faults are a common feature of active folding on the Oregon shelf. We made several DELTA dives on this type of fault off the Tillamook Bay area and southeast of Daisy Bank. These dives confirmed the active nature of these faults as previously postulated (Goldfinger et al., 1992) on the central shelf in water depths of 180-150 m. We documented several active flexural slip thrust faults with overhanging scarp morphology developed in poorly consolidated material. These scarps offset the Holocene transgressive sediments (i.e., post-20 Ka features). It is unlikely they survived the inner shelf erosive wave action during the last low stand of sea level. We have previously linked some of these folds and associated faults to Oregon's coastal bays, and suggested that these active folds may be partly or solely responsible for documented co-seismic subsidence and salt marsh burial (Goldfinger et al., 1992). Confirmation of the active nature of these folds by direct observation, along with onshore mapping by other investigators, supports the premise that upper plate folding and faulting plays a significant role in the vertical tectonics of a number of Oregon's coastal bays.

Several strike-slip faults in different localities were studied in detail in the field program. We recorded sidescan images and made submersible dives on two active strike-slip faults: (1) fault B on the uppermost continental slope-outer shelf off the central Oregon coast (Goldfinger et al., 1992); and (2) Coquille fault on the continental shelf off Bandon, OR along the southern Oregon coast. Fault B truncates the southern flank of a structural uplift named Daisy Bank on the uppermost continental slope. The fault zone was observed as a WNW-trending vertical shear zone with vertical scarps locally 10 m in height. Submersible observations confirmed the trend, dip, and slip-sense of this fault as hypothesized by Goldfinger et al. (1992a,b). A second similar fault bounds the northern slope of the bank. The orientation of secondary shear fractures on both fault segments suggests left-lateral motion, thus the uplift of Daisy Bank may be due to the

compressional zone between these two faults. Gentle deformation of unconsolidated Holocene transgressive sand and mud deposits (Kulm et al., 1975) indicates both these faults are currently active.

We mapped a series of WNW trending left-lateral strike-slip faults on the inner shelf off the mouth of the Umpqua River. These faults cut probable Elkton Formation rocks of Eocene age, and also displace the surficial trangressive sands (Figure 2a). The Coquille fault is a similarly active, NNW-trending strike-slip fault, with open fractures and scarps observed from the submersible in 85 m water depth (Figure 2b). Preliminary analysis of the main fault and secondary structures confirm the Coquille fault as a right-lateral strike-slip fault. Nearby reflection profiles suggest 3-5 km of right lateral separation of NNE trending fold axes.

4. Vertical Tectonics of the Oregon Continental Shelf

SeaBeam swath bathymetry and sidescan sonar images of Heceta Bank off central Oregon identified two Pleistocene shorelines (i.e., wave cut platforms and sea cliffs) in water depths of 115-130 m, and 190-210 m. The shorelines are about 25 km in length, and the latter is better defined than the former. The shallower shoreline approximates the latest Pleistocene eustatic sea level lowstand at about 20 Ka. The deeper shoreline lies some 65-85 m below this lowstand and is tilted down to the south. Sediment samples were collected on the platform with the aid of the submersible for dating. Paleo-water depths of sedimentary rocks indicate that Heceta Bank has undergone an average of 900-1000 m of post-Miocene uplift (Kulm and Fowler, 1974). The largest amount of uplift on the Oregon shelf occurs in late Miocene and early Pliocene strata from Heceta Bank. However, the deepest shoreline suggests subsidence has occurred along the seaward flank, possibly sometime during middle to late Pleistocene time. Likewise, paleo-water depths of sedimentary strata comprising Nehalem Bank to the north and Coquille Bank to the south indicate several hundred meters of uplift along the outer shelf during the Pliocene, but 100 and 200 m of subsidence on their seaward flanks, respectively, is documented during the Pleistocene (Kulm and Fowler, 1974). The vertical movements of these three outer shelf banks are complex but consistent over a distance of 325 km.

Reports (also cited in text)

Appelgate, B., Goldfinger, C., MacKay, M., Kulm, L.D., Fox, C.G., Embley, R.W., and Meis, P.J., 1992, A left lateral strike slip fault seaward of the central Oregon convergent margin: Tectonics, v. 11, p. 465-477.

Goldfinger, C., Kulm, L.D., Yeats, R.S., et al., 1992, Neotectonic map of the Oregon continental margin and adjacent abyssal plain, Oregon Department of Geology and Mineral Industries, Open File Report O-92-4.

Goldfinger, C., Kulm, L.D., Yeats, R.S., Appelgate, B., MacKay, M.E., and Moore, G.F., 1992a, Transverse structural trends along the Oregon convergent margin: Implications for Cascadia earthquake potential and crustal rotations, Geology, v. 20, p. 141-144.

Goldfinger, C., Kulm, L.D., Yeats, R.S., Appelgate, B., MacKay, M.E., and Cochrane, G.R., 1992b, Active strike-slip faulting and folding of the Cascadia plate boundary and forearc in central and northern Oregon, U.S.G.S. Professional Paper 1560, Earthquake Hazards in the Pacific Northwest, in press.

MacKay, M.E., Moore, G.F., Cochrane, G.R., Moore, J.C., and Kulm, L.D., 1992. Landward vergence and oblique structural trends in the Oregon margin accretionary prism: Implications and effect on fluid flow, Earth and Planetary Science Letters, v. 109, p. 477-491.

References

Kulm, L.D., Roush, R.C., Harlett, J.C., Neudeck, R.H., Chambers, D.M., and Runge, E.J., 1975, Oregon continental shelf sedimentation: Interrelationships of facies distribution and sedimentary processes, Journal of Geology, v. 83, p. 145-175.

Kulm, L.D. and Fowler, G.A., 1974, Oregon continental margin structure and stratigraphy: a test of the imbricate thrust model, in Burke, C.A., and Drake, C.L., eds., The geology of continental margins: New York, Springer-Verlag, p. 261-284.

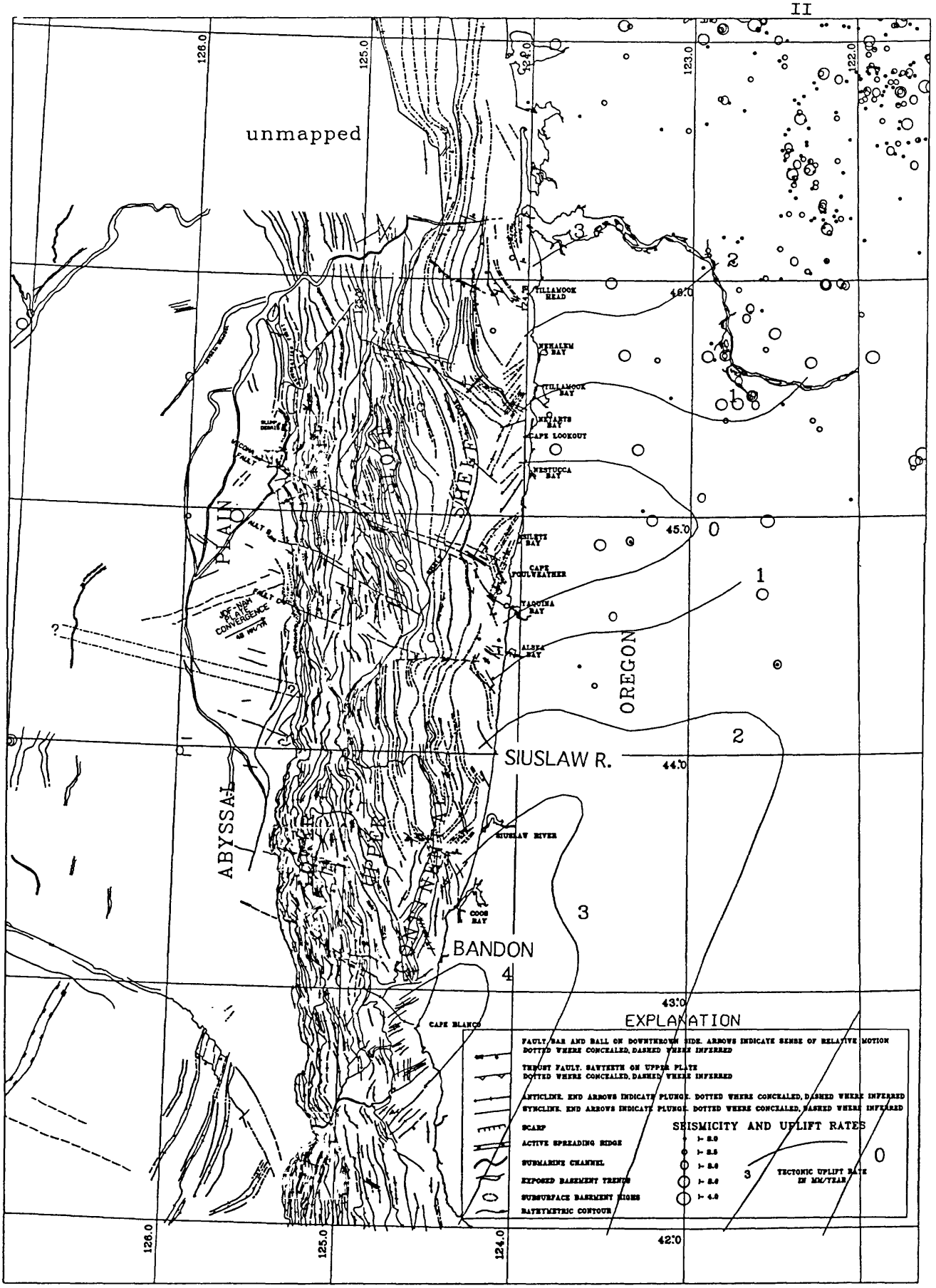

Figure 1. Neotectonic map of the Oregon continental margin showing structure, geodetic uplift rate contours, and seismicity. After *Goldfinger et al.*, 1992b, seismicity from *Kulm et al.*, 1984.

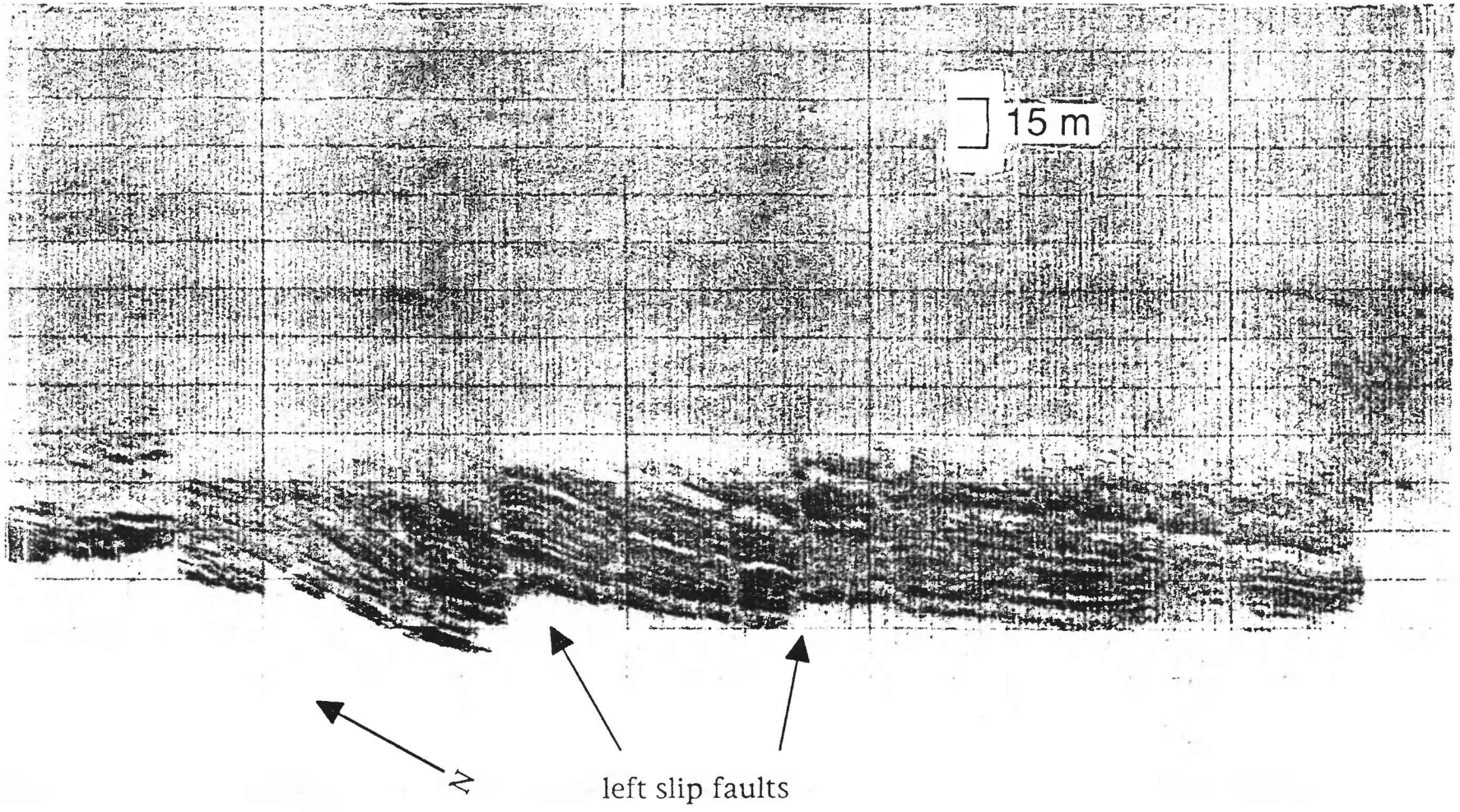

Figure 2a. 50 kHz sidescan record showing closely spaced left lateral strike-slip faults offsetting bedrock ridges of probable Elkton Formation off the Siuslaw River, southern Oregon. Strike-slip motion confirmed by mapping the same sense of offset on both limbs of a syncline. Water depth 90 m.

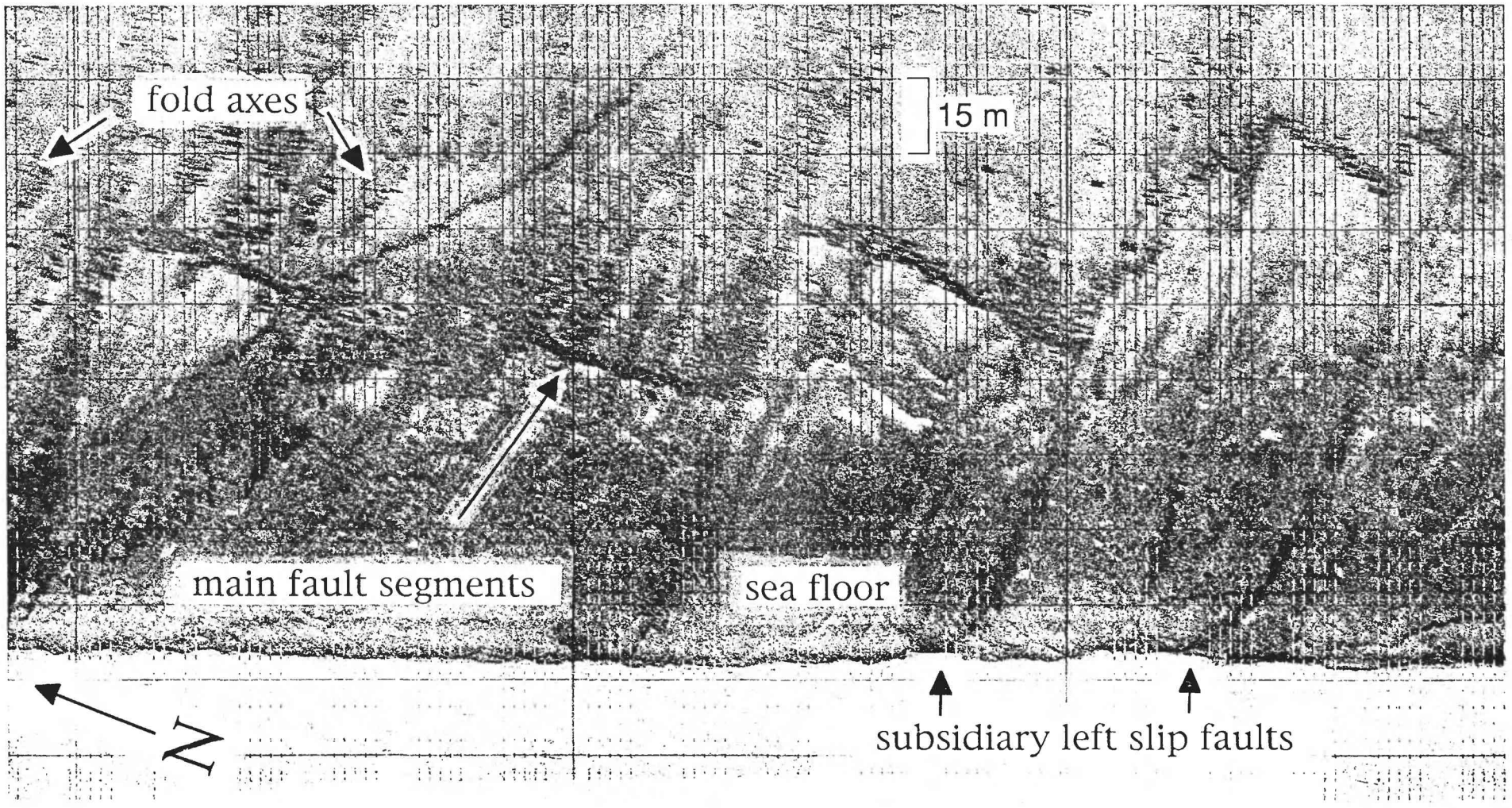

Figure 2b. 50 kHz sidescan record of the Coquille fault off Bandon, Oregon. En echelon main rupture segments trend north, while trend of the zone is NNW. Subsidiary WNW trending left-lateral faults are also clearly visible, as are active folds, establishing the direction of maximum compressive stress. Water depth 85 m.

Alaska Seismic Studies

9930-70023

John C. Lahr, Christopher D. Stephens,
Robert A. Page, and Kent A. Fogleman
Branch of Seismology
U. S. Geological Survey
345 Middlefield Road
Menlo Park, California 94025
(415) 329-4744

Investigations

1. Cooperated with the Geophysical Institute of the University of Alaska (UAGI) and the USGS National Earthquake Information Center (NEIC) in the operation of the Alaska Earthquake Information Center (AEIC) in Fairbanks. The AEIC is responsible for recording and analyzing Alaskan earthquake data and disseminating earthquake information and advisories to government agencies and to the public. As part of AEIC, continued lead role in collection and analysis of data from the high-gain short-period seismograph network extending across southern Alaska from the volcanic arc west of Cook Inlet to Yakutat Bay, and inland across the Chugach Mountains.

2. Cooperated with the Branch of Igneous and Geothermal Processed, UAGI, and the Alaska Division of Geological and Geophysical Surveys in operating the Alaska Volcano Observatory (AVO). Under this program, we have principal responsibility for monitoring the seismicity of Redoubt and Spurr, the recently active northern Cook Inlet volcanoes.

3. Cooperated with the Branch of Engineering Seismology and Geology and the UAGI in operating 13 strong-motion accelerographs in southern Alaska, including 11 between Icy Bay and Cordova in the area of the Yakataga seismic gap.

Results

1. For the time interval July 1991-June 1992, AEIC processed more than 7200 event triggers, of which 5187 were caused by earthquakes in southern and central Alaska (Figures 1 and 2). Seventeen of the earthquakes had magnitudes of 4.5 or greater, with the largest of these being a 5.9 ML shock on May 5 located 139 km deep beneath Iliamna volcano in a zone where earthquakes of similar size commonly occur. The largest shallow (depth above 30 km) earthquake was a 5.0 m_b (NEIS) shock on March 8 located along the Fairweather fault system northwest of Glacier Bay in southeastern Alaska. Of note is the persistence of aftershock activity in the northern Gulf of Alaska where two magnitude 7-class earthquakes occurred in 1987-88 (Lahr and others, 1988), a cluster of small earthquakes along the Transition fault zone near 58.75°N, 141.5°W, and the pesistence of shallow crustal activity beneath northern Cook Inlet about 75 km west-southwest of Anchorage. No unusual seismicity patterns were noted in and around the Yakataga seismic gap.

2. Focal mechanisms were compiled for nearly 1000 earthquakes that occurred between January 1987 and April 1992 in the area 60°-62.5°N latitude, 146°-153°W longitude. The more reliable solutions show a remarkably consistent pattern of stress orientation in the subducted plate beneath southern Alaska (Figure 3). Beneath Prince William Sound and the Chugach Mountains to the north, where the shallow subducted plate plunges northwestward at a low angle, the axes of least-compressive-stress (T-axes) tend to be subhorizontal and oriented west-east to northwest-southeast, with the general trend of the axes becoming more northerly to the north, roughly paralleling the change in the downdip direction of the subducted plate. The focal mechanisms of these events vary and range from normal to oblique-normal to strike-slip faulting. As both the depth and dip of the subducted plate increase, the dips of the T-axes also tend to systematically increase, so that the axes remain approximately aligned in the downdip direction of the Wadati-Benioff seismic zone within the descending plate to depths of at least 150 km. These observations are consistent with a model of the subducted plate acting as a stress guide transmitting upward the pull from deeper parts of the sinking slab. Evidence that this stress field may extend seaward of the trench is found in the northwestward orientation of T-axes determined for the sequence of two magnitude 7-class earthquakes in the northern Gulf of Alaska in 1987-88 (Lahr and others, 1988). The orientations of the axes of maximum-compressive-stress (P-axes) tend to be more variable. At depths less than about 65 km the axes tend to orient normal to the plane of the seismic zone; below 65 km the axes systematically rotate into the plane of the seismic zone and parallel the strike direction of the zone, and this tendency increases with depth (Kissling and Lahr, 1991). Many of the focal mechanisms for earthquakes in the overthrust North American plate have P-axes that are compatible with maximum subhorizontal compression aligned approximately in the direction of plate convergence.

3. Increasing seismic unrest at Spurr Volcano alerted AVO seismologists to magmatic activity beneath the volcano that culminated on June 27, 1992 in an explosive eruption at the historically active Crater Peak vent, which was the site of the last eruption in 1953. AVO issued a formal warning of a potential eruption one day before it occurred. The earliest indication of unrest was a swarm of shallow, high-frequency volcano-tectonic earthquakes (VT's) that occurred beneath Crater Peak in August 1991, the first swarm recorded at this location in ten years of monitoring. In the ensuing months levels of seismicity increased throughout the caldera, and notices of the increased activity were disseminated by AVO. In early June 1992, discontinuous episodes of tremor began following a brief swarm of VT's beneath Crater Peak. About 19 h before the June 27 eruption, continuous tremor started and persisted until about 4.5 hours before the eruption when a vigorous swarm comprising VT's and a few long-period events (LP's) began. The explosion blew away a seismic station located on the crater rim. Within several days after the eruption the level of seismic activity gradually declined to slightly elevated levels. A second explosive eruption occurred on August 18, but unlike the first event it was not preceded by significant seismic activity energetic enough to be recognized on the closest stations operating at that time (at distances greater than 4 km). The plume from this eruption was carried over Anchorage where as much as 3 mm of ash was deposited, disrupting aviation and commerce. After the August eruption, the seismic activity declined again but not to the level preceding August 18. In fact, at depths below 20 km the activity increased and suggested that magma was being replenished in the system. The crater rim station recorded the onset of continuous tremor starting a few hours before a third explosive eruption on September 17 and enabled AVO to issue an advance warning of the eruption. This explosion was followed by days of vigorous tremor

and in mid-November by an intense swarm of shallow events that led to an eruption alert but did not result in an eruption.

4. Earthquakes within a zone of seismicity beneath the Copper River delta area are being relocated using a model based on velocity structures determined for nearby TACT seismic profiles. Most of the well-recorded seismicity is concentrated near the top of a mid-crustal high-velocity (6.9 km/sec) layer that, in adjacent areas to the south and west, has been inferred to correlate with subducted lower crustal rocks of the Yakutat terrane. Typical focal mechanisms for these earthquakes are compatible with oblique reverse faulting controlled by compressive stress aligned approximately with the northwestward direction of plate convergence. However, the dips of the most northerly dipping nodal planes are probably too steep for these events to be associated with slip on the interplate thrust. Below about 20 km depth the rate of seismicity is much lower and the focal mechanisms generally have T-axes aligned in a northwest-southeast direction, which is characteristic of earthquakes in the Wadati-Benioff seismic zone in adjacent areas to the west. Relatively few earthquakes are located in the upper crust, but among them is the largest (by one magnitude unit) earthquake recorded by the regional network in this area since 1972, a magnitude 4.3 ML shock on September 15, 1989 that was followed by a significant aftershock sequence.

5. A patch of earthquake epicenters near Waxell Ridge marks the approximate center of the Yakataga seismic gap (see Figure 1). For many years the nature of this seismicity has remained uncertain due to poor local station coverage. However, with new data available since two additional seismographs were installed north of the Waxell Ridge, and with some velocity control available from nearby TACT seismic profiling, both the distribution and focal mechanisms of this seismicity can now be studied in more detail. In the southern part of this patch, many of the better constrained hypocenters tend to be concentrated in a diffuse zone between about 20 and 30 km depth that may lie at or near the top of the subducted plate. Offset from this zone by about 30 km to the northeast is a cluster of hypocenters centered at a depth of about 27 km. Focal mechanisms for earthquakes in this cluster are highly consistent and compatible with almost pure thrusting on a northward-dipping plane. Thus, this seismicity may be occurring at a weak spot on the interplate thrust. Near the hypocenter of the 1979 St. Elias earthquake (7.4 M_w; Estabrook and others, 1992), which is located about 50 km to the east, a similarly isolated cluster of seismicity was active for at least several years prior to the mainshock (Stephens and others, 1980). By analogy, the earthquake cluster at the northeast corner of the seismicity patch in the Waxell Ridge area may indicate a possible location for rupture initiation during a future large earthquake in the Yakataga gap.

6. Among the more significant computer software developments are: a new program (SPLAY) to display and interactively scroll through SSAM spectral data using a color VGA or super VGA monitor; a new version of the online event detection program XDETECT (version 3.0) that allows coeval triggers on multiple subnets which may have some stations in common; implementation of an automatic calibration analysis program to monitor and record station operational status; and changes to the event triggering algorithm in XDETECT to correct computational errors that tended to desensitize the algorithm.

7. Only one of the SMA units that were serviced had a trigger (Middleton Island), but the record has not yet been processed to check for an earthquake signal.

References

Estabrook, C.H., J.L. Nábělek, and A.L. Lerner-Lam, 1992, Tectonic model of the Pacific-North American Plate Boundary in the Gulf of Alaska from broadband analysis of the 1979 St. Elias, Alaska, earthquake and its aftershocks, J. Geophys. Res., v. 97, p. 6587-6612.

Lahr, J.C., R.A. Page, C.D. Stephens, and D.H. Christensen, 1988,Unusual earthquakes in the Gulf of Alaska and fragmentation of the Pacific plate, Geophys. Res. Lett., v. 15, p. 1483-1486.

Plafker, G., and K. Jacob, 1986, Seismic sources in Alaska, *in* Hayes, W.W., and P.L. Gori, eds., A workshop on evaluation of regional and urban earthquake hazards and risk in Alaska, U.S. Geol. Surv. Open-File Report 86-79, p. 76-82.

Reasenberg, P. and D. Oppenheimer, 1985, FPFIT, FPPLOT, and FPPAGE: Fortran computer programs for calculating and displaying earthquake fault-plane solutions, U.S. Geol. Surv. Open-File Report 85-739, 109 p.

Stephens, C.D., J.C. Lahr, K.A. Fogleman, and R.B. Horner, 1980, The St. Elias, Alaska, earthquake of February 28, 1979: Regional recording of aftershocks and short-term pre-earthquake seismicity, Bull. Seismol. Soc. Amer., v.70, p. 1607-1633.

Reports

Brocher, T. M., M. J. Moses, M. A. Fisher, C. D. Stephens, and E. L. Geist, 1991, Images of the plate boundary beneath southern Alaska, in Continental Lithosphere: Deep seismic reflections, AGU Monograph, Geodynamic Series, v. 22, p. 241-246.

Chouet, B.A., R.A. Page, C.D. Stephens, J.C. Lahr, and J.A. Power, Precursory swarms of long-period events at Redoubt Volcano, Alaska (1989-1990), Alaska: Their origin and use as a forecasting tool, submitted to J. Volcanol. Geotherm. Res.

Dawson, P.B., B.A. Chouet, R.A. Page and J.C. Lahr, 1992, A post-eruptive seismic survey of Redoubt Volcano, Alaska (abs.), Seismol. Res. Lett., v. 63, p. 67.

Jolly, A.D., R.A. Page, C.D. Stephens, J.C. Lahr, J.A. Power, and G.R. Cruse, 1991, Seismicity in the vicinity of Mt. Spurr Volcano, south-central Alaska, based on a revised velocity model (abs.), EOS (Trans. Am. Geophys. Un.), v. 72 (44 supplement), p. 567.

Kissling, E., and J.C. Lahr, 1991, Tomographic image of the Pacific Slab under southern Alaska, Eclogae geol. Helv., v. 84, p. 297-315.

Lahr, J.C., B.A. Chouet, C.D. Stephens, J.A. Power, and R.A. Page, Earthquake classification,

location and error analysis in a volcanic environment: Implications for the magmatic system of the 1989-1990 eruptions of Redoubt Volcano, Alaska, submitted to J. Volcanol. Geotherm. Res.

Moore, J. C., John Diebold, M. A. Fisher, J. Sample. T. Brocher, M. Talwani, John Ewing, R. von Huene, C. Rowe, D. Stone, Chris Stephens, and Dale Sawyer, 1991, EDGE deep seismic reflection transect of the eastern Aleutian arc-trench layered lower crust reveals underplating and continental growth, Geology, v. 19, p. 420-424.

Page, R.A., N.N. Biswas, J.C. Lahr, and Hans Pulpan, 1991, Seismicity of continental Alaska, in, Slemmons, D.B., E.R. Engdahl, M.D. Zoback, and D.D. Blackwell, eds., Neotectonics of North America, The Geological Society of America, Boulder, CO, CSM V-1, p. 47-68.

Page, R.A., J.C. Lahr, B.A. Chouet, J.A. Power, and C.D. Stephens, Statistical forecasting of repetitious dome failures during the waning eruption of Redoubt Volcano, Alaska, February-April 1990, submitted to J. Volcanol. Geotherm. Res.

Page, R.A., J.C. Lahr, C.D. Stephens, K.A. Fogleman, T.M. Brocher, and M.A. Fisher, 1992, Seismicity and stress orientation in the Alaska subduction zone after the great 1964 earthquake and speculation on the origin of a giant asperity [abs], in Wadati Conference on Great Subduction Zone Earthquakes, September 16-19, 1992, Fairbanks, Alaska, p. 31-32.

Power, J.A., J.C. Lahr, R.A. Page, B.A. Chouet, C.D. Stephens, D.A. Harlow, T.L. Murray, and J.N. Davies, Seismic evolution of the 1989-90 eruption sequence of Redoubt Volcano, Alaska, submitted to J. Volcanol. Geotherm. Res.

Rogers, J.A, and W.M. Kohler, 1992, XDETECT Version 2.01 Technical Reference, U.S. Geol. Surv. Open-File Report 92-364, 28 p.

Stephens, C.D., B.A. Chouet, R.A. Page, J.C. Lahr, and J.A. Power, Seismological aspects of the 1989-1990 eruptions at Redoubt Volcano, Alaska: The SSAM perspective, submitted to J. Volcanol. Geotherm. Res.

Stephens, C.D., J.C. Lahr, R.A. Page, and K.A. Fogleman, 1992, Recent seismicity in and near the Yakataga seismic gap, southern Alaska [abs], in Wadati Conference on Great Subduction Zone Earthquakes, September 16-19, 1992, Fairbanks, Alaska, p. 30.

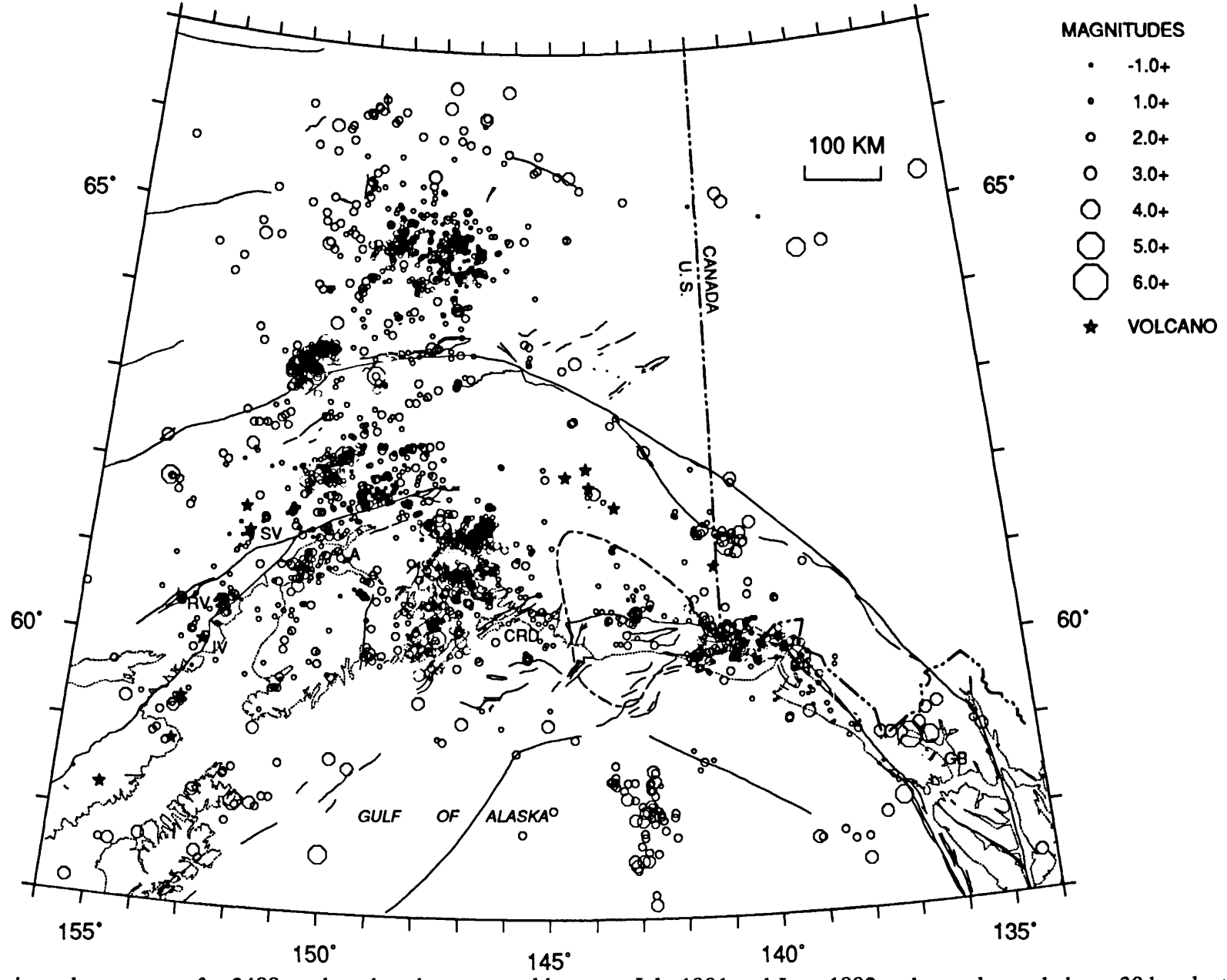

Figure 1. Preliminary hypocenters for 2488 earthquakes that occurred between July 1991 and June 1992 and were located above 30 km depth. Magnitudes are determined from amplitudes of seismic signals; the magnitude threshold for completeness varies across the region. Contour with alternating long and short dashes outlines inferred extent of Yakataga seismic gap. Neogene and younger faults (Plafker and Jacob, 1986) are shown as solid lines. A - Anchorage; CRD - Copper River delta; GB - Glacier Bay; IV, RV, SV - Iliamna, Redoubt and Spurr volcanoes.

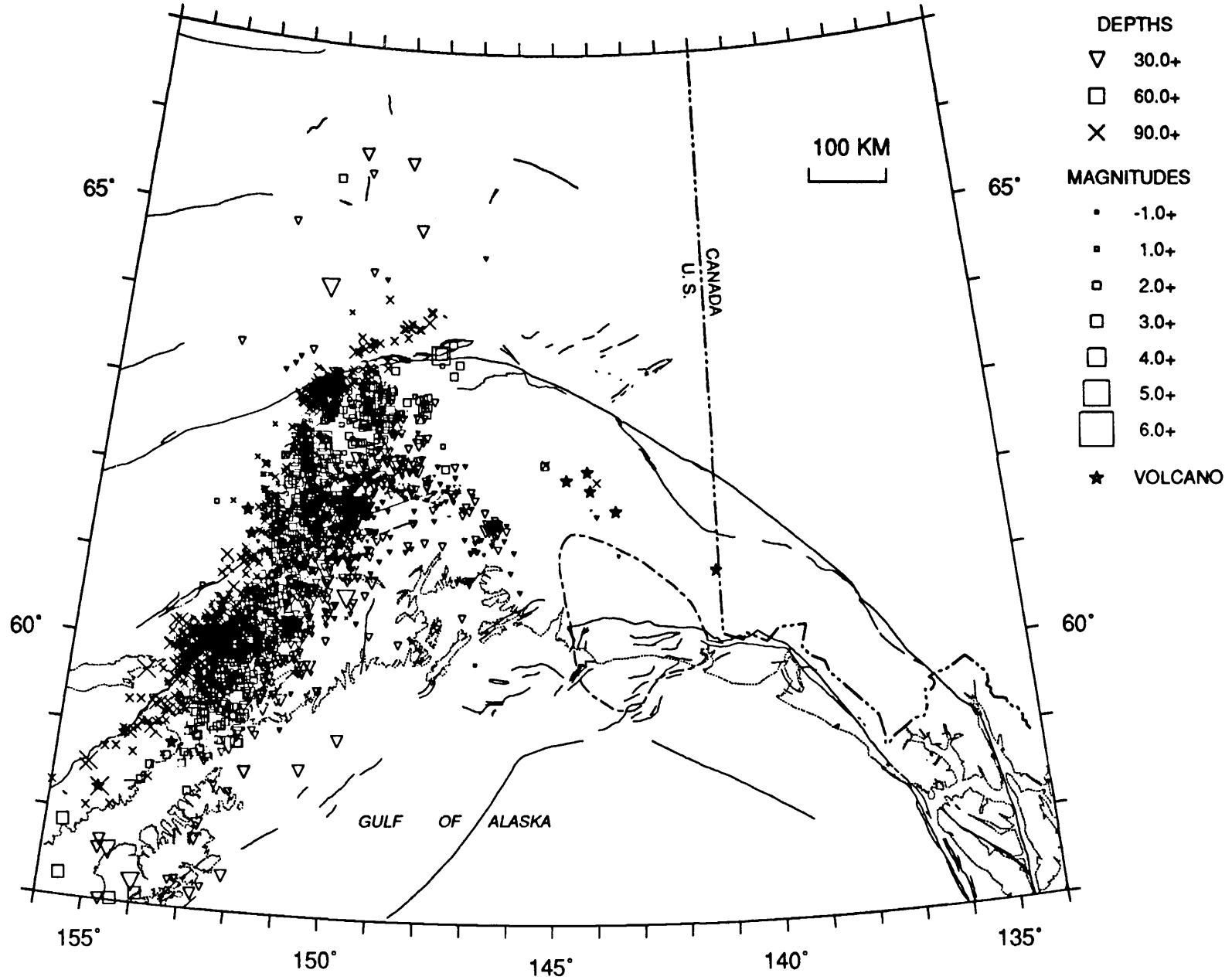

Figure 2. Preliminary hypocenters for 2699 earthquakes that occurred between June 1991 and July 1992 and were located at or below 30 km depth. See Figure 1 for details about magnitudes and identification of map features.

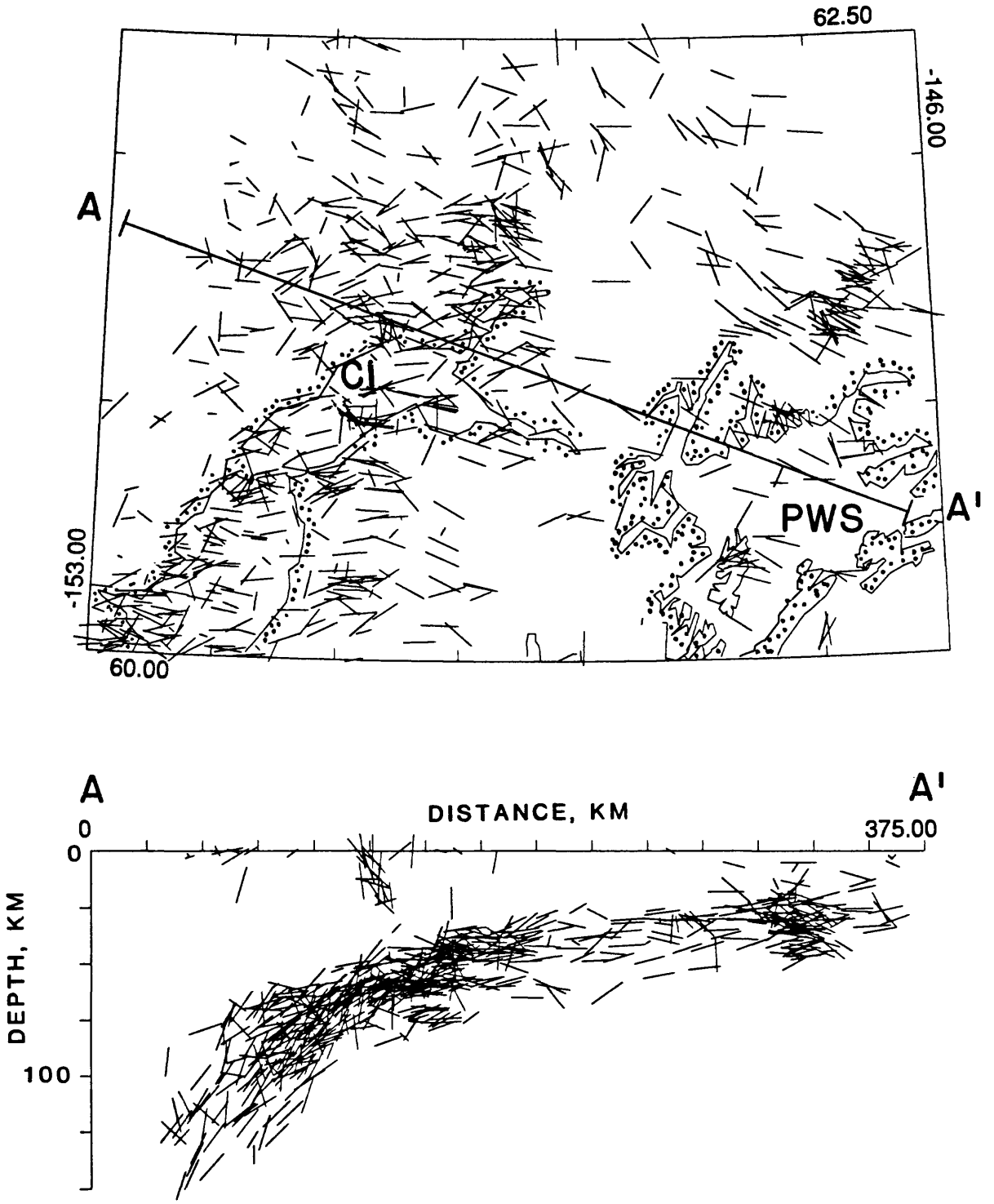

Figure 3. Orientation of T-axes for higher-quality focal mechanisms of 779 earthquakes. Unit-length axes are projected onto horizontal (*top*) and vertical (*bottom*) planes, so that shorter line segments correspond to nearly perpendicular axes. Focal mechanisms were determined using initial P-wave polarites and a modified version of the computer program FPFIT (Reasenberg and Oppenheimer, 1985), and were selected on the basis of having the 90% confidence regions for both the P- and T- axes cover less than 20% of the focal sphere. Line A-A' (*top*) shows the orientation of cross section (*bottom*), which is approximately perpendicular to the downdip direction of the Wadati-Benioff seismic zone in the subducting plate. CI - Cook Inlet, PWS - Prince William Sound.

POST-EARTHQUAKE STUDIES OF THE JUNE 28, 1992 LANDERS, CALIFORNIA, EARTHQUAKE

9910-01623

KENNETH R. LAJOIE
BRANCH OF ENGINEERING, SEISMOLOGY, AND GEOLOGY
U.S. GEOLOGICAL SURVEY
345 MIDDLEFIELD ROAD, MS/977
MENLO PARK, CALIFORNIA 94025
(415) 329-5641

Investigations

Post earthquake studies of June 28,1992 Landers earthquake. As part of joint USGS/CDMG effort mapped and analyzed surface fault rupture in Landers area.

Results

Surface fault rupture associated with the June 28, 1992 M_s 7.5 Landers earthquake extends 85 km from the Little San Bernardino Mountains in the south to the Rodman Mountains in the north. The rupture occurs along parts of several previously mapped north- to northwest-trending, subparallel faults (Eureka Peak, Johnson Valley, Homestead Valley, Emerson and Camp Rock), and along several unmapped north-trending faults connecting them. A 5-km gap in this otherwise continuous zone separates the northern end of the Eureka Peak fault and the southern end of the Johnson Valley fault. No surface rupture occurs on the east-trending Pinto Mountain fault, which runs through this gap. Southwest of the main rupture zone minor surface rupture occurs on the Lenwood fault and on the newly mapped Upper Johnson Valley fault. Northeast of the main zone rupture occurs on the Pisgah and Calico faults. Minor surface rupture also occurs on small faults northeast of Barstow. Surface rupture on the Eureka Peak, Lenwood, Upper Johnson Valley, Pisgah and Calico faults might reflect triggered, not primary, slip. Triggered slip did occur along the Indio segment of the San Andreas fault (40 km south of Landers) and along the entire length of the Superstition Hills fault (160 km southeast of Landers).

Displacement along the main faults is entirely right-lateral. Displacement along the connecting faults, with minor exceptions, is also right lateral. Thus, the connecting faults are not conjugate to the main faults, but are extensions of them. Horizontal displacement along the main faults is typically 2 to 3 m, but along the Emerson fault it reaches 5.5 m. Vertical displacement along the main faults is typically less than 0.3 m, but reaches about 2.0 m on the Emerson fault. In many places the sense of vertical displacement changes over short distances, and in some places it opposes general topographic relief.

Surface ruptures along the major faults generally follow topographic lineations and pre-existing fault scarps. However, at two places on the Emerson fault surface ruptures lie

up to 20 m from clearly expressed Quaternary scarps, possibly indicating local changes in stress. Most minor ruptures branching from the main faults follow no pre-existing geomorphic features, but along the Kickapoo fault there is clear geomorphic evidence of prior fault activity. In most places and on a wide range of scales surface ruptures are discontinuous, consisting of simple to complex patterns of en-echelon fractures and mole tracks. In some places, the rupture zone is over 100-m wide. Because of these complexities, few slip vectors could be measured precisely.

Surface rupture occurs along only on parts of the major faults. For example, it occurs only on the southern third of the Johnson Valley fault, and only on the northern halves of the Emerson and Camp Rock faults. Apparently, the numerous north-trending connecting faults transferred slip from part of one major fault to part of another. It is doubtful that this complex rupture pattern could have been predicted prior to the Landers event. Also, it is uncertain whether the same pattern occurred in the past or will occur again in the future. The pattern suggests that rupture started on the Johnson Valley fault and propagated northwestward. The pattern also suggests that the driving mechanism was a deep, northwest trending right-lateral couple that integrated parts of pre-existing faults at the brittle crustal surface. If correct, this model supports the conclusion of others that a major shear zone carries significant right-lateral motion between the North American and Pacific plates from the southern San Andreas fault across the Mojave desert into the western Great Basin. In effect, the Landers earthquake might reflect the northwestward propagation of the right-stepping transform system in the Gulf of California into the western Great Basin.

Reports

Staff (U.S. Geological Survey Menlo Park, CA 94025; California Division of Mines and Geology, Sacramento, CA 94518),1992, Pattern of Surface rupture associated with the June 28,1992 Landers Earthquake, EOS, v. 73, no. 43, p. 357. (Abs.)

Lajoie, K. R., 1992, Holocene Coastal Uplift in the Region of the 1992 Petrolia Earthquake, Northern California, EOS, v. 73, no. 43, p. 497. (Abs.)

McLaughlin, R.J., Lajoie, K. R., Castle, R. O. and Beutner, E. C., 1992, Tectonic Framework of the Mendocino Triple Junction of Northern California, EOS, v. 73, no. 43, p. 496. (Abs.)

Sebrier, M., McLaughlin, R. J., Lajoie, K.R. and Oppenheimer, D., 1992, Fault Kinemetics in the San Francisco Peninsula Area: is the 1989 Loma Prieta Earthquake Anomalous?, EOS, v. 73, no. 43, p. 4589. (Abs.)

Geodetic Strain Monitoring

9960-02156

John Langbein

Branch of Tectonophysics
U.S. Geological Survey
345 Middlefield Road MS/977
Menlo Park, California 94025
(415) 329-4853
langbein@shasta.wr.usgs.gov

Investigations

Two-color geodimeters are used to survey, repeatedly, geodetic networks within selected regions of California that are tectonically active. This distance measuring instrument has a precision of 0.1 to 0.2 ppm of the baseline length. Currently, crustal deformation is being monitored within the south moat of the Long Valley caldera in eastern California, across the San Andreas fault at Parkfield, California, at three locations near Palmdale, California on a section of the San Andreas fault that is within its Big Bend region, and at two locations near Pinon Flat, California. Periodic comparisons with other other two-color geodimeters are conducted both at Parkfield and at Mammoth Lakes. These intercomparisons measurements serve as a calibration to monitor the relative stabilities of these instruments.

Results

1. Long Valley Caldera

The line length changes measured using a two-color geodimeter still show high extension rates within the Long Valley Caldera. Figure 1 shows the line-length changes measured from mid 1983 to 27 monuments using our centrally located monument at CASA. The location of these baselines along with other baselines that are infrequently measured is shown in Figure 2.

The results from our measurements have been submitted for publication in *JGR*:

Abstract: Following the episodes of inflation of the resurgent dome associated with the May 1980 earthquake sequence (four M6 earthquakes) and the January 1983 earthquake swarm (two M5.2 events), seven years of frequently repeated two-color geodimeter measurements spanning the Long Valley Caldera document gradually decreasing extensional strain rates from 5 ppm/a in mid-1983, when the measurements began, to near zero in mid-1989. The corresponding seismic activity within the caldera persisted at a low rate of fewer than 10 M≥1.2 earthquakes per week from 1985 through November 1989 with no events exceeding M3.0. Early October 1989 marked a change in activity when measurements of the two-color geodimeter network showed a significant increase in extensional strain rate (9 ppm/a) across the caldera. The seismic activity began exceeding 10 M≥1.2

per week in early December 1989 and rapidly increased to a sustained level of tens of M≥1.2 per week with bursts having hundreds of events per day. Many events exceeded M3.0 and the largest event was M≈4. The 1989-91 inflation episode is the firs' have sufficient geodetic measurements in Long Valley to define the temporal relation between onset of an inflation episode and onset of brittle failure (earthquake swarm within the caldera). Here, the onset of events per day. Many events exceeded M3.0 and the largest event was M≈4. The 1989-91 inflation episode is the first time that we have sufficient geodetic measurements in Long Valley to define the temporal relation between onset of an inflation episode and onset of brittle failure (earthquake swarm within the caldera). Here, the onset of deformation preceded the onset of increased earthquake activity by more than two months. The seismicity rate began to decrease in mid-July 1990, consistent with a gradually slowing of extension across the caldera as measured by the two-color geodimeter. The recent episode of inflation can be modeled by a single Mogi point source located about 7 km beneath the center of the resurgent dome. In contrast, the deformation pattern observed between mid-1983 and mid-1989 is best reproduced by fault slip in the south moat, inflation at 6.5 km-depth near Casa Diablo Hot Springs and inflation beneath the resurgent dome. It appears that the source beneath the resurgent dome that was active for the earlier episodes is the primary source for the more recent episode. The model used to satisfy the line-length observations predicts 7.5 cm of uplift along leveling route along highway 395 from mid-1983 to mid-1989 and an additional 11 cm through the end of 1991. Thus the recent inflation episode represents a significant portion of the observed geodetic deformation with only little seismic energy release

During the summer of 1992, Dzurisin and co-workers of CVO releveled many of the routes within and near the Long Valley Caldera. Their observations show 11 cm of uplift during the interval between 1988 and 1992 which support the model of inflation derived from the two-color measurements.

2. Parkfield

Frequent measurements of a 17 baseline networks are made for a geodetic network near Parkfield, California. Approximately one-half of these baselines straddle the San Andreas Fault along the segment that last ruptured in 1966. The data from these baselines are shown in Figures 3a and 3b.

3. Southern California

Following the 1992 Landers earthquake, we used the two-color geodimeter to remeasure 3 out of our 5 networks in southern California. Below, is a compilation of the co-seismic strain changes inferred from the line-length changes. These networks were measured in the two-week interval following the 4 July holiday. To compute the co-seismic strain changes, the parameters of secular strain accumulation and a co-seismic strain change were simultaneously determined. The table below shows the results of this calculation. The error bars represent the one-standard deviation level and are computed on the basis of propagating the a-priori estimates of the data error through the inversion and the error bars are re-scaled by a factor representing the RMS misfit of the predicted to the observed length changes. The RMS misfit ratio of the misfits to the a-priori data error ranges between 1.34 and 1.82 mm/mm. The estimated error on the co-seismic strain changes could by considered "optimistic" since they represent offsets from extrapolating a linear trend. Had we differenced the lengths between the survey preceding and following the time of the Landers earthquake, the

standard errors would be larger.

The center of mass given for each network is a rough estimate. In reality, one should use the actual line-length change data to model the slip distribution of the Landers events. From the estimates of the strain changes for Pinon and Anza, which are located within 20 km of each other, the gradient in strain is significant because these networks are located near a node of the strain field.

Network period	Center of mass		Secular strain rate ppm/yr			Co-seismic strain ppm		
	longitude	latitude	$\dot{E}_{ee}$	$\dot{E}_{en}$	$\dot{E}_{nn}$	E_{ee}	E_{en}	E_{nn}
Pearblossom 1980-1992	-117° 51.7′	34° 27.7′	0.158±0.005	0.151±0.003	-0.200±0.005	-0.34±0.08	-0.18±0.06	0.14±0.08
Pinon 1986-1992	-116° 27.1′	33° 35.6′	0.142±0.020	0.127±0.013	-0.054±0.010	-0.46±0.28	-1.27±0.20	0.80±0.15
Anza 1988-1992	-116° 37.1′	33° 35.2′	0.189±0.027	0.071±0.021	-0.232±0.025	-0.22±0.13	0.19±0.09	1.85±0.12

4. Northern California

During the summers of 1991 and 1992, we measured the baseline lengths of 2 networks established in North California (Figure 4) to measure strain accumulation due to subduction of the Gorda Plate near Crescent City, California. From these line-length changes, a model of uniform strain is fit to the data from each of these networks:

Network	Secular strain ppm/yr			Principal strain Axis; Max. Compr. Degrees	ppm/yr Max. Compr.	Min Compr.
	$\dot{E}_{ee}$	$\dot{E}_{en}$	$\dot{E}_{nn}$			
Gorda	0.04±0.06	-0.01±0.06	-0.08±0.12	N5°E±28	0.08±0.12	-0.04±0.09
Scott	-0.30±0.08	-0.25±0.06	0.18±0.08	N67°W±5	0.41±0.09	-0.29±0.09

These estimates of strain rate are very preliminary since there was an instrument mal-function during the survey in 1992 which resulted in a length dependent offset. We have now enough test measurements which simulate the mal-function and we have incorporated a calibration curve into the adjustments of the line length data. Further testing and refinements of the calibration curve are necessary before the above results should be referenced.

We expect to remeasure these networks infrequently over the next few years in order to refine our estimates of secular strain. With two accurate measures of the strain rate provided by these networks, we can test the hypothesis of whether the Gorda Plate is locked beneath the North American Plate.

5. Publications

Langbein, J.O., D.P. Hill, T.N. Parker, and S.K. Wilkinson, An episode of re-inflation of the Long Valley caldera, eastern California; 1989-1991, *J. Geophys. Res.*, submitted

FIGURE 1. A plot of changes in line length for the baselines that use CASA as a common station. The line-length changes have been normalized to the nominal baselines length therefore transforming the displacements from units of mm to parts per million (ppm). The error bars represent plus or minus one standard deviation.

FIGURE 2. The location of the baselines that are measured using a two-color geodimeter are shown along with the location of the boundaries of the Long Valley caldera (solid line) and the resurgent dome (dashed line).

FIGURE 3a. Plot of the two-color geodimeter data for measurements of line-length changes since mid 1984 for those baselines that cross the San Andreas fault near Parkfield. The error bars represent one standard deviation of each observation. The data as plotted has had a linear trend removed and the computed secular rate is next to the plot of the residuals. Data are particularly noisy between April 1989 and May 1990 because of an intermittent, systematic error within the two-color geodimeter. See previous technical reports for a discussion of this problem.

FIGURE 3b. Same as Figure 3a except that these baselines do not cross the San Andreas fault.

FIGURE 4. Map showing the location of the two geodetic networks used to measure strain accumulation in northern California. The Gorda network consists of 13 baselines while the Scott network consists of 10 baselines.

LONG VALLEY NETWORK

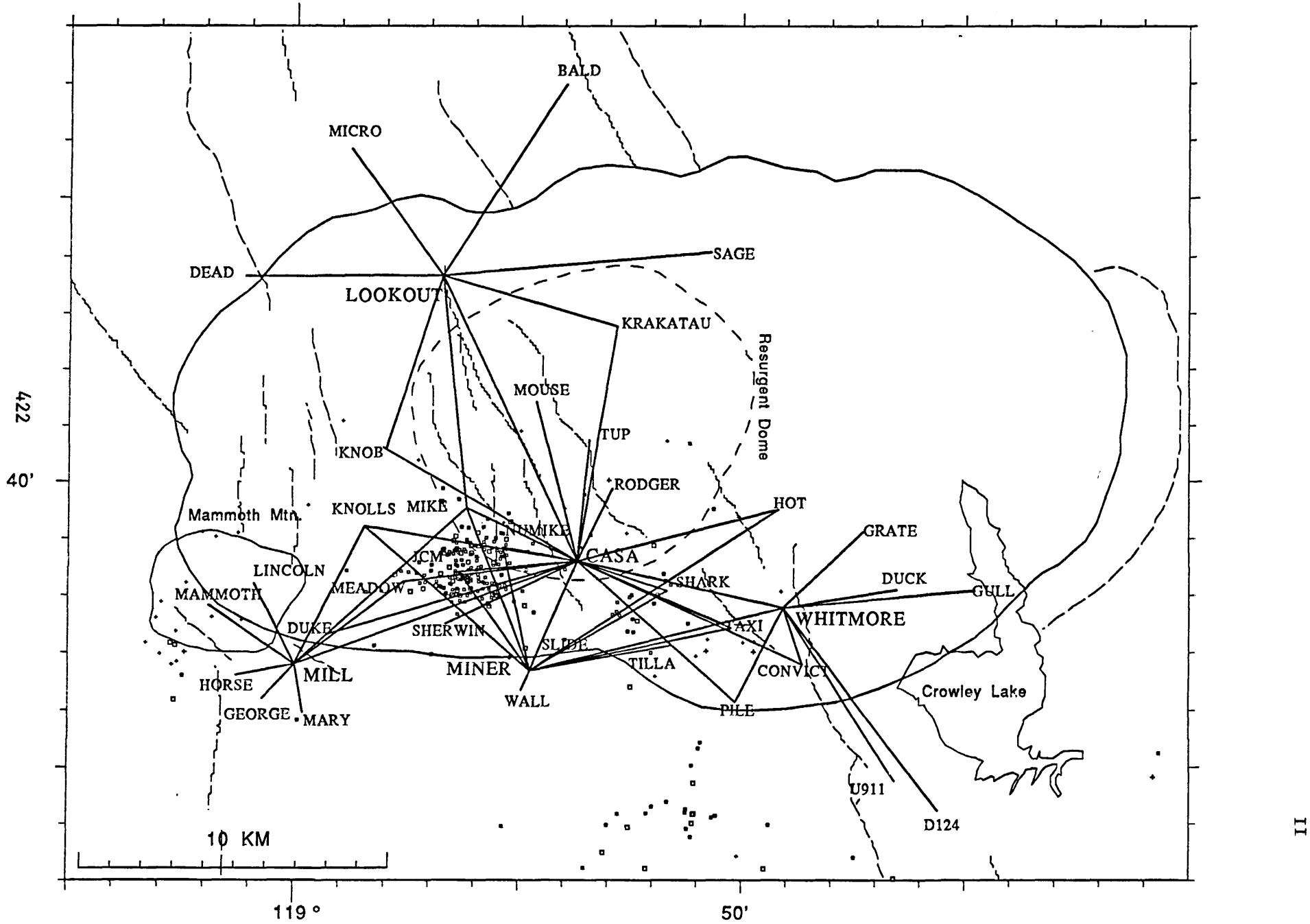

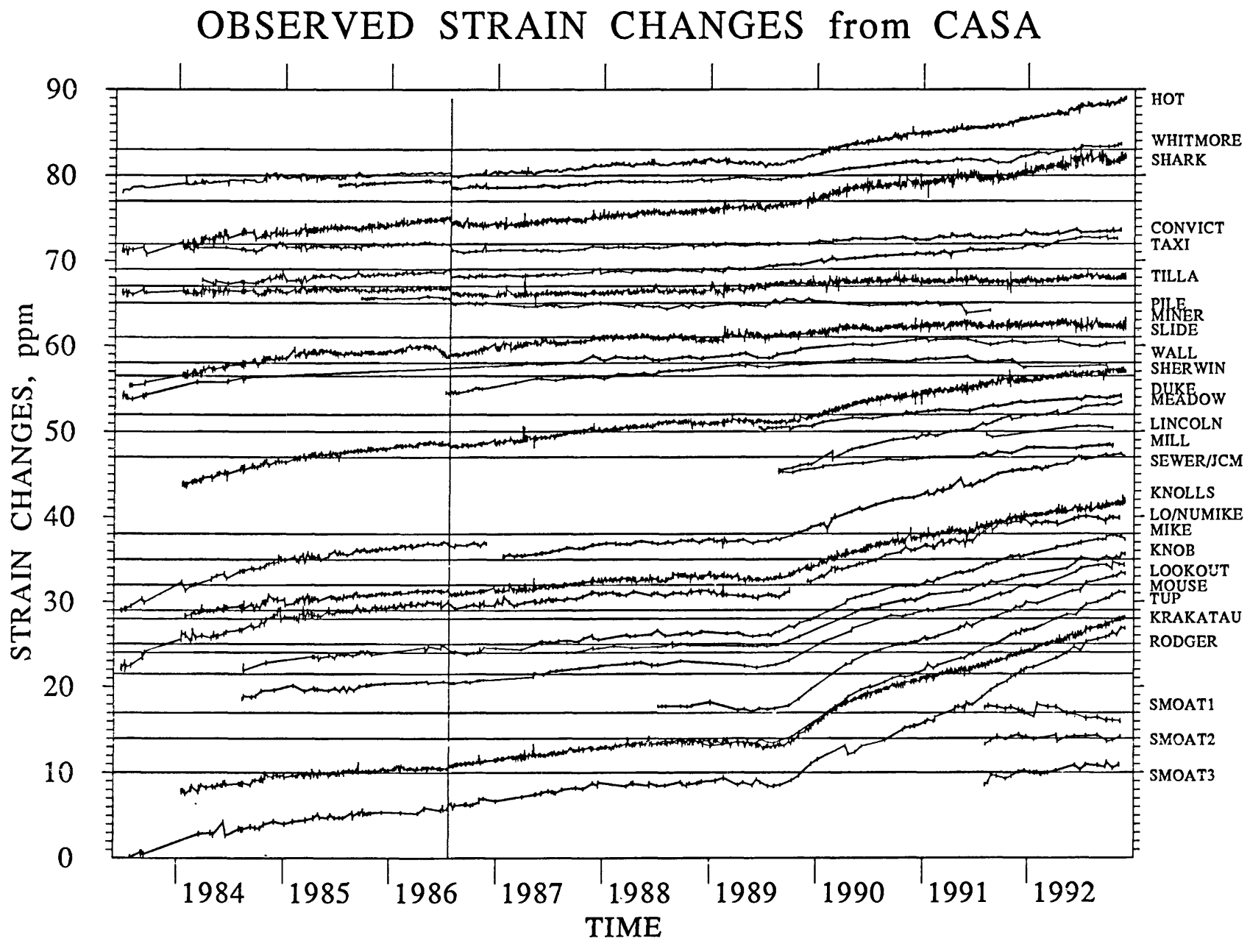
OBSERVED STRAIN CHANGES from CASA
STRAIN CHANGES, ppm
90
80
70
60
50
40
30
20
10
0
1984
1985
1986
1987
1988
1989
1990
1991
1992
TIME
HOT
WHITMORE
SHARK
CONVICT
TAXI
TILLA
PILE
MINER
SLIDE
WALL
SHERWIN
DUKE
MEADOW
LINCOLN
MILL
SEWER/JCM
KNOLLS
LO/NUMIKE
MIKE
KNOB
LOOKOUT
MOUSE
TUP
KRAKATAU
RODGER
SMOAT1
SMOAT2
SMOAT3

Parkfield; Fault crossing lines

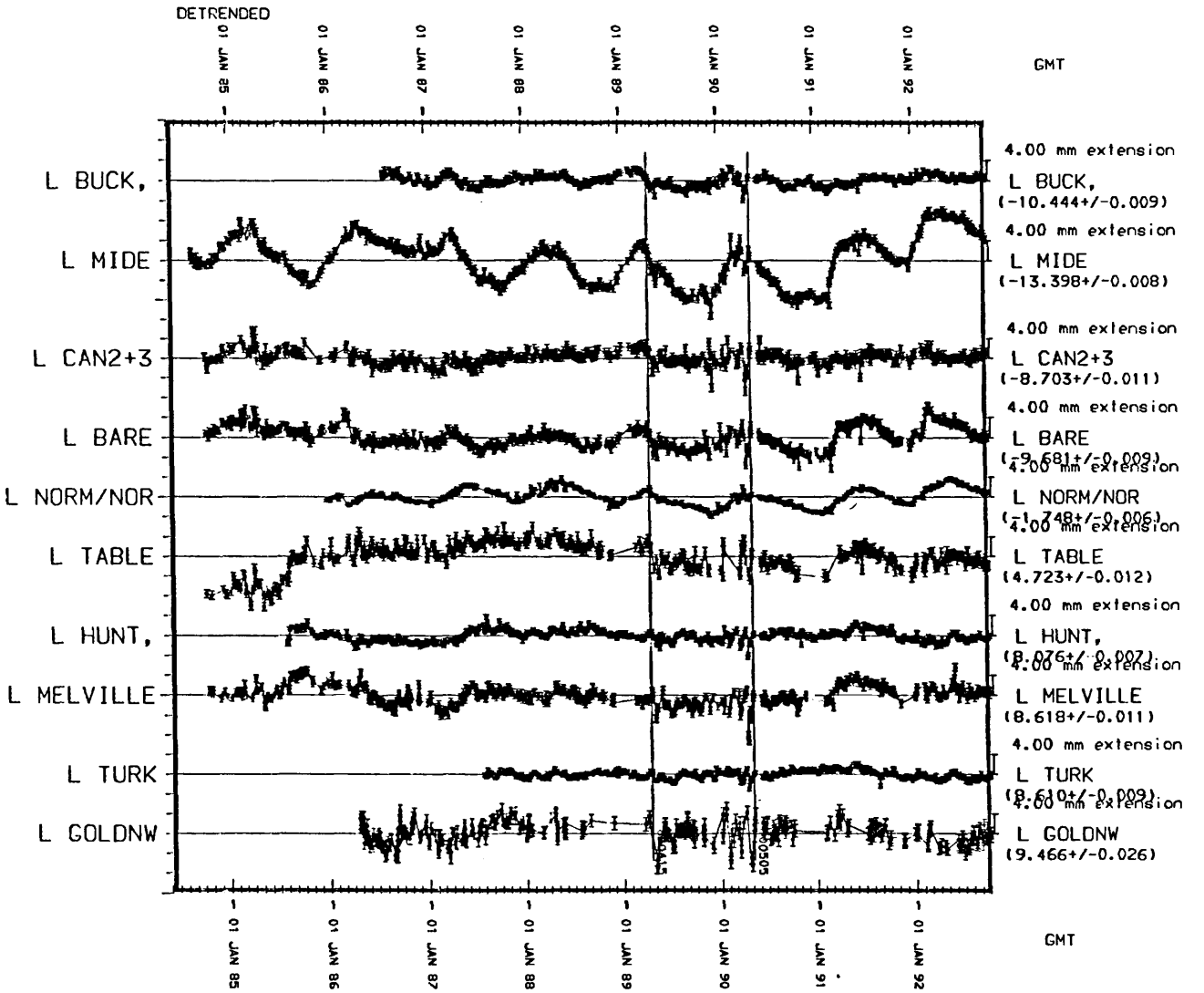

Parkfield; Fault crossing lines

Parkfield; non-fault crossing lines

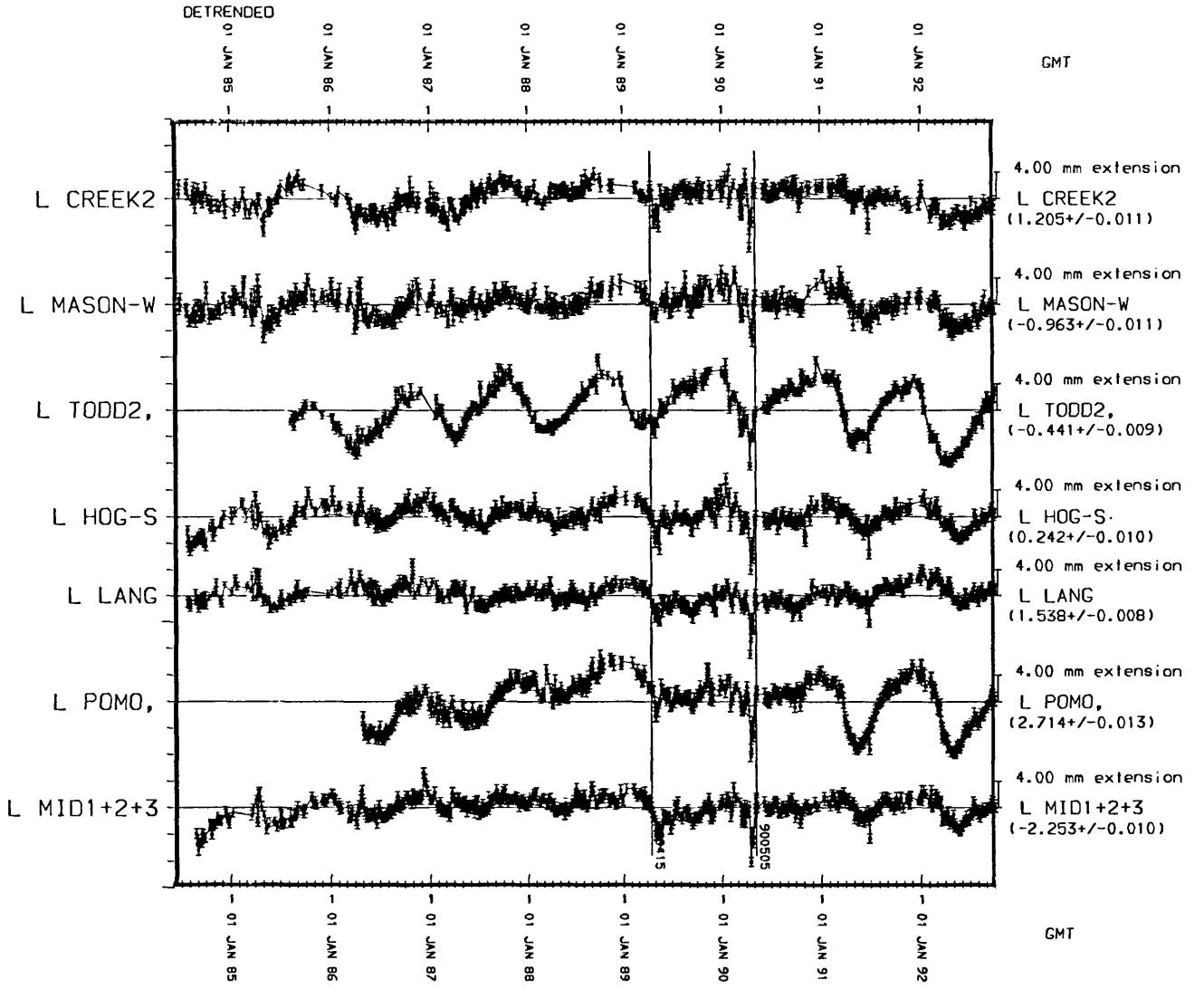

Parkfield; non-fault crossing lines

NORTHERN CALIFORNIA 2-COLOR NETWORKS

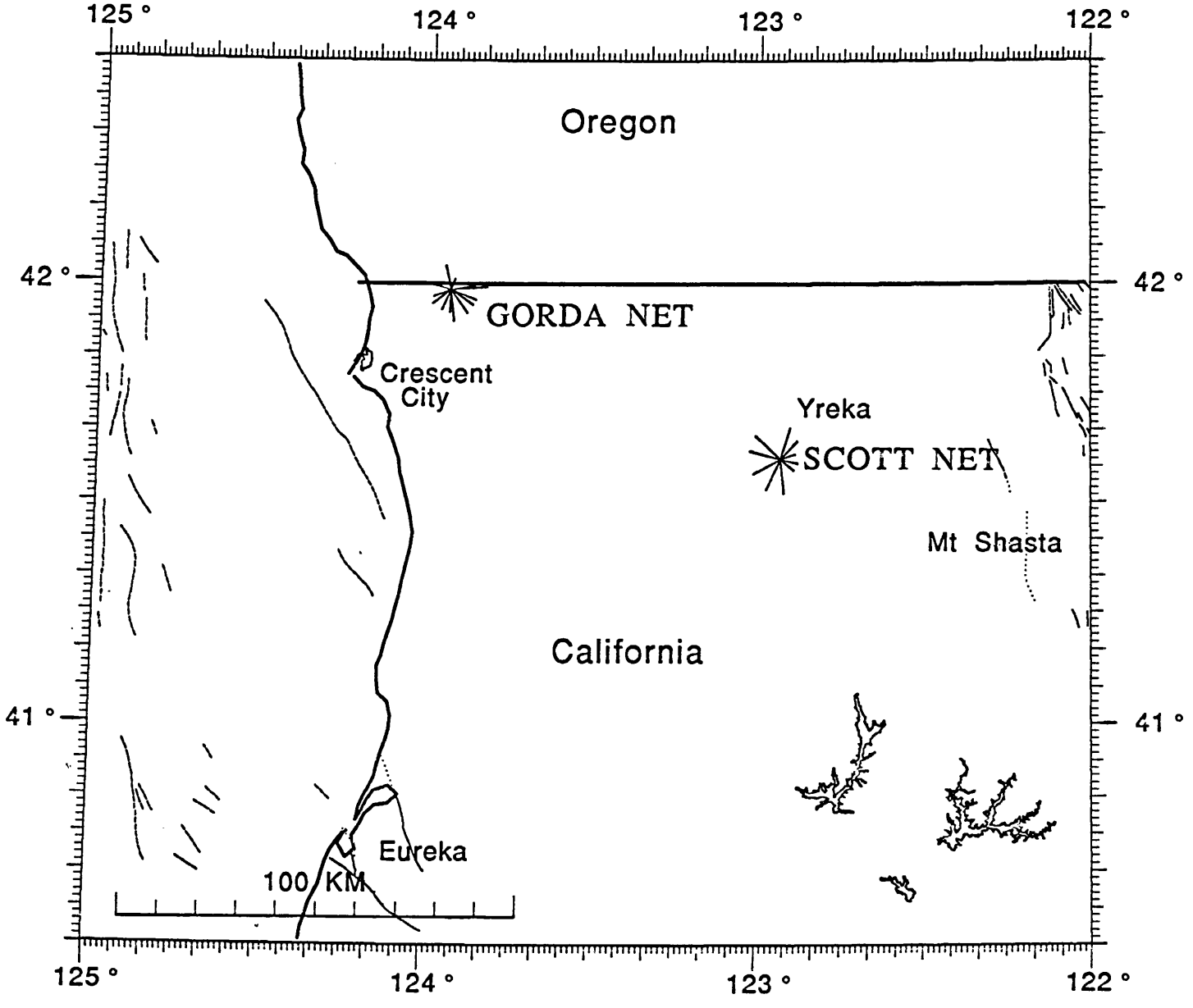

Parkfield Prediction Experiment

9960-04561

John Langbein

Branch of Tectonophysics
U.S. Geological Survey
345 Middlefield Road MS/977
Menlo Park, California 94025
(415) 329-4853

Investigations

This project coordinates the different experiments at Parkfield run by both USGS and non-USGS investigators. Some of the experiments are focused on the prediction in the short-term of the next Parkfield earthquake. Other experiments will document pre-seismic, the co-seismic, and post-seismic events. Both data from seismicity and from deformation are examined for significant events. This project has been examining the formal rules used in either calling an "alert" or "status-level".

Results

1. Significant Signals

The table summarizes the events in the past 1.75 years that meet established criteria to be called either an "alert" or "x-level status". For purposes of semantics, low-level signals which meet the "C" and "D" levels are called "status-levels", and the larger signals which meet the "A" and "B" levels remain as "alerts".

2. Parkfield in review workshop

From June 28 to 30, 1992 the Parkfield Working Group met at UC Santa Cruz to consider the future of the Parkfield Earthquake Prediction Experiment in light of the fact that the Parkfield mainshock has not yet occurred and that the 95% confidence window approved by the National Earthquake Prediction Evaluation Council would close at the end of the year. Despite this circumstance the working group reaffirmed its commitment to the Parkfield experiment as a critical part of the nations earthquake prediction program and reaffirmed their willingness to continue devoting time to it. The primary evidence of success of the Parkfield experiment was seen in the transfer of lessons learned at Parkfield over the broad range of monitoring techniques, scientific advances, and the alert scheme to other areas. As such the experiment has fulfilled part of its role as a prototype monitoring and short-term prediction experiment. However, much remains to be learned and, despite the debate over which is the correct model, all of the proposed statistical models conclude that Parkfield is the most likely place for a M6 earthquake in a region small enough to monitor in this way. And even if another area had similar mainshock probability, no other area has as much baseline data collected. The dense monitoring of varied networks was considered a critical aspect of

understanding anomalies on the various instruments and the group felt that Parkfield should be considered to be a National Earthquake Prediction Observatory and that future instruments should be tested there in order to allow comparison with the existing data. The major changes envisioned were expansion of the geodetic and strain networks in the northern part of the area in order to better image aseismic slip at depth near the expected hypocenter, expansion of real-time data transmission to Menlo Park to more of the monitoring networks in order to ease comparison between the various data sets, an online data repository to allow better access to the data by both the working group and the larger research community, and an expansion of shared technical support at Parkfield in order to save money.

3. Sensitivity of crustal deformation instruments to changes in secular rate

A paper was written examining the sensitivity of three of the Parkfield networks for determining the amount of changes in rate that would be significant.

Abstract. A variety of instruments (including borehole strainmeters, water wells, creepmeters, laser ranging and differential magnetometers) are used to monitor crustal deformation in areas that are prone to geologic hazards such as earthquakes and volcanic eruptions. In monitoring the deformation, one typically examines the data for either a change in rate, or a simple offset in the record. However, one needs to place a statistical confidence level that the detected signal differs from the background "noise". Calculation of the statistical confidence level may be done using the formalism of the *matched filter*. The output from a matched filter is the signal-to-noise ratio, ρ. Two ingredients are needed to form a matched filter: 1) The power density spectrum of the instrument and 2) the functional form of the signal that we desire to detect. Using the available crustal deformation data from the Parkfield, California earthquake prediction experiment, the background noise for individual instruments as a function of frequency, f, is estimated using the traditional method of the power density spectra. Except for two-color laser distance-ranging data, the power spectra for most of the instruments have a frequency dependence of f^{-n} where $2 \le n \le 3$. The power spectrum from laser ranging has a slight frequency dependence with $0 \le n \le 1$. The confidence level with which a hypothesized signal can be within the measurements is determined directly from the signal-to-noise ratio, with the numerator being a function of the signal and the denominator being a function of the power spectrum. Using a creepmeter as an example, a 0.04-mm change occurring over 1 hour, a 0.06-mm occurring over 10 hours, or 0.20-mm over 100 hours are all signals for which $\rho=2$ and therefore have only a 5% confidence that these signals could be background noise. The use of a single technique to determine the confidence for anomalous signals from all types of strain instruments might be suited to the Parkfield experiment where we can explicitly express a statistical confidence that a detected signal exceeds its background noise.

4. Publications

Langbein, J., E. Quilty, and K. Breckenridge, Sensitivity of crustal deformation instruments to changes in secular rate, *GRL*, in press, 1993.

Parkfield Working Group, The October 1992, Parkfield, California Earthquake prediction, *Science*, submitted, 1993.

Michael, A.J., and J. Langbein, Learning while waiting; Summary of the 1992 Santa Cruz Review Meeting, *EOS*, submitted, 1993.

Table. 1991 Parkfield alerts.

Date	Location	Description	Size	Level	Comments
910109	Parkfield	Earthquake	M 3.1	D	
910121	Cholame Valley	Earthquake	M 2.9	D	
910201	Middle Ridge	Creep	1.3 mm	D	
910204	Cholame Valley	Earthquake	M 2.8	D	Combine to C
910205	Middle Mtn	Earthquake	M 2.1	D	
910210	Middle Mtn	Earthquake	M 2.0	D	
910307	SW Trace (Hearst)	Creep	-5.4 mm	D	rain related
910311	Middle Mtn	Earthquake	M 1.8	D	
910319	XPK1 and XVA1	Creep	5 mm in 16 hours	B	raining
910319	XMM1	Creep	Surge 3.3mm in 7 days	D	Rain in past week
910322	Middle Mtn	Earthquake	M 2.2	D	
910327	X461	Creep	1.9mm in 7 days	D	rain in past week
910330	X461	Creep	2.9mm	D	Surge over past 10 days
910331	XMM1	Creep	0.8 mm in 30 minutes	D	
910331	Middle Mountain	Water well	9 cm	D	familiar combination, no C
910409	Middle Mountain	Earthquake	M 2.7	D	
910410	Middle Mountain	Earthquake	M 2.1	C	2 earthquakes M>1.5 in 72 Hrs
910412	Middle Mountain	Earthquake	M1.8 and M2	C	
910426	Middle Mountain	Earthquake	M 1.6	D	
910506	Middle Mountain	Earthquake	M 1.9	D	
910508	Middle Mountain	Earthquake	M 1.9	D	
910521	XMM1	Creep	0.7 mm in 30 min.	D	
910521	Middle Mountain	Water Well	4 cm	D	familiar combination
910711	Middle Mountain	Earthquake	M 2.0	D	
910722	Middle Mountain	Earthquake	M 1.6	D	
910726	Middle Mountain	Water Well	-12 cm	D	
910806	Slack Canyon	Earthquake	M 2.7	D	
910903	Middle Mountain	Earthquake	M 2.2	D	
910925	Middle Mountain	Earthquake	M 2.2	D	
911018	Parkfield	Earthquake	M 2.6	D	South end of M. Mtn.
911020	XMD1 & XMM1	Creep	2 events of 0.6mm in 1 hr	C	
911020	Middle Mountain	Water well	6 cm drop	D	
911108	Slack Canyon	Earthquakes	M 2.8?	D	
911201	Middle Mountain	Earthquakes	2 M>1	D	2 M1.0 in 72hrs
911218	Middle Mountain	Earthquake	M 2.3	D	

Note. Right lateral creep, water level rises, and compressive strain are positive.

1991 Combined Alert Totals: 1 B alert, 3 C alert, 29 D alerts.

Total alerts since beginning experiment: 1 B alert, 30 C alerts, 85 D alerts.

Table. 1992 Parkfield alerts.

Date	Location	Description	Size	Level	Comments
920127	Middle Ridge	Creep Event	0.9 mm	D	
	Middle Mountain	Water well		D	familiar combo
920224	Gold Hill	Earthquake	M 2.5	D	
920404	Middle Mountain	Earthquake	2 M >1.1	D	originally missed
920420	Middle Ridge	Creep Event	1 mm RL	D	Strain changes at Frolich
920420	Middle Mountain	Water well	13.7 cm drop	D	familiar combo
920529	Gold Hill	Earthquake	M 3.2	D	Strain change at GH dilatometer and water well
920603	Middle Mountain	Earthquake	M 1.5	D	
920916	Gold Hill	Earthquake	M 2.5	D	

Note. Right lateral creep, water level rises, and compressive strain are positive.

1992 Combined Alert Totals: 1 C alert, 9 D alerts.

Total alerts since beginning experiment: 1 B alert, 33 C alerts, 94 D alerts.

Microearthquake Data Analysis

3-9930-10053

W.H.K. Lee
U.S. Geological Survey
Branch of Seismology
345 Middlefield Road, MS 977
Menlo Park, California 94025
(415) 329-4781

Investigations

The primary focus of this project is the development of state-of-the-art computation for analysis of data from microearthquake networks. For the past twelve months I have been involved in:

(1) Implementing Seismic Instrumentation for Topical Volcano Studies

In collaboration with Gray Jensen and Sam Rodriquez, I am designing and implementing seismic instrumentation for topical volcanic studies. Two portable arrays (one telemetered and one hardwired) are being implemented to meet the scientific objectives of volcano research. These two portable arrays are based on PC-technology, and are designed to have a dynamic range of about 90 db. The hardwired array has 64 channels, and the digital telemetered array has up to 48 channels.

A shallow refraction experiment was carried out using the hardwired array in August, 1992 at the Zayante Vineyard (located in the epicentral area of the 1989 Loma Prieta earthquake) in collaboration with UC Santa Cruz. Excellent data were recorded using a sledge hammer as a source of compressional waves and an air-powered shear-wave generator as a source of shear waves. A data report of this experiment was released as Zayante Seismic Experiment Team (1992), and a paper will be presented at the Fall AGU National Meeting (Bonamassa, et al. 1992).

The hardwired array was also deployed in the Landers earthquake fault zone in October, 1992 in collaboration with the Southern California Earthquake Center. Up to 31 three-component geophones were recorded by two PC-based systems across and along the rupture zone of the 1992 Landers earthquake using about 12 km of cables. Several hundreds earthquakes were recorded. A detailed shallow refraction experiment using a sledge hammer and an air-powered chear-wave generator was also conducted. Excellent records of trapped waves in the fault zone were obtained. Because of the large amount of data

(about 2 gigabytes), it will take some time for us to process and analyze the data.

Descriptions of these two portable seismic arrays are being released in a series of Open-File Report; so far three have been released (Lee, 1992 a, b, c). The telemetered portable array is scheduled for field tests in the spring of 1993.

(2) Lecture Notes on PC-based Seismic Networks

A course on PC-based seismic networks was given to about 20 students in Menlo Park, CA from September 9 through 20, 1991. The purpose of this course was to show students how to operate a PC-based seismic network, carry out routine data processing, and perform basic data analysis. Twenty-one lectures were given and the lectue notes were edited by W.H.K. Lee and D.A. Dodge. These lecture notes were released as USGS Open-File Report 92-441, and contain the following separate lectures:

1. Regional seismic networks in California by J. P. Eaton.
2. PC-based seismic systems by W.H.K. Lee.
3. Seismometers theory and practice by J.P. Eaton.
4. Basic techniques for telemetry by J.C. VanSchaack.
5. Realtime seismic data acquisition by W.H.K. Lee.
6. The XDETECT program by W.H.K. Lee.
7. The TDETECT program by J.R. Evans.
8. Routine seismic network data processing by W.H.K. Lee.
9. Plotting seismograms and maps by R. Banfill.
10. Mathematics for earthquake location by W.H.K. Lee.
11. Local earthquake location programs by J.C. Lahr.
12. Computing travel time and derivatives by W.H.K. Lee.
13. Development of earthquake magnitude scales by J. P. Eaton.
14. Coda waves for magnitude and Q by W.H.K. Lee.
15. PCEQ and QCODA by C.M. Valdes.
16. Mathematics for waveform analysis by A. Lomax.
17. The SEISGRAM program by A. Lomax.
18. Focal mechanism: theory and history by P.A. Reasenberg.
19. The FPFIT program by D.H. Oppenheimer.
20. Mathematics for seismic tomography by W.H.K. Lee.
21. Applications of seismic tomography by H.M. Iyer.

Reports

Lee, W.H.K., and D.A. Dodge, (editors), 1992. "A course on: PC-based seismic networks", USGS Open-File Report 92-441, 535 pp.

Lee, W.H.K., (compiler), 1992a. Descriptions of seismic array components: Part 1. DIGGER, DIGIREC, and MULTIPLEXER, USGS Open-File Report 92-430 A and B, 276 pp. and 1 diskette.

Zayante, Seismic Experiment Team, 1992. Zayante seismic experiment: data report, USGS Open-File Report 92-561, A and B, 268 pp. and 4 diskettes.

Lee, W.H.K., (compiler), 1992b. Descriptions of seismic array components: part 2. software modules for data acquisition/processing, USGS Open-File Report 92-597, A and B, 313 pp, and 1 diskette.

Lee, W.H.K. (compiler), 1992c. Descriptions of seismic array components: Part 3. Software modules for data conversion, USGS Open-File Report 92-598, A and B, 106 pp. and 1 diskette.

Lee, W.H.K., 1992. PC-based seismic networks for monitoring earthquakes and volcanoes, (abstract), EOS, v. 73, p. 68-69.

Bonamassa, O., J.E. Vidale, W.H.K. Lee, and H.P. Liu, 1992, The relation between ground motions and near-surface geology, (abstract), EOS, v. 73, p. 338.

Northern and Central California Seismic Network Processing

9930-70013

Fredrick W. Lester
Branch of Seismology
U.S. Geological Survey
345 Middlefield, MS 977
Menlo Park, CA 94025
(415) 329-4747

Investigations

1. In 1966 a seismographic network (CALNET) was established by the USGS to monitor earthquakes in central California. In the following years the network was expanded to monitor earthquakes in most of northern and central California, particularly along the San Andreas Fault, from the Oregon border to Santa Maria. In its present configuration there are over 300 stations in the network, and more than 60 of those consist of more than one component. Also recorded are signals from more than 60 stations operated by other agencies or institutions, including the University of California, Berkeley, the University of Nevada, Reno, the California Institute of Technology, the California Department of Water Resources, and the Lawrence Livermore National Laboratory. The primary responsibility of this project is to monitor, process, analyze, and publish seismic data recorded from this network.

2. This project maintains a seismic data base of CALNET data for the years 1969 to the present on both computers and magnetic tapes for those office staff who are doing research using the network data.

3. Project staff often act as the primary spokesperson or authority when inquires are received from the press, the public, or scientists from both inside and outside the Geological Survey regarding earthquakes that have been recorded by the network. Inquires include simple questions about recent earthquakes in the region, such as the date and time of occurrence, the location, and the magnitude of the earthquake. Or they may be somewhat complex and require expert opinion or interpretation, such as the relationship of recent swarms of earthquakes to historical seismicity, and how each relates to the seismogenic potential of a region or fault.

4. As time permits research projects are undertaken by project personnel on some of the more interesting or unusual events or sequences of earthquakes that have occurred within the network, or related topics.

Results

1. Figure 1 illustrates most of the 20198 earthquakes located in northern and central California and vicinity during the time period October 1991 through September 1992.

   There were several significant earthquakes and their aftershocks that affected the network during this this time period. On April 25, 1992 a M7.1 earthquake occurred in the Cape Mendocino region of northern California. It was followed by two large aftershocks on April 26 that were magnitude 6.6 and 6.7. In the month following these large earthquakes more than 3300 aftershocks occurred and were located by this office, mostly by project staff. These were mostly within 50 to 60 kilometers of the larger events, forming an football-shaped aftershock zone centered on Cape Mendocino (Fig. 1).

On June 28 a magnitude 7.5 earthquake struck the region near Landers, in southern California. It was followed by a few hours later by a M6.6 quake in the region near Big Bear Lake, just north of the Landers epicenter. These two earthquakes were followed by thousands of smaller aftershocks, which are still occurring. While those earthquakes are beyond the region monitored by this office, they are still recorded by our automatic detection systems and must be processed, in at least a minimal way. Our detection system is triggered by most earthquakes in that sequence that are larger than magnitude 3.0. Since there have been several hundred of those the impact on our data processing has been significant.

On April 23, 1992 a magnitude 6.3 earthquake struck the Joshua Tree region of southern California. As with the Landers-Big Bear earthquakes those are outside of our monitoring region, but the magnitude 3.0 or larger events still trigger our network stations and therefore are recorded and must be processed. A few hundred of those recorded throughout the CALNET, and therefore impacted data processing in the project.

Work is currently underway on the publication of a catalog of earthquakes for northern and central California for 1991. The format is patterned after the format of the USGS-Caltech catalogs of southern California earthquakes that have been published in the last few years. Work on this publication is a joint effort between several projects and more than a dozen people. The catalog should be published by early 1993. It is our intention, after that time, to publish a yearly catalog on a regular basis within a few months of the end of each year. Data prior to 1991 will be published in yearly catalogs, as soon as time permits, in 1993. These catalogs will supersede previous catalogs for the years 1967 - 1978.

2. The 1992 catalog is relatively complete and correct through September 1992. We are currently adding events from the Cape Mednocino swarm in April and May that were missed in the routine detection and processing. These are earthquakes that are mostly smaller than magnitude 3.0. Quarry blasts still need to be identified for April through September.

3. More than 55 requests were received for seismic data which required computer searches of the data base. Most of the searches were for specific regions and time periods. Some were more complex requiring multiple searches and some interpretation. Data from these searches were most often distributed as printed listings, but but some were also sent as data files over electronic mail or files on magnetic tape.

   Telephone inquires were handled at a rate of 3 to 5 per day. Most of these required verbal responses that were of short duration, 10 minutes or less. The majority of these were simple requests for information about recent earthquakes, ongoing or past USGS research, maps and publications, and some interpretation of geologic information. During periods of higher than normal seismic activity the project may receive as many as 20 to 30 requests of this type per hour.

   Recognition of earthquake risk and related hazards has increased dramatically since the Loma Prieta earthquake of October 1989. A consequence of this has been an increase in insurance claims related to earthquakes that has resulted in an increase in insurance company requests for data searches for recent earthquake activity. Another consequence of that earthquake is the increasingly common request from homeowners or potential homeowners for information about all types of geologic hazards, particularly earthquake hazards, in the area around their homes or where they plan to purchase a home.

4. Due to the large number of earthquakes that occurred during this time period no staff members had time to pursue any research.

Reports

None

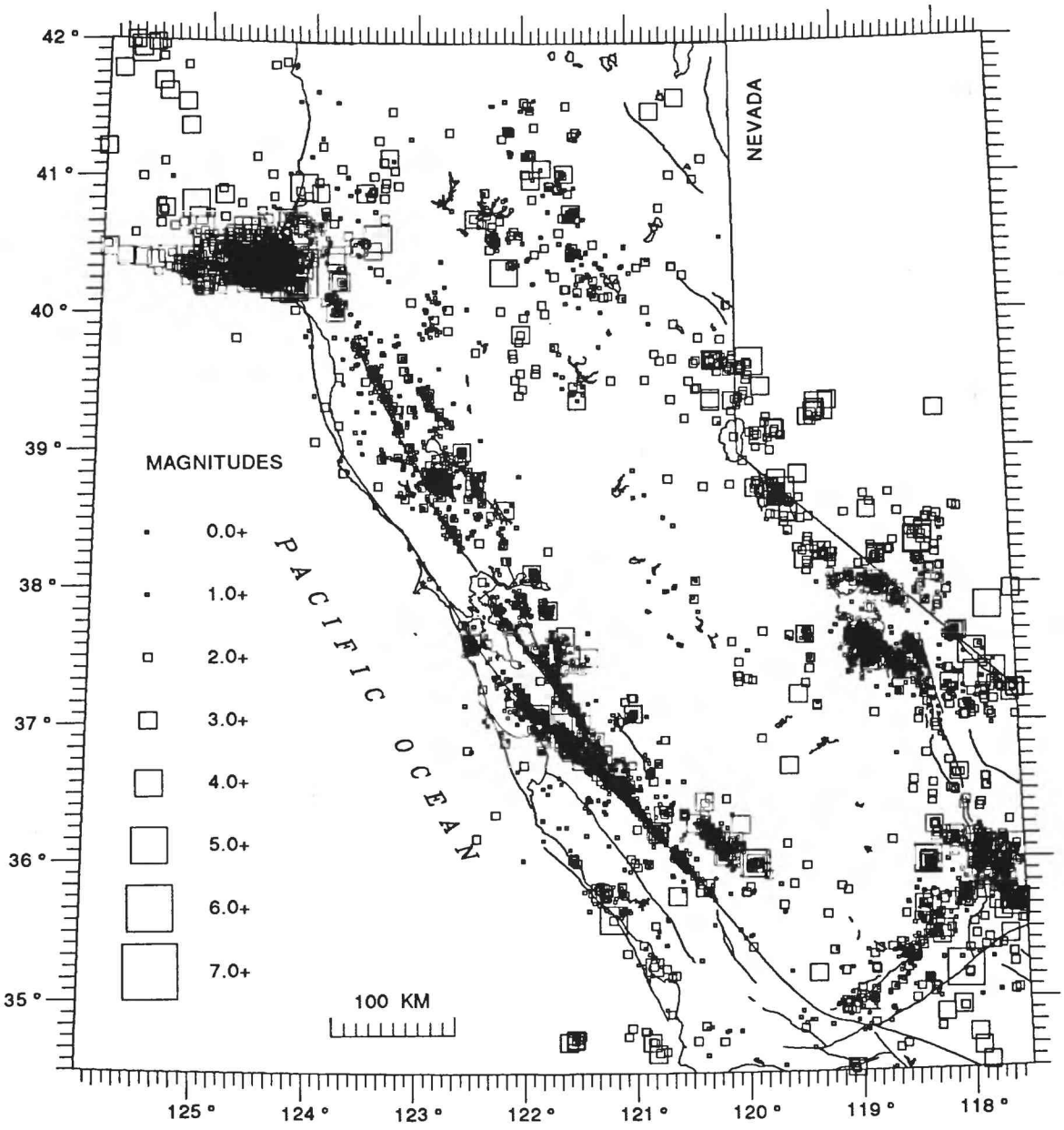

FIGURE 1. Seismicity for October 1991 - September 1992

Characterization of Range Front Deformation, Northeastern Margin of Santa Cruz Mountains, Southern San Francisco Bay Region, California

Award Number: 1434-92-G-2220

William R. Lettis, Gary D. Simpson, and Keith I. Kelson
William Lettis & Associates, Inc.
1000 Broadway, Suite 612
Oakland, CA 94607
(510) 832-3716

Investigations

Apparent coseismic ground deformation during the 1989 Loma Prieta earthquake is coincident with and/or subparallel to the system of faults along the northeastern margin of the Santa Cruz Mountains, indicating possible coseismic movement along the Sargent-Berrocal, Shannon, and Monte Vista faults. These faults displace the Pliocene and Pleistocene Santa Clara Formation, and locally deform overlying Quaternary surficial deposits and associated geomorphic surfaces adjacent to and in the communities of Los Gatos, Saratoga, Cupertino, and Los Altos Hills. Because the amount and timing of this deformation is poorly known, these faults pose a significant, heretofore undocumented, earthquake hazard to the southern San Francisco Bay region. We believe that a critical issue for evaluating the earthquake hazards along the range front is whether the Sargent-Berrocal, Shannon, and Monte Vista faults are a result of secondary coseismic deformation related to the San Andreas fault, or whether they are independent seismic sources. We anticipate that the results of this study will contribute to a better understanding of the structural and kinematic association of the range-front deformation with the San Andreas fault, and thus help estimate potential seismic hazards in the southern Bay region.

We are using two distinct, yet complementary, approaches to investigate the nature of deformation and seismogenic potential of faults along the range front between the towns of Los Gatos and Los Altos Hills. Our approach to assessing the style and pattern of deformation associated with the Sargent-Berrocal, Shannon, and Monte Vista faults is to conduct a quantitative geomorphic analysis of the range front and adjacent areas, and to delineate late Quaternary deposits and geomorphic surfaces. Age-estimates of these surfaces and deposits will yield data on the long-term rates of range-front deformation. Our approach to assessing the timing of deformation and fault-specific physical and behavioral characteristics is to conduct detailed paleoseismologic investigations at selected sites along one or more of these faults. The goal of this task is to obtain quantitative data that can be used to assess potential rupture lengths, fault segmentation, displacement per event, slip rate, sense of slip, and recurrence intervals for faults along the range front. We anticipate that this information will be used to evaulate whether the range-front structures are independent seismic sources or are solely related to deformation along the San Andreas fault.

Results

We are using three quantitative geologic and geomorphic analyses to define the style and patterns of Quaternary deformation along the range front. First, we are mapping late Quaternary fluvial

terraces along Los Gatos, Saratoga, and Stevens creeks, at a scale of 1:20,000, based on field reconnaissance and analysis of black-and-white aerial photographs taken in 1939. At this time, we identify a well-developed sequence of four major fluvial terraces along Los Gatos Creek, of which the oldest two are displaced by thrust faults at the base of the range. Second, we are utilizing the 1939 air photos and recent mapping by Wesling and Helley[1] to delineate alluvial fan surfaces along the range front. This mapping shows that an older fan surface at the range front is separated from younger fans to the northeast by a linear topographic scarp that is coincident with the mapped trace of the Shannon fault (Wesling and Helley, *ibid.*). This scarp extends across business and residential areas of Los Gatos, Saratoga, and Cupertino. Third, we are initiating construction of envelope, sub-envelope, and residual maps of the northeastern Santa Cruz Mountains that will help assess the locations and spatial variations of tectonic uplift. We are obtaining digital elevation models (DEMs) and appropriate software to construct these maps.

Based on preliminary field reconnaissance and analysis of existing reports, we have selected a preliminary site for paleoseismologic investigation of the Monte Vista fault in Cupertino. Through our ongoing analysis of aerial photography and field mapping, we are currently assessing whether this site is the most promising location for obtaining paleoseismologic information.

[1]Wesling, J.R., and Helley, E.J., 1989, Quaternary geologic map of the San Jose West quadrangle, California: U.S. Geological Survey Open-file Report 89-672, scale 1:24,000

Operation of Borehole Tiltmeters at Pinon Flat Observatory, California and Analysis of Secular and Tidal Tilt

14-08-0001-G1765

Judah Levine
Joint Institute for Laboratory Astrophysics
Campus Box 440
University of Colorado
Boulder, Colorado 80309
(303) 492 - 7785

Objectives: To install borehole tiltmeters at Pinon Flat Observatory in Southern California; to compare the performance our instruments installed at three different depths; to analyze the data at secular and tidal periods; and to compare our results with those obtained from other instruments at the same site.

Results: We currently have three instruments installed at Pinon Flat Observatory and all three have been operating during this report period. Our previous reports discussed our finite-element studies of the effects on the measured tilt resulting from a borehole that is not perfectly vertical and from the variation in the topography of the weathering layer boundary. Our calculations predicted that both of these effects would result in appreciable strain-tilt coupling. During this reporting period, we tested the predictions of these models by performing several different experiments in boreholes BOA (24 m deep) and BOB (36 m deep).

In the first series of experiments, we modified the instrument installed in BOB so that it could be operated at different depths within the borehole. In particular, we operated the instrument both below the weathering layer boundary and just above it. Our calculations predicted that this change in depth would change the sign of the difference between the signals recorded at BOA and BOB, and the observation was almost exactly what we had predicted.

In the second series of experiments, we studied the effect of different installation methods on the tilt signal. Our previous design used the side of the borehole as the reference for the tiltmeter; we changed the mounting brackets so that the reference for the instrument became the center of the bottom of the borehole and three points spaced symmetrically around the side of the casing near the top of the instrument compartment. (This is essentially the method used in the Askania instrument, and we implemented the change using retractable pins that are quite similar to the Askania design.) This latter coupling method is theoretically more sensitive to tilt-strain coupling than our initial design, but the theoretical advantage of our design can not be realized in practice if the borehole is tipped (as it almost always is). The results of this set of experiments also agreed very well with our models, and we are now

in the process of confirming this agreement with additional measurements along different azimuths in the same borehole.

Using the results of these measurements it is possible to install an instrument in borehole BOB so that the tilt-strain couplings due to the weathering layer and due to the mounting of the capsule very nearly cancel. We are testing this possibility with a third set of experiments that are currently underway. These experiments have been interrupted by a serious failure due to a recent lightning strike at PFO very close to our instruments. (Other instruments, including the Askania were also damaged by that strike.) We have just returned from a repair trip to PFO, and an additional repair trip will probably be necessary in the near future.

In addition to providing insight into methods of improving tilt measurements, our results suggest that it may be possible to construct a combined strainmeter-tiltmeter using two tiltmeters installed in the same borehole at different depths and along different azimuths. An installation of this kind could provide simultaneous measurements of both tilt and strain -- the sensitivity to local strain arises from the difference between the tilt-strain coupling coefficients of the two instruments and this difference allows us to both estimate the strain and remove it from the tilt records. Such a device would have certain technical advantages over borehole strainmeters: the instruments need not be installed permanently, for example, and the instrumental calibration is easier to perform and is likely to be more stable in time. We hope to make some preliminary tests of this idea early in 1993.

Summary of Data Collected: We acquire the data from our three instruments at PFO (2 channels/instrument) every 6 minutes. These same values are also transmitted to the PFO central recording trailer and are digitized and recorded there 12 times/hour.

Slip History of San Andreas and Hayward Faults

9910-04192

J. J. Lienkaemper
Branch of Engineering Seismology and Geology
U.S. Geological Survey
345 Middlefield Road, MS 977
Menlo Park, California 94025
(415) 329-5642

Investigations

Determine slip rates and earthquake recurrence times on San Andreas and Hayward Faults. Compare rates of geologically determined surface slip to rates of historic creep and geodetically determined deep slip. Analyze effects of structural complexity and fault segmentation upon inferring recurrence from slip rate. Participant in 1992 Landers Earthquake Investigation.

Results

1. Creep Rates, Hayward Fault. We report interesting results on creep rate for the initial 3 years (1989-1992) of precision monitoring of about 20 arrays established for observing afterslip expected in the next major earthquake on the Hayward Fault [*Lienkaemper, Galehouse, and Simpson,* 1992]. Creep rate along most of the fault since the 1989 Loma Prieta Earthquake (LPE) has averaged only half the long-term rate. At the southeast end where long-term rates have been about 9 mm/yr right-lateral, the post-LPE creep rate has been 2 mm/yr left-lateral. This reversal in the direction of creep rate is a predictable effect of modelled static stress changes and can be expected to continue for at least another 3 years at our southernmost array. North of central Fremont, creep is now returning to normal at some sites (where long-term rate is 5-6 mm/yr and creep is steady), but at many sites creep is still strongly retarded (where long-term rate is 3.5-5 mm/yr and behavior is episodic).

2. Holocene Slip Rates, Masonic Site. We submitted 8 more radiocarbon samples to refine the ages of the basal contacts of the early Holocene (unit G) and mid-Holocene (unit E) fan deposits. A serious problem at the NSF AMS facility delayed completion of this project. Age dating is still incomplete. Some new dates suggest that greater accuracy in unit-E slip rate is possible. Preliminary reports: *Lienkaemper and Borchardt* [1992a&b].

3. Map of Holocene traces of the Hayward Fault. USGS printed the new map of the Hayward fault [*Lienkaemper,* 1992] with financial support from the Second Conference on Earthquake Hazards in the Eastern San Francisco Bay Area. This map was introduced to the public for sale as a poster exhibit at the Conference. For the Conference I served on several committees and authored/co-authored/edited various volumes, papers, abstracts (omitted below, replaced by Proceedings) and field guide articles listed below.

Reports *(referenced using the abbreviated volume names below:)*

East Bay '92-Proceedings: Proceedings of the Second Conference on Earthquake Hazards, Eastern San Francisco Bay Area, March 25-29, 1992, California State University, Hayward; G. Borchardt, S.E. Hirschfeld, J.J. Lienkaemper, P. McClellan, P.L. Williams, and I.G. Wong, eds.: *California Division of Mines and Geology Special Publication 113.*

East Bay '92-Field Guide: Field Trip Guidebook of the Second Conference on Earthquake Hazards, Eastern San Francisco Bay Area, March 25-29, 1992, California State University, Hayward; Taylor, C.L., compiler, and Hall, N. T. and Melody, M., eds., 225 p.

East Bay '92-Program and Abstracts: Program and Abstracts of the Second Conference on Earthquake Hazards, Eastern San Francisco Bay Area, March 25-29, 1992, California State University, Hayward; Galehouse, J.S., ed., 91 p.

Borchardt, G., J. J. Lienkaemper, and K. Budding, in press, Holocene slip rate of the Hayward Fault at Fremont, California: *East Bay '92-Proceedings*.

Lienkaemper, J.J., 1992, Map of recently active traces of the Hayward Fault, Alameda and Contra Costa Counties, California: U.S. Geological Survey Miscellaneous Field Studies Map MF-2196, scale 1:24,000, 13 p. text.

Lienkaemper, J.J., 1992, Stop B-2, Contra Costa College and El Portal School: *East Bay '92-Field Guide*, p. 25-27.

Lienkaemper, J. J., 1992, Optional Stop A-4, Masonic Home slip rates: *East Bay '92-Field Guide*, p.173.

Lienkaemper, J. J., and G. Borchardt, in press, Holocene slip rate of the Hayward Fault at Union City: *East Bay '92-Proceedings*.

Lienkaemper, J. J., and G. Borchardt, in press, Hayward Fault: Large earthquakes versus surface creep: *East Bay '92-Proceedings*.

Lienkaemper, J.J. and J.C. Hamilton, 1992, Stop A-3, Holy Sepulchre fault scarp: *East Bay '92-Field Guide*, p. 151-156.

Taylor, C.L, and J.J. Lienkaemper, 1992, Contribution 6-2: Location of Hayward Fault traces in the Montclair Village area, Oakland, California; and Stop B-4, Montclair Park and Village: *East Bay '92-Field Guide*, p. 83-93.

CRUSTAL STRAIN

9960–70076

M. Lisowski, J.C. Savage, N.E. King, J.L. Svarc, M. Murray
Branch of Tectonophysics
U.S. Geological Survey
345 Middlefield Road, MS/977
Menlo Park, California 94025
(415) 329-4855

Investigations

The principal subject of investigation was the measurement and analysis of deformation in a number of tectonically active areas in the United States.

We list the networks surveyed during FY 92 along with some information about the surveys in Table 1. Many of the surveys were in response to magnitude 6 and 7 earthquakes in northern and southern California.

We used Geodolite (trilateration) and Global Positioning System (GPS) to survey the San Gabriel, Loma Monitor (three times), Fairweather, and Joshua (twice) networks. We surveyed the San Gabriel network several months after the Sierra Madre earthquake and the Joshua network two months before and one month after the Landers earthquake. The Lake San Andreas, Calaveras, and Black Mountain small aperture fault crossing trilateration networks were surveyed with the Geodolite. The Calaveras network was also surveyed with GPS.

We used GPS to survey the following networks: Juan de Fuca, Southern Oregon, Eureka, Southern California Monitor (twice), Parkfield Monitor (twice), Parkfield Regional, Parkfield Quad (three times), Farallon-Sierra, Long Valley-Mono Chain, Landers Profile, and five profiles in the San Francisco Bay Area. The Southern Oregon network and Landers Profile are new networks. Surveys of the Eureka network were in response to the Honeydew and Cape Mendocino earthquakes. As part of our response to the Landers earthquake we used GPS to measure part of the Mojave and all of the Landers trilateration networks. The Landers Profile was established to monitor post-seismic strain diffusion. We experimented with rapid static GPS surveys after the Cape Mendocino and Landers earthquakes. The Hayward fault crossing Richmond, East Bay, and Hayward short range trilateration networks were measured with GPS. We monitored deformation across the Hayward fault with two continuously recording GPS receivers. The sites also provide a reference for other measurements in the area.

The Juan de Fuca network survey was a cooperative effort with the Geologic Survey of Canada. We list only the part of the project in the U.S.A. in Table 1. The southern Oregon GPS survey was in cooperation with the University of Oregon. Not listed in the table is the rapid static survey of a 110-station network in Parkfield conducted by NASA's Jet Propulsion Laboratory in cooperation with the Crustal Strain Project.

Table 1. Field Surveys FY 1992

Project	Region/ Program	Survey Dates	Field Days	Tra-vel Days	Geod-olite Lines	GPS Station Days	Local Ties	GPS Sta-tions	Local Sta-tions	Rapid Static
Hayward Continuous	BAFEP	Continuous								
Juan de Fuca	PACNW	91/10/04-09	6	3		43	18	21	5	
Eureka-Honeydew Eq.	PACNW	91/10/11	2	1		6	1	6	1	
L. San Andreas	BAFEP	91/10/21&29	2		9					
Calaveras	BAFEP	91/10/22-23	2		17					
Black Mt.	BAFEP	91/10/24	1		14					
San Gabriel	SCAL	91/10/31-11/05	6	2	47	11	3	10	3	
S. Cal Monitor	SCAL	91/11/19-11/21	3	2		13	9	13	9	
S. Cal Monitor	SCAL	91/12/04-12/05	2	1		13	9	13	9	
Parkfield Monitor	CORE	91/12/06	1	1		5		5		
Calaveras	BAFEP	91/12/12	1			7		7		
Loma Monitor	CORE	91/12/17	1			7		7		
Richmond	BAFEP	91/12/18	1			4		4		
Hayward	BAFEP	91/12/20	1			5	1	6	1	
NBay Profile	BAFEP	92/02/11-02/13	3			18		14		
GG Profile	BAFEP	92/02/14	1			7		7		
CBay Profile	BAFEP	92/02/19-02/20	2			14		12		
Coso	VHAZ	92/02/25-02/27	3	2		12	1	7	1	
SBay Profile	BAFEP	92/03/04-03/06	4			22	1	19	1	
Farallon-Sierra	BAFEP	92/03/11-03/14	5	1		35	5	13	5	
Loma Profile+Monitor	BAFEP	92/03/17-03/19	3			20	1	16	1	
Loma Monitor	CORE	92/3/24	1		3					
Ricmond	BAFEP	92/03/25	1			2	1	1	1	
Parkfield Regional	CORE	92/04/11-04/14	1			24	4	20	2	
Joshua & Coach Monit	SCAL	92/04/24-04/27	7	2	45	17	2	9	2	
Eureka-Mendocino Eq.	PACNW	92/05/06-05/09	4	2		39	4	21	1	
S. Cal Monitor	SCAL	92/05/27-05/31	5	2		20	6	20	7	
Mendo Post-Seismic	PACNW	92/06/10-06/13	3	2		22	3	15	1	11
Fairweather	CORE	92/06/17-06/28	11	2	12	40		14		
Landers Eq. Resp 1	SCAL	92/06/30-07/02	9	2		42				
Landers Eq. Resp 2	SCAL	92/07/08-07/16	8	2	44	17				
Landers Eq. Resp 3	SCAL	92/07/29-08/06	8	2		20	3	52		39
Long Valley-Mono Chain	VHAZ	92/07/11-07/16	6	2		43		35		
Southern Oregon	PACNW	92/08/26-09/03	9	3		86	3	75	4	
Loma Monitor	CORE	92/09/22	1			8	2	5	2	
Parkfield Monitor	CORE	92/09/23	1	1		6		6		
Loma Monitor	CORE	92/09/22	1			6	2	5	2	
		Totals	126	35	191	634	79	458	58	50

We have established an internal data archive using a 10 gigabyte capacity rewriteable magneto-optical jukebox for easy access and permanent storage. We plan to archive all native format and RINEX format GPS data collected by the Crustal Strain project along with data from some of the global tracking sites. The archive currently includes only data collected since October 1992. The project data archive will simplify processing the data as well as collecting and transmitting the RINEX files to the Southern California Earthquake Center and to the USGS-Berkeley data archives.

Results

1. *Coseismic Displacement Associated with the 1992 Landers Earthquake ($M_s = 7.5$)*

The rupture associated with the 1992 Landers earthquake ($M_s = 7.5$) extended along the west edge of a 60 x 50 km trilateration network that had been surveyed two months before the earthquake and was resurveyed a month after it. The coseismic displacement field within the network was calculated from the changes observed in the trilateration network supplemented by the absolute displacements measured at four GPS stations and other less timely trilateration measurements. Stations near the rupture were displaced by as much as 3 m. The observed changes are reproduced reasonably well by dislocation modeling in which the Landers rupture is represented by 8 vertical fault segments, each extending from the surface to 9 km depth. A slightly better fit is obtained if we allow the depth of the model faults to vary. Two additional segments represent the Big Bear and Eureka Peak faults. The average modeled right-lateral slip on the Landers rupture is about 5 m. However, the residuals for the best-fit slip distribution are about four times greater than expected from measurement error. Given that uncertainty, a broad range of slip models furnish acceptable fits to the data (one model is shown in Figure 1). The large residuals are attributed to inelastic deformation (principally sympathetic slip on numerous unmodeled faults) within the fault blocks assumed to be elastic in the model.

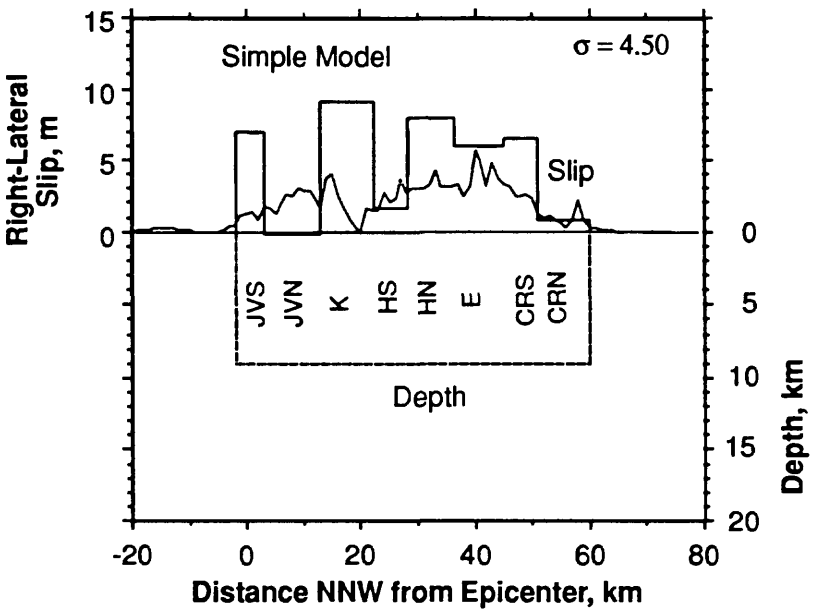

Fig. 1. Distribution of slip along the Landers rupture inferred from the fit to trilateration data. Fault segments are identified as follows: Johnson Valley South (JVS) Johnson Valley North (JVN), Kickapo (K), Homestead South (HS), Emerson (E), Camp Rock South (CRS), and Camp Rock North (CRN).

2. *Deformation in the Epicentral Area of the Landers, California, Earthquake in the Decade Prior to the Earthquake*

A 55-km-aperture trilateration network that spans the epicenters of the 1992 Joshua Tree ($M_s = 6.1$) and Landers ($M_s = 7.5$) earthquakes was surveyed in 1974, 1975, 1977, 1979, 1980, 1981, 1988, and in 1992 after the Joshua Tree earthquake but before the Landers earthquake. No premonitory anomaly is obvious in these data. The velocity field determined from these measurements shows a northwest-southeast extension north of the San Andreas fault in addition to the right-lateral shear across the fault. That velocity field suggests a pull-apart basin connecting the San Andreas fault south of Indio and the Camp Rock-Emerson fault farther north. The Landers earthquake ruptured northward diagonally across this basin before turning northwest along the Camp Rock-Emerson fault. A 6-line monitor net located 15 km from the epicenter of the Joshua Tree earthquake and 35 km from the epicenter of the Landers earthquake was surveyed several times each year between 1982 and 1990 and surveyed again in 1992 after the Joshua Tree earthquake but before the Landers earthquake. After allowance was made for coseismic offsets associated with the North Palm Springs and Joshua Tree earthquakes, no significant change in strain rate before the Landers earthquake was identified.

3. *Inferred Depth of Creep on the Hayward Fault, Central California*

A relation between creep rate at the surface trace of a fault, the depth to the bottom of the creeping zone, and the rate of stress accumulation on the fault is derived from Weertman's 1964 friction model of slip on a fault. A 5 ± 1 km depth for the creeping zone on the Hayward fault is estimated from the measured creep rate (5 mm/yr) at the fault trace and the rate of stress increase on the upper segment of the fault trace inferred from geodetic measurements across the San Francisco Bay area. Although fault creep partially accommodates the secular slip rate on the Hayward fault, a slip deficit is accumulating equivalent to a magnitude 6.6 earthquake on each 40 km segment of the fault each century. Thus, the current behavior of the fault is consistent with its seismic history, which includes two moderate earthquakes in the mid-1800's.

4. *The Parkfield Prediction Fallacy*

The Parkfield earthquake prediction is generally stated as a 95% probability that the next moderate earthquake there should occur before January 1993. That time limit is based on a two-sided 95% confidence interval. Because at the time of the prediction (1985) it was already clear that the earthquake had not occurred prior to 1985, a one-sided 95% confidence interval would have been more appropriate. That confidence interval ended in October 1991. The Parkfield prediction was based on an extrapolation of 5 of the 6 events in the 1857–1966 earthquake sequence; the 1934 event was omitted because it did not fit the regularity exhibited by the other data. The fallacy in the prediction is that it did not take account of other less-contrived explanations of the Parkfield seismicity (*e.g.*, not excluding the 1934 event). Even if the Parkfield earthquake should occur in the near future, it would be better explained by less-contrived hypotheses.

5. *Coulomb Plasticity Within the Fault Zone*

A well-developed fault zone is represented by as layer of granular material (fault gouge) confined between two competent fault blocks. Slip on such a fault involves plastic shearing of the fault gouge. That is, the fault gouge behaves as a Coulomb material, and the plastic flow is accomplished by slip on the two sets of Coulomb shears appropriate to the stress state and the frictional properties of the gouge. Neither set of Coulomb shears is coplanar with the fault zone. This explains the observation of Mandl that slip in such a fault model occurs when the plane of maximum shear in the gouge is parallel to the fault plane. The fault appears to slip as if friction on the plane of the fault were less than on planes of other orientations, whereas, in fact, the apparent slip is simply a consequence of Coulomb plasticity in the gouge (*i.e.*, cooperative slip on the two sets of Coulomb shears). The explanation requires that the apparent coefficient of friction on the fault μ_a is related to the coefficient of internal friction μ by $\mu_a = \sin(\tan^{-1}\mu)$. *Lockner et al., Eos,73*, 511, 1992] show that values of μ_a and μ measured at various normal stresses do indeed satisfy this relation.

6. *Coseismic Displacement Models for the 1992 Cape Mendocino, California, Earthquake from GPS and Coastal Uplift Observations*

Horizontal and vertical displacements due to the Cape Mendocino earthquake ($M_s = 7.1$) was recorded by Global Positioning System (GPS) surveys. Observed changes between pre-earthquake surveys in 1989 and 1991 and a survey one month after the earthquake are corrected for secular motions as derived from 1981–1989 trilateration surveys. The 1991 survey included the subset of the network near the 1991 Honeydew earthquake ($M_b = 6.0$). The observed coseismic displacements relative to the northernmost site are shown in Figure 2. The maximum displacements were measured at a site 5 km NE of the epicenter, which moved 400 ± 20 mm to the WSW and subsided by 160 ± 80 mm. Die-off of intertidal marine organisms provide an independent measure of coastal uplift.

Our preferred coseismic displacement model, estimated from both the coseismic geodetic and uplift data, indicates that 2.7 m of nearly pure thrust motion occurred on a shallow dipping (12°) fault plane that is consistent with the location of the mainshock hypocenter (10.5 km depth), focal mechanism, and distribution of aftershocks. We assume uniform slip on a rectangular, planar fault embedded in an elastic half-space. To determine the best-fitting model, we performed a Monte Carlo search for the parameters describing the location and geometry of the fault plane and estimated the magnitude and rake of the slip. The scatter of the residuals for the best-fitting model was 2.2 times observational errors. The range of other acceptable models suggest that our estimates of the dip and depth of the fault are well constrained and that the geodetic moment was $3.0 \pm 0.5 \times 10^{26}$ dyne-cm, which is about 60% of the moment estimated from seismic data. The preferred model predicts a maximum coastal uplift of about 800 mm, which is consistent with but somewhat less than the observed uplift of marine organisms; non-uniform slip models that concentrate moment release offshore are likely to provide a better fit to the uplift and seismic moment observations.

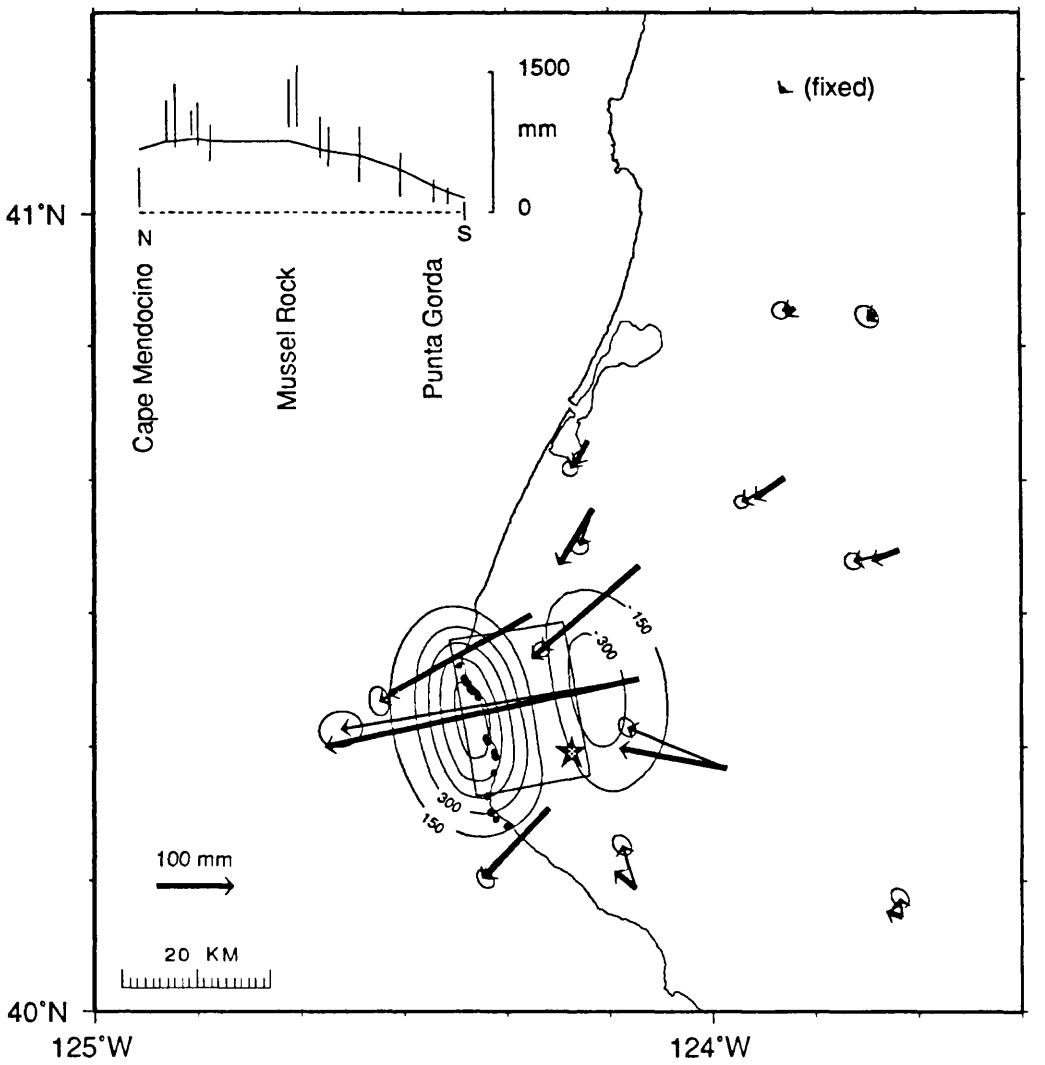

Figure 2. Horizontal and vertical displacements for the Cape Mendocino earthquake (epicenter shown with a star). The light vectors with 95% confidence region ellipses are the GPS measured displacements relative to the northernmost site. The dark vectors are the modeled displacements. The surface projection of the model fault is outlined with a rectangular box. The contours show the modeled uplift. The graph compares the uplift deduced from the die-off of marine organisms along the coast at the positions marked by black dots with that from the dislocation model.

7. *Continuous GPS Across the Hayward Fault*

In September 1991 the U. S. Geological Survey began continuous GPS monitoring of a north-south trending 8.1 km baseline that crosses the Hayward fault. This segment of the fault last ruptured in a major earthquake in 1868, and is now a zone of high seismicity and creep. We operate codeless dual-frequency Ashtech LM-XII receivers at 30 second sampling, archive daily files, and process seven-hour sessions with the Bernese version 3.2 software. Figure 3 shows the results through November 22, 1992. For this

short baseline, the broadcast orbit yields satisfactory results (Fig. 3). The rms scatter about the best linear fit is 2.2 mm in the north, 2.9 mm in the east, 10.4 mm in the vertical, and 2.1 mm in baseline length. The vertical rate of change is implausibly high.

We made several equipment changes, some of which introduced offsets in the time series. The offsets are removed by solving simultaneously for average slope and offsets at given times in a least squares adjustment. The largest offset is associated with the conversion to a forced center antenna mount. We experimented with borrowed P-code receivers for one month in the summer of 1992. A major firmware upgrade (1992.6) for the codeless receivers significantly reduced the L2 cycle slips and noise.

We made significant progress toward automating the data reduction. Data are downloaded automatically. We use PhasEdit, adapted by Jeff Freymuller of Stanford, to remove most of the low elevation angle noise. The Bernese automatic cycle slip detector fixes most of the remaining problems. As a result, our manual data cleanup time has gone from 2 hours to about 30 minutes.

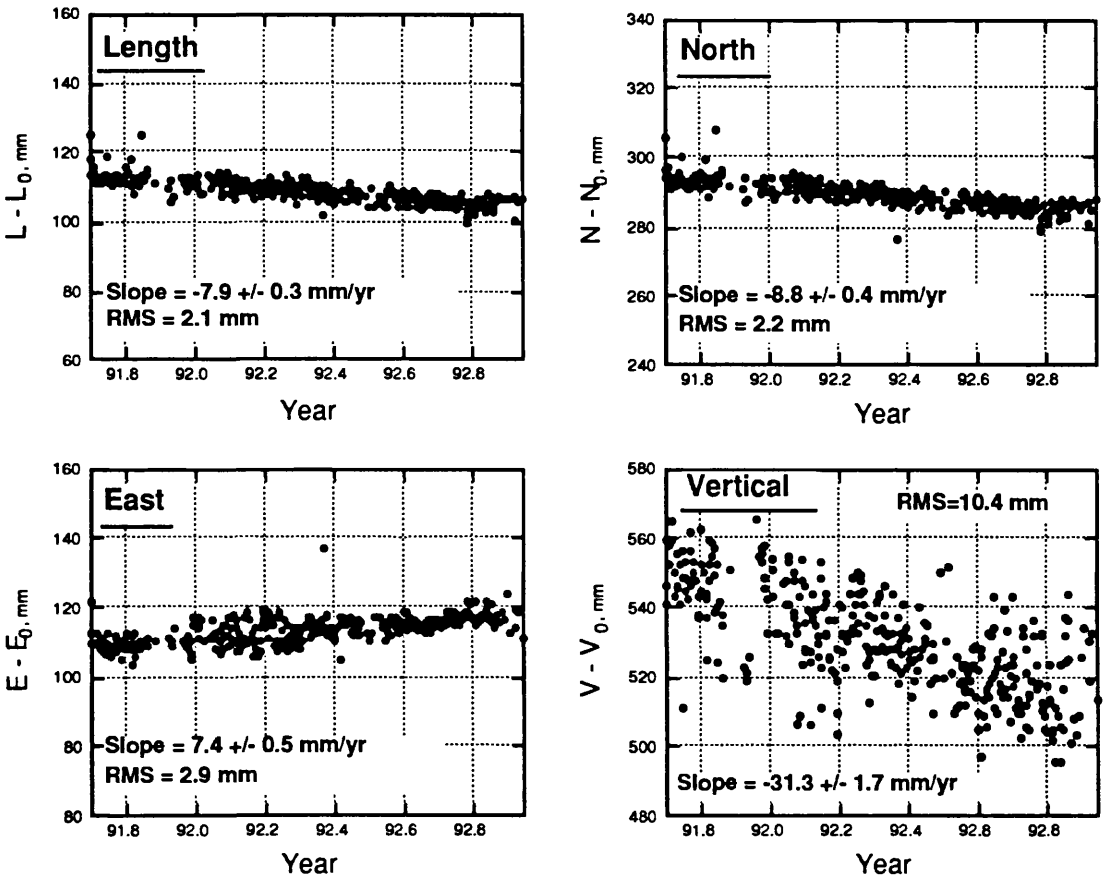

Figure 3. Length and vector components as a function of time for the 8.1 km baseline between the continuously recording GPS receivers near the Hayward fault. Uncertainties are one standard deviation as derived from the rms scatter about a weighted linear fit.

Reports

Savage, J.C., and W.Thatcher, Interseismic deformation at the Nankai Trough, Japan, subduction zone, *J. Geophys. Res. 97*, 11,117–11,135, 1992.

Savage, J.C., The uncertainty in earthquake conditional probabilities, *Geophys. Res. Lett.*, *19*, 709–712, 1992.

Savage, J.C., M. Lisowski, and W.H. Prescott, Strain accumulation across the Wasatch fault near Ogden, Utah, *J. Geophys. Res.*, *97*, 2071–2083.

Nonlinear velocity inversion for subsurface imaging of the Hosgri fault, offshore California

Agreement No. 14-08-0001-G-N2210

John N. Louie
Seismological Laboratory
The University of Nevada
Reno, NV 89557-0141
(702) 784-4219 louie@seismo.unr.edu

30 November 1992

Annual Technical Report

Motivation

The geometry and tectonics of the Hosgri fault have been the subject of intense debate. Opposing models have been developed that characterize the Hosgri as being dominated by either compressional (Crouch et al., 1978; Namson and Davis, 1990) or trans-tensional tectonics (DiSilvestro et al., 1990; Hanson and Lettis, 1990) over its history. These theories conflict on the nature of the neotectonic motion of the Hosgri, leaving the seismic potential of this major fault in doubt. Other points of contention have centered on the validity of structural models and/or interpretations of geologic features.

Our Investigations

Performing post- and pre-stack migration of data obtained from the NE-oriented seismic reflection line RU-3 (McIntosh et al., 1991) helps determine the character of the Hosgri Fault. A suite of post-stack images calculated at different migration velocities were produced for analysis. The stacked data show the best images of the stratigraphy within the Santa Maria basin near the Hosgri (figure 1). Our pre-stack migration utilized the Kirchhoff summation method (Louie and Qin, 1991). This method takes into account strong lateral variations in seismic velocity across the fault, for which any stacking process gives incorrect results. We derive the velocity model used in performing the Kirchhoff migration from a simulated-annealing (Rothman, 1985) Monte-Carlo inversion of RU-3 first-arrival picks, developed by Pullammanappallil and Louie (1992). Previous attempts to image structure within the fault zone (Shih and Levander, 1989) suffered from lack of constraint on velocities. Our model (figure 1) constrains lateral velocity variations to 2 km depths with 0.2 km/s accuracy, and is a consistent superset of the stacking velocities.

Results to Date

Results from the post-stack migration indicate thinning of Miocene-Pliocene sedimentary deposits northeastward, as they lap onto the south-west limb of the Point San Luis anticline (figure 1). The sediments, characterized by prominent reflections, are terminated and displaced upward on the north-east side of the Hosgri Fault Zone (HFZ). On the post-stack images, the HFZ is primarily characterized by columns of diffractions and truncations of reflectors. The pre-stack migration (figure 1) images the fault plane and characterizes it as dipping from 50-60 degrees to the NE.

Our images (figure 1) indicate upward-thrust pre-Miocene rocks on the NE side of the Hosgri Fault truncating Miocene to post-Miocene sedimentary reflectors underthrust on the SW side of the fault. The combination of the post-stack and pre-stack migrations

gives good control on both sedimentary and fault-plane structures. Further work will concentrate on eliminating the arcing artifacts in the pre-stack migrations with coherency criteria similar to those used by Louie and Qin (1991), and on enhancing fault-plane reflection strength with additional pre-processing of the unstacked data.

Reports submitted for publication:

Honjas, B., J. Louie, and S. Pullammanappallil, 1992, Results of post and pre-stack migrations imaging the Hosgri fault, offshore Santa Maria basin, CA: presented at the Amer. Geophys. Union Fall Meeting, San Francisco, Dec. 7-11.

Pullammanappallil, S. K., and J. N. Louie, 1992, Inversion of seismic reflection travel times using a nonlinear optimization scheme: submitted to *Geophysics*, 30 August.

References

Crouch, J. K., Bachman, S. B., and Shay, J. T., 1984, Post-Miocene compressional tectonics along the central California margin: *in* Crouch, J. K., and Bachman, S. B., Eds., Tectonics and Sedimentation Along the California Margin, Pacific Section, Soc. Economic Paleontologists and Mineralogists, **38**, 37-54.

DiSilvestro, L. A., Hanson, K. H., Lettis, W. R., and Shiller, G. I., 1990, The San Simeon/Hosgri pull-apart basin, south-central coastal California (abstract): EOS Trans. Am. Geophys. Union, **71**, 1632.

Hanson, K. L., and Lettis, W. R., 1990, Use of ratios of horizontal to vertical components of slip to asses style of faulting — Hosgri fault zone, California (abstract): EOS Trans. Am. Geophys. Union, **71**, 1632.

Louie, J. N., and Qin, J., 1991, Subsurface Imaging of the Garlock Fault, Cantil Valley, California, J. Geophys. Res., **96**, 14461-14480.

McIntosh, K. D., Reed, D. L., Silver, E. A., and Meltzer, A. S., 1991, Deep structure and structural inversion along the central California continental margin from EDGE seismic profile RU-3: J. Geophys. Res., **96**, 6459-6474.

Namson, J., and Davis, T. L., 1990, Late Cenozoic fold and thrust belt of the southern Coast Ranges and Santa Maria Basin, California: Am. Assoc. Petrol. Geologists Bull., **74**, 467-492.

Rothman, D. H., 1985, Non-linear inversion, statistical mechanics, and residual statics estimation: Geophysics, **50**, 2784-2796.

Shih, R.-C., and Levander, A. R., 1989, Pre-stack layer-stripping reverse-time migration (abstract): EOS Trans. Am. Geophys. Union, **70**, 1222.

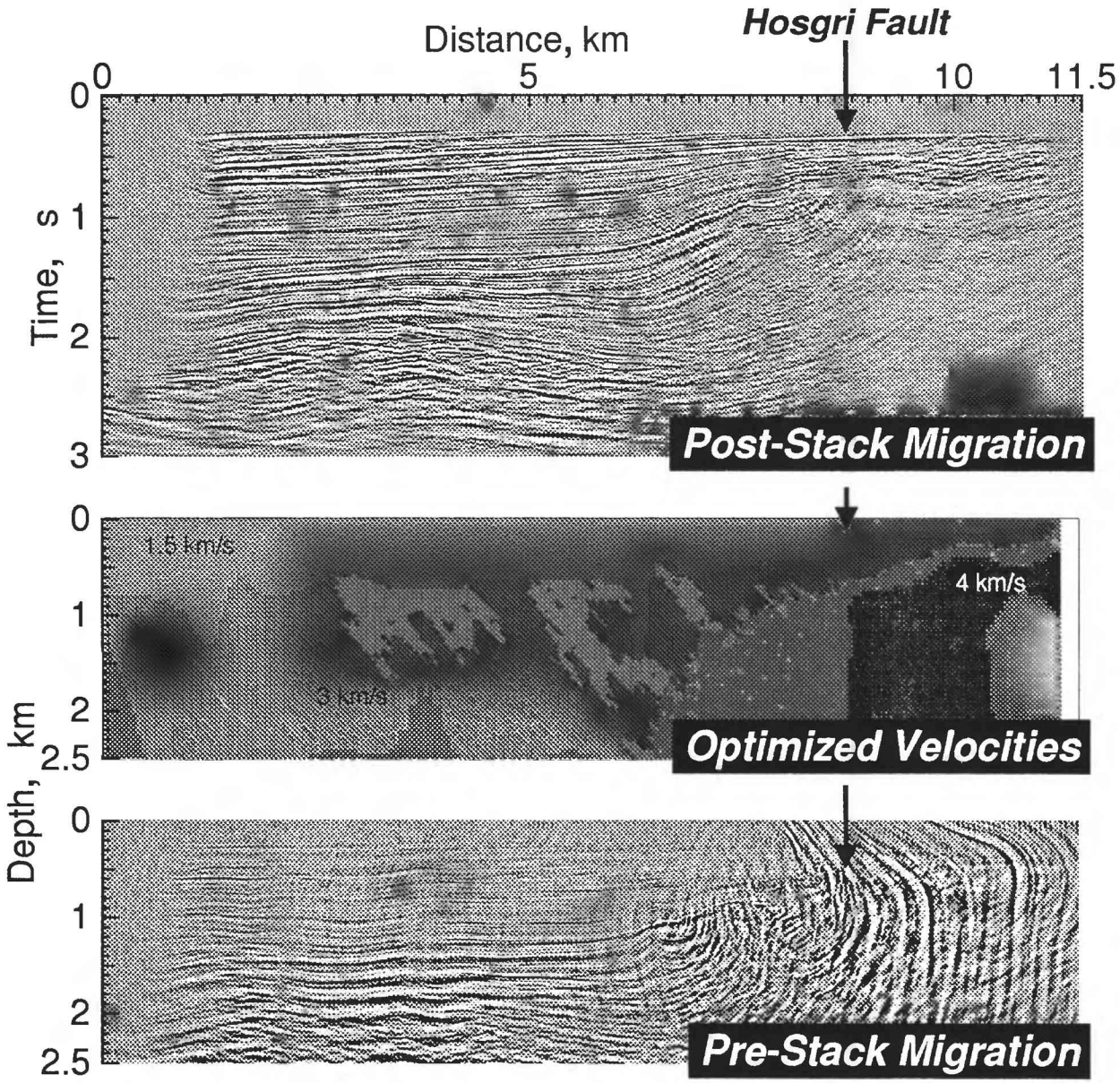

FIGURE 1: Analysis of seismic reflection data previously acquired by the EDGE Consortium and Rice University crossing the offshore Hosgri fault near San Luis Obispo, California. The top image is a common-midpoint stacked section, after F-K migration. It is similar to the stacks published by McIntosh et al. (1991) and shows the details of basin stratigraphy. However, strong lateral velocity variations near the Hosgri fault (arrows) disrupt the stacked image nearby. The middle image shows the result of a non-linear, curved-ray velocity inversion using picked first arrival times and a simulated-annealing optimization method. Having found estimates of the lateral velocity contrasts, we can then compute a pre-stack migration of the reflection data that accounts for these contrasts. The resulting lower image has almost as much detail on the basin sediments, but is much more accurate near the Hosgri fault. The arrow points to steep, east-dipping fault-plane relfections, with truncated basin stratigraphy below.

CRUSTAL VELOCITY STRUCTURE AND GROUND RESPONSE IN THE PACIFIC NORTHWEST - COAST RANGES THROUGH CASCADES

Project Number: 9930-03791
Project Co-P.I.'s: James Luetgert, Walter D. Mooney
Institution : U.S. Geological Survey, Branch of Seismology
Address: 345 Middlefield Road / MS 977
Menlo Park, CA 94025
Telephone: 415-329-4763/4764

This project is a continuation of the investigation of lithospheric velocity structure and ground response in the Pacific Northwest begun in 1991 with collection of seismic refraction/wide angle reflection data in the Puget Sound/Willamette lowland region funded by NEHRP and DCS.

Despite the importance of the Pacific Northwest as a region of seismic and volcano hazard, and as a laboratory of active tectonic processes, limited deep seismic profiling has been conducted in the region. Our present knowledge of the structural framework of the Pacific Northwest is largely based upon projections of surface geology to depth, inferences from gravity, aeromagnetic and magnetotelluric data, limited seismic reflection data and observed patterns of seismicity. Seismic characterization of a portion of the Pacific Northwest, the Puget Sound/Willamette lowland region, has begun as a result of field work completed in September, 1991.

We have continued to investigate the geophysical framework of this region by proceeding with the analysis and interpretation of the data collected in 1991 (Figure 1). The 1991 field program consisted of three seismic refraction/wide angle reflection profiles: a 300-km-long N-S profile on the eastern flank of the Puget Sound Basin of Washington; a second 330-km-long N-S profile on the west flank of the Willamette Lowland of Oregon; and a 140-km-long cross-strike (E-W) profile across the central Oregon Coast Ranges and Willamette Lowland. A total of 24 large bore-hole shots were fired, and recording was accomplished with more than 500 portable seismographs from the USGS, Stanford, IRIS/PASSCAL, and the GSC, Ottawa. In addition, two 96-channel seismic reflection spreads were deployed by the University of Wyoming. These data, in consort with other geological and geophysical data, will provide a model of the velocity and structure of both the upper crust and the lower crust/upper mantle through this region.

During FY92, the data collected in September, 1991, have been collated, distributed to University collaborators, and an Open-File Report is in final preparation. Preliminary modeling of crustal velocity structure has begun and has already yielded intriguing results. P-wave velocities in the upper crust from the north-south profile along the eastern side of the Puget Basin (Figure 2) show that the basin is deepest toward the center of the profile and is relatively shallow at the north and south ends. Upper crustal velocities greater than 6 km/s underlie the basin and are found as shallow as 5 km in depth. Velocities rise from 6.3 to 6.7 km/s to 7.1 km/s across a mid-crustal gradient zone near 25 km depth. Crustal thickness is approximately 45 km along the length of the profile.

The Coast Ranges of western Oregon constitute a large portion of the Cascades forearc. In central Oregon, the Coast Ranges consist of a thick accumulation of basalt and associated marine sediments; pre-Tertiary crust is apparently missing. The

seismic refraction/wide angle reflection profile was recorded along the west flank of the Willamette Lowland of Oregon. These profiles provide more than 330 km of deep seismic data, which define the crustal and upper mantle structure in unprecedented detail. The N-S seismic profile in Oregon indicates a substantially thicker crust (more than 30 km) than appears in many previous geophysical interpretations (Figure 3). The average crustal velocity is high (6.8 km/s or greater), and is indicative of substantial amounts of mafic rocks in the deep crust, in agreement with the positive Bouguer gravity anomaly. Strong wide-angle reflections from depths of 40+ km may be from the subducting Juan de Fuca plate.

More than forty rock samples have been collected along the 1991 profiles and laboratory velocity measurements have begun (N. Christensen) The crustal seismic velocities determined from the 1991 Oregon seismic refraction data are in excellent agreement with laboratory velocity measurements made at high pressure on rock samples collected in the Coast Ranges. The following presentations of early results have been made.

Luetgert, J.H., Mooney, W.D., E. Criley, G.R. Keller, J. Gridley, K. Miller, A. Tréhu, J. Nabelek, S.B. Smithson, C. Humphreys, N.I. Christensen, R. Clowes, and I. Asudeh, 1991. Crustal Architecture of the Pacific NW: The 1991 Seismic Field Experiment, EOS, 72:44:323.

Luetgert, J.H., Mooney, W.D., E. Criley, G.R. Keller, J. Gridley, K. Miller, A. Tréhu, J. Nabelek, S.B. Smithson, C. Humphreys, N.I. Christensen, R. Clowes, and I. Asudeh, 1992. Crustal velocity structure of the Pacific NW: The 1991 Seismic refraction/wide-angle reflection experiment, GSA Abst. with Programs, 24:5:66.

Mooney, W.D., J.Luetgert, E. Criley, G.R. Keller, J. Gridley, K. Miller, A. Tréhu, J. Nabelek, S.B. Smithson, C. Humphreys, N.I. Christensen, R. Clowes, and I. Asudeh, 1991. The 1991 Pacific Northwest Seismic Field Experiment, EOS, 72:44:326.

Trehu, A. M., J.N. Nabelek, S. Azevedo, T.M. Brocher, J. Luetgert, W.D. Mooney, I. Asudeh, R. Clowes, G.R. Keller, K. Miller, and Y. Nakamura, 1992. Crustal Structure of the Cascadia Subduction Zone Beneath Western Oregon, GSA Abst. with Programs, 24:5:66.

Luetgert, J.H., Mooney, W.D., A. Tréhu, N.I. Christensen, and I. Asudeh, 1992. Crustal Structure of the Oregon Coast Ranges from 1991 Seismic Refraction Data, EOS, 73:43:526.

Trehu, A. M., J.N. Nabelek, S. Azevedo, T.M. Brocher, J. Luetgert, W.D. Mooney, I. Asudeh, R. Clowes, Y. Nakamura, S.B. Smithson, and K. Miller, 1992. A Crustal Cross-section across the Cascadia Subduction Zone in Central Oregon, EOS, 73:43:391.

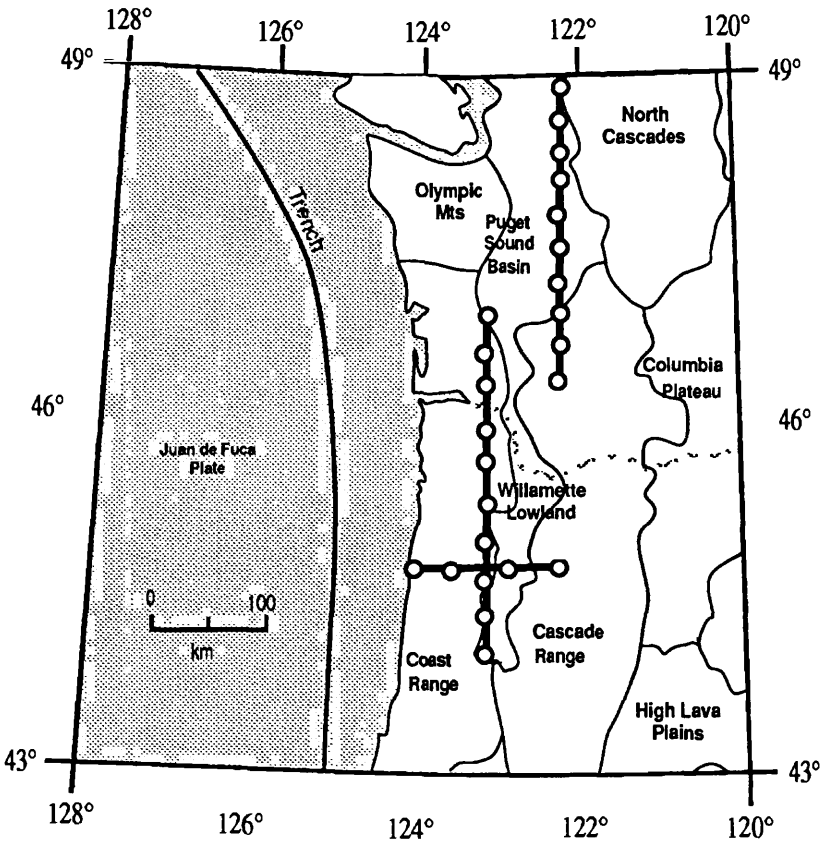

Figure 1: Locations of shotpoints and recording arrays used for the 1991 Pacific NW seismic refraction/wide-angle reflection experiment.

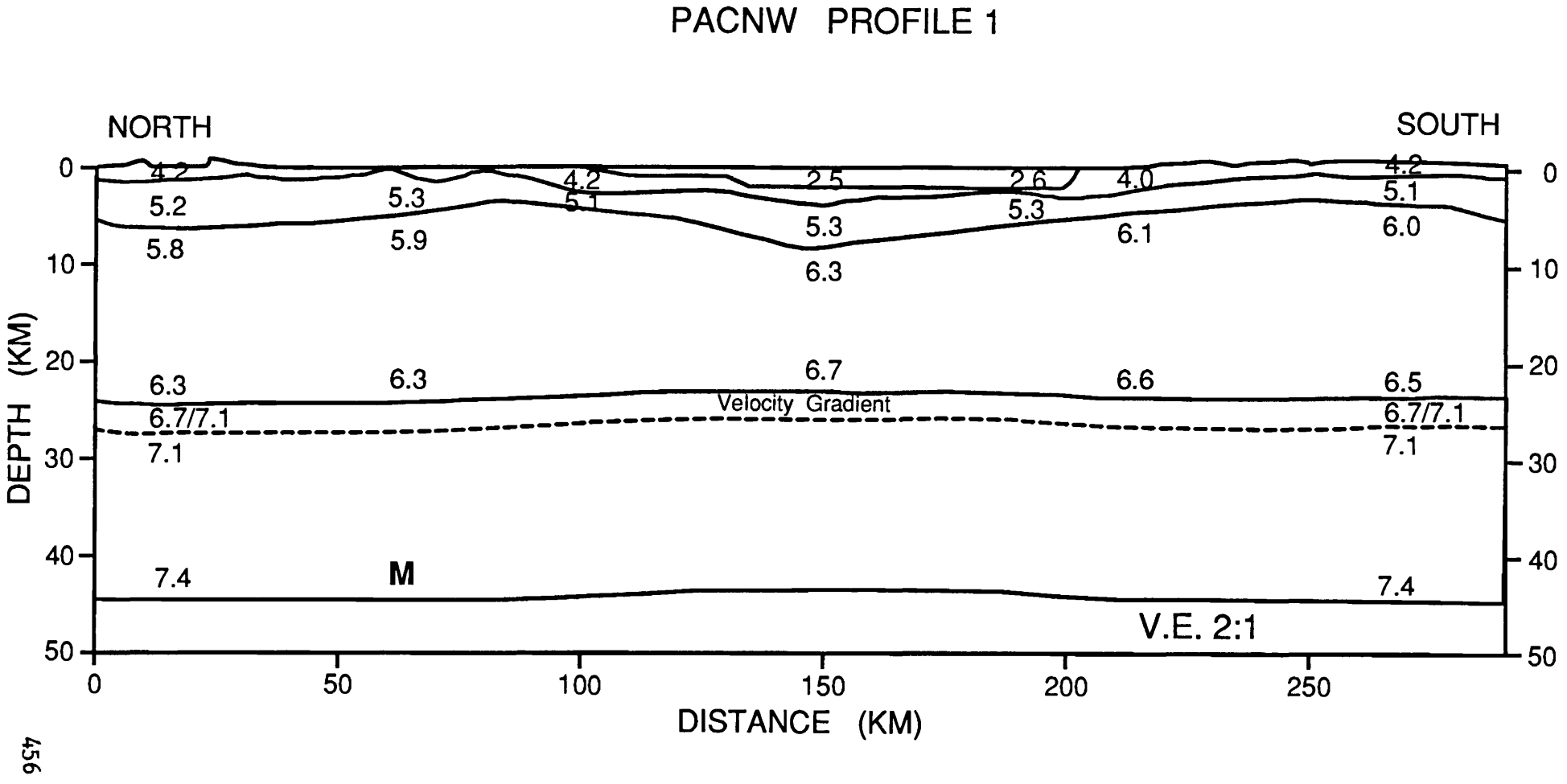

Figure 2: Preliminary velocity model for PACNW profile 1; located at the eastern edge of the Puget Basin in Washington State.

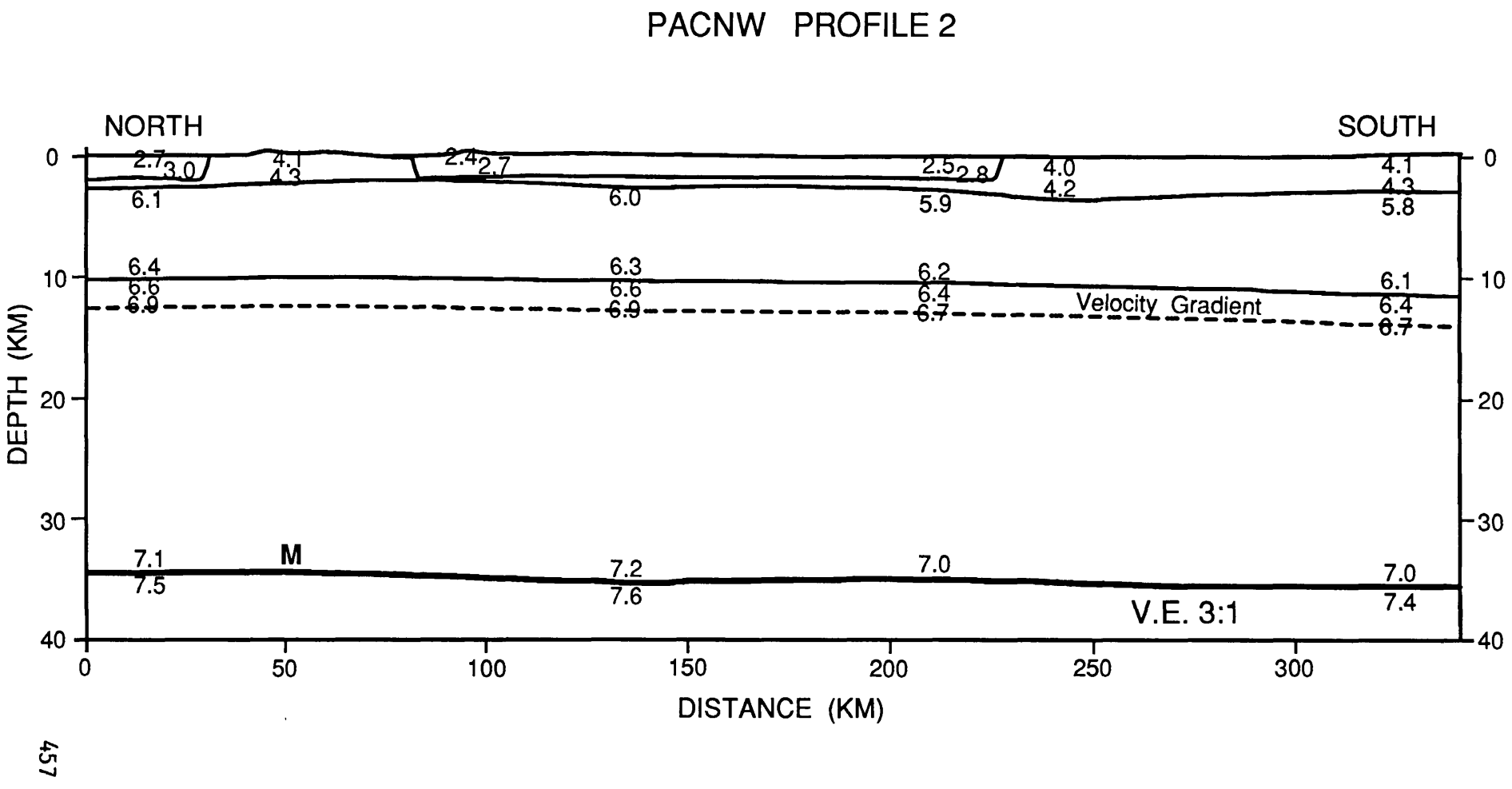

Figure 3: Preliminary velocity model for PACNW profile 2; located at the western edge of the Willamette Valley in Oregon State.

TEMPORAL AND SPATIAL BEHAVIOR OF LATE QUATERNARY FAULTING, WESTERN UNITED STATES

9950-04540

Michael N. Machette
Branch of Geologic Risk Assessment
U.S. Geological Survey, Box 25046, MS 966
Denver, CO 80225-0046
(303) 273-8612

PURPOSE OF PROJECT

To define regional variations in the time-space distribution of late Quaternary paleoseismic activity as a guide to understanding the accumulation and release of strain on extensional faults in the Western United States. Our main objective is to study selected historic faults to interpret the paleoseismic and neotectonic history in regions of active faulting, especially in the Central Nevada seismic belt (CNSB). In addition, at least one-half of FY 92 was spent on a new International Lithosphere Program (ILP) project entitled "World Map of Major Active Faults, Western Hemisphere." Project members are Michael N. Machette, Richard L. Dart, and Kathleen M. Haller.

INVESTIGATIONS

1. This summer, Machette, Haller, and Kelvin Berryman (visiting scientist from New Zealand Geological Survey) completed describing and sampling six large exploratory trenches that were excavated in Pleasant Valley, south of Winnemucca, Nev. Four of the trenches cross surface ruptures of the 1915 Pleasant Valley earthquake (estimated Richter magnitude $7^3/_4$) in order to investigate the timing of prehistoric faulting. Two additional trenches were located on nearby pre-1915 fault scarps; one on a valleyward strand of the Tobin Scarp and a second that is to the north along the frontal fault of the Sonoma Range in Grass Valley. Detailed topographic/geologic maps were made of the trench sites using an EDM Total Station on loan from S.G. Wesnousky of the University of Nevada-Reno. Samples were taken for TL and ^{14}C dating and tephrochronologic studies.

2. In January 1992, we were asked by ILP to help compile the World, North American, and United States maps of major active faults in support of a new Global Seismic Hazards Assessment Program (GSHAP). This work began in earnest in mid-1992 with a carefully chosen list of participants for the Western Hemisphere. We are enlisting technical experts from Canada, the United States, and Mexico/Central America that are known to be both productive and knowledgeable, and to have strong national contacts. For the United States, the compilation will be done by the USGS in Denver, under the direction of this project. Given the limited time to produce the North American map (two to three years at the most), the project must be limited to just those elements needed for the GSHAP. The number of features to be included on the map were reduced at an initial GSHAP planning meeting in San Francisco (Dec. 1991) and further modified at the 1992 meeting in Rome.

Assembling the fault map and database for the United States (and North America) will involve:

1) General supervision and interpretation of geologic/tectonic information (M.N. Machette),
2) Data compilation and entry for the fault catalog (all personnel) and the design and management of the database (K.M. Haller), and
3) Digitization and manipulation of data (file transfer, transform projections) using ARCINFO software on a Sun-workstation (R.L. Dart).

By the end of FY 92, we had obtained digital files for California, Nevada, Utah, Montana, Colorado, and parts of New Mexico. The California faults were scanned on the Menlo Park Scitex using a specially prepared version of Jennings' 1992 fault map. The files for the other states come from sources within the USGS or state geological surveys.

Our strategy is to assemble a large body of data on the Quaternary faults in the U.S. portion of North America. Although many authors have compiled maps, few have taken the time to fully document their maps with databases, particularly in computer form; thus, fault data in catalog form is relatively sparse. However, the state of Utah will soon publish an excellent catalog and Malcolm Clark (USGS) continues to compile a catalog of slip-rate data for California. Overall, we suspect that there are catalog data for about 20% of the faults on the U.S. map.

The customers for these products include internal (USGS) to external NEHRP scientists, as well as scientists, engineers, planners with state and local governments, universities, and consulting firms. We are using ARC Info on a SUN-platform for the map preparation and are compiling fault data on a relational database (FoxBase, MicroSoft Corp.) on the Macintosh. However, because most of the intended users do not have Macintosh computers, we intend to supply the data in a DOS and/or Windows version of the database. We hope to write the database, a run-time version of the program, and the digital map files to CD-ROM for easy access at low user cost.

3. Crone and Machette completed two comprehensive manuscripts that describe the results of their 1991 Gilbert Fellowship field studies of the 1988 earthquakes at Tennant Creek, Australia (Crone and others, 1992) and Marryat Creek, Australia (Machette and others, 1993). These manuscripts discuss the implications of long-recurrence intervals for intraplate faulting. They will be published as USGS Bulletins that contain lithologic/structural logs of six exploratory trenches, detailed site maps, plots of scarp profiles, and preliminary results of TL and ESR dating.

RESULTS

1. Last summer we spent about 5 weeks logging trenches across surface ruptures of the 1915 Pleasant Valley earthquake, south of Winnemucca, Nev., and nearby prehistoric scarps. These trenches revealed evidence of 2-3 faulting events during late Pleistocene time (10-130 ka). The first and most important conclusion of our study is that earthquakes of similar magnitude to the 1915 Pleasant Valley earthquake must have long recurrence intervals (*i.e.*, many tens of thousands of years). The two trenches along the Pearce scarp (at Miller Basin and just south of Siard Canyon) crossed large (>6- to 13-m-high) scarps on alluvium believed to be of pre-late Pleistocene age (>130 ka). The two trenches along the Tobin scarp, which is a right-stepping, northward extension of the Pearce scarp, crossed a 8-m-high scarp on pre-late(?) Pleistocene alluvium and colluvium at Sheep Creek and a small (0.5-m-high) scarp on pre-late(?) Pleistocene alluvium just south of Jim Creek near the northern end of the Tobin scarp. At all of these sites, we found no evidence of pre-1915 faulting events on surfaces of Holocene or latest Pleistocene (<15 ka) age. No trenches were excavated along the China Mountain and Sou Hills scarps (the distal sections of the 1915 ruptures) because evidence of prior faulting is sparse and discontinuous, recorded on bedrock or steep hillslopes, or is restricted to small (<1-m high) scarps on old alluvium.

Two additional trenches were excavated to investigate the history of subjacent faults that were not activated during the 1915 Pleasant Valley earthquake. A long, deep trench was placed across a 9-m-high scarp that is about 1 km valleyward of the Tobin scarp in the northern part of Pleasant Valley. The other trench was across a 4.4-m-high scarp of the range-front fault of the Sonoma Range near Elbow Canyon about 12 km south of Winnemucca in Grass Valley. The history of faulting along the Sonoma Range is particularly interesting in that it may show if late Quaternary faults in the Grass Valley near Winnemucca were part of an integrated prehistoric analog of of the CNSB, or whether the seismic belt has included the China Mountain, Tobin, Pearce, and Sou Hills fault blocks in late Quaternary time. We are suspucious that the recent rupturing along China Mountain is defining a relatively new NE-oriented rupture path.

The tectonic stratigraphy in these trenches is dominated by loess (eolian silt) and fine sand derived from Quaternary lake deposits and local debris flows that postdate and commonly lie on middle(?) Pleistocene alluvium; as a result, these trenches presented a special challenge to map and decipher previous faulting events owing to a lack of distinguishing lithologies, sedimentary features, and organic matter. The following discussion briefly summarizes results of our trenching.

Miller Basin Trench

Three colluvial wedges and a fourth unit of colluvium were found in this trench. The wedges become progressively more lenticular with time as a result of increasing scarp height, such that the post-1915 wedge extends across most of the 13-m-high scarp. The oldest colluvium lies on alluvium of probable pre-late Pleistocene age (>130 ka) age. The second and third wedges are separated by a moderately well developed soil (Av, Btk horizons) that probably required tens of thousands of years to form. The fault zone is at least 9 m wide and consists of a main shear zone (70° W dip) that was active in 1915 (and earlier), and associated minor faults, the most basinward of which is a high-angle reverse fault. The bulk of sediment on the downthrown side of the fault is derived from debris-flows and loess and have no correlative on the upthrown block. No organic material or tephra were found in this trench.

South of Siard Canyon Trench.

The 1915 scarp at this site is large (ca. 2-3 m) and comprises about 1/2 of the total scarp height (5.8 m) at the site. However, the upper surface is steep (10° slope) and may represent earlier faulting events. The total surface offset here is probably about 10 m. Three colluvial wedges and a fourth tectonically derived unit were found in the trench, however these material are concentrated in a healed graben that was exposed in the midslope position of the scarp. The oldest tectonic material fills a portion of the graben. The third wedge fills a meter-wide fissure and is characterized by abundant organic matter and/or basaltic ash (see also Sheep Creek trench). The two younger wedges are lenticular and contain many sedimentary packages. The main shear zone is about 1.5 m wide, dips 53-66° W., and daylights high on the scarp. The entire fault zone is about 18 m wide and forms a deep graben, which was entirely filled by debris flows and loess prior to reactivation in 1915. Pods of Mazama ash (6,845±50 ^{14}C yr B.P.; Bacon, 1983) are concentrated within the graben and except for one problematic exposure, the Mazama seems to be deformed by only one faulting event (1915). All of the material in the 3.5-m-deep trench across the graben is either debris flows or loess. A buried soil at 1.4 m depth (valleyward of the graben) probably correlates with the upthrown surface above the scarp and is covered by loess. This soil has a strong accumulation of clay in gravel, suggesting considerable antiquity. The abundant organic material in the fissure fill and the tephras were sampled for dating/correlation.

Sheep Creek Trench

R.E. Wallace found Mazama ash exposed in the fault scarp at Sheep Creek along of the Tobin scarp and argued that the ash is faulted by only the 1915 earthquake. On this basis, the minimum recurrence interval for surface faulting along the Tobin scarp is at least 6,800 yr; however, we suspect that it may be substantially longer (several tens of thousands of years?). To evaluate the fault's recurrence interval, a trench was placed across a large composite fault scarp that is superposed on a 10-15° west-facing hillslope, about 50 m south of Sheep Creek.

The main faulting is concentrated in a 1-2-m wide zone and an adjacent back tilted half graben. The 1915 and prior faulting event (2nd) resulted in a colluvial wedge comprised of slump blocks and finely laminated wash-slope sediment. The next older events (3rd and 4th) are characterized by large slump blocks comprised of well developed Bt and Btk horizon material. Interspersed within the blocks is a prominent clean mafic ash(?) that was probably emplaced after the 4th faulting event and prior to the 3rd event. Considering that there are three faulting events recorded after deposition of the ash and that the faulted land surface appears old based on soil development, the ash may be correlative with the pre-late Pleistocene Wadsworth ash bed(A.M. Sarna-Wojcicki, oral commun., 1992). The Wadsworth is a mafic ash in the upper part of the pluvial in the Eetza Alloformation of Lake Lahontan in west-central Nevada (Davis, 1978). The Eetza was deposited during oxygen isotope stages 6 and 10, and thus could be as young as 130 ka (end of stage 6), although Sarna-Wojcicki and others (1991) estimated an age of 155 ka for a correlative ash from Tule Lake in northern California. If the correlation of the Sheep Creek ash and the Wadsworth ash bed is substantiated, then the recurrence interval for faulting at the Sheep Creek site is about 65-75 ky.

Upper Jim Creek Trench

This trench crossed a small scarp (total height of about 0.5 m) that had been nearly healed prior to the 1915 event. However, if one walks along the scarp you can detect the presence of a pre-1915 scarp, however subtle. A shallow graben that extends almost 20 m west of the main fault was found to be at least 2 m deep and filled mainly with loess. The well developed soil on the upthrown surface (Av/Bt/Cox profile) was not found in the graben, but is evident valleyward of the antithetic fault beneath about 1.5 m of loess. These relations suggest about 2-2.25 m of net thrown across the fault zone. The number of faulting events recorded in this trench is problematic owing to the thick fill of loess and the absence of easily recognizable colluvial wedges that were probably the result of individual <1-m displacements. If prior faulting events had displacements similar to the 1915 event (0.7 m from trench log), then only 3 events are needed to form the scarp and graben found at this site. If the surface is a of pre-late Pleistocene age, which seems to be the case for most surfaces that have large scarps and well developed soils, then recurrence intervals are on the order of 50 ky or longer. However, the site is near the northern end of the Tobin scarp and thus may not record all of the events that occurred at the Sheep Creek site or along the Pearce scarp to the south. The downdropped surface can be traced west to the Lower Jim Creek site (see next description), where the surface also has a well developed soil profile.

Lower Jim Creek Trench

This trench crossed a 9-m-high scarp having a maximum slope angle of about 17°. No faulting occurred along this fault in 1915, although the scarp joins the Tobin scarp just north of Sheep Creek. The trench revealed evidence for 3 or 4 events in the late(?) Pleistocene, the youngest of which occurred before the most recent episode of loess deposition (latest Pleistocene to Holocene time). There is about 3 m of fill on the downdropped side of the fault, and another 2 m of disturbed fluvial gravels are preserved within a narrow graben. The fill averages about 25 percent gravel, whereas the source material on the upthrown block is almost entirely sandy gravel. Therefore, about 3/4 of the fill is probably derived from eolian deposits and 1/4 is derived from erosion of the fault scarp.

Elbow Canyon Trench

This trench is along a prehistoric fault scarp that parallels the western front of the Sonoma Range. Wallace (1979) considered this scarp to be of latest Pleistocene age (ca. 12 ka) on the basis of its morphology. The trench crossed a 4.4-m high scarp having a maximum slope angle of about 14.5° and revealed evidence for 3 events in the late(?) Quaternary (past 130 ka); however, the most recent event probably predates the desiccation of Lake Lahontan at about 12 ka. The lake's highest shoreline is about 5 km to the west of the trench site, and the lake undoubtedly supplied the bulk of the eolian material found in the trench. At the base of the trench, we found a large block of soil that had collapsed from the fault's free face during the oldest event; the preservation of this delicate block indicates that it was soon buried by colluvium. Samples from the intact Av horizon at the former top of this block will provide a TL date for the third (oldest) event, and thus allow us to calculate a minimum recurrence interval and slip rate at this site.

Summary of Trenching Investigations

Our preliminary interpretations from the trenching lead us to believe that large-magnitude surface-rupturing events occur on long time intervals (many tens of thousands of years) along the eastern side of Pleasant and Grass Valleys. This conclusion contrasts markedly with the historic pattern of surface-rupturing in the northern part of the CNSB. Careful dating of paleoseismic events will be required to document whether or not ancient episodes of temporal earthquake clustering occured in the CNSB. In addition, regional fault studies may show that seismic belts (such as the CNSB) may move back and forth through regions, allowing temporal clustering on long time frames.

From the materials exposed in our trenches, it seems obvious that the use of fault scarp morphology for discriminating times of faulting in the western Basin and Range province is handicapped by two problems. First, many fault scarps are probably not eroded in a closed system (as often modeled) but instead are buried by eolian materials derived from distant sources (tens to hundreds of km away). Second, most scarps more than 3-4 m high are probably the result of multiple faulting events and thus scarp height will be a compound value, whereas scarp slope will be related to the most recent faulting event. One must be careful in applying morphometric analysis to multiple-event scarps; chances are good that young scarps will seem too old (Holocene will look like late Pleistocene) and old scarps will seem too young (owing to the compound nature of the scarps). We are optimistic that our trench mapping and sampling for dating and tephrochronologic correlation will allow us to decipher the approximate timing of prehistoric faulting events along the Pleasant Valley scarps and nearby faults. The results of this study will be compared to paleoseismic histories being developed by Bell and dePolo on the 1934 Cedar Mountain scarps, by Bell on the 1954 Dixie Valley scarps, and with work planned by Wesnousky on the 1954 Fairview Peak scarps, in order to better understand the temporal and spatial patterns of prehistoric seismicity along the northern part of the CNSB.

2. No modern map of active faults exists for the entire United States, either in paper or digital form. The proposed map of the United States (and probably North America) will be compiled and digitized at 1:250,000 scale (AMS quadrangles). This scale will allow eventual output at state map scales (commonly 1:500,000 to 1:750,000) without serious loss of information. We favor the AMS quadrangles because they are uniformly available, are near the maximum size of personal-computer digitizer tables, and have been used as a base for many of the state compilations of Quaternary faults in the Western United States (*e.g.*, Utah and Nevada).

In addition to fault location and style, our maps will depict times of most recent movement and slip rate as a proxy for fault activity. Our age scheme allows some flexibility owing to differing levels of understanding and the fact that the age of some faults can only be inferred from stratigraphic relations. Five ages of movement can be shown on the U.S. map using colors (colors tentative):

Red	Historic (date, generally <200± years),
Orange	Holocene (<10 ka) to post-latest Pleistocene (<15 ka),
Green	Late Quaternary (<130 ka),
Blue	Late and middle Quaternary (<730 ka), or
Black	Quaternary (<1.6 Ma).

TABLE 1. Status of Quaternary fault data for different regions of the United States
*[*Quality: ***A***, good; ***B***, adequate; ***C***, poor or nonexistent]

State/region	Regional Map	Database Type	Main Contacts
Alaska	***A***. Digital, 1992	***A***. Text, unpublished	Plafker
Washington	***B***. Compiled, 1991	***C***. Uncompiled	Walsh
Oregon	***B***. Part digital, 1992	***B***. Partial; text, 1992	Weldon, Pezzopane
California	***A***. Recompiled, 1992	***B***. Partial; text, 1984	CDMG, USGS
Nevada	***A***. Digital, 1991	***C***. Uncompiled	Dohrenwend
Idaho	***C***. Uncompiled	***C***. Uncompiled	Haller
Montana	***B***. Part digital, 1992	***C***. Uncompiled	Stickney
Utah	***A***. Digital, 1992	***A***. R-base, 1992	Hecker
Arizona	***B***. Nondigital, ca. 1987	***B***. Partial; text, ca. 1987	Pearthree
New Mexico	***B***. Part digital, ca. 1987	***B***. Partial; text, ca. 1987	Machette
Colorado	***B***. Digital, ca. 1987	***B***. Partial; text, ca. 1987	Colman, Kirkham
Texas	***B***. Nondigital, 1992	***C***. Uncompiled	Collins
Mid-Continent	***C***. Uncompiled	***C***. Uncompiled	Crone, Obermeier
Eastern U.S.	***C***. Uncompiled	***C***. Uncompiled	Prowell, Talwani

Three ranges of slip rates (mm/yr or m/ky), depicted by fault-line thickness, will be used on the map to differentiate rates of activity:

>5 Faults at plate boundaries and along subduction zones (San Andreas fault, Cascadia subduction zone),

1-5 Lesser strike-slip and major extensional faults (Garlock and Wasatch faults), or

<1 Most extensional and intraplate faults.

3. The results from our Gilbert Fellowship research on intraplate faulting in Australia (1986 Marryat Creek, Machette and others, in press; 1988 Tennant Creek earthquakes Crone and others, 1992) show that these historic intraplate earthquakes reactivated ancient faults. However, there was no clear evidence of fault-scarp derived colluvium in the Quaternary deposits in any of the six trenches, nor is there any compelling geomorphic evidence of prehistorical faults scarps at any of the sites. TL age estimates from eolian sand at Tennant Creek are as old as 61±5 ka (John Prescott, University of Adelaide, Australia). These relations indicate that the historical earthquakes were associated with faults that had ruptured in the past, but that the recurrence interval for surface-rupturing earthquakes on these faults is probably measured in time increments of tens of thousands of years and possibly hundreds of thousands of years or more. These investigations of historical intraplate faulting and our brief observations of a trench across the 1968 Meckering (Western Australia) fault scarp suggest that Australian intraplate faults have long repeat times; with this in mind, the concept of recurrence intervals may not be appropriate for earthquakes that occur in the 'stable' interiors of continents. Perhaps hazard assessments in Australia and other continental interiors should be based on models where moderate- to large-magnitude earthquakes occur at any time on suitably oriented faults, rather than only on faults having Quaternary movement.

REFERENCES CITED

Bacon, C.R., 1983, Eruptive history of Mount Mazama and Crater Lake caldera, Cascade Range, U.S.A.: Journal of Volcanology and Geothermal Research, v. 18, p. 57-115.

Davis, J.O., 1978, Quaternary tephrochronology of the Lake Lahontan area, Nevada and California: Nevada Survey Archeological Research Paper 7, 137 p.

Jennings, C.W., 1992, Fault activity map of California: California Division of Mines and Geology Open-File Report 92-03, scale 1:750,000 (preliminary version of second edition).

Sarna-Wojcicki, A.M., Lajoie, K.R., Meyer, C.E., and Adam, D.P., 1991, Tephrochronologic correlation of upper Neogene sediments along the Pacific margin, conterminous United States, *in* Morrison, R.B., ed., Quaternary nonglacial geology; Conterminous U.S.: Geological Society of America, The Decade of North American Geology, v. K-2, p. 117-140.

Wallace, R.E., 1979, Map of young fault scarps related to earthquakes in north central Nevada: U.S. Geological Survey Open-File Report 79-1554, 2 plates, 1:125,000 scale.

REPORTS

Crone, A.J., Machette, M.N., Bowman, J.R., 1992, Geologic investigations of the 1988 Tennant Creek, Australia, earthquakes—Implications for paleoseismicity in stable continental regions: U.S. Geological Survey Bulletin 2032-A, 51 p., 2 plates.

Machette, M.N., and Haller, K.M., 1992, Late Quaternary faulting in the Western United States—Evidence of geologically recent extension of the northern Basin and Range province: Kyoto, Japan, 29th International Geological Congress Abstracts with Programs, p. 398.

Machette, M.N., Personius, S.F., and Nelson, A.R., 1992, The Wasatch fault zone, USA: Accepted for Special Issue of Annales Tectonicae, 58 ms. p., 22 figs., in press.

Machette, M.N., Crone, A.J., Bowman, J.R., 1993, Geologic investigations of the 1986 Marryat Creek, Australia, earthquake—Implications for paleoseismicity in stable continental regions: U.S. Geological Survey Bulletin 2032-B, 54 ms. p., 19 figs., 8 tables, 1 plate, in press.

Trifonov, V.G., and Machette, M.N., 1993, The World Map of Major Active Faults Project (14 p.), *in* P.W. Basham and D. Giardini, eds., The Global Seismic Hazards Assessment Program (GSHAP): Proceedings of the GSHAP Planning Meeting, Rome, Italy, June 1-3, 1992.

Analysis of Seismic Data from the Rose Canyon and Elsinore Fault Zones

Project Number 1434-92-G2173

Harold Magistrale
San Diego State University
Department of Geological Sciences
San Diego, California 92182
(619) 594-6741

The purpose of this work was to analyze existing phase data of earthquakes along the Elsinore and the Rose Canyon fault zones, as recorded on the USGS-Caltech southern California seismic network, in order to relate seismicity patterns to geologic structures. Arrival times were inverted for hypocenters and one- and three-dimensional P and S wave velocity structures.

Rose Canyon fault zone.

Earthquakes from the period of 1983 to 1990 are examined. Most happened in the three distinct time-space clusters of 6/85, 8-10/86, and 9/87 under the San Diego Bay. The 6/85 swarm contained three $M_L \approx 4$ earthquakes and many smaller events. It forms a southwest dipping hypocenter blob 2 to 11 km deep under the central San Diego Bay that is elongate in a northeast direction. First motion focal mechanisms indicate oblique slip (reverse plus left lateral) on northeast striking planes. The 1986 events include an 15 km deep M_L 4.6 strike slip earthquake under the south San Diego Bay. Prior to that event was a three month long swarm of M_L 2.0-3.5 events further west whose epicenters form a northeast trend on strike with the 1985 and 1987 swarms. The 9/87 events were all $M_L<3$. The epicenters form a short, northeast trending, southwest plunging, 5 to 14 km deep lineation just abutting the south edge of the 1985 blob. Focal mechanisms again show oblique slip on northeast striking planes. The 1985 and 1987 earthquakes were in clusters that dip to the southwest yet many of the earthquakes occurred on northeast striking faults. These earthquakes appear to be located on northeast striking faults, similar to those mapped at nearby Point Loma, where those faults intersect the northwest striking, southwest dipping Rose Canyon fault zone. The dip of the earthquake clusters thus reflects the dip of the Rose Canyon fault zone. The 1985 and 1987 clusters occurred at places where no earthquakes had previously been located (within the limits of location accuracy and detection threshold) since at least 1934. The maximum earthquake depths found here (up to 15 km) are much deeper than those found previously, implying a greater fault width and correspondingly larger potential earthquakes.

Elsinore fault zone.

Relocations of several thousand earthquakes between 1981 and 1991 along the Elsinore fault zone identify a fault east of, and parallel to, the Elsinore fault defined by an alignment of hypocenter clusters (Fig. 1). The fault defined by the microseismicity coincides in part with the Earthquake Valley and Agua Tibia faults (EQVAT) as mapped on the state geologic sheets. The hypocenter clusters represent activity

concentrated near fault steps and conjugate fault intersections. Where the EQVAT fault ends to the south and north seismicity shallows and becomes diffuse. These areas mark steps where slip is transferred to and from the EQVAT fault from the Elsinore fault; the steps have prominent topographic expressions. A prominent northeast striking seismicity lineation defines the left lateral Sawtooth Ridge fault near the south end of the EQVAT fault. An M 5.1 event in June 1940 occurred near the intersection of the Sawtooth Ridge feature and the Elsinore fault, the largest event in the Elsinore fault zone since 1910. Aftershocks paralleled the Sawtooth Ridge fault. Currently, both the Elsinore and the Earthquake Valley-Agua Tibia faults are active. The three-dimensional velocity model images relatively slow velocities between the Elsinore and EQVAT faults, interpreted as a component of down to the east motion across the primarily strike slip Elsinore fault.

Report published:

Magistrale, H. (1992). Relocation of 1983-1990 earthquakes near San Diego, California (abstr.), *Seismol. Res. Lett.*, **63**, p.68.

Figure 1. Relocated earthquakes along the Elsinore fault zone. Newly defined EQVAT fault shown by heavy line. Symbol size scaled to earthquake magnitude.

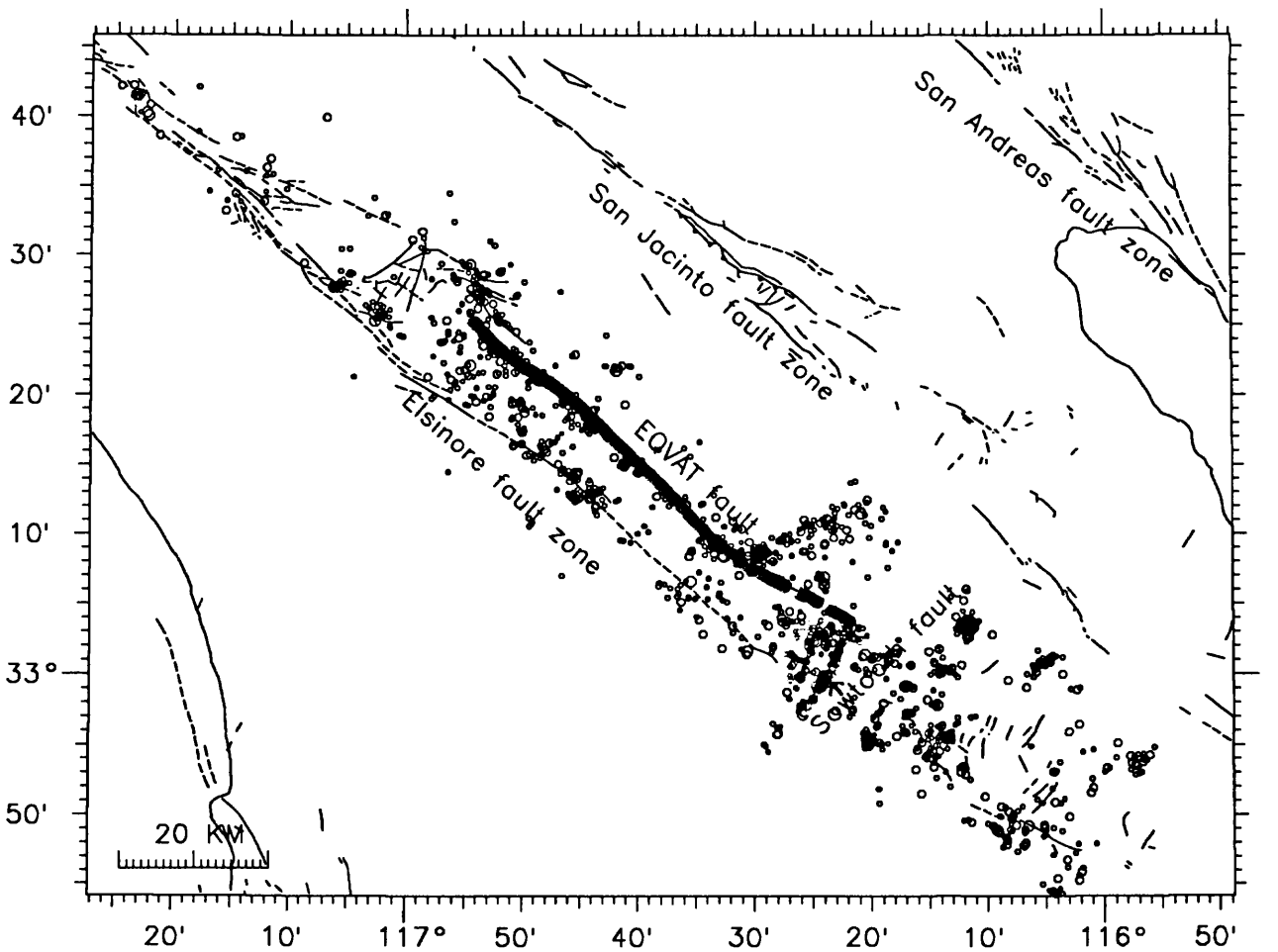

Instrumentation to Improve the Washington Regional Seismograph Network
1434-92-G-2195 S.D. Malone and R.S. Crosson, P.I.s

Geophysics Program
University of Washington
Seattle, WA 98195
(206) 543-8020
March 1, 1992 - Sept. 30, 1992

Introduction

This contract is for the purchase and installation of four new, high quality broad-band digital seismograph stations as an addition to the Washington Regional Seismograph Network. It also includes funding for the development of the data acquisition process and integration of these data into the routine data collection and analysis procedures. In addition to the four stations funded under this contract we have a prototype station already in hand, and will also incorporate data from the USNSN station at Newport, WA. On completion 18 months from now, there will be 7 high quality seismograph stations operating in the Pacific Northwest (5- operated by us, one by USNSN, NEW and one by the GSN, COR).

Progress

Development efforts have proceded on schedule. Funding for this project was received on March 1, 1992 and equipment was ordered as soon as possible. Three of the four new data loggers were received in October; the seismometers have not yet been delivered.

Our prototype broad-band station was operated in a test configuration in Seattle for several months and then moved to Longmire (LON) near Mount Rainier in May, where it has been operating on the same pier as the DWWSSN station. Sites for three of the four new stations have been selected and permits obtained (Liberty- LIB, Tolt Resevoir- TOT, Satsop- SAT). Selection of the final site is still to be done; it will be near Port Townsend, WA. Site construction, including power and telephone service, has been completed for the site near Liberty, WA. Figure 1 shows the current analog telemetry network configuration as well as the existing and planned new broad-band station locations.

We adapted the *GOPHER* dial-up system from IRIS to access our new broad-band stations and have now recovered data from 68 events recorded on our prototype station at LON. In other software development, we are developing the capability to archive our trace data in SEED format so that it can be all be stored at the IRIS Data Management Center and be easily available to anyone, along with the rest of the global data. We have developed a SEED writer for trace data from our analog telemetry network, and tested it at the IRIS DMC.

We have completed all conduit, antenna mounting hardware, and power access requirements for installation of the VSAT communications link from Seattle to the USNSN; through which we plan to receive data from the USNSN station at Newport, WA (NEW), and also possibly other stations they will install later. We await installation of satellite communications by the USGS, initially planned for June, 1991.

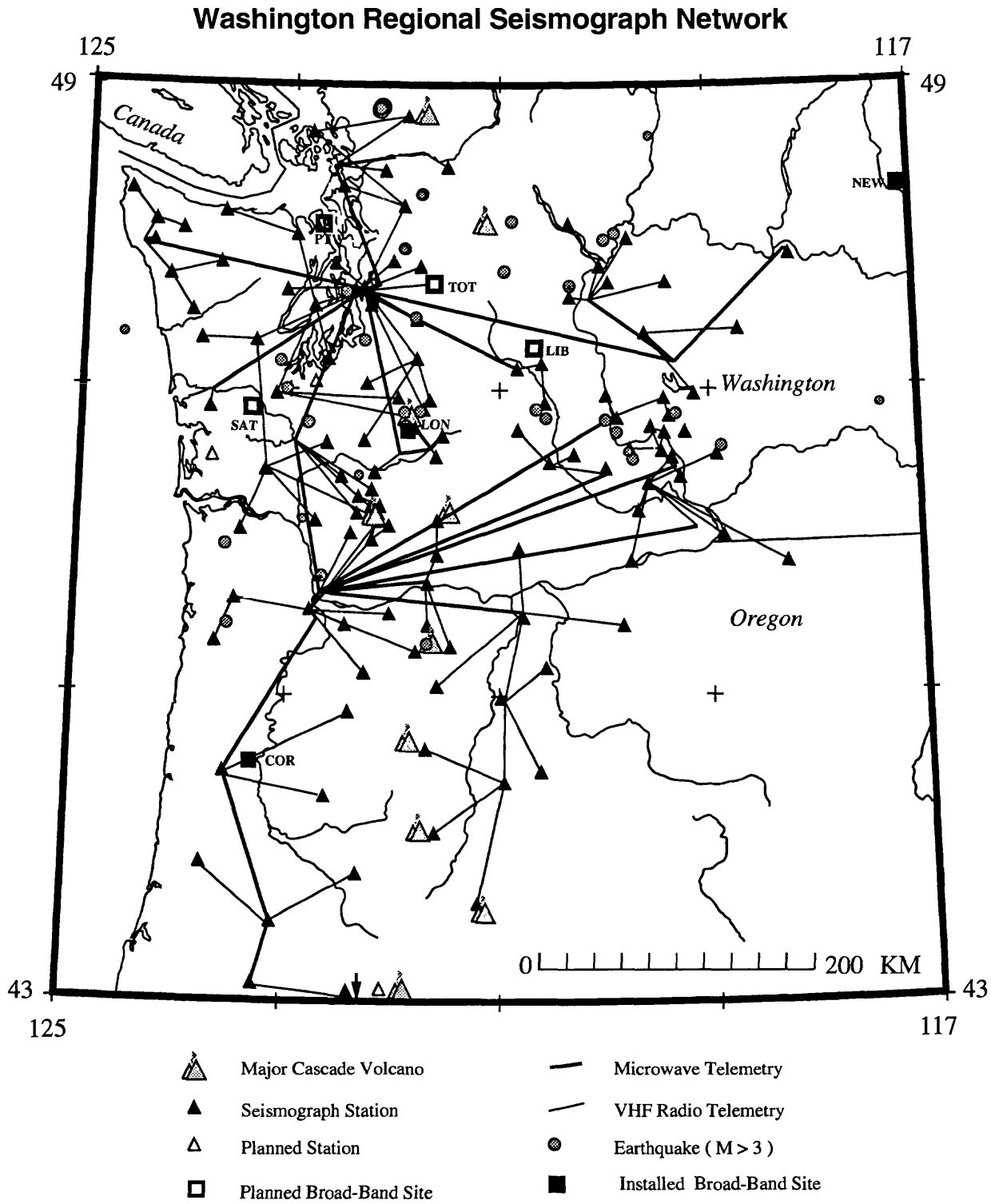

Figure 1. Map showing WRSN stations, telemetry and state of new broad-band stations

QUANTITATIVE ANALYSIS OF LANDFORMS: A WAY TO DELINEATE ACTIVE TECTONIC STRUCTURES

Agreement No. 1493-92-G-2229

Larry Mayer
Department of Geology
Miami University
Oxford, Ohio 45056

(513) 529-3241

ABSTRACT

Analysis of landforms in the New Madrid seismic zone using digital elevation data at 30 degree-, 3 degree-resolutions, and digitized planforms, indicates that several topographic features exist, with different wavelengths, that may be related to processes other than simple fluvial erosion. Landform analysis is based on image processing of digital elevation data within the context of geomorphological hypothesis testing, and the study of river planforms. These studies indicate that surface deformation of the scale and style of the Tiptonville dome may exist in several places in the region. Larger wavelength features are inferred to exist as well. Although theses larger features, are at present, defined only by their apparent effects on river pattern, they do coincide with a significant topographic blocking boundary that extends from Newport southeastward past the southern tip of Crowley's Ridge and across the embayment.

INTRODUCTION

Quantitative studies of topography are being carried out using digital elevation data, digitized representations of fluvial features such as river planforms, slope breaks, and valley morphometry, and SAR and SPOT images. The primary purpose of these studies is the delineation of tectonic features with topographic expression in the New Madrid area. By means of quantitative analysis of landforms we hope to

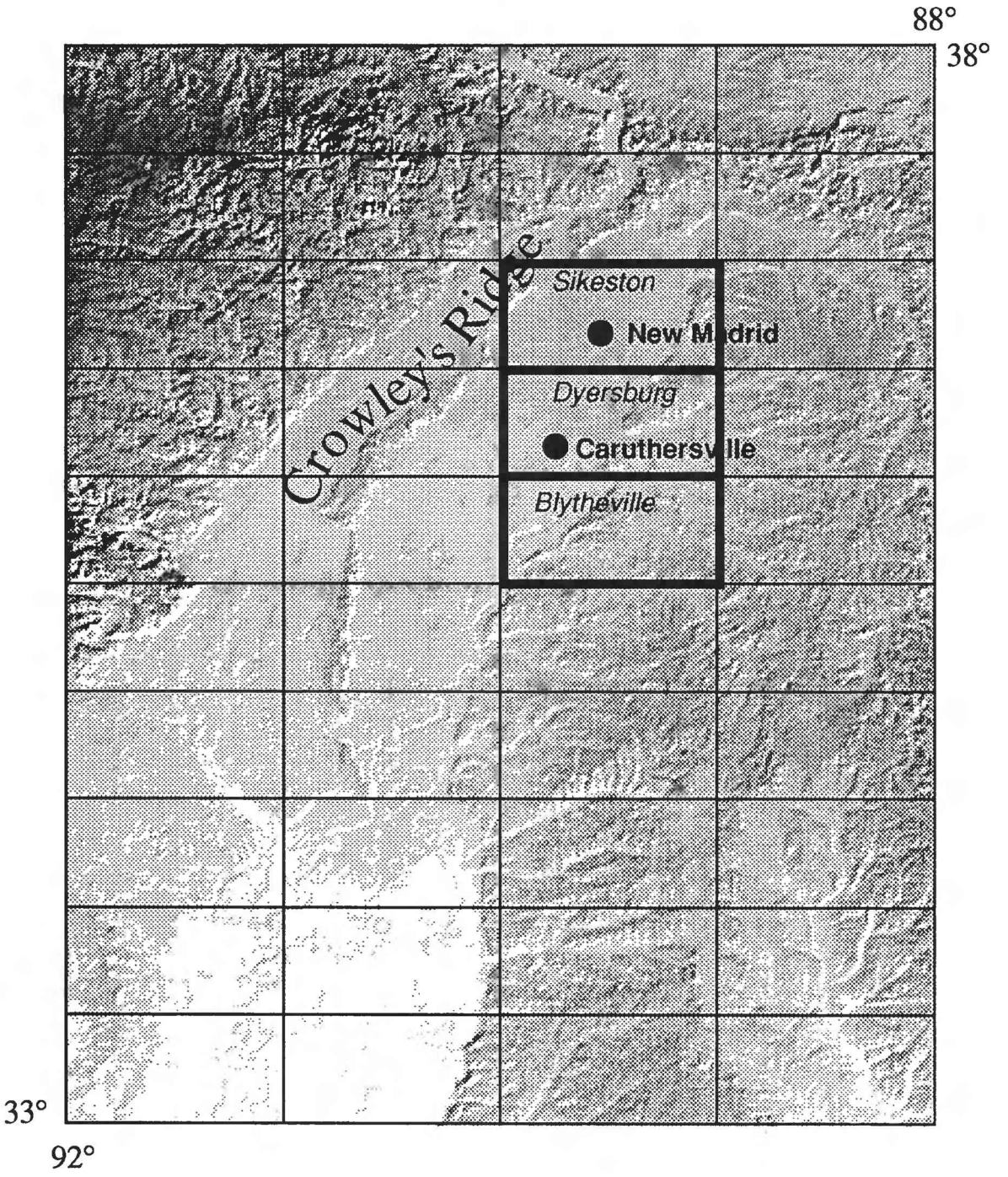

Figure 1. Digital topographic map image from 30 arc-second data showing features cited in text and location of individual 3 arc-second quadrangles. This image was produced with a simple spatial convolution.

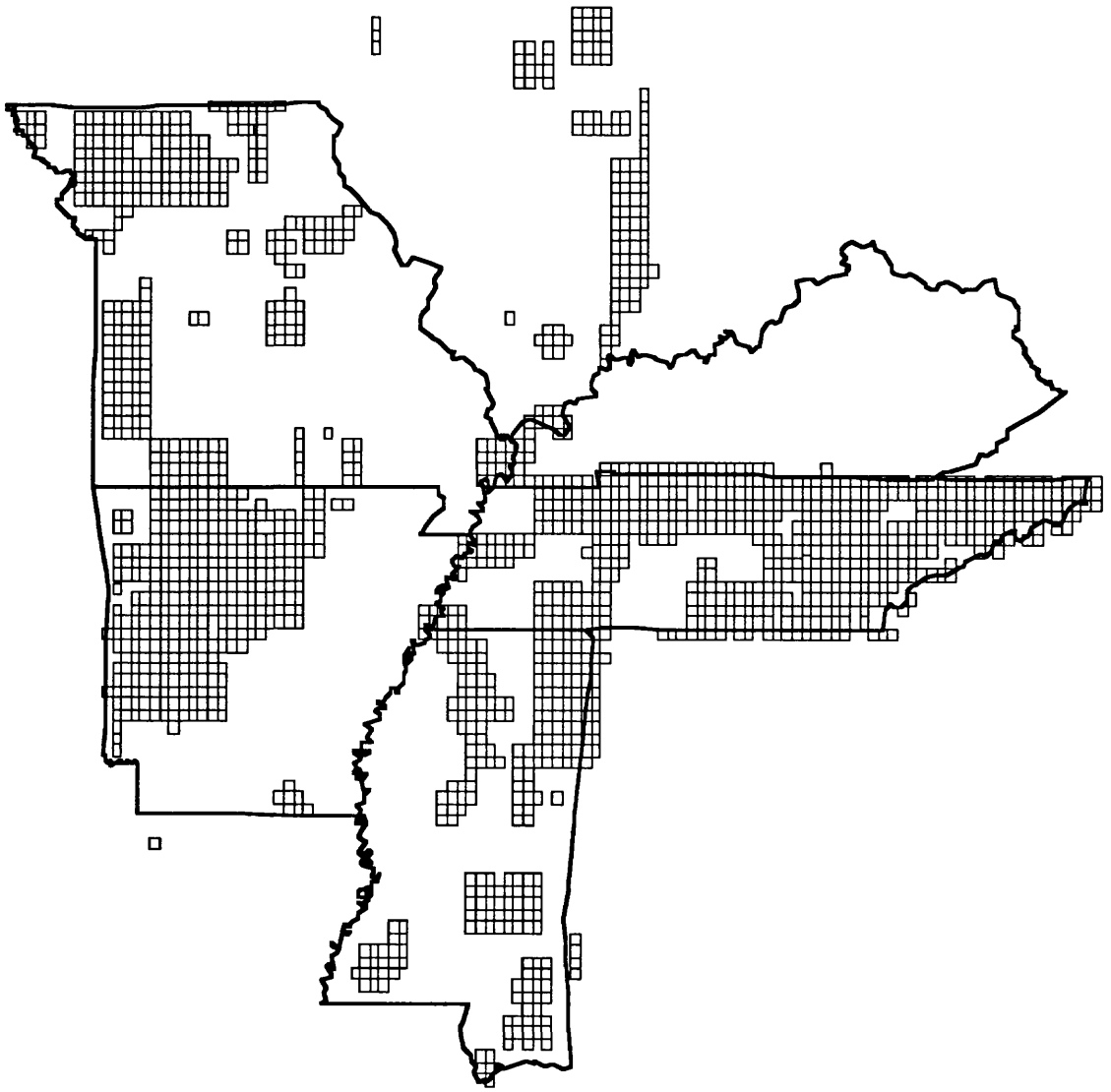

Figure 2. Index map to 7.5 DEMs for the region.

better document the history and geometry of strain and to identify potential seismic sources.

The main assumption of topographic studies is that tectonic strain deforms the surface. Surface deformation may or may not be associated with earthquakes. The challenge to the geomorphologist is the recognition of a deformed landform despite its presence in a dynamic surface environment. Another assumption is that the expression of topographic deformation has a finite survival time, which is dependent on the particular surface environment. For example, a fault scarp can be reasonably easy to recognize on a hillslope or piedmont, but it is rapidly altered by the action of a river. On the other hand a dynamic environment, one where new geomorphic surfaces are frequently generated, also provides morphostratigraphic data that can be helpful in identifying surface deformation.

Surface deformation occurs at different wavelengths. At one end of the spectrum are short wavelength features such as fault scarps that distribute vertical or horizontal strain over a very short distance measured perpendicular to strike. At the other end of the spectrum are long wavelength features such as uplifts or depressions that have vertical displacements distributed along great distances. The detection of both short and long wavelength surface deformation is sometimes directly observable and sometimes can only be inferred. The definition of surface deformation as a phenomenon with a specific wavelength or amplitude permits quantitative treatment of topographic data using digital image processing in the spatial domain.

DIGITAL ELEVATION DATA AND DIGITIZED PLANFORMS

Digital data were obtained for the study area to maximize geographic coverage and spatial resolution. The raw data tapes are downloaded onto a DEC Vax minicomputer and then transferred to the Geomorphology Computer Laboratory's Macintosh LAN using the file-transfer protocol. Locally, the data are stored on either a Ricoh optical (250M) or Bernoulli (90M) drive. Computer programs were written to convert the USGS digital elevation data sets into ASCII numeric files that could be analyzed using statistical and imaging software. The data coverage consists of both 30 arc-second and 3 arc second coverage (Fig. 1). Forty separate 1 degree by 30 minute quadrangles have been processed. The geographic coverage for 7.5 minute DEMs is very spotty (Figure 2).

The planforms of streams and the loess bluffs were obtained by digitizing these features from 1:250,000 scale and

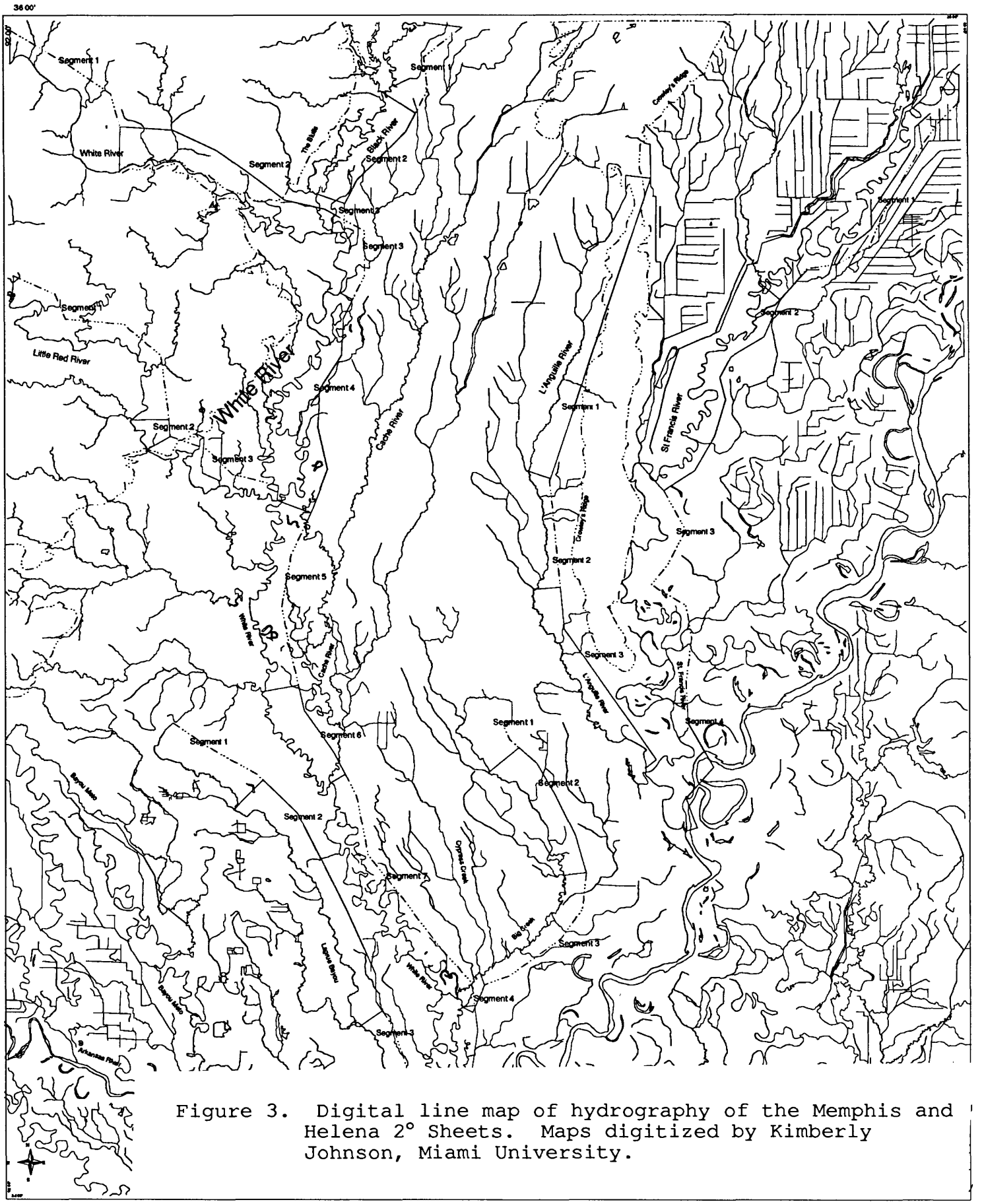

Figure 3. Digital line map of hydrography of the Memphis and Helena 2° Sheets. Maps digitized by Kimberly Johnson, Miami University.

1:24,000 scale topographic maps respectively using a digitizing board with a 1000 lines/inch resolution. Digitized stream networks taken from the Memphis and Helena 1:250,000 scale maps are shown on Figure 3. We are now in the process of downloading and converting hydrological features from the USGS in Golden and converting them to a locally compatible format.

IMAGING OF DIGITAL ELEVATION DATA

Imaging of digital elevation data is based on standard processing techniques within the contexts of geomorphological hypothesis testing. For example, to identify areas that are anomalously high in elevation, a density slice is used. In the present context, the elevation of the Mississippi river floodplain and meander belt are morphostratigraphic data. The lower part of the density slice is set to river floodplain level. The upper part of the density slice is set at progressively higher elevations in order to identify maximum local departure from river level. This technique clearly identifies known tectonic uplifts such as the Tiptonville Dome. The usefulness of using density slicing and thresholding of digital elevation data is that it addresses a simple geomorphic hypothesis. Russ (1982; especially Figs. 4,7) used essentially the same hypothesis when he documented the relationships between the Lake County uplift, including the Tiptonville dome, to the channel levees of the Mississippi. For the same area as Russ (1982) discussed, the digital image shows Tiptonville dome and Reelfoot Lake clearly (Fig. 4).

Density slicing reveals interesting dome-like features in many places within the region shown on Figure 1. Low features are also identified. Within the area corresponding to the Dyersburg 1:100,000 scale quadrangle are two pertinent features (Fig. 5). The first informally referred to as the Caruthersville anomaly appears to be a high area that has been trimmed by the Mississippi. On the other side of the river, towards the bluffs is a low area which is informally referred to as the Dyersburg low. Both of these anomalies are, like the Tiptonville Dome, difficult to explain with fluvial processes alone.

Farther south, within the area defined as the Blytheville 1:100,000 scale quadrangle are a pair of anomalies adjacent to one another and with opposite sense of vertical strain (Fig. 5). These topographic features, like the ones to the north, are comparable in size to the Tiptonville Dome. They also are all loosely paired in the sense that a positive anomaly (higher than expected) is closely associated geographically with a negative anomaly (lower than expected).

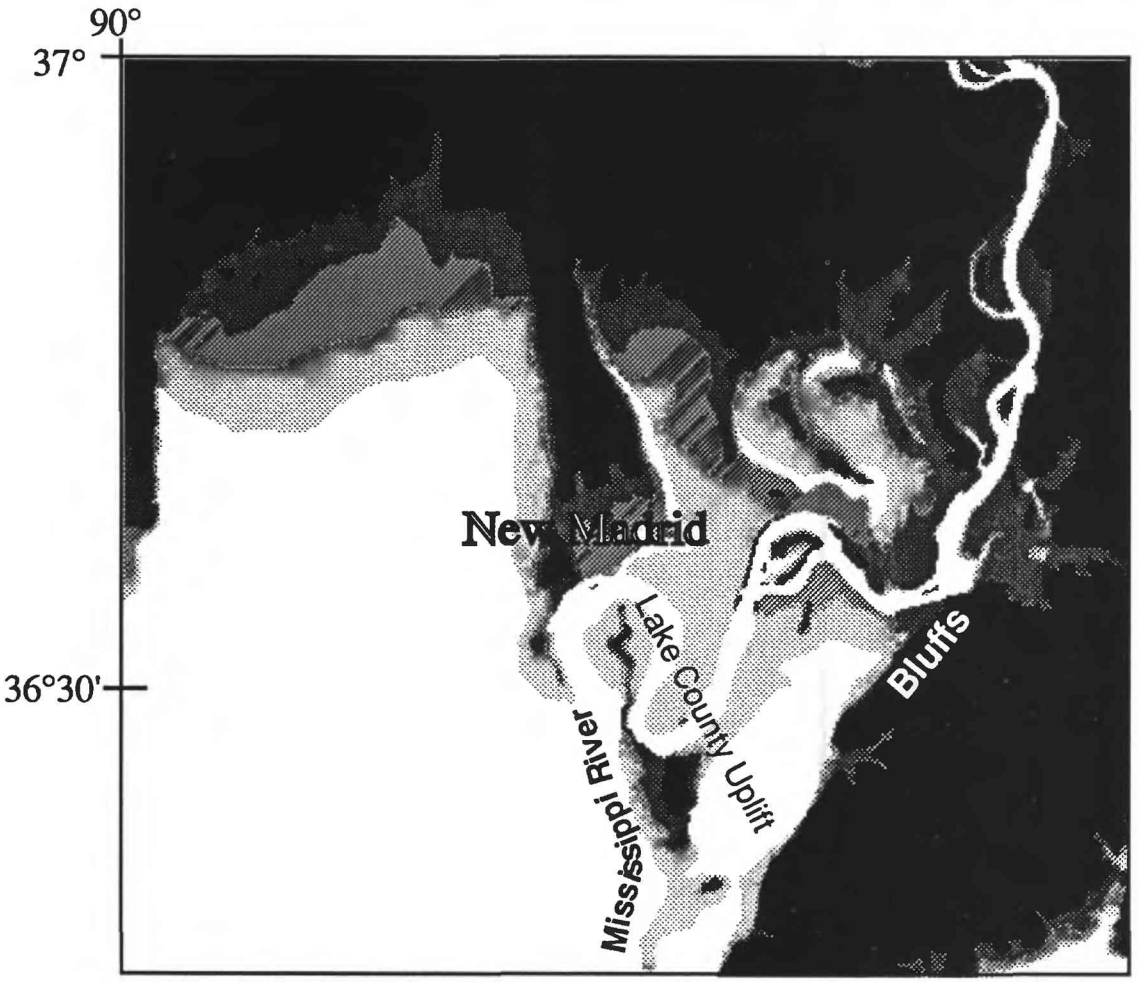

Figure 4. Digital topographic map image from 3 arc-second data showing the areas corresponding to the Sikeston 1:100,000 scale map and portion of Blytheville map. The Tiptonville dome is easiliy recognized and the broader boundary of the Lake County Uplift identifyable as a higher area relative to the that on the west of Sikeston Ridge.

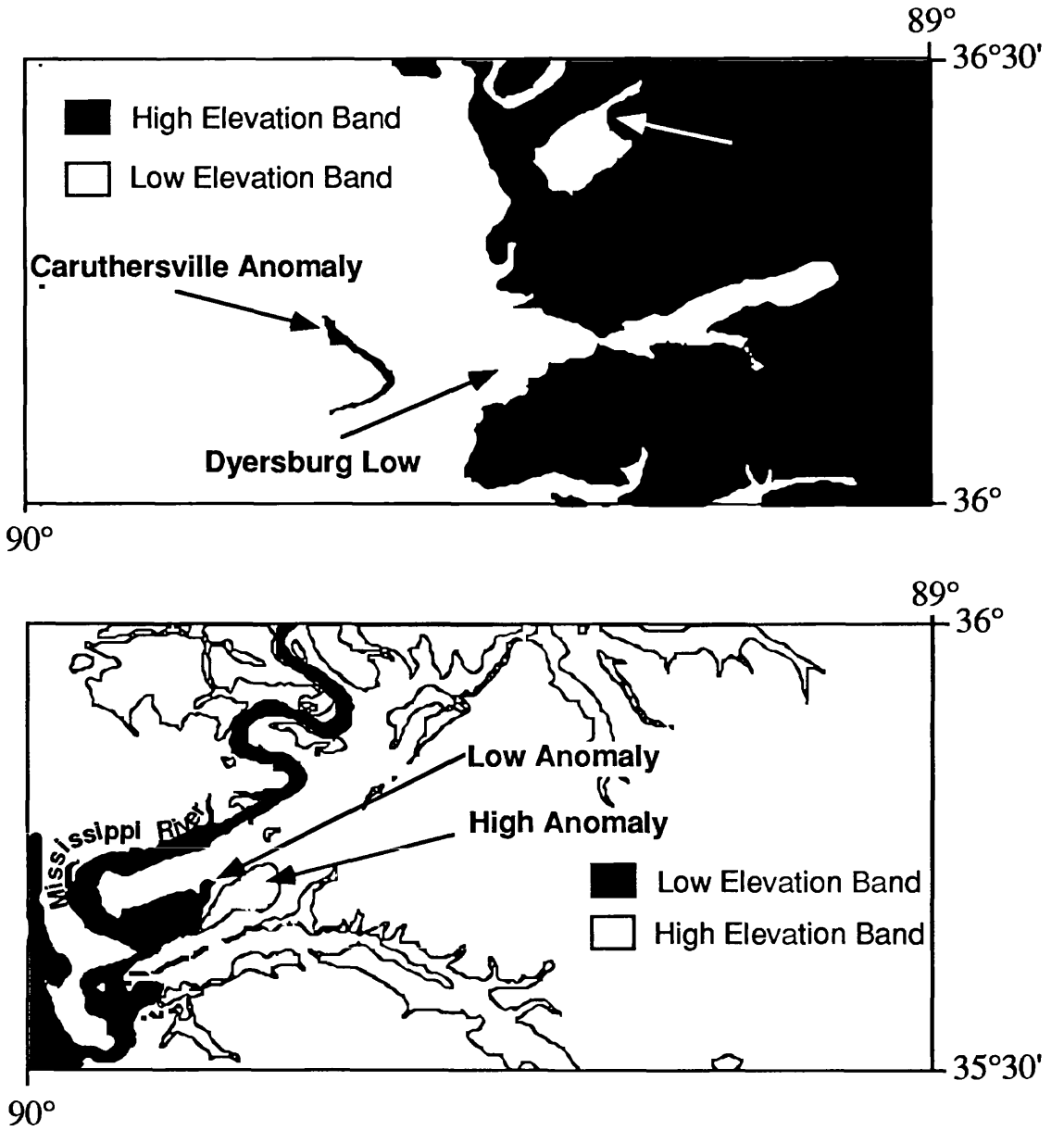

Figure 5. Digital topographic map images from 3 arc-second data showing the areas corresponding to the Dyersburg 1:100,000 scale map (TOP) and Blytheville 1:100,000 scale map (BOTTOM). Anomalous topographic features analogous to the Tiptonville dome are found in each area.

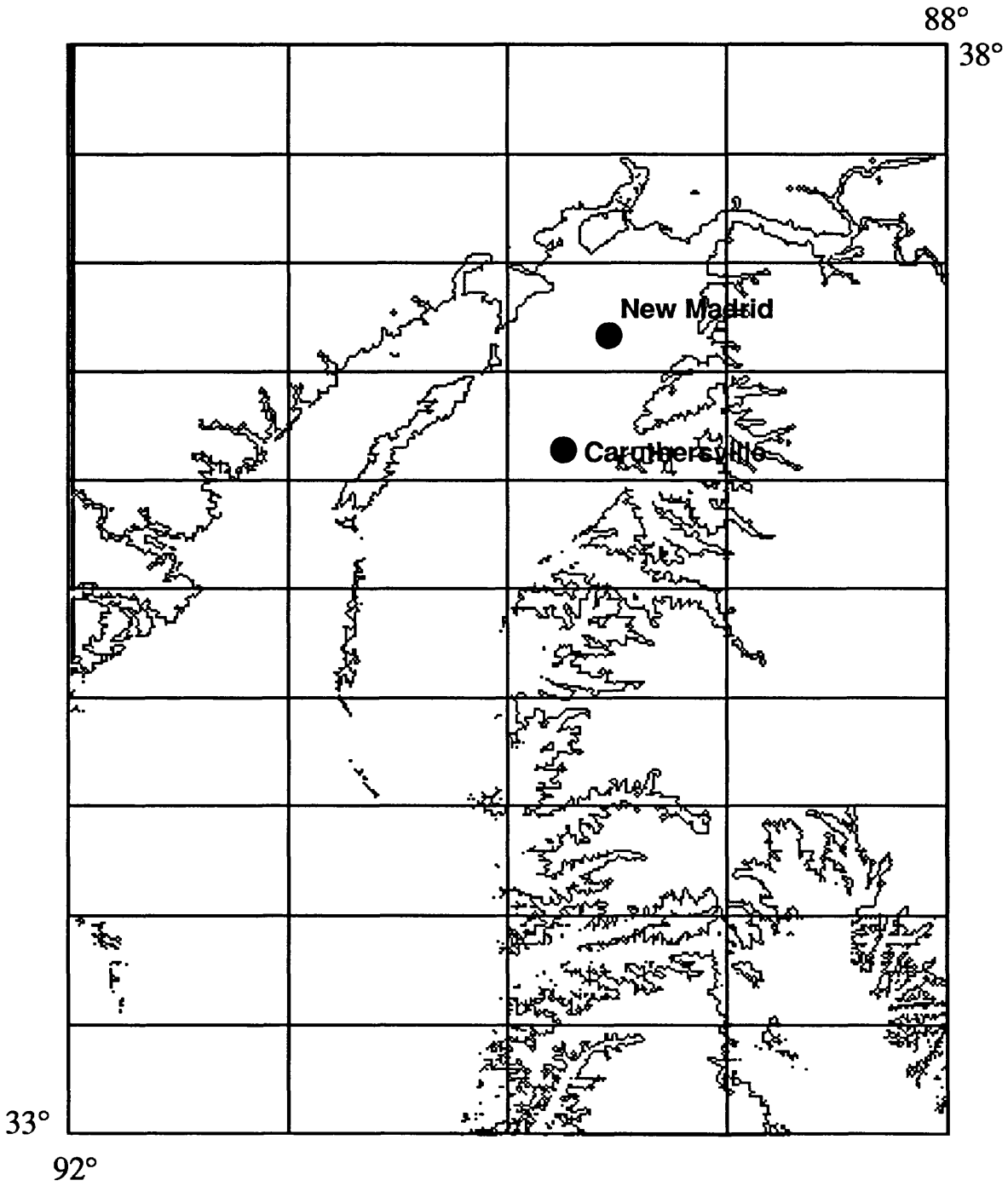

Figure 6. Digital topographic map image from 30 arc-second data showing high western boundary of the Mississippi embayment relative to the eastern boundary. This image was produced by thresholding and boundary tracing.

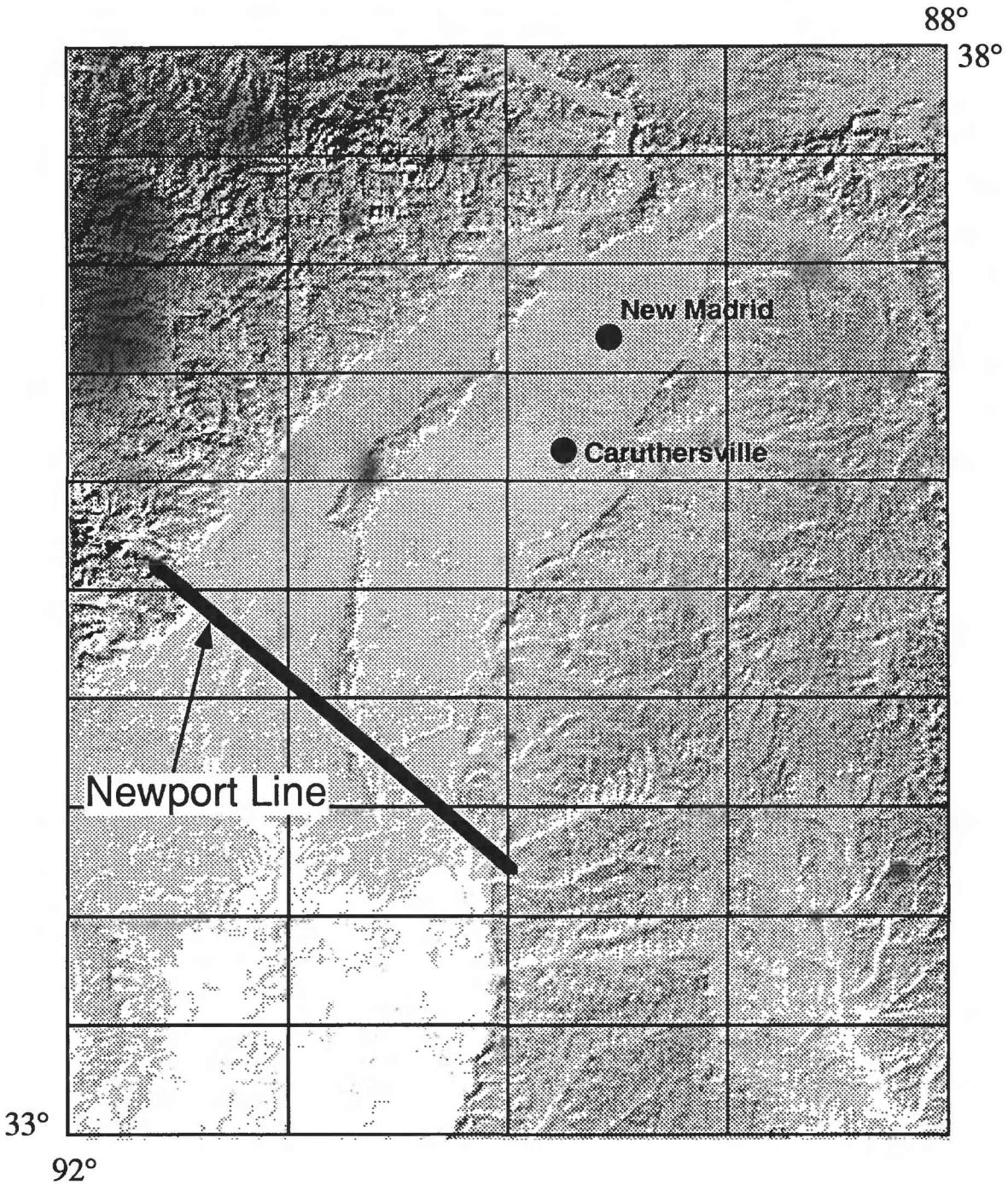

Figure 7. Digital topographic map image from 30 arc-second data showing location of the Newport line. On this image it appears as a topographic lineament.

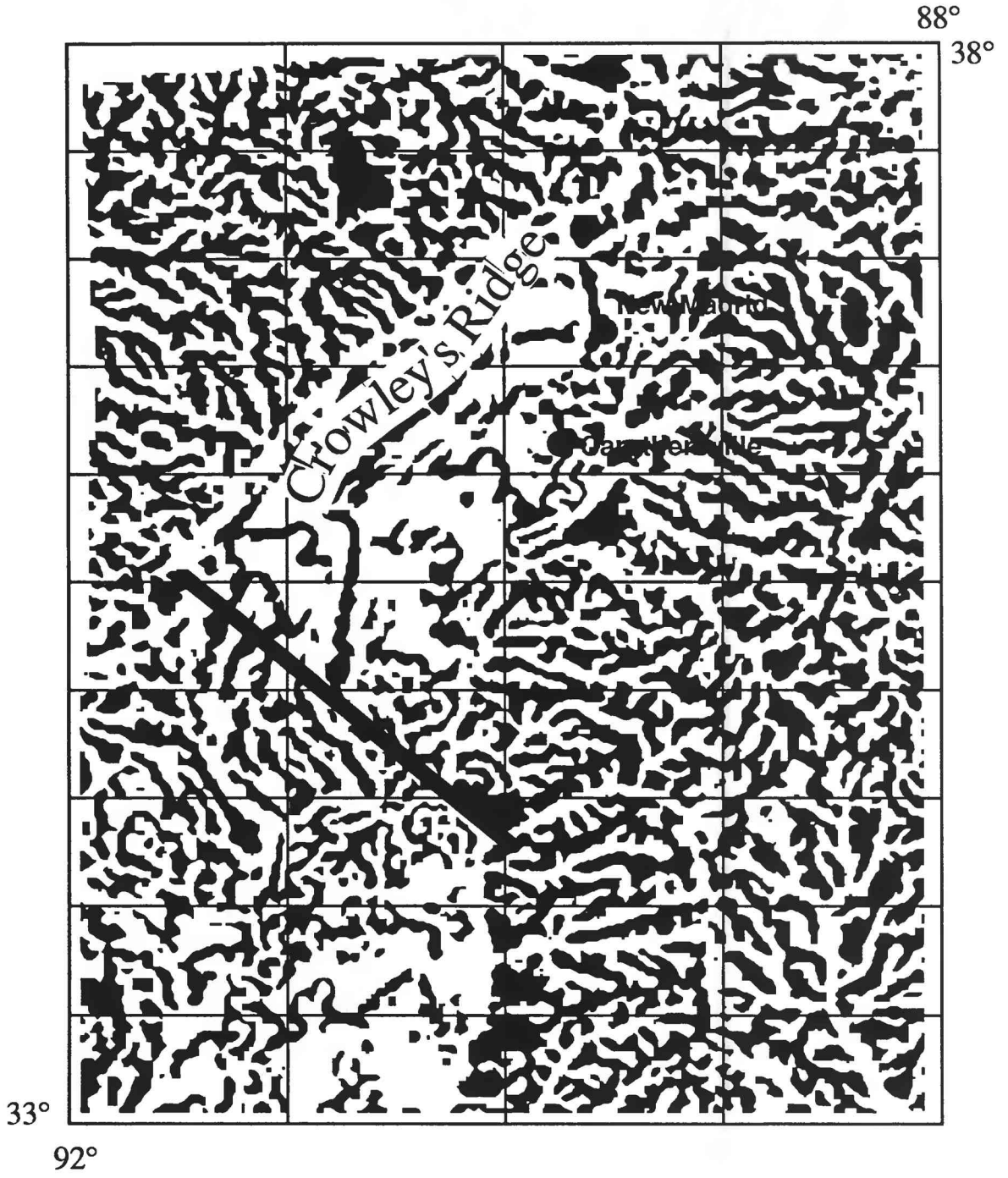

Figure 8. Digital elevation data processed from 30 arc-second files showing topographic blocking, or regionalized patterns of relief. Here the Newport line appears as a boundary separating distinct block textures.

Thresholding and edge detection is a convenient method to identify contours on a digital elevation image. A regional perspective using this view clearly shows that the western side of the embayment is much higher that the eastern side and that a horizontal slice through both regions traces a highly dissected eastern embayment boundary relative to the west (Fig. 6). The significance of the topographic difference is not yet clear, however, it becomes particularly intriguing towards the north where the Mississippi river itself skirts the boundary between these two distinct physiographic regions.

Even farther to the south and within the embayment there several topographic lines of evidence suggesting active control of surface patterns. In particular is a linear feature, here informally referred to as the Newport line, is a boundary between the narrower upper and wider lower Mississippi embayments. The Newport line appears to be a lineament on the digital images that emphasize short wavelength topography (Fig. 7).

Topographic blocking refers to the notion that the texture of topography and the relative scaling of topographic elements is related to the scale and perhaps depth of the forces generating topography. Rigorous methods to delineate blocking have not been proposed, however blocks can be described in ways that are reproducible. For example, since blocks represent regionalizations of topography, image smoothing at larger and larger scales could delineate a pattern related to blocking. A box filter whose dimensions represent the spatial extent of the smoothing function was used. The digital elevation data were first passed through an 18 by 18 pixel smoothing box filter and then thresholded until a stable block pattern appeared. That block pattern is shown on Figure 8. The Newport line appears to be a line separating distinct topographic textures.

Imaging of the loess bluffs on the eastern side of the Mississippi river also indicates that dome-like topographic features may exist there as well. These features are recorded as bluff edges where the drainage flows eastward away from the Mississippi river. Delineation of these features is ongoing.

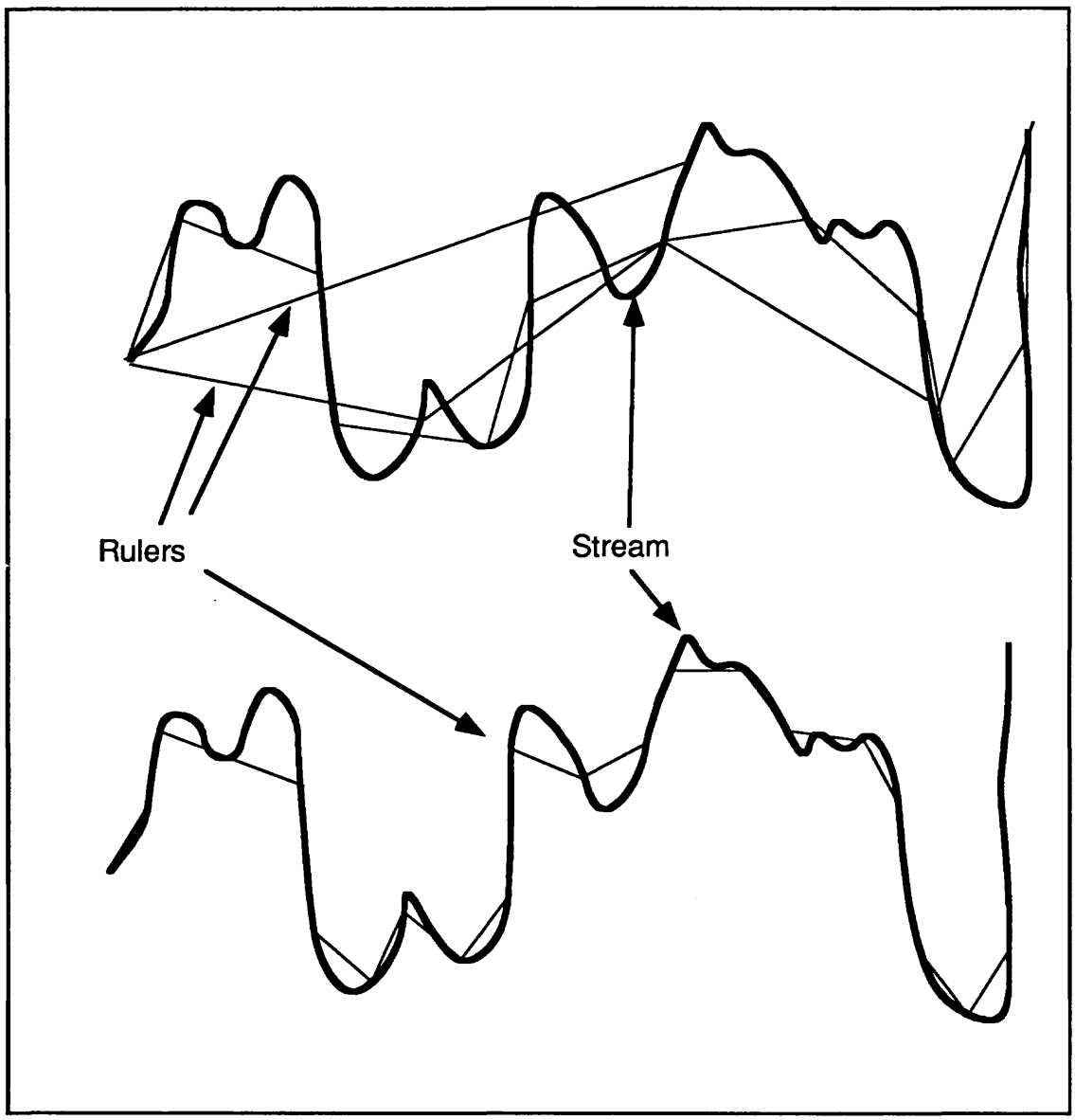

Figure 9. Cartoon illustrating "Richardson Analysis". The rulers used to measure stream length are systematically shortened to determine the rate of apparent increase in length as a function of scale. This technique can be used to identify the changes in the scale of wavelength patterns and to quantify river sinusosity.

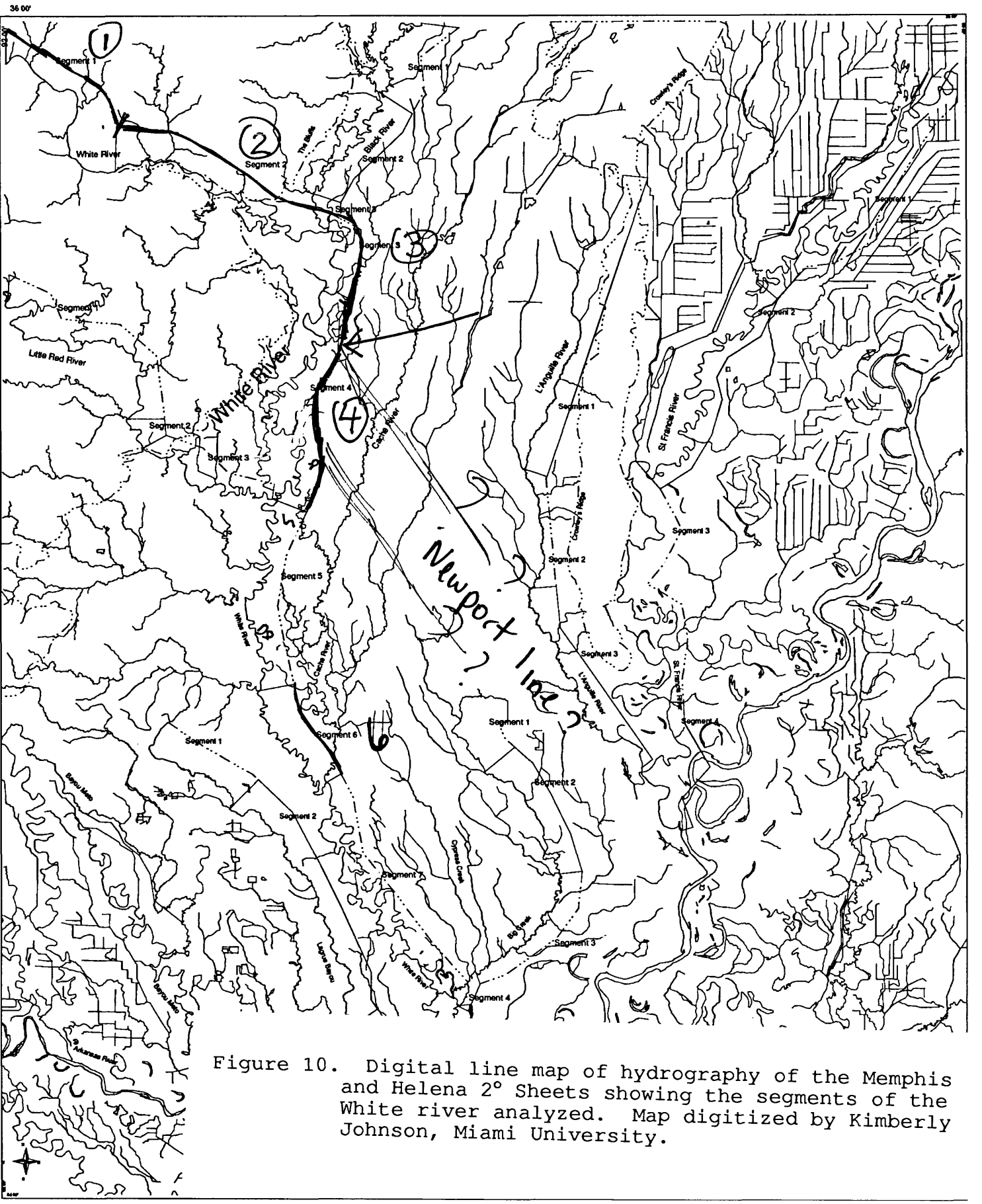

Figure 10. Digital line map of hydrography of the Memphis and Helena 2° Sheets showing the segments of the White river analyzed. Map digitized by Kimberly Johnson, Miami University.

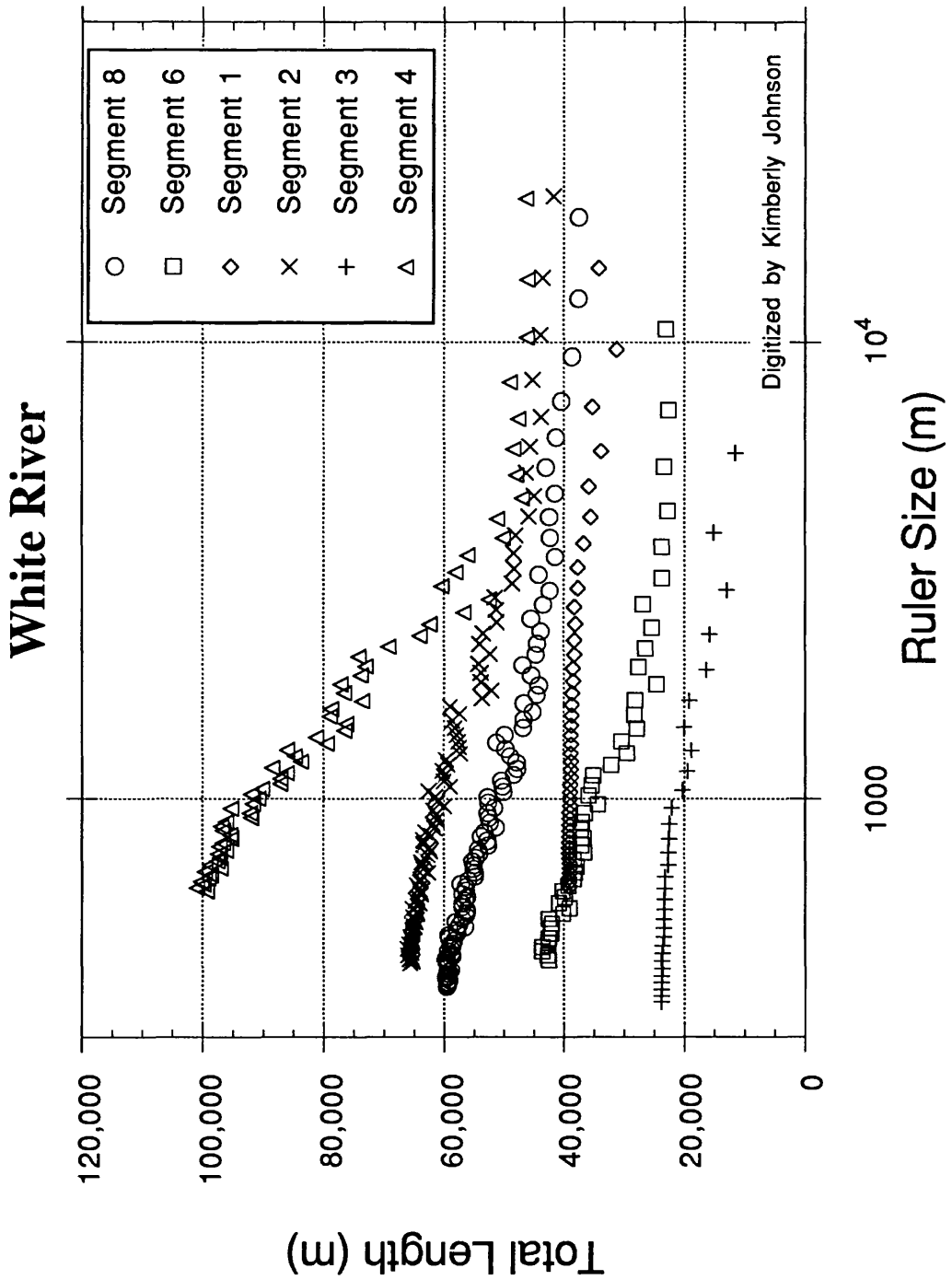

Figure 11. Richardson analysis of the meandering characteristics of the White River. Data that have little change with ruler size are relatively straight features. Steeply sloping patterns indicate rapid increase in sinuosity at that particular scale. Stream reach 4 has the steepest slope and also crosses the Newport line.

ANALYSIS OF PLANFORMS

River planforms that meander can adjust to active deformation of their channels by altering the sinuosity of the channel. Changes in sinuosity compensate for changes in channel slope. However a single river may have a variable sinuosity due to non-tectonic factors such as dominant sediment load. The wavelength and scale of their meander bends may provide a deeper insight to distinguishing between tectonic and non-tectonic changes in sinuosity. In any event, the coincidence of river pattern changes with other topographic features should be sought in order to further confirm the nature of the feature.

Richardson analysis is a technique based on the notion of statistical self-similarity which allows one to quantify how a planform is changing in a way more meaningful than simple sinousity. Basically the technique uses a systematically changed scale to calculate a length of an object thereby measuring the scale at which variation occurs (Fig. 9). It essentially describes the scale dependent sinuosity if a river. A useful demonstration is given using the White River, which drains into the Mississippi embayment from the west (Fig. 10). The White River also crosses the Newport line. Figure 11 is a summary of its scale dependent sinuosity. Note how one reach of the White River in particular is very different from the rest in that the rate of its increase in sinousity with decreasing scale is very rapid (Fig. 11). This reach is the reach which crosses the Newport line. Similar analyses are underway for numerous other meandering streams in the area.

REFERENCE

Russ, D.P., 1982, Style and significance of surface deformation in the vicinity of New Madrid, Missouri: in Makeown, F.A. and Pakiser, L.C., editors, Investigations of the New Madrid, Missouri, earthquake region, U. S. Geological Survey, Professional Paper 1236, p. 95-114.

REPORTS

Mayer, Larry, Tectonic geomorphology of the New Madrid seismic zone based on imaging of digital topographic data: Geological Society of America Abstracts with Programs, submitted for publication in 1993.

Mayer, Larry, Topographic Analysis for tectonic geomorphology using digital image processing of elevation data from the Mississippi Embayment and adjacent areas: Geological Society of America Abstracts with Programs, submitted for publication in 1993.

Mayer, Larry, Rates and scales of topographic change in response to tectonic perturbations as suggested from computer simulation using DEMs: Third International Conference on Geomorphology, submitted for publication in 1993.

Johnson, K.A., and Mayer, Larry, Analysis of river planforms in the New Madrid region and possible relations to tectonic warping across the loess bluffs and within the meander belt of the Mississippi river: Geological Society of America Abstracts with Programs, submitted for publication in 1993.

Church, Amy, and Mayer, Larry, Morphologic characteristics of upland bluffs east and west of Crowley's ridge in the New Madrid area: Geological Society of America Abstracts with Programs, submitted for publication in 1993.

Assessing the Paleoseismic Activity of the Brigham City Segment, Wasatch Fault Zone, Utah; Probable Site of the Next Major Earthquake on the Wasatch Front?

Award No. 1434-92-G-2205

James P. McCalpin
Department of Geology
Utah State University
Logan, UT 84322-4505
303-586-3217

Steven L. Forman
Byrd Polar Research Institute
The University of Ohio
1090 Carmack Rd.
Columbus, OH 43210-1002
614-292-6085

Investigations

During August, 1992, we excavated 9 backhoe trenches across multiple fault scarps of the Wasatch fault zone (WFZ) at Brigham City, Utah. These seven parallel scarps (Fig. 1) displace the surface of a delta built into Lake Bonneville during the occupation of the Provo Shoreline (ca. 13-14 ka). The scarps potentially record all paleoseismic events of the WFZ in the last 13-14 ka, a time span which is twice as long as that covered by current paleoseismic evidence (Personius, 1991). The Brigham City segment is thought to be unique for two reasons: 1) it has the longest elapsed time since surface rupture of any of the 5 Holocene segments of the WFZ, and 2) paleoseismic events may have occurred in closely-spaced pairs separated by longer time intervals (Nishenko and Schwartz, 1990). The objective of trenching is to date at least 6-10 paleoearthquakes in the last 13-14 ka, refine recurrence intervals, and confirm if paired clustering has occurred more than once.

Methods

Four trenches (1-4 in Fig. 1) were excavated on July 1, 1992. These trenches were logged between July 1 and July 15, but little datable material was found. Accordingly, a second round of trenching occurred on July 16, when trenches 5 through 9 (Fig. 1) were excavated. Total trench length is now about 900 feet. Four radiocarbon samples were collected during logging of the second set of trenches from July 29-Aug. 7, 1992. These numerical ages help to constrain the ages of faulting events on several of the seven scarps (Fig. 2).

Because organic material was scarce, but dating events is critical to project goals, we are using two other dating methods to control event timing. First, detailed soil profile sampling was performed by Dr. Margaret Berry, Southern Illinois University, to

characterize the soil catena relationships on fault scarps and fluvial scarps. Comparison of soil development on fault scarps with soils on dated stable geomorphic surfaces may yield a first approximation of the ages of latest faulting. Second, eight samples for luminescence dating were collected from four trenches on Sept. 25-26, 1992. Some of these samples may be subjected to optically-stimulated luminescence (OSL) dating if thermoluminescence (TL) dating reveals a large component of relict signal.

Results

1) Scarps C and H are not underlain by faults. Trenches 1 and 8 on scarp C both reveal unfaulted deltaic topset beds extending across the scarp, overlain by a thick, monolithic colluvial wedge. The soil developed on this wedge is somewhat better developed than the soil on the Provo delta surface, indicating that the scarp was formed at about the same time as the delta. Personius (pers. comm., 1992) suggests that this scarp may be a fluvial scarp, which formed by lateral ersoion when the delta surface was active. A similar fluvial scarp exists on the delta about 1 km south (Personius, 1990).

Scarp H, at least at the location of trench 6, was formed about 13,010$\pm$460 yr B.P. Immediately afterward it was buried by a landslide (cls on Fig. 1) that fell onto the delta surface. The landslide is clearly not faulted in the trench, nor do the underlying lacustrine sediments appear faulted. Personius (Pers. comm., 1992) speculates that scarp H is a fluvial scarp cut by a small tributary to the NE of trench 6, back when the delta surface was active.

2) The latest event dated in trench 5 (ca. 3420$\pm$60 yr B.P.) is probably the same (latest) event dated by Personius (1991) at 3600$\pm$500 yr B.P. at a site several km to the north. The penultimate event dated by Personius (at 4700$\pm$500 yr B.P.) has not been identified in our trenches.

3) Gravelly delta surfaces are sterile environments in regard to datable carbon. So far, datable carbon has been found only in trenches where a younger unit (such as landslide or alluvial fan) overlies the deltaic gravels. In addition, thick loesses amenable to luminescence dating are absent, even in grabens. Several trenches expose thin (5-10 cm) buried Av soil horizons that are somewhat enriched in silt. These soils are the best targets found so far for luminescence dating (see F numbers on Fig. 2).

Future Work

We anticipate that a third round of trenching may be necessary in spring, 1993. Three target sites have already been identified. The existing trenches will be left open (winter, 1993) until the first round of luminescence samples have been dated.

References

Personius, S.F., 1990, Surficial geologic map of the Brigham City segment and adjacent parts of the Weber and Collinston segments, Wasatch fault zone, Box Elder and Weber Counties, Utah: U.S. Geological Survey Miscellaneous Investigations Map I-1979, scale 1:50,000, with inset at 1:10,000.

Personius, S.F., 1991, Paleoseismic analysis of the Wasatch fault zone at the Brigham City trench site, Brigham City, Utah and Pole Patch trench site, Pleasant View, Utah: Paleoseismology of Utah, vol. 2, Utah Geological and Mineral Survey, Special Studies 76, Salt Lake City, Utah, 39 p.

Nishenko, S.P. and Schwartz, D.P., 1990, Preliminary estimates of large earthquake probabilities along the Wasatch fault zone, Utah: EOS, AGU Transactions, v.71, no 43, p.1448.

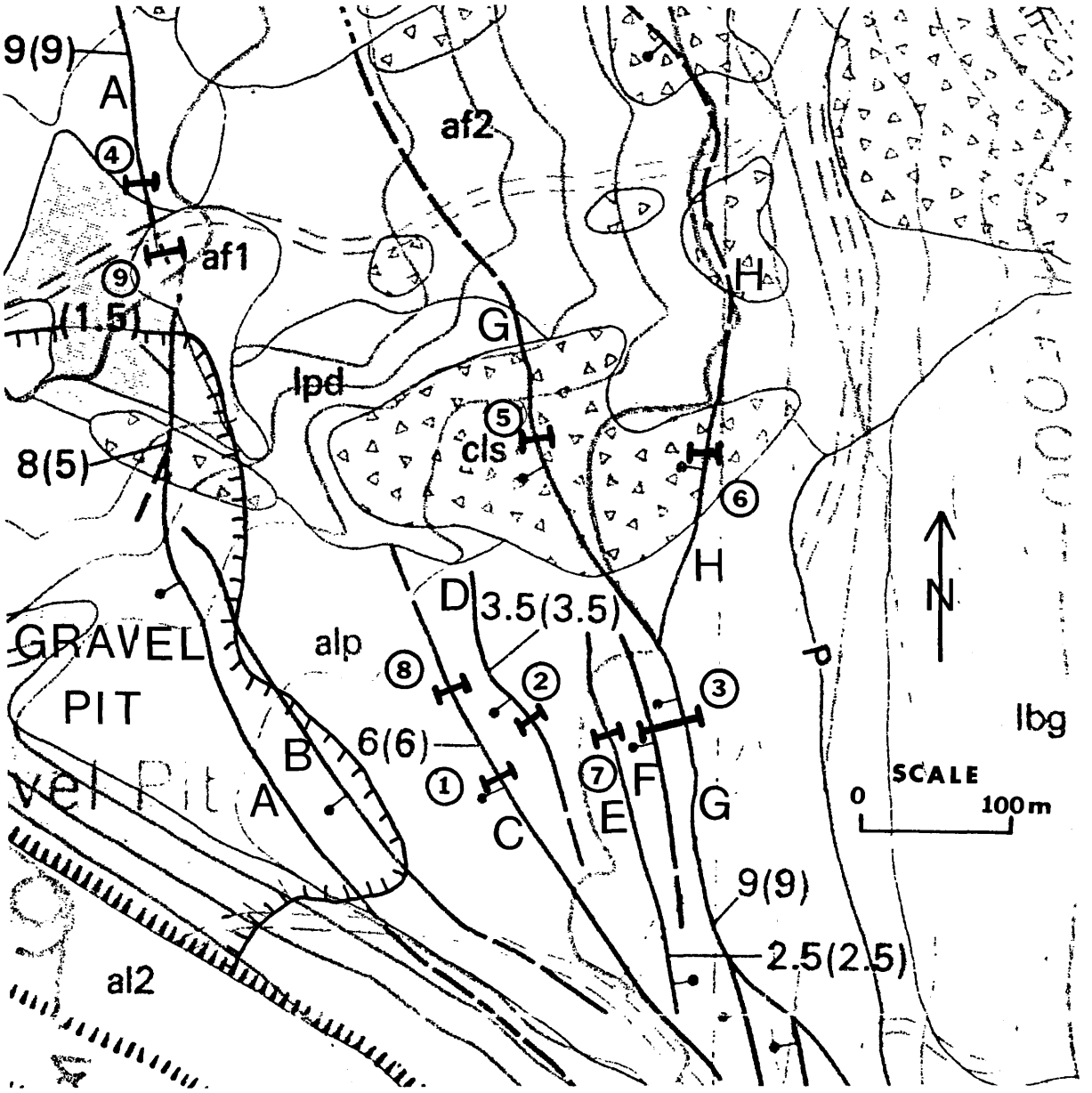

Fig. 1. Surficial geologic map of the Brigham City trench site (from Personius, 1990). Fault scarps are shown by heavy lines, with ball on downthrown side. Map units: alp, Provo topset deltaic beds;lpd, Provo foreset deltaic beds; cls, landslide; af2, older alluvial fan; af1, younger alluvial fan; al2, Holocene alluvium. Large numbers show scarp height, with surface offset in parentheses (both in m). Scarps are lettered from W to E. Trenches are shown by heavy bars, labelled by circled numbers.

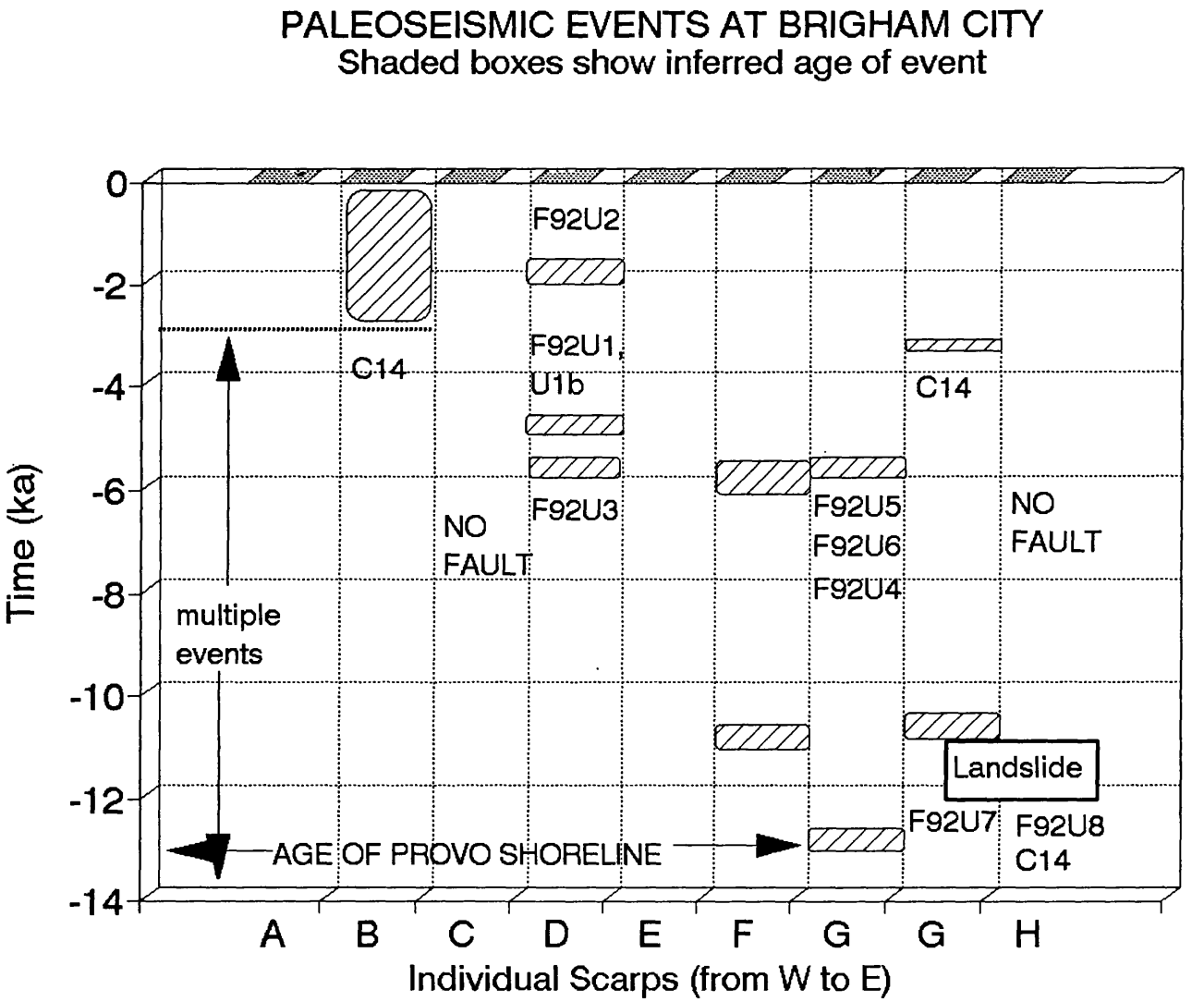

Fig. 2. Time/space diagram showing inferred paleoseismic events at the Brigham City trench site. C14 indicates position of dated radiocarbon sample. The overall time position of events is mainly inferred from degree of soil development, assuming: 1) a Bt horizon takes roughly 5 ka to form, and 2) a Bw horizon takes at least 2 ka to form. Numbers such as F92U2 show inferred age range of thermoluminescence samples that have not yet been dated. This diagram will be updated as TL samples are analyzed during winter, 1993.

ACTIVE MARGIN TECTONICS, PACIFIC NORTHWEST REGION

9910-04492

P. A. McCrory

Branch of Engineering Seismology and Geology
U. S. Geological Survey
345 Middlefield Road, MS 977
Menlo Park, California 94025
(415) 329-5677

Investigations

This research project addresses the problem of how the Cascadia subduction margin of the Pacific Northwest responds tectonically to varying rates of convergence with the objective of understanding whether a history of convergence, if coupled with a history of regional tectonism, can partially explain the timing, style, and rates of regional deformation. This problem can be approached both spatially and temporally in the Pacific Northwest as active convergence rates vary along the margin. Current research utilizes the technique of geohistory modeling to discern the record of tectonism in late Cenozoic rocks and sediments along the southern Washington margin, along with more traditional geologic techniques to quantify fault movement and tilting of strata.

Although current seismic activity is low along the Cascadia margin, geodetic data indicates interseismic strain accumulation reflecting compression between the Juan de Fuca and North American plates and the Holocene paleoseismic record in the Pacific Northwest reveals cycles of episodic large earthquakes and coseismic downwarping of coastal marshes. Upper Cenozoic rocks and sediments in this region also record a history of intense and episodic tectonism that reflects convergence between the Juan de Fuca and North American plates. Field investigations in coastal Washington have identified several sites with geomorphic and stratigraphic evidence of youthful folding, faulting, uplift or subsidence. Strata at these sites are being examined in detail to quantify recent tectonic deformation.

Field investigations during FY 92 included completion of stratigraphic description and sampling of the Cape Elizabeth section of the Quinault Formation; sampling and description of Quaternary deposits adjacent to the Raft River; reconnaissance of Quaternary deposits exposed in the seacliffs from Iron Springs to Pacific Beach and from Queets River to Kalaloch.

Lab investigations during FY 92 included microscope analysis of microfossils collected from Quinault Formation and tephra analysis of tuffaceous clasts from faulted Quaternary deposit near Raft River.

Results

1. The sedimentary sequence exposed at Cape Elizabeth displays evidence of syndepositional deformation such as slumping, liquifaction, and sand venting which may be related to paleoseismic shaking. Contacts between the Quinault Formation and the underlying and intruding accretionary prism rocks (Hoh Formation) indicate diapirism post-dated deposition of the Quinault Formation, continued into the late Quaternary and may be ongoing.

2. Investigated an exposure of severely tilted Quaternary strata that may be related to paleoliquifaction features documented along the Copalis River.

3. Continued analyses of sedimentary rock samples collected in southern Washington in FY89 for age and uplift data.

4. Rock samples collected in FY 91 have been processed for microfossil analyses.

Reports

McCrory, P. A., 1992, Quaternary deformation along the Washington margin of the Cascadia subduction zone: Evidence from the Raft River area: GSA Abstracts with Programs, Cordilleran Section, v. 24, p. 69.

McCrory, P. A., 1992 , Isopach map of upper Quaternary deposits in the Gulf of Catalina area, California: U. S. Geological Survey MF-2212 Map Series, scale 1:250,000.

SEISMIC WAVE MONITORING AT PARKFIELD, CALIFORNIA

14-08-0001-G1703

T.V. McEvilly, R. Clymer, E. Karageorgi, M. Antolik, R. Nadeau, P. Johnson
Seismographic Station, University of California, Berkeley, CA 94720
and
Earth Science Div, Lawrence Berkeley Lab, Berkeley, CA 94720

INTRODUCTION

Two programs of seismic wave analysis continue: Earthquake recording with the high-resolution seismic network (HRSN), begun in December, 1986, and controlled-source monitoring with HRSN begun in June, 1987.

The HRSN (Figure 1) consists of ten, 3-component, borehole seismometers surrounding the 1966 Parkfield epicenter. Data-acquisition features digital telemetry with 125-Hz bandwidth and 16-bit resolution, and can operate in external-trigger (i.e., controlled-source) or event-trigger (earthquake) modes. Five low-gain recorders with similar parameters, on loan from the IRIS PASSCAL instrument pool, are also installed. Network characteristics are summarized in Karageorgi *et al.*, 1992.

INVESTIGATIONS

1) Earthquakes.

Local microearthquakes of magnitude about -0.5 to about +1.8 are routinely recorded on scale by the high-gain, telemetered system, extended to near M5 at the five low-gain sites. (The M4.7 event on October 20, 1992 within the nucleation zone recorded on-scale at three of the five low-gain sites, and clipped only the S-wave at the other two.) A 3-D velocity model (Michelini and McEvilly, 1991) and a high-precision relative hypocenter location procedure for clustered events with similar waveforms have been developed for use in high-resolution analyses of local earthquakes. Clustered events are being studied for evidence of temporal changes in fault zone processes and properties, including anisotropy. Studies are underway in source scaling, failure processes, fault zone structure, and material properties within the Parkfield nucleation zone. All of these parameters plus the vibrator-generated wavefields are subject to analyses for temporal changes that may be premonitory to the expected M6 event.

With the October, 1992 A-level alert, we increased the coverage of the HRSN with installation of seven temporary surface sites using 3-component recorders. Five of the sites are to the north of the present array, and two between the EAD and GHI sites at the south end. These recorders were obtained under the IRIS RAMP program, and will operate into January, 1993.

2) Controlled-source monitoring with HRSN.

From June, 1987 through October, 1992, the HRSN has been illuminated 42 times with S-waves of three polarizations at (presently) seven source positions throughout the study zone, using a shear-wave Vibroseis source, in an on-going monitoring program (Figure 1). The resulting data are searched for temporal variations of wave propagation characteristics throughout the nucleation zone. Data reduction is accomplished at the Center for Computational Seismology (CCS) in the Earth Sciences Division of the Lawrence Berkeley Laboratory (LBL). This work was reported by Karageorgi, *et al.*, 1992.

DATA COLLECTED

Earthquake data are archived as IEEE-format binary files on magnetic tape with simple headers. These will soon be converted to a standard SEGY format. We have archived some 1500 local events.

Six vibrator data sets have been collected and the data reduced

in this project year. Data after routine processing (edit, stack, correlation, gather by source site) are archived in SEGY format on magnetic tape.

RESULTS

Earthquake Studies:

Event analysis: Local Parkfield events are now picked and located with the 3-D model within a month of occurrence.

Clustering analysis: When located with high-resolution methods, more than half of the 1500 local microearthquakes recorded to date are seen to have occurred as members of some 80 clusters of 1-12 highly similar sources on small patches typically about 100m in extent throughout the 30-km Parkfield zone, in both creeping and locked sections. The total area of all the clusters constitutes only a small fraction of the fault zone approaching failure at Parkfield. Many clusters span the five years of data collection. Waveforms are remarkably coherent to frequencies of 50-100 Hz. This coherency provides the opportunity for precise relative timing of P and S arrivals among the cluster members, based on the slope of the cross-spectral phase. Timing precision to better than 0.5 msec yields relative hypocenter locations of cluster members uncertain apparently to about 10m. The archived clusters are presently the basis for various on-going studies of fault zone processes. A paper on the clustering analysis has been submitted (Nadeau, *et al.*, 1992).

Characteristics of seismicity: To first order, the pattern of earthquake locations has remained constant throughout network operation, although the rates of activity change, apparently in concert throughout the region. Parkfield earthquakes yield a b-value of about 0.9 that has not changed significantly during operation of the network.

Magnitude scaling and source parameter variations: The distinct clusters or 'nests' of microearthquakes, typically 100 m or less in dimensions, recorded with high bandwidth, provide a natural laboratory for investigating the scaling of source parameters with magnitude, and the details of the slip process within the fault zone. We are reviewing earthquake mechanisms at Parkfield for evidence of a non-double-couple (tensional or reverse-slip) component. A study earlier this year of S-to-P spectral ratios below the corner frequency gave evidence for non-shear rupture in some (but not all) events, which we interpret to be indicative of a significant component of tensional failure. We have begun to map the source mechanism character and its variation throughout the fault zone.

The October, 1992 sequence of some 100 events larger than about M=-0.5 involved much of the fault zone at Parkfield (Figures 2 and 6), but the energy release was mainly concentrated along a 3 km long segment of the fault surface stretching southeastward at 8 km depth from the 1966 hypocenter into the expected M6 rupture zone. This segment had been inactive throughout the 5 years of monitoring with the HRSN. The SE end of the 3 km segment was particularly energetic, containing a nest of 12 events that included the M4.7 shock ($0.5<M<4.7$). Two other large events (M3.9 and 3.3) fell on the same trend halfway between the SE nest and the 1966 hypocenter. The sequence clearly appears to represent a failed attempt to rupture the M6 asperity SE of the nucleation point at the 1966 focus.

The SE nest of events provides an excellent data set for source scaling studies and for close scrutiny of the waveforms for possible effects of changes in material properties or source mechanisms associated with the M4.7 occurrence, since there are small events in the nest before and after it. The tight clustering of the events eliminates the problem of differing path effects among the cluster members. Preliminary results show:

SCALING: The M4.7 event is clearly and substantially different in source dimension and time function from all the others, which are very similar over the magnitude range -0.5 to 4.0i (Figure 3). Corner frequency increases with decreasing magnitude (around 40Hz and 100Hz for M~1.8 and M~0.5-1.0, respectively (Figure 4).

TEMPORAL CHANGES: There are no obvious differences between foreshocks and aftershocks of the M4.7 event at the M1.5 - 1.9 range.

MECHANISM: An initial computation of low-frequency S/P spectral ratios suggests that the foreshock selected (M1.5) shows no evidence of non-shear source.

Assessment of temporal changes in wafeform polarizations: The clusters, each with nearly identical repeating waveforms and locations, distributed throughout the fault zone, are being used to monitor the nucleation zone for precursory changes in material properties. Most effort to date has gone into study of the stability of waveform polarization applying a vector linearity trace formalism to a cluster about 2 km NW of the 1966 hypocenter at about 10 km depth. It was found that a suite of small events within the cluster (M 0.5) produced apparent temporal variability of polarization on certain paths due to higher attenuation (and therefore lower S/N) on the NE side of the fault. Choice of window lengths and consideration of nodal plane geometry did not explain the variations. However, choice of more energetic events (M 1.5) produces apparent stability of waveforms over time on the several paths analyzed. Preliminary results also indicate that travel times are stable.

There appears to be evidence of anisotropy (S-wave splitting) in the trace polarization displays, with the fast direction parallel to the fault zone, in agreement with results obtained in vibrator studies using HRSN (Karageorgi, *et al.*, 1992) and the Varian Well Vertical Array (Daley and McEvilly, 1991). Further studies will attempt to characterize the spacial extent and consistency of the anisotropy with clustered and unclustered events, and search for temporal variations.

Controlled-Source Studies.

The final working data sets for analysis are "time gathers": one source into one receiver gathered across calendar time, producing 720 files, each containing, at present, up to 42 similar traces. The time gathers are then examined for variations in waveform parameters.

Most displays show only seasonal variations in various properties (travel time, amplitude, spectral properties). Seasonal variations are due to very near-surface moisture changes under the vibrator (Clymer and McEvilly, 1981).

Karageorgi, *et al.*, 1992 describes the analysis techniques and their application to a subset of paths through the expected nucleation zone, and illustrates the types of anomalies found. In the past year, we have extended the analysis to the entire dataset in order to better characterize the prominent travel-time anomaly in the vicinity of source site 2, south-west of the 1966 epicenter, that began in mid 1988, and continues through October, 1992 (Figure 5 and 6). No significant change was found in the anomaly with special surveys run during the October, 1992 M4.7 sequence.

References

Clymer, R.W., and T.V. McEvilly, 1981. Travel time monitoring with VIBROSEIS, *Bull. Seism. Soc. Amer*, 71, 1902-1927.

Publications

Daley, T.M. and T.V. McEvilly, Shear wave anisotropy in the Parkfield Varian Well VSP, *Bull. Seism. Soc. Am.*, 80, 857-869, 1990.

Michelini, A. and T.V. McEvilly, Seismological studies at Parkfield: I. Simultaneous inversion for velocity structure and hypocenters using B-splines parameterization, *Bull. Seism. Soc. Am.*, 81, 524-552, 1991.

Karageorgi, E., R. Clymer and T.V. McEvilly, Seismological studies at Parkfield. II. Search for temporal variations in wave propagation using Vibroseis, *Bull. Seism. Soc. Am.*, 82, 1388-1415, 1992.

Foxall, W., A. Michelini and T.V. McEvilly, Three-dimensional velocity structure and rupture characteristics of the Santa Cruz mountain zone, in *The Loma Prieta, California, Earthquake of October 17, 1989,* USGS Open-file Rept. (submitted), 1992.

Submitted:
Nadeau, R., M. Antolik, P. Johnson, W. Foxall and T.V. McEvilly, Seismological studies at Parkfield. III. Microearthquake clusters in the study of fault-zone dynamics

Ph. D. Theses

Michelini, A., Fault Zone Structure Determined Through the Analysis of Earthquake Arrival Times, 1991.

Foxall, W., Fault-Zone Heterogene Slip and Rupture Models of the San Andreas Fault Zone Based upon Three-Dimensional Earthquake Tomography, 1992

Papers Presented on Parkfield Research - 1992

Seismological Society of America 1992 Annual Meeting, Santa Fe, New Mexico, April 13-15, 1992.

T.V. McEvilly, High-frequency observations of microearthquakes in active fault zones

T. M. Daley and T. V. McEvilly, Joint VSP and microearthquake tomography for fault zone structure

R. M. Nadeau, M. Antolik and T. V. McEvilly, A search for temporal changes in travel times and polarization at Parkfield using earthquake sources

P. A. Johnson, M. Antolik, W. A. Peppin, W. Foxall and T. V. McEvilly, Structure and rupture processes of the fault zone at Parkfield from the spectra of microearthquakes

E. D. Karageorgi, R. W. Clymer and T. V. McEvilly, Shear-Wave propagation in the San Andreas fault zone Monitored with Vibroseis.

1992 Fall AGU, San Francisco, 07-11 Dec.

R. Nadeau and T.V. McEvilly, An Assessment of Temporal Changes in P- and S-Coda Polarizations at Parkfield Using Microearthquake Sources.

M. Antolik and T.V. McEvilly, An Analysis of the 1987-92 Parkfield Seismicity Based on Data From the High-Resolution Borehole Network.

P.A. Johnson and T.V. McEvilly, Magnitude Scaling and Source Parameter Variations of Microearthquakes at Parkfield.

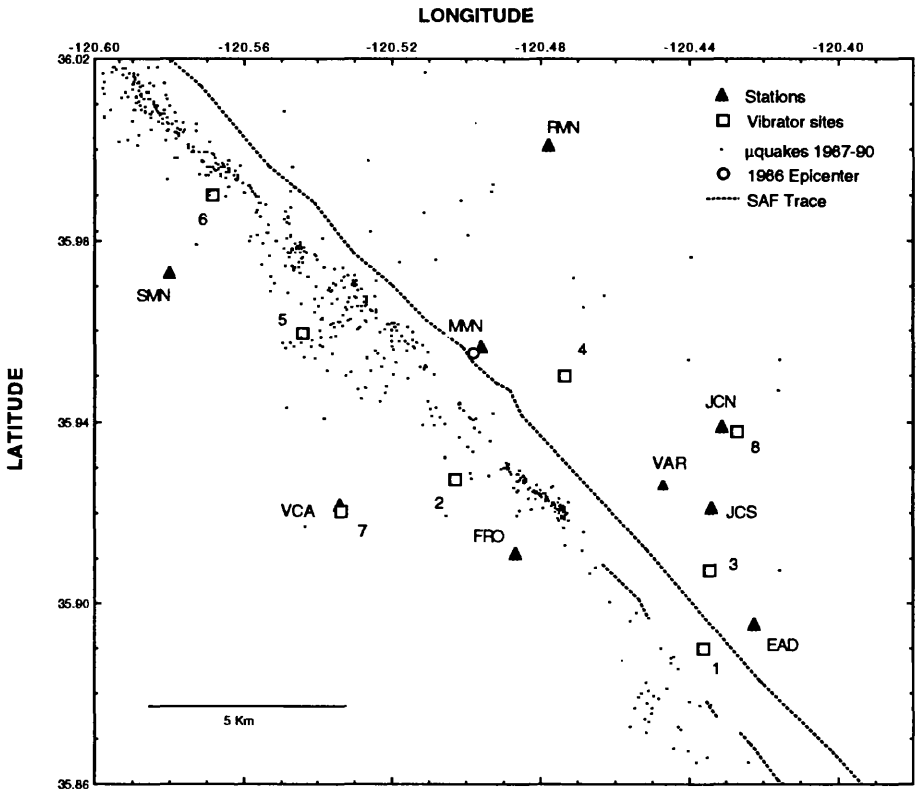

Figure 1. Location map showing the borehole seismometer network, vibrator positions (VPs) and microearthquake seismicity for 1987-1990.

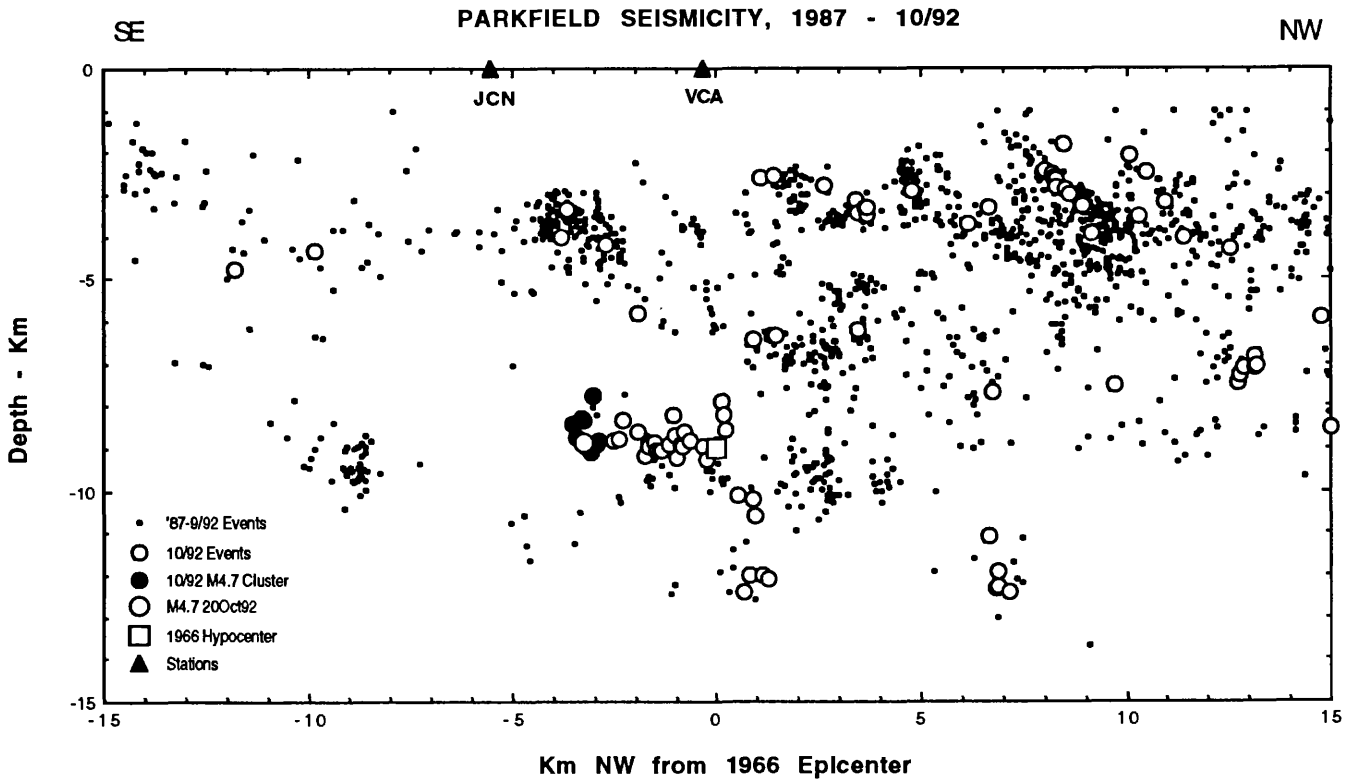

Figure 2. Cross section with seismicity along the San Andreas Fault, showing the October, 1992 earthquake sequence.

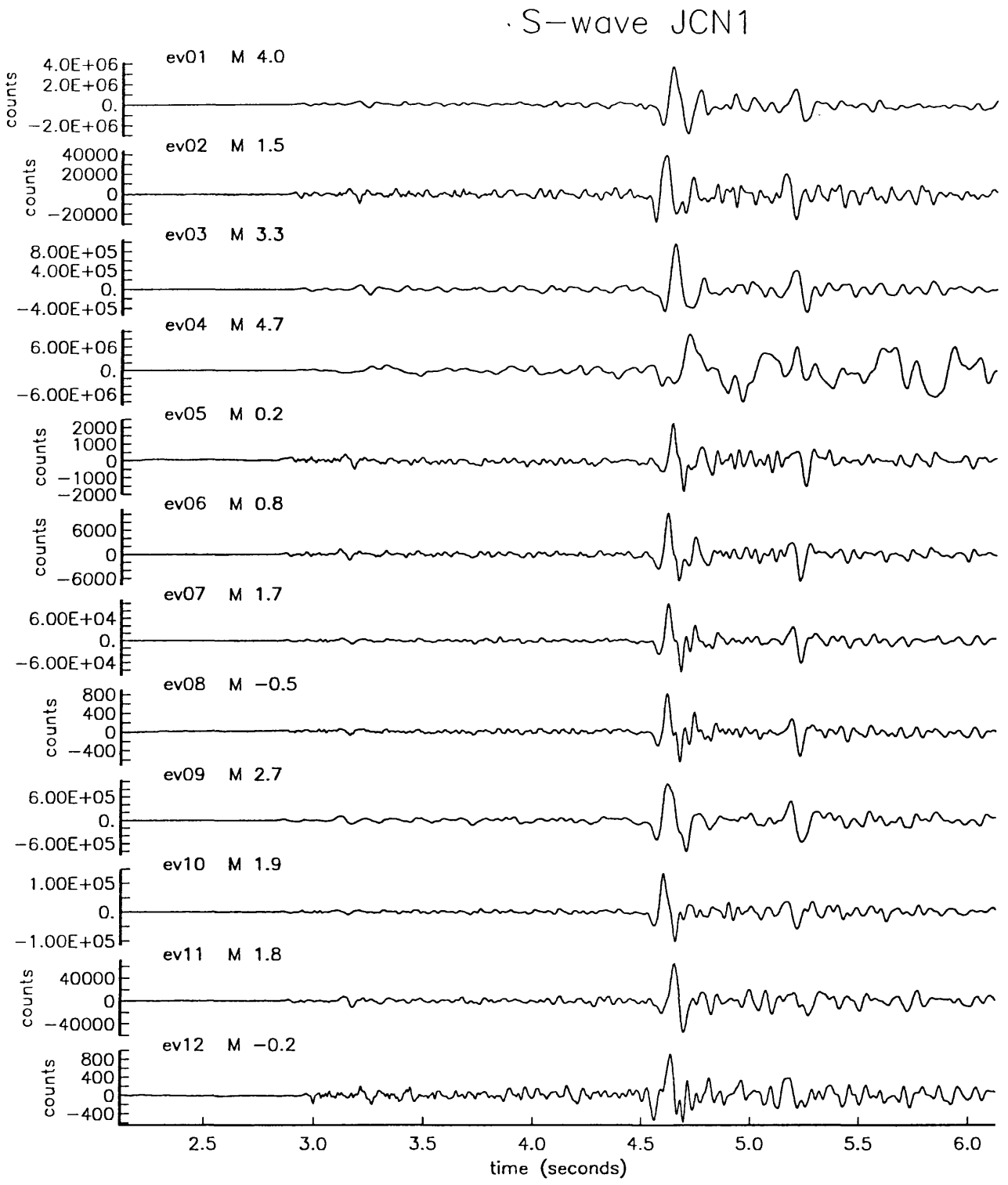

Figure 3. Set of nested events at the M4.7 focus in the October 1992 sequence, shown in chronological order.

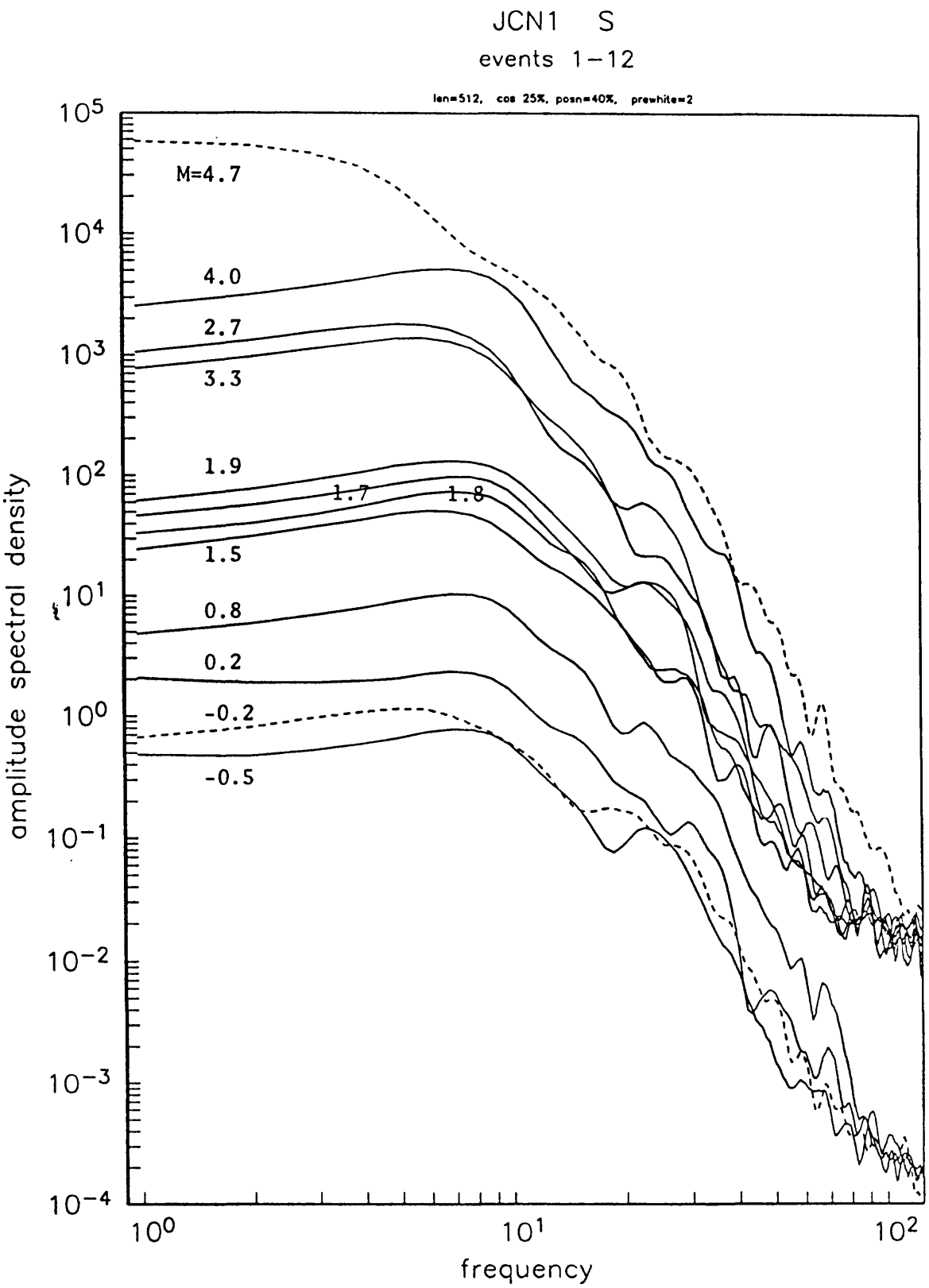

Figure 4. S-wave spectra for suite of events in the October 1992 M4.7 sequence.

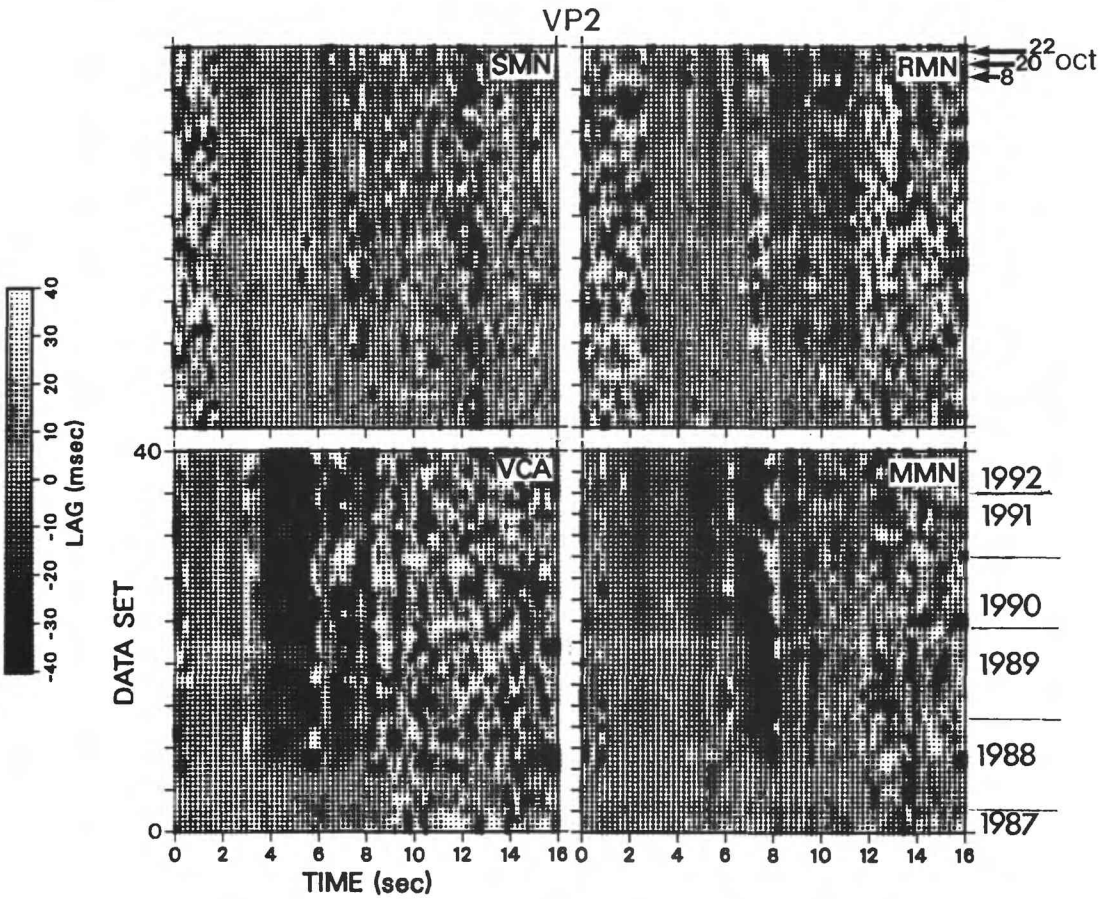

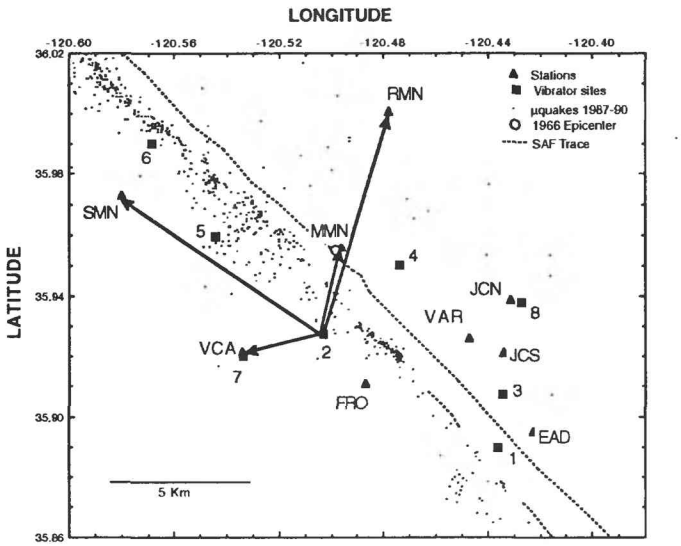

Figure 5. Travel-time variations relative to a reference trace (arbitrarily chosen, here in mid 1988) measured across the repeated 16-sec seismograms in a moving window for several paths from vibrator site two.

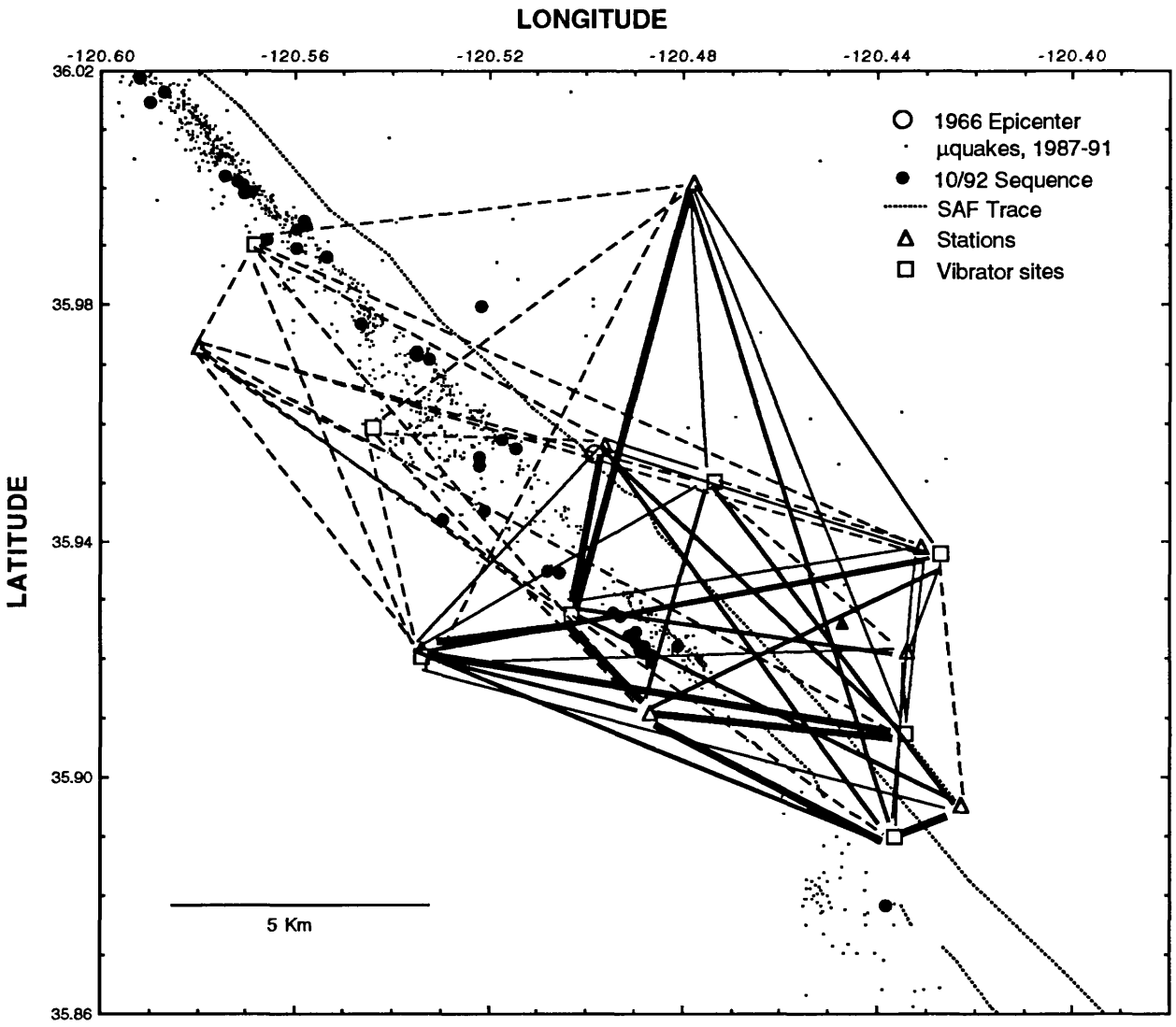

Figure 6. Paths showing velocity anomaly. Heavy solid lines show paths with strong travel-time advance of later phases (concentrated primarily SE of Middle Mountain); dashed paths are stable, light solid paths show marginal indication of anomaly.

U.S. DEPARTMENT OF THE INTERIOR
U.S. GEOLOGICAL SURVEY

NATIONAL EARTHQUAKE HAZARDS REDUCTION PROGRAM, SUMMARIES OF TECHNICAL REPORTS VOLUME XXXIV

Prepared by Participants in

NATIONAL EARTHQUAKE HAZARDS REDUCTION PROGRAM

Compiled by

Muriel L. Jacobson

The research results described in the following summaries were submitted by the investigators in September 1991 and cover the period from April 1991 through October 1, 1991. These reports include both work performed under contracts administered by the Geological Survey and work by members of the Geological Survey. The report summaries are grouped into the four major goals of the National Earthquake Hazards Reduction Program.

Open File Report No. 93-195

The data and interpretations in these progress reports may be reevaluated by the investigators upon completion of the research. Readers who wish to cite findings described herein should confirm their accuracy with the author.

EARTHQUAKE HAZARDS REDUCTION PROGRAM

CONTENTS - VOLUME I

Goal I - Understanding what happens at the earthquake source

Why and how does a segment of a geologic fault suddenly slip and produce an earthquake? What physical conditions within the Earth control where and when an earthquake occurs?

Goal II - Evaluating the potential of future earthquakes

Where are future earthquakes likely? How large will they be? How often will they occur? When will they occur? Where are future earthquakes unlikely?

EARTHQUAKE HAZARDS REDUCTION PROGRAM

CONTENTS - VOLUME II

Goal II - Evaluating the potential of future earthquakes

Where are future earthquakes likely? How large will they be? How often will they occur? When will the occur? Where are future earthquakes unlikely?

Goal III - Predicting the effects of earthquakes

During an earthquake of a certain magnitude, how severely and for how long will the ground shake? Where will hillsides slide, and flatlands fissure and crack? On what types of ground will earthquake damage be concentrated? Which faults will offset the Earth's surface? By how much? Which coastlines will be elevated or submerged? Where will destructive sea waves be generated? What losses to structures are expected?

Goal IV - Using research results

What new hazard reduction strategies become possible as understanding of earthquake phenomena advances? What scientific information is needed and can be furnished to practitioners in the engineering, land-use planning and emergency managements communities? How can such information be most effectively communicated to these practitioners?

BAY AREA DIGITAL SEISMIC NETWORK

14-08-0001-G2122
T.V. McEvilly, R. Clymer, P. Johnson
Seismographic Station, Dept. of Geology & Geophysics and
Earth Sciences Division, Lawrence Berkeley Laboratory
University of California, Berkeley, CA 94720

Goals

The purpose of the Hayward Fault Network (HFN) in the San Francisco East Bay is to provide high resolution , high frequency (1000 samples per second), wide dynamic range(24-bit digitization), 3-component, on-scale seismic data for earthquakes of magnitude $0 < M < 7.0$ for detailed studies of the Hayward fault. From our experience managing the Parkfield High-Resolution Network, with similar dimensions to the HFN, we believe we can accomplish this goal even in a noisy urban environment, given carefully designed sensors and deep borehole emplacement.

The HFN is a joint effort with the USGS. The network as envisioned will consist ultimately of 24-30 stations, 12-15 each north and south of the San Leandro seismic gap, managed respectively by UCB and USGS. Other sites are being drilled and instrumented by Lawrence Livermore National Lab (LLNL) in conjunction with the State of California Transportation Department (CALTRANS) in the south Bay. Identical sensors, designed and constructed at UCB/LBL, are being installed in the entire network. Recording and telemetry equipment will differ between north and south, but the resulting data will be shared in near real time and archived with CALNET data in common format in the Bay Area optical mass store facility at Berkeley, also operated jointly by UCB and the USGS, and will thus be made promptly available to the research community.

FY 92 Accomplishments

During the past fiscal year, we have reviewed, designed, and selected state-of-the-art technology for sensors, signal processing, central network control, and telemetry. Sensors for the initial ten stations (five each north and south) have been fabricated, most have been installed, and delivery of field- and central-site recording and control equipment is imminent. The initial network configuration (Figure 1) should be operational in early 1993. In the interim, sites may be instrumented with event recorders.

1) **Sensor design.** Our Parkfield experience (and basic physics) has shown us that velocity sensors are insufficient for our purposes because they do not see ground noise above 15 or 20 Hz (Figure 2) in quiet deep borehole sites. We have therefore chosen as our primary sensor the Wilcoxon Model 731 low noise accelerometer. This sensor has good signal-to-noise ratio for M 1.0 earthquakes and a very wide dynamic range. Three components of these accelerometers with 3dB bandwidth 0.05 - 600 Hz and 0.5 g full-scale covers the magnitude range from ~0.5 to 7+ (in boreholes at depths greater than 100 m), delivering flat acceleration response over the bandwidth. In addition, three velocity geophones are included for two reasons: (1) to cover the bandwidth 5-15 Hz for M<1.0, where the geophone has lower intrinsic noise (the only range where the geophone noise is better than the accelerometer), and (2) redundancy in the non-recoverable borehole sensor package should the active accelerometers fail at some time.

(Normally the two geophone horizontals will not be recorded). Figure 3 compares waveforms and spectra at Berkeley of the two types of borehole sensors at 180 m depth in the Hayward fault zone on the UCB campus, and the 80 sps VSP channel from the STS1 vertical component in the BKS vault on the surface a short distance away, illustrating the signal strength at high frequencies.

2) **Installation**. We have fabricated the sondes in two diameters (for holes <3" and <4") and provided them also to the USGS and LLNL. Six of these have been installed in "holes of opportunity" drilled by the USGS strainmeter program. Three more have been installed by Caltrans, two for LLNL at the Dumbarton Bridge in the South Bay, and one for UCB at the east end of the Oakland Bay Bridge. Two more will soon be installed in existing boreholes on UC property, and perhaps one in south Oakland (not shown in Figure 1). The network, as presently funded, will thus include 9 or 10 UC/USGS sites, plus the two LLNL sites, all installed at depths of about 150-200 m.

3) **Data recorders.** For the northern network, we have chosen the Quanterra recorder with 24-bit digitizers on 4 channels (3 accelerometers, 1 vertical velocity geophone), sampling at 1000 sps. Event data will be telemetered to a central site, with local field-site 2-GByte DAT-tape backup recording, remote parameter setting from the central site, and remote and local triggering protocols.

   We expect this system to survive a major local earthquake and record the aftershock sequence without communication to the central site for up to 5 days. The DAT tape is designed for simple field tape changes without the need for complicated interaction via laptop or handheld terminals.

   Five Quanterra dataloggers are presently on order, with imminent delivery expected.

4) **Telemetry.** Full 2-way telemetry will be over the new PacBell Advanced Digital Network (ADN). Continuous telemetry of selected channel(s) at a chosen data rate will allow network trigger control at the central site, with triggered events multiplexed into the 56KB data line as required. Total throughput is yet to be determined, though 38Kbps should work with the planned workstation receiving hardware.

5) **Central acquisition/control.** A workstation-based central system will control the network, defining network triggers (from the continuous telemetry) and requesting data streams, monitoring state of health and state of local event triggers, and routing events to appropriate analysis/archiving queues, including that interrogated in near real-time by USGS, and accessing complementary data from CALNET and the southern Hayward Fault Network from Menlo Park. A SPARCstation 10 is on order and we expect initial delivery before the end of the year.

   Event declaration can occur in one of two user-specified ways. Declaration can occur in the central receiving system with a subsequent broadcast to the net sites for specific transmission windows (given the event start time, determined at the center). The other option is for declaration to occur at the individual sensor sites for unsolicited event transmission. In this case, event declarations will be telemetered also, for central system use.

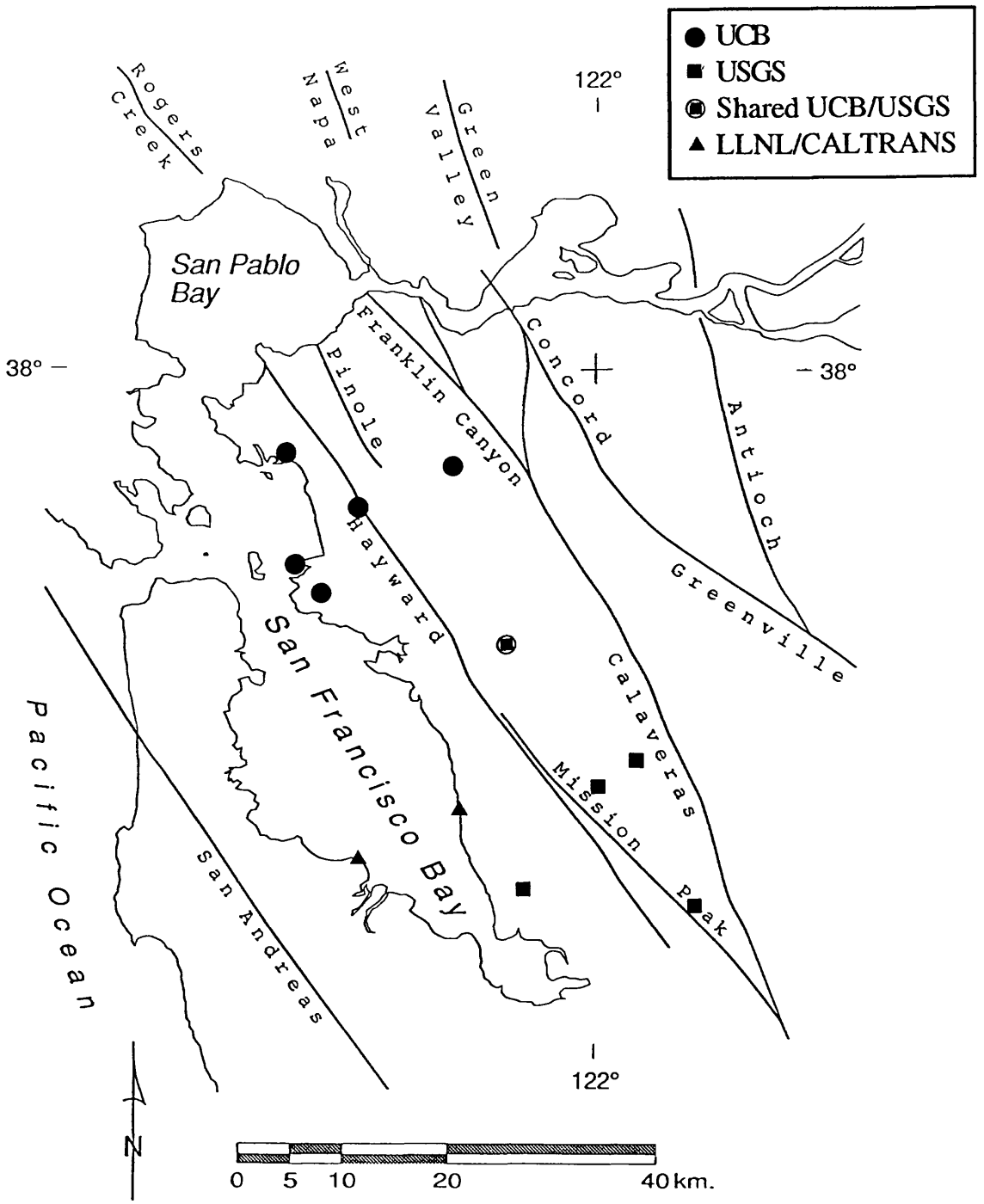

Figure 1. Hayward Fault Digital Network.

Figure 2. Equivalent Ground Noise for L-22D, HS-1, and Wilcoxon Geophones Operating into the AMP-01

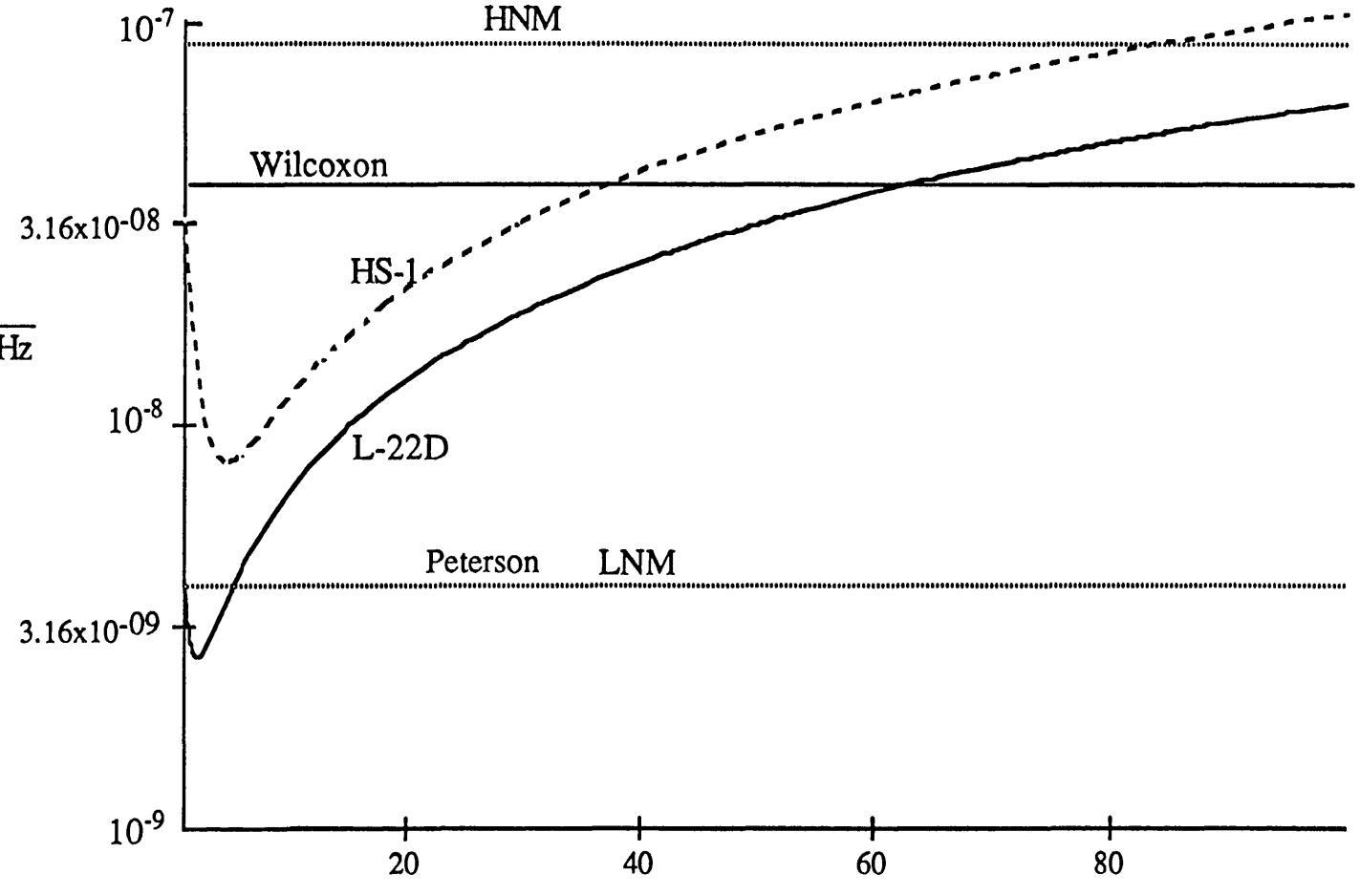

P.W. Rodgers, 4/92

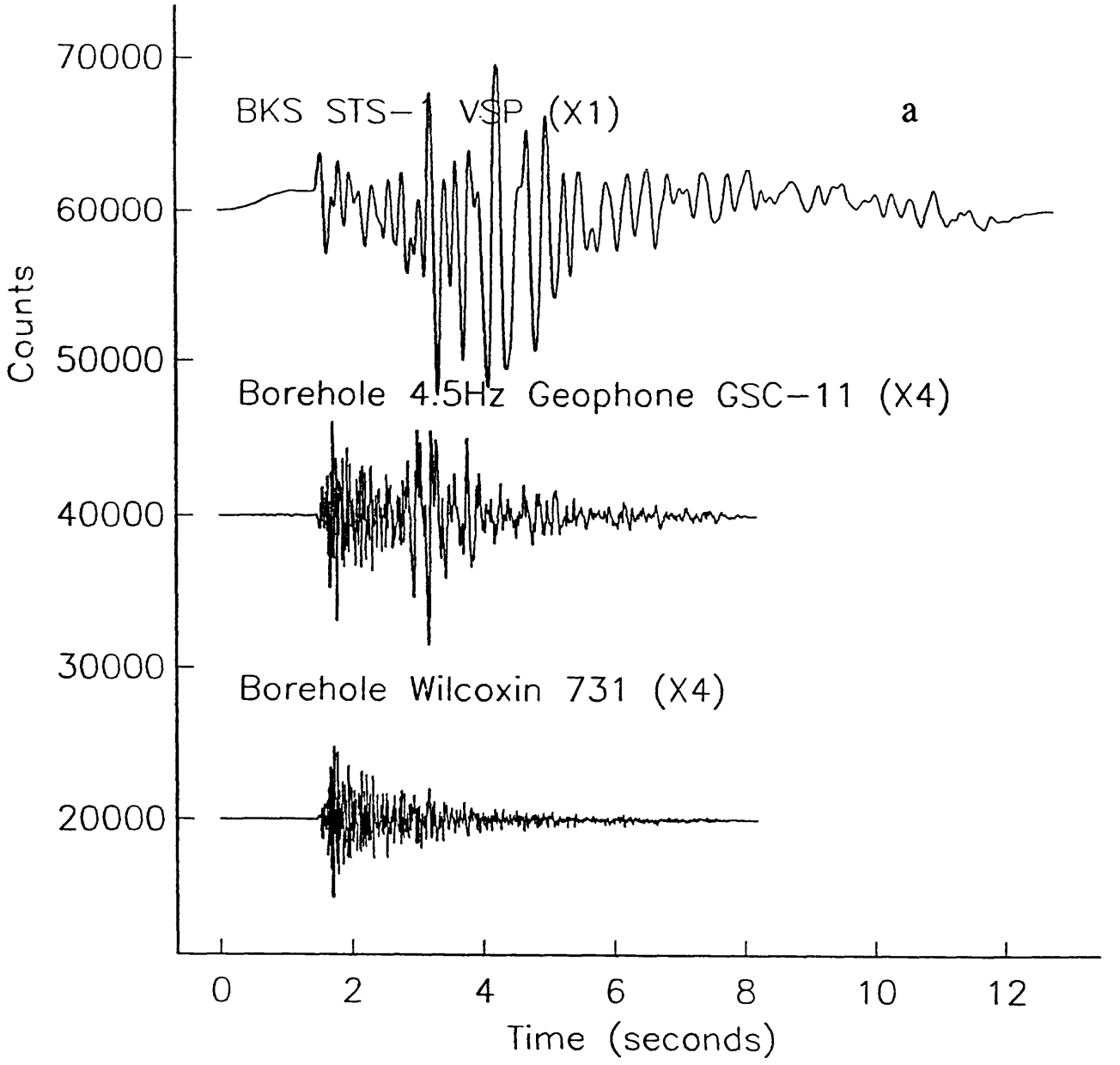

Figure 3. Comparison of surface and subsurface vertical recordings of a local M 1.7 event (10 January 1992). Two borehole sensors at 180 m depth in the Hayward fault zone on the UCB campus (GSC-11 geophone and Wilcoxon 731 accelerometer) and one surface sensor (STS-1) located in the BKS vault a short distance away. (3a) Time series (unprocessed recordings). (3b) Spectra (power spectral density) -next page.

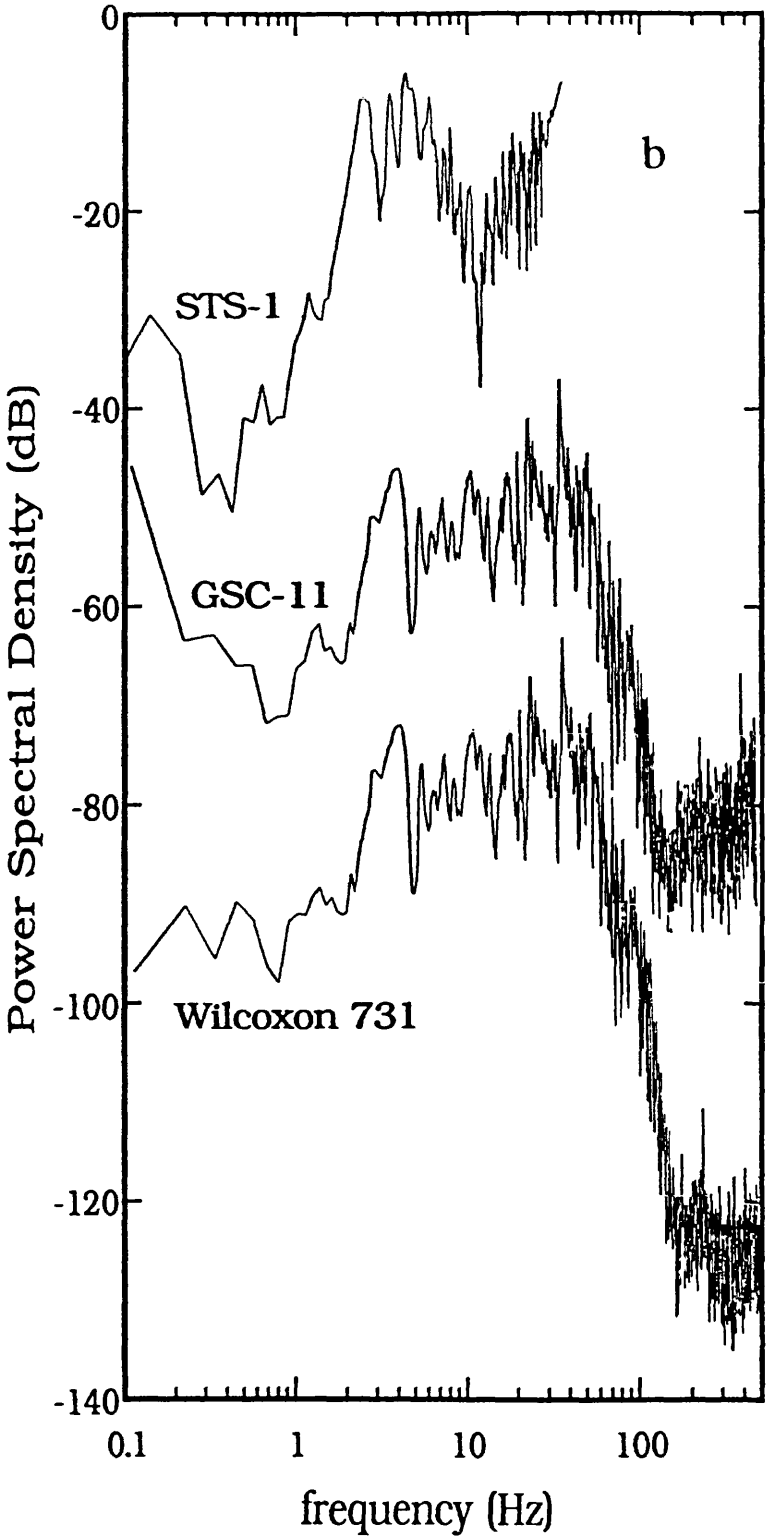

Figure 3b. Spectra of traces shown in Figure 3a. Ordinate origin is arbitrary. The geophone and accelerometer spectra have been artificially offset down 20 and 40 dB, respectively. Note the extended useful bandwidth (to higher frequencies) of the borehole accelerometer.

MARINE SEISMIC INVESTIGATIONS OF THE EAST BAY FAULTS

14-08-0001-G2123
T.V. McEvilly, D.L Jones, E. Karageorgi, Janine Weber Band
Seismographic Station, Dept. of Geology & Geophysics and
Earth Sciences Division, Lawrence Berkeley Laboratory
University of California, Berkeley, CA 94720

Data

The investigation of the crustal structure and complex fault geometries of the Bay Area is the main focus of the BASIX (Bay Area Seismic Imaging Experiment) research program. The BASIX profiling cruise conducted in September 1991 provided coverage across the Coast Ranges from the Sacramento River delta into the San Francisco Bay and through the Golden Gate. Data were collected by deploying daily a complex survey geometry of up to 100 buoyed receivers and two non-coincident 15 km-long passes of the airgun ship through the line. Three land receiver arrays were also deployed to complement the marine data.

The BASIX project has been a multi-institutional and multi-program exercise conducted cooperatively with Dr. Jill McCarthy of USGS. In addition to the UC Berkeley involvement, Stanford and Pennsylvania State universities participated along with Lawrence Berkeley Laboratory, and resources were supplemented by CALTRANS, NSF and DOE. In addition, the investigation bears directly on several other research efforts underway in the San Francisco Bay area. Under the related NSF CALCRUST-North program, approximately 172 miles of high-quality industry reflection data in the area have been purchased for study of the East Bay region, and these results will complement the BASIX effort.

Processing

We have processed data from the north-eastern section of the profile, from the Sacramento River Delta into San Pablo Bay. The processing steps for the generation of the initial stacked sections of the BASIX line involve trace editing, sorting to CDP gathers and preliminary velocity analysis. The complexity of the source-receiver geometry and editing of traces contaminated by the current-generated noise has been a challenging aspect of the data processing, especially in view of the need to combine successive night's data where they overlap to obtain the maximum possible CDP fold. The resulting data quality on preliminary stacks is very good in the Delta and Suisun Bay waters at the east end of the survey. Strong tidal currents contaminated other parts of the data with noise and greatly complicated the receiver geometry, but the high CDP-fold coupled with further velocity analysis is expected to yield usable sections.

Interpretation

Geologic interpretation, guided by well log analysis, is an attempt to shape the known surface geological data and seismotectonics into a working model of the broad plate boundary system that encompasses the Bay Area..

The study area lies at the juncture of three large terranes: the Elder Creek (EC), the Del Puerto (DP), and the Central Valley (CV, part of the Sierran Block), a region crucial to understanding the nature and style of tectonism along the western margin of the Coast Ranges. Characteristic tectonic wedges at

Dunnigan Hills to the north and at Kettleman Hills to the south are located east of the bounding fault. In contrast, the wedge identified on the BASIX line lies beneath the Pittsburg/Kirby Hills thrust fault. The wedges imply a strong east-west compression of the Coast Ranges, in agreement with recent interpretations of surface geological mapping. South of the Sacramento River, CV abuts the Del Puerto terrane. The junction of DP with EC and CV terranes appears to occur under the river between Pittsburg and Benicia. The fault zone identified beneath the river on the high resolution uniboom data is seen in the BASIX section as a 1 km wide zone of thrust slivers that cut all but the youngest river deposits at Pittsburg. The same fault is seen on the CALCRUST lines 3, 6, and 11 miles north of the river, where it appears to daylight as the Kirby Hills fault. The fault changes from a steeply east-dipping multiple-splaying thrust zone at the river to a west-verging thrust dipping 30 degrees where it crosses the line 11 miles north, soling in a decollement interpreted at 2.5 to 3 sec. Our data show no other major faults to the east.

Recent Presentations

Karageorgi, E.D., J. Weber Band, and K Williams, Tectonic style of the San Francisco Bay region from CALCRUST and BASIX reflection profiles, *EOS*, **73**, 404, 1992 (abs.). (1992 Fall Am. Geophys. Union meeting).

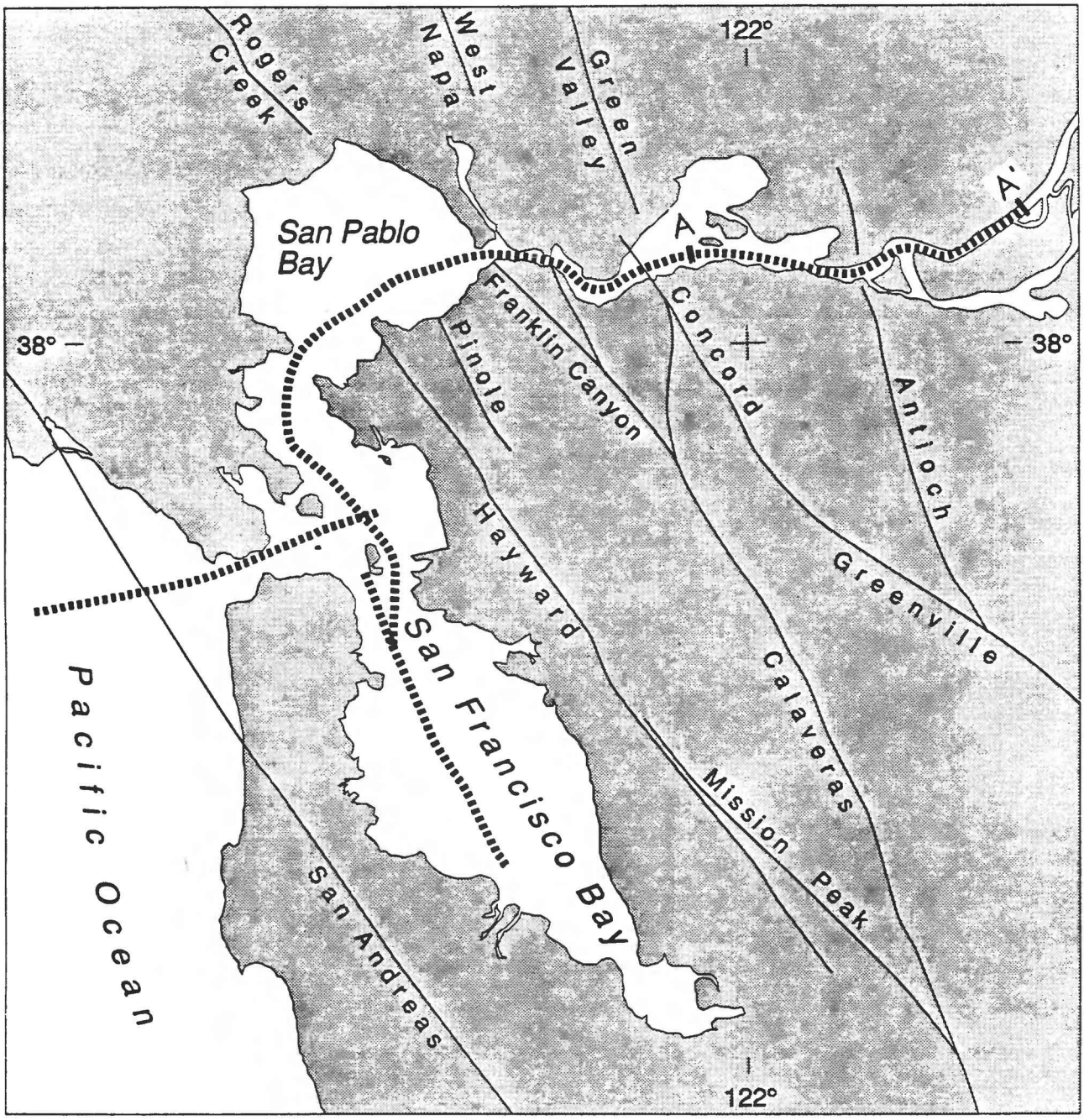

Figure 1. BASIX profile line..

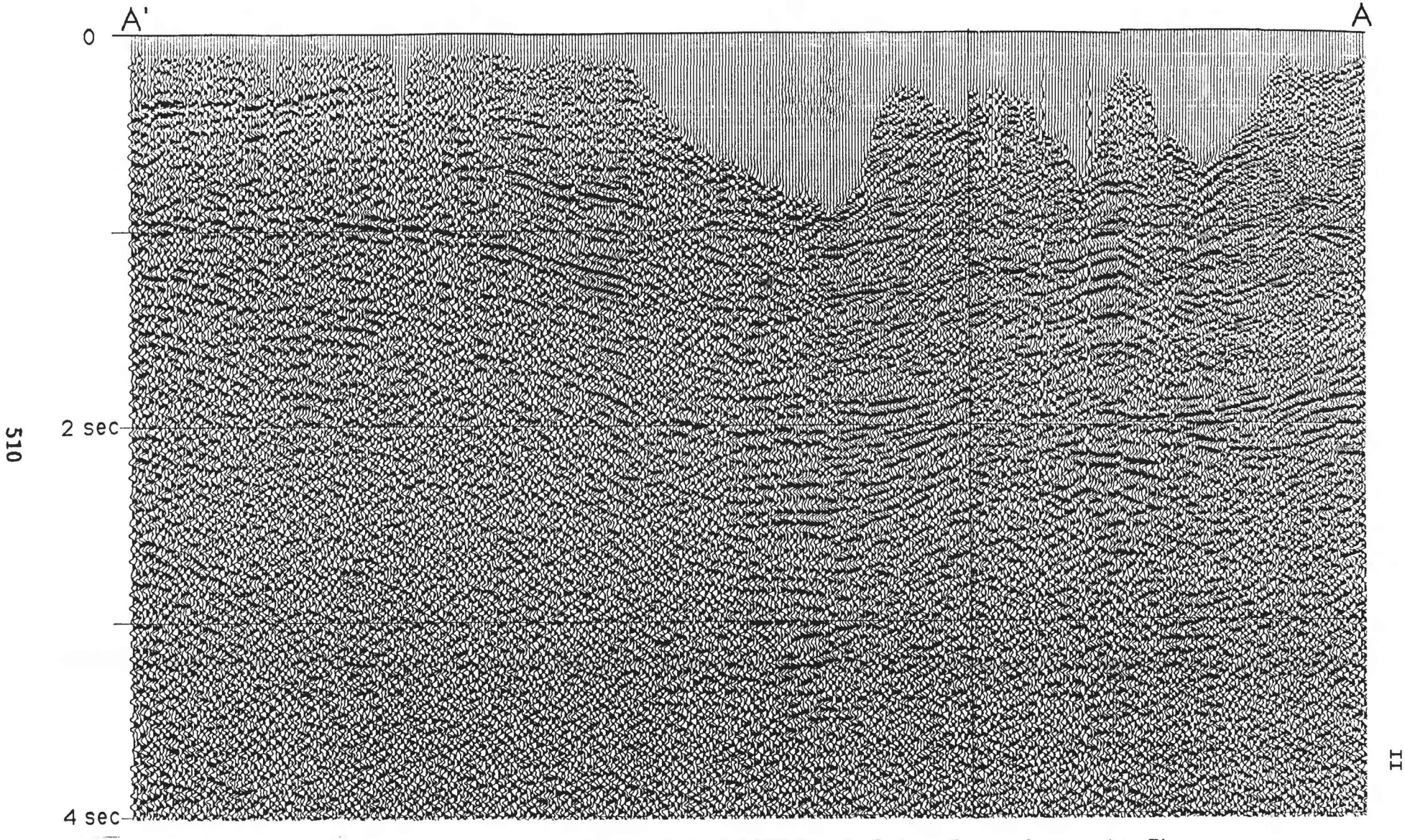

Figure 2. CDP stack of the eastern portion of the BASIX line, in Suisun Bay, referenced to Figure 1. Note that west is on the right.

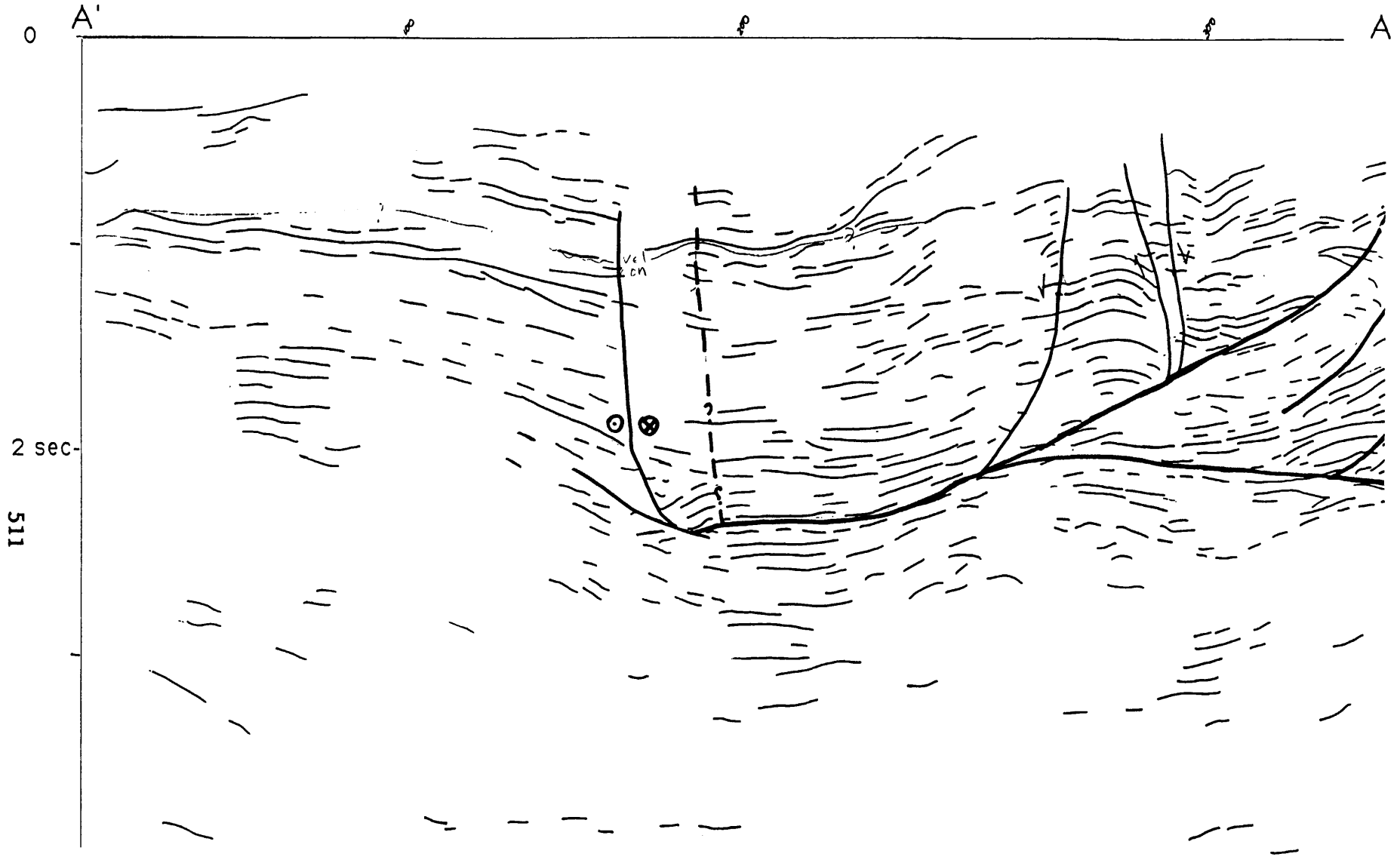

Figure 3. Preliminary interpretation of the section in Figure 2.

Slip Rate Studies of the Garlock and Owl Lake Faults

Sara F. McGill
California State University
San Bernardino

1. Highway 14 Site (Figure 1):

The photogrammetric map of this site (Figure 2) shows a channel offset 60 ± 5 meters left-laterally with little or no (< 1 m) vertical displacement. These measurements are from points surveyed along the top of the geomorphic expression of the northeastern wall of the channel. With the help of field assistants Joseph Stroud and Michael Slates, I logged and interpreted both walls of each of two trenches excavated at this site during April and May 1992. Trench 1 crossed the northeastern wall of the channel on the southeastern side of the fault. This trench revealed the location and trend of the buried portion of the channel wall (Figure 3). The second trench crossed the Garlock fault zone near Trench 1. Trench 2 revealed the location and trend several fault strands within a 15-m wide fault zone. Judging from the degree of disruption of the older alluvium in Trench 2, the northwesternmost strand within the fault zone appears to have had the most displacement.

During November and December 1992, two new trenches (Trenches 3 and 4, in Figure 2) will be excavated and logged at this site. Trench 3 will cross the channel wall northwest of the fault. This trench will reveal the buried channel wall that is correlative to the one exposed in Trench 1. Trench 4 will cross the fault zone near Trench 3 and will provide details of the fault zone geometry in that area.

The relationships observed in Trenches 1-4 will allow a more informed measurement of the offset of the channel than can be made geomorphically. They will also lay the ground work for future three-dimensional excavations at this site to follow the base of the buried channel wall to its actual intersection with each of the fault strands.

Over 100 charcoal samples were collected from Trenches 1 and 2. Five samples have been submitted for AMS radiocarbon dating. The stratigraphic positions of three of these samples are shown in Figure 3. Three of the samples submitted for dating are from the older alluvium into which the channel incised and will provide a maximum age for the offset channel wall. Two samples were from colluvium that buries the channel fill and will provide a minimum age for the offset channel wall. I have not yet found any charcoal from within the channel fill. If charcoal within the channel fill is found in Trench 3 or 4 this will provide and even tighter minimum age for the offset channel wall.

2. Owl Lake fault site (Figure 1):

At this site a terrace riser on the eastern side of an incised channel has been left-laterally offset (Figure 4). The channel has incised late Tertiary or early Quaternary conglomerate, sandstone and claystone on the northern side of the fault and has incised Late Quaternary alluvial fan deposits on the southern side of the fault. With the help of a student assistant, Joseph Grant, I surveyed points along the top of the terrace riser between

Qt_2 and Qt_3 south of the fault, along the top of the eastern channel wall north of the fault and along the top and base of the fault scarp. Within about 50 meters south of the fault, the terrace riser has been mantled by colluvium derived from the fault scarp. Projecting the unmantled segment of the top of the terrace to the fault suggests that the top of the terrace riser intersects the fault about 55 meters east of the point on the channel wall north of the fault with the same elevation.

If no vertical slip had occurred, the left-lateral displacement of the terrace riser would be about 50 m. The presence of a 4-6 meter high, southward facing fault scarp east of the channel, however, indicates that significant vertical displacement has occurred. The point on the channel wall north of the fault that correlates with the top of the terrace riser is probably 4-6 meters higher than the elevation of the riser at the southern edge of the fault zone. If vertical displacement of the terrace riser is 5 meters, then the left-lateral displacement of the riser is about 43 meters. If erosion has significantly shifted the channel wall north of the fault eastward, then the left-lateral offset may be larger than 43 meters.

Dr. Ronald Dorn and I also collected surface samples from six boulders on the Qt_3 terrace. Dr. Dorn extracted organic material from the weathering rind beneath a coating of rock varnish on two of the samples and had it radiocarbon dated. The resulting ages are 29,490 ± 270 and 30,820 ± 280 radiocarbon years B.P. These ages represent the time at which organisms living within the weathering rind of the rock were killed by being covered with rock varnish (Dorn, oral comm.). Varnish begins to form on a surface within about a hundred years after exposure to the atmosphere (Dorn and Whitley, 1984; Dorn and others, 1988). Complete covering of the rock surface with varnish is probably necessary to kill the organisms inhabiting the weathering rind, however, so the reported ages are minimum estimates of the age of abandonment of the Qt_3 terrace. Dorn (1989) has shown, however, that radiocarbon dates on organic material extracted from the basal layers of rock varnish are < 10% younger than radiocarbon dates on charcoal, shells and tufa for several different surfaces of Holocene and Late Quaternary age.

Thus, deposition probably ceased on the Qt_3 surface, and it became permanently exposed within a few thousand years before 30,000 $_{14}$C-yr B.P. Abandonment of the Qt_3 surface was most likely caused by incision of the offset channel, so the age of abandonment of the Qt_3 surface probably approximates the age of formation of the offset terrace riser between Qt_2 and Qt_3. If this is the case, then the ~43 m of left-lateral slip occurred over the past 30-33 ka or so, yielding a preliminary left-lateral slip rate estimate on the order of 1.3-1.4 mm/$_{14}$C-yr.

References:

Dorn, R. I. and D. S. Whitley, 1984, Chronometric and relative age determination of petroglyphs in the western United States, Association of American Geographers Annals, v. 74, p. 308-322.

Dorn, R. I., M. Nobbs, and T. A. Cahill, 1988, Cation-ratio dating of rock engravings from the Olary Province of arid South Australia, Antiquity, v. 62, p. 681-689.

Dorn, R. I., A. J. T. Jull, D. J. Donahue, T. W. Linick, and L. J. Toolin, 1989, Accelerator mass spectrometry radiocarbon dating of rock varnish, Geological Society of America Bulletin, v. 101, p. 1363-1372.

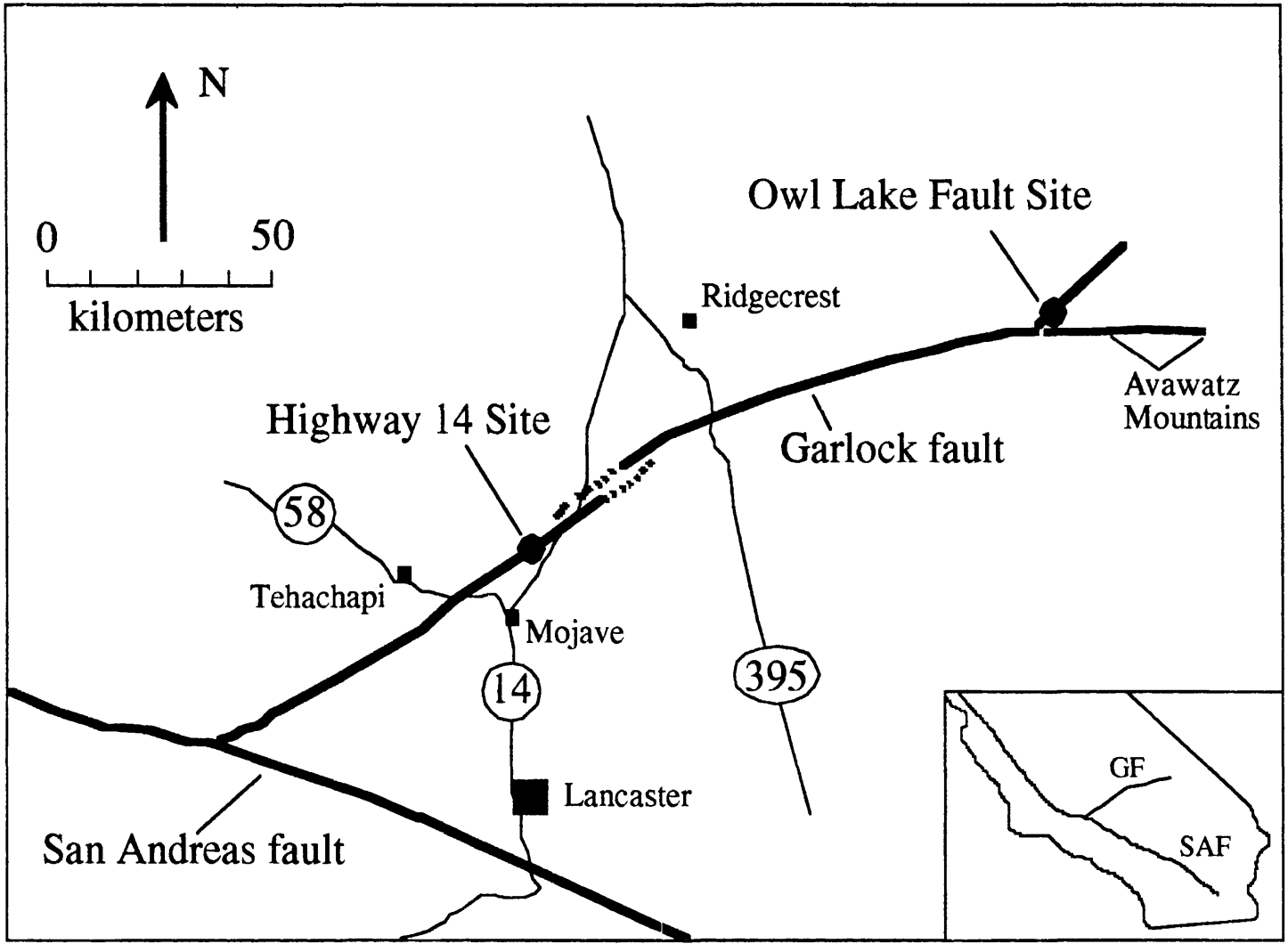

Figure 1: Reference map showing location of Highway 14 and Owl Lake Fault Sites.

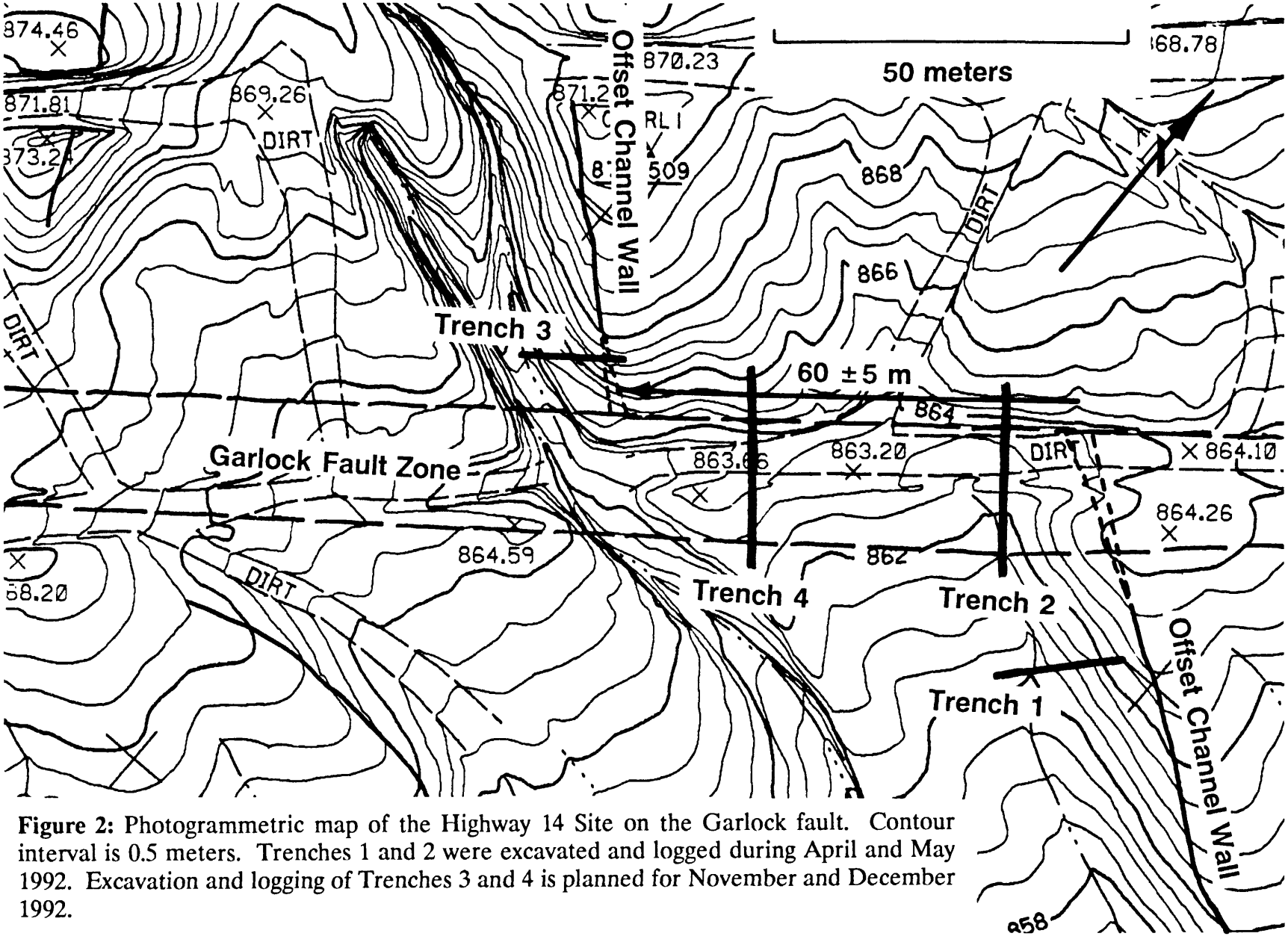

Figure 2: Photogrammetric map of the Highway 14 Site on the Garlock fault. Contour interval is 0.5 meters. Trenches 1 and 2 were excavated and logged during April and May 1992. Excavation and logging of Trenches 3 and 4 is planned for November and December 1992.

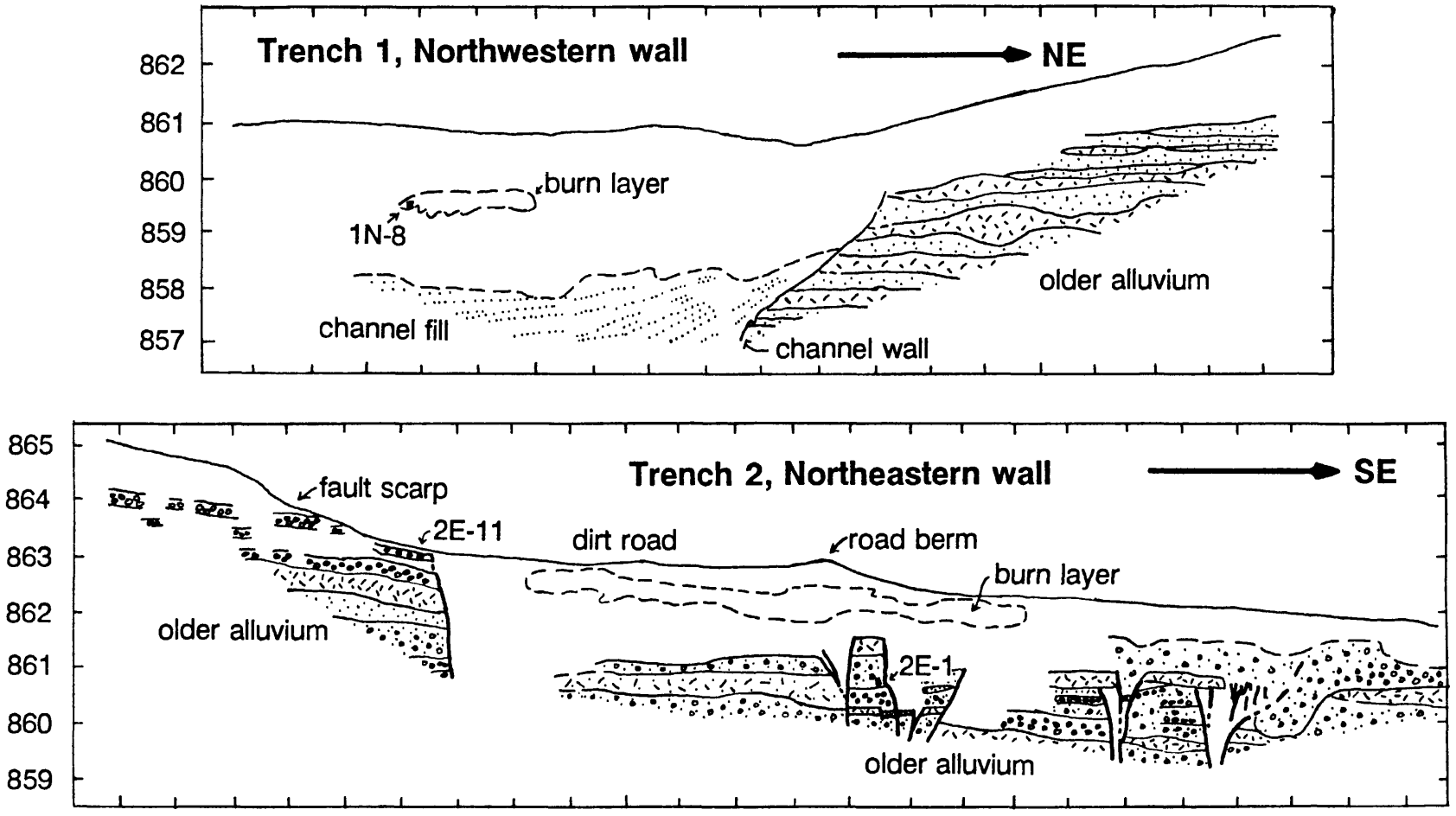

Figure 3: Cross sections along Trenches 1 and 2. Trench 1 crosses the northeastern wall of the offset channel southeast of the fault. Trench 2 crosses the Garlock fault zone near Trench 1. Blank areas are massive. 1N-8, 2E-1 and 2E-11 are charcoal samples that have been submitted for radiocarbon dating. Tick marks along sides of each cross section are spaced 1 m apart. Elevations along left side of each cross section are in meters above sea level. Absolute elevations are approximate (± 5 m).

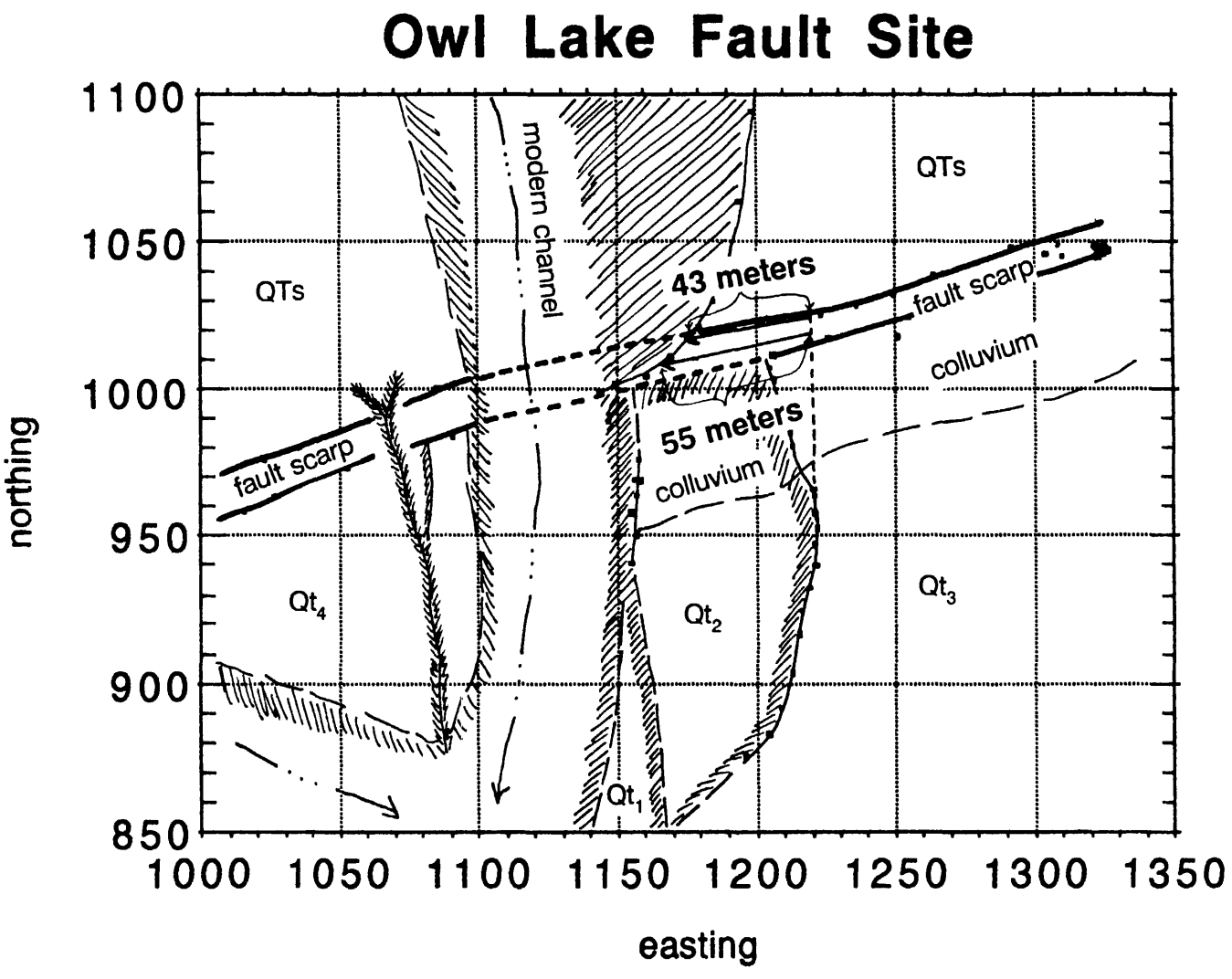

Figure 4: Sketch map of the Owl Lake Fault Site with surveyed points along the top of the eastern wall of the offset channel and along the top and base of the fault scarp. QTs, Late Tertiary or Early Quaternary conglomerate, sandstone, and claystone; Qt_1 to Qt_4, progressively higher and older Late Quaternary alluvial terraces.

Parkfield Earthquake Prediction Experiment: Earthquake Seismology

9930-02098

Andrew J. Michael
Branch of Seismology
U.S. Geological Survey
345 Middlefield Road, MS/977
Menlo Park, California 94025
(415)329-4777

Investigations:

The principal subject of investigation is an attempt to understand the structure and behavior of the seismogenic zone at Parkfield, California in order to better understand the physical processes that control the earthquake generation cycle in that area. In addition we have been attempting to apply these ideas to other areas to determine if we have uncovered processes that are generally applicable or if they are specific to the Parkfield area. To accomplish this we have maintained a detailed catalog of Parkfield hypocenters and focal mechanisms and determined a three-dimensional velocity model of the Parkfield region. This velocity modeling work is in collaboration with Donna Eberhart-Phillips.

Another important Parkfield activity this year has been organizing a review of the Parkfield experiment in anticipation of the end of the 95% confidence window for the long term prediction in January, 1993. John Langbein, Peter Malin, and myself organized a three day review meeting for the Parkfield Working group at UC Santa Cruz in June 1992. The report for this meeting was given to the NEPEC appointed review panel for their use and will be submitted to EOS in the near future.

Finally, in October of 1992 the Parkfield experiment underwent its first A level alert and public short-term earthquake warning. This event showed that our real-time processing techniques were capable of responding quickly to a possible foreshock (the State of California released its warning only 33 minutes after the foreshock occurred) and that the public education effort around Parkfield was successful. This was demonstrated by the positive response to the alert despite the fact that the mainshock did not occur.

Due to the high level of earthquake activity around the state of California during 1992 much of this years principal activities have centered around areas other than Parkfield. After the April 1992 M_S = 7.1 Cape Mendocino earthquake I organized a group of 10 institutions that installed a total of about 35 portable digital 3 to 6 component seismic stations in and around the epicentral region. This data is now being used for a variety of studies, perhaps the most important of which is an attempt to get accurate focal depths for the aftershocks in order to determine their relationship to the megathrust.

On June 28 the Landers earthquake occurred and triggered seismic activity up to 1250 km away which is far beyond the usual aftershock zone. We have been studying this activity in order to determine the mechanisms that could cause such distant

triggering.

On a more theoretical level I have been investigating the best way to undertake and justify research on earthquake prediction by comparing it to the history of weather prediction. Currently in earthquake prediction there are two avenues being pursued. The first is a search for patterns of precursory behavior with little or no regard for physical models. This appears, at times, to be desirable because it is clearly an attempt at earthquake prediction. The other avenue appears less direct and is the attempt to understand the underlying physical causes of earthquakes. The same two avenues were pursued in meteorology and the second avenue turned out to be the successful one. By analogy it suggests that basic studies of earthquake processes are justified as part of an earthquake prediction program.

Results

The June 28, 1992 M_S = 7.5 Landers earthquake triggered seismicity far beyond the aftershock zone at distances of up to 1250 km. The times and locations of the earliest events may help constrain the mechanism responsible for such remote triggering. However, the mainshock seismogram may obscure the earliest events and prevent them from being identified or located. Due to attenuation the mainshock seismograms become deficient in high frequencies as epicentral distance increases, while the local events are deficient in low frequencies due to their small source dimensions. Thus a high-pass filter will tend to enhance signals from the local events relative to the "noise" from the mainshock. Experimentation has shown that this is best done with a 5 to 30 Hz bandpass filter on the data recorded by the Northern California Seismic Network (NCSN).

When filtered the low gain vertical components within the NCSN reveal triggered events starting within the S coda at both Long Valley and the Geysers Geothermal areas. Other stations at similar distances did not show triggered events, which demonstrates that these events are not artifacts of the filtering or large aftershocks near Landers. The low gain components were chosen to minimize clipping; however, tests show that the same events can also be detected by filtering the more numerous clipped high gain NCSN stations. By using more stations we can identify more events and get locations. The onset of activity in these two areas came about 30 seconds after the S arrival which coincides with the arrival of surface waves which can produce dynamic stress of a few tens of bars. Thus, this result helps to link these events to the dynamic stresses produced by the surface waves.

At Long Valley Caldera there were thirteen events during the first 10 minutes of which 11 within a few hundred meters of each other. The two others were within at least a km of that spot, but the exact locations have not been determined. At the Geysers the 19 events in the same time period were spread throughout a volume with about a radius of 5km. Further work on the locations and magnitudes is expected during FY93.

Bends and offsets in faults have been proposed as features that affect the propagation of earthquake ruptures and result in fault segmentation. To investigate the physical causes of this observation, we have reanalyzed the earthquakes in the Parkfield region within a three-dimensional velocity model. The Parkfield segment is

particularly interesting because of its historical record of repeated earthquakes that begin under Middle Mountain near a 5° bend in the surface trace of the San Andreas fault and end near the 1 km wide right-stepping offset in the surface trace through Cholame Valley.

However, relocations of the background seismicity from 1984 to 1990 have shown that these earthquakes lie on, or close to, a single plane and does not follow these surface complications in the fault trace. This result is in contrast to the results originally obtained from the 1966 aftershock sequence. Eaton *et al.* (1970, BSSA, pp. 1151-1197) suggested that the fault became more complicated through Cholame Valley and that this might account for the southeastern termination of the 1966 event. However, relocations of the aftershocks using more accurate JHD techniques, such as VELEST, suggest that the fault that was active during the aftershocks is the same essentially planar fault that is active during the current background seismicity. Along these lines, more obvious and abrupt offsets in the faults that made up the Landers earthquake did not act as a barrier to the rupture.

Reports:

Eberhart-Phillips, D. M., Michael, A. J. , The 1991 active seismic experiment in the Loma Prieta, California region: shallow seismicity and fault structure, abstract, EOS, 72, 311.

Michael, A. J. ,Eberhart-Phillips, D. M., 1991 , Fault geometry at the surface and at seismogenic depth near Parkfield, California, abstract, EOS, 72, 483.

Michael, A. J., 1992, Three's a crowd in California, Nature, 357, 111-112.

Eberhart-Phillips, D.M., Michael, A.J, 1992, Three-dimensional velocity structure and seismicity in the Parkfield region, central California, J. of Geophys. Res., submitted.

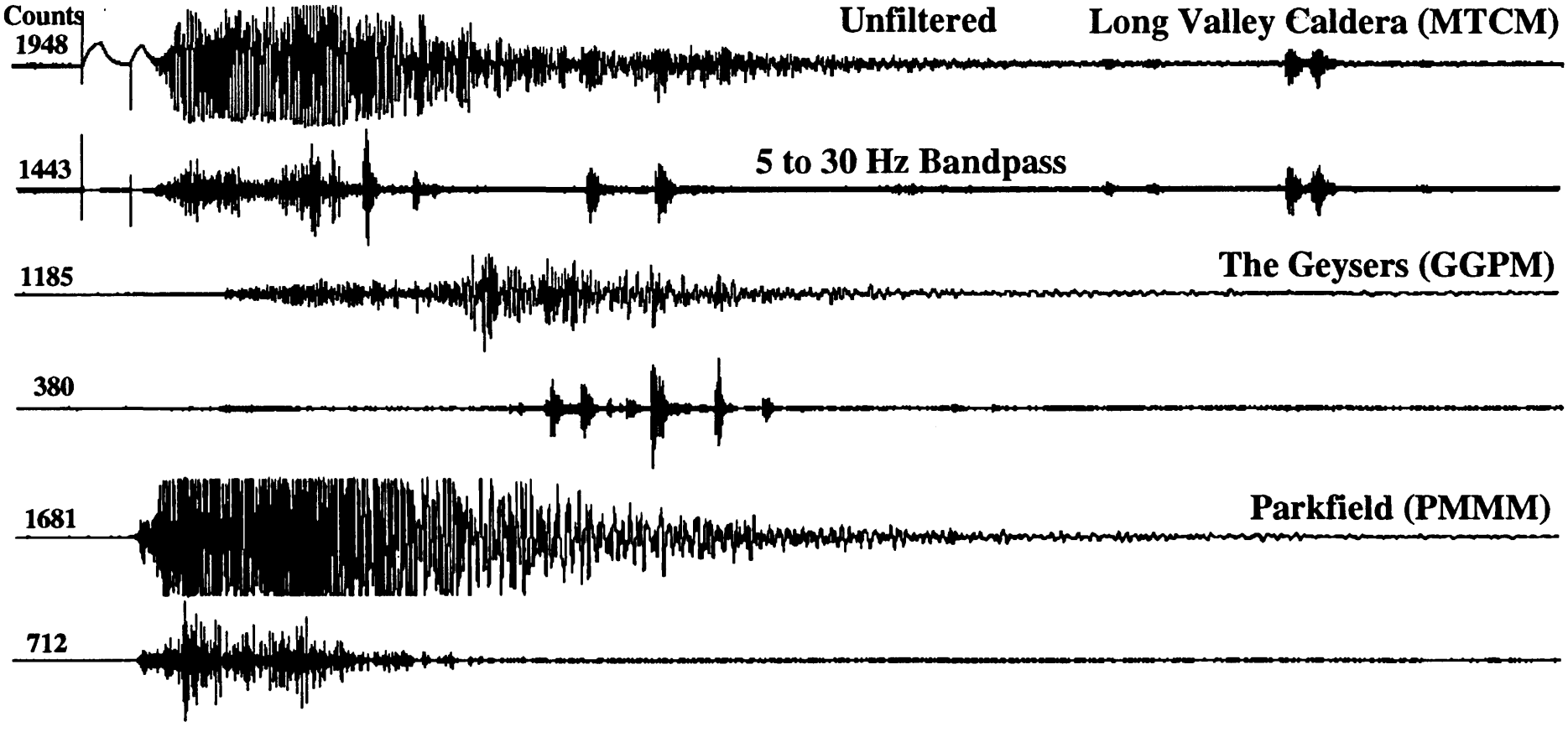

Figure 1. Filtered and unfiltered low-gain vertical seismograms of the Lander's earthquake recorded at Long Valley Caldera, the Geysers, and Parkfield. The filtered traces at the first two sites show local earthquakes beginning 30 seconds after the S arrival.

Analysis of stress drops, rupture lengths, and slip distributions, along the northern segment of the New Madrid seismic zone

Agreement No. 1434-92-G-2231

Kevin L. Mickus
Department of Geography, Geology and Planning
Southwest Missouri State University
Springfield, MO 6580

(417)-836-6375

Investigations Undertaken

This research focuses on the analysis of small earthquakes ($M<3.5$) along the northern segment of the New Madrid seismic zone for stress drops, rupture lengths, and slip distributions from 1980 to present. The technique of Mori and Frankel (1990) for removing the path and site effects of small events by using co-located aftershocks will be used to estimate the rupture lengths and stress drops. The deconvolved data will be analyzed for slip distributions using the technique of Mori and Hartzell (1990).

Results

Research has been completed on the 75% of the first phase of the project. The seismograms of five main events and ten aftershocks have been obtained from St. Louis University. The digital data from the Panda experiment coordinated at Memphis State University have not been released. Each of the main events and aftershocks were recorded on at least 5 stations and at most 22 stations. The seismograms for all stations for each main event and all nearby aftershocks were examined for the quality of the P-wave first motions and the if the aftershock had a similar waveform as the main event. Because some aftershocks were small ($M=1.6$) the quality of the seismograms were poor for many stations, so only a small portion of the stations were used for analysis. For example, a main event ($M=2.6$) recorded on 1/21/86 was recorded on twenty-three stations and two aftershocks ($M=2.0$ and 1.6) were recorded on 14 and 18 stations, respectively. After examining all the seismograms, I found that nine stations could be used for further analysis.

To determine if the main events and their associated aftershocks are indeed co-located (with 1 km), I next performed a relocation of all events using a 3-D relocation algorithm developed by Shedlock and Roecker (1988). This was done because the hypocenter locations provided by St. Louis University are based on a one-dimensional velocity model determined in 1975 by Otto Nuttli and there have been several seismic refraction, reflection and 3-D velocity models determined from the inversion of travel time residuals (Al-Shukri and Mitchell, 1987) performed in the New Madrid area, so a more accurate velocity could be used. The relocation of some events agreed with those of St. Louis University but some were deeper by 20%, which agree with the results of Al-Shukri and Mitchell (1987). Not all aftershocks were within 1 km of the main event and had to be discarded from further analysis.

The events remaining after being relocated were processed using the technique of Mori and Frankel (1990). The aftershocks were used as an empirical Green's function to deconvolve out site and path effects from the main event. Each event was Fourier transformed and then the main event was divided by the aftershock and the result was then inversed Fourier transformed. The final result will then analyzed for stress drops and rupture lengths. This step has not been performed yet.

The final step in the analysis will be to analyze the deconvolved main events for slip distributions. A source inversion algorithm developed by Mori and Hartzell (1990) will be used to determined the fault planes and slip distributions. This will be performed next Spring.

Reports

There have been no published reports or talks given to date. An abstract will be sent to Geological Society of America's north-central meeting in December and a talk will be given next March. This talk will cover the stress drops and rupture lengths. An abstract concerning the slip distributions will be sent to Spring 1993 American Geophysical Union meeting.

References

Al-Shukri, H., and Mitchell, B.J., 1988, Reduced seismic velocities in the source zone of New Madrid earthquakes: Bull. Seis. Soc. Am., v. 78, p. 1491-1509.

Mori, J., and Frankel, A., 1990, Source parameters for small events associated with 1986 North Palm Springs, California earthquake determined using empirical Green functions: Bull. Seis. Soc. Am., v. 80, p. 278-297.

Mori, J., and Hartzell, S., 1990, Source inversion of the 1988 Upland, California earthquake: determination of a fault plane for a small event: Bull. Seis. Soc. Am., v. 80, p. 507-518.

Shedlock, K.M., and Roecker, S.W., 1987, Elastic wave velocity structure of the crust and upper mantle beneath the North China basin: J. Geoph. Res., v. 92, p. 9327-9350.

Recognition of the Effects of the 1811-1812 New Madrid Earthquake in the Sediment Record of Reelfoot Lake: Technical Report

Award number 1434-92-G-2232

Dr. June E. Mirecki
Department of Geological Sciences
Memphis State University
Memphis, TN 38152
(901) 678-4358
MIRECKIJ@MEMSTVX1

Investigations Undertaken

The principle objective of this investigation is to characterize the effects of the 1811-1812 New Madrid Earthquakes, as preserved in the lacustrine sediment archive of Reelfoot Lake. Because it is difficult to discern the physical effects of seismic-induced deformation, especially under subaqueous conditions, we will attempt to define the 1811-1812 "earthquake horizon" using geochronologic (C-14, Pb-210) and palynologic tools. The hypothesis is that several palynologic indicators of land-use change should be useful for definition of the earthquake horizon. These effects are not necessarily co-seismic, but the timing of these changes (such as extensive regional deforestation and subsequent agricultural activity after 1840) will be useful in bracketing any earthquake effects in the lacustrine sediment record.

Results Obtained

1. 10 vibracores were taken from the periphery of lower Blue Basin in Reelfoot Lake during the months of April and October 1992 (Fig. 1). Cores ranged in length between 1 and 2 meters. Similar lithologic sequences were observed in most cores, consisting of a dense, compact clayey silt overlain by organic-rich mud (Fig. 2). Occasional sand layers are observed in some cores.

2. Grain-size analysis of selected cores is proceeding, in order to characterize the core for subsequent paleomagnetic, palynologic and geochronologic studies. The sand-sized fraction of selected cores (Moultrie Field and Blue Basin Livingston cores, collected by USGS and MSU in 1991) are being examined for the presence of anthropogenic particles as an additional relative indication of time.

3. Subsamples of selected cores were submitted for paleomagnetic analysis.

4. Cores have been x-radiographed.

Reports Published

No reports have been published to date.

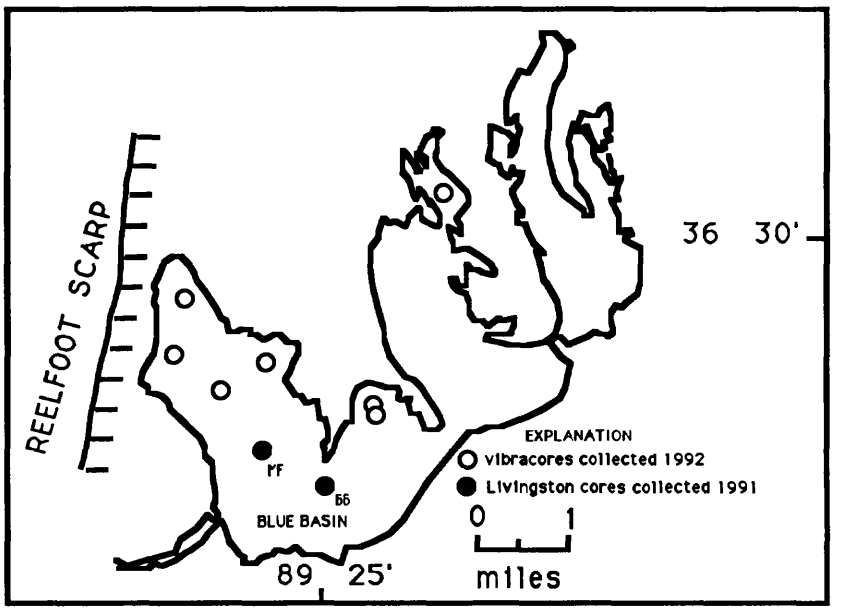

Figure 1. Location of all cores collected for preliminary work (1991) and for this project (1992) from Reelfoot Lake, Obion and Lake Counties, TN.

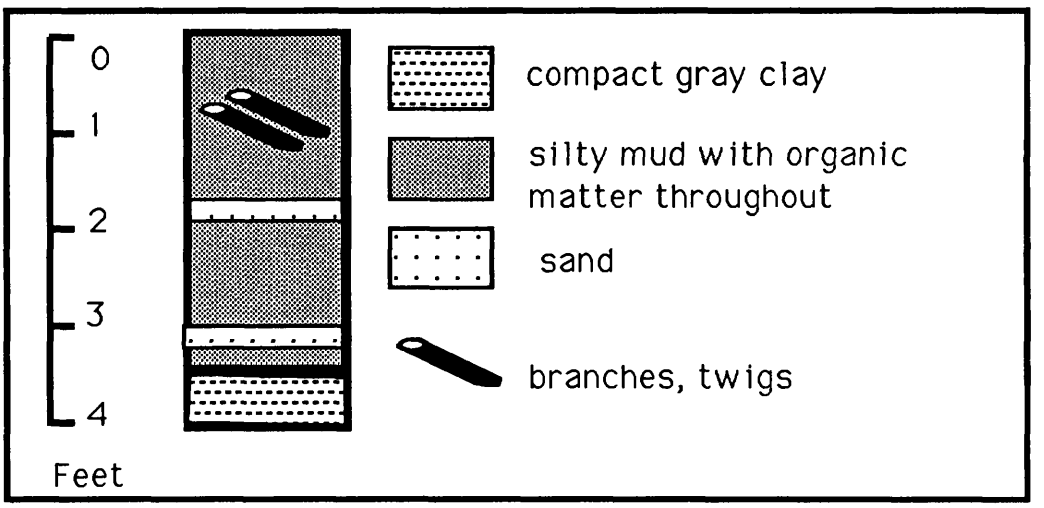

Figure 2. Typical stratigraphic section from Reelfoot Lake cores collected in 1992. All cores range in length from 1-2 meters, and show a less compact, organic-rich silty mud overlying a dense, blue silty clay.

Loma Prieta Data Archive Project

1434-92-G-2228

Jack P. Moehle and Katherine A. Frohmberg
Earthquake Engineering Research Center
University of California
1301 South 46th Street
Richmond, CA 94804
(510)-231-9401
e-mail: katie@eerc.berkeley.edu

Introduction

Under the general editorship of the U.S. Geological Survey (USGS), the National Earthquake Hazards Reduction Program (NEHRP) is issuing the official report to Congress describing the post-earthquake investigation of the October 17, 1989, Loma Prieta, California earthquake. That report will synthesize results of earthquake research funded and performed by a wide range of investigators. These investigators have produced or gathered a variety of data sets generated by the earthquake or produced as a result of research into the earthquake. Of necessity, the NEHRP report will not be a suitable medium for distributing this extensive data.

The nonprint data is extremely important to organize and preserve since it will not be published in the open literature and, unless preserved, will be lost to future scholarship. The Loma Prieta earthquake is the first major earthquake in the San Francisco Bay Area since 1906 and is the first to occur in a highly populated, heavily instrumented area. The data will form an important baseline for research into future earthquakes in this area and elsewhere.

The National Information Service for Earthquake Engineering (NISEE) at the Earthquake Engineering Research Center (EERC) was charged by the National Science Foundation in 1971 to gather and disseminate information in earthquake studies, particularly earthquake engineering. As a result of the Loma Prieta earthquake, NISEE founded the National Clearinghouse for Loma Prieta Earthquake Information in 1990. The clearinghouse has gathered data from a wide variety of sources and published the Loma Prieta Clearinghouse Catalog listing 1500 sources of information on or about the earthquake.

Investigations Undertaken

NISEE has established the Loma Prieta Data Archive to gather, organize, and issue the raw data associated with the Loma Prieta earthquake in one coherent format. In particular, NISEE will

* **identify** the data sources produced as a result of the earthquake
* **gather** them together
* **organize and issue** the data on CD-ROM with a printed user's guide
* **deposit** the guide and CD-ROMs in selected national and university libraries throughout the country as well as distribute them at cost to anyone interested
* **publicize and disseminate** the archive to researchers worldwide

The data from the Loma Prieta earthquake is extremely important to preserve since this earthquake occurred in a heavily populated area where there were a great number of strong-motion instruments. There is more data available for study from this earthquake than for any significant earthquake in recent history. Therefore, experimental data will used as a baseline for future research in the Bay Area and other locations. In addition, making this data generally available will allow for independent verification of results by other researchers.

Results Obtained

The project is still in the data gathering stage. By December 31, 1992, the bulk of the data will have been submitted. It will then be manipulated for issuance on the CD-ROM.

Reports Published

A printed guide to the data will be issued in late 1993/early 1994 as an addendum to the U.S. Geological Survey (USGS) Professional Paper series which will constitute the NEHRP Report to Congress. The CD-ROMs themselves will be distributed by NISEE at cost.

SEISMIC REFRACTION STUDIES OF THE NEW MADRID SEISMIC ZONE

9930-02102
Walter D. Mooney
Rufus D. Catchings
Seismology Branch
U.S. Geological Survey
345 Middlefield Road, MS 977
Menlo Park, CA 94025
(415) 329-4764

INVESTIGATIONS:

1. The objective of this project is to understand the physical properties of the New Madrid seismic source zone based on recently recorded high-resolution seismic refraction profiles and related geophysical data.

2. This study is closely coordinated with other geophysical studies. Specifically, our seismic refraction profiles were recorded coincident with seismic reflection, magnetotellurics, high-resolution magnetics, and gravity data.

RESULTS:

Geophysical studies of the New Madrid Seismic Zone (NMSZ) have made impressive progress toward understanding the origin and risks associated with this intra-continental seismic zone ever since the Reelfoot Rift (Fig. 1) was identified using potential field data. Major advances followed the acquisition within the Mississippi Embayment of 100's of kms of seismic reflection data by industry. This reflection data documents the correlation of the seismicity with a highly faulted and deformed zone known as the Blythville Arch (and to the NE, the Pascola Arch).

The correlation of the New Madrid axial seismic zone with the Blytheville and Pascola arches (Fig. 1) brings us close to a fundamental understanding of the physical causes of seismicity within the NMSZ: it appears that the geologic structures within the arches are weak due to effects that may include: repeated deformation, igneous intrusion, diapirism, and/or thermal and hydrothermal alteration. A recent study that compares the Blytheville arch with existing (1980-vintage), sparse seismic refraction data indicates that the waves that pass through the arch are strongly attenuated, but this study was unable to identify the physical mechanism for this attenuation, or reliably determine seismic velocities within the arch (Hamilton and Mooney, 1990).

The goal of this project is to determine, with high-resolution, the compressional and shear-wave velocity and seismic attenuation properties of the Blythville arch. In combination with other data, we will develop a physical model for the arch and of the seismicity of the NMSZ. When completed, this integrated geophysical study of the New Madrid seismic zone will contribute

important criterion for deliminating high-risk seismic source zones throughout the eastern U.S.

We have begun a detailed analysis of high-resolution seismic refraction data across the New Madrid fault zone in the vicinity of Blythville, AK. (Fig. 1; "FY92 profiles"; Fig. 2 and 3).

2. (A) W. Mooney and R. Catchings lead the field project during October/November 1991. A long-distance profile was recorded from Memphis to St. Louis, and a pair high-resolution refraction profiles were recorded across the New Madrid fault. The following institutions were major participants in the 1991 field project:

U.S. Geological Survey
University of Wyoming
University of Tennessee, Knoxville
University of Texas - El Paso
Lamont-Doherty Geological Observatory

In addition, the following institutions provided significant field assistance, or recorded data of their own with permanent network or portable seismographs:

Memphis State University
Saint Louis University
Purdue University (field assist.)
University of Kansas (field assist.)

(B) All data have been played back, merged, and written to an industry-standard "SEG-Y" digitial data tape (Fig. 2 and 3). This turned out to be a difficult task because the presently-available instrumentation in the US is limited to about 100-200 channels per instrument type. In the 1991 New Madrid project, six types of instruments were used, necessitating considerable pre-processing prior to merging.

(C) Catchings and Mooney (1992) presented results based on the interpretation of the long-distance profiles. (New Madrid Special Session, SSA meeting, Santa Fe, N.M.).

3. Data Interpretation: The data were recorded with acquisition parameters that permit the use of a seismic inversion method (W. Lutter's USGS code), rather than interactive trial-and-error fitting, thereby giving quantitative resolution estimates on the seismic velocity models. The structural complexity of the Blytheville arch will necessitate the use of some more sophisticated wave propagation modeling methods (finite differences). Art Frankel and Harley Benz have agreed to take the lead on this effort. Interpretaion will be coordinated with complementary MT, potential field, and seismic reflection studies (Denver USGS and R.M. Hamilton, USGS, Reston, VA.).

4. Relation to non-Geological Survey Programs:

** The seismic networks in the area have made use of the explosions fired in this study to further calibrate the velocity structure; we will work closely with the staff of these networks to ensure optimal use.

** We have coordinated with Jer-Ming Chiu (Memphis State University), who took advantage of the mobilization of a large field to conduct an add-on seismic experiment to complement this study.

REPORTS

Catchings, R. D. and W. D. Mooney, 1992, Velocity and Q models of the Mississippii embayment, Seis. Soc. America, Santa Fe, April, 1992, (abst. in Geophy. Res. Lett., in press).

Mooney, W.D. and Meissner, R., 1992, Multi-genetic origin of lower crustal reflectivity: a review of seismic reflection profilin the continental lower crust and Moho, in: The Continental Lower Crust, D. Fountain, R. Kay, and R. Arculus, editors, Elsevier, Amsterdam 45-84.

Holbrook, W.S, Mooney, W.D., and Christensen, N.I., 1992, Seismic velcoity structure of the lower continental crust, in The Continental Lower Crust, D. Fountain, R. Kay, and R. Arculus, editors, Elsevier, Amsterdam, 1-43.

Durrheim, R. A. and Mooney, W. D., 1991, Archean and Proterozoic crustal evolution: evidence from crustal seismology, Geology, 19, 606-609.

Catchings, R.C. and Mooney, W.D., 1991, Basin and Range crustal and uppermost mantle structure, Northwest to central Nevada, Jour. Geophys. Res., 96, 6247-6267.

Fuis, G.S. and Mooney, W.D., 1990, Lithospheric structure and tectonics from seismic refraction and gravity data, in: R.E. Wallace, editor, The San Andreas Fault System, California, U.S. Geological Survey Prof. Paper 1515, 207-236.

Hamilton, R.M. and Mooney, W.D., 1990, Seismic-wave attenuation associated with crustal faults in the New Madrid Seismic Zone, Science, 248, 351-354.

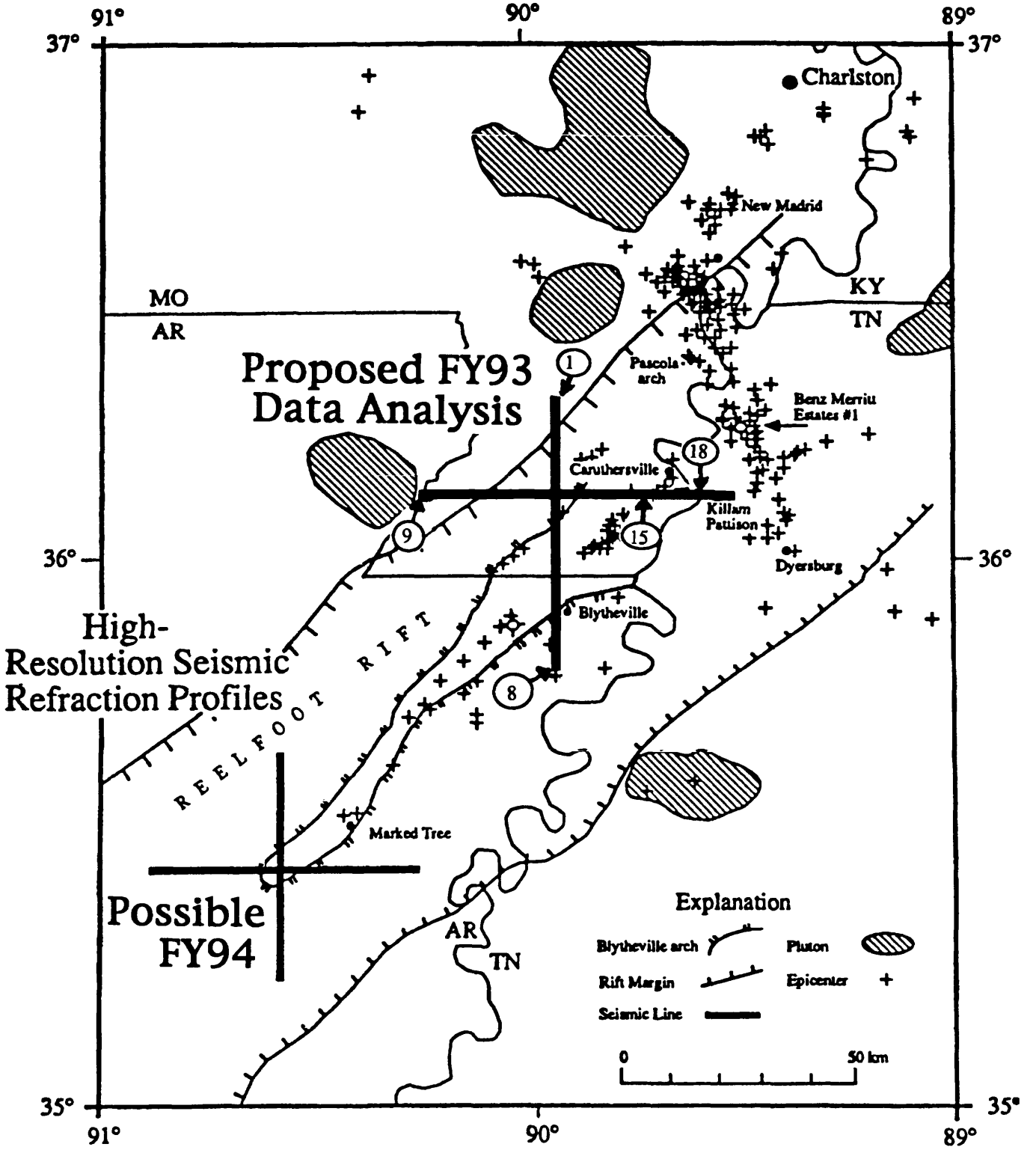
91°
90°
89°
37°
36°
35°
Charlston
New Madrid
MO
AR
KY
TN
Proposed FY93
Data Analysis
Pascola arch
Benz Merriu Estates #1
Caruthersville
Killam Pattison
Dyersburg
Blytheville
High-Resolution Seismic Refraction Profiles
REELFOOT RIFT
Marked Tree
Possible FY94
Explanation
Blytheville arch
Rift Margin
Seismic Line
Pluton
Epicenter
0
50 km
1
9
18
15
8

Figure 1.

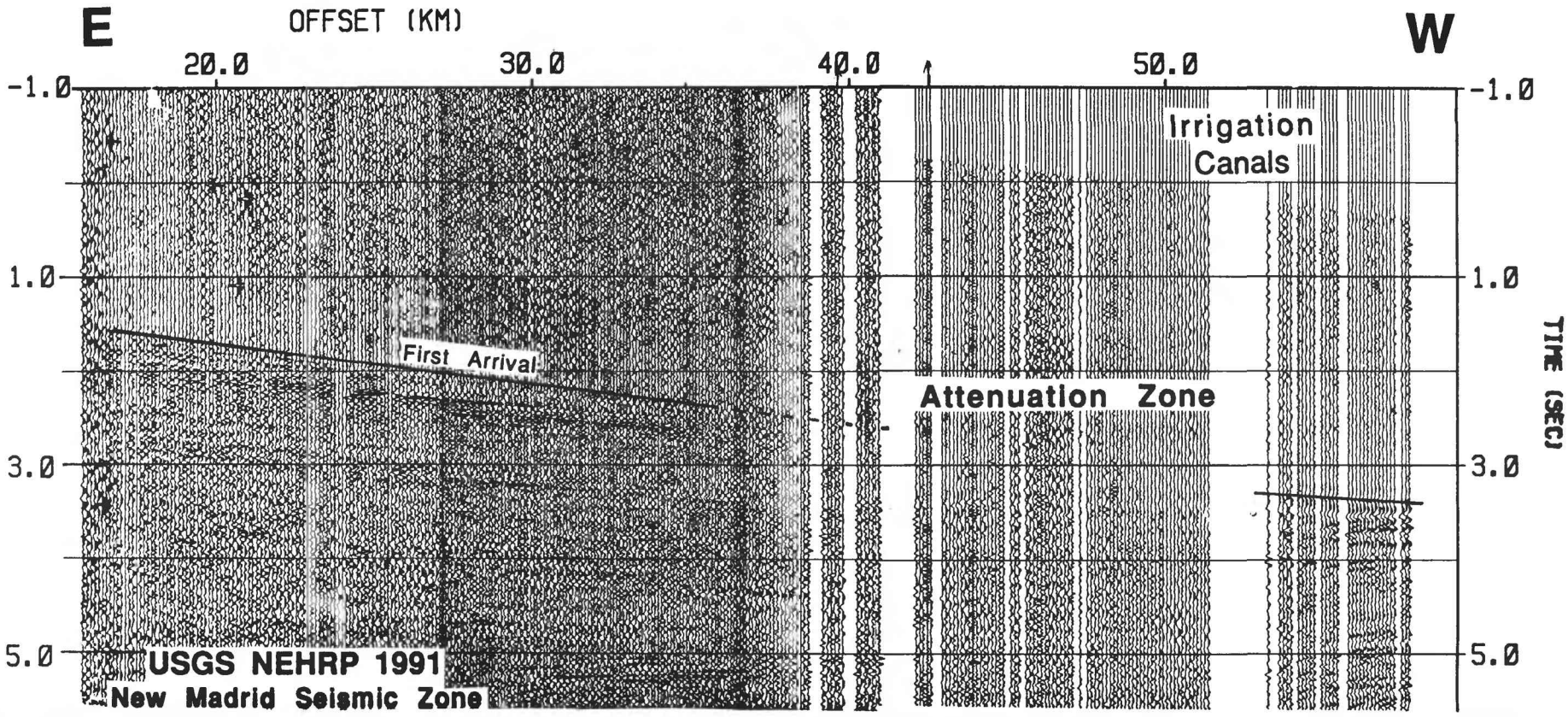

Figure 2. Seismic refraction data collected by the USGS in 1991 across the New Madrid seismic zone on the east-west profile of Figure 1 (shot point 18). Increased offset to the West; reduction velocity 8 km/s, not the usual 6 km/s due to shallow high-velocity carbonates.

These data show clear attenuation of first-arrival energy as the Blytheville arch is crossed. We propose to interpret these two-component (vertical and in-line) data in terms of the laterally varying compressional and shear wave velocity structure. Our results will help define the physical properties of the New Madrid fault zone.

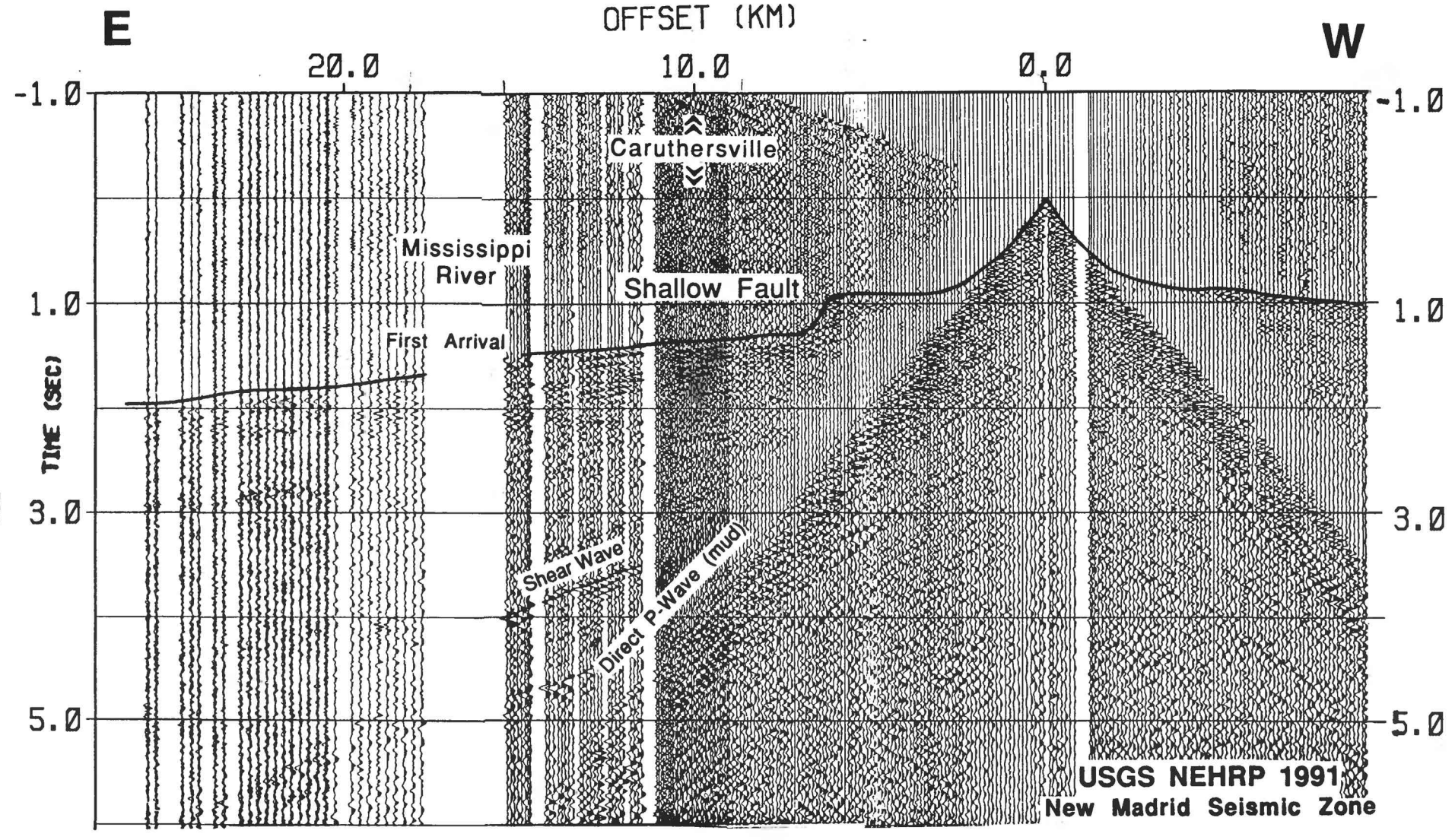

Figure 3. Seismic refraction data for east-west profile for shot point 15 located above the seismic lineament (Fig. 1). This profile shows a significant and abrupt traveltime delay 6 km to the east of the shot point, signifying a shallow basement offset (down to the east). This basement offset correlates with the arch. This figure and the previous one show typical data quality (i.e., not the best) for the eighteen shots recorded during the 1991 New Madrid seismic refraction experiment.

Annual Report
Southern California Earthquake Project
(9930-01174)

J. Mori, T. Heaton, L. Jones,
D. Eberhart-Phillips, L. Hwang, R. Dollar,
D. Given, C. Koesterer, L. Wald

Branch of Seismology
U.S. Geological Survey
525 S. Wilson Ave. Pasadena CA 91106
818-405-7821

INVESTIGATIONS

This report covers most of the (old) Seismology Branch activities in the Pasadena Office of the U.S. Geological Survey for FY1992. This large project is involved in a wide range of tasks from field maintenance of instruments and seismic data processing through efforts in developing real-time earthquake information systems and basic research. Tasks for the FY1992 proposal were divided into 3 categories.

- Seismic Data Collection
- Earthquake Hazards Monitoring and Public Information
- Earthquake Research

The work carried out in all three categories was dominated by the intense sequence of earthquakes that occurred at Joshua Tree (M6.1 on April 23), Landers (M7.5 on June 28), and Big Bear (M6.5 on June 28). These 3 damaging earthquakes along with the tens of thousands of aftershocks severely tested the capabilities of the Project. Personnel, instrumentation, and computer systems were generally successful in meeting the challenge. There was practically no loss of data. Scientists were able to watch the aftershock sequences develop in real-time and release quick information to government agencies and media. Over 90 Gbytes of seismic data provide numerous new opportunities for research.

Seismic Data Collection

A major responsibility of the Project is to maintain and operate the large (220 site) seismic network, thus a substantial part of the Project's resources (Personnel and Operating Expenses) are used for instrument maintenance. The network provides the primary data for hazard monitoring in southern California and data for much of the research done by the project scientists. Responsibilities for hardware (instrument sites, radio telemetry, microwave and telephone links, computer cluster) and software (on-line recording system, off-line data processing, real-time earthquake information systems) are shared jointly with Caltech.

In addition to maintaining the network, we continue to try and improve our seismic recording capabilities by installing new sites in sparsely instrumented areas, adding Force-Balance-Accelerometers (FBA) to improve on-scale recordings of larger earthquakes, and installing broadband TERRAscope instruments with large dynamic range. FBA components and the TERRAscope data are crucial for both the development of better real-time information systems and the on-going research of seismic waveforms.

Routine analysis of the data is also carried out cooperatively with Caltech and includes, interactive timing of phases, location of hypocenters, calculation of magnitudes and preparation of the final catalog. Phase data are stored on magnetic disks and waveform data

are archived on magnetic tape and an optical mass storage device. These data are readily available to other USGS and university users.

Earthquake Hazard Monitoring and Public Information

An important part of monitoring earthquakes in a populated region such as southern California, is the ability for scientists to have access to quick and accurate locations and magnitudes. This enables them to release timely information to government officials and the media following felt and damaging earthquakes. Also, real-time locations and magnitudes are useful for watching large aftershock sequences develop providing possible information on forthcoming activity. To facilitate the response, we have worked on the reliability and speed of applications to improve the automated event locations and magnitudes. In addition to hypocenters and magnitudes of the earthquakes, we are developing further real-time utilizations such as, alarms for unusual activity in special study areas, designation of likely areas of damage from future large earthquakes, and rapid assessment of earthquake probabilities.

Earthquake Research

The FY1992 proposal listed 6 areas of research which utilized seismic data from the network to study diverse topics, mainly specific to southern California, but having applications to more general seismological problems. Research results were produced in all of these areas of investigation.

Earthquake Mechanics

We proposed to analyze significant earthquake sequences as they occurred in southern California. The 1992 Joshua Tree-Landers-Big Bear (JTLBB) earthquakes were the strongest seismic activity in California in 40 years and has provided much new data for many studies in the years ahead. The large number of aftershocks along the 100 km Landers rupture and the 25 km Big Bear rupture along with associated seismicity in the surrounding region provide a detailed and complex picture of the fault structures. Focal mechanism studies with correlation of the seismic and geological features (particularly large surface faulting of the Landers earthquake) provide insight into the local tectonics and regional stress fields.

Foreshock and Aftershock Statistics

We proposed to continue analysis of the statistical characteristics of foreshock and aftershock distributions. Using a combination of short-term probabilities of earthquake occurence based on these statistics and specific knowledege about characteristic seismicity of certain faults, along with long-term probabilities of damaging shaking from the geologic history of the faults, we are developing a computer program (STEP) to calculate and display real-time probabilites of strong ground shaking. The program maps the probability that an earthquake will generate shaking exceeding 0.10 g in the next 24 hours on a color display of southern California.

Since both the Joshua Tree and Landers earthquakes had foreshocks, we have looked more carefully at the temporal and spatial distribution of these earthquakes to see if they had any distinguishable characteristics. One interesting observation is that the foreshocks before both Joshua Tree and Landers tended to be tightly clustered in space. To quantify the degree of clustering, we determined a "closeness" parameter by calculating the average of $(\frac{1}{distance})$ for every pair of events in a given time window. A running average of this parameter was calculated for the Joshua Tree aftershock sequence which eventually lead into the Landers earthquake. We investigated the possibility that the foreshocks before Landers were significantly more clustered than the rest of the Joshua Tree aftershocks.

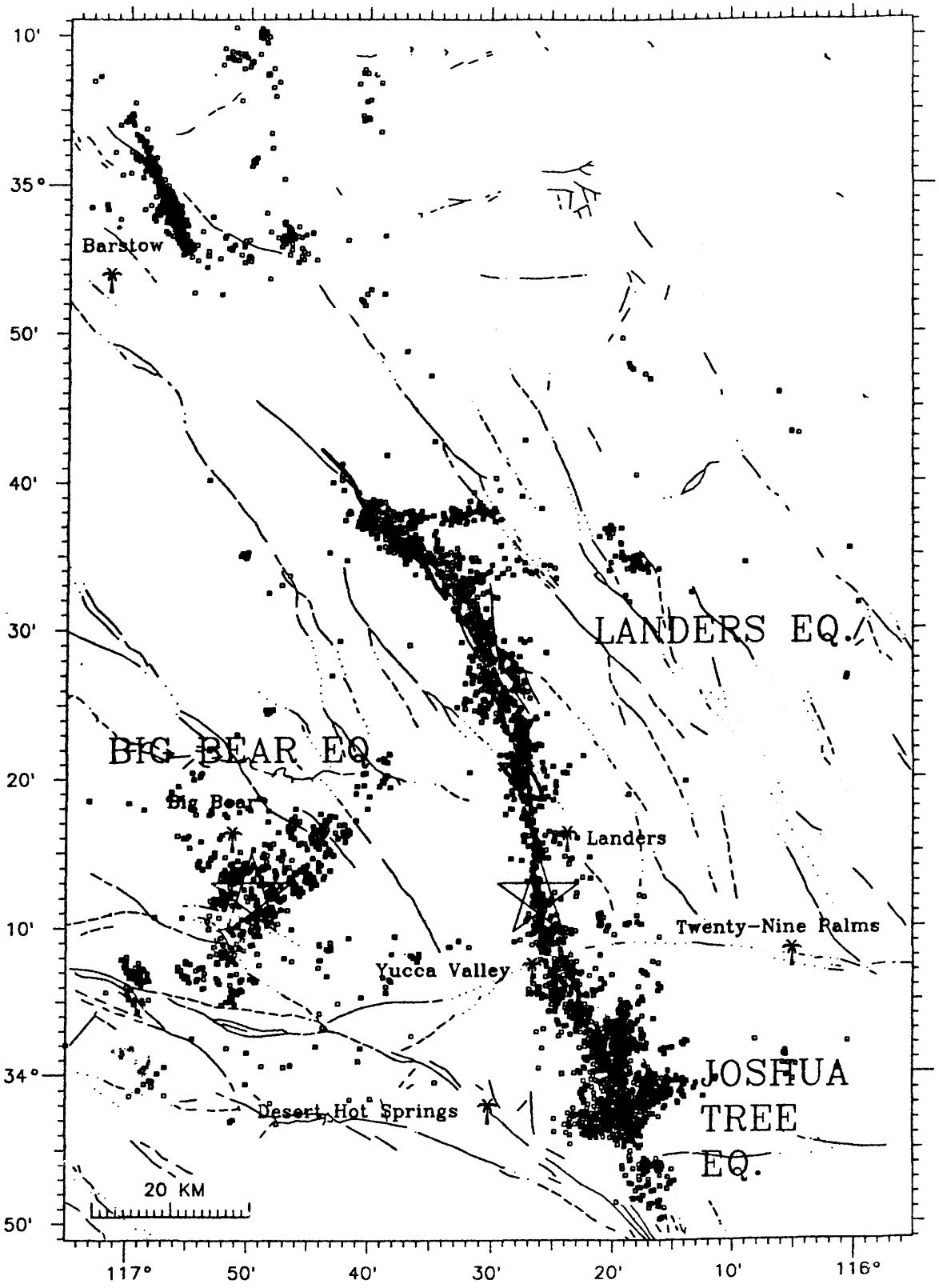

Earthquake locations for the Joshua Tree - Landers - Big Bear sequence.

Short-Period Waveform Studies

We proposed array studies of short-period waveforms to infer structures of the Earth on a variety of scale lengths. Three different types of waveforms studies were carried out using the network data.

Network recordings of local microearthquake in the epicentral region of the 1988 (M4.6) and 1990 (M5.2) Upland earthquakes were cross-correlated to identify similar earthquake groups and study their spatial variability. The P-waveforms from 3 permanent sites that are closest to the aftershock region were bandpass filtered between 1 to 10 Hz and 1 sec of data are cross-correlated. This time window includes the initial P-wave as well as secondary phases. The resulting cross-correlation values are then organized into equivalence class groups - groups of associated events that meet a minimum cross-correlation value criteria. The spatial distribution of the equivalence groups is used to infer small scale structures in the region of the earthquakes.

S-wave codas were studied for events recorded at distances of 5 to 150 km in order to estimate the intrinsic and scattering attenuation. We used a recent formulation by Hoshiba (1991) which uses the time decay of the coda envelope and the amplitude of the direct S wave to estimate both the intrinsic and scattering attenuation. We analyzed several aftershocks of the 1990 Upland earthquake which were recorded at close distances (5 -10 km) by portable instruments and larger distances by the permanent network. We looked for distance dependence to the instrinsic and scattering attenuation which could be used to infer the depth dependence for the two types of attenuation.

Teleseismic P and PcP waves recorded on several hundred stations in California were analyzed to study deep structure of the Earth. Stacked record sections from earthquakes in Fiji were constructed to examine the variations of the PcP arrival compared to the direct P. The variations (or lack of) in relative arrival times and amplitudes are used to resolve details in the core-mantle boundary.

Source Parameters of Small Earthquakes

We proposed to study source parameters (moment, stress drop, energy, fault planes) of small earthquakes (M 3.5 to 4.5) which are well recorded by low-gain components of the network. Using a smaller event as an empirical Green function, one can successfully remove complicated site and path effect from short-period waveforms so that source properties can be resolved. This technique was used to obtain stress drop and rupture directivity in the Joshua Tree foreshock.

Site Response in Basin Structures

Utilizing the broad-band TERRAscope station at Pasadena (PAS), we proposed a study of the characteristics of seismic waves that propagate across the Los Angeles Basin. 30 earthquakes at distances of 2 to 40 km from PAS were studied and events with paths that cross the Basin were compared to events that did not cross the Basin. Effects of frequency-dependent amplifications and phase conversions at the basin-basement interface are related to potential strong-motions from large earthquakes.

Three-Dimensional Velocity Structures

We proposed analysis of crustal structure across the San Gabriel Mountains and Mojave section of the San Andreas Fault. Following the Landers earthquake, the area of focus for the study concentrated on the region around the fault rupture in the Mojave desert. In order to calibrate the crustal structure and obtain a better estimate of the Landers mainshock and aftershock depths, a seismic experiment was conducted (with cooperation from other personnel of the Seismology Branch) to provide explosive sources along the fault rupture. One shot was located near the mainshock epicenter. The second shot was located 40-km north near the southern end of the Camp Rock Fault section of the rupture.

We deployed 42 3-component Reftek instruments in a 110-km long profile approximately paralleling the trend of the rupture. The instruments recorded 160 earthquakes as well as these shots. Five additional instruments were deployed at distributed sites to enhance network coverage, including reoccupation of three of the 1979 USGS Homestead Valley stations.

Using the abundunt aftershocks plus data from two calibration explosions the local velocity structure near the fault and station corrections are determined. More accurate aftershock distribution along with the velocity structure itself help identify physical properties of the fault.

RESULTS

Seismic Data Collection

Data collection during FY1992 included locating and archiving (with Caltech) over 30,000 earthquakes. Seismicity, dominated by the M6.1 Joshua Tree (6000 events) and M7.5 Landers - M6.5 Big Bear (> 20,000 events) sequences, is summarized in the 1991 and 1992 (in preparation) Network Bulletins. The number of earthquakes process in FY1992 was more that 3 times the number of typical years.

The FY1992 proposal lists several instrumental improvements for the network, of which not all were possible because of budget constraints and the extra work caused by the JTLBB sequence. We were able to:

- Install FBA's at 3 permanent sites to increase on-scale recordings of larger earthquakes.
- Expand the microwave telemetry system, which reduced costs of renting telephone lines.
- Carry out site and instrument preparation for the a broadband TERRAscope station near Superstition Hills. Station should be in operation in FY1993.
- Install 3 semi-portable stations in the JTLBB region each with 4 component of velocity sensors and 3 component FBA's were added to the telemetry system in response to the recent activity.

There were significant improvements to user access to the network data. The work done in conjunction with the Southern California Earthquake Center (SCEC) and Caltech, enabled the network waveform data from 1983 through part of 1992 (including much of the JTLBB sequence) to be accessible from an optical mass storage device to users over INTERNET. This data set currently consists of over 150 Gbytes of waveforms.

There were improvements to continuous recording system of the network data on the 4mm tape drives. Data from about 200 teleseismic and local events were provided to USGS and university researchers from this system.

Earthquake Hazard Monitoring and Public Information

Progress was made in the software systems which automatically determine and broadcast earthquake locations and magnitudes. We now have a moderately reliable system, which sends locations and preliminary magnitudes over computer mail and to pocket pagers within 5 minutes of significant earthquakes. More accurate (although time consuming) magnitudes are determined for larger earthquakes and update messages follow several minutes later, if necessary. Graphic displays of these real-time data were particulary useful for watching the aftershock sequences develop following the Joshua Tree and Landers - Big Bear earthquakes.

Although the high rates of seismic activity during both of these sequences overloaded parts of the online recording system and hampered quick release of information, there was no data loss and scientists were able to provide preliminary information within 20 minutes. After the initial computer problems during the first few hours were solved, the automatic location and magnitude determinations became invaluable for providing quick information to scientists tracking the aftershock sequence and to government agencies and media following the numerous felt aftershocks.

In response to the Joshua Tree and Landers earthquakes, 16 GEOS instruments were deployed, in cooperation with the (old) Branch of Engineering Seismology and Geology, to collect waveform data for studying source and site effects from the aftershocks. Several instruments which were installed following the Joshua Tree earthquake were fortunate to record near-field strong-motions for the M7.5 Landers event. There was also a coordinated effort with university scientists deploying 19 SCEC Reftek instruments in the JTLBB area.

Project scientists spent a large amount of their time (20% - 50%) during the subsequent month responding to hundreds of requests for TV, radio, and newspaper interviews. There were also meetings with state and local governments agencies to discuss emergency responses and public forums to discuss safety issues.

During FY1992 project scientists gave over 70 talks to a wide variety of public, civic, community, professional and school groups.

Earthquake Research

Earthquake Mechanics

The thousands of well-located earthquakes of the JTLBB sequence, which includes 10 M5 and over 100 M4 events, has shown many interesting features which are summarized as follows:

- The Joshua Tree aftershocks show a 15 km north-northwest trending rupture with off-fault "wings" which are similar to the aftershocks of the 1979 Homestead Valley sequence.
- Aftershocks of the Landers earthquake show a 100 km rupture which trends northwards in the southern part of the aftershock region and bends toward the northwest in the northern part. The aftershocks correlate well with the observed surface displacements on the a number right-stepping *en echelon* faults. From south to north these faults are the Eureka Peak, Johnson Valley, Landers, Homestead Valley, Emerson, and Camp Rock faults.
- On the northwest end of the Landers rupture the observed surface rupture extends about 7 km further along strike than the aftershocks.
- The aftershocks to the Big Bear earthquake show a 25 km northeast trending rupture that is more diffuse than the Landers aftershock distribution, although the focal mechanism indicates that this event also occurred on a steeply dipping fault. There was no observed surface rupture and the trend of the aftershocks does not correspond to any geologically mapped faults in the immediate area.
- There is a 20 km lineament of aftershocks northeast of Barstow. This has been a relatively active area for aftershocks. The main Landers rupture probably did not extend to this area.
- One of the larger aftershocks was the M5.5 event 25 km east of the Landers rupture, on or near the Pisgah fault.
- Aftershocks along the Big Bear trend and the Joshua Tree - Landers trend extend southward close to the San Andreas fault, although there appears to have been very few events actually on the San Andreas.

- The Joshua Tree and Landers events occurred on right-lateral strike-slip faults and the Big Bear event occurred on a left-lateral strike-slip fault.
- There was a good agreement between the slip along the fault inferred from analyzing the TERRAscope data and the observed amount of fault slip observed by geologists.
- There was a large increase in seismicity in the Owens Valley and Coso regions (200-300 km to the north) associated with the Landers sequence. A M5.6 earthquake near the town of Mojave (220 km north of Landers) and a M3.9 earthquake felt in Pasadena (160 km west of Landers) also appear associated with the JTLBB sequence.

Foreshock and Aftershock Statistics

STEP (Short-Term Earthquake Probabilities), a program to map the daily probability of damaging earthquake shaking in southern California has been updated and modified. In STEP, the probability that a damaging earthquake (aftershock or even bigger mainshock) will follow earthquakes recorded by the real-time processing system in southern California is automatically calculated and displayed. First, the possibility of damaging aftershocks to recent main- shocks is determined using the model of Reasenberg and Jones (1989). Second, the probabilities are further modified because of the possibility that earthquakes recorded in the last few days will be foreshocks to larger events using the generic probabilities for southern California. Third, for earthquakes within 10 km of the Imperial, San Jacinto or San Andreas faults, the probability that they are foreshocks to the characteristic earthquake for that fault is calculated using the formulation of Agnew and Jones (1991). STEP was completed and tested this year. Modifications have recently been made so that the probability of a damaging aftershock is now distributed over the whole aftershock zone rather than assigned solely to the epicenter. The continuing Landers aftershocks have been taken into account in calculating the probability that an earthquake near the San Andreas fault will be a foreshock to a characteristic earthquake. Also, the possibility that an earthquake on one segment of a major fault could grow onto an adjacent segment is now included. The real-time display shows daily probabilities mapped for southern California with different colors for different orders of magnitude from 10^{-6} to 1.

The results of the closeness analysis which measured the degree of clustering for the Joshua Tree aftershock sequence, shows that the foreshocks during the 12 hours prior to the Landers earthquake on June 28th was one of the tightest spatial clusters. There was another cluster on June 17th which was also close to the epicenter of the Landers mainshock. Both of these clusters of earthquakes appear spatially more localized than the rest of the events in the Joshua Tree aftershock sequence, suggesting this may be a discriminant for foreshocks.

Short-Period Waveform Studies

The cross correlation of P waveforms at 3 sites near the Upland earthquakes showed optimal clustering values that ranged from 0.87 to 0.97. The resulting equivalence groups tend to be dominated by events associated with the 1990 earthquake due to its higher number of aftershocks. Events prior to the 1990 earthquake, but not those associated with the 1988 aftershock sequence, correlate well with post-1990 activity perhaps suggesting a change in stress state between the 1988 and 1990 events. Equivalence groups cluster in discrete zones along the fault plane and have dimensions on the order of 5 km or less. Correlation values also change dramatically at approximately 5 km depth suggesting the influence of local crustal structure or a change in fault orientation. The variation in correlation values also can be associated with mapped faults. Their pattern indicate that the fault plane rupture dimensions for the 1990 event may have been partially structurally controlled. Equivalence groups with first motion polarity opposite to that of the mainshock were also identified. These events tended to ring the main fault plane, similar to focal mechanism studies that

show a ring of thrust mechanisms around a core of strike-slip mechanisms. This appears to indicate local stress re-adjustments along the edges of the mainshock rupture.

The S-wave coda analysis gave estimates of the intrinsic and scattering attenuation for path that varied in length from 5 to 150 km. Theses results showed the whole-path intrinsic and scattering Q were approximately equal, with values of 50 to 500 in the distance range of 5 to 30 km and values of 500 to 1000 at greater distances. There is a fairly clear increase for the Q values with distance in the 5 to 30 km range. This is interpreted to reflect the increase of Q with depth. At close distances the waves travel only through the shallow portions of the crust. For farther distances the Q values reflect waves that travel mainly through the deeper portions of the crust, but also pass through the shallow crust on the way to the receiver site.

Record sections for deep earthquakes from Fiji were put together using data from both the Southern and Northern California Seismic Networks. Waveforms that were stacked over stations that were within 20 km epicentral distances of each other, show a PcP arrival the varies in amplitude across the array. This variation is interpreted to be due to lateral homogeneities on the core-mantle boundary. The bounce point for PcP is near Hawaii, so this is a region where one might expect to observe significant structure on the core-mantle boundary.

Source Parameters of Small Earthquakes

The empirical Green function technique was used to remove site and path effects from the P-wave seismograms of the M4.6 foreshock to the M6.1 Joshua Tree earthquake. The resulting source time functions recorded at 4 stations show that the foreshock ruptured toward the north with a duration of about 0.3 sec. For typical fault models this implies the rupture extended several hundred meters to the north and stopped quite close the eventual hypocenter of the mainshock 2 hours later. The foreshock had a relatively high stress drop of 200-300 bars. Similar analysis of some of the larger aftershocks show that the stress drops are relatively low compared to the foreshock.

Site Response in Basin Structures

The broadband data recorded at PAS show that events that have a significant portion of their path through the deeper portions of the Los Angeles Basin have strong spectral peaks at 1.5-1.6 hz for the P waves and 2.5-2.6 hz for the S waves. These amplifications are consistent with simple models of the basin with a sediment depth of 2.2 km. In general, the P- and S-wave spectra have similar characteristics indicating they are modified caused by the same basin structures. These frequency-dependent amplitude observations have a systematic effect on the M_L's determined at PAS.

Three-Dimensional Velocity Structures

Preliminary modelling has been done using the arrival times of the calibration shots at the permanent stations to obtain a 1D velocity model and station corrections appropriate for the Landers area. With this model the Landers mainshock relocates at 7 km depth, at the base of the foreshocks whose relocations cluster from 4 to 7 km depth. Variation in the resulting station corrections shows that the crust is heterogeneous and improved results will be obtained with 3D modelling. Continuing analyses of these data will involve solving for the 3D velocity structure and making record sections of the shots and earthquakes to image secondary arrivals. Improved earthquake hypocenters will be compared to the mapped rupture in order to interpret fault structure at depth.

Other

During FY1992 Project scientists were also involved with studies on:

- Effects of material heterogeneities on the deformations observed for the 1989 Loma Prieta earthquake.
- 3D velocity structures and seismicity at Parkfield, California.
- Long-period atmospheric waves from volcanic eruptions recorded on TERRAscope stations
- Shock waves from sonic booms recorded on the network.

REPORTS

This is a list of papers and reports published or submitted by project scientists during FY1992. There were also 31 abstracts.

Bryant, A. S. and L. M. Jones, Anomalously deep crustal earthquakes in the Ventura Basin, southern California, *J. Geophys. Res.*, 97, 437-448, 1992.

Eberhart-Phillips, D., Local earthquake tomography: Earthquake source regions, in *Seismic Tomography: Theory and practice* edited by H.M. Iyer and K. Hirahara (in press), 1992.

Eberhart-Phillips, D. and A.J. Michael, Three-dimensional velocity structure, seismicity, and fault structure in the Parkfield region, central California, *submitted to J. Geophys. Res.*, 1993.

Eberhart-Phillips, D. and W. D. Stuart, Material heterogeneities simplifies the picture: Loma Prieta, *Bull. Seismol. Soc. Am.*, 82, 1964-1968, 1992.

Ekstrom, G., R.S. Stein, J.P. Eaton, D. Eberhart-Phillps, Seismicity and geometry of a 110-km-long blind fault, 1:the 1985 Kettleman Hills, California, earthquake, *J. Geophys. Res.*, 97, 4843-4864, 1992.

Hauksson, E., K. Hutton, K. Douglass, L.M. Jones, Earthquake Atlas of Southern California 1987-1990, in *Engineering Geology in Southern California - 1992 Edition*, ed. by R. Proctor and B.W. Pipkin, Southern California Section of the Assoc. of Engineering Geologists, Los Angeles CA (in press).

Hutton, L.K. and L.M. Jones, Local Magnitudes and apparent variations in seismicity rates in southern California, *submitted to Bull. Seismol. Soc. Am.*.

Hwang, L., Microearthquake spectral amplification in the Los Angeles Basin region as observed at PAS, submitted to *Bull. Seismol. Soc. Am.*, 1993.

Jones, L.E., J. Mori, D.V. Helmberger, Short-period constraints on the proposed transition zone discontinuity, *J. Geophys. Res.*, 97, 8765-8774, 1992.

Kanamori, H. and J. Mori, Harmonic excitation of mantle Rayleigh waves by the 1991 eruption of Mount Pinatubo, Philippines, *Geophys. Res. Lett.*, 19, 721-724, 1992.

Kanamori, H., J. Mori, E. Hauksson, T.H. Heaton, L.K. Hutton, L.M. Jones, Determination of earthquake energy release and M_L using TERRAscope, *submitted to Bull. Seismol. Soc. Am.*

Kanamori, H., J. Mori, B. Sturtevant, D.L. Anderson, T. Heaton, Seismic excitation by space shuttles, *Shock Waves, An International Journal*, 2, 89-96, 1992.

Landers Earthquake Response Team, Near-field investigations of the June 28, 1992, Landers, California, earthquake, *Science, in press*, 1993.

Mori, J., Determination of fault planes from rupture directivity: Search for cross faults in the San Jacinto fault zone, California, *submitted to J. Geophys. Res.*, 1993.

Mori, J., J. Filson, E Cranswick, R. Borcherdt, R. Amirbekian, V. Aharonian, L. Hachverdian, Near-surface measurements of P- and S-wave velocities from the dense three dimensional array at Garni, Armenia, *submitted to Bull. Seismol. Soc. Am.*, 1993.

Mori, J. and A. Frankel, Correlation of P wave amplitudes and travel time residuals for teleseisms recorded on the southern California seismic network, *J. Geophys. Res.*, 97, 6661-6674, 1992.

Mori, J., K. Hudnut, L. Jones, E. Hauksson, K. Hutton, Rapid Scientific Response to Landers Quake, *EOS, Transactions American Geophysical Union*, 73, 417-418.

Wald, D.J., D.V. Helmberger, T.H. Heaton, Rupture model of the 1989 Loma Prieta earthquakes from the inversion of strong-motion and broadband teleseismic data, *Bull. Seismol. Soc. Am.*, 81, 1540-1572, 1991.

Wald, L. A., Southern California Earthquake Center, USGS Yearbook Fiscal Year 1991, in press.

Wald, L.A., L. K. Hutton, L.M. Jones, D. D. Given, K. Douglass, J. Mori, E. Hauksson, H. Kanamori, The southern California network bulletin, January-December, 1991, U.S. Geological Survey Open-File Report 92-335, 1992.

Wald, L.A. and L. M. Jones, LEAP: Local Earthquake Analysis Programs for Southern California Seismic Network Data, U.S. Geol. Surv. Open-File Report 92-577, 1992.

Experimental Tilt and Strain Instrumentation

9960-01801

C.E. Mortensen
Branch of Tectonophysics
U.S. Geological Survey
345 Middlefield Road, MS 977
Menlo Park, California 94025
(415) 329-4856

Investigations

1. There are currently 135 Data Collection Platforms (DCP's) that transmit a variety of data to the Direct Readout Ground Station (DRGS) in Menlo Park. Sixty-six of these DCPs transmit data at 10-minute intervals on two exclusively assigned random channels, which are being utilized under a special agreement with NESDIS. The remainder of the DCPs report at standard 3 or 4-hour intervals as assigned by NESDIS. This system transmits data from all types of low-frequency instruments including dilatometers, creepmeters, strainmeters, water-level meters, magnetometers, tiltmeters, and related measurements. One of the first DCP's installed has been in continuous operation, with no repairs and little maintenance, for more than 3000 days

   A Direct Readout Terminal (DROT) that receives the GOES DCS data stream through a domestic communications satellite (DOMSAT) has been installed. Data quality has improved greatly as the DROT is less directly affected by the condition of the spacecraft than the DRGS. The DRGS serves as a backup system.

2. Networks of tiltmeters, creepmeters and shallow strainmeters have been maintained in various regions of interest in California. A network of tiltmeters located at seven sites monitor crustal deformation within the Long Valley caldera. Roger Bilham of the University of Colorado and Jon Beaven of Lamont-Doherty installed a very long baseline tiltmeter in Long Valley. This project provided three DCP's to collect the data and return it to Menlo Park via GOES satellite. We also monitor the data received to keep track of deformation within the caldera, comparing results frequently with the USGS tiltmeter array.

   Other tiltmeters are located in the San Juan Bautista and Parkfield regions. Creepmeters located along the Hayward, Calaveras and San Andreas faults between Berkeley and the Parkfield area are maintained in cooperation with the Fault Zone Tectonics project. A shallow strainmeter is located near Parkfield, while observatory type tiltmeters and strainmeters are sited at the Presidio Vault in San Francisco, and a tiltmeter is installed in the Byerly Seismographic Vault at Berkeley. Data from these instruments are telemetered to Menlo Park via the GOES satellite.

3. A system to backup the satellite telemetry system with non-volatile, solid-state memory and dialup or dedicated telephonic communications path has been developed. Included in this system is the capability to lock the DCP timing to a radio time standard. This feature enables more efficient utilization of the assigned satellite bandwidth. The system is known as the Companion because of its interfacing role with satellite DCP's. The system is currently deployed at the Long-baseline tiltmeter at Long Valley caldera.

4. A low-cost, short-haul digital telemetry system utilizing UHF radios, packet controllers and off-the-shelf digital data converters, is currently in use in Parkfield monitoring the tilt of monuments that support the reflectors that constitute the 2-color laser network. This system, components for which cost less than $1500 per site, automatically polls the remote sites and transfers the data to a computer file, calculating the mean and standard error in the process. The system, including the tiltmeters, can easily be removed and transported to other locations.

5. Conducted advisory activities for the Regional Interagency Steering Committee (RISC), which is convened bimonthly by FEMA to accomplish and coordinate regional planning for earthquake preparedness and response. Coordinated scientific input to emergency responders following the Cape Mendocino earthquakes in April and the Landers/Big Bear earthquakes in June. Served on the State/Federal Hazard Mitigation Survey Team for the Landers/Big Bear earthquake disaster.

6. Continued drafting an operational plan for USGS, Office of Earthquakes, Volcanoes and Engineering (OEVE), participation in the Federal response to a catastrophic earthquake in the San Francisco Bay Area under a PL 93-288 disaster declaration.

Results

1. Conducted regional monitoring of deformation in Central California, Parkfield, and the Long Valley caldera areas. Maintained and operated instruments and associated telemetry systems in those regions.

2. Provided recommendations that were incorporated into the *Interagency Hazard Mitigation Team Report for the June 28, 1992 Landers and Big Bear Earthquakes*. This report was compiled in response to Federal Disaster Declaration FEMA-947-DR-CA.

Reports

Mortensen, Carl E., 1992. Planning for a USGS contribution to emergency response in the Bay Area: Proceedings of the Second Conference on Earthquake Hazards in the Eastern San Francisco Bay Area, California Division of Mines and Geology Special Publication 113, in press.

Geology of Southwestern California

9540-70220

D. M. Morton and V. R. Todd
Branch of Western Regional Geology
University of California
Riverside, CA 92521

G. L. Dixon
Branch of Western Regional Geology
6770 S. Paradise Road
Las Vegas, NV 89119-3721

J. C. Matti
Branch of Western Regional Geology
Gould-Simpson Building #77
University of Arizona
Tucson, AZ 85721

R. E. Powell
Branch of Western Regional Geology
W904 Riverside Avenue, Room 117
Spokane, WA 99201-1087

A. W. Ward
Branch of Western Regional Geology
2255 North Gemini Drive
Flagstaff, AZ 86001-1698

J. A. Bartow
Branch of Western Regional Geology
345 Middlefield Road, MS 975
Menlo Park, California 94025
415-329-4910

Investigations

The goal of this project is to produce geologic maps of a series of 12 1:100,000-scale quadrangles in southwestern California. It is a subset of a larger undertaking of the Southern California Areal Mapping Project (SCAMP), a cooperative effort with the State of California Division of Mines and Geology, with a goal of producing geophysical and geologic maps for the onshore 20 1:100,000-scale quadrangles of southwestern California. Procedure for producing the maps is initial compilation of existing map data, prioritizing geologic-map deficient areas, and final map release in digital GIS form (ARC/INFO). In addition to the 1:100,000 scale

quadrangles, larger-scale maps will be produced in areas of relevant complexity which require the larger scale to properly resolve the geology; most of the larger-scale geologic maps will be at a scale of 1:24,000. Project members were involved in post earthquake mapping of ground rupture produced by the Landers earthquake.

Results:

Geologic mapping of the Elsinore fault zone in the vicinity of Murrieta-Temecula and Lake Mathews areas were completed. A review of evolution of the San Andreas fault was completed for Annual Reviews of Earth and Planetary Sciences. Initial compilation of the El Cajon 1:100,000-scale was completed. Geologic mapping was completed in the Robers Lake area.

Reports:

Matti, J.C., Morton, D.M., Cox, B.C., Carson, S.E. and Yetter, T.J., 1992, Geologic map of the Yucaipa quadrangle, southern California: U.S. Geological Survey Open File Report 92-446.

Matti, J.C., Morton, D.M., and Cox, B.F., 1992, San Andreas fault system in the vicinity of the central Transverse Ranges province, southern California: U.S. Geologic Survey Open-File Report 92-354

Powell, R.E., and Weldon, R.J.,1992, Evolution of the San Andreas fault: Annual Reviews of Earth and Planetary Sciences, v. 20, p. 431-468.

Sieh, K.E., and Matti, J.C., 1992, The San Andreas fault system between Palm Springs and Palmdale, southern California: Field-trip guidebook, *in:* Earthquake Geology, San Andreas fault system, Palm Springs to Palmdale: Publication of the Southern California Section, Association of Engineering Geologists, p. 1-12.

Distribution and Dating of Prehistoric Earthquake Liquefaction in the Wabash River Valley of the Central U.S.

Agreement No. 14-08-0001-G2117

Patrick J. Munson and Cheryl Ann Munson
Indiana University
and
Ned K. Bleuer
Indiana Geological Survey
Bloomington, Indiana 47405

(812)855-0528

History of Research

The occurrence of large-scale, earthquake-induced liquefaction centered within the Wabash River Valley of southwestern Indiana and southeastern Illinois was first documented in 1990 by S.F. Obermeier (USGS) and the Principal Investigators. That preliminary study discovered Holocene-age paleoliquefaction features (dikes, sills, and buried sand-blows) exposed in river cutbanks and the walls of sand and gravel pits at 7 sites within a 100 km diameter area in the lower Wabash Valley (Obermeier et al. 1991).

On the basis of the 1990 findings we sought and were awarded a USGS NEHRP grant for research designed to determine the distribution of earthquake-induced paleoliquefaction features in the lower and central Wabash Valley of Indiana and to make initial assessments of the dating of these features.

1991 Research

The project began in June 1991, and was originally planned to be completed by May 1992. During summer and fall of 1991 we systematically surveyed, by boat, all eroding cutbanks of the central and lower Wabash River from 80 km north to 100 km south-southwest of Vincennes, Indiana and the lower White River to a point 50 km east of Vincennes, Indiana. This survey covered 426 river-km, which contain 226 eroding cutbanks (with combined lengths of 160,000 m), and resulted in the discovery of an additional 17 paleoliquefaction sites. These sites, combined with the 7 sites discovered in 1990, have a total of 187 paleoliquefaction features. Also discovered during the 1991 survey were 10 buried prehistoric archaeological sites and 12 radiocarbon samples (both archaeological and non-archaeological) that stratigraphically pre-date, post-date, or are penecontemporaneous with paleoliquefaction features. The 1991 findings are summarized by Munson et al. (1992) and Obermeier et al. (1992b).

However, the 1991 survey demonstrated that the geographic distribution of paleoliquefaction features in the Wabash Valley was much larger than the area that had been projected on the basis of the 1990 research.

Consequently, supplementary funding was awarded to continue the survey and initial assessments through December 1992.

1992 Research

During 1992, the survey was extended northward on the Wabash River to 210 km north-northeast of Vincennes, northeastward on the West Fork of White River and its tributaries to 190 km northeast of Vincennes, and eastward on the East Fork of White River and its tributaries to points 150 km east and east-northeast of Vincennes. The 1992 survey covered 729 river-km, which contain 862 eroding cutbanks (with combined lengths of almost 188,000 m), and resulted in the discovery of 39 additional paleoliquefaction sites (which contain in aggregate 109 paleoliquefaction features). Buried archaeological sites were found stratigraphically post-dating or pre-dating liquefaction features at 9 of the newly discovered sites, and radiocarbon samples (both archaeological and non-archaeological) were found post-dating or pre-dating liquefaction features at 14.

In 1992 we also returned to 23 of the 24 paleoliquefaction sites that had been discovered in 1990 and 1991 for the purpose of re-examining the exposures after spring flooding had scoured them of slump and weedy vegetation. Resurvey resulted in the discovery of additional paleoliquefaction features at 5 of the sites (including, in 3 instances, features larger than those previously observed), as well as previously unrecorded post-dating archaeological deposits at 2 sites, and additional radiocarbon samples in stratigraphic association with liquefaction features at 6 sites. By the end of the 1992 field season, radiocarbon samples had been collected from 27 of the 63 paleoliquefaction sites; samples pre-date liquefaction at 13 sites, post-date at 9, both pre- and post-date at 3, and are penecontemporary ($\pm$1,000 years?) at 2.

In addition to greatly increasing the numbers of paleoliquefaction sites and samples of datable materials, another result of the 1992 research was the development of a preliminary classification of the near-surface floodplain sediments that are exposed in the river cutbanks. Floodplain deposits throughout the valleys of the Wabash River and White River are generally similar; unconsolidated sand and gravel extends from bedrock (commonly 15 to 46 m below the floodplain surface) upward to 2-7 m below the floodplain surface. The sand and gravel facies, which are the source materials for liquefaction features, are generally capped by alternating, thin, plane-bedded sand and silt facies 1-2 m in thickness; these are overlain by massive clayey silt to sandy silt facies 1-5 m in thickness. The water table is generally high, and even during periods of extended drought rarely drops more than a few meters below the top of the highest sand and gravel facies. Consequently, the thick, saturated, granular materials, overlain by 2-7 m of fine-grained sediments, are moderately to highly susceptible to liquefaction and formation of sand-blows during strong earthquake shaking.

Despite the general similarities of the floodplain sediments, differences are evident among the exposures of these sediments, primarily in minor differences in elevations of their surfaces, pedogenesis, and presence-absence of buried soil horizons. These differences appear to be largely or

entirely age-correlative, and a four-part division (Table 1) is supported by stratigraphic relationships, association with archaeological materials of known ages, and a limited number of radiocarbon dates. However, given (a) that all four classes are at least moderately susceptible to liquefaction, and (b) that numerous and extensive exposures of all four occur throughout the surveyed sectors of the river valleys, then the presence or absence of liquefaction features in sediments of different ages is relevant to the dating of the causal earthquake(s). Moreover, differences in presence-absence and sizes of liquefaction features in sediments of the same age but in different geographic sectors of the valleys are relevant to interpretations of the magnitude(s) and epicentral area(s) of the prehistoric earthquake(s).

Results and Preliminary Interpretations

Our research in Indiana, as well as surveys by S. F. Obermeier in southeastern Illinois, has demonstrated that paleoliquefaction features are common in the Wabash Valley and are comparable to the features formed by historic large earthquakes in the Charleston, South Carolina and New Madrid, Missouri areas (cf. Obermeier et al. 1990). Very large dikes (>60 cm wide), often with extensive sand-blows, occur at four sites within a 20 km radius of Vincennes, Indiana (Fig. 1), and numerous dikes as large as 15 cm in width occur 100 to 120 km to the south, east, and north of Vincennes. Beyond a radius of 120 km, sizes and frequencies of dikes markedly decrease. No liquefaction features were discovered (in Indiana) at distances greater than 140 km from Vincennes, despite the examination beyond this distance of many thousands of meters of excellent exposure in liquefaction-susceptible deposits. Noting, again, that sediments susceptible to liquefaction (and exposures of these sediments) are extensive throughout the surveyed area, the distributional data suggest that the paleoliquefaction features in the Wabash Valley resulted from one or more very strong earthquakes centered in the general vicinity of Vincennes.

Furthermore, all of the largest and most widely distributed liquefaction features penetrate sediments that are apparently Early Holocene in age, suggesting that many (possibly all) of these features date near the Early Holocene-Middle Holocene boundary, perhaps shortly after 7,000 BP. The most parsimonious explanation would be that the features that penetrate the earliest Holocene (>9,000 BP) and Late Pleistocene sediments resulted from the same earthquake, but the possibility remains that they were caused by one or more earlier strong earthquakes; this possibility will be addressed in future research.

There is less equivocation regarding strong earthquake shaking in the more recent past in the Wabash Valley. Examination of almost 280,000 m of exposures of Middle(?) and Late Holocene sediments has resulted in the discovery of only 3 paleoliquefaction sites, where are exposed, in aggregate, only 10 small (1-10 cm wide) dikes. All of these sites are located within a 35 km radius of Vincennes. An anaerobically-preserved log from deposits that stratigraphically pre-date liquefaction at one site has been radiocarbon dated 4440 $\pm$ 80 BP (ISGS-2314).

Contributions to Related Research

The information resulting from this study of distribution and sizes of paleoliquefaction features in Indiana has significantly contributed to a preliminary estimate of magnitude of prehistoric earthquakes in the Wabash Valley Seismic Zone (Obermeier et al. 1992a). Additionally, many of the paleoliquefaction sites discovered by the survey are the locales of ongoing, USGS NEHRP-sponsored research by J. R. Martin and E. C. Pond; this geophysical investigation addresses the composition, thickness, and seismic properties of the sediment pile underlying the liquefaction features so that levels of input (rock) vibration and soft-sediment amplification can be estimated.

References Cited

Munson, P.J., Munson, C.A., Bleuer, N.K., and Labitzke, M.D., 1992, Distribution and dating of prehistoric earthquake liquefaction features in the Wabash Valley of the central U.S.: Seismological Research Letters (in press).

Obermeier, S.F., Bleuer, N.K., Munson, C.A. Munson, P.J., Martin, S.M., McWilliams, K.M., Tabaczynski, D.A., Odum, J.K., Rubin, M., and Eggert, D.L., 1991, Evidence of strong earthquake shaking in the lower Wabash Valley from prehistoric liquefaction features: Science, v. 251, p. 1061-1063.

Obermeier, S.F., Jacobson, R.B., Smoot, J.P., Weems, R.E., Gohn, G.S., Monroe, J.E., and Powars, D.S., 1990, Earthquake-induced liquefaction features in the coastal setting of South Carolina and in the fluvial setting of the New Madrid Seismic Zone: U.S. Geological Survey Professional Paper 1504.

Obermeier, S.F., Martin, J.R., Frankel, A.D., Youd, T.L., Munson, P.J., Munson, C.A., and Pond, E.C., 1992a, Liquefaction evidence for strong Holocene earthquakes(s) in the Wabash Valley of southern Indiana-Illinois, with a preliminary estimate of magnitude: U.S. Geological Survey Open-File Report 92-406.

Obermeier, S.F., Munson, P.J., Munson, C.A., Youd, T.L., and Martin, J.R., 1992b, Liquefaction evidence for strong Holocene earthquake(s) in the Wabash Valley of Indiana-Illinois: Seismological Research Letters (in press).

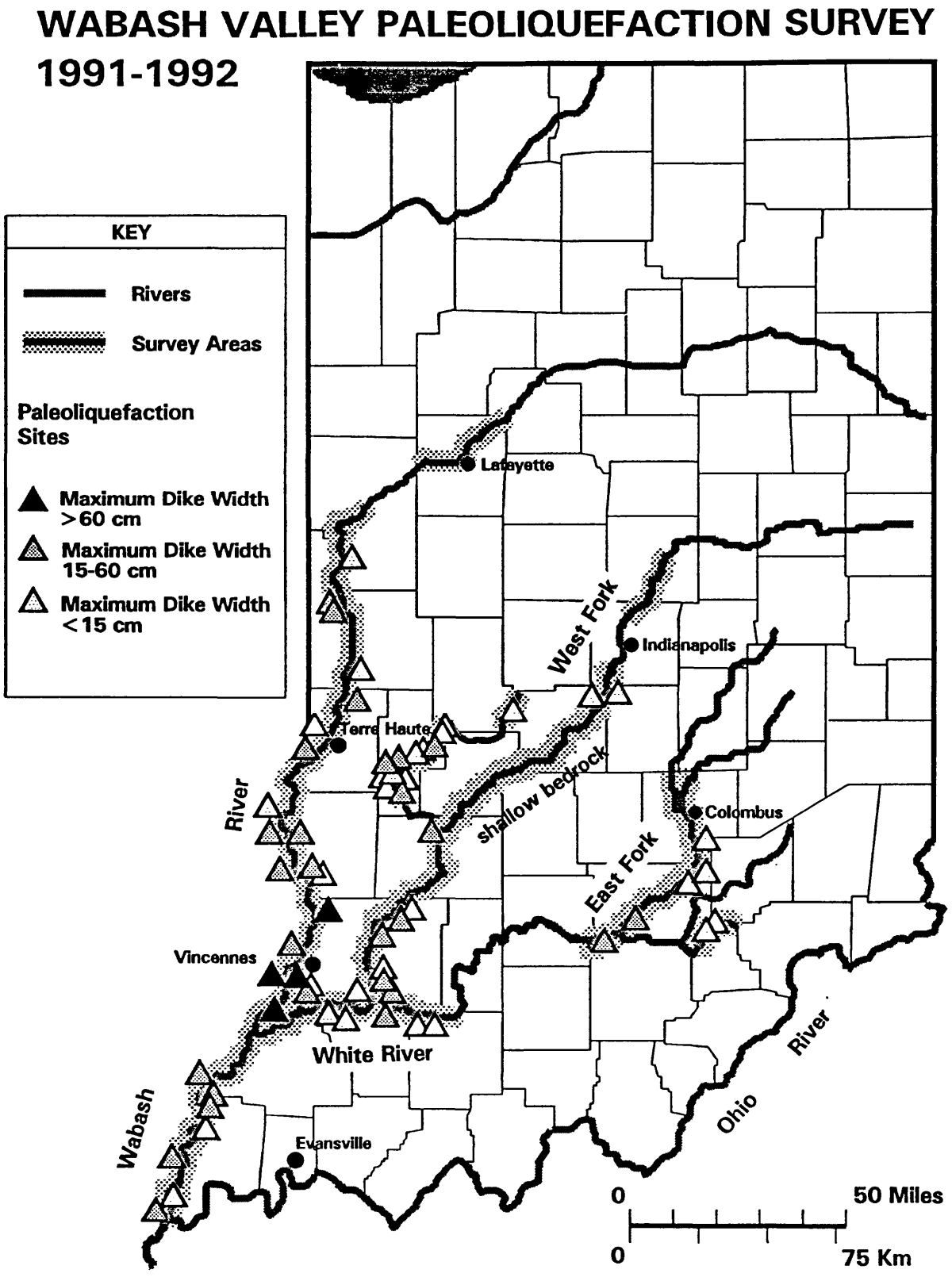

Figure 1. Map showing areas searched for liquefaction features, and locations of paleoliquefaction sites.

Table 1: SUMMARY OF EXAMINED EXPOSURES, THROUGH NOVEMBER 1992

Preliminary Exposure Class*	Number of Exposures	Total** Length (m) of Exposures	Number of Paleo-Liquefaction Sites	Number of Paleo-Liquefaction Features	Number of Liquefaction Features per 1000 m
1	59	17,050	6	17	1.0
2a	100	27,840	40	217	7.8
2b	68	22,355	14	52	2.3
3	345	130,215	3***	10	0.1
4	516	149,760	0	0	0.0
Total	1,088	347,180	63	296	---

* Preliminary exposure classification:
- 1 Late Pleistocene low terrace or high floodplain (15,000-10,000 BP?).
- 2a Early Holocene floodplain (10,000-7,000 BP?) with top of sand-gravel strata below mean summer low river level.
- 2b Early Holocene floodplain (10,000-7,000 BP?) with top of sand-gravel strata above mean summer low river level.
- 3 Middle-Late Holocene floodplain (7,000-1,500 BP?).
- 4 Late Holocene-Historic floodplain (<1,500 BP?).

** Total length of exposures based on survey of 1,155 km along stream channels (or 2,310 km stream banks).

*** All paleoliquefaction sites in Class 3 exposures are within 35 km radius of Vincennes, Indiana.

Element II

PALEOSEISMOLOGY AND QUATERNARY DEFORMATION OF COASTAL OREGON

9950-04180

ALAN R. NELSON and STEPHEN F. PERSONIUS

Branch of Geologic Risk Assessment
U.S. Geological Survey
MS 966, Box 25046
Denver, CO 80225
(303) 273-8592

INVESTIGATIONS

The project consists of two components: Nelson's study of coseismic changes in late Holocene sea level as revealed by tidal-marsh stratigraphy, and Personius' study of fluvial terrace remnants along major Coast Range rivers to determine styles and rates of late Quaternary deformation. Both components will help define the potential hazard from great subduction earthquakes in the U.S. Pacific Northwest.

RESULTS

Coseismic changes in late Holocene sea level

Has subduction of the Juan de Fuca plate beneath the North America plate in the Pacific Northwest produced great (M>8) earthquakes during the late Holocene? Records of the past 200 years yield no evidence of great plate-interface earthquakes in the Cascadia subduction zone. But along the coasts of Oregon and Washington peaty, tidal-wetland soils are interbedded with mud in estuarine stratigraphic sequences, and the submergence (relative rise of sea level) of some of these soils seems too widespread (>100 km), too large (>1 m), and too sudden (<10 years) to be attributed to any process except coseismic subsidence. How large were the Cascadia plate-interface earthquakes that produced coastal subsidence and how often did they occur? Such questions are critical for earthquake hazard assessment in the Pacific Northwest.

Nelson's research in FY92 focused on the following two questions:

(1) Were the peaty units interbedded with estuarine mud in late Holocene marsh stratigraphic sequences in Oregon and Washington submerged and buried during the same 50- to 300-yr-long periods?

Peaty stratigraphic units may have been submerged and buried during great (M>8) subduction earthquakes, smaller upper-plate earthquakes, or by aseismic processes. Precise radiocarbon dating should help distinguish among these alternatives by showing whether units at different sites were submerged at different times (Atwater and others, 1991; Nelson, 1992).

In FY91 we demonstrated that multiple accelerator mass spectrometer (AMS) ^{14}C analyses of carefully selected and extensively pretreated plant macrofossils from the tops of peaty units can significantly improve the precision of estimates of the times when peaty units were submerged (Nelson and others, 1992). The precision with which submergence times can be estimated is now chiefly limited by the shape of the ^{14}C calibration curve during the period of interest--typical 95% confidence intervals on calibrated ages range from 50 to 300 yr. However, even for events that occurred during periods when the relation between ^{14}C yr and calendar yr was very non-linear, our AMS ages are better estimates of event times than most conventional ^{14}C ages because we limit our AMS samples to above-ground plant parts collected within 3 mm of the upper contact of peaty units (e.g., Nelson, 1992).

The youngest (250 BP) buried peaty unit most likely to have been submerged coseismically at seven coastal sites between southern Oregon and central Washington was selected as the first target of our regional high-precision AMS dating project. Samples from this unit are the rooted stem and leaf bases of individual salt marsh plants thought to have been suddenly submerged about A.D. 1700. Analyses of the 64 marsh plant AMS samples that were delayed due to alleged sulfur contamination are now being completed at the AMS accelerator facility in New Zealand.

After we receive the complete results of the analyses of the 250 BP samples we will analyze high-precision samples from similar units dated at about 1500 BP at 2 sites and at 1700 BP at 4 sites. At sites were rooted marsh-plant fossils can be collected in outcrop we will probably analyze 5 samples per unit. If rooted fossils cannot be found we will analyze 2-3 carefully selected samples of detrital plant material at the upper contact of the units. Our results with detrital samples suggest that more than 3 separate analyses from the same unit are not justified at most sites.

(2) *Were most of the peaty units in marsh stratigraphic sequences in the Pacific Northwest submerged and buried during coseismic subsidence or were many of these units buried by aseismic coastal processes?*

One of the central concerns of our marsh stratigraphic studies in Oregon discussed in earlier reports (FY89-91) and publications (Nelson and Personius, in press; Nelson, in press), was the degree to which marsh stratigraphic sequences in the Pacific Northwest were similar to those of some passive continental margins, such as the U.S. Atlantic coast (e.g., Fletcher and others, 1991; van de Plassche, 1991; Thomas and Varekamp, 1991) or northwest Europe (e.g., Shennan, 1986; 1992; Streif, 1987), and, therefore, whether many buried peaty stratigraphic units in the Pacific Northwest might have an aseismic origin. Nelson's FY92 studies with Ian Shennan, Antony Long, and other sea-level researchers at the Department of Geography, University of Durham, show that this concern is justified--much more extensive stratigraphic and paleontologic studies will be required to demonstrate a coseismic origin for many units at most sites before we can estimate the recurrence and magnitude of plate-interface earthquakes.

Nelson found that the lithologies and stratigraphy of intertidal deposits in eastern England and western Scotland are much like the deposits at similar sites in the Pacific Northwest. For example, along the north shore of the Humber River estuary outcrops show a woody peat containing rooted tree stumps that is overlain by decimeters of lower intertidal or subtidal mud. In most places the upper contact of the peat is abrupt (<1 mm), but in a few places the contact is gradational (1-2 cm) indicating that submergence of the peat was rapid but not sudden. Microfossil analyses are needed to confirm the rapid rise interpretation. Near Arisaig in western Scotland, a 2-to-50-cm-thick sand sheet thins upvalley and abruptly buries a freshwater bog peat over an area of a square kilometer. Many erosional and load structures at the sand-peat contact and marine diatoms in 2-3 cm of silt overlying the sand indicate sudden deposition of the lower

part of the sand sheet during breaching of barrier bars near the mouth of the valley. Criteria described by Atwater (1992) for coseismic subsidence deposits in southern Washington included abrupt transgressive contacts marked by centimeters of sand over high intertidal or supratidal peat overlain by decimeters of lower intertidal or subtidal mud. This type of stratigraphy has not been described from England or Scotland. However, some peaty units at almost all sites in the Pacific Northwest and all units at many sites in southern Oregon lack these criteria, and so, on the basis of field evidence, many units in the Pacific Northwest are very similar to peaty units in Britain and elsewhere.

During his studies in Britain Nelson was particularly impressed with the difficulty in correctly interpreting the environment of deposition of intertidal units without detailed field lithologic descriptions and supporting pollen and diatom data. Paleoseismologists in the Pacific Northwest have probably underestimated the importance of brackish and freshwater lagoonal environments and transitional salt-marsh--freshwater-wetland environments in estuarine sequences, at least at some sites. For example, the structure of the organic-rich matrix and the orientation of detrital herbaceous organic material and fine rootlets in some buried peaty units at our Winchester Creek site in Coos Bay, Oregon, suggest that some units accumulated in standing brackish water behind a temporary barrier, and, therefore, do not have any direct elevational relation to a specific intertidal zone. If so, Nelson's (in press) inference that several of these peaty units are coseismically submerged marsh soils may be incorrect and the stratigraphic sequence at that site may have little or no coseismic significance.

Abrupt erosional contacts, particularly at the top of peaty units are more common in sequences on the coasts of passive continental margins than recognized by many coastal researchers in the Pacific Northwest. For this reason, microfossil analyses across abrupt contacts are required at key sites to help distinguish between an erosional or sudden submergence origin for the contacts. The rooted leaves and stems of delicate marsh plants that protrude into mud or sand beds that abruptly overlie peaty units, such as those described by Atwater and Yamaguchi (1991), are convincing evidence of sudden submergence, but such well-preserved fossils have been found at only a small number of well-exposed outcrops. If pollen analysis through an abruptly truncated peat shows evidence of gradually rising water levels and if diatom evidence in overlying mud indicates continuing submergence, then even a widespread abrupt contact may indicate minor erosion of the peat rather than coseismic subsidence. Although initial microfossil work in the Pacific Northwest is a step in the right direction (e.g., Darienzo and Peterson, 1990; Jennings and Nelson, 1992; Hemphill-Haley, 1992; Bucknam and others, in press; Nelson and Kashima, in press), more detailed studies will be required to determine the environment of deposition and processes of burial of many stratigraphic units in marsh sequences along the outer coasts of Washington and Oregon.

Deformation of fluvial terraces

Personius is completing his analysis of fluvial terraces in the Oregon Coast Range. This analysis has two main objectives: (1) to search for active folds and faults, and (2) to analyze stream (bedrock) incision rates for evidence of differential uplift. Both aspects of this research are aimed at helping to define intermediate-term (late Peistocene and Holocene) rates and styles of deformation in the on-land portion of the forearc of the Cascadia subduction zone. Such information can help define the tectonic settings of tidal-marsh and geodetic studies in the region.

A single example of an active structure has been found in the central Coast Range, a north-trending anticline in Eocene bedrock on the Siuslaw River that has warped the overlying fluvial terraces. However, there is no evidence that this or any other structure has been active in late Pleistocene or Holocene time. The poor preservation of terraces in the Coast Range indicates

that other active structures may have gone undetected, but the presence of an undeformed, relatively continuous latest Peistocence-early Holocene terrace along most rivers precludes the presence of rapidly deforming Holocene structures. The large area affected by the anticline on the Siuslaw River (over 20 km wide) indicates that active folds should be easy to detect on profiles of older stream terraces.

The exact relationship between stream incision rates and uplift is unknown. However, most of the rivers examined have concave stream profiles, and TL and radiocarbon ages indicate no significant differences between short and long-term incision rates on individual rivers. These relations indicate that bedrock incision rates are probably roughly in equilibrium with rates of regional uplift. In addition, there are no significant differences in incision rates in east-west transects along the Umpqua and Siletz Rivers, which supports the conclusion that there is no pervasive regional tilting of the Coast Range. However, there are significant differences in bedrock incision rates between rivers. Rates on the Smith and Siuslaw Rivers are lower than rates on the Umpqua River to the south and Siletz River to the north, but perhaps the most striking differences are the very high incision rates on the Siletz River. Incision rates on the three southerly rivers are 0.2-0.4 mm/yr, whereas incision rates on the Siletz River are 0.7-0.8 mm/yr. Climate in the region is relatively uniform and all these rivers flow through similar bedrock, so a tectonic cause for these differences appears likely.

Several geologic and geodetic studies have discussed evidence of both east-west and north-south trending deformation in western Oregon (Adams, 1984; Mitchell and others, 1991; Kelsey and others, 1992), but the relationship between this deformation and active subduction is still poorly understood. Personius' results indicate that differences in incision rates in the central Coast Range may be the result of folding associated with long-term, north-south directed compression in the overriding North American plate, and(or) may reflect the presence of a segment boundary in the underlying Juan de Fuca plate somewhere between the Siletz and Siuslaw Rivers in central western Oregon. The north-trending anticline on the Siuslaw River indicates some localized component of east-west compression in Quaternary time as well.

Personius' research in FY 92 focused on the following question:

(1) How do the rates of bedrock incision along streams in the northern Oregon Coast Range compare to those along streams in the central Coast Range, and what do possible variations in incision rates tell us about differences in the subduction process along the Cascadia zone?

This aspect of Personius' work is an extension of his previous research in the central Coast Range. Fieldwork in FY92 focused on stream terraces in the northern Coast Range, primarily on the Nestucca and Nehalem Rivers. Northern Coast Range rivers also are flanked by late Pleistocene and Holocene terraces and are incising their channels into bedrock, so charcoal samples from several terrace exposures were collected and have been submitted for radiocarbon dating. The resulting ages will be used to define incision rates that will be compared to rates from central Coast Range rivers. The expected north-south variations in incision rates may have significant implications for the interpretations of the tectonic settings of coastal marsh sites in Oregon and Washington, and raise questions about the relative roles of uplift and subsidence in the earthquake cyle during late Holocene events. The FY92 work will result in a regionally extensive dataset of incision/uplift rates for a period of time (40-10 ka) that is intermediate between previous studies of 80-125 ka marine terraces, and historic geodetic data.

REFERENCES CITED

Adams, John, 1984, Active deformation of the Pacific Northwest continental margin: Tectonics, v. 3, no. 4, p. 449-472.

Atwater, B.F., 1992, Geologic evidence for earthquakes during the past 2000 years along the Copalis River, southern coastal Washington: Journal of Geophysical Research, v. 97, no. B2, p. 1901-1919.

Atwater, B.F., Stuiver, Minze, and Yamaguchi, D.K., 1991, Radiocarbon test of earthquake magnitude at the Cascadia subduction zone: Nature, v. 353, p. 156-158.

Atwater, B. F., and Yamaguchi, D. K., 1991, Sudden, probably coseismic submergence of Holocene trees and grass in coastal Washington State: Geology, v. 19, p. 706-709.

Bucknam, R.C., Hemphill-Haley, E., and Leopold, E.B., Abrupt uplift within the past 1700 years at southern Puget Sound, Washington: Science, (in press).

Darienzo, M.E., and Peterson, C.D.., 1990, Episodic tectonic subsidence of late Holocene salt marshes, northern Oregon coast, central Cascadia margin, U.S.A.: Tectonics, v. 9, p. 1-22.

Fletcher, C.H., Van Pelt, J.E., Sherman, J., and Brush, G.S., 1991, High-resolution sea-level and climate history of the middle to late Holocene from wetland sediments of Delaware Bay: Geological Society of America Abstracts with Programs, v. 23, no. 5, p. A352.

Hemphill-Haley, E., 1992, Diatom micropaleontology of Holocene intertidal sediments in coastal southwest Washington: Ph.D. thesis, University of California, Santa Cruz.

Kelsey, H., Mitchell, C.E., Weldon, R.J., II, Engebretson, D., and Ticknor, R., 1992, Latitudinal variation in surface uplift from geodetic, wave-cut platform and topographic data, Cascadia margin: Geological Society of America, Abstracts with Programs, v. 24, no. 5, p. 37.

Mitchell, C.E., Weldon, R.J., II, Vincent, P., and Pittock, H.L., 1991, Active uplift of the Pacific Northwest margin: EOS (Transactions, American Geophysical Union) v. 72, no. 44, p. 314.

Plassche, Orson van de, 1991, Late Holocene sea-level fluctuations on the shore of Connecticut inferred from transgressive and regressive overlap boundaries in salt-marsh deposits, *in* Gayes, P.T., Lewis, R.S., and Bokuniewicz, H.G., eds., Quaternary coastal evolution of southern New England: Journal of Coastal Research, special issue no. 11, p. 159-179.

Shennan, Ian, 1986, Flandrian sea-level changes in the Fenland. I--The geographical setting and evidence of relative sea-level changes: Journal of Quaternary Science, v. 1, p. 119-154.

Shennan, Ian, 1992, Late Quaternary sea-level changes and crustal movements in eastern England and eastern Scotland--an assessment of models of coastal evolution, *in* Ota, Yoko, Nelson, Alan R., and Berryman, Kelvin, eds., Impacts of tectonics on Quaternary coastal evolution: Quaternary International, v. 15/16, p. 161-173.

Streif, Hansjorg 1987, Barrier islands, tidal flats, and coastal marshes resulting from a relative rise of sea level in East Frisia on the German North Sea coast, *in* van der Linden, W. J. M., Cloetingh, S. A. P. L., Kaasschieter, J. P. K., van de Graaff, W. J. E., Vandenberghe, J., and van der Gun, J. A. M., eds., Coastal lowlands: geology and geotechnology: Dordrecht, Kluwer Academic Publishers, p. 213-223.

Thomas, E., and Varekamp, J.C., 1991, Paleo-environmental analyses of marsh sequences (Clinton, Connecticut): evidence for punctuated rise in relative sea level during the latest Holocene: Journal of Coastal Research, v. 11, p. 125-158.

REPORTS

Jennings, A.E., and Nelson, A.R., 1992, Foraminiferal assemblage zones in Oregon tidal marshes--Relation to marsh floral zones and sea level: Journal of Foraminiferal Research, v. 22, p. 13-29.

Nelson, A.R., 1992, Discordant ^{14}C ages from buried tidal-marsh soils in the Cascadia subduction zone, southern Oregon coast: Quaternary Research, v. 38, p. 74-90.

Nelson, A.R., Contrasting styles of late Holocene relative sea-level change revealed by tidal-marsh stratigraphy, south-central Oregon coast, Cascadia subduction zone, *in* Fletcher, C.P., and Wehmiller, J.F., eds., Quaternary coasts of the United States--Marine and lacustrine systems: Society for Sedimentary Geology Special Publication no. 48, (in press).

Nelson, A.R., and Manley, W.F., 1992, Holocene coseismic and aseismic uplift of Isla Mocha, south-central Chile, *in* Ota, Yoko, Nelson, Alan R., and Berryman, Kelvin, eds., Impacts of tectonics on Quaternary coastal evolution: Quaternary International, v.15/16 , p. 61-76.

Nelson, A. R., and Personius, S. F., The potential for great earthquakes in Oregon and Washington--An overview of recent coastal geologic studies and their bearing on segmentation of Holocene ruptures, central Cascadia subduction zone, *in* Rogers, A. M., Walsh, T. J., Kockelman, W. J., and Priest, G. R., eds., Earthquake hazards in the Pacific Northwest of the United States: U.S. Geological Survey Professional Paper 1560, (in press, released in preliminary form as USGS Open-File Report 91-441-A).

Nelson, A.R., Ota, Yoko, Stafford, T.W., Jr., Umitsu, Masatomo, Kashima, Kaoru, and Matsushima, Yoshiaki, 1992, High-precision accelerator-mass-spectrometer radiocarbon dating of buried tidal-marsh soils--An approach to estimating the frequency and coastal extent of subduction zone earthquakes in Oregon and Washington, *in* Weiss, A.J., compiler, Proceedings of 19th Water Reactor Safety Meeting: U.S. Nuclear Regulatory Commission, Office of Nuclear Regulatory Research, NUREC/CP-0119, p.?

Nelson, A.R., 1992, Great subduction-zone earthquakes in the Pacific Northwest?--Differentiating coseismic from nontectonic tidal-marsh deposits along the Oregon coast: Proceedings of the 35th Annual Meeting of the Association of Engineering Geologists, October 2-9, 1992, Long Beach, California, p. 284-290.

Nelson, A.R., and Kashima, Kaoru, Diatom zonation in southern Oregon tidal marshes relative to vascular plants, foraminifera, and sea level: Journal of Coastal Research, (in press).

Personius, S.F., 1992, Stream incision rates and Quaternary deformation in the Oregon Coast Range: Geological Society of America, Abstracts with Programs, v. 24, no. 5, p. 74.

Personius, S.F., Age and origin of fluvial terraces in the central Coast Range, western Oregon: U.S. Geological Survey Bulletin 2038, (in press), 68 ms. p., 35 figs., 2 tables.

Personius, S.F., Kelsey, H.M., and Grabau, P.C., in press, Regional stream aggradation in the central Oregon Coast Range during the Pleistocene-Holocene transition: (Branch Approval 11/12/92; submitted to Quaternary Research) 32 ms. p., 9 figures, 1 table.

Paleoseismic and Geoarchaeologic Investigations Along the San Andreas Fault, Fort Ross State Historic Park, California

Award No. 14-08-0001-G2076

Jay S. Noller, William R. Lettis, and Keith I. Kelson
William Lettis & Associates
1000 Broadway, Suite 612
Oakland, California 94607
(510) 832-3716

Kent Lightfoot
Archaeological Research Facility
Department of Anthropology
University of California
Berkeley, California 94720

Investigations

We are developing new paleoseismic techniques that incorporate archaeological methods to determine the timing and recurrence of moderate- to large-magnitude earthquakes, slip rate, displacement per event on the northern segment of the San Andreas fault at Fort Ross State Historic Park, California. In the Fort Ross area, the San Andreas fault is geomorphically well expressed and there is excellent documentation of deformation associated with the 1906 San Francisco earthquake. The study area contains a rich and varied archaeological record that date to the middle Holocene. We are assessing middle to late Holocene activity of the fault based on offset cultural, geologic, and geomorphic features that are dated by radiometric and obsidian-hydration methods, and by diagnostic artifacts.

Geomorphic, archaeologic, and geologic investigations have been conducted at two sites in the Fort Ross State Historic Park, California. These investigations have involved surficial geologic and geomorphic mapping, surficial and shallow subsurface archaeologic surveys, sampling of subsurface deposits through hand-auger drilling, and paleoseismic trench excavations. Objectives of the program are to obtain data on the amount and rate of slip on the fault via offset archaeological sites and the timing of past earthquakes via offset stratigraphy exposed in trenches across the fault.

Results

Our current research focuses on two archaeologic sites that straddle the fault: Archae Camp (CA-SON-670) and "Murley" sites. Archae Camp is a multi-component archaeological deposit of about 4000 m^2 in extent that is transected by and offset along its western margin by the fault. At

this location the fault is defined by a single strand that ruptured in 1906, offsetting a nearby fence. The well-studied site is located above a 5-m-high, west-facing scarp. Our investigations show one surface and possibly as many as four buried cultural horizons that are present west of and up to 60 m north of the main site. We interpret the western components to be offset remnants of the main site. Preliminary dates show that these offset remnants are possibly as old as 3,000 yr B.P. We are awaiting the results of additional radiocarbon and obsidian-hydration dating to place constraints on timing of site materials. Margins of the site and the offset components, important as piercing lines across the fault, have been defined by a matrix of shallow shovel and auger holes, augmented by earlier trench excavations.

Additional subsurface investigations were conducted at the "Murley" site, located near Kolmer Gulch in the northern part of the park. Investigations of the subsurface extent of the archaeologic site has been conducted through a matrix of hand-auger borings. Stratigraphic analysis of the surface and subsurface investigations are currently being completed. Samples from these boreholes are being analyzed for physical and chemical tracers of the archaeological sites.

Reports

Noller, J.S., Lightfoot, K., Wickens, K.A., Kelson, K.I., Wake, T., and Parkman, E.B., 1992, Preliminary results of geoarchaeologic investigations along the northern San Andreas fault zone, Fort Ross State Historic Park, California: Proceedings of the Society for California Archaeology, vol. 6, 12 pp.

Noller, J. S., Lettis, W.R., Kelson, K.I., and Lightfoot, K., 1992, Holocene Activity of the Northern San Andreas Fault as Determined by Paleoseismic and Archaeologic Methods [Abstract]: 1992 AGU Fall Meeting, Eos, v. 73.

PALEOSEISMIC LIQUEFACTION STUDIES--COASTAL WASHINGTON STATE AND WABASH VALLEY SEISMIC ZONE
9950-04485

Stephen F. Obermeier
Branch of Geologic Risk Assessment
MS 922, U.S. Geological Survey
Reston, Virginia 22092
703-648-6791

The purpose of this project is to determine where prehistoric earthquake shaking has been strong enough to form liquefaction-induced features. Relict liquefaction-induced features normally take the form of sand- or gravel-filled dikes and sills. These features are commonly preserved in the recent geologic record.

Field searches for evidence of relict liquefaction were conducted this past year in two regions: the Wabash Valley Seismic Zone (of southern Illinois and Indiana) and near the coast of Washington State.

WABASH VALLEY SEISMIC ZONE

Background

The Wabash Valley Seismic Zone is a zone of diffuse seismicity centered about the Wabash Valley of Illinois and Indiana. Many small and slightly damaging earthquakes have occurred here during the 200 years of historic record. The Wabash Valley region has extensive alluvial lowlands, ranging in age from late Wisconsinan to modern. The alluvium is sand-rich, and the ground-water table has been high throughout much of the Holocene. Althogether, the setting of the valley has been conducive to formation and preservation of prehistoric liquefaction features for thousands of years. Laterally cutting rivers expose clean outcrops at many places.

Investigations

Hundreds of kilometers of outcrop throughout southern Illinois and Indiana have been examined for evidence of earthquake-induced liquefaction. Search areas were mainly in stream banks, but walls of man-made ditches and sand and gravel pits were also searched. Major streams searched were the Wabash, White, Embarras, Kaskaskia, and Eel Rivers. Significant portions of the Ohio River were also searched.

Results

Hundreds of planar, nearly vertical sand- and gravel-filled dikes that are interpreted to have been caused by earthquake-induced liquefaction have been discovered throughout southern Illinois and southern Indiana. These dikes range in width from a

few centimeters to as much as 2.5 m. The largest dikes are centered about the general area of Vincennes, Indiana; dikes strongly tend to decrease in size and abundance in all directions from the vicinity of Vincennes. Dikes are present more than 100 kilometers from Vincennes. Preliminary studies indicate that it is highly possible that many, if not all, of the dikes were formed by a single large earthquake that took place in the Vincennes area sometime between 5,000 and 7,500 years ago. Engineering-seismologic analysis, based on comparison of liquefaction effects with those of historic earthquakes in the Central and Eastern United States, indicates that the magnitude of the prehistoric earthquake was on the order of M 7.5.

REPORTS

Obermeier, S. F., Martin, J. R., Frankel, A. D., Youd, T. L., Munson, P. J., Munson,C. A., and Pond, E. C., 1992, Liquefaction evidence for strong Holocene earthquake(s) in the Wabash Valley of southern Indiana-Illinois with a preliminary estimate of magnitudes: U.S. Geological Survey Prof. Paper 1536, 28 p.

Obermeier, S. F., Bleuer, N. K., Munson, C. A., Munson, P. J., Martin, W. S., McWilliams, K. M., Tabaczynski, D. A., Odum, J. K., Rubin, M., and Eggert, D. L., 1991, Evidence of strong earthquake shaking in the lower Wabash Valley from prehistoric liquefaction features: Science, v. 251, p. 1061-1063.

COASTAL WASHINGTON STATE

Background

Coastal Washington has been almost completely devoid of historic earthquakes. The only occurrences have been scattered small events. Yet there is the possibility that great earthquakes occur here periodically. Atwater (1987, 1992) estimates that at least two episodes of coastal subsidence have occurred in Washington State during the past 2,000 years. Strong evidence indicates that one episode occurred 300 years ago, and moderately strong evidence indicates that another episode occurred 1,400 to 1,900 years ago. Buried lowlands indicative of this coastal subsidence have been postulated as originating from the action of great subduction earthquakes (M~8 to 9.5). The earthquakes are hypothesized to occur along the Cascadia subduction zone, where the oceanic (Juan de Fuca) plate is being subducted beneath the continental (North American) plate. To test this explanation, a search for relict liquefaction features was initiated.

Investigation

The search areas (Fig. 1) are designated in two categories: the Columbia River and smaller rivers. A major part of the search in the rivers was near the coast where shaking should have

been strongest. Most searching in smaller rivers was in the Humptulips and Chehalis Rivers.

Results

Many islands in the lowermost Columbia River were searched between the towns of Astoria and Longview (Fig. 1). These islands originated as braid bars, on a grand scale. The islands are flat, poorly drained, and swampy. Large portions are submerged during very high tides. Strong currents and wave pounding are severely eroding many islands and, as a result, are sculpting clean, vertical clay-rich banks as much as 2 meters in height, which extend from water level to top of the bank. Age at the base of the exposed clay-rich cap is probably less than 1,000 years, which is based on a radiocarbon age (640 $\pm$ 60) on tuberous plants (genus scirpus) found in their growth position, just above the base. Therefore, the sediments are old enough to record shaking associated with Atwater's 300-year old downdropping, but probably not old enough for the eposide 1,400 to 1,900 years ago.

At many places sand is exposed immediately beneath the clay cap. Grain sizes range from fine- to- medium-grained, clean sand to clayey, silty fine sand. Clean sands appear to be widespread and commonplace. Altogether, conditions on many islands are nearly ideal for formation of large liquefaction-induced features. Not only is the cap thin, but the ground-water table has almost certainly been at or within a meter or so of the ground surface since the islands formed.

About 15 km of clean banks were searched for liquefaction features. More than a hundred sand-filled dikes have been found in scattered islands. The dikes vented onto a paleosol, and about 1 m of silt and clay subsequently was laid down on the vented sand. For the following reasons, all dikes are thought to have been caused by the coastal downdropping event 300 years ago: (1) the radiocarbon ages of sticks collected on the surface of venting are in the proper range; (2) trees on sediments above vented sand have the same maximum ages (about 200 years); (3) dikes increase in abundance toward the coast; (4) dike sizes (widths) increase toward the coast.

Only very small dikes in the Columbia River islands occur as far as 60 km inland from the coast. Such features likely formed at an acceleration level on the order of 0.1 g, on the basis of threshold accelerations observed worldwide for highly susceptible sediments (National Research Council, Committee on Earthquake Engineering, 1985).

No clear-cut liquefaction-induced dikes were found in banks of smaller rivers. At least 100 km of smaller rivers were searched (Fig. 1). More than 20 km of river banks were eroded so cleanly that even very small dikes (1 cm in width) would have been observed. At many places there are two or three pedological

profiles stacked on top of one another, each separated by a meter or so of silt and clay. Therefore, on the basis of well-developed pedological profiles in the deposits along the banks, ages of many kilometers of deposits exposed in the banks much predate the 300-year old downdropping event.

Beneath a thin clay-silt cap, sandy gravels occur at almost all places. Depth to semilithified to lithified bedrock seems to range from a few meters to about 30 meters. Thus there appears to be little opportunity for amplification or dampening of shaking at depth.

The sandy gravels of the smaller rivers are so coarse-grained that very strong shaking probably would be required to cause liquefaction features to form. Still, comparison of grain-size data shows coarser gravels (based on data in Andrus and Youd, 1987) formed large dikes and vented large quantitites of sand and gravel to the surface during the 1983 Borah Peak, Idaho, earthquake (M 7.3). Peak accelerations at the Borah Peak liquefaction sites are thought to be 0.4 to 0.6 g (Andrus and Youd, 1987). Thus, it would seem that a great earthquake directly beneath the coast of Washington, causing very strong shaking, should have formed at least some small, but unequivocal liquefaction-induced features in the sandy gravels. None has been found, though.

References Cited

Andrus, R. D. and Youd, T. L., 1987, Subsurface investigation of a liquefaction-induced lateral spreads, Thousand Springs Valley, Idaho: U.S. Army Waterways Experiment Station Mis. Paper GL-87-8, 106 p.

Atwater, B. F., 1987, Evidence for great Holocene earthquakes along the outer coast of Washington State: Science, v. 236, p. 942-944.

Atwater, B. F., 1992, Geologic evidence for earthquakes during the past 2,000 years along the Copalis River, southern coastal Washington: Journal of Geophysical Research, v. 97, no. B2, p. 1901-1919.

National Research Council, 1985, Liquefaction of soils during earthquakes: Washington, D. C., National Academy Press, 240 p.

Figure 1. Map showing search area for paleoliquefaction features. River banks that were searched are shown with heavy linework. Islands in the Columbia River were searched mainly between 30 to 60 km inland from the coast. On these islands, dike abundance and dike sizes increase toward the coast. Dikes appear not to occur further inland than about 60 km from the coast. Islands searched are probably about 800 to 1,000 years old.

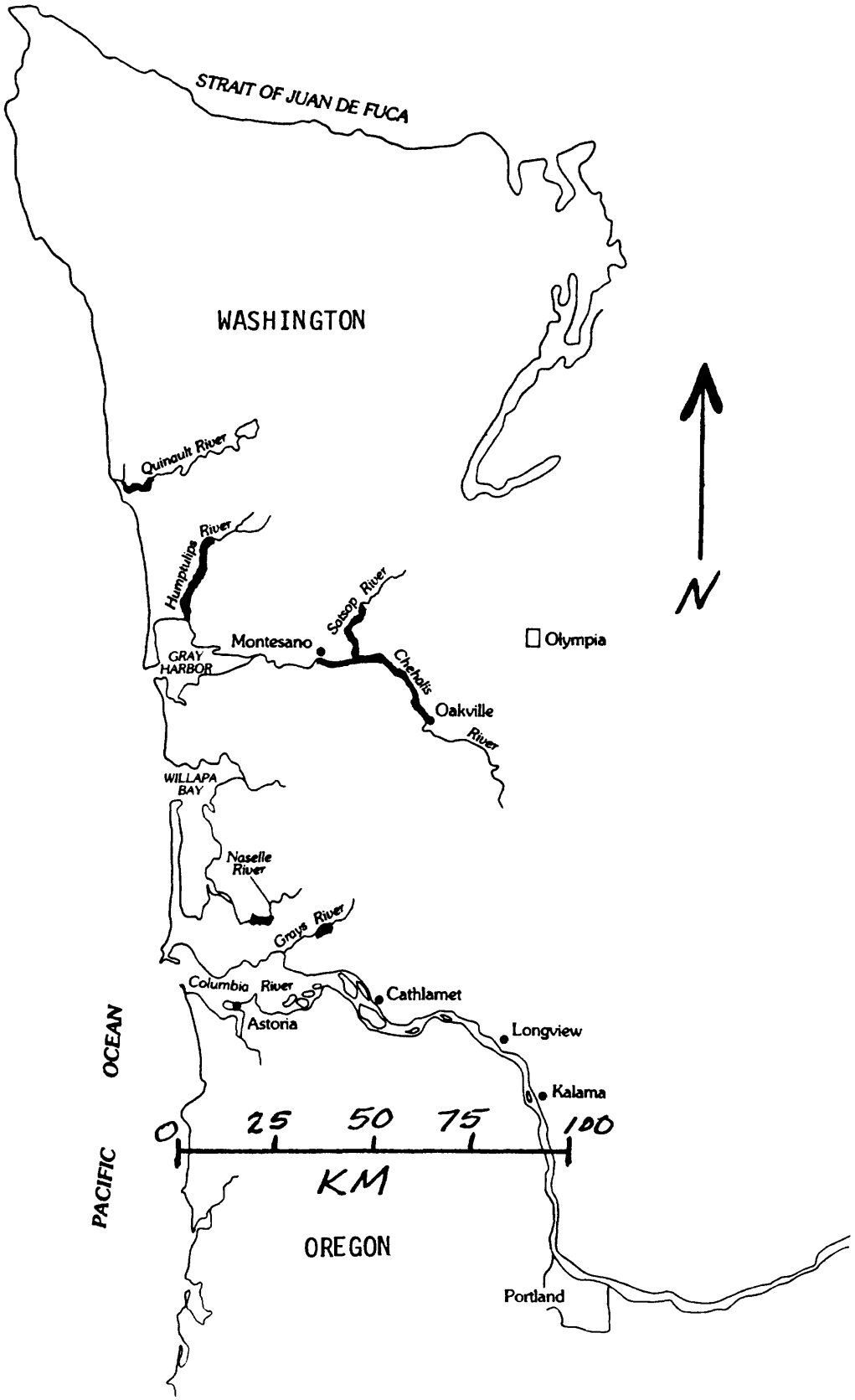
STRAIT OF JUAN DE FUCA
WASHINGTON
Quinault River
Humptulips River
Satsop River
Montesano
GRAY HARBOR
Chehalis River
Oakville
Olympia
N
WILLAPA BAY
Naselle River
Grays River
Columbia River
Cathlamet
Astoria
Longview
Kalama
PACIFIC OCEAN
0 25 50 75 100
KM
OREGON
Portland

Earthquake Potential Evaluation of the Northern Oquirrh Fault Zone, Central Wasatch Front, Utah

Award No. 1434-92-G-2218

Project Summary

Susan S. Olig, William R. Lund, and Bill D. Black
Utah Geological Survey
2363 S. Foothill Dr.
Salt Lake City, UT 84109
(801) 467-7970

Investigations

This project is a paleoseismic investigation of the northern Oquirrh fault zone, which bounds the west side of the Oquirrh Mountains, roughly 35 km from downtown Salt Lake City (figure 1). Previous geomorphic investigations indicated that fault scarps offset the Provo shoreline of Lake Bonneville and were probably formed 9,000 to 13,500 years ago (Barnhard, 1988; Barnhard and Dodge, 1988). However, constraints on the minimum age were not conclusive. The purpose of this study is to better characterize the timing and size of prehistoric surface-rupturing earthquakes along the fault zone by:

1. interpretation of aerial photographs and detailed mapping of the surficial geology at proposed trench sites,

2. profiling of fault scarps,

3. excavating and logging trenches across fault scarps at two different sites, and

4. dating material from key stratigraphic units to best constrain the timing of surface-rupturing earthquakes.

Results (April 15, 1992 through October 1, 1992)

Two trenches near the mouth of Big Canyon were excavated and logged (figure 1). There is a wide graben at this site, formed by a large west-facing main scarp, 12 to 18 meters high, and a small antithetic scarp. Net vertical displacements range from 4 to 6.8 meters. Stratigraphy is similar in both trenches, with pre-Lake Bonneville alluvial-fan gravels exposed on the upthrown east side of the fault and Lake Bonneville transgressive, deep-lake, and regressive deposits overlain by a debris-flow deposit on the downthrown side of the fault. A 2- to 3-meter-thick colluvial wedge overlies the debris-flow deposit at the base of the scarp and is in turn overlain by unfaulted colluvium and a moderately developed modern soil that drapes the scarp. Radiocarbon ages for bulk soil samples collected from the faulted debris-flow deposit, directly beneath the colluvial wedge, are

6840 ±100 yr B.P. and 7650 ±90 yr B.P., indicating that the most recent surface-rupturing earthquake was younger than previous age estimates based on scarp morphology. Our preliminary interpretations of the Big Canyon trench exposures are that one large surface-rupturing earthquake occurred after 7,000 years ago and no surface-rupturing earthquakes occurred between 7,000 and 30,000 years ago. We are excavating another trench across unfaulted alluvial-fan sediments at this site in an attempt to constrain the minimum age of the most recent surface-rupturing earthquake.

We are also planning to excavate trenches at a site about 2.5 km south of the Big Canyon site in an attempt to constrain the timing of the penultimate surface-rupturing earthquake on the northern Oquirrh fault zone. In addition to the report cited below, we conducted field reviews to quickly disseminate available information to local government officials, the media, and the engineering and geologic community.

Reports

Olig, S. S., in press, Prehistoric earthquakes on the northern Oquirrh fault zone, Tooele County: Utah Geological Survey, Survey Notes (Fall, 1992).

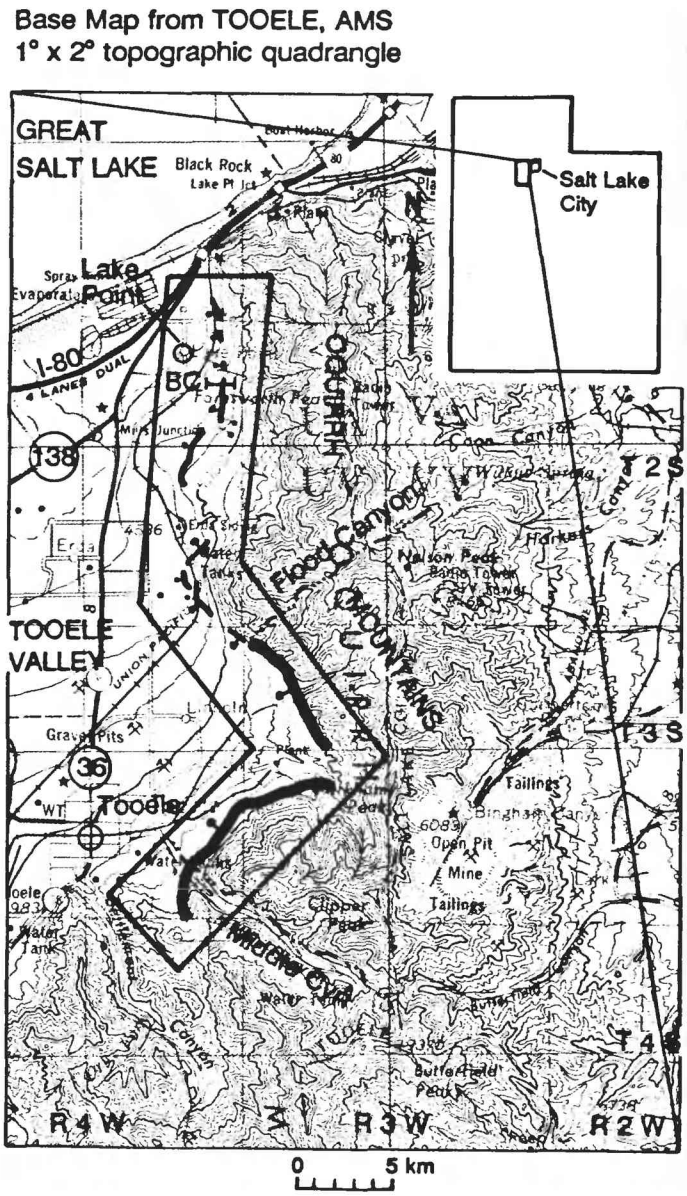

Figure 1. Location map of the northern Oquirrh fault zone, Tooele County, Utah, and the Big Canyon trench site, labeled BC (modified from Barnhard, 1988).

Array Studies of Seismicity

9930-02106
David H. Oppenheimer
Branch of Seismology
United States Geological Survey
345 Middlefield Road - MS 977
Menlo Park, California 94025
415-329-4792

Investigations

1. Consolidation and clean-up of phase data of central California Seismic Network (CALNET) from 1968 through present.
2. Prototype development of GIS-based seismicity maps.
3. Seismicity of the East San Francisco Bay region.
4. Seismicity of the April 25, 1992 Cape Mendocino earthquake.

Results

1. The last phase of the reprocessing of CALNET earthquake data collected since 1968 continued (see previous Semi-Annual Reports). We have examined earthquake locations with an RMS>0.5 s between 1967 and 1989 to ascertain the reason for the poor locations. Quality checking of duplicate event identifiers was performed. Software has been developed to identify likely explosions in the catalog using criteria of known quarry locations, time-of-day, day-of-week, depth, and percent of compressional first-motion readings. The entire catalog of earthquakes will be re-processed such that explosions will be tagged with appropriate identifiers.
2. Because the catalog of earthquakes recorded by the CALNET between 1967 and 1992 now exceeds 320,000 earthquakes, with each year adding an additional 15,000 earthquakes, it is no longer practical nor desirable to publish bulletins of all earthquakes recorded by the network. Instead, most seismologists prefer to have the data in digital form. However, for the non-seismologist, there is a need for maps of earthquakes recorded by the network. To address this need, we have generated raster-scan images of the 1:250,000 scale USGS topographic base maps for central California and have imported these scans into ARCINFO, a GIS system for that enables us to overlay the seismicity on the digitized topographic base. The resulting map series will have the same scale and boundaries as the maps of the Geologic Atlas of California published by C.D.M.G. Explanatory text, cross sections, select focal mechanisms, and bibliography will accompany the maps. A prototype map for the San Jose Quadrangle is in preparation and should be completed by the end of the year.
3. Three reports describing the seismotectonics, fault structure, and segmentation of active faults in the East an Francisco Bay regions were produced for the proceedings of the Second Conference on Earthquake Hazards in the eastern San Francisco Bay Area. The first report reviews the seismicity of the East Bay since 1969, which indicates that four classes of faults are active: 1) major NW-trending, vertical, right-lateral strike-slip faults that apparently accommodate the relative Pacific-North American plate motion across the region. Faults typical of this class in-

clude the Hayward, Calaveras, Concord, and Greenville faults; 2) NE-trending, vertical, left-lateral strike-slip faults that occur within right step-over regions between endpoints of major faults. These step-over faults also tend to produce earthquake swarms; 3) north-trending, vertical, right-lateral strike-slip faults, such as the source of the M_L5.7 Mt. Lewis earthquake; and 4) reverse faulting on NW-oriented planes. This complex pattern of faulting is the result of low shear strength on the major faults and the related fault-normal horizontal compression. The principal, northwest-oriented, vertical, right-lateral strike-slip faults are required by geodetic studies to play the dominant role in the release of tectonic strain over time.

The second report focuses on the seismicity of the Hayward fault, which poses a major seismic hazard to the San Francisco Bay region. Analysis of seismicity recorded by the University of California at Berkeley since 1910 and the USGS since 1969 indicates that earthquakes of $M_L <$ 4.5 occur on or adjacent to the Hayward fault from Point Pinole to the juncture of the Hayward and Mission faults. South of this juncture the Hayward fault is aseismic for approximately 15 km where shallow (<4 km) $M < 3$ seismicity resumes for about 13 km until the Hayward fault intersects the Calaveras fault near the epicenter of the 1984 Morgan Hill earthquake. Cross sections of seismicity indicate that the Hayward fault is nearly vertical over most of its length, and the width of the seismogenic zone is less than 13 km. We attribute non-vertical distributions of seismicity to systematic mislocations arising from un-modeled velocity variations across the fault. Focal mechanisms are generally consistent with right-lateral motion on a vertical fault, but near San Leandro secondary faults adjacent to the Hayward fault exhibit oblique reverse, right-lateral motion. Gaps in seismicity may indicate main shock rupture zones, but uncertainties in earthquake locations and focal mechanisms make it difficult to determine whether most earthquakes occur on the Hayward fault or on small, reverse faults immediately adjacent to the fault. As a consequence, the seismicity data are insufficient at present to be able to recognize the segment boundaries of the 1836 and 1868 *M*7 earthquakes and to unambiguously forecast where future main shocks might occur.

The third report similarly focuses on the seismicity of the Calaveras fault north of the Calaveras Reservoir and south of Danville, which has been virtually been aseismic since 1969. By comparison with the seismic behavior of the Calaveras fault south of the reservoir and the fault segment that ruptured during the Loma Prieta earthquake, we infer from the lack of earthquakes that the northern Calaveras fault is locked and accumulating elastic strain energy. The slip rate of this segment of the fault is approximately 6 mm/yr, and there is no indication of surface creep. The length of the seismic gap is approximately 40 km and the width of the fault inferred from the maximum depth of earthquakes is 10 km. We consider the potential of an earthquake occurring on this segment over the next 30 years for two equally plausible rupture scenarios. If the entire northern Calaveras fault ruptures at one time, the expected magnitude (*M*) would be approximately *M*7, but there is insufficient information at present to calculate reliable probabilities. Alternatively, the fault could rupture in two or more *M*6 earthquakes, as suggested by the occurrence of three moderate earthquakes between 1858 and 1864, with a probability of 0.18. Although the probabilities have large uncertainties, we believe the geologic and geophysical data indicate that the northern Calaveras fault is a significant seismic hazard for the San Francisco Bay region.

4. On April 25, 1992 at 18:06 (UTC) a *Ms* 7.1 earthquake occurred near the town of Petrolia, California. The main shock was followed the next day by two large aftershocks (M_s 6.6 at 07:41 and M_s 6.7 at 11:41) located offshore 30-40 km west of Petrolia. These three earthquakes and

more than 2000 aftershocks occurred in the vicinity of the Mendocino Triple Junction (MTJ), where the Pacific (PA), North American (NA), and southern Juan de Fuca, or Gorda (GD), plates meet. Our preliminary findings indicate these earthquakes involved plate scale processes including coseismic slip on the southernmost part of the Cascadia megathrust. This sequence provides a unique opportunity to witness the coseismic movement of these three plates.

The main shock hypocenter locates onshore, 4 km east of Petrolia, at a depth of 10.5 km. Its focal mechanism indicates nearly pure thrust on a N12°W trending fault plane dipping 13° to the ENE, and aftershock locations clearly image the slip plane. The hypocenter locates at the southeast end of the aftershock zone, indicating that the fault ruptured unilaterally to the west. The aftershocks less than 12 km deep outline a trapezoidal region that extends seaward 5-10 km and which is bounded on the south by the Mendocino fault (MF) and on the northeast by a NW trend of earthquakes. The location, depth, and orientation of the main shock rupture plane is consistent with the absence of observed surface faulting.

The two large aftershocks locate 30 km seaward from the mainshock at depths near 20 km and both have strike-slip mechanisms with planes striking SE and dipping steeply to the SW. The second large (M_S 6.7) aftershock occurs within a similarly oriented trend of smaller aftershocks, which confirms this as the slip plane, but the first large (M_S 6.6) aftershock apparently locates 5 km north of the trend and has no aftershocks associated with it. Although no large shocks ruptured the MF during this sequence, a considerable number of aftershocks occurred on the eastward projection of the fault. The seismicity on the MF indicates that all of the aftershock activity for this sequence is bounded on the south by a near vertical structure that extends to depths of 25 km. If this is the boundary between the Gorda and Pacific plates, then the lack of any aftershocks within the Pacific plate suggests that the main shock represents strain release primarily between the Gorda and North American plates.

A comparison of the seismicity of the Cape Mendocino sequence and the pre-main shock seismicity recorded by local networks demonstrates that the principal faults which ruptured during the main shock and large aftershocks were inactive during the period 8/74-4/92. Moreover, the focal mechanism and aftershocks of the Cape Mendocino main shock indicate motion on a thrust fault parallel to, but 7 km more shallow than the pre-main shock seismicity. The seismicity gap between the slip plane of the main shock and the pre-main shock seismicity most likely reflects the aseismic crust of the Gorda plate, and the inception of seismicity at a depth of 17 km coincides with the top of the Gorda mantle, which due to its more mafic composition remains brittle at these temperatures.

Reports

1. Oppenheimer, D.H., I. G. Wong, and F. Klein, The seismicity of the Hayward fault, California, *in* Borchardt, G., et al., eds., Proceedings of the Second Conference on Earthquake Hazards in the Eastern San Francisco Bay Area, California Division of Mines and Geology Special Publication 113, *in press*, 1992.

2. Oppenheimer, D.H., and A. G. Lindh, The potential for earthquake rupture of the northern Calaveras fault, *in* Borchardt, G., et al., eds., Proceedings of the Second Conference on Earthquake Hazards in the Eastern San Francisco Bay Area, California Division of Mines and Geology Special Publication 113, *in press*, 1992.

3. Oppenheimer, D.H., and N. Macgregor-Scott, The seismotectonics of the eastern San Francisco Bay region, *in* Borchardt, G., et al., eds., Proceedings of the Second Conference on Earthquake Hazards in the Eastern San Francisco Bay Area, California Division of Mines and Geology Special Publication 113, *in press*, 1992.

4. Andrews, D. J. and D. H. Oppenheimer, The Mission fault: A magnitude 6+ thrust or reverse-slip earthquake can be expected, *in* Borchardt, G., et al., eds., Proceedings of the Second Conference on Earthquake Hazards in the Eastern San Francisco Bay Area, California Division of Mines and Geology Special Publication 113, *in press*, 1992.

5. Oppenheimer, D.H., F.W. Klein, and J.P. Eaton, The first 20 years of CALNET, The Northern California Seismic Network, U.S. Geological Survey Open-File Report 92-209, 33pp., 1992.

6. McLaughlin, R., D.H. Oppenheimer, E.J. Helley, and M. Sebrier, The Lexington fault zone: A north-south link between the San Andreas fault and range front thrust system, Geol. Soc. Amer. Abs. with Prog., 1992.

7. Zandt, G., W.R. Walter, H.M. Benz, D.H. Oppenheimer, D. Verdonck, and K.P Furlong, Tectonics of the Mendocino triple junction region from seismic tomography and earthquake source mechanisms, EOS, Trans. Amer. Geophys. Union, 73, 496, 1992.

8. Oppenheimer, D.H., and J.P. Eaton, The seismicity of the 1992 Cape Mendocino, CA, earthquake, EOS, Trans. Amer. Geophys. Union, 73, 497, 1992.

9. Sebrier, M., R. McLaughlin, K. Lajoie, and D. Oppenheimer, Fault kinematics in the San Francisco peninsula area, Is the 1989 Loma Prieta earthquake anomalous?, EOS, Trans. Amer. Geophys. Union, 73, 589, 1992.

Variations in Electrical Properties Induced by Stress Along the San Andreas Fault at Parkfield, California

Grant 14-08-0001-G1357

Stephen K. Park
Tien Chang Lee
Institute of Geophysics and Planetary Physics
University of California
Riverside, California 92521

(714)787-3438

Introduction

We are monitoring fluctuations of resistivity with telluric currents in Parkfield. The array uses grounded telephone lines as dipoles (Figure 1). The analysis and relevant results through early 1990 are discussed in Park [1991]. We look at daily fluctuations of the telluric coefficients relating Dipoles 1 through 6 to the reference dipoles of Dipoles 7 and 8. Thus, we are looking at relative variations, rather than absolute ones. Changes in the telluric coefficients are directly related, albeit through the response of a complex, heterogeneous earth, to changes of resistivity.

Discussion of Data

Results of the analysis for the past nine months for Dipoles 1 through 6 are shown in Figures 2 through 7. We plot the projection of the daily fluctuation of the telluric coefficient onto the major and minor eigenvectors (upper and lower plots for each dipole, respectively) and the coherency as a measure of the data quality. Based on fluctuations of the projections for all of 1988 and 1989, standard deviations for the daily projections were calculated. The 95% confidence intervals (approximately 2σ) are shown with dashed lines in Figures 2 through 7. These projections are further smoothed with a nine day running average which is weighted by the inverse of the square of the coherency (which is a measure of the relative noise). The error bars for each daily point are standard errors calculated from this running weighted average.

Significant deviations can be identified in one of two ways. First, points which lie outside the 95% confidence intervals can be significant. Second, deviations for which the error bars are not overlapping may be significant. For example, the minor projection on Dipole 3 increases beyond the confidence interval between Days 34 and 38 in 1992 (just before the gap; Figure 4) and returns to within its usual bounds on Day 46 (just after the gap; Figure 4). However, the error bars also grow quite large between Days 34 and 38, so this is probably not a significant deviation. The variations on the minor projection for Dipole 2 during this same time are probably significant, in comparison. However, the data quality on Dipole 2 is poor during the first four months of 1992 so this significant deviation is poorly recorded.

This year has been characterized by the relative lack of significant deviations. In

particular, only one has been observed. This was on Dipole 2 between Days 130 and 140 and was seen on both projections (Figure 3). Note that the error bars for Days 130 and Days 140 do not overlap, so this is a real variation. We currently have no explanation for this variation. Other than this, the signals have shown no variations and this is consistent with the lack of other activity in Parkfield (at least until September). The increase of seismic activity beginning in late September and continuing until the present is not accompanied by changes in resistivity. The M4.7 earthquake occurred on Day 294 and while our data do not extend past Day 297, we see no obvious precursory or coseismic change (Figures 2 through 7). Dipoles 4 (Figure 5) and 6 (Figure 7) exhibit the beginnings of decreases in the minor projections, but these drops are not significant yet by the criteria outlined above.

We have seen a general degradation of data quality over the past several years as other experiments have been added to Halliburton Ranch. These experiments have introduced electronic noise to our system which appears to be picked up by our telephone lines in the recording room. We have now acquired a new computer and data acquisition system and are in the process of redesigning our electronic circuits in order to eliminate these noises.

Conclusions

This year has been characterized by a relative absence of activity, even during the most recent seismic events. While the lack of coseismic or precursory signals is disturbing, a review of electrical phenomena which have been reported as precursors shows that the recent seismic activity in Parkfield is still below the threshold for detectablility (Park et al., 1992).

Reports Published

Park, S.K., Quantification of errors for the Parkfield array, in Roeloffs, E. (ed), Proceedings of the Joint US-PRC Conference on Focused Earthquake Prediction Experiments, San Juan Bautista, September, 1991.

Park, S.K., M.J.S. Johnston, T.R. Madden, F.D. Morgan, and H.F Morrison, Electromagnetic precursors to earthquakes in the ULF band: A review of observations and mechanisms, submitted to Reviews of Geophysics, 1992.

Figure 1 - Telluric monitoring array in Parkfield, California. Dipoles 1 through 8 are created electronically by differencing potentials from five electrodes (Ff, Hq, Hr, Tf, and Lc). Symbols referred to elsewhere in the text are: MM = Middle Mountain ; PK = town of Parkfield; DL = Donalee tensor strain meter; and EA = Eades tensor strain meter.

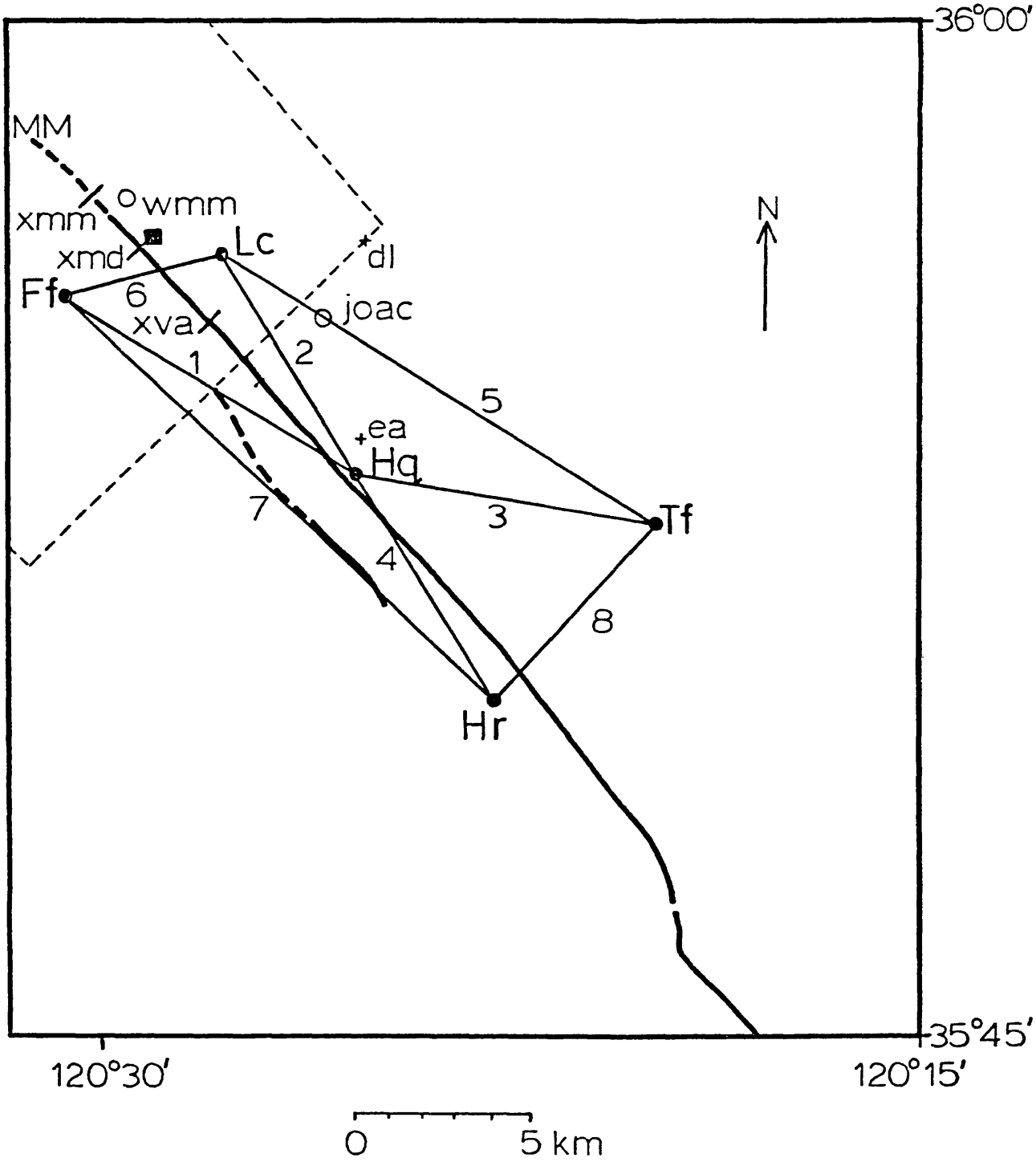

Figure 2 - Residual analysis for Dipole 1 for the past nine months. The first plot is the projection of the residual on the major eigenvector with a scale of +2% to -2% and the second is the projection on the minor eigenvector with a scale of +5% to -5%. Coherencies are between the signal predicted using the telluric coefficients and the measured signals are shown between .998 and 1.000. 95% confidence intervals are shown with dashed line on the projection plots.

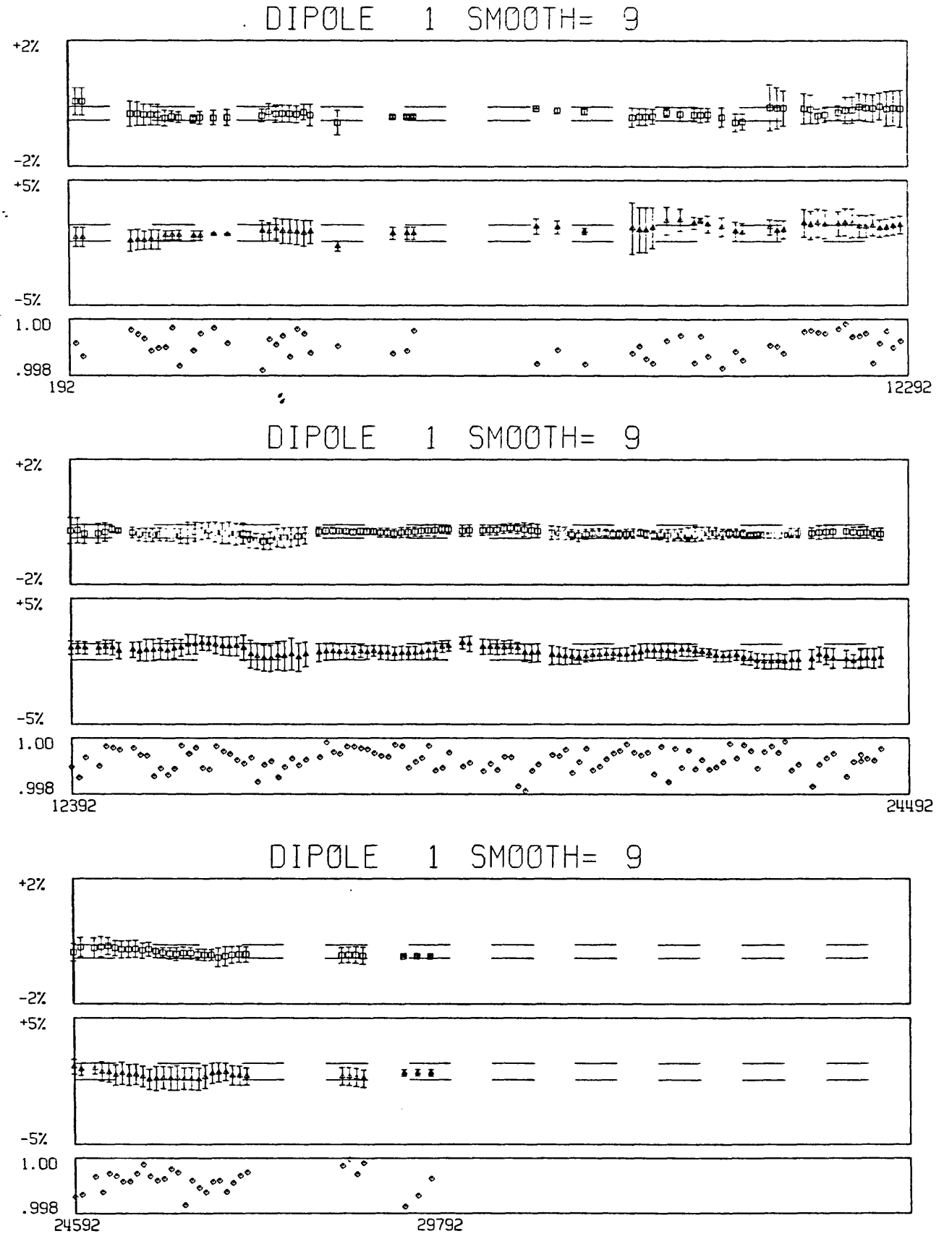

Figure 3 - Residual analysis for Dipole 2 for the past nine months. See caption of Figure 2 for explanation.

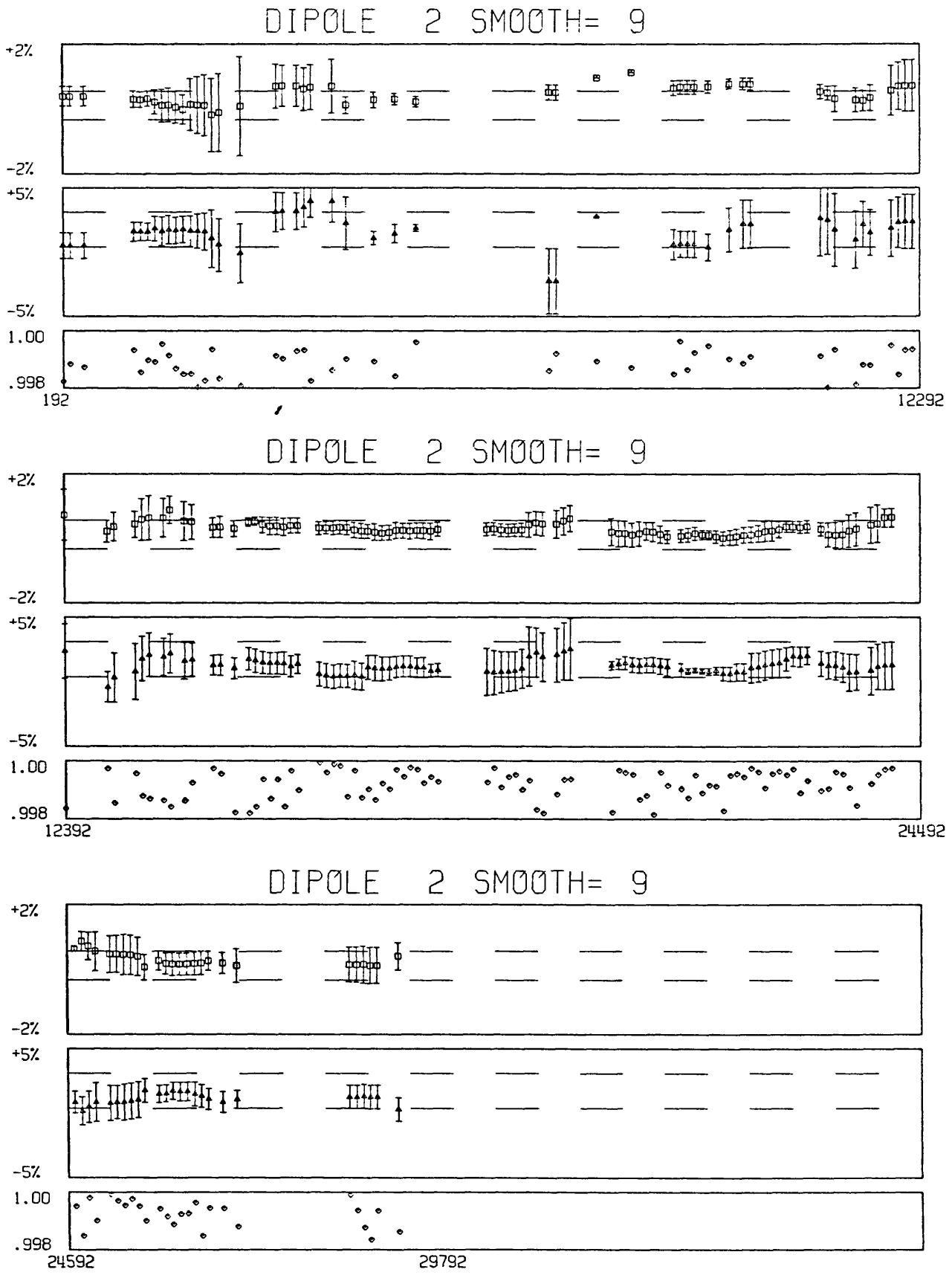

Figure 4 - Residual analysis for Dipole 3 for the past nine months. See caption of Figure 2 for explanation.

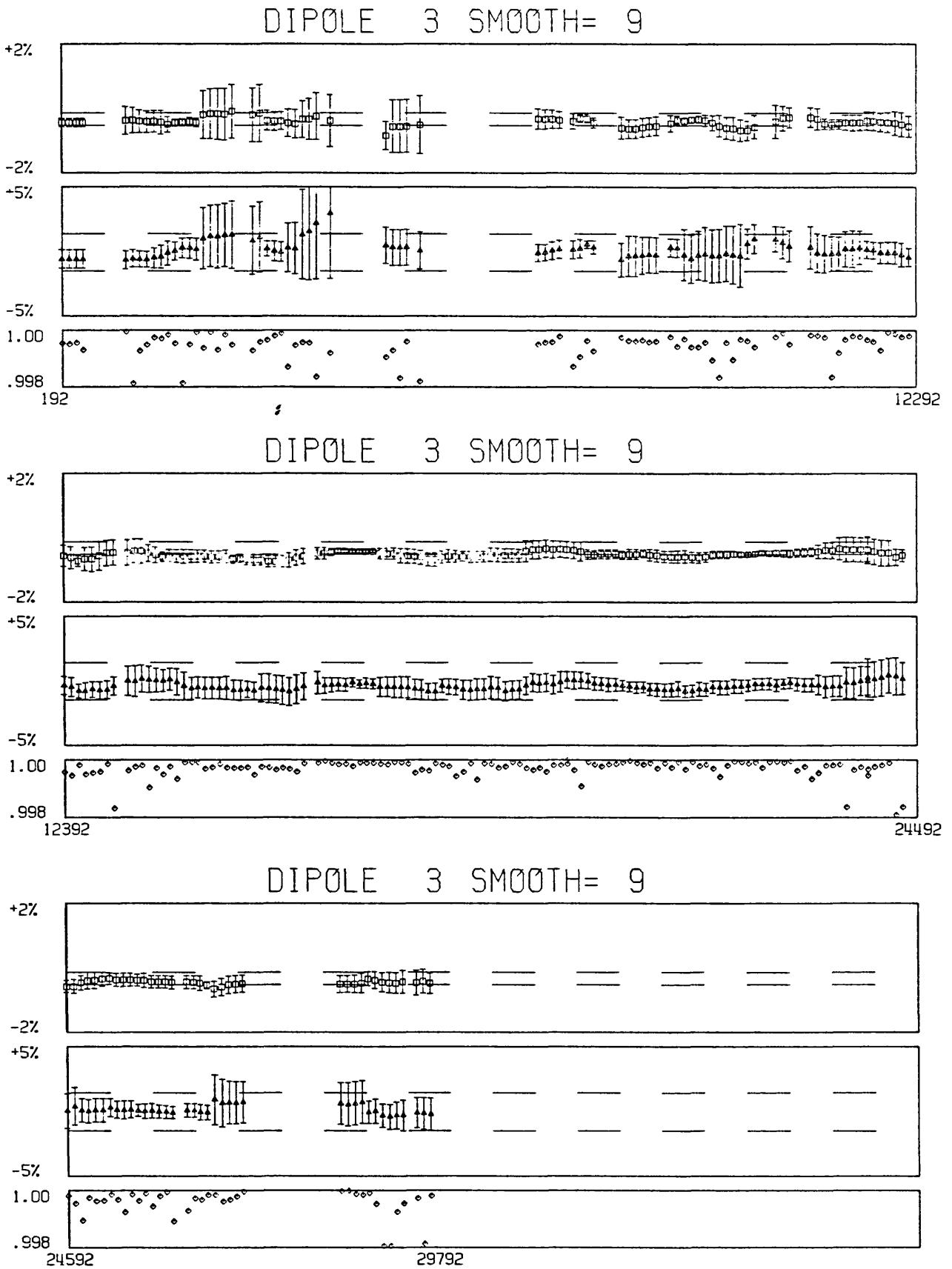

Figure 5 - Residual analysis for Dipole 4 for the past nine months. See caption of Figure 2 for explanation.

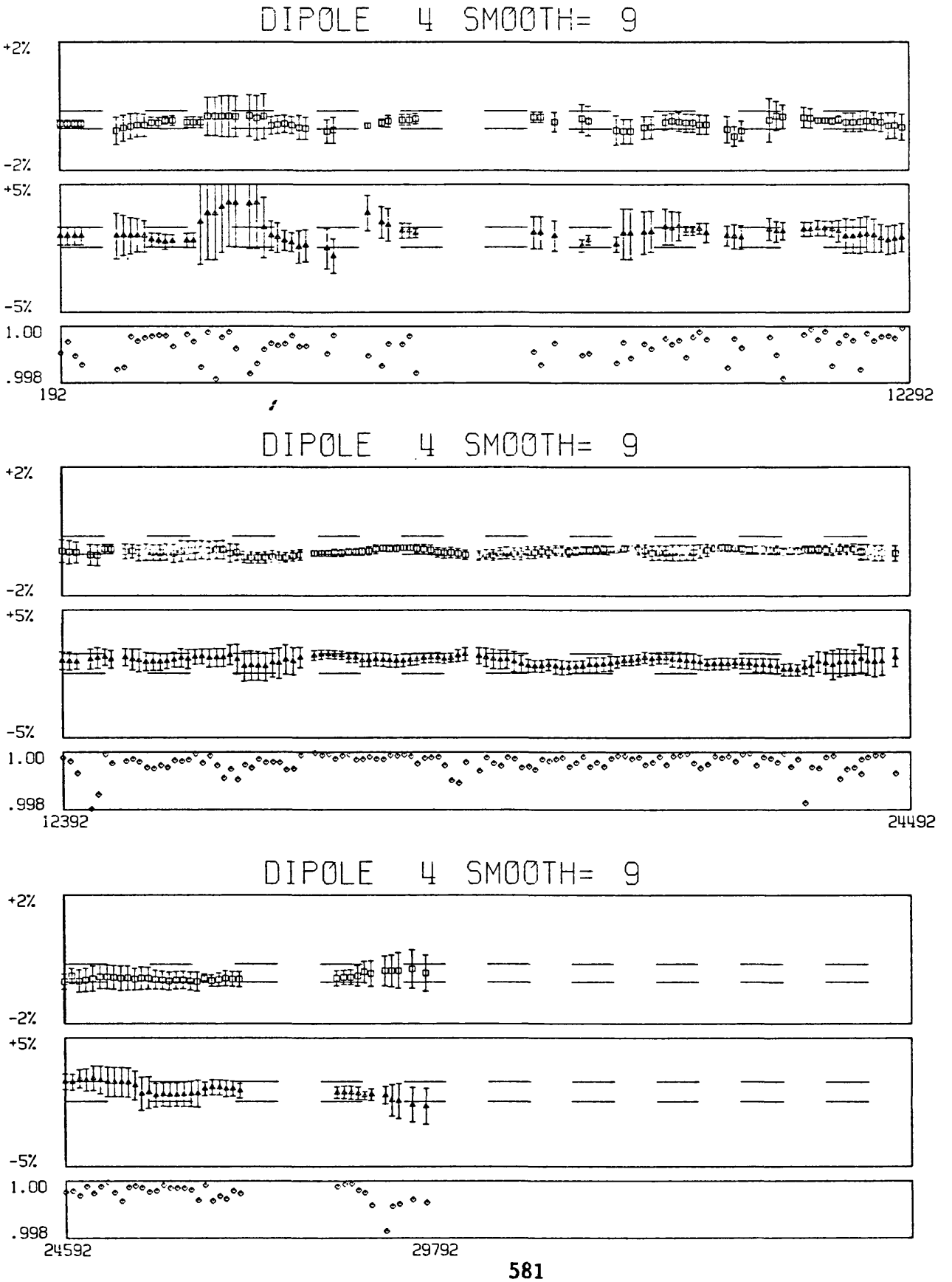

Figure 6 - Residual analysis for Dipole 5 for the past nine months. See caption of Figure 2 for explanation.

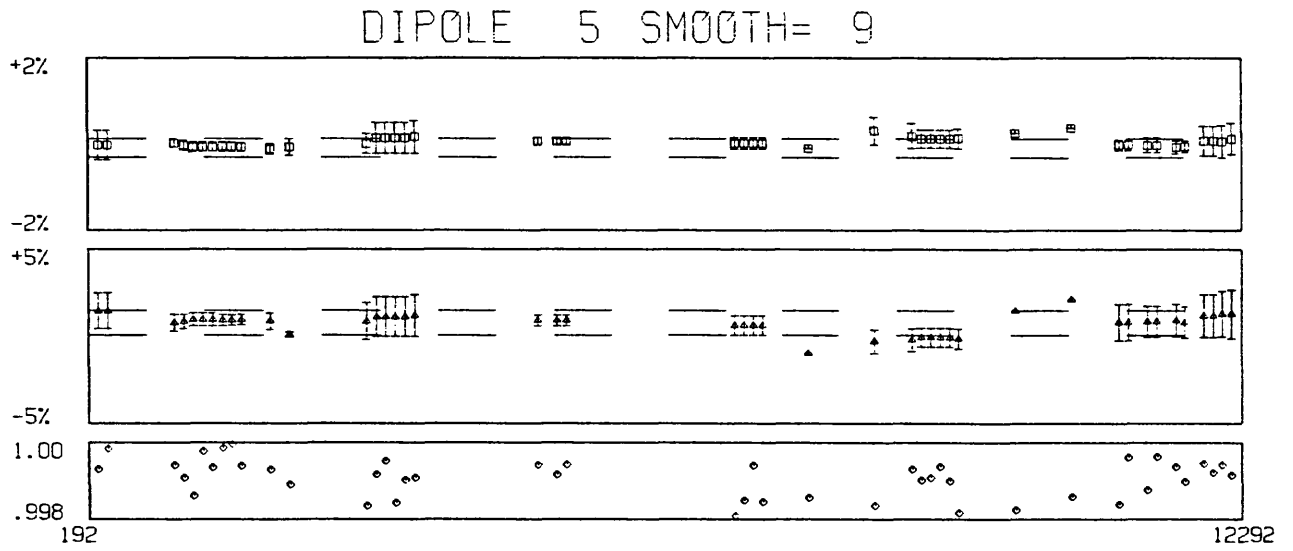

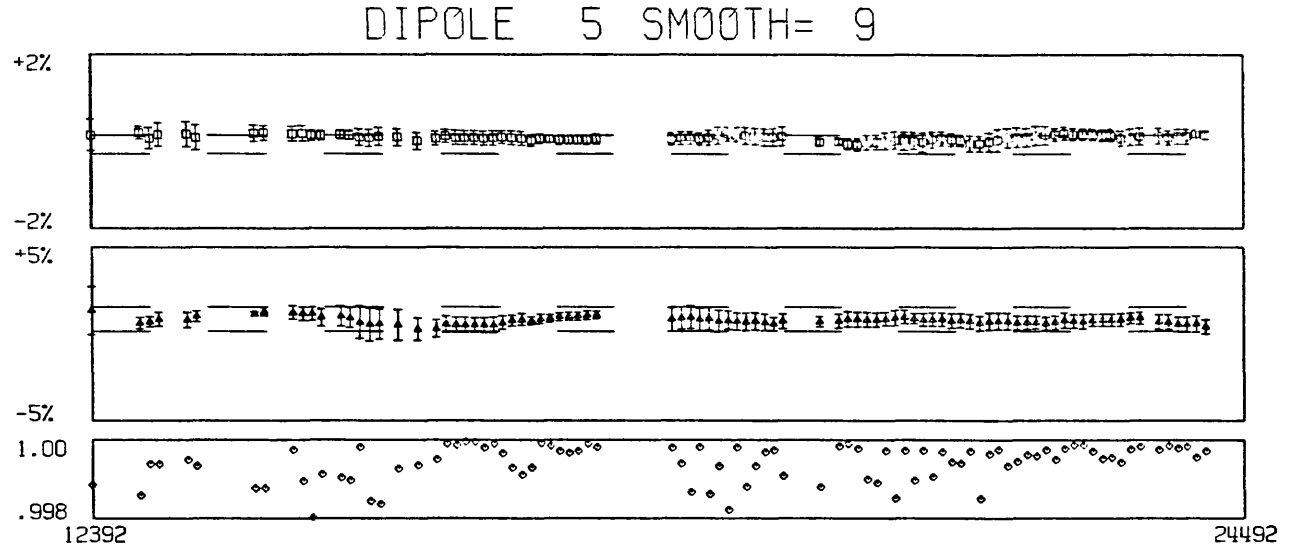

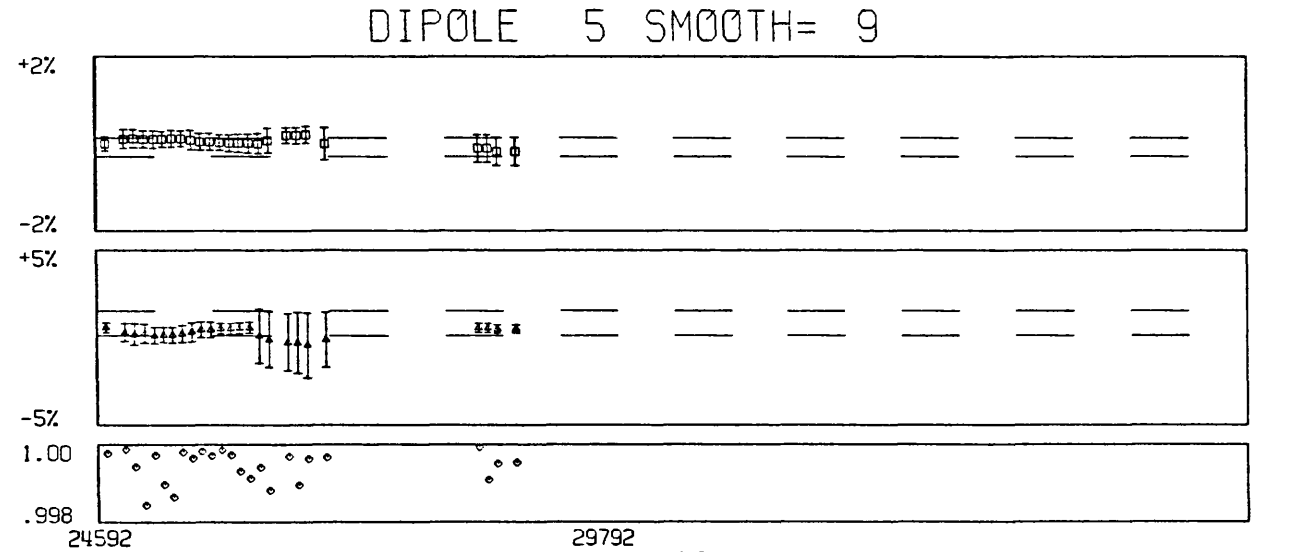

Figure 7 - Residual analysis for Dipole 6 for the past nine months. See caption of Figure 2 for explanation.

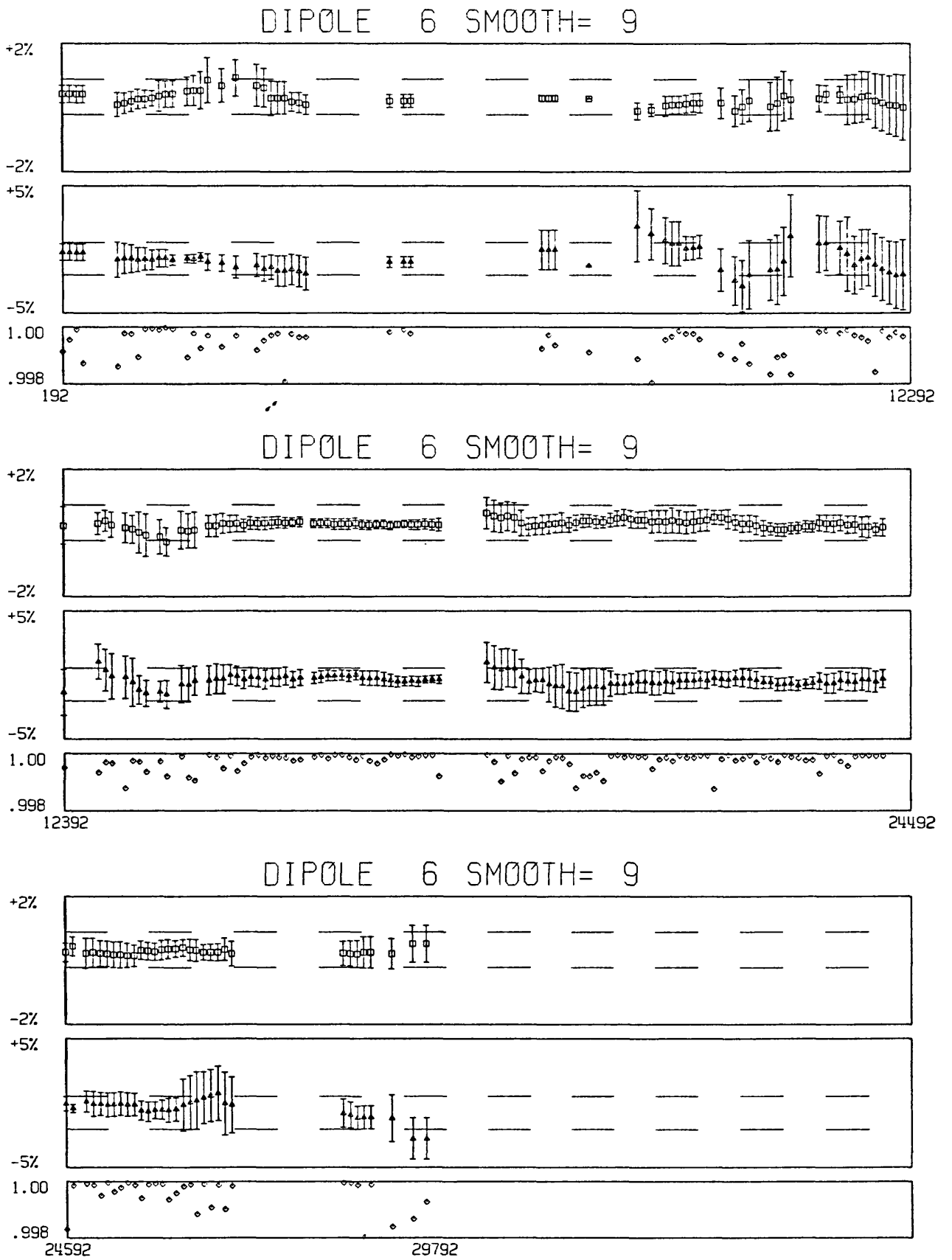

ALASKA GEOLOGIC EARTHQUAKE HAZARDS
9310-01026

George Plafker
Branch of Alaskan Geology, MS-904
345 Middlefield Road
Menlo Park, CA 94025
415-329-8920

Investigations

1. Continue studies of the recurrence intervals for great tectonic earthquakes and the seismic cycle associated with the eastern Aleutian subduction zone (with Ken LaJoie and Meyer Rubin, U.S.G.S.). Recent fieldwork has been focussed mainly on elucidation of the earthquake cycle and recurrence intervals in the Copper River Delta region, which has the most complete paleoseismologic record within the focal region of the great 1964 Alaska earthquake, and has one of the finest subduction zone paleoseismologic records in the world. On-going office and laboratory work involve completing radiocarbon dating of fossil plants, study of diatoms for paleoenvironmental data, and compilation of stratigraphic sections for a final publication on the Copper River delta studies.

2. Evaluate the limits of precision of the radiocarbon method for dating paleoseismologic events and in deducing interseismic displacement histories.

Results

Paleoseismicity and Seismic Cycle from the Copper River Delta, Alaska

The Copper River delta was uplifted during the March 27, 1964 Alaska earthquake (9.2 M_w) at which time about 2+ m of coseismic uplift resulted in abrupt conversion of intertidal mud flats as much as 4 km wide into subaerial marshes. The Copper River delta stratigraphy records at least seven, and possibly eight, pre-1964 sudden uplifts that are interpreted as coseismic events (Fig. 1). Each event was followed by gradual interseismic subsidence and marine transgression. As a consequence, the upper 11.5 m of the stratigraphic sequence consists of multiple thin (10–30 cm) beds of fresh-water peat with sharp basal contacts that grade upward into thicker (1–3 m) beds of varved(?) intertidal silt containing marine diatoms and the rooted remains of salt-tolerant sedge. Each peat and silt pair is interpreted to reflect a complete earthquake cycle consisting of an abrupt coseismic uplift above the highest-tide level during which fresh-water peat formed, followed by gradual resubmergence and burial beneath intertidal sediment. The thickness of silt layers indicates that coseismic uplifts for the pre-1964 events are ≥1–1.75 m, suggesting that the causative tectonic earthquakes were large and were probably comparable in mechanism and size to the 1964 event.

^{14}C dating of plant fossils indicates a record of about 5,600 years during which 13.5 m of silt and peat accumulated on the delta (Fig. 2). The last two pre-1964 uplift events (I and II), which are exposed in surface sections, are dated by ^{14}C as most probably in the range 750-640 and 1400-1270 calibrated years b. p., respectively. Deeper peat layers sampled in the subsurface by hand auger reflect uplift events tentatively dated at approximately 2350-2100 (III), 3010-2760 (IV?), 3700-3390 (V?), 4070-3920 (VI?), 4820-4640 (VII?), and 5610–5300 (VIII?) calendar years b. p. Repeat times for earthquakes that have uplifted the delta area average about 750 years for the 5600-year stratigraphic record.

^{14}C dating of plant fossils in the intertidal silt between peat layers indicates interseismic average sediment accumulation rates as high as 4.4 mm/yr. They probably represent minimum interseismic subsidence rates, which are presently 6.8 ± 1.1 mm/yr at nearby Cordova (Savage and Plafker, 1991). The long-term average subsidence rate (coseismic uplift plus interseismic subsidence) is about 0.9 mm/yr for 5600 yrs, assuming an average 1.5 mm/yr eustatic sea level rise. These data require a seismic cycle at Copper River delta in which interseismic subsidence plus eustatic sealevel rise is equal to or larger than coseismic uplift. With Steven Ward (U.C. Santa Cruz), we are evaluating the contribution to this subsidence by late Holocene sedimentation in the Copper River delta.

Precision of Radiocarbon Dates

We continue to evaluate the precision of the 119 ^{14}C dates for Copper River delta plant material by replicate analyses from the same sample either by the same laboratory or by two different laboratories. Conventional dates are by the U.S. Geological Survey in Reston and Menlo Park and by the University of Arizona; all AMS dates were run at the University of Arizona. These data indicate that (1) AMS dates on peat and intertidal sedge fossils tend to be younger than conventional dates by as much as 300 radiocarbon years in the upper part of the section; (2) Duplicate AMS dates for 3 peat samples differ by 200-520 radiocarbon years and for 2 sedge samples they differ by 35-100 years; (3) Differences between AMS and conventional dates are 150-500 (average 280) radiocarbon years for 6 peat samples, 10-300 years (average about 140) for 7 sedge samples , and 130 years for one wood sample; and (4) Duplicate conventional ages by Arizona and Reston for a single wood sample differ by about 100 radiocarbon years.

REFERENCES

Plafker, George, 1990, Regional vertical tectonic displacement of shorelines in south-central Alaska during and between great earthquakes: Northwest Science, v. 64, p. 5, p. 250-258.

Savage, J.C., and Plafker George, 1991, Tide-gage measurements of uplift along the south coast of Alaska: Journal of Geophysical Research, v. 96, no. B3, p. 4325-4335.

Stuiver, M. and Reimer, P. J., 1986, A computer program for radiocarbon age calibration: Radiocarbon, v. 28, p. 1022-1030.

REPORTS

Plafker, George and Rubin, Meyer, 1992, "Yo-Yo" tectonics above the eastern Aleutian subduction zone: coseismic uplift alternating with even larger interseismic subsidence [expanded abs.]: Proceedings of the Wadati Conference on Great Subduction Earthquakes, Geophysical Institute, University of Alaska, Fairbanks, Alaska, p. 90-91.

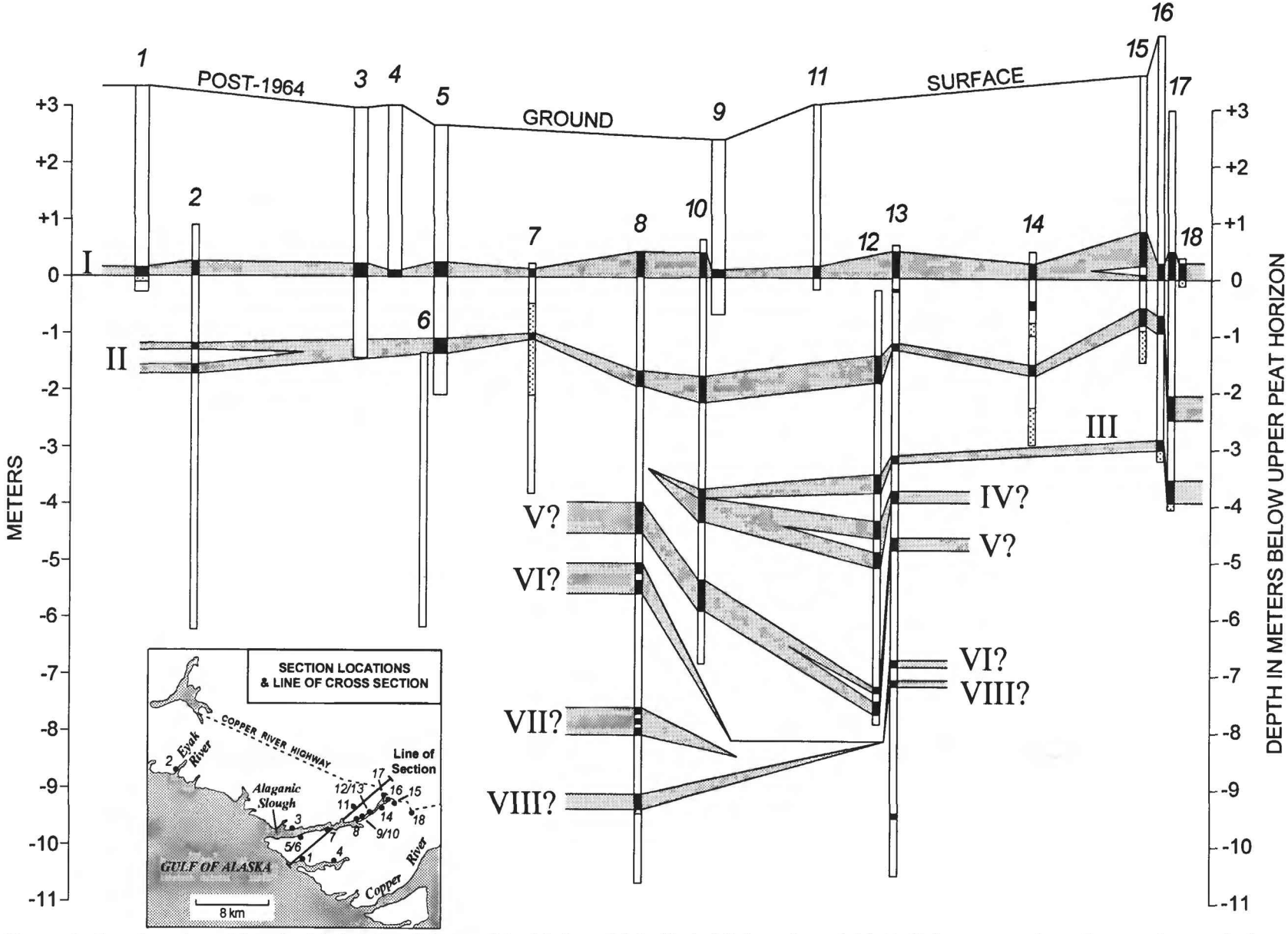

Figure 1. Stratigraphy of interbedded subaerial peat (black), intertidal silt (white), and sand (dotted) in measured sections and auger holes on the Copper River delta. Numbered holes and sections correspond to localities shown on index map. Sections referenced to base of upper peat layer; correlation of peat layers is based on stratigraphic position and ^{14}C age. The abrupt change from intertidal silt below to subaerial peat is interpreted as due to coseismic uplift during paleoseismic events (Roman numerals I - VIII) comparable in mechanism to the 1964 Alaska earthquake

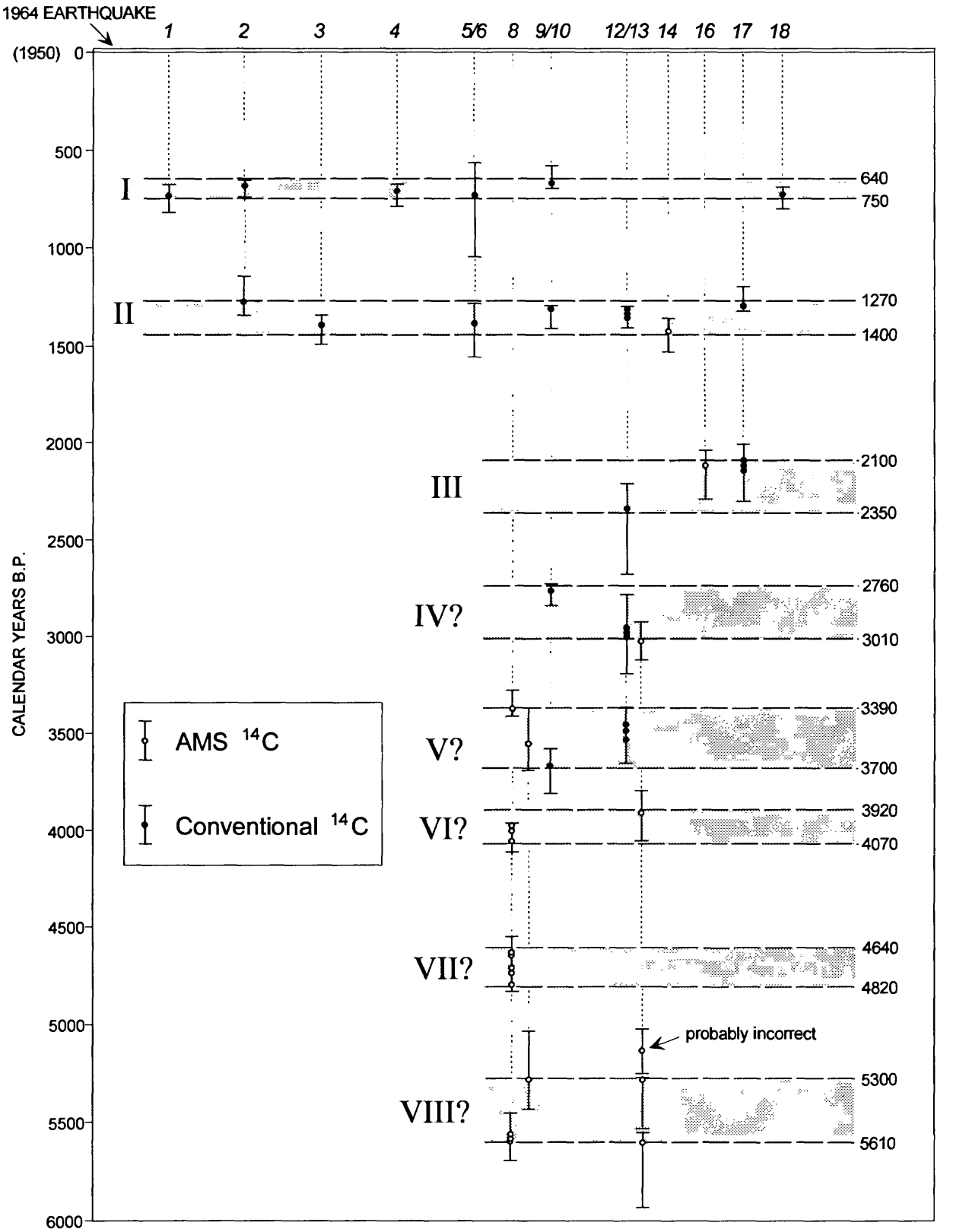

Figure 2. Inferred pre-1964 coseismic uplift events at the Copper River delta and their most probable calendar age ranges based on ^{14}C ages of samples that bracket these events. Numerals above the upper gray band indicate measured sections and auger holes shown in Figure 1. Open and filled circles represent the intersection of the sample radiocarbon age with the calendar age calibration curve of Stuiver and Reimer (1986); attached bars indicate the maximum error limits at 1σ confidence level. Gray bands bracket the most likely age ranges for pre-1964 paleoseismic events (Roman numerals I - VIII).

Quaternary Chronostratigraphy and Deformation History, Los Angeles Basin, California

9910-04555

Daniel J. Ponti
Branch of Engineering Seismology and Geology
U.S. Geological Survey
345 Middlefield Road MS 936
Menlo Park, CA 94025
(415) 329-5679

Investigations

1. Amino-acid geochronology, faunal correlations, and uplift history of the Palos Verdes Peninsula and Signal Hill areas, Los Angeles basin, California.
2. Post-earthquake investigations and analysis of surface fault rupture, Landers/Big Bear earthquakes of June 28, 1992 (with other USGS and CDMG staff members).

Results

1. Interpretation of a recently defined chronostratigraphy for marine Pleistocene deposits in the southwestern Los Angeles basin indicates that the Palos Verdes Hills have experienced a long and complex history of uplift as the result of several million years of displacement along one or more blind faults. In contrast, the uplift history of Signal Hill appears much simpler. Rapid uplift of Signal Hill began no earlier than ~200,000 years ago and probably signifies the inception, at the surface, of a positive flower structure that defines a left-step within the Newport-Inglewood zone of deformation.

   The uplift characteristics of the Palos Verdes and Signal hills are derived by comparing the chronostratigraphy of these two areas to that which underlies the intervening Torrance and Long Beach plains (Figure 1). Sediments beneath the Torrance and Long Beach plains preserve a nearly continuous record of marine deposition from late Miocene through early Pleistocene, with shoaling of the basin beginning in the Pliocene. The uppermost ~100 m comprise the Upper Wilmington chronozone. Within this unit is evidence for two marine regressions separated by a transgression, a probable reflection of glacio-eustatic sea level change. The top of the Upper Wilmington is marked by an unconformity which we interpret to represent subaerial exposure of the ocean floor as a result of a drop in sea level that occurred ~600,000 years ago (oxygen isotope stage 16). There is little evidence for much deformation of the Upper Wilmington chronozone within the Torrance and Long Beach plains. Near the Pacific Coast Highway in Wilmington, the top of the Upper Wilmington chronozone is near the elevation of current sea level, but over most of the region stream erosion has carved channels into the Upper Wilmington to an elevation of -30 to -40 m. Subsequent continental deposition (the Lakewood Formation of the California Division of Water Resources, 1961) and marine transgressions have largely filled these channels; these deposits lie within the Harbor through Lower Bent Spring chronozones. The most recent marine incursion into the Torrance plain occurred ~330,000 years ago. Younger marine sediments, deposited during a sea-level high stand ~220,000 years ago, appear to blanket the Long Beach plain. The tops of all marine deposits in the Torrance and Long Beach plains occur near present sea level; therefore, vertical tectonism during the last 600,000 years in this area has been negligible.

   At Signal Hill, a thin veneer of Harbor-age marine sediments unconformably overlies the Upper Wilmington chronozone, suggesting that a small amount of uplift did initiate after its deposition.

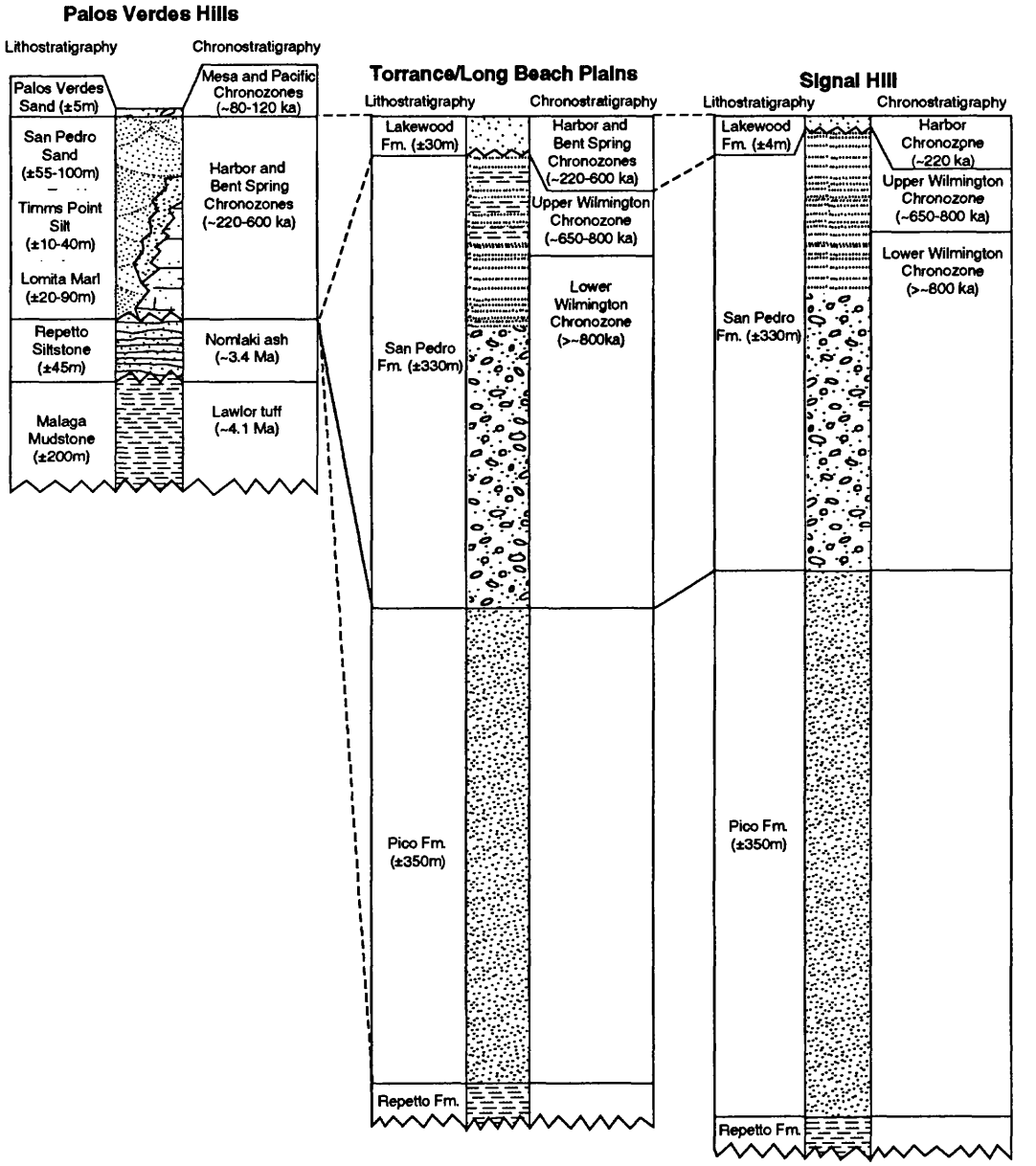

Figure 1. Correlation diagram of composite sedimentary marine sections in the southwestern Los Angeles basin; sections are hung on the top of the Harbor chronozone. Lithostratigraphy and stratigraphic thicknesses modified from DeLong(1941), Woodring and others (1946), Poland and others (1956, 1959), and California Department of Water Resources (1961). Chronostratigraphy modified from Ponti (1989); ages of the Lawlor tuff and Nomlaki ash are from Sarna-Wojcicki (personal communication, 1988).

However, the rate of uplift had to have been quite low in order for erosion to be able to keep the top of Signal Hill below sea level prior to ~200,000 years ago. In the last ~200,000 years the rate of uplift increased at least threefold, to an approximate maximum of 0.56 mm/yr, and may be continuing at this rate.

A significant aspect of the Palos Verdes Hills stratigraphy is the absence of all late Pliocene through lower Pleistocene deposits, suggesting that the region of the present Palos Verdes Hills stood high and received little or no sediment during that time. The presence of schist clasts and displaced shallow-water fauna in the Repetto Siltstone also indicates that the proto-Palos Verdes Hills had reached wave base ~3.4 m.y. ago.

Amino-acid age estimates of the youngest marine terraces in San Pedro yield an uplift rate of ~0.35 mm/yr for the last ~120,000 years; this uplift is likely the result of offset along the right-reverse Palos Verdes fault. However, details of the mid-Pleistocene stratigraphy exposed in the Palos Verdes Hills suggests a complicated faulting geometry (at least within the shallow subsurface) and raises doubts as to whether the late-Pleistocene-Holocene rate has been constant through time. A thick section of Bent Spring and Harbor-age marine sediments (Lomita Marl, Timms Point Silt and San Pedro Sand) occurs only along the northern and eastern flanks of the hills and records the formation of an apparent structural depression that was no more than 2 km wide and at least 100 m deep. This trough was fairly short-lived; it did not exist prior to ~500,000 years ago and has been deformed and uplifted within the last 300,000 years. One possible explanation for this trough (Figure 2) is that it reflects the initiation of a ramp on the Palos Verdes thrust. The broader uplift of this region characteristic of the last ~300,000 years, however, suggests that displacement has ceased or slowed on the ramp, or that the dip of the fault decreased as it continues to propagate toward the surface.

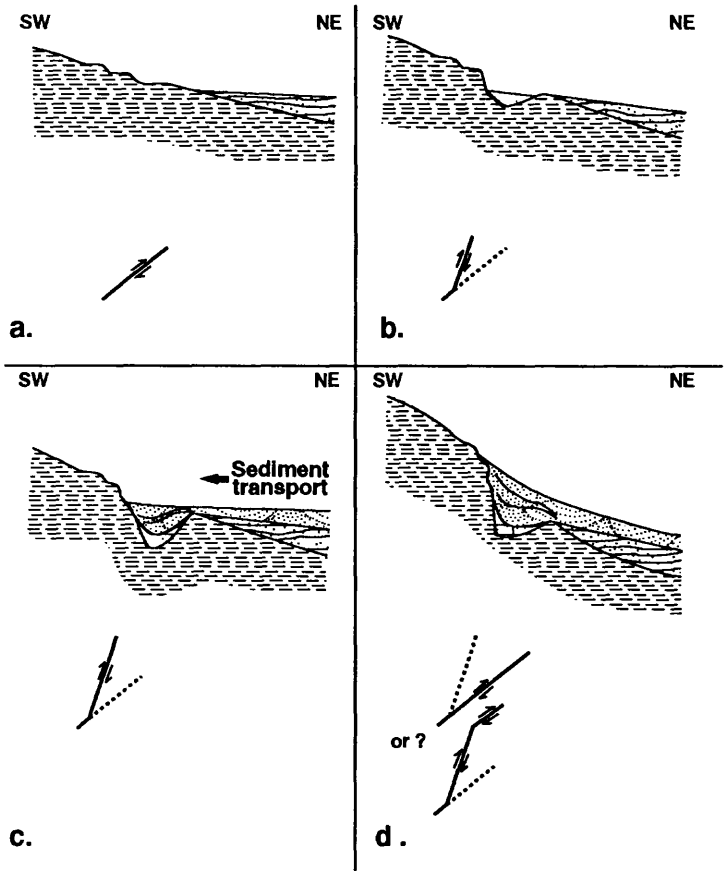

Figure 2. Conceptual diagrams illustrating a possible mechanism for formation of a structural trough and deposition of mid-Pleistocene sediments along the northeastern margin of the Palos Verdes Hills. a.) Prior to ~500,000 years ago, broad uplift of the Palos Verdes Hills results from offset of a blind oblique thrust fault; lower Pleistocene marine sediments are deposited off the northeast flank in a broad subsiding region overlying the footwall block of the thrust. b.) Trough inception (ca. 500,000 years ago) occurs along the margin of the hills as a result of inception of a ramp off of the buried thrust. Trough fills with marine waters, but is initially cut off from major sediment supply which is derived from the San Gabriel Mountains to the north. Lomita Marl is deposited within the trough. c.) Trough growth (ca. 500,000-300,000 years ago) continues as a result of upward propagation of the thrust ramp. River sediments derived from the San Gabriel Mountains are transported across the Torrance plain and deposited in the trough as a delta front which progrades from NW to SE, eventually filling the trough. The San Pedro Sand and Timms Point Silt represent the proximal and distal facies, respectively, of this delta complex. d). From ~300,000 years ago to present, the northeast margin of the Palos Verdes Hills is once again subject to broad uplift; the trough is uplifted above sea level and warped to the northeast, either as a result of secession of slip on the thrust ramp and a return to offset on the main buried fault, or to the shallowing of the dip of the fault plane as it continues to propagate toward the surface.

2. The M_S 7.5 Landers earthquake of June 28, 1992 produced more than 80 km of complex right-lateral surface rupture that trends northwest between the Little San Bernardino Mountains on the south and the Rodman Mountains on the north. The primary rupture propagated from south to north, incorporating overlapping portions of four major mapped faults (Johnson Valley, Homestead Valley, Emerson, and Camp Rock) and numerous smaller connecting faults. Sub-parallel faults to the west and east of the main rupture (Old Woman Springs, Lenwood, Upper Johnson Valley, Calico and Pisgah faults) exhibited small amounts of right-lateral slip locally (probably triggered), and a peculiar set of N-NE trending normal faults in the Newberry Springs area also exhibited small displacements. Triggered displacements of a few centimeters were also observed far to the south along portions of the San Andreas fault in the Mecca Hills, Indio Hills, and at Durmid Hill, locally on the Coyote Hills fault, and along much of the Superstition Hills and East Elmore Ranch faults in the Imperial Valley.

Most of the surface rupture occurred in zones ranging from a few meters to more than 100 m wide. These zones generally follow subdued pre-existing topographic lineations and fault-line features, although small segments of the main rupture and many of the minor splays had no preexisting topographic expression. Segments of the various faults with well-expressed fault geomorphology commonly did not rupture in this event. Complex fracture patterns representative of duplexing and flower-structures occur at scales from a few meters to a few kilometers. It is doubtful that the overall pattern of faulting exhibited in this event could have been predicted prior to the earthquake, and the great breadth of the zone of faulting in many locations along the rupture was clearly not expected.

The distribution of right-lateral displacement along the rupture reveals two slip maxima (Figure 3): one, of almost 5 m, occurs approximately 15 km north of the epicenter, where the rupture crosses over from the Johnson Valley to the Homestead Valley fault, and the other (~6 m) occurs on the Emerson fault just to the south of the Bessemer Mine Road. Along most of the rupture, right-lateral

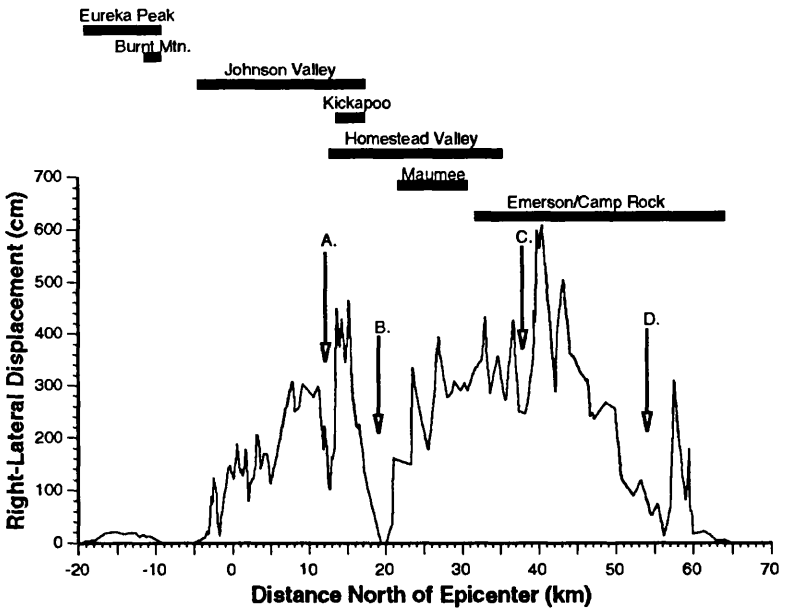

Figure 3. Distribution of right-lateral surface displacement along the length of the rupture associated with the Landers Earthquake of June 28, 1992. Black bars show the extent of the various faults that ruptured in the event. Where faults overlap, the curve reflects the cumulative right-lateral slip across the overlapping structures. Arrows show locations of major slip gaps: A.) Southern end of broad step-over zone between the Johnson Valley and Homestead faults. B.) Major westward deflection of the Homestead fault around the northern end of a bedrock high, and initiation of incipient cracking at the southern end of the Maumee fault. C.) Southern end of 10 km-long zone containing numerous fault splays that branch off of Emerson fault, forming an incipient negative flower structure associated with an apparent right step to the southern extension of the Camp Rock fault. D) Region of extensive graben formation as fault strikes more northerly and slip is transferred the Camp Rock fault.

displacement ranges between 2 and 3 meters. The slip-distribution curve is not smooth, but is punctuated by numerous peaks and valleys. Some of the smaller variations are due to measurement errors that are an inevitable consequence of the complex nature of the fault zone, but there are several areas where the slip drops abruptly and significantly. These "slip gaps" occur in areas where significant changes occur in the faulting character or fault geometry. For example, one gap occurs at the southern end of the Kickapoo fault where it branches from the Johnson Valley fault; another occurs on the Homestead Valley fault where there is a ~40° westward bend in the fault strike; a third occurs about 5 km south of Bessemer Mine Road at the southern end of a 10 km long zone that contains numerous splay and conjugate faults. The reasons for these "slip gaps" are not clear, but perhaps they reflect regions of fundamentally different material properties within the upper crust. These asperities may act to stop rupture propagation along a given structure, and perhaps serve to divert rupture from one structure to an adjacent one, thus accounting for the overall complexity of the faulting pattern.

Reports

Ponti, D.J., and Lajoie, K.R., 1992, Chronostratigraphic implications for tectonic deformation of Palos Verdes and Signal Hills, Los Angeles basin, California: *Proceedings of the 35th Annual Meeting of the Association of Engineering Geologists*, p. 617-620.

Staff (U.S. Geological Survey Menlo Park, CA 94025; California Division of Mines and Geology, Sacramento, CA 94518), 1992, Pattern of surface rupture associated with the June 28, 1992 Landers Earthquake, *EOS*, v. 73, no. 43, p. 357-358.

Crustal Geophysics of Seismically Active Regions

Thomas L. Pratt
Branch of Geologic Risk Assessment
MS 966, Denver Federal Center
Denver, Colorado 80225
303-273-8606

Puget Sound

During FY 1992 three high-resolution reflection seismic profiles acquired in Lake Washington were reprocessed to examine the shallow (1.0 km or less) structure. The data were acquired by Sam Harding. The new data processing included pre-stack partial migration (DMO) and post-stack migration to enhance dipping reflectors, a more careful mute selection to image the water bottom, and more frequent velocity picks.

The final images (Fig. 1) show an acoustically transparent zone in the central third of the profiles which is interpreted to be a ridge of Oligocene and older volcanic and sedimentary 'basement' rocks cropping out nearby. The structure is bounded on both flanks by distinct reflectors dipping at approximately 20 to 25 degrees away from its center. To the north, the dipping reflector obviously forms the southern edge of a thick sedimentary sequence previously defined from drillhole data and termed the Seattle Basin. To the south, the dipping reflector may form the northern margin of another layered sequence, but a distinct unconformity separating these strata from overlying younger sediments suggests that there are two different-aged sequences.

The northern dipping reflector correlates with a major east-west-trending geophysical anomaly interpreted as the Seattle Fault. It appears that a fault-bounded ridge of basement rocks trending westerly across Puget Sound, and imaged as the transparent zone on these profiles, is currently being uplifted, as indicated by recent (circa 1,500 years or less) uplift of wave-cut terraces at Restoration Point on the west side of Puget Sound. The dipping surface imaged on the seismic data flanking the north side of the basement structure is either a part of the Seattle fault itself, either the main fault or a splay, or is an erosional surface formed on the edge of the fault block. The dipping reflector imaged to the south on the seismic data does not correlate with a known fault, so its interpretation is more problematic. Earthquakes recorded by the present seismometer array, though not well located, align with these dipping structures and may indicate that the basement rocks are borded by active faults.

Work in FY 93 will concentrate on reprocessing the remaining USGS profiles crossing the structure in Puget Sound and obtaining and reprocessing 1971-vintage industry seismic reflection data to obtain an image of the deeper structures.

New Madrid

Work in FY 1992 consisted of initial reprocessing of seismic reflection data purchased earlier from Dow Chemical Company and completion of several reports concerning earlier work. The key part of the reprocessing effort was use of an extended

correlation technique to retrieve partially-recorded reflections from the data. The resulting seismic profiles consist of 14 sec data - enough to image lower crustal features.

Results of this initial effort are promising: clear reflections in the 9.5 to 11.5 sec range were obtained. Figure 1 shows a portion of an east-west transect crossing the southeast border of the Reelfoot rift near Memphis Tennessee. The seismic section shows a subhorizontally-stratified lower crust (25 to 33 km depths) with individual reflections continuous laterally for 5 km or more. The reflections may represent mafic underplating or mafic intrusives which have been hypothesized from refraction data and from the presence of the Reelfoot rift above. The reflections do not have an arrival time appropriate for them to be multiply-reflected energy, so they appear to be primary reflections.

Work in FY 1993 will concentrate on processing a series of profiles across the Reelfoot rift west of Memphis to examine the relationship between the rift and the lower crustal reflections. Crossing seismic profiles will also be reprocessed to determine the attitude of the lower crustal reflectors. If time permits, a second set of profiles near the seismic zone will also be processed and interpreted.

Southern California

We obtained 23 km of high-resolution seismic reflection data in the San Jacinto Graben, in conjunction with Dr. Steven Park and Dr. Tien-Chang Lee of University of California, Riverside. The data acquisition and processing was completed on a timely schedule and has been turned over to Drs. Park and Lee for interpretation and publication by their students.

Reports:

Luzietti, E.A., Kanter, L.R., Schweig, E.S., Shedlock, K.M., and VanArsdale, R.B., in press, Shallow deformation along the Crittenden County fault zone near the southeastern boundary of the Reelfoot rift, northeast Arkansas, Seismological Research Letters.

Odum, J.K., Shedlock, K.M., Michael, J.A., Worley, D.M., and Luzietti, E.A., 1991, A seismic reflection survey of the northwestern boundary of the Reelfoot rift near Marston, Missouri, EOS, Supplement to October 29, 1991 p. 429-430 (abstract).

Stephenson, W.J., Odum, J., Shedlock, K.M., Pratt, T.L., and Williams, R.A., 1992, Mini-Sosie high-resolution seismic method aids hazards studies, EOS, v. 73, p. 473-476.

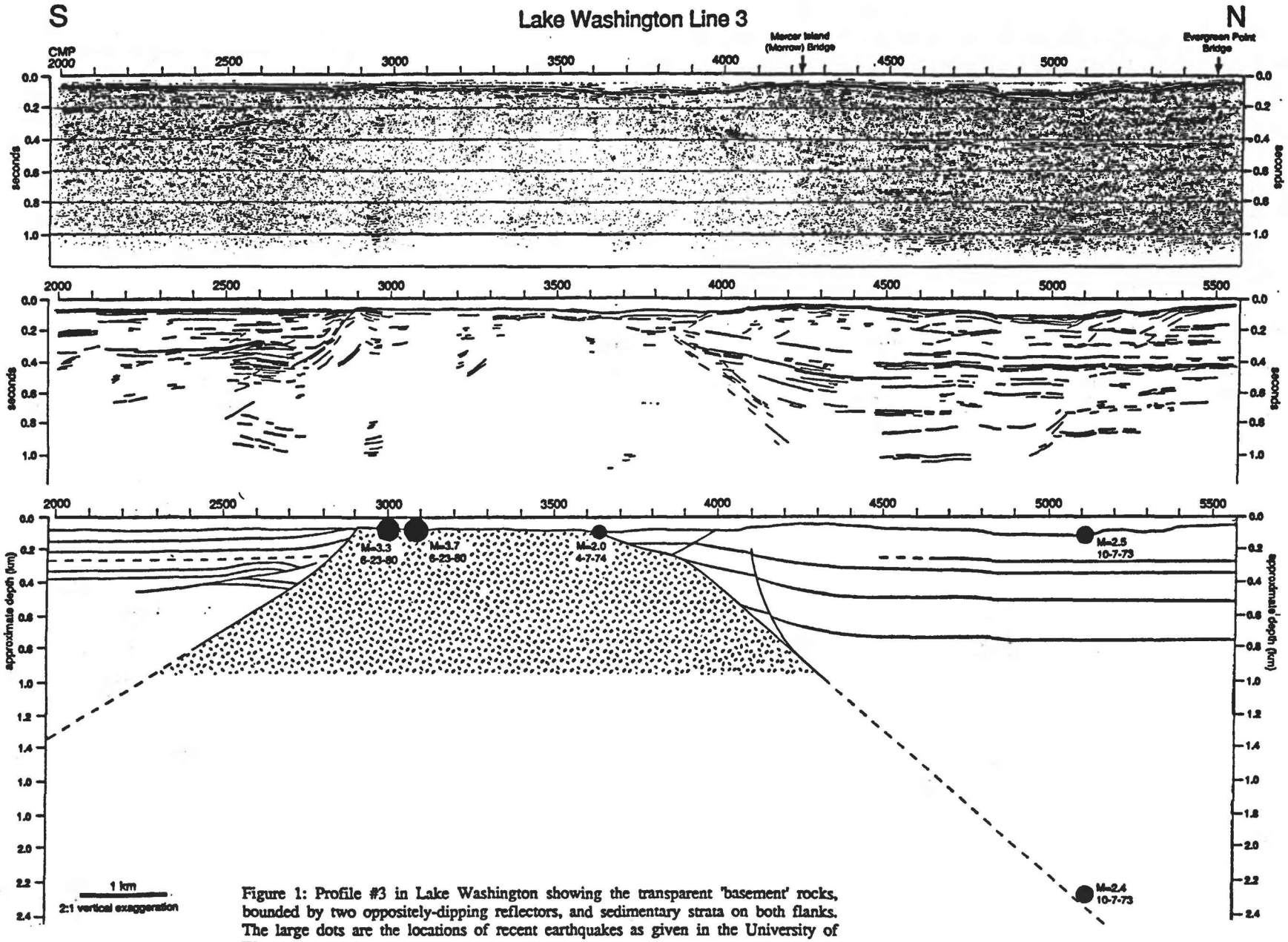

Figure 1: Profile #3 in Lake Washington showing the transparent 'basement' rocks, bounded by two oppositely-dipping reflectors, and sedimentary strata on both flanks. The large dots are the locations of recent earthquakes as given in the University of Washington catalog.

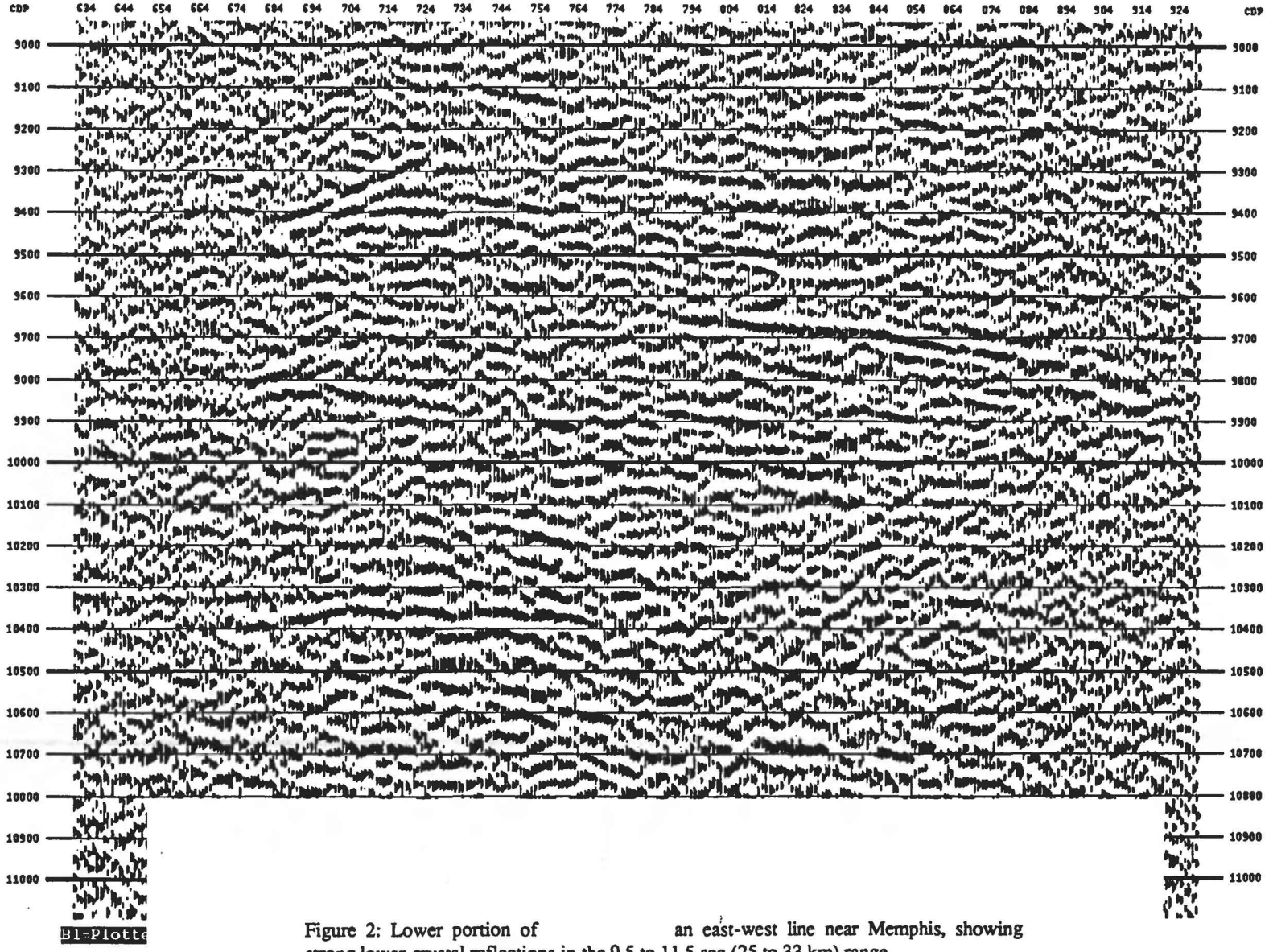

Figure 2: Lower portion of an east-west line near Memphis, showing strong lower-crustal reflections in the 9.5 to 11.5 sec (25 to 33 km) range.

NORTHERN SAN ANDREAS FAULT SYSTEM: PALEOSEISMIC AND SLIP RATE STUDIES IN NORTHERN AND CENTRAL CALIFORNIA

9910-04483

Carol Prentice
Branch of Engineering Seismology and Geology
U. S. Geological Survey
345 Middlefield Rd, MS 977
Menlo Park, CA 94025
415-329-5690

Investigations

1) Investigations of the San Andreas and related faults in northern and central California to determine timing of prehistoric earthquakes and average Quaternary slip rates. 2) Investigations of the behavior of the San Andreas fault in the Loma Prieta region in 1906. 3) Investigations of the Septentrional fault to determine timing of prehistoric earthquakes. 4) Post-earthquake investigations of the 25 April 1992 Cape Mendocino, California and the 28 June 1992 Landers, California earthquakes.

Results

1) Studies of excavations at two sites have yielded paleoseismic data for faults of the San Andreas system in northern and central California: on the Carrizo Plain along the San Andreas fault in central California, and along the Maacama fault near Ukiah, CA. Sites within a third region, the peninsula segment of the San Andreas fault, are being evaluated for paleoseismic and slip rate potential.

An excavation across the San Andreas fault on the Carrizo Plain in central California has yielded evidence for at least six late Holocene earthquakes. The most recent earthquake is known from historical records to have occurred in 1857. This study shows that an earthquake prior to 1857 occurred after the deposition of a unit with a corrected radiocarbon age of 1365 +/- 165 AD. The third event back occurred before the deposition of a unit formed in 1190 +/- 80 AD. All six events occurred after the deposition of a unit that is about 3000 years old. These data imply a long recurrence interval for this fault segment.

An excavation in Talmage, near Ukiah, California, exposed a sequence of marsh, fluvial and lacustrine deposits overlying a paleosol developed on Pleistocene(?) gravel. The Maacama fault, clearly expressed in the older gravel, has not caused any brittle deformation of the overlying Late Holocene section. The section instead has been folded across the fault zone. Relationships indicate that only one folding event has occurred. Results of radiocarbon dating show the folding occurred. after about 1500 AD. These data suggest an earthquake large enough to cause surface deformation has occurred on the Maacama fault in the last few hundred years.

Sites with high potential for yielding paleoseismic and slip-rate information have been identified along the peninsula segment of the San Andreas fault using large-scale color aerial photographs. Each site has accumulated sediments in the last few thousand years that may record the history of late Holocene earthquakes on this segment of the San Andreas fault.

2) Investigations following the Loma Prieta earthquake of October, 1989, included mapping of ground fractures and study of historical archives to compare the effects of the 1906 earthquake in this region with the effects of the 1989 earthquake. In this region in 1906, as in 1989, many large ground cracks occurred in the Summit Road and Skyland Ridge areas. Left-lateral offset was documented (off the main trace of the San Andreas fault) in 1906 near the Morrell ranch; a smaller amount of left-lateral offset occurred on this same fracture as a result of the 1989 earthquake. Virtually no surface rupture occurred along the San Andreas in 1989; careful study of historical documents strongly suggests that surface rupture did occur in 1906, though none of the reported values of offset is reliable. Field work and analysis of aerial photographs show a youthful, through-going fault for this region and trenches in two localities clearly show late Holocene surface rupture. These studies indicate that fault behavior in 1989 was significantly different than in 1906.

3). A study along the Septentrional fault in the Dominican Republic has yielded data constraining the time of the most recent earthquake along the major North American Caribbean plate-boundary fault. The most recent earthquake occurred at least 430 and probably more than 730 years ago, implying a high earthquake potential for the Septentrional fault.

4) Post-earthquake investigations of the 25 April, 1992 M7 Cape Mendocino and the 28 June 1992 M7.4 Landers earthquakes were conducted immediately following the occurrences of these events. Reconnaissance of the Cape Mendocino area showed no evidence of fault surface rupture associated with this earthquake. However, the coastline was raised approximately 1 m in the area south of Cape Mendocino. Large, complicated, right-lateral surface rupture on several northwest-trending strike-slip faults accompanied the Landers earthquake.

Reports

Prentice, C.S., Ground ruptures in the Loma Prieta region:1989 and 1906 compared. Contributed to the USGS Loma Prieta Professional Paper.

Galehouse, J.S., Sowma-Bawcom, J.A., and Prentice, C.S., 1992, The Maacama fault: Preliminary creep and paleoseismic data, Mendocino County, California [abs.]: EOS, Transactions of the American Geophysical Union, v. 73, n. 43, p. 123.

Prentice, C. S., Mann, P., Taylor, F. W., Burr, G., and Valastro, S., Jr., Paleoseismicity of the North American—Caribbean plate boundary (Septentrional fault), Dominican Republic: Geology, *in press*.

Prentice, C. S., Mueller, C., Keiffer, D., and Sims, J., The 25 April 1992 Cape Mendocino earthquake: coastal uplift, liquefaction, landslides and strong motion: Earthquakes and Volcanoes, *in press*.

CALIFORNIA EARTHQUAKE STUDIES

9930-02103

Paul A. Reasenberg

Branch of Seismology
U.S. Geological Survey
345 Middlefield Road - MS 977
Menlo Park, California 94025
415-329-5002

Investigations

1. The M7.5 Landers, California, Earthquake: Implications for Earthquake Hazard in Southern California
2. Remote Seismicity Triggered by the M7.5 Landers, California, Earthquake of June 28, 1992.

Results

1. The M7.5 Landers, California, Earthquake: Implications for earthquake hazard in southern California

The aftershock pattern for the Landers and Big Bear earthquakes was used to estimate the probability of an aftershock occurring in a given magnitude range and time period (Reasenberg and Jones, *Science*, **243**, 1173-1176, 1989). The chance of more aftershocks capable of damage ($M \geq 5$) over the next three years is high (95 percent). Such events pose little risk in most of the Landers rupture zone because of its low population density, but could cause significant additional damage in the more populated Big Bear area.

The same model was used to estimate the probability of another large ($M \geq 7$) earthquake. This approach employs a scaling relationship to model the functional form of regional seismicity, and adjusts parameters to fit the local rate, magnitude distribution and recent history of earthquakes in the region. The model predicts an extra probability associated with the Landers event of 3.6 percent and 8 percent for the one-year and five-year periods beginning September 1, 1992, respectively. Assuming that the Poisson rate for southern California (which has been estimated by David Jackson to be 1 percent per year) is based on independent (as opposed to triggered) earthquakes, then the rate of triggered events associated with the Landers earthquake can be added to the rate of independent events for southern California.

2. Remote Seismicity Triggered by the M7.5 Landers, California, Earthquake of June 28, 1992.

Coworkers: D.P. Hill, A.J. Michael, R.W. Simpson, W.L. Ellsworth, S. Walter and M. Johnston (U.S. Geological Survey); R. Smith, S.J. Nava, W.J. Arabasz, J.C. Pechmann (University of Utah); J. Gomberg (U.S. Geological Survey, Denver); J.N. Brune, D. DePolo (University of Nevada, Reno); G. Beroza (Stanford University); S.D. Davis; J. Zollweg (Boise State University)

An intense, widespread and sudden increase in seismicity began within minutes after the Landers earthquake at numerous remote sites in western United States (Figure 1). At each site the increased seismicity is easy to recognize when compared to the previous local seismicity (Figure 2). Furthermore, the simultaneity of the Landers earthquake and the seismicity surges at these sites convinces us that the Landers earthquake was the cause (in the sense of triggering) of the increased remote seismicity.

Increased seismicity occurred at distances up to 1250 km (17 rupture lengths) from the Landers earthquake. The most distant sites of triggered seismicity were in Yellowstone National Park (1250 km) and near Cascade, Idaho (1100 km). The most intense triggering occurred along the western and southern margins of the Great Basin and along the eastern California shear zone. Earthquakes were apparently triggered in the southern Cascade Range, near Lassen Peak and Mount Shasta. The largest triggered earthquake (M 5.6) was located near Little Skull Mountain, Nevada. Triggered earthquakes were also recorded at the Geysers geothermal area, 100 km north of San Francisco. All of these sites have a history of persistent seismicity and most are characterized by recent volcanism and geothermal activity. The San Andreas fault system did not produce a surge of triggered seismicity, nor did the Wasach fault zone, Utah.

The simultaneity of the remote seismicity surges and the Landers earthquake was observed at some sites by filtering certain Calnet seismograms of the Landers main shock coda. Use of a 5 to 30 Hertz bandpass filter reduced the long period surface waves while relatively enhancing the short period waves from small, local earthquakes. With this method, Andy Michael (USGS) found that the local seismicity at Long Valley caldera and the Geysers geothermal area began within 40 seconds after the local arrival of the Landers S wave, during the passage of the surface wave train.

Postseismic compressional strain rate recorded by the dilatometer at Devil's Postpile, located at the western edge of Long Valley caldera closely resembles the seismicity rate within the caldera. Both the seismicity surge and strain rate pulse measured at Long Valley lasted about 5 days.

The static stress changes produced by the Landers earthquake were estimated by Robert Simpson (USGS) with a model dislocation in an elastic halfspace. At distances greater than about 300 km, these stress changes are smaller than daily tidal stress fluctuations (order 10^{-2} bar). At distances of 500 and 1000 km, modeled static stress changes are on the order of 10^{-3} bar and 10^{-4} bar, respectively. Thus, static stress changes seem too small to be a likely explanation for all of the triggering.

Dynamic stresses associated with the passage of the Landers surface waves were estimated at several sites by Greg Beroza (Stanford University) from particle velocities recorded by unclipped, broadband seismographs. Stresses associated with the fundamental mode Rayleigh wave, with period in the range 5 to 20 sec, are on the order of 1 to a few bars at distances up to about 500 km. Corresponding stresses at seismogenic depths may be an order of magnitude greater. While dynamic stresses are an attractive candidate for explaining the remote triggering, they can be only a partial explanation because, while the surface waves died down after about 10 minutes, the triggered seismicity lasted for hours and days. Additional mechanisms under consideration that might "stretch out" the time of the triggering effect include some kind of non-linear interaction between the dynamic stresses and crustal magma (for example, exsolution of magmatic gasses); non-linear interaction between the dynamic stresses and crustal pore fluids (hydraulic pumping); interaction between the dynamic stresses and a non-linear fault zone rheology (i.e., direct "working" of the fault); and propagating aseismic movement on an interconnected network of faults initiated by near-source stresses. At present no single explanation seems fully satisfactory.

Reports

Reasenberg, P.A., D.P. Hill, A.J. Michael, R.W. Simpson, W.L. Ellsworth, S. Walter, M. Johnston, R. Smith, S.J. Nava, W.J. Arabasz, J.C. Pechmann, J. Gomberg, J.N. Brune, D. DePolo, G. Beroza, S.D. Davis; J. Zollweg, Remote Seicmicity Triggered by the M7.5 Landers, California, earthquake of June 28, 1992 (abstract), EOS, v. 73, p. 392 (1992).

The Landers Earthquake Sequence and Future Seismic Hazards in Southern California: A Progress Report, NEPEC/CEPEC/SCEC Ad-hoc Working Group, 1992.

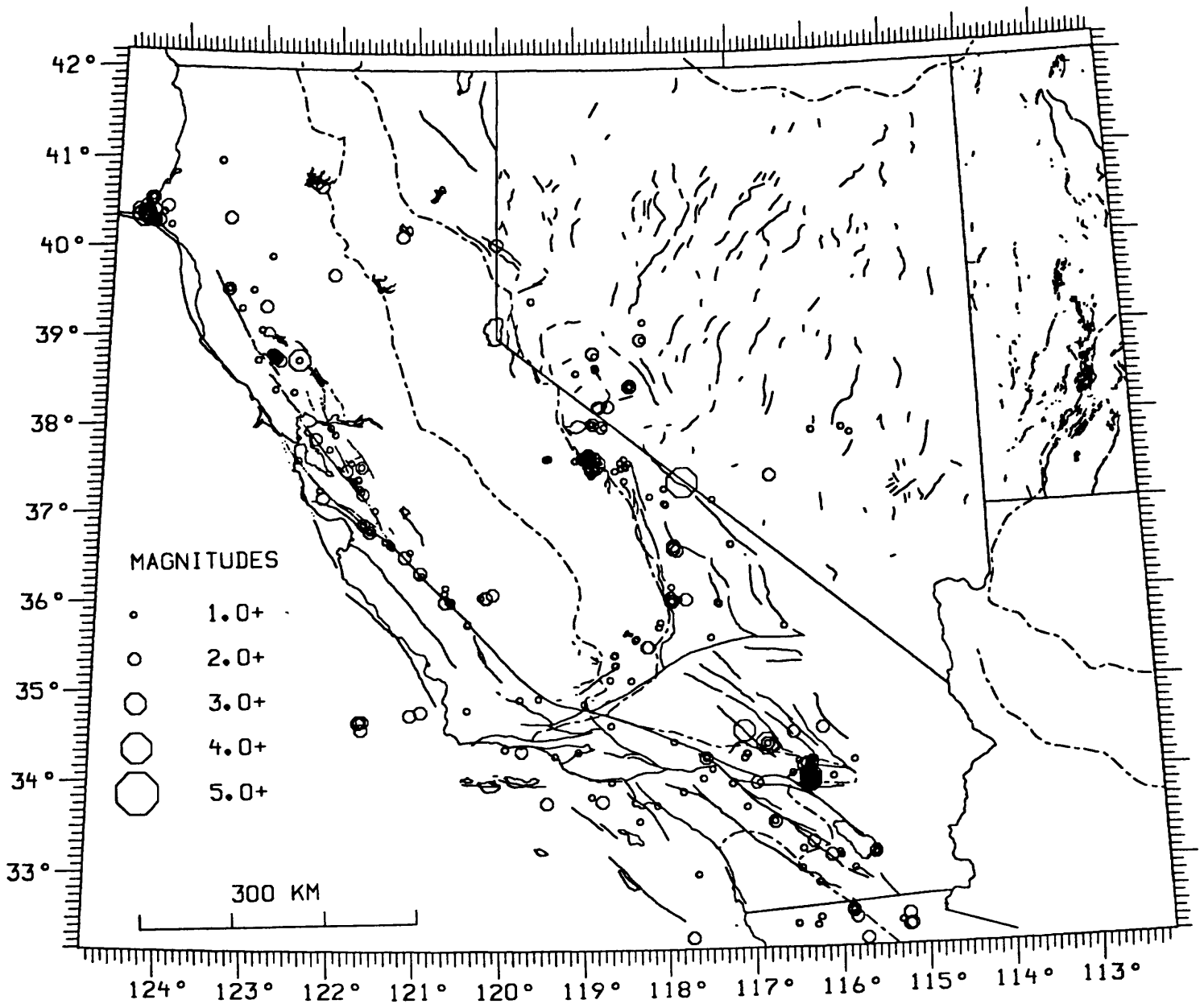

Figure 1a. Map showing earthquake activity in the 10-day period immediately before the Landers earthquake.

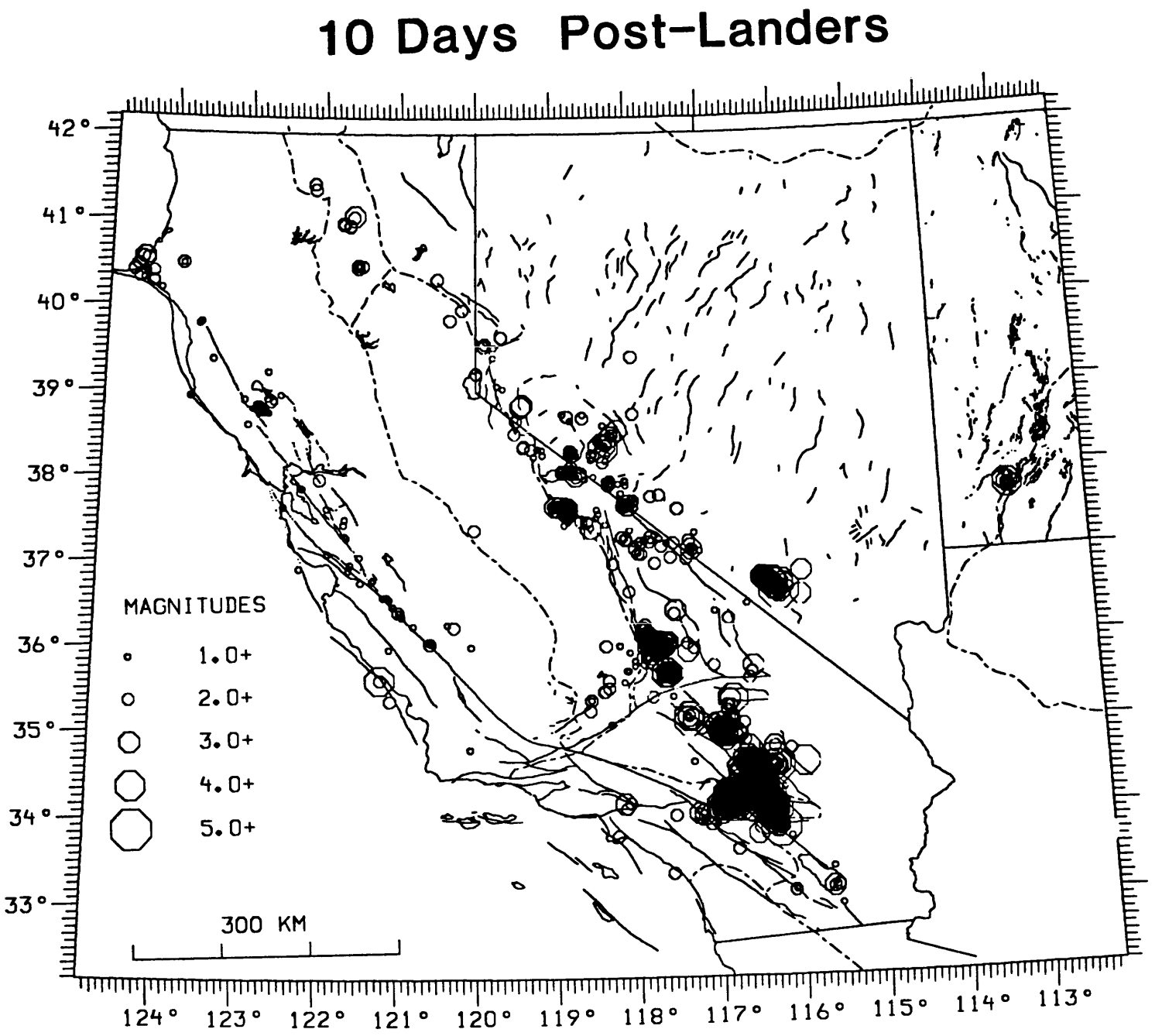

Figure 1b. Map showing earthquake activity in the 10-day period immediately after the Landers earthquake.

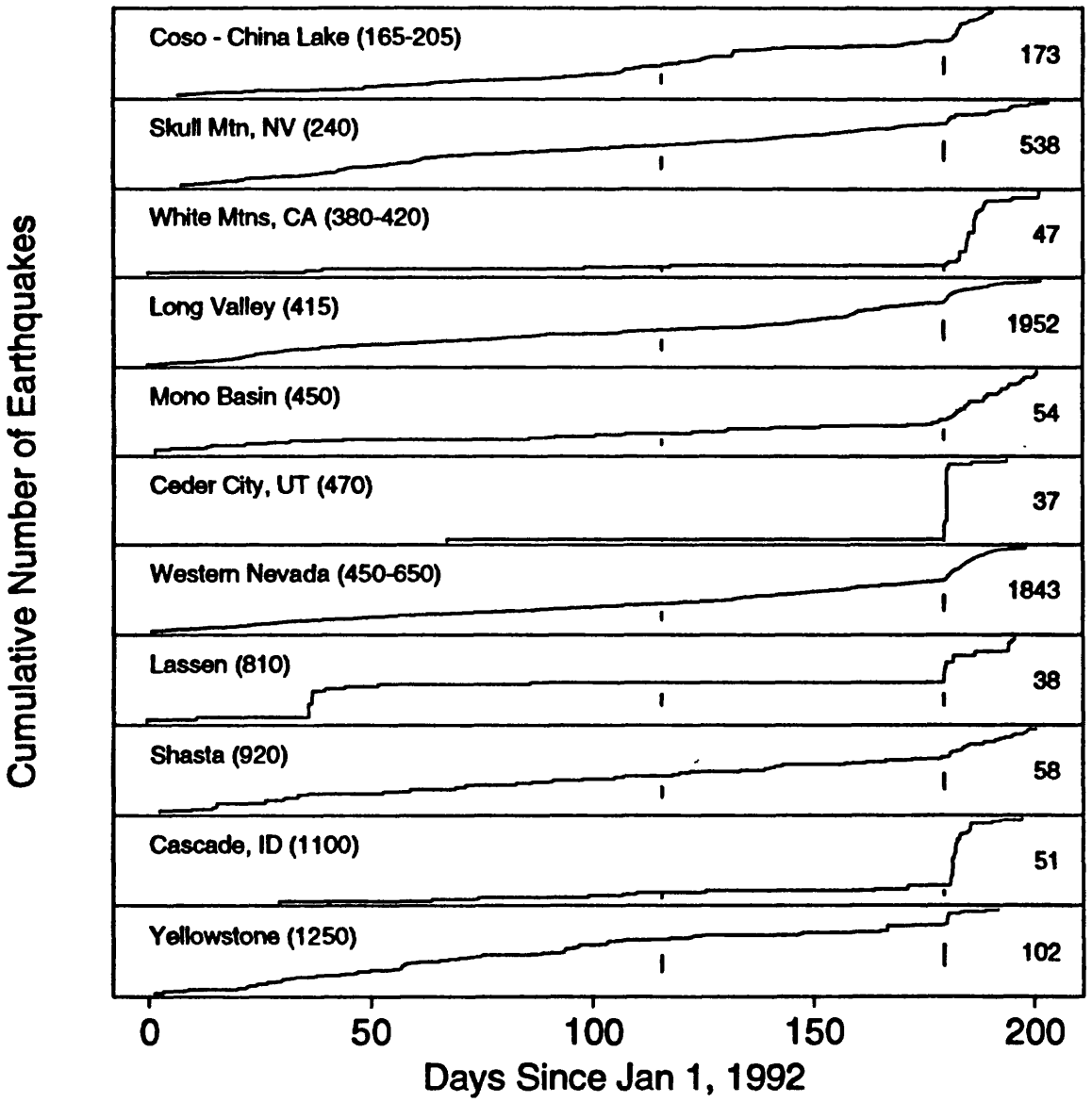

Figure 2. Cumulative number of earthquakes in selected zones, beginning January 1, 1992. Numbers in parentheses are distances (km) from Landers earthquake. Total number of earthquakes in each zone is shown at right. Vertical lines mark times of the Cape Mendocino (M = 7.1) and Landers (M = 7.5) earthquakes.

Analysis of Crustal Deformation Along the Southernmost Segment of the San Andreas Fault System, Imperial Valley, California: Implications for Earthquake Prediction

14-08-0001-G1679

R.E. Reilinger
Earth Resources Laboratory
Dept. of Earth, Atmospheric, and Planetary Sciences
Massachusetts Institute of Technology
Cambridge, Massachusetts 02142
(617) 253-7860

INVESTIGATIONS

This project involves using geodetic observations in conjunction with other geophysical and geological information to investigate contemporary tectonic processes along the southernmost segment of the San Andreas fault system. Our primary effort during the present contract period focused on continuing analysis and interpretation of 1986 to 1991 GPS measurements in the Imperial Valley-Salton Trough with emphasis on temporal and spatial patterns of regional strain accumulation.

RESULTS

We continue to concentrate on reduction, analysis, and interpretation of the 1986-1991 GPS observations (Figure 1). Initial results from the 1986-1989 observations are reported in two papers recently published in JGR (Larsen et al., 1992; Larsen and Reilinger 1992), and those from the 1989 - 1990 are presented by Reilinger and Larsen (1993).

At present we are focusing our attention on reducing and analyzing GPS observations collected prior to, and following the 1992 Joshua Tree and Landers/Big Bear earthquakes. These data will be used to constrain better pre-. co-, and post-seismic deformations for these events. These efforts are in collaboration with other participants in the STRC consortium, SCEC, and the USGS.

PUBLICATIONS

Reilinger, R., and S. Larsen, Present-day crustal deformation in the Salton Trough, southern California, (in) *NASA Crustal Dynamics Project AGU Monograph*, in press, 1993.

Larsen, S., R. Reilinger, H. Neugebauer, and W. Strange, Global Positioning System measurements of deformation associated with the 1987 Superstition Hills earthquake: Evidence for conjugate faulting, *J. Geophys. Res.*, 97, 4885-4902, 1992.

Larsen, S., and R. Reilinger, Global Positioning System measurements of strain accumulation across the Imperial Valley, California: 1986-1989, *J. Geophys. Res.*, 97, 8865-8876, 1992.

Gilbert, L. E., et al., A comparison of STRC90 and STRC91 campaign results: Strain in the Coachella Valley, southern California, *EOS, Trans. Am. Geophys. Union, 72,* 117, 1991.

Figure 1. GPS stations observed during the period 1986 to 1991 by the STRC Consortium.

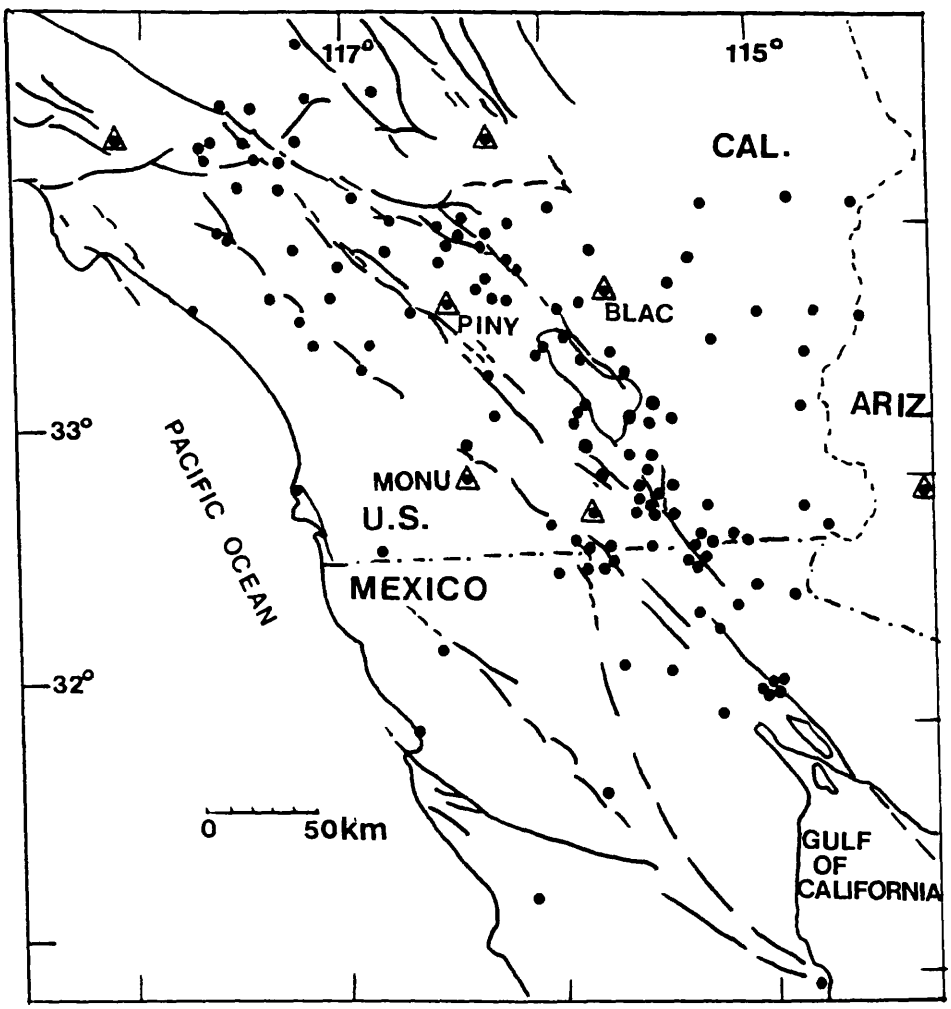

NEW MADRID SEISMIC ZONE CONODONT STUDIES

9590-04553

John E. Repetski and David J. Weary
Branch of Paleontology and Stratigraphy
U.S. Geological Survey
970 National Center
Reston, Virginia 22092
(703) 648-5486

Investigations

Project goals are to document and clarify the age, correlations, and stratigraphic relations of the Late Cambrian and Ordovician strata in the Reelfoot Rift basin/graben and related nearby areas by means of conodonts (marine microfossils) from available subsurface materials and surrounding outcrop belts. The resulting biostratigraphic framework will improve significantly knowledge of details of timing and magnitude of tectono-sedimentary episodes or pulses in the graben area for this time interval of widespread tectonic activity, details not provable from seismic data alone. Additionally, age-dating of lithologically similar bedrock units in structurally disturbed or poorly exposed areas within the greater New Madrid Seismic Zone will aid the ongoing mapping and structural geological investigations in the region.

During FY 92, we have extracted and (or) analysed conodonts and other microfossils from more than 300 samples from some key available and on-hand drillholes in and adjacent to the Reelfoot basin. These wells include the Dow Chemical #1 Garrigan and #1 Wilson holes, USGS Fort Pillow well, and Dupont GHS well. We have searched for and acquired additional key subsurface samples and data, and important surface sections for microfossil investigation. New well samples were obtained from Amoco #1 Burmah Haynes, Illinois Power #2 Morrell, and Maguire #1 J.B. More drillholes. More than 100 samples were collected from outcrops from more than 15 surface sections. Laboratory processing and analysis of this newly acquired data are underway.

We are coordinating these biostratigraphic efforts with related ongoing bedrock mapping, physical stratigraphic, structural/tectonic, geophysical, paleomagnetic, and geochemical and mineral resources research studies within USGS and cooperating agencies and institutions. Timely updates of this study and its generated data, and preliminary interpretations, are being shared with cooperating scientists, and reports on these findings, both by this project and jointly co-authored with collaborating workers, have been released and (or) presented at public meetings.

Results

1. *Dow Chemical #1 Garrigan and #1 Wilson (both Mississippi County, Arkansas), and USGS Fort Pillow (Lauderdale Co., Tennessee) drillholes.*

Approximately 300 samples were processed for conodonts and other microfossils from these three holes -- Garrigan (locality DG on Fig. B): 126 samples; 60-ft composites; cuttings -- Wilson (DW on Fig. B): 153 samples; 60-ft composites; cuttings -- Ft. Pillow (FP on Fig. B): 20 samples; 1-ft splits; core. Processing has been completed.

Conodonts indicate that the top of the Paleozoic strata in the Wilson and Fort Pillow wells is at or very near the top of the Lower Ordovician (Ibexian Series). Moreover, the rocks and faunas at this level in these two drillholes are quite different from most coeval adjacent outcrop successions: they indicate cooler and (or) deeper marine facies and thus that this area had more open communication with the open ocean to the (paleo) south and had limited influence from the restricted-circulation shallow cratonic seas immediately to the west, north, and east. The remaining upper, middle, and lower Ibexian faunas are more typical of those of the adjacent shallow, warm-water carbonate platform areas, and reasonably confident correlations can now be made. Figure A shows the setting, relative to the stratigraphic framework for the U.S. southern Midcontinent, of the early Paleozoic succession in the southeastern segment of the Reelfoot basin, based on the conodonts and other microfossils from the Wilson and Fort Pillow wells.

Joint study of the Garrigan microfossils and and sedimentology by this project and by D.S. Collins and M.E. Taylor (USGS, Golden and Denver) and A.R. Palmer (Boulder, CO) has shown that the stratigraphy in the Garrigan well, located near the crest of the Blytheville arch, is anomalous relative to both the adjacent carbonate platforms and the segment of the Reelfoot basin east of the Blytheville arch. The Garrigan sediments are dominantly siliciclastic rather than carbonate. The sedimentation rate, determined by fossil-based age dates in both wells, was more than double in the area of the Garrigan drillhole (assuming no significant thickness perturbations due to structural disturbances) than that for the carbonate facies in the vicinity of the Wilson drillhole during the Late Cambrian and earliest Ordovician.

The thermal alteration levels of the conodonts in the Wilson and Fort Pillow wells are higher than would be expected under most extant models of Reelfoot basin history. The levels observed could reflect the effects of burial under a greater thickness of post-Early Ordovician, pre-Cretaceous, strata than has been postulated by most workers. However, the effects of post-Early Ordovician, pre-Cretaceous (Cretaceous strata were not anomalously heated), hydrothermal fluids passing through these Reelfoot basin strata, or, alternatively, a higher-than-normal geothermal gradient locally during that time interval, must also be considered. To address this important aspect of Reelfoot basin evolution, we are coordinating our conodont thermal and chemical alteration studies for this region with fluid inclusion and other geochemical investigations being conducted by D.L. Leach and colleagues (USGS-Denver; Branch of Geochemistry).

2. *Other drillholes.*

Four very small samples were obtained from near or at the top of the

Paleozoic part of the Maguire #1 J.B. More well near Danceyville, Haywood Co., Tennessee (locality DA on Fig. B). The lithology is dark argillaceous limestone, similar to the cooler/deeper facies at the top of the Ibexian in the Wilson and Fort Pillow wells. Lab processing has begun.

Conodonts from eighteen productive samples from the Dupont GHS well, Humphreys Co., Tennessee (loc. GHS on Fig. B), and 14 from the Illinois Power #2 Morrell well, Montgomery Co., IL, were identified and preliminarily analysed, in cooperation with T.H. Shaw (Queens College, NY), R.D. Norby (Illinois State Geol. Survey), and W.C. Sweet (Ohio State Univ.). Data from these drillholes are helping to unravel the very complex stratigraphy of the peritidal, generally restricted-circulation facies tracts that make up the Middle Ordovician of the southern Midcontinent, including the part of the New Madrid Seismic Zone north of the Pascola arch.

3. *Surface bedrock investigations.*

Collecting of selected bedrock samples for conodont age-dating and facies interpretation in and related to the greater New Madrid Seismic Zone was initiated during fieldwork late in FY 92, in conjunction with other USGS, State Geological Survey, and university projects and colleagues. Samples of non-dated or poorly-dated Lower Ordovician formations were collected along Interstate 44 in Missouri, in conjunction with the transect study being conducted by T.L. Thompson and C. Robertson (Missouri Geol. Survey). More than 50 samples from eastern Missouri, from Scott to Jefferson Counties, ranging from Early Ordovician to Mississippian in age, were collected, for collaborative study with and/or in support of projects by A. Schultz and R. Harrison (USGS - bedrock mapping and structural studies), J.T. Dutro (USGS), R.L. Ethington (Univ. Missouri-Columbia), R. D. Norby (Illinois State Geol. Survey), and T.H. Shaw (Queens College-CUNY)(stratigraphic studies). Specific study areas include the St. Genevieve and Jackson fault zones. Lab processing of these samples had begun by the end of FY 92.

4. *Collaboration with magnetostratigraphic study.*

A coordinated sampling program for detailed paleomagnetic and biostratigraphic data through the Lower and Middle Ordovician of the Ozark platform to western Illinois basin was initiated. The cooperating group comprises: A) USGS - this project (micropaleontology; biostratigraphy); B) University of Kansas Geology Dept. (paleomagnetism; NSF-funded project, M.R. Farr, principal investigator; and C) University of Missouri-Columbia Geology Dept. (stratigraphy; Ordovician studies group, R.L. Ethington, principal investigator).

Paleomagnetic study of closely-spaced samples through measured sections of Ordovician sedimentary strata in northern Arkansas by M.R. Farr and his students has demonstrated the potential for establishing a useful magnetostratigraphy through this interval by identifying an apparently consistent pattern of paleo-polarity reversals. This magnetostratigraphy, based on non-unique events (polarity reversals), must of necessity be calibrated into a stratigraphic framework based on unique events (biotic events and (or) absolute

age-dating) in the host rocks. The Paleozoic (marine sedimentary) rocks of this region are not amenable to a detailed radiometric dating framework, but fossils, particularly conodonts, can provide a stratigraphy with sufficiently fine resolution for calibration, control, and ultimately correlation of the polarity sequences as these are established throughout the region.

During FY 92, two of the northern Arkansas measured sections that were used for the initial paleomagnetic study of the Everton Formation (Middle Ordovician) were sampled in detail for conodonts and other microfossils. Processing of the 50± samples is complete; conodonts were recovered in ~90% of these macrofossil-poor dolostones. Preliminary analysis of the recovered faunas indicates the probability of recognizing at least two or three "time lines" through this (early Whiterockian age) interval based on the conodonts.

Additional work during FY 92 consisted of identifying and sampling additional outcrop sections to extend this joint study stratigraphically (both downward and upward) and geographically. Another 50± samples were collected in northeastern Arkansas and southeastern Missouri, immediately adjacent to or within the New Madrid Seismic Zone and related fault zones, in order to gain conodont-based control for these sections that will be drilled for paleomagnetic study early in FY 93. Lab processing to extract the conodonts from these samples has begun. When a polarity reversal magnetostratigraphy is established for well-controlled surface sections it may become another important stratigraphic tool that can be applied to this and other regions.

Reports

Repetski, J.E., 1992, Lower Ordovician stratigraphy and facies in and adjacent to the Reelfoot basin, southern midcontinent, U.S.A. [abs.], *In* Goldhaber, M.B., and Eidel, J.J. (eds.), Mineral Resources of the Illinois Basin in the Context of Basin Evolution, St. Louis, MO, Jan. 22-23, 1992, Programs with Abstracts: U.S. Geological Survey, Open-File Report OF 92-1, p. 51.

Collins, D.S., Taylor, M.E., Repetski, J.E., and Palmer, A.R., 1992, New sedimentologic and paleontologic data for the Dow Chemical #1 B.L. Garrigan drill hole, Mississippi County, Arkansas: U.S. Geological Survey, Open-File Report 92-6, 38 p.

Repetski, J.E., 1992, Lower Ordovician conodonts from the Reelfoot basin, southern midcontinent, U.S.A. [abs.]: Geological Society of America, North-Central Section Meeting, Abstracts with Programs for 1992, v. 24, no. 4, p. 61.

Repetski, J.E., Taylor, M.E., Collins, D.S., Palmer, A.R., Wood, G.D., and Tobin, R.C., 1992, Integrating paleontology, geothermometry, and sedimentology in determining the history of the Reelfoot basin, southern midcontinent, U.S.A. [abs.], *In* Lidgard, S., and Crane, P.R. (eds.), Fifth North American Paleontological Convention, Field Museum of Natural History, June 28-

July 1, 1992, Abstracts and Program, The Paleontological Society, Special Publication No. 6, p. 243.

Derby, J.R., Hinch, H.H., and Repetski, J.E., 1991, Lithology, stratigraphy, and age of the Arbuckle Group in the Amoco SHADS No. 4, a continuous core from grassroots into basement, Rogers County, Oklahoma: Oklahoma Geological Survey, Special Publication 91-3, p. 69-82.

Repetski, J.E., and Weary, D.J., 1992, Conodont studies in the New Madrid Seismic Zone, *In* National Earthquake Hazards Reduction Program, Summaries of Technical Reports Volume XXXIII: U.S. Geological Survey, Open-File Report 92-258, p. 573-577.

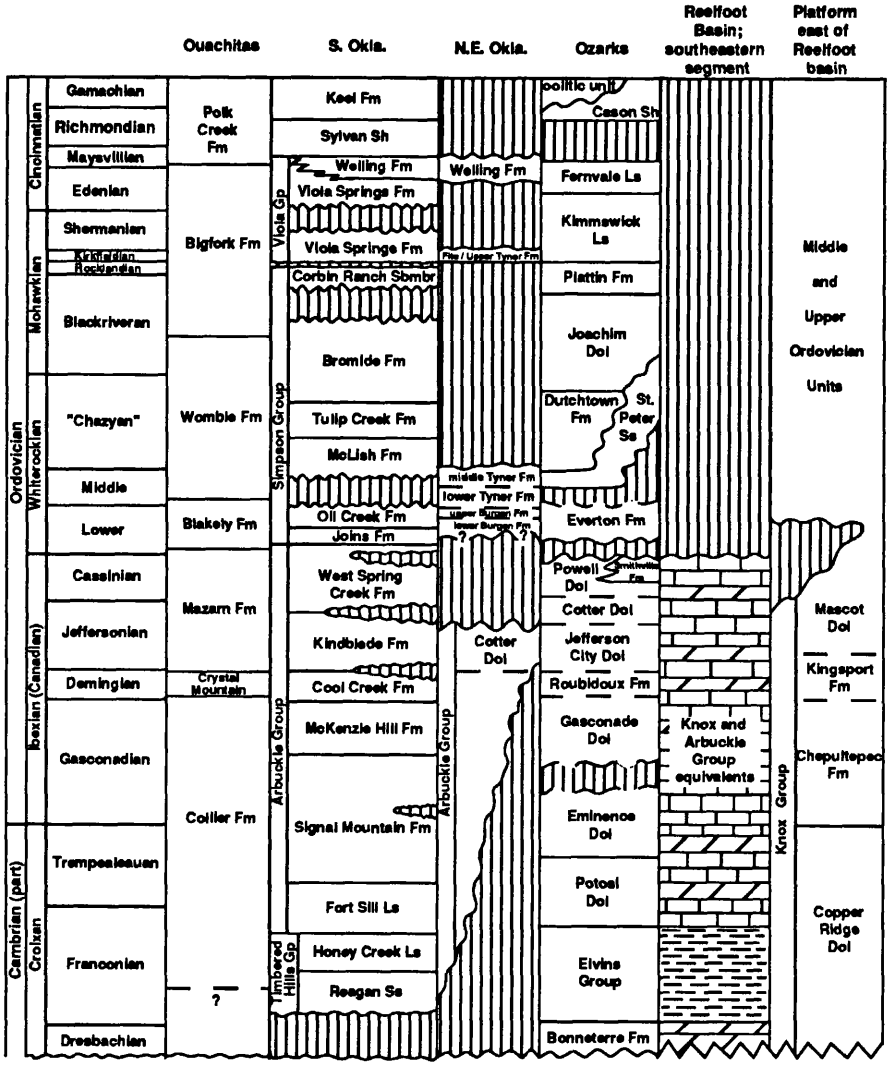

Figure A. Correlation chart for major Upper Cambrian and Ordovician successions in U.S. southern Midcontinent. Southeastern Reelfoot basin stratigraphy is based on microfossils from Dow Chemical #1 Wilson and USGS Fort Pillow drillholes.

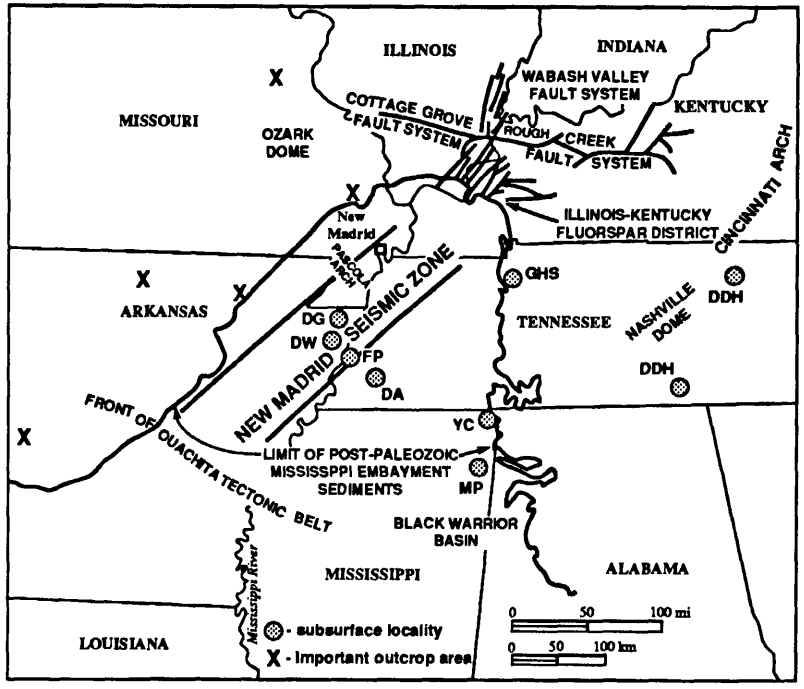

Figure B. Map showing Paleozoic study sites and areas in and related to New Madrid Seismic Zone.

An Integrated Study of the San Miguel Fault Zone, Northern Baja California, Mexico

1434-92-G2223

Thomas Rockwell
C. Kenji Hirabayashi
Dept. of Geological Sciences
San Diego State University
San Diego, CA 92182
(619) 594-4441

Objective: The primary purposes of this study are to resolve the slip rate and determine the timing of past earthquakes on the San Miguel fault in Baja California. These data will further our knowledge of how slip is distributed in southern California and how much slip is being fed directly into the the Tijuana-San Diego area. It is also of interest because the fault has historically been the most seismically active structure in peninsular Baja California though the total slip on the fault has been estimated at less than 1 km.

Results: We have been mapping along the rupture trace of the 1956 earthquake and can make several important tentative conclusions at this time. It should be pointed out, however, that the contract began only this Fall (September) and we are in the early stages of data collection.

First, an alluvial deposit that is bisected by the 1956 rupture is offset a total of 22±3 m. The soils developed in the alluvium suggest an age of 50-120 ka, thereby yielding a long term slip rate of a ~0.2-0.5 mm/yr. Second, in this same area, total slip on the fault is less than 1 km, based on offset of a Cretaceous pluton. Slip in 1956 in this area was about 50 cm. Taken together, these data suggest: 1) the San Miguel fault has probably been active for much of the Quaternary, but at a low slip rate. It is not a newly activated fault zone; and 2) the probable return time for 1956-type surface ruptures is on the order of 1-3 ka.

We have identified several potential trench sites that will be investigated this January and February. We hope to directly date the past several earthquakes.

FLUID PRESSURE AND EARTHQUAKE GENERATION

9960-04451

Evelyn Roeloffs, Eddie G. Quilty
Branch of Tectonophysics
U.S. Geological Survey
5400 MacArthur Blvd.
Vancouver, WA 98661
(206)696-7693

Investigations:

1. The project carried out real-time monitoring and processing of water level data from Parkfield, California, as part of the Parkfield Earthquake Prediction Experiment. Water level data are processed in real time to remove tidal and barometric fluctuations, and the processed data are automatically screened for anomalous signals.

2. Research is carried out on the utility of water wells in earthquake prediction experiments.

3. Hydrologic effects of the Landers earthquake were investigated.

Results:

1. In cooperation with the USGS Water Resources Division, water level data from a network of 11 sites near Parkfield, California, were collected throughout the reporting period. Site locations are shown in Figure 1. Raw water level, barometric pressure, and rainfall data are shown in Figures 2a-c.

In the Middle Mountain (MM) well near Parkfield, water level changes associated with fault creep on the San Andreas fault continue to be observed, as they have been at this site since recording there began in 1987 (Roeloffs et al., 1989).

2. Because there were many reports of water level anomalies following the June 1992 Landers earthquake, E. Roeloffs spent several days in southern California and several more days back in the office compiling reports. No unusually large water level changes were found in the epicentral area. Gas bubbling in city water supply wells in San Bernardino was investigated; the gas bubbles were analyzed and found to be air slightly enriched in carbon dioxide. Significant water level changes at larger distances from the epicenter did take place and research is currently in progress to use these data to learn more about how earthquakes affect groundwater.

Reports:

Roeloffs, E., and E.G. Quilty, "Water level changes preceding and following the August 4, 1985 Kettleman Hills, California, earthquake", submitted to J. Geophys. Res.

Roeloffs, E., "A reported streamflow increase prior to the October 18, 1989 Loma Prieta, California, earthquake", to appear in U.S. Geological Survey Professional Paper on the Loma Prieta earthquake.

Rudnicki, J.W., J. Yin, and E.A. Roeloffs, "Analysis of water level changes induced by fault creep at Parkfield, California", accepted by J. Geophys. Res.

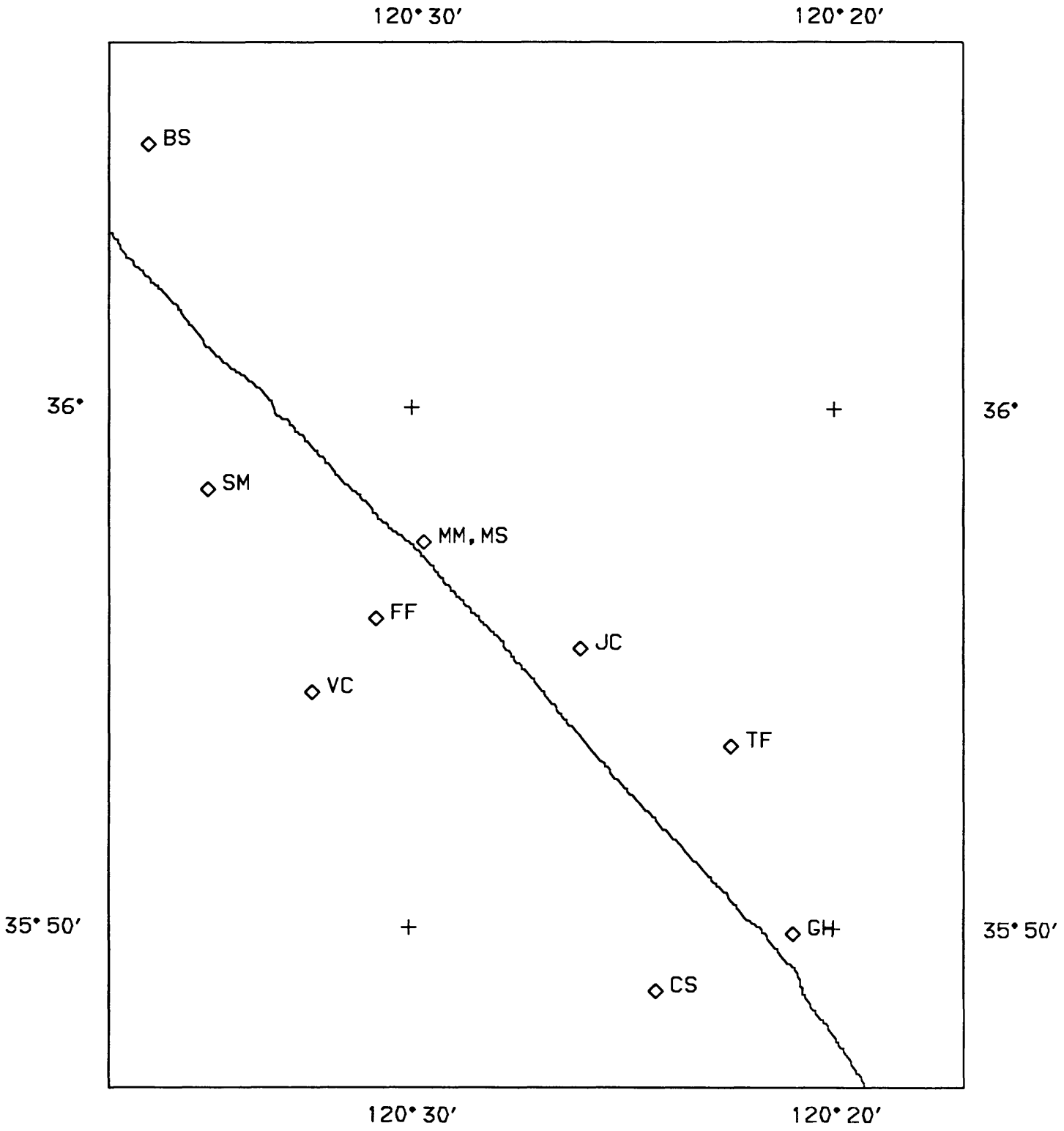

Figure 1. Map showing water wells near Parkfield California, monitored as part of the Parkfield Earthquake Prediction Experiment.

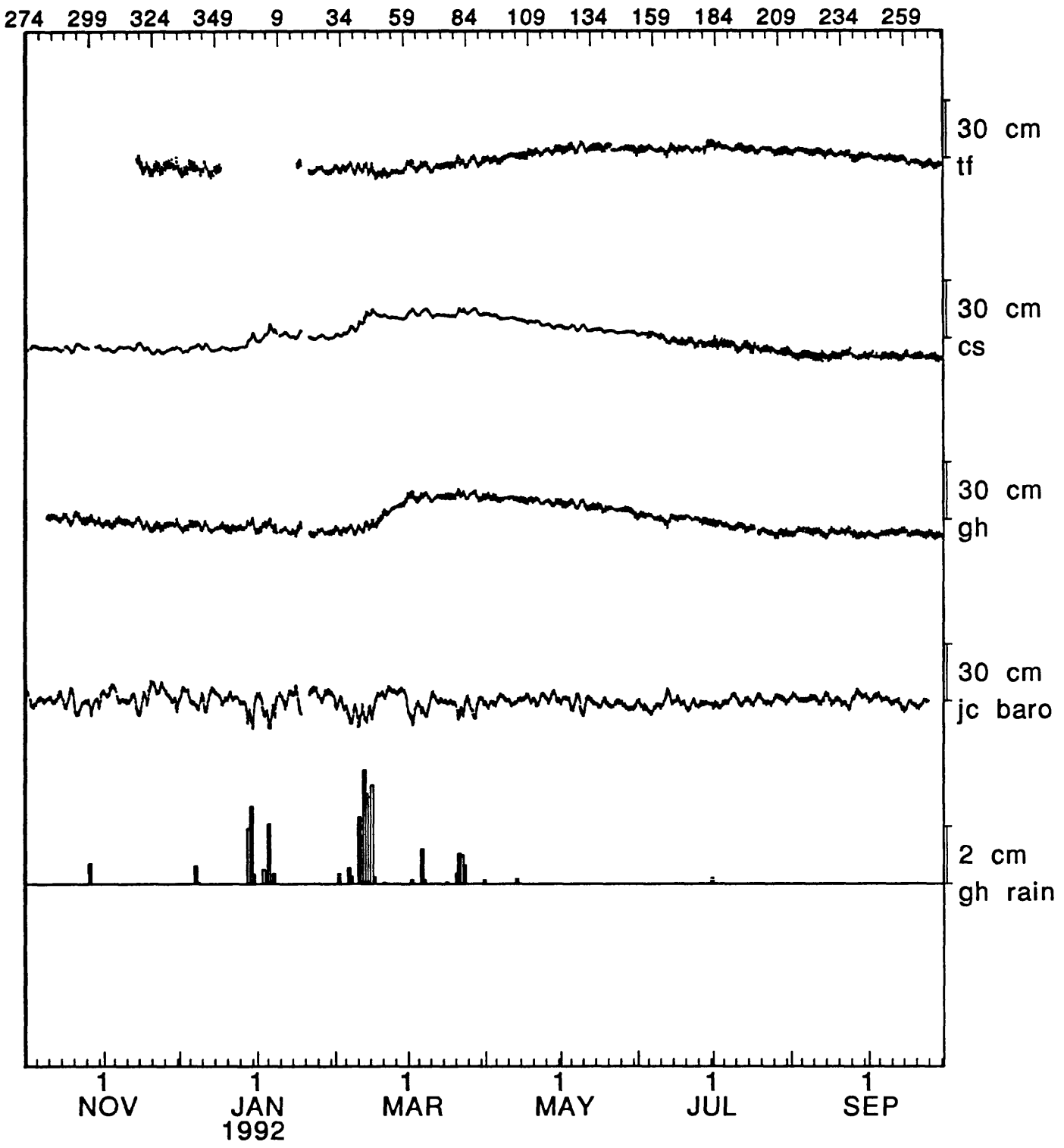

Figure 2. (a) Water level, barometric pressure, and rainfall records. Hourly values are plotted for water level and barometric pressure. Water level is in centimeters above an arbitrary datum. Barometric pressure is in centimeters of water with respect to an arbitrary datum. Bars indicate total rainfall in a 24 hour period. Site names are indicated at right.

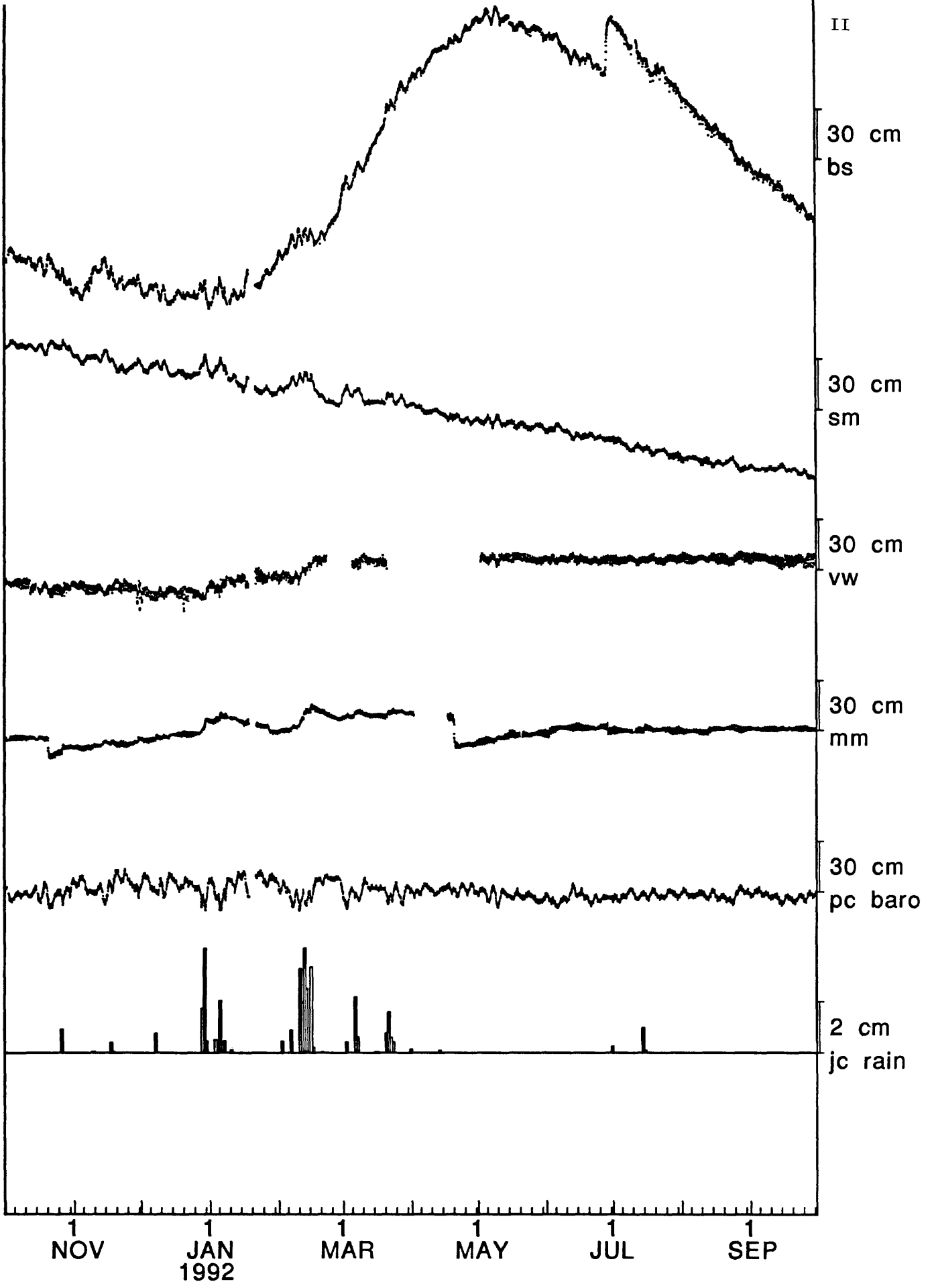

Figure 2. (b) Water level records plotted as in Figure 2(a).

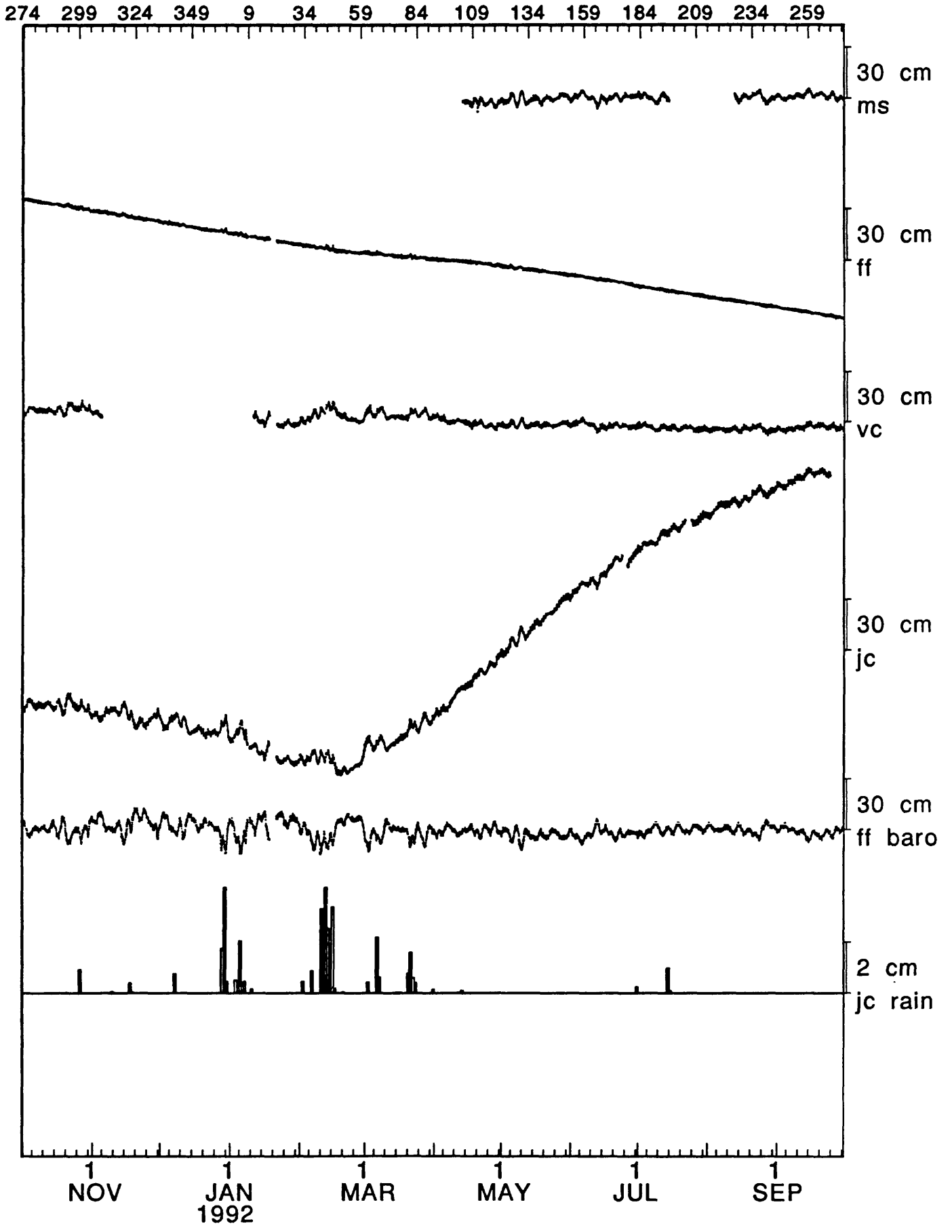

Figure 2. (c) Water level records plotted as in Figure 2(a).

USGS/UCB Seismic Data Center

Project Number: 14-08-0001-G2118

Barbara Romanowicz
Seismographic Station, University of California at Berkeley
475 Earth Sciences Building
Berkeley, California 94720

(510) 643-5690

Objectives

This project consists in establishing a joint UC Berkeley/USGS Menlo Park Northern California Database for earthquake related digital data. The database resides on a 330 Gbyte mass-storage device accessible "on-line" to outside users through Internet and other computer networks. The database is designed to contain seismological waveform data from:

1) The USGS/Menlo Park Northern California CalNet "CUSP" collection.
2) The Berkeley Digital Seismic Network (broadband data).
3) The USGS/UCB Hayward Fault network.
4) Other seismological stations and networks as will appear appropriate (e.g. subsets of the Geoscope and IRIS datasets; strong motion data collections).
5) Historical data digitized from the Berkeley collection of paper records.

It will also contain other types of data, such as GPS data acquired by USGS/Menlo Park and UC Berkeley, so as to span the entire frequency spectrum and dynamic range relevant to the study of earthquakes and deformation in northern and central California.

Results

Hardware

The database resides on a mass-storage system consisting of a SONY WORM jukebox (capacity 330 Gbytes) attached to a front end SUN-Sparc 2 computer system. The hardware/software configuration is designed so as to match the system acquired at Caltech for the Data Center of the Southern California Earthquake Center, in order to achieve optimal compatibility and sharing of resources.

The following hardware items have been purchased with funds from USGS award number 14-08-0001-G2080, and are currently operational:

1) SONY 330 Gbyte jukebox, two drives and controllers and 50 platters.
2) AMASS software, which implements a cached UNIX filesystem for files stored on the SONY jukebox.
3) Ten magnetic disk drives (capacity 1.3 Gbytes each).
4) One Exabyte 8500 5.0 Gbyte 8-mm tape drive.
5) One HP DDS DAT tape drive.

The following operational hardware has been purchased with matching funds from the University of California:

1) Two Sparcstation 2 computers with 200 Mbyte disk, 64 Mbyte memory.
2) Two SUN ELC diskless workstations.

The primary Data Center computer consists of one Sparcstation 2, the SONY jukebox with AMAS software, seven 1.3 Gbyte disk drives and the tape drives. The other workstations are used for support services associated with the Data Center.

Data currently available

1) UCB broadband data

The UCB Seismographic Station acquires continuous and triggered 24-bit digital broadband datastreams from Quanterra dataloggers at eight stations in northern and central California, using continuous telemetry and dial-up (Figure 1). All continuous and triggered data from September 1991 to the present are available through the data center. Ongoing continuous and triggered data are made available on a daily basis.

Over the next several months, we will be loading both currently telemetered and archived data from UCB's 16-bit digital broadband data loggers. This dataset ranges from 1986 to the present.

2) USGS CalNet event data

The CalNet dataset consists of two distinct but inter-related datasets. The first dataset consists of the CUSP "grm" and "mem" files. The "grm" files contain the event waveforms, and the "mem" files contain waveform descriptors and event parameters derived by the Menlo Park CUSP event processing system. The second dataset consists of the CalNet phase and catalog files, which contain phase pick information and updated event parameters that have been derived by more precise crustal models. This dataset draws extensively on pick information from the CUSP events as well as events triggered by the stand-alone Menlo RTP systems, and contains updated event parameters for all northern California events that meet the catalog's inclusion criteria. Since neither dataset is a proper subset of the other, both will be available at the Data Center (Figure 2).

The Data Center has currently loaded all of the available CUSP "mem" files in both CUSP and ASCII forms from 1984 through August 1992.

Since the "mem" files are not easily usable on systems without CUSP processing software, the Data Center is deriving an ASCII representation of the important parameters in the "mem" files.

We have begun loading the waveform data ("grm" files) for the CalNet data, starting in 1992 (presently over six months of 1992 are available). This process will take a number of months to complete, since the original tapes must be read and copied at Menlo Park before the data is shipped to UCB and loaded onto the mass-store. Procedures have been established for loading and retrieving waveform files. The Data Center is loading the waveforms as rapidly as they are received from USGS.

Software

The Data Center currently has interim programs for extracting broadband data from the on-line archive. Data can be extracted in one of two formats -- as either Steim-1 SEED data records or as full SEED volumes. Information is currently being loaded into a database system designed by IRIS in order to provide instrument response and complete indexing of time intervals for all broadband data.

In collaboration with USGS Menlo Park and Caltech, programs have been developed to load, index, store and extract the CUSP "mem" files, CUSP "grm" files, and CalNet phase and catalog files. Programs are currently being adapted to provide easy search and extract capability of event and phase data from the CalNet phase and catalog files. CalNet "grm" files can either be retrieved in their native form, or can be converted to time series in AH format. We intend to continue to work with USGS Menlo Park staff to investigate better methods of storing and retrieving the CalNet phase and catalog data.

The Raina db_VISTA Data Manager database toolkit is being purchased with University of California funds to support the database and query program developed by IRIS for the broadband dataset. A complement of development software (C, C++, FORTRAN, X11) is provided by the Berkeley campus-wide software licenses. All hardware purchasing and software development at UCB has been performed by the Seismographic Station computer systems manager, Douglas Neuhauser. Data is currently being loaded by Seismographic Station staff.

Reports Published

Bogaert, B., D. Neuhauser, A. Walter, B. Romanowicz, 1992, The USGS/UCB Northern California Seismic Data Center, *EOS Trans. AGU*, 73, 371.

Dataflow for UCB Broadband Data

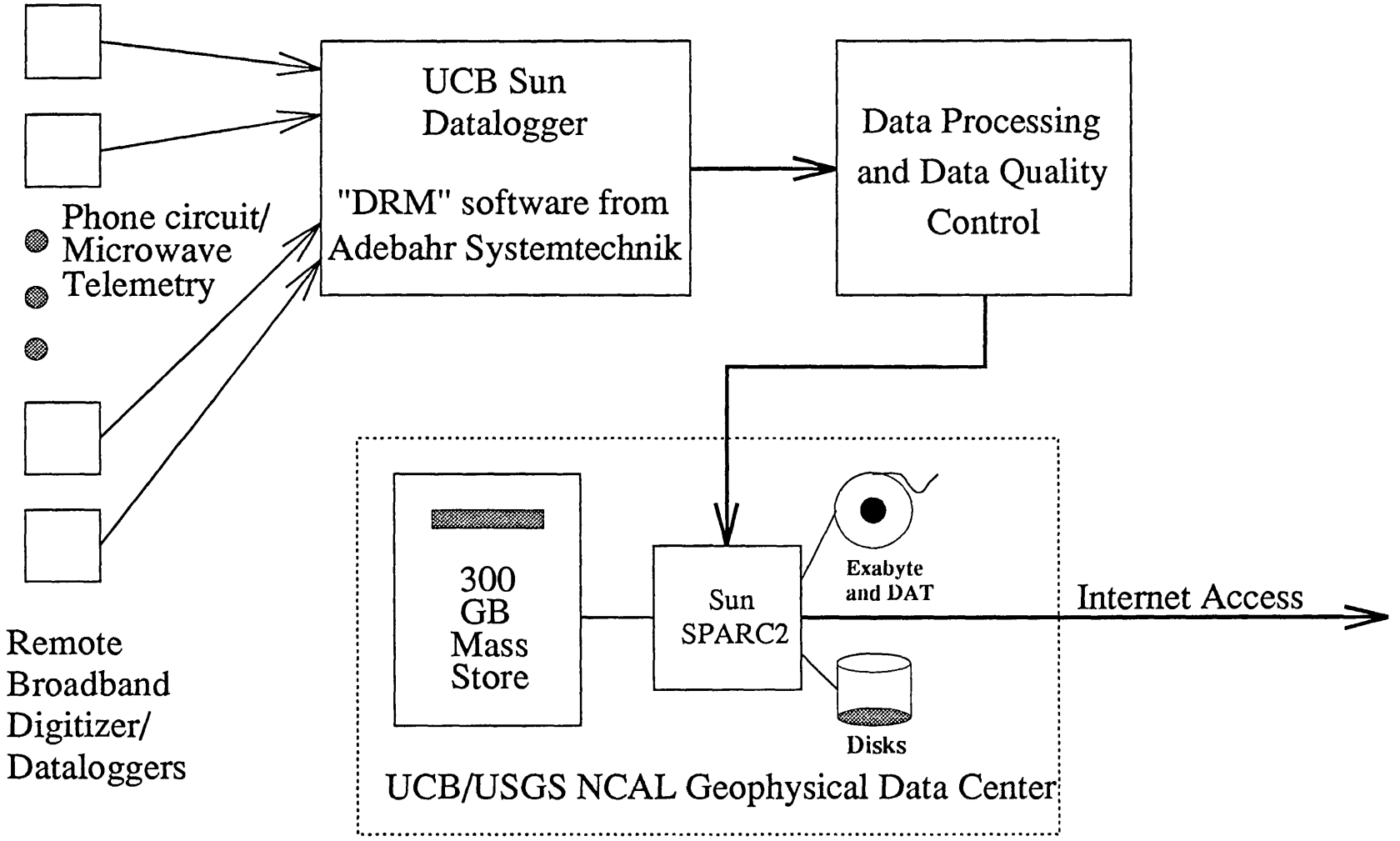

FIGURE 1

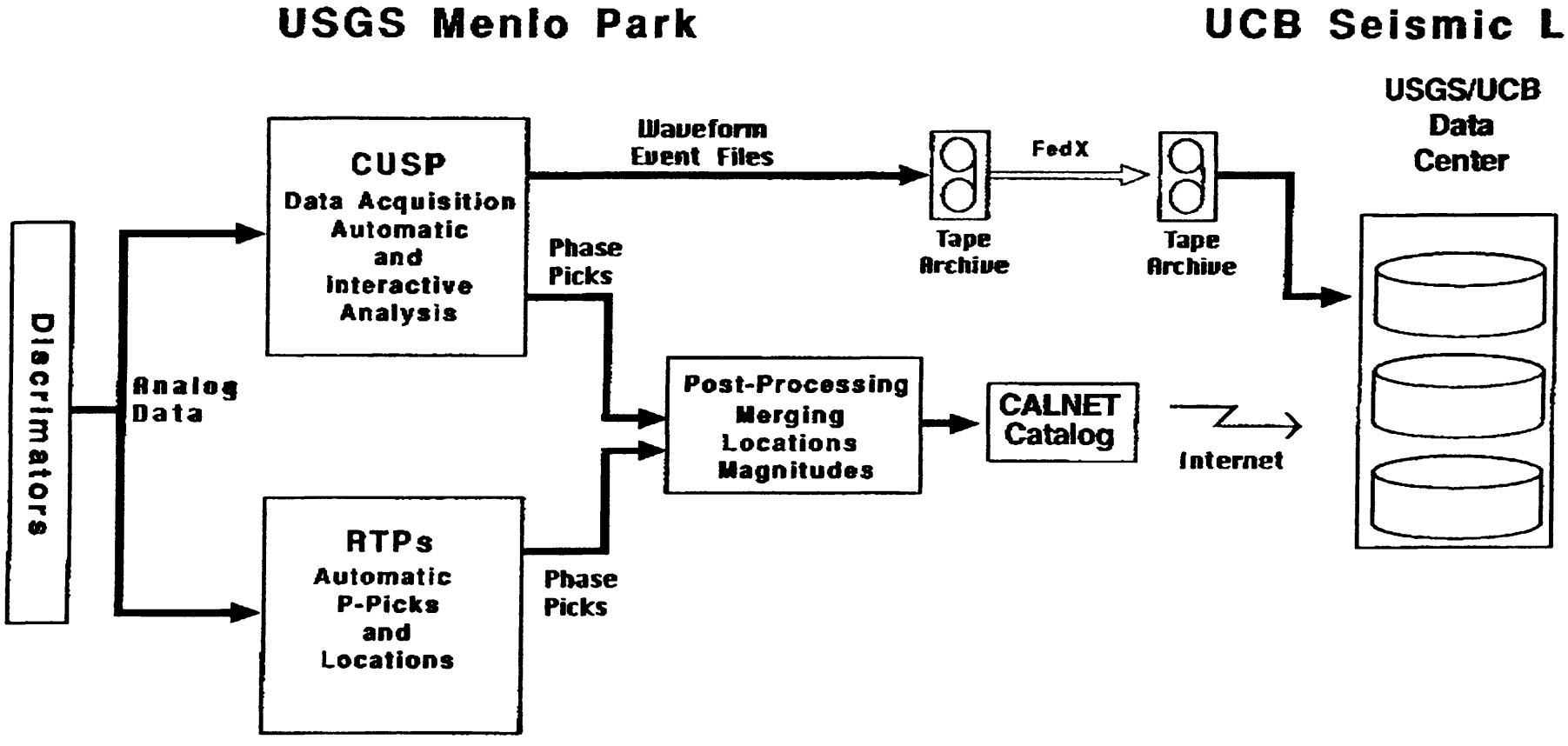

CALNET- UCB DATAFLOW

FIGURE 2

Accessing the UCB/USGS Seismology Data Center 92/12/07

The UCB/USGS Seismology Data Center is accessible via the Internet. Initially, the data center will establish individual accounts for each user accessing the data center. In the future we may migrate to a single publicly-accessible account similar to the IRIS bulletin board system. It is assumed that users are either familiar with or will obtain their own support on the use of the Unix operating system. The data center cannot provide consulting support on questions not directly related to the data center.

Host Name:	brkseis20.berkeley.edu
Internet address:	128.32.146.106
Computer:	Sun SPARCstation 2
Operating system:	SunOS (Unix)

To request an account at the data center:

1. Use telnet to connect to brkseis20.berkeley.edu. Depending on your local computer configuration, you may have to use the Internet address of the machine instead of the hostname:

```
telnet brkseis20.berkeley
```

or

```
telnet 128.32.146.106
```

2. Login to special account "bulletin", which has a password of "board".

3. Select the option to request an account. It is currently the only option available, other than "quit". You will be prompted for information such as your name, address, institutional affiliation, email address, and phone number.

4. You should be contacted within 2 working days with your account information. If you do not hear within this time period, please contact:

Douglas Neuhauser
Seismographic Station
Earth Science Building,
University of California, Berkeley CA 94720
510-642-0931

5. This computer account is to be used strictly for accessing and retrieving data explicity provided by the data center. Any other use consititutes fraud.

See the sample session on the next page for an account request.

Sample session to the UCB/USGS Seismology Data Center

```
telnet brkseis20.berkeley.edu
Trying 128.32.146.106 ...
Connected to brkseis20.berkeley.edu.
Escape character is '^]'.


SunOS UNIX (brkseis20.berkeley.edu)

login: bulletin
Password:
Last login: Mon Dec  7 11:14:13 from brkseis10.berkel

******************************************************************************
                UCB/USGS Seismology Data Center
******************************************************************************
Welcome to the UCB/USGS Northern California Seismology Data Center.
Your host is: brkseis20.berkeley.edu

Type "man info" to get more information about available resources.
******************************************************************************
Welcome to the UCB/USGS Seismology Data Center


Enter 'a' to request an account
Enter 'q' to QUIT

Enter your selection: a



          UC Berkeley Seismographic Station / USGS
                   Seismology Data Center


User ID request form:
Please answer the following questions:
(Terminate each reply with a 'return'.)
(Type a control-D to abort account request.)

Full Name: Joe Smith
Institution/Organization/Company: Podunk U, Dept of Seismology
Full Address (1 line): 123 Earth Sciences Building, Podunk U, Podunk, NY 14882
Office Phone #: 800-555-1212
Internet/Bitnet address (0=none): joesmith@geo.podunk.edu
preferred user ID name: joesmith

request logged...
You should be contacted at the above address with information
about your account.  If you have not heard by the end of two
working days, please resubmit your request, and if that
does not work, please call 510-642-0931 or 510-642-3977
Thank you.

Enter 'a' to request an account
Enter 'q' to QUIT

Enter your selection: q
Connection closed by foreign host.
```

Determination of the Recurrence Interval for Large Earthquakes In the New Madrid Seismic Zone Using Paleomagnetic Methods

14-08-0001-G1929

Stephen L. Salyards
Geophysics Program, Physics Department
New Mexico State University
Las Cruces, NM 88003

Objectives

This past year two goals were emphasized in the continuation of this work. Last year I demonstrated the ability of liquefaction features generated in 1811-1812 to record the magnetic field at that time. This year I progressed to sampling liquefaction features of unknown age and showed that their magnetic field directions are compatible with their formation in 1811-1812. Second, last year I developed a preliminary Holocene magnetic secular variation curve for the New Madrid region and this year I sampled additional sections to test the curve and provide redundancy to increase the master curve's certainty.

Results Obtained

The results from the liquefaction studies have proved to be quite interesting and the results have gone beyond simply correlating and dating earthquakes to providing information on the dynamics of the liquefaction process. I found that comparison of the magnetic susceptibility of the liquefied sand with probable source regions provides information on the source and development of liquefied sediments.

William Lettis and Keith Kelson of W. A. Lettis and Associates excavated a trench across the Reelfoot Scarp in northeast Tennessee. In cooperation with them, I collected samples from three different liquefaction features. Only one of the three features, a dike cutting the "topstratum," had a clear stratigraphic indication of its age. While this dike was easily attributable to the 1811-1812 earthquakes, two diapiric sand bodies showed no eruption onto a ground surface and therefore no clear evidence of age. The stratigraphic position was consistent with recent emplacement and attributed to 1811-1812.

The lack of clear age information provided an opportunity to test paleomagnetic correlation as a paleoseismologic tool. Last year I demonstrated that sands can preserve the magnetic field at the time of liquefaction: sands that were erupted onto the ground surface in the 1811-1812 events were indistinguishable from the magnetic field direction measured in St. Louis in 1819 [Salyards, 1992]. If the paleomagnetic direction of these diapirs also agreed with the 1819 magnetic field direction then this would support the paleoseismological conclusion of emplacement in 1811-1812.

Eight samples were collected from each diapir and demagnetized using our standard stepwise demagnetization sequence (Alternating field at 1, 2, 3, 4, 6, 8, and 10 mT and thermal demagnetization beginning at 100° C and progressing in 50° steps to at least 600°C). The bulk susceptibility of each sample was measured before heating and at 50° or 100° steps through the demagnetization process. In addition, rock magnetic tests, such as anhysteritic remanent magnetization (ARM)

acquisition and demagnetization and isothermal remanent magnetization (IRM) acquisition and demagnetization, were preformed on samples to characterize the magnetic carriers. In all cases, single-domain magnetite appeared to be the carrier of the primary magnetic component with little or no chemical overprint.

In both diapirs the region of 95% confidence of the mean contains the magnetic field direction for 1819 in St. Louis (Figure 1). This supports that conclusion that these features formed in the historical earthquakes of 1811-1812 and not an earlier event.

If the magnetic susceptibilities of the samples from the first diapir are plotted in depth order (Figure 2) a clear increase in magnetic susceptibility with depth is seen. This could be due to (1) variation in the source material; (2) variation in the selective entrainment of grains; (3) settling or physical process after diapir emplacement and before dewatering; (4) chemical alteration of the sand. Since the magnetic studies show no sign of chemical alteration the last explanation is presently being disregarded although future measurements may again make it a candidate. Comparison of the magnetic susceptibilities of the diapir, probable source sand, and host sand show that the top of the source sand has a susceptibility similar to the probable source while the base has a susceptibility closer to the host sand. If the variation is not due to selective mobilization of different size grains, then variation in the source material is the most likely explanation for the variation. Specifically, the upper part of the diapir must have originated from the probable source sand, while the lower part of the diapir must have come from the host sand. In the mid-regions of the diapir mixing of sand from the two regions must have occurred. Grain-size distribution comparison should help determine if selective entrainment of grains occurred, or if the proposed mixing model is a better explanation.

Reports Published

Salyards, S. L., 1992, Paleomagnetics of liquefied sands from the 1811-1812 New Madrid earthquakes: Seis. Res. Lett., in press

Papers presented

Salyards, S. L., 1991, Quality of the magnetic direction of liquefied sands from the 1811-1812 New Madrid earthquakes: Geol. Soc. Amer., Abstracts with Programs, v. 23, n. 5, p. 92.

Salyards, S. L., 1992, Paleomagnetic evidence of 1811-1812 liquefaction along the Reelfoot Scarp, New Madrid seismic zone, Tennessee: Geol. Soc. Amer., Abstracts with Programs, v. 24, n. 7, p. 206.

Figure 1
Least Squares Equal Area Plot
Reelfoot Trench, Liquefaction features

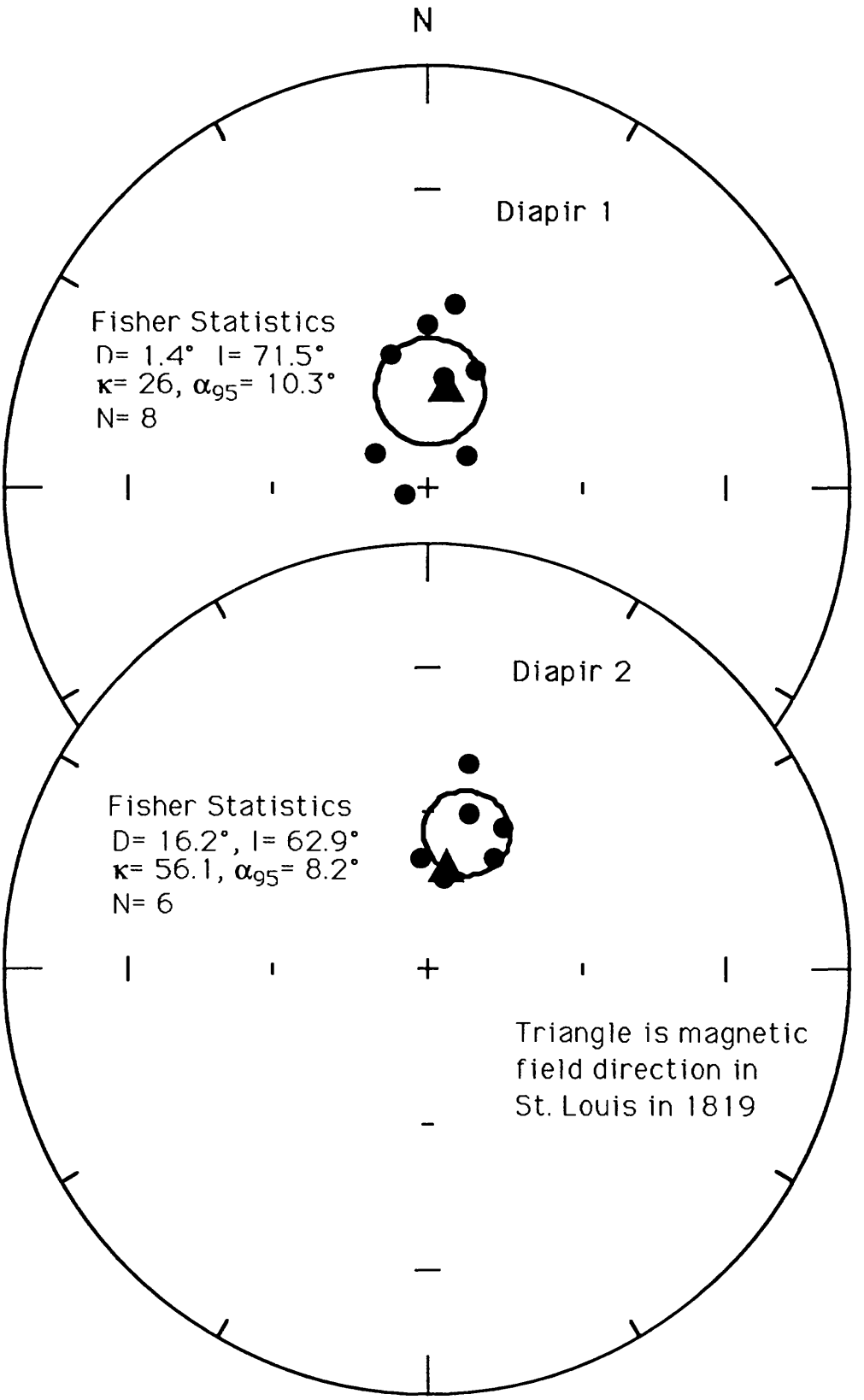

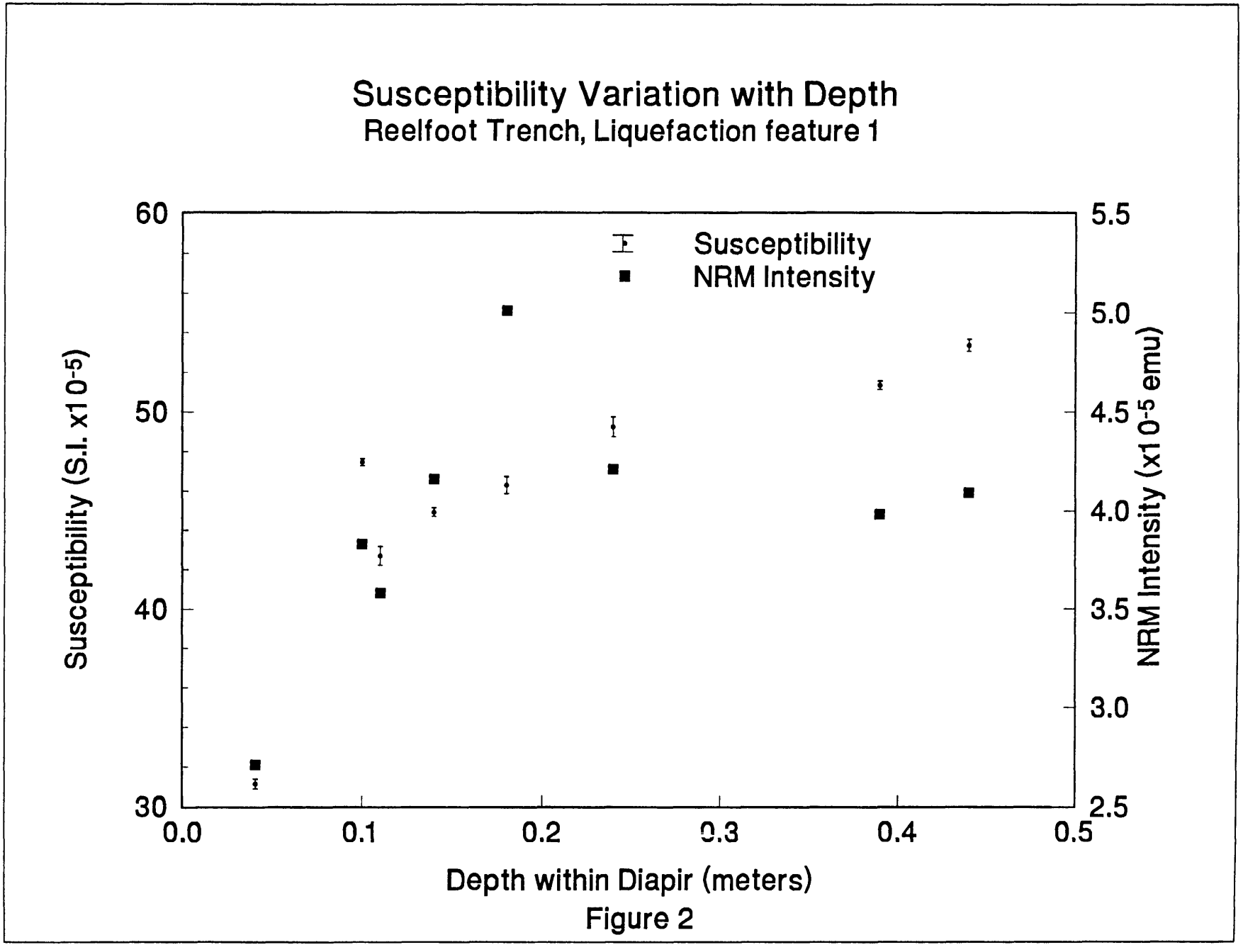
Susceptibility Variation with Depth
Reelfoot Trench, Liquefaction feature 1
Susceptibility
NRM Intensity
Susceptibility (S.I. x10-5)
NRM Intensity (x10-5 emu)
60
50
40
30
5.5
5.0
4.5
4.0
3.5
3.0
2.5
0.0
0.1
0.2
0.3
0.4
0.5
Depth within Diapir (meters)

Figure 2

Paleomagnetic Studies of the Kinematics of Non-brittle Deformation of Fault Zones

1434-92-G-2215

Stephen L. Salyards
Department of Earth and Space Sciences
University of California, Los Angeles
Los Angeles, CA 90024

Objectives

The purpose of this research is to understand the mechanical relationship between fault zone deformation, as measured using paleomagnetic rotations, and fault slip. One of the integral questions associated with this problem is the grain-scale deformation of the rock or sediment.

Results obtained

Preliminary results are now finished for two sites and similar behavior is seen.

The first site is an outcrop of medium cemented sandstone with three faults exposed in the outcrop. The faults have >5, 1, and 1.75 meters of offset respectively from west to east (Figure 1). Grain-scale deformation is present in the sand near the faults, but the amount, and distance of deformation is directly related to the amount of offset on the faults. The deformation does decrease rapidly away from the faults with about 4 meters of more anisotropic material adjacent to the fault with largest offset.

The second site is along the surface rupture of the 28 June 1992 Landers earthquake. At this location along the Emerson fault cultural features show that sub-meter blocks rotated by up to 45°. Magnetic anisotropy measurements of the uncemented sediments from several points across the fault zone shows almost no significant change in the anisotropy. The only samples with a significantly different anisotropy were in a rare exposure of fault gouge. These samples had a magnetic foliation parallel to the fault plane.

This preliminary work suggests that more than a few centimeters to meters from the main fault trace sediment deformation is not a significant factor and that paleomagnetic rotations may be best converted to fault offset using a model of finite size rigid blocks.

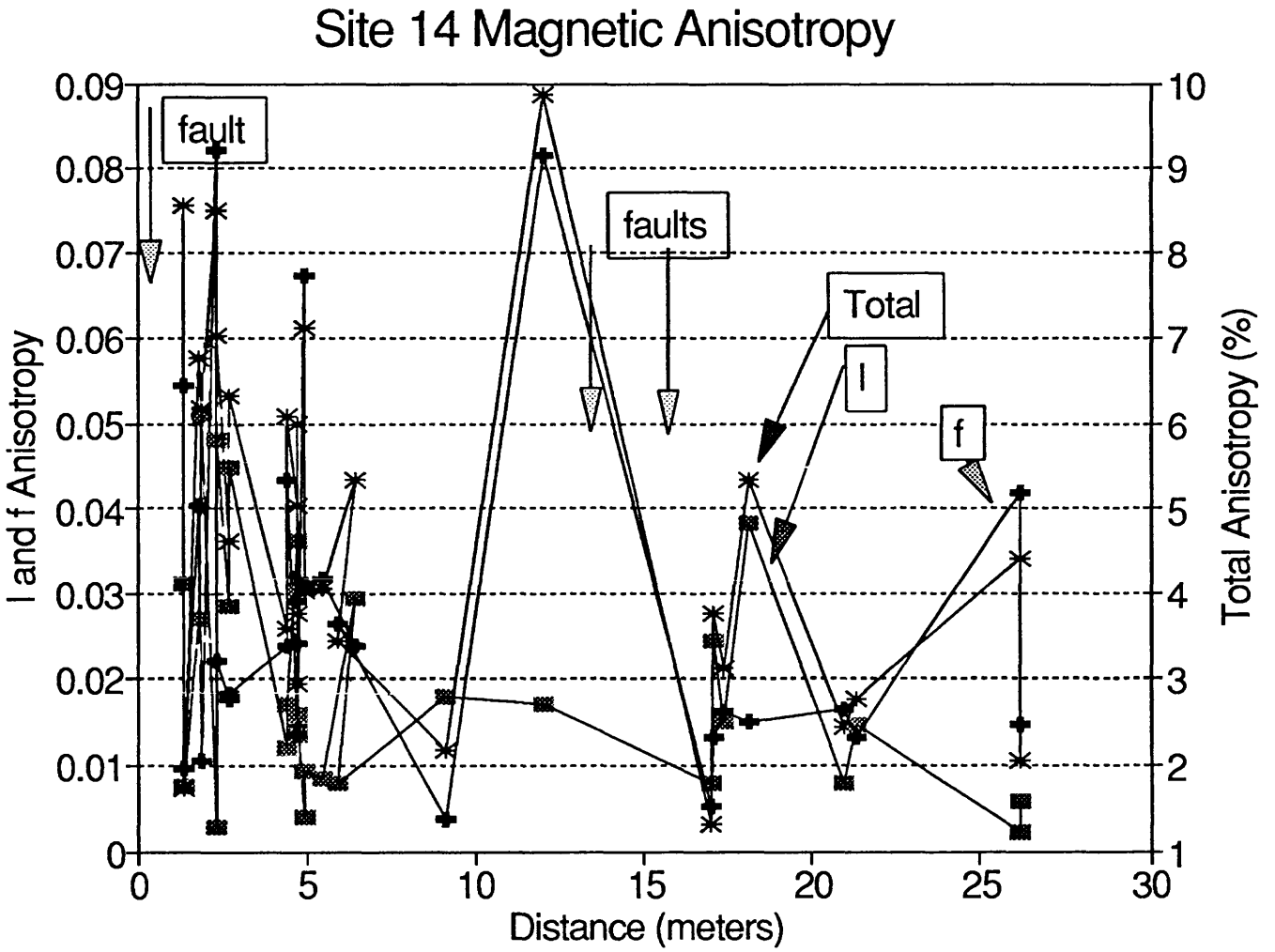

Figure 1

Magnetic anisotropy of sandstones adjacent to active faults with a few meters of offset. The figure shows the total anisotropy and the lineation and foliation anisotropies of the sandstone. There is a general increase in anisotropy near the faults with anisotropy increases further from the faults with increasing offset on the faults.

Quaternary Tephrochronology in the Western Region in Support of Earthquake Hazards Reduction Studies

9540-70020

Tephrochronology Project (of the Western Region)
A. M. Sarna-Wojcicki, C. E. Meyer, and Elmira Wan
Branch of Western Regional Geology, MS 975
345 Middlefield Road; Menlo Park, CA 94025
Tel.:415-329-4930; FAX: 459-4936

Investigations

The Tephrochronology project provides stratigraphic correlation and age control to studies of active faults and neotectonics in the Western Region by means of chemical analysis and numerical age dating of tephra (volcanic ash and tuff layers). Currently ongoing studies are with:

1. Michael Rymer (BESG, Menlo) on the geologic structure, transpression, and neotectonics of the San Andreas Fault in the Salton Trough, California, using the Bishop ash bed as a chronostratigraphic marker.
2. Ray Wells and John Hillhouse (BWRG, Menlo), and Wayne Thatcher (BTTP, Menlo), on Plio-Pleistocene rotations across the San Andreas Fault System and paleomagnetic constraints on inelastic strain accumulation within the central Coast Ranges of California.
3. Eldridge Moores, Randy Southard, Jeff Unruh, and Lewis Munk (Univ. of California, Davis; USGS EQHRP contract), on kinematics of Quaternary blind thrusting in the southwestern Sacramento Valley of California.
4. Marith Reheis (BCRG, Denver) on Neogene displacement of the Fish Lake Valley Fault Zone, the northern extension of the Furnace Creek Fault Zone in eastern California and western Nevada, and late Neogene tectonics of Fish Lake Valley.
5. John Bell (Nevada Bureau of Mines and Geology, Reno, NV), on the seismicity and active faulting in the Walker Lane seismic gap region of central Nevada.
6. Richard Madole (GRA, Denver), on the age and paleoseismic significance of the Ribbon Cliff landslide of the Columbia River, central Washington, as it relates to the location of the epicenter of the North Cascade earthquake of December 14, 1872.

7. Gary Mann (BPMG, Menlo), on the age of morphologically young fault scarps within the Wallawa Fault Zone, southeastern Washington.

8. Earl Brabb (BWRG) and Davey Jones (Univ. of Calif., Berkeley), on the age and correlation of early Neogene tephra layers, for age control in tectonic and chronostratigraphic studies of the eastern San Francisco Bay area.

9. Malcolm Pringle (formerly of BIG) on laser-fusion $^{40}Ar/^{39}Ar$ dating of late Neogene tephra layers as chronostratigraphic horizons in the western U.S.

10. With Kevin Johnson, Hawaiian State Museum of Natural History, Honolulu, HI, on new experimental geochemical methods of chemically "fingerprinting" individual glass shards for minor and trace elements, using the ion probe.

11. Atilla Aydin (Stanford Univ.), to provide age constraints on deformed late Neogene alluvium offset by major strike-slip faulting during the June 28, 1992, Landers earthquake in the Mojave Desert.

Results (refer to corresponding numbers, above)

For interim results of ongoing studies 1 through 6, see our previous report in vol. XXXIII.

3. The Dunnigan Hills are a low, gentle, northwest trending, linear range of hills situated incongruousy among the flat bottomlands of southwestern Sacramento Valley. Identification of the late Pleistocene Olema ash bed (55-75 ka) in a tectonically warped stream terrace from these hills provides a new age constraint for this anticlinal flexure, one situated above a presumed blind thrust at depth, and demonstrates the youthfullness of this feature. This thrust system is seismogenic, as inferred from historic seismicity and subsurface data in this area.

9. We have obtained new laser-fusion $^{40}Ar/^{39}Ar$ ages on the Bishop ash bed and Tuff of Taylor Canyon, two widespread late Neogene tephra layers in the western U.S. The Bishop ash bed and tuff were erupted from the Long Valley caldera east of the central Sierra Nevada, the Tuff of Taylor Canyon, a complex of several tuffs, was erupted from the Glass Mountain area, just east of Long Valley.

The new age for the Bishop ash bed, 0.759 ±0.002 Ma, is based on about 80 individual determinations of individual sanidine crystals or groups of a few small crystals, and is precise (±0.3%). This result provides a new, precise constraint on the Brunhes/Matuyama Chron boundary (B/MC), which is identified a short distance stratigra-

phically below the Bishop ash bed at many sites. Our new estimate of the age of the B/MC boundary based on interpolations and extrapolations from dated chronostratigraphic markers above and below the B/MC boundary is 0.775 ±0.004 Ma, in reasonable agreement with recent data reported from other areas, although on the young side.

Ages on the Tuff of Taylor Canyon, a group of tephra layers erupted during a relatively brief period of activity, range from 1.92 to 2.22 Ma. At Fish Lake Valley, 70 km to the east of Glass Mountain, the Tuff of Taylor Canyon is interbedded with the Huckleberry Ridge ash bed, which we have redated at 2.06 Ma, an age in good agreement with the stratigraphic relations of the latter to the Tuff of Taylor Canyon beds.

10. Kevin Johnson, using the Woods Hole ion probe, has analyzed individual volcanic glass shards from several of our control samples that were collected from well-dated and identified tephra layers. Results indicate that individual glass shards can be chemically "fingerprinted" for a large suite of major, minor, and trace elements, and that there is good agreement between the ion probe data and that of other analytical techniques such as instrumental neutron activation, X-ray fluorescence, and electron-microprobe. This analytical advance makes it possible to analyze rare, disseminated volcanic glass shards in sediments and sediment cores, and extends the potential of tephrochronologic age control to all sediments that contain even trace amounts of volcanic shards.

11. We have identified the Nomlaki Tuff (Member of the Tehama and Tuscan Formations) in deformed sediments offset by the Emerson fault during the Landers earthquake of June, 1992. We suspected that this might be the younger Bishop ash bed, but analysis indicated it was the older, 3.4 Ma unit (K-Ar). This finding suggests that there is a long history of late Neogene deformation on the Emerson fault.

Reports (funded wholly or in part by EQHRP)

Aydin, A., and 8 others, (incl. Sarna-Wojcicki), Surface rupture associated with the June 28 1992 Landers, California, earthquake along the north-central Emerson fault and its neotectonic significance. Abs., American Geophysical Union, San Francisco, Dec.., 1992, Accepted.

Rieck, H.J., Sarna-Wojcicki, A.M., Meyer, C.E., and Adam, D.P., 1992, Magnetostratigraphy and tephrochronology of upper Pliocene to

Holocene record in lake sediments at Tulelake, northern California. Geological Society of America Bulletin, v. 104, p. 409-428

Mann, G.M., and Meyer, C.E., Late Cenozoic structure and correlations to seismicity along the Olympic-Wallowa lineament. Geological Society of America Bulletin, accepted.

Sarna-Wojcicki, A.M., 1992, Long-term displacement rates of the San Andreas Fault System in northern California from the 6-Ma Roblar tuff. *In* Program and Abstracts, Second Conference on Earthquake Hazards in the Eastern San Francisco Bay Area, California. California State University, Hayward, March 25-29. P. 60.

Sarna-Wojcicki, A.M., and Pringle, M.S., Jr., Laser-fusion 40Ar/39Ar ages of the Tuff of Taylor Canyon and Bishop Tuff, E. California-W. Nevada. Abs., American Geophysical Union, San Francisco, Dec., 1992. Accepted.

HYDROGEN AND OTHER NON-RADON GEOCHEMICAL MONITORING

Project # 9970-02773 (FY92)

Motoaki Sato
Branch of Lithospheric Processes
U.S. Geological Survey, MS-959, Reston, VA 22092
(703) 648-6766, FAX (703) 648-6789

INVESTIGATIONS

Soil hydrogen concentration is monitored by using fuel-cell sensors along the San Andreas and Calaveras faults in central California. A borehole about 2 meter deep is dug at the fault trace and the sensor is placed at 1.5 meter depth. The hole is then completely filled with coarse sand to minimize the ambient temperature and barometric pressure effects on the sensor signal. An isolation amplifier is inserted between the sensor output and the telemetry unit to prevent possible ground-loop noise during heavy rain. There are four soil hydrogen monitoring sites in the Hollister area and seven sites in the Parkfield area (Fig. 1). Duplicate sensors are installed 17 meters apart at five sites in the Parkfield area. All these sites are adjacent to creep-meters to share the satellite-based telemetry units.

Also continuously monitored are water conductivity, dissolved CO_2, and dissolved H_2 of pumped water from two wells, one drilled into the San andreas fault zone and the other about 500 meters from the fault in Parkfield. These experiments share the water pumping system and the telemetry units with the radon monitoring project.

RESULTS

Soil Hydrogen

Telemetered soil hydrogen data from eleven sites are compositely plotted as time-series in Fig. 2 (from 1 October 1991 to 1 April 1992) and Fig. 3 (from 1 April 1992 to 1 October 1992). The cumulative rain data recorded at Middle Mountain are also shown at the top of both figures. The signal changes marked "s.s." in Fig. 3 are the result of servicing of the sensor and *in situ* test with a calibration gas mixture (1000 ppm H_2). The full sensor responses are not shown in the figure. The data from the San Juan Bautista site are not plotted because the site developed a problem in electronics or cable connections in the summer of 1991 and attempts to locate the problem were unsuccessful due primarily to severe time shortage for field maintenance work, travel funds being available only for a total of 10 days during FY92.

As easily recognizable in Fig.s 2 and 3, the diurnal variations of the sensor signals are extremely small as the result of the replacement of isolation amplifiers with new products (Analog Devices 5B30 series isolated signal conditioner) in previous years. Except for the Cienega Winery site which still uses the old 284J amplifier, even the worst sites show variations less than 20 ppm H_2 equivalency during quiescent periods. The stable baselines make it possible to use the raw data (in point plots) to examine anomalies as shown.

Parkfield #1 and #2 sensors showed irregular changes starting on 10 February 1992, in coincidence with the start of heavy rainfalls and a large (5 mm) right lateral creep event at the same location as shown in Fig. 4. Although the exact patterns are different between the two sensors which are 50 feet apart, the changes were roughly concurrent. The signal changes of the #1 sensor are much more limited in time and magnitude than those of the #2 sensor. The #1 sensor was rebuilt and tested *in situ*

after burial on 24 Sept. 1991, so it was probably operating properly. The sand-filled borehole for this sensor is barely 1.5 meter deep because of obstruction by rocks, whereas the hole for the #2 sensor is about 2 meter deep. It is possible that a small difference in depth or in channeling makes a difference in the local soil hydrogen concentration in a minor event (about 100 ppm or less; the atmospheric H_2 concentration is 0.5 ppm). What really caused the minor anomalies is not clear. The signal of the #1 sensor returned to the baseline by 10 March, but minor irregular changes of the #2 sensor lingered on until mid-April. Rainfalls were frequent in the area until 23 March, but the persistency of the irregular changes of the #2 sensor for few more weeks beyond this date is puzzling.

Site maintenance was performed in early July right after the Parkfield Workshop held at Santa Cruz. The peaks marked "s.s." in Fig. 3 were the results of in-ground test of the sensors with a calibration gas mixture. The full extent of the sensor responses are not shown in the figure. These peaks are completely artificial and should be ignored. Some sensors (*eg* Gold Hill #2, Twisselman Ranch) exhibit a voltage depression to negative values immediately after a brief exposure to H_2 gas, followed by a gradual return to the baseline, as seen at the bottom of Fig. 3. This behavior is probably caused by the penetration of H_2 into the interior of the cell and resulting absorption of H_2 into the interior platinum coating of the cell assembly. Currently an improved sensor design to eliminate this effect is being tested in cooperation with a commercial vender.

Several minor (< 100 ppm) peaks of similar shapes were recorded by the Gold Hill #2 sensor stating on 28 July and ending in September. This was not reproduced by the #1 sensor, which was installed in 1982 and does not have the in-ground calibration provision. The last anomaly recorded by this sensor was in mid-July 1991. The #1 sensor probably needs reinstallation.

Before the M_L5.4 New Idria EQ (earthquake) of 25 Oct 1982 and the M_L6.7 Coalinga EQ of 2 May 1983, the Parkfield and Slack Canyon sites recorded a few thousand ppm peaks months in advance of the quakes (Sato et al., 1986, JGR, **91**,12315). Soil H_2 anomalies of comparable magnitudes were recorded at these and/or other sites along the San Andreas and Calaveras faults prior to the M_L5.7 Kettleman Hills EQ of 4 Aug 1985, M_L5.8 Tres Pinos EQ of 26 Jan 1986, M_L5.8 Mt. Lewis EQ of 31 March 1986, M_L5.2 Coalinga EQ of 14 Feb 1987, and M_L7.1 Loma Prieta EQ of 16 Oct 1989 (manuscript in preparation). The precursory times were dominantly less than 1 month and seem to be shorter for closer sites. If an earthquake of a similar magnitude is going to occur in Parkfield as generally anticipated, I expect soil H_2 anomalies of at least several hundred ppm will be recorded at multiple sites in the southern cluster of the monitoring network within a few months before the earthquake.

Water Geochemistry

Water geochemistry monitoring had serious problems in this reporting period due to the termination of field support by the local technical personnel for low-frequency experiments, budgetary restriction for me to spend an extended period of time in the field, and the lack of enthusiasm by the radon monitoring project, which initially agreed to take care of the well water pumping, to continue experiment in Parkfield.

Taylor Ranch: The telemetered records of water conductivity, dissolved CO_2, and dissolved H_2 obtained between May 1991 and May 1992 are shown in Fig. 5. The water flow record for the radon monitor is also shown in the figure because it gives information on the water supply condition. Before September 1991, the experimental system was running smoothly. In September and October 1991, the water supply became erratic. Even though my monitoring system has an automatic flow control device, the monitored parameters were affected with the stop-and-go water supply. The main PVC pipe broke on 22 Nov 1991 because the PVC pipe joint could not support the increased weight of the pipe line, which was lengthened every time the water level became deeper and the main pump had to be lowered.

Basically the well could not produce enough water needed (1 gallon/min for radon and 1/4 gallon/min for water geochemistry) in recent draught condition. In December 1991 I got the contractor started on the pipe replacement job and Chi-Yu King supervised the completion of the job. For durability, 3/4 " galvanized steel pipes are used for the new pipe line. The job was completed on 10 Jan 1992. The temporary increase of dissolved H_2 was due to the evolution of this gas by the reaction of water with the surface of the new steel pipe. On April 23, the pump went dry because the water level in the well became lower than the pump. This apparently caused excess stress on the dual metering pump (for fixing the water-air ratio for degassing) and its motor burned up. The entire system was shut down by the field crew. When I checked the site on July 3 the main pump was pumping the water to the conductivity meter because the radon monitor has been shut down and the total water demand has drastically been reduced. At my request, Rich Liechte turned the telemetry system back on August 3. So presently I am getting the conductivity data together with the soil hydrogen data from this site. There has been interesting changes in the conductivity since August 1992, but I have been unable to visit the site to determine how reliable the conductivity data are by on-site inspection and calibration. Other monitors can be turned back on with a few days of work. If the radon monitor is going to be put back into operation, however, the steel pipe must be extended by 100 feet or so to guarantee enough water supply. This is up to the radon project.

Miller Ranch: Telemetry went down between 15 Oct 1991 and 26 Feb 1992 and again on 2 Aug 1992. It has not been back since. The main pump went down before July 1992. The water conductivity and dissolved CO_2 channels in the telemetry were off scale for an unknown reason, though the voltages measured at the telemetry input were normal and being recorded on the on-site recorder. The problem is that I can not get the chart-paper from the recorder. For these reasons, the data are not shown in this report.

REPORTS

Sato M., 1991, Hydrogen and other non-radon geochemical monitoring: in NEHRP Summaries of Technical Reports v. XXXIII, USGS Open-file Report 92-258, 593-598.

Sato M., 1992, Anomalous changes in soil H_2 recorded in the Parkfield area since 1982: Eos, Trans. AGU, 1992 Fall Mtg., p. 397.

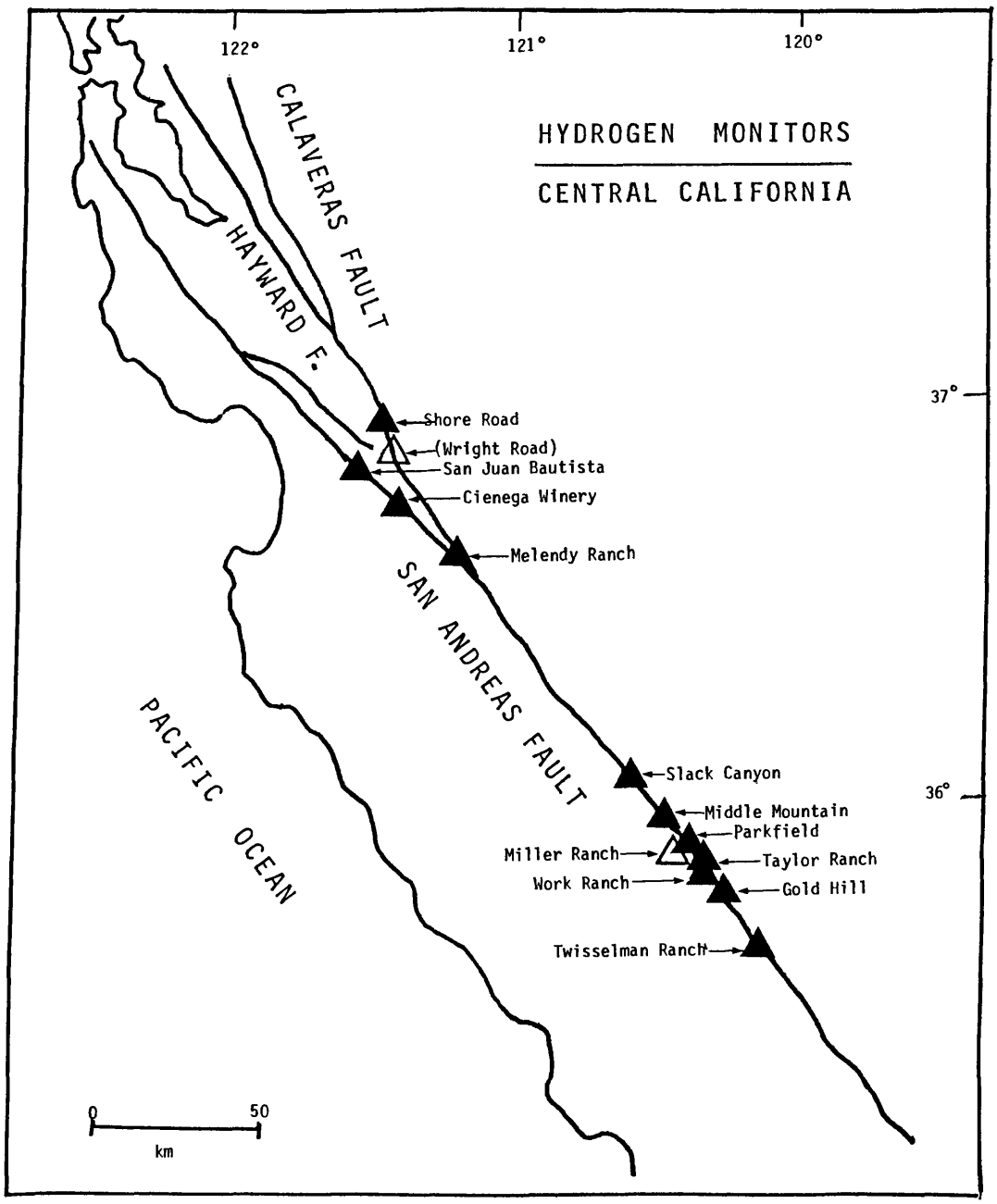

(FIG. 1) A map showing the locations of soil hydrogen monitoring sites in central California (filled triangles). The Wright Road site is no longerin operation. The Miller Ranch site is for water geochemistry only.

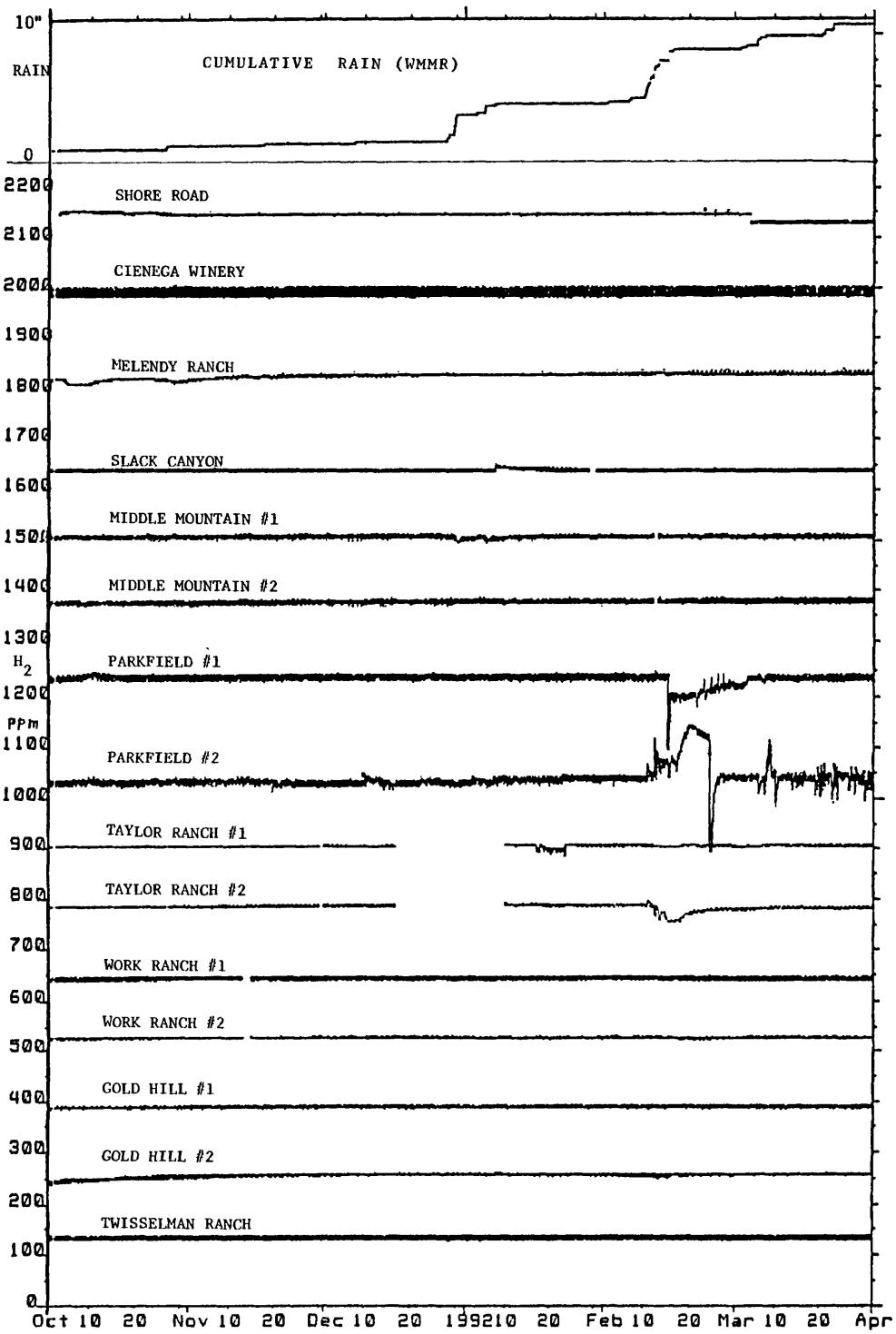

(FIG. 2) Soil hydrogen data recorded in central California between 1 October 1991 and 1 April 1992. The hydrogen concentration scale is in ppmv. The plots are composite and the relative levels of H_2 are arbitrary.

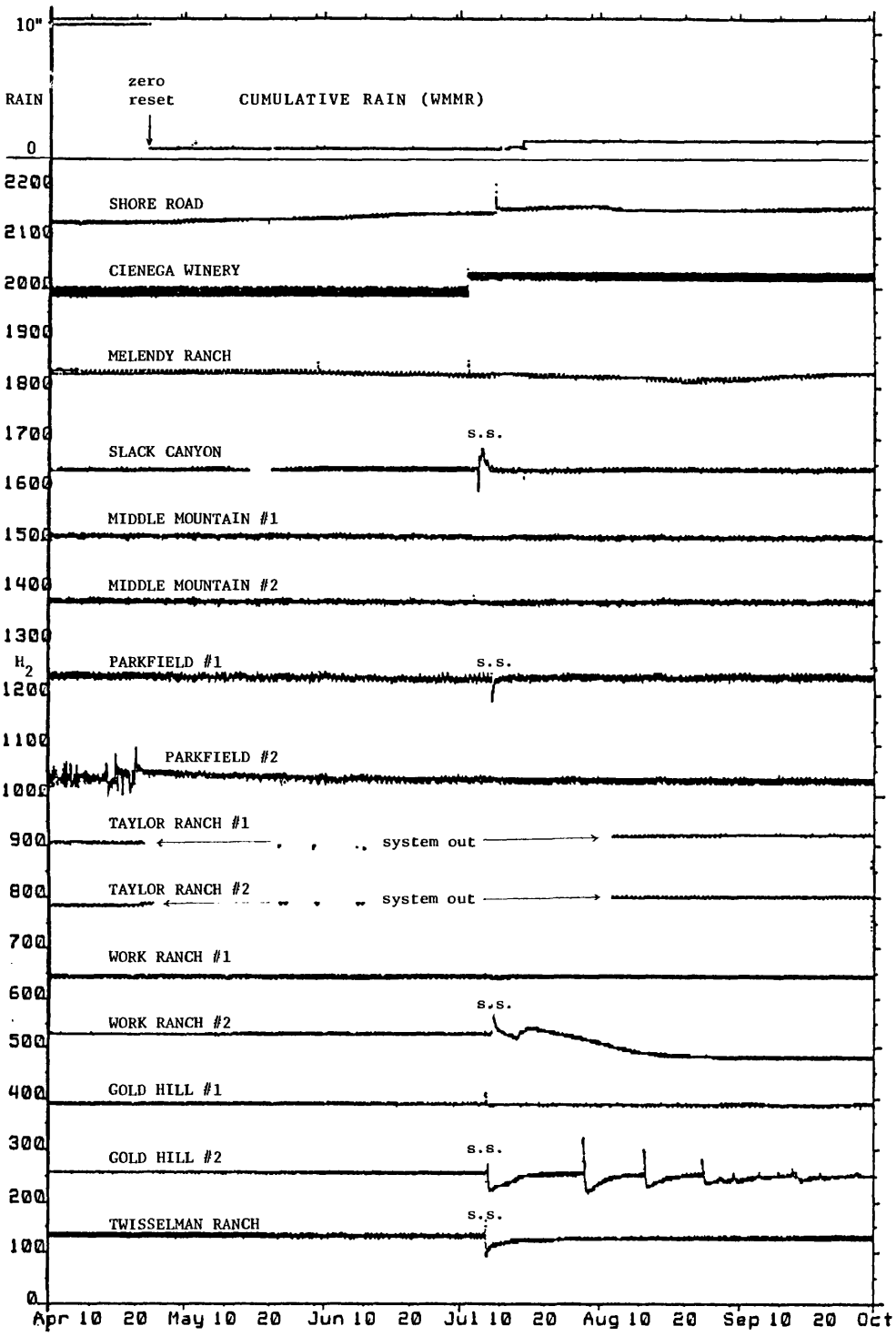

(FIG. 3) Soil hydrogen data recorded in central California between 1 April 1992 and 1 October 1992. The hydrogen concentration scale is in ppmv. The plots are composite and the relative levels of H_2 are arbitrary. The top trace is cumulative rain monitored at Middle Mountain. The notation "s.s." indicate servicing of the sensor and testing with calibration gas mixture.

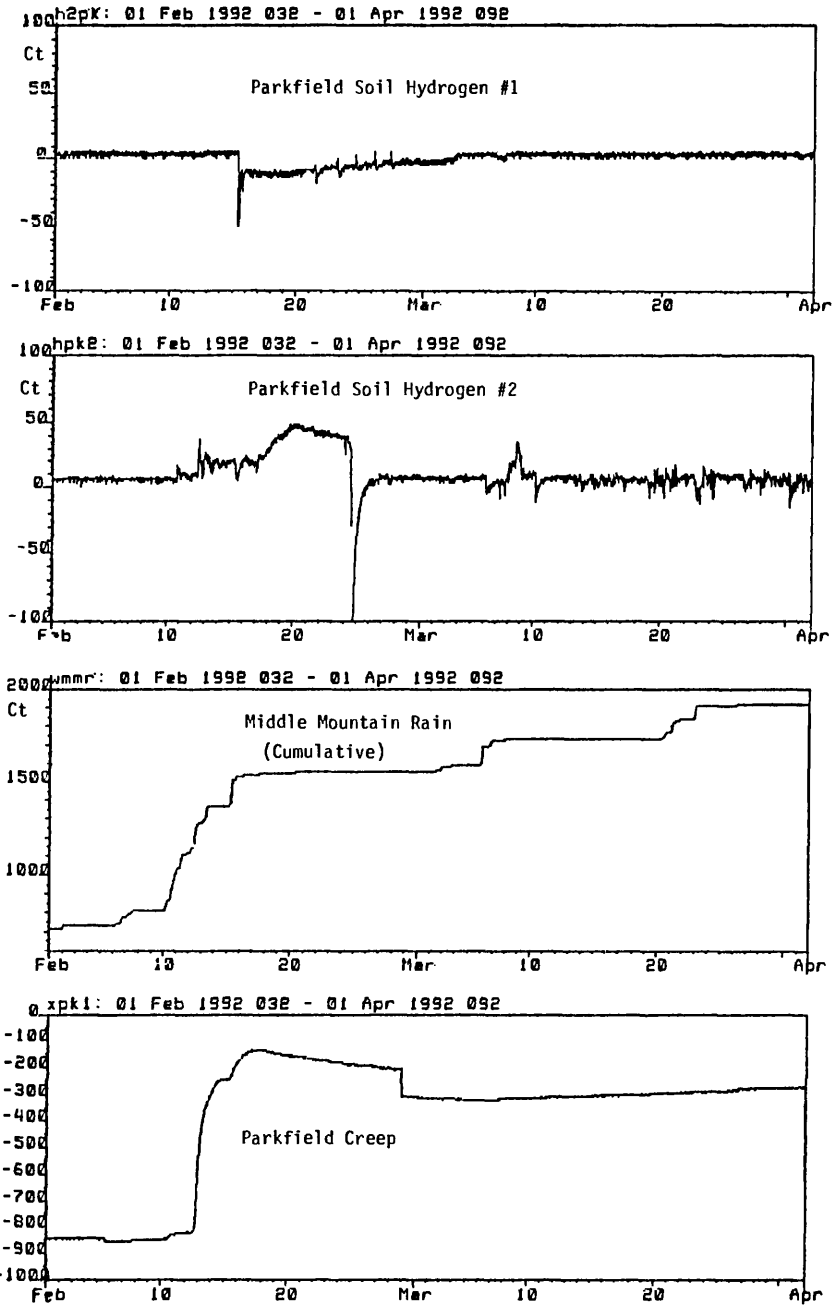

(FIG. 4) Time-coincidence relations between the rain and soil hydrogen sensors #1 and #2 and fault creep signals recorded at Parkfield (XPK1 site) in February and March 1992. Vertical axes are all in telemetry count.

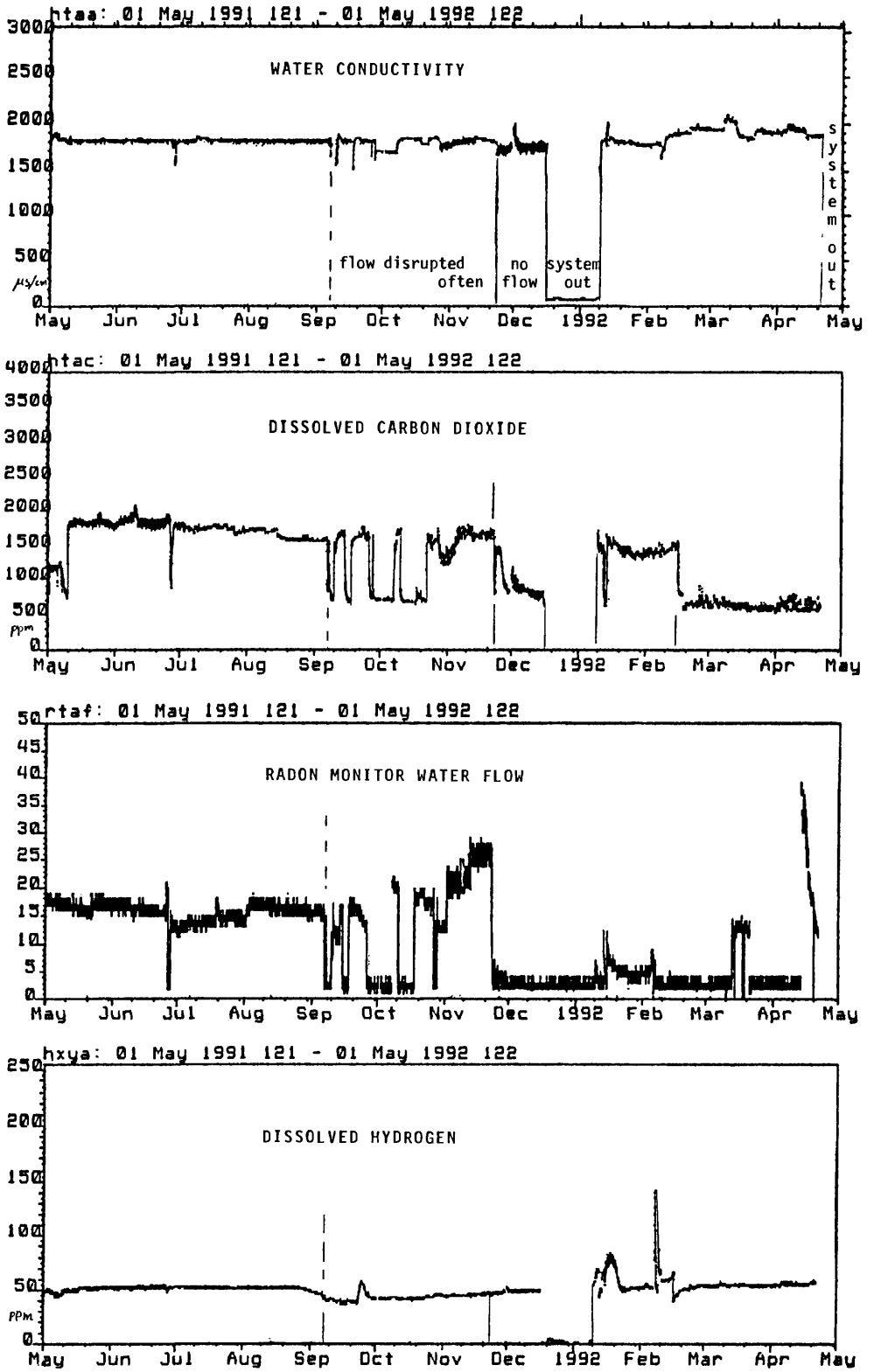

(FIG. 5) Water geochemistry data recorded at the Taylor Ranch site in a year period between 1 May 1991 and 1 May 1992.

SURFICIAL AND BEDROCK GEOLOGY IN THE MID-CONTINENT MISSISSIPPI VALLEY AND NEW MADRID SEISMIC ZONE

9510-10210
ART SCHULTZ, Project Chief
Branch of Eastern Regional Geology
U.S.Geological Survey
926 National Center, Reston, VA 22092
703-648-6501

INVESTIGATIONS

Research during FY 92 included geologic mapping and topical studies throughout the study area from St.Louis to Memphis with combined funding from the National Geologic Mapping Program and the National Earthquake Hazard Reduction Program,.

MAPPING INVESTIGATIONS

Geologic mapping in FY 1992 concentrated on three general areas. In southeast Missouri, detailed mapping in the Thebes area concentrated on structures that deform rocks and sediments of Paleozoic through Pleistocene(?) age. Detailed and reconnaissance mapping along the Ste. Genevieve fault was carried out along its length in Missouri. Detailed mapping and reconnaissance mapping in the St. Louis area concentrated on the Cap au Gres fault-fold and related structures. Portions of the Eolia 7.5 min. quadrangle were mapped in detail and the surficial and bedrock geology of the St. Louis 1:100,000 scale map was compiled from existing sources.

TOPICAL INVESTIGATIONS

A. Continuing study of deformation along the Ste. Genevieve fault zone included detailed mapping across the fault zone, quantification of mesoscopic (outcrop) deformation along the fault, and microstructural studies of deformed rocks from the fault zone.

B. Surface and sub-surface investigations of the Cap au Gres fault-fold and related structures in the St. Louis area, based on detailed and reconnaissance mapping and compilation of surface and sub-surface data, were completed.

C. Surficial geologic framework studies continued in the Memphis area with focus on loess and valley fill stratigraphy. Surface samples were collected and analyzed for age dating. Core drilling east and west of Crowleys Ridge near Memphis was completed and samples are now under study.

RESULTS

A. Ste. Genevieve fault zone: The Ste. Genevieve fault zone has been described as a high-angle block fault resulting from vertical uplift of Proterozoic basement,(Nelson and Lumm, 1985), as a left-lateral, strike-slip or transpressive wrench fault (Clendenin and others, 1987), as an extension of the Northeast Missouri Tectonic Zone (Simms and others, 1987), and as a continental transform fault associated with Reelfoot rifting (Kisvarsanyi, 1984).

New detailed mapping across the Ste. Genevieve fault zone in southeast Missouri has documented deformation styles characteristic of complex strike-slip faulting. The width of the fault zone and the number of fault strands changes along strike,

often within kilometer spacing. The orientation of rocks within the deformation zone is highly variable along strike and the amount of stratigraphic offset, the sense of stratigraphic offset and the intensity of mesoscopic deformation changes across individual fault strands along strike. These data were used to constrain several cross-section models showing the fault zone as complex flower structures. Orientation analysis of outcrop and map-scale 2nd order structures, such as clusters of contractional, extensional and strike slip faults, suggest left-lateral oblique strike slip as the dominant motion on the Ste. Genevieve fault. Microstuctures in quartzite, sandstone, and dolomite document cataclasis as the dominant deformation mechanism associated with faulting. In fault rocks, minor intracrystalline deformation consists of enhanced twinning in dolomite, undulose extinction, deformation banding and recrystallization.

Field and micro-structural evidence of multiple extensional-compressional (transtensional-transpressional?) episodes of fault movement consists of overprinting veins and tectonic stylolites. Evidence of multiple non-coaxial deformation consists of multiply deformed folds in the fault zones. These folds occur in lens shaped horses between fault strands and have non-parallel axial surfaces and steeply plunging axes. At one location, slickolite surfaces of variable orientation indicate that pressure-solution slip along fault and bedding surfaces occurred during tectonism. The mechanical significance of these features along the Ste. Genevieve fault is still under investigation; however, in one instance, slickolites were oriented sub-parallel to fold axes indicating multiple deformation periods associated with changes in stress orientation during strike-slip faulting.

Continued, focused detailed mapping in the Weingarten, Mo area of the Ste. Genevieve fault and synthesis of our structural data will be the FY93 agenda. At present, we concluded that our studies support regional-scale models relating the Ste. Genevieve fault to long-lived, recurrent activation associated with Reelfoot and New Madrid tectonism. Because documented seismicity has occurred in the vicinty of the Ste. Genevieve fault zone, we feel an analysis of the structural fabric will permit a comparison of past strain history with present stress conditions.

B. Memphis area: As part of our mapping and geologic framework studies in the Memphis area, two sites in the Mississippi Valley were core drilled to depths of 100-175 foot depths in order to define the three dimensional stratigraphic setting of the area, and to define surficial map units. Pleistocene(?) through Holocene fluvial and loessial deposits were recovered and description and sampling of the material is underway. The core hole locations occur on both the west and east side of Crowleys Ridge, thus these data may prove useful in constraining recent tectonic models that interpret the Ridge as a neo-tectonic feature.

C. Thebes area:

Geologic mapping of the Thebes 7.5 min. quadrangle, Missouri and Illinois (Thebes Gap area) has identified numerous north-

northeast- and northeast-striking faults that have had a long-lived and complex structural history. The faults are vertical and are located in an area of moderate recent seismicity at the northern margin of the Mississippi embayment, approximately 45 km north of the New Madrid seismic zone. Similar fault orientations, as well as recent seismicity and close proximity, clearly suggest a structural relationship between deformation in the Thebes area and tectonism associated with the New Madrid seismic area.

Following is a preliminary outline of tectonic events for the Thebes quadrangle:

1. Late Precambrian-Early Cambrian

Normal faulting is inferred from location of the area along the margin of the Reelfoot rift; no rocks of this age are exposed in the area.

2. Middle Ordovician

A episode of faulting during the Middle Ordovician is indicated by an increase in thickness of the Ordovician Girardeau Limestone in the vicinity of one fault, extreme variations on an erosional surface on top of the Ordovician Kimmswick Limestone across several faults, differential offset between Ordovician and younger formations on several faults, and west-northwest-striking fault-propagation folds found only in Ordovician-age rocks. Motion of the northeast-trending faults is left-lateral strike-slip. Evidence consists of a left-lateral strike-slip fault exposed in Grays Point quarry that is constrained in time by deposition of the Ordovician Cape La Croix Shale in a small graben on the structure (C. W. Clendenin, 1992, personal commun.). This fault was later reactivated by multiple pulses of dextral strike-slip motion (Diehl et al., in press.). Additional left-lateral fracture patterns are found only in Ordovician-age rocks at several locations in the Thebes quadrangle. The vergence direction between the dominantly north-northeast-striking faults in the Thebes area and the northeast-trending Reelfoot rift is indicative of a left-lateral ancestry to these structures.

3. Post-Middle-Devonian--pre-Cretaceous

On the Missouri side of the Mississippi River, in the vicinity of Chalk Bluffs, strongly faulted and rotated beds of the Devonian, Silurian, and Ordovician age are overlain above an angular unconformity by gently dipping, nondeformed Cretaceous strata. Although only constrained as post-Middle-Devonian--pre-Cretaceous, this deformation is probably the result of multiple periods of tectonism that include the Ouachita orogeny. Nearby, small pull-apart grabens that contain breccia blocks of Ordovician, Silurian, and Devonian rocks occur along right-stepping fault strands. This is indicative of right-lateral, strike-slip faulting.

4. Tertiary

Multiple episodes of deformation in the Thebes area involve Cretaceous, Paleocene, Eocene, and Pliocene-Pleistocene(?) age rocks, as well as Paleozoic units. A period of minor extension, indicated by numerous conjugate sets of normal faults with minor offset, affected Cretaceous and early Tertiary rocks. This was

followed by major right-lateral, strike-slip faulting that cuts all Tertiary units, including the Pliocene-Pleistocene(?) Mounds Gravel. En echelon north-south folds, east-west antithetic R' shears, and drag folds indicate right-lateral motion. Positive and negative flower structures are commonly revealed in cross section. Horizontal and subhorizontal slickenside striations and mullions on fault surfaces are numerous. Beds of Cretaceous and Tertiary units (including Pliocene-Pleistocene Mounds Gravel) are strongly rotated (as much as 90 degrees) adjacent to major faults. Some high-angle, strike-slip fractures have developed after rotation of beds. In some outcrops, older Tertiary units have been rotated more than younger units. Right-stepping fault strands have produced pull-apart basins where Tertiary strata was deposited.

5. Quaternary and Recent

Stewart (1942) showed that loess was involved in faulting in an area approximately 6 km southwest of the Thebes quadrangle. Although not conclusive, there are other suggestions that faults cut the loess deposits which largely cover the uplands of the Thebes area. At several locations, loess may be interpreted to be offset by known faults however, the blanket-like and unconsolidated nature of loess precludes a definitive fault explanation without drilling, trenching or seismic data. Other supporting evidence for recent faulting consists of visible traces of known faults on SLAR images. This is a proposed topic to be addressed via drilling and trenching during the next year.

Other suggestions for the fault deformation of Quaternary deposits is found in Mississippi River alluvium in the Thebes Gap area. Recent drilling by Union Pacific Resources shows thickening of Quaternary alluvium across known faults. One drill hole penetrated approximately 160' of alluvium which is more than 50' in excess of what the U.S. Mississippi River Commission (Fisk, 1945) indicates is present in the river channel, and is more than twice the thickness delineated in nearby drill holes. This anomalously thick section lies between two known faults and suggests that they have been active during the Quaternary.

There is moderate present-day seismicity in the Thebes quadrangle and vicinity (Stover, 1987, 1988; Stover and Brewer, 1991). On 9/26/90, an earthquake of magnitude 4.8 (md) occurred just west of the Thebes quadrangle; focal mechanism analysis indicated that motion was right-lateral strike slip with a north-northeast azimuth (Chiu, 1990).

D. Eolia quadrangle:

Preliminary results indicate that the Cap au Gres structure, a faulted monoclinal flexure, bifurcates westward into multiple structures, one of which is the Lincoln fold. This interpretation is supported by regional structural contours on the top of the Ordovician St. Peter Sandstone. Timing of deformation is constrained only as post-Osagean (Mississippian). Quaternary glacial till and loess cover structures with no apparent offset.

E. St. Louis 30X60 min. quadrangle:

The bedrock geology of the St. Louis 30X60 min. quadrangle has been compiled at 1:100,000 scale. Accompanying the

compilation is a review of stratigraphy of the area, a magnetic anomaly map, seven cross sections based on existing well data, and a structural interpretation. Field work in the vicinity of Alton, Illinois was performed to supplement the compilation and mapping done by Rubey (1952), and to study a series of strike-slip faults exposed along the river bluffs. Subsurface data, drill records and geophysical surveys, have been used to model the tectonics of the area.

References Cited

Chiu, J., 1990, A high resolution PANDA experiment in the central New Madrid seismic zone (abs): Geological Society of America Abstracts with Programs, v. 22, no. 7, p. A17.

Clendenin, C.W., Niewendorp, C.A., and Lowell, G.R., 1987, Reinterpretation of faulting in southeast Missouri: Geology, v. 17, no. 3, p. 217-220.

Diehl, S.F., Throckmorton, C.K., and Clendenin, C.W., in press., Significance of recurrent fault movement at Grays Point quarry, southeast Missouri (abs): Geological Society of America North-Central Section Abstracts with Programs

Fisk, H.N., 1945, Geological investigation of the alluvial valley of the lower Mississippi River: War Department, Army Corps of Engineers, 78 pp.

Kisvarsanyi, E.B., 1984, contribution to Precambrian Geology No. 14, Part B, Missouri Department of Natural Resources, 19p.

Nelson, W.J., and Lumm, D.K., 1985, Ste. Genevieve fault zone, Missouri and Illinois: Illinois State Geological Survey Contract/Grant Report 1985-3, 94p.

Rubey, W.W., 1952, Geology and mineral resources of the Hardin and Brussels quadrangles, (Illinois): U.S. Geological Survey Professional Paper 218, 179 pp.

Simms, P.K., Kisvarsanyi, E.B., and Morey, G.B., 1987, Geology and metallogeny of Archean and Proterozoic basement terranes in the northern midcontinent, U.S.A.-and overview: U.S. Geological Survey Bulletin 1815, 15p.

Stewart, D.R., 1942, The Mesozoic and Cenozoic geology of southeastern Missouri: Missouri Geological Survey and Water Resources, unpublished manuscript in Missouri Department of Natural Resources Archives, 115 pp.

Stover, C.W., 1987, United States earthquakes, 1983: U.S. Geological Survey Bulletin 1698, 196 pp.

Stover, C.W., 1988, United States earthquakes, 1984: U.S. Geological Survey Bulletin 1862, 179 pp.

Stover, C.W., and Brewer, L.R., 1991, United States earthquakes, 1985: U.S. Geological Survey Bulletin 1954, 170 pp.

REPORTS PUBLISHED

Schultz, A.P., Baker, G.S., and Harrison, R.W., 1992, Deformation associated with the Ste. Genevieve fault zone and Mid-Continent tectonics(abs): Geological Society of America Abstracts with Programs, v. 24, no. 7, p. A181.

Harrison, R.W., and Schultz, A.P., 1992, Faulting at Thebes Gap, Missouri-Illinois: implications for New Madrid tectonism: Geological Society of America Abstracts with Programs, v. 24, no. 7, p. A191.

Harrison, R.W., and Schultz, A.P.(compilers), in press, Bedrock and surficial geologic map of the St. Louis 30X60 min. quadrangle: U.S. Geological Survey Miscellaneous Field Studies Map MF-xxx, text, 2 map sheets and accompanying cross sections and figures.

Markewich, H.W., Millard, H.T.,Jr., Pavich, M.J., Rodbell, D.T., Rich, F.J., Rutledge, E.M., Ward, L., VanValkenburg, S., and Wysocki, D., 1992, Chronostratigraphic and paleoclimatic data for Quaternary loessial and fluvial deposits in the Mississippi River Valley of Arkansas and Tennessee: Geological Society of America Abstracts with Programs, v. 24, no. 7, p. A50.

Maat, P.B., Markewich, H.W., McGeehin J.P, Millard H.T., Jr., Pavich, M.J., Reynolds, R.L., Rich, F.J., Rodbell D.T., Rosenbaum, J.G., Ruben, Meyer, Rutledge, E.M., Van Vakenburg, S.G., Ward, L. B., Wysocki, D.A., in press, Progress report on chronostratigraphic and paleoclimatic studies, middle Mississippi River Valley, eastern Arkansas and western Tennessee: U.S. Geological Survey Open-File Report 93-xxx.

GEOMORPHIC EVALUATION OF THE NEW MADRID SEISMIC ZONE

Award Number 14-08-0001-G2119

S.A. Schumm and Karin J. Fischer
Resource Consultants & Engineers, Inc.
P.O. Box 270460
Fort Collins, Colorado 80527

PURPOSE OF PROJECT

This study will use geomorphic techniques in an attempt to identify areas of past and active tectonics in the New Madrid Seismic Zone (NMSZ) between Hickman, KY and Osceola, AR. This will be accomplished by identifying anomalous reaches of Mississippi River and anomalous channel, drainage network, and drainage-ditch patterns and longitudinal profiles. Project members are Stanley A. Schumm and Karin J. Fischer.

INVESTIGATIONS

Data have been collected on Mississippi River dimensions and patterns for the period 1765 to 1930. High and low-water profiles have been obtained for the period from about 1960 to 1988.

Topographic maps have been used to study drainage patterns and the morphology of Crowleys Ridge north of Jonesboro.

Topographic surveys completed in 1924 of the Little River Drainage District are being analyzed to determine if there are anomalous gradient changes that can be associated with surface deformation.

RESULTS

Mississippi River

The Mississippi River between Cairo and Helena can be divided into 14 reaches based upon channel pattern, sinuosity variability since 1765, and valley slope (Figure 1). Analysis of Mississippi River data suggest that the river is controlled in some reaches by geologic controls. For example, the marked change of gradient of the 1974 and 1988 low-water profiles (Figure 2) and the change of Mississippi River pattern and valley slope below New Madrid coincides with a fault mapped near that location (Heyl and McKeown, 1978). The geomorphic evidence strongly supports the interpretations of Heyl and McKeown.

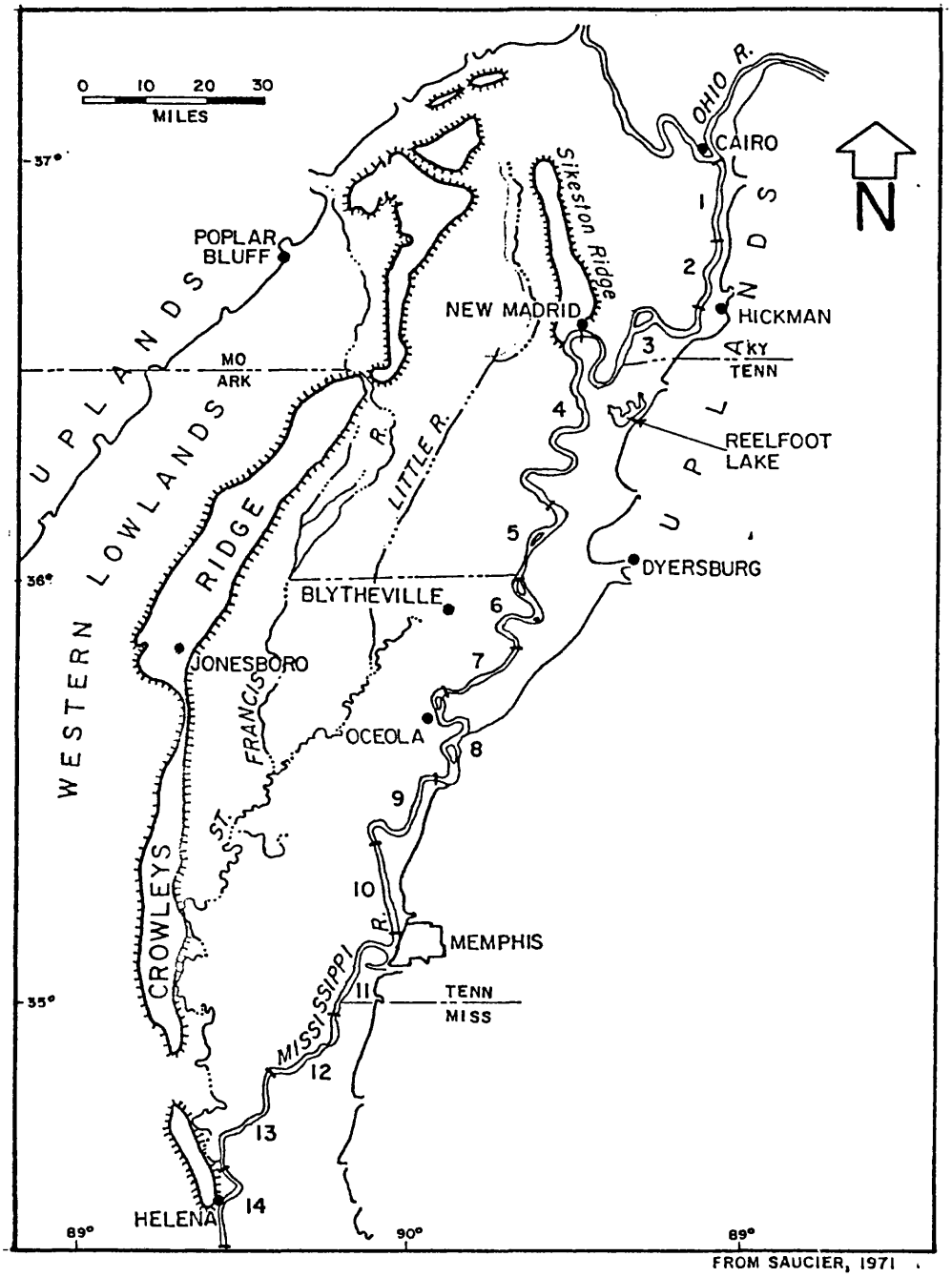

Figure 1. Index map of study area showing numbered Mississippi River reaches.

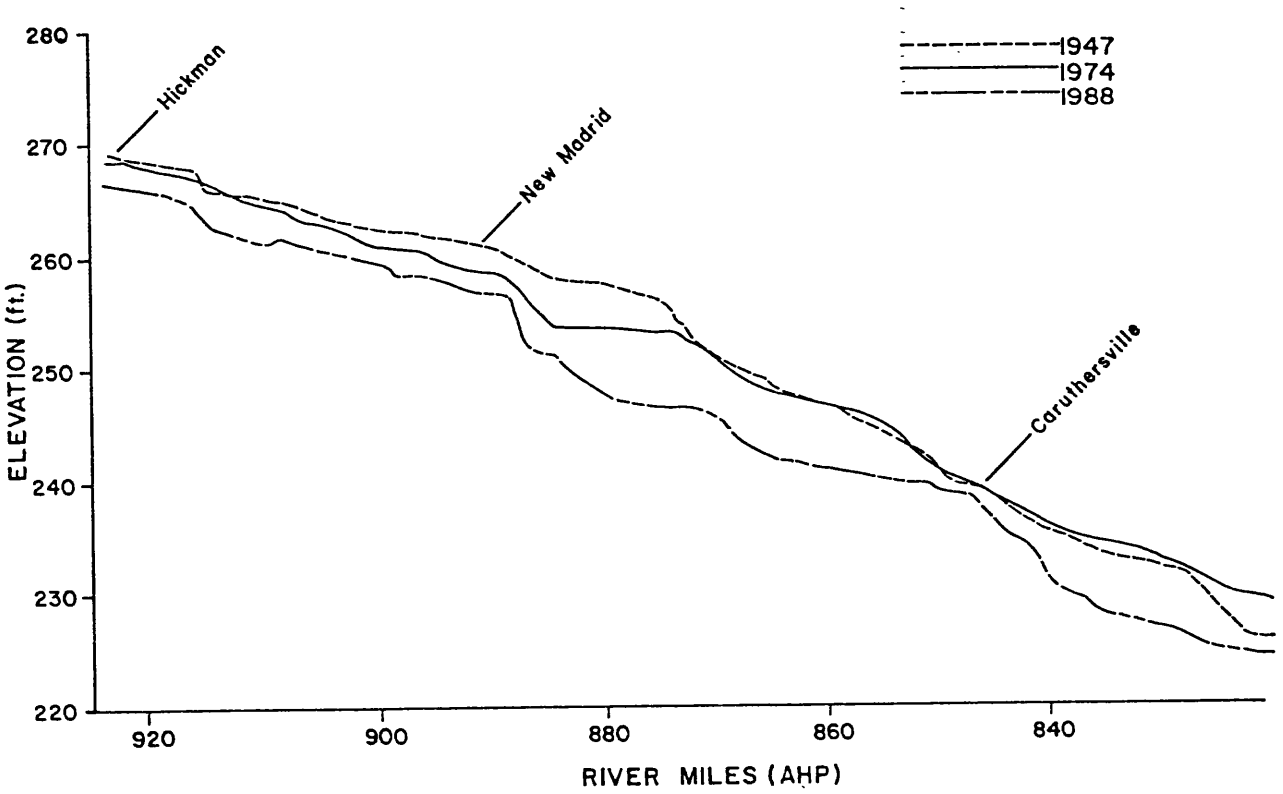

Figure 2. Mississippi River low-water profiles.

Alluvial Valley

The rivers of the Mississippi River alluvial valley show marked changes of flow direction that are atypical of alluvial rivers. Angular bends suggest influences other than hydrologic on Little River, St. Francis River, and Black River. For example, between Lonestar and Bragg City, the width of the floodplain of Little River narrows, and there is an abrupt turn to the west near Wardell.

Preliminary results suggest that drainage ditch profiles have been affected by surface deformation in the Little River Drainage District.

Cross sections of Crowleys Ridge north of Jonesboro strongly suggest that the Ridge is structurally controlled. North of Jonesboro it appears to be a fault block with the major scarp on the west and the bulk of the Ridge drainage is to the east. Between Rector to the St. Francis River water gap, the drainage is equally divided to east and west, but north of the St. Francis River, the scarp is to the east and drainage is to the west. These observations support the conclusions of Cox (1988a, b) and Van Arsdale (1991, 1992) that the Ridge is faulted at and to the south of Jonesboro.

In summary, numerous Mississippi River, Black River, St. Francis River, and Little River anomalies have been identified in the Mississippi Embayment between Hickman, Kentucky to the north and Osceola, Arkansas to the south. Individual anomalies may be related to subsurface faulting or other types of deformation such as uplift or downwarping, as well as to differential compaction over structures or the effects of groundwater withdrawal. Cox (1988b) suggested that the southern end of the northern segment of Crowley's Ridge near of Jonesboro is faulted and that it is part of a northwest-southeast megatrend. An extension of this trend coincides with the boundary between Mississippi River Reaches 9 and 10 south of the study area (Figure 1)

Other anomalies occur along lines that suggest other major structural controls. For example, a line extending from the Caruthersville bend intersects the Little River anomalous bend and then continues to the northwest through the St. Francis River water gap. Another trend extends from the faulted Barfield Bend area, which is the boundary between Mississippi River Reaches 5 and 6 (Figure 1) to the Little River and then through Crowley's Ridge at the structural boundary, near Rector.

REFERENCES

Cox, R.T., 1988a, Evidence of Quaternary ground tilting associated with the Reelfoot Rift zone, northeast Arkansas: Southeastern Geology, v. 28, p. 211-224.

Cox, R.T., 1988b, Evidence of late Cenozoic activity along the Bolivar-Mansfield tectonic zone, Midcontinent, USA: The Compass, v. 65, p. 207-213.

Heyl, A.V., and McKeown, F.A., 1978, Preliminary seismotectonic map of central Mississippi Valley and environs: U.S. Geological Survey Miscellaneous Field Studies Map, MF-1011.

Van Arsdale, R., 1991, Tectonic deformation revealed in baldcypress trees at Reelfoot Lake, Tennessee: Report prepared for Division of Engineering, Office of Nuclear Regulatory Research, U.S. Regulatory commission, Contract No. NRC-04-90-111, 12 p.

Van Arsdale, R.B., 1991, Preliminary study of the subsurface structure of Crowley's Ridge, northeast Arkansas (abstr.) Program and Abstracts 63rd Annual Meeting, Eastern Section, Seismological Soc. America, p. 58.

Van Arsdale, R.B., Schweig, E.S., Kanter, L.R., Williams, R.A., Shedlock, K.M., and King, K.W., 1992, Preliminary shallow seismic reflection survey of Crowley's Ridge, northeast Arkansas: Seismological Soc. America, Bull., in press.

SEISMOTECTONICS OF THE CENTRAL UNITED STATES

9950-01895

Eugene S. Schweig, III
U.S. Geological Survey
c/o Center for Earthquake Research and Information
Memphis State University
Memphis, TN 38152
(901) 678-2007

INVESTIGATIONS

This project addresses major gaps that currently exist in our understanding of the tectonic setting, seismic source zones, and recurrence intervals of damaging earthquakes in the central U.S., and the integration of surface and subsurface data into seismotectonic models. 1992, the first year of this project, was largely dedicated to 1) analysis of trenching and surface mapping data collected in the Bootheel lineament area during 1991 and publication of results; 2) excavations and examination of drainage ditches in areas most likely to exhibit paleoliquefaction features; and 3) continuing analysis of shallow seismic reflection data collected in the New Madrid seismic zone during 1990 and 1991.

RESULTS

Analysis of trenching and surface mapping data collected in the Bootheel lineament — The Bootheel lineament is a 135-km-long feature that may represent ground rupture that occurred as a consequence of the 1811-1812 New Madrid earthquakes. The morphology and en echelon pattern of the north-northeast-trending lineament are suggestive of strike-slip displacement on a buried fault. Two long and one very short trenches were excavated across the Bootheel lineament toward the end of 1991. In 1992 a paper on the results of these studies was completed (Schweig et al., 1992a). Vertically displaced strata were observed in one of these trenches, but the displacement could be due to collapse caused by the removal of liquefied sand from below. Shear zones exposed in the two other trenches, however, do not appear to be directly related to liquefaction and may represent near-surface deformation associated with deeper seated deformation.

Excavations and examination of drainage ditches in areas most likely to exhibit paleoliquefaction features — In collaboration with Martitia Tuttle of Lamont-Doherty Geological Observatory, we found at least three sites with evidence strongly suggestive of pre-1811 earthquake-induced liquefaction. Two of the sites were in Army Corps of Engineers drainage ditches, just north of the Missouri/Arkansas border (Sites 1 and 2, Figure 1). The features we have found are complex, multi-generation structures. In the most promising site (Figure 2), there is evidence for four liquefaction events. The de-

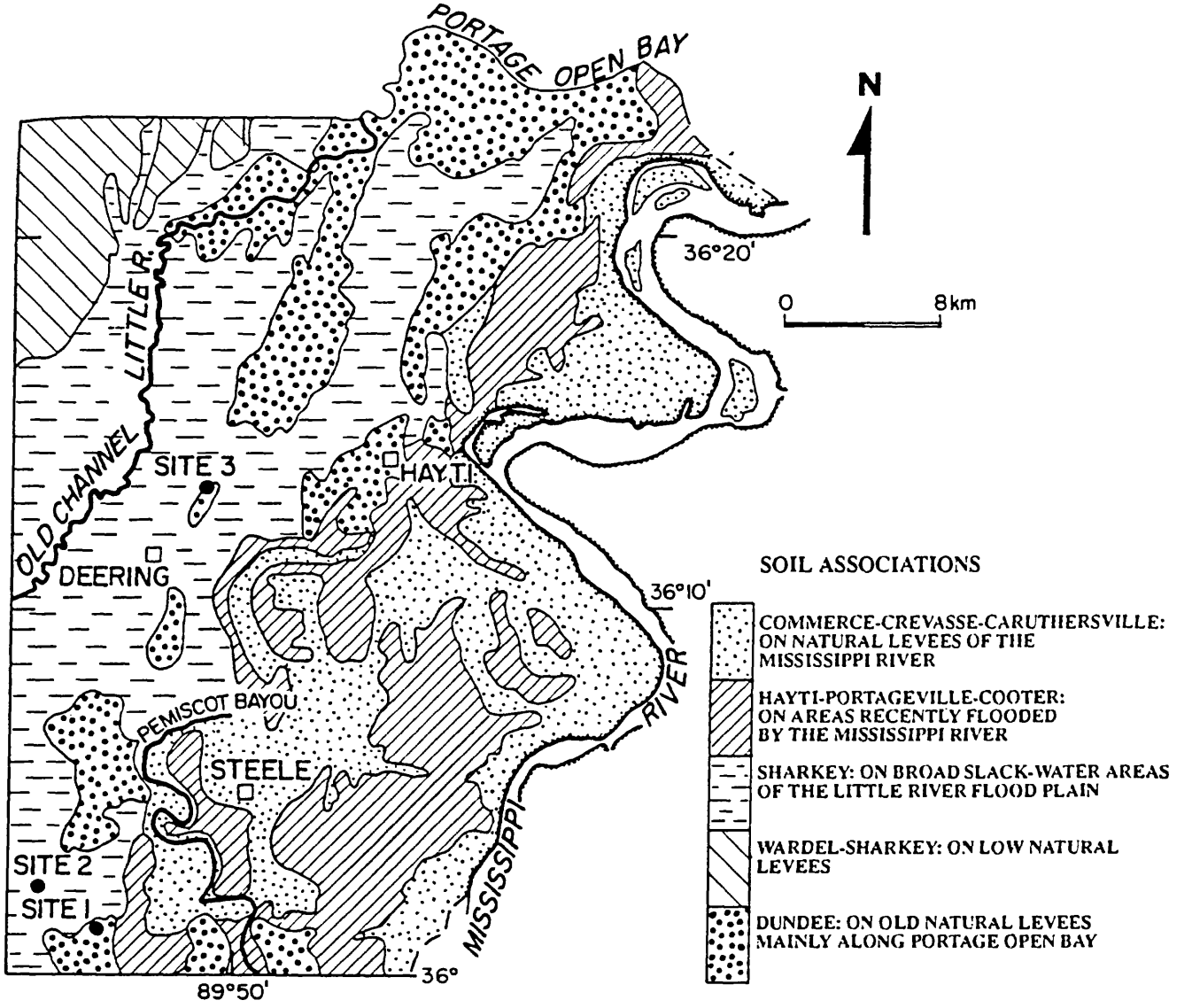

Figure 1. Map of soil associations in Pemiscot County, Missouri (Brown, 1971, Soil survey of Pemiscot County, Missouri: U.S. Department of Agriculture) and the locations of sites where we have found liquefaction that may predate the 1811-1812 earthquakes. Features at Sites 2 and 3 are described in the text and in a log of Site 2 is shown in Figure 2.

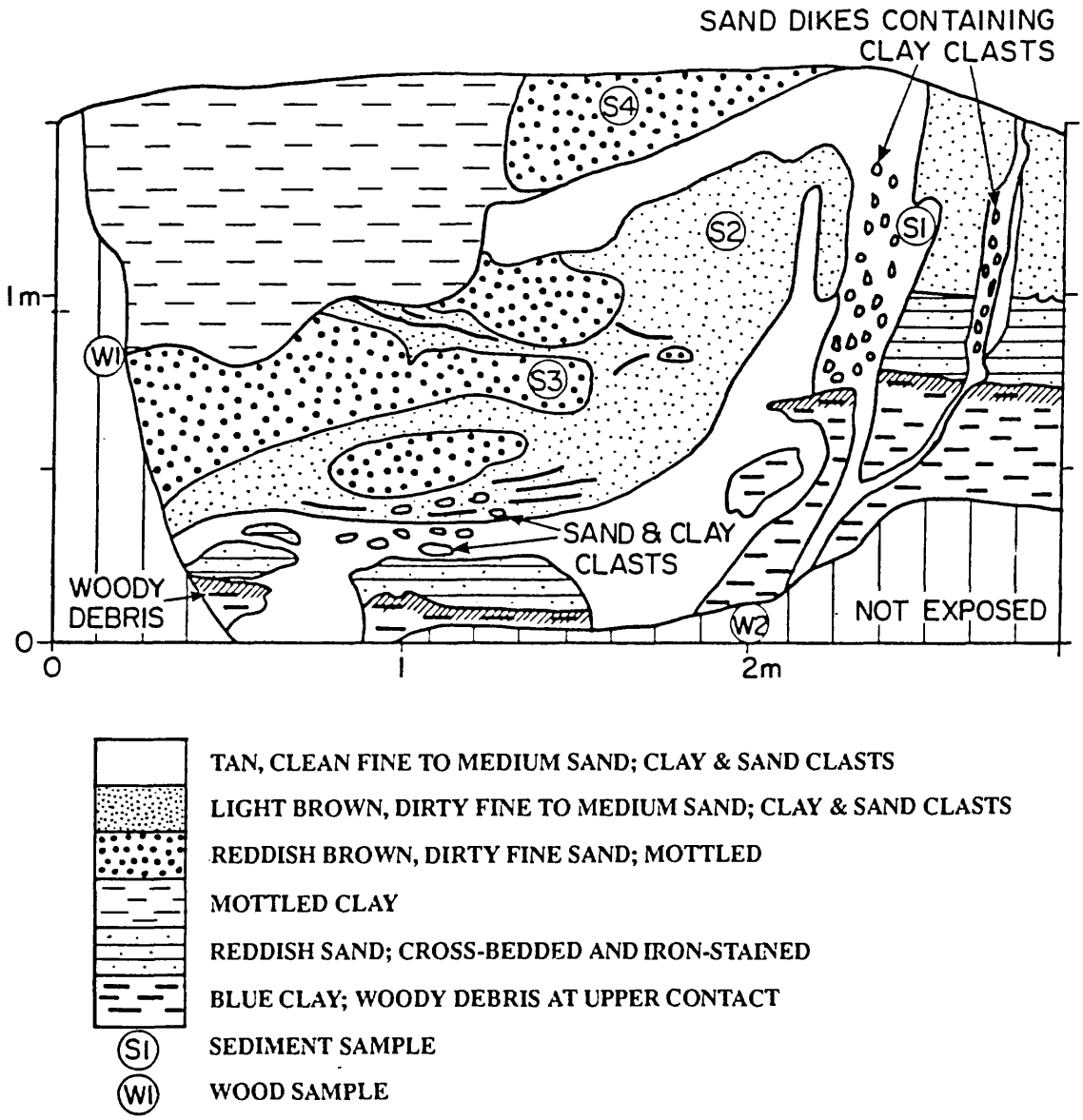

Figure 2. Log of exploratory trench near the Missouri-Arkansas border. At least three generations of liquefaction features occur at this location. The older two generations exhibit pedologic characteristics indicative of advanced (pre-1811) age. Radiocarbon dating of wood removed from the paleosol beneath the section yielded an age of 4,930±160 C-14 years (sample W1). Sample W2, which is younger than the older two generations of liquefaction, yielded an age of 205±81 C-14 years.

posits show increasing soil development and decreasing pH with increasing age as suggested by cross-cutting relationships. The youngest event is likely dates from 1811-1812. The oldest two events cannot be distinguished using these criteria and may be nearly contemporaneous in age. New ^{14}C age determinations show that all of the liquefaction deposits are younger that about 5,000 years old (sample W2, Figure 2), and that the older three formed prior to 205 ± 81 C-14 years BP (sample W1, Figure 2), yielding a minimum age of about 125 years (or about 1825 AD). Thus, we have not yet conclusively demonstrated a pre-1811 origin for these deposits.

We also excavated a 100-m-long trench across the Bootheel lineament in an area where the lineament shows its most prominent geomorphic expression, a 1-m-high scarp (Site 3 in Figure 1). Although this trench had to be abandoned because of a major problem with collapse of the walls, we were able to collect some data in this very unusual exposure. The material at the surface, which has been mapped by earlier investigators as 1811-1812 extruded sand, actually displays a well-developed soil. An Indian midden was dug into the surface and contained pottery that is clearly pre-1811. We found no clear evidence for faulting along the scarp, nor any evidence for material differences on either side as might be expected if it were a fluvial scarp. Thus, we do not yet know the genesis of the scarp, but suspect it predates the 1811-1812 events. Several dikes were seen terminating about 10-20 cm below the surface, although none actually penetrate to the ground surface. All of these dikes have significant soil development, some more than others, suggesting two generations of dike intrusion; both generations appear older than typical 1811-1812 liquefaction. Unfortunately, no datable material was found that could establish the ages of these dikes before the trench had to be closed.

Analysis of shallow seismic reflection — In collaboration with Kaye Shedlock (USGS), Roy VanArsdale (University of Arkansas), Lisa Kanter (Memphis State University) and Gene Luzietti (formerly USGS), shallow seismic reflection data (Mini-SOSIE) were collected in 1990 and 1991 along the Bootheel lineament, Crowley's Ridge, the Crittenden County fault zone, as well as several other targets in northeastern Arkansas, southeastern Missouri, and western Tennessee. This project is primarily responsible for lines collected along the Bootheel lineament (Schweig et al., 1992b). In particular, the Bootheel lineament survey was undertaken to determine if the lineament can be shown to be associated uniquely with subsurface faults with geologically recent offset.

We have interpreted the 1990 data to show a complex zone of strike-slip faulting and gentle folding consisting of multiple flower structures, with deformation at least as young as an Eocene/Quaternary unconformity. Some deformation appears to continue into the Quaternary section. Processing of the 1991 data is not yet complete, due to the large volume of data collected by the USGS that year. A preliminary stack of a very high resolution reflection line using a shotgun source, however, appears to confirm offset horizons at the Eocene/Quaternary unconformity and above.

REPORTS:

Ellis, M. A. and Schweig, E. S., III, 1992, Tectonic setting of active deformation and the 1811-1812 earthquakes in the New Madrid region (abstract): Seismological Research Letters, v. 63, p. 50.

Marple, R. T., and Schweig, E. S., III, 1992, Remote sensing of alluvial terrain in a humid, tectonically active setting: the New Madrid seismic zone: Photogrammetric Engineering and Remote Sensing, v. 58, p. 209-219.

Schweig, E. S., III and Ellis, M. A., 1992a, Distributed faulting along the Bootheel lineament — smoothing over the rough spots in the New Madrid seismic zone (abstract): Seismological Research Letters, v. 63, p. 50.

Schweig, E. S. and Ellis, M. A., 1992b, The Bootheel lineament, the 1811-1812 New Madrid earthquake sequence, and modern seismicity (abstract): Geological Society of America Abstracts with Programs, v. 24, p. A153.

Schweig, E. S., III, Marple, R. T., and Li, Y., 1992a, An update of studies of the Bootheel lineament in the New Madrid seismic zone, southeastern Missouri and northeastern Arkansas: Seismological Research Letters, v. 63, p. 277-284.

Schweig, E. S., III, Shen, F., Kanter, L. R., VanArsdale, R. B., Luzietti, E. A., Shedlock, K. M., and King K. W., 1992b, Shallow seismic reflection survey of the Bootheel lineament area, southeastern Missouri: Seismological Research Letters, v. 63, p. 285-296.

SALTON TROUGH TECTONICS AND QUATERNARY FAULTING

9910-01292

ROBERT V. SHARP
BRANCH OF ENGINEERING SEISMOLOGY AND GEOLOGY
U.S. GEOLOGICAL SURVEY
345 MIDDLEFIELD ROAD, MS 977
MENLO PARK, CALIFORNIA 94025
415/329-5652

Investigations

1) Geologic mapping of the southeastern San Jacinto fault splays in the Western Imperial Valley.

2) Post-1987 afterslip on the Superstition Hills fault and the eastern Elmore Ranch fault.

3) Triggered fault displacements in the Imperial Valley following the 1992 landers earthquake.

4) Surface faulting associated with the 28 June 1992 Landers earthquake.

Results

1) Geologic mapping at 1:24,000 scale of the Kane Spring NW quadrangle is about 70 per cent completed. This is one of the most complexly faulted areas within the broad zone of Quaternary shearing in the southeastern San Jacinto fault zone.

2) After a lapse of 316±5 days, during which most of the Superstition Hills fault continued to creep at a slow rate($\leq$0.3 mm/mo.), a relatively large creep event with surface fracturing occurred along a 22-km length of the fault. Only the southernmost kilometer remained unbroken. The maximum right-lateral slip was about 1.3 cm. Although the Wienert fault (a right-stepover southeastward continuation of the Superstition Hills fault) is known to be right-laterally creeping as well, creep events large enough to produce surface fractures have not yet been identified on it.

During this report period, the eastern branch of the Elmore Ranch fault only locally showed apparently steady background creep up a maximum rate of about 0.2 mm/mo. No creep events with surface fractures were detected until the third day

after the 28 June Landers earthquake when an apparently triggered offset was observed. Although fracture-producing movements had previously been documented on this fault, none had been simultaneous with surface offsets along the Superstition Hills fault until the 28 June displacement.

3.) Three historically active faults in western Imperial Valley slipped at the surface in association with the M_s 7.5 Landers earthquake. New right-lateral displacement took place along nearly all of the 1987 rupture on the Superstition Hills fault (22 of 23 km) and a small segment of the 1968 Coyote Creek fault rupture (2.5 of 30 km) near the Ocotillo Badlands. The northeast-trending eastern branch of the Elmore Ranch fault slipped left-laterally over 6.5 km of its 9.5 km-long 1987 surface break. In the order of naming, the maximum horizontal slip components observed were 1.3, 1.3, and 0.7 cm, respectively. These maxima are similar to those of previously triggered slip events in the region. Fracturing on the Superstition Hills fault was observed 1.3 hours after the Landers mainshock, and it was not present during the previous evening. By their similar freshness, the other breaks are judged to be coseismically triggered rather than due to pre-Landers creep events. No evidence of triggered slip was found along the Imperial, Wienert, Superstition Mountain, west strand of the Elmore Ranch, or Extra faults.

Time elapsed since the earlier known creep events for each fault are 39 ± 5, 1685 ± 2, and 299 ± 15 days, respectively. Although the Superstition Hills fault was thus at a freshly lowered stress state, it nevertheless slipped again when triggered, as did the Imperial fault before and during the 1987 Superstition Hills earthquake sequence. Triggered slip on a northeast-trending fault is novel in this event, but earlier post-1987 slip measures on the eastern Elmore Ranch fault had already established its creeping behavior and dominance in the group of left-lateral conjugate breaks. The spatial correlation of triggered movements with afterslip along faults remains intact.

4) The mapping of the extensive surface rupturing and the measurement of displacement in this team effort are reported elsewhere in this volume.

Reports

Sharp, R.V., 1992, Surface faulting in the Imperial Valley triggered by the 1992 Landers, California, earthquake [abs.]: EOS, AGU Fall Meeting, San Francisco, December 1992.

Staff, U.S. Geological Survey, 1992, Pattern of surface ruptures associated with the 28 June 28, 1992, Landers earthquake [abs.]: EOS, AGU Fall Meeting, San Francisco, December 1992.

11/92

Systems Analysis of Geologic Rate Processes:

SPACE-TIME MODELS, COUPLED OSCILLATORS, AND GENETIC CODES: NONLINEAR DYNAMICS OF EARTHQUAKE RECURRENCE PATTERNS

9980-70138

Herbert R. Shaw
Branch of Igneous and Geothermal Processes, U. S. Geological Survey
MS-910, 345 Middlefield Road, Menlo Park, CA 94025
(415) 329-5245

Objective: The objective of this project is to develop models that explain the earthquake process in terms of emerging concepts of nonlinear dynamics. Examples of this approach have been given in many previous Technical Reports of NEHRP, and in papers cited here. The crucial question in the evaluation of earthquake recurrence patterns is spatiotemporal scaling. Recent collaboration with Bernard Chouet (EVE-SIS) on magma-related seismicity in Hawaii has demonstrated that a model of nonlinear coupled oscillations explains a wide range of magma-tectonic recurrence phenomena, ranging from long-period earthquakes to the periodic growth of the Hawaiian Ridge (Shaw and Chouet, 1991). The scaling is logarithmic and universal, resembling the power-law scaling of a self-organized critical-state process, which is shown to be equivalent to the critical golden mean nonlinearity (CGMN) of coupled oscillator systems in the limit of low-dimensional strange attractors (Shaw and Chouet, 1988, 1989; Chouet and Shaw, 1991). The universality implied by this model supports an earlier conjecture by Shaw (1980) that the moment release of magma rise is in approximate balance with the release of seismic moment, averaged over the global spatiotemporal scales of the volcanic and earthquake cycles. A global test of this model requires systematic, and as yet unavailable, frequency data for Circumpacific volcano-tectonic activity over several orders of magnitude in time—from the seismic frequency at least to the mean characteristic recurrence time of Circumpacific volcano-edifice growth ($< 10^{-1}$ sec to $> 10^5$ yr). The present report considers the feasibility of analyzing Circumpacific seismic activity as a system of coupled oscillators of the CGMN type.

Results: In the model of Shaw (1980) seismic tremor both signals and manifests the initiation of tectonic failure cascades emanating from mantle processes. These cascades encompass a very wide fractal spectrum of seismic and subseismic frequencies, where subseismic refers to so-called "slow earthquakes" and general plasticoviscous magmatectonic deformation cycles that include the dissipative motions of mantle melting (Shaw, 1969). In conjunction with prior studies of seismic tremor by Bernard Chouet (EVE-SIS), we have developed a hierarchical description and nonlinear dynamical model of the tremor process (Chouet and Shaw, 1991; Shaw and Chouet, 1988; 1989; 1991) which also stands for a generalized description of the earthquake process as it relates to global tectonism. Central to nonlinearly coupled seismomagmatic and seismotectonic processes (TMMT of Shaw and Chouet, 1991) is the phenomenon of self-organized criticality, manifested in its simplest form by the CGMN singularity spectrum of sine-circle maps (Shaw, 1987, 1991; Shaw and Chouet, 1988, 1989). Self-organized criticality represents the collective action of many interior crises in the phase space of low-dimensional strange attractors (e.g., Chouet and Shaw, 1991) relative to systems of unstable periodic attractors interior to the respective chaotic attractors (core attractors) of local dynamical processes. Each interior crisis of a subsystem of attractors is characterized by power-law dependence of frequencies, $1/\tau$, relative to its proximity to a critical frequency in the neighborhood of an unstable natural nonlinear frequency of the system (Ditto et al, 1989; Shaw, 1991, p. 118 ff). A condition of steady or quasisteady state critical self-organization in a global system, such as the magmatectonic cascade just described, constitutes an ensemble average of a large number of such interior crises. Natural systems have a potentially infinite number of dynamical degrees of freedom, but the action of self-organization and

the universality parameters associated with local systems of attractors and their crises results in a reduction of the effective degrees of freedom to relatively low dimensions (Chouet and Shaw, 1991). In the steady-state limit of self-organized critical-state processes, the infinite-dimensional cascade acquires a simplicity analogous to the one-dimensional CGMN spectrum of Shaw and Chouet (1988, 1989).

The phenomenon of interior crises appears to explain an aspect of seismotectonic signatures that other workers have described in terms of Poissonian properties of the earthquake process (e.g., Nishenko and Buland, 1987). Power-law behavior of recurrence times is characteristic near the critical transition between chaotic and periodic dynamics—the CGMN condition described in Shaw and Chouet (1988, 1989), or the so-called "border of chaos" of Bak and Tang (1989) and Bak and Chen (1990)—but the recurrence time, τ, obeys lognormal statistics at a constant value of the average intermittency ($1/\tau$; cf. Ditto et al., 1989, Fig. 4). The latter behavior is analogous to the distributions of Circumpacific earthquake recurrence intervals of Nishenko and Buland (1987). Interpreted according to the concept of interior crises and self-organization, therefore, this class of characteristic earthquakes represents events scaled to a characteristic global critical frequency for earthquake instabilities. A power-law distribution of plate segments, faults, and earthquake magnitudes for the global system implies a spectrum of recurrence frequencies related to a system-wide critical frequency associated with the largest rupture lengths (or moments) that can exist on a finite Earth of given rheological properties and dynamical dissipation rates. Within the time frame of historical observations and earthquake hazard assessments for human activities, the relevant critical frequency would correspond to the intermittencies in a complete catalog of the greatest earthquake events (cf. Kanamori, 1986). Over shorter times, smaller geographic regions, and smaller magnitudes, the spatio-temporal scaling of events is renormalized to fractal fault-length budgets analogous to those described by Shaw and Gartner (1986, 1987). According to models of critical self-organization and/or chaotic crises, the scaling of recurrence frequency spectra would be analogous to that described by Shaw and Chouet (1989). In that case, frequency bundles (local spatiotemporal patterns of events) are expected to resemble the self-similar logarithmic scaling of frequencies described by Shaw and Chouet (1991, p. 10,205; cf. Fein et al., 1985).

The simplest numerical model of two coupled oscillators is given by the sine-circle function, a tunable phase-bias/coupling-strength (dissipative) algorithm, which is graphically expressed by recurrence relations shown by the iterated points of a circle map (see Shaw, 1987, 1991). Expressed in another way, the recursive circle maps of nonlinearly coupled periodic functions are analogous to nonlinear clocks in which the hands trace out the relative cyclicites of the coupled oxcillators. An analogy with the seismicity of the Circumpacific "ring of fire" is suggested by the notion of a global critical frequency of seismotectonic deformation waves (temporally analogous to the slower hand of a two-handed nonlinear clock) relative to the intermittency of great earthquakes (the faster hand of the clock) during the seismotectonic cycle. This analogy is simplistic because the surface trace of the deformation cycle—the fundamental "circle" of the process—is driven by the vertical moment distribution of magmatic transport in the model of Shaw (1980). Nonetheless, the resolved toroidal motion at the Earth's surface is analogous to a rotation about a pole normal to a mapping of the Circumpacific earthquake distribution. In that simple sense, then, the distribution of earthquakes is analogous to the iterations of a circle map, and these iterations are analogous to the integrate-and-fire motions of the escapement that controls the rotation of the faster hand of the nonlinear clock mechanism. The effect of nonlinear coupling—compared to a linear-periodic clock mechanism with uniform and constant increments of time—causes the faster hand to progress in an irregular fashion relative to the slower hand (i.e., the hypothetical ramp function of an integrate-and-fire escapement mechanism has "teeth" that are unevenly spaced as well as uneven in heights). Such a nonlinear mechanism possesses all of the dynamical regimes of the sine-circle map (Shaw, 1987, Figs. 1 and 2), including (1) a regime of mode locking (nonlinear-periodic resonance), (2) the critical-state transition regime (e.g., the CGMN condition), and (3) the chaotic regime (aperiodic behavior with periodic windows, the latter identifying the conditions of interior crises and chaotic-bursting types of transient chaotic intermittencies).

This circle-map/nonlinear-clock metaphor applied to Circumpacific seismicity suggests that we might look for characteristic dynamical regimes of the above types. Regime-1 behavior would

consist of periodic seismic cycles in which the intracycle intermittency is repeated at intervals p/q, where p is the seismotectonic frequency (the "slow" hand of the clock) and q is the earthquake frequency (the "fast" hand). For example, a value of $p/q = 1/19$ means that there are 19 irregularly spaced earthquake events during one seismic cycle, while a value of $p/q = 3/19$ means that there are 19 irregularly spaced earthquake events every 3 seismotectonic cycles, and so on. Unfortunately, the possible permutations for large cyclicities make it difficult to identify repeat periods unless the catalog of events exceeds the larger of the frequencies by orders of magnitude. Regime-2 behavior would resemble the singularity spectra of Shaw and Chouet (1989) in which the event frequencies scale logarithmically in universally distributed frequency bundles, as in Shaw and Chouet (1991). Regime-3 behavior would permit many types of chaotic crises, each with its own characteristic power-law scaling of recurrence periods (implying that the underlying seismotectonic cycle could be far more complex than a simple sinusoid).

With these regimes in mind, a preliminary examination was made of the distribution of large Circumpacific earthquake events plotted in the form of circle maps, using the data of Kanamori (1983, 1986). Although the progressions of events around the Circumpacific "circle" correspond well to the concept of a nonlinear clock mechanism, the number of events is insufficient to draw conclusions concerning the dynamical regime among the three types outlined above. It seems likely that all three will be represented at different spatiotemporal scales but that the general scaling for all earthquake magnitudes may well correspond to the universal CGMN regime in a manner analogous to seismovolcanic behavior in Hawaii (Shaw and Chouet, 1991).

References:

Bak, P. and C. Tang, Earthquakes as self-organized critical phenomena, *J. Geophys. Res., v. 94*, p. 15,635-16,637, 1989.

Bak. P. and K. Chen, Predicting earthquakes, in L. Lam and H. C. Morris, eds., *Nonlinear Structures in Physical Systems: Pattern Formation, Chaos, and Waves*, p. 113-118, New York, Springer-Verlag, 1990.

Chouet, B. and H. R. Shaw, Fractal properties of tremor and gas-piston events observed at Kilauea Volcano, Hawaii, *J. Geophys. Res., v. 96*, p. 10,177-10,189, 1991.

Ditto, W. L., S. Rauseo, R. Cawley, C. Grebogi, G.-H. Hsu, E. Kostelich, E. Ott, H. T. Savage, R. Segnan, M. L. Spano, and J. A. Yorke, Experimental observation of crisis-induced intermittency and its critical exponent, *Phys. Rev. Letters, v. 63*, p. 923-926, 1989.

Fein, A. P., M. S. Heutmaker, and J. P. Gollub, Scaling at the transition from quasiperiodicity to chaos, *Physica Scripta, v. T9*, p. 79-84, 1985.

Kanamori, H., Global seismicity, in, *Earthquakes: Observation, Theory, and Interpretation*, p. 596-608, Bologna, Italy, Soc. Italiana di Fisica, 1983.

Kanamori, H., Rupture process of subduction-zone earthquakes, *Ann. Rev. Earth Planet. Sci., v. 14*, p. 293-322, 1986.

Nishenko, S. P. and R. Buland, A generic recurrence interval distribution for earthquake forecasting, *Bull. Seis. Soc. Am., v. 77*, p. 1382-1399, 1987.

Shaw, H. R., Rheology of basalt in the melting range, *J. Petrology, v. 10*, p. 510-535, 1969.

Shaw, H. R., Mantle convection and volcanic periodicity in the Pacific: Evidence from Hawaii, *Geol. Soc. Am. Bull., v. 84*, p. 1505-1526, 1973.

Shaw, H. R., The fracture mechanisms of magma transport from the mantle to the surface, in R. B. Hargraves, ed., *Physics of Magmatic Processes*, p. 201-264, Princeton NJ, Princeton Univ. Press, 1980.

Shaw, H. R., The periodic structure of the natural record, and nonlinear dynamics, *Eos, v. 68*, p. 1651-1665, 1987.

Shaw, H. R., Magmatic phenomenology as nonlinear dynamics: Anthology of some relevant experiments and portraits, in G. V. Middleton, ed., *Nonlinear Dynamics, Chaos, and Fractals: With Applications to Geological Systems*, p. 97-149, Toronto, Geol. Assoc. Canada, Short Course Notes, v. 9, 1991.

Shaw, H. R. and A. E. Gartner, On the graphical interpretation of paleoseismic data, *U.S. Geol. Survey, Open File Rep. 86-394*, 1986.

Shaw, H. R. and A. E. Gartner, Earthquake distributions as multifractal singularity spectra, *U. S. Geol. Survey, Unpub. Res. Rept.*, 1987.

Shaw, H. R. and B. Chouet, Application of nonlinear dynamics to the history of seismic tremor at Kilauea Volcano, Hawaii, *U. S. Geol. Survey, Open File Rep. 88-539*, 1988.

Shaw, H. R. and B. Chouet, Singularity spectrum of intermittent seismic tremor at Kilauea Volcano, Hawaii, *Geophys. Res. Lett., v. 16*, p. 195-198, 1989.

Shaw, H. R. and B. Chouet, Fractal hierarchies of magma transport in Hawaii and critical self-organization of tremor, *J. Geophys. Res., v. 96*, p. 10,191-10,207, 1991.

Utilizing Compressive Growth Structure for Calculating Slip Rates on Buried Thrust Faults
1434-92-G-2192

John H. Shaw and John Suppe
Dept. of Geological and Geophysical Sciences
Princeton University
Princeton, NJ, 08544
(609) 258-3261

Active Blind Thrusting

In previous investigations we have identified and mapped several active blind thrust faults in the eastern Santa Barbara Channel, California (Suppe et al., 1991; Shaw et al., 1992A). Slip above a ramp in the Channel Island thrust has folded the overlying hangingwall rock along the Offshore Oak Ridge trend. Deformed near-seafloor sediments along the fold trend, imaged in seismic reflection profiles, suggest that the underlying fault has slipped in the Quaternary and may pose a significant earthquake hazard to the nearby populated areas of southern California (Shaw et al. 1992A). Based on empirical relationships between earthquake magnitude and fault rupture area (Kanamori and Anderson, 1975), we estimate that one segment of the Channel Island thrust is capable of generating a Ms=7.1 earthquake.

Sediments deposited near the Offshore Oak Ridge fold trend during the active slip history of the underlying fault (syntectonic or growth strata) quantitatively record the rates of fold growth and fault slip (Suppe et al., 1992). The kink-band (fold limb) widths of growth strata in cross section (***Lo***) equal the amount of fault dip-slip since deposition of the syntectonic units (Figure 1B). Sediments deposited earlier in the slip history of the underlying fault record wider kink-band widths between sets of axial surfaces (***A-A'***) than do sediments deposited later. Therefore, growth strata form narrowing upward kink-bands, or growth triangles, above bends in blind thrust faults (Suppe et al., 1992). Analysis of a growth triangle along the Offshore Oak Ridge trend suggests that the underlying Channel Island thrust is slipping in a northeast-southwest direction (***S***, Figure 2A) at a rate of ≈1.3 mm/year (Suppe et al., 1991; Shaw et al., 1992A). The thrust ramps upward beneath the Offshore Oak Ridge trend and approaches the seafloor south of Santa Cruz Island.

Lateral Fault Slip Distribution Through Time

The fold limb (kink-band) width (***L***) of the Offshore Oak Ridge trend between axial surfaces ***A-A'*** equals the total dip-slip on the underlying Channel Island thrust (Figure 2A). Mapped along trend, the axial surfaces indicate that total fault slip (***S***, Figure 2A) reaches a maximum of ≈12 km along the center of the trend and decreases laterally in both directions (Shaw et al., 1992A). During this past year, we have constructed axial surface maps through syntectonic strata to document the lateral distribution of slip on the underlying Channel Island thrust through time (Figure 2) (Shaw et al., 1992B). Because the fold limb widths of syntectonic strata record the amount of fault slip since their deposition, the difference in map view kink-band widths of two growth horizons equals the amount of fault slip between the deposition of the units (Figure 1B). By mapping axial surfaces in progressively younger growth strata,

we can document the lateral distribution of slip on the Channel Island thrust since the early Pliocene.

Axial surface mapping from three correlated time horizons along the Offshore Oak Ridge trend defines slip on the underlying Channel Island thrust through time. Segments of the total kink band (*A-A'*) equal slip patches on the underlying thrust between deposition of the dated growth horizons (Figure 2B). Prior to 3 m.a., fault slip was greatest beneath the center of the fold trend and decreased laterally toward the east. During more recent time intervals (3.0 - 1.0 m.a.), slip occurred along the eastern extent of the fault at an approximately constant rate as denoted by the roughly constant width of slip patches along strike. Therefore, the Channel Island thrust has not propagated laterally over this mapped segment since 3.0 m.a. In the last ≈1 million years, the slip patch is of greatest width along the eastern edge of the fold trend (Figure 2B). This may suggest that the underlying Channel Island thrust has slipped at a slightly higher long-term rate over this eastern segment since 1 m.a. If this is the case, an earthquake that ruptured the entire mapped segment of the thrust (Shaw et al., 1992A, B) may nucleate in this patch of higher slip rates near the Ventura-Oxnard coast (Figure 2A).

References

Corbett, E.J., Johnson, C.E., 1982, The Santa Barbara, California, Earthquake of 13 August, 1978, Bulletin of the Seismological Society of America, vol.72, no.6, p. 2201-2226.

Gawthrop, W., 1975, Seismicity of the central California coastal region: U.S.G.S. Open-file Report 75 - 134, p.87.

Kanamori, H., and Anderson, D.L., 1975, Theoretical basis of some empirical relations in seismology, Bulletin of the Seismological Society of America, vol. 65, no. 5, p. 1073 -1095.

Larsen, S., 1991, Geodetic measurements of deformation in southern California, doctoral dissertation, California Institute of Technology.

Larson, K., 1990, Precision, accuracy, and tectonics from the Global Positioning System, doctoral dissertation, University of California, San Diego.

Luyendyk, B. P., Hajik, E, J., Crippen, R. E., and Simonett, D. A., 1982, Side-Scan sonar and high-resolution reflection maps of the Santa Barbara Channel seafloor, California Sea Grant Program Report no. T-CSGCP-006, Institute of Marine Resources, University of California, La Jolla.

Luyendyk, B. P., Hajik, E, J., and Simonett, D. A., 1983, Side-Scan sonar mapping and computer-aided interpretation in the Santa Barbara Channel, California, Marine Geophysical Research, vol. 5, no. 4, p. 365-388.

Mount, V.S., 1989, State of Stress in California and a seismic structural analysis of the Perdido Fold Belt, Northwest Gulf of Mexico, Doctoral Thesis, Princeton University.

Shaw, J.H., Bischke, R.E., and Suppe, J., 1992A, Evaluation of the use of compressive growth structure in earthquake hazard assessment, NEHRP Technical Reports, v. XXXIII, U.S.G.S. Open-file Report 92-258, p. 619-622.

Shaw, J.H., Genovese, P., and Suppe, J., 1992B, Geometry and lateral slip distribution along large thrust fault systems, Geological Society of America Abstracts with Programs, V. 24, no. 7.

Suppe, J., Bischke, R.E., and Shaw, J.H., 1991, Evaluation of the use of compressive growth structure in earthquake hazards assessment, NEHRP Technical Reports v. XXXII, U.S.G.S. Open-file Report 91-352, p. 192-195.

Suppe, J., Chou, G.T. and Hook, S.C., 1992, Rates of folding and faulting determined from growth strata, in *Thrust Tectonics*, K.R. McKlay ed., Unwin Hyaman, Publisher.

Yeats, R. S. and Olson, D.J., 1984, Alternate fault model for the Santa Barbara, California, Earthquake of 13 August 1978, Bulletin of the Seismological Society of America, vol. 74, no. 5, p.1545-1553.

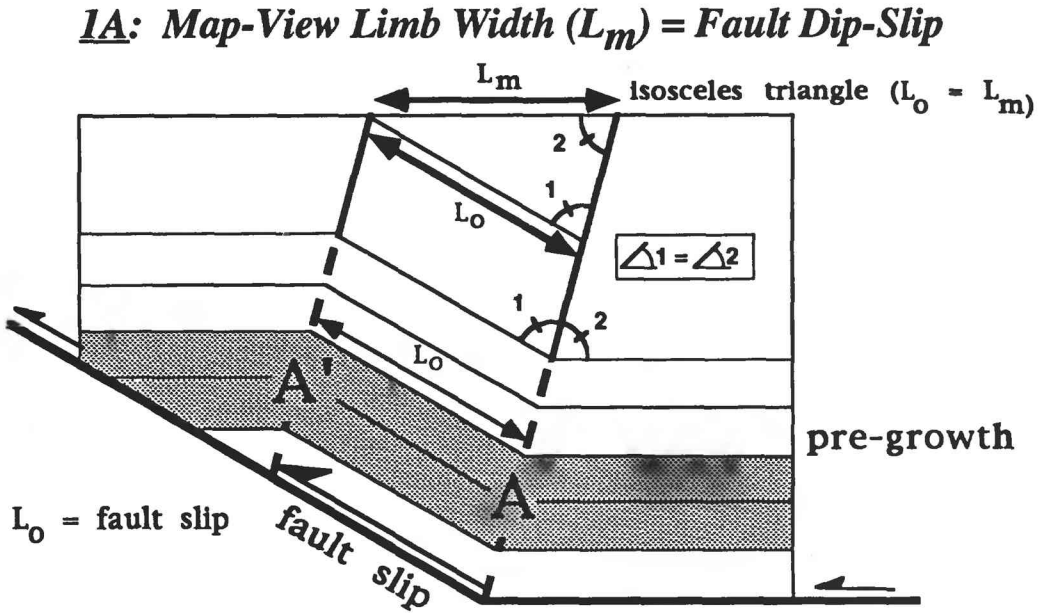

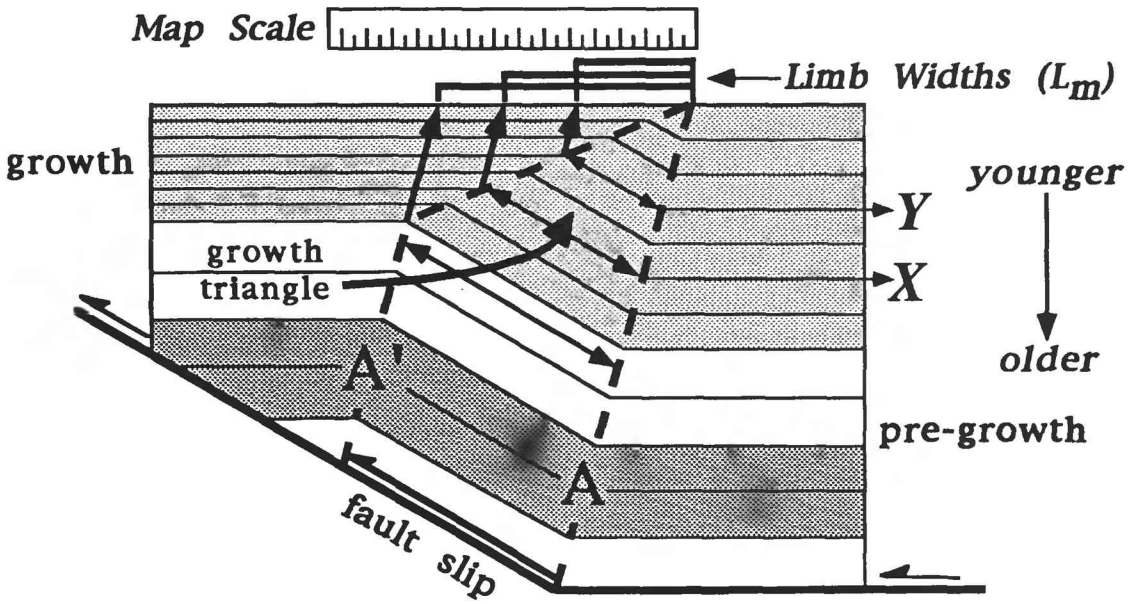

Figure 1A: The parallel projection method of axial surface mapping generates kink band widths in map view (*Lm*) equal to fold limb widths in cross section (*Lo*) when axial surfaces (dashed lines) bisect fold limbs and kink bands are bounded by horizontal strata. For simple ramps in decollements, these limb widths (*Lo*) equal dip-slip on the underlying fault. **1B:** Fold limb widths of syntectonic (growth) strata record the amount of fault slip since their deposition, forming narrowing upward kink-bands, or growth triangles, in cross section. The difference between map-view limb widths (*Lm*) of different growth horizons equals the amount of fault slip between the deposition of the mapped growth strata. Axial surface mapping in growth section through a series of cross sections (or seismic reflection profiles) documents the lateral distribution of fault slip through time (see Figure 2B). *A-A'* are axial surfaces like those mapped in Figure 2.

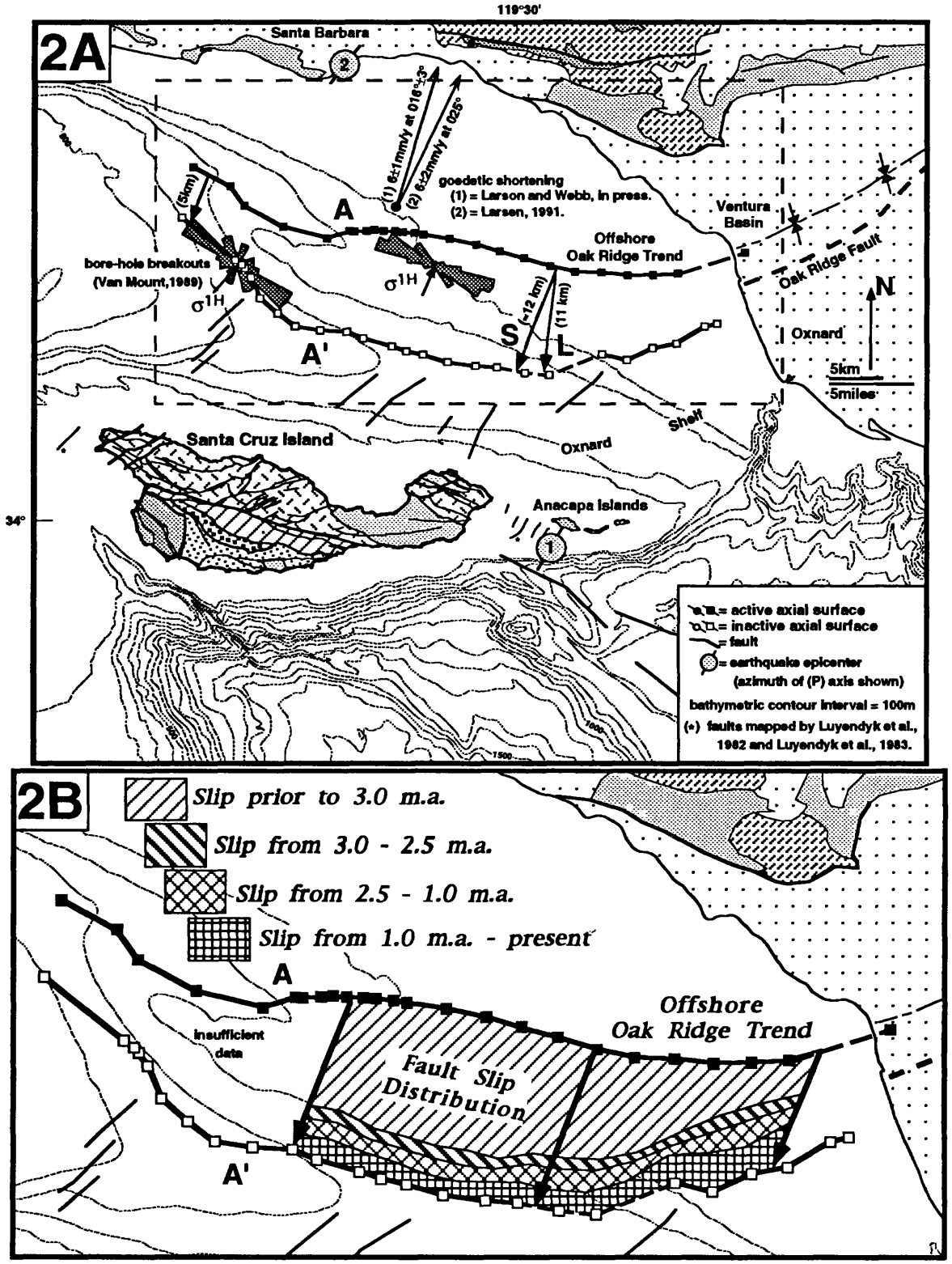

Figure 2A: An axial surface map of the Offshore Oak Ridge kink band (*A-A'*), Santa Barbara Channel, California. The map-view kink band width (*L* between *A-A'*) records the total dip-slip on the underlying Channel Island blind thrust (see Figure 1). Oblique, left-lateral thrusting (*S*≈12km) on the underlying thrust fault, suggested by the axial surface map pattern, is consistent with present day stress directions, tear fault orientations, earthquake P-axes, and the measured geodetic shortening direction. *σ1H* = estimate of the trace of the maximum compressive stress that is perpendicular to borehole breakout directions. Epicenter (1) - 1978 M = 5.1 Santa Barbara earthquake, Corbett and Johnson, 1982; Yeats and Olson, 1984; (2) 1973 Ml = 5.0 Anacapa earthquake, Gawthrop, (1975). The dashed box outlines the map area of Figure 2B. **2B:** Axial surface mapping from syntectonic strata records the lateral distribution of fault slip through time (denoted by the patterned slip patches). Since 3 m.a., fault slip has occurred along the eastern length of the fault at a roughly constant long-term rate as denoted by the roughly constant widths of slip patches along strike.

Low Frequency Data Network

Semi-Annual Report - Project Number 9960-10096

S. Silverman
Branch of Earthquake Geology and Tectonophysics
U. S. Geological Survey
Menlo Park, California 94025
415/329-4862

Investigations

[1] Real-time monitoring, analysis, and interpretation of strain, creep, magnetic, tilt and other low frequency data within the San Andreas fault system and other areas for the purpose of understanding and anticipating crustal deformation and failure.

[2] Enhancements to satellite-based telemetry system for reliable real-time reporting and archiving of crustal deformation data.

[3] Development and implementation of backup capablities for branch workstations.

[4] Specialized monitoring, including automated alerts, and display of data relevant to specific regions such as Parkfield and Mammoth.

Results

[1] Data from low frequency instruments in Southern and Central California have been collected and archived using the Low Frequency Data System. In the six months measurements from over 100 satellite platforms have been received via satellite telemetry and subsequently archived by Low Frequency Network computers for analysis.

[2] The project has operated a configuration of two Sun workstations for use as data archiving, monitoring, and analysis systems. Both workstations receive satellite telemetry in near real-time from a PC-based system which acts as a satellite downlink. Data from the Network are available to investigators in near real-time and software for data display and analysis is available. Tectonic events, such as creep along the fault, can be monitored while still in progress.

[3] The project uses a 1.8 meter satellite receiver dish installed in Menlo Park for retrieval of near real-time surface deformation data from California and South Pacific islands. The GOES geostationary satellite in conjunction with a domestic communications satellite provide the telemtry which makes possible a reliable real-time data collection system. Further expansion of the number of platforms monitored, particularly in the San Francisco Bay area is ongoing.

[4] The project continues to take an active part in the Parkfield Prediction activities. Automated alerts for signals which may indicate anomolous tectonic activity notify personnel in realtime. Data collection and computer operations are automatically monitored for abnormal activity and project members are paged for in the event of problems with either.

[5] As part of the Bay Area region study, new display facilities have been developed to provide improved monitoring and other graphic displays. An area of Menlo Park Building 7 has been upgraded to provide better facilities for public outreach and media communications.

Segmentation Model For the Northern Calaveras Fault, Calaveras Reservoir To Walnut Creek

Contract # 14-08-0001-G2140

Gary D. Simpson, William R. Lettis and Keith I. Kelson
William Lettis & Associates
1000 Broadway, Suite 612
Oakland, California 94607
(510) 832-3716

ABSTRACT

On the basis of geomorphic expression and structural relations, we evaluate the location and physical segmentation of the northern Calaveras fault. North of Calaveras Reservoir, four fault segments are identified: the Calaveras Reservoir, Sunol, San Ramon, and Alamo segments. These segments range in length from 7 to 23 kilometers and are defined primarily by geomorphic expression, fault geometry, seismicity, intersecting structures, and range-front orientation. The fault is characterized by relatively short, distinct fault segments, reflecting the relative immaturity of the fault zone as a through-going fault system. If the identified segments represent independent fault rupture segments, the northern Calaveras fault probably ruptures in moderate magnitude (M $6\pm1/2$) earthquakes similar to historical events on the Calaveras fault south of Calaveras Reservoir. If two or more segments rupture during a single event, empirical regressions suggest maximum magnitudes ranging from M 6 1/2 to 7 1/4. The location and nature of the northern termination of the Calaveras fault and its structural association with the Concord and Hayward faults is not clear. Geomorphic evidence of recent fault activity progressively dies out north of Danville. The fault does not extend as a prominent feature to the Walnut Creek basin and thus transfer of strain to the southern Concord fault cannot be accommodated via a simple en echelon pull-apart basin model. Strain may be transferred to the Concord fault via distributed deformation in the northern San Ramon Valley, as partially reflected by the Danville and Alamo earthquake swarms, as well as potentially to the central and northern Hayward fault via a restraining stepover reflected in uplift of the Oakland Hills.

INTRODUCTION

The northern Calaveras fault zone extends from Calaveras Reservoir on the south to the vicinity of Walnut Creek on the north. Through part of this area it traverses the western margin of the densely populated San Ramon Valley, including the rapidly developing towns of Pleasanton,Dublin, San Ramon, Danville and Alamo. Location of the fault, however, is poorly constrained through much of this reach due to poor geomorphic expression and concealment by large late Quaternary landslides. In addition, little is known about the rate and distribution of geologic slip along the northern Calaveras fault, or about its northern termination and structural association with the Concord fault to the northeast and Hayward fault to the west. The sparsity of these data make it difficult to estimate the probability for future large earthquakes on the fault (WGCEP, 1990). In short, the northern Calaveras fault zone is the most prominent, potentially hazardous fault within the Bay region for which insufficient information is available for reliable earthquake hazard analysis.

The northern Calaveras fault zone (Figure 1) dies out northward between Las Trampas Ridge and Walnut Creek. Existing structural models postulate that slip along the northern Calaveras fault may transfer onto the Concord fault via a right en echelon step-over or right releasing bend (Page, 1982; Oppenheimer and MacGregor-Scott, 1991), or that slip may progressively decrease northward and is transferred across the East Bay Hills to the Hayward fault (Aydin, 1982). Evidence for the right step-over or releasing bend includes the spatial coincidence of the northern end of the Calaveras fault and the southern end of the Concord fault (Page, 1982; Dibblee, 1980), and the presence of northeast-trending seismicity across the northern San Ramon Valley (Oppenheimer and MacGregor-Scott, 1991, Oppenheimer and Lindh, this volume). This model implies a continuous Calaveras-Concord fault system, the presence of extensional strain in the step-over region, and significant lateral slip on the Calaveras fault extending into the Walnut Creek basin. Alternatively, slip on the northern Calaveras fault may progressively decrease northward, and be transferred across the uplifting East Bay Hills to the Hayward fault. This slip transfer may occur on mapped structures such as the Mission, Las Trampas, and Bollinger faults, or it may occur on low-angle detachment faults at depth. In this scenario, the Concord fault is unrelated to the Calaveras fault, and may represent a continuation of the northern Greenville fault across a left-restraining step-over occupied by the Mt. Diablo uplift.

Relative to the Calaveras fault south of Calaveras Reservoir, which is associated with contemporary seismicity and has generated several moderate-magnitude earthquakes (Oppenheimer and others, 1990), the northern Calaveras fault is seismically quiescent and may represent a seismic gap (Oppenheimer and Lindh, this volume). The fault probably ruptured in 1861, when a reported 13-kilometer-long fissure occurred along the western margin of San Ramon Valley from San Ramon south to Dublin (Figure 1; Toppozada, 1981). The exact location of surface rupture is not known. Based on historical accounts of damage and felt reports, Toppozada (1981) assigned a Modified Mercalli Intensity of VIII for the earthquake, and estimated a magnitude of 5.6. This magnitude designation, however, is small relative to the documented length of surface rupture. Based on comparisons with world-wide earthquakes (see below), we believe the 1861 earthquake may have been as large as M6.4. In addition, two significant earthquake swarms have been documented in San Ramon Valley adjacent to the northern Calaveras fault, the 1970 Danville and 1990 Alamo swarms, with maximum magnitudes of 4 to 4.5 (Figure 1). Focal mechanisms and epicenter locations for these swarms show left-lateral movement on unmapped northeast-trending faults within San Ramon Valley and the foothills southwest of Mt. Diablo (Oppenheimer and MacGregor-Scott, 1991). The seismic potential of the northern Calaveras fault is highlighted, in part, by a northward progression of earthquakes along the central segment of the Calaveras fault (Oppenheimer and others, 1990). Because the most recent event (1988 M5.1 Alum Rock earthquake) occurred just south of the northern Calaveras fault, there is an increased probability for at least a moderate magnitude event occurring on the northern Calaveras fault near Calaveras Reservoir.

In this study, we evaluate the location and physical segmentation of the northern Calaveras fault zone between Calaveras Reservoir and Walnut Creek (Figure 1) via compilation of a tectonic map, aerial photograph interpretation, field reconnaissance, and detailed mapping of Quaternary units along parts of the fault north of Sunol Valley. In conjunction with paleoseismic investigations near Calaveras Reservoir (Kelson and others, this volume), we are attempting to develop a better understanding of the northern Calaveras fault and its role in the tectonic framework of the eastern San Francisco Bay region. Our study will help assess the likelihood of future moderate- to large-magnitude earthquakes on the fault.

SEGMENTATION OF THE NORTHERN CALAVERAS FAULT

Based on compilation of published and unpublished data, interpretation of 1939, 1966, and 1974 aerial photographs, and limited Quaternary mapping, we have assessed the geomorphic and structural character of the northern Calaveras fault. The fault in this region is generally subtly expressed, concealed by large landslides, and commonly parallel to ridge-forming Tertiary sedimentary strata. It is typically expressed by linear range-fronts, deflected drainages, topographic saddles and scarps, groundwater barriers, vegetation lineaments, and tonal contrasts. Unfortunately, urban development along much of the western margin of San Ramon and Ygnacio Valleys has disturbed many of the prominent features visible on 1939 aerial photographs.

We identify four segments along the Calaveras fault north of Calaveras Reservoir based primarily on geomorphic expression, fault geometry, seismicity, intersecting structures, and range front orientation. From south to north, the segments are informally named the **Calaveras Reservoir**, **Sunol**, **San Ramon**, and **Alamo** segments (Figure 1). These segment designations are consistent with those of Page (1982), who used turning points in fault strike to qualitatively assess stress changes within individual segments. A discussion of segment boundaries, fault morphology, and characteristics of individual segments follows.

Calaveras Reservoir segment. Unlike northwest-trending segments to the north and south, the 7-km Calaveras Reservoir segment trends roughly north-south and occupies a 1.5- to 3.0-kilometer-wide releasing double bend between the southern end of Calaveras Reservoir and the southern end of Sunol Valley (Figure 1). The southern end of this segment is defined by an approximately 20° change in fault orientation at the southern end of Calaveras Reservoir, and by an intersection of the fault zone with a prominent trend in microseismicity that diverges from the Calaveras fault toward the mapped trace of the Mission fault (Wong and others, this volume). This microseismicity trend may reflect a fault zone at seismogenic depths along which slip is transferred from the central Calaveras fault to the southern segment of the Hayward fault (Wong and others, 1991; Andrews, 1991). The northern end of the Calaveras Reservoir segment is defined by a 20° to 25° northwesterly bend in the fault trace near the southern end of Sunol Valley.
The most pronounced lineament along this reach of the fault zone is a prominent linear scarp at Leyden Creek (Kelson and others, 1991; this volume). This linear scarp aligns with a topographic saddle and linear drainage at the northern end of Calaveras Reservoir, but cannot be traced to the north where the fault trace is coincident with lithologically-controlled topography. Based on the presence of a prominent contrast in basement lithology coincident with the scarp and evidence of multiple late Holocene faulting events (Kelson and others, this volume), we interpret this to be the active trace of the Calaveras fault.

The Calaveras Reservoir segment is unlikely to produce an independent large-magnitude earthquake because of its short length (7 kilometers) and location within a releasing bend of the fault zone. Rather, the segment primarily represents our uncertainty in locating the juncture of the central and northern Calaveras fault zones. The fault segment is most likely to rupture along with a neighboring segment to either the north or south. The Calaveras Reservoir segment could, therefore, form the end point of ruptures from either direction, but a throughgoing rupture is unlikely. In any case, multiple late-Holocene events are documented near the northern end of the Calaveras Reservoir segment at Leyden Creek (Kelson and others, this volume).

Sunol segment. The Sunol segment of the northern Calaveras fault extends for a distance of 9 kilometers along the eastern margin of Sunol Valley, from the northwesterly bend defining the northern end of the Calaveras Reservoir segment, to the southern end of Pleasanton Ridge (Figure 1). Although the Calaveras fault is poorly expressed geomorphically in the southern part of Sunol Valley, it forms a prominent linear range front along the northeastern margin of the valley. The mapped trace of the Sinbad fault (CDWR, 1974) forms the southwestern margin of Sunol Valley, a steep linear range front marked by several faceted spurs. The apparent en echelon nature of the

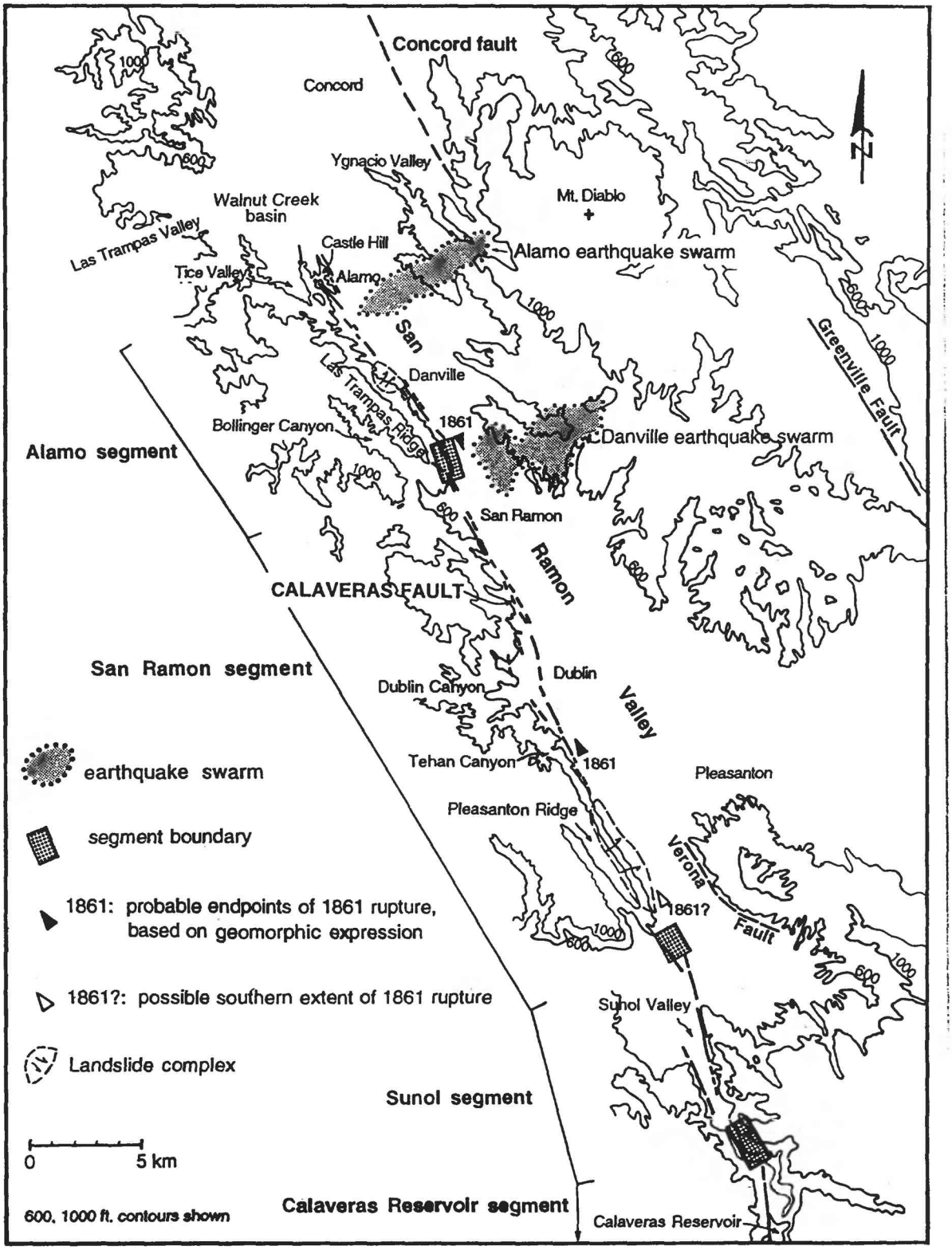

Figure 1. Segmentation model for the northern Calaveras fault; shaded boxes depict uncertainty in the location of segment boundaries. Map also shows generalized topography, possible endpoints of the 1861 rupture, and locations of the Danville and Alamo earthquake swarms. Calaveras fault traces based on interpretation of aerial photographs, field reconnaissance, and compilation of consultants reports. Concord, Verona, and Greenville faults approximately located based on CDMG mapping.

opposing linear range fronts bordering a subsiding basin suggests that the valley may be a pull-apart basin formed by a 0.7- to 1.5-km-wide right step. Subsidence of Sunol Valley is indicated by Quaternary gravels beneath the valley floor at a lower elevation than the bedrock sill at the northern end of the valley, and by the lack of stream terraces bordering Alameda Creek on the flat valley floor. Based on geomorphic expression, the Sunol segment consists of several N12°-15°W-trending fault strands in a relatively narrow, less than 250-m-wide zone. At the northern end of the valley, a northward diverging fault trace marked by a tonal lineament trends approximately N40°W toward Pleasanton Ridge. Trench exposures along this lineament show displacements of probable Holocene deposits along this trace near Interstate 680 (J. VanVelsor, personal communication, 1991).

Definition of the northern segment boundary is based primarily on a reversal in sense of apparent vertical separation between Sunol Valley and Pleasanton Ridge. Within Sunol Valley, the fault forms a prominent west-facing escarpment reflecting a component of up-on-the-east vertical separation. North of Sunol Valley, the fault traverses the east side of Pleasanton Ridge, suggesting a component of up-on-the-west vertical separation. This segment boundary also coincides with the closest approach of the Verona fault, and possibly the southern termination of rupture during the 1861 earthquake (as described below).

San Ramon segment. The San Ramon segment of the northern Calaveras fault, the longest of the segments defined by our study, extends for a distance of 23 kilometers from Pleasanton Ridge to north of San Ramon (Figure 1). At the south end of the segment, the fault is concealed by large Quaternary landslides along much of the southern part of Pleasanton Ridge. North of the landslide complex, the fault is well-expressed by a clear linear depression, vegetation and tonal lineaments, sag ponds, and several deflected drainages near Tehan Canyon. Location of the fault is documented between Dublin Canyon and Tehan Canyon by several unpublished trench studies (Burkland and Associates, 1973a, b; Purcell, Rhoades & Associates, 1989). The fault trends approximately N22°W through this reach and, on the basis of geomorphic expression, is confined to a 250-m-wide zone.

Published accounts of the 1861 earthquake (Toppozada, 1981) suggest that fault rupture occurred entirely along the San Ramon segment. Based on the strong geomorphic expression of the fault between San Ramon and Tehan Canyon, and on historical accounts of the length of ground rupture, we believe the 1861 rupture extended across Dublin Canyon, and may have extended southward to Tehan Canyon (Figure 1). Because there are abundant landslides obscuring the fault trace along Pleasanton Ridge, it is possible that fault rupture extended south of Tehan Canyon in 1861. Based on geomorphic expression and the findings of Toppozada (1981) the northern extent of the 1861 rupture probably coincides with the northern end of the San Ramon segment, near Danville (Figure 1).

Dublin Canyon is the southernmost major drainage crossing the San Ramon segment (Figure 1). The Calaveras fault forms a series of linear, faceted range fronts along the foothills directly north and south of Dublin Canyon. The fault trace defined by these range fronts makes a 700- to 800-m right step or bend across the canyon (Figure 1). Northward divergent lineaments south of Dublin Canyon, and a series of springs and tonal contrasts in the foothills to the north, suggest that the fault zone is up to a kilometer wide through this bend. A low topographic scarp was present on the Dublin Canyon alluvial fan prior to development and a fault is identified in several consultants' trenches and in the Martin Creek channel (Carpenter, 1975). Most previous workers suggest that the scarp represented surface rupture associated with the 1861 earthquake. North of Dublin Canyon, geomorphic expression of the fault defines a narrow 400-m-wide, N25°W-trending zone.

The right-step or bend at Dublin Canyon may define a further segmentation point within the San Ramon segment. For our initial model however, we have not placed a boundary here because of the lack of multiple lines of evidence supporting such a designation. Other than the bend in the fault

trace, there are no other characteristics indicative of a segmentation point (e.g., changes in seismicity, intersecting structures, etc.). In addition, the width of the bend or step is probably not sufficient to define a segment boundary. Finally, based on the length of rupture, presence of the low scarp crossing the Dublin Canyon fan, and prominent geomorphic expression of the fault continuing to the south, it is likely that the 1861 event ruptured across this step.

San Ramon Canyon forms another large drainage along the East Bay Hills range front north of Sunol Valley (Figure 1). The fault zone is geomorphically well defined north and south of San Ramon Canyon by topographic saddles, scarps, and linear fronts, and is identified in several consultants' trenching studies. As at Dublin Canyon, the fault makes an apparent right step or bend across San Ramon Canyon (Figure 1). The zone of fault-related lineaments diverges northward (to a maximum width of 600 m) through the 800-m-wide step, then converges to the north to form a narrow zone along the northeast side of Las Trampas Ridge. Rogers and Halliday (this volume), however, suggest that the trace of the Calaveras fault north of San Ramon Canyon may be even farther east than previously assumed, which would make the width of the right step even greater. About 2.5 km north of San Ramon Canyon, the fault makes an approximately 10° northwesterly bend to N35°W.

The northern boundary of the San Ramon segment is located just north of San Ramon Canyon (Figure 1); it is defined by a number of factors, including changes in seismicity and fault orientation, and the presence of intersecting structures within the East Bay Hills. This location is coincident with the intersection of a northeast-trending left-lateral fault defined by the 1970 Danville earthquake swarm (Figure 1). In addition, this boundary is marked by an approximately 10° change in fault strike, and the mapped intersection of the more northwesterly-trending Las Trampas and Bollinger Canyon faults (Dibblee, 1980; Wagner, 1978). The northern boundary is also directly (2.5 km) north of the $\geq$0.8-kilometer-wide right bend or step in the fault across San Ramon Canyon.

Alamo segment. The Alamo segment extends for 9 kilometers from the north end of the San Ramon segment to the vicinity of Castle Hill. The southern and northern ends of the fault segment are defined, in part, by the apparent intersection of northeast-trending, left-lateral faults within San Ramon Valley delineated by the 1970 Danville and 1990 Alamo earthquake swarms, respectively (Figure 1). In general, this segment of the northern Calaveras fault is characterized by the diffuse microseismicity bordering its northeastern side, as opposed to the relatively aseismic areas around and along the San Ramon segment (Oppenheimer and others, this volume). North of San Ramon Canyon, the Calaveras fault is located at the base of a well-defined range front, and is expressed by a narrow (less than 300-m-wide) zone of topographic and tonal lineaments, although large landslides obscure the fault west of Danville (Figure 1). The fault zone becomes increasingly diffuse near the south end of Castle Hill (Figure 1). Based on available data and geomorphic expression, the northern extent of the northern Calaveras fault can not be definitively located. Previous workers (Herd, 1978; Dibblee, 1980) mapped the fault along two linear drainages at the southern end of Castle Hill that trend to the west-northwest toward Tice Valley. Trenching studies, however, failed to uncover an active fault within these drainages. Based on field reconnaissance and interpretation of aerial photographs of the Walnut Creek basin, we found no geomorphic features indicative of Holocene fault activity north of Castle Hill. The northeastern side of Castle Hill is marked by several conspicuous linear fronts and apparent shutter ridges, but no previous worker has mapped the fault this far north along the San Ramon Valley margin. Late Quaternary deposits within Las Trampas Valley (Figure 1) have no fault-related features, and there is no apparent deflection of Las Trampas Creek. Therefore, we place the northern boundary of the Alamo segment, and therefore, the northern termination of the Calaveras fault, near Castle Hill. This designation defines a 9-km-long segment. Because of its diffuse structural character, the Alamo segment is probably not an independent source of large-magnitude earthquakes. This segment, in part, represents our uncertainty in locating the northern end of the Calaveras fault.

Because of poor geomorphic expression and lack of data on the amount and distribution of slip along the northern Calaveras fault, it is not possible to determine the nature of the structural relationship between the Calaveras and Concord faults. From a strictly geomorphic perspective, the Walnut Creek/Ygnacio Valley basin is the most likely location for slip transfer between the two faults; the overall morphology here would be consistent with a simple pull-apart basin. There is, however, no evidence of active faulting along the western margin of the Walnut Creek/Ygnacio Valley basin to support this model. Alternatively, Oppenheimer and MacGregor-Scott (1991) postulate that slip is transferred between the Calaveras and Concord faults via short, northeast-trending left-lateral faults defined, in part, by the Alamo and Danville earthquake swarms. However, there is no prominent geomorphic expression of these faults within San Ramon Valley, and the series of topographic and structural highs (Alamo Ridge, Sherburne Hills, Sugarloaf Hill, Shell Ridge) northeast of Danville and Alamo are not typical features for an extensional strain field within a releasing stepover. The broad distribution of strain across the stepover may inhibit development of features indicative of faulting. At the very least, the left-lateral faults associated with the Danville and Alamo swarms represent conjugates to the northern Calaveras fault (Oppenheimer and MacGregor-Scott, 1991), and indicate that some degree of active right-lateral slip is occurring on the Alamo segment.

ESTIMATES OF MAXIMUM MAGNITUDE

Earthquake magnitudes for the fault segments defined in this study (and all possible groups of segments) are estimated based on empirical relations comparing rupture length or rupture area with magnitude (Table 1; Wells and Coppersmith, 1992; Slemmons, 1982; Bonilla and others; 1984; Wyss, 1979). The empirical relations are statistical regressions based on historical earthquakes that provide a means for estimating earthquake magnitudes based on comparisons within a large regional or world-wide database.

Table 1.

Proposed fault segments for the northern Calaveras fault with associated lengths, rupture areas, and magnitudes.

	rupture length vs. magnitude				**rupture area vs. magnitude**		
Segment	length	W&C	B,M,L	S	area[1]	W&C	W
	(km)	(M_w)	(M_s)	(M_s)	(km^2)	(M_w)	(M_w)
CR-SUN	16	6.5	7.0	6.3	192	6.3	6.4
CR-SUN-SR	39	6.9	7.2	6.8	468	6.7	6.8
SUN	9	6.2	6.8	6.0	108	6.1	6.2
SUN-SR	32	6.8	7.2	6.7	384	6.6	6.7
SUN-SR-AL	41	6.9	7.2	6.8	492	6.7	6.8
SR	23	6.7	7.1	6.6	276	6.5	6.6
SR-AL	32	6.8	7.2	6.7	384	6.6	6.7
CR-SUN-SR-AL (all)	48	7.0	7.3	6.9	576	6.8	6.9

W&C = Wells and Coppersmith (1992); B,M,L = Bonilla, Marks, and Lienkaemper (1984); S = Slemmons (1982); W = Wyss (1979)

CR = Calaveras Reservoir; SUN = Sunol; SR = San Ramon; AL = Alamo

[1] area calculated assuming vertical fault, 12 km depth (conservative estimate based on Danville earthquake swarm, see Oppenheimer and Lindh, this volume)

Assessment of maximum magnitudes for the northern Calaveras fault is dependent on whether the segments defined in this study represent independent rupture segments or whether two or more segments may rupture in a single event. Due to the strong heterogeneity in fault characteristics, we believe it is highly unlikely that the entire northern Calaveras fault will rupture in a single event. Maximum magnitudes for individual segments range from about M 6 1/4 to 6 1/2 and from M 6 1/2 to 7 for groups of two or three segments rupturing simultaneously.

It should be noted that, based on intensity reports and distribution, Toppozada (1981) estimated the 1861 earthquake to be approximately M5.6. Assuming a rupture length of 13 km (8 miles), the empirical relations described above suggest an earthquake of M6.4 or greater. Based on historic accounts, this earthquake apparently ruptured only a part of the San Ramon segment. The likely location of the northern end of rupture, north of San Ramon (Toppozada, 1981) agrees well with the location of our segment boundary in this area. The south end of the rupture, probably south of Dublin along Pleasanton Ridge, however, does not appear to coincide with any feature or change in fault characteristic that would suggest a segmentation point. Rupture may have continued undetected farther south along Pleasanton Ridge, where it is obscured by landslides.

CONCLUSIONS

North of Calaveras Reservoir, we identify four segments along the northern Calaveras fault. The two principal segments, the Sunol and San Ramon segments, have lengths of 9 and 23 kilometers, respectively. Based on the continuity and geomorphic expression of these segments, both may be potential sources for moderate- to large-magnitude earthquakes. The Calaveras Reservoir and Alamo segments, 9 and 7 kilometers respectively, are unlikely to represent independent seismogenic sources due to their short lateral extent and/or diffuse expression. However, these segments may act as the termination or nucleation points for earthquakes extending from or onto neighboring segments. Based on published empirical relations, maximum magnitude estimates range from 6 1/4 to 7 for individual segments and groups of segments, respectively, to 7 1/4 if the entire 48-kilometer length of the northern Calaveras fault should rupture in a single event.

Based on available data, field exposures, and geomorphic expression, the northern Calaveras fault terminates along Las Trampas Ridge before reaching the Walnut Creek basin. Slip may transfer to the Concord fault across a right en echelon stepover, but the location and nature of this transfer is still unclear. Overall geomorphic expression suggests that the Walnut Creek/Ygnacio Valley areas may be an extensional pull-apart basin, although there is no evidence that the Calaveras fault extends far enough to the north. Seismicity suggests the transfer of slip may occur across a diffuse zone in the northern San Ramon Valley.

ACKNOWLEDGEMENTS

This research is supported by the U.S. Geological Survey (USGS), Department of the Interior, under USGS award number 14-08-0001-G2140. The views and conclusions contained in this document are those of the authors and should not be interpreted as necessarily representing the official policies, either expressed or implied, of the U.S. Government.

REFERENCES

Andrews, D.J., 1991, The Mission link between the Hayward and Calaveras faults, north-central California: Eos, v. 72, no. 44, p. 446.

Aydin, A., 1982, The East Bay Hills, A Compressional Domain Resulting from Interaction Between the Calaveras and Hayward-Rodgers Creek Faults: in Hart, E.W., and others, eds., Proceedings of the Conference on Earthquake Hazards in the Eastern San Francisco Bay Area, California of Mines and Geology Special Publication 62, p. 11-22.

Bakun, W.H., Clark, M.M., Cockerham, R.S., Ellsworth, W.L., Lindh, A.G., Prescott, W.H., Shakal, A.F., and Spudich, P., 1984, The 1984 Morgan Hill, California earthquake: Science, v. 225, no. 4659, p. 288-291.

Bonilla, M.G., Mark, R.K., Lienkaemper, J.J., 1984, Statistical Relations Among Earthquake Magnitude, Surface Rupture Length, and Surface Fault Displacement: Bulletin of the Seismological Society of America, v. 74, No. 6, p. 2379-2411.

Burkland and Associates, 1973a, Geologic and seismic hazards investigation, Tehan Canyon School site, Alameda Co., California, Unpublished consultants report on file at California Division of Mines and Geology.

_____, 1973b, Geologic and seismic hazards investigation, Foothill reservoir site, Pleasanton, Alameda Co., California. Unpublished consultants report on file at California Division of Mines and Geology.

California Department of Water Resources, 1974, Evaluation of groundwater resources: Livermore and Sunol Valleys: California Department of Water Resources Bulletin 118-2, 153 p.

Carpenter, D.W., 1975, Unpublished letter report on file with Alquist-Prilo report no. 65 at California Division of Mines and Geology.

Dibblee, T.W. Jr., 1980, Preliminary geologic map of the Walnut Creek Quadrangle, Contra Costa County, California: U.S. Geological Survey Open-File Report 80-351.

Hart, E.W., 1984, Evidence of surface faulting associated with the Morgan Hill earthquake of April 24, 1984: in Bennett, J.H. and Sherburne, R.W., eds., The Morgan Hill, California, Earthquake, California Division of Mines and Geology Special Publication 68, p. 161-184.

Herd, D.G., 1978, Quaternary faulting along the northern Calaveras fault zone: U.S. Geological Survey Open-File Report 78-307, 5 map sheets.

Kelson, K.I., Lettis, W.R., and Simpson, G.D., 1991, Paleoseismic investigations along the northern Calaveras fault, Alameda County, California: Geological Society of America Abstracts with Programs, v. 23, no. 2, p. 41.

Kelson, K.I., Lettis, W.R., and Simpson, G.D., this volume, Late Holocene paleoseismic events at Leyden Creek, northern Calaveras fault.

Montgomery, D.R., Jones, D.L., 1992, How Wide is the Calaveras fault zone? - Evidence for distributed shear along a major fault in central California: Geology, v. 20, p. 55-58.

Oppenheimer, D.H., and MacGregor-Scott, N.G., 1991, Seismic Potential of the East San Francisco Bay Region of California: Geological Society of America Abstracts with Programs, v. 23, no. 2, p. 85.

Oppenheimer, D.H., Bakun, W.H., Lindh, A.G., 1990, Slip partitioning of the Calaveras Fault, California, and Prospects for Future Earthquakes: Journal of Geophysical Research, v. 95, no. B6, p. 8483-8498.

Oppenheimer, D.H., and Lindh, A.G., this volume, The Potential for Earthquake Rupture of the Northern Calaveras Fault.

Page, B.M., 1982, The Calaveras Fault Zone of California, An Active Plate Boundary Element: in Hart, E.W., and others, eds., Proceedings, Conference on Earthquake Hazards in the Eastern San Francisco Bay Area, California Division of Mines and Geology Special Publication 62, p. 175-184.

Purcell, Rhoades & Associates, 1989, Geologic fault investigation, 4440 Foothill Road, Pleasanton, California, unpublished consultants report on file with the City of Pleasanton.

Slemmons, D.B., 1982, Determination of design earthquake magnitudes for microzonation: Proceedings of Third International Earthquake Microzonation Conference, v. 1, p. 119-130.

Toppozada, T.R., 1981, Preparation of isoseismal maps and summaries of reported effects for pre-1900 California earthquakes: California Division of Mines and Geology Open-File Report 81-11.

Van Velsor, J., 1991, personal communication of results of CalTrans fault study of Hwy 680-84 interchange.

Wagner, R., 1978, Geologic map of Las Trampas Ridge Quadrangle: unpublished Ph. D. thesis, University of California, Berkeley, California.

Wells, D.L., and Coppersmith, K.J., 1992, Updated empirical relationships among magnitude, rupture length, rupture area and surface displacement: Seismological Society of America, 1992 Santa Fe meeting.

Wong, I.G., Hemphill-Haley, M.A., and Wright, D.H., 1991, What and where is the Mission fault in the eastern San Francisco Bay Area, California?: Seismological Research Letters.

Wong, I.G., and Hemphill-Haley, M.A., this volume, Seismicity and faulting near the Hayward and Mission faults.

Working Group on California Earthquake Probabilities (WGCEP), 1990, Probabilities of large earthquakes in the San Francisco Bay Region, California: U.S. Geological Survey Circular 1053, 51 p.

Wyss, M., 1979, Estimating maximum expectable magnitude of earthquakes from fault dimensions: Geology, v. 7, no. 7, p. 336-340.

Parkfield Area Tectonic Framework

9910-04101

John D. Sims
Branch of Engineering Seismology and Geology
U.S. Geological Survey
345 Middlefield Road, MS 977
Menlo Park, California 94025
(415) 329-5653

Investigations Undertaken

1. Late Holocene and historic slip rates in the Carrizo Plain and Parkfield segments of the San Andreas fault
2. Earthquake recurrence intervals determined from earthquake-induced liquefaction structures formed in unconsolidated sediments
3. Late Holocene and historic creep rate on the Green Valley fault, northern San Francisco Bay area

Results Obtained

1. Continued work on the Carrizo Plain at the Phelan site. We determined the dates of the past 6 earthquakes on the Carrizo Plain as well as the slip per event for the last two events. Work is progressing on extending the slip per event to the older events in the last six earthquakes. The date of individual events and their maximum slip at the Phelan site are listed in the table below.

Event	Date (AD)	Slip per Event
I	1857	7.5 m
II	1616	7.5 m
III	1376	?
IV	1169	?
V	1011	?
VI	845	?

Our network of surveyed quadrilaterals, established on the San Andreas, White Canyon, Red Hills, Gold Hill, and Gillis Canyon faults in the Parkfield-Cholame area, totals 19 quadrilaterals. Fifteen quadrilaterals lie across the San Andreas, 2 on the White Canyon, and one each on the Red Hills and Gold Hill faults. These quadrilaterals are resurveyed every 2 months to gain background information on the sites prior to the next Parkfield earthquake.

2. The M_L 7.1 of 25 April 1992 earthquake, whose epicenter is near the town of Petrolia 53 km south of Eureka, induced scattered liquefaction in flood plain deposits of the Eel, Mattole, and Salt Rivers (Fig. 2). Two large aftershocks of this earthquake did not induce liquefaction although they were well above the threshold for the induction of liquefaction. The earthquake series is notable for the

fact that liquefaction was not more widespread. The liquefaction that did occur is notable for the coarseness of the material that was expelled on the ground surface. Recent damaging earthquakes with epicenters near Eureka occurred 7 March 1992 (M 5.3), 17 August 1991 (M 6.0), and 16 January 1990 (M 5.3). No earthquake-induced liquefaction is reported for any of these earthquakes.

Aerial and ground reconnaissance identified the principal areas of liquefaction in the epicentral area. Liquefaction primarily occurred in active flood plain deposits of the Mattole River between its mouth and the town of Honeydew. Isolated sandblows and groups of sandblows erupted onto the active flood plain of the Eel River. Isolated patches of sandblows erupted along the banks of the Salt River between Port Kenyon and Ardylia Corners 2 km north of Ferndale. Other isolated patches of liquefaction occurred near the town of Bull Creek (Fig. 2).

The most extensive liquefaction occurred in the epicentral area near Petrolia in modern floodplain deposits of the Mattole River. Fissures opened primarily in the modern active floodplain of the river, and sandblows erupted along them (Fig. 3). These fissures did not develop in response to lateral spreading, but solely to intense shaking and probable settling of the unconsolidated fluvial deposits in the river channel. Sandblow deposits are generally <6 to 8 cm thick and average about 3 to 4 cm thick. The characteristic feature of the sandblows in the Mattole River deposits is the coarse grain size of the erupted material. Fine to medium gravel is common and on the average makes up about 8 to 20 weight percent of the erupted material (Fig. 4). The grain size distribution of the erupted sediments is notable in that it is bimodal. The bimodal nature of the deposits suggests that the gravel component may not have been present in the liquefied layer but was entrained from coarse overlying deposits by the moving liquefied sand.

The fissures along the Mattole River are all parallel to subparallel to the axis of the river. The fissures occur in sets of *en echelon* fractures that cut longitudinal and point bar deposits in the river. There is no evidence that these fissures are associated with lateral spreading of the surficial deposits.

Isolated occurrences of liquefaction in the modern deposits of the Mattole River occur between Petrolia and Honeydew. At the confluence of Bundle Prairie Creek about 2.5 km southwest of Honeydew is a concentration of sandblow deposits that erupted along fissures parallel to the river axis. The general grain size of material erupted from the fissures is finer than the sandblows near Petrolia and the mouth of the Mattole River (Fig. 2). However, the grain-size distribution of the Honeydew sandblow cone deposits is bimodal which suggests entrainment of the coarser mode by liquefied sand (Fig. 5).

Local liquefaction accompanied by lateral spreading occurred along the Salt River. One site was excavated in cooperation with the USDA Soil Conservation Service office in Eureka. Small sandblow cones composed of fine- to medium-grained sand and silt erupted along fissures developed in lateral spreads. The lateral spreads were parallel to the river channel and had a total vertical separation of 0.5 m. The top of the liquefied layer lay between 2.3 to 2.5 m below the ground surface.

The liquefaction structures consisted of surface sandblow cones and subsurface sand dikes. The sandblow cones were about 1 to 3 m in diameter and up to 15 cm thick at the vent. Individual cones commonly coalesce with adjacent cones that erupted along a single fissure. Fissure lengths were about 2 to 12 m long. The subsurface dikes were about 2 to 10 cm wide, nearly vertical, planar features. Multiple anastomosing sand dikes are frequently observed in the vicinity of a stepover in an en echelon fissure system. In rare cases in the stepover region of en echelon fissures the sand dikes do not extend all the way to the surface. The sandblow cones are are composed of fine to medium sand. Grain size analysis shows that the sand grains are unimodally distributed (Fig. 6). The cones all exhibit several fining upward components that suggests episodic eruption and accumulation of sediment.

3. The Green Valley fault stretches from the Carquinez strait northwestward at least 30 km to Wooden Valley. However, plots of earthquake epicenters suggest that the fault extends northwestward for at least another 22 km. The fault was first mapped as an active fault by Sims and others(1973) as an active fault. Later mapping by Frizzell and Brown (1976) further detailed the geomorphic features that delineate the fault. The Green Valley fault is the northernmost active fault of the San Andreas transform System in the bay area and is related to the Concord fault as either a stepover or splay. Faults with strikes similar to the Green Valley lie in the Clear Lake area (Sims, oral commun., 1974 cited in Frizzell and Brown, 1976).

Two man made features are offset by the Green Valley Fault. A power line built in 1922 is offset 280 ± 10 mm and a fence built prior to 1862 is offset about 250. These two offsets yield modern slip rates of between 5.5 and 2.25 mm/yr (Frizzell and Brown, 1976). Seismic activity on the fault is nearly coincident with the mapped trace.

Several trench sites were found and one approved by the land owners in October 1991. The site consists of an alluvial fan terrace at the junction of two intermittent streams. The trace of the fault is clearly expressed in the alluvial fan terrace by several moist spots accompanied by green vegetation. On nearby hillsides low scarps are easily identifiable. An abandoned stream channel that is subparallel to the present active stream is present also on the alluvial fan terrace. The stream channelappear to be offset or truncated at the mapped trace of the fault.

Trenching investigations proceeded and seven trenches were opend at the site. The trenches revela that the Green Valley fault traces extend up into the modern soil and an offset abandoned channel that contains abundant charcoal. The channel is offset across the fault 1.2 - 1.5 m. Radiocarbon age dates received 23 November 1992 are as follow:

Sample Number	Unit	Uncalibrated ^{14}C Age
GV1-6	Older Fan	2815±75
GV2-25	C-5/6	655±55
GV2-35	C-11	1935±95
GV3-7	C-u	510±55
GV3-15	Older Fan	300±100
GV3-16	C-9	885±70
GV3-20	C-8	2530±70
GV5-26	C-4	1310±75
GV7-4	C-4	modern
GV7-11	C-3	465±65
GV7-29	C-4	655±65

Preliminary examination of the dates suggests reworking from older units is common. The older fan deposits into which the offset channel is incised are dated at 2815±75 yr B.P. The offset channel contains carbon that ranges in age from 2530±70 yr B.P. to modern. However there is a cluster of dates 510±55, 655±55, 465±65, and 655±65 yr B.P that suggest the age of the offset channel to be in the range of 510±55 to 655±55 yr B.P. Final interpretation of the age of the channel and slip rate on the Green Valley fault awaits recipet of the remaining four radiocarbon dated and complete analysis of the dates from the trenches in the light of the radiocarbon dates.

Reports Published

Sims, J.D., and Garvin, C.D., 1992, Sandblows and sand dikes developed in the 1989 Loma Prieta earthquake, and 1990 and 1991 aftershocks: Implications for paleoseismicity studies: submitted to Geological Society of America Abstracts with Program, v. 24, no. 3, p. .

Sims, J.D., and Garvin, C.D., in press, Recurrent liquefaction at Soda Lake, California induced by the 1989 Loma Prieta Earthquake and 1990 and 1991 aftershocks: Implications for Paleoseismicity Studies: Submitted to Geological Society of America Bulletin.

Sims, J.D., and Garvin, C.D., in press, Observations of multiple liquefaction events at Soda Lake CA during the 1989 Loma Prieta earthquake abd its aftershocks *in* Holzer, T. L., ed., The 1989 Loma Prieta Earthquake, Vol. II: Strong Ground Motion and Ground Failure,: U.S. Geological Survey Professional Paper

Digital Data Analysis

9920–10112

Stuart A. Sipkin
Branch of Global Seismology and Geomagnetism
U.S. Geological Survey
Box 25046, Mail Stop 967
Denver Federal Center
Denver, Colorado 80225
(303) 273–8415

Investigations

1. **Moment Tensor Inversion.** Apply methods for inverting body phase waveforms for the best point-source description to research problems.

2. **Other Source Parameter Studies.** Apply methods for inverting body phase waveforms for distributed kinematic and dynamic source properties.

3. **Aftershock Source Properties.** Examine mainshock and aftershock source properties total-time earthquake occurrence.

4. **Earth Structure.** Use long-period and broadband body phases to study lateral heterogeneity, attenuation, and scattering in the crust and mantle.

5. **Network Activity.** Participate in international endeavors aimed at increasing the installation, deployment, and operation of modern worldwide digital seismic networks, especially within areas where seismic-station coverage is poor, for the routine reporting of earthquake arrival-time information.

6. **Data Services.** Provide seismological data and information services to the public and to the seismological research community, particularly data from the Global Digital Seismograph Network (GDSN) on SEED tapes, Network-Day tapes, Network-Event tapes, and Network-Event CD–ROMs.

7. **NEIC Monthly Listing.** Contribute both fault-plane solutions (using first-motion polarity) and moment tensors (using long-period body-phase waveforms) for all events of magnitude 5.8 or greater when sufficient data exists. Contribute waveform/focal-sphere figures of selected events.

Results

1. **Moment Tensor Inversion.** A paper listing the moment-tensor solutions for 114 moderate- to large-size earthquakes occurring in 1990 has been published and a paper listing the moment-tensor solutions for 108 moderate- to large-size

earthquakes occurring in 1991 is in press. We are currently implementing a procedure for the rapid estimation of moment-tensor solutions using near-real-time USNSN, GTSN, and IRIS/GSN data. A paper analyzing an anomalous tsunamigenic seismic event near Tori Shima, Japan, in which we hypothesize that the causative process was magma injection, is in press. This paper represents the first widely accepted demonstration of magma injection inducing teleseismically observed, long-period seismic radiation.

2. **Other Source Parameter Studies.** Linear and nonlinear methods of waveform inversion are being implemented to derive the distributions of rupture time and/or fault slip as a function of position on the earthquake fault. These methods can be applied to either teleseismic or strong-motion data sets, although a joint inversion including both types of earthquake data provides a maximum constraint on the recovered rupture history. Seismograms recorded through a wide range of frequencies are used whenever possible to retrieve significant details of the coseismic slip pattern. The results of a linear inversion method to recover the distribution of fault slip for the 1989 Loma Prieta, California, earthquake using teleseismic body waves has been published. A paper detailing the application of this technique to two large Mexican subduction-zone earthquakes has been submitted for publication. Studies in progress include a teleseismic body-wave analysis of the 1979 Petatlan, Mexico, earthquake and a simultaneous inversion of the local strong ground motions, teleseismic body waves, and long-period Rayleigh waves recorded for the 1985 Chile earthquake.

3. **Aftershock Source Properties.** A study comparing the locations of the aftershocks following the 1979 Petatlan, Mexico, earthquake with the pattern of mainshock slip derived from a finite-fault inversion is currently in progress. Preliminary results suggest that the two clusters of intense aftershock activity observed in the source region occur at the edges of a single circular source zone.

4. **Earth Structure.** Data sets of long-period and broadband shear-wave data have been assembled for the purpose of studying lateral heterogeneity, attenuation, and deep discontinuities in the earth. While trying to recover broadband ground displacement, we discovered that, when deconvolving an instrument response, unless one is explicitly takes into account the properties of the filters being used, either bias or increased uncertainty in the results can be introduced, especially when taking integral measures of the displacement pulse. A new optimal method for deconvolving the instrument response has been developed that avoids the pitfalls inherent in the methods currently used. A paper quantifying the bias introduced and presenting this new deconvolution method has been published. Two papers detailing mantle discontinuity structure and regional variation of attenuation beneath China are in preparation.

5. **Network Activity.** Current programs focus on the MIDAS (Middle America Seismograph) Consortium, formed to promote the installation of a real-time, satellite-based, digital seismic network in Middle America. Also, there is an

ongoing collaboration with Instituto de Geofisica personnel at the Universidad Nacional Autonoma de Mexico to promote the deployment of a Mexican network of digital, broadband seismometers. This network will monitor seismicity throughout Mexico on a real-time basis.

6. **Data Services.** FORTRAN software to read and extract digital data from station tapes (1976–1979) and network day tapes (1980–1987) has been developed and distributed to the research community worldwide. Users are supported on a variety of computers. A new Standard for the Exchange of Earthquake Data (SEED) has been created and tapes are now being produced (1988 to present) and distributed by the Albuquerque Seismic Laboratory. FORTRAN software has been developed to read and extract the digital data from the SEED tapes and this software is being made available to the research community. Event tapes have been produced from network day tapes for data from 1980 through 1987 for all events with magnitude 5.5 or greater. Data from the event tapes are reformatted and sent to a CD–ROM mastering facility for replication. Nine volumes have been produced, covering 1980 through March 1987. The CD–ROMs are being distributed to over 200 universities across the United States and geophysical research institutions worldwide. Negotiations have been completed concerning the production of the first Federation of Broadband Digital Seismograph Network (FDSN) CD–ROM. Retrieval software, SONIC (C) and CDRETRV (FORTRAN), has been developed for the IBM/PC/AT/386 compatibles and distributed, allowing easy access to the digital data.

7. **NEIC Monthly Listing.** Since January 1981, first-motion fault-plane solutions for all events of magnitude 5.8 or greater have been contributed to the Monthly Listings. Since July 1982, moment-tensor solutions and waveform/focal-sphere plots have also been contributed. In the last year solutions for 112 events have been published. An atlas of European seismicity is in preparation. A catalog of first-motion focal mechanisms for 1988 and 1989 is in publication.

Reports

Eliutin, A., Ben Sari, D., Chinnery, M., Meyers, H., Massé, R.P., Gvishiani, A., and Lishner, J., 1991, Enhancement of Earth science research and educational capabilities in the developing nations through the use of compact disc technology—Report on the pilot project, Publication No. 199 of the International Lithosphere Program: National Oceanic and Atmospheric Administration, National Geophysical Data Center, Boulder, Colorado, 35 p.

Hartzell, S.H., Stewart, G.S., and Mendoza, C., 1991, Comparison of L1 and L2 norms in a teleseismic waveform inversion for the slip history of the Loma Prieta, California, earthquake: Bulletin Seismological Society of America, v. 81, no. 5, p. 1518–1539.

Kanamori, H., Ekström, G., Dziewonski, A., Barker, J.S., and Sipkin, S.A., 1992, Seismic radiation by magma injection—An anomalous seismic event near Tori Shima, Japan: Journal of Geophysical Research (in press).

Massé, R.P., 1992, United States National Seismograph Network: U.S. Geological Survey Yearbook, Fiscal Year 1991, p. 58–59.

Mendoza, C., 1992, Coseismic slip of two large Mexican earthquakes from teleseismic body waveforms: Implications for asperity interaction in the Michoacan plate-boundary segment: Journal of Geophysical Research (submitted).

Revenaugh, J., and Sipkin, S.A., 1992, Mantle discontinuity structure beneath China based on multiple-ScS reverberation mapping [abs.]: EOS (American Geophysical Union, Transactions) (in press).

Sipkin, S.A., 1991, Regional variation of attenuation in China from analysis of multiple-ScS phases [abs.]: EOS (American Geophysical Union, Transactions), v. 72, no. 44, p. 317.

Sipkin, S.A., and Lerner-Lam, A.L., 1992, Pulse-shape distortion introduced by broadband deconvolution: Bulletin Seismological Society of America, v. 82, no. 1, p. 238–258.

Sipkin, S.A., and Needham, R.E., 1992, Moment tensor solutions estimated using optimal filter theory: Global seismicity, 1990: Physics of the Earth and Planetary Interiors, v. 70, no. 1–2, p. 16–26.

Sipkin, S.A., and Needham, R.E., 1992, Moment tensor solutions estimated using optimal filter theory: Global seismicity, 1991: Physics of the Earth and Planetary Interiors (in press).

Sipkin, S.A., and Revenaugh, J., 1992, Regional variation of attenuation in China from analysis of multiple-ScS phases [abs.]: EOS (American Geophysical Union, Transactions) (in press).

Seismicity, Ground Motion, and Crustal Deformation Wasatch Front, Utah, and Adjacent Intermountain Seismic Belt

14-08-0001-G1762

R.B. Smith, W.J Arabasz, J.C. Pechmann, and C.M. Meertens*
Department of Geology and Geophysics
University of Utah
Salt Lake City, Utah 84112-1183
(801) 581-6274

Investigations: October 1, 1991 - September 30, 1992

1. Apparent decrease of stress drop with seismic moment for small earthquakes in Idaho: An artifact of attenuation.
2. Determination of the nature and rate of deformation along the Wasatch fault using the Global Positioning System.
3. Estimates of earthquake magnitude potential of active faults in the Intermountain Seismic Belt from paleoseismic surface rupture data.
4. The March 16, 1992, M_L 4.2 Western Traverse Mountains earthquake, Utah: Possible slip on the Wasatch fault.
5. Earthquakes near Cedar City, Utah ($M_L \leq 4.1$), June 28-29, 1992, and their possible relation to the M_s 7.5 Landers, California, earthquake.
6. The M_L 5.8 St. George, Utah, earthquake of September 2, 1992: A normal-faulting earthquake with very weak aftershock activity.
7. Review and synthesis of earthquake hazards of southwestern Utah.

Results

1. We have made new measurements of attenuation of seismic waves from aftershocks of the 1983 M_s 7.3 Borah Peak, Idaho, earthquake. The results show that attenuation can fully account for an apparent decrease of stress drop with seismic moment (M_o) previously observed for aftershocks of $M_o \leq 2 \times 10^{21}$ dyne-cm. To make these measurements, we used high quality USGS 3-component digital recordings of 61 aftershocks with $M \leq 3.5$ and $M_o \leq 3 \times 10^{21}$ dyne-cm. The attenuation parameter t* (the ratio of travel time over quality factor, Q) was calculated from the slopes of log-linear displacement spectra of P- and SH-wave pulses at frequencies below the apparent corner frequency. Average t* values of 0.03 for P waves and 0.06 for SH waves indicate high attenuation, despite short epicentral distances ($\leq$ 40 km) and

---

*J.D.J. Bott, G.E. Christenson, W.L. Hardman, D.B. Mason, and S.J. Nava also contributed significantly to the work reported here.

recording sites on bedrock. Forward modeling in the time domain shows that this high attenuation causes significant broadening of SH-wave pulses shorter than 0.5 seconds duration (Figure 1). If not properly accounted for, this pulse broadening causes overestimation of source radii for small earthquakes and hence underestimation of stress drops. This systematic error is large enough to produce the observed deviation from constant-stress-drop scaling for the Borah Peak aftershocks.

The t* measurements were inverted for three-layer Q models for P and SH waves, allowing for different amounts of attenuation in the top layer beneath each seismograph station. Q is low but varies for both P (21 to 56) and SH waves (12 to 22) in the top layer (0.0-1.64 km depth), increasing in the second layer (1.64-6.95 km) to 103 for P waves and 405 for SH waves. For depths greater than 6.95 km, Q_P and Q_{SH} are high, 274 and 1000 respectively, but poorly constrained for SH waves due to lack of data at large epicentral distances. In the uppermost layer, Q_P/Q_{SH} varies from 1.5 to 3.7, ratios usually considered to indicate high levels of water saturation. The ratio is reversed in the two lower layers to ~0.3, indicating less water saturation at depth. Most of the attenuation occurs in the near surface and the amount varies with receiver location.

Numerous other studies have found apparent decreases of stress drop with M_o for small earthquakes. Our results confirm the hypothesis that high attenuation in the shallow crust can explain this phenomenon, at least in the Borah Peak region.

2. We have completed the first part of a two-year project to measure deformation rates along the Wasatch fault using Global Positioning System (GPS) technology. Activities included (1) field reconnaissance of benchmarks and training of personnel, (2) a 2½-week GPS field campaign in May 1992, and (3) subsequent data processing. The field work was a collaborative effort involving 12 participants from the University of Utah and 19 from the Utah Geological Survey, the Salt Lake County Surveyor's Office, the U.S. Bureau of Land Management, the Utah Department of Transportation, and 6 other government agencies and universities. Thirty-two horizontal trigonometric and trilateration stations (Figure 2) were observed for the first time with GPS. Each station was occupied for two days or for two 12-hr consecutive sessions. A continuously-tracking Trimble 4000 SST dual-frequency GPS receiver was operated on the University of Utah campus in Salt Lake City during the campaign, and four other Trimble 4000 SST receivers were used for field measurements. The processed measurements have average uncertainties of 3-4 mm in the horizontal and 10-12 mm in the vertical—typical of what can be achieved in a high-precision GPS survey using improved orbits, long tracking times (>6 hrs), and careful surveying techniques. The GPS measurements will be compared with surveys done using conventional triangulation (in 1938 and 1962) and with laser trilateration (beginning in 1972) to determine long-term strain rates.

3. We have used a worldwide set of 16 normal-faulting earthquakes to develop regressions of surface-wave magnitude on maximum surface displacement and surface rupture length. Application of the resulting formulas to paleoseismic surface rupture parameters for 29 of the best-studied Intermountain Seismic Belt faults shows that magnitudes predicted by displacement are consistently larger than those determined from lengths. This discrepancy can be attributed primarily to a tendency for workers to overestimate prehistoric single-event surface

displacements and to underestimate surface rupture lengths. Regressions based on the product of these two quantities are more physically justifiable, have generally better statistics, and predict magnitudes that represent a compromise between the diverging errors plaguing estimates from the other regressions. The weighted least-squares regression of this form derived from the 16 historical earthquakes is

$$M_s = 0.47 \log (d_{sM} L_s) + 6.1$$

where M_s is surface wave magnitude, d_{sM} is maximum surface displacement in meters, and L_s is the average of the straight-line and trace lengths of the surface rupture in km. A trivariate regression of M_s on L_s and d_{sM}/L_s produced an equation that is identical to the above bivariate equation within the limits of resolution of the coefficients, indicating that L_s and d_{sM} scale similarly with M_s.

We used the relation given above to estimate magnitudes of late Pleistocene and Holocene earthquakes on 39 segments of 29 faults in the Intermountain Seismic Belt for which the necessary data are available. The results suggest that the largest earthquake likely to occur in the region for *either* single- or double-fault-segment rupture is $M_s=7.3$. The standard error is ±0.3, so that there is a 32% statistical chance that some of the faults could generate magnitudes as great as $M_s=7.6$. This calculation suggests that the $M_s=7.5$ to 7.6 Hebgen Lake, Montana earthquake may represent the largest earthquake likely to occur in the ISB. The six central segments of the Wasatch fault, which cross an urban corridor of 1.6 million people, has repeatedly produced earthquakes with estimated magnitudes from $M_s=7.1$ to 7.3. This size range is likely to characterize future earthquakes on those segments.

4. An M_L 4.2 earthquake occurred on March 16, 1992, at 12.5 ± 1.5 km depth beneath the Western Traverse Mountains south of Salt Lake City, Utah. The epicenter of this earthquake is at the western edge of a prominent ENE-WSW-trending band of seismicity, where small earthquakes have occurred episodically since at least 1971. This band of seismicity appears to coincide with the boundary between the Salt Lake City segment of the Wasatch fault to the north and the Provo segment to the south. This segment boundary is located at a major bend in the surface trace of the fault which is called the Traverse salient. Unfortunately, the three-dimensional distribution of the associated seismicity band cannot be determined with the available data because the focal depth control on most of the hypocenters is poor.

The focal mechanism for this earthquake shows dominantly normal faulting on a fault dipping moderately to the SW (38° ± 4°) or to the E (56° ± 2°). The surface projection of the SW-dipping nodal plane lies within one kilometer of the surface trace of the Wasatch fault at the western edge of the Traverse salient, where the local strike of the fault is similar to the NW strike of the nodal plane. Therefore, it is possible that the Western Traverse Mountains earthquake occurred on the Wasatch fault at the Traverse salient. This observation is significant because there have been very few instrumentally-located earthquakes that could be interpreted to lie on the Wasatch fault, even though this fault has produced numerous Holocene surface-faulting earthquakes. It is equally possible, however, that this earthquake occurred on a small unrecognized fault or a buried fault with no clear surface expression, as do most of the small- and moderate-sized earthquakes in Utah.

5. A series of more than sixty earthquakes, the largest of M_L 4.1, occurred near Cedar City in southwestern Utah on June 28 and 29, 1992—beginning within 40 minutes of the M 7.5 Landers, California, earthquake. The earthquakes clustered ~11 km NW of Cedar City along the NW margin of Cedar Valley, broadly within the Hurricane fault zone and within an area of Pleistocene volcanic activity. The June 28-29 activity may have occurred on a NE-trending buried fault inferred by others from gravity data to form the NW boundary of the Cedar Valley block. The occurrence of the Cedar City earthquakes so soon after the Landers main shock, taken together with nearly simultaneous increases in seismicity at more than a dozen other sites in the western U.S., suggests that these earthquakes may have been remotely triggered by the Landers event. Collaborative work with USGS scientists investigating this possibility is continuing.

6. An M_L 5.8 earthquake occurred in SW Utah on September 2, 1992, 8 ± 1 km ESE of the center of the city of St. George. The shock was the largest in the Utah region since 1975 and the largest in the St. George area since 1902. The earthquake caused surprisingly little damage to St. George (population ~28,500) and other nearby communities, although it triggered a massive, destructive landslide 45 km away. No surface faulting was observed. Our focal mechanism for this earthquake indicates normal slip on a N-striking fault dipping 46° ± 5° E or 46° ± 6° W. A focal depth of 15 ± 2 km was determined by Terry C. Wallace (University of Arizona) from analysis of teleseismic waveform data.

The main shock had no foreshocks ($M_L \geq 2.0$) and has had remarkably few aftershocks for an event of this size. Only one aftershock of $M_L \geq 2.0$ has occurred as of this writing (3 months after the main shock)—an M_L 2.7 event on September 10. The University of Utah deployed a variety of portable seismographs, including 5 telemetered stations and one 3-component digital station, to supplement the sparse coverage of the regional seismic network in this area (nearest station 75 km). Hypocenters of 20 microaftershocks, constrained by data from the portable seismographs, define a 20-km-long zone extending from 5 to 18 km depth which shallows to the east of the main shock focus. This aftershock distribution implies that the W-dipping nodal plane of the focal mechanism is probably the slip plane. The surface projection of this nodal plane lies close to the surface trace of the Hurricane fault, a major W-dipping normal fault with a late-Quaternary slip rate of 0.30 to 0.47 mm/yr which lies along the western margin of the Colorado Plateau. Our data suggest, but do not prove, that the St. George earthquake resulted from buried slip on the Hurricane fault.

7. Parts of southwestern Utah lie within the southern Intermountain Seismic Belt, which in this region trends SW from Scipio through Richfield, Cedar City, and St. George. Historical earthquakes have reached magnitude 6 to 6½, mostly near Richfield and Elsinore. Geologic studies indicate that late Quaternary deformation (faulting, folding, and uplift) has occurred in southwestern Utah, and many potentially seismogenic geologic structures are present. Faults potentially capable of rupturing the surface, with accompanying tectonic subsidence and strong ground shaking, are found throughout the area, but are concentrated in the Intermountain Seismic Belt. Prehistoric earthquakes in the magnitude 7 to 7½ range have occurred throughout the area and could occur in the future.

Reports and Publications

Arabasz, W.J., J.C. Pechmann, and E.D. Brown (1992). Observational seismology and the evaluation of earthquake hazards and risk in the Wasatch front area, Utah, in *Assessment of Regional Earthquake Hazards and Risk Along the Wasatch Front, Utah,* P.L. Gori and W.W. Hays (Editors), *U.S. Geol. Surv. Profess. Paper 1500-A-J,* D1-D36.

Arabasz, W.J., S.J. Nava, and J.C. Pechmann (1992). Earthquakes near Cedar City, Utah, June 28-29, 1992, *Wasatch Front Forum (Utah Geological Survey) 8, No. 2,* 4-7.

Arabasz, W.J., J.C. Pechmann, S.J. Nava, and T.C. Wallace (1992). EERI special earthquake report: St. George, Utah, September 2, 1992, *EERI Newsletter 26, No. 10,* 6-7.

Bott, J.D.J. (1992). Apparent decrease of stress drop with seismic moment for small earthquakes in Idaho: An artifact of attenuation, *M.S. Thesis,* University of Utah, Salt Lake City, Utah, 78 pp.

Bott, J.D.J. and J.C. Pechmann (1992). Apparent decrease of stress drop with seismic moment for small earthquakes in Idaho: An artifact of attenuation, *Seism. Res. Lett. 63,* 58.

Christenson, G.E. and S.J. Nava (1992). Earthquake hazards of southwestern Utah, in *Engineering and Environmental Geology of Southwestern Utah,* K.M. Harty (Editor), *Utah Geol. Assoc. Pub. 21,* 123-137.

Mason, D.B. (1992). Earthquake magnitude potential of active faults in the Intermountain seismic belt from surface parameter scaling, *M.S. Thesis,* University of Utah, Salt Lake City, Utah, 110 pp.

Pechmann, J.C. (1992). Focal mechanism and seismotectonic setting, in *The March 16, 1992* M_L 4.2 Western Traverse Mountains Earthquake, Salt Lake County, Utah, G.E. Christenson (Compiler), *Utah Geological Survey, Open-File Rept. 255,* 3-7.

Pechmann, J.C., S.J. Nava, and W.J. Arabasz (1992). Seismological analysis of four recent moderate (M_L 4.8 to 5.4) earthquakes in Utah, *Utah Geological Survey, Contract Rept. 92-1,* 107 pp.

Pechmann, J.C., S.J. Nava, and W.J. Arabasz (1992). Four moderate (M_L 4.8 to 5.4) earthquakes in Utah, 1987 to 1989, *Seism. Res. Lett. 63,* 38.

Smith, R.B. and W.J. Arabasz (1991). Seismicity of the Intermountain seismic belt, in *Neotectonics of North America,* D.B. Slemmons, E.R. Engdahl, M.D. Zoback, and D.D. Blackwell (Editors), *Geol. Soc. Am., Decade Map Vol. 1,* 185-228.

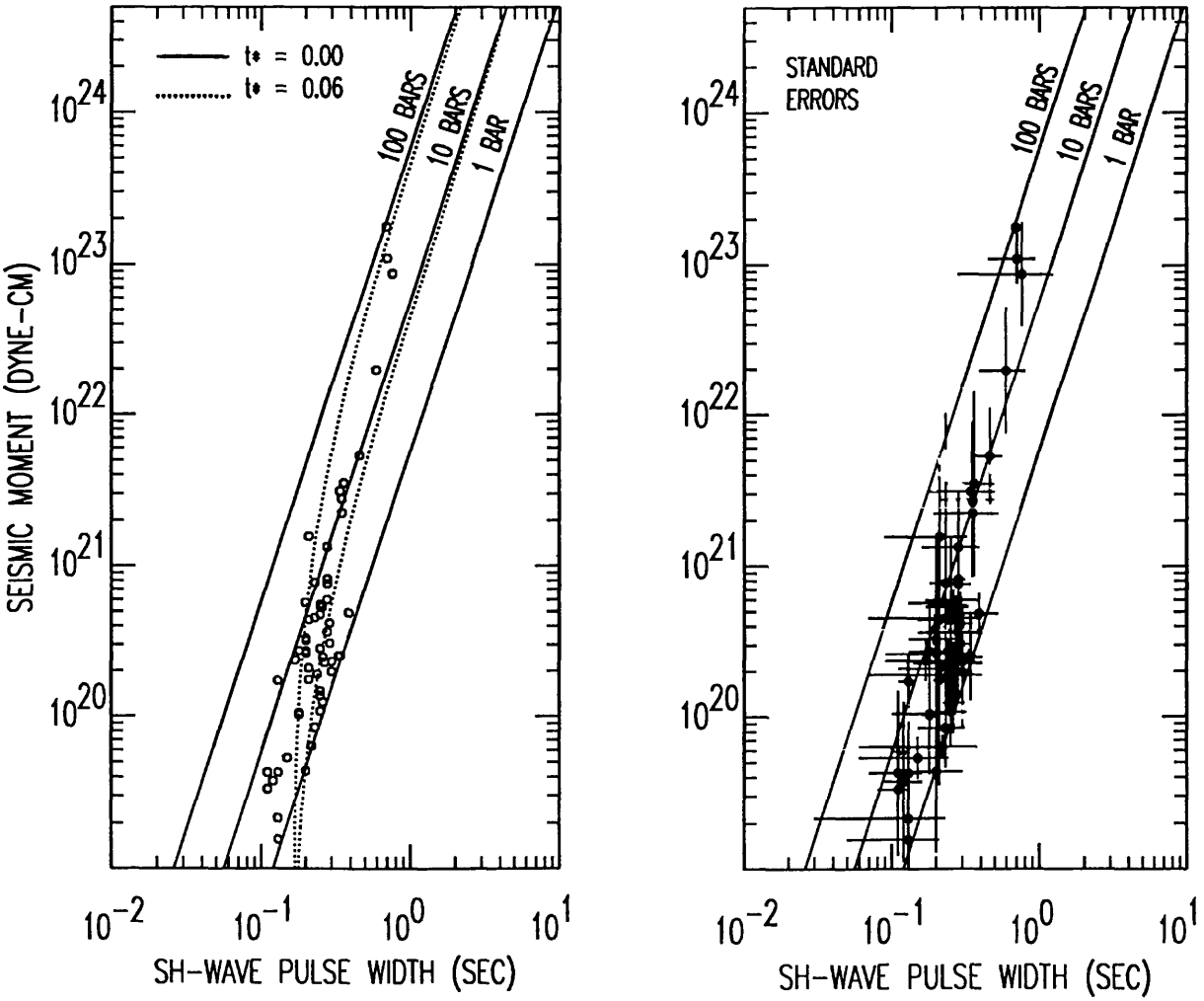

Figure 1. M_o versus SH-wave pulse width for Borah Peak aftershocks. The M_o values were calculated from the areas beneath the SH-wave displacement pulses. Each data point plotted is the average of at least two measurements from different stations. The error bars on the right plot show the standard deviations of these averages. The solid lines show the relation between M_o and SH-wave pulse wide predicted by the circular source model of Cohn et al. (1982, JGR 87, 4585-4594) for constant stress drops of 1, 10, and 100 bars. The dotted lines on the left plot show how the M_o-pulse width relations for stress drops of 10 and 100 bars are modified by attenuation for $t^* = 0.06$, the average value that we measured for SH waves. Note that the data are well fit by constant-stress-drop scaling with stress drops of 10 to 100 bars if the measured attenuation of $t^* = 0.06$ is accounted for.

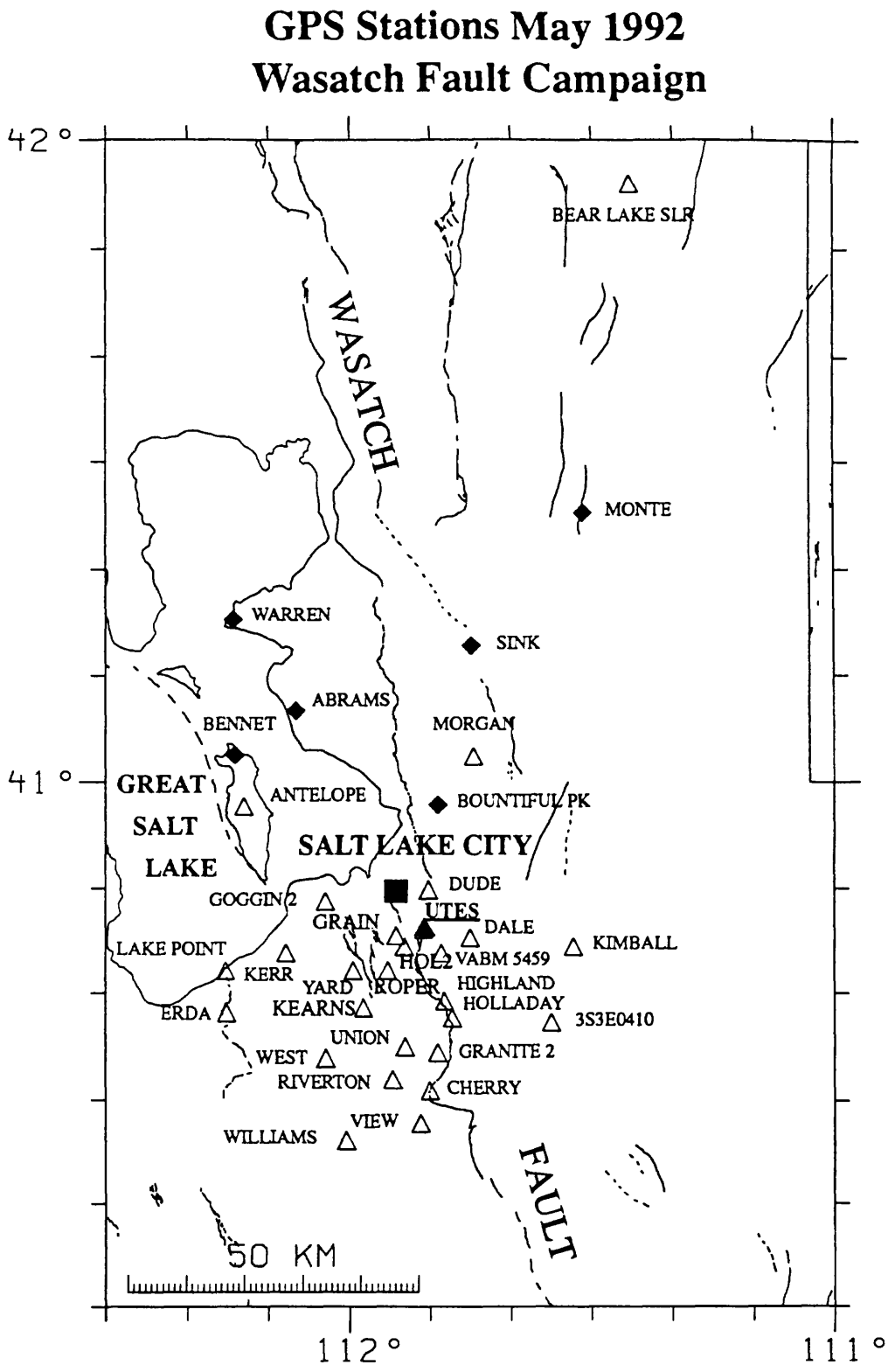

Figure 2. Map of GPS stations occupied in the May 1992 Wasatch Fault GPS Campaign in north-central Utah. Solid diamonds are U.S. Geological Survey geodelite-measured trilateration sites. The open triangles are 1st order horizontal triangulation sites. The fixed station UTES (solid triangle) was operated continuously during the 17-day survey. Young faults are shown by solid or dashed lines.

5 Dec 92

Annual Technical Report XXXIV

Modeling and Monitoring Crustal Deformation

9960-70116

Ross S. Stein, Wayne Thatcher, Grant A. Marshall, and Gillian R. Foulger

Office of Earthquakes, Volcanoes, and Engineering
345 Middlefield Road, MS 977
Menlo Park, California 94025

rstein@isdmnl.wr.usgs.gov
Tel 415/329-4840
Fax 415 329 5163

INVESTIGATIONS

1. We calculated the failure stress changes on the San Andreas fault system caused by the 1992 Landers earthquake sequence, to infer the effect on great earthquake occurrence.

2. We tested the sensitivity of the Loma Prieta coseismic geodetic deformation to different strategies for inversion of the fault slip geometry.

3. We are analyzing the coseismic deformation associated with the 1992 Cape Mendocino earthquake, the 1954 Dixie Valley and Fairview Peak, Nevada, earthquakes, and have carried out a 100-km-long GPS first epoch campaign to measure the extension of the U.S. Basin and Range.

RESULTS

Landers Earthquake Stress Changes. The largest earthquake to strike southern California during the past four decades did not rupture the San Andreas fault, but instead slipped faults within the eastern California shear zone. We show that several smaller shocks which occurred near the Landers event during the preceding 17 years increased stress at the future Landers epicentral site and along much of the eventual rupture path. Similarly, we argue that the Landers earthquake and its aftershocks have changed the stress along the San Andreas fault system, bring the San Andreas fault significantly closer to failure near San Bernardino, a site that has not sustained a large shock since 1812. Stress also increased on the San Jacinto fault near San Bernardino and on the San Andreas fault southeast of Palm Springs. Unless creep or moderate earthquakes relieve these stress changes, the next great earthquake on the southern San Andreas fault is likely to be advanced by 1 to 2 decades. In contrast, stress on the San Andreas north of Los Angeles dropped, potentially delaying the next great earthquake there by 2 to 10 years (Stein, G.C.P. King, and J. Lin).

Loma Prieta Earthquake Deformation. Leveling surveys conducted before and after the Loma Prieta earthquake provide observations of the coseismic elevation changes. These data are used to define the spatial pattern of elevation change, and to deduce the faulting geometry and distribution of slip. Both planar and curved (listric and negatively listric) faults produce elevation changes consistent with the observations. Using an elastic halfspace, we treat the data as correlated observations and find that 60% of the observed signal can be modeled with a planar rupture surface that extends from 6- to 12-km depth, is 32 km in length, 7 km wide and dips 64°s southwest. With a slip magnitude of 3.6 m, this model fault produces a geodetic moment of 2.6×10^{19} N•m. A larger thrust component is found northwest of the epicenter (rake=144°) and a larger strike-slip component is found southeast of the epicenter (rake=157°). Models with larger rake variations (>40°) reduce marginally the fit to the data, but require a moment of only 1.8×10^{19} N•m. The rupture plane lies 2 km southwest of the aftershock zone. When a low-modulus layer or wedge model is added for consistency with the seismic P-wave velocity structure, the fault deepens and locates adjacent to the aftershock zone, coming within 1.5 km of the hypocenter (G. Marshall, R. Stein, and W. Thatcher).

1992 Cape Mendocino Earthquake. Working with Humboldt County, California State Office of Emergency Services, the Federal Emergency Management Agency, the National Ocean Survey, and the U.S. Coast Guard, we have coordinated resurvey of 350 km of leveling lines in the epicentral region of the Cape Mendocino earthquake. These observations, due in late December, will be processed and analysed to infer the location, geometry, and slip of the earthquake, and to identify sites of coastal uplift, hazards to navigation, and damage to roads, pipelines, and lifelines. Using coseismic observations of coastal uplift from *Carver et al* [1992], we find a geodetic moment of at least 1.8±0.1E26 dyne-cm (M_W=6.8). When we further constrain the fault to be as small as possible and to come within 2 km of the mainshock hypocenter, we obtain a moment of 4.4±0.3E26 dyne-cm (M_W=7.1), pure thrust slip of 10.5±0.7 m, a fault length of 13 km, and a fault tip extending about 4 km offshore. The southern edge of the fault is close to the latitude of the main shock, but we must await additional observations to constrain the northern limit of the rupture and the full landward extent of the fault (G. Marshall, R. Stein).

Measurement of Coseismic and Secular Basin and Range Extension. We have emplaced a highly redundant 63-station Global Positioning System (GPS) network extending from eastern California to eastern Utah, straddling U.S. Highway-50. The network is designed to detect the rate and orientation of continental extension over a 5-year time span. We hope to resurvey nearly 100-year-old triangulation stations along this network this year, to learn if detectable shear strain has occurred anywhere along the network. In addition, we are analyzing the vertical and horizontal geodetic deformation that accompanied and followed the 1954 Dixie Valley and Fairview Peak earthquakes in Nevada, developing new tools to identify and remove survey errors (G. Foulger, W. Thatcher, K. Hodgkinson, M. Mofton, G. Marshall, B. Julian, and R. Stein).

REPORTS PUBLISHED OR SUBMITTED DURING THIS PERIOD (excluding abstracts):

Ekström, G., R. S. Stein, J. P. Eaton, and D. Eberhart-Phillips, Seismicity and geometry of a 110-km-long blind thrust fault, 1, The 1985 Kettleman Hills, California, earthquake, *J. Geophys. Res., 97,* 4843-4864, 1992.

Hill, D.P., and W. Thatcher, An energy constraint for frictional slip on misoriented faults, *Bull. Seismol. Soc. Am., 82,* 883-897, 1992.

Marshall, G.A., and R.S. Stein, Geodetic leveling observations associated with the October 18, 1989, Loma Prieta earthquake and their use to infer fault slip geometry, in press, *USGS Prof. Pap. on Loma Prieta Earthquake,* 80 p., 1992.

Southern California Earthquake Center Ad-hoc Working Group Report to National Earthquake Prediction Evaluation Council (one of many authors), The Landers earthquake sequence and future seismic hazards in southern California, in press, *U.S. Geological Survey Open-File Rep.*, in press, 80 pp, 1992.

Savage, J.C., and W. Thatcher, Interseismic deformation at the Nankai Trough, Japan, subduction zone, *J. Geophys. Res., 97,* 11,117-11,135, 1992.

Stein, R. S., and G. Ekström, Seismicity and geometry of a 110-km-long blind thrust fault, 2, Synthesis of the 1982-1985 California earthquake sequence, *J. Geophys. Res., 97,* 4865-4883, 1992.

Stein, R. S., P. Briole, J.-C. Ruegg, P. Tapponnier, and F. Gasse, Contemporary, Holocene and late Quaternary deformation of the Asal rift, Djibouti: Implications for the mechanics of slow-spreading ridges, *J. Geophys. Res., 96,* 21,789-21,806, 1991.

Stein, R. S., G. C. P. King, and J. Lin, Change in failure stress on the southern San Andreas fault system caused by the 1992 Magnitude=7.4 Landers earthquake, *Science, 258,* 1328-1332, 1992.

Consolidated Digital Recording and Analysis

9930-03412

S.W Stewart, A. W. Walter
Branch of Seismology
U. S. Geological Survey
345 Middlefield Road, MS/977
Menlo Park, California 94025
(415) 329-5515

Investigations.

There are between 25-50 regional seismic networks in the U.S., consisting of 1200-1500 seismic stations. The two largest regional networks are the Northern and Central California Seismic Network (CALNET) operated by the USGS (Menlo Park) in central California, and the Southern California Seismic Network operated jointly by Caltech and the USGS (Pasadena). CALNET consists of more than 300 sites and 500 instruments, while the Southern California Seismic Network has at least 200 sites and 300 instruments. These two networks combined account for about one-half of the existing seismic stations and about three-quarters of the existing data volume of digitized waveforms from all regional seismic networks in the U.S.

This project supports the Earthquake Hazards Reduction Program in the following ways.

(1) We have developed and now provide software systems to automate the acquisition and processing of local, regional and teleseismic earthquake waveforms from large, regional seismic networks. For example, the CALNET earthquake network in north-central California and the Caltech/USGS Cooperative Southern California earthquake network are producing masses of data in nearly identical formats because they are using computer-based data acquisition and analysis systems developed by this project.

(2) We support the focused monitoring experiment currently being carried out at Parkfield, California. The same software/hardware system used for large regional networks is used at the Varian and Haliburton monitoring sites at Parkfield.

The following networks (or network operators) are now using CUSP software:

- Northern California Seismic Network (CALNET)
- Southern California Seismic Network
- Hawaii Volcanos Observatory, Hawaii
- Parkfield Prediction Experiment (Varian site)
- Parkfield Prediction Experiment (Haliburtion site)
- University of Nevada (Reno)
- Idaho National Engineering Laboratories (INEL)
- University of Southern California

Hardware for these systems is based upon the Digital Equipment Corporation (DEC) VAX series of micro-computers. Currently, this includes the VAX 785, microVAX II, VAXstations 2000, 3100 and 3200, and VAX 4000 series.

Software is based upon the DEC/VMS operating system, the CUSP database system, and the GKS graphics system. VMS is a major operating system, well documented and developed, and has a rich variety of system

services that facilitate our own system development. CUSP is a state-driven database system designed for systematically processing large numbers of earthquakes recorded by large local seismic networks. It was developed by Carl Johnson formerly of the USGS. GKS is an international-standard graphics analysis package that provides interactive input facilities as well as graphical output to a workstation. We use the DEC implementation of GKS.

The transfer of Bob Dollar from Menlo Park to Pasadena in March, 1992, raises some questions, as yet unanswered, as to how the "official" version of the CUSP system (realtime and offline analysis) will be maintained in an efficient and timely manner.

Results:

1.CUSP software development and installation:

1.1 All elements of a complete package for Realtime processing of Regional Seismic Network Data were completed and installed at the sites listed in (2) below. These elements are collectively referred to as the CUSP system, version 1.0, and include:

RT: the Real_Time data acquisition system; this system performs both online earthquake detection and pre-processing. The pre-processing steps include automatic P-phase picking and calculation of a hypocenter.

TIMIT: an interactive graphics program to process earthquake traces; this program can handle seismic waveforms recorded on different regional networks, merged from several sources, each with different digitizing rates and different instrument characteristics. For example, Quanterra 24-bit waveform data from Caltech can be merged and displayed along with 16-bit waveform data from the CALNET and Southern California earthquake networks. The former QED earthquake editor is a subset of the TIMIT system.

STNMAP: an interactive graphics program to display the station locations and epicenter of each earthquake. The analyst can select subsets of the stations and trial hypocenters for more detailed analysis.

1.2 The CUSP 9-track tape ARKIVE process was converted to run on DAT and EXAbyte tape streaming devices. This results in greatly reduced volumes of tape to be used for arkiving.

1.3 A backup system for the CUSP Realtime Data Acquisition system was completed and brought on-line. In addition to providing complete backup to the primary realtime system, it has two EXabyte tape sub-systems for continuous digital recording of the CALNET earthquake network. Data retrieval from these tape sub-systems is being developed and tested now.

2. Making CUSP data files available to UNIX users:

2.1 To make the CUSP data more readily available to the scientific community, we spent considerable time making general-purpose routines to convert seismic data from one format to another, including CUSP-to-SEGY, SEGY-to-CUSP, CUSP-TO-SAC and CUSP-to-AH/XDR. format. The latter includes decimation filtering for processing teleseismic data. The CUSP-to-AH software is used extensively by other investigators in the Seismology Branch for teleseismic studies.

2.2 The VAX/VMS versions of the CUSP database libraries, and the data conversion filters (see '3.' above) were converted to AH/XDR format to run under UNIX, In addition, those CUSP applications that require access to the event files database also were converted to run under UNIX.

2.3 The continuous digital recording referred to in section 1.3 above will make it possible to retrieve longer portions of teleseismic waveforms than is now practical.

Reports:

None.

INFLUENCE OF THE SOUTHERN WASHINGTON CASCADES CONDUCTOR ON VOLCANISM AND TECTONISM

9980-04028

Donald A. Swanson
Branch of Igneous and Geothermal Processes
U.S. Geological Survey
Department of Geological Sciences AJ-20
University of Washington
Seattle, WA 98195
(206) 553-5587

Investigations

The East Canyon Ridge 7-1/2-minute quadrangle (figs. 1 and 2), near the eastern edge of the Southern Washington Cascades Conductor (SWCC; Stanley and others, 1987, 1990), was mapped geologically at a scale of 1:24,000. In addition, parts of the Tower Rock (Swanson, 1991), McCoy Peak (Swanson, 1992a), French Butte (Swanson, 1989), and Blue Lake (Swanson, 1992b) quadrangles were field checked and modified where necessary. The geologic map of the East Canyon Ridge quadrangle will be released as an open-file report after chemical analyses and thin sections are received and evaluated, most likely in 1993.

This work is part of an ongoing cooperative effort with Roger Ashley and Russ Evarts (Branch of Western Mineral Resources, U.S. Geological Survey, Menlo Park) to define the development of the Cascade Range along an east-west transect in the Mount St. Helens area (fig. 1). The SWCC, an anomalous electrical conductor at intermediate depth within the crust, underlies that part of the transect area between Mount St. Helens and Mount Adams. One goal of the cooperative effort is to compare and contrast volcanism and tectonism above the SWCC with that beyond the limits of the SWCC.

Improved understanding of the nature and influence of the SWCC is important in order to define and evaluate earthquake hazards in the area. The western margin of the SWCC coincides with the St. Helens seismic zone (Weaver and Smith, 1983; Grant and others, 1984; Grant and Weaver, 1986), which "could, under certain assumptions, be capable of generating a magnitude 7.0 earthquake" (Weaver and Smith, 1983, p. 10,380). The northeastern margin of the SWCC includes a north-northwest-trending zone of seismicity near Mount Rainier (Weaver and Malone, 1987; Stanley and others, 1987) and the epicentral area of the 1981 Goat Rocks earthquake (magnitude 5.0; Zollweg and Crosson, 1981; Weaver and Smith, 1983).

Results

The East Canyon Ridge quadrangle contains a suite of volcanic rocks ranging in age from late Oligocene to Quaternary. Lava flows, pyroclastic flows, and diamictites of andesite and basaltic andesite, with minor dacite and rhyolite, comprise the Tertiary section. These rocks were intruded by numerous dikes, sills, and related intrusions and then folded along a north-northwest-trending anticline (the Yozoo Creek anticline) that diagonally crosses the Blue Lake quadrangle (fig. 2).

The folding took place before about 12 Ma, the approximate age (from zircon fission-track counts) of a suite (the Kidd Creek suite of Marso and Swanson, 1992) of hornblende andesite-dacite and hornblende diorite-quartz diorite dikes and sills that intrude the older rocks (fig. 2). This hornblende-bearing suite forms a subvolcanic complex with a large radial dike swarm (Swanson, 1990, 1991) centered in the northeast part of the McCoy Peak quadrangle. The pattern of the radial dikes,

and their systematic subvertical orientation, indicate that they were intruded after folding, which produced dips of 30–50° (in places, possibly disturbed by faulting, even 85°). In addition, several other bodies (chiefly sills) of hornblende diorite in the northern part of the East Canyon Ridge quadrangle, though clearly part of the Kidd Creek suite, may reflect the presence of other smaller volcanoes, all other evidence for which has been eroded away.

The distribution of the Kidd Creek intrusive suite is of interest relative to the eastern limit of the SWCC. From reconnaissance work, the suite occurs only a little farther east than the eastern edge of the Blue Lake and East Canyon Ridge quadrangles, which roughly coincides with the margin of the SWCC (figs. 1 and 2). Future work in the adjoining Hamilton Buttes quadrangle will test this idea.

The hornblende-bearing intrusions in the Blue Lake quadrangle are restricted to the area south of the North Fork Cispus River (fig. 2). In the adjacent Tower Rock quadrangle, the intrusions are similarly restricted to the area south of the Cispus River downstream from the mouth of the North Fork. No significant faulting is evident along these rivers. The rather sharp northern limit in distribution of the hornblende-bearing suite might reflect some kind of crustal control not manifested at the surface, such as a blind fault or hidden structure in the SWCC.

Regional uplift and associated erosion followed intrusion of the hornblende-bearing suite. The timing and duration of the uplift is unknown but might be continuing today. My unpublished reconnaissance study of the paleogradient of the Tieton Andesite, an 80-km long, 1-Ma intracanyon flow in the Tieton River drainage on the east flank of the Cascades (fig. 1), suggests uplift of the Cascade axis of about 4.7 m/km in the past one million years. Whether this implies that uplift is continuing in the map area is unclear.

The Pin Creek fault zone (fig. 2), a north-northwest-trending zone first recognized by Hammond (1980), cuts obliquely across the northwest corner of the East Canyon Ridge quadrangle (fig. 2). The fault zone may control the course of the Cispus River for several kilometers upstream from the mouth of the North Fork Cispus River (Swanson, 1991). At least some of the motion within the Pin Creek fault zone was in a dextral sense, as indicated by subhorizontal slickensides on stepped surfaces and minimal roughness in a right-lateral direction. Other surfaces show steeply plunging slickensides, however. Direct evidence for faulting has been found only in the Tower Rock quadrangle, and even there marked flattening of attitudes in the volcanic rocks on either side of the fault zone suggests that the zone may in part be a broken monocline on the west flank of the Yozoo Creek anticline, perhaps a transpressional feature. The age of most recent movement in the fault zone is not known. All breccia zones contain calcite and zeolite and give the appearance of being of Tertiary age. Exposures are poor, however, and the possibility of Quaternary displacement cannot be discounted.

In the East Canyon Ridge quadrangle, the Pin Creek fault zone is expressed by a zone of steeply dipping Tertiary volcanic rocks, a large rhyolitic intrusion that probably postdates the deformation that caused the steep dips, and a cluster of young high-K_2O basaltic vents (schematically shown in figure 2), most of which are of phreatomagmatic origin. No direct evidence of faulting has been found. Just north of Spud Hill, a low-K_2O basalt flow erupted from far east of the mapped area about 21,500 years ago (the basalt of Spring Creek; Swanson, 1991) not only occupies the floor of the Cispus River valley but also occurs as much as 43 m higher on the flank of the valley. This could reflect displacement of the flow by a hidden fault. However, scattered exposures of the flow at intermediate elevations, and the presence of a semi-continuous blanket of river gravel capping the eroded flow top, together suggest most strongly that the high elevation records a "high-lava" mark or "bath-tub ring" left after the flow drained downstream and later erosion removed much of the flow from the main valley floor.

The Pin Creek fault zone cannot be traced into the southern part of the East Canyon Ridge quadrangle. Instead it seems to die out, as indicated by rapid shallowing of dips, about half way into the quadrangle. The southern part of the quadrangle is underlain chiefly by lava flows with gentle dips that reflect the interplay of primary attitudes and the Yozoo Creek anticline.

A moderate-size, partly subglacial volcano (Blue Lake volcano) composed of high-K_2O olivine basalt formed during the Hayden Creek Glaciation (probably about 140 ka) in the valley of the Cispus River in the western part of the Blue Lake quadrangle (fig. 2). The basalt along the Pin Creek fault zone in the East Canyon Ridge quadrangle is of similar composition but probably slightly younger age (fig. 2).

The high-K_2O olivine basalt at Blue Lake volcano also lies at the northeast end of a zone of similar olivine basalt that extends southwestward from Blue Lake volcano to beyond the southern limit of the McCoy Peak quadrangle (fig. 2; Swanson, 1992). Significantly, this suite of basalt, which includes at least one flow with modal aegirine-augite, a K_2O content of about 2.3 percent, and a very unusual trace-element composition (R.M. Conrey and D.A. Swanson, unpub. data), is the most potassic known in the southern Washington Cascades except for the Simcoe volcanic field, which occupies a behind–the–arc setting. Whether the SWCC influences the composition of the basalt is a question for future work.

To summarize, work in the East Canyon Ridge and adjacent quadrangles has found several features unusual for the southern Washington Cascades that may reflect the presence of the SWCC: an extensive hornblende-bearing suite of intrusive rocks; possible control by the SWCC on the distribution of this suite; and high-K_2O olivine basalt of late Quaternary age that is anomalous in this intra-arc setting. The Pin Creek fault zone may also localize some of this young basalt. Continued study of the several quadrangles already completed, and of those targeted for future work, will address these issues.

Reports

Marso, J.N., and Swanson, D.A., 1992, The intrusive suite of Kidd Creek: a middle Miocene magmatic event in the Cascade arc of southern Washington: Geological Society of America Abstracts with Programs, v. 24, n. 5, p. 67.

Swanson, D.A., 1992a, Geologic map of the McCoy Peak quadrangle, southern Cascade Range, Washington: U.S. Geological Survey Open-File Report 92-336, 36 p., map scale 1:24,000.

____ 1992b, Geologic map of the Blue Lake quadrangle, southern Cascade Range, Washington: U.S. Geological Survey Open-File Report, map scale 1:24,000, in preparation.

Swanson, D.A., and Evarts, R.C., 1992, Tertiary magmatism and tectonism in an E-W transect across the Cascade arc in southern Washington: Geological Society of America Abstracts with Programs, v. 24, n. 5, p. 84.

References Cited

Grant, W.C., and Weaver, C.S., 1986, Earthquakes near Swift Reservoir, Washington, 1958–1963: seismicity along the southern St. Helens seismic zone: Bulletin of the Seismological Society of America, v. 76, p. 1573-1587.

Grant W.C., Weaver, C.S., and Zollweg, J.E., 1984, The 14 February 1981 Elk Lake, Washington, earthquake sequence: Bulletin of the Seismological Society of America, v. 74, p. 1289-1309.

Hammond, P.E., 1980, Reconnaissance geologic map and cross sections of southern Washington Cascade Range: Portland, Oreg., Publications of Department of Earth Science of Portland State University, scale 1:125,000.

Marso, J.N., and Swanson, D.A., 1992, The intrusive suite of Kidd Creek: a middle Miocene magmatic event in the Cascade arc of southern Washington: Geological Society of America Abstracts with Programs, v. 24, n. 5, p. 67.

Stanley, W.D., Finn, Carol, and Plesha, J.L., 1987, Tectonics and conductivity structures in the southern Washington Cascades: Journal of Geophysical Research, v. 92, p. 10,179-10,193.

Stanley, W.D., Mooney, W.D., and Fuis, G.S., 1990, Deep crustal structure of the Cascade Range and surrounding regions from seismic refraction and magnetotelluric data: Journal of Geophysical Research, v. 95, p. 19,419-19,438.

Swanson, D.A., 1989, Geologic maps of the French Butte and Greenhorn Buttes quadrangles, Washington: U.S. Geological Survey Open-File Report 89-309, scale 1:24,000, 25 p.

____, 1990, Trends of middle Tertiary dikes in and north of the Dark Divide Roadless area, southern Washington Cascades: Eos, Transactions of the American Geophysical Union, v. 71, p. 1144.

____, 1991, Geologic map of the Tower Rock quadrangle, southern Cascade Range, Washington: U.S. Geological Survey Open-File Report 91-314, scale 1:24,000, 26 p.

____, 1992a, Geologic map of the McCoy Peak quadrangle, southern Cascade Range, Washington: U.S. Geological Survey Open-File Report 92-336, 36 p., map scale 1:24,000.

____ 1992b, Geologic map of the Blue Lake quadrangle, southern Cascade Range, Washington: U.S. Geological Survey Open-File Report, map scale 1:24,000, in preparation.

Weaver, C.S., and Malone, S.D., 1987, Overview of the tectonic setting and recent studies of eruptions of Mount St. Helens, Washington: Journal of Geophysical Research, v. 92, p. 10,149-10,154.

Weaver, C.S., and Smith S.W., 1983, Regional tectonic and earthquake hazard implications of a crustal fault zone in southwestern Washington: Journal of Geophysical Research, v. 88, p. 10,371-10,383.

Zollweg, J.E., and Crosson, R.S., 1981, The Goat Rocks Wilderness, Washington, earthquake of 28 May 1981: Eos, Transactions of the American Geophysical Union, v. 62, p. 966.

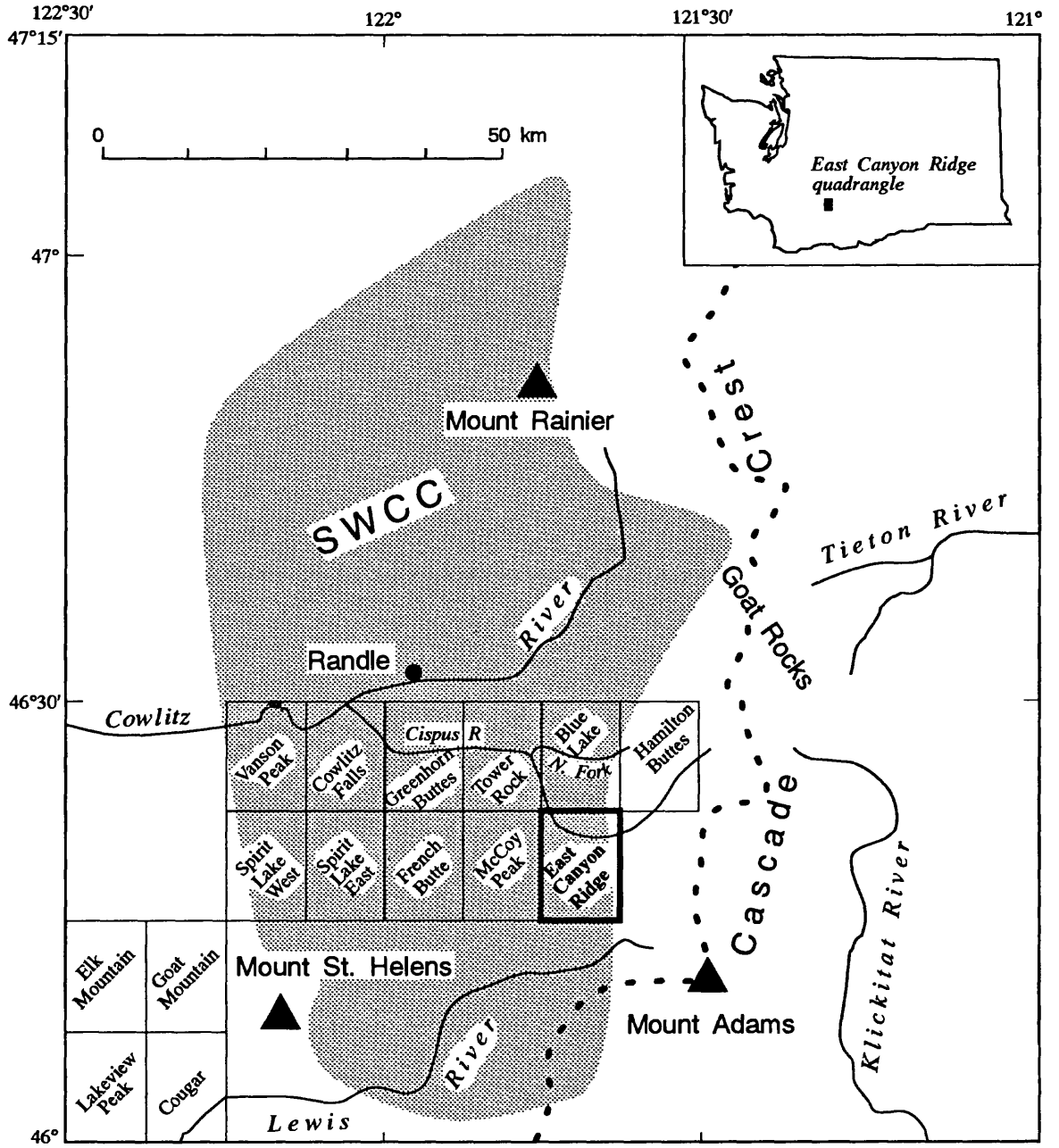

Figure 1. Map showing locations of East Canyon Ridge quadrangle and other quadrangles being mapped in the southern Washington Cascades relative to the Southern Washington Cascades Conductor (SWCC). The quadrangles west of longitude 122° are being mapped by Russ Evarts and Roger Ashley (U.S. Geological Survey, Menlo Park), and those east of longitude 122° by me.

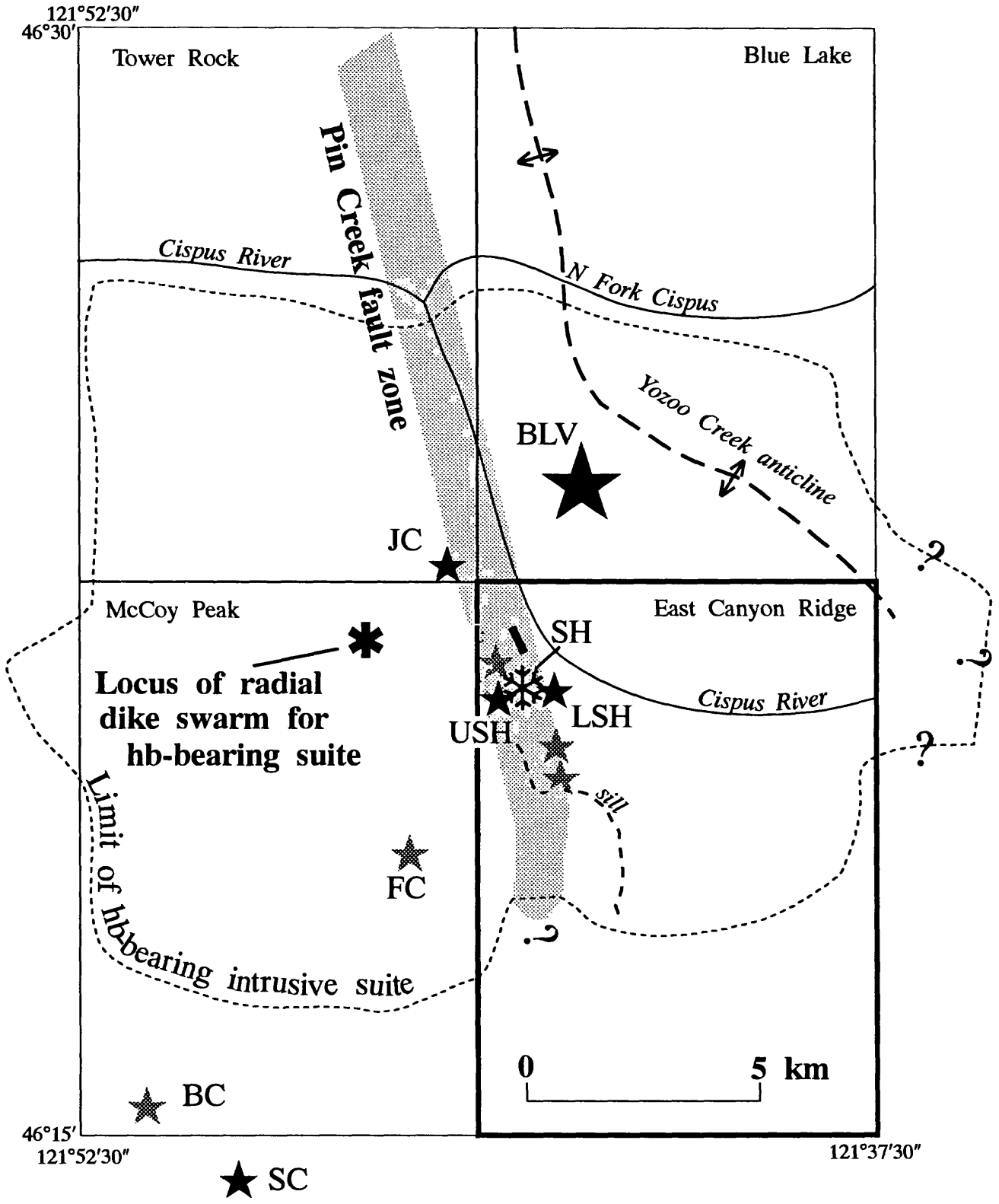

Figure 2. Map showing Pin Creek fault zone relative to late Pleistocene basaltic vents (stars, shaded where minor), locus of 12 Ma radial dike swarm of hornblende-bearing dacite, undated rhyolite intrusive dome (snowflake), sill that crosses Pin Creek fault zone without offset, and site of possible but unlikely offset of 21.5-ka basalt flow that fills Cispus valley (short heavy line just north of rhyolite intrusive dome. BLV, Blue Lake volcano; JC, Juniper Creek; SH, Spud Hill rhyolite; LSH, lower Spud Hill; USH, upper Spud Hill; FC, Falls Creek; BC, Basin Camp; SC, Snagtooth Creek.

Nearfield Geodetic Investigations of Strain across Faults in Southern California

14-08-0001-G1690

Arthur G. Sylvester
Department of Geological Sciences, and
Institute of Crustal Studies
University of California
Santa Barbara, California 93106-9630
(805) 893-3156
arthur@magic.ucsb.edu

OBJECTIVE

The long-term, fixed purpose of this investigation is to search for and monitor the spatial and temporal nature of nearfield displacement across active and potentially active faults. Thus, we document pre-, co- and post-seismic displacement and aseismic creep, if any, especially where seismographic, paleoseismic and geomorphic evidence indicates current or recent fault activity. The geodetic arrays range in length from 300 m to 7000 m and are intermediate in scale, therefore, between the infrequent, regional geodetic surveys traditionally done by the National Geodetic Survey, and point measurements by continually recording instruments such as creepmeters, tiltmeters, and strainmeters. All leveling is done according to First Order, Class II standards, and horizontal surveys are done to First Order standards.

RESULTS

We releveled three level lines in the third week of June, 1992, across the San Andreas fault in the Parkfield area, specifically: OWENS RANCH, CAR HILL, and TURKEY FLAT. None of these lines revealed height changes since the previous surveys in July 1989 with the limits of our uncertainty.

We were awakened the morning after we returned from Parkfield by the Landers earthquake. We scurried out there and installed four fault crossing quadrilaterals to detect afterslip. The quadrilaterals are located at the north end of the surface rupture on the Camp Rock fault where we measured 3.9 m of coseismic slip, at Galway Lake Road where we measured 6.1 m of coseismic slip, at Bodick Road where we measured 3 m of coseismic slip, and at the end of San Andreas Street in Yucca Valley where we measured 20 cm of coseismic slip. We also remeasured Tom Rockwell's quadrilateral at Aberdeen Road before it was destroyed by vandals. We reset the damaged bench marks and have continued to resurvey the array. All these arrays were in place and measured within 48 hours of the main shock on 28 June, and we have remeasured most of them at least two more times to September 9, 1992. We have 14 measurements on the San Andreas Road array to November 7, 1992. Apertures of the arrays range from 10 m (San Andreas Road) to 160 m (Galway Lake Road). The San Andreas Road site is the only one we have south of the Pinto Mountain fault, whereas all the others are north of that fault.

As of November 1992, we have not measured any afterslip in any of the arrays that exceeds the uncertainty of the measurements (3 mm), except at San Andreas Road where we measured 20 mm of afterslip between July 1 and September 9. We measured an additional 2 mm at that array on November 7. The total measured afterslip represents 15% of the coseismic slip at the site. We speculate that all available stored elastic strain was expended at the time of the main shock, precluding afterslip. Moreover, the alluvial cover is thin, precluding the usual postulated adjustment of the alluvial cover by afterslip to abrupt slip at depth.

When we failed to detect significant afterslip on any of the Landers fault segments, we turned our attention to the Coachella Valley segment of the San Andreas fault from Whitewater Canyon southeast to Durmid Hill to see if the Landers earthquake had perturbed it. We established new level lines and strain

quadrilaterals across the fault at Morongo Canyon, Thousand Palms, and Box Canyon. We resurveyed all our existing arrays, including those at WHITEWATER CANYON, MIRACLE HILL, PAINTED CANYON, BOX CANYON, CORVINA BEACH, NORTH SHORE, and BAT CAVES. No height changes occurred in the level lines since they were last surveyed in March 1992. That means that the southern San Andreas segment was not perturbed by the Landers earthquake, at least within the limits of detection by our methods (± 2 mm horizontal; ± 0.5 mm/km vertical).

We also established a quadrilateral across the Calico fault 2 km southeast of Newberry Springs and two doubly braced quadrilaterals and a leveling array across the Pisgah fault where it is crossed by old Route 66 near Hector. Apertures across the well defined strands of each fault are about 100 m each. All of the quadrilaterals were surveyed with our TC2000 total station distance meter, and most of the leveling was done with our N3000 automatic level. As of this writing, we have surveyed the arrays across the Calico and Pisgah faults only once, but the seismic activity has ceased on these faults, and we would not expect to find displacement since the arrays were established in late July 1992.

We resurveyed two level lines and quadrilaterals (SNORT and AIRFIELD) at China Lake where seismic activity increased dramatically shortly after the Landers earthquake, with four M 4+ earthquakes and one M 5+ earthquake. We found no changes at the level of our uncertainty (± 2 mm horizontal; ± 0.5 mm/km vertical).since our last surveys there in 1987.

We resurveyed two level lines in Long Valley (McGEE CREEK and YMCA) together with one line in the north end of Owens Valley (SILVER CANYON). We found no significant changes in the McGEE CREEK and SILVER CANYON lines, but the YMCA array has tilted 18 microradians SW since 1986, that is, 3 microradians/year.

Lastly, in October 1992, we resurveyed two of our horizontal strain quadrilaterals across the Santa Cruz Island fault. Preliminary analysis of the data indicates no horizontal slip along the fault to an uncertainty of ± 2 mm since 1980.

REPORTS

Sylvester, A. G., J. Feltman, L. Hasbargen, T. Bruskotter, D. Korengold, S. Dougherty, G. Bawden, and L. Mitchell, 1992. Negligible afterslip with 28 June 1992 M 7.5 Landers earthquake and no nearfield triggered slip on southern San Andreas fault, California. EOS, Transactions of the American Geophysical Union 73, 380.

Sylvester, A. G., 1992. Nearfield interseismic vertical strain on the central Garlock fault, southern California, 1984-1991. Geophysical Research Letters 19 (10) 1037-1040.

Quaternary Framework of Earthquake Studies

9540-10010

John C. Tinsley
Branch of Western Regional Geology
345 Middlefield Road MS-975
Menlo Park, California 94025
415-329-4928

William R. Dupré
Department of Geology
University of Houston
Houston, TX 77004
713-749-3710

Investigations

1. Liquefaction hazards in the Monterey Bay Area, Central California: Geologic and geographic aspects of liquefaction-related ground failure were emphasized in the analyses of extensive data collected since the October 17, 1989 Loma Prieta earthquake. The main goal was to evaluate mapping criteria to distinguish susceptible geologic deposits from non-susceptible deposits. A set of 6 digital maps (1:24,000) showing the surficial geology of the Monterey Bay area as mapped by Dupré and Tinsley (1980) was prepared from scans. These maps are being edited and the quality of the digital renditions is being compared to the 1:62500-scale published maps to be sure the quality is sustained at the larger scale, prior to publication. Overlays showing the distribution and character of liquefaction-related ground failures are in the editorial stage of preparation and evaluation using computer-based geographical information techniques to study probabilities of sustaining ground failure.

2. Ground Motion Arrays, Southern California: Drilling, sampling and casing operations were completed during October and November, 1992, at 6 instrument sites that comprise an array extending from Whittier to Cerritos College. Five of the holes were drilled to a depth of approximately 100 feet and will be instrumented with a free-field strong motion instrument. One hole was drilled to a depth of 300 feet and will be instrumented with a sensor placed in the hole and a second sensor at the ground surface. A second 300 foot-deep hole was constructed at Central Fire Station in San Bernardino. (See report by Charles Mueller and others, this volume, for additional information concerning the ground motion arrays.)

Results

1. Studies of liquefaction-induced ground failure are directed towards two goals: 1) Improving understanding of material properties as controlling factors in genesis

of lateral spreading and 2) evaluating means of mapping and predicting liquefaction and lateral spreading ground failures. The ground failures in the Monterey Bay region are important because they give revealing insights into the effectiveness with which surficial mapping can be used to forecast the locations of ground failures. The Dupré and Tinsley (1980) mapping was produced according to the methodology developed by Youd and others (1975) and detailed further by Youd and Perkins (1978). Thus, the 10/17/89 earthquake provided the first objective test of regional hazard mapping of liquefaction-related ground failures, and a test of the Youd and Perkins' approach.

Laboratory work is completed on more than 350 geotechnical samples obtained during FY 199-1992, including Standard Penetrometer Testing, grain-size distribution, Atterberg limits, moisture content, radiometric dating and stratigraphic description of samples taken during 1989-1992; these data have been installed into a geotechnical database management system (GTGS) and are being prepared for release to data repositories concerning the Loma Prieta earthquake.

Radiocarbon samples submitted in 1990-1992 for dating using accelerator mass-spectrometer techniques have been received and results support the reigning paradigm that the youngest cohesionless deposits (those that are historical or just a few hundred years old) have the greatest susceptibility to liquefaction, a trait noted by Youd and Perkins (1978) and exploited by Dupré and Tinsley (1980) and Tinsley and others (1985) in published liquefaction potential mapping in the Monterey Bay area and in the Los Angeles region.

The location of lateral-spread ground failures and other sites of liquefaction manifest by sand-boil activity during the Loma Prieta earthquake were chiefly restricted to laterally accreted depositional facies, with special emphasis on point-bar facies (a heretofore not well-recognized finding) along the lower meandering reaches of the coastal streams. The Salinas, Pajaro, and San Lorenzo rivers in the Monterey Bay area, a coastal setting wherein response by rivers to stable or slowly rising Holocene sea levels relative to the land has been the deposition of locally extensive areas of point-bar, levee, and channel deposits bounded by vertically accreted floodbasin and floodplain deposits. The vertically accreted facies were effectively immune to lateral spreading ground failure and lateral spread ground failure during the 1989 earthquake, in stark contrast to marked effects mapped in the laterally-accreted facies.

Facies analysis of zones of failure continues in the coastal zone, where a complex interplay of longshore bars, eolian dune deposits, and historical changes in the location of rivers and bay mouths make a more complicated stratigraphic picture compared to the purely fluvial setting.

Of the 47 lateral spreads mapped in the Monterey Bay area south of the epicenter of the 10/17/89 Loma Prieta earthquake, 46 were observed to occur in areas mapped by Dupré and Tinsley as having a very high or high susceptibility to liquefaction. Tinsley and Dupré (1992) analyze the depositional facies apparently involved in the ground failures and conclude that the point bar facies was most often the facies associated with ground failure. Fluvial channel deposits and estuarine channels also were highly susceptible to ground failures.

Miscellaneous Field Studies Map MF-1199 (Dupré and Tinsley, 1980) showing geology and liquefaction potential in the southern Santa Cruz and northern Monterey County areas has been reprinted and is available through the U.S. Geological Survey's distribution outlets as of October, 1991.

See report by Holzer and others, this volume, for additional information concerning liquefaction-related studies.

2. Drilling operations went quite smoothly and without awkward incidents. No chemical contamination was found in the spoils, so efforts to locate sites free of groundwater or soil pollution problems were successful. The completion of the study awaits analyses of soil samples, analysis of the P-wave and S-wave profiling obtained using down-hole techniques, and installation and testing of the instrumentation. Unfortunately, irregularities in funding continue to plague this study, so additional time is going to be required in order to complete it.

References cited

Dupré, W.R. and Tinsley, J.C., 1980, Geology and liquefaction potential, northern Monterey and southern Santa Cruz Counties, California: U.S. Geological Survey Miscellaneous Field Studies Map MF-1199, 1:62,500.

Tinsley, J.C., Youd, T.L., Perkins, D.M., and Chen, A.T.F., 1985, Evaluating liquefaction potential in Ziony, J. I. (ed), Evaluating earthquake hazards in the Los Angeles region -- an earth science perspective: U.S. Geological Survey Professional Paper 1360, p. 263-316.

Youd, T.L. and Perkins, D.M., 1978, Mapping liquefaction-induced ground failure potential: Proceedings of the American Society of Civil Engineers, Journal of the Geotechnical Engineering Division, v. 104, no. GT4, p. 433-446.

Tinsley, J.C. and Dupré, W.R., in press, Liquefaction hazard mapping, depositional facies, and lateral spreading ground failure in the Monterey Bay area, central California *in* Proceedings of Japan-U.S. Conference on Earthquake Hazards and Liquefaction Countermeasures, 4th, Honolulu, Hawaii, May, 1992 (Director's Approval Received June, 1992).

Reports:

Tinsley, J.C. and Dupré, W.R., in press, Liquefaction hazard mapping, depositional facies, and lateral spreading ground failure in the Monterey Bay area, central California *in* Proceedings of Japan-U.S. Conference on Earthquake Hazards and Liquefaction Countermeasures, 4th, Honolulu, Hawaii, May, 1992 (Director's Approval Received June, 1992).

EXPERIMENTS ON ROCK FRICTION CONSTITUTIVE LAWS APPLIED TO EARTHQUAKE INSTABILITY ANALYSIS

USGS Contract 14-08-0001-G-1364

Terry E.Tullis
John D. Weeks
Department of Geological Sciences
Brown University
Providence, Rhode Island 02912
(401) 863-3829

INVESTIGATIONS:

1. New results on the frictional behavior of serpentine.
2. New results on the frictional behavior of powdered granite simulated fault gouge.
3. Three-dimensional fault modelling.
4. Dynamic fault rupture modelling.

RESULTS:

1. We have found in previous room-temperature experiments on both roughened bare surfaces and powder, that the antigorite polymorph of serpentine undergoes a transition from velocity weakening at fast velocities to velocity strengthening at slow velocities. This behavior is well described by a two-mechanism model (described in detail in Volume XXXIII) which produces the observed behavior through the interaction of two constitutive laws: (1) a rate-weakening state-variable law using two state variables, and (2) a flow law with friction linearly dependent on log(velocity); both the constitutive parameters and the number of state variables remain constant over the entire range of experimental velocities.

We have extended this study to include the lizardite polymorph of serpentine. We have results from two room-temperature experiments on powdered lizardite serpentinite (grain size < 90 μm) on quartzite forcing blocks; normal stress was 25 MPa, and velocities ranged from 10.0 to 0.001 μm s^{-1}. Figure 1 shows the steady-state coefficient of friction for both the serpentine and lizardite polymorphs. The coefficient of friction of the lizardite serpentinite is quite low (~0.3) over the range of velocities tested, while that of the antigorite serpentinite is similar to other silicates (~0.7); we presume this difference is due to the crystalline structure of the serpentine polymorphs. These results suggest that the presence of lizardite on a

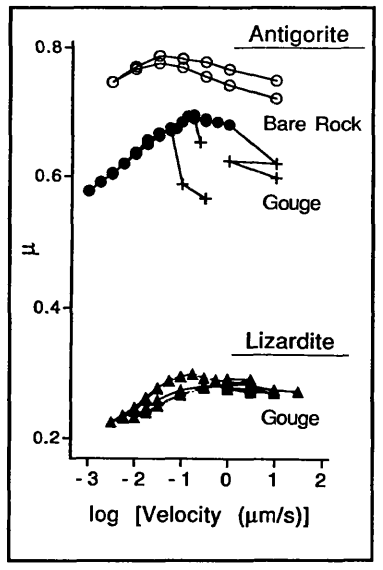

Figure 1. Steady-state coefficient of friction of antigorite and lizardite polymorphs of serpentine plotted as a function of log (Velocity), showing the velocity strengthening (positive slope) at low velocity, and velocity weakening (negative slope) at higher velocity. In addition, the overall frictional strength of lizardite is very low. In portions of the San Andreas fault containing serpentine, if the polymorph controlling the fault strength is lizardite, this could help explain the observed low strength of the fault.

fault would result in stresses about half that expected from typical crustal rocks. Like antigorite, the lizardite serpentinite displays state-variable-type behavior at fast velocities and flow-type behavior at slow velocities. At fast velocities, the two lizardite experiments differ from each other: one slid by stick-slip sliding and the transition to flow behavior occurred at a low velocity, the other slid stably and displayed a higher transitional velocity. We believe these differences may be caused by differing water content in the two experiments. In the slow-velocity flow regime, the magnitude of the velocity-strengthening response of the lizardite is remarkably similar to that of the antigorite serpentinite. This suggests that the velocity dependence at slow velocities of both polymorphs has a common origin, despite the contrast in strength.

2. Previous results have shown that the steady-state velocity dependence (**a-b**) of granite at room temperature in the velocity range of 1 - 10 μm s^{-1} is a function of displacement and sample starting configuration. Initially bare surfaces can have either negative or positive values of (**a-b**) initially but evolve rapidly with displacement to velocity weakening and remain velocity weakening. In contrast, sliding on 1 mm thick layers of simulated granite gouge shows a more complicated evolution with displacement: initially velocity strengthening, decreasing to velocity neutral or velocity weakening, then returning to velocity strengthening. The evolution of the velocity dependence of simulated gouge, though unexpected, is not due to machine effects.

The transitions in velocity dependence in simulated gouge correlate with transitions in gouge microstructure and with the size of changes in gouge layer thickness which accompany changes in sliding velocity. The evolution of frictional strength, steady-state velocity dependence, and sample thickness are illustrated in Figure 2. Changes in sliding velocity at short displacement are accompanied by relatively large changes in the derivative of gouge thickness with displacement (dH/dδ). Changes in dH/dδ diminish with further displacement and mimic the decrease in the observed velocity dependence; these are accompanied by a decrease in frictional strength. The minimum change in dH/dδ coincides with the most negative velocity dependence and the minimum frictional strength. Microstructures at this range of displacement show a single localized shear zone at the layer boundary. With further displacement the velocity dependence again becomes positive, the frictional strength increases, and large changes in dH/dδ are again associated with velocity steps. This corresponds with a widening of the deformation zone. We interpret the correlation between velocity dependence, friction, gouge microstructure and change in dH/dδ as strong evidence that the transitions in velocity dependence with displacement in simulated gouge are real. Changes in dH/dδ

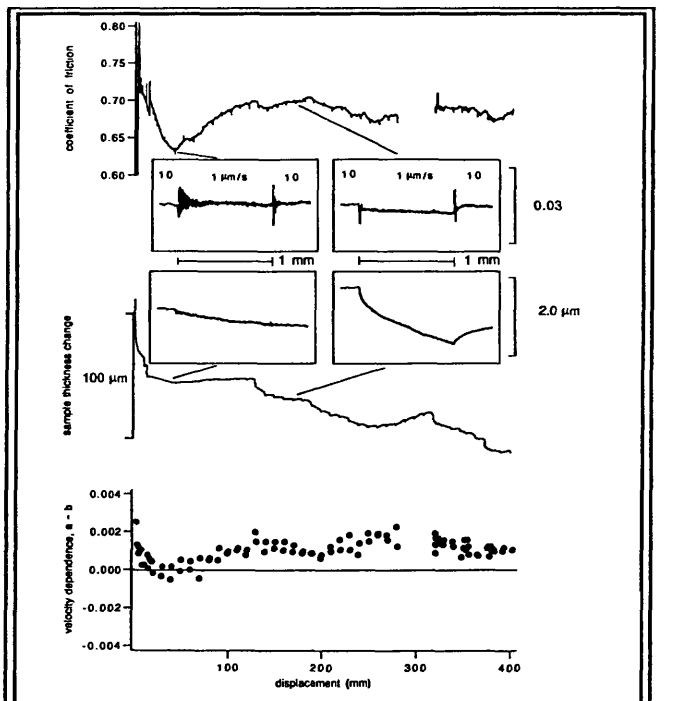

Figure 2. Development of frictional strength, sample thickness, and steady-state velocity dependence (**a-b**) with sample displacement. Insets show details of response of friction and thickness to velocity changes at two points, the first at the point of minimum strength and most negative **a-b**, the second in the portion of the experiment at large displacement showing the velocity strengthening response.

and gouge microstructure throughout initially bare experiments are similar to those observed in the velocity weakening displacement range of simulated gouge experiments. The size of the change in dH/dδ apparently reflects the amount of gouge which participates in the deformation. Contrary to the results of Marone and Scholz, the magnitude of the observed dH/dδ is not large enough to account for all of the observed velocity strengthening in simulated gouge experiments (see Figure 3).

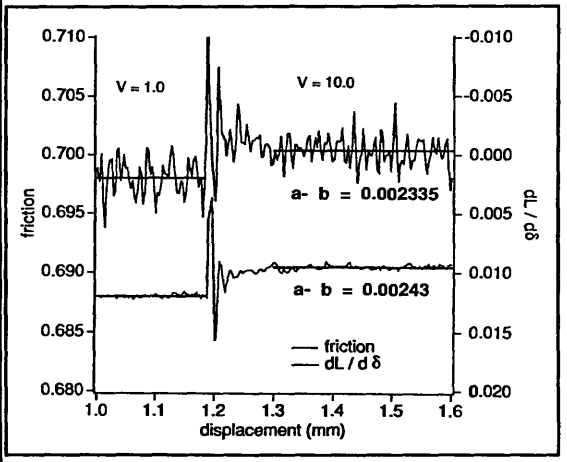

Figure 3. Plot of frictional strength (lower trace) and dH/dδ (upper trace) plotted as a function of displacement at the time of a velocity jump from 1 to 10 μm s^{-1} late in an experiment. This is a velocity jump equivalent to the one detailed in the left inset in Figure 2. The derivative dH/dδ is plotted at a scale equivalent to its contribution to frictional strength, so the two traces can be directly compared. Solid horizontal lines superimposed on the two traces show the average values before and after the velocity jump, and the **a-b** labels indicate the equivalent frictional velocity dependence. These values are nearly identical, indicating that the change in dH/dδ is not sufficient to account for the difference between the observed velocity strengthening in gouge experiments and the observed velocity weakening in initially bare surface experiments.

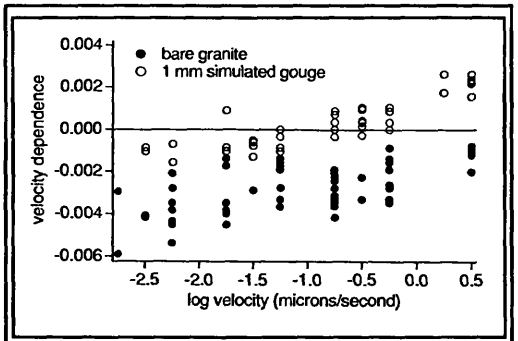

Figure 4. Steady-state velocity dependence for sliding on granite bare surfaces (circles) and 1 mm layer of simulated granite gouge (squares) plotted as function of velocity. These data were taken at a total displacement of about 250 mm, well after the gouge layer had returned to velocity strengthening for 1 to 10 μm s^{-1} velocity jumps, as can be seen by the positive values for the open circles at the right end of the figure. The gouge and bare surfaces have a roughly parallel trend with the bare surface data displaced to more negative values, such that it is velocity weakening at all velocities, while the gouge shows velocity weakening at lower velocities, and velocity strengthening at the high velocities where we and others have concentrated our efforts.

While we have concentrated on velocity changes from 1 to 10 μm s^{-1} in order to facilitate comparison with work done in other labs, we find that this velocity range is not representative of the entire range of velocities (Figure 4). We find that **a-b** becomes increasingly negative at lower velocity, so that even when sliding on simulated gouge layers at large displacement **a-b** is negative. This is in contrast with the results for 1 to 10 μm s^{-1}at large displacement described above.

3. The behavior of three-dimensional instability models of Parkfield earthquakes can be used to gain insight into what might be expected during the various parts of the seismic cycle for actual Parkfield earthquakes. In particular, the changes that occur in the model prior to a simulated earthquake can be studied to determine whether they could be detected by the existing array of instruments at Parkfield in the presence of ambient noise. This approach can give some insight into the most appropriate locations for various types of instruments and the required sensitivity and signal-to-noise levels for these instruments to be useful for purposes of intermediate- and short-term earthquake prediction.

Using a model to help understand real faults is only useful if the behavior of the model is realistic. For application to precursory changes this requires that the constitutive behavior of the model fault be similar to that of the real fault, and in particular that the role played by time and slip velocity in

determining fault strength be realistic. Although we do not know the constitutive behavior of real faults, guidance provided by laboratory studies of rock friction constitutive behavior suggest using the rate- and state-variable constitutive law of Dieterich and Ruina. As shown by Tse and Rice, fault models using this law are realistic in terms of the magnitudes of stress drop and the proportions of slip that occur during the different parts of the seismic cycle. More stringent comparisons should be available after the Parkfield earthquake occurs.

Accelerating slip at depth in the hypocentral region occurs prior to the mainshock in the models, its magnitude and timing depending on model parameters. Monitoring of microseismicity may be the most sensitive way to detect this slip. Other geophysical techniques may be able to detect the associated stress changes. Model results show, in agreement with observations on several other earthquakes, that the premonitory changes are too small to detect with sensitive strain meters at distances from the fault larger than several times the fault depth. Arrays of high sensitivity strain meters located near the ground surface within a distance about equal to the depth of the accelerating slip may be able to detect premonitory changes above the noise in the final year before the earthquake.

4. Seismological observations of short slip duration (rise time) on faults during earthquake rupture are not consistent with existing models of dynamic rupture. In these models, the leading edge of rupture stops only when a strong region is encountered and slip at an interior point ceases only when waves from the stopped edge of slip propagate back to the interior point. In contrast, seismological evidence suggests that the duration of slip is too short for waves to propagate to the nearest edge of the rupture surface, even if the distance used is an asperity size instead of the entire rupture. This leads to the question of what controls slip duration, if not dimensions of the fault or asperities?

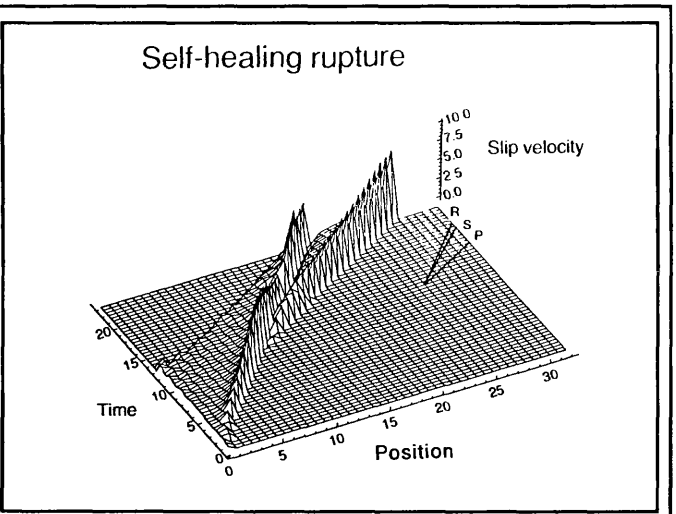

Figure 5. Plot of the variation of dimensionless slip velocity with time for half of a bilaterally symmetric shear crack with self-healing rupture. The velocity of compressional (P), shear (S) and Rayleigh (R) waves are labelled. A rupture, initially forced to propagate at half the Rayleigh velocity, begins propagating spontaneously at approximately the Rayleigh velocity and undergoes the transition to super-Rayleigh velocity just as a purely slip weakening case would. Behind the rupture front, slip occurs over a finite width or slip band. The velocity of the trailing edge of the slipping region does not propagate at the same speed as the front of the band. It appears that the slip velocity peak associated with the Rayleigh velocity will eventually be consumed by the trailing edge of the slip band.

We have modelled dynamic rupture propagation of faults numerically using the boundary element method of Andrews [1985], incorporating simple friction laws with slip velocity dependence. These models demonstrate that rise time, rupture propagation velocity, and stress drop can depend on the frictional constitutive law imposed on the fault. With negative velocity dependent friction, the fault restrengthens as the velocity behind the rupture front decreases, and can eventually lead to healing. We have modified the slip-weakening friction law commonly used in studies of dynamic rupture such that the fault strength depends exponentially on the negative of normalized slip velocity after the initial slip weakening has taken place. If the velocity dependence is

weak, the propagation of rupture is identical to the slip weakening case. If the velocity dependence is stronger, rupture propagation resembles the slip weakening case, but spontaneous healing occurs. The healing edge of rupture nucleates well behind the rupture front and travels more slowly than the rupture front for the entire simulation. If the velocity dependence is even stronger, the propagation velocity of the rupture front is reduced and the healing edge of the rupture achieves a constant velocity equal to the velocity of the rupture front (Figure 5). This leads to a propagating band of slip having a constant width and rise time independent of the eventual fault size. In all cases of healing rupture, the residual stress increases with distance behind the healing edge so that the final stress drop is much less than the dynamic stress drop, in agreement with some seismological observations of rupture.

REPORTS:

Papers:

Power, W. L. and Tullis, T. E., The contact between opposing fault surfaces at Dixie Valley, Nevada and implications for fault mechanics, *J. Geophys. Res, 97*, 15425-15435, 1992.

Power, W. L. and Tullis, T. E., A review of the fractal character of natural fault surfaces with implications for friction and the evolution of fault zones, *Fractals and Their Application to Geology*, Paul Lapointe, Ed., *Geol. Soc. Am. Special Paper*, in press, 1992.

Reinen, L. A., and Weeks, J. D., Determination of rock friction constitutive parameters using a least squares inversion method, *in revision, J. Geophys. Res.*

Reinen, L. A., Weeks, J. D., and Tullis, T. E., Two mechanism model for frictional sliding of serpentinite, *Geophys. Res. Let., 19*, 1535-1538, 1992.

Weeks, J. D., Constitutive laws for high velocity frictional sliding and their influence on stress drop during unstable slip, *in revision, J. Geophys. Res.*

Abstracts:

Beeler, N. M., Weeks, J. D., and Tullis, T. E., Evolution of velocity dependence of granite with displacement, *EOS Trans AGU Fall Meeting Supplement, 73*, 511, 1992.

Park, S. K., Eberhart-Phillips, D., Jackens, R. C., Michael, A. J., Roeloffs, E. Simpson., R. W., Wentworth, C. M., Foxall, W., Malin, P. E., and Tullis, T. E., 1992, Three-dimensional integration of diverse geophysical models at Parkfield using a geographic information system, *Eos Trans. AGU, 73, Fall Meeting Abs. Supp.*, 396.

Reinen, L. A., Tullis, T. E., and Weeks, J. D., The frictional behavior of serpentine: implications for aseismic slip on oceanic transform faults, *EOS Trans AGU Fall Meeting Supplement, 73*, 550, 1992.

Reinen, L. A., Weeks, J. D., and Tullis, T. E., Interaction of two mechanisms during frictional sliding of serpentinite, *EOS Trans AGU Spring Meeting Supplement, 73*, 310, 1992.

Reinen, L. A., Weeks, J. D., and Tullis, T. E.,1992, Velocity dependence of serpentinite friction promotes aseismic slip on faults, *Geol. Soc. America Abstracts with Programs, 24*, A323.

Reinen, L. A., Weeks, J. D., and Tullis, T. E., Comparison of the frictional constitutive behavior of antigorite and lizardite serpentine polymorphs, *EOS Trans AGU Fall Meeting Supplement, 73*, 511, 1992.

Stuart, W. D., and Tullis, T. E., Instability model for repeated Parkfield $M_W = 6$ earthquakes, *EOS Trans AGU Fall Meeting Supplement, 73*, 406, 1992.

Tullis, T. E., Beeler, N. M., and Weeks, J. D., Frictional healing of dynamic earthquake rupture, *EOS Trans AGU Fall Meeting Supplement, 73*, 388, 1992.

Tullis, T. E. and Stuart, W. D., Premonitory changes prior to a model Parkfield earthquake, *EOS Trans AGU Fall Meeting Supplement, 73*, 396, 1992.

Weeks, J. D., and Tullis, T. E., High-resolution measurement of displacement in rock friction experiments, *EOS Trans AGU Fall Meeting Supplement, 73*, 565, 1992.

Re-Evaluation of Large Historic Earthquakes in the San Francisco Bay Area Using New Primary Sources

Agreement No. 1434-92-G-2201

Martitia Tuttle and Lynn Sykes
Lamont-Doherty Geological Observatory
Palisades, New York 10964
(914) 359-2900

Introduction

For a study funded by the U.S. Geological Survey the year following the 1989 Loma Prieta earthquake, we began to re-evaluate data on large historic earthquakes, including the 1836, 1838, 1865, 1868, and 1890 events, that had occurred in the San Francisco Bay area. That study included (1) reviewing published work on the large 19th Century earthquakes, (2) canvassing archives in the San Francisco Bay area for materials that may contain new data pertaining to the historic events, (3) reviewing primary sources at several of those archives for descriptions of ground shaking and damage resulting from historic earthquakes, (4) and comparing effects and intensities of the 1838 and 1865 events as well as isoseismal maps of the 1865 and 1868 events with those of modern earthquakes. We used the 1989 Loma Prieta, 1984 Morgan Hill and 1979 Coyote Lake earthquakes to calibrate the locations and magnitudes of the historic events under consideration.

In a subsequent project funded by the U.S. Geological Survey in February 1992 which builds on our previous study, we have (1) focussed our archival search in areas where new data could greatly improve our understanding of the locations and magnitudes of the historic earthquakes, (2) developed magnitude-felt area relationships for the San Francisco Bay area, (3) evaluated the repeat time of the Loma Prieta segment of the San Andreas fault, and (4) considered the relationship between stress changes and moderate-size seismicity in the Bay area. The progress and results of this project are presented below.

Archival Search

During the course of our research, the intensity of ground shaking at New Almaden has surfaced as a critical point for determining the location of the 1865 event. Based on a newspaper report that several houses were thrown down, New Almaden was assigned a MMI (modified Mercalli intensity) of IX and was thought to have experienced the most intense shaking during the 1865 earthquake (Toppozada et al., 1981). Relatively high intensity of ground shaking in San Jose as well as in New Almaden suggest that the 1865 earthquake was centered in the eastern foothills of the Santa Cruz Mountains or in the Santa Clara Valley (Tuttle and Sykes, 1992a). Since the Loma Prieta earthquake, it has also been suggested that the 1865 earthquake was

located near the epicenter of the 1989 earthquake (Sheffels et al., 1990; Stover et al., 1990) and that the 1989 earthquake may have been a "duplicate" of the 1865 event (McNutt and Toppozada, 1990). Intensity assignments of the 1865 earthquake for several localities in the meizoseismal area were re-interpreted and now more closely resemble those of the 1989 earthquake (McNutt and Toppozada, 1990). For example, the 1865 intensity in New Almaden has been down-graded from a MMI IX (Toppozada et al., 1981) to a MMI VII-VIII (McNutt and Toppozada, 1990). It was postulated that the damage in New Almaden during the 1865 event was anomalously high because of poor building construction.

Because the location of the 1865 earthquake is significant in terms of characterizing the behavior of the San Andreas fault in the San Francisco Bay area, we have directed our search for new information bearing on the intensity of ground shaking in New Almaden in 1865. Tuttle has visited the New Almaden Museum and Historical Park and has begun to review the collection on the New Almaden Mine housed at the Special Collections of Stanford University. The construction in New Almaden probably varied a great deal depending on the use and occupancy of the buildings. The homes of the manager and supervisors were fairly well-constructed; whereas, construction of the the miners' homes may have been substandard. For example, a large brick and wooden structure, known as "Casa Grande", where the manager of the mine lived for many years was built prior to 1860 and still stands today. Therefore, it is important to determine, if possible, which buildings were damaged during the 1865 earthquake.

A new account of damage attributed to the 1865 earthquake was found during the initial review of the New Almaden Mines collection at Stanford. In a letter written on November 14, 1865, the general manager of the mines, Samuel F. Butterworth, states that "furnaces nos. 4,5, 6 are slightly damaged" by the earthquake. In several letters written to Butterworth in October 1865, the mine superintendent, James A. Nowland, requests supplies including cement for repairing the furnaces. In addition, a reference to the 1868 earthquake has also been found. In a letter written to J.A. Mayo on October 23, 1868, S.F. Butterworth states that he is glad to learn "that the mine is not seriously damaged by the earthquake." Our review of this collection will be completed in December 1992 and we hope to find additional references to effects of the 1865 and 1868 earthquakes in New Almaden.

For both the 1865 and 1868 earthquakes, intensity data exists for many localities in the San Francisco Bay area. However, there are almost no data for these two events in the vast area south of San Juan Bautista and east and southeast of San Jose. As a consequence, the isoseismals for MMI < VII are very poorly defined in these areas. During the course of our research on historic earthquakes, we have become aware of letters and diaries of settlers of central California not previously used in earthquake research. Several of these letters and diaries are in the holdings of small archives, historical trusts and libraries scattered throughout central California. M. Ryan, a consulting archivist and historian working with us on this project, recently visited the San Benito County Historical Museum, the Milliken Museum in Los Banos, the San Luis Obispo County Museum, the Santa Barbara Historical Society. During these visits, Ryan reviewed the letters and diaries of early American settlers and searched for new information about the 1865 and 1868 events. We have also come to recognize

the potential for gaining new information about the early 19th century earthquakes from the letters and diaries of the California missionaries. Therefore, Ryan also visited the Santa Barbara Mission Archives while in Santa Barbara. References to earthquakes were found in several spanish documents. Copies of these documents have been sent to an experienced translator, S. Gurcke. A report summarizing the findings of visits to archives mentioned above is expected from Ryan by December 1992.

Magnitude-Felt Area Relationships

We have developed magnitude-felt area relationships specifically for the purpose of improving estimates of the size of historic earthquakes in the San Francisco Bay area. These relationships are based on the three largest modern earthquakes to occur in this area, the 1989 Loma Prieta, 1984 Morgan Hill, and 1979 Coyote Lake events and were developed for felt areas of MMI V and VI. These intensities and felt areas were chosen because they occurred close enough to the earthquake epicenters to be relatively well defined, yet far enough away from the epicenters so as not to be greatly influenced by variations in rupture depths and local rock and soil conditions. M_W rather than the local magnitude M_L was used as a standard here. Nevertheless, the M_W and M_L magnitudes are nearly identical for each of three calibration events.

The relationships thus developed are:

$$M_W = 1.65 \log A_{(V)} - 1.20,$$
$$M_W = 1.00 \log A_{(VI)} + 2.44, \qquad (1)$$

where $A_{(V)}$, for example, is the area in square kilometers shaken at intensity V or greater. The felt areas we used represent total inferred area (land and offshore areas combined). Isoseismal maps of the historic earthquakes (Toppozada et al., 1981) were re-evaluated, new data on intensities added, and in all three cases, the intensity data were re-contoured. Magnitude estimates based on these relationships of the 1865, 1868, and 1890 earthquakes are presented in Table 1. We plan to further improve the magnitudes estimates of these and other historic earthquakes by including additional modern events in our regression of magnitudes and felt areas.

Repeat Time of the Loma Prieta Segment

If the Loma Prieta segment of the San Andreas fault zone (but not necessarily exactly the same fault or portions of a fault in this complex transpressional restraining bend) ruptured in 1838, 1906 and 1989, its average repeat time and the standard deviation are 76 $\pm$ 11 years (Fig. 1). If it ruptured in 1865 and not in 1838, the repeat time would be shorter, about 62 years, and the uncertainty would be $\pm$ 30 years. In our opinions, the data favor the 76 year average repeat time and its associated smaller standard deviation.

While the reverse component of fault motion in the 1989 event appears to be more atypical of the behavior of the Loma Prieta segment in large earthquakes, the

release of horizontal right-lateral shear strain is probably a much more common occurrence as suggested by the 1906 and 1989 events and the rate of long-term horizontal slip of 1.9 ± 0.4 m per century (Segall and Lisowski, 1990; Working Group on California Earthquake Probabilities, 1990). Therefore, the first order behavior of the Loma Prieta segment, or release of horizontal shear strain, appears to be reflected in the 76 ± 11 year repeat time that we obtain. Several studies, especially inversions based on horizontal and vertical geodetic data and aftershock locations, indicate that significant rupture in the 1989 earthquake extended to a depth as shallow as 4 km. Hence, a near-vertical fault above that zone does not appear to have the potential of rupturing in a large event over the next few decades, whereas a shallow-dipping thrust or reverse fault extending from the top of the 1989 rupture zone to the northeast does have that potential.

TABLE 1

FELT AREAS (KM^2)AND MOMENT MAGNITUDES OF LARGE EARTHQUAKES ASSOCIATED WITH THE SAN ANDREAS FAULT SYSTEM IN THE SAN FRANCISCO BAY AREA

Date	A_{VI}	M_{VI}	A_V	M_V	M_W
October 17, 1989	31,300	6.94	73,000	6.84	6.92
April 24, 1984	3,930	6.04	33,900	6.29	6.15
August 6, 1979	2,440	5.83	14,300	5.67	5.74
April 24, 1890	5,180	6.16	43,200	6.49	6.32 ± 0.16
October 21, 1868	38,400	7.03	55,100	6.64	6.84 ± 0.20
October 8, 1865	17,400	6.69	35,800	6.33	6.51 ± 0.18

M_{VI} and M_V calculated using Equation (1).
M_W = average moment magnitude and its standard error of the mean for the three oldest events, and calculated values from log (M_O) = 1.5 M_W + 9.1 using the following seismic moments in units of N-m: 1989, 3.0×10^{19} (Hanks and Krawinkler, 1991); 1984, 2.1×10^{18}; 1979, 5.1×10^{17} (Dziewonski et al., 1990).

Relationship between Stress Changes and Moderate-Size Seismicity

S. Jaumé and Sykes have begun modelling stress changes in the region in response to the earthquakes of 1868, 1906, and 1989 and to compare them with changes in moderate-size seismicity before and after these earthquakes (Jaumé and Sykes, 1992a). Figure 2 is an example of stress changes associated with the great 1906 earthquake and seismicity in the 25 years before and after that earthquake. The stress changes were modelled by a dislocation in a three-dimensional elastic medium (Fig. 3; Erickson, 1986). Stress changes were mapped onto vertical planes striking N32°W (strike of plane of maximum shear in San Francisco Bay region, Lisowski et al., 1991)

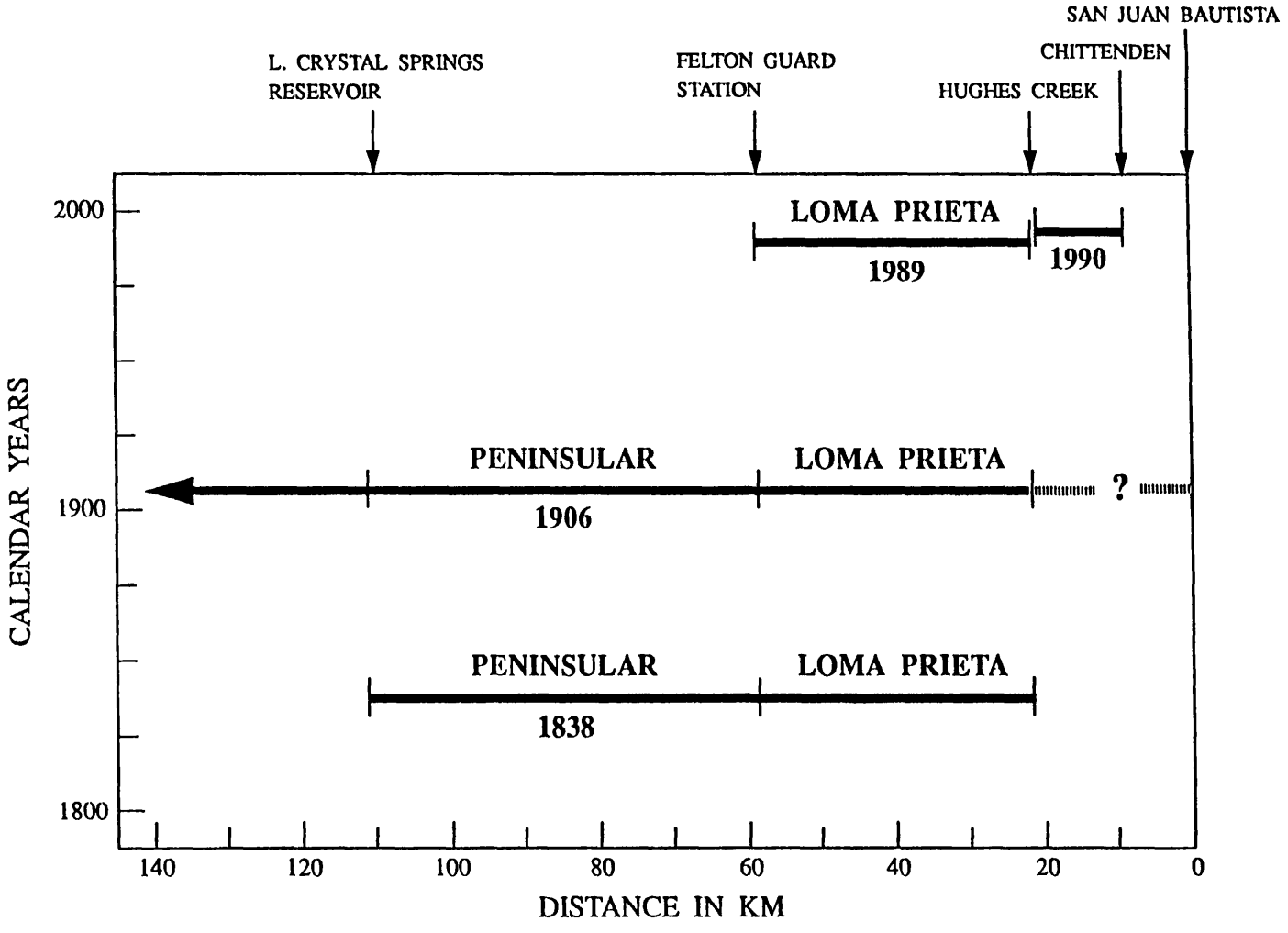

Figure 1. Space-time diagram of ruptures of the San Andreas fault between Bolinas and San Juan Bautista illustrating the 76 $\pm$ 11 year repeat time for the Loma Prieta segment. Distances along fault are measured from San Juan Bautista.

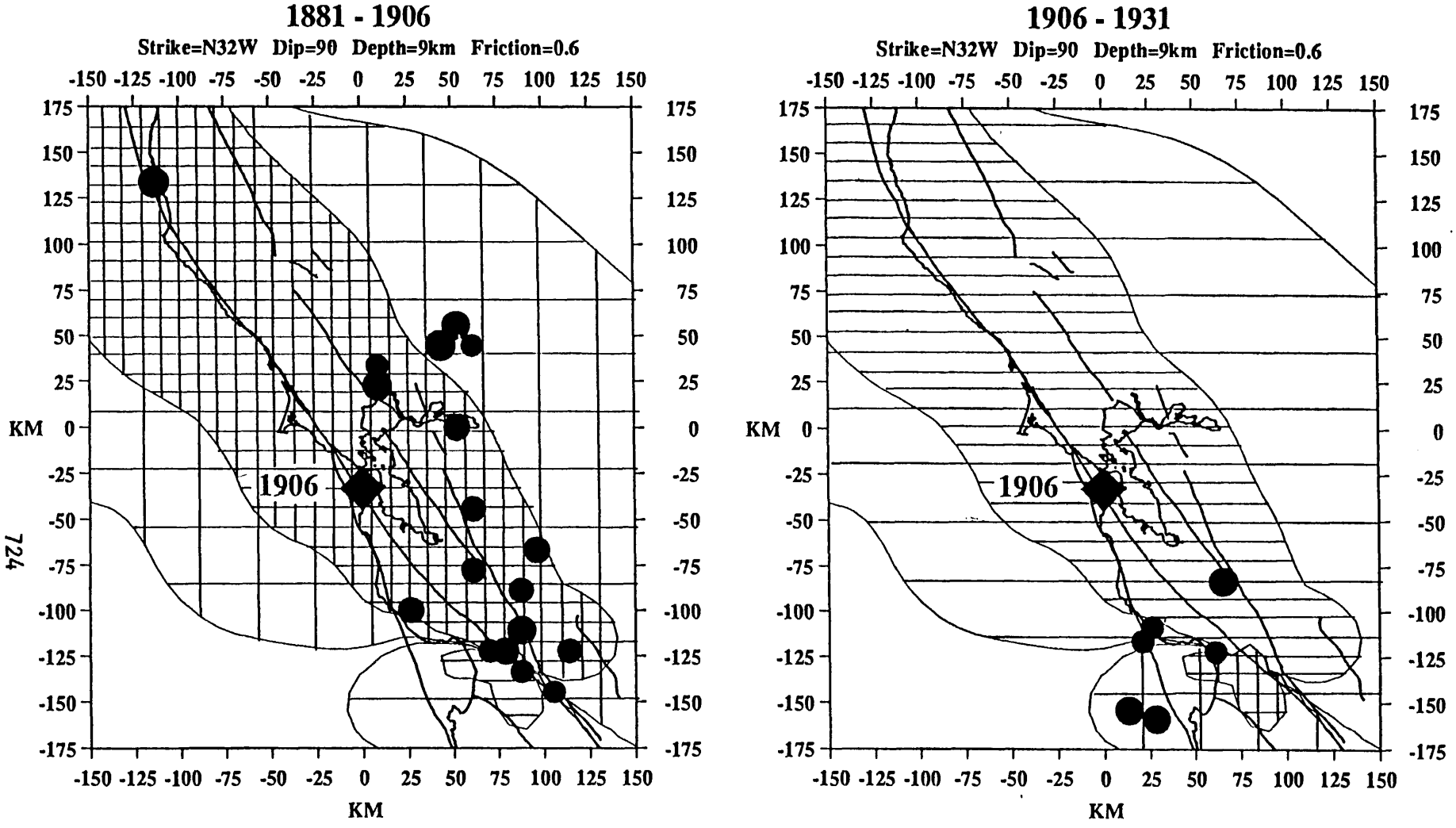

Figure 2. Maps showing effective stress changes (CFF - see text) due to the great 1906 earthquake and moderate (M≥5.5) seismicity in the 25 years before (left) and 25 years after (right) 1906. The closely spaced pattern represents regions that are calculated to have experienced a greater than 1 bar stress change and the widely spaced pattern represents regions that experienced 0.1-1.0 bar stress change. The crossed pattern represents stress increases and the horizontal line pattern represents stress decrease. Most of the seismicity before 1906 occurred in regions expected to be more highly stressed by the strain accumulation associated with that great earthquake. Following 1906, the overall rate of seismicity drops, but several earthquakes occur in regions that should have experienced large stress drops at the time of the 1906 earthquake. Earthquake locations are from Toppozada et al. (1981) and Toppozada and Parke (1982).

at a depth of 9 km (average depth of mainshock hypocenters on Calaveras fault, Oppenheimer et al., 1990) assuming a coefficient of friction of 0.6. We follow Reasenberg and Simpson (1992) in defining a change in the Coulomb Failure Function (CFF),

$$\Delta CFF = \Delta\tau + \mu\Delta\sigma_{eff}, \qquad (2)$$

where $\Delta\tau$ is the decrease in shear stress, μ is coefficient of friction, $\Delta\sigma_{eff}$ is the change in effective normal stress on the planes in question.

As illustrated in Fig. 2, almost all of the moderate seismicity prior to the great 1906 earthquake occurs in regions expected to be more highly stressed by strain accumulation for that earthquake. Indeed, most of the active strike-slip faults sub-parallel to the San Andreas fault and situated broadside to it should be moved towards failure before a 1906 type event. Similar maps for the 1868 and 1989 earthquakes show large stress changes over more restricted regions, consistent with the accelerated seismicity before those events (Sykes and Jaumé, 1990). Following the 1906 earthquake, activity shuts off as expected in the entire area to the north of the Loma Prieta segment, i.e., opposite those segments that experienced the largest displacements in 1906. Some moderate seismicity to the south, i.e., the 1911 event, occurred in regions which would be expected based on dislocation models to have moved away from failure as a result of the occurrence of the 1906 earthquake.

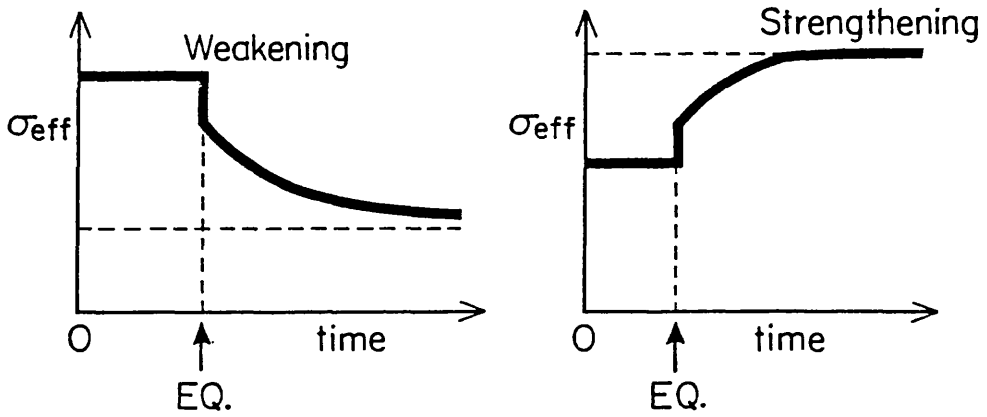

Figure 3. Two examples of changes in effective normal stress as a function of time for nearby faults following the occurrence of a major (M~7) earthquake. Instantaneous changes in normal stress are opposed by changes in fluid pressure. If diffusion occurs in response to fluid pressure changes, further changes in effective normal stress will occur with time.

The region between the Loma Prieta section of the San Andreas fault and the southern Calaveras, Mission, and southern Hayward faults is characterized by southwest dipping thrust and reverse faults to the northeast of the San Andreas and northeast dipping faults of that type to the west of the Calaveras and Hayward faults. The buildup of stress prior to large or great earthquakes along the San Andreas moves broadside-portions of nearby strike-slip faults like the Calaveras closer to failure and inhibits the occurrence of moderate-size shocks along thrust and reverse faults in the area. The occurrence of a major or great event on the San Andreas reverses this process, promoting failure along certain thrust and reverse faults, as well as along adjacent segments of the San Andreas, and inhibiting moderate-size events along nearby strike-slip faults situated broadside to the major event. This is the one region in which moderate-size shocks did not completely turn off after the 1906 event.

The fault that ruptured in the 1865 event, which we think was not the San Andreas, could have been moved closer to failure by the 1838 event on the San Andreas if it was a thrust or reverse fault of appropriate orientation. If the 1911 shock was associated with rupture of one of the reverse faults to the west of the Calaveras fault, then the occurrence of the great 1906 earthquake would have promoted rather than inhibited slip on that fault. Hence, we could see a change from moderate-size strike-slip events in the area surrounding the Loma Prieta shock in the few decades before 1989 to more reverse and thrust events in the coming decades.

The June 28, 1992 (M=7.5) Landers earthquake is the largest to strike southern California in the past 40 years. Based on our experience in modeling stress changes associated with large earthquakes in the San Francisco Bay area, we are also considering stress changes due to the Landers earthquake sequence (Jaumé and Sykes, 1992b). In particular, we have focussed our attention on changes in stress acting on the San Andreas fault where it passes through the San Gorgonio Pass. In summary, we find that (1) the San Andreas fault in that region was moved towards failure by decreases in normal stress across the fault, and (2) the fault will be further weakened with time by the effect of fluid diffusion (Fig. 3).

Publications

Jaumé, S.C. and L.R. Sykes, 1991, A model for the seismic strain cycle in the San Francisco Bay region (abs.), EOS, Trans. Amer. Geophys. Union, 71, p. 1448.

Jaumé, S.C. and L.R. Sykes, 1992a, Changes in moderate seismicity in the San Francisco Bay region and stress changes due to large and great earthquakes (abs.), EOS, 1992 Spring Meeting Supplement, p. 197.

Jaumé, S.C. and L.R. Sykes, 1992b, Changes in the state of stress on the southern San Andreas fault resulting from the California earthquake sequence of April to June 1992, Science, (submitted).

Sykes, L.R. and S.,C. Jaumé, 1990, Seismic activity on neighboring faults as a long-term precursor to large earthquakes in the San Francisco Bay area, Nature, 348, p. 595-599.

Tuttle, M.P. and L.R. Sykes, 1992a, Re-evaluation of several large historic earthquakes in the vicinity of Loma Prieta and Peninsular segments of the San Andreas Fault, California, Bull. Seismol Soc. Amer. , 82, p. 1802-1820.

Tuttle, M. and L. Sykes, 1992b, Re-evaluation of the 1838, 1865, 1868 and 1890 Earthquakes in the San Francisco Bay area, *in* Borchardt, G. Editor, Proceedings of Second Conference on Earthquake Hazards in eastern San Francisco Bay Area, California Division of Mines and Geology Special Publication 113, (*in press*).

Tuttle, M.P., L. Sykes, and S. Jaumé, 1990, Historic earthquakes along the Loma Prieta segment of the San Andreas fault, EOS, 71, p. 1448.

Additional References Cited

Armbruster, J.G. and L. Seeber, 1991, A mechanically modeled seismicity precursor of the Loma Prieta, California earthquake (abs.), EOS 1991 Fall Meeting Suppl., 310.

Dziewonski, A.M., G. Ekstrom, J.H. Woodhouse, and G. Zwart, 1990, Centroid-moment tensor solutions for October-December, 1989, Phys. Earth Planet Inter., 62, p. 194-207.

Erickson, L., 1986, Master's thesis, Stanford University, Stanford, California.

Hanks, T.C. and H. Krawinkler, 1991, The 1989 Loma Prieta, California, earthquake and its effects: Introduction to the special issue, Bull. Seismol. Soc. Amer., 81, p. 1415-1423.

Lisowski, M., J.C. Savage, and W.H. Prescott, 1991, The velocity field along the San Andreas fault in central and southern California, J. Geophys. Res., 96, p. 8369-8389.

McNutt, S.R. and T. R. Toppozada, 1990, Seismology of the 17 October 1989 earthquake, *in* McNutt, S. and R. Sydnor, eds., The Loma Prieta (Santa Cruz Mountains), California earthquake of 17 October 1989, Calif. Div. Mines and Geol., Special Publication 104, p. ll-27.

Oppenheimer, D.H., W.H. Bakun, and A.G. Lindh, 1990, Slip partitioning of the Calaveras fault, California, and prospects for future earthquakes, J. Geophys. Res., 95, p. 8483-8498.

Reasenberg, P.A. and R.W. Simpson, 1992, Response of regional seismicity to the static stress change produced by the Loma Prieta earthquake, Science, 255, p. 1687-1690.

Segall, P. and M. Lisowski, 1990, Surface Displacements in the 1906 San Francisco and 1989 Loma Prieta Earthquakes, Science, 250, p. 1241-1244.

Sheffels, B.M., W.L. Ellsworth, and A.G. Lindh, 1990, An assessment of an early forecast for the Loma Prieta earthquake, EOS, 71, 290.

Stover, C.W., B.G. Reagor, F.W. Baldwin and L.R. Brewer, 1990, Preliminary isoseismal map for the Santa Cruz (Loma Prieta), California, earthquake of October 18, 1989 UTC, USGS Open-File Report 90-18, 24 pp.

Toppozada, T. R., C.R. Real, D. L. Parke, 1981, Preparation of isoseismal maps and summaries of reported effects for pre-1900 California earthquakes, USGS Open-File Report 81-11 SAC, 182 pp.

Working Group on California Earthquake Probabilities, 1990, Probabilities of large earthquakes in the San Francisco Bay region, California, USGS Circular 1053, 51 pp.

FIELD EXPERIMENT OPERATIONS

PROJECT 9930-01170
JOHN VAN SCHAACK
BRANCH OF SEISMOLOGY
U. S. GEOLOGICAL SURVEY
MENLO PARK, CALIFORNIA

This project is responsible for a number of activities associated with the Earthquake Hazards Reduction Program: Personnel maintain and operate a number of portable recording systems used in earthquake aftershock studies, install and maintain radio telemetry systems used to transmit network data to the Centers, install new seismic stations for special topical studies, maintain all the VHF, UHF, and microwave radios used in the California networks, and manage all the radio frequencies used by the Office of Earthquakes Volcanoes and Engineering.

Seventeen 5-day magnetic tape portable recording systems were deployed for about 3 months in southern California and Arizona for the PACE 3 teleseismic experiment. Personnel from this project are now digitizing the tape for analysis.

Experiments were conducted to attempt to transmit digital data from University of California and Stanford University long period seismic stations through the U.S.G.S. operated microwave system to Berkeley. At the present time three stations are operating in this mode. Results are very encouraging as all three stations are operating satisfactorily with data transmission rates of about 15K baud over voice band channels.

Through verbal cooperative agreements with the U.S. Army Corps of Engineers, Sacramento District, we have been able to extend our microwave facilities along the west side of the Sierras from Oroville Dam to Lake Isabella east of Bakersfield. With this extension we are now better able to monitor the western side of the Sierras and reduce our telemetry costs.

We have installed an 80 foot antenna tower at the Office headquarters in Menlo Park. This tower will allow us to harden our seismic network so that we can remain operational after a large earthquake in the Bay Area. Most of the network data will come to the office directly by radio and will not depend on commercial carriers.

PALEOSEISMOLOGICAL STUDIES IN THE WESTERN LOWLANDS, SOUTHEAST MISSOURI

14-08-0001-G1931

James D. Vaughn
Missouri Department of Natural Resources
Division of Geology and Land Survey
P.O. Box 250
Rolla, MO 65401
(314) 368-2155

INVESTIGATIONS

1. Documentation of a prehistoric, surficial sandblow in the Western Lowlands of southeast Missouri.
2. Investigation of liquefaction features in a ditch on the John Clodfelter farm (Site JC-1) in southwest Stoddard County, Missouri.
3. Reconnaissance of 180 km of river banks in the Western Lowlands of southeast Missouri and northeast Arkansas.
4. Core drilling of two scarps near paleoearthquake sites in the Western Lowlands of southeast Missouri.
5. Investigation of a swarm of sandblows on a late Wisconsinan terrace in the Eastern Lowlands north of Paragould, Ark.
6. Investigation of anomalous depressions five km north-northwest of New Madrid, Mo.

RESULTS

1. The surficial prehistoric sandblow (solid triangle in fig. 1) was investigated via three shallow backhoe trenches excavated normal to the long axis. Near the apex of the sandblow, trench walls revealed three soil morphological characteristics indicative of a pre-1811 age: (a) absence of original bedding in the sandblow except at a depth of about 50 cm in the lowermost throat of the vent, (b) dominant brownish color (10YR 5/4 and 5/6) in the horizon of the sandblow which underlies the plow layer, and (c) absence of a buried A horizon immediately beneath the sandblow. In contrast, 1811-12 sandblows typically have observable bedding immediately beneath the A horizon and are intermittently underlain by buried A horizons of the pre-earthquake surface soils (Haller and Crone, 1986; Obermeier, 1989, 1990; Wesnousky and Leffler, 1992).

Tiny pieces of highly carbonized wood obtained from the upper 10 cm of the soil buried by this prehistoric sandblow yielded a calibrated radiocarbon age of AD 770-1020 (AA-8204). It is likely that the dated material was remnants of woody roots killed by the sandblow or else woody debris buried by the sandblow. If this is correct, the age date provides a maximum age which is very close to the paleoearthquake's timing. The plausibility of such an interpretation is strengthened by the large overlap of the AD 770-1020 age date with a calibrated paleoearthquake timing of AD 539-991 reported by Saucier (1991).

2. Liquefaction features at Site JC-1 in southwest Stoddard County, Mo., include a swarm of clastic dikes and sills believed to have been produced by the 1811-12 earthquakes and by at least one strong paleoearthquake. The presumed 1811-12 intrusions have a youthful appearance marked by light color, relict bedding, minimal diagenesis, and an absence of translocated clay. On the other hand, the inferred pre-1811 intrusions have stronger marks of diagenetic and pedogenetic alternation such as iron-oxide cementation, brownish colors, and translocated clay. Organic materials recovered at one of the dike locations will be submitted for radiocarbon assays to establish a minimum and maximum age for the event.

3. By use of a motor boat, approximately 180 km of the Current, St. Francis, and Black Rivers in northeast Arkansas and southeast Missouri were field searched for liquefaction features. In southeast Missouri, very low water levels limited the search to about 15 km of the St. Francis and Black Rivers where good bare-bank exposures were rare. In northeast Arkansas, on the other hand, approximately 25-50 percent of Current River and Black River had bare exposures of sandy point-bar deposits, sandy to clayey natural levee deposits, and fine-grained floodplain deposits.

The search in southeast Missouri resulted in discovery of only one clastic dike of presumed 1811-12 age in Holocene deposits along the St. Francis River in west-central Stoddard County, Mo. This dike extended from a sandy point-bar source bed near the water level of the river up through about 2.0 m of sandy to silty natural levee deposits. Youthfulness of the dike is inferred from its fresh appearance and lack of appreciable diagenetic or pedogenetic alteration.

Reconnaissance of Current River and Black River in northeast Arkansas extended from the Missouri-Arkansas line to a point on Black River about 40 km north of Newport. Approximately 15 clastic dikes and a possible buried sandblow were found in fine-grained floodplain deposits in the reach between the confluence with Little Black River and Pocahontal, Ark. South of Pocahontas, fine-grained deposits were devoid of liquefaction features.

Some of the liquefaction features identified in the banks of Current River north of Pocahontas have marks of weathering indicative of a pre-1811 age. At one location, three dikes are relatively unweathered in the lower 2.0 m of the section; but they are brownish and more weathered in the 1.0-1.5 m of brown loamy sediments which immediately underlie the well-drained, well-developed surface soil (a Hapludalf). This coincidence of the weathered dike zone with a zone of brown, weathered host sediment implies a probable prehistoric age. Small pieces of wood obtained from a bed of gray silty clay cut by the dikes will be submitted for radiocarbon assay, which will provide a maximum age for the event. Currently, however, no organic materials have been found for determination of a minimum age.

At a second location about 10 km north of Pocahontas, a clastic dike was traced up the bank from the waterline to a silty bed a few centimeters beneath a weathered, dome-shaped sand body. Although the texture of the dike and sand body were similar, origin of the sand body is ambiguous

because no eruptive vent was found. It should be noted, however, that two-dimensional vertical exposures of sandblows rarely exhibit a direct connection of the feeder dike, eruptive vent, and sandblow (for example, see Haller and Crone, 1986).

4. Core drilling across two scarps near a paleoearthquake site in the Western Lowlands (near the northernmost star in fig. 1) yielded inconclusive results. A line of six-meter-deep cores across a scarp located 5.0 km northeast of the paleoearthquake site failed to reveal any stratigraphic offset indicative of coseismic deformation. At a second site 0.5 km southwest of the paleoearthquake site, a line of similar cores revealed a complex assemblage of sandy, silty, and clayey beds which contained two clastic dikes; however, the apparent lack of one or more distinct marker beds prevented detection of any significant displacement across the meter-high scarp. Because of the existence of several zones of perched water beneath the scarp, I elected to defer excavation of a backhoe trench until drier conditions occur and a short line of high resolution seismic reflection can be run.

5. A swarm of surficial sandblows on a late Wisconsinan terrace about 25 km northeast of Paragould, Ark., (fig. 1, surface Pvl_4) was briefly investigated with a soil probe and in a hand-dug trench. Several of the sandblows were found to have a 15-20 cm thick Ap horizon underlain by a brownish (10YR 5/4 and 5/6) C1 horizon, morphologies which may represent more than 200 years of pedogenesis. Wood obtained from the periphery of tubular intrusions within the upper 10 cm of the Alfisol buried by one of the sandblows had a radiocarbon age of 11,790 $\pm$ 110 yr B.P. (UA-6561). However, because bedding planes were present in the lower third of the sandblow (which precludes thousands of years of pedogenesis), it is likely that the dated wood originated in deeper sediments and was carried upward in the liquefied sand. Additional investigation of a couple of these sandblows via backhoe trenching is planned to attempt to obtain additional materials for age dating.

6. Three circular to oblong depressions located on Sikeston Ridge about 5.0 km north of New Madrid (fig. 1) were investigated via a soil probe and a backhoe trench to determine the likely origin. Initial soil-probe results suggested that one of the depressions might be a prehistoric earthquake crater that got reactivated in 1811-12. The backhoe trench, however, exposed soil and stratigraphic relationships indicative of a non-earthquake, anthropogenic origin. It appears that these anomalous depressions were excavated some years ago either for prospective ponds or else as small borrow pits.

References

Autin, W.J., S.F. Burns, B.J. Miller, R.T. Saucier, and J.I. Sneed, 1991, Quaternary geology of the Lower Mississippi Valley, in Morrison, R.B., ed., Quaternary nonglacial geology: conterminous U.S., Geological Society of America, v. K-2, p. 547-582.

Haller, K.M., and A.J. Crone, 1986, Log of an exploratory trench in the New Madrid seismic zone near Blytheville, Arkansas: U.S. Geological Survey Miscellaneous Field Studies Map MF-1858.

Nuttli, O.W., 1979, Seismicity of the Central United States, in Hathaway, A.W., and C.R. McClure, eds., Geology in the siting of nuclear power plants: Geological Society of America, Reviews in Engineering Geology, v. 4, p. 67-93.

Obermeier, S.F., 1989, The New Madrid earthquake: an engineering-geologic interpretation of relict liquefaction features: U.S. Geological Survey Professional Paper 1336-B, 114 p.

Obermeier, S.F., R.B. Jacobson, J.P. Smoot, R.E. Weems, G.S. Gohn, J.E. Monroe, and D.S. Powars, 1990, Earthquake-induced liquefaction features in the coastal setting of South Carolina and in the fluvial setting of the New Madrid seismic zone: U.S. Geological Survey Professional Paper 1504, 44 p.

Russ, D.P., 1982, Style and significance of surface deformation in the vicinity of New Madrid, Missouri, in McKeown, F.A., and L.C. Pakiser, eds., Investigations of the New Madrid, Missouri, earthquake region: U.S. Geological Survey Professional Paper 1236, p. 95-114.

Saucier, R.T., 1991, Geoarchaeological evidence of strong prehistoric earthquakes in the New Madrid (Missouri) seismic zone. Geology v. 19, pp. 296-298.

Stover, C.W., B.G. Reagor, and S.T. Algermissen, 1979, Seismicity map of the state of Missouri: U.S. Geological Survey, Miscellaneous Field Studies Map MF-1155.

Wesnousky, S.G., and L.M. Leffler, 1992, The repeat time of the 1811 and 1812 New Madrid earthquakes: a geological perspective. Bull. Seism. Soc. Amer. v. 82, no. 4, pp. 1756-1785.

Reports

None this reporting period

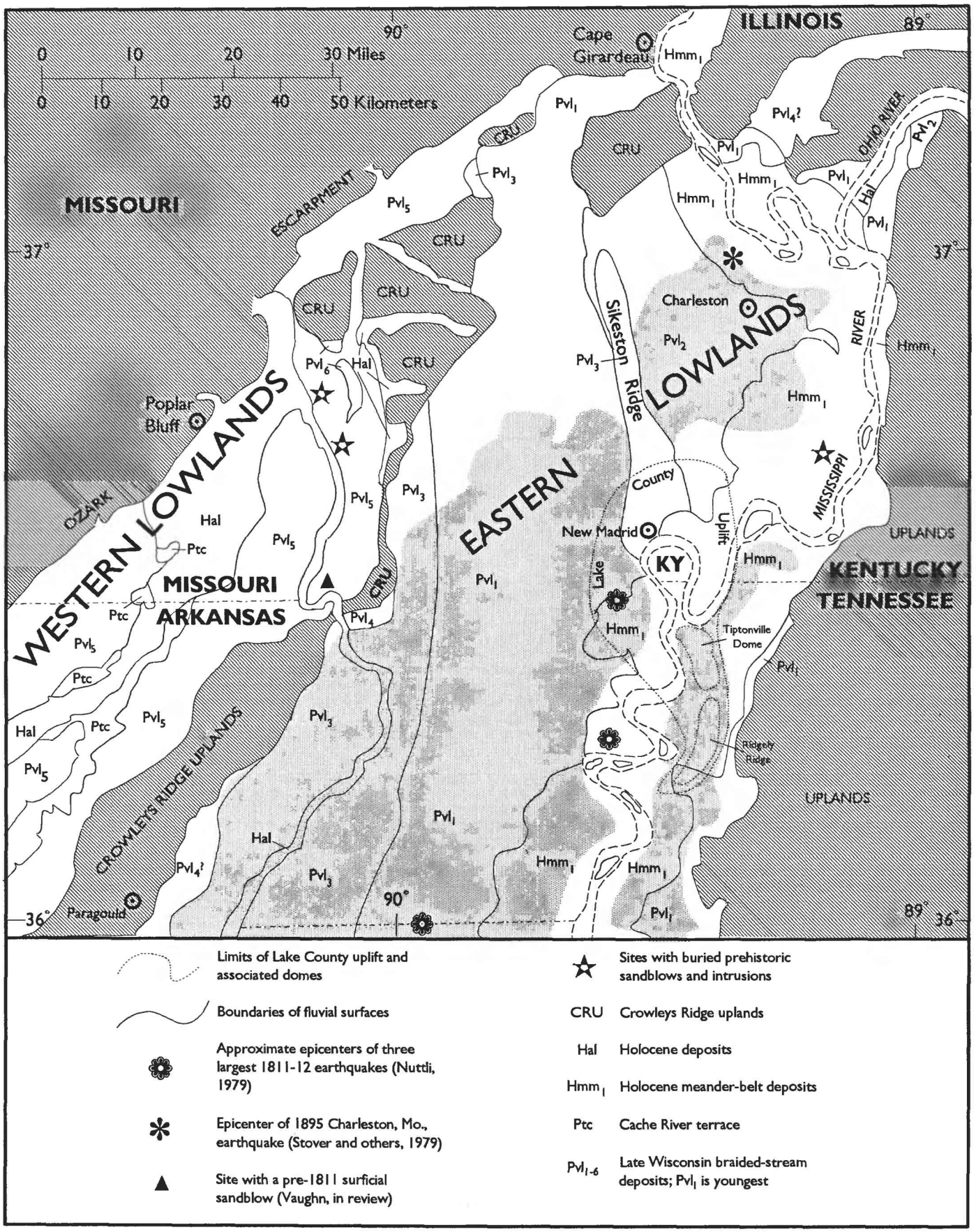

Figure 1. Map of the study area showing the major fluvial surfaces, major surficial sandblow deposits (stippled areas), uplands (hachured areas), and paleoearthquake sites. Adapted from Russ (1982); Obermeier (1989); Autin and others (1991, Plate 6); and Saucier, (1991); with modifications by the author.

Geothermal Seismotectonic Studies

9930-02097

Craig S. Weaver
Branch of Seismology
U.S. Geological Survey
at Geophysics Program AK-50
University of Washington
Seattle, Washington 98195
206-553-0627

Investigations

1. Continued analysis of the seismicity and volcanism patterns of the Pacific Northwest in an effort to develop an improved tectonic model that will be useful in updating earthquake hazard assessments in the region. (Weaver, Yelin, co-authors from Menlo Park and Golden)

2. Continued acquisition of seismicity data across the Pacific Northwest, with emphasis on monitoring the Cascadia subduction interface, the Cascade volcanoes, and the Mount St. Helens area including the St. Helens zone. (Weaver, Yelin, Norris, UW contract)

3. Study of earthquake catalogs for the greater Parkfield, California region for the period 1932-1992. This work is in the final phase, with most effort devoted to final revision of a manuscripts and final checking of the revised earthquake catalog. (Meagher, Weaver)

4. Study of estuaries along the northern Oregon coast in an effort to document probable subsidence features associated with paleosubduction earthquakes. This work is scheduled for completion during FY93. (Grant)

5. Study of seismically recorded rockslides and avalanches on Cascade volcanoes. This work is now largely focused on honing the revisions to a manuscript that has been through peer review. (Norris)

6. The project provides leadership to the USGS NEHRP Pacific Northwest regional focus and serves as one of the local focal points for public information about the USGS activities in the area. (Weaver, Grant, Yelin, Meagher, Norris)

7. Study of historical seismicity at Lassen Peak. This project is investigating earthquake swarms that occurred at Lassen Peak in 1946 and 1950. The study seeks to determine the nature of the swarms (rate of occurrence of events greater than magnitude 2.0, variation in S-P times, variations in amplitude ratios) and compare these results with similar parameters determined from better-monitored seismic swarms in the Long Valley area. (Meagher, Norris, Weaver)

Results

1. Studies of seismicity in the Parkfield region

One of the major conclusions of our study of earthquakes in the greater Parkfield region is that the pattern of background earthquake activity at magnitudes 3.5 and greater, has been stationary over time. We have used this result and our assessment that in the immediate vicinity of Parkfield that we have a complete earthquake catalog above magnitude 3.5 from 1932 to 1969 to which we have appended the modern catalog drawn from dense regional networks installed since 1969 to plot a time-distance plot of seismicity along the Cholame-Middle Mountain section of the San Andreas fault (Figure 1). Our catalog of events greater than magnitude 3.5 from 1932 to 1992 includes 109 events in the boxed area in Figure 1 (circles are our locations from 1932-1969, squares are USGS locations from 1970 to 1992). As reported previously, in examining our locations we concluded that our epicentral errors are small along the strike of the San Andreas, but larger perpendicular to the fault (this is seen by the tendency for locations from 1932-1969 to fall on either side of the fault).

Along the 40 km section of the San Andreas marked by A-A' in Figure 1, we have plotted a time-distance plot (Figure 2). The immediate aftershocks following the 1934 and 1966 events are clearly observed; each mainshock was followed by events along a 30 km length of the San Andreas. The years following each mainshock show some differences. Whereas the immediate aftershocks for the 1934 event were of greater average magnitude than those following 1966, there were more events in the first 15 years following the 1966 event compared to the 1934 quake. Finally, the October 1992 activity at Parkfield bears some resemblance to that in the mid-1950's. Notice that along the San Andreas north of Middle Mountain (at 10 km in Figure 2) there were no earthquakes located from about 1942 until the early 1950's. The October 1992 activity was the first of magnitude 3.5 or greater since the early 1980's.

2. Investigations of earthquake swarms at Lassen Peak

Although the earthquake sequences that occurred in 1946 and 1950 near Lassen Peak in the Cascade Range of northern California are some of the largest instrumentally recorded sequences to occur near a Cascade volcano, they have not been examined since they were first reported in the annual earthquake catalogs published by the University of California at Berkeley (UCB). In 1946 several earthquake sequences were reported including a magnitude 5.0 event on July 7. The 1950 sequence began with a magnitude 5.5 earthquake on March 20 that was located by UCB within Lassen Volcanic National Park. This event was followed by approximately 7000 aftershocks within 20 days. On November 14, 1950 another event occurred at Lassen Peak with a reported magnitude of 4.6. This event was followed by 1700 aftershocks within the next 8 days.

The events were recorded on the 3-component station Mineral (MIN) operated by UCB; MIN is located 15 km southwest of Lassen Peak. We scanned the MIN records for the years 1946 and 1950 and read P arrival times, S-P times, maximum amplitude, and duration for all events with coda durations greater than 20 seconds (382 for 1946, 962 for 1950). Local magnitudes had been calculated by UCB for 93 events in the 1950 swarms and only for the main shock in 1946. We calculated approximate magnitudes for the remaining events using a linear relation obtained from a least-squares regression of the P-coda data versus the corresponding UCB magnitudes.

Our results include: 1) the March and November 1950 sequences consist of well-defined mainshock-aftershock sequences with few foreshocks, whereas the 1946 activity is more swarmlike in character. 2) the sequences do not show obvious signs of a volcanic "signature" such as low-frequency events or harmonic tremor. 3) most S-P values area between 1.8 and 3.2 seconds, indicating that the dimension of the hypocentral volumes of the 1946 and 1950 sequences are less than 15 km in diameter.

Reports

Weaver, C. S. and K. M. Shedlock, 1991, Estimates of seismic source regions from considerations of the earthquake distribution and regional tectonics in the Pacific Northwest, *U.S. Geol. Surv. Open-File Rep. 91-411-R,* 15pp. (Funded by Earthquake Hazards)

Weaver, C. S. and K. M. Shedlock, (in press), Estimates of seismic source regions from considerations of the earthquake distribution and regional tectonics in the Pacific Northwest, *U.S. Geol. Surv. Prof. Pap. 1560,* A. Rogers, W. Kockelman, G. Priest, and T. Walsh, eds., (34 pages, 10 figures). (Funded by Earthquake Hazards)

Yelin, T. S., 1992, An earthquake swarm in the north Portland (Oregon) Hills: More speculations on the seismotectonics of the Portland basin (abs), *1992 Abstracts with Programs, Cordilleran Section, Geological Society of America, v. 24,* p. 92.

Wells, R. E. and C. S. Weaver, 1992, Rotating crustal blocks and big earthquakes in western Oregon and Washington (abs), *1992 Abstracts with Programs, Cordilleran Section, Geological Society of America, v. 24,* p. 89.

Stanley, W. D., Finn, C. A., Williams, J. L., and C. S. Weaver, 1992, Tectonics and seismicity of the Mount Rainier region (abs), *Eos, Trans. Am. Geophys. U., v. 73, no. 43 supplement,* p. 526.

Norris, R. D., Meagher, K. L., and C. S. Weaver, 1992, The 1936, 1946, and 1950 earthquake sequences at Lassen Peak, California (abs), *Eos, Trans. Am. Geophys. U., v. 73, no. 43 supplement,* p. 399.

Meagher, K., L., Norris, R. D., and C. S. Weaver, 1992, Progress report: Investigation of the 1946 and 1950 earthquake sequences at Lassen Peak, California (abs), *Eos, Trans. Am. Geophys. U., v. 73,* (in press).

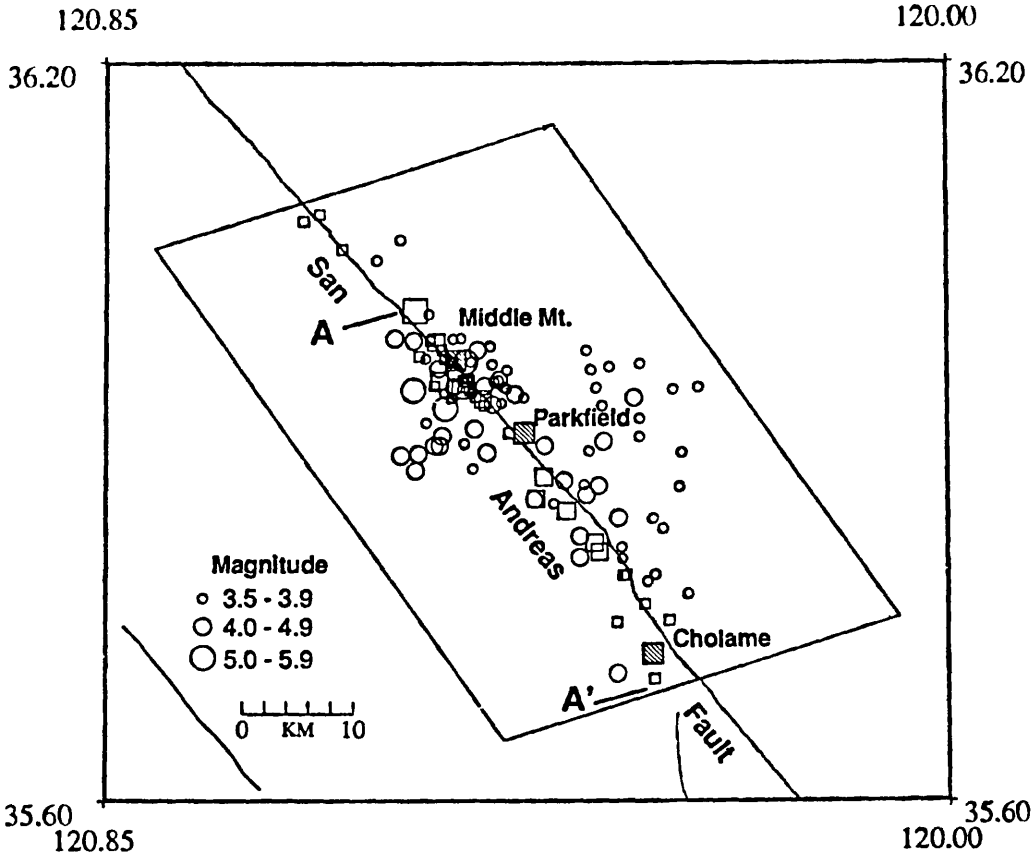

Figure 1: Seismcity of the Parkfield area, 1932-1992. Circles are events prior to 1970, squares are events from 1970 through 1992. Distance marked by A-A' shown Figure 2.

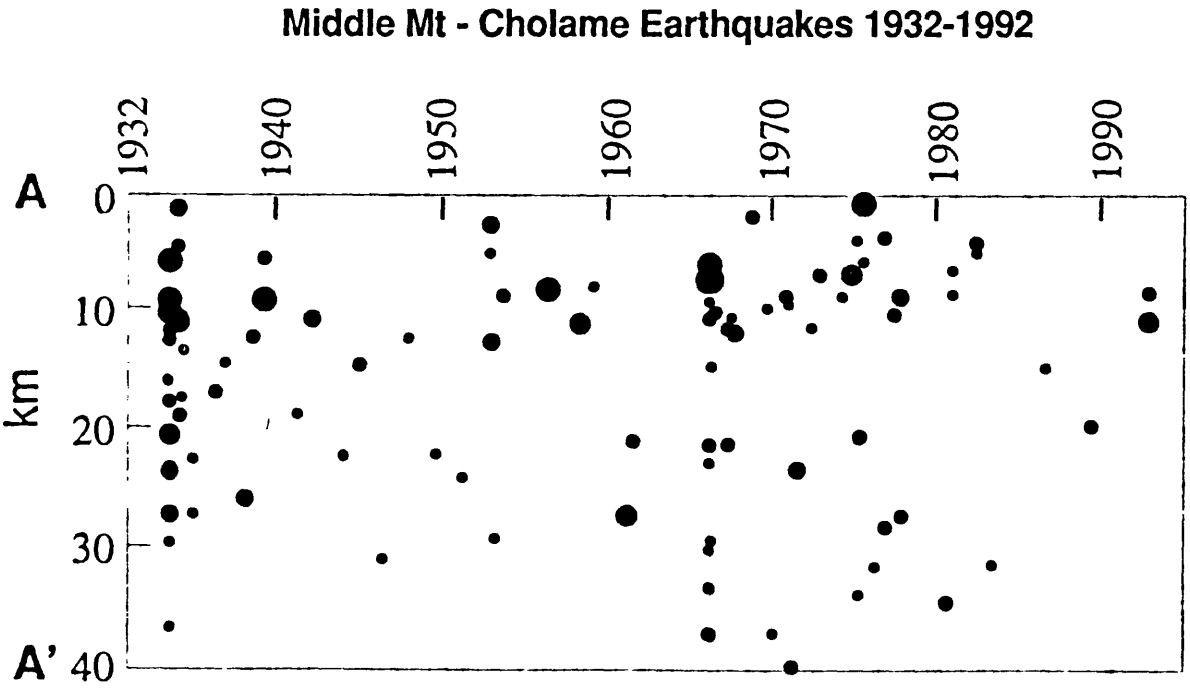

Figure 2: Time-fault distance plot along the strike of the San Andreas fault near Parkfield. Same magnitude scaling as in Figure 1. The 10 km tic is approximately at Middle Mountain.

Plio-Pleistocene Rotations across the San Andreas Fault System- Paleomagnetic Constraints on Inelastic Strain Accumulation

9540-70090

Ray Wells, John Hillhouse, Andrei Sarna-Wojcicki, and Wayne Thatcher
Branches of Western Regional Geology and Tectonophysics
345 Middlefield Road, MS 975
Menlo Park, California 94025
415-329-4933

Investigations

We have sampled widespread Plio-Pleistocene tephra units in the Bay area for paleomagnetic study of rotations. These tephras were deposited quickly and may represent uniformly magnetized sheets which could provide ideal strain markers for deformation studies across the San Andreas system. These studies could place useful bounds on the relative proportion of permanent strain to elastically-restored deformation in the San Francisco Bay region. Our main target is the Roblar Tuff (6 Ma), which crops out between the San Andreas and Green Valley Faults. We have sampled several known localities (Sebastopol, Petaluma, Sears Point, Berkeley Hills, Pinole, Lafayette and Green Valley) to test for tectonic rotation. We have also studied 4 additional localities in the Huichica, Lawlor (4 Ma), and Rockland tuffs (400 ka) to establish characteristic paleomagnetic signatures and their possible value in studies of rotation rate.

Results

Paleomagnetic results from six of eight localities (140 samples) of the Roblar tuff indicate a stable normal polarity remanence that passes a modified fold test. Two sites were clearly overprinted by present field directions. Near Sebastopol in the Roblar quarry, a thick (~15 m) columnar-jointed tuff of similar age and composition may represent proximal ash-flow facies of the Roblar tuff. We interpret its well-defined direction (Dec=002°, Inc=44°, a_{95}=2°, N=16) to be a characteristic TRM (thermal remanent magnetization). To the NW and SE the tuff thins to as little as 2 m, and it is interbedded with marine, fluvial and estuarine sedimentary rocks. Site-mean directions from redeposited tuff are similar to the TRM direction, but the dispersions are greater, suggesting acquisition of a DRM (depositional remanent magnetization) or PDRM (post-DRM). Although the directions pass a fold test, there is an inherent uncertainty in the results because the pre and post- tilt directions are close to the present axial dipole field direction.

If we accept the fold test as definitive, then the directional similarity among most sites after correction for tilt of beds indicates little differential rotation across the region (except for one site rotated 39° clockwise adjacent to the Rogers Creek fault). The directions are in accord with those of *Mankinen* [1989] from the nearby 3-8 Ma Sonoma Volcanics, which also show no rotation. This implies that the majority of dextral shear strain is being accommodated by movement on the major right-lateral faults, rather than by deformation distributed within blocks between the faults. The relative proportion of permanent simple shear strain to elastically stored deformation, as measured by geodetic methods, is constrained to be less than 5%. Thus, geodetic measurements of relative velocities across the San Francisco Bay area should approximately equal the sum of the geologically determined slip rates across individual faults. The late Cenozoic distribution of simple shear deformation inferred from the paleomagnetic data is also consistent with a crustal model of relatively strong blocks separated by weak faults.

References

Mankinen, E. A., 1989, Revised paleomagnetic pole for the Sonoma Volcanics, California: Geophysical Research Letters, v. 16, p. 1081-1084.

Reports

Haeussler, P.J., Wells, R.E., Hillhouse, J.W., Sarna-Wojcicki, A., and Thatcher, W., 1991, Are there vertical axis rotations in the San Francisco Bay Region? Implications from Paleomagnetic studies: EOS, Transactions, American Geophysical Union, v. 72, p. 125.

Tectonic Framework and Geology of the San Francisco Bay Region

9540-70210

Carl M. Wentworth and Earl E. Brabb
Branch of Western Regional Geology
U.S. Geological Survey
345 Middlefield Road
Menlo Park, CA 94025
(415) 329-4950/5140

INVESTIGATIONS

The principal activities, which were pursued as part of a larger Regional Geology project that is focussed on the Bay region, included mapping of Quaternary deposits and of bedrock structure and stratigraphy, geologic compilation at 1:100,000, development of digital techniques for the compilation and analysis of geologic maps, cooperative work with other projects, and participation on the regional team (BAFEP).

RESULTS

Mapping of Quaternary deposits along the east side of San Francisco Bay (Helley) has been extended through 10 quadrangles that will be incorporated into 1:100,000 compilation. This work reveals remnants of Bay margin terraces and upraised oyster beds at several localities that stand about 6 m above present high water. These probably indicate tectonic uplift relative to probable Sangamon marine deposits in the subsurface beneath the south bay. The maps can be used to derive liquefaction potential of a substantial area around San Francisco Bay.

Mapping the top of the Pleistocene alluvial fill in the Bay trough delineates a seismic impedence boundary within the Quaternary sedimentary prism in the Bay trough. Cooperative work is underway with WRD (Sacramento) to pursue this opportunity.

Quaternary deposits over six 1:24,000 quadrangles on the eastern flank of the Diablo Range have been mapped under contract by William Lettis and Associates. This work extends Lettis' thesis mapping northward from the northeastern part of the San Jose 1:100,000 sheet. The maps can be used to prepare maps of liquefaction susceptibility and aid evaluation of the location and history of a prominent thrust fault on the eastern flank of the Diablo Range.

Isotatic gravity and aeromagnetic maps of the East Bay area prepared by R. Jachens and A. Griscom have been digitally overlain on a working version of areal geology at 1:100,000 to show the relations between the geology and distinctive geophysical anomalies in the vicinity of the Hayward, Calaveras and other faults.

Cores recovered by Malcolm Johnson from holes drilled in the vicinity of the Hayward fault were examined by Jones and Brabb for microfossils; samples were collected and submitted for paleontologic analysis.

A Professional Paper manuscript on the tectonics of the Loma Prieta area is in the final stages of preparation (McLaughlin and Clark). Structural analysis of the active fold and thrust belt east of the San Andreas fault here indicates ~5 km of shortening, ~6 km of uplift, and ~8 km of reverse slip since the Miocene. This deformation is attributed to reactivation since the Miocene of a wedge of Franciscan rocks originally obducted onto the continental margin in the

Paleocene.

Work in the Silver Creek area by Jones, Graymer, and Brabb indicate that thrusting is more important than previously recognized. Two distinct late Cenozoic non-marine sequences have been overridden by Franciscan assemblage and Coast Range ophiolite; one of the thrusts roots in the Calaveras fault. These relations help support a model in which the major strike-slip faults migrate eastward through time along midcrustal detachments.

Digital compilation of new and existing geologic maps continues to interact with the development of ALACARTE and needed digital procedures. The user interface ALACARTE for controlling the commercial geographic system ARC/INFO was released (Fitzgibbon and Wentworth, 1991), and a preliminary routine for preparing earthquake cross sections in ALACARTE-ARC/INFO was written (Wentworth and Mark).

Cooperative work by volunteers and others included Jones' collaboration with Brabb, Clark's collaboration with McLaughlin and Brabb in the southern Bay region, Coleman's work on serpentinites, and mapping by B. Page in the Lick Observatory quadrangle. Volunteers Larry Dickerson, Mary Bowen, and Neil Foley have been working with Brabb to expand the extensive files of drill holes in the Bay region compiled earlier by Engineering Geology Branch scientists. Walter Hensolt has been using this information to prepare a depth to bedrock map.

REPORTS

Fitzgibbon, T.T., and Wentworth, C.M., 1991, ALACARTE user interface - AML code and demonstration maps, Version 1.0 (part A); installation manual (Fitzgibbon, part B), user manual (Wentworth and Fitzgibbon, part C): U.S. Geological Survey Open File Report 91-587.

Helley, E.J., and Miller, D.M., 1992, Geologic map of the Newark 7.5 minute quadrangle, Alameda County, California: U.S. Geological Survey Open-File Map 92-312, map scale 1:24,000.

Helley, E.J., and Nakata, J.K., 1991, Geologic map of the Gilroy quadrangle, California: U.S. Geological Survey Open-File Map 91-278, map scale 1:24,000.

Jones, D.L., Brabb, E.E., and Blake, M.C. Jr., in press, Terrane accretion in a transpressive setting, a model from the California Coast Ranges (abs): Kyoto, Japan, International Geological Congress, Proceedings with Abstracts.

McLaughlin, R.J., Clark, J.C., Brabb, E.E., and Helley, E.J., 1991, Geologic map and structure sections of the Los Gatos 7 1/2 minute quadrangle, Santa Clara and Santa Cruz Counties, California: U.S. Geological Survey Open File Map 91-593, 1:24,000.

McLaughlin, R.J., Kistler, R.W., Wooden, J.L., and Franck, C.R., 1992, Coast Range Ophiolite of the Sierra Azul block southwest of Los Gatos, California (abs): Pacific Section, AAPG-SEPM-SEG-EMD, Program and Abstracts, Sacramento, California.

McLaughlin, R., Oppenheimer, D., Helley, E.J., and Sebrier, M., 1992, The Lexington fault zone: a north-south link between the San Andreas fault and range front thrust system, Los Gatos, California (abs.): Geological Society of America, Abstracts with Programs, v. 24, no. 5, p. 69.

Seiders, V.M., and Cox, B.F., 1992, Place of origin of the Salinian block, California, as based on clast compositions of Upper Cretaceous and lower Tertiary conglomerates: U.S. Geological Survey Professional Paper 1526.

Slip Distribution of the 1954 Fairview Peak and Dixie Valley Earthquake Ruptures

Agreement No. 1434-92-G-2183

Steven G. Wesnousky
Center for Neotectonic Studies
MS 168
Mackay School of Mines
University of Nevada, Reno
Reno, Nevada 89557-0135
(702) 784-1382

Objective

The Fairview Peak and Dixie Valley, Nevada earthquakes of December 16, 1954 produced a 90 km long zone of complex surface faulting in north-central Nevada. Ongoing field studies of coseismic surface offsets associated with these earthquakes seek to provide information important to our understanding of the mechanical behavior of earthquakes and analysis of seismic hazard in the western United States. Specifically, the distribution of coseismic slip for these Nevada earthquakes, examined in the context of geometrical and geological features of the fault, will provide insight to processes that control variation in slip and rupture termination for large earthquakes. Furthermore, resolution of strike-slip verses normal slip components on these historic ruptures has bearing on our understanding of the kinematics of Basin and Range extension.

Progress

Accomplishments of fiscal year 1992 include completion of detailed mapping and measuring surface offsets along roughly 80 km of 1954 Fairview Peak earthquake ruptures and about 25 km of the 1954 Dixie Valley earthquake ruptures. Mapping is being done on large scale (1:10,000 and 1:12,000) low sun-angle aerial photos. In addition, 1:24,000 scale orthophotos (maps) and accompanying tables are being compiled to index and describe evidence for the amount and character of coseismic slip during the 1954 events.

Additional work planned

Three projects are planned for Spring and Summer 1992:

1) complete mapping and measuring surface offsets for the 1954 Dixie Valley earthquake rupture.
2) complete and submit for publication a report and map of the 1954 surface ruptures describing and interpreting surface offsets and slip distribution.
3) excavate and log two exploratory trenches across the Fairview Peak fault zone in the vicintiy of Bell Flat.

Piñon Flat Observatory: A Facility for Studies of Crustal Deformation

14-08-0001-G1764

Frank K. Wyatt, Duncan Carr Agnew,
and Hadley O. Johnson
Institute of Geophysics & Planetary Physics
Scripps Institution of Oceanography
University of California, San Diego
La Jolla, CA 92093-0225
(619) 534-2411

This grant supports the operation of Piñon Flat Observatory (PFO) as a research center for the study of crustal deformation. Through this grant, the U.S. Geological Survey provides 50 percent of the funding needed both for running the 160-acre facility and for maintaining the reference-standard instruments there. Matching funds are provided by a grant from the National Science Foundation. The work done at PFO includes establishing the accuracy of instruments designed for measuring various geophysical quantities by comparing results from them with data from the best available continuously recording deformation monitors. Such comparison then provides for an accurate record of strain and tilt changes in the area near the observatory, between the active San Jacinto fault and southern San Andreas fault systems. All of this effort is intended to foster development of precision instrumentation and from this an improved understanding of the earth. Particularly for crustal deformation studies, more accurate measurements are needed for a better understanding of the mechanics of faulting. The site continues to be utilized by roughly 20 different research teams.

In this period, the most important event has been the Landers earthquake sequence (**Figure 1**). The shaking from this event at 5 AM local time awakened nearly everyone in southern California and by 6 AM—even without knowing all the details of the source—we were on the road to the observatory. Since PFO is only 65 km from the epicenter, we knew several of the instruments wouldn't be working. We arrived at PFO two hours later and spent the day working on all the sensing systems—no small task with aftershocks every few minutes. This attention to the equipment was well worth while, since the next day began with an early-morning telephone call from Dr. Lucile Jones of the USGS to Dr. Agnew (at home), asking about the strain data from PFO. In the previous 24 hours aftershocks of the Big Bear event had extended as far south as the San Andreas fault, leading to concern that rupture on that fault might be imminent. An inspection of the telemetered records showed that a strain change of unprecedented rapidity was in fact occurring, with the amount of change in the previous day being about what we normally see in a year. Later that day we were asked to send PFO strain data to a meeting of CEPEC,[1] as the PFO strain records were the best

[1] The California Earthquake Prediction Evaluation Council, meeting in emergency session.

clue as to whether or not some instability might be developing. Some hectic data editing culminated in an evaluation that the rate of postseismic strain, while still rapid, was decreasing. This reduced the immediate concern, though not the interest in how these strains were evolving.

Figure 2 shows two days of data on either side of the Landers earthquake for the three laser strainmeters with the coseismic offsets removed—roughly the same data span sent to CEPEC. After the Landers earthquake (the first laser strainmeter comes on about 80 minutes after the shock) the NW-SE strain rate went from its usual value, generally tracking the long-term geodetic signal, to an unprecedentedly high one. **Figure 3** shows a much longer span of data for the three strain records (200 days); here and in all the data plots we show the records both with earth tides left in (for scale) and removed (to show the signals). This figure shows how the initial rapid change in strain gradually leveled off, reaching a total amount (for the NW-SE instrument) of ~8% of the coseismic strain change. Similar transients are visible on the other two strainmeters. **Figure 4** shows the same span of data from the long-base tiltmeters; the NS tilt also shows a decaying transient, while the EW record instead shows an abrupt change in long-term tilt rate. **Figure 5** shows the long-base tilt data for a slightly shorter time span, for comparison with the Askania borehole tiltmeter (KUB); there is a striking agreement between these completely different instruments, adding credibility to all the signals of perturbed strain at the observatory.

We are pursuing various explanations for this deformation. Two effects that we think can be eliminated early on are that these effects are purely instrumental (they appear on too many different types of instruments), and that this is some kind of viscoelastic adjustment (the time constant would seem much too short). The remaining possibilities are local changes in the water table, which would probably not give the large spatial scale implied by these data, and aseismic slip on faults, driven by the static strain changes from the Landers and Big Bear earthquakes. Frictional models of faulting all show some amount of deep afterslip following the actual earthquake rupture—typically amounting to ~5% of the coseismic moment in 24 hours—so this is physically reasonable. While we have not yet been able to identify the faults that would cause this signal, there are a number of candidates that could cause the dilatational event recorded on all the strainmeters; most probably many faults contributed, making identification difficult. We are continuing to work on this and are optimistic that a synthesis of the PFO data with the near-field postseismic GPS measurements (which we helped in) will give a better picture of where this deformation may and may not have come from. One thing we do know is that unlike earlier events, where the postseismic signal could easily be assigned to ongoing sympathetic slippage on or at the edge of the rupture surface, the PFO signals for the Landers/Big Bear earthquake require a more complicated pattern of postseismic adjustment.

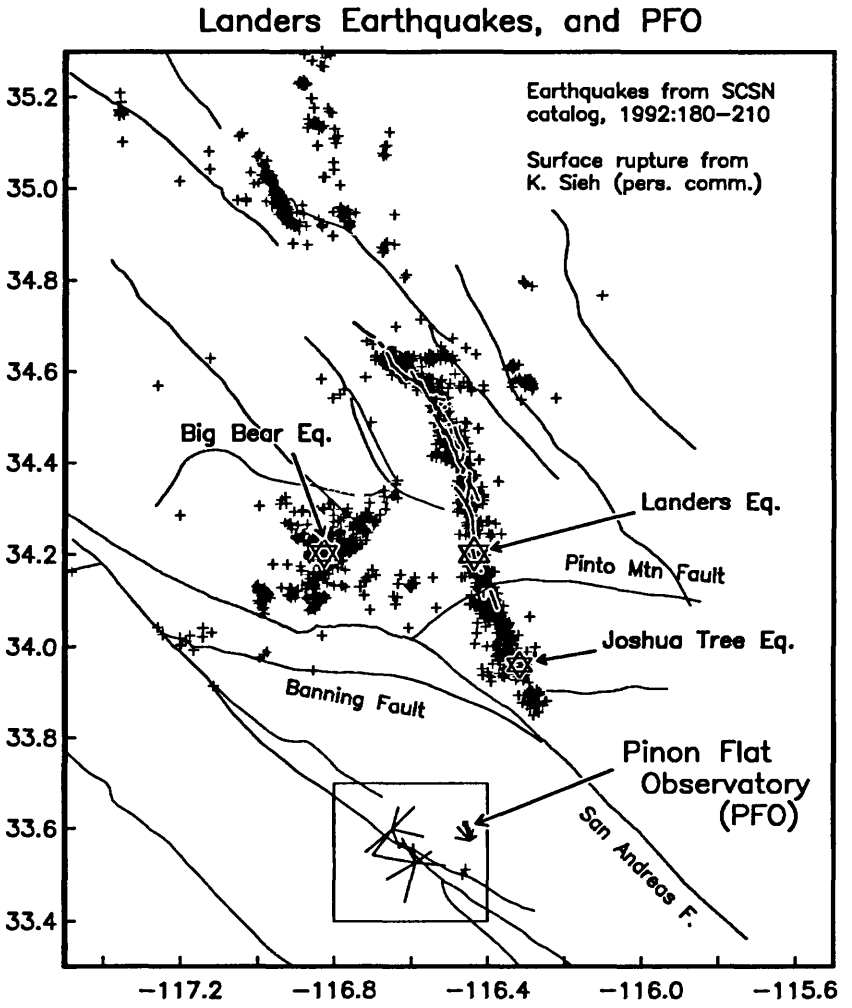
Landers Earthquakes, and PFO
Earthquakes from SCSN catalog, 1992:180–210
Surface rupture from K. Sieh (pers. comm.)
Big Bear Eq.
Landers Eq.
Pinto Mtn Fault
Joshua Tree Eq.
Banning Fault
Pinon Flat Observatory (PFO)
San Andreas F.
35.2
35.0
34.8
34.6
34.4
34.2
34.0
33.8
33.6
33.4
−117.2
−116.8
−116.4
−116.0
−115.6

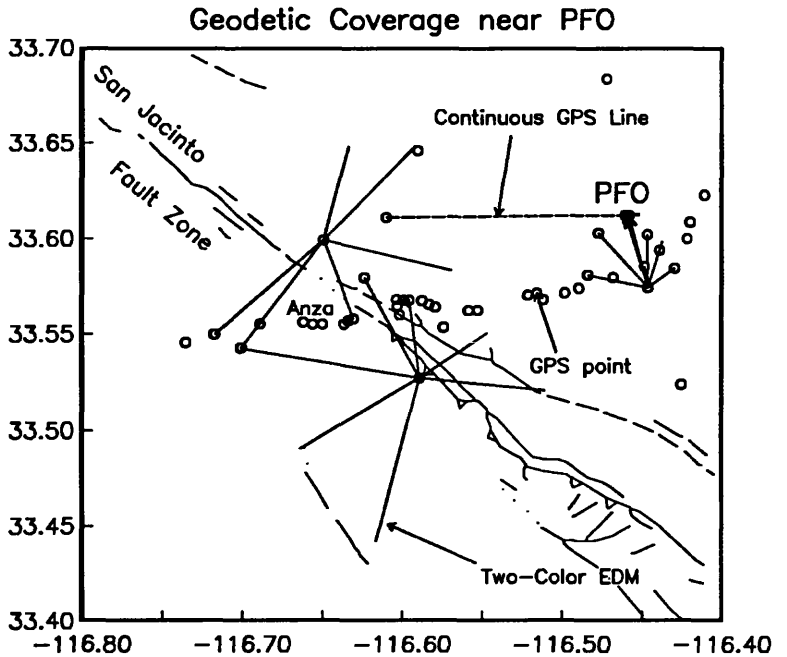
Geodetic Coverage near PFO
San Jacinto Fault Zone
Continuous GPS Line
PFO
Anza
GPS point
Two−Color EDM
33.70
33.65
33.60
33.55
33.50
33.45
33.40
−116.80
−116.70
−116.60
−116.50
−116.40

Figure 1

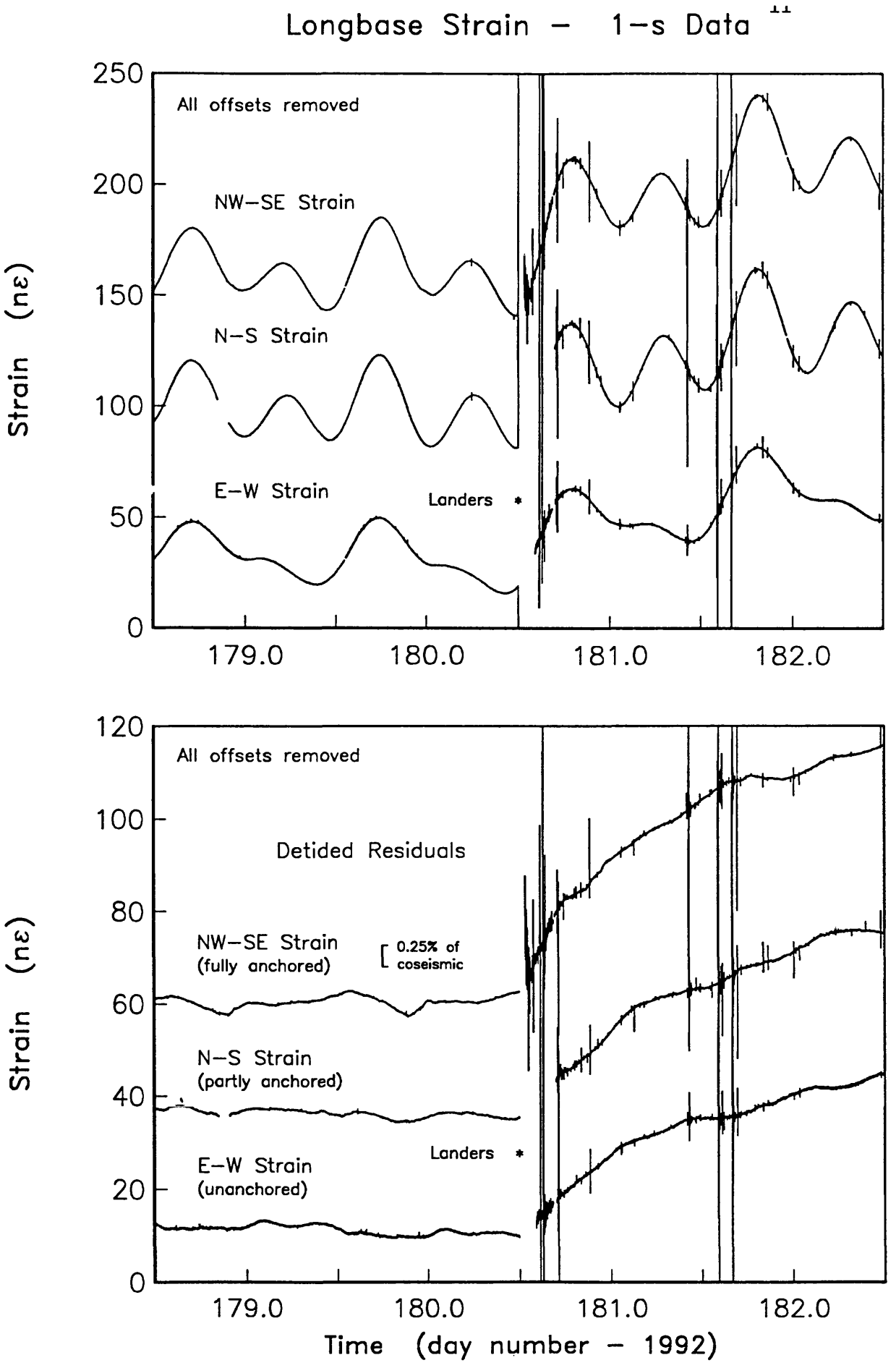
Longbase Strain – 1–s Data
All offsets removed
NW–SE Strain
N–S Strain
E–W Strain
Landers
Strain (nε)
250
200
150
100
50
0
179.0
180.0
181.0
182.0
All offsets removed
Detided Residuals
NW–SE Strain
(fully anchored)
0.25% of coseismic
N–S Strain
(partly anchored)
E–W Strain
(unanchored)
Landers
120
100
80
60
40
20
0
Time (day number – 1992)

Figure 2

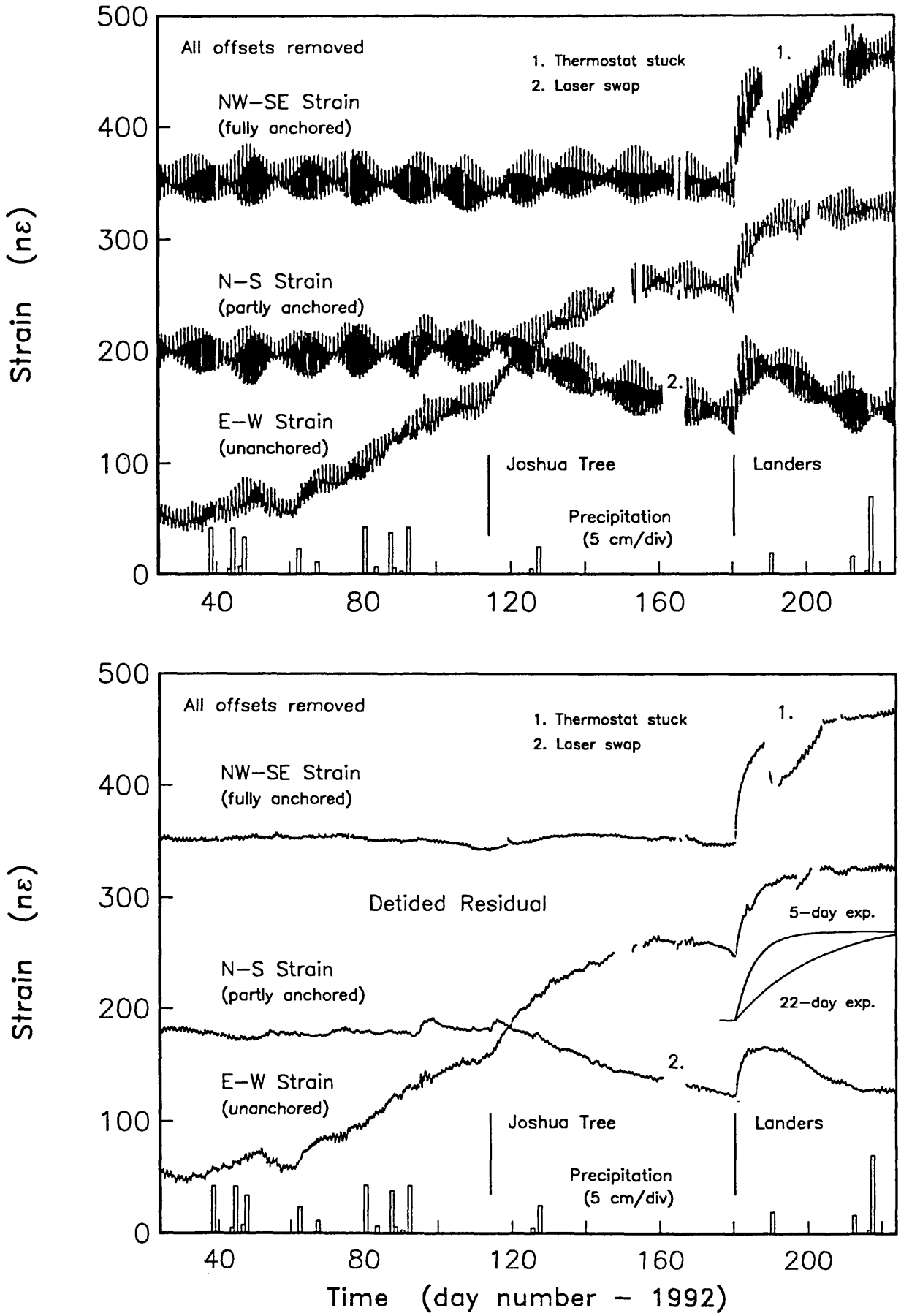
Longbase Strain
All offsets removed
1. Thermostat stuck
2. Laser swap
NW–SE Strain
(fully anchored)
N–S Strain
(partly anchored)
E–W Strain
(unanchored)
Joshua Tree
Landers
Precipitation
(5 cm/div)
Strain (nε)
Detided Residual
5–day exp.
22–day exp.
Time (day number – 1992)

Figure 3

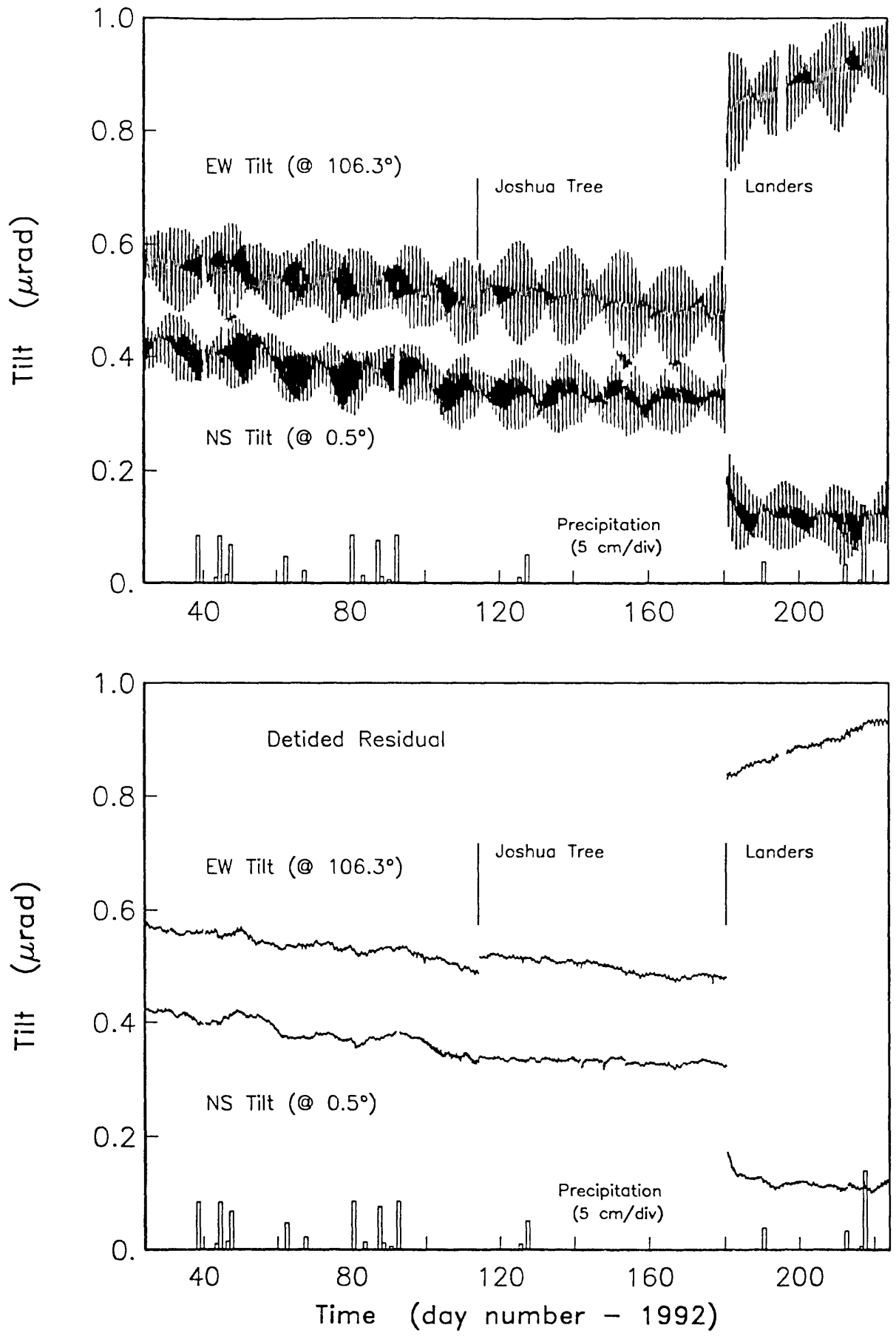
Longbase Tilt
Tilt (μrad)
1.0
0.8
0.6
0.4
0.2
0.
EW Tilt (@ 106.3°)
Joshua Tree
Landers
NS Tilt (@ 0.5°)
Precipitation
(5 cm/div)
40
80
120
160
200
Detided Residual
Time (day number − 1992)

Figure 4

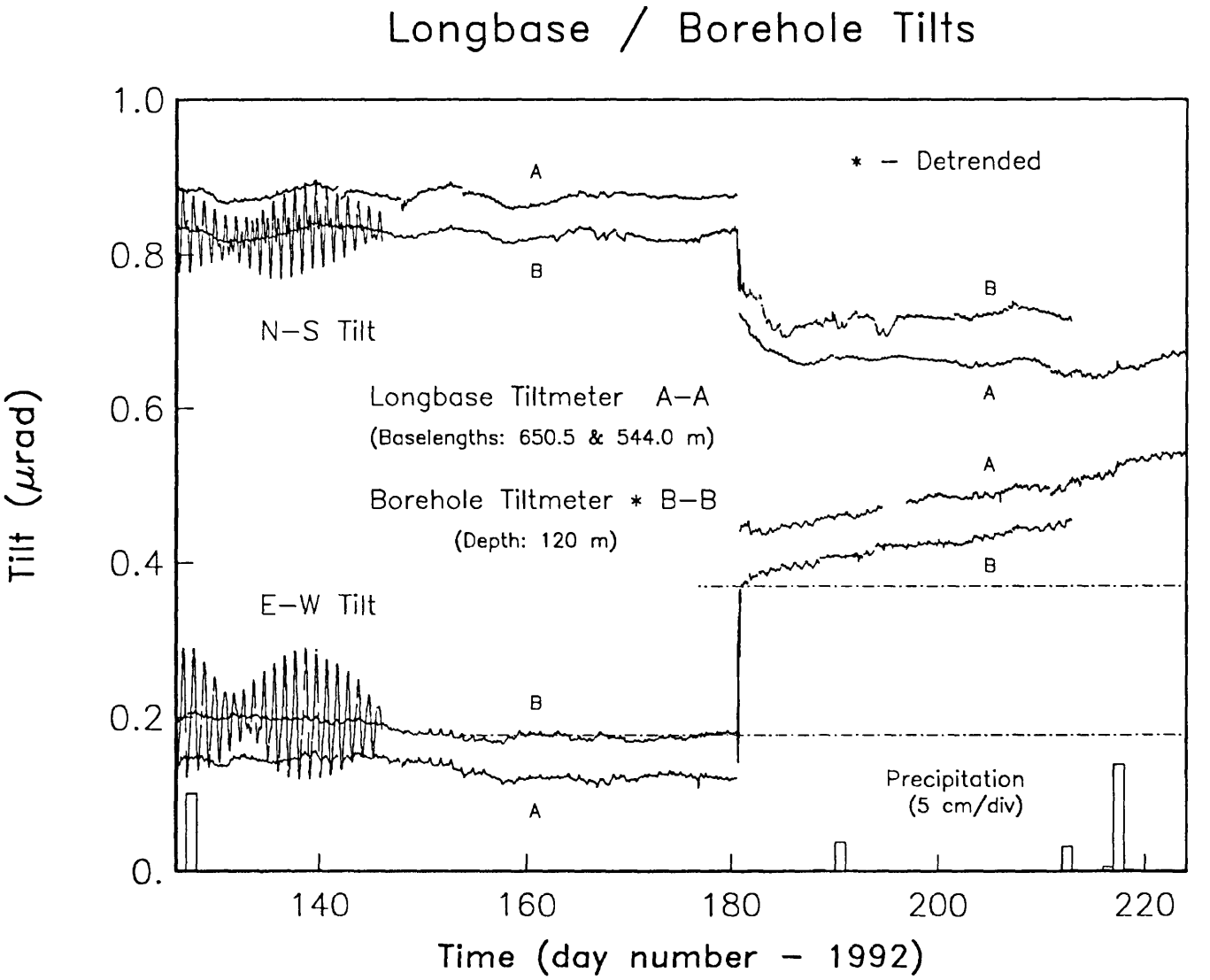
Longbase / Borehole Tilts
1.0
0.8
0.6
0.4
0.2
0.
Tilt (μrad)
* – Detrended
A
B
N–S Tilt
Longbase Tiltmeter A–A
(Baselengths: 650.5 & 544.0 m)
Borehole Tiltmeter * B–B
(Depth: 120 m)
E–W Tilt
Precipitation
(5 cm/div)
140
160
180
200
220
Time (day number – 1992)

Figure 5

Deformation Monitoring of the Southernmost San Andreas Fault

14-08-0001-G1786

Frank K. Wyatt, Hadley O. Johnson, and Duncan Carr Agnew
Institute of Geophysics and Planetary Physics
University of California, San Diego
9500 Gillman Drive, La Jolla, California 92093-0225
(619) 534-2411

Based on our good fortunes in building and running an optical-fiber monument anchor in the Coachella Valley, we decided in early 1991 to propose a long baselength strainmeter for the area. Stable anchoring of end monuments had proven an essential element for the instruments situated on the granites of Piñon Flat Observatory (PFO); the initial optical fiber experiment had been designed to establish if similar anchoring was possible in the clayey material of the Coachella Valley. In the proposal we made the argument that a strainmeter (or tiltmeter), run in parallel with the laser strainmeters at Piñon Flat Observatory—but in a completely different geological and tectonic setting—should prove highly enlightening in trying to understand crustal deformation in the period range of minutes to months. The optical anchor study (discussed in detail last year) convinced us that a ~500 m-long Coachella Valley strainmeter, anchored to depths of about 20 m, had a good chance of giving meaningful results. This year's grant has thus supported two efforts: (1) the continued operation of our fiber-optic anchoring experiment on the Coachella segment of the San Andreas Fault—specifically, on the western flank of Durmid Hill, near the termination of the San Andreas Fault and its junction with the Brawley Seismic Zone—and (2) the construction phase of a long baselength strainmeter.

The ongoing optical fiber experiment involves measuring the differential vertical motion of four points in the ground from depths of 1.65 m to 48 m. The primary goal of this experiment was to determine the appropriate depth (if any) for anchoring long-base instruments. Over the past 1½ years we have found that ground between 5 m and 8 m depths (and presumably above these depths) can be quite unstable, showing motions as much as 0.5 cm in response to surface wetting. In contrast the deformations over the interval of 23 m to 48 m (a span eight times greater than above) have proven quite stable, with little more than an apparently steady secular extension of 0.2 mm/yr. This and other measurements suggest that ~20 m is deep enough for stable anchoring. We are still running this experiment as it continues to provide insights into the behavior of the material in the valley and because operating it, in conjunction with the many construction trips to the area, demands little effort on our part.

Our design for the long-base instrument at Durmid Hill (hereafter DHL) was based on two goals: (1.) To construct a high-quality long-base strainmeter that is as low-maintenance as possible. (2.) To make the instrument as "portable" as possible. Though this may seem an odd notion for to something so substantial, we sought in our design to make sure that everything not sunk in the ground could be removed and re-installed elsewhere. This aspect of the design is in keeping with our expectation that the installation at Durmid Hill is not to turn into a permanent one.

The small size of the original fiber-optic anchor allowed us to place it on private property and work closely with the land owners. This went so well we felt that the DHL installation should be as near as possible to continue the benefit of their help; experience had convinced us that this would make the instrument much more reliable—a paramount consideration in this field. Having chosen a preferred location we began discussions with the land owners, the California State Park system, in September 1991. Surveying for the specific site within Section 14 (Figure 1) began in January 1992. Our "use" permit was issued on February 19, 1992, and we began heavy-equipment work at the site the next day, with drilling commencing the week after this.

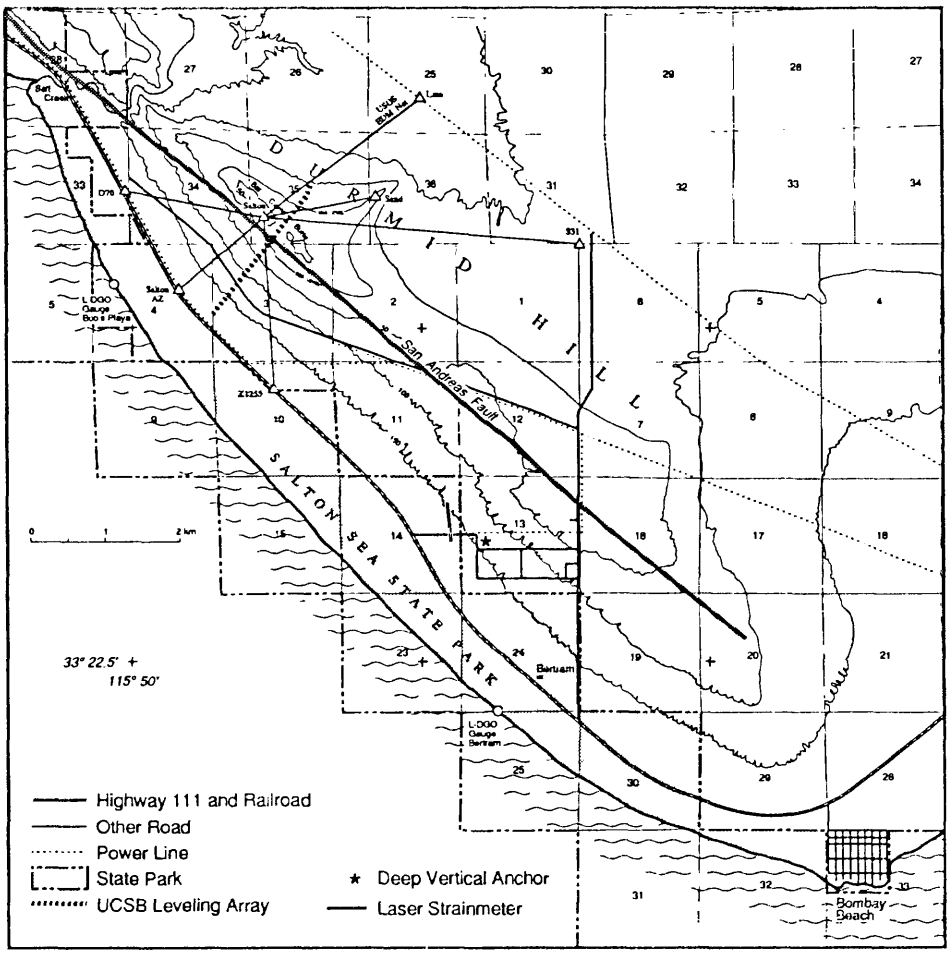

Figure 1.

The major constraint in siting the equipment was avoiding the larger gullies that dissect the surface; the largest of these are 30′ deep and twice as wide: impressive just to look at, dangerous to get too near, and much too big to bridge. Our final choice involved may tradeoffs, but put the south end close to the end of the powerline serving the nearby houses, with the instrument running 524 m from there at an azimuth of N5°W, 45° to the local fault-strike.

Serious construction began in March 1992 and by the start of May we felt we were in a good position to complete the instrument by year's end, but a number of unexpected events conspired to thwart this plan. The most redeeming of these was the Lander's earthquake sequence of late June. This along with the others—our sad loss of Leo Weuve at PFO and the ill-health and eventual disability-loss of our lead field engineer for this project—has meant that we are only now completing construction at the site. Unfortunately the winter rains mean we can't expect the work to go quickly. It is absolutely impossible to work at the site any time after the ground has become wet; "gumbo" sticks to vehicle tires within only few feet of driving causing them to become frozen no matter what is tried (not to mention what happens to your shoes and feet).

Figure 2 is a schematic drawing of one end of the laser strainmeter. This instrument is identical in principle to the existing laser strainmeters at PFO: a Michelson interferometer with one of its optical arms spanning an extended path, which needs be evacuated to remove the effects of variations in the index of refraction of air. However, the new instrument does differ in a number of ways from what has been done before. The entire installation is to be buried; while this has made

the construction much more difficult, it will provide better thermal stability, immunity to vandalism, and all-in-all should provide for a much better measure of strain.

Strainmeter End-Vault DHL - Side View

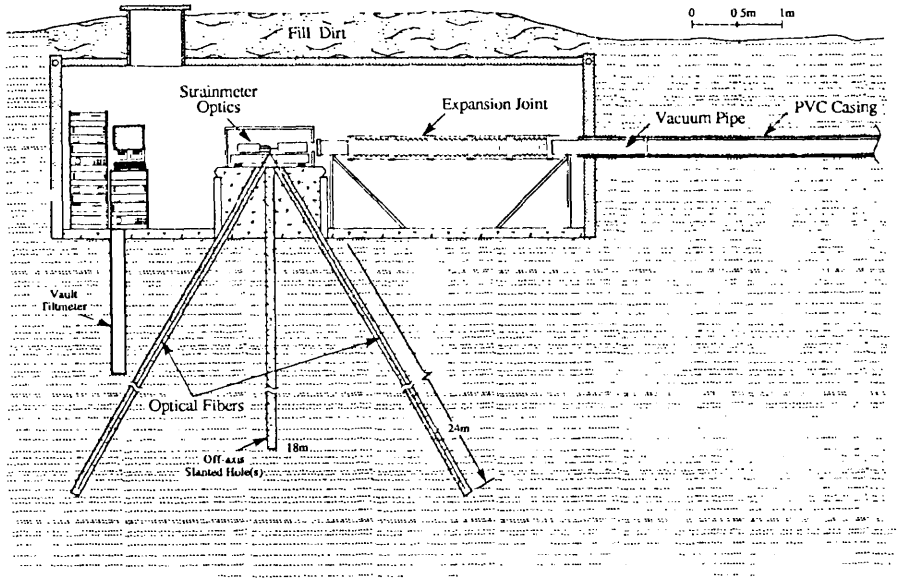

Figure 2.

The vaults have been built from damaged shipping containers, which has turned out to be a very economical approach. At each end concrete pads have been formed to support optical tables on which two interferometers will be installed. One will be for the primary sensor, the horizontal strainmeter, while the other would monitor the lengths of two optical fibers extending downward in inclined boreholes to a depth of 25.6 m. These fibers will serve to anchor the strainmeter to more stable points at depth, in the manner of the original optical anchor of Wyatt *et al.* (*BSSA*, 1982). The vacuum pipe is to be installed inside a buried PVC casing. Halfway between the two vaults we will build a center shelter where the sections of vacuum pipe can be inserted into the PVC pipe-conduit—"cartridge" loaded in both directions; this will also house the system's main vacuum pump.

Our first step in site construction was to build a road and a series of bridges to permit heavy-equipment vehicle access to the two ends of the instrument. The top panel of Figure 3—a profile along the line of the strainmeter—shows how flat the surface is, except for five 1-3 m-deep washes we needed to pass. We bridged these by adding fill over wash-bottom culverts made from 55-gallon drums welded end-to-end (100 all totaled). Sand and soil was piled on the culverts to raise the bridge levels up to grade. We expect these bridges to last though all but a "10-year" flash flood. (We did have a substantial rain do an impressive job of removing *all* signs of one temporary ~3 m by 4 m by 5 m earthen-filled bridge.)

We next drilled four holes (inclined at 35° from vertical) at each end: two along the strainmeter axis, with open casings inserted, and two off-axis holes simply for additional mechanical anchoring of the end piers. The drilling equipment was a dual-wall rotary rig with a "drag" bit, designed to fully support and isolate the side-walls during the drilling operation. Despite this we did suffer from some well-bore collapse as the drill casings were removed, losing, in one important case, several meters of open hole. All eight holes were cemented using pressurized grout injected at the bottom of the boreholes, sweeping fresh grout upwards to the surface. (In one case the grout actually found a separate route to the surface, spewing out there first before issuing from the well-

bore.) Borehole-casing depths for the on-axis holes were 25.6 m; for the off-axis holes, 20.4 m.

We planned the major construction (trenching for the vacuum-pipe casing) for April and May, based on the absence of rains in the last ten years of weather recordings. We started trenching the last week in March only to be forced off the site, with the trench one-third dug, by a 3-cm+ downpour. The last two-thirds of the trench was dug with a massive "trench excavator." In doing the first third, we had crossed everything from loose aeolian sand, to rock-hard-until-wetted clays, to meter-thick hard siltstone that a regular backhoe could not break. Most of the strata throughout this area are of order ½-2 m thick, with all manner of strike and dip, often spanning the complete spectrum of composition and strength over a few meters. Some of the material was so weak (floury) that agitation with your feet was enough to excavate it, while other material was flint hard. Without question, our fondest and most bizarre memory of this period was the appearance, on—and spreading across—our desolate access road, of *MTV*, Michael Jackson, giraffes, oxen, and scores of support people for the two-week filming of a music video in a custom-built Mexican village. Getting our equipment through this required some special diplomacy.

Surveying for the trenching was done in part by leveling and in part with a T-2 theodolite, stationed at one end of the strainmeter line and aimed at a target at the other. This use of the theodolite for trenching was a calculated gamble that we wouldn't overdig too much; we knew that the daytime near surface air temperature gradient would cause the sight-line between the ends to be below the correct level in the middle. Early on we found we were going to have to work very hard to install a truly straight pipe: even 2 m above the ground, daytime vertical deflections of the line-of-sight amounted to as much as 8 cm, with horizontal deflections reaching 5 cm, and both of these varying by up to 50% over a few minutes. Even nighttime refraction on our 524 m baseline was substantial, though with the opposite sign. Only when we had a fairly good breeze at night could we be confident we were looking along a straight line. In the end we were forced to survey-in a number of "range sights" which allowed us to see immediately how distorted a viewing path we had at any given moment; if the seeing problems were severe we could move the theodolite forward (closer to the work at hand) to reduce the magnitude of the effects. We also leveled over successive short baselines, to verify the pipe's vertical position (which included compensating for the earth's curvature).

As the trenching progressed (four days worth) it became clear we could not use the native material for backfilling around the casing. The spoils were nearly impossible to move by hand and unlikely to provide the PVC casing with the uniform support it needed so it might handle the load of backfilled material without deforming. In the end we settled on hauling in 166 yd^3 of sand—yep, sand to the desert—in total, some 230 tons of sand which we actually positioned by hand. Supports for the casing at the washes and near entrances to the vaults was another problem. We needed to ensure that the casing would not move, knowing the clay-rich surface material was likely to heave of order 1-3 cm with each rainfall. Our solution was to build strong support bridges for the casing, each anchored to ~1 m depths in a number of places; the anchors for these consisted of 2-cm diameter rebar, driven until we exhausted ourselves.

Another task we undertook before assembling the casing pipe was to install power and signal wiring in the trench. In addition to this we installed an empty 6-cm diameter PVC casing for future use. The trenching effort being so great, and the trench bottom so manicured, we felt it prudent to lay some groundwork for further instrumentation. Indeed, another UCSD research team, one working on development of a long-baseline seafloor tiltmeter, volunteered their labor to install the pipe in exchange for possible use of the conduit and end-vaults at a future date.

Assembly of the vacuum-pipe casing took the day-time hours of two days, the nights being reserved for aligning the pipe, which ended up requiring a total of four late-night efforts. The casing was quite stiff and most sections came with a natural 1-3 cm bow which presented us with a problem. Our design goal was for a pipe straight to within 0.5 cm over short distances, to make it

easy to slide in the vacuum pipe (hence the stringent requirements on surveying technique). We did not need to hold this line over the longer distances since the vacuum-pipe aperture will allow more deviation than this, but to keep the vacuum pipe from being able to shift laterally within the PVC we wanted to make the vacuum pipe a relatively tight fit—and this set our requirement that the PVC be very straight locally. Shimming the pipe as we went and backfilling with sand, we were able to remove most of the bow in the pipe; independent measurements of the pipe position (Figure 3) show that we achieved the desired 0.5 cm straightness throughout.

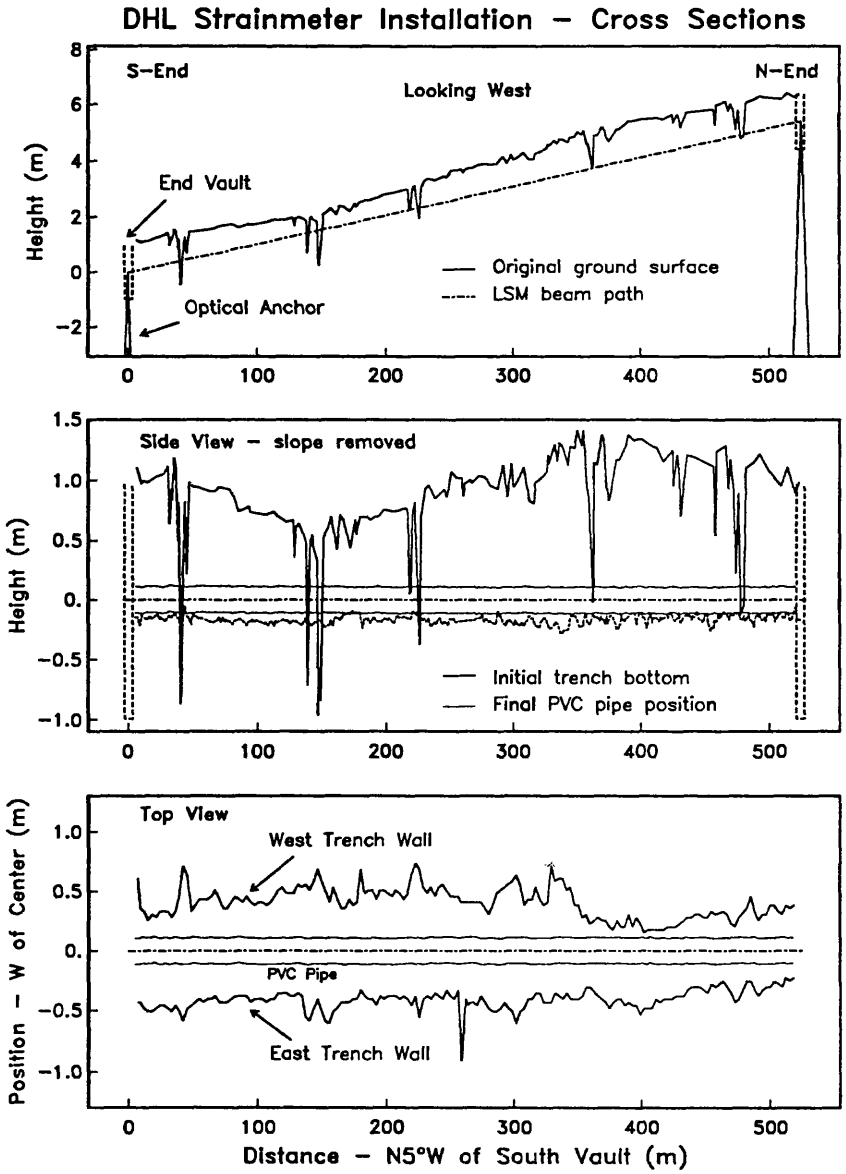

Figure 3.

At this juncture we feel we have completed nearly all the work at the site that will require heavy equipment and massive amounts of hand labor; we have also completed almost all the design work on the optical and vacuum-system components. It is now a mostly matter of completing the end vaults machining the various elements, and bolting them all together.

Subsurface Geology of Northern Los Angeles Fold-and-Thrust Belt and the Eastern Ventura Basin

Contract Number: 14-08-0001-G1967

Robert S. Yeats, Department of Geosciences, 104 Wilkinson Hall, Oregon State University, Corvallis, OR 97331-5506, (503-737-1226)

Investigations. A structure-contour map of the base of the Pleistocene gravels (Figure 1) has been revised to incorporate additional water-well, oil-industry biostratigraphic, and Metro Rail boring data. Other structure-contour maps on the top Repettian Stage, the Miocene-Pliocene contact, the upper Puente-middle Puente Formation contact (within the upper Miocene), and the Santa Monica fault strands are under construction. Several detailed cross sections are under construction (by Tsutsumi west of the Newport-Inglewood fault zone [NIFZ] and by Hummon and Schneider [Figure 2] east of the NIFZ) in preparation to balance cross sections across the northern Los Angeles basin. The well base map, 3 panels at a scale of 1:6,000, is nearly complete. Cheryl Hummon is concentrating on deformation of Pleistocene strata. This work was published in a special volume of the Association of Engineering Geologists (Hummon et al., 1992a) and has been submitted to Geology (Hummon et al., 1992b).

Yeats et al. (1992) have finished a paper on the details and timing of structures in the east Ventura basin. This paper has been accepted by the American Association of Petroleum Geologists. A companion paper (Huftile et al., in prep.) balances cross sections to determine the convergence rate across the basin. A paper on the convergence rates across the central Ventura basin (Huftile and Yeats, 1992) has been submitted to the Journal of Geophysical Research.

Results. The base of the Pleistocene gravels is the youngest horizon that can be contoured extensively over the entire area, and its age is critical to determining rates of deformation. Ponti (1989) found that the base of the Pleistocene San Pedro Formation in the subsurface of the southwest Los Angeles basin is considerably older than it is at the type locality in San Pedro. Our best estimate now, prior to obtaining direct dates, is that the base of the gravels was deposited between 800-1,600 ka. Our revised map of the base of the Pleistocene gravels is shown in Figure 1. The Wilshire arch, Hollywood basin, and Los Angeles trough all terminate westward against the NIFZ. However, the structure previously mapped as the Wilshire arch to the west of the NIFZ is now recognized as a monocline, with a steep south-facing flexure which is expressed as a set of young fault scarps (Dolan and Sieh, 1991). The boundary between the Wilshire arch and Hollywood basin is in part marked by the North Salt Lake fault shown in Figures 1 and 2, which is parallel to the Hollywood fault to the north. The steep south flank of the Wilshire arch is underlain by two en-echelon fault-propagation folds, the Las Cienegas anticline and the East Beverly Hills anticline. Figure 2 is an unbalanced cross section. Note that the North Salt Lake fault has normal separation. The inset shows that there is no thinning of the Puente, Repetto, or middle-lower Pico formations across the Wilshire arch, implying that the Wilshire arch did not begin to form until after the deposition of the middle Pico Formation.

For several years, convergence rates across the Ventura basin were based on the assumption that active high-angle reverse faults (Oak Ridge, Red Mountain, San Cayetano) flatten to horizontal at the brittle-plastic transition, a décollement at the base of the seismic zone. However, Bryant and Jones (1992) found earthquakes at 20-30 km depth beneath the Ventura basin. The deep keel on the base of the seismogenic zone implied by these earthquakes is difficult to reconcile with the décollement model. The Moho is also depressed 7-10 km indicating crustal thickening. 2.7 years of GPS data suggest convergence of 7 mm/y (Donnellan, 1991; Donnellan et al., 1992), about a third of the rate based on the décollement model. If the reverse faults do not flatten at the base of brittle crust but instead continue into the lower crust as ductile shear zones, horizontal shortening would be based on the fault slip rates times the cosine of the fault dip, resulting in a convergence rate closer to that based on GPS. The keel at the base of the seismic zone would be explained by downward displacement of the central Ventura basin between opposing reverse faults, a process dominant in the basin for the past several million years (Yeats and Huftile, 1992).

References cited.

Bryant, A. S., and Jones, L. M., 1992, Anomalously deep crustal earthquakes in the Ventura basin, southern California: Jour. Geophys. Res., v. 97, p. 437-447.

Dolan, J. F., and Sieh, K. E., 1991, Structural style and geomorphology of the Santa Monica-Hollywood fault system: Constraints on kinematics of recent fault movement: EOS, Trans. Am. Geophys. Union, v. 72, p. 319-320.

Donnellan, A., 1991, A geodetic study of crustal deformation in the Ventura basin region, southern California: unpub. Ph. D. dissertation, California Inst. Tech., Pasadena, California, 220 p.

Donnellan, A., Hager, B. H., and King, R. W., preprint, Rapid north-south shortening of the Ventura basin, southern California:

Ponti, D. J., 1989, Aminostratigraphy and chronostratigraphy of Pleistocene marine sediments, southwestern Los Angeles basin, California: unpub. Ph. D. dissertation: Univ. Colorado, boulder, Colorado, 409 p.

Reports.

Hummon, C., Schneider, C. L., Yeats, R. S., and Huftile, G. J., 1992a, Active tectonics of the northern Los Angeles basin: An analysis of subsurface data, in Stout, M. L., ed., Proc. of the 35th Annual Meeting: Assoc. Eng. Geol., p. 645-654.

Hummon, C., Schneider, C. L., Yeats, R. S., and Huftile, G. J., 1992b, The Wilshire arch: Active tectonics of the Los Angeles basin, California: submitted to Geology.

Huftile, G. J., and Yeats, R. S., 1992, Convergence rates across a displacement transfer zone in the western Transverse Ranges near Ventura, California: submitted to Jour. Geophys. Res.

Huftile, G. J., Yeats, R. S., and Huafu, L., 1992, Convergence rates across the east Ventura basin: in prep.

Yeats, R. S., Huftile, G. J., and Stitt, L. T., 1992, Late Cenozoic tectonics of the east Ventura basin, Transverse Ranges, California: accepted by the Am. Assoc. Petrol. Geol.

Yeats, R. S., and Huftile, G. J., 1992, Alternate model for convergence across the Ventura basin, California: EOS, Trans. of Am. Geophys. Union, v. 73, p. 590.

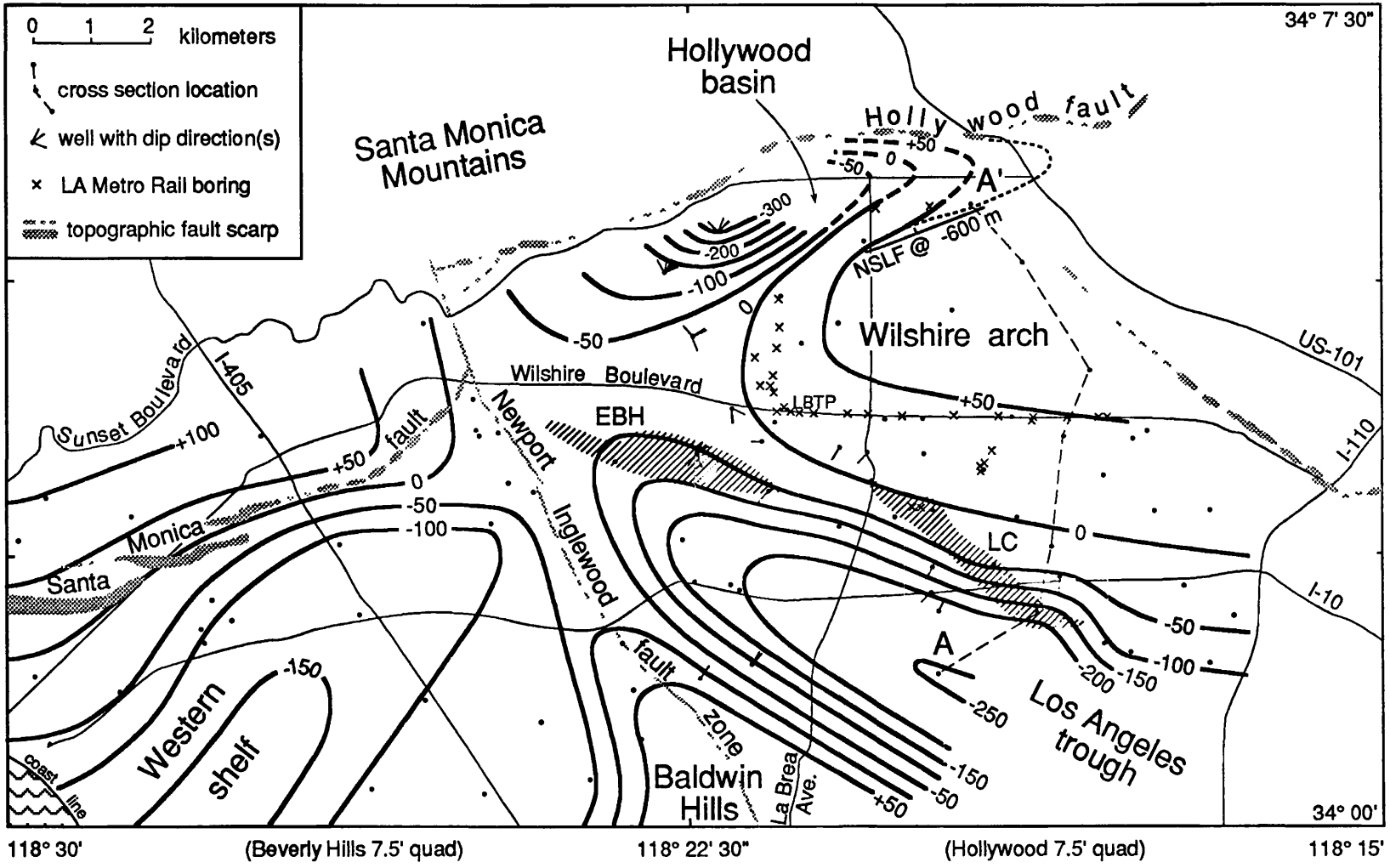

Figure 1. Structure contours on the base of the Quaternary marine gravels, based primarily on correlation of oil-well electric logs. Dashed contours at eastern end of Hollywood basin are estimated form groundwater studies. The +50 m structure contour on the Wilshire arch is the approximate edge of the marine Pleistocene gravels, which are not present over the highest part of the Wilshire arch. In the Hollywood basin, the same contact is indicated by a dotted line. Diagonal-lined areas show the extent of the East Beverly Hills (EBH) and Las Cienegas (LC) SW-vergent anticlines. Stippled areas are topographic fault scarps from Dolan and Sieh (1991). NSLF is the North Salt Lake fault at the -600 m structure contour. LBTP indicates the location of the La Brea tar pits. Cross section location for Figure 2 (A-A') is shown.

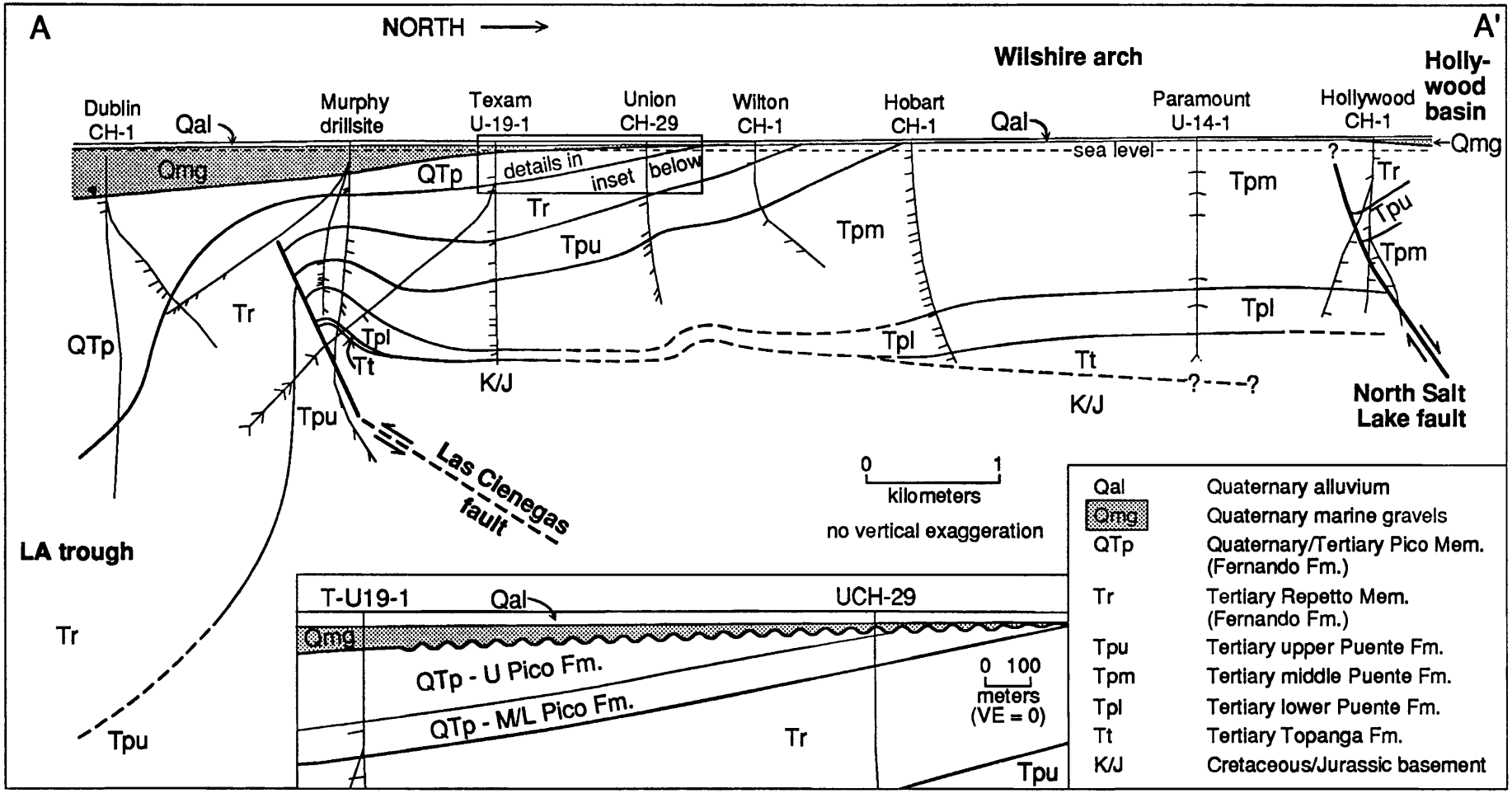

Figure 2. Cross section (not balanced) across the Wilsire arch and Las Cienegas fault (location shown on Figure 1). Formation dips on wells are from dipmeter data (single tick marks) and core dips (double dip symbol). The inset shows details of the unconfomable contact between the Quaternary marine gravels (Qmg) and the underlying Pico strata (QTp), showing that uplift on the Wilshire arch began after deposition of the M/L Pico Formation.

CONSTRAINTS ON INTRAPLATE DEFORMATION

9930-02669

Mary Lou Zoback
Seismology Branch
U. S. Geological Survey
345 Middlefield Road, MS 977
Menlo Park, CA 94025
(415) 329-4760

INVESTIGATIONS:

1. Frictional faulting analysis of well-constrained earthquake focal mechanisms and independently-derived stress orientation data from a variety of areas around the world to place limits on possible pore pressure conditions at depth.

2. Utilizing stress orientation data to investigate local stress anomalies that may be responsible for localizing intraplate seismicity.

3. Investigation of the stress state and style of deformation in the Basin and Range province.

4. Maintaining and updating a global compilation of contemporary in-situ stress data compiled as part of the World Stress Map Project, an international collaborative effort including over 30 scientists from over 25 different countries and lead by the project chief.

RESULTS:

1. A dense cluster of seismicity (mostly M_L=1.2-2.8) within the southern Rhine graben, Germany, has yielded well-constrained focal mechanisms which range from nearly pure normal to nearly pure reverse faulting. Master event locations indicate that the earthquakes are all occurring within a 2 km source region centered about 12 km depth. The largest event recorded in the sequence is M_L=4.7.

One way of explaining the observed diversity of focal mechanisms is if near-lithostatic pore pressure exists throughout the source region. In this case, small differences in relative stress magnitudes can cause marked changes in the style of faulting. However, if the differences between the vertical and horizontal stress magnitudes are small enough so that these axes can exchange, permutations of the two horizontal axes should also be possible. The uniform orientation of the P- and T-axes of these events (contained in planes striking 145° (±10°) and 55° (±10°) respectively) argues against a uniform high pore pressure explanation. This P-axis orientation is identical to the mean P-axis direction of the dominantly strike-slip earthquakes which occur throughout the southern Rhine graben/Black Forest region and also

coincides with the maximum horizontal stress direction inferred from wellbore breakouts and in-situ stress measurements in the region.

Alternately, using the fault slip inversion method of Gephart, it can be shown that the observed slip vectors in a representative subset of the events are consistent with a single strike-slip stress tensor with σ_1: azi= 150°, pl=10°, and the relative magnitude of σ_2 about halfway between σ_1 and σ_3. However, an analysis of the conditions for slip using this stress tensor (with a constant frictional coefficient = 0.65) indicate a wide range in pore pressure values, from close to hydrostatic (0.40 lithostatic) for the strike-slip events to 0.90 lithostatic for the dip-slip events. At depths of 12 km, this corresponds to pore pressures ranging between 127-286 MPa.

2. Analyses of occurrence of intraplate seismicity invariably show a correlation with "continental rifts" or crustal zones with a history of extensional tectonics. Preliminary modeling suggests that the presence of a dense body in the lower crust beneath rifts can generate a significant local compressive stress which may be a factor influencing both the style and likelihood of intraplate seismicity. Perhaps one of the best examples of a local stress rotation and intraplate seismicity related to lateral variations in crustal structure beneath rifts occurs in central Brazil. Two moderate earthquakes in this region have occurred along the northern margin of the E-W trending Precambrian Amazona rift (08/05/83, m_b=5.5, d=45 km, P: 329/07 T: 184/82 and 12/14/63, m_b=5.1, d=23 km, P: 14/10 T: 264/62) . These thrust events indicate N-S compression, a 90° local stress rotation relative to the regional E-W compression observed throughout the South American plate and strongly suggest a causal relationship. Gravity data indicate an enormous (about 100 km wide) lower crustal dense rift pillow beneath the Amazonas rift. Finite element modeling with Randy Richardson of Univ. of Arizona (Zoback and Richardson, in prep.) indicates that this rift pillow is capable of generating a compressive stress field in the crust of 80-200 MPa, with the maximum stress oriented perpendicular to the axis of the rift. This local compressive stress must be greater than the regional horizontal stress differences to cause the observed 90° rotation. A similar rift pillow effect may be associated with other ancient intraplate rift zones.

3. The NW- to N-trending Walker Lane Zone (WLZ) is located along the western boundary of the northern Basin and Range province and the Sierra Nevada. This zone is distinguished from the surrounding Basin and Range province on the basis of irregular topography and evidence for both strike-slip and normal Holocene faulting events. Inversion of slip-vectors on active faults, historic fault offsets, and earthquake focal mechanisms indicate two distinct Quaternary stress regimes within the WLZ both of which are characterized by a consistent WNW σ_3 axis: a normal faulting regime with a mean σ_3 axis of N100°E and an R value ($R=(\sigma_2-\sigma_1)/(\sigma_3-\sigma_1)$) of 0.65, and a younger strike-slip faulting regime with a mean σ_3 axis of N115°E and an R value of 0.19 (R=0 indicates a stress regime transitional between strike-slip and normal faulting) which is compatible with historic fault offsets and earthquake focal mechanisms. Both the Quaternary extensional and strike-slip stress regimes reactivated inherited Mesozoic and Cenozoic structures and also produced new faults. The present-day strike-slip stress regime has produced strike-slip, normal oblique-slip and normal dip-slip historic faulting.

Previous workers have explained the complex interaction of active strike-slip, oblique, and normal faulting in the WLZ as a simple consequence of a single stress state with a consistent WNW σ_3 axis and transitional between strike-slip and normal faulting (R ~ 0 in both regimes) with minor local fluctuations. New slip data in Plio-Quaternary deposits together with cross-cutting dip slip and strike-slip striae on fault surfaces in Pleistocene volcanic rocks support previous results from Owens Valley [Zoback, 1989] that indicate a distinct change from

extensional tectonics to strike-slip tectonics with a roughly constant WNW $\sigma 3$ axis which may have occured in Late Pleistocene time. The change from a normal faulting to a strike-slip faulting stress regime can be interpreted in terms of a temporal and/or lateral variation in the magnitude of the maximum horizontal stress ($\sim\sigma_{NNE}$). The location of the WLZ between the deep-seated regional extension of the Basin and Range and the right-lateral strike-slip regional tectonics of the San Andreas fault zone is probably responsible for the complex interaction of tectonic regimes in this transition zone. Geologic control on the timing of the change is too poor to determine if there has been a single recent absolute change in stress magnitude or if there is an alternating or cyclic variation.

4. For the past 6 years the project chief, Mary Lou Zoback, has headed a global program to compile and interpret intraplate tectonic stress data, the World Stress Map Project, as part of the International Lithosphere Program. This collaborative effort involves over 40+ scientists in over 30 countries, and has resulted in over 6500 reliable determinations of tectonic stress orientations and relative stress magnitudes globally. Efforts in the past year and a half have largely been focused on producing a special issue of JGR on the World Stress Map project (published in July 1992) and the accompanying release of the entire dataset on floppy diskettes through the NGDC (National Geophysical Data Center, NOAA). The special issue of JGR includes 20 papers (2 of which I am first author of and are listed below) and a large size color plate of maximum horizontal stress orientations on a base of average global topography. Digital preparation of the color separates for the plate as well as continued monitoring of the compilation of the diverse types of information that are utilized as tectonic stress indicators took up much of my time and fortunately this compilation effort is largely now complete.

REPORTS

papers:

Burchfiel, C. B., Lipman, P. W., and Zoback, M. L., 1992, Introduction, *in* Burchfiel, B. C., Lipman, P. W., Zoback, M. L., eds., Cordilleran Orogen: Conterminous U. S., Boulder, CO, Geological Society of America, Geology of North America, v. G-3, p. 1-9.

Zoback, M. L., 1992, First- and second-order patterns of stress in the lithosphere: the World Stress Map project: Journal of Geophysical Research, v. 97, p.11703-11728.

Zoback, M. L., 1992, Stress field constraints on intraplate seismicity in eastern North America: Journal of Geophysical Research, v. 97, p. 11761-11782.

Zoback, M. L., McKee, E. H., Blakely, R. J., and Thompson, G. A., 1992, Significance of middle Miocene tectonic and igneous features in the western United States--large scale rotations in northern Nevada?: in review, Geological Society of America Bulletin.

Bellier, O., and Zoback, M. L., 1992, Recent state of stress change in the Walker Lane zone, western Basin and Range province-U.S.A.: in review, Tectonics.

abstracts:

Zoback, M. L., Zoback, M. D., and K.-P. Bonjer, 1991, High pore pressure gradients-an explanation of diverse focal mechanisms within a small source region, EOS (Trans. American Geophysical Union), v. 72, p. 512.

Bellier, O., and Zoback, M. L., 1991, Implications of young strike-slip and normal slip on subparallel faults in the western Basin and Range province, EOS (Trans. American Geophysical Union), v. 72, p. 461.

Zoback, M. L., 1992, Using stress orientations to constrain tectonic stress magnitudes at depth, EOS (Trans. American Geophysical Union), v. 73, p. 298.

Zoback, M. L., and Zoback, M. D., 1992, Episodic release of high pore pressure, an explanation of rapid short-term rates of intraplate seismicity, EOS (Trans. American Geophysical Union), v. 73, p. 306.

REGIONAL AND NATIONAL SEISMIC HAZARD AND RISK

9950-01207

S.T. Algermissen, E.V. Leyendecker, D.M. Perkins, P.C. Thenhaus,
M.G. Hopper, S.L. Hanson, L.M. Highland, N.Dickman, P. Powers

Branch of Geologic Risk Assessment
U.S. Geological Survey
Denver Federal Center
M.S. 966, P.O. Box 25046
Denver, CO 80225

Investigations

1. The first stage in a project aimed at the development of a relatively simple method of approximating the response spectrum of ground motion at any point in the contiguous United States has been completed. The results have broad application to the seismic design provisions of building codes.

2. A complete probabilistic ground-motion hazard mapping system for Macintosh personal computer systems has been completed using USGS ground-motion hazard mapping software and commercial map-plotting applications to aid the dissemination of ground-motion hazard mapping technology and techniques.

3. Investigation of standard geologic site condition corrections for use in national building-code maps was done using a world-wide strong-motion data base. Project personnel participated in the NCEER Site Effects Workshop on selection and specification of standard site conditions for use in national building codes.

4. Investigations of peak acceleration data were completed for saturating magnitude scaling, distance-dependent magnitude scaling, magnitude-dependent distance scaling. Data was tested for consistency in magnitude and distance slices.

5. In conjunction with work conducted for DOE, the role of alternative probabilistic model parameters and methodologies on the wide variability in LLNL, EPRI, and USGS probabilistic ground motion results in the eastern United States were investigated. Historical intensity data was used to assess which results in this range might be more likely to be correct and what might be the source of the discrepancies.

6. The effect of various estimated recurrence rates for Pacific Northwest subduction zone earthquakes on probabilistic ground motion hazard values was investigated.

7. An investigation of the historical intensity distribution of the 1872 earthquake in the Pacific Northwest was completed.

8. An investigation and report was completed on earthquake hazards to the Seattle public schools.

9. A poster showing a color Landsat image of the New Madrid seismic zone region is being prepared for wide public distribution.

10. An earthquake preparedness guide for the central United states is in preparation as a public outreach publication.

11. A study on hypothetical earthquakes for the New Madrid seismic zone was updated and is in review.

Results

1. *Seismic spectral response maps*

For the contiguous United States, new probabilistic equal hazard spectral acceleration maps for periods of 0.3 and 1.0 sec have been developed and published. These maps are for periods of interest of 50 and 250 years, with a 10 percent chance of being exceeded (fig. 1). These maps may be used for the construction of approximate response spectra for the earthquake design provisions of buildings codes and for various other earthquake mitigation applications. Detailed investigations of the spectral responses at 10 major United States cities indicate that response spectra developed using only two spectral ordinates serves as a very useful approximation to spectra derived from more comprehensive (and lengthy) study of spectral shapes (fig. 2). The results have been published in the Proceedings of the 10th World Conference on Earthquake Engineering.

2. *Seismic hazard computation on a Macintosh personal computer*

The USGS computer program used in the estimation of probabilistic ground-motion hazard, SEISRISK III, has previously been adapted for use on IBM or IBM-compatible personal computers (Arnold, 1990). We have recently adapted SEISRISK III to a Macintosh II computer system and have further developed utility programs for seismicity catalog manipulation, seismicity parameter estimation and hazard map plotting in order to create a complete hazard mapping system for a Macintosh personal computer (fig. 3). The system has been installed at the Geological Research and Development Center in Bandung, Indonesia, and at the Philippine Institute of Volcanology and Seismology in Manila with the cooperation of the Agency for International Development, Office of Foreign Disaster Assistance under the auspices of The International Decade for Natural Hazard Reduction. The compact and relatively inexpensive system allows, for the first time, complex probabilistic ground-motion hazard calculations and mapping to be performed in a "desk-top" environment.

3. *Magnitude and site conditions*

Found magnitude-dependent site condition effects for hard rock, shallow soils, and deep, soft soils. Other site conditions are not discriminable from one another.

4. *Magnitude saturation*

Found magnitude saturation for distance ranges less than 30 km. Found magnitude-dependent distance attenuation. Testing several typical functional forms found in the literature for regression of ground motion, found none of them well represent the behavior actually in data smoothed in distance slices. Was able to extract data in which it was possible to have high confidence as well as to suggest replacement data levels upon the application of a distance-dependent magnitude saturation paradigm. Was able to confirm observed and paradigm data properties through simulation of a patchy fault model.

5. *Earthquake catalog discrepancies*

Found that major source of discrepancy in LLNL and EPRI hazard assessment at low hazard values to be due to EPRI use of low background maximum magnitudes, and choice of attenuation functions. Also there was some contribution due to lack of constraint in consultants estimates of future Richter-Law *a*- and *b*-values. Discrepancy in LLNL and USGS estimates was found to be due to assignment of moment magnitude values based either on historical intensity or M_S together with employment of random-vibration model attenuation function for moment magnitude.

Intensity data suggests either one-unit increase in site effect for worst site conditions in eastern U.S., compared to western U.S. or that moment magnitude attenuation functions for the eastern U.S. do not use a high enough stress drop.

6. *Ground motion from Pacific Northwest subduction zone earthquakes*

Found that assuming the Pacific Northwest subduction zone earthquakes are limited to magnitude 8.5 events with a recurrence of once every 500 years produces little effect on 500-yr return period ground motion maps, because of the spatial spreading of the effects of these earthquakes over the possible locations over the range of expected subduction occurences. On the other hand, assuming a magnitude 9.2 event produces considerable increase in hazard along the coastal portions of the Pacific northwest, from northern California to northern Washington.

7. *Reevaluation of 1872 earthquake in the Pacific Northwest*

Reevaluation of intensity data for the 1872 earthquake indicated that the maximum Modified Mercalli intensity (MMI_O) was IX and the epicenter was near Lake Chelan, in central Washington State. Previous analyses by five different researchers had determined MMI_O's of VII to X and epicenter locations ranging from central Washington to British Columbia. Comparison of our interpreted isoseismal map to the works of the other researchers on the basis of intensity assignments and intensity attenuation curves revealed that, although the maps are different, the intensity attenuation is similar within the limits of the available data for the 1872 earthquake. Consideration of the five interpretations of the intensity data together with our own review of the data leads us to believe that the epicenter of the 1872 main shock was located in the vicinity of Lake Chelan within a 100-km radius of the point, 47.8° N., 120.2° W. This area includes Lake Chelan and the town of Wenatchee.

8. *Earthquakes and the Seattle public schools*

A report on exposure to earthquake hazards for the Seattle public schools is in review. It includes four hazard maps showing surficial geology, areas of artificial fill, recent seismicity (fig. 4), and hypothetical seismicity patterns for two postulated magnitude 7.5 earthquakes. The report also contains a review of earthquake mechanisms in the Pacific Northwest, historical seismicity, and construction data for Seattle public school buildings.

9. *New Madrid seismic zone poster*

A poster showing a Landsat image of the New Madrid seismic zone in the central United States is nearing completion. It will be published as the cover image for the journal EOS along with an accompanying article.

10. *Earthquake preparedness guide for central U.S.*

An earthquake preparedness guide for the central United States is being written, and will be published as an outreach product next year.

11. *Hypothetical earthquakes for the New Madrid seismic zone*

Sections of a report on hypothetical earthquakes in the New Madrid seismic zone have been completed and are in review for a USGS Bulletin. The sections include detailed studies of the historic earthquake effects at seven representative cities in the area, as well as projections for the distribution of intensities in the cities and in the region for possible future large earthquakes.

Reports

Algermissen, S.T., and Leyendecker, E.V., A technique for uniform hazard spectra estimation in the U.S.: Madrid, Spain, Proceedings, Tenth World Conference on Earthquake Engineering, v. 1, July 19–25, 1992, p. 391–397.

Algermissen, S.T. and Hopper, M.G., 1993, Maps of hypothetical intensities for the region, *in* Hopper, M.G., and Obermeier, S.F., eds., Estimation of earthquake effects in the New Madrid seismic zone: U.S.G.S. Bulletin, in review, 15 ms p.

Algermissen, S.T., and Thenhaus, P.C., A worldwide earthquake risk management program—A progress report: [abs. invited] EOS, Transactions of the American Geophysical Union, 73 (14), Spring Meeting Supplement, p. 205.

Highland, L.M., and Michael, J.A., 1993, Exposure to hazards from earthquakes for Seattle public schools: U.S.G.S. MF map, in review.

Highland, L.M., and Michael, J.A., 1993, New Madrid seismic zone poster (tentative title): U.S.G.S. poster, in review.

Hopper, M.G., 1993, Introduction, *in* Hopper, M.G., and Obermeier, S.F., eds., Estimation of earthquake effects in the New Madrid seismic zone: U.S.G.S. Bulletin, in review, 13 ms p.

Hopper, M.G., 1993, Intensity attenuation patterns, *in* Hopper, M.G., and Obermeier, S.F., eds., Estimation of earthquake effects in the New Madrid seismic zone: U.S.G.S. Bulletin, in review, 12 ms p.

Hopper, M.G., 1993, Historical seismicity of the Mississippi Valley and its effects on seven cities *in* Hopper, M.G., and Obermeier, S.F., eds., Estimation of earthquake effects in the New Madrid seismic zone: U.S.G.S. Bulletin, in review, 55 ms p.

Hopper, M.G., Algermissen, S.T., Perkins, D.M., Brockman, S.R., Arnold, E.P., 1993, The December 14, 1872 earthquake in the Pacific Northwest: in press, 40 ms p.

Hopper, M.G., and Obermeier, S.F., 1993, Glossary, *in* Hopper, M.G., and Obermeier, S.F., eds., Estimation of earthquake effects in the New Madrid seismic zone: U.S.G.S. Bulletin, in review, 5 ms p.

Rogers, A.M., Perkins, D.M., and Campbell, K.W., 1992, Shortcomings of the world-wide peak acceleration data set that may affect strong-motion regression analyses: Abstract to the Seismological Society of America meeting, Santa Fe, N.Mex., April 14–16. p. 1.

Thenhaus, P.C., and Algermissen, S.T., 1992, Ground-motion hazard implications of alternative earthquake recurrence models in northern California [abs. invited]: EOS, Transactions of the American Geophysical Union, 73 (14), Spring Meeting Supplement, p. 206.

U.S. Geological Survey, 1992, Review of earthquake hazard assessments of plant sites at Paducah, Kentucky, and Portsmouth, Ohio, Administrative report to DOE. Four of the nine chapters present sensitivity studies and investigations of differences in probabilistic ground motion hazard estimates by EPRI, Livermore Labs and USGS methodologies.

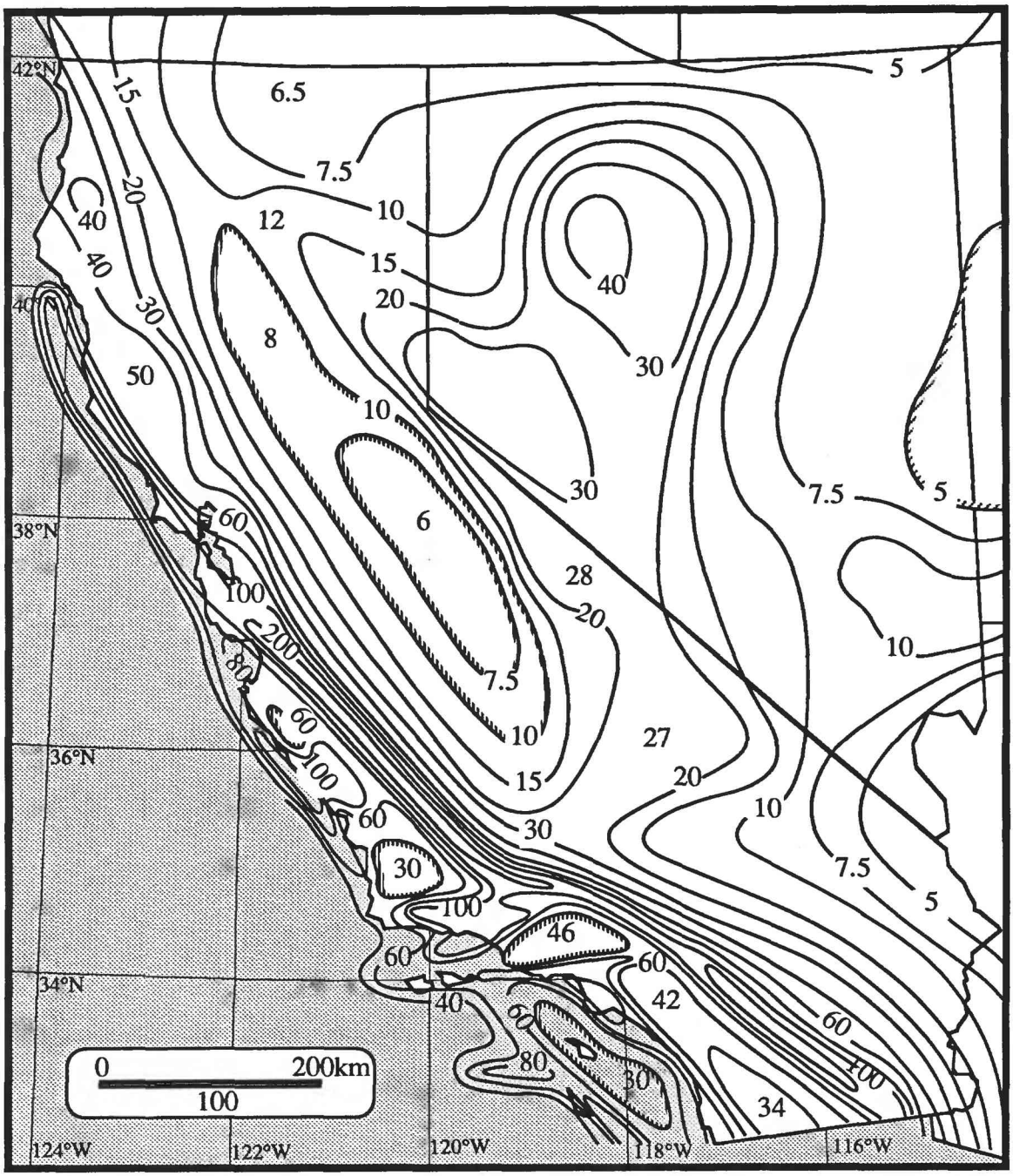

FIGURE 1. Ground motion map of California and Nevada showing spectral response acceleration (in percent) for 1.0 sec period, 5% damping, and 10% probability of exceedance in 50 years. This map is an example of the series of spectral response maps completed and published.

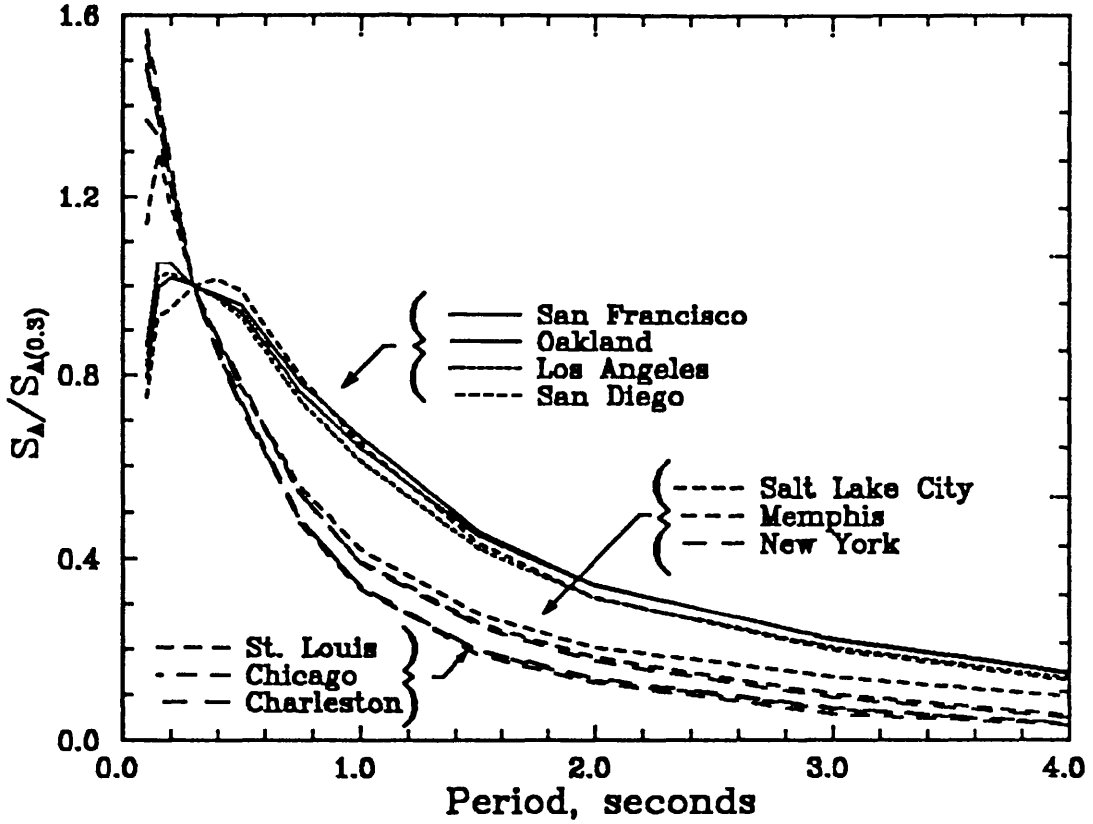

FIGURE 2. Normalized response spectra for ten cities for 5% damping for an exposure time of 50 years and a 90% probability of nonexceedance.

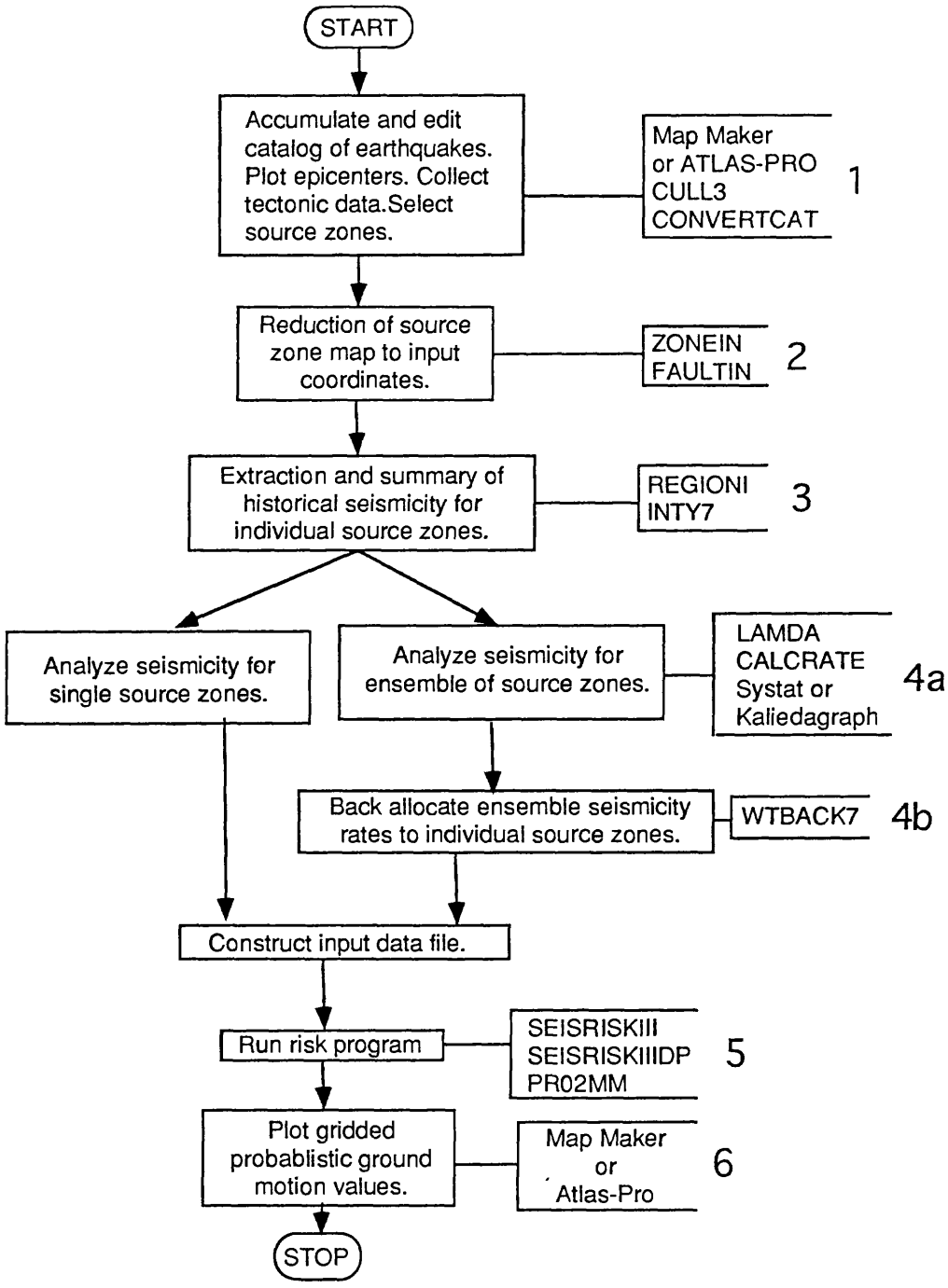

FIGURE 3. Application programs for analyzing probabilistic ground-motion hazard from earthquakes.

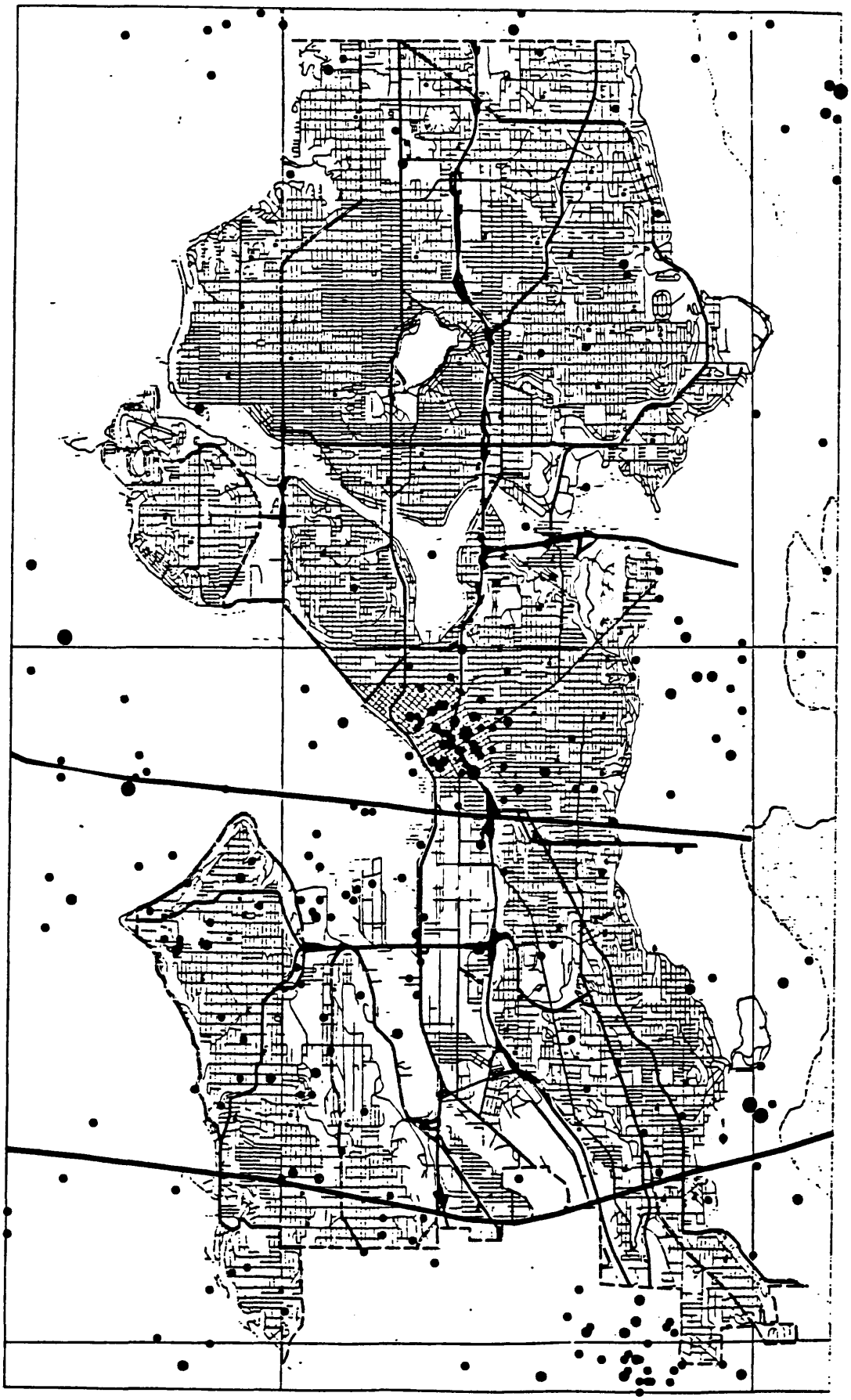

FIGURE 4. Map of the city of Seattle showing recent seismicity (1974–1990, magnitudes ≤3.0). Lines represent gravity anomalies indicating possible earthquake-generating structures at depth.

WORLD WIDE EARTHQUAKE RISK MANAGEMENT

9960-53500

S.T. Algermissen, E.V. Leyendecker,
P.C. Thenhaus, and S.L. Hanson

Branch of Geologic Risk Assessment
U.S. Geological Survey
Denver Federal Center
M.S. 966, P.O. Box 25046
Denver, CO 80225

Investigations

1. Pilot studies of seismic hazard and risk in Sulawesi Province, Indonesia were undertaken. A program of training and transfer of technology was conducted with the Geological Research and Development Centre, Bandung, Indonesia.

2. Investigations on the regional ground-motion hazard of the Philippines were initiated and technology transfer and training of counterpart personnel were begun at the Philippine Institute of Volcanology and Seismology (PHIVOLCS).

3. A post-earthquake damage investigations were conducted following the 12 October 1992, Dahshûr, Egypt, earthquake (m_b 5.9).

4. Regional assessments of ground motion in Chile, including site response, have been completed.

5. Pilot studies of seismic hazard and risk in Morocco have been started.

Results

1. *Seismic hazards and risk in Indonesia.*

Earthquake ground motions in North Sulawesi on soft soil that have a 90 percent probability of not being exceeded in 50 years are estimated to be 0.46 g (46 percent of the acceleration of gravity) at Palu, 0.31 g at Gorontalo, and 0.27 g at Manado (Fig. 1a, b). Estimated ground motions for rock conditions for the same probability level and exposure time are 56 percent of those for soft soil. The hazard estimates are obtained from seismic sources that model the earthquake potential to a depth of 100 km beneath northern and central Sulawesi and include the Palu fault zone of western Sulawesi, the North Sulawesi subduction zone, and the southern most segment of the Sangihe subduction zone beneath the Molucca Sea. An attenuation relation based on Japanese strong-motion data and considered appropriate for subduction environments of the western Pacific was used in determination of expected ground motions.

Field investigations following the 18 April 1990 North Sulawesi earthquake (M_S 7.3) established the Modified Mercalli intensity (*MMI*) distribution throughout Kodya Gorontalo (the Mayorial province of Gorontalo). The total number of masonry houses (permanent and semi-permanent dwellings) within the *MMI* V isoseismal was approximated from housing counts obtained from a sampling of 18 villages. From the post-earthquake damage investigation and from comparisons to masonry construction in the United States, a vulnerability curve was constructed for masonry housing in Gorontalo. Assuming an average value for a house of $1,053, total economic loss to masonry housing from the 18 April 1990 earthquake is estimated at $1,198,578,

or a 9.6 percent economic loss to the masonry dwelling stock of Gorontalo. Simulation of the earthquake history for the past 31 years within 300 km of Gorontalo indicates an average annual loss to masonry housing of $358,609, or $30 on a per house basis. Catastrophe potential (a worst-case loss) for masonry housing in Gorontalo that has a 90 percent probability of not being exceeded in 250 years is estimated to be $3,083,525, or an economic loss equivalent to 25 percent of the total value of the masonry dwelling stock of Gorontalo. These results were presented at the second US-ASIA Conference on Engineering for Mitigating Natural Hazards Damage, June 22-26, Yogyakarta, Indonesia, and a comprehensive jounal paper is in press.

2. *Cooperative study in the Philippines*

A cooperative seismic hazard and risk investigation of the Philippines with the Philippine Institute of Volcanology and Seismology (PHIVOLCS) was begun in May, 1992. A Macintosh computer system, transferred as part of the program, was installed at PHIVOLCS and personnel trained on its use and the use of 17 application programs for analyzing probabilistic ground-motion hazard from earthquakes. Compilation and analysis of seimological, geologic and tectonic databases for the Philippine region is in progress.

3. *1992 Dahshûr, Egypt, earthquake*

Figure 2 is a preliminary map of the Modified Mercalli intensity (*MMI*) distribution of the Dahshûr, Egypt, earthquake of 12 October 1992 (m_b 5.9; NEIS, PDE 11/5/92) based on a four-day reconnaissance tour of damaged areas. Areas of inspection were along Highway 2 on the west side of Nile River valley as far south as Girza; on the east, along Highway 54 as far south as Atfih; west along Highway 22 between Cairo and (Lake) Birket Qãrun; and in Cairo. The southern extent of the isoseismals is based on interviews with staff members of the Geological Survey of Egypt knowledgeable of earthquake effects in the villages of Tâmiya, El Rôda and El Faiyûm. The smoothed contours of the isoseismal map represent the highest predominant levels of *MMI* with regard to building damage and, therefore, do not preclude isolated higher intensities and common lower intensities than the generalized level of intensity shown on the map. Intensity assessments were not based on geologic effects of the earthquake because of the known wide variation in the threshold shaking required to produce these effects and their strong dependence on local geotechnical properties of soils, water content, and degree of slope. The western and eastern excursions of the isoseismals are queried to reflect uncertainty in their locations in desert regions characterized by very low population concentrations and little development.

In general, *MMI* VII effects were widespread in the villages of the Nile valley to approximately 80 km south of Cairo, which includes most of the populated area of the Giza governorship (Fig. 1). One- and two-story adobe dwellings performed poorly and were the primary cause of the more than 500 earthquake fatalities. Fallen adobe walls and collapsed roofs that had been supported by cross timbers were common. The considerable damage to adobe dwellings warranted *MMI* VII assessments at many villages in the Nile valley. Brick-firing kilns with masonry smoke stacks approximately 20 m to 30 m tall are scattered throughout the Nile valley but none was known to be toppled in the earthquake. Only one stack was observed to be cracked; it was near the village of Girza. This observation generally limits a maximum *MMI* assessment to some level lower than VIII for most of the affected area of the Nile valley. However, maximum *MMI* VIII effects were observed in the village of Manshiyat Fâdil on the west side of the Nile River, approximately 20 km south of the National Earthquake Information Service epicenter at 29.89° N., 31.22° E. (PDE, 11/5/1992). The principal bases for this assessment were the fall of unreinforced masonry walls of dwellings and the more widespread damage and collapse in adobe dwellings than in nearby villages. Newer one- and two-story reinforced concrete-framed dwellings with masonry infill walls performed well with no damage or only hairline cracking at the contact of the concrete frame with the infill masonry wall. Two older dwellings of apparently similar construction were, however, severely cracked. Coincident with this intensity assessment, sandblows of a limited extent were observed in the cultivated fields

neighboring Highway 2 just south of Manshiyat Fâdil. The roadway itself reportedly settled 1.5 m along a distance of perhaps 100 m but was repaired and in use at the time of the inspection.

The northeast-trending elongation of the isoseismals in Figure 2 is due to the north-trending belt of population and development along the Nile valley and the very sparse settlement of neighboring desert regions. The isoseismal shapes should not, therefore, be used to infer properties of a fault rupture, such as concentration of damage along strike of a hypothetical fault rupture or focusing of ground motion at the terminal ends of rupture.

4. Probabilistic maximum ground accelerations maps (for average ground) have been prepared for a 50-year period of interest, 10 percent chance of exceedance, for all of Chile. Fifty-year maps have been prepared both with (fig. 3) and without attenuation variability. Probabilistic maximum Modified Mercalli intensity maps have been prepared for central Chile and site response factors (in terms of intensity) have been developed for five classifications of surficial geological materials. These site corrections have been incorporated into the 50-year probabilistic intensity map (fig. 4). Probabilistic earthquake dwelling loss (risk) studies are currently under way for central Chile.

Acceleration response spectra (5% damping) have been developed for Santiago and Valparaíso, Chile (fig. 5).

5. Geological, seismological, and engineering data for pilot earthquake hazard and risk investigation of Morocco have been collected and are being reviewed.

Reports

Algermissen, S.T., and Thenhaus, P.C., A worldwide earthquake risk management program—A progress report: [abs. invited] EOS, Transactions of the American Geophysical Union, 73 (14), Spring Meeting Supplement, p. 205.

Hanson, S. L., Thenhaus, P.C., Chapman-Wilbert, M., and Perkins, D.M., 1992, Analyst's manual for USGS seismic hazard programs adapted to the Macintosh computer system: U.S.G.S. Open-File Report 92-529, 64 p., 1 computer diskette.

Joyner, William B., Boore, David M., Algermissen, S.T., 1992, Quantifying the variability of ground-motion estimates for seismic hazard calculations: Submitted to the Bulletin of the Seismological Society of America, 5 ms pages.

Thenhaus, P.C., 1992, Intensity distribution of the 12 October 1992 Dahshur, Egypt, earthquake: Earthquake Engineering Research Institute Newsletter, December issue, in press

Thenhaus, P.C., 1993, Overview of Nazca plate subduction and central Andean tectonics: Geologica Revista, in press.

Thenhaus, P.C., Effendi, I., and Kertapati, E.K., 1992, Probabilistic seismic hazard estimates in North Sulawesi Province, Indonesia, *in*, Chiu, A.L., and Danuatmodjo, A.S., eds., Proceedings of the Second U.S.-Asia Conference on Engineering for Mitigating Natural Hazards Damage: June 22-26, Yogyakarta, Indonesia, p. E15-1 to E15-8.

Thenhaus, P.C., Hanson, S.L., Effendi, I., Kertapati, E.K., and Algermissen, 1993, Pilot studies of seismic hazard and risk in North Sulawesi Province, Indonesia: Earthquake Spectra, v. 9, no. 1, in press.

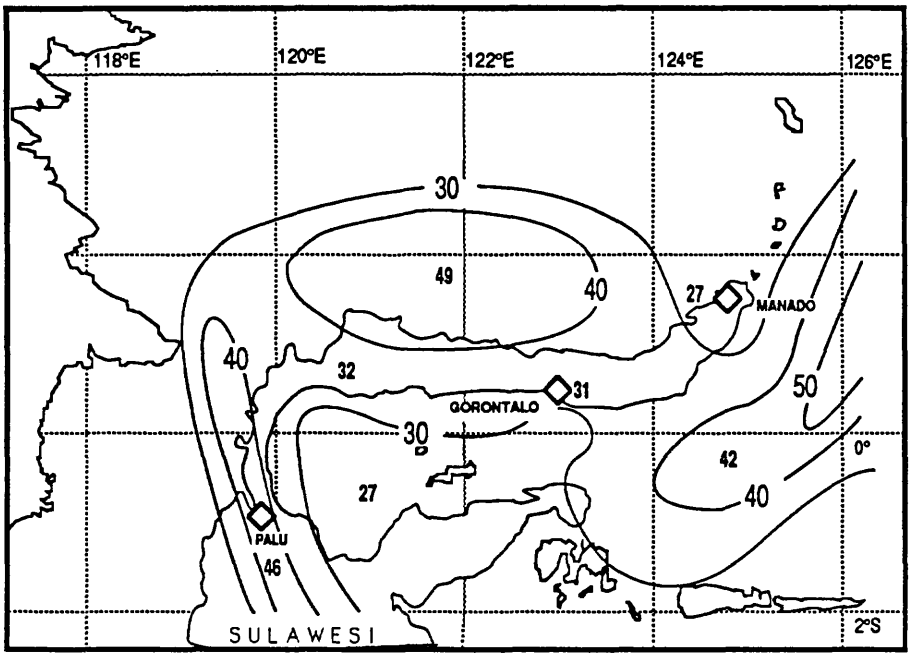

FIGURE 1a. Peak horizontal acceleration in soft-soil having a 90% probability of not being exceeded in 50 years. Contours are in percent of gravity (%g).

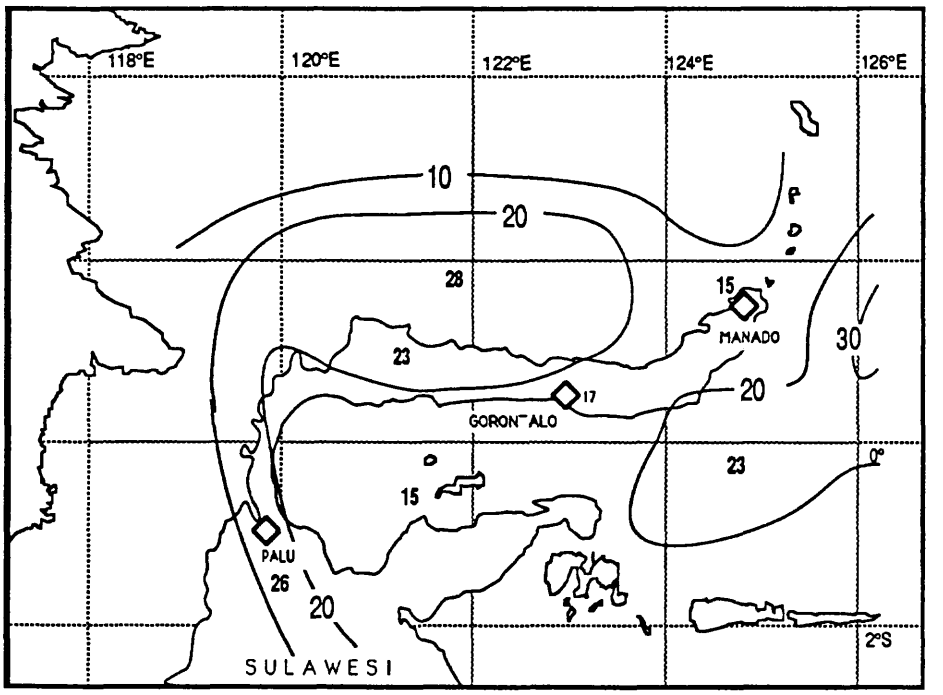

FIGURE 1b. Peak horizontal acceleration in rock having a 90% probability of not being exceeded in 50 years. Contours are of gravity (%g).

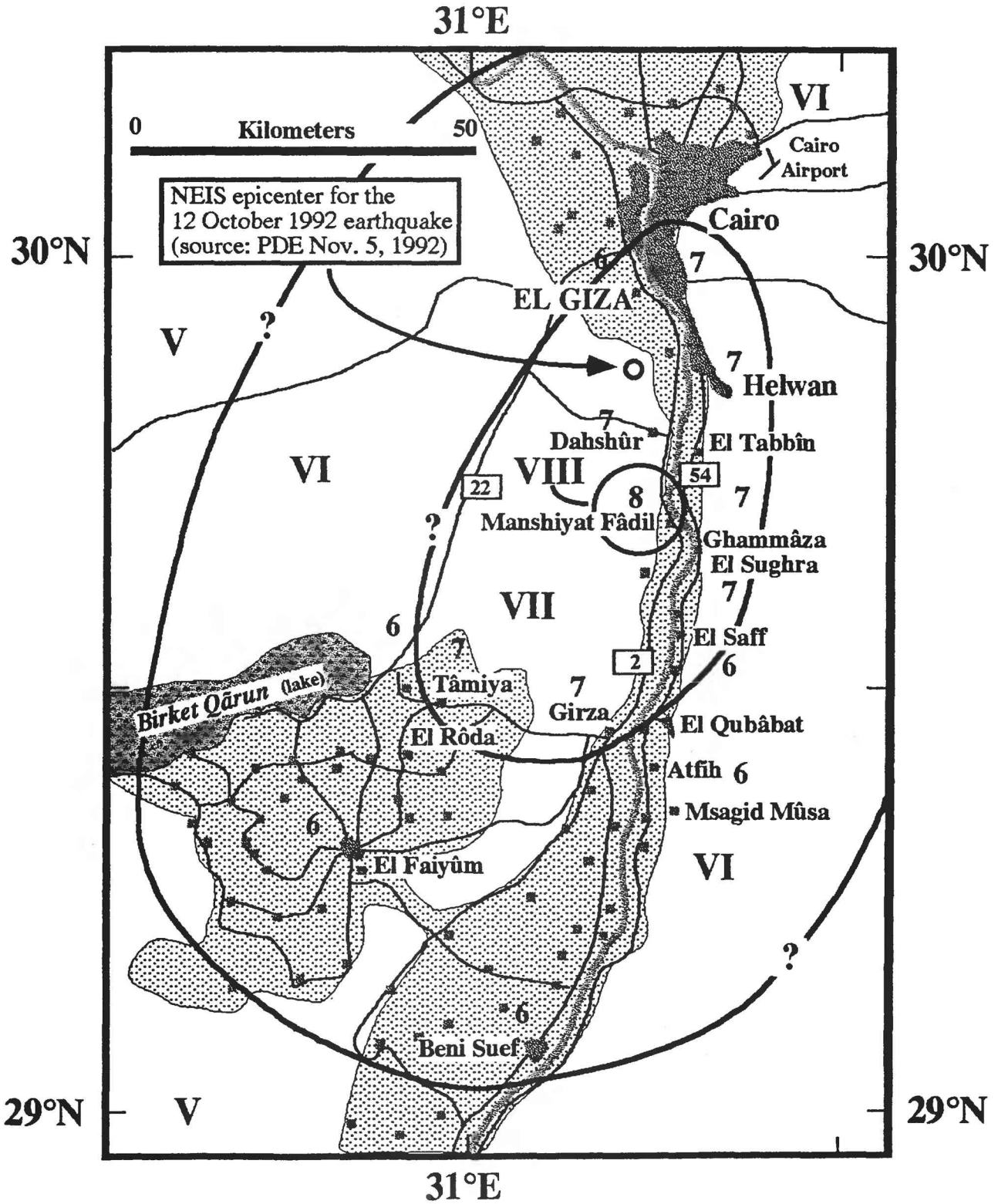

FIGURE 2. Modified Mercalli intensity (*MMI*) distribution of the Dahshûr, Egypt, earthquake of 12 October 1992.

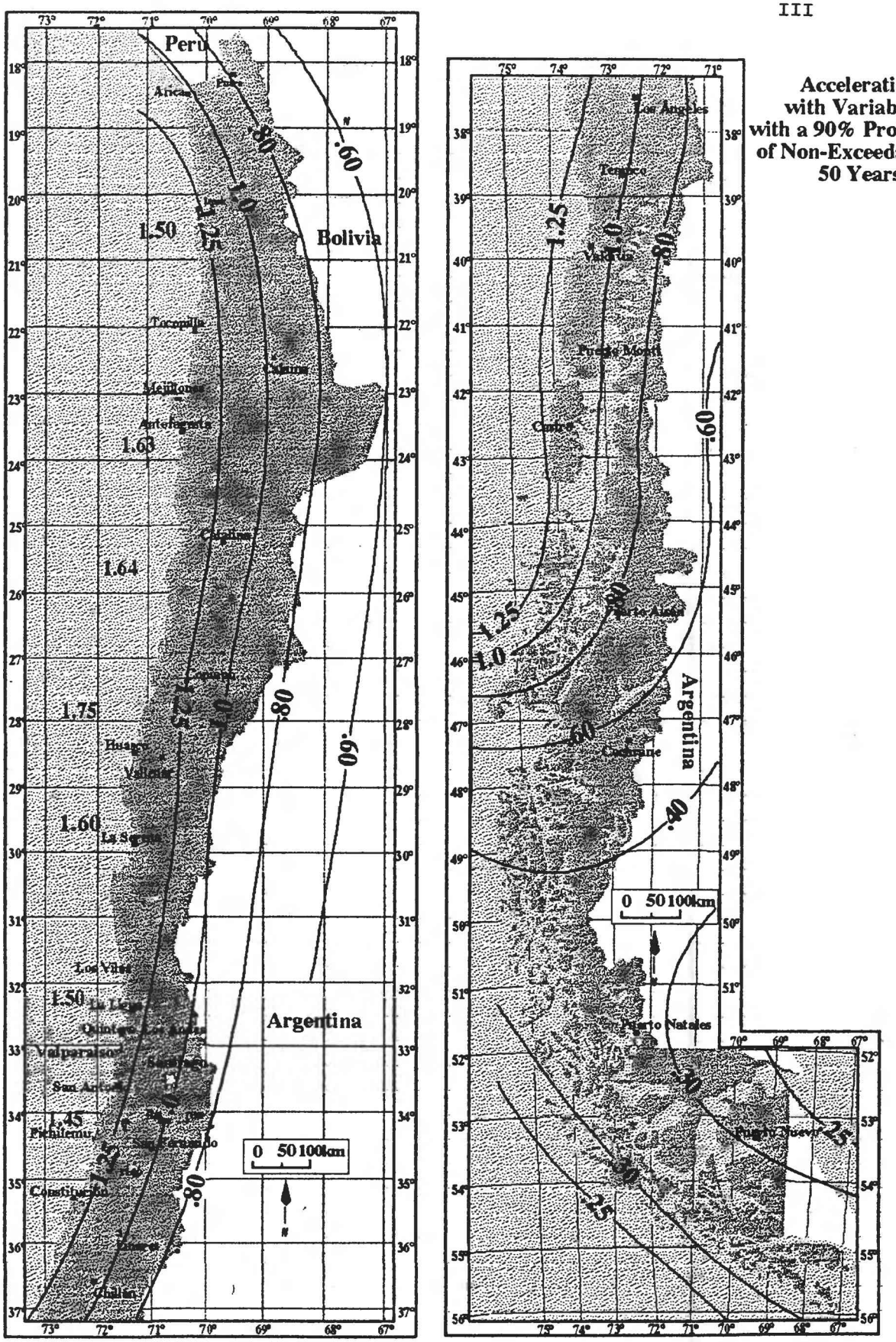

FIGURE 3. Probabilistic ground motion acceleration map of Chile for a 50-year time period of interest. The ground motions mapped have only an estimated 10% chance of being exceeded in 50 years. Maps of this type are widely used as design maps in the earthquake resistant design provisions of building codes.

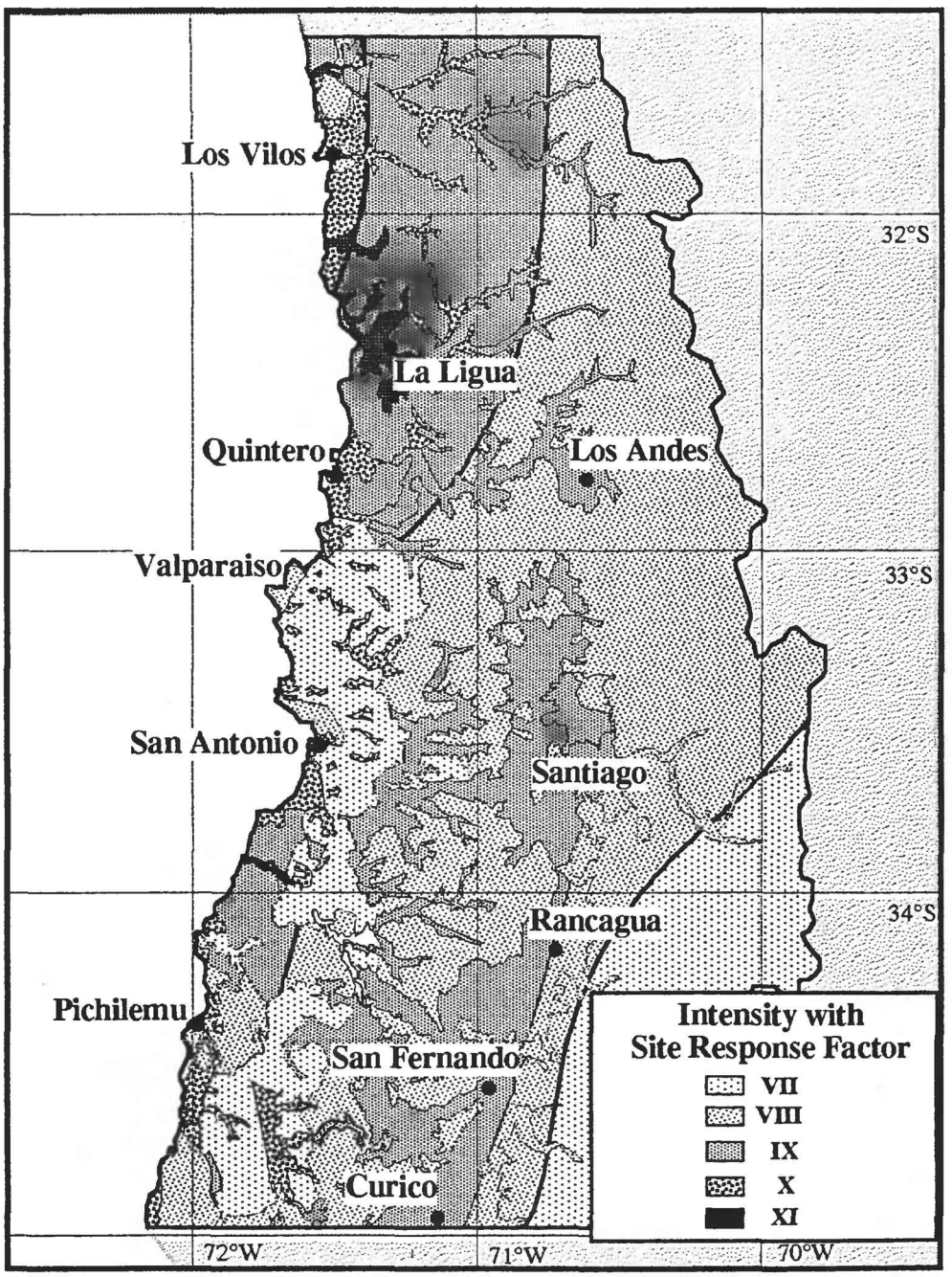

FIGURE 4. Probabilistic ground motion intensity map of Chile for a 50-year time period of interest. This map includes the effect of near surface materials. This kind of map is valuable in disaster preparedness, mitigation, land use planning and earthquake risk (loss) studies because it represents an estimate of the maximum damage (and consequently loss) that is expected to occur in the period of time considered in the mapping.

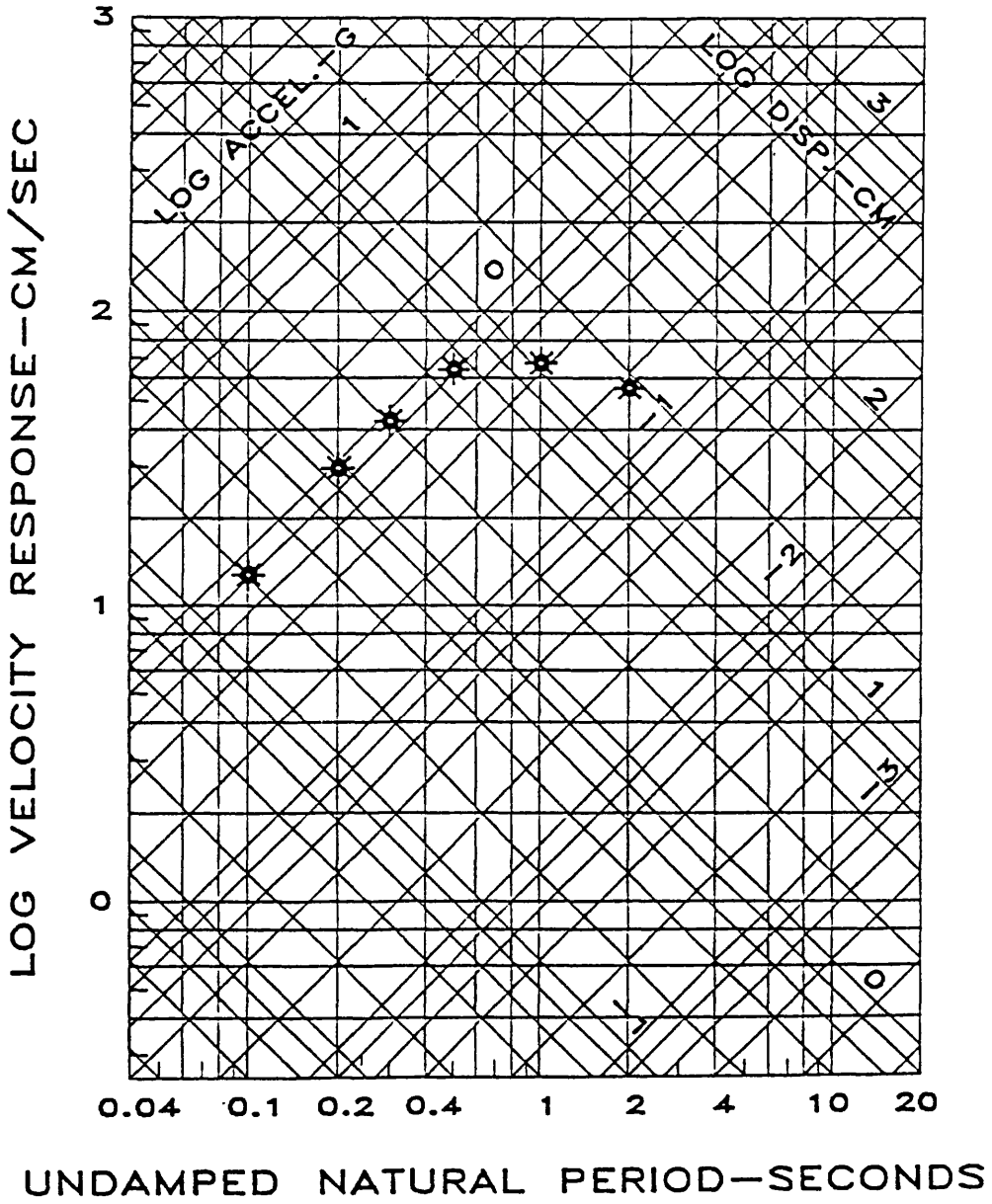

FIGURE 5. Probabilistic (equal hazard) maximum spectral response in 50 years (10 percent chance of exceedance) for Santiago, Chile.

Physics of the Earthquake Process

9910-01915

D. J. Andrews
Branch of Engineering Seismology and Geology
U.S. Geological Survey
345 Middlefield Road, MS 977
Menlo Park, California 94025
(415) 329-5606

INVESTIGATIONS

1. The junction of the Hayward and Calaveras faults
2. Dynamic shear rupture in a compacting and dilating fault zone at high fluid pressure

RESULTS

1.

I spoke at the Second Conference on Earthquake Hazards in the Eastern San Francisco Bay Area in March 1992 on the Mission fault system linking the Hayward and Calaveras faults.

2.

Blanpied et al. (Nature, vol. 358, p. 574, 1992) found in an experiment with a sawcut "fault" containing a layer of saturated "gouge" at hydrothermal conditions that a pressure seal forms in the country rock, that shear strain induces compaction in the gouge, and that fluid pressure rises sufficiently to allow sliding at low apparent friction. They suggest that shear-induced compaction may be an instability mechanism for earthquakes.

I have incorporated a poro-elastic-plastic constitutive relation into a dynamic finite difference program in two-dimensional plane strain. When shear stress reaches a frictional yield condition, plastic shear strain is prescribed to be accompanied by plastic volumetric strain, which is initially compaction. Fluid pressure increases in compaction. The resulting decrease in effective pressure causes shear behavior to be strain-weakening. Mode 1 and mode 2 deformation are coupled. A region of elevated fluid pressure (analogous to a Griffith flaw) will propagate dynamically if its aspect ratio is larger than a critical value. If the initial rate of compaction is as large as the rate of shearing, then the ratio of length to thickness of the critical region may be as small as about 10. If the thickness is limited by the fault zone thickness, then the shear behavior is slip-weakening, and the critical crack length is 10 or more times the fault zone thickness. Calculated dynamic motion is similar to that in a slip-weakening model.

As shearing continues after the initial compaction, one may reasonably hypothesize a gradual dilatation due to geometrical mismatch of the sliding surfaces. The decrease in fluid pressure causes an increase in frictional shearing stress. Slip stops at any given point in model calculations when dilatation causes shear traction to rise to its initial value. As the rupture propagates farther, the slip velocity pulse approaches a constant shape with a constant duration, shorter than for a crack solution.

REPORTS

D. J. Andrews, D. H. Oppenheimer, and J. J. Lienkaemper, 1992, The Mission link between the Hayward and Calaveras faults: submitted to Journal of Geophysical Research.

D. J. Andrews, D. H. Oppenheimer, and J. J. Lienkaemper, 1992, The Mission link between the Hayward and Calaveras faults: Proceedings of Second East Bay conference on earthquake Hazards, to appear.

D. J. Andrews, 1992, Dynamic shear rupture in a compacting and dilating fault zone at high fluid pressure (abstract): EOS Transactions AGU, vol. 73, p. 387.

A Dynamic Geographic Information System (GIS) To Forecast Economic Effects of Earthquakes

9112-10300

R.L. Bernknopf and P.L. Gori
Office of the Chief Geologist and
Branch of Geologic Risk Assessment
U.S. Geological Survey
Reston, VA 22092
703-648-6726

Investigations

1) Develop probability fomulation of damage function with earthquake faulting, expected ground shaking, and liquefaction using GIS information at 1:24,000 scale derived from ongoing mapping activities in Santa Clara County, CA and demogrphic and cultural data collection activities.

2) Develop a map portfolio that illustrates hazards zones with means and variances to represent levels of hazard and statistically test the economic impact of hazards-related regulations as proposed in the California Division of Mines and Geology (CDMG) urban hazards mapping program.

3) Update hazards map portfolio information with earthquake induced slope failue data from the Loma Prieta earthquake.

4) Update hazards map portfolio information with earthquake-induced liquefaction data from the Loma Prieta earthquake.

Results

We arrived at a preliminary probability of earthquake-induced liquefaction in Monterey County,CA based on topographic data, geologic unit age, and a geologic attribute called percent sand in a surficial geologic unit.

We discussed how to use of the above types of probability maps with representatives of CDMG, Santa Clara County and the City of Palo Alto. Uses which interested these jurisdictions related to regulation and planning for future density of residential and commercial development.

GROUND MOTION PREDICTION FOR CRITICAL STRUCTURES

9910–01913

D. M. Boore
W. B. Joyner
Branch of Engineering Seismology and Geology
U. S. Geological Survey
345 Middlefield Road, MS 977
Menlo Park, California 94025
415/329-5616 or 415/329-5640

Investigations

1. Determine the values of κ and $\Delta\sigma$ in the stochastic model of ground motion by fitting the model to empirical ground motion relations.

2. Determine velocity and attenuation in boreholes at sites that recorded the 1989 Loma Prieta earthquake.

3. Develop procedures for the regression analysis of data.

4. Develop a database of ground motion data.

Results

1. A good overall fit of theoretical ground motions to observed response spectra for periods ranging from 0.1 to 2 secs and magnitude from 5.5 to 7.5 is obtained with values of $\Delta\sigma$ and κ close to 70 bars and 0.02 sec, respectively.

2. Velocities were obtained at a number of strong motion sites, and attenuation was measured using several techniques at Gilroy site 2, situated on alluvium. The average shear-wave attenuation over the upper 120 m at the site is given by $Q = 10$.

3. Rigorous procedures for the regression analysis of strong motion data was developed. By using proper weighting matrices, unbiased results can be obtained with either one- or two-stage procedures when applied to data whose distribution in magnitude and distance space is non-uniform.

4. The groundwork for a PC-based strong motion database was laid, with the development of auxiliary programs ('scripts') to aid in selecting and maintaining the data. A superset of earthquakes for which digital strong-motion data are available was created, and initial efforts were made to winnow out those earthquakes which will not provide data that meet our standards for inclusion in regression analyses.

Reports

Boore, D. M., W. B. Joyner, and L. Wennerberg (1992). Fitting the stochastic ω^{-2} source model to observed response spectra in western North America: Tradeoffs between $\Delta\sigma$ and κ, *Bull. Seism. Soc. Am.* **82**, 1956–1963.

Gibbs, J. F., T. E. Fumal, D. M. Boore, and W. B. Joyner (1992). Seismic velocities and geologic logs from borehole measurements at seven strong-motion stations that recorded the Loma Prieta earthquake, *U. S. Geol. Surv. Open-File Rept.* **92 – 287**, 139 pp.

Joyner, W. B. and D. M. Boore (1993). Method for regression analysis of strong-motion data, *Bull. Seism. Soc. Am.* (in press).

Boore, D. M. and W. B. Joyner (1993). Empirical prediction of strong ground motion, *Proceedings of Structures '93 Congress, Irvine, California*, (in press).

ANELASTIC WAVE PROPAGATION

9910-02689

ROGER D. BORCHERDT
BRANCH OF ENGINEERING SEISMOLOGY AND GEOLOGY
U.S. GEOLOGICAL SURVEY
345 MIDDLEFIELD ROAD, MS 977
MENLO PARK, CALIFORNIA 94025
415/329-5619

Investigations

- Development of methodologies for predictive mapping of potential hazards due to strong ground shaking using GIS technology.
- Development of site classification and empirically based site coefficients for building code consideration.
- Model soil response using general multi-layer and viscoelastic models for incident inhomogeneous wavefields *via* modern computer packages such as *Mathematica.*

Correlations between measured weak- and strong-motion amplifications, mean shear velocity to depths of 30 m, and geologic characteristics are used to classify geologic units for purposes of predictive mapping and deriving spectral amplification factors for design. Geologic maps in a GIS data base are used to prepare maps of *amplification capability*, intensity, *excedent opportunity*, and intensity *excedent potential.* A methodology for definition of spectral study zones for strong ground shaking in terms of a specified *critical level* for excedent potential has been developed. Such maps provide a rigorous basis for seismic zonation to economically mitigate future earthquake hazards. Site classification and empirical basis for site response factors F_a and F_u have been incorporated into recommendations of National Workshop on Site Response Estimation.

Reports

Borcherdt, R.D., and Glassmoyer, G., 1992, On the characteristics of local geology and their influence on ground motions generated by the Loma prieta earthquake in the San Francisco Bay region, California: Bulletin of the Seismological Society of America, v. 82, p. 603-641.

Borcherdt, R.D., 1992, Characterization of potential geographic variations in ground shaking for purposes of mapping ground failure potential: Proceedings, Association of Engineering Geology, Annual Meeting, Los Angeles, CA.

Borcherdt, R.D., 1992, Characterization and predictive GIS mapping of strong ground shaking for earthquake hazard reduction in urban areas: Proceedings, 3rd US/Japan Workshop on Urban Earthquake Hazard Reduction.

GENERAL EARTHQUAKE OBSERVATION SYSTEM (GEOS)

9910-03009

ROGER D. BORCHERDT
BRANCH OF ENGINEERING SEISMOLOGY AND GEOLOGY
U.S. GEOLOGICAL SURVEY
345 MIDDLEFIELD ROAD, MS 977
MENLO PARK, CALIFORNIA 94025
415/329-5619

Investigations

1. Complete acceptance testing for 100 portable, broad-band, high-resolution digital data acquisition systems.

2. Provide maintenance and field support for use of GEOS in a wide variety of active and passive seismic experiments.

3. Develop capabilities for field retrieval, processing, and archival of large volumes of GEOS data.

4. Conduct Eurasian Seismic Studies Program.

Results

1. Acceptance testing has been nearly completed by J. Sena and R. Aikens on 55 new GEOS II systems, which include design modifications for:

   a) Expanded data buffer (1 M/sample),
   b) Extended gain 84 db; 16 bit resolution),
   c) Tape controller for new 16 Mbyte tape cartridges,
   d) Software drivers for mag tape controller,
   e) Software for RS 232 for use in the satellite, radio, and telephone telemetry and data transfer to field computer, and
   f) Software for incorporating design modifications, teleseismic trigger, and field playback.

2. GEOS maintenance laboratory under direction of J. Sena together with field support of G. Sembera and C. Dietel has facilitated the execution of several experiments within the last year, including experiments at Parkfield, Anza, Armenia, Petrolia (CA), Landers (CA), San Bernardino (CA), South Carolina, and San Francisco (CA).

3. Playback and processing capabilities have been developed. Work is underway to improve speed.

14. A portable, high-resolution, dense three-dimensional array consisting of 12 sites with three-component, 1.0 Hz seismometers has been installed in and around a two-dimensional tunnel with its longest dimensions being 200 m at the Garni Observatory, Armenia. The sites are arranged in a nested tripartite configuration with expanding interstation spacings near 60, 120, 240, and 480 meters. Signals are routinely recorded at 200 sps on time-synchronized GEOS recorders with maximum signal resolution of 96 dB. Simultaneous recording *via* pc-based data acquisition system is coupled to GEOS recorders and permits synchronized digitization and simultaneous tape playback and analysis capability. Array continues to operate successfully with data playback conducted by G. Glassmoyer as tapes are received from Armenia. Array has yielded an especially large dataset including local regional, and more 134 teleseismic events up to distances of 139 degrees.

Reports

None.

(See other projects, *e.g.* Borcherdt *et al.*, 9910-02089, 9910-02689; McGarr; Fletcher; Boatwright; Mueller; and Liu for additional reports based on GEOS data sets.)

INTEGRATED GROUND RESPONSE, LIQUEFACTION AND STRUCTURAL RESPONSE STUDIES (Market Street Area, San Francisco, California)

9910-NEW

R.D. BORCHERDT, H.P.-LIU, E. ŞAFAK, AND R.E. WARRICK
BRANCH OF ENGINEERING SEISMOLOGY AND GEOLOGY
U.S. GEOLOGICAL SURVEY
345 MIDDLEFIELD ROAD, MS 977
MENLO PARK, CALIFORNIA 94025
415/329-5619

Investigations

Conduct long-term, integrated experiments to resolve major issues concerning behavior of "soft soil" deposits and response of modern high-use structures under damaging levels of ground motions. Major topics in earthquake engineering will be investigated, such as:

1. Quantification of nonlinear in-situ soil response at soft sites with and without anticipated liquefaction-induced failure, and

2. Improved quantification of soil-structure and structural response parameters under damaging levels of shaking.

These experiments are being executed with the installation of Borehole arrays at three sites in the Market Street area of San Francisco, upgrade of instrumentation in the Chevron building and planned upgrade of pertinent free-field sites.

Results

1. Drilling has been completed for installation of the borehole arrays at the three sites near Market Street, San Francisco, California. Instrumentation installation is nearing completion at Embarcadero-Market Street site and is planned for the other sites.

2. Chevron Building instrumentation upgrade has been completed.

CHARACTERISTICS AND SEISMIC RESPONSE OF THE DEEP OLD BAY CLAY DEPOSITS IN THE EAST SAN FRANCISCO BAY AREA

1434-92-G-2177

Jonathan D. Bray[1] and Jean-Lou A. Chameau[2]
[1]School of Civil Engineering, Purdue University
West Lafayette, IN 47907-1284
(317) 494-5032
[2]School of Civil Engineering, Georgia Institute of Technology
Atlanta, GA 30332-0355
(404) 894-2201

INVESTIGATIONS

Project Summary

The localized patterns of heavy damage during the 1989 Loma Prieta earthquake demonstrate the importance of understanding the seismic response of deep clay deposits. At deep stiff clay sites in the Oakland area, peak ground accelerations were amplified by a factor of 2 to 4, and spectral accelerations at some frequencies were amplified by a factor of 4 to 8. The amplified ground motions contributed to the collapse of the Cypress elevated highway and the damage of hundreds of buildings in the Oakland area. This research program will evaluate the seismic response of deep stiff clay sites, validate existing analytical procedures with respect to such deposits, and assess the seismic hazards resulting from future earthquake shaking in the heavily populated Oakland area.

Work Performed

Research was initiated on this project prior to the May 1, 1992 USGS start date by utilizing other internal and external funding to secure and test soil samples retrieved from other USGS and CALTRANS sponsored drilling programs and to compile soil data developed by related studies (e.g. Rogers and Figuers 1991, Dickenson and Seed 1992). Much of this preliminary work is documented in Bray et al. (1992).

Since the official project initiation date of May 1, 1992, the following work has been performed:

- Soil borings were completed at the Oakland 2-story office building site (SMIP Code #224) and at the Emeryville Pacific Park Plaza site (USGS Station #1662). The first boring was terminated at a depth of 391 ft. and the second boring was terminated at a depth of 202.5 ft. Forty-three high quality soil samples were retrieved from these sites. In addition, with funds provided by CUREe and EPRI, Agbabian Associates

personnel performed in situ soil velocity measurements using a suspension logging system at the Oakland 2-story office building site. The in situ shear wave velocity (V_s) measurements will be useful in evaluating the laboratory small strain shear modulus (G_{max}) measurements (since $G_{max} = \rho V_s^2$, where ρ = the soil's mass density) and in evaluating the effects of sample disturbance. Although not in the initial scope of work, in situ pressuremeter tests were attempted at the Oakland site, but the tests were unsuccessful. Preliminary soil boring logs have been developed for each of the two deep boreholes advanced in July 1992. The boring logs are being edited as the engineering index property and soil classification tests are performed.

- The laboratory testing, which will characterize the Old Bay Clay's engineering properties, has commenced. A complete range of engineering index property tests, strength and consolidation tests, and dynamic tests are being performed to characterize the dynamic properties of the Old Bay Clay and to develop understanding and soil property correlations useful for estimating the dynamic properties from more routine test data. A battery of laboratory tests on ten soil samples is well underway.

RESULTS

Observed Seismic Response of Deep Clay Deposits

The amplification of higher period ground motions is one of the most critical effects of the seismic response of clay soil sites. Whereas this effect is recognized at soft clay (e.g. Young Bay Mud) sites, it has not received as much attention at deep stiff clay sites. The response spectra of ground motions recorded at three "non-Young Bay Mud" sites in Oakland, however, show considerable spectral amplification of long period motions (see Fig. 1). If the stiffer clay deposit is sufficiently deep, longer period ground motions can also be produced at deep stiff clay sites. The observed amplification at the Oakland Outer Harbor site (see Fig. 2) shows this effect. Hence, deep stiff clay sites have the potential for producing heavy damage in a wide range of buildings (2 to 15 story) having predominant periods close to that of the underlying deposit.

Field Investigation

Sufficient data is available to develop preliminary characterizations of three sites in the Oakland area. Soil borings have been completed at all three sites through field work conducted by the U.S. Geological Survey and this research team, and initial testing on retrieved soil samples by Purdue-Georgia Tech researchers as well as some seismic shear wave velocity measurements have been performed. Using this information, the generalized soil profiles shown in Fig. 3 have been developed.

Laboratory Testing

Water contents and Atterberg limits of the soil deposit at the Oakland 2-story building site are shown in Fig. 4. The overconsolidation ratio of the retrieved samples

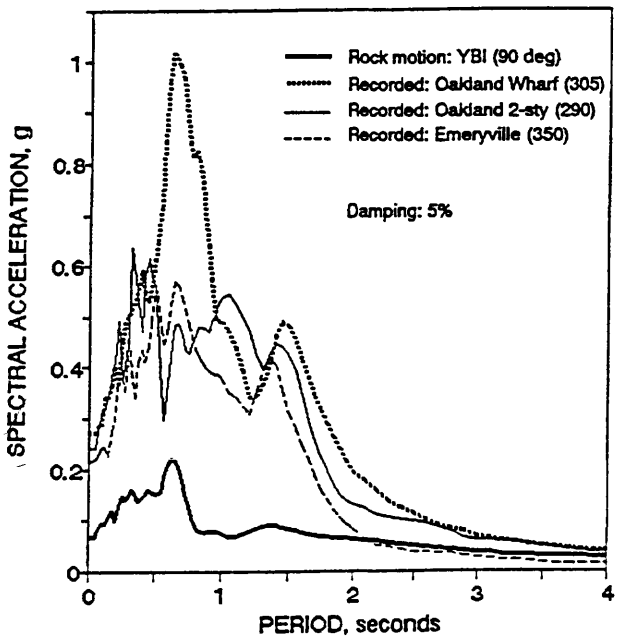

FIG. 1 -- Response spectra for three deep soil sites in the Oakland area: 1989 Loma Prieta earthquake

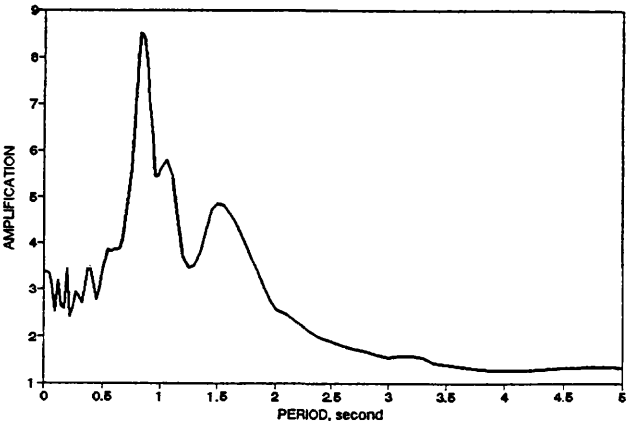

FIG. 2 -- Observed amplification at the Oakland Outer Harbor Site (i.e. recorded "deep soil" spectral acceleration/nearby recorded "rock" spectral acceleration)

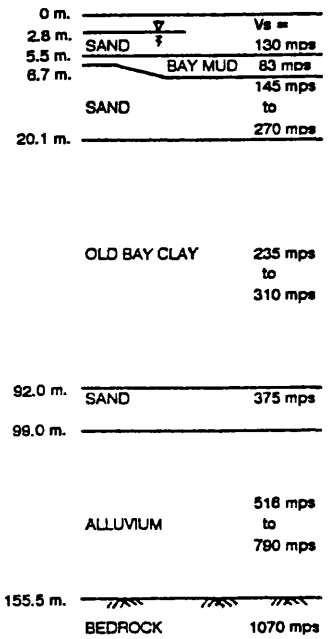

(a) Oakland Outer Harbor

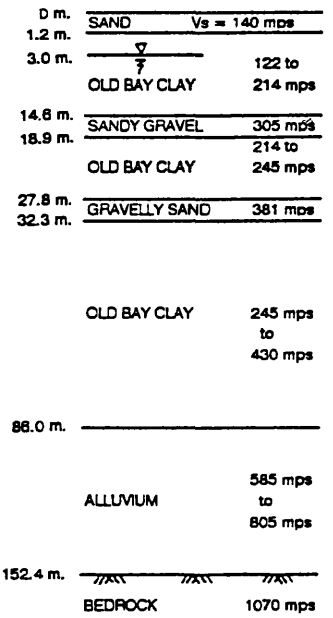

(b) Oakland 2-story Building

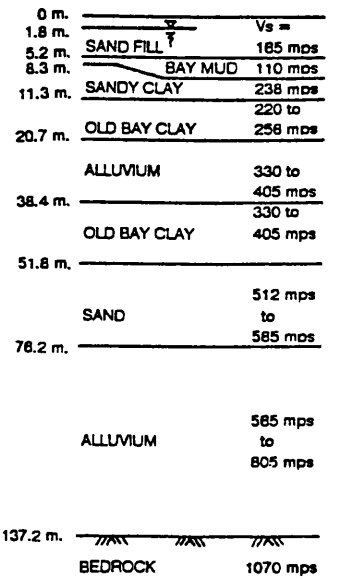

(c) Emeryville

FIG. 3 -- Soil profiles used in dynamic response analyses

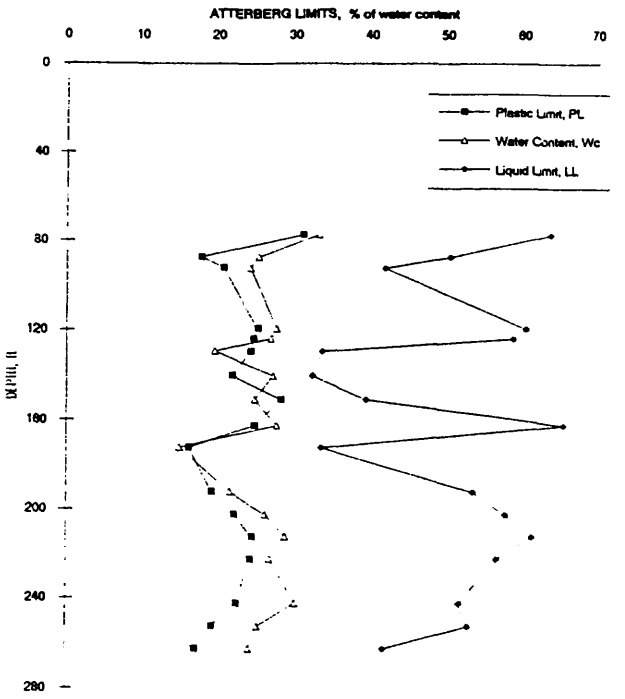

FIG. 4 -- Water contents measured at Oakland 2-story building site

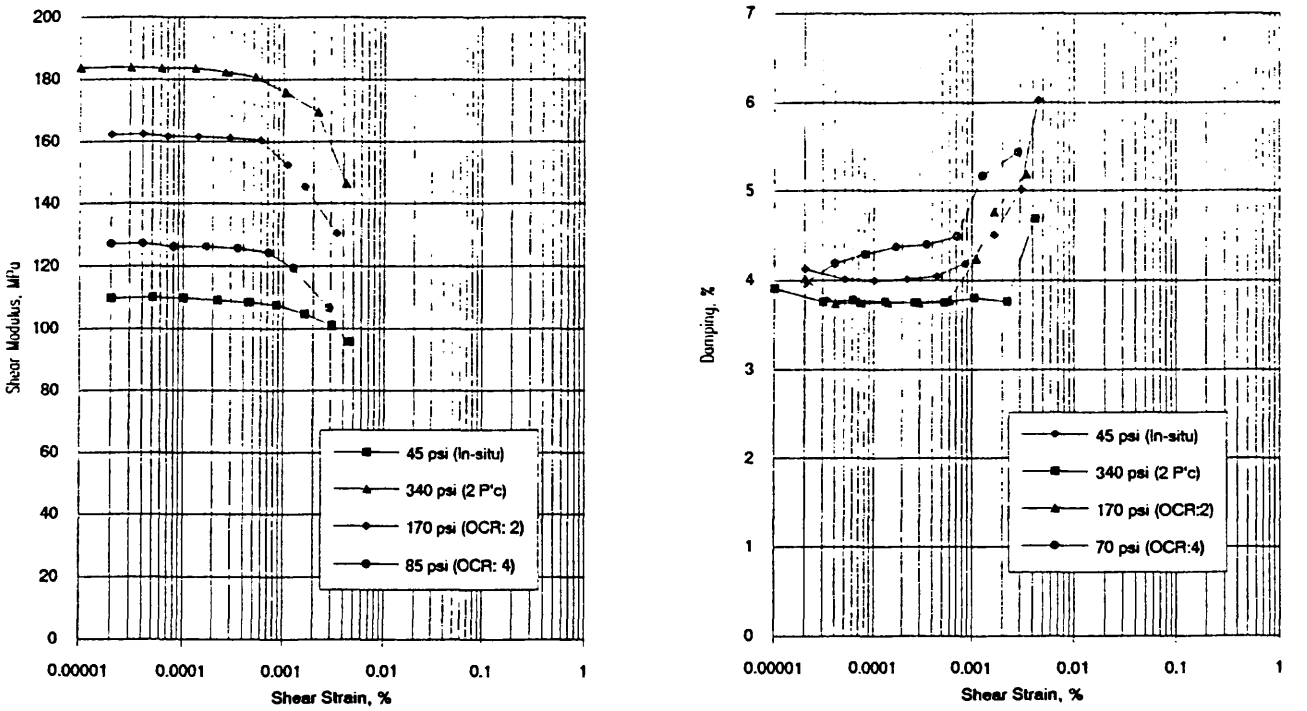

FIG. 5 -- Resonant column test results for sample #20 (depth = 75 ft.) at the Oakland 2-story building site

appears to be in the range of 2 to 4. Representative high pressure resonant column test results performed at different confining pressures and overconsolidation ratios are shown in Fig. 5.

Preliminary Site Response Analyses

The results of preliminary one dimensional seismic wave propagation analyses using the program SHAKE (Schnabel et al. 1972) further suggest that deep stiff clay deposits can produce significant amplification of the peak ground acceleration and longer period motions (Bray et al. 1992). As shown in Fig. 6a, the 1-D seismic response analysis was able to capture the tendency of this deep stiff clay site to amplify motions, and the computed response spectra is in fair agreement with the recorded motion. The computed motions at this site, however, were strongly dependent on the selection of reasonable dynamic soil properties. For example, as shown in Fig. 6b, minor variations in the shear wave velocity used to establish the "small strain" shear moduli of the Old Bay Clay deposit did produce significant variations in the computed response. Hence, it is imperative that the nonlinear strain-dependent shear moduli and damping properties of the Old Bay Clay be adequately characterized. Comparatively little test data (both static and dynamic) currently exists, however, for this critical soil deposit. This research project will address this shortcoming.

The SHAKE computed motion fits the general trends indicated by the recorded horizontal motions at the Oakland 2-story building site (see Fig. 7), except at frequencies near 1 Hz. Near this frequency, the spectral accelerations predicted by the 1-D seismic response analysis is less than half of that indicated in the recorded motions. The results of the Emeryville seismic site response analyses show a similar tendency of under-estimating the recorded motions at periods within the range of 1 to 1.5 seconds (Fig. 8). It is not known if this is a failure of the analytical procedures, or if soil-structure interaction or three-dimensional effects produced higher spectral accelerations in the recorded motions near this frequency. The results of the seismic response analyses are quite sensitive to the characteristics of the input rock motion so it is likely that the use of the Yerba Buena motion may have contributed to this discrepancy.

Further Work

The laboratory testing on the retrieved samples will be completed by April 30, 1993 as originally scheduled. Provided that the proposed second year funds are obtained, these research work items will be completed in the second year of the research program:

- Data Analysis and Synthesis: Integrate the newly developed information with that previously existing to characterize the distribution, properties, and behavior of the Old Bay Clay.

- Seismic Response Analysis: The recorded motions at well-documented sites provide an exceptional opportunity to use the observed performance as a field laboratory to evaluate the effects that the Old Bay Clay dynamic soil properties have on the ground motions. In addition, efforts will be made to estimate the influence of the

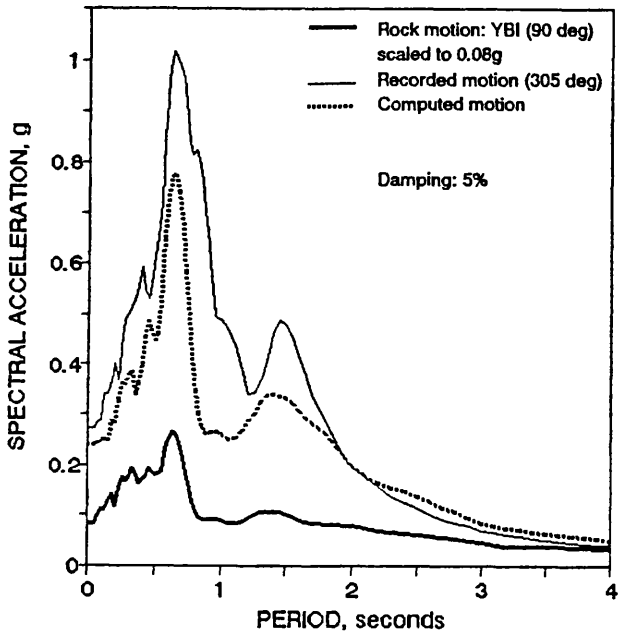

(a) Baseline Case

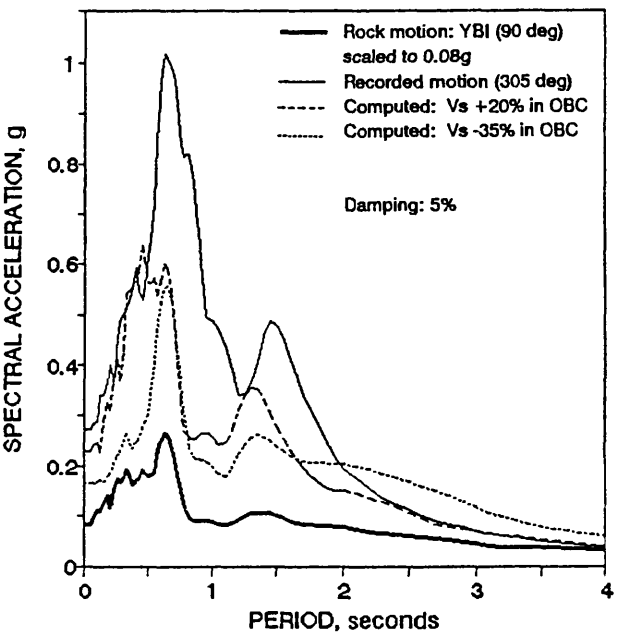

(b) Sensitivity of Variations in V_s

FIG. 6 -- SHAKE computed response spectra: Oakland Outer Harbor

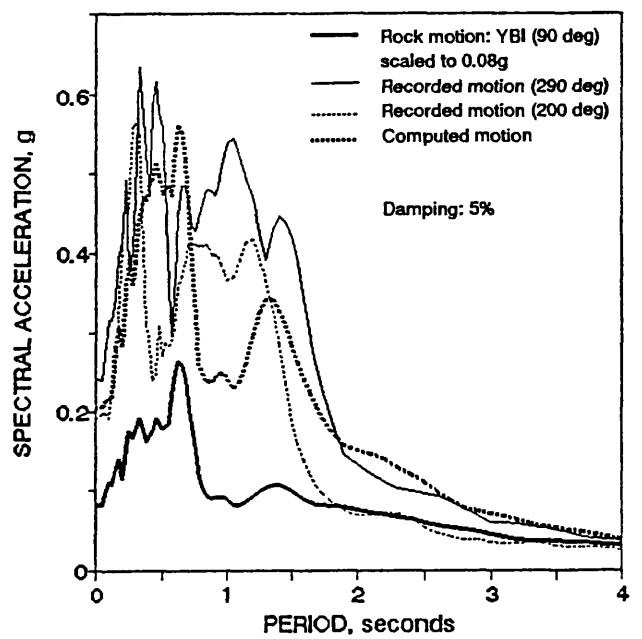

FIG. 7 -- SHAKE computed response spectra: Oakland 2-story Building

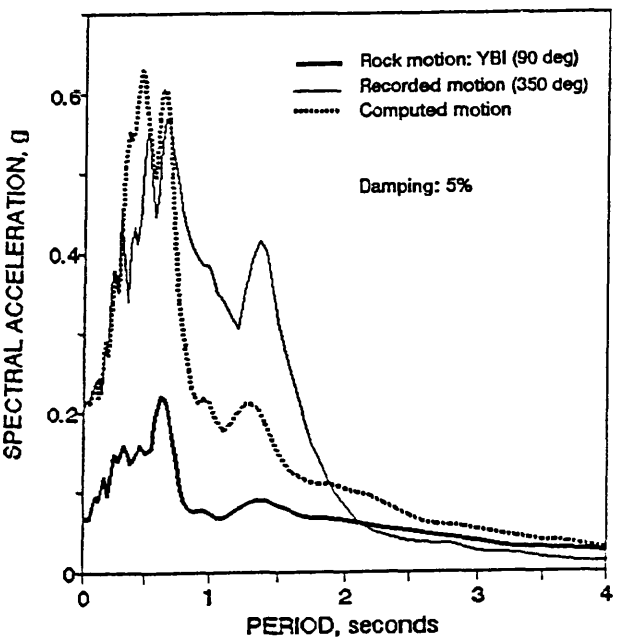

FIG. 8 -- SHAKE computed response spectra: Emeryville

complex geology and bedrock topography on the recorded motions.

- Seismic Hazard Assessment: Consolidate previous studies, test results and analyses into an overall assessment of the expected behavior of deep Old Bay Clay sites during future earthquake events.

RELATED PUBLICATIONS

J. D. Bray (1992), "Geotechnical Considerations in Earthquake Engineering", Proceedings of the National Earthquake Training Conference, Jackson, Tennessee, November 9-12.

J. D. Bray, J. L. Chameau and S. Guha (1992), "Seismic Response of Deep Stiff Clay Deposits", Proceedings of the First Canadian Symposium on Geotechnique and Natural Hazards, Vancouver, May 6-9, pp. 167-174.

REFERENCES

Dickenson, S. E. and Seed, R. B. (1992), "Correlations of Shear Wave Velocity and Engineering Properties for Soft Soil Deposits in the San Francisco Bay Region", Rpt. No. UCB/EERC-92/xx, Univ. of Calif. Berkeley, in press.

Rogers, J. D. and Figuers, S. H. (1991), "Engineering Geologic Site Characterization of the Greater Oakland-Alameda Area, Alameda and San Francisco Counties, California", Final Report to the NSF, BCS-9003785, Dec. 30.

Schnabel, B., Lysmer, J. and Seed, H. B. (1972), "SHAKE, A Computer Program for Earthquake Response Analysis of Horizontally Layered Sites", EERC Report 72-12, University of California, Berkeley, December.

NATIONAL STRONG-MOTION NETWORK: DATA PROCESSING

9910-02757

A.G. BRADY
BRANCH OF ENGINEERING SEISMOLOGY AND GEOLOGY
U.S. GEOLOGICAL SURVEY
345 MIDDLEFIELD ROAD, MS 977
MENLO PARK, CALIFORNIA 94025
415/329-5664

Investigations

1) Cataloging all strong-motion records from the USGS National Strong-Motion Network, and decisions on further digitizing and processing for the following earthquakes:

*	M_L6.1		Joshua Tree, southern Cal.	22 April 1992
*	M_S7.0,	M_L6.4	Cape Mendocino, nth. Cal.	25 April 1992
			(and two aftershocks on 26 April 1992)	
*	M 7.4		Landers, southern Cal.	28 June 1992
*	M 6.5		Big Bear, southern Cal.	28 June 1992

2) We are preparing a Network Operations Manager using Paradox, a commercial database software package, to assist field technicians in the sister project: National Strong-Motion Network: Operations.

3) We continue to develop the capabilities of our processing programs, including a streamlined version for export to user pc's.

Results

1) Continued digitizing and processing of strong-motion records, including copying and preparing records for contracted digitization and preparing ASCII tapes for distribution, *via* NGDC/NOAA, to outside organizations. We often supply outside organizations with small numbers of specific processed records on MS-DOS formatted disks as requested.

   At this time, there are three sets of earthquake records being processed: The Cape Mendocino event and its two aftershocks, the Landers event, and the Big Bear event. All are currently being digitized by L.S. Associates in San Jose.

   To assist the user in locating the positions of stations and records, we have adapted mapping software to produce relevant maps for preliminary earthquake reports and any subsequent reports needing displays of our active stations for a given area.

2) Continued work on a Network Operations Manager using Paradox. Paradox is a relational database software package which we are using to facilitate the gathering of data in the field. With the Network Operations Manager, we can enter, *via* portable computer in the field, data related to the installation and inspection of strong-motion accelerographs. Reports can then be easily generated with up-to-date statistics on all USGS-maintained accelerographs, including special reports for our reimbursable projects. Past histories of each station can be examined on site by technicians, enabling them to see recurring problems easily. A special report is generated, which includes the results of an epicentral distance calculating program. A table of station epicentral distances from a given event is generated for use in our preliminary earthquake reports.

3) We continue to develop the capabilities and general usefulness of the AGRAM computer programs. We use this software for our own strong-motion record processing and we also distribute portions of it to organizations outside the Survey. In May of this year, we published the Basic Accelerogram Processing program named BAP, together with several of the more important support programs, as two Open-File Reports. One report (#92-296A) is the printed User's Manual for the software, the other (#92-296B) is the software itself, in a form suitable for IBM-style PC computers.

   The new BAP computer program is a streamlined version of several older processing programs. It is easier to use and easier to install on other computers (that is, other than the VAX), than are the predecessor programs. BAP will calculate velocity and displacement from an input acceleration time series or it will calculate acceleration and displacement from an input velocity time series. The program will make linear baseline corrections, apply instrument correction, filter high frequency and/or low frequency content from the time series, calculate the Fourier amplitude spectrum, and calculate response spectra. It will also plot the results after each processing step.

   The most immediate reason for writing the new program was to provide processing software that would handle the 4000+ digitized strong-motion time series that were published on the Strong-Motion CD-ROM this year (as USGS DDS #7). The time series on the CD-ROM are in a relatively unprocessed form. They would be of little use to many of the organizations that purchase the CD-ROM unless we also distribute software that can process the data. Organizations that are collecting new strong-motion records of their own but that lack personnel with training or experience in record processing will also be more likely to process their records with satisfactory results if the USGS processing software and user's guides are available to them.

   Documentation is an important aspect of this effort. The BAP User's Manual is the sole reference given in the Strong-Motion CD-ROM for processing all its records. The User's Manual provides processing guidelines that should be of help to those who are using software other than BAP to do the actual processing. Consequently, this documentation must cover <u>why</u> and <u>when</u> different features of BAP should be used, in addition to the nuts-and-bolts of <u>how</u> to use it. This software is for people who are not necessarily steeped in strong-motion record processing requirements and techniques, and that means the documentation must be very thorough. The software is also for

people who are impatient with computer problems and are reluctant (or unable) to telephone the author for assistance. As such, the software and its documentation must be much more robust and thorough than software that is used only in-house.

References

Converse, April M., and Brady, A. Gerald, 1992, BAP: Basic Strong-Motion Accelerogram Processing Software; Version 1.0: U.S. Geological Survey Open-File Report No. 92-296A, 175 p.

Converse, April M., 1992, BAP software distribution diskettes: U.S. Geological Survey Open-File Report No. 92-296B (two 1.44 Mbyte PC diskettes.)

Seekins, L.C., Brady, A.G., Carpenter, C., and Brown, N., 1992, Digitized Strong-Motion Accelerograms of North and Central American Earthquakes 1933-1986: USGS Digital Data Series DDS-7 (one CD-ROM disk.)

NATIONAL STRONG-MOTION NETWORK: ENGINEERING DATA ANALYSIS

9910-02760

A.G. BRADY
BRANCH OF ENGINEERING SEISMOLOGY AND GEOLOGY
U.S. GEOLOGICAL SURVEY
345 MIDDLEFIELD ROAD, MS 977
MENLO PARK, CALIFORNIA 94025
415/329-5664

Investigations

1) The Loma Prieta earthquake has raised two issues related to the performance of engineered structures. Firstly, some soft soil sites or sites with deep layers of softer sediments provided damaging amplified ground motions while others did not, and secondly, very few thoroughly instrumented structures were seriously damaged. The implications for code upgrades are studied.

2) An understanding of the structural behavior of tall buildings during earthquakes can be gained by both children, who have no experience, and adults with no dynamics training, by using models designed for response demonstrations.

Results

1) If the resonant amplifications are dominant at a specific site, then this site will suffer large, damaging motions only if the resonant frequencies and the input frequencies of the earthquake coincide, and if the input amplitudes are sufficiently high. There exists no way of estimating the predominant frequencies or their possible range for large damaging earthquakes. The structural engineering profession is wise to limit its treatment of the seismic component of codes to a general one. For example, there is no justification at present, nor in the foreseeable future, for treating any soft soil in high seismicity regions differently from other soft soil. Although the understanding of the seismological and geophysical aspects of the most recent multiple-recorded earthquake (in the present case, Loma Prieta) has grown considerably in recent years, the ability to predict the effects of the next remain in question. There are not enough data, and there have not yet been enough earthquakes, for the situation to be any different.

The Loma Prieta earthquake provided strong-motion accelerograms from 137 ground and structural stations throughout the epicentral area, the San Francisco Bay Area and surrounding areas. Data are available from 47 structural stations: 37 multi-story buildings, four dams, three bridges, a gymnasium, an elevated rail and a wharf. It is the intelligent analysis of recordings from strong damaging motion that will decrease the seismic hazard in the years ahead, as well as the much more frequently occurring visual inspection and subsequent interpretation of damaged structures. As structures have become more complex, architecturally and geometrically, so has our interest heightened in their behavior during strong motion. Only a few records from earthquakes other than Loma Prieta have been recovered from structures suffering structural damage from earthquake shaking, and fewer still from structures with extensive instrumentation. These records offer the real opportunity of correlating earthquake input, nonlinear structural motion, and documented damage. The structural engineering community and the building code writers need more of these correlations. The successful design of structures for seismic effects, apart from following the relevant building codes, is dependent on the ability to understand how a completed structure will respond to a future earthquake, how this response builds, and how the behavior changes from the expected when critical sections suddenly lose a fraction of their strength. The structural engineering community and particularly that segment of it that is responsible for changes to building codes cannot wait for a database of pairings of measured dynamics and inspected damage. There exists a risk in attempting to consider changes to a code on the basis of a specific dynamics-damage trend in that no such trend can yet be considered reliable.

2) Representative models of two types of buildings (one with stiff columns and one with stiff floors) illustrating dynamic resonant behavior when excited by hand, were designed and built. The mass at each floor level and the stiffness of the columns were chosen in order that the frequency of the second mode was close to 5 cycles per second so that both the first and second modes could be excited by hand. Persons unfamiliar with the dynamic resonant response of tall buildings have gained a measure of understanding when shaking these models. The experience should develop a level of confidence in the builder and participant should either be in a tall building during an earthquake, sensing both these resonances and other violent shaking.

References

Brady, A.G., 1991, Recorded structural response during the M7.1 Loma Prieta earthquake: Proc., 23rd Joint Meeting UJNR Panel on Wind and Seismic Effects, Tsukuba, Japan, p. 143-147.

Brady, A.G., 1992, Desk-top model buildings for dynamic earthquake response demonstrations: Proc., 24th Joint Meeting UJNR Panel on Wind and Seismic Effects, Gaithersburg, Maryland, p. 435-443.

FAULT ZONE TECTONICS

9960-01188

Katherine S. Breckenridge, F. Brett Baker
Branch of Tectonophysics
U.S. Geological Survey
345 Middlefield Road, MS 977
Menlo Park, California 94025
(415) 329-4849

Investigations

[1] We operate 23 alinement arrays along the San Andreas fault near Parkfield, and 38 creepmeters along the San Andreas, Calaveras, and Hayward faults in central California. The creepmeters are generally 10 to 30 meters long, with 28 of the sites on GOES satellite telemetry, recording data every 10 minutes. The remaining 10 sites are read during quarterly maintenance trips.

[2] Data are cleaned of telemetry and manually induced errors and appended to the long-term archive on a quarterly bases.

[3] Data are monitored in realtime to detect events and anomalous movement near Parkfield and San Juan Bautista.

Results

[1] Alinement arrays were re-occupied, testing a procedure to perform surveys with a single person. Guidelines developed were not adopted. Instead the alinement array function of the project will be terminated for lack of resources. In the future, sites will be measured on an as-needed basis by other geologists within the branch.

Voltage parameters developed during the creepmeter calibration exercise in May 1991 have been implemented in a simple spreadsheet to facilitate and improve comparison of manual and telemetered data. In the past year this tracking mechanism has resolved rate discrepancies at 3 sites and revealed a faulty amplifier at 1 site.

[2] Long-term data sets for Parkfield are updated through mid-November 1992, while data for San Juan Bautista and Hayward are current through September 1, 1992. Table 1 compares long-term slip rates with the rate over the last 12 months at each site. Discussions are underway with members of the UC Berkeley - USGS cooperative seismic data archive committee to include USGS creep data in the archive, providing wider availability of data to researchers.

[3] Realtime monitoring continues on the southern Calaveras fault near Hollister and along the San Andreas fault from San Juan Bautista to south of Parkfield. Movement on the Calaveras fault continues to be significantly lower than the established long-term rates. As seen in figure 3 this rate reduction pre-dates the Loma Prieta earthquake, appearing in 1988 at XSH1 and as early as 1986 at HLC1. On the San Andreas fault south of San Juan Bautista (figure 4) afterslip triggered by the Loam Prieta earthquake is decaying, and instruments are returning to rates that approximate long-term slip in the area. XMR is the exception, where the slip deficit which began in August 1988 continues. At the Cienega Winery (CWC) about 4.0 mm of right lateral slip was triggered by the Landers earthquake of

6/28/92.

The past year at Parkfield featured characteristic slip at most sites (figure 5). Gold Hill (XGH1) is one exception, recording almost no slip since mid-1991. Another exception is Middle Ridge (XMD1) where strong left-lateral movement during the rainy season, coupled with a slower rate and smaller events, accounts for a significantly reduced rate in the past year. The Landers quake triggered about 0.5 mm of slip at XMM1 and XVA1, and about 1.5 mm in a slow event at CRR1. XSC1, which normally moves about 0.3 to 0.5 mm/week, recorded no slip for about 10 days after the quake. In 1989 the site was still for 3 days after Loma Prieta. Other coseismic steps ranged from -0.06 mm to 0.3 mm.

Instruments along the Hayward fault in Hayward are not telemetered. However periodic measurements indicate normal movement at the 4 sites (figure 6).

Table 1: Long-term and Short-term rates

For the rates below, LTR refers to the long-term rate, determined by least-squares fit. Site abbreviations ending in ".m" are instruments where only quarterly manual measurements are available. All entries are arranged in north-to-south order along the fault.

Hayward Fault			Calaveras Fault		
Site	LTR	12 mos.	Site	LTR	12 mos.
hwr2.m	4.4	3.1	xsh1	11.1	4.6
hww1.m	3.2	3.8	hlc1.m	8.3	-0.9
hwe1.m	0.9	0.8	hld1.m	1.9	-0.9
hwp1.m	3.6	0.3			

San Andreas Fault		
Site	LTR	12 mos.
xsj2	6.5	7.3
xhr2	14.0	13.5
cwc3	10.7	13.1
xfl1	7.2	6.8
xmr1	17.6	13.7
mrw1.m	16.8	16.8
bit1.m	17.3	12.7
xmp2.m	13.9	24.6
xsc1	21.5	22.2
xmm1	13.4	17.5
xmd1	14.4	1.3
xva1	8.7	8.8
xrsw	0.6	0.7
xpk1	7.9	9.9
xta1	8.1	9.0
wkr1	6.6	7.7
xhsw	-1.8	1.5
crr1	3.4	0.6
xgh1	3.4	1.2
x461	1.0	0.8

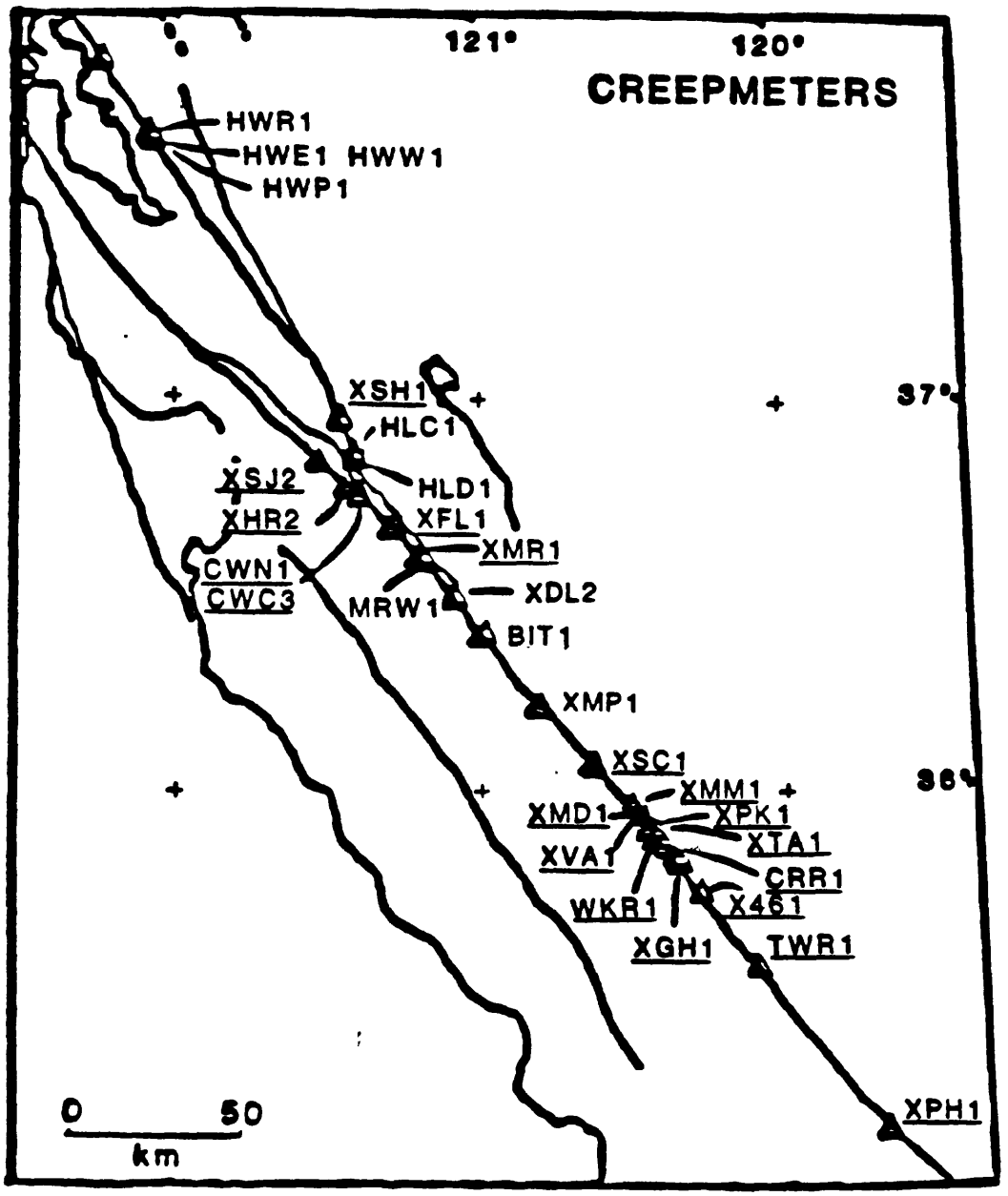

FIGURE 1

USGS creepmeter stations in northern and central California. Instruments with underlined names transmit on telemetry. NOT SHOWN: XRSW, XHSW on the Southwest Fracture near Parkfield (See Figure 2). Strong-motion creepmeters are located in vaults at XMM1, XMD1, XVA1, XTA1, X461, XRSW, and XHSW.

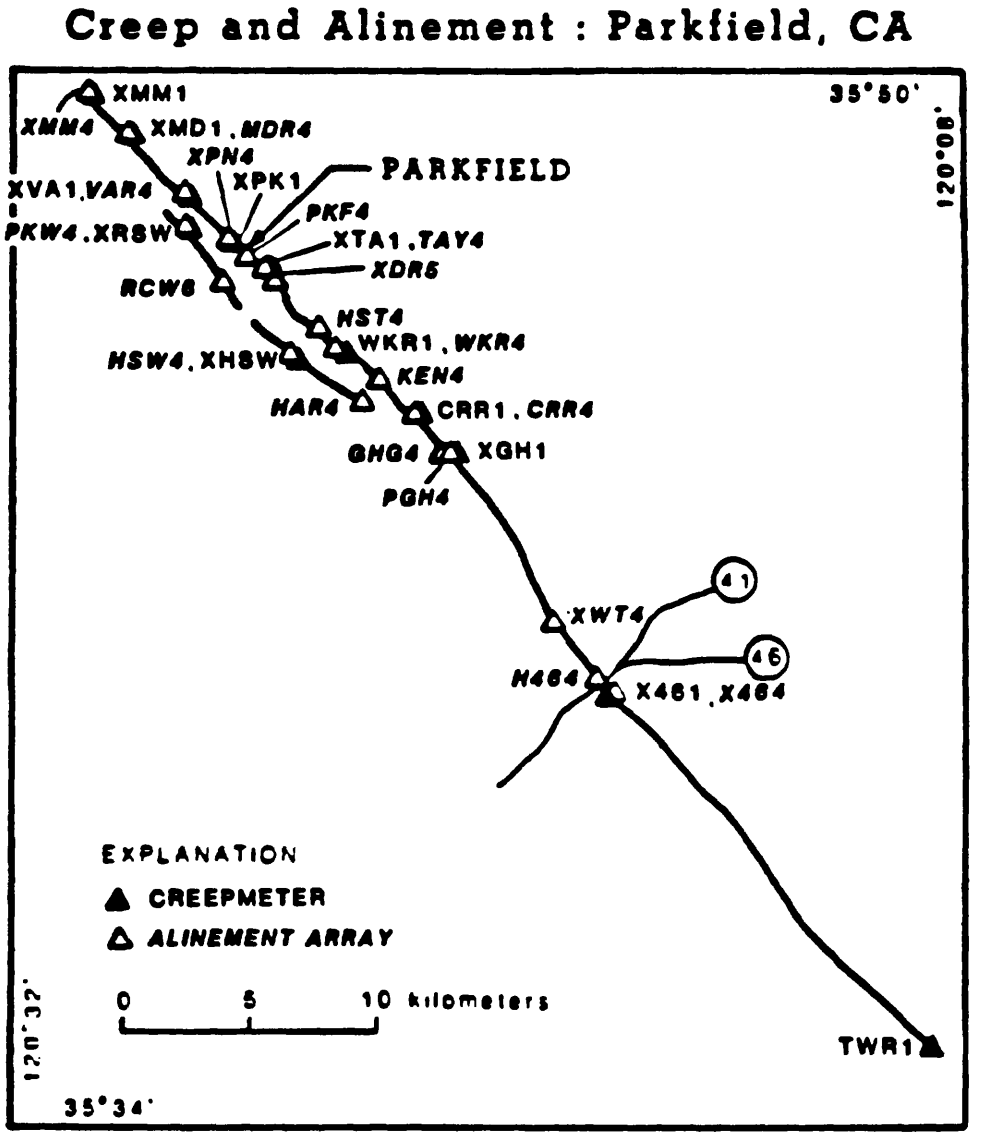

CREEPMETER AND ALINEMENT ARRAY SITES IN PARKFIELD
MARCH 1988

FIGURE 2

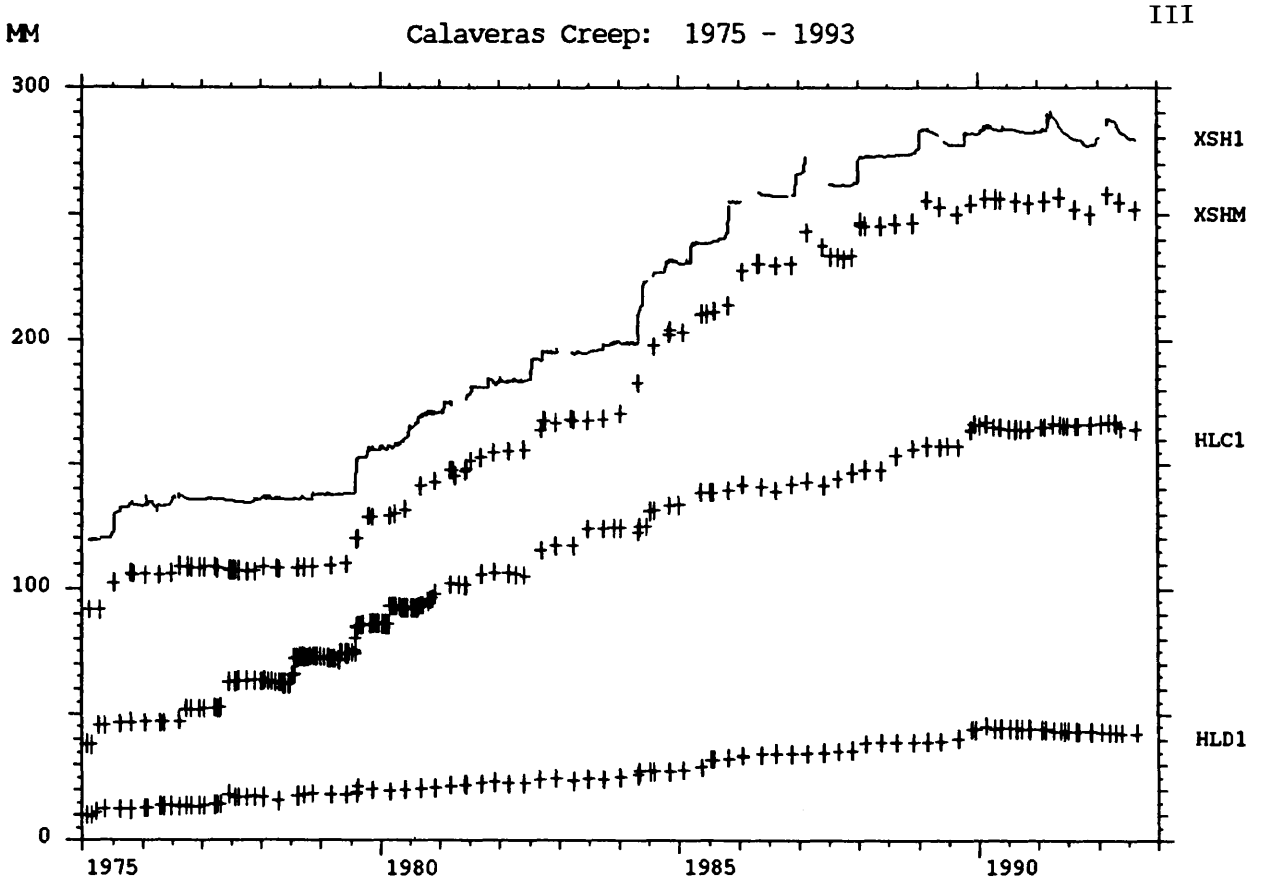

Figure 3. Long-term slip along the Calaveras fault near Hollister, in north-south order. Plus-signs represent periodic measurements. Both manual and telemetered data are shown for Shore Rd., XSHM and XSH1 respectively.

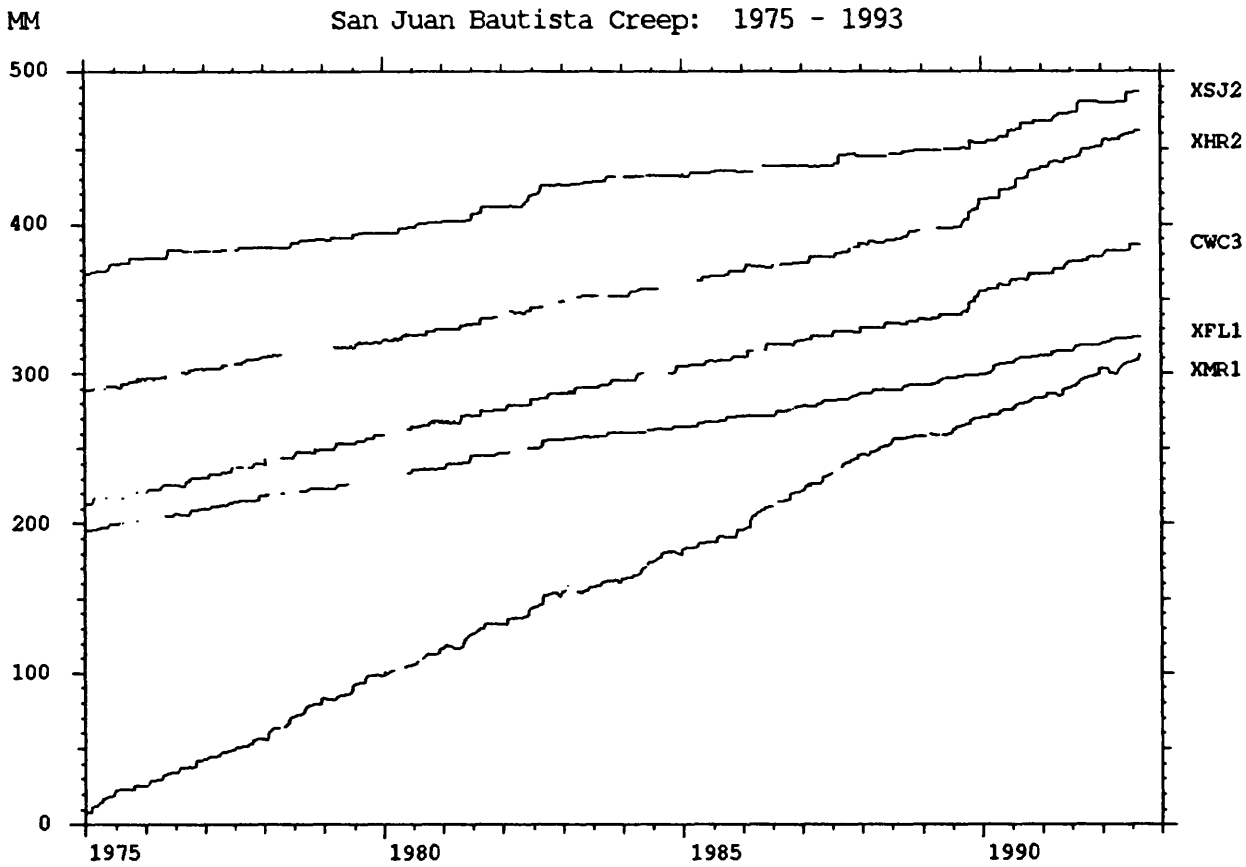

Figure 4.

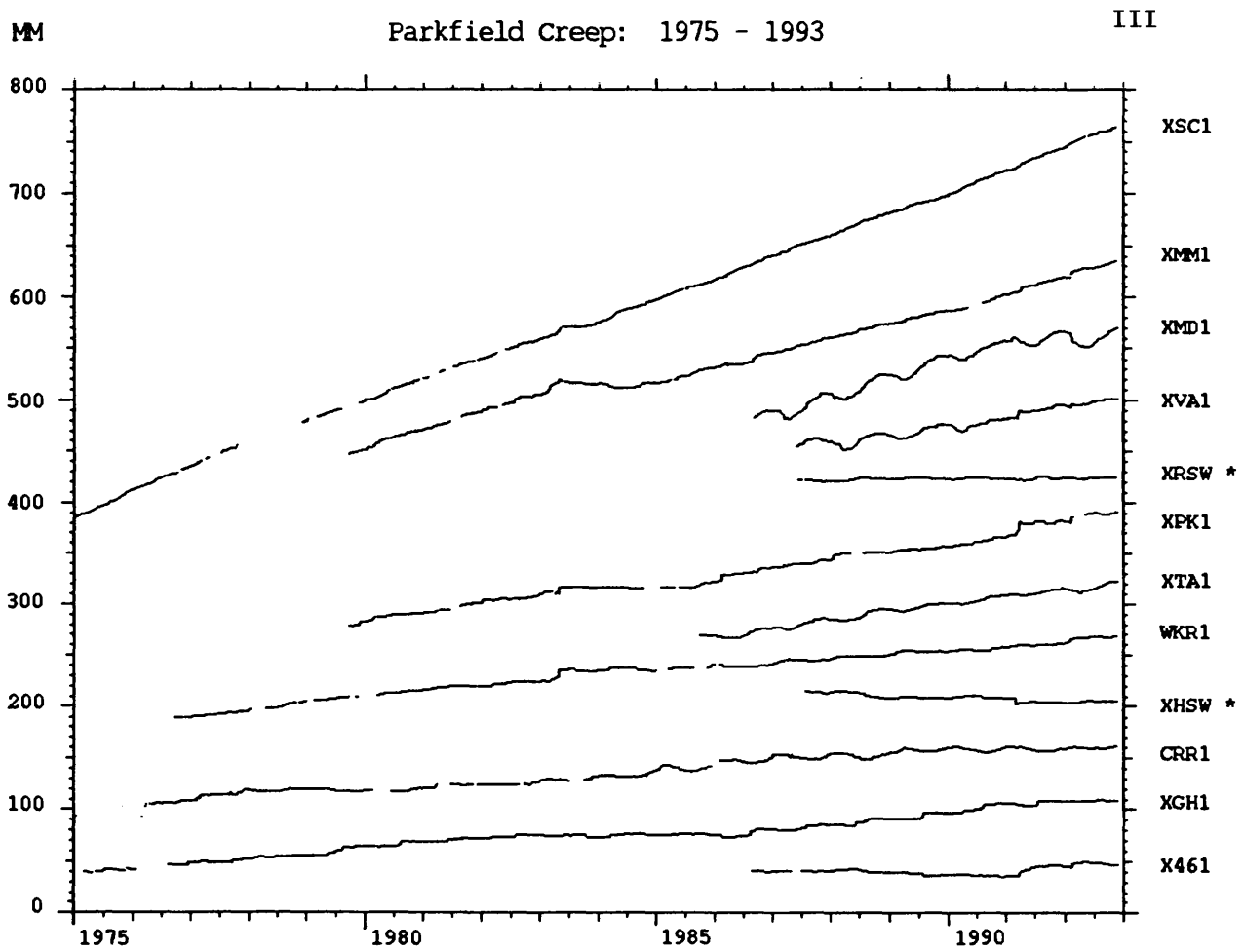

Figure 5.

* On Southwest Trace

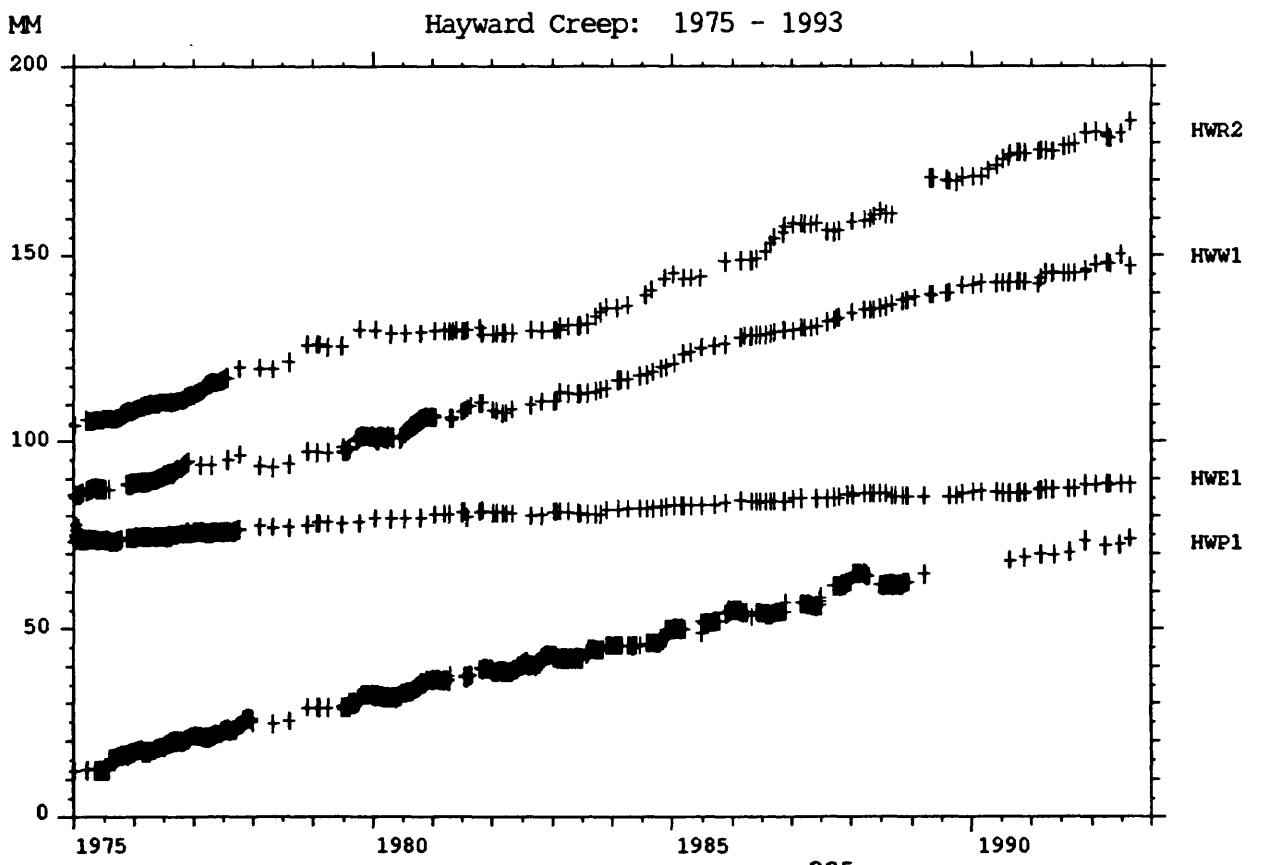

Figure 6.

CENTRAL UNITED STATES STRONG-MOTION INSTRUMENTATION

9910-04428

MEHMET ÇELEBI
BRANCH OF ENGINEERING SEISMOLOGY AND GEOLOGY
U.S. GEOLOGICAL SURVEY
345 MIDDLEFIELD ROAD, MS 977
MENLO PARK, CALIFORNIA 94025-3591
415/329-5623

Summary

During this fiscal year, allocated funds have been used to purchase necessary hardware for instrumentation of a building and also to deploy free-field accelerographs in five new sites in the New Madrid seismic area. The building to be instrumented is selected through an advisory committee in the New Madrid area. Digital free-field accelerographs have been deployed in Lepanto and Blytheville (Arkansas), Poplar Bluff (Missouri), and Paris and Union City (Tennessee).

Investigations

1. Strong-motion instrumentation in the Central United States is supplemented during the fiscal year by five digital strong-motion accelerographs deployed as free-field stations in Lepanto and Blytheville (Arkansas), and Paris and Union City (Tennessee).

2. A building in St. Louis, Missouri, is selected by the local Advisory Committee for instrumentation. Permit for instrumentation is obtained. Hardware is purchased and implementation is completed.

Results

1. Digital accelerographs deployed at free-field will allow rapid assessment of the parameters related to the strong shaking when there is a strong-motion event.

2. Instrumented building will provide important data on the response of a structure in a critical seismic zone.

Engineering Subsurface Information, Criteria, and GIS Data Base for Regional Earthquake Hazard Evaluation in the Northern Mississippi Embayment Region

Agreement No. 1434-92-G-2197

T. S. Chang, W. Y. Chung, A. C. Johnston, H. T. Kung, and R. Patri
Center for Earthquake Research and Information
Memphis State University
Memphis, TN 38152

(901) 678-2007

Research Background

This report presents the progress and some preliminary results of a regional seismic hazard study for the areas in the central United States. The study is conducted on the basis of the engineering subsurface information gathered throughout the study area, state-of-the-art knowledge and technology in the earthquake engineering, and the results of previous related studies. The key research elements include:

(1) computer data base of existing engineering bore hole data,
(2) measurements of dynamic properties of sedimentary soils in the study area,
(3) regional seismic hazard evaluations for developing engineering seismic hazard maps of liquefaction potential, earthquake-induced earth movements, and seismic soil types, and near surface site response spectrum information for site-related earthquake resistance design, and
(4) development and application of computerized GIS using the study results.

Soil Data Collection, Compilation, and Presentation

In addition to the soil data in the Shelby County area, data of about 4,400 engineering logs were collected for the 20 less populated counties in West Tennessee (see Table 1). The soil data used in the study is the existing subsurface information available in the local communities from sources including private consulting companies, local government agencies, and the Army Corps of Engineers.

Table 1. Distribution of Boring Logs in West Tennessee

Name of the County	No. of Boring Logs
Lake	288
Lauderdale	299
Obion	289
Dyer	678
Tipton	316
Weakley	287
Gibson	277
Crockett	157
Haywood	125
Fayette	139
Henry	141
Carroll	114
Madison	669
Hardeman	116
Henderson	109
Chester	15
McNairy	89
Benton	27
Decatur	36
Hardin	218
Total	4389

For the interpretation of the collected soil data, a grid system consisting of rectangular cells with equal size of 3 minutes in both latitude and longitude was applied to a map that was based on the USGS (1:250,000) topographic maps. The number of boring logs collected in each cell in the study area is shown in Figure 1. A computer data system was developed for the soil data base in the study area.

Regional Earthquake Hazard Evaluation

The regional earthquake hazard evaluation in this project includes the following studies: (1) generation and processing of synthetic earthquake time histories, (2) dynamic properties of soils, (3) seismic site response, and (4) liquefaction and the corresponding earthquake-induced earth movements potential.

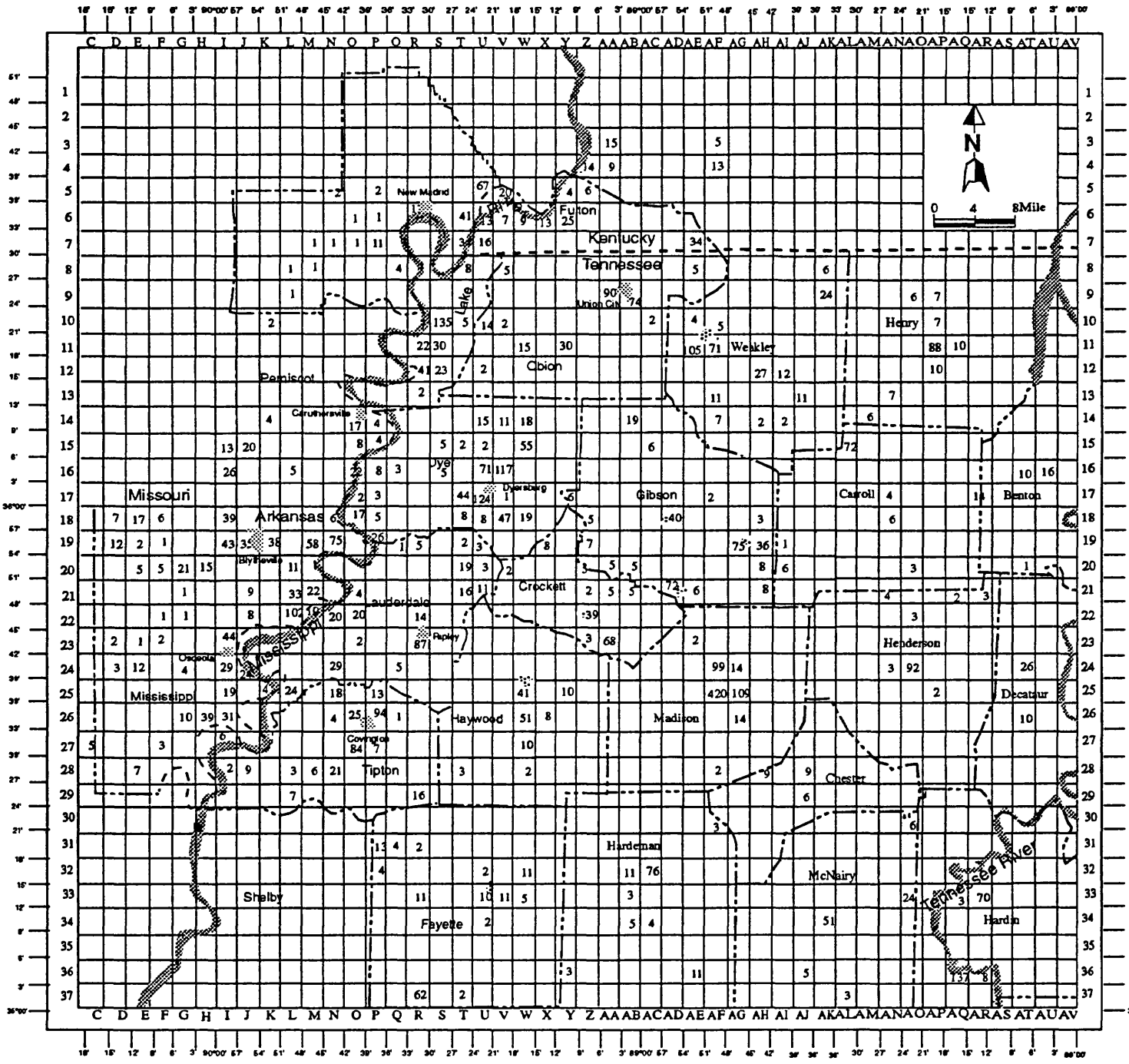

Figure 1 Number and Boring Location in West Tennessee

(1) Synthetic earthquake time history: A seismologically-based model used by previous researchers has been employed in this study to provide a preliminary estimate of the earthquake accelerations in the study area. Appropriate subsurface parameters were selected to produce earthquake ground accelerations at "soft rock" for the study. The velocity-density contrast between the near-surface soft rock level and the underlying "hard rock" was taken into account to produce amplified ground motion time histories for "soft rock" situation. By using the synthetic earthquake time histories described above, the near-surface soil response for selected sites can be computed using the selected representative soil logs in the study area.

In addition to the synthetic earthquake time history, common ground surface acceleration of 0.1g and 0.2g are also used for the seismic hazard evaluation in the study area without the effect of distance between the assumed epicenter and the evaluated sites.

(2) Dynamic properties of soils: The low-strain elastic and high-strain nonlinear behaviors of soils in the study area were obtained in the laboratory from 78 resonant column tests on 35 soil samples. The parameters for describing the strain-dependent nonlinear behavior of various types of soils (alluvial sand, terrace sand and gravel, Jackson fine sand, silty clay, Jackson clay, and loess) were determined for creating the soil model for the seismic site response study.

(3) Seismic site response: The results of the seismic site response study include peak ground acceleration, elastic site period, average shear-wave velocity, near-surface response spectrum, and seismic soil type of the site.

(4) Liquefaction and corresponding earthquake-induced earth movements potential: Liquefaction potential of the sites in the study area are evaluated on the basis of the established evaluation criteria including Seed's field criteria and the pore-pressure-development criteria from a previous study at CERI. The average and possible range of earth movements corresponding to assigned liquefaction risk are estimated and are shown in a series of earth movement potential maps.

Results

Summaries of earthquake-induced settlement in the Memphis and central NMSZ areas are shown in Tables 2 and 3 and Figure 2. Results indicate that the average earthquake-induced settlements in the central NMSZ and Memphis areas are almost the same for very low, low and high

Table 2 Summary of results of earthquake-induced estimated settlements in the Memphis area (A total of 518 sites).

Ground Surface Acceleration	Liquefaction Potential Index (PL)	Number of Sites (%)	Settlement Range (in)	Number of Sites (%)
0.1 g	PL = 0 (no liquefaction)	503 sites (97%)	< 0.5	432 sites (86%)
			0.5 - 2.5	72 sites (14%)
	PL > 0 (liquefaction)	15 sites (3%)	< 0.5	0 site (0%)
			0.5 - 12	12 sites (80%)
			> 12	3 sites (20%)
0.2g	PL = 0 (no liquefaction)	416 sites (80%)	< 0.5	359 sites (86%)
			0.5 - 2.5	57 sites (14%)
	PL > 0 (liquefaction)	102 sites (20%)	< 0.5	0 site (0%)
			0.5 - 12	92 sites (90%)
			> 12	10 sites (10%)
Estimated from Seismic Hazard Curve	PL = 0 (no liquefaction)	362 sites (70%)	< 0.5	305 sites (84%)
			0.5 - 2.5	57 sites (16%)
	PL > 0 (liquefaction)	156 sites (30%)	< 0.5	5 sites (3%)
			0.5 - 12	135 sites (87%)
			> 12	16 sites (10%)

Table 3 Earthquake-induced estimated settlement range for various liquefaction risks on the basis of liquefaction potential index PL for the Memphis area.

Liquefaction Potential	Liquefaction Risk	Settlement (in)	
		Average	Possible Range
PL = 0	very low (no liquefaction)	1.0 ± 1	< 0.01 to 3
0 < PL ≤ 5	low	2.5 ± 1.5	1/2 to 9
5 < PL ≤ 15	high	6.0 ± 2	3 to 14
15 > PL	very high	> 8	5 to 18

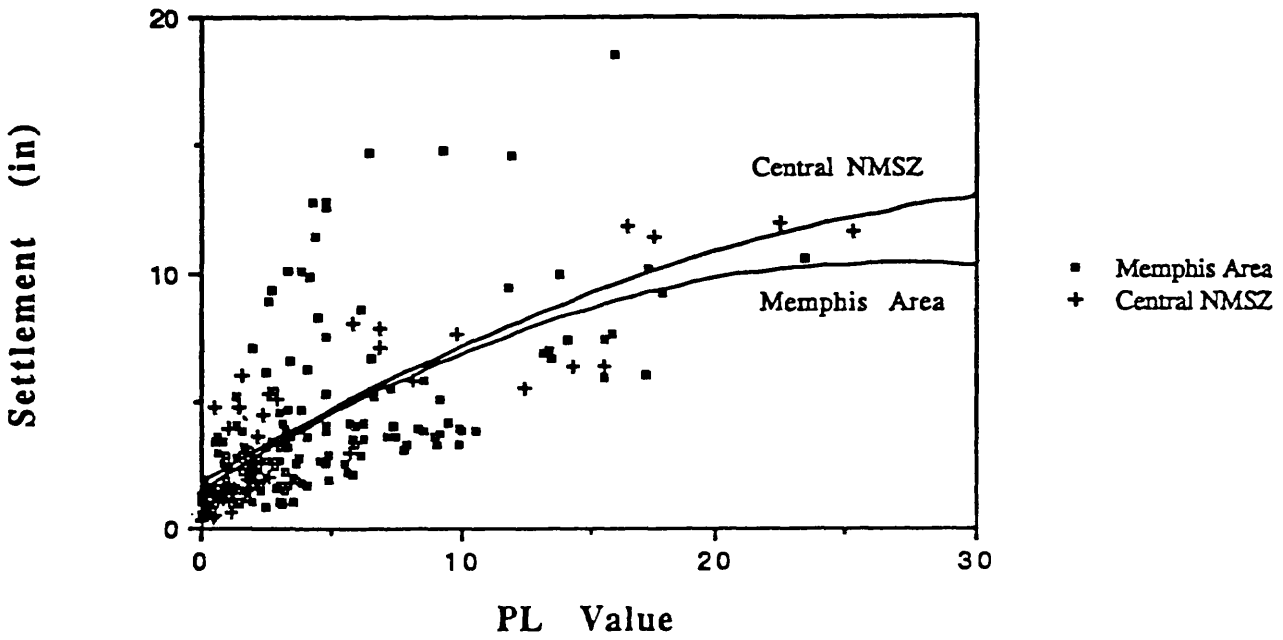

Figure 2 Earthquake-induced settlement potential as a function of liquefaction potential index PL for the central NMSZ and the Memphis Area.

liquefaction potential, however, the central NMSZ area may experience settlements 1 to 2 inches greater for the very high liquefaction potential sites. Results also indicate that a catastrophic landslide that will threaten lives and properties is unlikely to occur in most of the Memphis area. Only a few Memphis suburban areas have slopes steep enough to produce landslide or creep-type lateral movements triggered by earthquakes. In these rolling areas, lateral movements, not necessarily mass landslide, are estimated to be from less than 1 ft to in the order of 3 ft depending upon the thickness of the liquefiable soil layer, slope angle, and ground surface acceleration. Figures 3 and 4 present the earthquake-induced earth movement potential in the Memphis area subjected to a common ground surface acceleration of 0.2g for settlement and lateral slope movement, respectively.

Geographic Information System (GIS)

Results and the derived seismic hazard maps and the soil data base are included as part of the GIS in the study area.

Reports

The first year of the project produced one technical report and one technical paper as follows:

(1) Chang, T.S., Chang, K.P, Chung, W.Y. and Johnston, A.C. (1992) "Earthquake Hazard Evaluation in the Central New Madrid Seismic Zone." CERI technical report submitted to the USGS, May, 1992.
(2) Chang, T.S. and Chang K.P. (1992) "Earthquake-induced Earth Movements Potential in the Memphis Area." Paper to be included in the proceedings of 1993 national Earthquake Conference, Memphis, Tennessee, May, 1993.

The final report of the project for FY 1992 and two technical papers resulting from the project will be prepared for publication in 1992-1993.

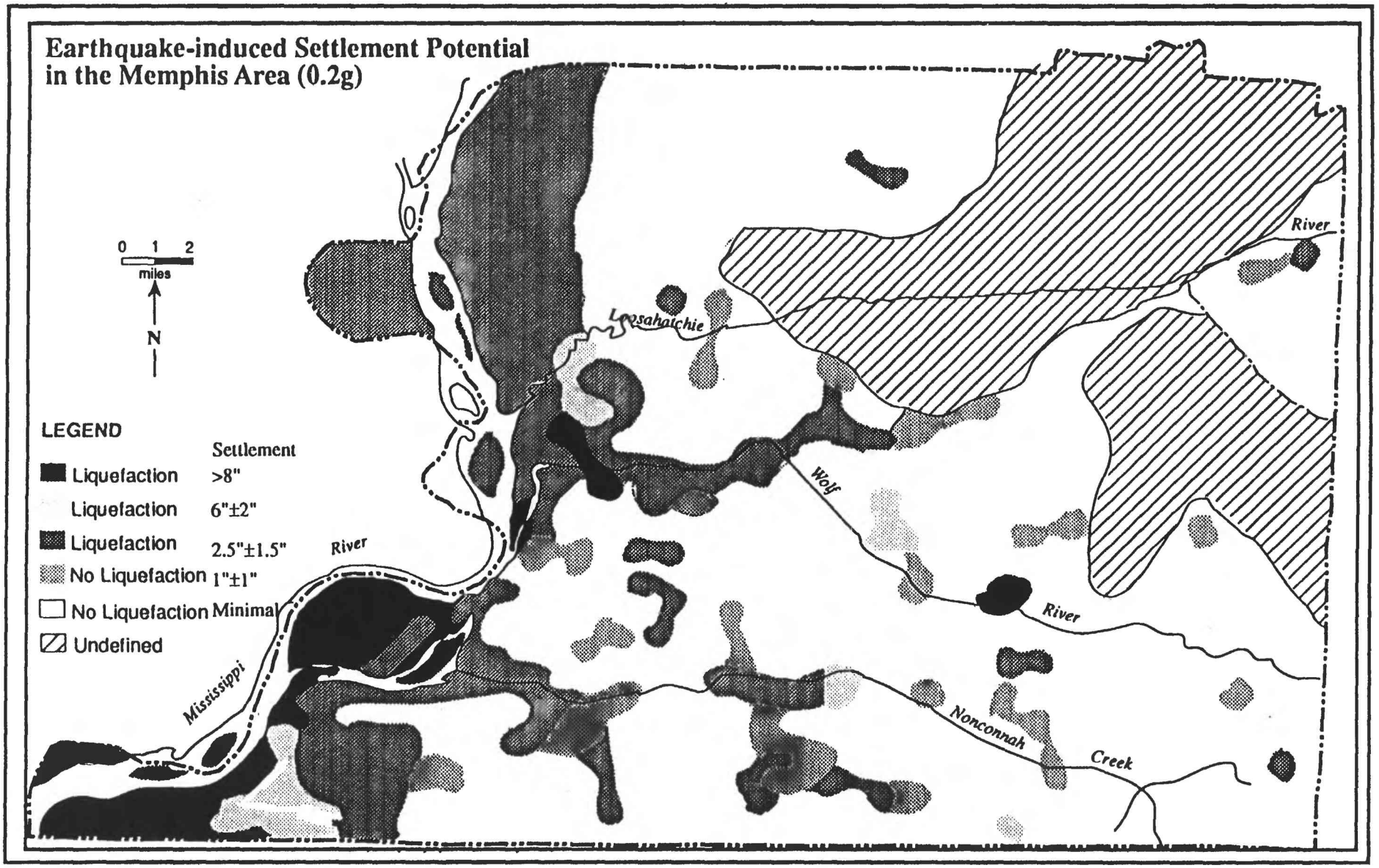

FIGURE 3 Earthquake-induced settlement potential for common ground accelararation of 0.2g in the Memphis area

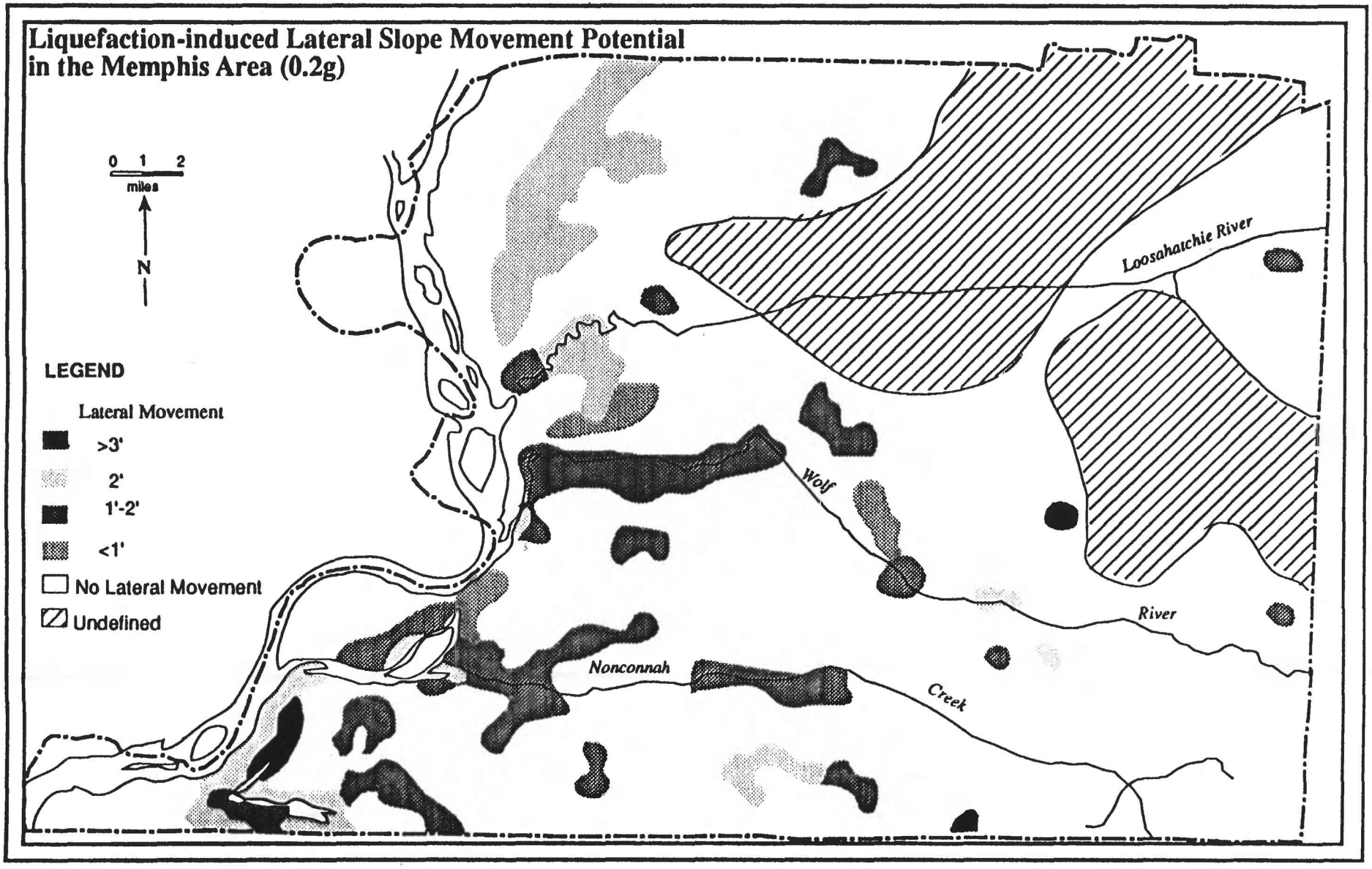

FIGURE 4 Liquefaction induced lateral slope movement potential for a common ground surface accelaration of 0.2g in the Memphis Area

Inventory and Preliminary Seismic Vulnerability Assessment of Essential Facilities for GIS Data Base in the Southern New Madrid Seismic Zone

Agreement No. 1434-92-G-2198

T.S. Chang, H. T. Kung, S. Pezeshk, and K. C. Yiak
Center for Earthquake Research and Information
Memphis State University
Memphis, TN 38152

(901) 678-2007

Research Background

This interdisciplinary study is conducted to obtain information about the damage risk imposed to the existing essential facilities in the northern Mississippi embayment region from the New Madrid seismic zone (NMSZ) earthquakes. Results of the study, including a Geographic Information System (GIS), will provide information for regional earthquake preparedness and response plans for reducing seismic risk and saving lives in the event of moderate NMSZ earthquakes (M = 6 to 7). This report presents the progress and some preliminary results of the seismic evaluation for the selected facilities (schools, fire stations, hospitals, and main river-crossing bridges) in West Tennessee, and the procedure of developing the GIS using the evaluation results and data collected from these selected facilities.

Methods and Procedures

A cost-effective preliminary seismic vulnerability evaluation system was developed for the study. This system uses existing data (site, subsurface condition, foundation, and structure) and the results of a quick on-site documentation of target facilities. This evaluation system also provides feasible measures for identifying some potentially hazardous facilities that require further detailed seismic vulnerability evaluation and/or intensive maintenance. The flow chart for the facility seismic vulnerability evaluation used in the study is shown in Figure 1.

Data Collection of the Existing Facilities

The selected essential facilities in the study area, 20 counties in west Tennessee, include 174 public schools, 179 fire stations, 97 main river-

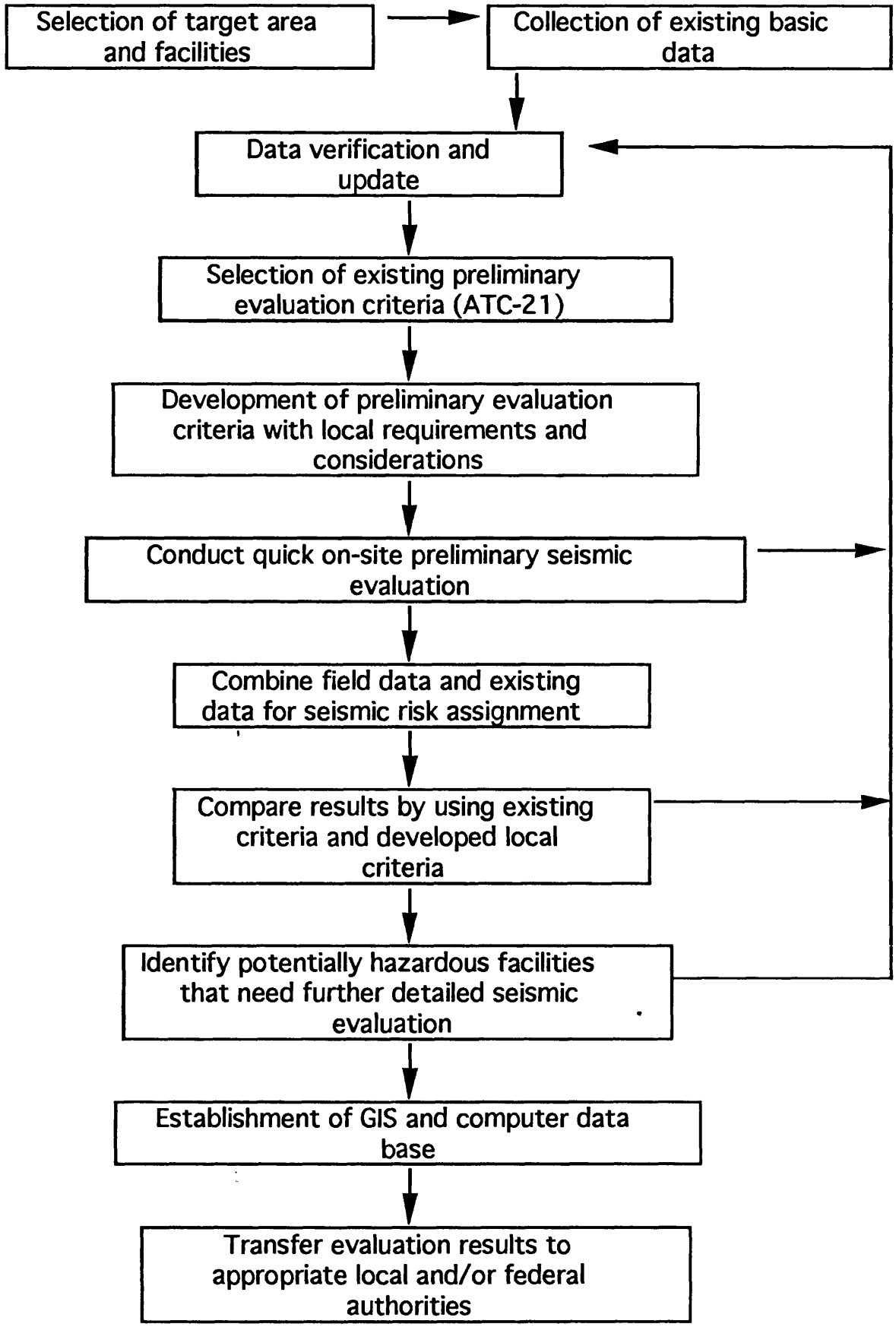

Figure 1 Procedure for Facility Seismic Vulnerability Assessment

crossing bridges, and 19 main hospitals (see Table 1). Location of the target facilities is shown in Figures 2 and 3. Basic data for each facility were collected through West Tennessee Emergency Management Agency (TEMA), City and County governments, and private sectors. All the facility data were verified by each County's emergency management agency, board of education, fire department, and regional hospital administrator, and Tennessee Department of Transportation. The basic data for each facility include site and structure information, history, capacity, and operational information. The picture documentation of each facility is also completed as part of the basic facility data.

Development of a Quick On-Site Facility Evaluation System

The preliminary evaluation system was first developed by the MSU earthquake engineering research team and then was finalized in a technical meeting held at CERI on June 5, 1991. The attendees at the meeting included professionals from universities and government agencies. The evaluation criteria used for fire stations, schools, and hospitals included (1) site conditions (soil type, liquefaction potential), (2) past performance of various structures and foundations, (3) age of facility, (4) type of structure, (5) type of material, (6) detailing, construction, and current conditions, (7) seismic code adoption, (8) mass, stiffness, strength, and shape irregularities in plan and elevation, and (9) structure/structure separation. The evaluation criteria used for bridges included (1) super structure: continuity, number of joints, bearing type, alignment of the bridge, year built, seismic retrofit, shape irregularity, height of pier or column, and girder support length; (2) site and foundation: soil type, liquefaction potential, and abutment height; and (3) importance: detour length, and average daily traffic.

The primary, regular, and secondary criteria for evaluating seismic vulnerability of facilities were identified in the technical meeting then a predetermined evaluation index score (a total of 100 points) was applied to the evaluation criteria with a rational point/weight to each criterion reflecting the effect on facility seismic damage caused by earthquakes. Some improvements of the evaluation form have been made for the study in West Tennessee. Figure 4 shows an example of evaluation form used for the river-crossing bridges.

On-Site Preliminary Seismic Vulnerability Evaluation

An engineering crew of 3 faculty and 4 students, organized into two groups, conducted the preliminary seismic vulnerability assessment by

Table 1 Summary Of Evaluated Essential Facilities In West Tennessee

COUNTIES	SCHOOLS	FIRE STATIONS	HOSP.	BRIDGES	OTHERS*	TOTAL FAC.
BENTON	5	6	1	0	1	13
CARROLL	11	5	2	9	0	27
CHESTER	6	8	0	2	0	16
CROCKETT	8	4	0	3	0	15
DECATUR	5	6	1	3	1	16
DYER	13	13	1	8	0	35
FAYETTE	8	14	1	8	5	36
GIBSON	20	15	3	10	0	48
HARDEMAN	9	10	1	4	0	24
HARDIN	2	5	0	0	0	7
HAYWOOD	7	10	1	5	0	23
HENDERSON	8	9	1	8	1	27
HENRY	6	5	0	6	0	17
LAKE	3	2	0	1	0	6
LAUDERDALE	6	7	1	4	0	18
MCNAIRY	8	12	1	0	0	21
MADISON	24	20	2	7	1	54
OBION	11	9	1	9	2	32
TIPTON	8	11	1	2	0	22
WEAKLEY	6	8	1	8	1	24
TOTAL	174	179	19	97	12	481

* VOCATIONAL, HEAD START, ACADEMY, and KINDERGARTEN

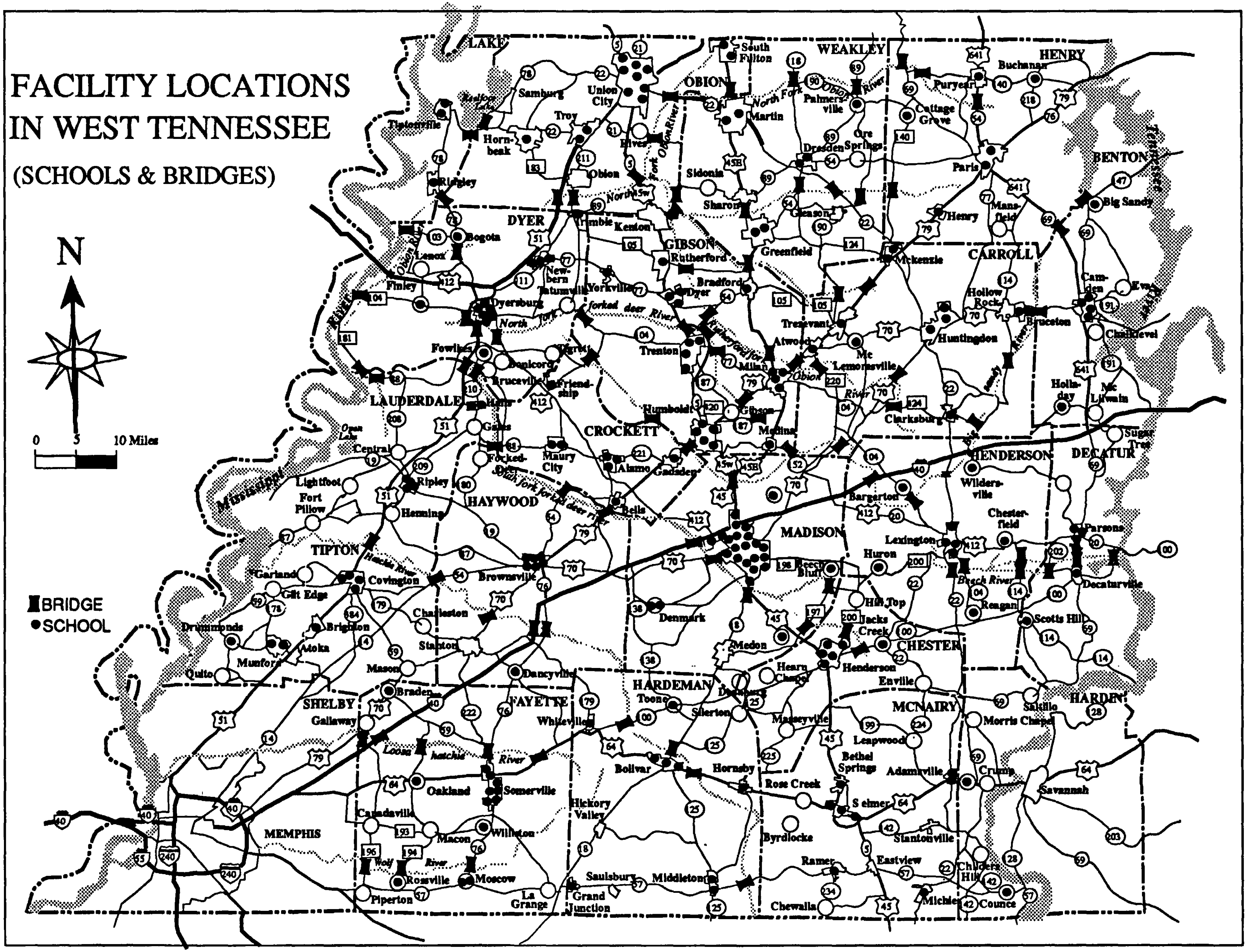

FIGURE 2 Locations of essential facilities in West Tennessee (Schools & Bridges)

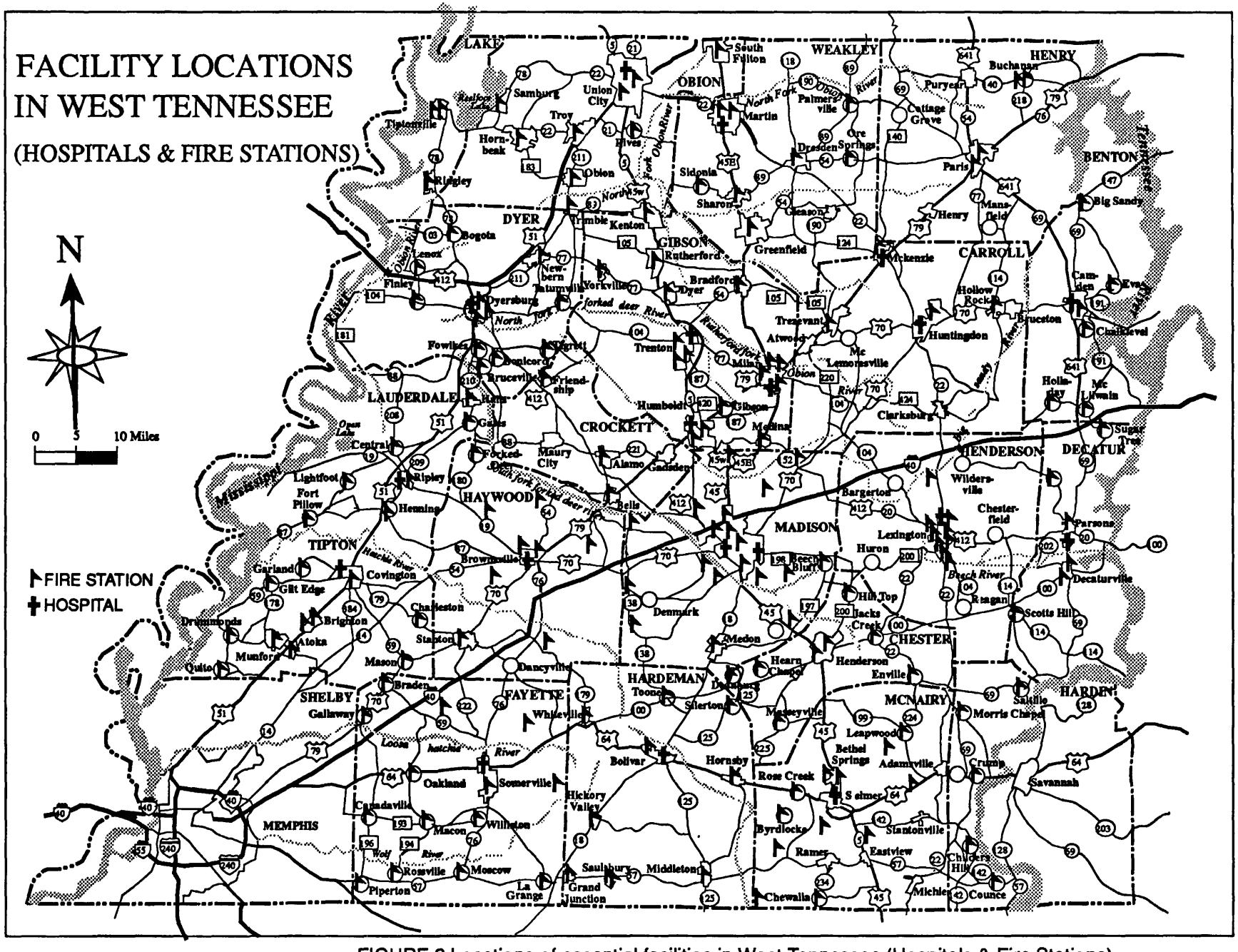

FIGURE 3 Locations of essential facilities in West Tennessee (Hospitals & Fire Stations)

GENERAL

Bridge Number: _____ Picture No. _____

Location: _____

ADT _____ Detour Length: _____ Essential Bridge: Yes: ___ No: _____

Length: _____ Inspector Name: _____ Year Built: _____

Engineer (Designer): _____ Width: _____

SUPERSTRUCTURE:

Material and Type: _____

Number of Spans: _____

BEARING

Actual Support Length : _____ Minimum Required Support Length (N_d): ___

$N_d = 12 + 0.03L + 0.12H$ (inches)

L = Length of bridge deck to the adjacent expansion joint

H = Average of Height of Columns supporting the bridge

STRUCTURE					Final score
1. Super Structure:		Continuous	Non-Continuous		
(5pts)		5	0		
2. Number of Expansion Joints ____		<=1	2	3	>=4
(5pts)		5	4	4	3
3. Bearing Type	Rocker	Roller	Elastomeric Bearing Pad		Sliding
(5 pts)	0	1	4		5
4. Alignment of the Bridge		Straight	Skewed(<20^0)	Skewed(>20^0)	Curved
(5 pts)		5	4	1	1
5. Year Built		Before adoption of EQ Code		After adoption of EQ Code	Don't know
(10 pts)		0		10	0
6. Seismically Retrofitted:		Yes	No		
Bonus points		10	0		
7. Classification (differential stiffness, different pier heights, etc.)				Regular	Irregular
(5 pts)				5	0
8. Height of the Piers or Columns		< 15 ft	> 15 ft		
(5 pts)		5	0		
9. Actual Support Length > Minimum Required Support Length (N_d)				Yes	No
(10 pts)				10	0
10. Visible Damage		Major Damage		Minor Damage	No Damage
(10 pts penalty)		-10		-5	0
Final Structural Score					

IMPORTANCE				Final score
1. Detour Length	>4 miles	2-4 miles	< 2 miles	
(10 pts)	0	5	10	
2. ADT	<2000	2000 - 10,000	> 10,000	
(10 pts)	10	5	0	
Final Importance Score				

FOUNDATION				Final score
1. Soil profile type	SL2	SL3	SL4	
(10 pts)	10	5	3	
2. Liquefaction potential	Low	Moderate	High	
(10 pts)	10	5	0	
3. Abutment Height (ft)	0-15	15-30	<30	
(10 pts)	10	5	0	
Final Foundation Score				

SEISMICITY				Final score
1. Seismicity	5,6,7	3,4	1,2	
(100 pts)	0	50	100	

TOTAL SCORE

Total Score = (Structural Score + Foundation Score + Importance) X 0.8 + Seismicity X 0.2

Total Score =

FIGURE 4. Typical Evaluation Form for Bridges

using the collected basic facility data, picture document, and the developed preliminary seismic evaluation form. Approximately it took 5 months to complete field examination of each individual selected facility in west Tennessee. The itemized seismic score of each evaluation factor of the facilities is also documented for future reference. The results of the evaluation reveal the technical integration of design and construction of the existing facilities in the region in terms of earthquake resistance.

Preliminary Results

Results of the field works are being organized and analyzed. Comparing with the results of the evaluations in the Shelby County, Tennessee, we anticipate some differences among the facilities between the two study areas. In average, many of the facilities were inadequately designed and constructed for seismic resistance in this earthquake-prone area. Relatively speaking, general conditions of the evaluated bridges and hospitals may be more vulnerable to earthquake in West Tennessee than in the Memphis area. From the field observations, the following are noted:

(1) Most of the evaluated school structures were constructed of unreinforced concrete block with brick as an external veneer.
(2) One of the major types of construction of the evaluated fire stations is wood frame built on shallow foundation (trench and slab-on-grade) without adequate considerations in earthquake resistance. A good number of the evaluated fire stations is constructed of unreinforced concrete block.
(3) The major structural types of hospitals include unreinforced concrete block, steel frame, and reinforced concrete.
(4) A number of evaluated bridges have wood pile/pier supporting the main span steel and/or concrete girders. This kind of mixed mass and stiffness in a bridge is a major concern for earthquake risks.

Development and application of Geographic Information System (GIS)

Interpretation of GIS on essential facilities in the previous study for the Shelby County proves to be very useful, therefore, we apply the GIS to the current study. This GIS consists of digitized spatial information and attribute file of each evaluated facility. GIS has the capability to overlay, compare, and analyze several maps in digital form with speed and efficiency, and is convenient and productive in data management. It is easy to produce special purpose maps at selected scale and tabular analysis reports. There are many potential applications of the developed

GIS in earthquake engineering, regional seismic emergency management, and others. The two applications being conducted as part of the project are (1) 3-D computer model for facility evaluation and seismic hazard maps and soil data management, and (2) regional emergency management such as optimal route selection between schools and designated hospital under various emergency scenarios.

Reports

The first year of the project produced one technical report and four technical paper as follows:

(1) Chang, T.S., Kung, H.T., Pezeshk, S. and Yiak, K.C. (1992) "Inventory and Preliminary Vulnerability Assessments of Essential facilities in Memphis and Shelby County." CERI technical report submitted to the USGS, April, 1992.
(2) Chang, T.S., Kung, H. T. and Pezeshk, S. (1992) "Application of GIS in Seismic Evaluation of Essential Facilities." Paper accepted to be published in International Journal of Computer Application in Engineering.
(3) Pezeshk, S., Chang, T.S, Yiak, K.C. and Kung, H.T. (1992) " Seismic Vulnerability Evaluation of Bridges in Memphis and Shelby County." Pending, Professional Journal of Earthquake Engineering Research Institute, Earthquake Spectra.
(4) Chang, T.S, Pezeshk, S., Yiak, K.C. and Kung, H.T. (1992) " Seismic Vulnerability Evaluation of Essential Facilities in Memphis and Shelby County." Pending, Professional Journal of Earthquake Engineering Research Institute, Earthquake Spectra.

The final report of the project for FY 1992 and technical papers resulting from the project will be prepared for publication in 1992-1993. The final report of the project will be submitted to the USGS as indicated in the proposal.

NATIONAL STRONG-MOTION INSTRUMENTATION NETWORK

9910-02764, 9910-02765

Ed Etheredge, Ron Porcella, and Dick Maley

Branch of Engineering Seismology and Geology
NATIONAL STRONG-MOTION PROGRAM
345 Middlefield Road, MS 977
Menlo Park, California 94025
(415) 329-5667

Investigations

The National Strong-Motion Program (NSMP) in cooperation with federal, state, and local agencies and advisory engineering committees, designs, develops, and operates an instrumentation network in 41 states and Puerto Rico. Program goals include: (1) recording of potentially damaging ground motion in regional networks, and in closely spaced sensor arrays; and (2) monitoring the structural response of buildings, bridges and dams using sensors placed in critical locations. The present cooperative network consists of approximately 1,000 recording units installed at 620 ground sites, 30 buildings, 5 bridges, 56 dams, and 2 pumping plants.

New Instrumentation

Structures - extensive instrumentation

1) 42-story steel frame building in San Francisco. Twelve data channels added to existing 12-channel system. Instrumentation updated with digital recorders and new acceleration sensors.

2) 43-story steel frame building in St. Louis, MO. Twelve data channels in the structure with digital recorders and a nearby triaxial ground motion recorder.

3) 4-story reinforced concrete Palo Alto VA Hospital. Twelve channels in the structure with digital recorders and a nearby triaxial ground motion recorder.

Landslide arrays

1) Chantry Flat Forest Station near Los Angeles. Three triaxial acceleration sensors located on and off of the slide and two extensometers, with all data transmitted to digital recorders

2) La Honda near San Francisco. Two triaxial acceleration sensors located on and off of the slide, two extensometers, and three piezometers, with all data transmitted to digital recorders.

Ground stations

1) Stanford Linear Accelerator	2
2) Richmond, CA	1
3) Pasadena - USGS	1
4) Los Angeles	1
5) Lake Success - Corps of Engineers	1
6) Sepulveda, CA, VA Hospital	1
7) Palo Alto, CA, VA Hospital	1
8) St. Louis, MO	1
9) CA Landslide arrays	2

Seismic Alarm Devices - acceleration threshold monitors with integrated alarm indicators.

Installed at Corps of Engineers facilities in the following states

Arizona	1
California	7
Idaho	1
Montana	1
Washington	4

Earthquake Records

1) Petrolia, California ML = 6.9 4/25/92
9 ground motion records
Peak ground acceleration, .49 g at Centerville

2) Joshua Tree, California ML = 6.1 4/22/92
> 45 records
Peak ground acceleration, .53 g at Fun Valley

3) Landers, California M = 7.5 6/28/92
> 170 records
Peak ground acceleration, .29 g at Indio

4) Big Bear, California M = 6.5 6/28/92
>150 records
Peak ground acceleration, .30 g at Forest Falls

Projects in planning or underway

1) Hawaii
Five ground motion stations to be installed in cooperation with the state of Hawaii Office of Civil Defense and the Structural Engineering Association.

2) Olympia

Install digital, 13-channel structural instrumentation system in the new Natural Resources building in Olympia in cooperation with the Washington State Division of Geology.

3) Alaska

3 new ground stations in Fairbanks in cooperation with the Univ. of Alaska.

3 new ground stations in Anchorage in cooperation with the Borough's Geotechnical Advisory Committee.

4) Oregon

Instrument four bridges (one base isolated) with the Oregon Department of Transportation.

5) San Francisco

Plan and install 36 sensor digital recording system in the U.S. Court of Appeals and Post Office building under renovation, including a base isolation system.

6) Ground motion arrays under further development

White Mountain gap Nevada (with UNR)
Northwest Nevada Region
San Bernardino, CA
San Francisco Bay Area, CA
Seattle, WA (with advisory committee)

Reports:

CATALOGUE OF U.S. GEOLOGICAL SURVEY STRONG-MOTION RECORDS, 1989, USGS Circular 1084, J.C. Switzer and R.L. Porcella, 34 p.

CATALOGUE OF U.S. GEOLOGICAL SURVEY STRONG-MOTION RECORDS, 1990, USGS Circular 1093, J.C. Switzer and R.L. Porcella, 24 p.

U.S. GEOLOGICAL SURVEY STRONG-MOTION RECORDS FROM THE NORTHERN CALIFORNIA (PETROLIA) EARTHQUAKE OF APRIL 25, 1992, Preliminary report, National Strong-Motion Program Staff, 7 p.

U.S. GEOLOGICAL SURVEY STRONG-MOTION RECORDS FROM THE SOUTHERN CALIFORNIA (JOSHUA TREE) EARTHQUAKE OF APRIL 23, 1992, Preliminary report, National Strong-Motion Program Staff, 8 p.

SELECTED ACCELEROGRAMS FROM U.S. GEOLOGICAL SURVEY STATIONS THAT RECORDED THE LANDERS (YUCCA VALLEY) AND BIG BEAR EARTHQUAKES OF JUNE 28, 1992, Preliminary report, National Strong-Motion Program staff, 13 p.

SITE RESPONSE AND SEISMIC HAZARD IN PROVIDENCE, RHODE ISLAND

Agreement No. 1434-92-G-2166

Karen M. Fischer
Department of Geological Sciences
Brown University
Providence, Rhode Island, 02912

401-863-1360

Susan E. Hough
U. S. Geological Survey
525 S. Wilson Ave.
Pasadena, California, 91106

818-405-7224

Many heavily populated coastal cities in the northeastern United States are built on bedrock valleys filled with partially unconsolidated Holocene sediments. In this study we assess the potential for seismic site response in typical glacial valleys that lie beneath Providence, Rhode Island.

Ground Motion Observations

We deployed portable seismic instruments at 8 sites within Providence. Seven stations were located in two sediment-filled bedrock valleys that intersect beneath downtown Providence, and one was on an adjacent bedrock highland with minimal sediment cover. We recorded ground motion from two types of sources: pile-drivers at a local construction site and ambient microtremors. Data were collected in 9 minute windows over a two-day period, using Kinemetrics 5 s sensors and EDA PRS-4 recorders.

At valley sites we found peaks in both pile-driver and ambient microtremor frequency spectra in the range of 2.0-3.5 Hz. In contrast, recordings from the bedrock reference site contain little energy in this frequency range. While the spectral shapes and amplitudes at each site are approximately uniform in time for frequencies of 5 Hz and less, at frequencies of 5 Hz and more, the pile-driver spectral patterns contain regularly spaced large amplitude peaks that are quite distinct from the microtremor spectra. These observations argue that the 2.0-3.5 Hz peak is a robust feature of ambient noise in the valleys and is not sensitive to the details of local noise sources. Because the 2.0-3.5 Hz peak is observed at the valley stations but not at the bedrock reference site, it may be explained by resonance within the valley sediment columns.

Modeling Sediment Resonance

We constrained the geologic structure beneath our study area with 147 borehole logs from four recent construction projects and 43 older borehole and well-log measurements compiled by the U.S. Geological Survey. These data yield a detailed three-dimensional map of bedrock depth and identify two sediment layers: a mixture of unconsolidated artificial fill and fluvial sediments on top of thin lenses of consolidated glacial till.

In order to obtain a quantitative estimate of sediment and bedrock velocity structure, we collected data over two 12-sensor refraction lines. The first recorded a pile-driver hit at distances of 340 to 400 m, and the resulting travel-times indicate a bedrock P-wave velocity of 3500 ± 800 m/s. Bedrock beneath the entire study area and adjacent highland is a sandstone/conglomerate [*Bierschenk*, 1959]. The second refraction line recorded stacked sledge-hammer hits at distances of 1 to 96 m. These travel-times indicate an average sediment P-wave velocity of 1440 ± 100 m/s.

We compared the spectra observed at each site to the resonances predicted by models containing a layer of sediment over bedrock. Depth to bedrock was determined by borehole data at or adjacent to each site. Precise S-wave velocities were not constrained observationally, but for the bedrock we assumed a Poisson's ratio of 0.25, and assigned the S-wave bedrock velocity a value of 2020 m/s. Sediment velocities were allowed to vary from 350 to 450 m/s. To compute the theoretical response of the sediment column, we used the one-dimensional reflection matrix technique of Kennett and Kerry [1979]. The 2.0-3.5 Hz spectral peak observed at each site is matched by the frequency of fundamental resonance predicted for the sediment layer. Slightly higher sediment velocities are required at sites of greater bedrock depth (45-50 m). This result may reflect real variation in sediment velocity, or the effects of two-dimensional basin structure [e.g. *Bard and Bouchon*, 1985].

If earthquake site response is similar to the basin resonances apparently excited by pile-drivers and microtremors, the unconsolidated sediment layers under downtown Providence have the potential to amplify earthquake ground motion at frequencies that are potentially damaging to 2-5 story buildings and other engineered structures.

References

Bard, P.-Y. and M. Bouchon (1985). The two-dimensional resonance of sediment-filled valleys, *Bull. Seism. Soc. Am.* **75**, 1985.

Bierschenk, W. H. (1959). Ground-water resources of the Providence Quadrangle, Rhode Island, *Rhode Island Geological Bulletin 10*, Rhode Island Water Resources Coordinating Board.

Kennett, B. L. N. and N. J. Kerry (1979). Seismic waves in a stratified half space, *Geophys. J. R. astr. Soc.* **57**, 557-583.

Publications

Fischer, K. M., and S. E. Hough (1992). Site response in Providence, Rhode Island: Constraints from ambient noise measurements, *Seis. Res. Lett.*, in press.

Gonzalez, E., K. M. Fischer, S. E. Hough, C. Nelsen, and X. Yang (1992). Site Response in Sediment-filled Glacial Valleys: A Case Study from Providence, RI, Trans. Am. Geophys. Union. **73**, 338.

Prediction of Strong Ground Motion in Sedimentary Basins Using Numerical Simulations

9910-04482

A. Frankel

Branch of Engineering Seismology and Geology
U.S. Geological Survey
345 Middlefield Rd., MS 977
Menlo Park, CA 94025
(703) 648-4119

Investigations

1. Study seismic wave propagation in realistic, three-dimensional models of sedimentary basins using numerical simulations, to evaluate seismic shaking in such basins from future large earthquakes.

2. Analyze data from 14 GEOS seismic recorders deployed in the San Bernardino Valley to record aftershocks of the Landers-Big Bear earthquake sequence. Three dense arrays with apertures of about 200m were deployed to measure the direction of propagation and apparent velocity of seismic waves propagating in the valley.

Results

1. To date, I have simulated ground motions in two sedimentary basins using a 3-D finite difference program. 3-D models were developed for the Santa Clara and San Bernardino valleys based on water well data and, where available, seismic refraction results. The first simulation considered ground motions in the Santa Clara Valley for a magnitude 4.4 aftershock of the Loma Prieta earthquake. This simulation showed the conversion of incident S-waves to Love waves along the southern margin of the valley. These surface waves greatly increase the amplitude and duration of shaking within the valley. They were observed in recordings of this aftershock from the Sunnyvale dense array. The simulation shows large amplitudes where Rayleigh waves impinge on the northeast edge of the valley. In the simulations, some of this Rayleigh wave energy is reflected westward across the valley.

I have also simulated motions in the San Bernardino Valley for hypothetical magnitude 5 and 6.5 earthquakes along the San Andreas Fault. The simulations show that the basin efficiently traps seismic waves. The anelasticity of the alluvium will likely be the key factor controlling the duration of shaking in the valley. The simulations

demonstrate that surface waves are reflected back into the basin as they impinge on the edges of the basin. The location of the largest velocities in the basin is sensitive to the direction of rupture propagation, radiation pattern, and asperity position.

2. The recordings of the Landers-Big Bear aftershocks provide insights on the seismic response of the San Bernardino Valley. A Big Bear aftershock with M4.9 produced motions in the valley with periods of about 2 sec that were sustained for about 60 sec. Array analysis indicates that these motions are mostly surface waves travelling from a direction different from the source. This observation implies that future large earthquakes near San Bernardino could excite damaging ground motions (periods 1-2 sec) with duration of over 60 sec. A 3-D simulation for another Big Bear aftershock produces seismograms that are more similar to the observed duration and spectral ratios than synthetics derived from a 1-D (flat-layered) model.

Reports

Frankel, A., Three-dimensional simulations of ground motions in the San Bernardino Valley, California, for hypothetical earthquakes on the San Andreas Fault, submitted to *Bull. Seism. Soc. Am.,* 1992.

Frankel, A., S. Hough, G. Glassmoyer, E. Sembera, C. Dietel, and L. Hwang, Seismic response of the San Bernardino Valley to Landers-Big Bear aftershocks: implications for seismic hazard to buildings, *EOS Trans. Amer. Geophys. Union,* v. 73, p. 382, 1992.

Frankel, A. and J. Vidale, A three-dimensional simulation of seismic waves in the Santa Clara Valley, California, from a Loma Prieta aftershock, *Bull. Seism. Soc. Am.,* v. 82, 2045-2074, 1992.

Frankel, A., L. Hwang, and G. Coats, Three-dimensional simulations of ground motions in the San Bernardino and Santa Clara valleys, California, from earthquakes on the San Andreas Fault, *EOS Trans. Amer. Geophys. Union,* v. 72, p. 339, 1991.

Frankel, A., S. Hough, P. Friberg, and R. Busby, Observations of Loma Prieta aftershocks from a dense array in Sunnyvale, California, *Bull. Seism. Soc. Am.,* v. 81, 1900-1922, 1991.

Mori, J. and A. Frankel, Depth dependent scattering shown by coherence estimates and regional coda amplitudes, *EOS Trans. Amer. Geophys. Union,* v. 71, p. 344, 1991.

STRONG GROUND MOTION STUDIES IN THE OLYMPIA, WASHINGTON AREA

Agreement No. 14-08-0001-A0509

Wendy J. Gerstel and Stephen P. Palmer
Washington Division of Geology and Earth Resources
P.O. Box 47007
Olympia, WA 98504-7007
(206) 902-1450

INTRODUCTION

A multidisciplinary approach is being used to study the distribution of strong ground shaking from earthquakes in the vicinity of Olympia, Washington. The primary objective of the investigation is to provide a hazard zonation map delineating areas exhibiting significant earthquake ground motion amplification. Methods of investigation incorporate map compilation and field verification of the distribution of late glacial and glaciolacustrine sediments, data from water well logs and geotechnical borings, and down-hole shear wave logging. The investigation is based on the premise that historically strong ground shaking (and associated damage) experienced in the 1949 and 1965 Puget Sound earthquakes corresponds to areas underlain by thick accumulations of poorly consolidated upper Pleistocene glacial lake and associated fluvial deposits.

Olympia experienced significant damage during the 1949 and 1965 Puget Sound earthquakes. Mercalli intensity VIII effects were common during the 1949 event, and intensity VII effects were reported during the 1965 event. A strong-motion accelerometer situated in the downtown Olympia area registered a peak ground acceleration (PGA) exceeding 0.30 g in 1949. During the 1965 earthquake a PGA of 0.20 g was measured in Olympia at an epicentral distance of approximately 90 km. Strong-motion accelerometers in Seattle and Tacoma (epicentral distances of 65 km) registered only a 0.08 g PGA. Clearly the Olympia accelerometer data is influenced by significant local ground-motion amplification effects.

PRESENT INVESTIGATION

Four basic tasks constitute the multidisciplinary approach to the project. The first is to define the surface and subsurface distribution of Quaternary stratigraphic units and Tertiary bedrock through field observations and compilation of existing and new drilling information, including three borings recently drilled as part of this investigation. These holes penetrated earlier Pleistocene consolidated sands and clays, later Pleistocene advance(?) and recessional(?) weakly consolidated sands and gravels, and latest Pleistocene deltaic sands and silts, and Holocene Deschutes River flood sediments, respectively. The second project task is measuring shear wave velocities in these recently drilled borings to obtain characteristic shear velocities within these stratigraphic units.

A third task assimilates the field information to establish geologically constrained shear velocity profiles with which to model ground motion amplification using the computer program SHAKE. In the fourth and final task the results of the computer modeling are compared to the historic distribution of elevated Mercalli intensities from the 1949 and 1965 earthquakes. Comparison will also be made to areas of significant small-strain ground motion amplification documented by King and others (1990) in the Olympia area.

RESULTS

Detailed mapping to date has revealed extensive exposures of massive and laminated sands, silts, and gravels in areas of Olympia previously mapped as Vashon recessional outwash by Noble and Wallace (1966). From the observation of foreset beds as well as the character of the deposits we attribute these sediments to glaciolacustrine deposition (primarily deltaic) rather than outwash. The primary dip of the foreset beds is towards the north, indicating northward flowing currents and a sediment source from the south. Outwash originating from the continental ice sheet would have been transported from the north in southward flowing drainage systems.

Thick sequences (greater than 50') of homogenous gray sands and gravelly sands are exposed in the Deschutes River banks as well as in the drill hole penetrating the sediments underlying the adjacent flood plain. Although Bretz believed the Deschutes River to be a minor stream carrying no glacial sediments into Lake Russell (Bretz, 1913), we believe quite the opposite. The thickness and character of the sediments in this area suggest that the Deschutes River may have been a major source of sediment into the Lake Russell basin in the vicinity of Olympia. We have seen similar, but slightly coarser, deltaic sequences along Woodland Creek in the Lacey area that may have originated from a different drainage system to the southeast.

The existence of these glaciolacustrine sediments is consistent with earlier theories that ice blocked drainage to the north creating Lake Russell (Bretz, 1910) and adjoining lakes to the south of the ice terminus. The fluctuating lake levels and shifting drainages allowed for the deposition of deltaic deposits up to an elevation of approximately 160-180' (Bretz, 1913).

Existing shear wave velocity data in the Puget Sound suggest that Quaternary deposits that have been overridden by the Fraser and earlier Pleistocene glaciations typically have velocities of 3000 ft/sec and greater. These high-velocity sediments are effectively bedrock with regard to overlying soil-column amplification of earthquake ground motions. The shear velocity contrast between these consolidated Pleistocene deposits and the underlying Tertiary bedrock has not been established. Late- and post-glacial deposits in the Olympia area have shear velocities ranging from 500-1750 ft/sec. We have concluded that the extent and thickness of these deposits will be important factors in determining areas with significant shallow ground motion amplification. Preliminary correlation of 1949 and 1965 Mercalli intensity data with the late- and post-glacial geology suggests that the areas of strongest ground shaking occur where the thickness of these deposits exceeds 100-200 ft.

Ihnen and Hadley (1987) used 3-D ray tracing to model the distribution of strong ground motion from the 1965 Seattle earthquake. Their model worked well where they incorporated

depth to bedrock data, but was unsuccessful where these data were lacking (i.e, the Olympia area). Their work suggested that strong shaking in the West Seattle-Lower Duwamish Valley area (delineated by areas of significant building damage and ground failures) was primarily due to the steeply sloping bedrock interface beneath this area. Although a similar dipping bedrock interface exists beneath the Olympia area, the localized nature of heightened ground shaking (as determined by Mercalli intensity data) suggests that amplification may have a near-surface origin.

REFERENCES

Bretz, J. H.; 1910, Glacial lakes of Puget Sound: Journal of Geology, v. 18, no. 5, p. 448-458.

Bretz, J. H.; 1913, Glaciation of the Puget Sound region: Washington Geological Survey, Bulletin No. 8, 244 p.

Ihnen, S. M.; Hadley, D. M., 1987, Seismic hazard maps for Puget sound, Washington: Seismological Society of America Bulletin, v. 77, no. 4, p. 1091-1109.

King, K. W.; Tarr, A. C.; Carver, D. L.; Williams, R. A.; Worley, D. M., 1990, Seismic ground response studies in Olympia, Washington, and vicinity: Bulletin of the Seismological Society of America, v. 80, no. 5, p. 1057-1078.

Noble, J. B.; Wallace, E. F., 1966, Geology and ground-water resources of Thurston County, Washington; Volume 2: Washington Division of Water Resources Water-Supply Bulletin 10, v. 2, 141 p., 5 plates.

Near-Surface Lithologic and Seismic Properties

9910-01168

J.F.Gibbs
W.B.Joyner
Branch of Engineering Seismology and Geology
U.S.Geological Survey
345 Middlefield Road, MS 977
Menlo Park, California 94025
(415)329-5631 or (415)329-5640

Investigation :

Measurement of seismic velocity and attenuation to determine the effect of local geology on strong ground motion and to aid in the interpretation of seismic source parameters.

Results :

1. P- and S-wave measurements have been made in boreholes at seven locations in the Los Angeles area as part of a study of the Whittier Narrows earthquake ground motions (Mueller, Tinsley, and Rogers, USGS). Measurements were made at 2.5 meter intervals in boreholes that range in depth from 30 to 90 meters.

2. P- and S-wave measurements have also been made at Embarcadero Plaza in San Francisco California where downhole accelerometers are being installed (Borcherdt, USGS). Measurements were made at 2.5 meter intervals, in two boreholes to a depth of 45 and 80 meters.

3. We continue to study the attenuation effects of Quaternary alluvium using borehole measurements at strong-motion station Gilroy #2 located near the town of Gilroy, California. Q_s values determined, using spectral ratios and amplitude decay methods, are near 10 for the upper 115 meters of alluvium of Santa Clara Valley, California. A paper will be submitted to BSSA.

Reports :

Gibbs, James F., Thomas E. Fumal, David M. Boore, and William B. Joyner (1992). Seismic velocity and geologic logs from borehole measurements at seven strong-motion stations that recorded the Loma Prieta earthquake, U.S. Geological Survey Open-file Report 92-287.

Gibbs, James F., (1992). The attenuation of seismic shear waves in Quaterary alluvium from borehole measurements and local earthquakes, Santa Clara Valley, California, Seism. Res. Letters, 63 1, 1992.

Seismic Slope Stability

9950-70075

Edwin L. Harp
Randall W. Jibson
Branch of Geologic Risk Assessment
U.S. Geological Survey
Box 25046, MS 966
Denver, Colorado 80225

Raymond C. Wilson
David K. Keefer
Branch of Geologic Risk Assessment
U.S. Geological Survey
345 Middlefield Road
Menlo Park, California 94025

Investigations undertaken:

Loma Prieta Earthquake

Landslides and coseismic fractures have been mapped, investigated, and analyzed within the epicentral area of the 1989 Loma Prieta, California, earthquake. Slope stability analyses, trenching studies of landslide scarps and coseismic fractures, and monitoring of post-earthquake slope movements as part of a FEMA funded, U.S. Army Corps of Engineers study has been overseen in an advisory capacity to evaluate the present and future hazard to residents within the epicentral area. Efforts within the past year have been concerned with finalization and completion of the multi-disciplinary report.

Rockfall Susceptibility

Criteria for seismic rockfall susceptibility have been developed for both regional and site-specific application. Regional criteria have been formulated to allow slopes and materials to be categorized in a generalized regional sense to provide for large area overview in terms of the potential hazard from rockfall hazard. Site specific criteria have been developed and calibrated against past earthquake-triggered rockfalls to provide means to assess relative probabilities of rockfall generation in future earthquakes. This criteria is based upon rock-mass fracture characteristics that can be rapidly assessed and plotted allowing rockfall susceptibility of large areas to be evaluated and statistically compared.

Instrumentation Sites

Two sites, one in the San Francisco Bay area and one in the greater Los Angeles area have been selected in which instruments have been deployed to collect strong-motion, displacement, and pore-pressure data from active landslides likely to be reactivated in a future earthquake. Surface accelerometers have been installed both on and off the landslide masses, pore-pressure transducers (piezometers) within the slide masses below the water table, and extensometers across headwall scarps and lateral shear surfaces of the slides. During future earthquakes, surface accelerations, pore-water pressures, and displacements will be recorded simultaneously. The successful recording of such data will greatly enhance

the understanding of the physics of the interaction between seismic inertial forces and the landslide-triggering and movement process.

A site in the Santa Cruz Range near La Honda, California has been instrumented to record future earthquake effects on a landslide within the San Francisco Bay area. The landslide selected was one that showed slight displacement (0.5 cm) along its lateral shear surfaces in response to the Loma Prieta earthquake. In southern California, a site at Chantry Flat north of Santa Anita Canyon on a deep-seated landslide mass that was reactivated (≈ 15 cm displacement in its lower midsection) in the 1991 Sierra Madre earthquake has been instrumented. The site at Chantry Flat has been instrumented with three accelerometers, one on the landslide reactivated during the 1991 Sierra Madre earthquake, one on the ancient surrounding landslide mass, and one on stable bedrock. Two extensometers have been deployed across the 1991 scarp. Bedrock conditions at the site precluded installation of piezometers and inclinometer casing with existing in-house drilling capabilities. These will be installed as a cooperative part of the external NEHRP program if outside investigators are successful in obtaining funds.

The La Honda site has been instrumented with two surface accelerometers, one on the slide mass and one adjacent to it on stable ground, four piezometers at various depths, and two extensometers, all to be recorded simultaneously after being triggered by a seismic event. Other piezometers and displacement meters recording on a long term basis (to be installed in the future) will provide displacement and pore-pressure data for several hours or days after shaking stops.

Paleoseismicity

More than 200 landslides in the New Madrid seismic zone have been analyzed from several perspectives. Most recently, we analyzed the results of detailed geological and geotechnical site investigations of two representative landslides to determine the likely conditions leading to failure.

Results obtained:

Loma Prieta Earthquake

Work has been completed on an open-file report documenting the landslides and coseismic fractures triggered by the 1989 Loma Prieta, California, earthquake and assessing the present and future landslide hazard to residents within this area. Work is nearing completion on a multi-article professional paper chapter documenting and interpreting these effects.

Rockfall Susceptibility

Reports on regional and site-specific criteria have been completed and submitted for publication. These criteria provide methods to assess and evaluate the seismic rockfall potential on a regional basis (for example, within a county) and on a site specific basis (for example, whithin rock cliffs next to a potential development site or along a highway right-of-way). These criteria will give engineers and planners useful tools with which to assess seismic rockfall hazard and to make development and zoning decisions.

Instrumentation Sites

Sites have been selected in both the San Francisco Bay area and in southern California close to active faults likely to generate at least a magnitude 5-6 earthquake within the next ten years. The equipment was installed during summer 1992. The accelerometers at Chantry Flat in southern California were triggered by the Landers, California, earthquake of June 28, 1992 and have all produced records. Ground motion at Chantry Flat during this earthquake was not sufficiently large to produce measurable displacements within the instrumented landslide mass.

Paleoseismicity

We have developed an approach for determining if old landslides of unknown origin were more likely to have formed seismically or aseismically. A static stability analysis of aseismic conditions is conducted to determine if failure could have occurred under any reasonable set of conditions, such as ground-water fluctuations. If aseismic failure can be reasonably ruled out, a dynamic analysis using Newmark's sliding-block method is conducted to determine the minimum shaking conditions required to cause the observed failure. Such analyses can thus ascertain if a landslide was seismically triggered and, if so, the likely shaking conditions leading to failure. We also developed a general empirical relationship between landslide displacement, earthquake shaking intensity, and the dynamic stability of a landslide, as measured by its critical acceleration. This relationship is applicable in paleoseismic studies: if an old landslide can be shown to have been seismically triggered, and if the landslide movement can be dated, the date and shaking intensity of the triggering earthquake can be estimated. This approach also has application in seismic hazard analysis: the performance of slopes of known stability can be estimated under a postulated set of shaking conditions.

Reports Published:

Harp, Edwin L., and Noble, Marlene A., (in press), An engineering rock classification to evaluate seismic rock-fall susceptibility and its application to the Wasatch Front: Association of Engineering Geologists Bulletin, 49 ms. p., 19 figs., 5 tables.

Harp, Edwin L., (in press), Origin of fractures triggered by the earthquake in the Summit and Skyland Ridge areas and their relation to landslides, in Keefer, David K., ed., The Loma Prieta, California, Earthquake Of October 17, 1989: U.S. Geological Survey Professional Paper (Chapter on Landslides and Stream Channel Change), 36 ms. p., 13 figs., 1 pl.

Keefer, D. K., Griggs, G.B., and Harp, E.L.,(in press), Large landslides in the Summit Ridge area, Santa Cruz, California, in Keefer, David K., ed., The Loma Prieta, California, Earthquake Of October 17, 1989: U.S. Geological Survey Professional Paper (Chapter on Landslides and Stream Channel Change), 71 ms. p., 39 figs.

Keefer, D.K., and Manson, M.W., (in press), Landslides produced by the 1989 Loma Prieta, California, earthquake--Regional distribution and characteristics, in Keefer, David K., ed., The Loma Prieta, California, Earthquake Of October 17, 1989: U.S. Geological Survey Professional Paper (Chapter on Landslides and Stream Channel Change), 49 ms. p., 16 figs., 3 pl.

Keefer, David K., 1992, The susceptibility of rock slopes to earthquake-induced failure, in Stout, Martin L., ed., Proceedings of the 35th Annual Meeting Association of Engineering Geologists 1992, p. 529-538.

Jibson, R.W., and Keefer, D.K., 1992, Analyzing the origin of landslides in the New Madrid seismic zone, *in* Stout, M.L., ed., Proceedings of the 35th Annual Meeting of the Association of Engineering Geologists, p. 521-528.

Jibson, R.W., and Keefer, D.K., 1992, Analysis of the seismic origin of a landslide in the New Madrid seismic zone: Seismological Research Letters, v. 63, no. 4 [in press].

Jibson, R.W., and Keefer, D.K., 1993, Analysis of the seismic origin of landslides—examples from the New Madrid seismic zone: Geological Society of America Bulletin, v. 105 [in press].

Jibson, R.W., and Keefer, D.K., Analysis of the origin of landslides in the New Madrid seismic zone, *in* Shedlock, K.M. and Johnston, A.C., eds., Investigations of the New Madrid Seismic Zone: U.S. Geological Survey Professional Paper [accepted].

Jibson, R.W., Prentice, C.S., Langer, C.J., Rogozhin, E.A., and Borissoff, B.A., The 29 April 1991 Racha earthquake in the Republic of Georgia—seismology, structural damage, and ground failure: Seismological Society of America Bulletin [submitted—in review].

Jibson, R.W., Predicting earthquake-induced landslide displacements using Newmark's sliding block analysis: Transportation Research Record [accepted].

Hazard Potential and Paleoseismic Implications of Liquefaction-Induced Landslides Along the Wasatch Front, Utah

Agreement No. 14-08-0001-G2058

Kimm M. Harty, Mike Lowe, and Gary E. Christenson
Utah Geological Survey
2363 S. Foothill Dr.
Salt Lake City, Utah 84109

(801) 467-7970

BACKGROUND AND SUMMARY OF OBJECTIVES

Thirteen late-Pleistocene/Holocene liquefaction-induced landslides have been identified along the Wasatch Front by previous researchers. The goal of this study is to further constrain the timing of these landslides, to determine if they have experienced recurrent movement, and to evaluate their hazard potential. If recurrent movement can be shown, local governments are more likely to consider this in development on these features, or look for an area-wide mitigation strategy to reduce the risk. A further objective, identified during the course of the study, is to determine whether some of these 13 features may, in fact, be related to other processes such as differential subsidence or other effects of a fluctuating shallow water table and artesian conditions. Techniques used to investigate the features include air-photo interpretation, geologic and geomorphic mapping, and trench excavations. All radiocarbon dates are from standard radiocarbon dating of bulk soil samples. The dates were calendar calibrated (Stuiver and Reimer, 1986) and rounded to the nearest decade. Where appropriate, we subtracted 300 years from radiocarbon ages prior to calendar calibration to account for the mean residence time of carbon in the buried soil.

INVESTIGATIONS UNDERTAKEN

Geomorphic mapping at 1:10,000 or 1:20,000 scales and reconnaissance field checking was completed for all the landslides. Both internal geomorphic features such as shear scarps, ridges, hummocks, and depressions, and external regional features such as river terraces, deltas, and major and minor shorelines of Lake Bonneville were mapped.

Eleven excavations were completed on the following five landslides: "North Ogden" (Weber County); "North Salt Lake" and "Farmington Siding" (Davis County); and "Springville/Spanish Fork" and "Beer Creek" (Utah County). The trenches were logged and bulk soil samples were taken for radiocarbon dating. Only three trenches (one on the North Ogden landslide and two on the Farmington Siding landslide) contained evidence for liquefaction

and material suitable for radiocarbon dating. Cities and counties in the landslide areas cooperated in the investigations by providing backhoes for the trench excavations.

RESULTS OBTAINED

Box Elder County Landslides

Six areas of lateral-spread or flow landslides were mapped in Box Elder County (Oviatt, 1986a,b; Personius, 1988). Most of these landslides were inferred to have occurred approximately 12,000-13,000 years ago, based on undeformed lacustrine shorelines that cut the surfaces of the slope failures at approximately 1,347-1,353 m elevation (Oviatt, 1986a,b; Personius, 1988). Geomorphic mapping suggests that most of these landslides are rotational slumps or complex landslides, rather than liquefaction-induced lateral spreads or flow slides. Most of the main scarps of the landslides are on steep slopes, and some of the failures have multiple back-tilted minor scarps characteristic of slumps. Most of the failures formed in Lake Bonneville gravels, and many of the deposits consist of isolated knolls of gravel that lie on undisturbed finer lake sediments, suggesting that the slope failures flowed or spread out into the lake.

Because most of these landslides are cut by a single Lake Bonneville shoreline, they were likely synchronous events, perhaps triggered by an earthquake as proposed by Oviatt (1986a,b). However, it may be that these landslides are simply earthquake-induced landslides rather than liquefaction-induced landslides. No evidence of liquefaction was observed in exposures of the landslide deposits, but this does not preclude its existence. Tilted bedding was observed in some stratified sand and gravel deposits, but this can be explained by slumping of landslide blocks. Because the landslides occur on steep slopes, liquefaction is not necessary to account for the failures.

North Ogden Landslide

The approximately 30 km^2 North Ogden lateral spread was first identified by Miller (1980), and subsequently mapped in parts by Personius (1988) and Nelson and Personius (1990), but little information was available regarding the age of this landslide. We excavated two trenches into the North Ogden landslide. Stratigraphic relationships in a trench placed across the main scarp suggest that the landslide likely failed as a flow slide rather than as a lateral spread. A second trench excavated into a hummock on the main body of the landslide showed evidence of liquefaction and a means to constrain the timing of at least one liquefaction event. In this trench, we found numerous sand-filled fractures in fine-grained mud-flow, or possibly flow-slide deposits that post-date the Lake Bonneville cycle. We believe the sand was injected into fractures due to liquefaction during an earthquake. Radiocarbon dates on of the buried soils constrains the date of

occurrence of the liquefaction event as sometime after 7,860 [± 250] cal. yr B.P.

Severely deformed and contorted bedding was also observed in the trench that may be related to as many as two liquefaction-induced flow slides. The first of these flows occurred prior to 7,860 [± 250] cal. yr B.P. The second flow, which contained isolated blocks of stratified Lake Bonneville sediments, occurred after 7,860 [± 250] cal. yr B.P. but sometime prior to 3,390 [± 230] cal. yr B.P.

East Ogden landslide

Faults, tilted beds, and sand dikes exposed in trenches on the East Ogden landslide at Weber State University were first described by Pashley and Wiggins (1972). They attributed the features to a large translational landslide similar to the Turnagain Heights landslide that occurred during the 1964 Anchorage, Alaska, earthquake. Woodward-Clyde Consultants (1985) examined faults exposed in a building excavation on a scarp at the Weber State University campus and determined that the faults may represent seismically-induced slumping or lateral spreading, or gravity-induced subaqueous landsliding that may have occurred when the level of Lake Bonneville was high and the deposits were saturated. This event occurred prior to the deposition of Provo-age nearshore sands about 11,000-13,000 years ago, as the sands were exposed in the foundation excavation and were not faulted (Woodward-Clyde Consultants, 1985). Nelson and Personius (1990) mapped this scarp as the main scarp of the East Ogden landslide, but concluded that parts of the landslide postdate the Provo shoreline whereas other parts probably predate the Bonneville shoreline. The East Ogden landslide is heavily urbanized, and we were unable to identify a trench site that would help determine the age(s) of the landslide.

West Kaysville Landslide

This feature is west of the city of Kaysville, and was first mapped as a lateral-spread landslide by Miller (1980). Anderson and others (1982) also mapped the landslide as a failure by lateral spreading, and recognized a poorly developed Gilbert shoreline cut across its surface. The landslide is buried on the northwest and southeast margins by alluvial-fan sediments, and has a main scarp that is difficult to distinguish in the field, but that is visible on 1:10,000-scale aerial photographs. The presence of the Gilbert shoreline across the surface of the feature indicates it formed prior to about 10,000 years ago.

Farmington Siding Landslide Complex

The Farmington Siding landslide complex was first mapped by Van Horn (1975), who described longitudinal ridges and undrained depressions on the surface of the landslide complex; and faults, folded beds, and injected sand in exposures of the interior. The landslide complex was mapped as three separate slope failures by

Nelson and Personius (1990), and as one or two separate landslides by other workers (Van Horn, 1975; Miller, 1980; Anderson and others, 1982; Chen and Associates, 1986). The Gilbert shoreline is mapped by Anderson and others (1982) as crossing the southern part of the landside complex, but not the northern part. Thus, the southern two landslides, as mapped by Nelson and Personius (1990), probably occurred more than 10,000 years ago. Organic clay immediately overlying landslide deposits in Farmington Bay, which correspond to the younger, northern Farmington Siding landslide, gave a radiocarbon age estimate of 2,930 [± 70] yr B.P. (Everitt, 1991). This date is similar to dates from the penultimate surface-faulting earthquake on the Weber segment of the Wasatch fault zone (Nelson, 1988; Forman and others, 1991; McCalpin and others, in preparation).

To resolve the age of landsliding, we excavated one trench on one of the older landslides, and two trenches on the younger landslide. Bedded lacustrine sediments exposed in the trench across a hummock on the older landslide were slightly back-tilted, presumably due to landsliding, but no material suitable for age dating was obtained from the trench. We excavated two trenches across a wedge-shaped mound near the main scarp of the younger landslide. In one of the trenches, a block of soil incorporated into the landslide deposit gave a radiocarbon age estimate of 4,630 [± 340] cal. yr B.P., indicating that the landslide formed sometime after this date. In the second trench, a radiocarbon age estimate from a buried soil that formed on the landslide indicates that it occurred sometime prior to 2,650 [± 225] cal. yr B.P. These dates bracket the age estimate obtained by Everitt (1991).

North Salt Lake Landslide

This landslide is mapped as two separate lateral spreads by Van Horn (1982) and Anderson and others (1982). Anderson and others (1982) excavated two shallow test pits on the northern, younger landslide, and one test pit on the older landslide. The test pit on the older landslide showed no evidence of liquefaction or disturbed bedding. The test pits on the younger landslide showed minor bedding disturbance in the form of 1-2 cm offsets in marker beds (Anderson and others, 1982). We excavated two narrow trenches down the slope of a 2.5-meter-deep land drain that crosses both landslides. No evidence of liquefaction or sediment deformation was observed in either of the two trenches, each of which was on a separate landslide. Based on our investigation, the features, which may or may not be lateral-spread landslides, are both older than the Gilbert shoreline (approximately 10,000 years ago).

Springville/Spanish Fork Landslide

Situated between the cities of Springville and Spanish Fork, this feature was mapped by Miller (1982) and Machette (1989). It is mapped as a possible lateral-spread landslide by Miller (1982), and its age is estimated as Holocene to upper Pleistocene

(Machette, 1989). We excavated three trenches on this feature; one in the center of the deposit, another near the distal "toe" of the feature, and one across a previously unmapped lineament on the feature. The lineament is likely a Lake Bonneville shoreline that trends NE-SW, and can be traced for about 2.3 km. None of the trenches showed evidence of liquefaction, and only the trench excavated across the toe of the feature showed evidence of deformed bedding. In this trench, we observed minor offsets (< 1 cm) in a thin clay marker bed, suggesting brittle deformation.

Although dissected and eroded in places, the shoreline was not displaced by the landslide, and thus appears to post-date formation of the feature. However, surface topography on the feature, particularly depressions near the "toe", appear younger than a cross-cutting shoreline would suggest. We offer three explanations that may explain the apparent discrepancy: (1) post-Bonneville liquefaction-induced landsliding did not occur within all the areas mapped as a lateral spread by Miller (1982) and Machette (1989); (2) the feature is not a lateral spread, but liquefaction during earthquake ground shaking created surface depressions, giving the appearance of a lateral spread; or 3) the feature is not a lateral spread, but an area affected by differential subsidence or other conditions caused by a fluctuating shallow water table, spring discharge, and artesian ground-water flow. Evidence obtained thus far favors the latter explanation as the most plausible, but further study is needed to resolve the question.

Beer Creek Landslide

The Beer Creek landslide is north of the city of Salem, and was first mapped as a queried lateral-spread landslide by Miller (1982). He described ridges parallel to the possible landslide main scarps and subdued mounds, hummocks, and undrained depressions on the surface of the landslide. Machette (1989) remapped the feature, removing the queries, and noted that the horizontal bedding of the original lacustrine sediment commonly had been contorted or destroyed by the movement. We excavated a trench across the main scarp of the possible landslide, but did not find any material suitable for age dating, or information to confirm that the feature is a landslide.

CONCLUSIONS

Geomorphic mapping and trench excavations produced positive, negative, and in some cases inconclusive evidence for liquefaction and liquefaction-induced landsliding along the Wasatch Front. The hazard potential of the features evaluated in this study is variable because of the differences in failure mechanisms and uncertainty in origin of a number of the features. However, recurrent landsliding has likely occurred at least within the boundaries of the North Ogden and Farmington Siding landslides within Holocene time, and future recurrent movement on these and some of the other features can be expected and needs to be

considered by local governments during land-use evaluations.

REFERENCES CITED

Anderson, L.R., Keaton, J.R., and Ellis, S.J., 1982, Liquefaction potential map for Davis County, Utah: Utah State University Department of Civil and Environmental Engineering, and Dames and Moore Consulting Engineers unpublished report for the U.S. Geological Survey, 50 p.

Chen and Associates, 1986, Preliminary geotechnical investigation, Davis County Correctional Facility Site B, Farmington, Utah: Unpublished consultant's report for the Davis County Sheriff's Department, Salt Lake City, Utah, 11 p.

Everitt, Ben, 1991, Stratigraphy of eastern Farmington Bay: Utah Geological and Mineral Survey, Survey Notes, v. 24, no. 3, p. 27-29.

Forman, S.L., Nelson, A.R., and McCalpin, J.P., 1991, Thermoluminescence dating of fault-scarp-derived colluvium--deciphering the timing of paleoearthquakes on the Weber segment of the Wasatch fault zone, north central Utah: Journal of Geophysical Research, v. 96, no. B1, p. 595-605.

Machette, M.N., 1989, Preliminary surficial geologic map of the Wasatch fault zone, eastern part of Utah Valley, Utah County and parts of Salt Lake and Juab Counties, Utah: U.S. Geological Survey Miscellaneous Field Studies Map MF-2109, scale 1:50,000.

McCalpin, James, Forman, S.L., and Lowe, Mike, in preparation, Reinterpretation of Holocene faulting at the Kaysville trench site, Weber segment of the Wasatch fault zone: Manuscript in preparation.

Miller, R.D., 1980, Surficial geologic map along part of the Wasatch Front, Great Salt Lake Valley, Utah: U. S. Geological Survey Miscellaneous Field Investigations Map MF-1198, scale 1:100,000.

-----1982, Surficial geologic map along the southern part of the Wasatch Front, Great Salt Lake and Utah Valleys, Utah: U.S. Geological Survey Miscellaneous Field Investigations Map MF-1477, scale 1:100,000.

Nelson, A.R., 1988, The northern part of the Weber segment of the Wasatch fault zone near Ogden, Utah, in Machette, M.N., editor, In the footsteps of G.K. Gilbert--Lake Bonneville and neotectonics of the eastern Basin and Range Province: Geological Society of America Meeting Field Trip Guidebook, Utah Geological and Mineral Survey Miscellaneous Publication 88-1, p. 26-32.

Nelson, A.R., and Personius, S.F., 1990, Preliminary surficial geologic map of the Weber segment, Wasatch fault zone, Weber and Davis Counties, Utah: U.S. Geological Survey Miscellaneous Field Studies Map MF-2132, scale 1:50,000.

Oviatt, C.G., 1986a, Geologic map of the Honeyville quadrangle, Box Elder and Cache Counties, Utah: Utah Geological and Mineral Survey Map 88, scale 1:24,000.

----1986b, Geologic map of the Cutler Dam quadrangle, Box Elder and Cache Counties, Utah: Utah Geological and Mineral Survey Map 91, scale 1:24,000.

Pashley, E.F., Jr., and Wiggins, R.A., 1972, Landslides of the northern Wasatch Front, in Hilpert, L.S., editor, Environmental geology of the Wasatch Front, 1971: Utah Geological Association Publication 1, p. K1-K16.

Personius, S.F., 1988, Preliminary surficial geologic map of the Brigham City segment and adjacent parts of the Weber and Collingston segments, Wasatch fault zone, Box Elder and Weber Counties, Utah: U.S. Geological Survey Miscellaneous Field Studies Map MF-2042, scale 1:50,000.

Stuiver, Minze, and Reimer, P.J., 1986, CALIB & DISPLAY software: Radiocarbon, v. 28, p. 1022-1030.

Van Horn, Richard, 1975, Largest known landslide of its type in the United States--a failure by lateral spreading in Davis County, Utah: Utah Geology, v. 2, no. 1, p. 83-87.

----1982, Surficial geologic map of the Salt Lake City North quadrangle, Davis and Salt Lake Counties, Utah: U.S. Geological Survey Miscellaneous Investigations Series Map I-1404, scale 1:24,000.

Woodward-Clyde Consultants, 1985, Evaluation of fault activity and potential for future tectonic surface faulting--Allied Health Science Building site, Weber State College, Ogden, Utah: Unpublished consultant's report, 10 p.

EARTHQUAKE SOURCE AND EFFECT STUDIES

9950-04560

S. H. Hartzell, A. M. Rogers, J. S. Gomberg,
E. Cranswick, C. Langer

Branch of Geologic Risk Assessment
U.S. Geological Survey
Box 25046, MS 966, Denver Federal Center
Denver, CO 80225
(303) 273-8572

Investigations

1) Simultaneous inversion for source and site effects.

2) Estimation of near-source ground motions from a teleseismically derived rupture model. This study overlapped between FY 1991 and FY 1992 but was completed in FY 1992.

3) The spatial and temporal slip distributions for the 3 October, 1974 (M_W=8.0) Peru subduction zone earthquake and its largest aftershock on 9 November (M_S=7.1) are calculated and analyzed in terms of the inversion parameterization and tectonic significance.

4) An extremely wide-band (2 to 350 sec) waveform inversion is performed using the ground motion records for the 3 March 1985 (M_W=8.0) Chile earthquake to investigate the rise-time function on the fault for a major earthquake.

5) We examine a large peak acceleration data set (1,241 records from 180 earthquakes) in order to investigate the presence of magnitude-dependent distance scaling or distance dependent magnitude scaling.

6) Ms=5.6, Little Skull Mountain, Nevada earthquake of June 29, 1992. 16 portable seismographs were deployed on the Nevada Test Site from June 29-July 14, 1992. The field effort was coordinated with similar efforts by the University of Nevada, Reno and LLNL. Data from the portable seismographs, the permanent southern Great Basin Seismic network (SGBSN), and the U.S. National Seismograph Network (USNSN) are being analyzed to obtain basic parameters describing the main shock, its foreshocks and aftershocks, and its relationship to the Landers, CA earthquake. Modeling studies to explore mechanisms of remote triggering (by the Landers event) are also being conducted.

7) 2-D boundary-element modeling of the New Madrid seismic zone. One objective of this modeling study was to identify and characterize the most plausible causative faults of the 1811-1812 earthquakes. A second objective was to synthesize a tectonic framework for the region in a series of models of the elastic strain field constrained by the available morphologic (topography, sub-surface geologic structure) and seismologic data.

8) 3-D boundary-element modeling algorithm, program development. Together with M. Ellis of Memphis State University a computer program has been designed and written

to calculate 3- dimensional boundary element models of the elastic deformation field. The program utilizes the Green's functions of Okada (1992) that map planar dislocations in a half-space to the elastic displacement and displacement gradient field. The program is being applied to study tectonic deformation in the New Madrid seismic zone, the Death Valley region, and Tennent Creek, Australia.

9) Seismic tomography of the southern Great Basin. An NSF-funded study is underway to determine the 3-dimensional seismic velocity structure of the crust and upper-most mantle of the southern Great Basin using arrival time data recorded on the SGBSN. Knowledge of the velocity structure should provide strong constraints on the mechanism of extension in the region.

10) Supervision of upgrade of southern Great Basin seismic network (SGBSN).

11) U.S. National Seismograph Network/Regional network interfacing. Several activities were undertaken to develop tools that would enable regional networks to utilize USNSN facilities.

12) Seismicity study and USNSN site selection in southeast Oregon. In collaboration with personnel from the Branch of Seismology seven portable seismographs were deployed for approximately two weeks in southeast Oregon. The purpose of this investigation was to obtain a preliminary assessment of the seismicity and to select a site for a permanent USNSN station. The seismicity in this part of the Basin and Range province had previously never been monitored. The area also has significant hydrothermal activity and construction of a power plant is being considered. Thus, the USNSN site was chosen so that the telemetry might be shared by a regional seismic monitoring network that would be installed if power facilities were developed.

13) Joint USGS/Armenia Seismology Program.

14) Public Seismic Network.

15) PC-based field computer system for processing data recorded by portable autonomous digital seismographs.

16) Phased micro-array recordings of the 29 June Little Skull Mountain Earthquake (NTS) aftershock sequence.

17) Site Response in Santa Cruz, California.

Results

1) Aftershocks of the 1989 Loma Prieta, California, earthquake were used to estimate site response along the San Francisco Peninsula. A total of 215 shear-wave records from 24 sources and 21 sites were used in a linear inversion for source and site response spectra. The methodology makes no assumptions about the shape of the source spectrum. However, to obtain a stable unique inverse, a Q model and geometrical spreading factor were assumed, as well as a constraint on site response that sets the site response averaged over two specific stations to 1.0. A solution was obtained using a Chebyshev accelerated tomographic

method that damps out the contribution from small singular values and converges very rapidly to the least-squares solution. Site responses calculated by this formulation of the problem were compared with other studies in the same region that use different methodologies and/or data. The shear-wave site responses compared favorably with estimates based on an ω^2-constrained source model. Comparison with coda amplification factors was not as close, but still favorable considering that the coda values were determined for nearby locations with similar geology, and not the same sites. The extent of agreement between the three methods is encouraging considering the very different assumptions and data used.

2) A rupture model for the 1989 Loma Prieta earthquake obtained from inversion of teleseismic body waves was used to calculate the main shock, near-source, strong-ground motions. The effectiveness of both synthetic and empirical (aftershock) Green's functions was evaluated in terms of velocity response spectra over the period range from 0.1 to 10 sec. A strictly deterministic approach was used in the simulation of near-source ground motion with both the synthetic and aftershock Green's functions. A deterministic method has advantages in that it is simple to apply and there is no stochastic element to introduce variability in the solution. Response spectral values were very sensitive to the choice of the source-time function. Using a 1.0 sec triangular time function obtained from the teleseismic study gave good estimates of response spectra from 1 to 2 sec period for aftershock Green's functions and from 1 to 10 sec period for synthetic Green's functions. The limited long-period response of the aftershock summations was due to the restricted bandwidth of the recording sensor. Using a 0.5 sec Kostrov time function extended the bandwidth of validity of the aftershock summations to 0.1-2 sec and the synthetic Green's function summations to 0.3-10 sec period. The limited short-period bandwidth of the synthetic Green's function summations resulted from the lower frequency content (5Hz) and absence of accurate high-frequency propagation effects in the synthetic seismograms. Although the telseismic study could not distinguish between a 1.0 sec triangular time function and a 0.5 sec Kostrov time function, we felt justified in using the Kostrov function because it lies within our broader knowledge of earthquake source-time functions.

3) Teleseismic, WWSSN, P- and SH-waveforms are inverted to obtain the rupture histories of the 3 October and 9 November, 1974 Peru earthquakes. We demonstated that erroneous results are obtained if a parameterization is used that does not allow for a sufficiently complex source, involving spatial variation in slip amplitude, rise-time, and rupture time. The inversion method utilizes a parameterization of the fault that allows for multiple, sequential, rupture intervals that discretize the source rise-time and rupture time. Well-located aftershocks recorded on a local network help to constrain the geometry of the subduction zone. For the main shock a hinged fault is preferred having a shallow plane with a dip of 11° and a deeper, landward plane with a dip of 30°. A bilateral rupture is obtained with two major concentrations of slip, one 60 to 70 km to the northwest of the epicenter and a second 80 to 100 km to the south and southeast of the epicenter. For the primary source regions, rise-times vary from 6 to 18 sec. The slip distribution for the 9 November aftershock falls within a conspicuous hole in the main shock rupture pattern, near the hypocenter of the main shock. The 9 November event has a simple rise-time

function with a duration of 2 sec. Aftershocks recorded by the local network are shown to cluster near the hypocenter of the impending 9 November event and down-dip from the largest main-shock source region. Slip during the main shock is concentrated at shallow depths above 15 km and extends up-dip from the hypocenter to near the plate boundary at the trench axis. The significant amount of slip under the accretionary wedge of sediments is attributed to the relatively young age and high convergence rate of the subducted plate at the Peru trench, that results in good seismic coupling.

4) Several previous studies argue for short rise times compared to the time for a shear wave to traverse the width of a fault. However, the data used has covered a limited bandwidth, and short rise times are contradictory to some theoretical calculations for a dynamic rupture. The 1985 M_W8.0 Valparaiso, Chile, earthquake offers a good opporturity to estimate the source rise time funciton for a major earthquake. Three different sets of data are brought to bear on this question to form an extremely wide-band data set from 2 to 350 sec. The three data sets are: 1) locally recorded strong ground motion records, 2) broadband teleseismic body waves, and 3) teleseismic surface waves. Simultaneous inversion of these three data sets yields a model with peak slips of 2.8 meters and short rise times of about 15 sec. The inferred rupture model explains all three data sets very well, including the long-period Rayleigh waves. Thus, no evidence for preferential seismic-wave excitation can be found that would require a preferential frequency component of fault motion.

5) Because the magnitude and distance variables are strongly correlated in the data, we sought a means to isolate the magnitude and distance effects. After removing the first-order 1/R distance dependence, where R is closest distance to the fault, where available, or hypocentral distance, we computed mean peak acceleration in selected distance slices as a function of magnitude. We also evaluated mean peak acceleration in magnitude slices as a function of binned distance. Because of the large variability and sparseness in the data, parametric regressions in the distance and magnitude slices gave results excessively dependent on individual data points. Accordingly we used techniques of exploratory data analysis (i.e., LOWESS and DWLS smoothing, median polish, binning) to determine non-parametric fitted values in the distance slices. (magnitude slices exhibited too much variability for satisfactory fits tò anything but simple lines.) We also assumed some of the best controlled slices to be paradigm approximations to the true data behavior to fit expected data values in portions of the data where selection bias was present. This technique produced an alternative hypothetical data set extending the data range beyond that we considered acceptable in the original data.

We observed the following effects in the data. (1) For constant distance bins, peak accelerations saturate as a function of increasing magnitude for distance bins out to about 20 km. (2) At greater distances, we observed increased scaling with increasing magnitude, which could be termed anti- saturation. (3) Sampling bias may affect peak acceleration behavior especially for magnitudes below about M=5 and at the largest distance ranges in each slice. That is, we seem to be observing only the higher portions of the distribution of ground motion at distances corresponding to those which would yield ground motions near the level at which instruments are not triggered or that records are not digitized.

(4) Behavior in the constant magnitude slices broadly confirms the behavior observed in the distance slices. (5) Monte Carlo simulation of the data, based on a finite fault model composed fault patches that draw patch peak acceleration values from a statistical distribution, qualitatively confirms the hypothesis that magnitude and distance saturation behavior are a result of a combination of intrinsic statistical properties of the source, sampling properties of the strong motion data base, and geometrical aspects of finite sources and geometric spreading.

Given that observed peak acceleration behavior is a function not only of the physics of the earthquake source and ground motion propagation, but also of sampling bias, the proper functional form for regression analysis is unclear. We argue that for conventional regression studies, some functional forms are insensitive to the true behavior of the data and are hence relatively stable, though incorrect. Conversely, for complex functional forms, more capable of describing the true data behavior, the high amount of variability renders the fit excessively sensitive to selection amongst possible data sets. The high amount of variability renders us incapable of preferring one functional form over another. Thus, equations based on regression techniques may produce estimates of peak accelerations that will predict the existing data base adequately in terms of minimizing the sum of the errors squared but would not produce reliable estimates of future ground motions. On the other hand, use of binned smooth representations of the data and a method of fitting based on paradigm shapes defined by limited subsets of the data itself may be a means of overcoming some of the intrinsic sampling bias and scatter in the data.

6) Little Skull Mountain, Nevada earthquake of June 29, 1992. Aftershock data reduction, which includes combination of data from a variety of sources, is nearly complete and preliminary analyses (locations, focal mechanisms) are underway. Foreshock data has been analyzed and provide a strong, albeit circumstantial, evidence that this earthquake was triggered by the Landers, CA earthquake.

7) 2-D boundary-element modeling of the New Madrid seismic zone. The study was completed and a manuscript has been accepted by the JGR. Principal conclusions are that 1) the topography may be built by rupture of two, right-lateral, strike-slip faults separated by a compressional step, 2) the geometry and dimensions of these faults imply moment- magnitudes of 7.4 rather than greater than 8.0 as previously inferred for the 1811-1812 earthquakes, 3) the seismicity observed since the installation of modern networks are probably not aftershocks of the 1811-1812 events, 4) the Bootheel lineament does not appear to be a fault scarp of a major seismogenic fault, 5) the next major earthquakes are likely to nucleate at the ends of the current zone of greatest seismic activity.

8) 3-D boundary-element modeling algorithm, program development. The program is now operational, tested, and being applied. A user's manual has also been prepared.

9) Seismic tomography of the southern Great Basin. Data reduction has been completed and modeling is underway.

10) Supervision of upgrade of southern Great Basin Seismic network (SGBSN). The upgrade of the SGBSN included the installation of a USNSN station within the SGBSN and installation of six new state-of-the-art digital seismic stations and a telemetry node

that interfaces with the six stations and the USNSN satellite system. Software to receive these data from all of these stations and transmit commands to them was developed for use on SGBSN computers. On September 30, 1992 support provided by the DOE for continued operation and upgrade of the SGBSN was terminated.

11) U.S. National Seismograph Network/Regional network interfacing. In addition to demonstrating how a regional network might interface with the USNSN through the upgrade of the SGBSN (above), an electronic newsletter/bulletin board was established to exchange information and computer programs that would facilitate use of USNSN capabilities by regional networks.

12) Seismicity study and USNSN site selection in southeast Oregon. No local earthquakes were recorded during the deployment period. A USNSN station site was selected and noise levels at this site were measured and determined to be very low. A proposal was submitted to the Bureau of Reclamation (manages the land being considered for a hydrothermal power plant) which subsequently agreed to provide some financial assistance for the USNSN station operation.

13) In April-May 1992, as part of the joint USGS/Armenia Seismology Program which commenced following the USGS participation in the study of the 1988 Spitak Earthquake, a 5-week graduate course was taught entitled "Introduction to the Acquisition, Processing and Analysis of High-frequency Digital Seismograph Data for Strong Motion Studies" at the American University of Armenia, Yerevan, Armenia. While in Armenia, preliminary negotiations were initiated and conducted with various Armenian government officials concerning the transfer of responsibility for the Armenian side of the joint program from the Armenian Academy of Sciences to the new, post-Soviet organization, the National Survey for Seismic Protection (NSSP). These arrangements were particularly important for the continued operation of the Global Digital Seismic Network (GDSN) station at the Garni Geophysical Observatory, and they were subsequently formalized by J. Filson, BGSGM in August. As part of the new arrangement, a GEOS digital seismograph was installed at the NSSP Yerevan Seismic Station and the staff instructed how to operate it and how to analyze the data it recorded using PC-based software (an English/Russian language version of Cranswick, King and Banfill, 1989). Preliminary analyses of the data recorded by the three-dimensional GEOS array at the Garni Geophysical Observatory provide direct measurements of the P- and S-wave velocities of the near-surface and illustrate how the wavefield interacts with the surface. The array also indicates the presence of previously undetected microearthquake activity on the adjacent Garni Fault which has a historical record of macroseismic events and abundant geologic evidence of Holocene movement.

14) Following the 1990 AGU presentation, "A Proposal for a High-density People's Seismograph Array Based on Home Computers in the San Francisco Bay Area" (Cranswick and Banfill, 1990), work was done with various members of the public and the USGS to explore the possibilities of a Public Seismic Network (PSN). A prototype of the envisioned PSN system now exists in the form of a group of amateur seismologists centered in California who have connections with groups as far away as New Zealand. They perform all the basic functions of a PSN as originally proposed. They record seismograms from

event-triggered digital seismographs deployed in their own homes and upload the waveform timeseries via modem to a PC-based BBS where the records are available to other PSN members and the general public. On 28 June 1992, within a few hours of the Landers, California Earthquake, we were able to upload a seismogram of that event recorded by one of the PSN stations in San Jose, California, to computers at the USGS in Golden, Colorado, and give a copy of the seismogram to the National Earthquake Information Center. The PSN has BBSs operating in San Jose, Pasadena, and at the USGS in Menlo Park, California. The Los Altos High School, California, has been the site of a PSN seismograph station for the last year, and the PSN is embarking on a program to work with public schools throughout the State of California.

15) In the continuing development of field computer systems designed for the near-realtime processing of PADS data while recording in the field, we are now able to process the digital data recorded by RefTek PASSCAL PADSs in addition to those recorded by Sprengnether DR200 and USGS GEOS PADSs. The new software permits the ready interchange of waveform timeseries between the traditional DR100 Format for PADS data and the recently developed SUDS format, and it utilizes a database system to store and access station/instrument parameters such as instrument characteristics and clock corrections. The aftershock investigation of the Little Skull Mountain Earthquake provided an opportunity to test the prototype system of new PC-based hardware and software. We were able to effectively monitor and modify PASSCAL and DR200 PADSs operation and locate earthquakes they recorded while field data acquisition was in progress. Both IRIS and RefTek, Inc., have expressed considerable interest in this PC-based system, and the latter have contracted to develop it further.

16) To investigate how the conversion of body waves to surface waves contribute to the strong ground motions of sedimentary basins, a micro-array was deployed on flat-lying basin deposits within 12 km of the mainshock epicenter during the aftershock study conducted after the 29 June 1992 Little Skull Mountain Earthquake at the Nevada Test Site (NTS). The array consisted of a central three-component 2 Hz geophone surrounded by three vertical 4.5 Hz geophones at radial distances of 50 m. All six channels were recorded on the same timebase by one digital acquisition system at sample rates as high as 1000 sps. In one week of operation (3 - 10 July), the array recorded more than 100 local aftershocks and at least 10 aftershocks of the Landers Earthquake at regional distances.

17) Studies of the site response in Santa Cruz, California, reveal that the frequencies of the fundamental and second-mode site-resonance peaks observed in the strong motion records of Loma Prieta aftershocks can be explained by one-dimensional velocity models of the near-surface estimated from shallow reflection and refraction surveys conducted at or near the recording sites. The observed amplitudes, however, are significantly larger than those predicted by the models which suggests that the three-dimensional effects of the local conversion of body waves to surface waves may be responsible for much of the strong ground motion.

Reports

Banfill, R. (1992). PC-SUDS: the seismic unified data system for DOS, version 1.4 (October 1992), *Small Systems Support User Manual*, (produced in partial fulfillment of contract requirements).

Brockman, S., J. Brooks, D. Carver, E. Cranswick, J. Duggar, J. Gomberg, S. Harmsen, M. Meremonte, D. Overturf, K. Shedlock, T. VanDreser, D. Worley (1992). The June 29, 1992 Little Skull Mountain, Nevada earthquake, *EOS, Trans. Amer. Geophys. Union*, 73, p. 354.

Cranswick, E., M. Meremonte, D. Worley, J. Gomberg, D. Carver, J. Brooks, S. Harmsen, J. Duggar, T. Van Dreser, R. Banfill and C. Early (1992). Phased micro-array recordings of aftershocks of the 28 June 1992 Little Skull Mountain (NTS) Earthquake, *EOS (Trans., AGU)*, 73, 338.

Cranswick, E., B. Gardner, R. Banfill and S. Hammond (1992). Public Seismic Network and sedimentary basins: recording ground motions where the people live, *EOS (Trans., AGU)*, (submitted).

Ellis, M. and J. Gomberg (1992). 3D-DEF: A new three-dimensional boundary-element model, and applications to regions of active tectonics, *EOS, Trans. Amer. Geophys. Union*, 73, p. 124, 1992.

Glassmoyer, G., and R. Borcherdt [E. Cranswick is co-author of three chapters in this volume] (1992). Report on the dense three-dimensional array near Garni, Armenia as part of the Joint Eurasian Seismic Studies Program, *USGS Open-file Report*, (in preparation).

Gomberg, J., P. Bodin, S. Harmsen (1992). Was the Little Skull Mountain, Nevada earthquake of June 29, 1992 triggered by the Landers, California earthquake?, *EOS, Trans. Amer. Geophys. Union*, 73, p. 393.

Gomberg, J.(1992). Tectonic deformation in the New Madrid seismic zone: Inferences from boundary element modeling, *J. Geophys. Res.*, (in press).

Hartzell, S. H. (1992). Site response estimation from earthquake data, *Bull. Seism. Soc. Am.*, (in press).

Hartzell, S. H. (1992). Estimation of near-source ground motions from a teleseismically derived rupture model of the 1989 Loma Prieta, California, earthquake, *Bull. Seism. Soc. Am.*, 82, 1991-2013.

Hartzell, S. H. and C. Langer (1992). Importance of model parameterization in finite fault inversions: application to the 1974 M_W8.0 Peru earthquake, *J. Geophys. Res.*, (submitted).

Hill, D., P.A. Reasenberg, A. Michael, R. Simpson, J. Brune, D. dePolo, R. Smith, S. Nava, J. Gomberg, G. Beroza, W. Arabasz, S. Walter, M. Johnston, L. Jones, W. Ellsworth, and J. Zollweg (1992). Remote Seismicity Triggered by the M 7.5 Landers, California Earthquake of June 28, 1992, *Science*, (submitted).

Mendoza, C., S. H. Hartzell, and T. Monfret (1992). Wide-band analysis of the 3 March 1985 central Chile earthquake overall source process and rupture history, *Bull. Seism. Soc. Am.*, (submitted).

Meremonte, M., E. Cranswick, J. Gomberg, D. Worley, D. Carver, J. Brooks, D. Overturf, and T. Bice (1992). Report on seismologic field investigations of the 29 June 1992 Little Skull Mountain earthquake, *USGS Open-File Report*, (in preparation).

Mori, J., J. Filson, E. Cranswick, R. Borcherdt, R. Amirbekian, V. Aharonian and L. Hachverdian (1992). Near-surface measurements of P- and S-wave velocities from the dense three-dimensional array at Garni, Armenia, *Bull. Seism. Soc. Am.*, (in press).

Rogers, A. M. (1992). Shortcomings of the worldwide strong-motion data base: effects on peak acceleration regression analyses, (in review).

Rogers, A. M. (1992). Peak accelerations behavior from monte carlo simulations with a finite fault and sampling bias, (in preparation).

Williams, R.A., E. Cranswick and K.W. King (1992). Site response models from high resolution seismic reflection data, Santa Cruz, California, NEHRP report to Congress, *USGS Professional Paper*, (in review).

Williams, R.A., E. Cranswick and K.W. King (1992). Site response models from high resolution seismic reflection data, Santa Cruz, California, *EOS (Trans., AGU)*, 73, 352.

Geophysical Investigations of Possible Recent Ground Deformation and Neotectonism in White County, Illinois

Grant/project number: 1-5-27613-3310 INT 1434-92-G-2206

Paul C. Heigold and Timothy H. Larson
Illinois State Geological Survey
615 East Peabody Drive
Champaign, IL 61820

(217) 244-1309

In White County, Illinois (T5S R10E) there is a linear surficial feature called the Meadow Bank. This feature closely parallels the trace of the Herald-Phillipstown Fault on the West Franklin Limestone (Pennsylvanian) which is about one mile to the west. The Herald-Phillipstown Fault is one of the high-angle normal faults of the Wabash Valley Fault System.

In FY92 the data acquisition phase of a program to determine the nature of the Meadow Bank and its relationship, if any, to the Herald-Phillipstown Fault was initiated. This program includes seismic refraction surveying, vertical electrical soundings, and drilling and logging.

Further, an eye-witness account of a man living in the study area during the catastrophic New Madrid earthquake sequence of 1811-1812 mentions ground failure (cracks and sand blows) just to the east of the Meadow Bank. In an attempt to locate remnants of the ground failure and thus validate the account, constant-electrode-spacing resistivity profiling has been done in the northern half of section 35, T5S R10E.

Data Processing Section

9920-10142

Charles R. Hutt
Branch of Global Seismology and Geomagnetism
U.S. Geological Survey
Building 10002, Kirtland AFB-East
Albuquerque, New Mexico 87115-5000
(505) 846-5646

Investigations

1. IRIS/USGS Data Collection Center. The Incorporated Research Institutions for Seismology (IRIS) have designated the Albuquerque Seismological Laboratory (ASL) to be the data collection center (DCC) for a new global network of digitally recording seismograph stations. The data processing system at the ASL continues to be upgraded to increase its processing capability as new stations are added to the network.

2. Data Processing for the Global Digital Seismograph Network. All of the data received from the Global Digital Seismograph Network (GDSN) and other contributing networks is regularly reviewed, checked for quality, and archived at the ASL.

3. Network Volume Program. Data from the GDSN stations and other contributing networks are assembled into network volumes which are distributed to regional data centers and other government agencies.

Results

1. IRIS/USGS Data Collection Center. IRIS has initiated a program for the development, installation, and maintenance of a network of 60 or more seismograph stations around the world. The USGS has been assigned the task of installing and maintaining these stations, and processing the digital data they produce. At this time 19 of these stations have been installed with each one producing from 5 to 8 megabytes of compressed seismic data each day. As part of this program, IRIS has funded much of the new hardware required by the DCC to process this large amount of data. In addition, a new digital format know as the Standard for the Exchange of Earthquake Data (SEED) was developed by the USGS in cooperation with both IRIS and the Federation of Digital Broadband Seismograph Networks. This SEED format has been well received by the seismic community, and is rapidly becoming a standard for both recording and distributing seismic data around the world. A part of the new hardware furnished through IRIS for the DCC includes an optical jukebox memory system. Each optical platter, in the jukebox memory system, can store up to 6.4 gigabytes of

seismic data. All of the seismic data that has been received at the ASL over the past 20 years is now stored on these optical platters. This amounts to approximately 300 gigabytes of seismic information.

2. Data Processing for the Global Digital Seismograph Network. At the present time, the Data Processing Section at the ASL receives the data from a total of 59 digital recording seismograph stations. These include the 19 stations from the IRIS network, 8 DWWSSN stations, 2 SRO/ASRO stations, 10 stations from the China Digital Seismograph Network, 6 stations from the Terrescope Network in Southern California, 12 stations from the IRIS/IDA network supported by the University of California, San Diego, and 2 stations recently installed in Russia. All of this data is carefully processed at the ASL and reviewed for quality control which primarily includes timing problems and hardware problems which affect the quality of the data. After processing the data is stored on optical platters where it is immediately available to the seismic research community as requested.

3. Network Volume Program. The network volume program is a continuing program which assembles all of the data recorded by all the above listed networks for a specific calendar day or days onto one magnetic tape. This tape includes all the necessary station parameters, calibration data, transfer functions, and time-correction information for each station on the tape. All of the data in these network volumes are recorded in the new SEED format and copies are distributed to IRIS and to several university and government research groups for detailed analysis and further distribution. These tapes are assembled approximately 60 days after real time in order to provide a sufficient time frame for recording the data at the stations, forwarding this data to the ASL, and processing the data at the DCC. The amount of data produced by the various networks each day varies from 130 to 175 megabytes.

Maps of Potential Earthquake Hazards in the Urban Area of El Paso, Texas

Grant No. 1434-92-G-2171

Jeffrey R. Keaton
SHB AGRA, Inc. (formerly Sergent, Hauskins & Beckwith)
1617 E. Missouri Street, El Paso, Texas 79902
(915) 542-0046 [P.I.: (801) 266-0720]

Introduction

The El Paso metropolitan area, with a population exceeding 600,000, is located in the seismically active Rio Grande rift, but it currently is situated in Seismic Zone 1 of the Standard Building Code, and the general perception may be that potential earthquake losses are low. However, seven earthquakes have caused damage in El Paso since 1847, with Intensity VII being experienced once and and Intensity VI at least three times. At least 17 faults with evidence of Quaternary displacement are located within 100 km of El Paso; seven or eight of these have evidence of Holocene displacement. One of the major Holocene faults trends into downtown El Paso and probably extends across the Rio Grande into Ciudad Juárez, with a population of more than 1.2 million people. The broad valley east of downtown into which El Paso is expanding has been displaced and tilted by more than 20 faults which appear to be part of a major zone of deformation. Locally steep slopes in fractured bedrock and unconsolidated deposits may be subject to instability during earthquake shaking. Shallow groundwater in young alluvial sediments along the rapidly developing lower Rio Grande valley indicates part of the area may be susceptible to liquefaction-induced ground failure.

The objectives of the research are to 1) describe and map the distribution of earthquake hazards to which El Paso is exposed, and 2) advise El Paso City and County personnel about the risks commonly associated with these hazards and describe conceptual methods of dealing with the hazards and reducing the risks. The hazards addressed consist of 1) surface fault rupture, 2) tectonic deformation, 3) earthquake-induced landsliding, and 4) liquefaction-induced ground failure.

Investigations

This research consisted of five tasks and was based on existing data supplemented at selected locations along the Rio Grande floodplain.

Task 1 Compile and synthesize geologic, geotechnical, and groundwater data.
Task 2 Drill 10 borings to supplement subsurface soil and groundwater data at selected locations along the Rio Grande floodplain.
Task 3 Describe earthquake hazards and prepare maps showing a) traces of Quaternary and Holocene faults, b) the zone of tectonic deformation, c) areas susceptible to seismic landsliding, and d) areas of liquefaction-induced ground failure.
Task 4 Present the research results to the City of El Paso planning staff and other interested parties.
Task 5 Prepare and distribute the final report.

Tasks 1 through 4 have been completed; Task 5 is in progress and due by Dec. 31, 1992.

Results

Traces of the East Franklin Mountains fault and faults distributed in the Hueco Bolson east of El Paso have been compiled on a base map at a scale of 1:48,000. Reasonable parameters for the East Franklin Mountains fault consist of a 45-km fault length, a 10-km focal depth, a 65° fault dip, and a 3-m average displacement. These parameters result in a seismic moment (M_0) of 4.914 x 10^{26} dyne-cm, which corresponds to a moment magnitude (M_w) of 7.1. A 45-km rupture length yields surface wave magnitude (M_s) values of 7.0 to 7.2; a displacement value of 3 m yields M_s 6.8 to 7.3, depending on the equation used. A rupture length of 45 km yields a displacement of 2.17 m and a 3-m displacement yields a rupture length of 50.6 km. The values are in reasonable agreement; however, M_w 7.1 generally corresponds to about M_s 7.5.

The shape of the theoretical tectonic deformation associated with a maximum surface-faulting earthquake on the East Franklin Mountains fault was estimated on the basis of the parameters listed above. The profile of maximum deformation and tilt, shown in Figure 1 below, were used for contouring on the base map. The maximum predicted scarp height is 2.72 m and the maximum tilt is 0.178 m/km at a distance of 3.4 km east of the fault trace.

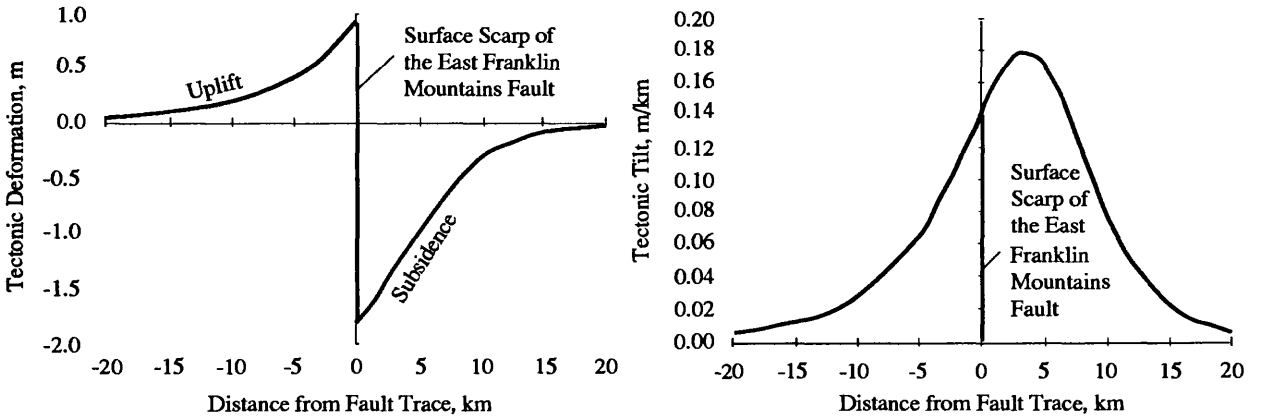

Figure 1. Tectonic deformation and tilt due to a hypothetical maximum earthquake on the East Franklin Mountains fault in the El Paso area.

Areas susceptible to seismic landsliding were evaluated by converting the Soil Survey of the El Paso area into a map of material strength and calculating the acceleration needed to reduce the factor of safety to unity for an infinite slope analysis. Ground slope was taken from 7.5-minute topographic quadrangles. Surficial materials were grouped into four strength categories: cohesionless alluvium ($c = 0$ psf; $\phi = 20°$); younger clayey alluvium ($c = 300$ psf; $\phi = 10°$); older clayey bolson deposits ($c = 800$ psf; $\phi = 10°$); and cemented older alluvial-fan deposits ($c = 5{,}000$ psf; $\phi = 30°$). The infinite slope analysis was done for a 10-foot-thick layer under two groundwater conditions: fully dry and fully saturated with seepage parallel to the slope. Critical accelerations are shown in Figure 2 for the cohesionless alluvium, younger clayey alluvium, and older clayey bolson deposits. Cemented alluvial-fan deposits and bedrock were considered too strong to slide, except where controlled by discontinuities, such as joints. Critical accelerations for these units plot beyond the limits of Figure 2. The arid climate in the El Paso area makes it unlikely for fully saturated conditions to exist to depths of 10 feet. Consequently, seismic landsliding does not appear to be a major earthquake hazard in El Paso.

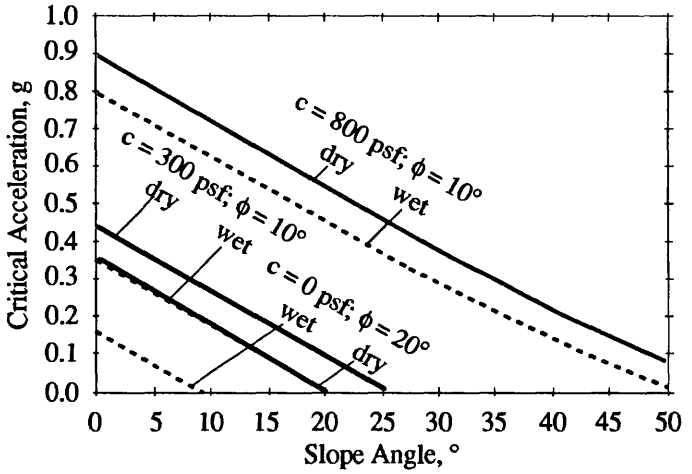

Figure 2. Critical accelerations for surficial deposits in El Paso.

Areas susceptible to liquefaction in the El Paso area are restricted to the floodplain of the Rio Grande. A reach approximately two miles long in downtown El Paso was lined with concrete over 20 years ago. The concrete lining effectively inhibits recharge of the shallow aquifer, and groundwater levels have declined to depths of 30 to 75 feet. The channel of the Rio Grande upstream and downstream of the concrete-lined reach continues to recharge the shallow aquifer. Standard penetration test blow-counts in sand and silty sand deposits below the water table indicate that liquefaction could occur in a few areas under accelerations < 0.10 g. Accelerations of 0.10 g to 0.30 g would be required to induce liquefaction is some parts of the areas where groundwater is less than 30 feet deep. However, substantial parts of the area have susceptible sediments that would require accelerations > 0.30 g for liquefaction to be a concern. The accelerations required to induce ground failure given the occurrence of liquefaction would be somewhat higher in most cases because most susceptible sediments do not occur in thick layers.

A major problem exists in relating the critical acceleration values for seismic landsliding and liquefaction to the probability they will occur. The published probabilistic acceleration maps indicate generally low values for El Paso (0.015 g with a 10 percent probability of being equalled or exceeded in a 50-year period and 0.09 g with a 10 percent probability in a 250-year period). However, a maximum earthquake (M_S 7.3) on the East Franklin Mountains fault could generate a peak horizontal acceleration of about 0.54 g at a site near the fault. About 2 km away from the fault, the peak acceleration could be about 0.50 g; 10 km away, the acceleration could be 0.30 g. In the Rio Grande rift, an earthquake up to about M 6 could occur without being attached to a specific known fault. Such an earthquake is known as the background earthquake. A site directly over the background earthquake could experience a peak acceleration of about 0.41 g. These scenario earthquake accelerations are deterministic rather than probabilistic. The recurrence of these earthquakes is unknown, but needs to be known to permit evaluate the likelihood of accelerations that could cause landsliding or liquefaction. The probabilistic and deterministic acceleration values for El Paso are summarized in Figure 3.

Products

The products of the research will be descriptions and maps showing the distributions of earthquake hazards (fault traces, tectonic deformation, seismic landsliding, and liquefaction-induced ground failure) in the urban area of El Paso. The results will be

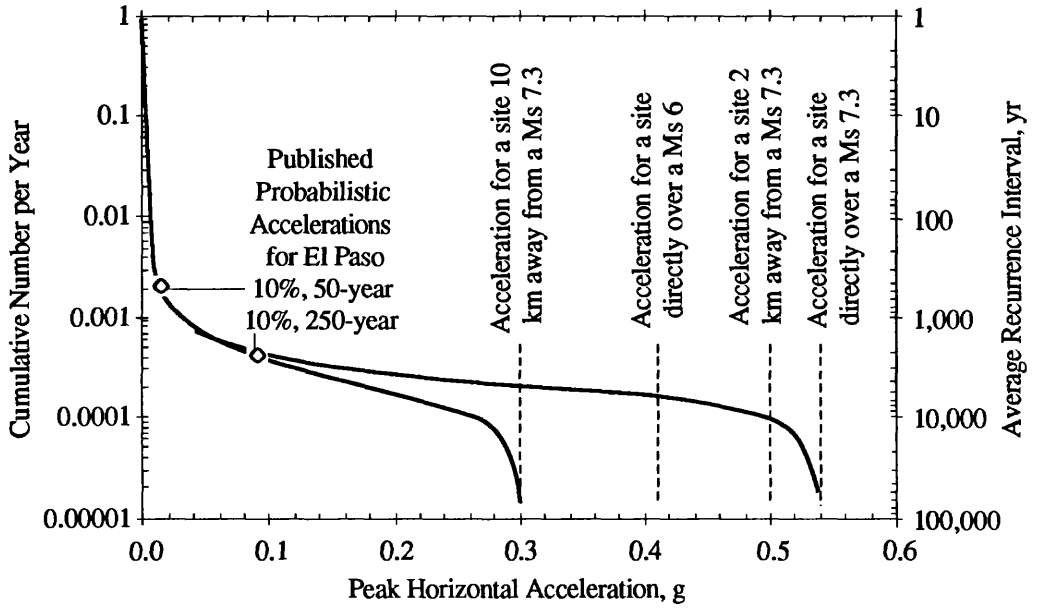

Figure 3. Acceleration recurrence data for El Paso.

translated into terms understandable and meaningful to city and county personnel who will be in positions to use the research to reduce potential earthquake losses.

Among the important implications of the research is the opportunity to change the general perception that Seismic Zone 1 adequately reflects the seismic risk in El Paso. The City of El Paso planning staff have some idea of earthquake hazards; in fact, they have a fault map overlay for the comprehensive plan. The plan notes that El Paso is an area of seismic activity and has numerous faults, some of which are active. The City of El Paso has no ordinance or code to accompany the fault map to allow them to use the information wisely, and such information is incompatible with the Seismic Zone 1 designation in the current Uniform Building Code. The planning staff indicates that the results of the research will be used initially to make siting decisions for new critical facilities, such as hospitals, fire stations, and schools. Subsequent use of the research results will be for decisions regarding changes in the city code regulating siting and construction of less critical facilities, such as commercial and residential developments.

SITE CHARACTERIZATION FOR EARTHQUAKE ENGINEERING STUDIES

9910-02413

Hsi-Ping Liu
Branch of Engineering Seismology and Geology
U. S. Geological Survey
345 Middlefield Road, MS 977
Menlo Park, California 94025
(415) 329-5643

Investigations

We have been setting up downhole arrays in urban areas and near nuclear power plants to study ground-motion amplification by sediments overlying bedrock.

Results

1. We revised and published a manuscript describing three-dimensional characteristics of site amplification in the Marina District of San Francisco.

2. In cooperation with project 9910-04481 (Integrated ground response, liquefaction and structural response studies, Market Street area, San Francisco), we contract-drilled six holes at the Embarcadero Center site, seven holes at the Bessie Carmichael School site, and seven holes at the Levi Plaza site. For the Embarcadero Center site and the Bessie Carmichael School site, a generalized sedimentary sequence from bottom up consists of Franciscan bedrock, Pleistocene Bay Clay, a sand layer, Holocene Bay Clay, and sand and artificial fill. The Pleistocene Bay Clay is missing from the sequence at the Levi Plaza site. The well log and borehole depths from the Bessie Carmichael School site are shown in Figure 1. The boreholes are to be instrumented with force-balance accelerometers and piezometers.

3. We installed a three-level vertical seismic array (bedrock, sediment, and surface) at the Savannah River Plant site in South Carolina in support of project 9910-03982.

4. As an OEVE outreach activity, we participated in an Wawona area ground water study in Yosemite National Park (project chief: Roger Borchers of USGS Water Resources Division). Specifically, we installed four units of three-component borehole seismometers in granite to monitor microearthquakes generated at the fracture front during a hydraulic fracturing experiment.

5. As another OEVE outreach activity, we provided a shear-wave source for scientists at the University of California at Santa Cruz in their study of the relation between ground motions and near-surface geology at a location in the Santa Cruz Mountains.

Reports

Liu, H.-P., Warrick, R. E., Westerlund, R. E., Sembera, E. D., and Wennerberg, L., 1992, Observation of local site effects at a downhole-and-surface station in the Marina District of San Francisco, *Bull. Seismol. Soc. Am.* , *82*, 1563–1591.

Bonamassa, O., Vidale, J. E., Lee, W., and Liu, H., 1992, The relation between ground motions and near-surface geology, *Eos (Trans. Amer. Geophys. Un.)*, *73*, 338.

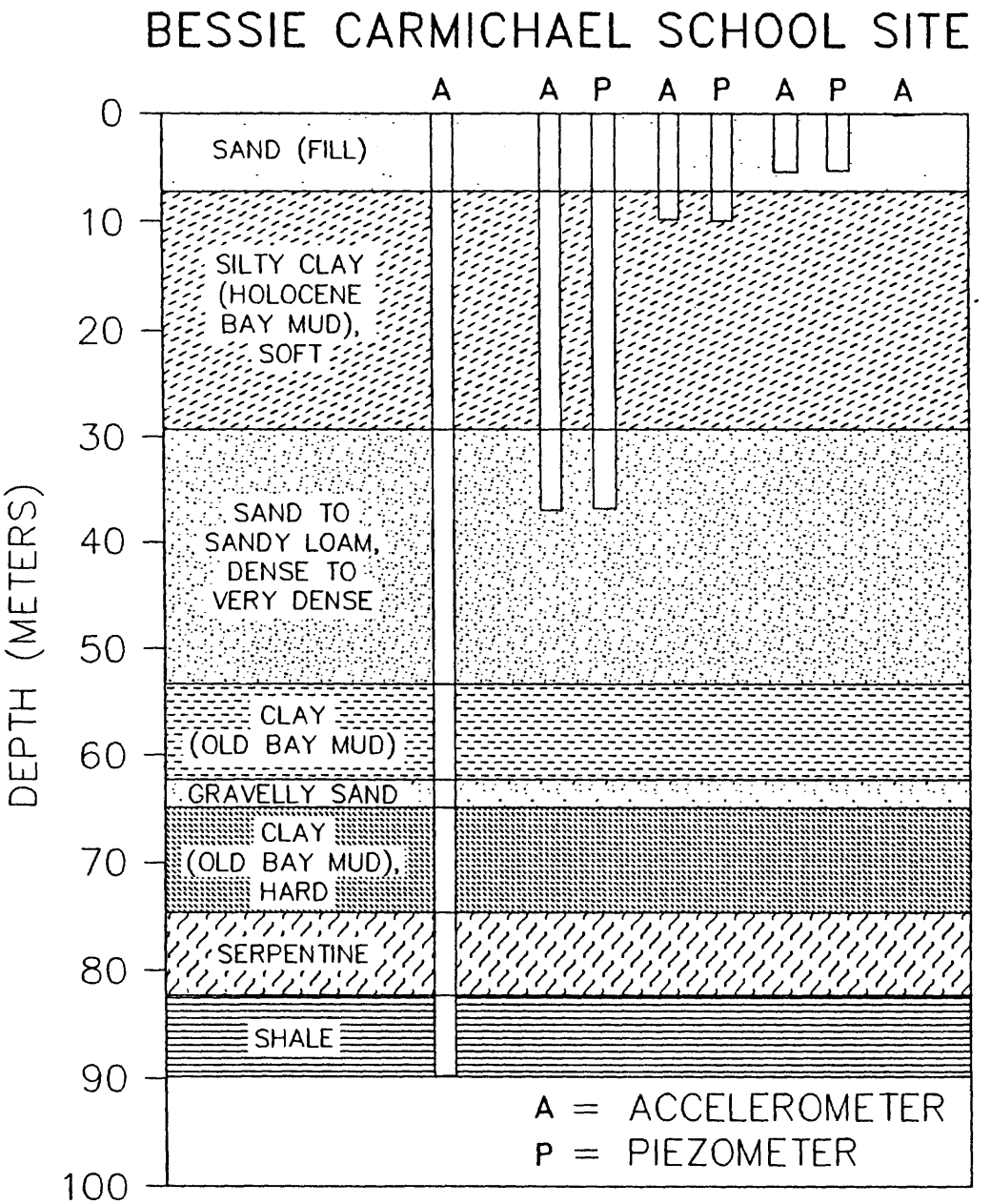

Figure 1. Well log and instrument-borehole depths at the Bessie Carmichael School site. Bessie Carmichael School is located at Folsom and Sherman streets in San Francisco near an elevated section of Freeway 101.

ROCK MECHANICS

9960–70036

D. Lockner, J. Byerlee, D. Moore, C. Morrow, R. Summers
Branch of Tectonophysics
U.S. Geological Survey
345 Middlefield Road, MS/977
Menlo Park, California 94025
(415) 329-4826

In cooperation with:

M. Blanpied, S. Hickman, and J. Savage
U.S.G.S.

D. Scott and C. Sammis
University of Southern California

L. Vernik
Stanford University
Stanford, California 94305

Investigations

Laboratory experiments are being carried out to study the physical properties of rocks at elevated confining pressure, pore pressure and temperature. The goal is to obtain data that will help us to determine what causes earthquakes and how to predict them. The relevant investigations cover a broad range of conditions. Stick-slip instabilities, which are the laboratory counterpart to earthquakes, are studied to understand both the dynamics of rupture and the processes leading to fault instability. Additional studies of permeability and chemical reactions that can occur in the crust at seismogenic depths are conducted to understand the large crustal system that loads earthquake-prone faults. Investigations are also underway to study conditions of borehole stability to aid in the interpretation of field data related to crustal stress measurements.

Results

Fault Strength at Hydrothermal Conditions.

Fault slip at hypocentral depths occurs at hydrothermal conditions, *i.e.*, at elevated temperature and elevated pressure of aqueous pore fluids. To determine the shearing strength and friction constitutive behavior of faults at these conditions, we have performed rate-stepping tests on sawcut cylinders of Westerly granite in triaxial shear at a range of

temperature (T = 23°–850°C), fluid pressures (P_{H_2O} = 0 to 100 MPa) and sliding rates (V = 0.01 to 5 μm/s). Effective normal stress ($\sigma_n{}^{eff}$) was 400 MPa. Surfaces contained 0.5 mm of crushed granite "gouge". All tests with P_{H_2O} = 0 ("dried"), and those with P_{H_2O} = 100 ("wet") below ~300°, show only a modest increase in friction ($\mu = \tau/\sigma_n{}^{eff}$) with increasing T, and a low sensitivity of μ to slip rate. In contrast, wet tests above ~300° show a marked reduction in μ with increasing T. For example, the addition of H_2O at 600°and 0.1 μm/s lowers μ from 0.8 to 0.5. These tests also show a strong, positive rate dependence of friction, which is expressed as a protracted evolution of strength following steps in slip rate. The mechanical results and temperature-strain rate conditions suggest the activation of a fluid-aided deformation mechanism above ~250° in tests with high P_{H_2O} = 0, which operates simultaneously with cataclastic flow. This mechanism stablizes slip by inducing rate strengthening and protracted strength transients, and may be responsible for the depth of the seismic-aseismic transition in the continental crust.

Experiments at high T show that a low-permeability seal can quickly form at hydrothermal conditions, trapping pore fluids within a porous fault zone. Wet samples slid at 600° and V = 0.1 μm/s show an initial strength peak of only μ = 0.42, followed by a rapid drop in strength to the remarkably low level of 0.20. Subsequent steps in externally-applied P_{H_2O} = 0 do not alter the shear stress, showing that there is no fluid communication through the granite country rock between the fault and the pore pressure system. Presumably, during the time before shearing commences (a few hours), static compaction of the heated gouge causes dissolved silica to precipitate in the gouge and nearby country rock, sealing the fluid pathways and perhaps elevating the pore pressure. The onset of shearing causes the porous gouge structure to compact further, rapidly raising the fluid pressure and lowering the effective stress, and leading to the loss of strength. Self-sealing may be important in natural fault zones, and could lead to overpressure that would account for the low shearing strength ($\mu \approx = 0.1$) inferred for some faults. The process may also provide a mechanism for nucleating intermediate-depth earthquakes. For instance, in a subducting lithospheric slab, solution-transport may create presure seals, allowing water-laden, porous sediments to be subducted to great depths while maintaining low effective stress. Subsequent shearing could raise fluid pressure and nucleate earthquake slip.

High Fluid Pressure and Fluid Partitions in Mature Fault Zones.

We present a model for the evolution of large crustal faults, such as the San Andreas, in which water that originally came from the country rock saturates the initially highly porous and permeable fault zone. During the shearing the fault zone compacts, and water then flows back into the country rock, but the flow is arrested by deposition of silicates to form seals between the fault zone and the country rock. Because of variations in temperature, mineralogical composition and the complex structure of the fault zone, a three dimensional network of seals will be formed in the fault zone itself so that the high pressure fluid will not be evenly distributed. As in deep oil resevoirs it will be confined to seal-bounded fluid compartments of various sizes and porosity that are not in hydraulic communication with each other or to the hydrostatic regime in the country rock. When the seal between two of these compartments is ruptured the sudden movement of fluid from the high pressure high porosity compartment to the low pressure, low porosity compartment will generate

an electrical signal. When the pore pressure in the two compartments reaches its final equilibrium state, which may be hours or days later, the average effective normal stress across them may be lower than it was initially and if the two compartments are large enough this may trigger an earthquake. During an earthquake many of the seals will be ruptured and the width of the fault zone will increase by failure of the geometrical irregularities on the fault. This newly created highly porous and permeable, but now wider fault zone will fill up with water and the process described above will be repeated. Thus, the process is an episodic one with the water moving in and out of the fault zone like the seismic pumping mechanism first described by Sibson. Each large earthquake should be preceded by an electromagnetic signal.

In a complimentary study we have considered the mechanical effects of a fault containing near-lithostatic fluid pressure in which fluid pressure decreases monotonically from the core of the fault zone to the adjacent country rock. This analysis shows that the maximum principal stress is oriented at a high angle to the fault in the country rock where the pore pressure is hydrostatic, and rotates to 45° to the fault within the fault zone where the pore pressure is much higher. This analysis suggests that on the San Andreas fault, where heat flow constraints require that the coefficient of friction for slip on the fault be less than 0.1, the pore fluid pressure on the main fault is 85% of the lithostatic pressure. The observed geometry of the subsidiary shears in the creeping section of the San Andreas are broadly consistent with this model, with differences that may be due to the heterogeneous nature of the fault.

The Effects of Fault Geometry on Fault Strength.

We have developed a model in which a well-developed fault is represented by a layer of granular material (fault gouge) confined between two competent fault blocks. Slip on such a fault involves plastic shearing of the fault gouge. That is, the fault gouge behaves as a Coulomb material, and the plastic flow is accomplished by slip on the two sets of Coulomb shears appropriate to the stress state and the frictional properties of the gouge. Neither set of Coulomb shears is coplanar with the fault zone. Generally, the initial plastic flow is self arresting, and increased shear stress is required to drive further shear. But as the shear stress is increased a stress state is reached in which the plane of maximum shear stress is parallel to the plane of the fault zone. Then the fault gouge shears at whatever rate is required to keep the shear stress across the fault from increasing further as was demonstrated experimentally by *Mandl et al.* [1977]. In a mature fault previous slip cycles have presumably left the fault gouge in a stress state such that the plane of maximum shear is parallel to the fault plane. Then unlimited shear deformation is possible at the shear stress corresponding to the onset of Coulomb failure, and the fault appears to slip as if friction on the plane of the fault appears to slip as if friction on the plane of the fault were less than on planes of other orientations.

Laboratory friction experiments lend support to this theoretical treatment of well-developed fault. A comparison of mechanical tests on granular fault gouge in different geometries reveals substantial variations in its apparent frictional strength. In triaxial tests on bulk cylinderical samples of natural fault gouge, the strain localizes to a well

defined shear band inclined at an angle of approximately 30° to the axis of compression. At a mean stress of 15 MPa, the residual coefficient of friction of the shear band is around 0.45. A thin layer of the same material at the same mean stress, when tested in the triaxial sawcut geometry, exhibits an apparent friction of around 0.6. This value is consistent with tests on layers of simulated quartz gouge in both the triaxial sawcut and double shear geometries. It appears that the frictional strength of gouge is larger in the layer tests than in the bulk tests.

Furthermore, the standard interpretation of the layer tests probably underestimates the intrinsic friction of the gouge. *Byerlee and Savage* [1992] have proposed that the strain in a gouge layer is actually accommodated by slip on internal (Riedel) shear bands that are inclined to the layer. The apparent friction of the layer as a whole is smaller than the true friction of the Riedel shears; if the apparent friction of the layer is 0.6, the friction of the Riedel shears is 0.75. We provide evidence for the veracity of Byerlee and Savage's theory, by applying it (in an extended form) to double shear tests which show a significant decrease in the apparent friction with increased rate of thinning. The thinning is unambiguous evidence that internal strain is occurring. The observed variation of apparent friction is quantitatively consistent with a constant friction of 0.75 on the Riedel shears.

We have carried the *Byerlee and Savage* [1992] analysis one step further. It has been shown both experimentally and theoretically that during the deformation of a Coulomb material in simple shear, the axis of principal compressive stress rotates to a limiting value of $\pi/4$ to the plane of the fault. The Coulomb failure planes on which slip actually occurs in this limiting state are oriented $\pm(\frac{\pi}{4} - \frac{\phi}{2})$ on either side of the axis of compression. These planes are the R1 and R2 Riedel shears that develop in fault gouge during friction experiments. Simultaneous slip on these two sets of Coulomb shears throughout the fault gouge produces the simple plastic shear flow in the gouge which permits the fault blocks to displace parallel to the fault surface. Microscopic deformation on the Coulomb shears satisfies the classical relation for the true coefficient of friction: $\mu = \tan\phi$. However, our analysis shows that the apparent macroscopic coefficient of friction of the fault system is given by

$$\mu_{\text{app}} = \sin\phi = \sin(\tan^{-1}\mu). \tag{1}$$

One important implication of equation (1) is that $\mu_{\text{app}} \leq 1$; an observational fact that has puzzled researchers for some time. Another consequence is that μ_{app} is less than the true value of μ; that is, friction of brittle materials as commonly measured on artificial faults in the laboratory is not a material property of the gouge, but rather a combination of the gouge properties and boundary constraints imposed by the test geometry. This analysis provides a straightforward explanation for the development of Riedel shears in laboratory experiments. In addition, it provides, for the first time, a link between internal friction μ_i of intact rock and friction of disaggregated material. As an example, we show that transformation of μ_i for intact Westerly granite using (1) successfully predicts observed sawcut friction μ_{app} (Figure 1). A final implication of this analysis relates to the stability of shear bands. Bifurcation theory generally assumes that shear localization is the result

of a change in material properties of the medium (e.g., strain weakening). However, equation (1) suggests that localized deformation in a shear band should occur at lower stress, and therefore be energetically favored over distributed shear, without requiring a divergence of material between the shear zone and the bulk material.

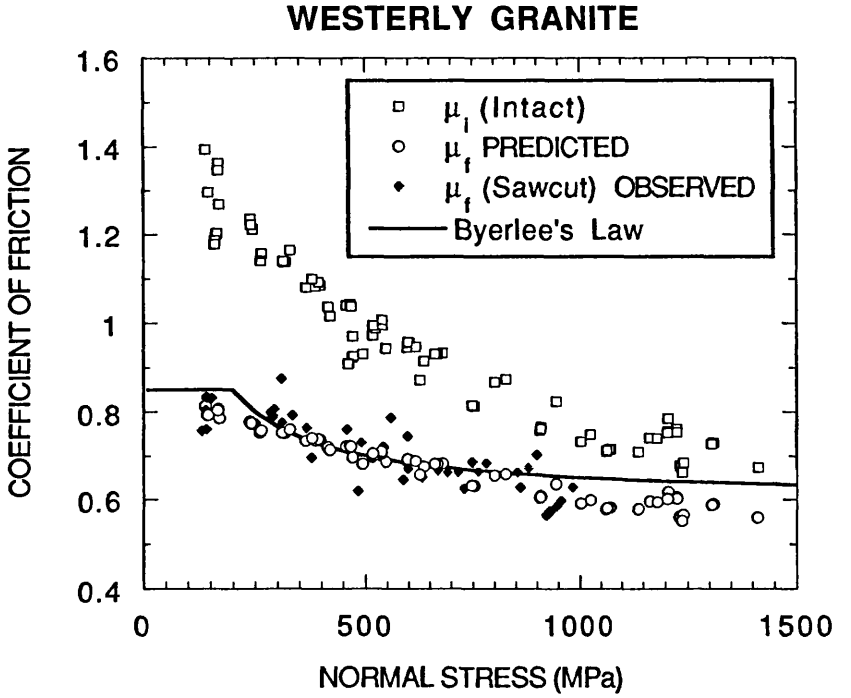

Figure 1. Application of equation (1) to internal friction data successfully predicts the observed sawcut friction values.

Microcrack Populations as Indicators of Stress Orientations Around a Developing Shear Fracture

We are investigating the evolution of microcracking associated with the formation of a shear fracture in Westerly granite at 50 MPa confining pressure. The sample studied is a cylinder 7.8 cm in diameter and 19.5 cm long, which contains a shear fracture that was arrested before completely traversing the sample during an experiment in which acoustic emission was recorded. Microcrack lengths and orientations were measured on images that were scanned into a computer from a microscope. Images from 9 locations around and in front of the fracture tip were examined. An image of the Westerly starting material also was studied, to separate pre-existing microcrack populations from those generated during the experiment. Analysis of acoustic emission hypocenters reveals an early stage of uniformly distributed microcracking in the sample. Upon nucleation of the shear fracture, the microcracking becomes concentrated in a process zone located directly in front of the fracture tip that migrates across the sample along with the propagating fracture. Microcracks associated with the early, distributed stage of acoustic emission have a preferred orientation that is parallel to the cylinder axis (loading direction). In contrast, microcracks generated in the process zone make angles to the shear plane of

30–40°, on average. In the immediate vicinity of the shear fracture, microcracks on the dilational side make larger angles to the shear than those on the compressional side. Crack densities are also 10–35% higher on the dilational side than on the compressional side. The markedly different orientations of microcracks associated with the distributed and the localized stages of acoustic emission reflect the rotation of the principal stresses in the region around the developing shear fracture. In addition, the orientations of microcracks in the vicinity of the shear are consistent with the theoretically predicted stress fields around mode II cracks; they therefore support the validity of the theoretical calculations and illustrate the sensitivity of the microcrack populations to the stress history of the sample.

Permeability of Core Samples From Deep Drill Holes.

Permeability measurements have been conducted on intact core samples from the Kola well, Russia, and the KTB pilot hole in Germany. Samples included granodiorites, basalts and amphibolites, extracted from depths of up to 11.6 km. These tests are intended to determine the pressure sensitivity of permeability, and to compare the effects of stress-relief microcracking on the matrix permeability of different rock types. Pore pressure, using distilled water, was fixed at the estimated *in situ* pressure assuming a normal hydrostatic gradient. Confining pressure was varied to produce effective pressures (confining - pore pressure) of 5 to 300 MPa.

The permeability of the basaltic samples was the lowest and most sensitive to pressure, ranging from around 10^{-20} to $10^{-23}m^2$ at effective pressures to only 60 MPa. In contrast, the granodiorite samples were more permeable and less sensitive to pressure, with permeability values ranging from 10^{-17} to $10^{-22}m^2$ at pressures to 300 MPa. Amphibolites displayed intermediate behavior. Petrographic evidence of abundant micro-fractures in the quartz-rich rocks, and their relative paucity in the quartz-poor rocks, supports the observed differences in permeability based on rock type and depth, and suggests a correlation between quartz content and stress-relief damage. As a result, stress-relief fractures dominate the permeability of the granodiorites at low pressures. By applying the Equivalent Channel Model of *Walsh and Brace* [1984] to the permeability data of the granodiorite samples, we can estimate the closure pressure of the stress-relief cracks, and thereby place bounds on the *in situ* effective pressure. This method is particularly useful for drillholes where the fluid pressure is not well constrained, such as at the Kola well. However, using crack closure to estimate *in situ* pressure is not appropriate for the basalt and amphibolite samples, because they are relatively crack free, and permeability is near or below the measurable lower limit at the estimated *in situ* pressure of the rocks.

Reports

The following recent publications are the result of studies conducted by or in cooperation with the Rock Mechanics project members.

Articles and Papers:

Blanpied, M. L., D. A. Lockner, and J. D. Byerlee, An earthquake mechanism based on rapid sealing of faults, *Nature*, 358 , 574–576, 1992.

Byerlee, J. D., The change in orientation of subsidiary shears near faults containing pore fluid under high pressure, *Tectonophysics*, 211 , 295-303, 1992.

Byerlee, J. D., The evolution of large fault systems, fluid pressure, and the implications for earthquake prediction, *Geology*, in press, 1992.

Byerlee, J. D. and J. C. Savage, Coulomb plasticity within the fault zone, *Geophys. Res. Lett.*, in press, 1992

Lockner, D. A., Room-temperature creep in saturated granite, *J. Geophys. Res.*, in press, 1992.

Lockner, D. A., Rock failure, In: *AGU Handbook of Physical Constants*, ed. T. J. Ahrens), in press, 1993.

Lockner, D. A. and J. D. Byerlee, Fault growth and acoustic emissions in confined granite, *J. Appl. Mech. Rev.*, 45 , S165–S173, 1992.

Lockner, D. A. and J. D. Byerlee, Precursory AE patterns leading to rock fracture, In: *Proceedings, Fifth Conference on Acoustic Emission/Microseismic Activity in Geological Structures and Materials*, (ed. H. R. Hardy), Trans-Tech Publications, Clausthal-Zellerfeld, Germany, 14, in press, 1992.

Lockner, D. A., J. D. Byerlee, V. Kuksenko, A. Ponomarev, and A. Sidorin, Observations of quasistatic fault growth from acoustic emissions, In: *Fault Mechanics and Transport Properties of Rocks*, (ed. B. Evans and T.-f. Wong), Academic Press, London, 3–31, 1992a.

Lockner, D. A., D. E. Moore, and Z. Reches, Microcrack interaction leading to shear fracture, In: *33rd U.S. Rock Mechanics Symposium*, (ed. J. R. Tillerson and W. R. Wawersik), Balkema, A. A., Rotterdam, 807–816, 1992b.

Moore, D. E. and J. D. Byerlee, Relationships between sliding behavior and internal geometry of laboratory fault zones and some creeping and locked strike-slip faults of California, *Tectonophysics*, 211 , 305–316, 1992.

Morrow, C. and J. Byerlee, Permeability of core samples from Cajon Pass Scientific Drillhole: results from 2100 to 3500 m depth, *J. Geophys. Res.*, 97, 5145–5151, 1992.

Morrow, C., B. Radney, and J. Byerlee, Frictional strength and the effective pressure law of montmorillonite and illite clays, In: *Fault Mechanics and Transport Properties of Rocks*, (ed. B. Evans and T.-f. Wong), Academic Press, London, 69–88, 1992.

Reches, Z. and D. A. Lockner, Nucleation and growth of faults in brittle rocks, *J. Geophys. Res.*, submitted, 1992.

Vernik, L., D. A. Lockner, and M. D. Zoback, Anisotropic strength of some typical metamorphic rocks from the KTB pilot hole, Germany, *Scientific Drilling*, 3, 153–160, 1992.

Abstracts:

Blanpied, M. L., D. Lockner, and J. Byerlee, Frictional sliding of granite at hydrothermal conditions: implications for fault strength and earthquake nucleation, In: *29th International Geol. Congress*, Kyoto, Japan, p. 166, 1992a.

Blanpied, M. L., D. Lockner, and J. Byerlee, Pressure seals, fault overpressure, and earthquake nucleation, In: *29th International Geol. Congress*, Kyoto, Japan, p. 168, 1992b.

Byerlee, J., The change in orientation of subsidiary shears near faults containing high pore fluid pressure, In: *29th International Geol. Congress*, Kyoto, Japan, p. 442, 1992.

Byerlee, J. D., Episodic flow of high pressure water in fault zones before earthquakes, *Eos, Trans. American Geophys. Union*, 73, p 387, 1992.

Hamajima, R., J. Byerlee, D. Lockner, and H. Koide, A numerical approach to frictional sliding of rock having fault gouge, In: *29th International Geol. Congress*, Kyoto, Japan, p. 167, 1992.

Lockner, D., J. Byerlee, and J. Savage, Limits of fault strength due to the constraints imposed by fault geometry, *Eos, Trans. American Geophys. Union*, 73 , p 511, 1992.

Lockner, D. A., Rock deformation and variations in complex resistivity and induced polarization, In: *Low Frequency Electrical Precursors to Earthquakes: Fact or Fiction?*, ed. by S. Park, Lake Arrowhead, Calif., 1992.

Lockner, D. A., D. Moore, and J. D. Byerlee, Microcrack interaction leading to shear fracture nucleation, In: *33rd U.S. Rock Mechanics Symposium*, Santa Fe, New Mexico, 1992.

Moore, D. E. and D. A. Lockner, Role of stress-induced cracking on the generation of a segmented fault, *Geol. Soc. of Amer. Abstracts with Programs*, 24, A157, 1992.

Moore, D. E. and D. A. Lockner, Microcrack populations as indicators of stress orientations around a developing shear fracture, EOS, Trans. American Geophys. Union, 73 , 515, 1992.

Morrow, C., S. Hickman, D. Lockner, and B. Khakaev, Permeability of core samples from the Kola Well, Russia, In: *6th International Symp. on the Observation of the Continental Crust through Drilling*, Paris, 1992.

Morrow, C., S. Hickman, D. Lockner, B. Khakaev, and T. Rckel, Permeability of core samples from deep drillholes; implications for estimating in situ pressure based on stress-relief cracks, *Eos, Trans. American Geophys. Union*, 73 , 499, 1992.

Scott, D., C. Sammis, D. Lockner, and C. Marone, The peak and residual strengths of shear bands in fault gouge, *Eos, Trans. American Geophys. Union*, 73 , 516, 1992.

Relative Earthquake Hazard Map of the Portland, Oregon Quadrangle.

14-08-0001-G2132

Ian P. Madin, Dr. Matthew Mabey
Oregon Department of Geology and Mineral Industries
800 NE Oregon St. # 28
Portland, OR 97232
503-731-4100

Investigations

The objective of the project is to develop a source-independent hazard map of the Portland quadrangle by creating a digital geologic and geotechnical model of the quadrangle and assessing the amplification, liquefaction and landsliding potential for each cell in the model. The geological model was developed by analysis and interpretation of an existing borehole database. Shear wave velocities for the units in the model were measured in purpose drilled boreholes, and software was written to automatically run amplification analyses on the geologic/geotechnical model. Subcontracted mapping of upland loess thickness was added to the program to provide data for the landslide analysis.

Results

Geologic Model

A raster based geologic model of the Portland quadrangle was developed using structure contour maps of the tops of the major geologic units in the area derived from a pre-existing borehole database. The structure contour maps were converted to Digital Elevation Models (DEM's) using a raster GIS package (IDRISI). The unit-top DEM's were overlaid with each other and a topographic DEM to develop a raster isopach image (Figure 1) for each geologic unit based on a 90 m cell. The set of images provides a complete three-dimensional model of the geology of the quadrangle, extending to local basement.

Shear Wave Velocity Logging.

We subcontracted with the Oregon Department of Transportation to drill 11 boreholes totalling 864 m for the purpose of collecting representative shear-wave velocities for the geologic units in the model. Ten of the holes were drilled in the Portland Quadrangle (Figure 2). The remaining hole was drilled 15 km southeast of the Portland quadrangle in order to obtain good data on a unit that is inaccessible (too deep) in the quadrangle. The holes were drilled with mud-rotary techniques, and cased with 2.5 " I.D. PVC flush joint pipe, grouted from top to bottom. Shear waves were generated by striking the end of a beam with a sledge and digitally recording the arrivals with a three component, downhole geophone. The downhole data was analyzed with custom-written software to obtain interval velocities for each geologic unit in the borehole. The representative velocities and associated geologic units are presented in Figure 3.

Amplification Analysis

Amplification potential over the area of the map was computed based on the average geotechnical properties for each geologic unit. These average values were determined from data gathered from the 11 previously mentioned boreholes. These data were supplemented with 24 other boreholes in the region in which shear wave velocities were measured. The geotechnical properties were then combined with the thickness data previously discussed.

The amplification response for each 90 meter square grid cell in the map was computed using the program *SHAKE88*, developed at the University of California, Berkeley. A computer program, *AUTOSHAK*, was composed which queries the GIS database to obtain the thickness of each geologic unit underlying a grid cell and then automatically generates an input file for *SHAKE88*. *AUTOSHAK* then automatically executes *SHAKE88*. After *SHAKE88* has completed its analysis *AUTOSHAK* resumes control and reads the output file from *SHAKE88* and extracts the information necessary to generate files of GIS data layers representing numerous site response parameters such as amplification and site period. This process is automatically completed for the entire grid coverage.

This type of analysis was repeated with 8 different time histories of acceleration. The Magnitudes of the events represented in the time histories ranged from $M_W=6.5$ to $M_W=8.1$ and the peak accelerations were scaled over a range of 0.05g to 0.30g. Numerous additional analyses are currently underway based on a 360m (1/4 resolution) grid size for the purpose of sensitivity analysis and error checking.

Liquefaction Analysis

Liquefaction susceptibility analysis was performed based on the simplified procedure of Seed and others by Dr. T.L. Youd and his students at Brigham Young University. The borehole database mentioned previously was used and the data it contained was supplemented by return visits to the original source material. The reliability and completeness of the data was then used to thin out the data set. The boreholes were then analyzed according to the simplified procedure to determine if the materials would liquefy in two scenario earthquakes, $M_W=6.5$ at 10 km and $M_W=8.5$ at 100 km. The total thickness of liquefiable material was also computed. These results were then extrapolated away from the boreholes based of the geology. Relative susceptibility classifications were assigned across the map on this basis. Lateral spread displacement predictions were also made based on regression equations developed from case history data from around the world.

Landslide Analysis

The landslide potential analysis will be based on the terrain slope derived from the U.S.G.S. 1:24,000 DEM and the thickness of the loess which overlies the Columbia River Basalt bedrock. The only area of significant topography in the quadrangle is the southwestern corner which is part of the Tualatin Mountains and consists of Columbia River Basalt bedrock overlain with a variable thickness of loess. The thickness of the loess material is being mapped based on borehole data and extensive seismic refraction profiling done under sub-contract by Dr. S.F. Burns, Dr. A. Johnson and their students at Portland State University. Other factors which influence slope stability such as vegetation and three dimensional geometry are being neglected, this simplification will be allowed for by a conservative approach to hazard delineation.

Reports

Madin, I.P., and Mabey, M.A., 1991, Seismic Hazard Mapping in the Portland Metro Area: Proceedings of the Fourth International Conference on Seismic Zonation, Stanford, California, August 1991. Earthquake Engineering Research Institute

Mabey, M.A., and Madin, I.P., 1992, Shear wave velocity measurements in the Willamette Valley and Portland Basin, Oregon. Oregon Geology, Vol. 54 No. 3, May, 1992.

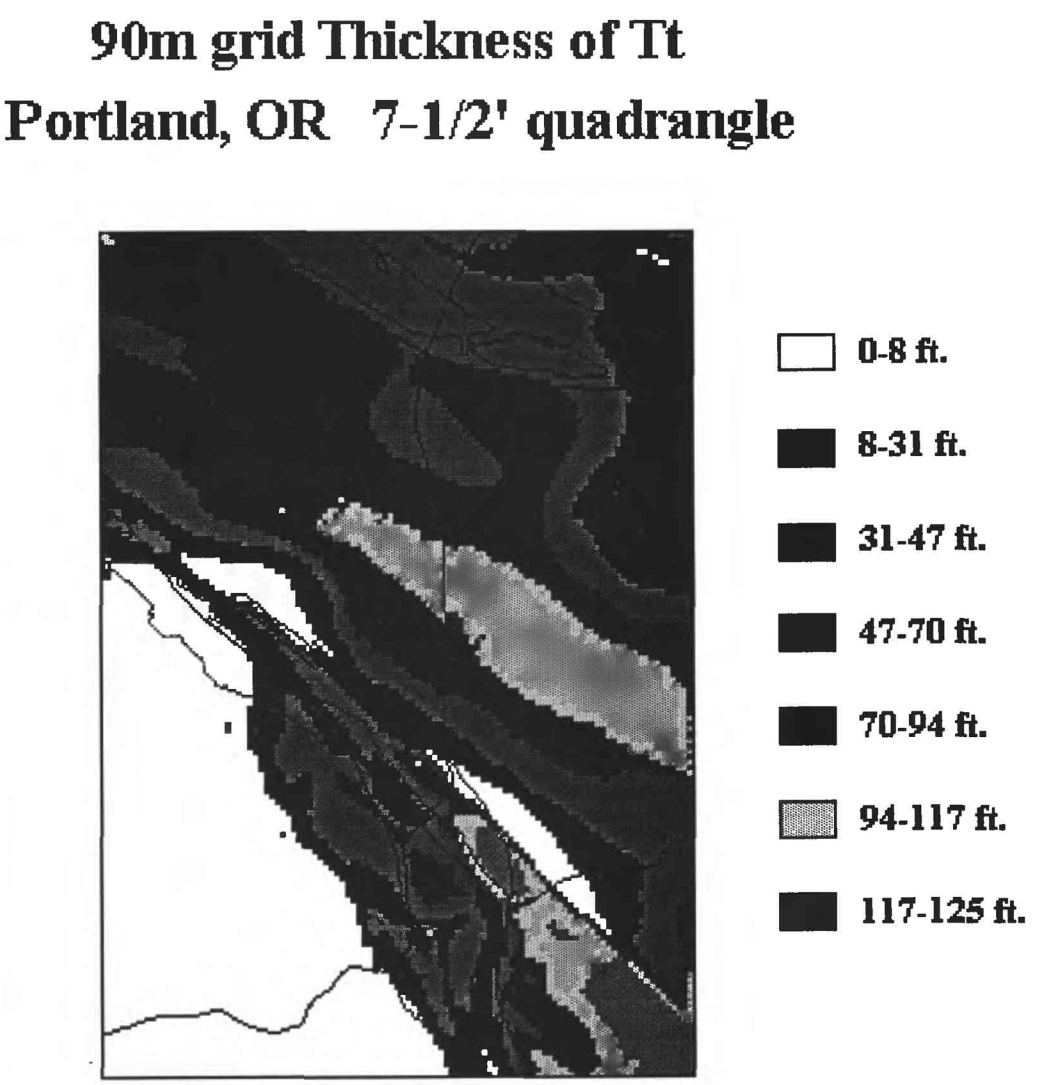

Figure 1. Example digital geologic model layer. Thickness and distribution of Unit Tt (Troutdale conglomerates) in the Portland quadrangle.

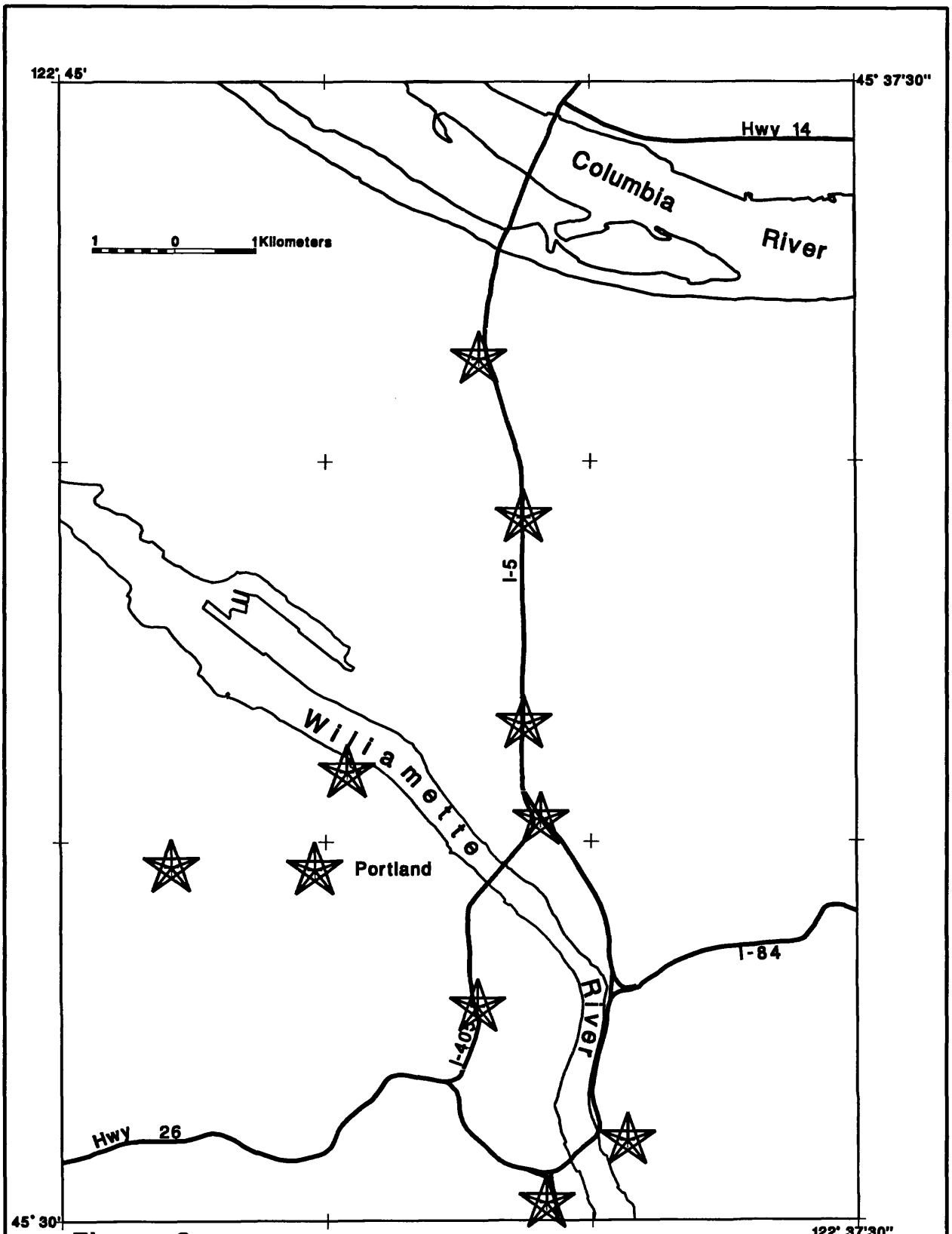

Figure 2. Stars indicate locations of boreholes drilled for shear-wave velocity logging within the Portland quadrangle.

Geologic Unit	Shear Wave Velocity
Unit Qal, Quaternary Alluvium sand, silt and clay.	Vs = 197 m/s +-30
Unit Ql, Quaternary Loess silt, very fine sand.	Vs = 288 m/s +-41
Unit Qff, Quaternary flood deposits, sand and silt.	Vs = 297 m/s +- 40
Unit Qfc, Quaternary flood deposits, gravel and boulders.	Vs = 513 m/s +- 43
Unit Tt, Pliocene Troutdale conglomerates.	Vs = 788 m/s +- 58
Unit Tsr, Pliocene Sandy River siltstones and sandstones	Vs = 750 m/s
Unit Tcr, Miocene Columbia River Basalt.	Vs = 1020 m/s +- 239

Figure 3. Representative shear wave velocities for the geologic model units of the Portland Quadrangle. Column is not to scale.

SCALING OF SEISMIC SOURCES

9910-04488

ART MCGARR
BRANCH OF ENGINEERING SEISMOLOGY AND GEOLOGY
U.S. GEOLOGICAL SURVEY
345 MIDDLEFIELD ROAD, MS 977
MENLO PARK, CALIFORNIA 94025
415/329-5645

Investigations

1. Seismic data recorded locally, both on the surface and underground, are analyzed to gain insight into the seismic source process, especially with regard to source scaling.

2. A special issue of *Pure and Applied Geophysics* entitled "Induced Seismicity" is in preparation.

Results

1. For three years, from early 1986 to early 1989, the USGS operated a seven-station seismic network in and around the Witwatersrand gold fields of South Africa. In addition to three continuously recording stations situated several hundred kilometers outside the gold fields, four GEOS digital event recorders were installed at the surface at each of the four most seismically active mining districts. During three short-term experiments, each of several weeks' duration, GEOS recorders were installed at underground sites within the two districts having the highest levels of seismicity. In November, 1986, two recorders were installed in the Western Deep Levels gold mine in the Carletonville district at depths of about 1800 and 3000 m. During two experiments in early 1988 and 1989, one GEOS unit was installed at a depth of 2065 m in the Vaal Reefs mine, Klerksdorp district, to record data in conjunction with the nearby GEOS recorder at the surface. Either ground velocity or acceleration were recorded at sampling rates of 400 per second during these three experiments.

   In the course of trying to determine seismic focal mechanisms for tremors, with moment-magnitudes ranging up to 3.3, it was found that the displacement waveforms recorded underground were incompatible with double-couple sources for the majority of events. Accordingly, a linear inversion technique was developed to determine the complete, six-component, moment tensor from waveforms recorded at several local stations, underground or surface. Although some inversions yield double-couple solutions, most show a substantial component of coseismic volumetric reduction; this reduction, $-\Delta V$, is presumably associated with the closure of the adjacent mine

2. As part of the 33rd U.S. Symposium on Rock Mechanics, Santa Fe, New Mexico, a Workshop on Induced Seismicity was held on June 10, 1992. This day-long workshop featured posters and discussion involving seismicity induced by deep mining, reservoir impoundment, liquid injection, and oil and gas exploitation. A pre-Workshop volume containing about 45 reports, abstracts, and extended abstracts was distributed to all participants several weeks before the Symposium and a special issue of PAGEOPH with about 25 papers on induced seismicity is in preparation.

Reports

McGarr, A., 1992, An implosive component in the seismic moment tensor of a mining-induced tremor: *Geophysical Research Letters,* p. 1579-1582.

McGarr, A., 1992, Moment tensors of ten Witwatersrand mine tremors, Pure and Applied Geophysics, accepted for publication.

McGarr, A. Çelebi, M., Sembera, E., Noce, T., and Mueller, C., 1991, Ground motion at the San Francisco International Airport from the Loma Prieta earthquake sequence: Bulletin of the Seismological Society of America, v. 81, no. 5, p. 1923-1944.

SOUTHERN CALIFORNIA SITE-RESPONSE INVESTIGATIONS

9910-04428

Charles S. Mueller
Branch of Engineering Seismology and Geology
U. S. Geological Survey
345 Middlefield Road, MS 977
Menlo Park, California 94025
(415) 329-5646

A. M. Rogers, Branch of Geological Risk Assessment, Golden, CO
J. C. Tinsley, Branch of Western Regional Geology, Menlo Park, CA

Investigations

The objective of this project is to investigate the influence of geologic structure on seismic ground motions in urban Southern California. We take a multi-disciplinary, multi-scale approach to the ground-motion problem, combining high-quality seismic waveform data, collected over a wide range of amplitudes and typical Southern California site conditions, with geological and geotechnical data.

The 1985 Michoacan and 1989 Loma Prieta earthquakes have reinforced well-known qualitative correlations between shaking and basin geometry and site geology, but the magnitude and predictability of site effects remains controversial (*e.g.*, can low-strain data be used to predict strong shaking?). A consensus now exists among seismologists and engineers that we must acquire the fundamental data that are needed to answer these questions and incorporate the results into engineering practice.

An array of eight wide-band, high-resolution (24-bit) digital seismographs will be installed in the Whittier-Norwalk and San Bernardino areas: six three-channel surface units and two six-channel borehole/surface units. The array is designed to provide data on the influence of geologic structure on ground-motion at scales from tens of kilometers (the Whittier-Norwalk array will extend from near the top of the Elysian Park antiform to near the deepest part of the Los Angeles basin) to tens of meters (borehole/surface sensors will be installed at the top and bottom of 300' boreholes at sites in Norwalk and San Bernardino where near-surface sediments are expected to respond nonlinearly during strong shaking). It will also provide a new real-time strong-motion monitoring capability in these populous areas.

Results

We have completed geotechnical drilling and data collection at all array sites: Cerritos College, Norwalk, police station (borehole/surface site, 300' borehole); Cerritos College physical sciences building (surface site, 100' borehole); Cerritos College gymnasium (surface site, 100' borehole); Los Alisos School, Norwalk (surface site, 100' borehole); St. Paul's School, Santa Fe Springs (surface site, 100' borehole); Lincoln School, Whittier (surface site, 100'

borehole); Hoover School, Whittier (surface site, 100' borehole); and Central Fire Station, San Bernardino (borehole/surface site, 300' borehole). P-wave and s-wave traveltime data were collected in each borehole using the apparatus developed by H.-P. Liu and others at the U. S. Geological Survey. Processing and analysis of these data is underway. Core samples collected during drilling are being analysed under the supervision of J. Tinsley; see his report in this volume for more information about the geotechnical work. The array hardware was received during the reporting period, and is currently undergoing testing in Menlo Park prior to deployment.

Reports

None.

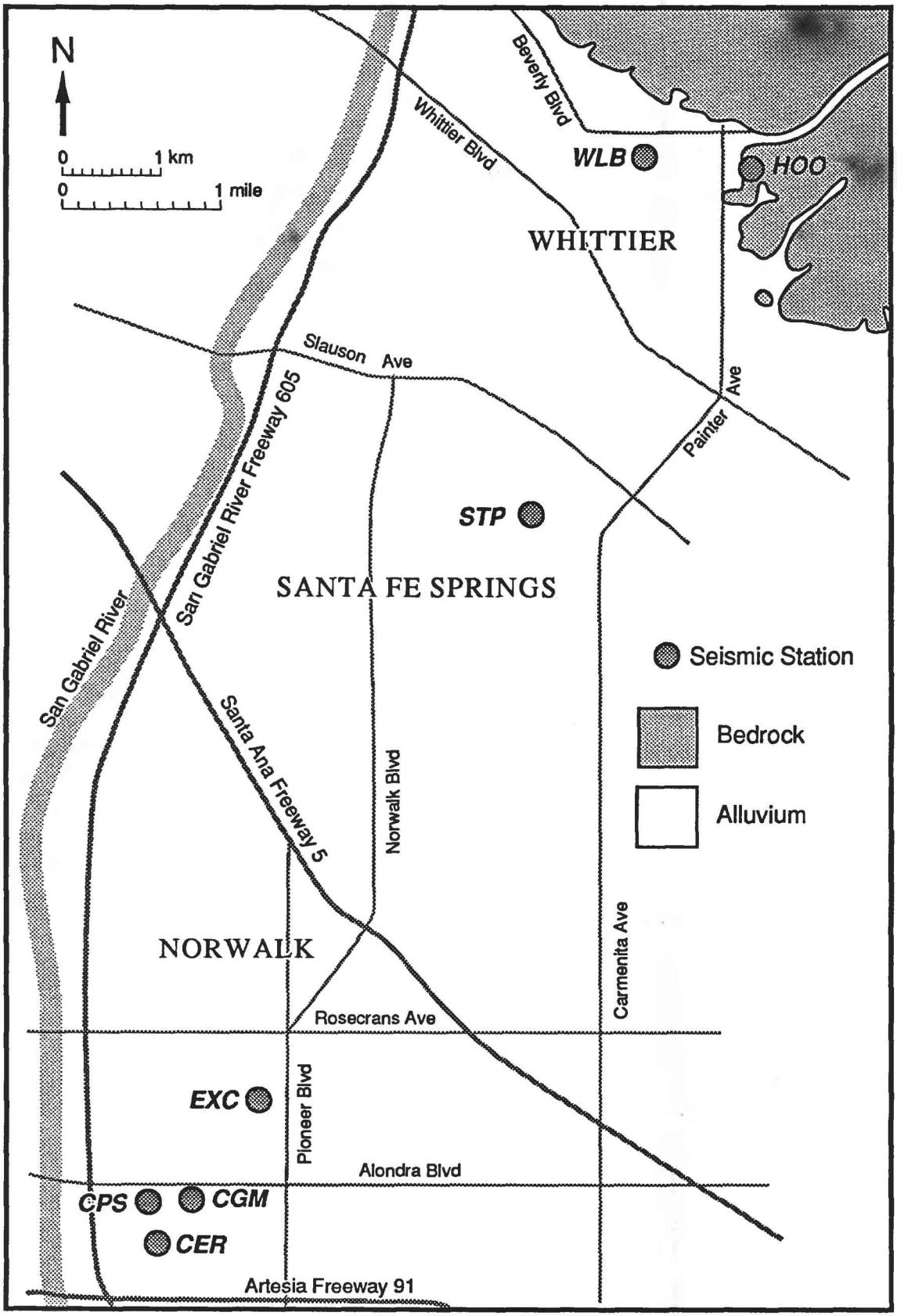

Map of the Whittier-Norwalk area showing the seismic array.

Liquefaction and Ground Failure in San Francisco: Site Investigation, Modeling, and Hazard Assessment for the Urban Environment

Grant No. 14-08-0001-G2128

Thomas D. O'Rourke and Harry E. Stewart
School of Civil and Environmental Engineering
Cornell University
265 Hollister Hall
Ithaca, NY 14853-3501
(607) 255-6470

INVESTIGATIONS UNDERTAKEN

There were four principal areas of soil liquefaction in San Francisco in 1906 and 1989, as shown in Figure 1. Recurrence of liquefaction during the 1989 Loma Prieta earthquake in the same locations as 1906 has critical implications for hazard mitigation in the City of San Francisco and, at the same time, provides an excellent opportunity to improve our modeling and prediction capabilities for the type of ground failure and deformation patterns caused by liquefaction. The problems of liquefaction are acute for San Francisco because the network of municipal water mains lying across liquefied ground is subject to numerous ruptures, which could result in the loss of water necessary to prevent the spread of fires. Catastrophic fire followed the 1906 earthquake and nearly followed the 1989 earthquake, due in part to lack of water.

This investigation is focused on the Mission District and South of Market areas of San Francisco, areas for which there was a substantial gap in knowledge between historic material and subsurface information. This gap left important questions unanswered as to the causes for past performance in earthquakes and also for evaluating future seismic performance, and provided a unique opportunity for a comparative analysis and evaluation of the four principal areas of liquefaction in San Francisco. Of great importance is the fact that these areas are urban sites which show the interaction between ground failure and infrastructure response, particularly of lifeline systems.

Site Exploration

Three sites in the Mission District and one site in the South of Market were explored in 1991. The sites were located in areas of historic liquefaction where little information about the subsurface conditions was available. Figures 2 and 3 show the locations of site exploration with respect to liquefaction features (O'Rourke, et al. 1992). An integrated program of CPT soundings, boreholes with SPT measurements and soil sampling, and seismic wave velocity profiling was performed to provide complimentary, yet independent, assessments of subsurface conditions.

The South of Market area is the site of the former Sullivan Marsh, a tidal marsh which was once contiguous with San Francisco Bay. Figure 2 shows the outline of the

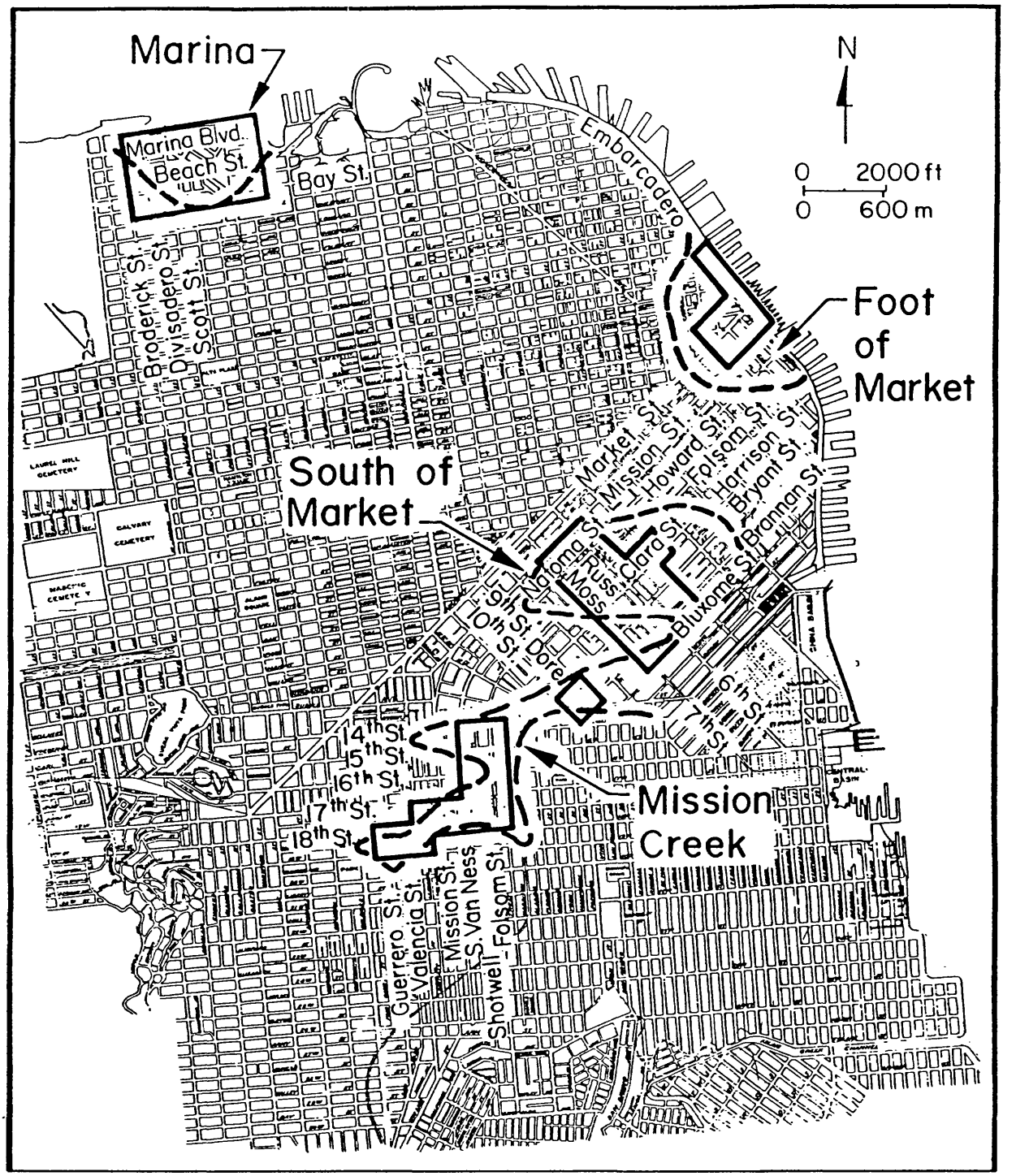

Legend: — — — Zones of Loose Fill Affected by Soil Liquefaction in 1906

——— Zones of Inspection after 1989 Earthquake

Figure 1. Principal areas of soil liquefaction in San Francisco in 1906 and 1989

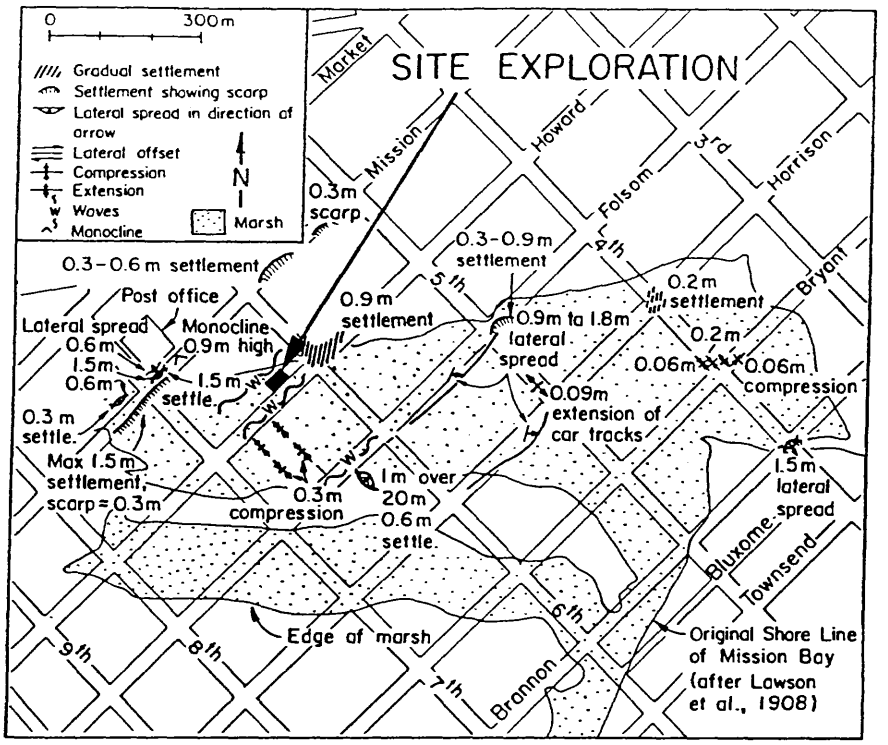

Figure 2. Plan view of the South of Market area with 1906 liquefaction-induced ground deformation

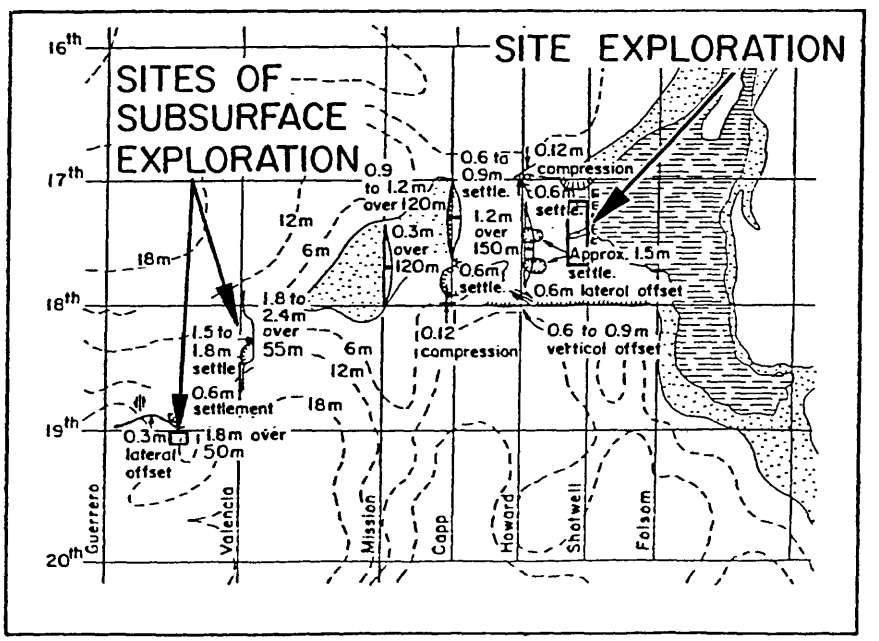

Figure 3. Plan view of 1906 liquefaction-induced ground movements and subsurface topography in the Mission Creek area

former marsh and of the original shoreline of Mission Bay to the south of Brannan Street. The ground displacements in the South of Market area mostly fall within the boundary of the former marsh. Investigations on Howard Street in the South of Market have resulted in subsurface data from 4 CPT soundings to depths of 15 to 20 m, a piezocone sounding to 18 m, a conventional boring with SPT measurements and sampling to bedrock at 70 m depth, and a downhole seismic shear wave velocity profile obtained with a seismic cone sounding to 20 m depth.

The Mission District was built over the marshes and deep ravines of Mission Creek. Figure 3 shows the outline of the former marsh, and dashed contours corresponding to the 1853 ground surface. Ground displacements in 1906 occurred within the upper marsh and ravine areas. Investigations on Shotwell Street in Mission Creek have resulted in subsurface data from 4 CPT soundings to 20 to 26 m depths, a conventional boring with SPT measurements and sampling to bedrock at 60 m depth, and a downhole seismic shear wave velocity profile obtained to 20 m depth. Investigations in Valencia Street have resulted in subsurface data from 2 CPT soundings to approximately 20 m depth and one conventional boring with SPT measurements and sampling to a depth of 20 m. Investigations on 19th Street west of Valencia Street have resulted in subsurface data from one CPT sounding to 29 m depth, 2 piezocone soundings to 14 m depths, one conventional boring with SPT measurements and sampling to bedrock at 35 m depth, and a downhole seismic shear wave velocity profile to a depth of 12 m.

Development of Subsurface Database

In addition to the subsurface explorations conducted for this project, approximately 150 borehole and sounding records in the Mission District and 310 records in the South of Market area were collected, reviewed, and summarized for stratigraphic changes to evaluate subsurface conditions in the two study areas. Subsurface data were obtained from both public and private sources, with extensive assistance from Harding Lawson Associates, Dames and Moore Inc., the City Engineer of San Francisco, and numerous independent geotechnical consultants.

RESULTS OBTAINED

An extensive and detailed database has been assembled for the Mission Creek and South of Market areas of San Francisco, including maps of bedrock surface contours, thickness of Holocene bay mud, fill thickness, groundwater depths, and surface gradients. In addition, maps of historic ground deformation, locations of soil liquefaction, and buried lifeline damage during the 1906 San Francisco and 1989 Loma Prieta earthquakes have been developed and correlated with the subsurface information.

It has been found that thickness of liquefiable soils is an excellent predictor of damage observed in San Francisco. Clean, poorly graded fill sands, found in Mission Creek and South of Market, are the main soil group, having low silt and clay content and low relative density. Thickness of filled ground below the current water table, referred to here as submerged fill thickness, is a very simple parameter to obtain, but successfully

explains the varying levels of liquefaction and ground deformation observed in San Francisco.

Mission Creek

Figure 4 shows contours of submerged fill thickness in the Mission Creek area. Submerged fills west of Shotwell Street are uniformly clean, poorly graded sand, typical of dune sand of loose to medium density. Hence, these materials are moderately to highly susceptible to liquefaction. Fills east of Shotwell Street are heterogeneous, primarily consisting of non-liquefiable soil, but with some local areas of dune sand.

For comparison, Figure 5 shows ground displacement features reported in the Mission Creek area following the 1906 earthquake. The map was developed further and refined in this project from the ground deformation maps of O'Rourke, et al. (1992). There is a close correspondence between the locations and spatial distributions of displacement and the locations and areal extent of liquefiable fill thickness.

During the 1989 Loma Prieta earthquake, moderate settlements, sand boils, and cracking were noted sporadically in the submerged fill zone east of Shotwell Street. The most severe liquefaction and associated building damage occurred within the block bounded by South Van Ness, Shotwell, 17th, and 18th Streets, which corresponds to a location of relatively thick liquefiable fill.

South of Market

Figure 6 shows contours of submerged fill thickness in the South of Market area. Submerged fills throughout the study area are, with a few isolated exceptions, slightly silty to clean, poorly graded sand of loose to medium density.

For comparison, Figure 7 shows ground displacement features reported in the South of Market area following the 1906 earthquake. Again, there is a close correspondence between the locations and spatial distributions of displacement and the locations and areal extent of liquefiable fill thickness. In particular, a strong correlation between ground deformation and thickness of liquefiable fill can be seen near 7th and Howard Streets, Dore and Bryant Streets, and 5th and Harrison Streets.

During the 1989 Loma Prieta earthquake, there was approximately 300 mm of liquefaction-induced settlement a half-block north of the intersection of 7th and Howard Streets. This movement ruptured a water main of the Auxiliary Water Supply System (AWSS) and contributed significantly to loss of water from the Jones Street Tank, thereby placing the AWSS out of service throughout the central business district of San Francisco (O'Rourke, et al., 1991). In 1989, liquefaction and significant settlements were observed near Dore and Bryant Streets, as well as at Townsend and 6th Streets. All these locations correspond to areas with thickness of liquefiable fill equal to or great than 4 m.

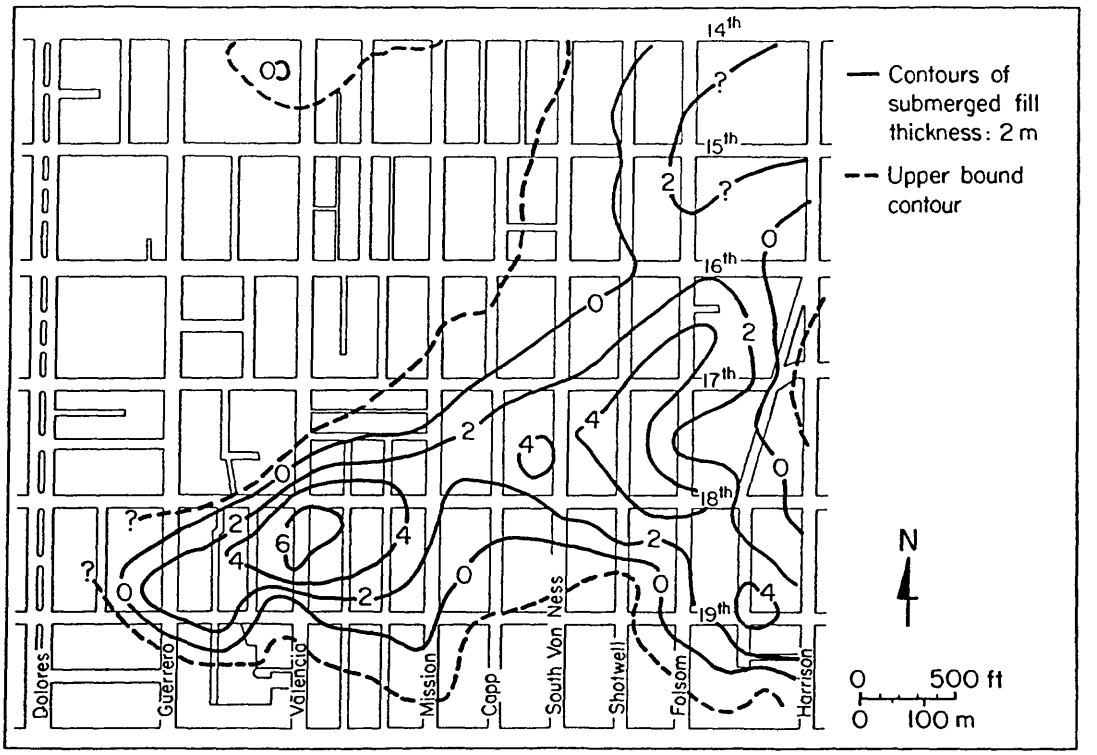

Figure 4. Contours of thickness of liquefiable fill in the Mission Creek area

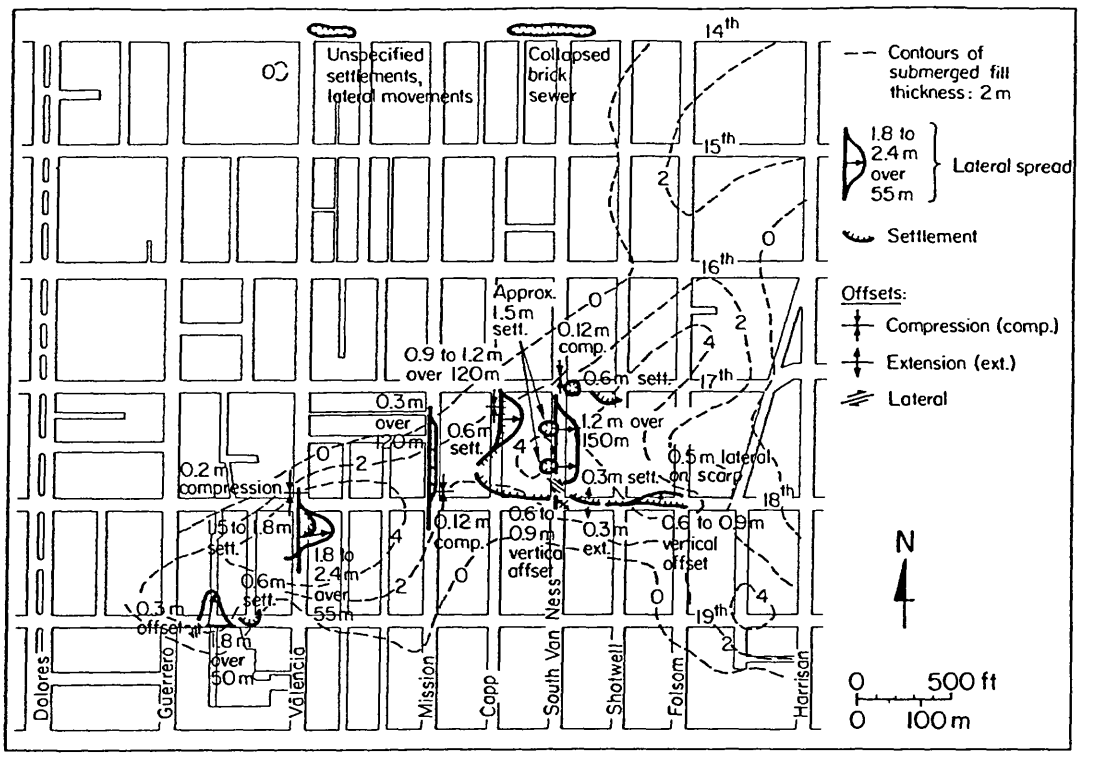

Figure 5. Map of liquefaction-induced ground deformation in the Mission Creek area following the 1906 San Francisco earthquake

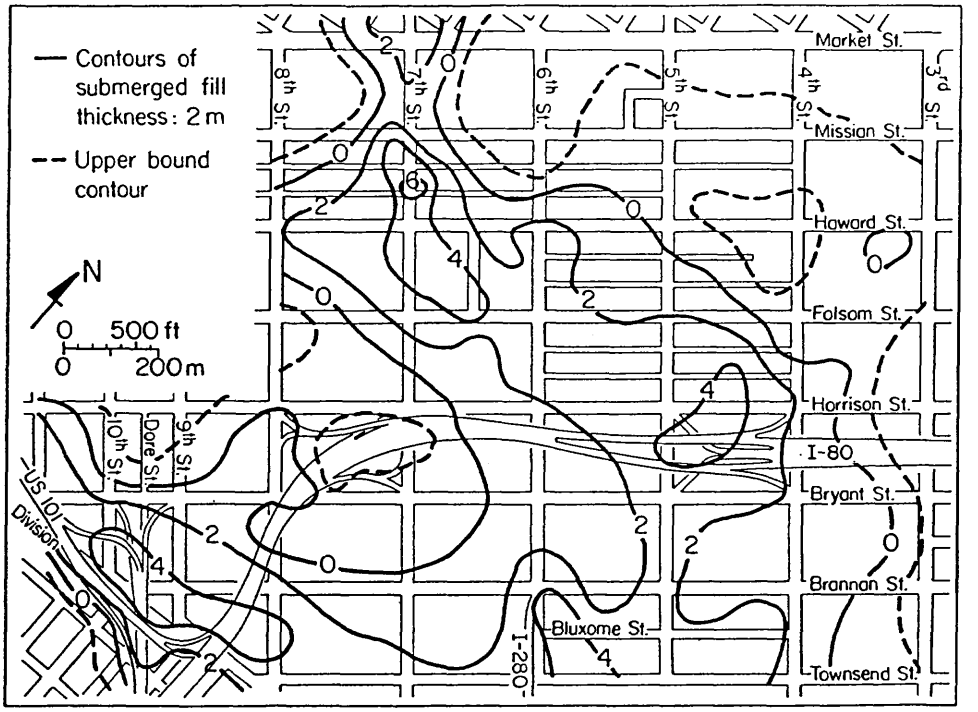

Figure 6. Contours of thickness of liquefiable fill in the South of Market area

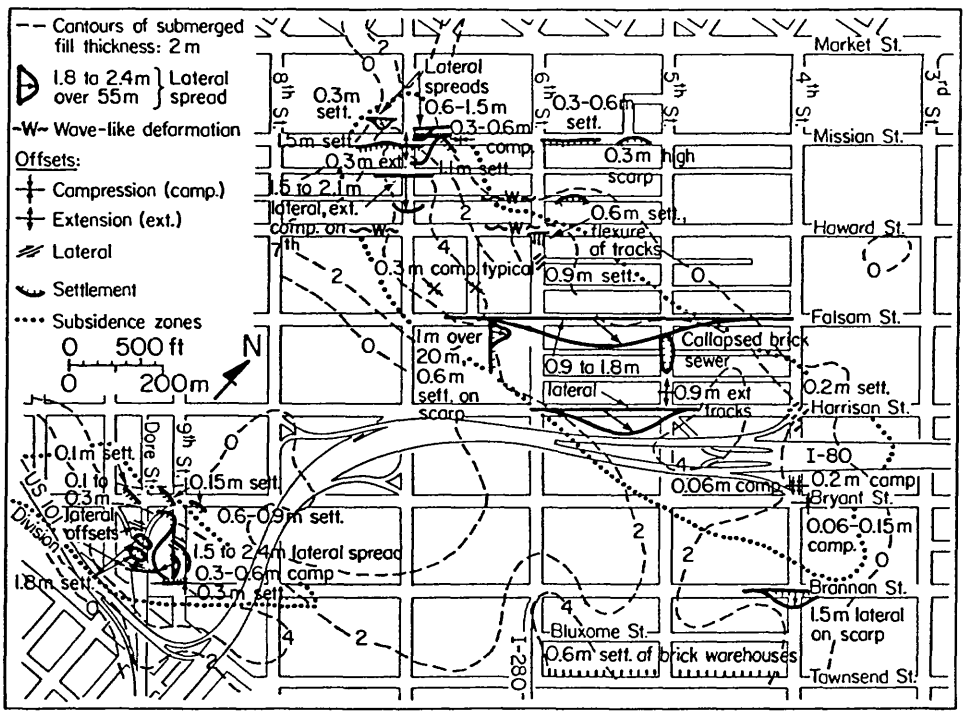

Figure 7. Map of liquefaction-induced ground deformation in the South of Market area following the 1906 San Francisco earthquake

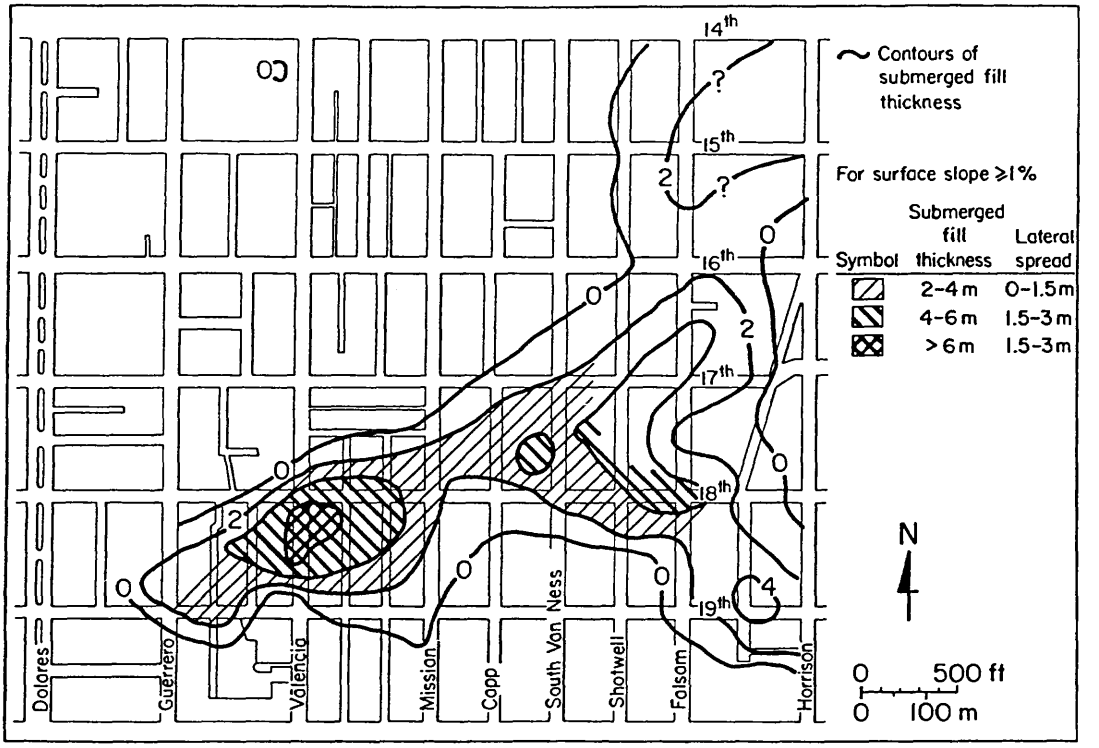

Figure 8. Graphical display of submerged fill thickness and indication of potential liquefaction severity in the Mission Creek area

Research Implications

The research findings have some very important implications for engineering and planning in areas of potential liquefaction. The research has shown that the thickness of liquefiable fill is a good index of the severity of liquefaction and the potential magnitude of ground deformation. This finding is corroborated by recent work on liquefaction-induced ground deformation during Japanese earthquakes (Hamada and O'Rourke, 1992), indicating that the thickness of a liquefiable natural deposit is the most important parameter which correlates well with the magnitude of ground deformation. Pease, et al. (1992) also have shown that thickness of liquefiable fill correlates very closely with damage to the water supply network in the Marina after the 1989 earthquake.

The thickness of liquefiable fill or natural sand deposit is a simple parameter which can be determined from computerized databases by subtracting the depth of the water table from the depth of loose to medium dense sand. A graphical display of this information provides a measure of the potential spatial distribution of liquefaction and ground deformation, which is of critical importance for evaluating liquefaction effects on buried lifeline systems.

The thickness of liquefiable fill is easily adapted to geographic information systems (GIS). Figure 8 provides an illustration of a potential GIS application in which various thicknesses of liquefiable fill for surface gradients exceeding 1% are accentuated in a graphical format to identify locations and potential magnitudes of lateral spreads, based

on 1906 observations. The plotting of this simple geologic parameter in relation to the built environment and lifeline network provides a useful vehicle for assessing urban hazards, microzoning for seismic hazard reduction, and planning for optimal lifeline performance during an earthquake.

REPORTS PUBLISHED

O'Rourke, T.D., Ed., "The Loma Prieta Earthquake, California of October 17, 1989 - Marina District", USGS Professional Paper 1551-F, U.S. Government Printing Office, Washington, DC, 1992.

O'Rourke, T.D., W.D. Meyersohn, H.E. Stewart, J.W. Pease, and M. Miyajima, "Site Response and Soil Liquefaction in San Francisco During the Loma Prieta Earthquake", Proceedings, 4th Japan-U.S. Workshop on Earthquake Resistant Design of Lifeline Facilities and Countermeasures Against Soil Liquefaction, Honolulu, HI, May 1992.

O'Rourke, T.D. and J.W. Pease, "Large Ground Deformations and Their Effects on Lifeline Facilities: 1989 Loma Prieta Earthquake", Case Studies of Liquefaction and Lifeline Performance During Past Earthquakes, Vol. 2, T.D. O'Rourke and M. Hamada, Eds., Technical Report NCEER-92-0002, National Center for Earthquake Engineering Research, Buffalo, NY, Feb. 1992, pp. 5-1 to 5-85.

O'Rourke, T.D., J.W. Pease, and H.E. Stewart, "Lifeline Performance and Ground Deformation During the Earthquake", U.S.G.S. Professional Paper 1551-F, T.D. O'Rourke, Ed., U.S. Government Printing Office, Washington, DC, 1992, pp. F155-F179.

REFERENCES

Hamada, M. and O'Rourke, T.D., Eds., Case Studies of Liquefaction and Lifeline Performance During Previous Earthquakes, Vol. 1, Technical Report NCEER-92-0001, National Center for Earthquake Engineering Research, Buffalo, NY, May 1992.

O'Rourke, T.D. and J.W. Pease, "Large Ground Deformations and Their Effects on Lifeline Facilities: 1989 Loma Prieta Earthquake", Case Studies of Liquefaction and Lifeline Performance During Past Earthquakes, Vol. 2, T.D. O'Rourke and M. Hamada, Eds., Technical Report NCEER-92-0002, National Center for Earthquake Engineering Research, Buffalo, NY, Feb. 1992, pp. 5-1 to 5-85.

O'Rourke, T.D., P.A. Beaujon, and C.R. Scawthorn, "Large Ground Deformations and Their Effects on Lifeline Facilities: 1906 San Francisco Earthquake", Technical Report NCEER 92-0002, Case Studies of Liquefaction and Lifeline Performance During Previous Earthquakes, Vol. 2, T.D. O'Rourke and M. Hamada, Eds., National Center for Earthquake Engineering Research, Buffalo, NY, May 1992, pp. 1-1 to 1-134.

O'Rourke, T.D., T.E. Gowdy, H.E. Stewart, and J.W. Pease, "Lifeline and Geotechnical Aspects of the 1989 Loma Prieta Earthquake", Proceedings, 2nd International Conference on Recent Advances in Geotechnical Earthquake Engineering and Soil Dynamics, St. Louis, MO, Mar. 1991, Vol. II, pp. 1601-1612.

Pease, J.W., T.D. O'Rourke, and H.E. Stewart, "Post-Liquefaction Consolidation and Lifeline Damage in the Marina District after the 1989 Loma Prieta Earthquake", Proceedings, 4th Japan-U.S. Workshop on Earthquake Resistant Design of Lifeline Facilities and Countermeasures Against Soil Liquefaction, Honolulu, HI, May 1992.

Wave Propagation and Amplification in Sedimentary Valleys: Refinement and Validation of a Method of Analysis

Award No. 1434–92–G–2168

Apostolos S. Papageorgiou
Department of Civil & Environmental Engineering
Rensselaer Polytechnic Institute
Troy, New York 12180–3590

(518) 276–6331

Objectives:

The objective of the project are the following:

(I) To extend and refine the discrete wavenumber boundary element method (DWBEM) so that it can be used to analyze the response of infinitely long sedimentary valleys of uniform (along the major horizontal axis) but arbitrary cross–section embedded in a half–space, to elastic body and surface waves incident with arbitrary angles with respect to the vertical and horizontal axes of the valley (Figure 1).

(II) To use the extended and refined discrete wavenumber boundary element method to study the frequency and time response of sedimentary valleys to elastic waves impinging in the underlying half–space with arbitrary angles with respect to the vertical and horizontal axes of the valleys.

(III) To use the method/model which was described in objective (I) to analyze the data recorded by the Gilroy array at the Santa Clara Valley, California, during the 1979 Coyote Lake, 1984 Morgan Hill and 1989 Loma Prieta earthquakes and their aftershocks.

Results:

So far we have successfully completed the mathematical formulation of the problem (Objective I) and we have transformed this formulation into an efficient computer code. We currently are in the process of completing Objective (II).

Our results so far have demonstrated that for nearly vertical incidence (i.e. $i \to 0^\circ$), the effect of the azimuthal angle of incidence φ amounts simply to a projection of the displacement components. In this case, the 3–D response can be obtained from knowledge of the in–plane and out–of–plane response of a 2–D model.

However, when the direction of incidence deviates considerably from the vertical and $\varphi \neq 0$, all three components of the response are strongly coupled. For instance, even for incident SH waves, when $i = 30^\circ$ and $\varphi = 30^\circ$ (Figure 2a), Rayleigh waves are induced and propagate inside the valley as well as Love waves. Complex patterns of motion with

prolonged duration are induced on the surface of the sediments due to the various interfering modes of propagation (Figure 2b).

Reports:

Papageorgiou, A.S. and D. Pei "Response of Cylindrical Alluvial Valleys of Arbitrary Cross–Section to Seismic Waves by the Boundary Element Method," 6th International Conference on Soil Dynamics & Earthquake Engineering, June 14–16, 1993, Bath, U.K.

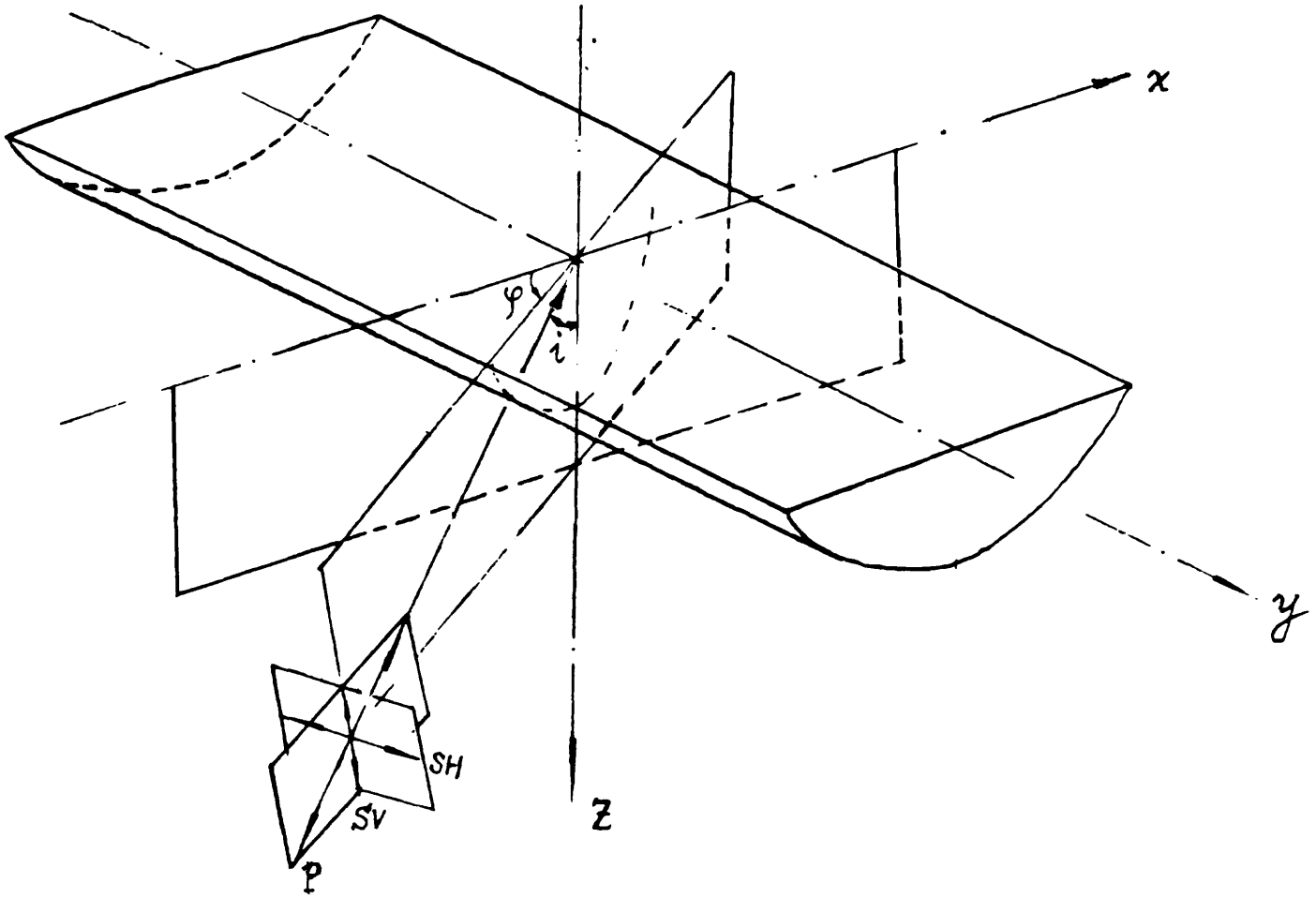

Figure 1: A two–dimensional model of a valley excited by a three–dimensional incident wave field. The azimuthal angle φ and the incidence angle i are in general non–zero. It should be pointed out that even though the geometry of the model is two–dimensional, the response is three–dimensional with the out–of–plane motions (y–component) being coupled with the in–plane motions (x,z components).

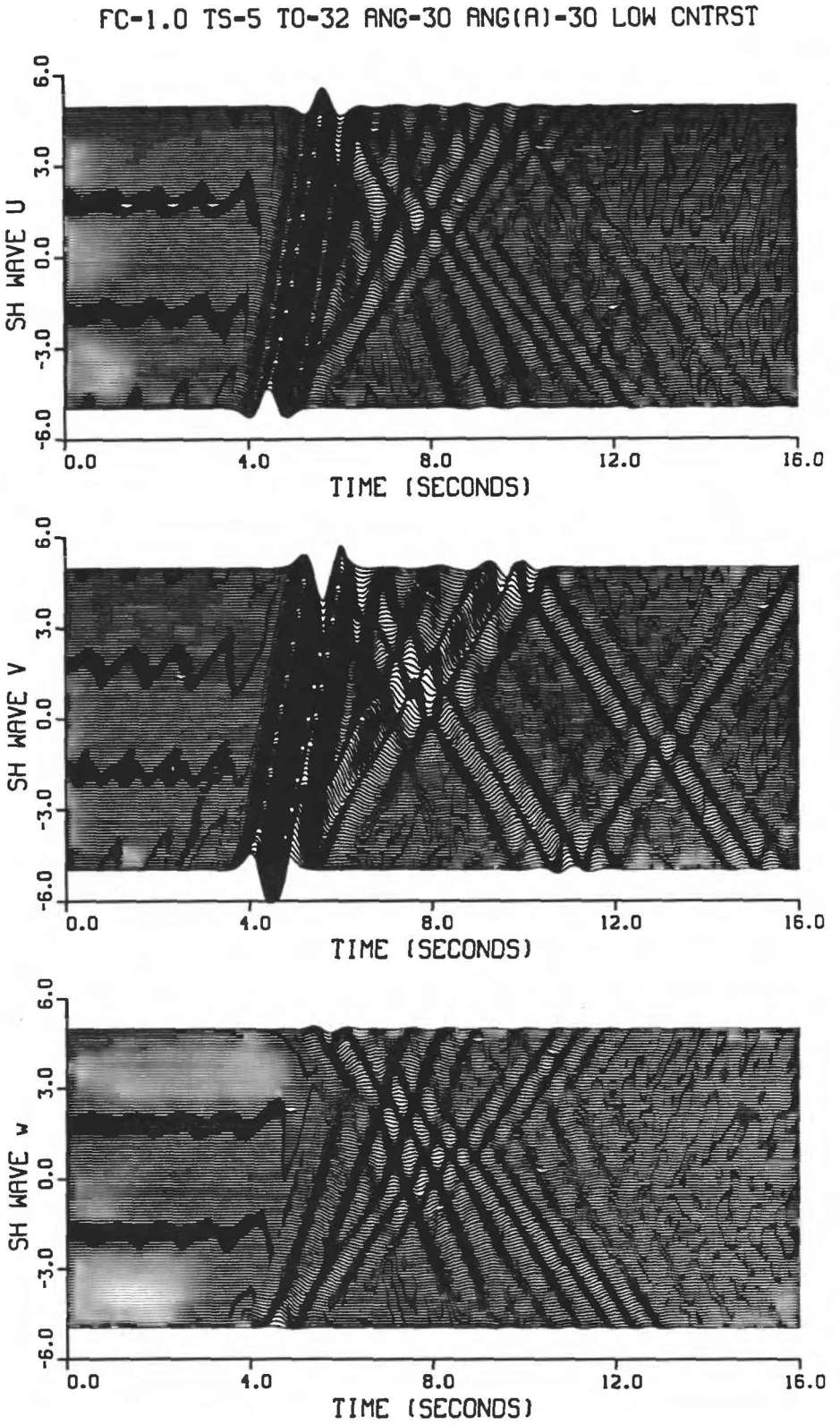

Figure 2a: Response of type 2 valley model (low contrast) of Bard and Bouchon (1980a,b) to incident SH waves. Angle of incidence $i = 30°$; azimuthal angle $\varphi = 30°$

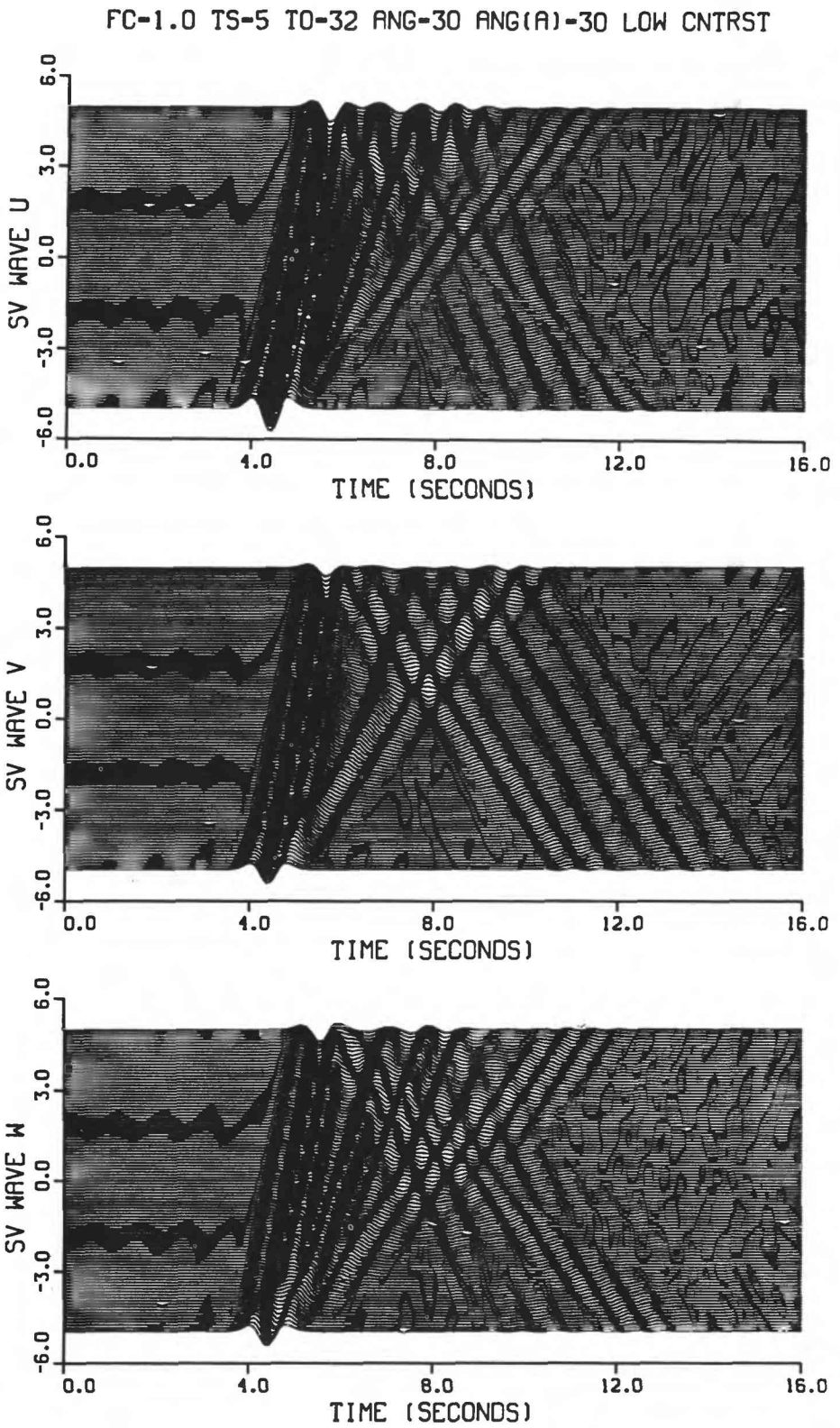

Figure 2b: Same as Figure 2a but for incident SV waves.

National Earthquake Information Service

9920–10022

Waverly J. Person
Branch of Global Seismology and Geomagnetism
U.S. Geological Survey
Denver Federal Center
Box 25046, Mail Stop 967
Denver, CO 80225
(303) 273–88500

Investigations and Results

The Quick Epicenter Determination (QED) continues to be available to individuals and groups having access to a 300- or 1200-band terminal with dial-up capabilities to a toll-free WATS number or a commercial telephone number in Golden, Colorado. It is also accessible via GEONET and public TYMNET. The QED has become one of our most popular ways of making near-real-time earthquake information available to the general public and scientists throughout the world. The time period of data available in the QED is approximately three weeks (from about two days behind real time to the current PDE in production). The QED program is available on a 24-hour basis, 7 days a week. From October 1, 1991 through September 30, 1992, there were 40,000 logins to the QED programs. A daily QED message, 7 days behind real time, is transmitted to many different agencies in the United States and throughout the world via electronic mail, including a scientific bulletin board operated by Dr. Francis Wu at the State University of New York at Binghamton. This bulletin board is accessible by anyone who is connected to BITNET. The daily QED message is also distributed to another 32 agencies via U.S. government communications (VADATS/DTS/AUTODIN), including worldwide distribution on the communications system of the World Meteorological Organization.

NEIS is making extensive use of electronic mail for data acquisition. Data are now being received via GEONET, TYMNET, internet, BITnet, DECNET/SPAN and uucp on a regular basis from several dozen agencies. Some of the agencies sending data to the NEIS via electronic mail included the following:

Universidad Autonoma de Mexico, Mexico City
Instituto Nazionale di Geofisica, Rome, Italy
Centre Seismologique Euro-Mediterraneen, Strasbourg, France
Kandilli Observatory, Istanbul, Turkey
Harvard University, Cambridge, MA (Centroid, Moment Tensor Solutions)
Graefenberg Observatory, Germany
Icelandic Meteorological Institute, Reykjavik, Iceland
Central Seismological Observatory, Obninsk, Russia
Seismological Survey, Ljubljane, Slovenia

Inst. of Seismology, Helsinki, Finland
Bureau of Mineral Resources, Canberra, Australia
Dept. of Scientific and Indust. Research, Wellington, New Zealand
Universidad Nacional de la Plata, Argentina
Project GEOSCOPE, Paris, France
Soviet Union
Chile
Czechoslovakia

In addition, the following agencies contribute data to the PDE program by computer file transfer or remove login via the computer networks:

USGS Alaska Seismic Project, Menlo Park
USGS/California Institute of Technology, Pasadena
USGS Fredericksburg Observatory, Corbin, Virginia
USGS Guam Observatory, Mariana Islands
University of California, Berkeley
University of Southern California, Los Angeles
University of Washington, Seattle
Northern Illinois University, DeKalb
Oklahoma Geophysical Observatory, Leonard

Data acquisition by electronic mail is in the process of being established with the Bureau Central Seismologique Francaise in France.

The following organizations are now receiving the automatically located earthquakes from the NSN system when an earthquake is located for specified magnitudes:

Recipient		Event Criteria
G. Smriglio, ING, Rome, Italy		>=5.5 worldwide
Duty Officer, ING, Rome, Italy		>=5.5 worldwide
S. Sipkin, USGS/NEIC		>=5.5 worldwide
J. Fyen, NORSAR, Norway		>=5.5 worldwide
Inst. of Geophysics, UNAM, Mexico		>=4.8 in/near Mexico
T. Heaton, CalTech, Pasadena		>=5.5 worldwide
	and	>=2.5 in CA or NV
L. Kong, PTWC, Honolulu		>=5.5 worldwide
U. Kradolfer, ETH, Zurich, Switz.		>=5.5 worldwide
USGS CalNet Duty Officer, Menlo		>=3.0 in CA or NV
Japan Meteorological Agency, Tokyo		>=5.5 worldwide
Union Pacific Railroad, Omaha NE		>=4.5 in contig. US

Telegraphic data are now being exchanged with the USSR on most larger earthquakes. The Soviet data are being received from the Central Seismological

Observatory, Obninsk, under the auspices of the World Data Center system. Our designation as World Data Center A for Seismology played a key role in permitting this exchange to be established.

Data from the People's Republic of China via the American Embassy continue to be received in a very timely manner and in time for the PDE publication. We continue to receive four stations on a weekly basis from the State Seismological Bureau of the People's Republic of China. The Bulletins with additional data are now being received by floppy disk in time for the Monthly.

Special efforts are being made to receive more data from the Latin American countries on a more timely basis. The increased availability of telefax is permitting much more interaction with Latin American countries than in the past, but there are still problems getting data on timely basis for many large earthquakes.

We have rapid data exchange (alarm quakes) with Centre Seismologique European-Mediterranean (CSEM), Strasbourg, France and Instituto Nazionale de Geofisica, Rome, Italy, and Sicily, and data by telephone from Mandaring Geophysical Observatory, Mundaring, Western Australia and Pacific Tsunami Warning Center in Honolulu. The geophysical laboratory in Papeete, French Polynesia contributes a single-station estimate of seismic moment within about 24 hours of a large event in the Pacific region. We also have the capability to dial into computers at the Bureau of Mineral Resources, Canberra, Australia, and Swiss Seismic Services at Zurich, and collect data on recent earthquakes. The Monthly Listing of Earthquakes is up to date. As of September 30, 1992, the Monthly Listing and Earthquake Data Report (EDR) have been completed through May 1992. The total number of events located for 1991 was 16,516, the second largest number for any given year. Radiated energy, moment tensor, P-wave first-motion and broadband depth solutions continue to be determined by the USGS when possible and published in the Monthly Listing and EDR for any earthquake having an m_b magnitude $\geq$ 5.8. Centroid moment tensor solutions contributed by Harvard University continue to be published in the Monthly Listing and EDR. Waveform plots are being published for selected events having m_b magnitude $\geq$ 5.8.

The Earthquake Early Alerting Service (EEAS) continues to provide information on recent earthquakes on a 24-hour basis to the Office of Earthquakes, Volcanoes, and Engineering; scientists; news media; other government agencies; foreign countries; and the general public.

One-hundred and eighteen releases were made from October 1, 1991 through September 30, 1992. The most significant earthquakes in the United States were as follows:

- On April 23, 1992, a magnitude 6.3 earthquake occurred in southern California. Thirty-two people were treated for minor injuries, and light to moderate damage occurred.

- On April 25, a magnitude 7.1 earthquake occurred near the coast of northern California. Ninety-eight people were injured and there was considerable damage in southwestern Humboldt County. Preliminary estimate of damage in the series of earthquakes was $66 million in U.S. dollars.
- On April 25, a magnitude 6.6 earthquake occurred near the coast of northern California, and on April 26, another magnitude 6.6 earthquake occurred in the same place.
- On June 28, a magnitude 7.6 earthquake occurred in southern California (Landers). One person was killed and at least 350 persons were injured. The Maximum Intensity was IX. The preliminary estimate of damage for this earthquake, plus the following magnitude 6.6 event at 15:05 UTC in Big Bear, was $92 million in U.S. dollars.
- On June 29, a magnitude 5.5 earthquake occurred at the California-Nevada border region. There was damage to the Department of Energy buildings at the Nevada Test Site and minor damage at Beatty, Amargosa Valley, and Mercury.
- On July 9, a magnitude 5.5 earthquake occurred in southern California. At least 16 people were injured, and additional damage occurred in the Big Bear Lake area.
- On August 7, a magnitude 6.5 earthquake occurred in the Gulf of Alaska. There were no reports of damage.
- On September 2, a magnitude 5.8 earthquake occurred in Utah. There was damage at Springdale, Hurricane, and New Harmony, as well as landslides in the Springdale area.
- On September 30, there was a magnitude 6.6 earthquake in the Andreanof Islands, Aleutian Islands. There were no reports of damage.

The most significant foreign earthquakes were as follows:

India

- On October 19, 1991, a magnitude 7.1 earthquake occurred. At least 2,000 people were killed, and more than 1,000 people were injured. The earthquake destroyed 10,000 buildings in the Chamali-Uttarkashi area.

Turkey

- On March 13, 1992, a magnitude 6.8 earthquake occurred. At least 498 people were killed, 2,000 were injured, and some were listed as missing. There were 2,200 houses which sustained heavy damage at Eyzincan.

The Netherlands

- On April 13, a magnitude 5.5 earthquake occurred (rare for this area). One person died from a heart attack in Bonn, Germany. Twenty people were injured, and there was some building damage (VIII) in Rosermond, Netherlands. Twenty-five people were injured, and buildings were damaged (VII) in Heinberg, Germany.

Pakistan

- On May 20, a magnitude 6.0 earthquake occurred. At least 36 people were killed and 100 were injured in the Peshawar and Kahat districts.

Cuba Region

- On May 25, a magnitude 7.0 earthquake occurred (a rare earthquake of this magnitude in the area). Forty people were injured, and there was some damage reported in the Manzanilla-Niguera area.

Kyrgyzstan

- On August 19, a magnitude 7.4 earthquake occurred. Sixty people were killed, not including the 14 killed by landslides in Tokek. Several villages, including Toulk, were destroyed (IX) in the Susamyrtau Mountains, and at least 8,200 dwellings were destroyed.

Near the Coast of Nicaragua

- On September 2, a magnitude 7.2 earthquake occurred generating a tsunami which killed at least 116 people; 68 people are still reported as missing. Many houses were destroyed, and fishing boats were destroyed along a 250 km strip of the west coast of Nicaragua.

Reports

Monthly Listing of Earthquakes, in Seismological Research Letters, Eastern Section, SSA, v. 62, no. 3 and no. 4, July through September 1990; v. 63, no. 1, October through December 1990; v. 63, no. 2, January through March 1991. Compilers: Jacobs, W., Chang, P., Lavonne, C., Minsch, J., Person, W., Presgrave, B., Schmieder, W.

Monthly Listing of Earthquakes and Earthquake Data Reports (EDR); 12 publications from June 1991 through May 1992. Compilers: Jacobs, W., Chang, P., Lavonne, C., Minsch, J., Needham, R., Person, W., Presgrave, B., Schmieder, W.

Person, Waverly J., Earthquakes, in Earthquakes and Volcanoes, v. 22, no. 6, March–April, May–June, July–August, September–October, November–December 1990; v. 23, no. 1, January–February, March–April 1991.

Person, Waverly J., Seismological Notes: Bulletin of the Seismological Society of America, v. 81, no. 6, November–December 1990, January–February 1991; v. 82, no. 1, March–April 1991; v. 82, no. 2, May–June 1991; v. 82, no. 3, July–August 1991; v. 82, no. 4, September–October 1991; v. 82, no. 5, November–December 1991.

Person, Waverly J., Jacobs, Jan M., 1992, Significant earthquakes of the world 1985–1989: U.S. Geological Survey Open-File Report 92–291, 32 p.

Person, Waverly J., Jacobs, Jan M., 1992, Significant earthquakes of the world 1990: U.S. Geological Survey Open-File Report 92–583, 9 p.

Person, Waverly J., Jacobs, Jan M., 1992, Significant earthquakes of the world 1991: U.S. Geological Survey Open-File Report 92–584, 9 p.

Preliminary Determination of Epicenters (PDE); 76 weekly publications from April 11, 1991 through September 24, 1992, numbers 12–91 through 35–92. Compilers: Jacobs, W., Chang, P., Minsch, J., Person, W., Presgrave, B., Schmieder, W.

Quick Epicenter Determination (QED) (daily): Distributed only by electronic media.

ANALYSES OF STRUCTURAL RESPONSE TO EARTHQUAKES
9910-02759

Erdal Şafak
U.S. Geological Survey. MS 922
12201 Sunrise Valley Drive
Reston, Virginia 22092
(703)-648-6534, FTS 959-6534

Investigations

1. Analyses of seismic recordings obtained from instrumented structures during the October 17, 1989 Loma Prieta earthquake.
2. Detection and identification of soil-structure interaction from recorded motions of buildings.
3. Investigation of the effects of source directivity and surface waves on structrural response in sedimentary basins.

Results

1. A set of acceleration records (14 channels) obtained from a 42-story steel-frame building (Chevron Building) in San Francisco during the $M_s = 7.1$ Loma Prieta earthquake of October 17, 1989 was analyzed. The response of the building is dominated by two modes: a translational mode in the weaker (southwest-northeast) principal direction at 0.16 Hz with 5-percent damping, and a translational-torsional mode along the east-west diagonal of the building's cross-section at 0.20 Hz with 7-percent damping.
2. Soil-structure interaction (SSI) can significantly alter the characteristics of recorded motions in buildings. The dominant frequency recorded in a building subjected to SSI is always smaller than the dominant frequencies of the fixed-base building, and of the foundation when no building is present. The presence of SSI can be detected by investigating the causality of the building's impulse response. The identification of SSI refers to extracting natural frequencies of the fixed-base building and the foundation from recordings of the foundation and upper stories. The ratio of the Fourier amplitude spectrum of top story accelerations to that of the foundation accelerations permits the identification of the natural frequency of the fixed-base building.
3. Structural response to 1-D and 3-D simulated motions in San Bernardino Valley, California from a hypothetical earthquake along the San Andreas fault with moment magnitude 6.5 and rupture length of 30 km is investigated. The results show that the ground motions and the structural response vary dramatically with the type of simulation and the location. In general, 1-D simulations underestimated the response and resulted in values as low as one-fifth of those of 3-D simulations. The difference in the structural response at three stations was found to be as high as a factor of six. The reasons for such large differences are the trapping of seismic waves in the basin, which cannot be accounted for by 1-D models, and the strong influence of source directivity.

Reports

1. E. Şafak (1992). Response of a 42-story steel-frame building to the $M_s = 7.1$ Loma Prieta earthquake, *Engineering Structures*, in print.

2*a*. Şafak, E. (1992). On identification of soil-structure interaction from recorded motions of buildings, proceedings of the *10th World Conference on Earthquake Engineering*, July 19-24, 1992, Madrid, Spain.

2*b*. E. Şafak (1992). Analysis of soil-structure interaction in buildings from vibration recordings, ASCE, *Journal of Engineering Mechanics*, submitted for publication.

3. E. Şafak and A. Frankel (1992). Structural response to 3-D simulated earthquake motions in San Bernardino Valley, California, ASCE, *Journal of Structural Engineering*, submitted for publication.

Heat Flow and Tectonic Studies

9960–70026

John H. Sass
Branch of Tectonophysics
U.S. Geological Survey
2255 North Gemini Drive
Flagstaff, AZ 86001
(602) 556-7226

Arthur H. Lachenbruch
Colin F. Williams
Branch of Tectonophysics
U.S. Geological Survey
345 Middlefield Road
Menlo Park, CA 94025
(415) 329-4879/4881

Investigations:

The investigation of the thermal regime of the southern Basin and Range has been completed and the manuscript will shortly be submitted for review.

Reconfiguration of laboratory calibration facilities, the transient heat-source conductivity apparatus, and development of a high-temperature thermal conductivity apparatus continued.

A joint study (with Daniel Pribnow of KTB) of thermal conductivities of both core and cuttings from KTB drillholes continued. Work was completed on a joint study of derivation of rock thermal conductivities from geophysical well logs, and a manuscript is in review for *GRL*.

Phase II of the Long Valley Exploratory Well was completed at a depth of 7588 ft (2313 m).

Thermal data were acquired from five strainmeter pilot holes near the Hayward fault. The resulting heat-flow values will be included in the ongoing study of the Coast Range heat-flow high and the San Andreas fault geotherm.

Temperature measurements were made in wells near the San Andreas fault in the Mojave Desert following the Landers earthquake sequence that began on June 28, 1992. Temperature measurements were also made at Yucca Mountain following the June 29 Skull Mountain event.

The thermal study of the Santa Maria Basin, California, was completed, and the resulting paper is in review for the *USGS Bulletin.*

A detailed investigation of the deep thermal regime of the northwestern Geysers geothermal field was initiated in an attempt to characterize the deeper, hotter parts of the system.

Temperature measurements were made in oil wells in Railroad Valley, Nevada, and in geothermal exploration wells near Ft. Irwin and Ridgecrest, California.

Characterization of the thermal regime of the Parkfield region was completed, and high-precision borehole-temperature monitoring in the area continued.

A manuscript on the thermal and hydrologic properties of oceanic crust in the Indian Ocean was completed and is in review for *JGR*.

Results:

Mojave-Sonora. More than 200 values of heat flow are now available from the crystalline terranes of southern California, the Basin and Range Province of Arizona, and Paleozoic sedimentary rocks of the southwestern Colorado Plateau (CP). Heat flow ranges from about 5 mW m^{-2} on the CP near Flagstaff, Arizona, to more than 150 mW m^{-2} in the crystalline rocks bordering the Salton Trough in SE California. The heat-flow pattern within this region is complex and appears to be controlled by regional physiographic and tectonic features. Unlike the adjacent Sierra Nevada Batholith where heat flow is a linear function of near-surface radiogenic heat production, no statistically significant correlation exists between these two quantities in the study area. This absence of correlation is attributable to the complex tectonic history, involving lateral movement of basement terranes, and heat sources and sinks of different strengths, ages, and durations. Contemporary and Neogene tectonism appears to be responsible for the very high heat flow (>100 mW m^{-2}) associated with the Salton Trough and its neighboring ranges, the Death Valley fault zone and its southward extension, and zones of shallow (<10 km) Curie isotherms (as inferred from aeromagnetic data) in west-central Arizona. Low (<60 mW m^{-2}) heat flow in the Peninsular Ranges and eastern Transverse Ranges of California may be caused by thermal transients related to subduction and compressional tectonics. Relatively low heat flow (67±3.5 mW m^{-2}) is also associated with the main trend of metamorphic core complexes in Arizona. This is a surprising observation in view of the fact that the processes related to their deroofing have positive thermal transients, with mantle contributions having time constants of tens of millions of years. The outcropping rocks in the core complexes have a low radioactive heat production (1.1 μW m^{-3}); only about half that for the other crystalline rocks in the region. Some, but not all of the nearly 20 mWm^{-2} deficiency related to the metamorphic core complexes can be related to this observation. The overall average heat flow for the presently quiescent southern Basin and Range province (82±3 mWm^{-2}) is not significantly different from that for the northern Great Basin, much of which has been actively extending over the past 10 m.y., and is several hundred meters higher in average elevation than the southern Basin and Range. Consideration of simple models for extension indicates that this is the expected result because of the long time constants governing the decay of thermal transients associated with province-wide extension.

Thermal conductivity of water-saturated crystalline rocks as a function of temperature. Scientific studies of the continental crust increasingly include the drilling of deep (~ 5 km) and "superdeep" (~ 10 km) research boreholes. Studies of the Earth's thermal regime rank among the most important scientific goals of these projects. To characterize adequately the variation of heat flow with depth in these boreholes, it is necessary to take account of the relation between thermal conductivity and temperature. A few systematic studies have been carried out on dry crystalline rocks, the most important of which remains the classic work of Francis Birch and Harry Clark in 1940. We have constructed an algorithm relating thermal conductivity to temperature based on the latter results. This empirical relation applies equally well to other experimentally determined

conductivity-temperature values irrespective of mineral composition. To our knowledge, no systematic studies of thermal conductivity as a function of temperature have been done on saturated rocks. Although crystalline rocks generally have little porosity (on the order of 1%, mostly fractures), significant errors in thermal conductivity can occur if the pore space is not mainteined in a saturated condition during measurement.

Collaboration with German deep drilling project (KTB). As outlined in our FY 1992 proposal, approximately 100 additional samples were collected from the pilot hole core. Disks were prepared in two or three orientations so as to characterize vertical, parallel, and perpendicular (to bedding) thermal conductivities. The initial results for the vertical component of conductivity were encouraging in that the majority of values were within 10% of one another (the combined uncertainties of the two techniques), but there were some disagreements that could not be readily explained. A re-examination of the algorithm used to calculate vertical conductivity from the KTB line-source method and a revised measurement strategy resulted in a much better agreement between the two sets of results. It is worth noting here that, without the cooperative study now under way, the shortcomings of the original algorithm would not have been readily apparent, and the improvements in both measurement strategy and interpretive procedures would most likely not have occurred.

The comparison of calculated anisotropies produced a very poor correlation. Typically, both line-source measurements and conductivity disks oriented parallel and perpendicular to the foliation were separated from each other by a few centimeters. This resulted in substantial uncertainties in anisotropy arising from significant differences in mineral composition between measurement sites. A similar problem was noted in the case of Cajon Pass (*Sass et al.,* 1992). Because of the uncertainty introduced by variations in mineralogy, the anisotropy can only be specified in general terms as an average for characteristic rock types.

Well-log measurements of compressional and shear velocity (V_p, V_s), density, and temperature from the 4 km-deep KTB Vorbohrung (pilot hole) were applied in a phonon conduction model for the thermal conductivity of a crystalline solid. The resulting conductivity estimates were compared with conductivities (k_{LAB}) measured on the nearly continous (91% recovery) core. Studies in other boreholes have shown the log-derived conductivity (k_{LOG}) to be within ±15% of k_{LAB} in predominantly isotropic crystalline rocks. The section penetrated by the KTB pilot hole includes both predominantly isotropic metabasites and highly anisotropic gneisses with foliation dips ranging from subhorizontal to nearly vertical. The predictions of the phonon model were accurate in the metabasites but inaccurate by 6% to 23% in the moderate to steeply dipping gneisses. These discrepancies between k_{LOG} and k_{LAB} correspond to depths at which laboratory measurements of V_s under *in situ* conditions deviate from the well log V_s. This suggests that full waveform sonic log determinations of V_s may not be reliable in dipping, anisotropic rocks. Alternatively, the laboratory V_s measurements may not be drawn from a representative sample, and the discrepancies may follow from errors in the phonon conduction model. Whatever the reason, the validation of the model in the metabasites confirms the utility of the phonon conduction approach in deriving *in situ* thermal conductivity in boreholes

for which even a small part of the penetrated section is composed of isotropic or weakly anisotropic rocks. The results also demonstrate that, if the cause of the discrepancy in anisotropic rocks is identified as following from errors in the well log measurements, the close relationship between thermal and elastic properties may provide a tool for deriving thermal conductivity profiles of the middle and upper crust from seismic studies of V_p and V_s.

Long Valley Exploratory Well. Phase II of drilling of the Long Valley Exploratory Well (LVEW) was completed on November 21, 1991, at a depth of 2313 meters (7588 ft). The hole was continuously cored from the bottom of the 13 3/8″ casing at 2080 m (6825 ft). The core was entirely within the Mount Morrison roof pendant, primarily metapelites with some quartzite and marble. Several temperature logs were obtained over the winter and spring. The temperature profiles indicate two thermally conductive zones within the Bishop Tuff, the upper zone (600–900 m) having a heat flow of about 120 mW m^{-2} and the lower (900–1500 m), a heat flow of about 100 mW m^{-2}. The temperature profiles below 1500 m indicate a thermal regime dominated by vertical water flow. In particular, the open corehole is isothermal at about 103°C, indicating vigorous water movement. Short-period injection tests suggested that the metasedimentary rocks in the corehole did not have high transmissivity by water-well standards. Fractures in the hole were, however, clogged to some degree by a gel consisting of drilling mud and rod grease so that a precise estimate of transmissivity could not be obtained. A resistivity log in the corehole confirms earlier suppositions that the large shallow low-resistivity unit identified from surface-based electrical and magnetotelluric studies is the result of graphite in the Mount Morrison roof pendant and is not the result of high temperatures.

Borehole televiewer surveys were run in the corehole before and after four sets of hydraulic fracturing tests between the depths of 2200 and 2260 m (7218 and 7415 ft). An impression-packer produced an image of the borehole wall at one of the test intervals. The televiewer data indicated several borehole breakouts with consistent orientations and suggestions of changes in the image of the borehole wall near two of the hydraulic fracturing intervals. Overall, the hydraulic fracturing pressures were at the very low end of the postulated breakdown and fracture reopening pressures. From the pressure-time records, it also appears that hydraulically induced fracturing occurred along pre-existing fractures in at least three of the four measurements. Detailed analyses await careful correlations among fracture, televiewer, and core data.

Between the depths of 1000 and 2080 m, several vertical seismic profiles were obtained with both compressional- and shear-wave vibrator sources. The seismic sources were deployed close-in and at distances of up to 2 km from the hole. Borehole gravimetric measurements closed out the logging schedule. A three-component seismometer package was installed in the 13 3/8″ casing at a depth of about 2000 m. Preliminary results indicate a very quiet, sensitive earthquake-monitoring capability. A water-level recorder is installed in a water well adjacent to LVEW, and water levels will be measured periodically in the deep well. Options for further work include a conventional 12 1/4″ hole to about 4000 m, as originally planned, and a continuously cored slimhole (3 7/8″ or 97 mm diameter) to the same depth.

Thermal disturbances in the wake of the Landers earthquake Observed changes in near-surface ground-water flow following earthquakes have been tied to a number of possible causes, including dynamic and static stress changes in aquifers, the expulsion of high-pore-pressure fluids from overpressured fault zones, and the abrupt enhancement of shallow crustal permeability. The surface rupture of the Landers earthquake passed within 10 km of ten existing Mojave Desert heat-flow sites and provided a unique opportunity to use thermal techniques to investigate both the magnitude and causes of earthquake-induced ground-water movement. Seven of these old holes were re-entered and logged in the weeks following the earthquake, and the resulting precision temperature logs were compared with pre-earthquake records. Temperature measurements in three shallow holes in the alluvium of the Yucca Valley region (including one hole located within 200 m of the surface rupture) revealed widespread small temperature decreases, generally less than 0.2°C, in the period three to four days after the earthquake. Abrupt increases in temperature of up to 2.1°C, requiring upward water movement of at least 100 m, were measured over a depth range of 300 m in LY2, a 700-m-deep well drilled into fractured crystalline rocks of the upper Lucerne Valley, approximately 5 km from the rupture. Because subsequent measurements show the disturbance decaying to 0.5°C within one month, this fluid movement probably ceased within a few hours after the earthquake. Temperatures were also measured in four newly acquired mining coreholes located more than 4 km northeast of LY2 and 40 to 800 m from the rupture. Temperatures in one of these wells show an advective disturbance of approximately 1°C at the intersection of a small fault with the wellbore.

Given the correspondence of the thermal anomalies with holes drilled into fractured basement rocks, the apparently "instantaneous" response to the earthquake at locations many kilometers away from the rupture, and the absence of any coherent trend of progressively larger anomalies closer to the rupture, it appears that the most likely explanation for these disturbances is the rapid movement of water along fractures reopened by the earthquake. At this time the data are not conclusive, but, by monitoring the decay of these disturbances through time and modeling both the development of the source signal and the return to equilibrium, it should be possible to determine both the nature and magnitude of the subsurface flow responsible for these anomalies.

Santa Maria. Equilibrium temperature logs have been recorded in 27 idle oil wells in the onshore Santa Maria, offshore Santa Maria, and western Ventura Basins. Thermal conductivities have been measured on 365 core and cuttings samples from an additional 26 wells in the region. From these data, conductive heat-flow values have been determined for the Guadalupe, Santa Maria Valley, Cat Canyon, Orcutt Hill, Lompoc, Zaca, Pt. Conception, and Pt. Arguello oil fields. Examination of these thermal data reveals a complex combination of advective and conductive processes dominating heat transfer within the province. Over much of the Santa Maria Valley, temperature gradients in the Plio-Pleistocene Careaga, Paso Robles, and Orcutt formations are depressed to nearly isotherm values. Geologic constraints and simple analytical models suggest that shallow groundwater flow accounts for most (if not all) of the heat loss within the shallow sediments. Temperature profiles in the older, underlying Foxen, Sisquoc, and Monterey formations are linear and yield conductive heat-flow values that are relatively constant with depth. Corrected heat-flow determinations for the deeper formations vary from 73

to 106 mW/m^2, with an average of 84 mW/m^2 for the entire region. These values are typical of the Coast Range heat-flow high to the north and contrast sharply with low heat flow (45 to 50 mW/m^2) in the central Ventura Basin to the south. Identification of Santa Maria heat flow with the Coast Range high extends the southern boundary of the high and provides compelling evidence for the persistence of high heat flow at least 20 Ma after cessation of subduction and the establishment of the transform margin. This suggests that the Coast Range high does not develop solely from asthenospheric upwelling in the wake of triple junction passage but may arise from a combination of sources within the crust and upper mantle.

Geysers Geothermal Field. During FY92, we continued a heat-flow study of the Geysers geothermal field, with the intention of characterizing heat and mass transfer processes both laterally and vertically within the reservoir. The Geysers field has recently experienced severe and unanticipated declines in reservoir pressure and steam supply. Reversal of these declines may depend upon the development of new comprehensive models of the nature and evolution of the Geysers steam field. Drilling has revealed a High Temperature Vapor Dominated Reservoir (HTVDR) directly underlying the producing Normal Vapor Dominated Reservoir (NVDR), but the nature of the transition from the NVDR to the HTVDR is unknown. The available data indicate that temperatures increase rapidly (>100°C/km) from the NVDR (~240°C) to the HTVDR (>350°C). It is unclear whether this reflects a transient response (perhaps due to recent magma injection) or steady-state heat transfer across an impermeable boundary. The problem, then, is to obtain high-resolution temperature and pressure logs over the entire depth range, but most importantly in the HTVDR. These can be combined with determinations of thermal conductivity under *in situ* conditions to provide information of the lateral and vertical variations of deep heat flow in and around the Geysers geothermal field. These data should, in turn, contribute to the greater understanding of the physics of the field, thus aiding both the design of remedial procedures and the development of evolutionary models for the entire Geysers geothermal system.

In collaboration with operators at the Geysers and investigators at Sandia National Laboratories, we have initiated a study of temperatures and pressures in wells penetrating the NVDR and the HTVDR. Temperature and pressure have been measured in two idle wells in an undisturbed section of the NW Geysers. The temperature data have been combined with thermal conductivity measurements on drill cuttings to develop a vertical profile of heat flow. Although the results confirm the conductive nature of heat transfer within the caprock, they also reveal a dramatic decrease in heat flow with depth (Figures 1 and 2). Modeling of these results is consistent with cooling or recession of the steam reservoir levels within the past 20,000 years. If this model is confirmed by other measurements, we may have a temporal record of the hydrothermal system changes recorded by fluid inclusions and alteration products.

Thermal Setting of the Parkfield Region Knowledge of the temperature variation with depth near the San Andreas fault is vital to understanding the physical processes that occur within the fault zone during earthquakes and creep events. Parkfield is near the southern end of the San Andreas fault's Coast Range segment, which has higher heat

flow than the Cape Mendocino segment to the northwest or the Mojave segment to the southeast. Boreholes were drilled specifically for the Parkfield experiment or converted from other uses at 24 sites within a few kilometers of the San Andreas fault near Parkfield. These holes, which range in depth from 150 to over 1500 m, were used mainly for the deployment of volumetric strain meters, water-level recorders, and other downhole instruments. We obtained temperature profiles from all of these holes, and we were able to estimate heat flow at 16 sites. For a number of reasons, primarily a paucity of thermal conductivities and rugged local topography, the accuracy of individual determinations was not high enough to document local variation in heat flow. Heat flow ranges from 60 to 90 mW m^{-2}, with a mean and 95% confidence limits of 74±3.5 mW m^{-2}, respectively. This is somewhat lower than the values of 83±2.5 for 39 previously published heat flows from the Coast Range segment of the San Andreas fault zone, but it is consistent with the regional broad zone of elevated heat flow with low values east of the fault in the Great Valley and the Sierra Nevada. The low heat flow close to the fault emphasizes the absence of a frictional thermal anomaly there and provides additional support for the notion of nearly fault-normal maximum compressive stress and a small component of shear stress along the fault.

Thermal and Hydrologic Properties of 150 Ma Oceanic Crust. With a few exceptions, knowledge of heat flow within the oceanic lithosphere comes from seafloor measurements using techniques that include sediment probes and coring. Borehole temperature-logging technology has been remarkably successful in continental boreholes and has only recently been exploited by the ODP community. Borehole temperature measurements are valuable because the data gathered allow us to investigate how heat transfer (conductive and/or convective) varies with depth. For this reason, fine-scale, high-resolution temperature profiles were measured in Hole 765D to document the thermal and hydrologic properties of 140 Ma oceanic crust in the Indian Ocean near the northwestern shelf of Australia. Three complete temperature logging runs were conducted employing the new temperature logging tool (TLT), which is now standard logging equipment aboard the JOIDES *Resolution*. The results indicate an average heat flow for the sediment section (0–932 mbsf) of 52.8±5.7 mW/m^2. This heat flow is slightly higher (~9 mW/m^2) than both the regional heat-flow measurements and the heat flow predicted by a conductive cooling model. Temperature profiles for the basalt section (932–1195 mbsf) are each associated with temperature inversions and intervals (10–50 m) of near-constant temperatures. The computed equilibrium temperature profile is thermally depressed in excess of a few degrees Celsius compared to an expected profile assuming a conductive and steady-state heat-flow regime. The major source of this thermal perturbation appears to be formation fluid that enters the borehole near the sediment/basalt interface and eventually flows downhole and into the basalt formation, presumably through open fractures. The flow is generally restricted to the upper 150 m of the basalts. Based on these thermal and hydrologic observations, the shallow section of the ocean crust at this site is believed to be permeable and slightly under-pressured (fluid pressure less than hydrostatic).

Reports:

Castillo, D. A., and Williams, C. F., Thermal and hydrologic properties of 140 Ma oceanic crust in Ocean Drilling Program Hole 765D, Argo Abyssal Plain, Indian Ocean, in review for *Journal of Geophysical Research.*

Deming, D., Catastrophic release of heat and fluid flow in the continental crust: *Geology,* v. **20**, p. 83–86, 1992.

Deming, D., Sass, J. H., Lachenbruch, A. H., and De Rito, R. F., Heat flow and subsurface temperature as evidence for basin-scale ground-water flow, North Slope of Alaska: *Geological Society of America Bulletin,* v. **104**, p. 528–542, 1992.

Lachenbruch, A. H., and Sass, J. H., Heat flow from Cajon Pass, fault strength, and tectonic implications: *Journal of Geophysical Research,* v. **97**, p. 4995–5015, 1992. (Also, Correction to "Heat flow from Cajon Pass, fault strength, and tectonic implications," *Journal of Geophysical Research,* v. **97**, p. 17,711, 1992.)

Pribnow, D., Williams, C. F., and Burkhardt, H., A well log-derived estimate of thermal conductivity of crystalline rocks penetrated by the 4 km KTB Vorbohrung, in review for *Geophysical Research Letters.*

Sass, J. H., Downhole science in the Long Valley Exploratory Well: *DOE Geothermal Program Review X,* San Francisco, March 24–26, 1992, *Abstracts,* p. 22, 1992.

Sass, J. H., Dunn, J. C., Rundle, J. B., and Eichelberger, J. C., Progress report on the Long Valley Exploratory Well, California (abstract): VI International Symposium on the Observation of the Continental Crust through Drilling, Paris, France, April 7–10, 1992, *Continental Scientific Drilling Programs Abstract Volume,* p. 237, 1992.

Sass, J. H., Galanis, S. P., Jr., and Lachenbruch, A. H., Thermal setting of the Parkfield region (abstract): *Eos,* v. **73**, p. 396–397, 1992.

Sass, J. H., Kennelly, J. P., Jr., Williams, C. F., and Lachenbruch, A. H., Thermal conductivity of water-saturated crystalline rocks as a function of temperature (abstract): *Thermal Properties of Crustal Materials Conference,* Bad Honnef, Germany, April 1–3, 1992.

Sass, J. H., Lachenbruch, A. H., Moses, T. H., and Morgan, Paul, Heat flow from a scientific research well at Cajon Pass, California: *Journal of Geophysical Research,* v. **97**, p. 5017–5030, 1992.

Sass, J. H., Rundle, J. B., and Eichelberger, J. C., Probing the center of Long Valley caldera, California (abstract): International Geological Congress, 29th, Kyoto, Japan, August 24–September 3, 1992, *Abstracts with Programs,* v. **3**, p. 837, 1992.

Williams, C. F., Galanis, S. P., Jr., and Barth, G. A., Thermal disturbances in the wake of the Landers earthquake (abstract): *Eos,* v. **73**, p. 364, 1992.

Williams, C. F., Galanis, S. P., Jr., Grubb, F. V., and Moses, T. H., Jr., The thermal regime of the Santa Maria Province, California, in press, *U.S. Geological Survey Bulletin.*

Zoback, M. D., and Lachenbruch, A. H., Introduction to Special Section on the Cajon Pass scientific drilling project: *Journal of Geophysical Research,* v. **97**, p. 4991–4994, 1992.

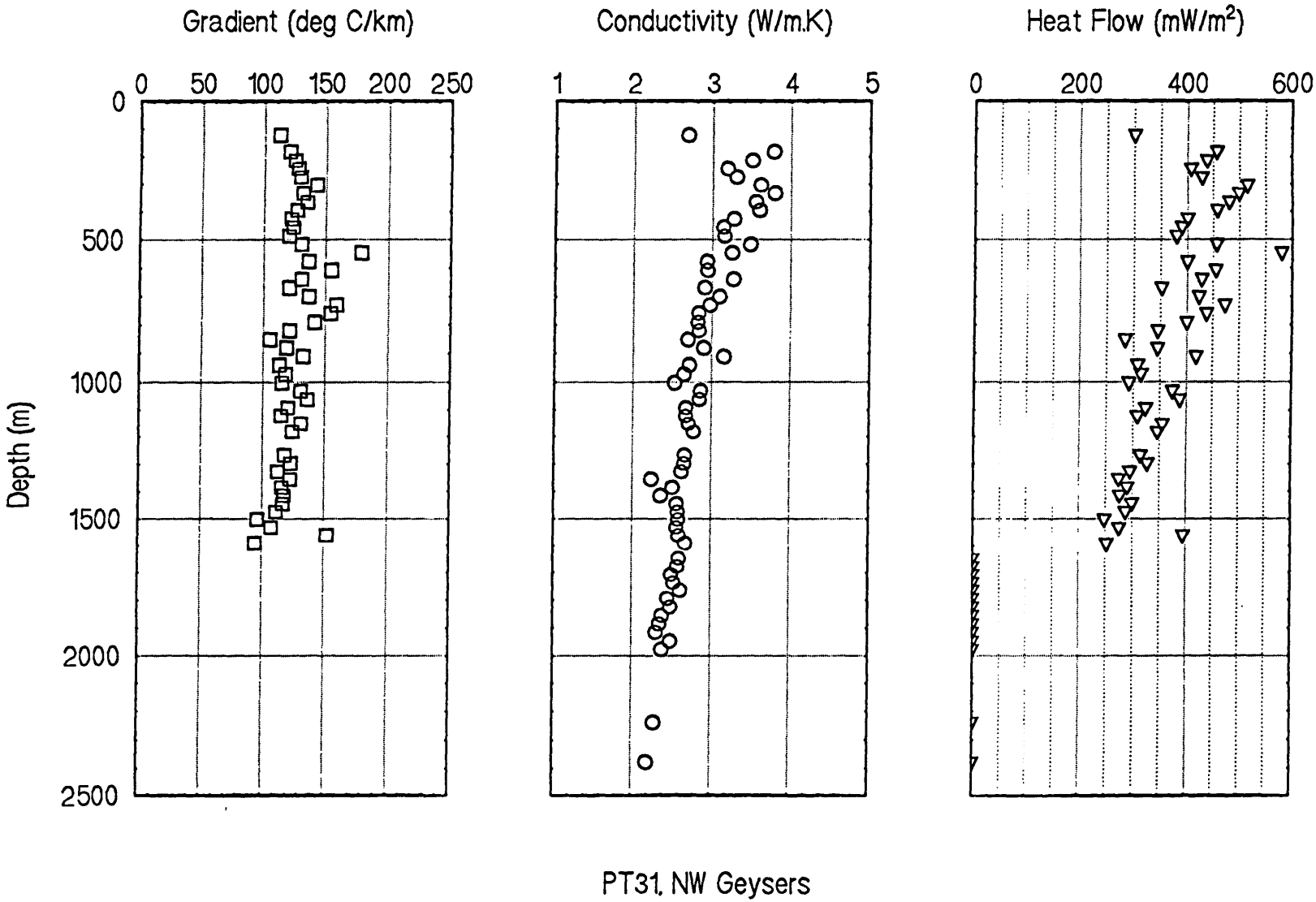

Figure 1 - Temperature gradient and thermal conductivity measurements in Prati 31, along with the resulting, topography-corrected heat flow. Note the steady decrease in heat flow with depth. This is consistent with a steady cooling of the reservoir over the past 20,000 years.

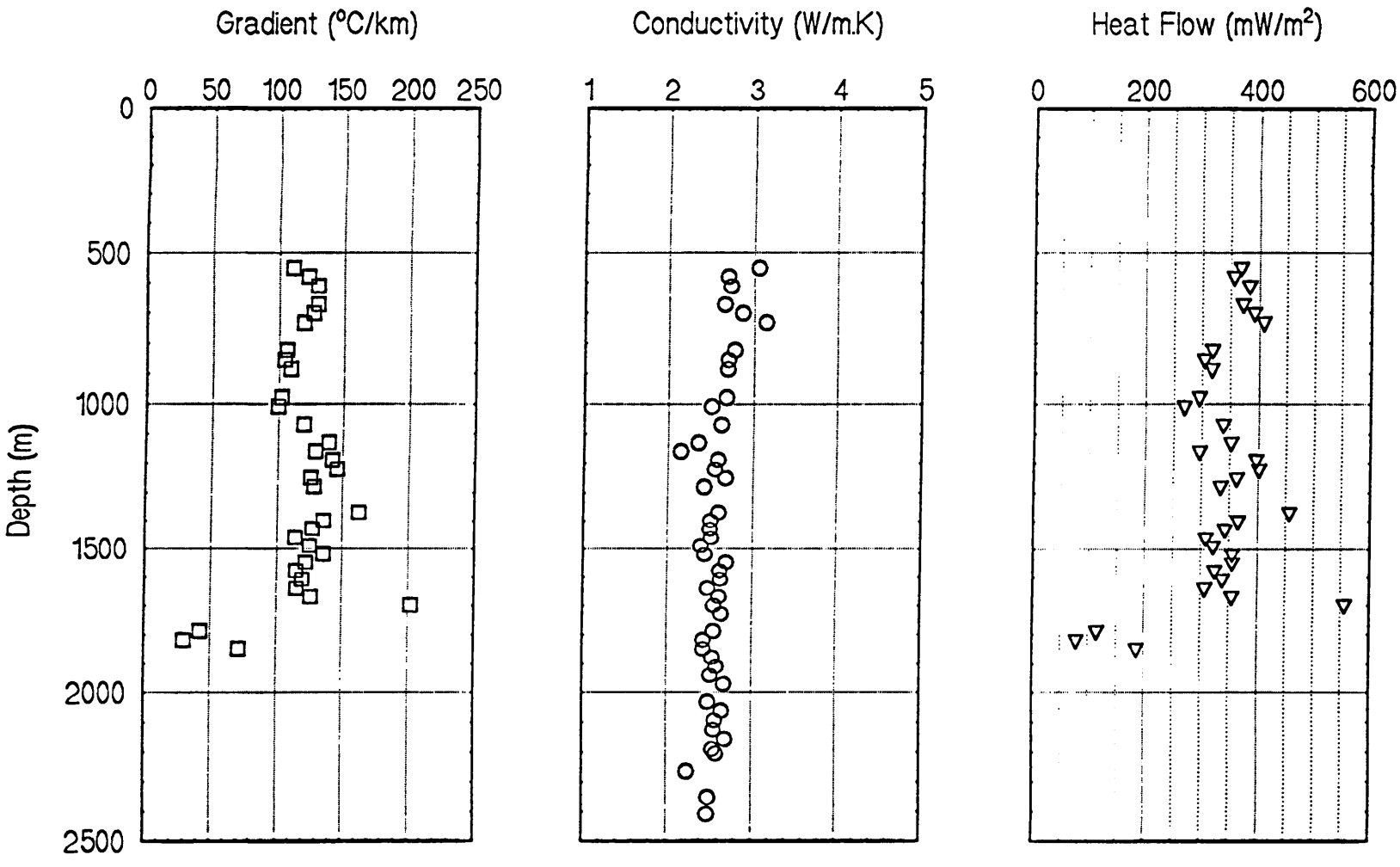

Figure 2 - Temperature gradient and thermal conductivity measurements in Prati 30, along with the resulting, topography-corrected heat flow. Note the decrease in heat flow with depth in the range of 500 to 1500 meters. New results in the region above 500 m (not plotted) confirm the trend, and are consistent with cooling of the reservoir over the past 20,000 years.

FAULT PATTERNS AND STRAIN BUDGETS

9960–10176

Robert W. Simpson
Branch of Tectonophysics
U.S. Geological Survey
345 Middlefield Road, MS/977
Menlo Park, California 94025
(415) 329-4865

Investigations

In collaboration with Ruth Harris, calculated the changes in static stress on southern California faults that resulted from the M7.5 Landers earthquake. Finished a report with Paul Reasenberg on the static stress changes on San Francisco Bay Area faults after the 1989 M7.1 Loma Prieta earthquake.

Results

We simulated the static stress changes associated with the M7.5 Landers earthquake of 28 June 1992 using dislocations in an elastic halfspace. The largest calculated stress changes (5–10 bars) on the San Andreas fault system occurred on the San Bernardino segment. Parts of this segment got increased right-lateral stress added and increased extensional stress, both of which would be expected to bring the region closer to failure in right-lateral strike-slip earthquakes.

A simple dislocation model was used to estimate long-term loading rates. In this model, the deeper aseismic reaches of the major faults from 15 km to 100 km were forced to slip at rates equal to long-term average slip rates. The resulting estimates of tectonic loading on the seismogenic layer (bars/yr) could then be compared with the Landers loading to yield an estimate, in years, for how much the stress changes may have advanced or delayed the next major earthquake on a segment. Although such loading models are far too simple to do justice to the fault complexities that exist along the San Bernardino segment, they suggest that the next large earthquake on this segment might have been advanced by 10–20 years by the added Landers stresses.

Simple models have also been used to investigate the possible effects of pore fluids and of a slipping horizontal detachment surface at depth. Preliminary results suggest that if these models have any validity, both the re-equilibration of pore fluids and aseismsic creep on a detachment may tend to increase the proximity of the San Bernardino segment to failure as time goes on.

Reports

Reasenberg, P.A., and Simpson, R.W., 1992, Response of regional seismicity to the static stress change produced by the Loma Prieta earthquake: *Science*, v. 255, p. 1687–1690.

Harris, R.A., and Simpson, R.W., 1992, Changes in static stress on southern California faults after the 1992 Landers earthquake: *Nature*, v. 360, p. 251–254.

TECHNICAL SUMMARY

"DEVELOPMENT OF ANALYSIS METHODS FOR EVALUATION OF SEISMIC STABILITY OF COASTAL BLUFFS IN THE SAN FRANCISCO BAY REGION"

AWARD NUMBER: 14-08-0001-G2127

PRINCIPAL INVESTIGATOR: Professor Nicholas Sitar
RESEARCH ASSISTANT: Scott A. Ashford
Department of Civil Engineering
University of California at Berkeley
Telephone: (510) 642-1262

This is a summary of the first year of a two year research program to evaluate the seismic response and stability of steep slopes in weakly cemented granular soils. The main objective of the research program is to develop practical analysis and design guidelines for evaluation of seismic stability of slopes in weakly cemented natural deposits, similar to those developed for the analysis of compacted soil embankments and dams by Makdisi and Seed (1978). The impetus for this work was the October 17, 1989, Loma Prieta Earthquake which caused extensive landsliding in the epicentral region and along the coastal bluffs from Seaside, south of Santa Cruz, to Daly City. While this research is specific to the coastal bluffs in the San Francisco Bay region, the methods developed will be applicable to analysis of seismic response of similar marine terrace bluffs along the coast of Southern California, Oregon, and Washington, and should be generally applicable to stability analyses of natural slopes.

RESULTS

During this first year of study, a review of available information was first performed to assess the available state of knowledge regarding: the behavior of weakly cemented soils under static and cyclic loading, observed modes of failure during seismic events, the influence of topographic effects on site response, and the use of the finite element method for slope analysis. A series of static numerical analyses was performed comparing a finite element model (FEM) to a photoelastic physical model. The purpose of this FEM study was to determine the effect of element size and shape on modelling stresses in steep slopes. The results indicate that much smaller elements are required when analyzing tensile stresses near free surfaces than are usually used in FEM slope analyses. In addition, data was collected on two prototype sites, in Daly City and near Santa Cruz, California. The geology of each site was evaluated, and borings were drilled at each site to help determine the subsurface stratigraphy. Each borehole was cased, and subsequently a shear wave velocity profile was developed for each site using the downhole method. In addition, the borehole in Daly City was gamma-logged to provide better resolution of the site stratigraphy. The casing installed at each location is designed for future installation of downhole strong motion instrumentation.

Makdisi, F.I. and Seed, H.B., "Simplified Procedure for Estimating Dam and Embankment Earthquake-Induced Deformations," *J. Geotech. Eng. Div., ASCE,* July 1978, pp. 849-867.

GROUND MOTION PREDICTION AND INVERSION IN REALISTIC EARTH STRUCTURES

9910-03010

PAUL SPUDICH
BRANCH OF ENGINEERING, SEISMOLOGY, AND GEOLOGY
U.S. GEOLOGICAL SURVEY
345 MIDDLEFIELD ROAD, MS/977
MENLO PARK, CALIFORNIA 94025
(415) 329-5654

Investigations

1. Investigation of the feasibility of recovering absolute stress levels from seismic radiation.

2. Identification of particular places at the edges of alluvial basins that scatter energy strongly into the basins.

Results:

1. This work determines the conditions under which it is possible to learn the absolute stress level at a subset of points on a fault from observation of the fault kinematics. Specifically, the points on a rupturing fault can be divided into two groups, those points at which the rake rotates during the rupture process, and those points at which the rake does not rotate. If it is true that sliding frictional traction is collinear with the instantaneous velocity of one side of a fault, then at the former group of points (having rotating rake) there is a unique absolute stress consistent with the motion, while at the latter group of points (having rakes that do not rotate) the absolute stress is unspecified by the motion. Published dislocation solutions for the 1979 Imperial Valley, 1986 North Palm Springs, 1987 Whittier Narrows, and 1989 Loma Prieta, California, earthquakes are examined for evidence of temporal rotations of rake at the hypocenters and largest asperities. The 1986 North Palm Springs earthquake shows evidence of a possible rake rotation at the hypocenter. This may imply a low absolute stress level.

2. In collaboration with Masahiro Iida of the Earthquake Research Institute of Tokyo, we have discovered that long duration ground motions recorded in the Coachella Valley, an alluvial valley in southern California, are caused by scattering of S waves incident upon particular places at the edge of the valley.

Our method uses single-station recordings of widely distributed earthquake sources to identify heterogeneities in the earth's crust that scatter energy into the early part of the observed S wave codas. We assume that ray theory accurately describes the propagation of body waves from the earthquake sources to the scatterers, but we assume no propagation mechanism between the scatterers and the seismic station. A grid of hypothetical scatterers is assumed to cover the earth's surface, and the strength of each scatterer is determined by an iterative inversion method. Our data are recordings of aftershocks of the 1986 North Palm Springs earthquake recorded at two seismic stations in the Coachella Valley, SMP and SUB, and at a station outside the valley, SMC. The technique is applied separately to each horizontal component of motion at each station. We identify a particular spot at the northwest end of the Coachella Valley that scatters waves into the S coda observed at SMP in the valley and SMC outside the valley. Although SUB is also in the valley, its coda appears to contain scattered waves from a different part of the valley edge. This study shows that laterally propagating waves are observable in the early coda, casting doubt on the use of 1-D techniques for estimating site responses. The observation of basin-edge scattering at SMC outside the basin implies that soil/rock transfer functions may be biased by contamination of the rock motions by basin-edge scattering. The northwest edge of the valley appears to be an especially strong scatterer of incident waves. If other basins have similar loci of strong scattering, perhaps these places can be identified using microearthquake seismograms and used to predict strong ground motions in the basins. Scattered energy at SMC is polarized, which may represent a mechanism by which directional site resonances arise.

Reports:

Spudich, P., 1992, On the inference of absolute stress levels from seismic radiation, *Tectonophysics*, v. 211, 99-106.

Spudich, P., and Iida, M., 1992, The seismic coda, site effects, and scattering in alluvial basins studied using aftershocks of the 1986 North Palm Springs, California, earthquake as source arrays, Bull. Seismol. Soc, Am., submitted.

STRONG MOTION INSTRUMENTATION FOR THE SAN FRANCISCO BAY REGION

9910-04428

PAUL SPUDICH, LEE K. STECK, EDWIN ETHEREDGE
BRANCH OF ENGINEERING, SEISMOLOGY, AND GEOLOGY
U.S. GEOLOGICAL SURVEY
345 MIDDLEFIELD ROAD, MS/977
MENLO PARK, CALIFORNIA 94025
(415) 319-5654

Investigations

The goal of this project is to acquire and deploy strong motion instrumentation to solve four major technical problems in the San Francisco Bay region. First, the pre-existing strong motion instrumentation layout was very irregular spatially, having large uninstrumented sections along major faults. Second, the previously deployed instrumentation was almost exclusively analog, leading to long processing times and delays in the release of the data, as well as diminished data quality owing to the occasional need for hand digitization. Third, the existing strong motion instrumentation was not co-sited with high gain instrumentation, meaning that very little weak and strong motion data were available from the same sites. Fourth, many existing strong motion instruments had no accurate time receivers on them, making their data difficult or impossible to use for certain types of modern seismological analysis.

Results

To accomplish these goals, 13 new digital Kinemetrics SSA-1 and SSA-2 accelerographs with FBA-23 accelerometers were purchased with FY 1991 money, and are ready to be deployed. In addition, 7 existing SMA-1's have been acquired from other experiments and with some refurbishing will also be available for re-deployment. Our current plans (Appendix 1) call for collocating 6 Kinemetrics SSA-2's at upgraded CALNET sites which will become part of the telemetered digital network. Five of these sites have been inspected and found satisfactory, and the sixth will be inspected soon. Three of the remaining 4 SSA-2's will be deployed at other CALNET sites around the San Francisco Bay region, while the fourth will be deployed in downtown Oakland. The last 3 new digital accelerographs, SSA-1's, will be collocated with joint telemetered-digital array and dilatometer sites at Coyote Hills Regional Park, Garin Ranch Regional Park, and at Mills Creek in Fremont. At Garin and Coyote Hills, our instruments will be deployed within an enclosure provided by the telemetered digital network, and special mounting hardware has been installed within this structure for our use. The 7 analog SMA-1's will be collocated at existing analog CALNET sites near the Rodgers Creek fault and along the peninsular segment of the San Andreas, along the Hayward fault, and at locations in Oakland. These sites have been inspected as well, and we have found that to collocate at most of these locations, enclosures will be required.

In addition to the acquisition of new instruments, 12 WWVB-PCB clocks were purchased to add time to existing analog strong motion instruments lacking clocks. These instruments are primarily located along the Calaveras fault. Additional purchases included 5 enclosures (T-huts) and 5 solar panels (plus mounting hardware) for instruments to be collocated with upgraded CALNET sites, 2 solar panels plus hardware for instruments collocated with dilatometer sites, and lastly, power control boxes for the new digital instruments.

To summarize, we have acquired strong motion instrumentation to significantly improve the coverage of major faults in the San Francisco Bay Region, including the North and South Hayward faults, the Rodgers Creek fault, the peninsula segment of the San Andreas fault, and the Calaveras fault. We have also purchased clocks to upgrade some existing strong motion stations to be compatible with modern seismological analysis methods. FY 1992 accomplishments have primarily been to purchase equipment and to visit sites and assess their feasibility. Progress in the deployment of the new digital instruments had been stalled somewhat while we waited for dilatometer holes to be drilled and for the upgraded CALNET sites to be decided upon and installed. To date, we have inspected six digital sites, and work is ready to begin on installing new accelerograph stations at these cooperative locations. In addition, site inspections have been performed for collocation at analog CALNET sites as well. A recent study of coherence at various dense seismic arrays has shown that to obtain coherent collocated weak and strong motion data, station spacings should be less than about 20-30 m. This observation has made it necessary for us to reconsider the use of existing structures at some sites, and to install more of our own seismic enclosures than originally anticipated. See Appendix 1 for details of the sites that have been selected for both new deployments and upgrades, and Appendix 2 for details of instrumentation purchased.

APPENDIX 1: Details of instrument locations

Six (6) Kinemetrics SSA-2's at Upgraded CALNET/ Telemetered Digital Net sites:
- Volmer Peak
- Point Molate
- San Leandro Hills
- Hamilton Air Force Base
- San Bruno Mountain
- Pacific Park Plaza (Emeryville)

Three (3) Kinemetrics SSA-2's at other CALNET sites:
- NCF, west of Cotati
- JEG, near El Granada
- JGB, near San Gregorio

One (1) Kinemetrics SSA-2 in downtown Oakland:
- near site of severe damage in the Loma Prieta earthquake

Three (3) Kinemetrics SSA-l's collocated at joint telemetered digital net dilatometer sites:
Garin Regional Park
Coyote Hills Regional Park
Mills Creek, Fremont

Seven (7) Refurbished Kinemetrics SMA-l's:
NBR Beebe Ranch, near Santa Rosa
CMC Mills College, Oakland
JRG Rodeo Creek, north of Santa Cruz
NTY Taylor Mountain, southeast of Santa Rosa
Mira Vista Country Club, Richmond
Union City, near Masonic Home
Downtown Oakland

APPENDIX 2: Equipment Purchases. FY 1991/92

1) Ten Kinemetric SSA-2s, which are 3-component 12 bit digital accelerographs, were purchased with internal FBA-23 accelerometers. A special external signal output plug was placed on these instruments so that the accelerometer output could simultaneously be recorded externally. It is anticipated that the joint Branch of Seismology/Lawrence Berkeley Laboratory telemetered digital array will digitize the accelerometer output at 1 ~bit resolution and incorporate this signal into their real-time data stream. A Kinemetrics WWVB-PCB clock was also purchased for each of these instruments.

2) Three Kinemetrics SSA-1 accelerographs, which are 4-channel, 3-component, 12-bit instruments, were purchased with internal FBA-23 accelerometers, and WWVB-PCB clocks.

3) Twelve WWVB-PCB clocks were purchased to add to existing analog strong motion instruments lacking time. These instruments are primarily located along the Calaveras Fault.

4) Miscellaneous seismic enclosures (5) and pads (5), power control boxes (13), and solar panels (7).

Reports:

None

The Undrained Residual Strength of Cohesive Soils and Landslides During Earthquakes

Contract Numbers: 14-08-0001-G1953 and 1434-92-G2178

Dr. Timothy D. Stark
Assistant Professor of Civil Engineering
University of Illinois at Urbana-Champaign
2217 Newmark Civil Engineering Lab.
Urbana, IL 61801
(217) 333-7394

and

Dr. I.M. Idriss
Professor of Civil Engineering
2097 Brainer Hall
University of California
Davis, CA 95616
(916) 752-5403

PROJECT SUMMARY

A significant number of landslides have occurred in cohesive soils during earthquakes. Most notably, seven major landslides occurred during the 1964 Alaskan earthquake and all involved large masses of Bootlegger Cove clay. A recent reevaluation of the Fourth Avenue slide in Alaska, showed that surface lateral movements were either several feet or less than six inches. In areas where the movements were greater than six inches, it is postulated that the shear strength of the Bootlegger Cove clay was reduced to the undrained residual value. Once the undrained residual strength was mobilized, several feet of lateral movement occurred.

The main objective of the research proposed was to investigate the undrained residual strength of cohesive soils and the occurrence of landslides during earthquakes. To achieve this objective, undrained torsional ring shear tests are being performed on undisturbed specimens of naturally occurring cohesive soils, including Bootlegger Cove clay. The results of ring shear tests on the Bootlegger Cove clay will be compared to the undrained shear strengths back-calculated for the Fourth Avenue slide, to estimate the strength mobilized at the time of sliding. The proposed investigation of the Fourth Avenue slide will greatly aid the understanding of the undrained strength loss that can occur during earthquake shaking.

SUMMARY OF RESEARCH RESULTS

Undrained ring tests on undisturbed and remolded specimens of thirteen naturally occurring cohesive soils have been conducted at various shear displacement rates and initial effective normal stresses. An electric variable speed motor was connected to the Bromhead ring shear apparatus using a pulley system. The existing gear box system was disconnected so

that shear displacement rates ranging from 20 to 900 mm/minute could be obtained using the pulley system. The specimen container was also modified to accommodate a 1.0 cm thick specimen so that an undrained condition could be obtained. It can be seen from Figure 1 that the undrained residual strength ratio, defined as the undrained residual strength divided by the undrained peak strength, is directly related to the clay fraction of the soil. These ring shear tests were conducted at a shear displacement rate of 400 mm/minute and an initial effective normal stress of 400 kPa. The undrained residual strength ratio initially has a value of approximately 1.0 and decreases to about 0.37 at a clay fraction of 20 percent. The undrained residual strength ratio remains essentially constant at 0.37 for clay fractions greater than 20 percent. This data implies that soils with a clay fraction greater than 20 percent are susceptible to a large undrained strength loss if sliding is triggered during an earthquake.

Figure 2 presents a relationship between the undrained residual strength and clay fraction at a shear displacement rate of 400 mm/minute and an initial effective stress of 400 kPa. It can be seen that the undrained residual strength decreases from a value of approximately 270 kPa to 75 kPa at a clay fraction of about 20 percent. The undrained residual strength remains essentially constant at 75 kPa for clay fractions greater than 20 percent. These values of undrained residual strength can be used to evaluate stability of cohesive slopes if sliding will be triggered during an earthquake.

The drained residual strength and the undrained residual strength measured for the thirteen naturally occurring cohesive soils are combined in Figure 3. The undrained tests were conducted at a shear displacement rate of 400 mm/minute and the drained tests at a drained displacement rate of 0.018 mm/minute. The initial effective normal stress in the drained and undrained tests was 400 kPa. The following observations can be made from Figure 3: (1) at clay fractions less than 5 percent the undrained residual strength is slightly larger than the drained residual strength, (2) for clay fractions between 5 and 35 percent the undrained residual strength is significantly lower than the drained residual strength, and (3) at clay fractions greater than 35 percent the drained and undrained residual strengths are essentially equal to 70 kPa. Therefore, if sliding is triggered in soils with a clay fraction between 5 and 35 percent, large rapid movements could result and continue after earthquake shaking has ceased.

CONCLUSIONS

In summary, the initial results of this research provides an insight into the cause of landslides in cohesive soils during earthquakes. These results have been accepted for publication in the Journal of Geotechnical Engineering published by the American Society of Civil Engineers. The following conclusions are based on the data of the undrained ring shear tests performed during the first phase of this study:

1.) The undrained peak strength ratio, i.e., the undrained peak strength divided by the effective consolidation stress, increased with increasing shear displacement rate. This suggests that cohesive soils will exhibit a greater initial resistance to sliding during an earthquake. However, subsequent conclusions will show that if sliding is triggered, there will be a large undrained strength loss that may increase lateral movements and propagate sliding.

2.) The undrained residual strength ratio, i.e., the undrained residual strength divided by the undrained peak strength, ranged from approximately 1 to 0.37 for clay fractions less than 20 percent. The undrained residual strength ratio remained essentially constant at 0.37 for clay fractions greater than 20 percent. This implies that soils with a clay fraction greater than 20 percent are susceptible to a 60 percent undrained strength loss if sliding is triggered during an earthquake.

3.) The magnitude of the undrained residual strength ranges from 270 to 75 kPa for clay fractions less than 20 percent. For clay fractions greater than 20 percent the undrained residual strength remains essentially constant at 75 kPa.

4.) The undrained residual strength is significantly lower than the drained residual strength for clay fractions between 5 and 35 percent. This implies that if sliding occurs during an earthquake there will be a large strength loss, which may increase the magnitude of the lateral displacements and possibly propagate the sliding. Clearly slopes involving cohesive soils should be designed such that the undrained residual strength is not mobilized.

During the next phase of the research undrained ring shear tests will be conducted on the Bootlegger Cove Clay from the Fourth Avenue landslide. The undrained ring shear test results will be compared to the undrained shear strengths back-calculated for the Fourth Avenue slide to estimate the strength mobilized at the time of sliding. If these strengths are similar, it will provide an insight into the undrained strength mobilized during earthquakes, and thus the cause of landslides in cohesive soils during earthquakes.

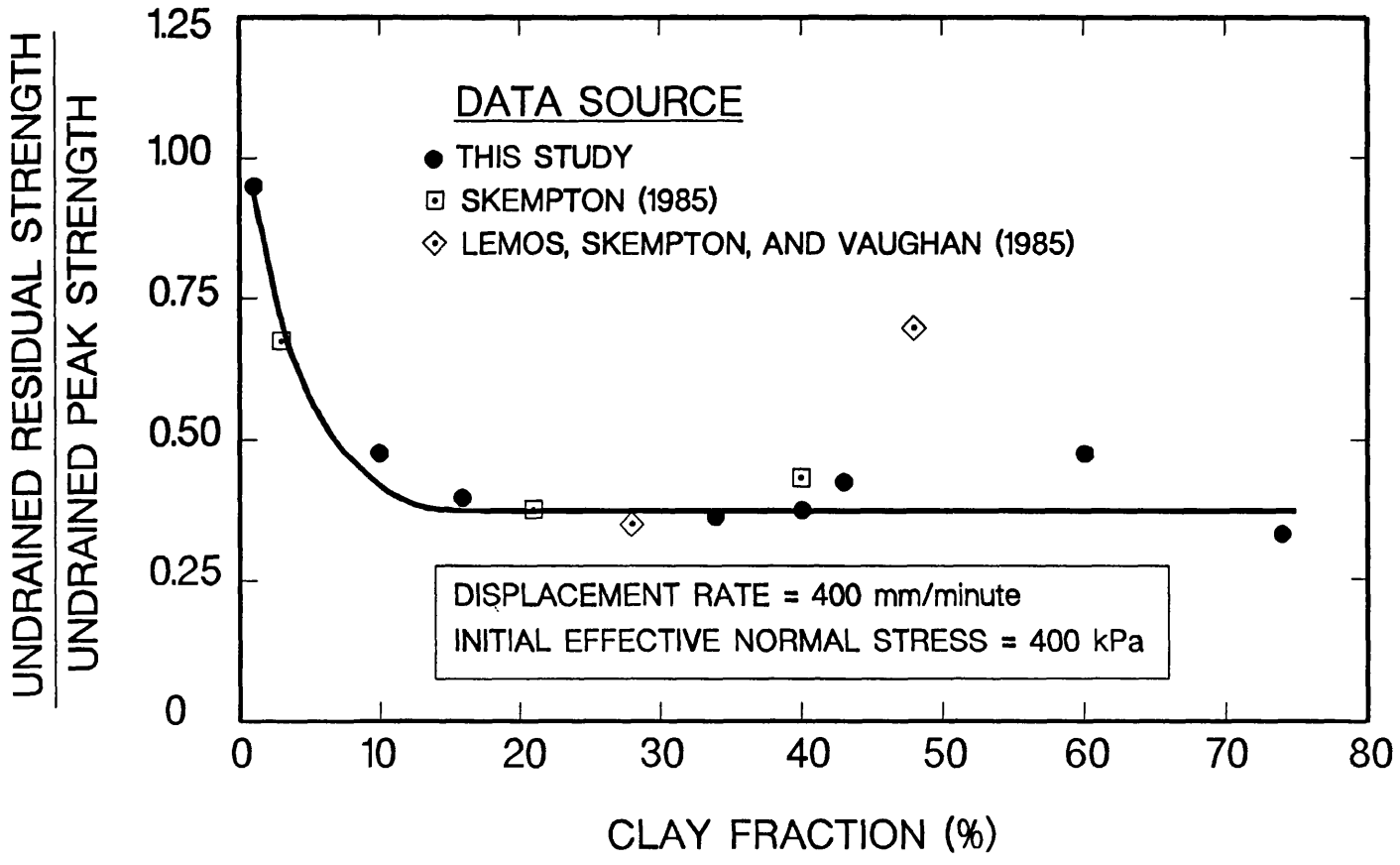

Figure 1. Relationship Between Undrained Residual Strength Ratio and Clay Fraction

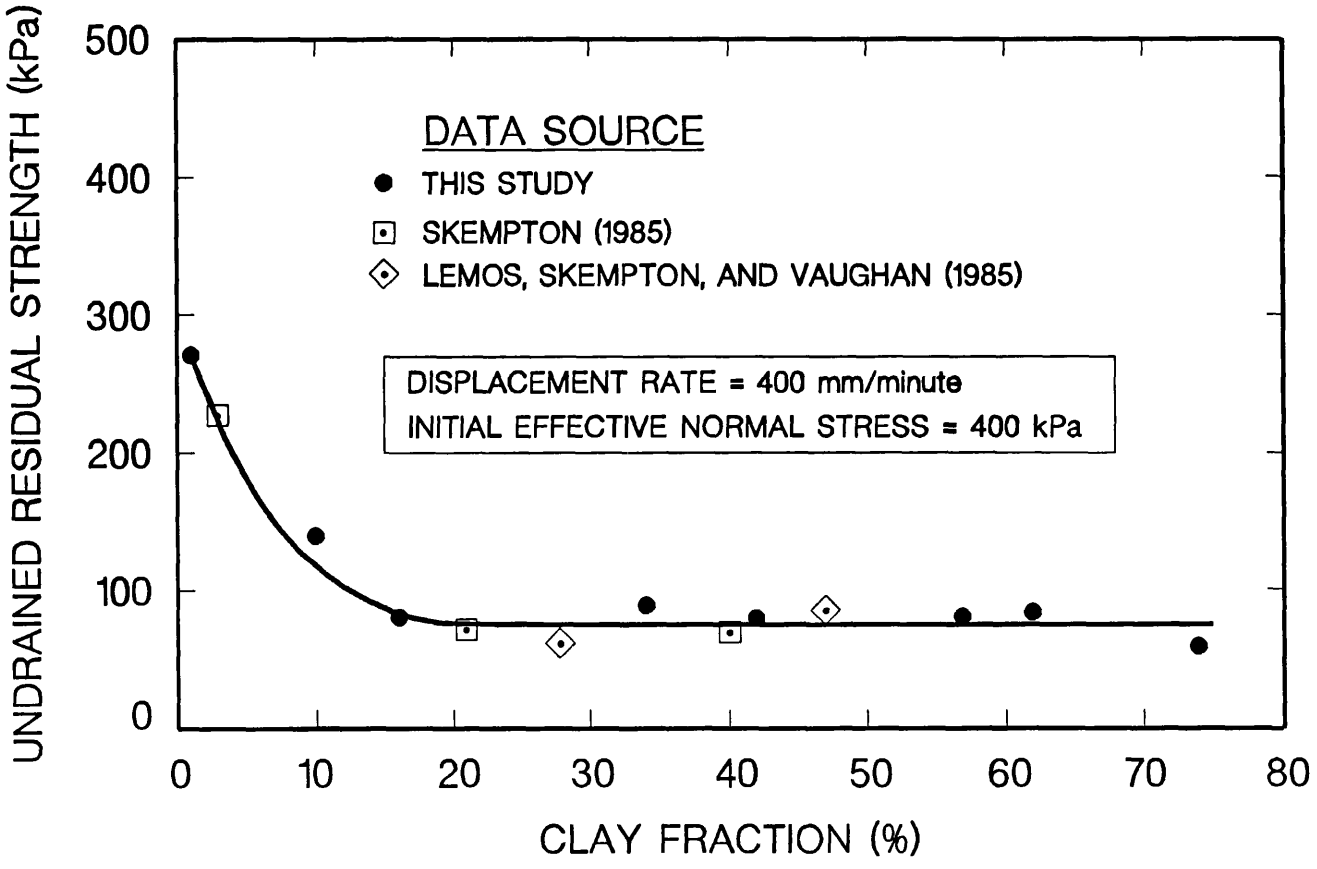

Figure 2. Relationship Between Undrained Residual Strength and Clay Fraction

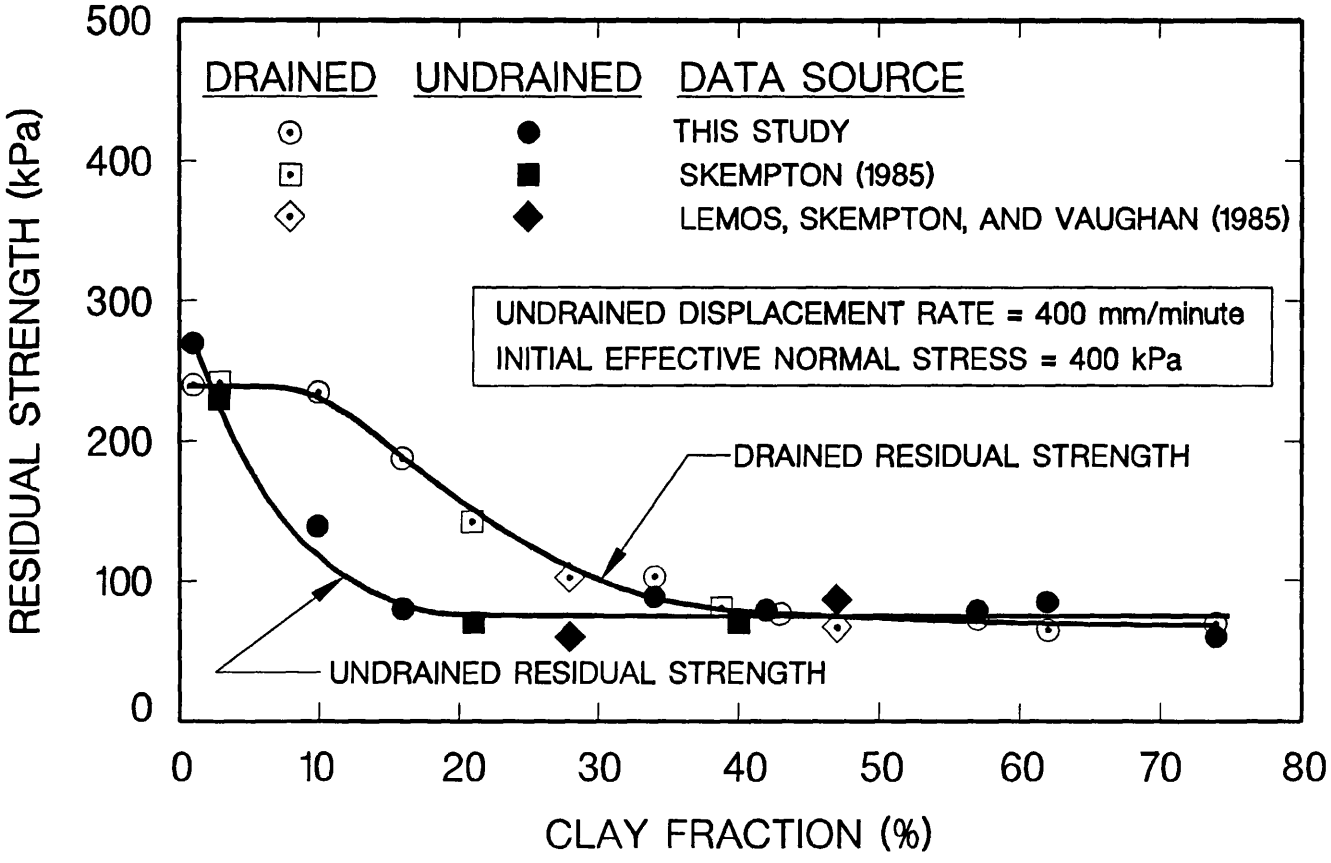

Figure 3. Comparison of Undrained and Drained Residual Strengths

SITE AMPLIFICATION OF STRONG GROUND MOTIONS AT PADUCAH, KENTUCKY

1434-92-G-2174

Ronald L. Street
Department of Geological Sciences
University of Kentucky
Lexington, Kentucky 40506-0059
(606) 257-4777

Investigation

Paducah, Kentucky, is one of the largest metropolitan areas within the New Madrid seismic zone. The city is founded on up to 160 m of unconsolidated sands, clays, silts, and gravels ranging in age from late Cretaceous to recent. For the past several years, personnel at the University of Kentucky have been involved in preparing a generalized microzonation map of the Paducah area with the goal of characterizing local site effects as a result of soil column amplification (Harris and Street, 1991a; 1991b).

In association with the microzonation of the Paducah, Kentucky, area, a geotechnical drilling program was carried out. The drilling strategy called for undisturbed Shelby tube samples to be collected at 3 m intervals. If Shelby tube samples could not be collected, split-spoon drive sampling was done. The units of interest for the drilling project were primarily the unconsolidated near-surface sediments (alluvium, loess, and lacustrine deposits).

The purpose of the drilling program was to determine geotechnical parameters at a representative site in each of the three zones delineated by the microzonation study, and to check the accuracy of interpretations made from surface seismic data used to characterize conditions at the sites (soil column geometry, shear wave velocity). Total depths for the holes ranged from 30 to 37 m, and all of the holes terminated below a regional unconformity, in more competent Tertiary or Cretaceous material. Figure 1 a map of the Paducah area with locations of the three boreholes marked, and Figure 2 presents generalized boring logs.

Data Analysis

Depths to the unconformity cut on Tertiary and Cretaceous material obtained through analysis of SH-wave refraction data were all within 4 m of those encountered by the boreholes. Because reasonable variations in relief on the unconformity surface are possible over relatively short distances, and the seismic data were not collected directly over the borehole sites, discrepancies in depth are not considered to be significant.

Using a relationship between shear wave velocity and blow counts from standard penetration testing (SPT-N values) presented by Suyama et al. (1987), estimates of shear wave velocity were made for the sediments tested by drive sampling. Shear wave velocities estimated from the SPT ranged from 315 to 510 m/s and shear wave velocity measurements from SH-wave refraction data for the corresponding sediments ranged from 285 to 485 m/s. Although some inconsistencies are present (probably due to lateral variations in the soil deposits), shear wave velocities estimated from SPT generally agree with the velocities measured from the SH-wave

seismic data.

Laboratory analyses were performed on the undisturbed samples by the Soils Lab at the University of Kentucky's Transportation Research Center. Shear wave velocities obtained from resonant column testing were on the order of 30% lower than those measured in situ by SH-wave refraction methods. Also, material damping ratios measured in the lab were considerably higher than those based on attenuation measurements made from field seismic data (Wang et al., 1992). A likely explanation is that the variances are due to the different strain levels under which the measurements were made. The refraction data were recorded at extremely low amplitude levels while the resonant column tests were performed using higher amplitudes, possibly approaching non-linear stress-strain conditions.

References

Harris, J. B., and Street, R. L., 1991a, Integrated seismic site characterization of the Paducah, Kentucky, area: Preliminary results: Proceedings of the 4th Symposium on the Application of Geophysics to Engineering and Environmental Problems, p. 24-37.

Harris, J. B., and Street, R. L., 1991b, Estimating site amplification effects using shallow seismic data: 61st Annual International Meeting of the Society of Exploration Geophysicists, Expanded Abstracts, p. 584-587.

Suyama, K., Imai, T., Ohtomo, H., Ohta, K., and Takahashi, T., 1987, Delineation of structures in alluvium and diluvium using SH-wave reflection and VSP methods, in Danbom, S. H., and Domenico, S. N., eds., Shear-wave exploration: Society of Exploration Geophysicists, Geophysical Developments No. 1, p. 165-179.

Wang, Z. M., Street, R., Harris, J. B., and Woolery, E. W., 1992, Q_s estimates for unconsolidated sediments in the upper Mississippi embayment (abs.): 64th Annual Meeting, Seismological Society of America, Eastern Section, Richmond, Virginia.

Reports

Harris, J. B., Street, R. L., and Kiefer, J. D., 1992, Microzonation and site amplification of seismic ground motions in the Paducah, Kentucky, area: Workshop presented to the city of Paducah, Kentucky, as part of the GEHSTAP (Governor's Earthquake Hazards and Safety Technical Advisory Panel) meeting of April 9, 1992.

Harris, J. B., Street, R. L., Kiefer, J. D., Allen, D. L., and Wang, Z. M., in press, Microzonation and site amplification of seismic ground motions in the Paducah, Kentucky, area: 1993 National Earthquake Conference, May 3-5, 1993, Memphis, Tennessee, 10 pp.

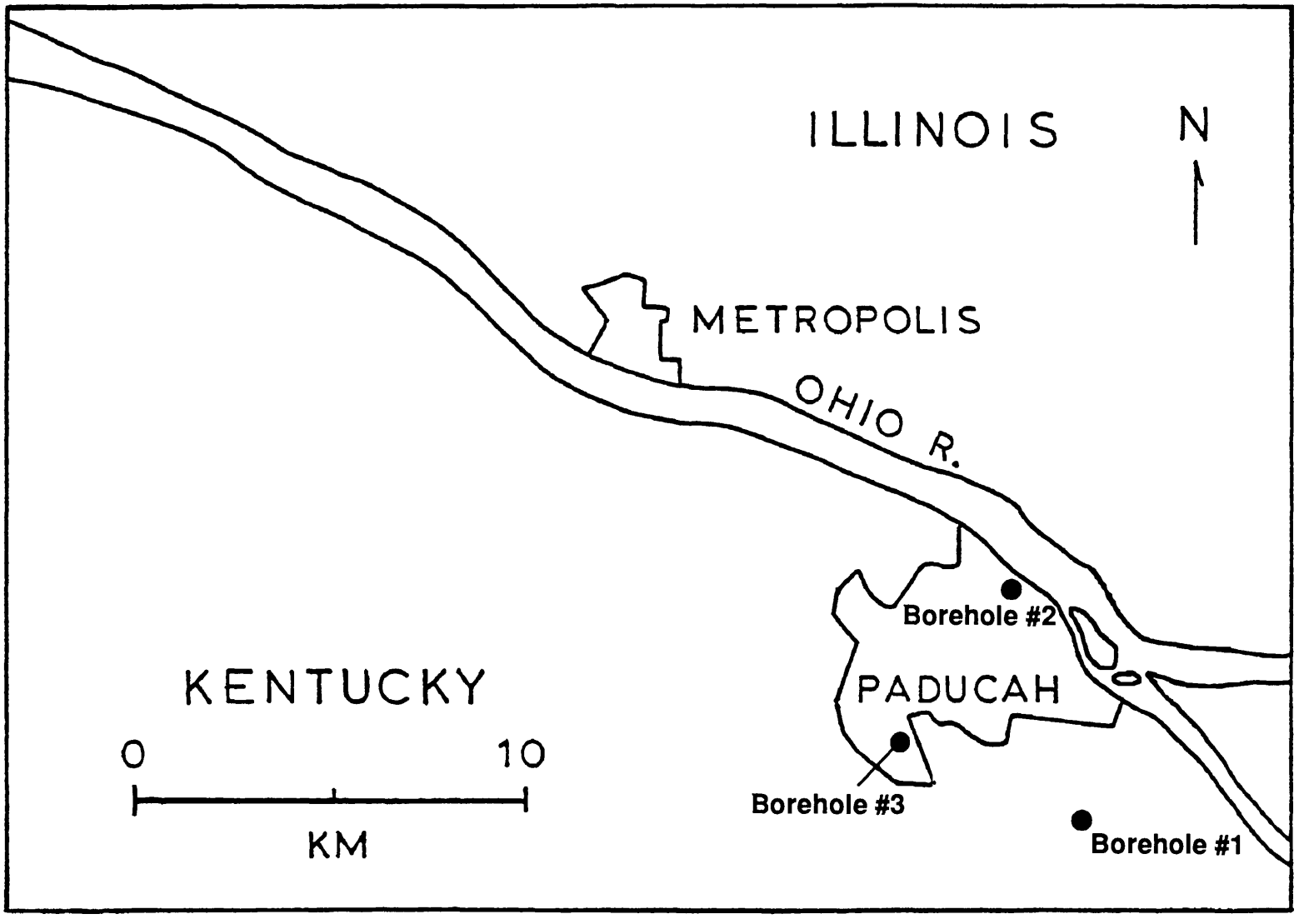

Figure 1. **Map of the Paducah, Kentucky, area showing the locations of three geotechnical boreholes used for characterization of the shallow subsurface.**

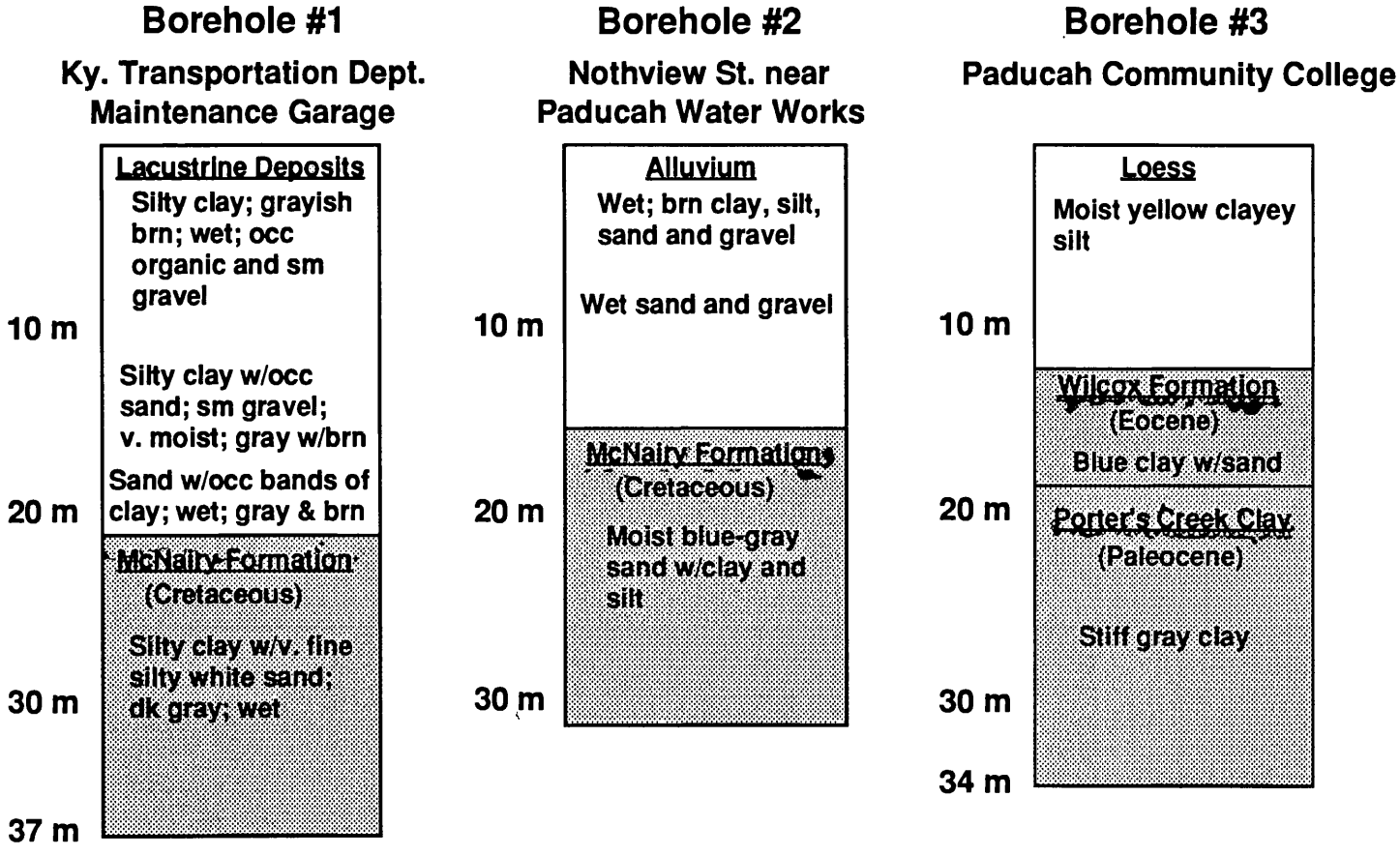

Figure 2. Generalized logs for the three geotechnical borings made in the Paducah, Kentucky, area. The locations of the boreholes are shown in Figure 1.

Earthquake Hazards Studies, Metropolitan Los Angeles
Western Transverse Ranges
9540-70050

R.F. Yerkes,
U.S. Geological Survey
Branch of Western Regional Geology (ORG)
Menlo Park, CA 94025
(415) 329-4946

R.H. Campbell
U.S. Geological Survey
Branch of Geologic Risk Assessment (OEVE)
Reston, VA 22092
(703) 648-6784

Investigation:

Digital geologic map, Los Angeles 1:100,000 quadrangle, a unit of the Southern California Mapping Project (1993 Prospectus, p. 7). This quadrangle contains the sources of the 1971 ML 6.6 San Fernando and 1987 ML 6 Whittier Narrows earthquakes, and other elements of the southern frontal zone of the Transverse Ranges. Continued processing digital data for eight 1:24,000 quadrangles that make up the southwest quarter of the Los Angeles quadrangle and completed six.: Calabasas, Canoga Park, Malibu Beach, Newbury Park, Thousand Oaks, and Topanga; Point Dume nearing completion, Triunfo Pass not yet compiled. Field mapped and checked critical areas with R.H. Campbell. Revised Canoga Park quad to accord with recently-completed study of Quaternary unit boundaries. Reviewed newly-published quadrangles of same areas by T.W. Dibblee. Compiled four quadrangles of northwest quarter: Moorpark, Oat Mountain, Santa Susana, and Simi; scanned and processed initial linework for Oat Mountain quadrangle.

Completed conversion from Prime-hosted PC-based terminal emulator to a stand-alone DG Aviion work station equipped with ARC 6.0.1. This version, in tandum with the Aviion version of Unix, is a disappointing step backward from version 5 with the emulator, and has resulted in severe losses due to downtime and repetition of efforts.

Reports:

None released.

LOS ANGELES, CA, QUADRANGLE, 1:100,000-SCALE, GEOLOGIC MAP COMPILATION AND DIGITAL DATABASE

9950-04063

R. H. Campbell
Branch of Geologic Risk Assessment
U.S. Geological Survey
MS 922, National Center
Reston, Virginia 22092
(703) 648-6784

Investigations

Compilation efforts in 1992 continue to focus on the eight 7.5-minute quadrangles that make up the southwestern quarter of the Los Angeles 1° x 30' quadrangle, where detailed geologic mapping done under predecessor USGS projects and new mapping by other USGS, CDMG, and University geologists; however, compilation has also begun for an additional 8 7.5-minute quadrangles in the northwestern quarter. The project is jointly funded by NEHRP and the National Geologic Mapping Program (NGM) and the work is a joint effort with the NGM Project of R. F. Yerkes (ORG, Branch of Western Regional Geology). Work on the compilation of the Los Angeles quadrangle is closely integrated with State of California (CDMG) efforts to prepare a similar compilation for the adjacent Lancaster 1° x 30' quadrangle under COGEOMAP, and is coordinated with USGS projects in other branches (including WRG, BPS, and PMG) that are contributing to the map compilation, seismological and regional geophysical studies, and paleontological studies. Project personnel are shared (approximately 60/40 in FY '92) with Landslide Probability and Risk investigations.

The map compilation uses GIS procedures to yield digital databases that will provide improved capabilities for the analysis of earthquake hazards and landslide risk. Several external factors affected the effort in FY 1992: (a) a hardware shift from PRIMOS-based Prime minicomputers to UNIX-based Data General file servers and work stations involved some delays for reconfiguring hardware and software, for learning a new operating system, and for transfer and testing of previously completed coverages; (b) the ongoing software shift from version 5.01 of ARC/INFO to version 6.1 requires some modifications to previously completed files and macros; and (c) the installation of ALACARTE as a menu control for ARC/INFO has greatly speeded digital preparation of the frames for various map layers.

Fieldwork in FY 1992, carried out jointly with R. F. Yerkes (BWRG), focused on the Topanga, and Canoga Park, CA, quadrangles, where geologic mapping by other workers joins published mapping by Yerkes and Campbell (1980), and was extended to include additional field checking of map compilations in the Newbury Park and Thousand Oaks 7.5' quadrangles.

Results

1. Twelve of the 16 7.5-minute quadrangles in the western half of the Los Angeles sheet are in various stages of compilation and preparation of digital map databases. (See also R. F. Yerkes, project 9540-70050)

2. Fieldwork in the Topanga Quadrangle established that low-angle faults and other Middle Miocene structural-stratigraphic elements identified to the west by Campbell and others (1965) can be identified and mapped in the eastern half of the quadrangle. Poorly exposed and poorly consolidated Late Miocene to Late Pleistocene deposits occur along the southern flank of the Santa Monica Mountains. Units of different ages include deposits having similar lithologic characteristics. Accurate discrimination of the different units will require additional detailed mapping.

3. The Point Dume quadrangle has been prepared in digital layers for (1) contacts, faults, and geologic units, (2) unit annotation, (3) structural symbols and annotation, and (4) structural axes; with a base map in three layers -- contours, streams and water boundaries, and roads; and a plot file including map marginalia, titles, color-, line-, and symbol-keys has been completed. One additional layer, for fossil collection localities, is being prepared.

4. Digital base map materials -- roads, hydrologic features, and contours -- were prepared from DLG's (roads and hydrologic features) and by scanning (contours) for the eight 7.5' quadrangle-panels that make up the northwest quarter of the Los Angeles 1:100,000-scale sheet.

5. Samples collected in FY 1991 for palynological study by N. Fredrickson (BP&S) were found to be barren of forms useful for correlation.

Reports - None released

Earth Structure and Source Parameters

9920–10102

George L. Choy
Branch of Global Seismology and Geomagnetism
U.S. Geological Survey
Denver Federal Center
Box 25046, Mail Stop 967
Denver, CO 80225
(303) 273–8424

Investigations

1. **NEIC reporting services.** The NEIC now uses broadband data to routinely compute source parameters such as depth from differential arrival times, radiated energy of an earthquake, and arrival times of late-arriving phases. These parameters are published in the Monthly Listing of the Preliminary Determination of Epicenters and in the Earthquake Data Report.

2. **Effects of Earth structure on source parameters.** To improve the accuracy of source parameters derived from waveform analysis, we are developing corrections for the effects of wave propagation in the Earth.

   A. **Body wave interactions with upper mantle structure.** With the proliferation of digitally recording broadband networks around the world (including the USNSN), new techniques must be developed for the interpretation of seismic phases recorded at regional distances. We are generating a data base of synthetic seismograms of body wave interactions with various upper mantle models of the Earth. A comparison of the differences in the theoretical seismograms will be used to infer regional upper mantle structure.

   B. **Effects of pulse distortion on reading arrival times of non-minimum travel-time phases.** From both theory and observation, it has been well documented that waveforms of body waves that propagate past internal caustics suffer severe phase distortion. The accuracy and/or resolution of tomographic inversions involving such phases may be affected by the accuracy with which arrival times of these phases are read.

   C. **Effects of attenuation on the computation of source parameters.** We are developing techniques to determine the depth- and frequency-dependence of attenuation in the Earth. Resolution of this frequency dependence requires analysis of a continuous frequency band from several Hz to tens of seconds. It also requires consideration of the contributions of scattering and slab diffraction to apparent broadening of a pulse.

D. **Use of differential travel-time anomalies to infer lateral heterogeneity.** We are investigating lateral heterogeneity in the Earth by analyzing differential travel times of phases that differ in ray path only in very narrow regions of the Earth. Because such phases often are associated with complications near a cusp or caustic, their arrival times cannot be accurately read without special consideration of the effects of propagation in the Earth as well as additional processing to enhance arrivals.

3. **Rupture process of large- and moderate-sized earthquakes.** We are using digitally recorded broadband waveforms to characterize the rupture process of selected intraplate and subduction-zone earthquakes. The rupture processes thus delineated are used to complement seismicity patterns to formulate a tectonic interpretation of the epicentral regions.

Results

1. **Reporting Services.** The NEIC now uses broadband waveforms routinely: (1) to resolve depths of all earthquakes with $m_b > 5.8$; (2) to resolve polarities of depth phases to help constrain first-motion solutions; (3) to present as representative digital waveforms in the monthly PDE's; and (4) to compute the energy radiated by earthquakes. In the Monthly Listings of the PDE covering the interval April 1991 to June 1992, depths using differential arrival times from broadband waveforms were computed for 118 earthquakes; radiated energies were computed for 159 earthquakes. The cumulative results of having computed radiated energy for over 400 earthquakes is being summarized in a paper describing global patterns of radiated energy release and apparent stress.

2. **Effects of Earth structure on source parameters.**

   A. **Body wave interactions with upper mantle.** Synthetic seismograms generated for P and S waves interacting with the upper mantle are sensitive to differences in velocity contrasts, velocity gradients, and attenuation at the 420- and 670-km discontinuities. Major contributions to waveform shape come from later arrivals such as interference head waves and cusp-diffracted waves. In waveform data with sufficient broad bandwidth, these features can be identified and used to infer acceptable models of the upper mantle. A Langer locked-mode method of synthesizing seismograms for local distances is being adapted for computation of synthetics out to regional distances.

   B. **Arrival times of pulse-distorted body waves.** Body waves that touch internal caustics in the Earth are distorted in a way that can be mathematically corrected by Hilbert transformation. As a significant amount of teleseismic data used by the NEIC is in digital form, this correction can now be routinely performed. An automated processing package combining the methods of Choy and Richards (1975) and Harvey and Choy (1982) is now being implemented to obtain distortion free broadband waveforms for routine processing by NEIC analysts.

C. **Attenuation in the Earth.** We are attempting to separate intrinsic attenuation from scattering in waveforms. We synthesize waveforms using a method that simultaneously models causal attenuation and source finiteness. Under the assumption that intrinsic attenuation can be described by minimum phase operators, we can attribute discrepancies in the waveforms to scattering.

D. **Lateral heterogeneity from differential travel times.** We are using a source-deconvolution technique to resolve differential travel times of body waves near cusps and caustics. Application of this algorithm to PKP waves sampling the inner core suggests that regional velocity variations exist within the upper 200 km of the inner core. In reading high-quality arrival times of branches of PKP, we are correcting for pulse distortion in the AB arrival. The accumulation of these data can be used to determine if pulse distortion phenomena have biased the historical catalogs which have seen extensive use lately in deriving models of lateral heterogeneity.

3. **Rupture processes.**

A. We have developed a method of computing radiated energy and acceleration spectrum from direct measurements of teleseismically recorded broadband body waves. We have applied this algorithm to the study of a series of shallow intraplate earthquakes that serve as earthquake analogs to earthquakes that might occur in northeastern North America. In addition to deriving acceleration levels and stress drops, we find that the shapes of acceleration spectra from intraplate earthquakes are systematically different from those of subduction zone earthquakes. These spectral differences are used to infer differences in the mechanics of rupture in intraplate and subduction zone environments. Large subduction zone earthquakes likely occur in thoroughgoing fault zones which serve as stress concentrators. Similar thoroughgoing fault zones are lacking in cratonic crust, thus restricting large intraplate earthquakes to relatively shallow depths.

B. Moderate-sized compressional earthquakes occurring in the outer rise have been observed to precede some large subduction-zone earthquakes. We are developing a methodology for using these possibly precursory events to constrain the state of stress seaward of large earthquakes prior to their rupture. Preliminary results from modeling an outer-rise earthquake that preceded the large 1985 Valparaiso earthquake indicate that the outer-rise earthquake was induced by an elevation of stress seaward of the interplate asperity of the 1985 Valparaiso earthquake.

Reports

Boatwright, J., and Choy, G.L., 1992, Acceleration source spectra anticipated for large earthquakes in northeastern North America: Bulletin of the Seismological Society of America, v. 82, p. 660–682.

Mueller, S., Choy, G.L., and Spence, W., 1992, Regional stress seaward of subduction zone asperities: Nature (submitted).

Global Seismicity Mapping

9920–10242

Susan K. Goter
Branch of Global Seismology and Geomagnetism
U.S. Geological Survey
Denver Federal Center
Box 25046, Mail Stop 967
Denver, CO 80225
(303) 273–8477

Investigations

1. **State Seismicity Maps.** Produce and distribute seismicity maps on shaded, elevation-tinted state map bases.

2. **U.S. Seismicity Map.** Produce and distribute a full-color map showing earthquakes plotted on a shaded, elevation-tinted base map of the U.S.

Results

1. **State Seismicity Maps.** The aim of the state seismicity maps is to provide the most complete picture possible of where earthquakes have occurred historically in relation to geographic, geomorphic and cultural features. This is accomplished by selecting or compiling an earthquake database that is then plotted and printed on a shaded, elevation-tinted base map.

   Since this project began in 1988, state seismicity maps have been completed for Alaska, California, Hawaii and Utah. A similar map for southern California has just been completed. This map displays over 140,000 earthquakes that occurred from 1978 through July 1992 (this includes the Landers and Big Bear earthquakes and many aftershocks). Also plotted on the map are large earthquakes (magnitude 5.5 and greater) that occurred from 1933 to July 1992. Both earthquake data sets were derived from the Southern California Seismographic Network Catalog, a cooperative project of the Seismological Laboratory of the California Institute of Technology and the USGS Branch of Seismology, Pasadena, CA.

   The resulting full-color maps are being distributed to the research community worldwide, as well as to each high school in the southern California.

2. **U.S. Seismicity Map.** Work was completed on a large (approximately 38" x 58") full-color map showing earthquakes in the U.S. from 1534 to 1990. Symbols are plotted at epicentral locations and symbol sizes are scaled into four magnitude categories. Earthquakes that occurred since 1970 are distinguished from earlier

events by the intensity of color of the epicentral symbol. Nearly 35,000 earthquakes are represented on this map. Also included is a table of 63 earthquakes of special interest because of their size or location. Earthquakes listed in the table are identified on the map by a bold circle labeled with the reference number.

The resulting posters are distributed to the research community worldwide, and are also available for purchase.

Reports

Goter, S.K., 1992, Southern California Earthquakes: U.S. Geological Survey Open-File Report 92–533.

Goter, S.K., Thelin, G.P., and Pike, R.J., 1992, Earthquakes in the Conterminous United States: U.S. Geological Survey Open-File Report 92–327.

LIQUEFACTION RESEARCH

2-9910-01629

THOMAS L. HOLZER AND MICHAEL J. BENNETT
BRANCH OF ENGINEERING GEOLOGY AND SEISMOLOGY
345 MIDDLEFIELD ROAD MS-977
MENLO PARK, CALIFORNIA 94025-3591
415/329-5637 OR 415/329-4890

JOHN C. TINSLEY III
BRANCH OF WESTERN REGIONAL GEOLOGY
345 MIDDLEFIELD ROAD MS-975
MENLO PARK, CALIFORNIA 94025-3591
415/329-4928

Investigations

Continued to refine methods for predicting and mapping the likely occurrence of ground failure by: *(a)* evaluating the liquefaction hazard mapping published by Dupré and Tinsley (1980) as MF-1199 (scale 1:62,500) and comparing the mapping to the 1989 field occurrences; and *(b)* conducting subsurface exploration in the Pajaro Valley of areas of lateral spread ground failures triggered by the Loma Prieta earthquake and of areas adjacent to failed areas which did not show evidence of ground failure.

Compiled at 1:100,000 scale all reported occurrences of liquefaction caused by October 17, 1989, Loma Prieta earthquake.

Edited Professional Paper Chapter 1551-B, Liquefaction during 1989 Loma Prieta earthquake.

Completed design of retrieval of pore-pressure transducer for liquefaction arrays in the Marina District and San Bernardino and initiated field testing prior to installation.

Results

Established that: *(1)* regional geologic and liquefaction hazard maps of the Monterey Bay area published by Dupré and Tinsley in 1980 correctly identified the relative susceptibility to liquefaction-related ground failure as tested by the 17 October 1989 Loma Prieta earthquake; and *(2)* fluvial channel, point bar, and estuarine deposits contained most of the lateral spread ground failures, with point bar deposits containing most. Of 47 lateral spreads mapped in the Pajaro and Salinas Valleys, 46 occurred within the areas delineated by Dupré and Tinsley (1980) as having high or very high susceptibility to liquefaction; one occurred

in an area mapped as having moderate susceptibility, and none occurred in areas having low susceptibility to liquefaction. A total of 120 cone penetration tests and 60 standard penetration tests have been conducted at 18 sites, 14 of which displayed liquefaction-related ground failure in the Monterey Bay area. In FY 92, we completed 72 cone penetration soundings and 26 standard penetration tests distributed among 8 sites between Watsonville and Salinas, California. Index properties of soils sampled in the areas of ground failure have been determined for comparison to soil properties in areas where ground failure did not occur. Supporting soils data and penetration test data are being entered into a geotechnical database using GTGS® software. We now have a good suite of basic soils engineering data to support analyses of the ground failures which we have studied in detail. Maps were digitized that depict the surficial geology and liquefaction hazards for six 1:24,000-scale quadrangles in the Pajaro and Salinas Valleys. Completed digitizing the distribution of lateral spread ground failures mapped following the Loma Prieta earthquake.

Maps and a descriptive table of liquefaction caused by the Loma Prieta earthquake have been compiled at a 1:100,000 scale and will be included as plates in Professional Paper 1551-B.

Twelve papers that describe field studies and analyses of liquefaction caused by the 1989 Loma Prieta earthquake were edited for Professional Paper 1551-B. Current engineering techniques for evaluating liquefaction potential were largely successful. Improved ground performed without failures during the earthquake although ground motions were generally less than design levels.

A system that permits retrieval of pore pressure transducers at liquefaction arrays has been designed and tested under static field conditions. A dynamic test is planned in the Fall of 1992. Permits have been obtained for installation of the Marina District liquefaction array and tentative sites have been identified in the San Bernardino area. Plans are to install the arrays once dynamic testing is completed.

LIQUEFACTION RESEARCH

2-9910-01629

Reports

1. Tinsley, J. C. and Dupré, W. R., 1992, [abstract] Geologic aspects of liquefaction-induced ground failure in the Monterey Bay area, California, during the 17 October 1989 Loma Prieta earthquake: Proceedings, EERI Annual Mtg, San Francisco, Feb., 1992, 2 p.

2. Dupré, W. R. and Tinsley, J. C., in press, Evaluation of liquefaction-hazard mapping in the Monterey Bay area, central California in Holzer, T.L., ed., Chapter B of Strong ground motion and ground failure, The Loma Prieta earthquake of October 17, 1989: USGS Professional Paper 1551-B.

3. Tinsley, J.C., and Dupré, W. R., 1992, Liquefaction hazard mapping, depositional facies, and lateral spreading ground failure in the Monterey Bay area, central California: Paper accepted for publication in Proceedings, 4th US-Japan Workshop on Earthquake Resistant Design of Lifeline Facilities and Countermeasures for Soil Liquefaction, 27-29 May, 1992, Honolulu, Hawaii, 15 pp. [US Sponsor: National Center for Earthquake Engineering Research, Buffalo, New York]

4. Tinsley, J.C., Dupré, W. R., Bennett, M. J., and Ellen, S. D., in press, Liquefaction-related ground failure in the Monterey Bay area during the Loma Prieta earthquake in Holzer, T.L., ed., The Loma Prieta earthquake of October 17, 1989: USGS Professional Paper 1551-B.

5. Tinsley, J.C., Bennett, M.J., Egan, J., Kayen R., and Kropp, A. eds, in press, Maps showing liquefaction-related ground failure caused by the Loma Prieta earthquake in the San Francisco and Monterey Bay areas, California (scale 1:100,000), in Holzer, T.L., ed., The Loma Prieta earthquake of October 17, 1989: USGS Professional Paper 1551-B.

Seismic Review and Data Services

9920–67032

Roger N. Hunter
Branch of Global Seismology and Geomagnetism
U.S. Geological Survey
Denver Federal Center
Box 25046, Mail Stop 967
Denver, Colorado 80025
(303) 273–8472

Investigations

This project distributes copies at cost of filmed seismograms from the World-wide Standardized Seismograph Network (WWSSN), the Canadian Standard Network (CSN), and various stations with historical (pre-1963) records.

Results

Four-hundred and ten station-months of WWSSN seismograms were processed during fiscal year 1992. The seismograms were received from the stations, reboxed, stamped, collated, sent to the contract photographer, returned from the photographer, and mailed back to the stations after the films passed quality control requirements. Copies of CSN seismograms on 35mm reels were received on schedule from the Geological Survey of Canada. No films of historical seismograms were added to the archives this year.

The number of active stations in the WWSSN continues to decline, partly as a result of the replacement of the 1960 vintage analog seismographs with modern broadband digital systems. The quality of the recent data from the active WWSSN stations is still very good because these stations are operated by well-trained staffs. Many of the closed or inactive stations were beset with financial, political, or cultural encroachment problems.

The government-owned camera broke down completely in September 1992, and since there are no funds to repair or replace it, we have ceased microfilming original seismograms. We will continue to copy existing microfiches as needed. Changes in branch funding will require a price increase in fiscal 1993.

We received 20 special orders for films, ranging from a few to several thousand seismograms. Approximately 48,000 filmed seismograms were copied and distributed to fill the orders.

Seismic Hazard Reduction Planning Process to Develop Policies and Programs for the City of Seattle

Agreement No. 14-08-0001-G1958

Seattle Planning Department
Room 200 Municipal Building
Seattle, WA 98104

Principal Investigator: Clifford Marks
(206) 684-8372

The objective of this project is to develop a Seismic Hazard Reduction Plan. This planning effort could serve as a model for other communities in the Puget Sound region, but is mainly intended to develop and adopt policies and programs to reduce earthquake damage and loss of life within the City of Seattle.

This project will incorporate the research work currently being funded by USGS's National Earthquake Hazard Reduction Program into the City's planning process and translate seismic hazard technical information into terms that are understandable to both the general public and decision makers.

A policy framework for defining acceptable risk will be established and preliminary seismic hazard reduction policies will be prepared. Building code and other land use regulatory changes may be recommended, and input into emergency response planning will be provided. The project is also intended to coordinate the activities of various City departments regarding seismic hazard reduction issues and to establish a uniform seismic information data base.

The first year of the work program consisted of the following tasks:

Task 1 Establish City Seismic Hazard Reduction Committee and Consolidate Seismic Hazard Data Used by City Departments

This first task consisted of the formation of a Seismic Hazard Reduction Committee to work with the Principal Investigator to ensure communication between departments on this project. This committee gives direction to the seismic hazard reduction planning activities carried out under this grant. Each department has submitted their priority issues to ensure that these are dealt with during the program. It is an objective of this seismic hazard reduction work program to establish a uniform data base concerning seismic information to be used by all City departments.

Task 2 Translate Technical Hazard Based Research Funded Under NEHRP Into Classifications for Risk Reduction Policies

This aspect of the work program has documented and incorporated the work currently being done by the USGS and its grantees as part of the National Earthquake Hazards Reduction Program. The objective is to provide information to the general public concerning this data as it applies to Seattle. A report, *Seismic Hazards in Seattle*, was published in June 1992, and translates seismic hazard technical information into terms that are understandable to both the general public and decision makers.

Task 3 Establish Framework for Acceptable Risk Analysis

The objective of this task is to establish a policy framework for defining acceptable risk. The City needs to address this risk issue in a formal manner. The product of this task was a working paper that provides a framework for risk and vulnerability analysis.

The second year of the work program consists of the following tasks:

Task 1 Identify Specific Buildings at Risk

The City has extensive information in its building department files concerning buildings that might be at seismic risk. The objective of this task is to gather this data in a systematic fashion and to put it in a form that can be easily retrieved and used in seismic hazard reduction planning. This data base will be used to evaluate risk, in general terms, and to document portions of the city that are most susceptible and should be noted in disaster response planning. It will also be used to prepare for post-earthquake response activities. This structure inventory and other information will be incorporated into and depicted on the City's Geographic Information System.

Task 2 Estimate Damage to Buildings, Structures, and Lifelines in Liquefaction-prone Areas

Since the most detailed hazard information available to date appears to deal with liquefaction potential, this area will be the subject of the most detailed work as part of the City's seismic hazard reduction planning effort during Year 2. The objective of this task is to evaluate the vulnerability of buildings and structures, especially critical ones in liquefaction-prone areas. Buildings in these areas may be classified by type and by age. Critical facilities have now been noted, such as hospitals, fire and police stations, bridges, schools, etc. This listing of critical facilities has now been incorporated into the City's GIS system and a map has been produced

combining the liquefaction-prone area information and the critical facility information. The information on susceptible structures will also be added to this mapping system.

Task 3 Establish Methodology for Ground-Shaking Hazards

The objectives of this task will be to determine the best approach for dealing with ground-shaking hazards, and to determine what can be accomplished with existing information. The proposed approach is to combine current mapping of earthquake intensity and geology with City land use/zoning maps. Ground acceleration data will be related to the general location of different building types which characterize different land use categories. A typology will also be established relating impacts on building type (e.g., high rise, single-family woodframe, unreinforced masonry, reinforced concrete) with areas subject to different ground response. The product of this task will be a working statement outlining the City's approach to dealing with ground shaking hazards.

Task 4 Develop Final Seismic Hazard Reduction Policies

This task will contain recommended additions or changes to City policies and regulations. These policies and regulations may include the following: comprehensive plan and land use policies; zoning, subdivision, environmental review, and environmentally critical area regulations; building code; development application review studies (e.g., geotechnical reports required in liquefaction-prone areas); capital improvement program; possible structural hazards abatement program; requirements for strong motion instrumentation on new or rehabilitated buildings; providing input into disaster response planning efforts; and making recommendations for pre-earthquake planning for post-earethquake recovery.

DATABASE MANAGEMENT

9910-03975

Charles S. Mueller
Branch of Engineering Seismology and Geology
U. S. Geological Survey
345 Middlefield Road, MS 977
Menlo Park, California 94025
(415) 329-5646

Investigations

1. Develop new techniques for playback, processing, management, and export of seismic waveform data, with emphasis on large aftershock datasets collected with portable digital seismographs (e.g.,GEOS).
2. Design and implement relational databases for strong-motion and aftershock data.

Results

1. New datsets collected, played back, and processed:
   Aftershocks of the 1992 Petrolia earthquake
   Aftershocks of the 1992 Joshua Tree earthquake
   Aftershocks of the 1992 Landers and Big Bear earthquakes
2. 1989 Loma Prieta aftershock dataset exported to:
   University of Connecticut
   University of California, Berkeley
   NOAA, National Geophysical Data Center
   Frank Hubach Associates (consultant)
   W. Johnson (consultant)
   California Department of Water Resources, Division of Dam Safety
   Projet Geoscope, Institut de Physique du Globe, FRANCE
   A. Nene (consultant)
   University of Nevada, Reno
   Pacific Gas and Electric, Geosciences Department
3. Other aftershock datasets exported:
   1983 Coalinga - to N. Abrahamson (consultant)
   1983 Coalinga - to U. C. Berkeley
   1986 North Palm Springs - to U. C. Santa Barbara

Probabilistic Earthquake Assessment

9920–80832

Stuart Nishenko and Jack Evernden
with Charles Bufe and James Dewey as Co-Investigators
Branch of Global Seismology and Geomagnetism
U.S. Geological Survey
Denver Federal Center
Box 25046, Mail Stop 967
Denver, CO 80225
(303) 273–8412

Investigations

Stuart Nishenko worked on probabilistic earthquake forecasts for the Wasatch Front, Utah with D. Schwartz (USGS, Menlo Park), an evaluation of the reliability of various types of probabilistic earthquake forecasts with Dave Perkins (USGS, Golden), and a rebuttal to the Kagan and Jackson paper on seismic gaps (JGR, 1991, 96, 21419–21431) with L. Sykes (L–DGO, Palisades, NY).

James Dewey worked with J. Healy (USGS, Menlo Park) and V. Kossobokov (International Institute for Earthquake Prediction Theory and Mathematical Geophysics, Moscow, Russia) to formulate and describe a test of the M8 earthquake prediction algorithm.

Charles Bufe worked with D. Varnes (USGS, Golden) and S. Nishenko on analysis of long-term seismicity patterns preceding and following large earthquakes. It is anticipated that this information will help to further define seismicity variations within the seismic cycle and refine earthquake forecasts in regions of high seismic potential.

C. Bufe planned and coordinated the second annual NEIC/OEVE/OIG international training course, "Understanding Earthquakes and Mitigating Their Effects."

Results

S. Nishenko and Lynn Sykes prepared a rebuttal to the Journal of Geophysical Research article by Kagan and Jackson on seismic gaps, noting that upon further examination, half of the earthquakes that K&J used to test the seismic gap hypothesis do not meet the selection criteria originally published by McCann, Nishenko, Sykes, and Krause (Pageoph, 1979, 117, 1082–1147). Examination of a revised catalog that meets these criteria as to mechanism, type of plate boundary, and range of magnitude indicates that elapsed time alone is not a powerful discriminant for classifying seismic potential in a system characterized by an order of magnitude variation in recurrence time.

The initial phase of data collection and analysis of the reliability of probabilistic earthquake forecasts was conducted with D. Perkins. An analysis of the 1991 Limon, Costa Rica tsunami, based on the responses obtained from the NEIC Tsunami Questionnaire, was conducted and an article was written for the USGS Professional Paper on the 1991 Costa Rica earthquake. Work continued on the analysis of Wasatch Front, Utah earthquake probabilities with D. Schwartz.

J. Dewey worked on preparing a rationale and description of M8 that is now being conducted jointly with Healy and Kossobokov. He participated in the May, 1992 meeting of the National Earthquake Prediction Evaluation Council (NEPEC), describing the M8 test to NEPEC members and seeking their advice on certain points of implementation.

C. Bufe and D. Varnes completed time-to-failure analysis of accelerating seismic release during the long-term seismic cycle and its included subcycles in the San Francisco Bay region. Bufe examined the space-time occurrence of large ($M \geq 7.5$) earthquakes in the Alaska-Aleutian region. This included analysis of accelerating seismic release preceding the great (M_W 8.7) 1957 central Aleutian Islands earthquake and the recent acceleration in the eastern Aleutians-Alaska Peninsula region.

The second annual NEIC/OEVE/OIG international training course, "Understanding Earthquakes and Mitigating Their Effects," was presented under the leadership of C. Bufe. The course, which provided an overview of applied earthquake seismology and engineering, was given on April 20–May 7, 1992, and consisted of two weeks of lectures in Golden followed by three concurrent four–day workshops, one of them in Albuquerque. The faculty were recruited primarily from the OEVE, although a number of key people came from other parts of the Geologic Division, from other agencies, and from academia. Participants were from Indonesia, Panama, Tunisia, Lebanon, Dominican Republic, Venezuela, Trinidad, Mexico, Argentina, United Kingdom, and Italy. The critique and feedback from the participants was quite positive. One purpose of the course is to foster ongoing communication and collaboration between USGS scientists and colleagues from around the world.

Reports

Bufe, C.G., 1992, Recent earthquakes and historical California-Nevada seismicity—The big picture [abs.]: EOS (American Geophysical Union, Transactions), v. 73, p. 373.

Bufe, C.G., and Varnes, D.J., 1992, Predictive modelling of the seismic cycle of the greater San Francisco Bay region: Journal of Geophysical Research, 29 p. (in final stages of revision).

Bufe, C.G., Nishenko, S.P., and Varnes, D.J., 1992 Clustering and potential for large earthquakes in the Alaska-Aleutian region [abs.]: Extended Abstract, Wadati Conference on Great Subduction Earthquakes, Fairbanks, Alaska, September 16–19, 1992, p. 129–132, also on CD–ROM.

Evernden, J.F., and S.P. Nishenko, 1992, Programs for prediction of ground motion resulting from worldwide earthquakes [abs.]: EOS, (American Geophysical Union, Transactions), v. 73, p. 73.

Healy, J.H., Kossobokov, V.G., and Dewey, J.W., 1992, A test to evaluate the earthquake prediction algorithm, M8: U.S. Geological Survey Open-File Report 92–401, 23 p., and 6 Appendices.

Nishenko, S.P., 1992, Wasatch Front, Utah earthquake probabilities, in Frizzell, V., Jr., ed., Proceedings of the National Earthquake Prediction Evaluation Council, June 11–12, 1991, Alta, Utah: U.S. Geological Survey Open-File Report 92–249, p. 16–19.

Nishenko, S.P., and Sykes, L.R., 1992, Comment on "Seismic gap hypothesis-ten years after," by Kagan and Jackson: Journal of Geophysical Research, 23 p. (in press).

Nishenko, S.P., and L.R. Sykes, 1992, Seismic gaps, seismic potential, and long-term probabilistic earthquake forecasts—A historic perspective [abs.]: Wadati Conference on Great Subduction Earthquakes, Fairbanks, Alaska, September 16–19, 1992, p. 40–42.

Nishenko, S.P., and Sykes, L.R., 1992, Seismic gap hypothesis test [abs.]: EOS (American Geophysical Union, Transactions), v. 73, p. 365–366.

Nishenko, S.P., Camacho, E., Astorga, A., Morales, L.D., and Preuss, J., 1992, The 1991 Limon, Costa Rica Tsunami, in Espinosa, A., Montero, W., Cardoze, N., and Camacho, E., eds., "The Limon, Costa Rica earthquake of April 22, 1991 and its aftershocks—A post-earthquake field study" U.S. Geological Survey Professional Paper xxxx 25 p.

Preuss, J., and Nishenko, S.P., 1992, The National Earthquake Information Center Tsunami Questionnaire: EOS, (American Geophysical Union, Transactions), v. 73, p. 267.

Data Processing, Golden

9950-02088

Robert B. Park
Branch of Geologic Risk Assessment
U.S. Geological Survey
Box 25046, MS 966, Denver Federal Center
Denver, CO 80225
(303) 273-8674

Investigations

The purpose of this project is to provide the day-to-day management and systems maintenance and development for the Golden Data Processing Center. The center supports Branch of Geologic Risk Assessment with a variety of computer services. The systems include a PDP 11/70, a VAX/750, a VAX/780, two MicroVAX's, two SUN servers, 5 SUN workstations, and a PDP 11/34. Total memory is 40 mbytes and disk space is approximately 7 G bytes. Peripherals include four plotters, ten mag-tape units, an analog tape unit, two line printers, 5 CRT terminals with graphics, and a Summagraphic digitizing table. Dial-up is available on all the major systems and hardwire lines are available for user terminals on the upper floors of the building. Users may access any of the systems through a Gandalf terminal switch. Operating systems used are RSX11 (11/34's), Unix (11/70), RT11(LSI's) and VMS (VAX's).

Results

Computation performed is primarily related to the Hazards program; however, work is also done for the Induced Seismicity and Prediction programs, as well as for DARPA, ACDA, and U.S. Bureau of Reclamation, among others.

The data center supports research in assessing seismic risk and the construction of national risk maps. It also provides capability for digitizing analog chart recordings and maps. Also, most, if not all, of the research computing related to the hazards program are supported by the data center.

The data center also supports equipment for online digital monitoring of Nevada and Colorado Western Slope seismicity. Also, it provides capability for processing seismic data recorded on digital cassette tape in various formats.

The computer center manages the local area network (LAN) providing central backup facilities, file services, and peripheral access for about 75 personal computers. This LAN management is accomplished with Path Works software.

United States Earthquakes

9920–10042

Glen Reagor and Lindie Brewer (for Carl Stover)
Branch of Global Seismology and Geomagnetism
U.S. Geological Survey
Denver Federal Center
Box 25046, Mail Stop 967
Denver, CO 80225
(303) 273–8406

Investigations

Five hundred and forty-eight earthquakes in 24 states and Puerto Rico were canvassed by a mail questionnaire for felt and damage data during the period October 1, 1991 through September 30, 1992. One hundred and eighty-eight earthquakes occurred in Alaska, 5 in Arizona, 1 in Arkansas, 235 in California, 8 in Colorado, 1 in Georgia, 4 in Hawaii, 17 in Idaho, 2 in Illinois, 1 in Kansas, 7 in Missouri, 4 in Montana, 20 in Nevada, 1 in New Mexico, 3 in New York, 1 in Ohio, 5 in Oregon, 3 in Puerto Rico, 1 in South Carolina, 1 in Tennessee, 2 in Texas, 15 in Utah, 1 in Virginia, 16 in Washington, and 6 in Wyoming.

Damage/felt surveys of the epicentral regions were made by Glen Reagor and Lindie Brewer for the April 25 and 26, 1992, Cape Mendocina, California, earthquakes and the Landers and Big Bear, California earthquakes (June 28, 1992). The data is used for evaluating damage caused by the earthquakes and mapping the extent of the felt area.

The Earthquake Data Base System (EDBS) continues to furnish seismic data to engineers, land-use planners, architects, oil company geophysicists, insurance companies, university programs, and private citizens.

Results

Thirteen earthquakes caused damage (MMI VI or greater) during this period. Moderate damage (MMI of VII–IX) was recorded for six California earthquakes; slight damage (MMI of VI) was reported for five earthquakes. Two earthquakes in Utah produced damage; slight (MMI of VI) damage was reported by one earthquake, and the other earthquake recorded moderate (MMI of VII) damage.

During this reporting period, seismicity searches on the EDBS has resulted in $9,906 in fees from non-government users. The following catalogs in the EDBS have been updated: the Preliminary Determination of Epicenters catalog (Monthly Listings) through 1991; the International Seismological Centre (ISC) catalog through August 1990.

The new mail intensity questionnaire (Earthquake Report Form 9–3013) was approved by the USGS. The project will begin to use the new forms in November 1992.

Version 2.0 of the Global Hypocenter Data Base CD–ROM has been approved. The distribution of the CD–ROM and the revised EPIC software is expected to be released in November 1992. A "DEMO DISK" has been created to simulate a CD–ROM data base for users who may be interested in the Global Hypocenter Data Base CD–ROM. The "DEMO DISK" is available on 5.25-inch 1.2M disk or the 3.5-inch high-density disk.

The Cape Mendocino, California, earthquakes on April 25 and 26, 1992 (magnitudes 7.1 M_S, 6.6 M_S, and 6.6 M_S) caused 98 injuries and over $66 million in damage. Together, the earthquakes were felt over a land area of approximately 86,000 sq km of California, Nevada, and Oregon. The most extensive damage occurred in Ferndale, Honeydew, Petrolia, Rio Dell, and Scotia. All of these communities were within a 50-mile radius of the three epicenters. A Modified Mercalli Intensity (MMI) of VIII was assigned to these communities.

The Landers and Big Bear Lake, California, earthquakes on June 28, 1992 (magnitudes 7.5 M_S and 6.6 M_S) caused 397 injuries and over $92 million in damage.

The Landers earthquake was felt throughout southern California, Nevada, southern Arizona, southern Utah, and in high-rise buildings as far north as Boise, Idaho, and as far east as Denver, Colorado. The heaviest damage occurred in the Landers, Yucca Valley, and Joshua Tree area. Primary ground rupture occurred on three faults that traversed this area. In this sparsely populated area, a MMI of IX was assigned to a wood-frame house that straddled a section of the ground rupture.

The Big Bear earthquake caused extensive damage in the mountain communities of Big Bear Lake, Big Bear City, Fawnskin, and Barton Flats—all in the Big Bear recreation area in the San Bernadino Mountains. The computed epicenter places the earthquake near the Barton Flats campground. A MMI of VIII was assigned to this earthquake.

Two in-house slide sets were made for the Cape Mendocino and Landers/Big Bear earthquakes. These slides have been presented in slide shows by USGS personnel to educational institutions, civic organizations (Rotary, Kawanis, and Senior Citizens) and government agencies such as FEMA. Selected slide sets were made available to Kelvin Berryman of the New Zealand Geological Survey. The best slides of our collection were furnished to Mike Rymer (USGS Menlo Park) for inclusion into a USGS Open-File Report (in progress). Earthquake photographs (8x10) were made for wall displays in the USGS offices located in Golden, Colorado, and Reston, Virginia, and the USGS booth at the December fall AGU meeting in San Francisco, California. Selected photographs of damage were used in the Cape Mendocino edition of "Earthquakes and Volcanoes."

Reports

Reagor, Glen, and Brewer, Lindie, The Cape Mendocino earthquakes, damage and intensity survey: Earthquakes and Volcanoes (in press).

Reagor, Glen, and Brewer, Lindie, The Cape Mendocino earthquakes of April 25 and 26, 1992: U.S. Geological Survey Open-File Report (in progress).

Stover, Carl W., and Brewer, R., 1991, United States Earthquakes, 1985: U.S. Geological Survey Bulletin 1954, 170 p.

Stover, Carl W., and Brewer, R., 1991, United States Earthquakes, 1986: U.S. Geological Survey Bulletin. Compilation of the publication continues. Director's approval as of 1/16/92.

Stover, Carl W., and Coffman, Jerry L., Seismicity of the United States, 1568–1989 (Revised): U.S. Geological Survey Professional Paper 418. Director's approval 2/28/92.

LATE QUATERNARY FAULTING, SOUTHERN SAN ANDREAS FAULT

9910-04098

Michael J. Rymer

Branch of Engineering Seismology and Geology
U.S. Geological Survey
345 Middlefield Road, MS/977
Menlo Park, CA 94025
(415) 329-5649
mrymer@isdmnl.wr.usgs.gov

Investigations

1. Mapping of Quaternary faults and adjacent geology in the Indio and Mecca Hills.

2. Paleomagnetic studies, with R. Weldon, J. Boley, and J. Stimac (University of Oregon), of late Pliocene and Quaternary deposits in the Indio and Mecca Hills to test for tectonic rotation.

3. Geologic investigation of the April, 1992, Joshua Tree earthquake in the Little San Bernardino Mountains, southern California.

4. Geologic investigation, with USGS and California Division of Mines and Geology staff, of the June, 1992, Landers, California, earthquake.

Results

1. Geologic mapping of the San Andreas fault zone in the Myoma and Thermal Canyon quadrangles in the Indio and Mecca Hills, respectively, is now complete. Parts of adjacent quadrangles (Cathedral City, Seven Palm Valley, East Deception Canyon, West Berdoo Canyon, Indio, and Mecca) are also mapped.

2. Significant progress was made in paleomagnetic studies of possible tectonic rotation in the Indio and Mecca Hills. We collected additional samples from our earlier paleomagnetic sections in the central and southeastern parts of the Indio Hills, approximately doubling the number of reverse-magnetic-polarity samples for each sample set. [We can not determine whether "normal"-magnetic-polarity samples are either actual normal samples with a normal magnetic overprint or are reverse samples dominated by a normal overprint. We, therefore, use only reverse magnetic polarity samples from which the normal overprint easily can be identified and removed.] The increased sample number provides for a greater statistical base. Interpretations of these two sections, by Boley and Weldon, indicate that the area near the southeast end of the Indio Hills (n=86) rotated counterclockwise about 7°±5°, and the section in the central Indio Hills (n=121) rotated about 12°±5° clockwise in the past approximately 1 Ma.

   Two new paleomagnetic sections were also sampled in this report period; both sections are in the Mecca Hills. The sections are Painted Canyon (n=25) and Sheep Hole

(n=99). The Painted Canyon section is a pilot study and currently is too small a sample set for meaningful statistical analysis. Interpretation, by Boley and Weldon, of the Sheep Hole section indicates no rotation, 0°±3°. Additional sampling in these sections will improve the statistical base.

3. Field investigations of the geologic structure in the western part of the Little San Bernardino Mountains following the M6.1 April 23 Joshua Tree earthquake confirm aerial photo interpretations that previously unmapped north-south faults are active and important structures in the tectonic setting of the area. Three such north-south faults, the Long Canyon, East Wide Canyon (EWCF), and West Deception Canyon (WDCF) faults, are geomorphically prominent and easily recognized in the field. The Joshua Tree earthquake resulted from movement on a 15-km segment of the WDCF. Holocene(?) motion on these faults is east-side-up right-lateral oblique slip, and these faults offset structures of the Dillon shear zone. Field and aerial photo interpretations following the June 28 Landers earthquake indicate that the EWCF and WDCF are structurally connected with the more northerly Burnt Mountain and Eureka Peak faults, respectively, that had surface rupture in the June earthquake. The north-south faults in the area thus are important structures not only for the Joshua Tree and Landers earthquakes, but also for partitioning slip from the San Andreas fault zone into the Mojave Desert region.

   Ground searches after the Joshua Tree earthquake revealed no surface rupture on the WDCF; however, surface fractures developed over a 1 1/2-km interval on the EWCF about 4 1/2 km to the west. Maximum right-lateral and vertical (east-side-up) slip values were 6 and 4 mm, respectively. These surface fractures are inferred to be triggered slip for the following reasons: The EWCF was aseismic and the fault plane dips about 60° to the west, away from the plotted seismicity. Most importantly, the surface fractures formed only locally in thin (<4 m thick) Holocene fluvial and colluvial deposits and not in underlying crystalline bedrock.

4. The Landers earthquake was the largest surface-rupturing event in the U.S. since 1906. Surface rupture, both primary and triggered, formed on four main faults and at least 12 other faults in southern California. Primary slip, defined by significant displacement values on seismically active faults, was centered on the Johnson Valley, Kickapoo, Homestead Valley, Emerson, and Camp Rock faults, all north of the Pinto Mountain fault, and on the Burnt Mountain and Eureka Peak faults south of the Pinto Mountain fault. Displacements on these faults was dominantly right lateral strike slip; the vertical component of slip, where present, amounted to only about 10 percent of the net slip. Maximum right-lateral slip values on the faults north of the Pinto Mountain fault were about 3 m for the Johnson Valley, Kickapoo, and Homestead Valley faults, about 5.6 m on the Emerson fault, and about 2 m on the Camp Rock fault; slip values on the Burnt Mountain and Eureka Peak faults were about 3 cm and 21 cm, respectively. Triggered slip developed on faults as far from the Landers epicenter as 160 km, in the Imperial Valley (discussed by R.V. Sharp). Triggered slip also developed along about 80 km of the southern San Andreas fault. Surface breakage there was discontinuous and amounted to as much as 2 cm of right-lateral slip. Triggered right-lateral slip also formed on faults nearer the epicenter and amounted to 2–5 cm.

Reports

Rymer, M.J., 1992, The 1992 Joshua Tree, California, earthquake: Tectonic setting and triggered slip [abs.]: EOS, Transactions, American Geophysical Union, v. 73, no. 43, p. 363.

Fault Segmentation: San Andreas Fault System

9910-03983

David P. Schwartz, Thomas E. Fumal, Suzanne Hecker, Thomas J. Powers
Branch of Engineering Seismology and Geology
U. S. Geological Survey
345 Middlefield Road, MS 977
Menlo Park, CA 94025
(415) 329-5651, *FAX* (415) 329-5143,5163

Investigations

The objective of the project is to quantify the behavior of the San Andreas fault and major parallel faults in the San Francisco Bay area and in southern California with regard to segmentation, recurrence, slip rate, and slip per event. These parameters form the basis for long-term probabilistic earthquake forecasting. At present the work involves paleoseismological studies on the Rodgers Creek fault zone in Sonoma County, the Santa Cruz Mountains segment of the San Andreas fault, and the Mojave segment of the San Andreas fault with emphasis on the Wrightwood site.

Results

1. Rodgers Creek fault zone (Schwartz, Hecker, Powers). Work during 1992 provided the first estimates of the timing of individual paleoearthquakes on this fault. Seven trenches were excavated parallel to and across the fault zone in fluvial deposits on the Triangle G Ranch, 25 km south of Santa Rosa. This is our second site on the fault.. The first, Beebe Ranch, was studied in FY 1989 and 1990. New radiocarbon dates from these trenches indicate that three surface faulting (M7) earthquakes occurred during approximately the past 1000 years. Preliminary constraints on the timing of these events suggest that they occurred at about 1000 AD, between 1200 and 1400 AD, and between 1650 and 1808 AD. Results at the two sites are encouragingly consistent. The investigation indicates that the elapsed time on the Rodgers Creek fault zone is the longest on any major Bay Area strike-slip fault segment (at least 184 years) and is near, at, or possibly beyond the average repeat time.

2. San Andreas fault zone, Santa Cruz Mountains (Schwartz, Powers). Logging was completed in three trenches excavated across the main trace of the San Andreas fault at Grizzly Flat, 9 km east of the 1989 Loma Prieta epicenter. The trenches exposed evidence of the past two large surface faulting events. The most recent event displaces all sediments and the ground surface and produced subvertical scarplets that are geomorphically fresh. Dendro-corrected radiocarbon dates on detrital charcoal indicate this event occurred after 1800 AD and it is interpreted as faulting from the 1906 earthquake. Structural relations suggest the penultimate event occurred shortly before 1636-1660 AD. These preliminary results suggest an interval of about 250 years, a value consistent with calculated repeat times for 1906-type earthquakes but longer

than 125 year average interval used by the 1990 Working Group to estimate probabilities for this part of the fault zone.

3. San Andreas fault zone, Wrightwood (Fumal). Analysis of the timing of individual earthquakes at this location on the San Andreas fault, using standard and high-precision radiocarbon dating on peats, continued. In 1992 our four year effort resulted in defining the timing of the five most recent events at the Wrightwood site. These are AD 1857, 1812, 1700, 1610, and 1460. The Wrightwood site contains two more events than Pallett Creek, 25 km to the north, for the same period of time. The 1610 event, and very likely the 1812 event, do not correlate with the event chronology at Pallett Creek and likely involved the San Bernadino Mountains segment of the fault. These events decrease the average recurrence interval on the southern San Andreas fault zone to about 100 years. The recognition of additional earthquakes in the paleoseismic record at Wrightwood resulted in a calculated 30 year probability increase to 80 percent for the southern San Andreas fault zone. These results were presented to NEPEC by R. Weldon, University of Oregon, our colleague in the study.

Reports

Fumal, T.E., Pezzopane, S.K., Weldon, R.J., and Schwartz, D.P., 1992, A 100 year average recurrence interval for the southern San Andreas fault at Wrightwood, California: *Science* (in press).

Schwartz, D.P., Pantosti, D., Hecker, S., Okumura, K., Budding, K.E., and Powers, T.J., 1992, The Rodgers Creek fault zone: fault behavior and earthquake potential (abs): Second Conference on Earthquake Hazards in the Eastern San Francisco Bay Area, p. 63.

Schwartz, D.P., Pantosti, D., Okumura, K., Powers, T.J., and Hamilton, J.C., 1993, Timing of past surface faulting earthquakes along the San Andreas fault in the Santa Cruz Mountains, Central California: U.S. Geological Survey Professional Paper: the Loma Prieta Prieta earthquake (in review).

EXPERIMENTAL AND ANALYTICAL INVESTIGATIONS OF FOUR GRAVELLY SITES WHICH LIQUEFIED DURING THE 1983 BORAH PEAK, IDAHO EARTHQUAKE

USGS 14-08-0001-G1779

Kenneth H. Stokoe, II, José M. Roesset and Ronald D. Andrus
The University of Texas at Austin
Department of Civil Engineering
ECJ 9.227
Austin, Texas 78712
(512) 471-4929

Investigation

The primary objective of this study is to characterize the gravelly sediments which liquefied during the 1983 Borah Peak, Idaho earthquake (M_S = 7.3). Since little information exists on the characteristics and field performance of gravelly materials subjected to earthquake shaking, this study will aid in the development of criteria for assessing the liquefaction susceptibility of gravelly soils. In August 1990 and September 1991, we conducted field investigations where liquefaction had occurred at three gently sloping sites along the Big Lost River and one more steeply dipping site along the Thousand Springs Creek.

Results

Three investigation sites along the Big Lost River are: 1) the lateral spread at the Pence Ranch, 2) the gravel bar just above Mackay Reservoir where Mr. Andersen was standing when the earthquake struck (called Andersen Bar herein), and 3) a side bar near the bridge onto the Goddard Ranch. The fourth site, along Thousand Springs Creek, is a lateral spread at the toe of the Elkhorn Fan on the Larter Ranch. Grain-size distribution curves of test pit samples taken from the layer most likely to have liquefied at each site are shown in Fig. 1. Shear wave velocities profiles determined by the Spectral-Analysis-of-Surface-Wave (SASW) and crosshole seismic methods are shown in Figs. 2 thru 5.

Pence Ranch--Liquefaction at the Pence Ranch site occurred in loose gravelly soils containing only a few percent fines. The degree of pore water pressure generation appears to have been controlled by a thick silty sand cap of low permeability that lies above the loose gravelly soils, as shown in Fig. 2. Investigations at Pence Ranch have been summarized in previous progress reports and in the papers by Andrus et al. (1991 and 1992).

Ratiocarbon dates of 3150±80 and 2460±60 years B.P. were obtained for soil samples taken from a depth of about 1 m. (The soil samples were dated at the University of Texas at Austin Radiocarbon Laboratory.) A piece of charcoal found in the same silty sand layer was dated at 3430±70 years B.P. (The charcoal sample was dated at the NSF Accelerator Facility at the University of Arizona and was partially funded by NSF grant EAR85-12761.)

Andersen Bar--Liquefaction at the Andersen Bar site occurred in loose gravelly soils containing only a few percent fines. Thin, interbedded layers of sandy silt appears to have aided in the development of high pore water pressures (see Fig. 3). Investigations at the Andersen Bar site have been briefly summarized in a previous progress report and in the paper by Andrus et al. (1992).

Goddard Ranch--Numerous sand boil deposits were observed in the low-lying areas on the Goddard Ranch. Shown in Fig. 4 are generalized soil and shear wave velocity profiles of the gravel side bar investigated. Liquefaction most likely occurred in the loose silty sand to clean sandy gravel between 2 and 4 m. The low permeability sandy silt layer just above the water table perhaps aided in the generation of pore pressures.

Larter Ranch--At the Larter Ranch site, liquefaction occurred beneath the coarse-grained Elkhorn fan in sandy gravel containing about 7 percent fines between the depths of 2 and 4.5 m (see Fig. 5). The high fines content would reduce permeability and, thus, prevent rapid pore water pressure dissipation. These finding were briefly discussed in a previous progress report and in the paper by Andrus et al. (1992).

Two liquefaction assessment charts based on V_S for sands are shown in Figs. 6 and 7 with results for each of the four gravelly sites. Both methods correctly predict liquefaction at all four gravelly sites.

REFERENCES

Andrus, R.D., Stokoe, K.H., II, and Roesset, J.M., (1991), "Liquefaction of Gravelly Soils at Pence Ranch During the 1983 Borah Peak, Idaho Earthquake," *Proceedings*, Fifth International Conference on Soil Dynamics and Earthquake Eng., Karlsruhe, Germany, pp. 251-262.

Andrus, R.D., Stokoe, K.H., II, Bay, J.A., and Youd, T.L., (1992), "In Situ V_S of Gravelly Soils which Liquefied," *Proceedings*, Tenth World Conference on Earthquake Engineering, Madrid, Spain, pp. 1447-1452.

Finn, W.D.L., (1991), "Assessment of Liquefaction Potential and Post-Liquefaction Behavior of Earth Structures: Developments 1981-1991. In. S. Prakash (ed.), *Proceedings*, Second ICRAGEESD II, St. Louis, MI, pp. 1833-1850.

Stokoe, K.H., II, Roesset, J.M., Bierschwale, J.G., and Aouad, M. (1989), "Liquefaction Potential of Sands from Shear Wave Velocity," *Proceedings*, Ninth World Conference on Earthquake Engineering, Tokyo, Japan, April, pp. 213-218.

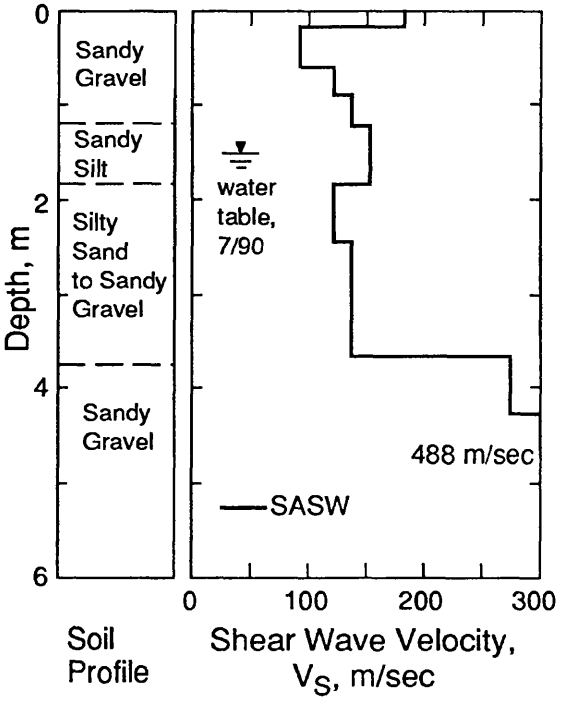

Fig. 4 - Shear wave velocity profile at Goddard Ranch.

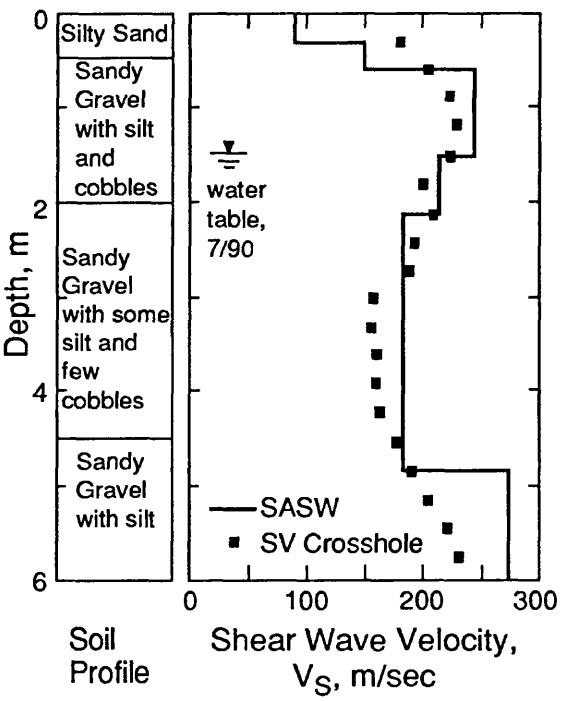

Fig. 5 - Shear wave velocity profiles at Larter Ranch (from Andrus et al., 1992).

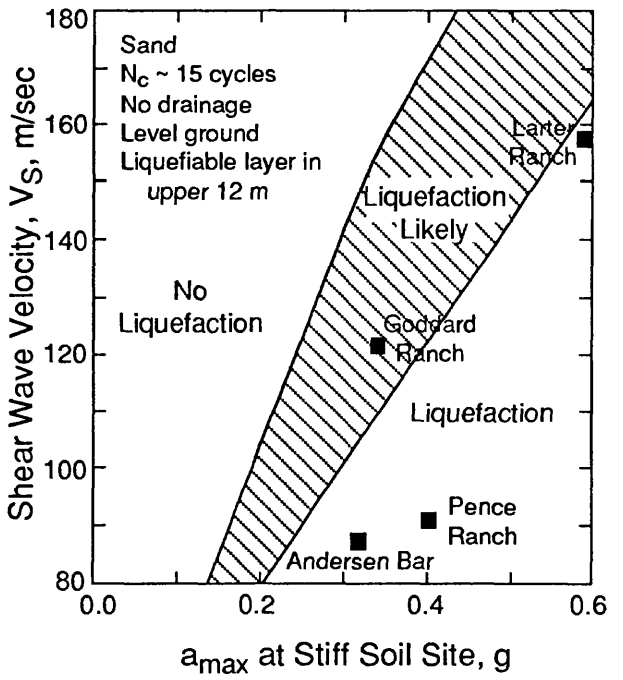

Fig. 6 - Liquefaction assessment chart based on shear wave velocity (Stokoe et al., 1989) with results from the four liquefaction sites.

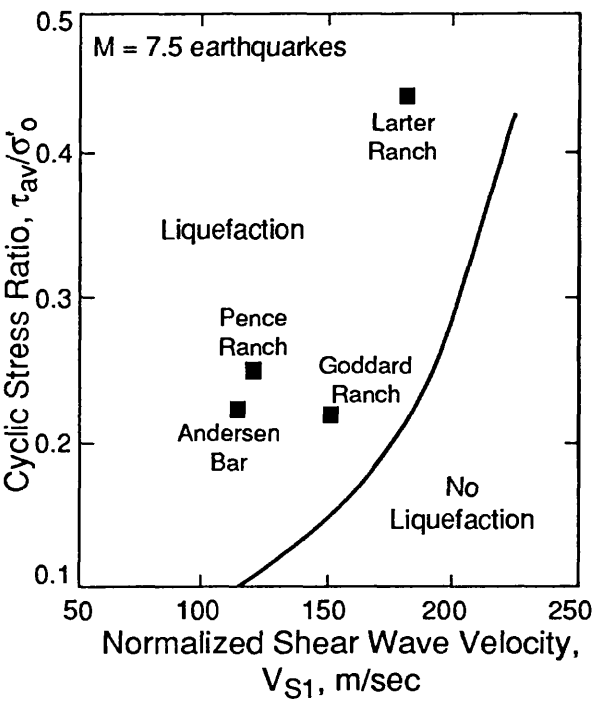

Fig. 7 - Liquefaction assessment chart based on normalized shear wave velocity (Finn, 1991) with results from the four liquefaction sites.

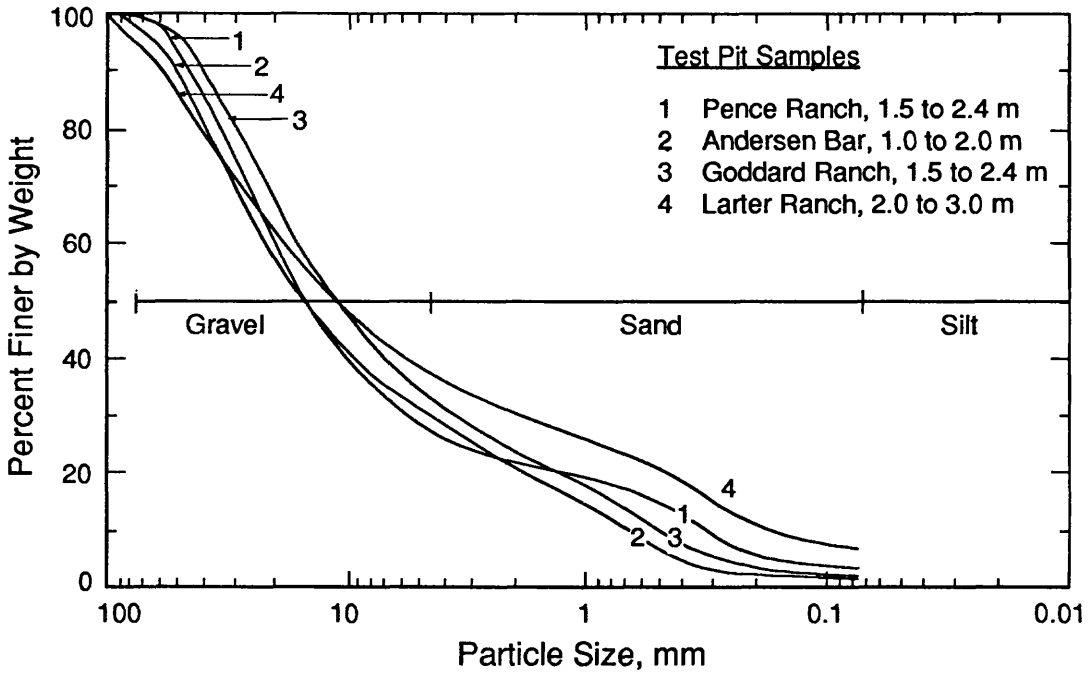

Fig. 1 - Grain-size distribution curves of test-pit samples taken from the critical layer at the four sites.

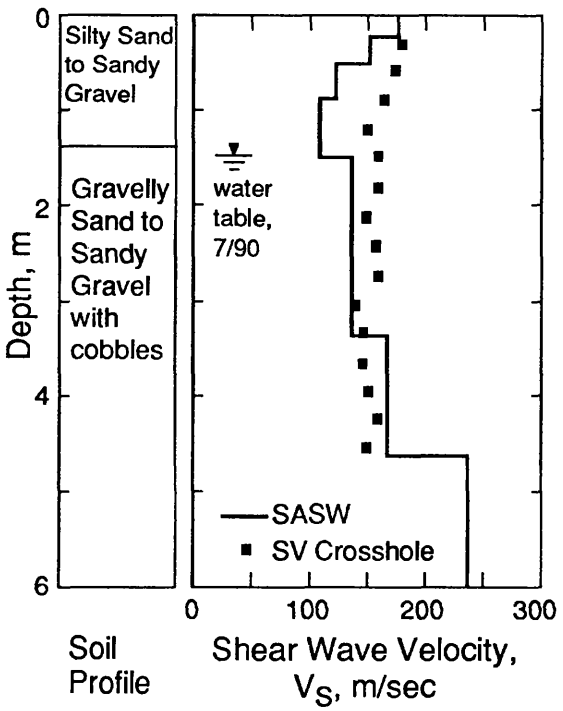

Fig. 2 - Shear wave velocity profiles at Pence Ranch (from Andrus et al., 1992).

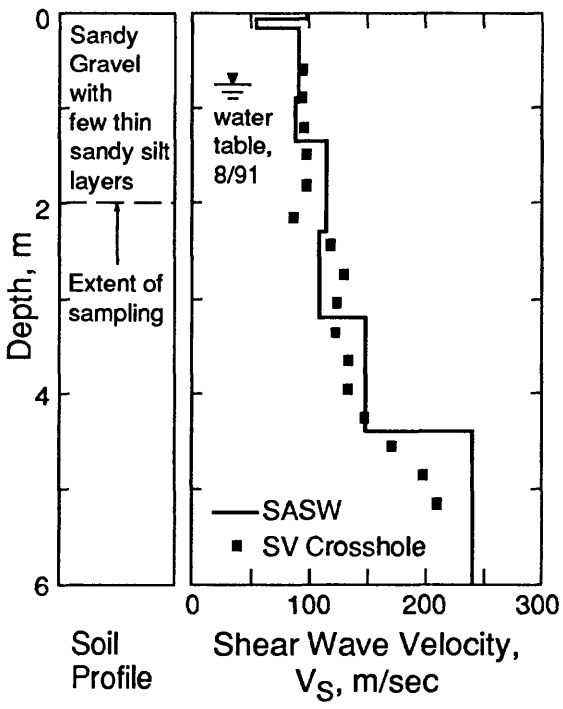

Fig. 3 - Shear wave velocity profiles at Andersen Bar (from Andrus et al., 1992).

COMPUTER GRAPHICS LABORATORY

9950-04541

A. C. Tarr
Branch of Geologic Risk Assessment
U. S. Geological Survey
MS 966, Box 25046, Denver Federal Center
Denver, CO 80225
(303) 273-8570

Investigations

The objective of this project is to provide computer graphics services (such as access to Geographic Information System (GIS) software) to USGS geological hazards investigators. These services include (1) consultation on digital spatial data base design and data acquisition, (2) training in the use of GIS methods, (3) assistance in the assembly of large spatial data sets, and (4) research into advanced spatial data analysis topics. In addition, the Laboratory manages a large Geological Hazards Data Base and assists in producing outreach products that require advanced graphics technologies. Personnel associated with this project are: S. R. Brockman, J. A. Michael, S. Rhea, A. Tarr, and R. Wheeler.

Specific investigations conducted during Fiscal Year 1992 were (1) Geologic Hazards Data Base, (2) Central U.S. and Pacific Northwest earthquake hazards data, (3) Colorado geologic hazards data, (4) SYBASE relational data base development, (5) ARC/INFO user interface development, and (6) Laboratory expansion.

Results

Geologic Hazards Data Base -- During FY 1992, the Geologic Hazards Data Base was managed and maintained by the Computer Graphics Laboratory in Golden, Colorado for the benefit of projects supported by the National Earthquake Hazards Reduction and Landslide Hazards Programs in the Central U.S., Pacific Northwest, and Colorado (Tarr, 1991a). The data in the Data Base consist principally of on-line ARC/INFO coverages and off-line native format data tapes containing USGS Digital Line Graph (DLG), Digital Elevation Model (DEM) files, and SPOT image files. The on-line data consist of working ARC/INFO coverages (approximately 1000 MB) and archived ARC/INFO coverages (approximately 500 MB). The archived coverages have been released by authors for informal distribution to other researchers while the working data are subject to revision and are only available by agreement with the authors. The on-line ARC/INFO data are accessible to local researchers over a LAN and to authorized remote users over Internet; in addition, the archived data sets are available to other research groups via anonymous ftp. For security reasons, the on-line data backup tapes and all the off-line data tapes are stored in a vault at the Central Region GIS Lab at the Denver Federal Center.

A catalog consisting of tabular listings of archived ARC/INFO data sets was produced for internal management of the growing data base. Later, graphics depicting each data layer were added to the listings. The resultant catalog proved to be a useful outreach product for distribution to USGS-supported projects.

Central U.S.-- During FY 1992, numerous geological and geophysical digital spatial data sets supplemented base data layers for eight 30- by 60-minute (1:100,000-scale) topographic quadrangles encompassing the New Madrid seismic zone. The base layers are hydrography, roads and trails, railroads, airports, pipelines, and power transmission lines. The thematic data layers include two instrumental earthquake catalogs, shallow reflection and Vibroseis shot lines, aeromagnetic and gravity anomalies, magnetotelluric profiles, seismic velocity, radon emanation, and various topographic and seismotectonic features. The source data for the new thematic data layers were provided by A. Crone, R. Dart, T. Hildenbrand, S. Rhea, D. Stanley, and R. Wheeler. Data layers portraying infrastructure elements at risk in the Central U.S. were generated by R. Wheeler and S. Rhea. These data included alignments of oil, gas, and petroleum products pipelines, railroads, limited access highways, large dams, and nuclear facilities. Soil profile classifications and liquefaction potential of Shelby County, Tennessee were provided by H. H. W. Hwang of Memphis State University. All of the new data sets were added to the Geologic Hazards Data Base.

The Geologic Hazards Data Base now contains data tapes for two SPOT satellite images of the Reelfoot Lake area and one SPOT Metroview of Memphis. The images were purchased for use as image backdrops for display of thematic data and for image processing experiments to enhance geomorphic features. The SPOT data are multispectral images of the New Madrid area acquired on March 6, 1987 and March 7, 1992 when the effect of vegetative cover was minimal.

Numerous maps and illustrations were produced in the Laboratory for use by various workers. Notable among these were a preliminary multi-sheet seismotectonic map (MF-Map series) of the New Madrid region (Rhea and Wheeler, in press) and three-sheet map of infrastructure elements at risk prepared by R. Wheeler and S. Rhea for a chapter in a USGS Professional Paper (see also Wheeler and others, in press). The seismotectonic map will show new geologic and geophysical information collected in the decade and a half since the previous seismotectonic map of the area (Rhea and others, in press). The Professional Paper chapter describes the data sets, notes spatial relations among them, and suggests likely social and economic impacts of a large New Madrid earthquake. Other maps of interest were of Shelby County, Tennessee and Memphis at 1:100,000 scale that portray soil profiles, liquefaction susceptibility, and infrastructure; the maps were prepared by A. C. Tarr in collaboration with H. H. W. Hwang of Memphis State University.

J. Michael and L. Highland arranged for the creation of a mosaic of the best Landsat images covering a 30 square degree centered on New Madrid, Missouri. Environmental Research Institute of Michigan (ERIM) prepared the mosaic in both

digital and graphic formats from 19 Landsat scenes. The mosaic will be used in future outreach products that require a high-resolution base. The nominal resolution of the mosaic is 100 m.

Pacific Northwest -- During FY 1992, new thematic data supplemented digital data base layers for three 30- by 60-minute (1:100,000-scale) topographic quadrangles encompassing the southern Puget Sound; these new data sets were contributed by L. Highland and T. Pratt and added to the Geologic Hazards Data Base. The base layers are hydrography, roads and trails, railroads, airports, pipelines, and power transmission lines. Thematic data layers now include the University of Washington catalog of instrumental seismicity, MM intensities for the 1965 Puget Sound earthquake, seismic response stations in the Olympia area, surficial geology, and Seattle schools. The surficial geology thematic data layer for the southern Puget Sound is approximately 65% complete as mapping of the northern half of the Tacoma quadrangle has not yet been completed. Base data layers, surficial geology, topographic contours, and slope map of Seattle were provided to the Seattle Planning and Engineering Departments for development of their earthquake response plan. Numerous illustrations, poster graphics, and maps were prepared by J. Michael for R. Bucknam, T. Pratt, and M. Cecil using data from the Geologic Hazards Data Base.

An experimental procedure using ARC/INFO was devised to produce a map of theoretical intensity modified for the effect of geology (Tarr, 1991b). The procedure used empirically determined radii of isoseismals and corrections for geologic unit type. The procedure may also be used with contours of acceleration on hard rock and correction factors other than geology.

Colorado Geologic Hazards -- Data sets pertinent to the needs of Earthquake Hazards Reduction and Landslide Hazards programs, in cooperation with the Colorado Natural Hazards Mitigation Council, were added to the Geologic Hazards Data Base during FY 1992. These data included base data layers for selected areas of the Front Range and Western Slope, the geologic map of Colorado and several 1:100,000 quadrangle maps in the Rockies, and digital topographic contour data for the Slumgullion debris flow near Lake City, Colorado. A series of digital Soil Conservation Service STATSCO soils series maps for Colorado were assembled using ARC/INFO. J. Michael used these Colorado digital soils data to prepare color eolian soils maps of eastern Colorado that are used by R. Madole in his arid lands research for the Global Change and Climate History Program.

Relational Data Base Development-- SYBASE relational data base management software (RDBMS) was procured and installed to provide the a tool for managing the various heterogeneous data bases in the Branch, including the GIS data in the Computer Graphics Laboratory and in the National Landslide Information Center and to gain access to the voluminous GEOBASE seismological data bases maintained by Lamont-Doherty Geological Observatory (SYBASE is the RDBMS of GEOBASE). S. R. Brockman heads the RDBMS development effort. One long-term

goal of this effort is to replace the INFO database engine in ARC/INFO with SYBASE if processing performance proves to be better or equal to INFO. Some performance degradation might be tolerated to achieve the benefits of Structured Query Language (SQL) capability. During FY 1992, a test application was conducted on the National Landslide Information Center's bibliographic data base to gain familiarity with data base design, SQL-generated data retrievals, and report writing. The test application was generally successful except for the report writing function of SYBASE which proved unsatisfactory; a replacement report writer is planned for FY 1993.

ARC/INFO User Interface -- MAPX 2.0, a utility for the production of complex thematic maps using ARC/INFO was replaced with an improved utility, XMAP 1.0, suitable for use with ARC/INFO Rev. 6.0.1. Numerous black-and-white illustrations and large-format color maps were composed during the reporting period using both MAPX 2.0 and XMAP 1.0.

Laboratory Expansion -- The number of projects requesting services from the Computer Graphics Laboratory increased substantially during the fiscal year, resulting in contention for the available hardware and software resources in the Laboratory. At the beginning of FY 1992, Laboratory computer resources consisted of two Sun Microsystems 4/75GX workstations and one Sun 3/60 workstation, 6.3 GB hard disk on-line storage, two single-seat and one three-seat node-locked ARC/INFO Rev. 5.0.1 licenses, an Exabyte 8mm tape drive for data base backups and data exchange, a Tektronix 4207 terminal, and an Altek AC40 digitizing tablet (36" by 48").

Because strong growth of GIS-related projects was anticipated in the future, a phased expansion plan was completed in FY 1992. The first phase included upgrades of the Sun 3/60 workstation to a Sun 4/75GX and the Sun operating system to SunOS v. 4.1.1 and OpenWindows 3. The second phase consisted of upgrading memory on the three Sun 4/75GX workstations to 64 MB, addition of 2 GB of hard disk on-line storage, and installation of ARC/INFO Rev. 6.0.1 on two of the workstations.

Reports Published

Brockman, S. R. and Bollinger, G. A., 1992, Q estimates along the Wasatch Front in Utah derived from S_g/L_g wave amplitudes: *Bulletin of the Seismological Society of America*, v. 82, pp. 135-147.

Brockman, S., Brooks, J., Carver, D., Cranswick, E., Duggar, J. Gomberg, J., Harmsen, S., Meremonte, M., Overturf, D. Shedlock, K., VanDreser, T., Worley, D., and Banfill, R., The June 29, 1992, Little Skull Mountain, Nevada earthquake [abs.]: *EOS*, Transactions of the American Geophysical Union.

Hopper, M. G., Algermissen, S. T., Perkins, D. M., Brockman, S. R., and Arnold, E. P., Director's approval, The December 14 , 1872, earthquake in the Pacific Northwest.

Odum, J. K., Shedlock, K. M., Michael, J. A., Worley, D. M., and Luzietti, E. A., 1991, A seismic reflection survey of the northwestern boundary of the Reelfoot rift near Marston, Missouri: *EOS*, Transactions of the American Geophysical Union, p. 429.

Rhea, Susan, and Wheeler, R. L., in press, Maps showing elements of infrastructure and seismic hazard in the central United States [abs.]: *EOS*, Transactions of the American Geophysical Union.

Rhea, Susan, Wheeler, Russell L., and Tarr, Arthur C., in press, Work sheets for seismotectonic map of the New Madrid 2° x 2° area [abs.]: *Seismological Research Letters.*

Tarr, A. C., 1991a, Geologic hazards data base. *Seismological Research Letters,* v. 62, p. 186-7.

Tarr, Arthur C., 1991b, GIS technology and its application to geologic hazards: *U. S. Geological Survey Yearbook Fiscal Year 1991,* p. 7-9.

Tarr, Arthur C., in press, A data base designed for urban seismic hazards studies, *in* Application of research from U.S. Geological Survey program of assessment of regional earthquake hazards and risk along the Wasatch Front, Utah, P. L. Gori, ed.: *USGS Professional Paper 1519,* pp. 82-90.

Wheeler, R. L., in press, Compressional reactivation of Iapetan extensional faults in southeastern North America [abs.]: *Seismological Research Letters.*

Wheeler, R. L., S. Rhea, and A. C. Tarr, in press, Seismotectonic and related maps of the central Mississippi Valley and environs: *Seismological Research Letters,* v. 63.

INDEX 1

INDEX ALPHABETIZED BY PRINCIPAL INVESTIGATOR

INDEX 2

INDEX ALPHABETIZED BY INSTITUTION

U.S. Geological Survey	Machette, M. N.	458
U.S. Geological Survey	McCrory, P. A.	490
U.S. Geological Survey	McGarr, A.	880
U.S. Geological Survey	Michael, A.	518
U.S. Geological Survey	Mooney, W. D.	528
U.S. Geological Survey	Mori, J.	534
U.S. Geological Survey	Mortensen, C. E.	544
U.S. Geological Survey	Mueller, C. S.	882
U.S. Geological Survey	Mueller, C. S.	951
U.S. Geological Survey	Nelson, A. R.	554
U.S. Geological Survey	Nishenko, S. P.	952
U.S. Geological Survey	Obermeier, S. F.	562
U.S. Geological Survey	Oppenheimer, D. H.	571
U.S. Geological Survey	Park, R. B.	955
U.S. Geological Survey	Person, W. J.	899
U.S. Geological Survey	Plafker, G.	584
U.S. Geological Survey	Ponti, D. J.	588
U.S. Geological Survey	Pratt, T. L.	593
U.S. Geological Survey	Prentice, C.	597
U.S. Geological Survey	Reagor, G.	956
U.S. Geological Survey	Reasenberg, P. A.	599
U.S. Geological Survey	Repetski, J. E.	607
U.S. Geological Survey	Roeloffs, E.	614
U.S. Geological Survey	Rymer, M. J.	959
U.S. Geological Survey	Safak, E.	904
U.S. Geological Survey	Sarna-Wojcicki,A. M.	633
U.S. Geological Survey	Sass, J. H.	906
U.S. Geological Survey	Sato, M.	637
U.S. Geological Survey	Schultz, A.	645
U.S. Geological Survey	Schwartz, D. P.	961
U.S. Geological Survey	Sharp, R. V.	661
U.S. Geological Survey	Shaw, H. R.	663
U.S. Geological Survey	Silverman, S.	671
U.S. Geological Survey	Simpson, R. W.	917
U.S. Geological Survey	Sims, J. D.	682
U.S. Geological Survey	Sipkin, S. A.	686
U.S. Geological Survey	Spudich, P.	920
U.S. Geological Survey	Spudich, P.	922
U.S. Geological Survey	Stein, R. S.	697
U.S. Geological Survey	Stewart, S. W.	700
U.S. Geological Survey	Stuart, W. D.	120
U.S. Geological Survey	Swanson, D. A.	703
U.S. Geological Survey	Tarr, A. L.	967
U.S. Geological Survey	Tinsley, J. C.	711
U.S. Geological Survey	Van Schaack, J.	728
U.S. Geological Survey	Weaver, C. S.	734
U.S. Geological Survey	Wells, R. E.	738
U.S. Geological Survey	Wentworth, C. M.	740
U.S. Geological Survey	Yerkes, R. F.	935
U.S. Geological Survey	Zoback, M.L.	759
Utah Geological Survey	Harty, K. M.	839
Utah Geological Survey	Olig, S. S.	568
Utah State University	McCalpin, J. P.	485

NO REPORTS RECEIVED

Investigators	Institutions
Beck, S.	University of Arizona
Bilham, R.	University of Colorado
Blackwell, R.	U. S. Geological Survey
Bogarert, B.	U. S. Geological Survey
Booker, J.	University of Washington
Carver, G.	Humboldt State University
Christensen, D.	University of Alaska, Fairbanks
Clark, S.	U. S. Geological Survey
Davies, J.	University of Alaska, Fairbanks
Day, S.	San Diego State University
Dieterich, J.	U. S. Geological Survey
Evan, B.	Massachusetts Institute of Technology
Fletcher, J.	U. S. Geological Survey
Gillespie, A.	University of Washington
Goldhaber/Potter	U. S. Geological Survey
Hager, B.	Massachusetts Institute of Technology
Hanks, T.	U. S. Geological Survey
Healy, J.	U. S. Geological Survey
Helliwell, R.	Stanford University
Irwin, P.	U. S. Geological Survey
Jacoby, G.	Lamont-Doherty Geological Observatory
Johnson, D.	Lamont-Doherty Geological Observatory
Julian, B.	U. S. Geological Survey
Keller, E.	University of California, Santa Barbara
Kirby, S.	U. S. Geological Survey
Lasmanis, R.	State of Washington
Lajoie, K.	U. S. Geological Survey
Lerner-Lam, A.	Lamont-Doherty Geological Observatory
Malin, P.	Duke University
Malnar, P.	Massachusetts Institute of Technology
Martin, J.	VA Technology
McGuire,	Risk Engineering, Inc.
Merritts, D.	Franklin/Marshall College
Moses, T.	U. S. Geological Survey
Nye	ADGGS
Pavlis, T.	University of New Orleans
Potter, C.	U. S. Geological Survey
Schuster, G.	University of Utah
Scott, R.	California Institute of Technology
Seeber, L.	Lamont-Doherty Geological Observatory
Segall, P.	U. S. Geological Survey
Sieh, K.	California Institute of Technology
Snavely/Wells	U. S. Geological Survey
Spudich, P.	U. S. Geological Survey
Su, W.	University of Illinois
Sykes, L.	Lamont-Doherty Geological Observatory
Weldon, R.	University of Oregon
Wyss, M	University of Alaska

☆U.S. GOVERNMENT PRINTING OFFICE: 1993-785-291/99064